PROCEEDINGS OF THE SIXTH INTERNATIONAL SYMPOSIUM ON LAND SUBSIDENCE
RAVENNA / ITALIA / 24 - 29 SEPTEMBER 2000

LAND SUBSIDENCE

Vol. I

Geological Issues
Fluid Removal
Solid Extraction
Remedies - Decision Making

Edited by

LAURA CARBOGNIN
GIUSEPPE GAMBOLATI
A. IVAN JOHNSON

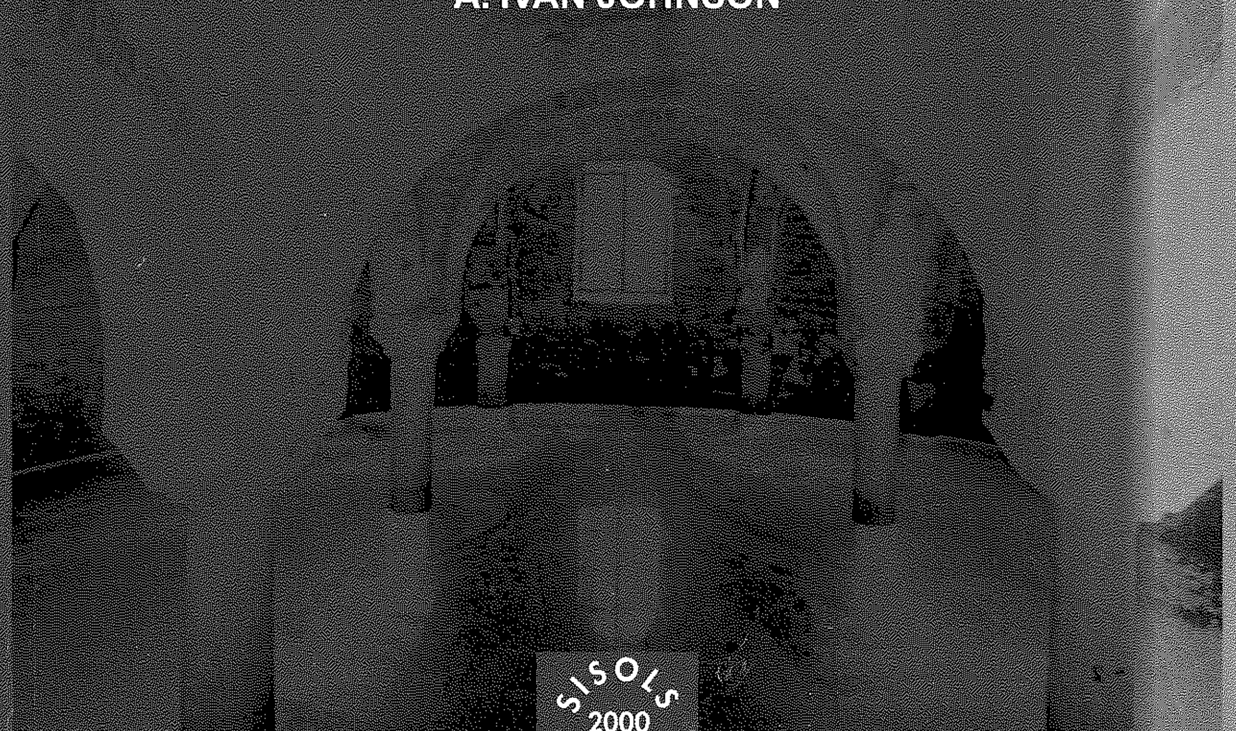

SISOLS 2000

LAND SUBSIDENCE

Vol. I

ISBN 88-87222-06-1

PROCEEDINGS OF THE SIXTH INTERNATIONAL SYMPOSIUM ON LAND SUBSIDENCE

RAVENNA / ITALIA / 24 - 29 SEPTEMBER 2000

LAND SUBSIDENCE

Vol. I

Geological Issues

Fluid Removal

Solid Extraction

Remedies - Decision Making

Edited by

LAURA CARBOGNIN
National Research Council, ISDGM, Venezia, ITALY

GIUSEPPE GAMBOLATI
University of Padova, DMMMSA, Padova, ITALY

A. IVAN JOHNSON
Arvada CO, USA

GNDCI

C. N. R.
National Group for the Pretection Against Hydrogeologic Catastrophies provided financial sponsorship for this publication.

Cover:
Ravenna, the Crypt of San Francesco's Church flooded.

The camera-ready copy for the papers was prepared by the authors and improved and completed at the C.N.R., - Istituto per lo Studio della Dinamica delle Grandi Masse (by Laura Carbognin and Jane Frankenfield Zanin), S. Polo 1364, 30125 Venice, Italy. Neverthless, in some cases, it was difficult to improve the quality of figures submitted by authors.

Printed by
"La Garangola", Via Montona, 4 - 35137 Padova, Italy
ISBN 88-87222-06-1

In honor of many years of research in land subsidence and very active participation in the UNESCO-IHP Working Group on Land Subsidence, this proceedings volume is dedicated to Doctor Laura Carbognin

This dedication provides high praise and Working Group recognition to Laura Carbognin for her long and dedicated participation in research, teaching, and writing about the subject of land subsidence during her activities with the UNESCO - IHP Working Group on Land Subsidence as well as during her position with the National Research Council of Italy (CNR).
Although the First International Symposium on Land Subsidence was convened in 1969, The UNESCO - IHP Working Group on Land Subsidence was not formally established until 1974 as one of the objectives of UNESCO's International Hydrological program (IHP-I). At that time Doctor Laura Carbognin was selected as a member of that Working Group and remained active in its affairs ever since. She assisted with the organization of all five UNESCO -sponsored subsidence symposia, and was local organizer of the Third edition convened in 1984 in Venice, and co-editor of the proceedings volume (published as IAHS Publication No. 151) resulting from that symposium. Laura also chaired this Sixth Symposium (SISOLS 2000) and is senior editor of the resulting proceedings.

Up to now Laura Carbognin has served for 31 years on the staff of the CNR at the Istituto per lo Studio della Dinamica delle Grandi Masse (ISDGM), where she joined the research staff in 1970 to work in the field of geostatistics. Presently, in the ambit of CNR, she is Director of Research.

During her career Laura had the responsibility for research concerning the understanding of environmental problems mainly related to land subsidence and coastal processes, especially for the lagoon of Venice and the North Adriatic Sea. Studies she and her colleagues performed, the first in Italy, on the subsidence in Venice and Ravenna, and on the environmental impact of this process, are of primary importance and of international interest. Within the framework of the ISDGM research activity, Laura has been involved in scientific studies concerning geomorphology, micropaleontology, water pollution, flooding and eustacy. In particular, the study on sea level rise made through a series of statistical analyses, partly original, has permitted definition of the eustatic trend for the last century, filtering out the influence of land subsidence during its occurrence.

For her innovating statistical approaches to environmental problems, she has received international recognition in the book "Italian Contributors to the Methodology of Statistics", 1987.
In addition to her research career, she has dedicated herself to training young scientists specializing in land subsidence studies, teaching courses and organizing national and international schools.

Laura Carbognin has been a prolific author of papers and reports, many of which have been on the subject of land subsidence.

In recognition of her scientific accomplishments, and because of her devoted participation and achievements in the activities of the UNESCO - IHP Working Group on Land Subsidence and its sponsored symposia, this proceedings volume resulting from the SISOLS 2000 of Ravenna, Italy is dedicated with great respect and appreciation to Laura Carbognin.

A. Ivan Johnson
Chairman, UNESCO-IHP W.G. on Land Subsidence

The Organizing Committee would like to express their appreciation to the many people who gave their time, effort and knowledge to produce a successful programme and enjoyable field trip.

The collaboration of the Scientific Advisory Board and the Local Working Committee is gratefully acknowledged.

Special thanks go to Mrs. Jane Frankenfield Zanin who provided the technical scientific secretarial job needed for the symposium and invaluable assistance in the publication of this proceedings volume.

The Editors would also like to express their thanks for the sponsorship and endorsement provided for the symposium by the following organizations and companies.

Sponsoring Organizations:

UNESCO
CNR (National Research Council of Italy)
ANPA (National Agency for the Protection of the Environment)
ARPA (Emilia Romagna Regional Agency for the Protection of the Environment)
ASSOMINERARIA
CVN (Consorzio Venezia Nuova)
Emilia-Romagna Regional Government
ENI-Agip
GNDCI (National Group for the Protection against Hydrogeologic Catastrophes)
IHP (International Hydrological Programme)
MED-Ingegneria
Municipality of Ravenna
NGC (Netherlands Geodetic Commission)
Romagna Acque
Solvay Chimica Italia S.p.A.
University of Ferrara
University of Padova

Endorsing Organizations:

IAHS / ICGW (International Association of Hydrological Sciences / International Commission on Ground Water)
AGID (Association of Geoscientists for International Development)
IAH (International Association of Hydrogeologists)
ISSMGE (International Society for Soil Mechanics and Geotechnical Engineering)
Ministry of Industry, Trade, and Handicraft of Italy
Ministry of the Environment of Italy

Organizing Committee

Laura Carbognin - Symposium Chairman
National Research Council, ISDGM, Venezia, Italy

Giuseppe Gambolati - Symposium Co-chairman
University of Padova, DMMMSA, Padova, Italy

A. Ivan Johnson, Chairman, UNESCO Working Group
Arvada, CO, USA

Scientific Advisory Board

James W. Borchers, U.S. Geological Survey, Sacramento, CA (USA)
Frans B.J. Barends, Delft Geotechnics, Delft, The Netherlands
Gianluigi Chierici, University of Bologna, Bologna, Italy
German E. Figueroa Vega, Coordinacion General de Los Proyectos de Abastecimiento de Agua Potable y Saneamiento del Valle de México, Mexico D.F.
Donald Helm, Morgan State University, Baltimore, MD, USA
Keith Prince, U.S. Geological Survey, Menlo Park, CA, USA
Francis Riley, U.S. Geological Survey, Menlo Park, CA, USA
Abdin M.A. Salih, Hydrological Sciences & Ecology, UNESCO, Cairo, Egypt
Andras Szollosi-Nagy, Director, Division of Water Resources, UNESCO, Paris, France

Local Working Committee

Alice Aureli, Division of Water Resources, UNESCO, Paris, France
Werther Bertoni, Geological Survey, Municipality of Ravenna, Ravenna, Italy
Giovanni Brighenti, University of Bologna, Bologna, Italy
Roberto D'Amico, ENI-Agip, Ravenna, Italy
Giancarlo Dossena, Assomineraria, Roma, Italy
Marco Gonella, MED-Ingegneria, Ferrara, Italy
Francesco Marabini, CNR-IGM, Bologna, Italy
Raffaele Pignone, Geological Survey, Emilia-Romagna Region, Bologna, Italy
Paolo Russo, University of Ferrara, Ferrara, Italy
Leonello Serva, ANPA, Roma, Italy
Pietro Teatini, University of Padova, Padova, Italy
Luigi Tosi, CNR-ISDGM, Venezia, Italy
Lucio Ubertini, Chairman, IHP National Committee, Perugia, Italy
Adriano Zavatti, ARPA, Bologna, Italy

Scientific Secretariat

Mrs. Jane Frankenfield Zanin, CNR-ISDGM, Venezia, Italy

CONTENTS

Vol. I

3 Solid extraction

4 Remedies - Decision Making

Vol. II

1 Measuring and Monitoring

Preface

Since the 1950s, there has been an ever increasing global awareness of problems related to the sinking of the land surface. The efforts by the scientific community were directed toward furthering the understanding and knowledge on both natural and anthropogenic causes, field and lab measurements, mechanisms, prediction techniques, effects and remedial measures. In the course of time, man realized that he could no longer follow a "use and discard" philosophy with underground resources. As a result, a need for a consistent policy of rational management of underground resources became evident. The seriousness of land subsidence was recognized by the United Nations Educational, Scientific and Cultural Organization (UNESCO) in 1969, when this problem was first included for study under the International Hydrological Decade (IHD), and later the International Hydrological Programme (IHP). This resulted in the organization of six International Symposia on Land Subsidence jointly sponsored by UNESCO, the International Association of Hydrological Sciences (IAHS), and other International and National Organizations that were held in 1969; 1976; 1984; 1991; 1995; and the Sixth International Symposium on Land Subsidence (SISOLS) in Ravenna, Italy in 2000.

SISOLS 2000 aimed to gather together members of the Scientific Community to review the advances achieved in the field of land subsidence, to present new research ideas, to exchange experiences, and to discuss a *sustainable approach* to land subsidence, intended to seek a compromise between the use of natural resources and mitigating negative effects caused by their exploitation. Issues include: the sustainable development of subsurface resources which may induce land subsidence, distinguishing natural subsidence from the anthropogenic one, predicting potential hot spots, in particular those located in coastal and low-lying flat areas, new monitoring techniques and advanced computer models to control and predict land subsidence phenomena. It is now recognized that decisions with respect to preventive or remedial land-subsidence strategies take place in a complex decision-making milieu in which there are many potentially-adversarial stakeholders. Negotiated settlements among these stakeholders depend on the results of technical analysis, but are heavily influenced by social, economic, legal, and political issues. The SISOLS 2000 program highlights the need for the integration of social policies that address resource management, land-use planning, industrial development, hazard mitigation, and environmental protection.

From the large number of contributions received, 68 have been selected and published in two separate proceeding volumes as follows:

Symposium topic	*Proceedings volume*
Geological issues	Volume I
Fluid removal	Volume I
Solid extraction	Volume I
Remedies - decision making	Volume I
Measuring and monitoring	Volume II
Theory and modeling	Volume II

The symposium was hosted by the Municipality of Ravenna at the beautiful Alighieri Theater inaugurated in 1852 in commemoration of the famous Italian poet Dante Alighieri (1265-1321) who is buried in Ravenna.

The one-day technical-environmental excursion to the Po Delta area, the largest expansion of land sinking in Italy, gave participants a chance to see and to visit one of the many beautiful natural reserves of Italy rich in flora and avifauna. The ENI-Agip Division contributed to making the trip possible through its sponsorship.

On Thursday afternoon, September 28, many representatives from local, regional, national and private agencies participated in the Round Table on problems connected with land subsidence problems in Italy.

Laura Carbognin
Symposium Chairman, National Research Council of Italy (CNR), Venezia, Italy

Giuseppe Gambolati
Symposium Co-chairman, University of Padova, Padova, Italy

A. Ivan Johnson
Chairman, UNSECO/IHP W.G. on Land Subsidence, Arvada, CO, USA

September, 2000

1 Geological Issues

SUBSIDENCE IN THE SYBARIS PLAIN (ITALY)

Claudio Cherubini
Istituto di Geologia Applicata e Geotecnica. Politecnico di Bari.
Via Orabona, 4, 70125 Bari, Italy

Vincenzo Cotecchia and Rosa Pagliarulo
Centro di Studio sulle Risorse Idriche e la Stabilità del Territorio
CNR, Via Orabona, 4, 70125 Bari, Italy.

Abstract

This research project describes the complex phenomena of subsidence in the Sybaris plain where the archaeological site is located. This phenomenon has been common since ancient times as the archaeological digs performed have led to the identification of three superimposed levels of occupancy, indicating continuous habitation from the sixth to the first century BC.

The phases of the geological evolution of the plain during the last 35,000 years have been identified on the basis of multidisciplinary surveys carried out on field and in the laboratory on samples taken from several boreholes. In particular piezocone tests have been performed for a depth of 100 meters. By means of the data collected, geotechnical classification of soils was possible. Carbon-14 dating has also been performed on samples of peat levels, carbon frustules and fossil remains up to a depth of 96 m below the actual ground level. Topographical surveys show about 20 cm soil subsidence ascertained at the IGM bench marks since 1950, mainly due to the withdrawal of the fresh water from the surface water table.

Keywords: land subsidence, sea level changes, alluvial plain, piezocone test.

1. INTRODUCTION

The CNR "Centro di Studio sulle Risorse Idriche e la Salvaguardia del Territorio" has been carrying out research on the archaeological site of Sybaris within the CNR Committee of Cultural Heritage Special Project. During the course of the research carried out until now, a complex phenomenon of subsidence has been found by means of a campaign of interdisciplinary investigations aimed at understanding the evolution of the area. Three main components have been found to be responsible for it: a) neotectonics; b) glacio-eustatic variations of the sea; c) compression of the sediments. (Cotecchia et al., 1994; Cherubini et al.,1994; Pagliarulo et al., 1995; Cotecchia & Pagliarulo, 1996). Archaeological research carried out in Sybaris, which began in 1879 and is still continuing, has led to the identification of three superimposed levels of occupancy, indicating continuous habitation from the sixth century BC (the ancient Greek town of Sybaris), then the third century BC (the Hellenistic town of Thurii) up to the first century BC with the Roman town of Copia, at a depth of between 7 and 3.5 metres from the present ground level. The finds are concentrated in different areas, Parco del Cavallo, Casa Bianca, Prolungamento strada and Stombi are some of those which have been found as being the ancient river courses of the rivers Crati and Coscile, with a single outlet today into the Ionic sea. (Fondazione Lerici, 1967), (Fig. 1)

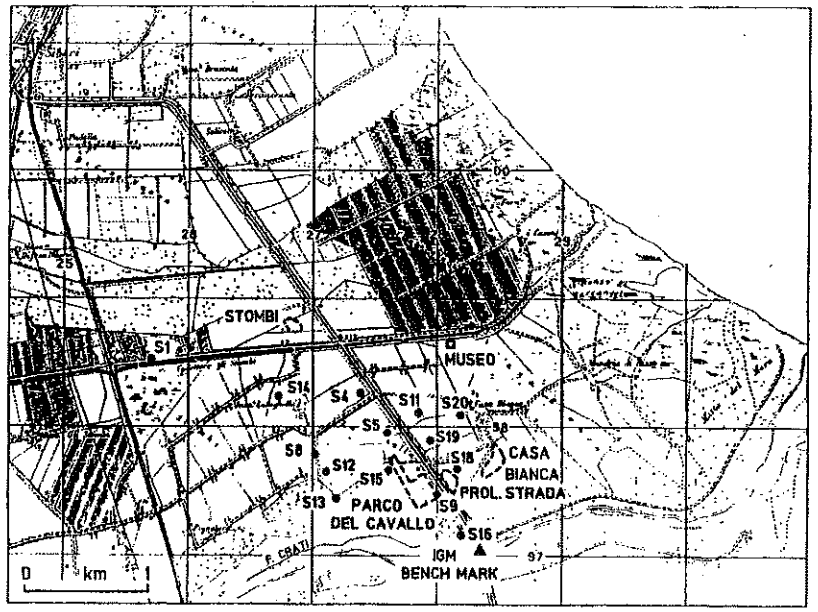

Figure 1. Location of archaeological sites and geomechanical borings drilled during the geognostic campaigns supported by CNR.

The archaeological site of Sybaris is located on the alluvial plain with the same name, crossed by the low valley of the river Crati and its tributaries. The plain is the terminal part of a graben, which runs in an ENE-WSW direction. The upper part of this depression is filled by alluvial deposits whose thickness is around 400 metres, consisting of sands, some of which are the finer clay-sandy variety, while others are coarser gravels that are anastomosed by frequent heteropic phenomena. Some peat levels are found at various depths. The neotectonic activity of the fault systems which border the graben has given rise to widespread lowering, called so because within the general raising of the southern Apennine chain, the raising level is lower than that of the surrounding areas.

2. CARBON-14 DATING AND DISCUSSION OF THE DATA

During the geognostic campaigns carried out 20 investigations were drilled with a variable depth from 10 to 120 metres from the current ground level. During the execution of these tests numerous samples were taken both for mineralogical-petrographic analysis and for ^{14}C dating. The presence and dating of consistent peaty levels found in the investigations (S1) in the Stombi area allowed extremely important considerations to be made regarding the glacio-eustatic variations of the sea along the Ionic coast. (Fig. 2).

The coastline in this area has undergone great changes since the end of the Pleistocene period and these have greatly influenced the sedimentation areas, which are being studied as well. The end of the Tyrrhenian was characterised by

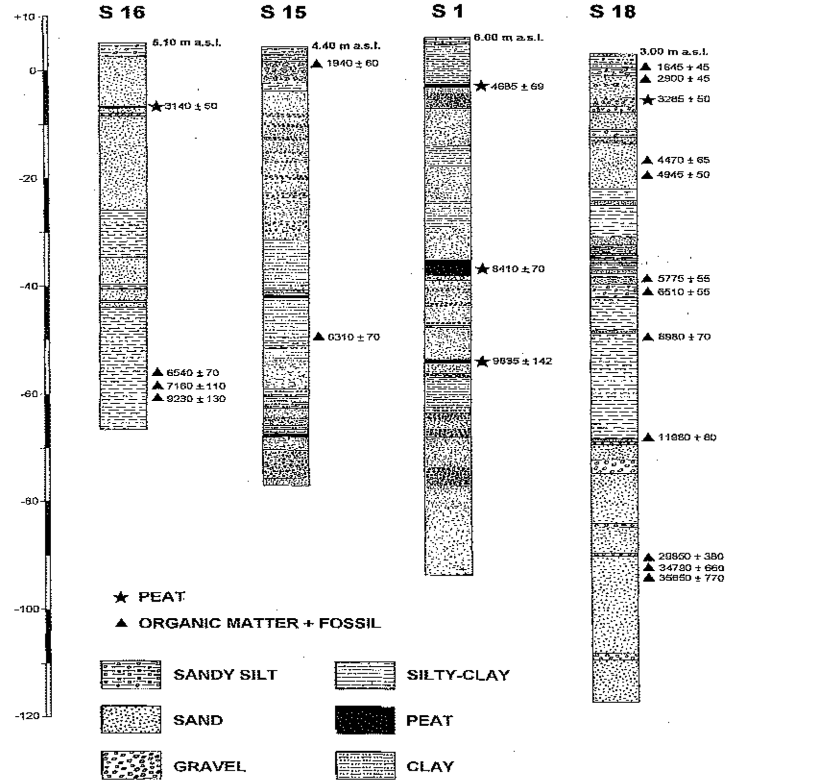

Figure 2. Soil profiles along the deepest boreholes indicating not calibrated absolute ages in yr BP obtained from ^{14}C dating.

Flandrian regression, which brought the sea level to approximately 100 metres below the current level. The subsequent equally rapid transgression about 6000 years ago brought the sea level more or less back to today's level. If it is considered that the area was in a marshy type transition in the period when the three levels of peat found in the S1 investigation were deposited, it can be deduced that the sea level must have been lower than the current level by between 4 and 40 metres. The size of these measurements is obviously just an estimate both for the significance to attribute to the diagram of the glacio-eustatic variations and because the effects of these variations cannot always be easily distinguished from the tectonic component. In a previous paper (Cotecchia et al., 1994), the total subsidence rate was calculated also considering the apparent subsidence due to glacio-eustatism. On the basis of these calculations, a considerable decrease in the speed of subsidence of the layers of the upper part of the ground was noticed. This trend is also confirmed by the data coming from other investigations.

If, as we have seen, comparing the age of the peat deposits with the glacio-eustatic variations of the sea is a mere indication, it is rather risky to correlate the values of the other datings obtained in the area with these diagrams for two reasons. The first because the absolute ages, as shall be seen below, were obtained by dating carbon frustules and remains of fossils, thus organic substances dissolved in the sediments and not primary deposits and secondly because the further one goes back in time the more uncertain the diagrams of the glacio-eustatic variation of the sea curves become. (Fig 3)

The absolute uncalibrated age of the carbon frustules and the remains of fossils were obtained by means of analysis with the Accelerator Mass Spectrometer (AMS), considering the small quantity of organic substances. The analyses were partly carried out in the Australian National Tandem for Applied

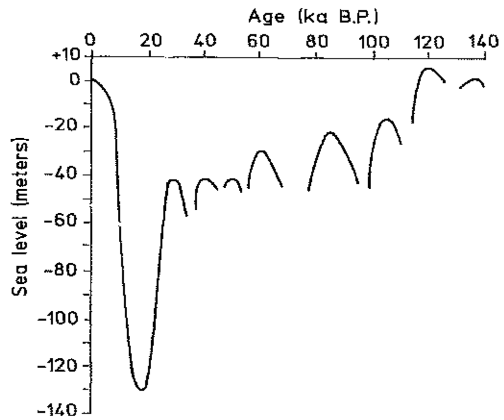

Figure 3. Sea level changes during Upper Pleistocene and Holocene (from Moore, 1982).

Research of Sidney and partly in the Department of Physics and Atmospheric Sciences at the University of Tucson, Arizona. The following considerations can be made by further analysing investigation S18, which reached 120 metres from

the ground level and was located in Casa Bianca, near one of the North-South roadways from the town of Thurii. The upper part of the stratigraphic column shows lithological characteristics which are typical of rearranged land resulting from the presence of layers with settlements, indeed at a depth of about -4.50 m compared to the ground level (the S18 investigation is located at 3 metres a.s.l.) the remains of buildings and various parts of ceramics were found. Moreover the absolute age of 2900 ± 45 yr BP of the sample taken at -4 m is entirely compatible with the Hellenistic age back to which the roadway of Thurii dates. Below this depth the different rock types become more frequent, changing rapidly from the clayey silts to fine quartz sands with large quantities of mica and from these to sandy silts between –35 and –45 metres from the ground level. Then down to a depth of –75 metres the sediments show more uniform lithologic features and the particle size becomes extremely fine. This variability indicates a depositing environment which varies from lagoonal to coastal, more precisely the area defined as intertidal. The lithology is almost totally uniform from a depth of –71.3 m from the ground level, whose absolute age is 11,980 ± 80 yr BP, down to the bottom of the borehole and consists of fine sands with large quantities of mica and full of organic substances, giving it its dark grey colour. The uniform sandy levels are interrupted by some gravelly layers with large blocks of granitic and gneissic rocks. The largest layer is located at approximately –75 m and is probably an ancient riverbed. In the S1 and S15 investigations, located further inland, a larger particle size was found more or less at the same depth.

3. GEOMORPHOLOGICAL EVOLUTION OF THE SYBARIS PLAIN

An attempt has been made to reconstruct the geological evolution of the Plain of Sybaris in the last 35,000 years on the basis of what has been set out before and by interpreting the sequence of deposits. Up until 35,000 yr BP Würmian glaciation was going on and thus even the Mediterranean area must have been affected by a cold climate. The deepest sand samples examined in investigation S18 show a rather fine high quartz content sediment with specks of muscovite and greatly altered granules of feldspar. Moreover, in terms of fauna content the samples were found to be sterile, but with a great deal of carbon frustules. In that time the sea level must have been about 40 metres lower than the present level and considering the cold and dry climatic phase there must have been a reasonably low alluvial material load. Sedimentation should have taken place very slowly as is demonstrated in the deepest layers of investigation S18, where only three metres were deposited in an extremely long period of time, changing from an absolute age of 29,850 ±380 yr BP at -93.3 m to 35,650 ±770 yr BP at -96 m.

Going towards the Upper Pleistocene it changed to a milder climatic phase than the previous one with a greater sedimentation speed and with rapid modifications in the sediment particle size. Around 20,000 yr BP Flandrian regression began and there was a colder and drier climatic phase, which culminated in about 11,000 yr BP with the cold period of the Younger Dryas. (Fig. 4).

In this period a stopping or a deceleration of sedimentation can be assumed. The climatic conditions changed with the Flandrian transgression, the temperature became milder and the sea level rose. As can be seen from the investigation logs, the lithological facies became more varied. The sedimentation environment varied from a typical sedimentary alluvial regime inland from the coastline, with marshy areas leading to the sedimentation of the peaty levels to a mixed coastal environment.

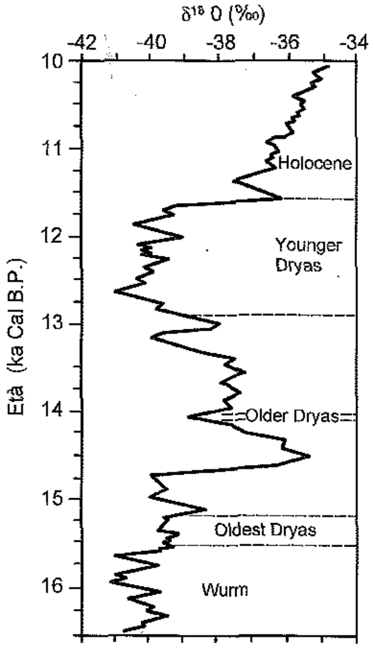

Figure 4. Late Glacial and Early Holocene δ^{18} O curve (from Orombelli & Ravazzi, 1996; modified)

As far as evolution during the Holocene is concerned, it can be seen that the ^{14}C age values are in line with the archaeological dating of the inhabited layers. The Roman town Copia overlooked the sea. The towpath now located at approximately 2.5 Km from the sea, had to be located on the seashore during Roman times. As mentioned in the previous paragraph, the amount of subsidence was much slower in the layers nearest to the current ground level compared to the deepest alluvial levels. Morphological variations resulting from variations in the Crati and Coscile river courses must also be taken into account. Historical sources indicate that the ancient town of Sybaris was located between the two rivers Crathis and Sybaris (now called Coscile). While the two rivers now have one single outlet, which has moved about 2.5 Km towards the sea since Roman times, they flow together a few kilometres upstream from the archaeological area

of Parco del Cavallo. The stream capture of the river Coscile by the river Crati cannot have influenced the historical evolution of the ancient inhabited layers of Sybaris, Thurii and Copia, since the two rivers still had separate courses as is evidenced by some geographical maps of Rizzi Zannoni Zotti of 1714, 1759 and 1783.

4. HYDROGEOLOGY

The deep boreholes sunk during the recent campaign have provided further information about the hydrogeology of the area. The permeability coefficients, derived in situ, vary from a maximum of about 10^{-3} cm/s to a minimum of around 10^{-7} ∏ 10^{-8} cm/s. The vertical variability of hydraulic conductivity is very great. The shallow water table, which affects archaeological levels more intimately, can be found at a mere 0.5 m bgl. This water table is dammed towards the shoreline by intruding seawater. At the present time, it is drained by a well-point system at the archaeological site to lower the groundwater level to an elevation of about mean sea level. In spite of this, the aquifer is not as yet affected by saltwater intrusion. Water for domestic use and for irrigation is pumped not rationally from the deepest water table. As a result, since 1950, some 20 cm soil subsidence ascribable to water extraction has been ascertained at the IGM bench mark located on the bridge over the Crati river. The presence of hydrogen sulfide and methane has been detected in boreholes drilled since the fifties. The local draw down of gas-pockets is likely to speed up the subsidence of the plain, as well. This indicates the chemical reduction of organic matter by the brackish fossil water confined in the deepest layers. This water is not thought to receive any natural recharge. Therefore, its extraction is likely to result in accelerated subsidence.

5. LABORATORY DATA

The S1 borehole is located next to a vertical along which a test was carried out with a piezocone (Fig. 5). As can be seen, the particle sizes and the consistence limits are rather variable. The latter in particular indicate medium or medium high plasticity with values of activity ranging between approximately 0.3 and 1.0. The same investigation showed clay values ranging from 0 to 50%, silt from 8 to 58% whereas the largest fractions (sand and sometimes gravel) range from 10 to 58%. The presence of gravel and pebbles becomes prevalent at greater depths (>70 m). The unite weights remain around 16 - 17 kN/ m^3. Some thin layers of peat a few decimetres thick can also be noted. The greatest quantities of fine material are found between 23 and 42 m. Similar variations to those found in investigation S1 were also found in investigation S15, while it was ascertained that a more significant presence of clay and lime was found between 30 and 72 m. As far as other features of the deposits are concerned, the permeability coefficient values of the finest materials was found to be around 10^{-8} cm/sec with slightly lower values in some cases. After evaluation of the K0 and comparison with the most widely accepted formulations concerning the dependence on F' these sediments can be considered as being normally consolidated ones. Further confirmation of the normal consolidation state of these sediments has been obtained from the study carried out in a previous work regarding a comparison of the state of the samples on site with the Intrinsic Compression Line (ICL) and with the Sedimentation Compression Line (SCL),

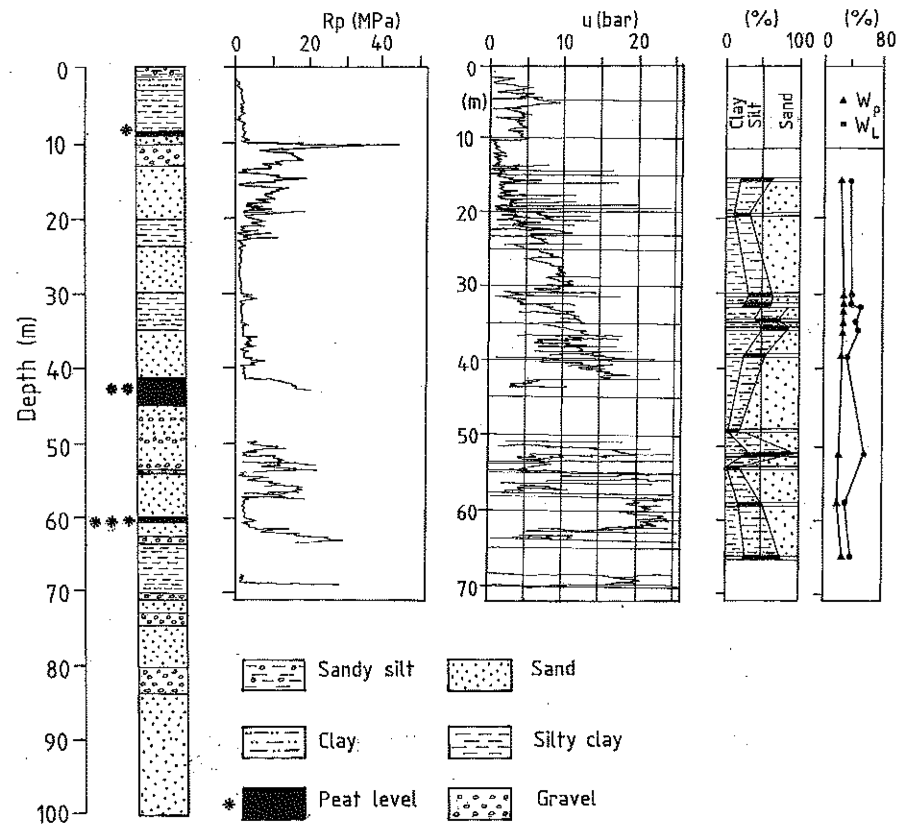

Figure 5. Soil profile, grain size distribution, consistency limits, tip resistance and pore pressures for borehole S1.

the sensitivity was also found to be below average. It was also possible to evaluate how these sediments are generally deposited in an environment characterised by high sedimentation speed.

6. IN SITU TESTS

A piezocone test was performed for a depth of about 100 m at Stombi, measuring the point resistance and the corresponding excess pore pressures. Unfortunately the lateral friction could not be read; this limits the possibilities offered by this kind of analysis to some extent. Figure 5 reports the diagrams of the as-read point resistance and excess pore pressures. It shows that coarse materials were come across between about 44 and 50 m in a short stretch prior to the 70 m mark. Fine grained materials occurred mainly at depths between 22 and 43 m, with minor presence at greater depths. The materials encountered by the borehole were then classified by the procedure proposed by Robertson (1990), (Fig. 6).

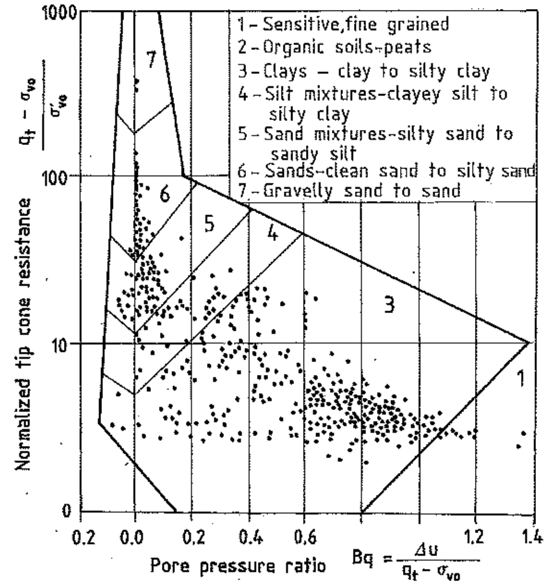

Figure 6. Robertson's nomogram (1990) for the results obtained using the piezocone.

It is readily apparent that there is a significant concentration of points in Zone 3, which includes clay and silty-clay ground, especially in the part where there is a B_q ratio of 0.6- 0.8, thus confirming that these are normally consolidated soils. There is also a concentration in fields 4, 5 and 6; this is characteristic of soils whose particle size distribution places them between clayey silts and sands, especially in those parts where B_q is fairly close to zero. The great variability of data can certainly be put down to the peculiar characteristics of the deposits, with a by-no-means negligible contribution from various factors influencing the test results to differing extents.

An evaluation has been made of the undrained shear strength Cu in the stretch between - 22 and - 43 metres on the basis of piezocone data, where a significant stiffer bed of clayey and soft silty clayey material is encountered. The expression adopted for the evaluation is:

$$C_u = \frac{q_c - \sigma_{vo}}{N_k}$$

where q_c is the point resistance; σ_{vo} is the total vertical load; $N_k = 15 \pm 3$.

The law found with $N_k = 15$ is of the type $C_u/\sigma'_{vo} = 0.24$. It is interesting to compare C_u calculated in this manner with the one derived by empirical relations using the Plasticity Index and the Liquid Limit. These relations have been applied by taking account of the minimum and maximum values encountered for PI and LL. They give 0.14 as the minimum value and 0.29 as the maximum one.

It should also be noted that according to Burghignoli & Scarpelli (1985), the values of C_u/σ'_{vo} for other types of soft Italian clays range from 0.15 to 0.40. Finally, an examination of four pressurimeter tests, performed in another borehole in the same area, has enabled an estimate to be made of the axial and shear moduli, reported in fig.7.

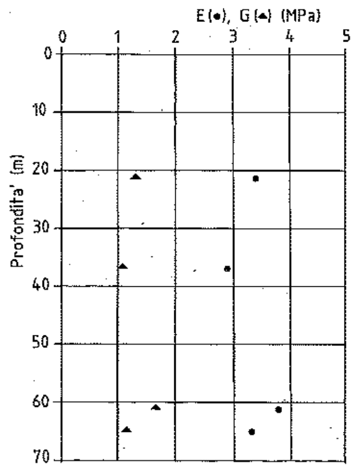

Figure 7. Values E and G obtained by the pressurimeter, as a function of depth (borehole S15).

The values obtained seem to match the materials investigated. This test also provides another way of evaluating the undrained shear strength C_u by means of the following empirical relationship involving initial pressure P_0 and limit pressure Pl for the upper 73 meters (Ghionna & Robertson, 1987; Giannaros & Christodoulias, 1990):

$$C_u = (Pl - Po)/5.5$$

The test conducted at the shallower depth gives a much higher value of C_u than that which might be expected on the basis of the piezocone results. The three tests conducted at greater depth point to a variation law of the following type:

$$C_u/\sigma'_{vo} = 0.17$$

the ratio being lower than that which emerges from the piezocone data.

Some authors (Mayne & Rix, 1993) have suggested some correlation between the tip of the penetrometer and the shear modulus G_{max} to small deformations. One of these relations is the following:

$$G_{max} = 42.9\ q_c^{\ 0.51}$$

with G_{max} and q_c in MPa.

The data from our areas indicated q_c as varying between 1 Mpa and 2.5 Mpa for the finest parts according to the depth, whereas it even reaches values of 20 Mpa for the coarsest levels, excluding crossing the gravel at depths of around 65-70 m. It is thus possible to determine values of G_{max} of between 42.9 Mpa and 68.5 Mpa for the clays, whereas the G_{max} of coarser grounds may reach the value of 198 Mpa.

7. CONCLUSIVE REMARKS

The investigations carried out until now on the Plain of Sybaris have indicated the geological – structural, geoclimatic and geotechnical circumstances responsible for the great subsidence affecting the ancient town of Sybaris and thus the Hellenistic town and the Roman one above it over the past two and a half thousand years. The ground level of ancient Sybaris was found in investigations and digs carried out until today below the water table approximately 2.5 metres below the current mean sea level with a relative variability of absolute distance depending on the differentiated measure assumed by the subsidence phenomena due to the lateral and vertical passage of differing sedimentary facies.

The bibliography mentions the previous papers in which the components which have led to the total subsidence of the ancient site, while this paper has concerned the reconstruction of the geomorphological evolution of the area from the Upper Pleistocene on the basis of the numerous ^{14}C datings carried out on organic substances present at different depths in the alluvial sediments levels and the reconstruction of the influence of climatic factors on depositing the sediments themselves. Reference has been made to the effect that the continual compression of the ground below the site over time may have had on the subsidence phenomena. The results obtained by means of in situ tests, using the piezocone in the first 100 metres of the sediments filling the plain, have shown the extreme variability of the soils with depth, the presence of significant percentages of fine grained soil, the low permeability of these fine soils and the state of normal consolidation of the sediments. Comparison of these results with the more precise laboratory findings showed a good agreement. The lithostratigraphic and geotechnical analyses both in situ and in the laboratory were found to have a satisfactory agreement. The whole analysis identifies the existence of a highly compressible mainly clayey layer which is discontinuous laterally from 35-40 metres of depth and possibly responsible for the great geotechnical subsidence which has occurred in the archaeological area of Parco del Cavallo. Thus the heterogeneous subsidence which, as has been mentioned, led to the presence of deep compressible levels and occasionally significant layers of peat like in the area of investigation S1, may have caused the faults in the inhabited layers such that they are no longer flat but undulating.

The research carried out not only represents a scientific advance regarding the knowledge of the subsidence phenomenon in the area, but also regarding the present and future management and visit to the archaeological digs. Water, invading the subsoil and the archaeological remains present in it are of special concern here. All the studies carried out will provide a guide as to the type action required to keep deep levels of archaeological interest free from groundwater.

REFERENCES

Burghignoli A. & Scarpelli G. (1985) Properties of Italian Clay Soils. A.G.I. *Geotechnical Engineering in Italy. ISSMFE Golden Jubilee.*

Cherubini C., Cotecchia V. & Pagliarulo R. (1994) Geological and geotechnical problems connected with the disappearance of the ancient city of Sybaris. *Science and Technology for cultural heritage*. Vol. 3, 95-112.

Cotecchia V.& Pagliarulo R.(1996) State of the art in geological, hydrogeological and geotechnical researches carried on the archaeological site of Sybaris. *Geologia Applicata e Idrogeologia*,Vol. XXX, 43-54.

Cotecchia V., Cherubini C. & Pagliarulo R. (1994) Geotechnical characteristic of outcropping deposits in the Sibari Plain. *Proceedings XIII International ICSMFE. New Delhi*. Vol. 1., 245-250.

Fondazione Lerici Politecnico di Milano and University Museum Philadelphia Pennsylvania (1967) The search for Sybaris 1960-1965. *Lerici Editori.*

Ghionna V. N. & Robertson P.K. (1987) Capability of in situ testing. *Atti delle Conferenze di Geotecnica di Torino. XIII Ciclo.*

Giannaros H. & Christodoulias J. (1990) Pressurimeter, laboratory and in situ test correlations for soft Cohesive soils. *6th International IAEG Congress.* Balkema Amsterdam , 371-376.

Mayne P.W. & Rix G.J. (1993) Gmax-qc relationships for clays. *Geotechnical Testing Journal.* Vol. 16 N.1, 54-60.

Moore W. S. (1982) Late Pleistocene sea level history. *Uranium series Disequilibrium: Applications to Environmental Problems. Ivanovich & Harmor (eds)* Clarendon press, Oxford, 481-494.

Orombelli G. & Ravazzi C. (1996) The Late Glacial and Early Holocene: chronology and plaleoclimate. *Il Quaternario. Italian Journal of Quaternary Sciences.* Vol. 9, Fasc. 2, 439-444

Pagliarulo R., Cotecchia F., Coop M.R., & Cherubini C. (1995) Studio litostratigrafico e geotecnico della Piana di Sibari con riferimento all'evoluzione morfologica e ambientale del sito archeologico. *Proc. I Convegno del Gruppo Naz di Geologia Applicata. Geologia Applicata e Idrogeologia. Vol. XXX,* 375-391.

Robertson P.K. (1990) Soil classification using the Cone Penetration Test. *Canadian Geotechnical Journal* 27, 151-159.

DISCOVERY OF SUBMERGED FIXED ARCHAEOLOGICAL STRUCTURES IN THE CROTONE COASTAL STRIP BETWEEN STRONGOLI MARINA AND LE CASTELLA (CALABRIA REGION, ITALY). CONSIDERATIONS ON COASTAL EROSION AND SUBSIDENCE PHENOMENA[1]

*A. Guerricchio, **L. Cantafora, **M. Guerricchio and **M. Ponte
* *Soil Conservation Department, University of Calabria – Contrada San Antonello – 87040 MONTALTO UFFUGO SCALO (CS) - ITALY*
** *External affiliate for underwater geoarchaeological investigations*

Abstract

The paper reports the results of underwater investigations made in the Crotone coastal strip between Strongoli Marina and Le Castella (along the Ionian Sea in Calabria). Numerous fixed archaeological structures have been found at depths of between 3 and 7-8 m; these consist in masonry works, old quarries, flight of steps (probable harbour-works) cut in calcarenites, flagstone paving of an old road on an islet.

These finds reveal the importance of such investigations in part of the Calabrian coast exhibiting signs of subsidence which may have been triggered, in the opinion of some people, by the extraction of gas from beneath the seabed. They demonstrate that the lowering of the shoreline is an ancient phenomenon in this area bound up with local lithological and tectonic conditions, as demonstrated also by precise topographic and GPS surveys.

Finally, at Punta Alice some recent marine works have modified longshore currents causing an increase in coastal retreat, due to erosion, and the submersion of structures built there, among which a pillbox fort of the second World War.

Keywords: Coastal Subsidence, Submerged Fixed Archaeological Structures, Ionian Calabria Coast, Coastal Gravitational Deformations.

1. INTRODUCTION

Finds of submerged, fixed archaeological structures are of great importance for understanding recent neotectonic episodes and/or subsidence phenomena, which may have played, or may still play, a decisive role in the stability of a coastal region or climatic variations (Schmiedt 1972; Vlora 1975; Cantafora 1986; Sovrintendenza

[1] Work performed with financial assistance from MURST 40% in 1994

Archeologica della Calabria 1988; Guerricchio et al. 1993, 1996 & 1997). On a par with such essential markers as marine terraces and/or wave-cut notches indicating old sea-levels, the foregoing indications bear witness to variations both in endogenous phenomena such as tectonic and isostatic ground-lowering and subsidence *latu sensu* (Guerricchio, Melidoro 1975; Guerricchio, Ronconi 1994 & 1995), as well as in those of an exogenous nature such as climatic variations (Ortolani, Pagliuca 1995) and eustatic oscillations (Cotecchia, Dai Pra, Magri 1974). Hence, once having excluded occurrences such as ground-sinking and/or collapse of land into the sea (Guerricchio, Melidoro 1975, 1986; Guerricchio 1987, 1988; Guerricchio et al. 1994) such submerged, fixed archaeological structures provide irrefutable evidence as to old sea levels at that particular moment of history.

The method based on the use of "archaeological indicators" has been adopted by various workers; Schmiedt (1972), for example, utilized evidence provided by sunken Roman fishing-boats to provide magisterial information on the rise in Tyrrhenian Sea levels during historic times.

The following text details the initial results of underwater geoarchaeological investigations conducted in the coastal strip between Punta Alice and Le Castella in the Crotone area of Calabria. These are of special interest from the soil conservation aspect and, hence, as regards protection of the coast which is mainly argillaceous and, as such, highly susceptible to erosion. Besides, recently, with scant regard to the evolutionary history of the relevant shoreline, almost considering it to have been virtually unchanged in the past and - in some respects - unchangeable in the future, subsidence phenomenon has been invoked to explain the breaking of the equilibrium, which has existed for centuries if not millennia, upsetting the introduction of man-made works.

2. PUNTA ALICE AREA

The Punta Alice plain consists mainly of sandy Holocene coastal deposits of littoral, eolian and alluvial origin (Fig.1). These deposits overlie reddish-brown sands and conglomerates with occasional levels of Upper Pleistocene cemented arenites, probably landslide fans, which - in turn - lie unconformably on the Santernian blue-grey clays that form the relative basement here.

More precisely, the littoral area in these parts consists of a 20-25 m wide strip of medium- to fine-grained sands, bounded by a belt of wandering dunes up to 70 m wide, also formed of medium- to fine-grained sands. This is followed landward by as much as 2 km of deposits, still laid down in an eolian environment, together with others of varied provenance (offshore bars, swamps and alluvial cones); the elevation of these deposits ranges from 2 to 15 m a.s.l., the lowest ones being the old swamps that occur within belts of dunes or higher bars. The village of Cirò Marina lies at an elevation of 5 m a.s.l., while the present Naval Lighthouse is at 6 m (Fig. 1).

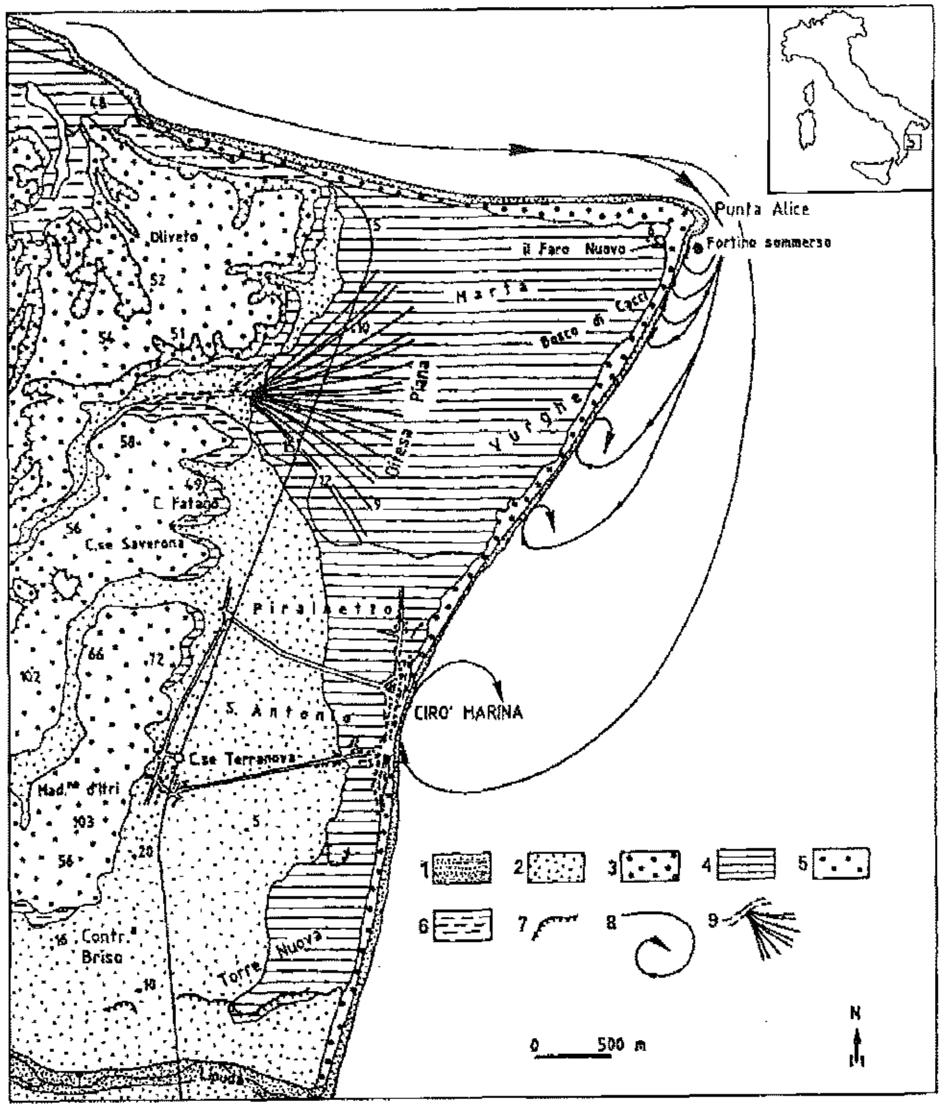

Figure 1. Geological and geomorphological map of Punta Alice area: 1 Beach sands, Present-day. 2 Sandy-pebbly terrace alluvials, Recent. 3 Wandering dunes and eolian sands, Recent. 4 Stabilized dunes and eolian sands, Holocene. 5 Reddish-brown sands and conglomerates with occasional levels of cemented arenites, Upper Pleistocene. 6 Blue-grey silty clays, Santernian. 7 Terrace rims. 8 Paths of longshore currents and coastal eddies. 9 Talus cone and traces of old valleys, Holocene.

From the landform aspect, the Punta Alice area is a low-lying triangular-shaped plain the northern edge of which runs approximately east-west, while the southern edge has a NNE-SSW trend (Fig.1).

The regime of the longshore currents is usually descendent, lapping the northern side of the Punta from west to east, then veering abruptly SSW at the Punta itself. This deviation along the shore creates disturbances in current flow, with the formation of large and small eddies. The latter, namely lower-order eddies, act on the littoral zone immediately to the south of the Punta, eroding the sandy beach and creating a series of short contiguous crescent-shaped bights. The higher-order eddies, instead, act farther south on the littoral strip flanking the town of Cirò Marina where they have produced the arcuate re-entrant identifiable on the 1954 aerial photographs. Here erosion has reduced the width of the sandy coastal strip and eliminated the more recent dune belt (Figs. 1 and 2a, b and c).

The regime of the longshore currents was considerably altered following construction of a jetty in the sixties. The jetty runs perpendicular on the northern side of Punta Alice from the Establishment to which runs the pipeline carrying brine from the salt deposits at Belvedere di Spinello (KR) (Fig. 2c). The alteration occurred despite the fact that the jetty was built on widely spaced supports, which theoretically should not have modified the current pattern. It is quite clear that immediately after construction of the jetty the current regime changed, more active eddies being formed immediately on the leeward side, namely just to the south of the Punta. Furthermore, owing to the increase in size, the zone of influence of the higher-order eddies was enlarged (Fig. 2c). Erosion was boosted significantly, leading to the rapid cutting-back of the shoreline for at least a hundred or so metres in only a few years (Fig. 2c). As is evident, the phenomenon also broadened the erosion belt on the beach at Cirò Marina (Fig. 2c) which is now protected by a T-shaped breakwater.

In the first zone, namely that immediately south of Punta Alice, this erosion process has led to the submersion of a small WW2 pillbox fort (Figs. 3a and b) which originally stood one metre above mean sea level - average elevation of the coastal strip - and some 80 m inland of the 1940's shoreline.

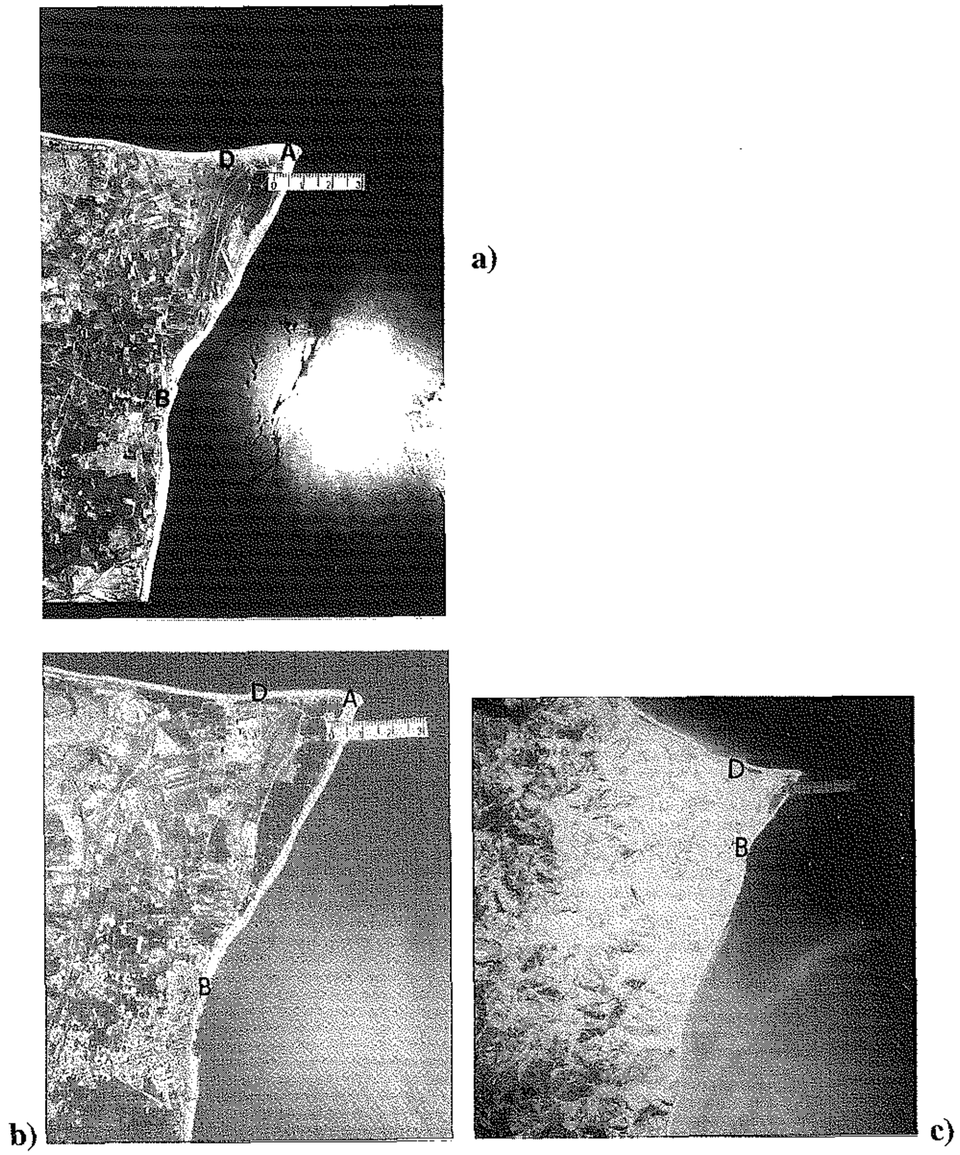

Figure 2. Aerial photographs taken in 1954 and 1980. Comparision of photos reveals marked changes in the coastal profile especially south of Punta Alice, indicated with the letter A in the figs. 2a, b and c. Retreat of coastal strip at Cirò Marina (B in figs. 2a, b and c) is pronounced. As is evident, the phenomenon post-dates construction of the jetty built perpendicular to the northern stretch of coast visible in D in the fig. 2c.

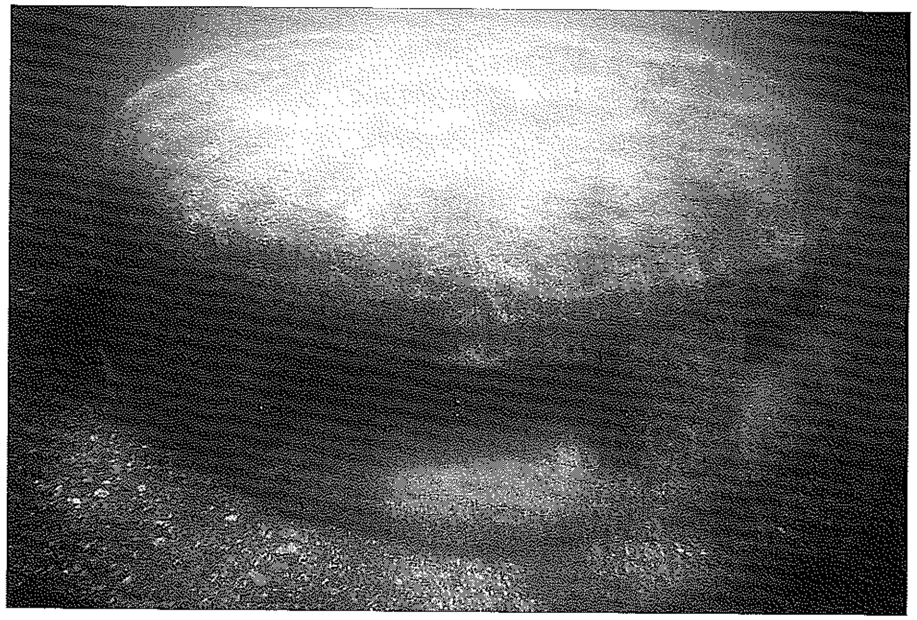

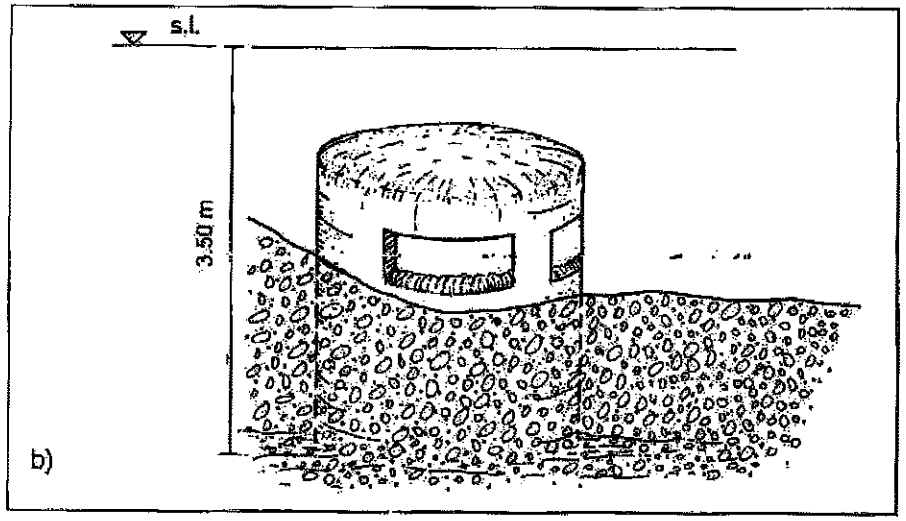

Figure 3 a) & b). Second World War pillbox fort. The structure now lies at a depth of 3.5 m in the sea near the present lighthouse south of Punta Alice, following a 70-m retreat of the shoreline in verv recent times.

The pillbox, which still remains perfectly upright, has been affected by coastal retreat. The base of the structure is now about 3.5 m below sea-level, while the domed top is under more than 1.7 m of water. The distance offshore was about 8 m when measured in August 1997.

Very close to Punta Alice, always along the same seabed which lies under between 3 and 5 m of water, are remains of an ancient landing (Fig. 4) and rock blocks that have been cut and squared (for columns, arches, etc.) now forming the ruins of what may once have been a lighthouse. Subsidence phenomenon is invoked to explain all these submerged remains instead of marine erosion due to the particular shape of Punta Alice and the longshore current.

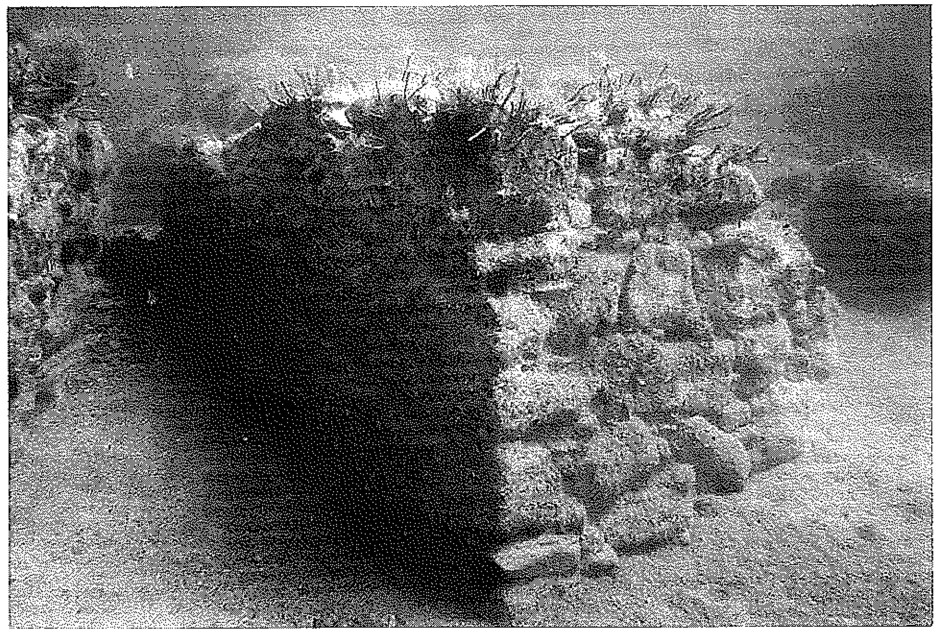

Figure 4. Punta Alice. Remains of a probable landing of the quay on which the ancient lighthouse standed.

3. SEA AREA OFF LE CASTELLA

The stratigraphic series here consists of a relative basement formed of Santernian blue-grey plastic clays with occasional levels and lenses of sands and silts unconformably overlain by Upper Pleistocene reddish-brown cemented sands and gravels. Interbedded sandstones, bioclastic sandstones with calcareous cement and calcarenites are also present locally, as are lenses of algal and biostromal limestones (Fig. 5). Cross-bedding is often to be seen, for instance in the Magna Grecian quarries lying SSE of the village of Le Castella, at the low cliff, which bounds the small peninsula here.

It is of fundamental importance to emphasize the presence in the coastal area of deposits exhibiting "competent" geomechanical behaviour overlying those classed as plastic.

To the east and WNW of the small peninsula, in the physiographic units comprising the low littoral zones, there are outcrops not only of pebbly deposits and beach sands *sensu stricto* but also of stabilized belts of dunes to the east and fixed alluvials to the west.

Landslide debris is frequent in the Blue Clay Formation; there are also eluvial-colluvial deposits in a somewhat arcuate depression in the sands and calcarenites to the NNW of Le Castella, corresponding to what is probably an old lateral spreading feature induced by the underlying clays eroded by the sea (Fig.5).

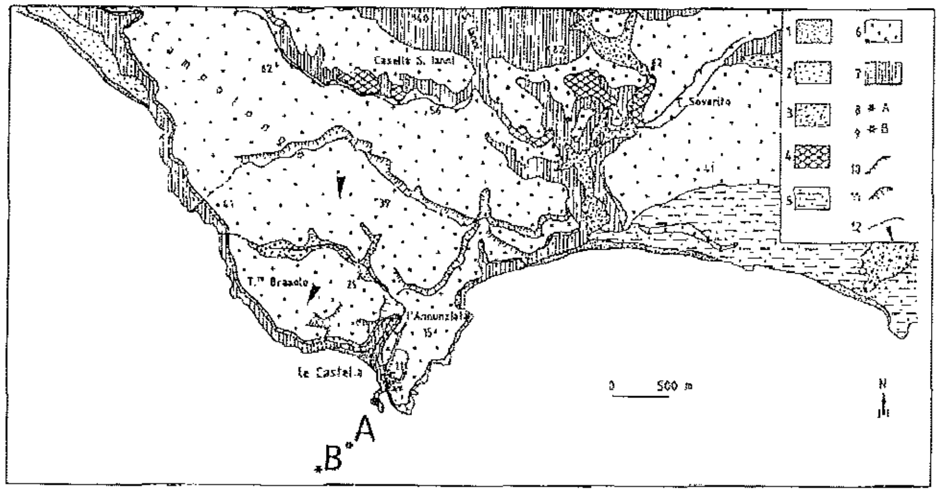

Figure 5. Geological and geomorphological map of Le Castella area: 1 Beach sands and pebbles, Present-day. 2 Sandy-pebbly terrace alluvials, Recent. 3 Eluvial-colluvial sandy-pebbly deposits, Holocene. 4 Landslide debris, Holocene. 5 Stabilized dunes and eolian sands, Holocene. 6 Reddish-brown conglomerates, sands and gravels with sandstone and calcarenite interbeds, Upper Pleistocene. 7 Blue-grey silty clays with occasional sandy levels, Santernian. 8 Seabed zone with flight of steps cut in the calcarenites, probably old harbour-works (A). 9 Seabed zone with flagstone-paved roadbed on remains of what is probably an old islet now under water (B). 10 Coastal landslip scarps. 11 Marine terrace rims. 12 Late Pleistocene shorelines, sometimes coinciding with breaks of the sandstone "slab". Arrows indicate direction of movement of broken masses.

The landform in these parts is characterised predominantly by a set of late Pleistocene terraces, at least three of which cut into the marine sands at Campolongo and Le Castella.

A continuous coastal landslide scarp, the result of marine erosion, borders the sandy cliff here. This cliff ranges from 60 to 9 m in height going from NW to SE.

The foot of the scarp is shrouded with debris, sand and sandstone boulders of various sizes. It is thought that one of these large rock masses formed the "cap" or cape rock on which the now highly distorted, partially-collapsed Aragonese Castle of Isola Capo Rizzuto was built. At shallow depth the cap rests on the blue-grey clays which outcrop at the bottom of the small cliff in the inlet to the east. Hence deformation of the castle structure was certainly induced by lateral spreading of the cemented sands and fissured, fractured sandstones resting on the submerged, plastic clays. This phenomenon, together with the marine erosion of the clays, was also responsible for the subsidence of the Magna Grecian ruins in the inlet along the western coast near the castle to a position several metres below sea level.

Also in this area, some 400 m WSW of the Aragonese Castle, a flight of eight steps each 20 cm high has been found carved in Pleistocene sandstone on the seabed at a depth of around 6 m (Fig. 6).

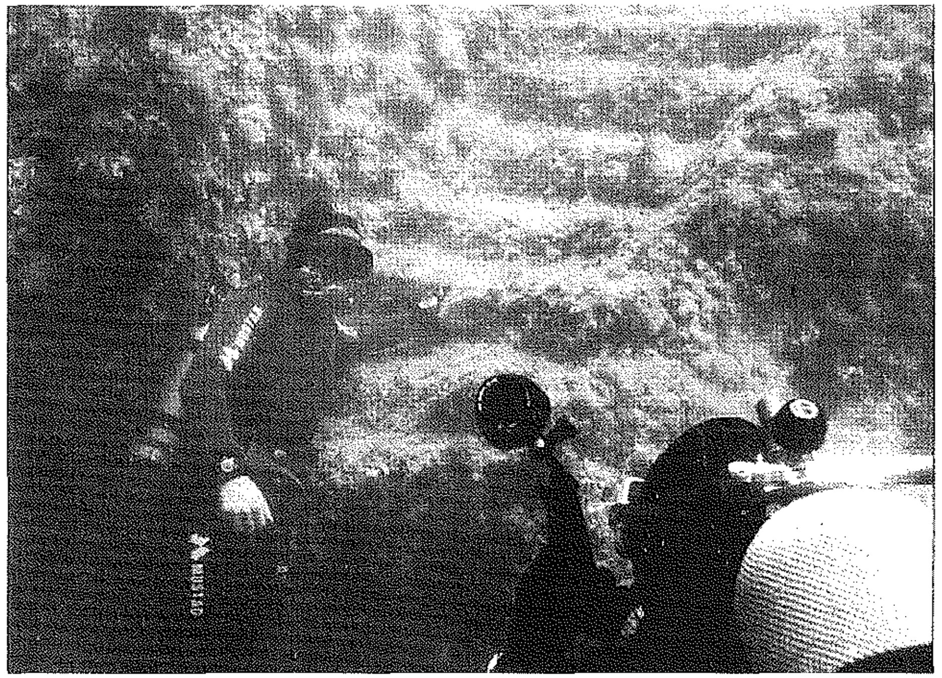

Figure 6. Flight of steps cut in Pleistocene calcarenites. Probably Magna-Grecian harbour-works, lying some 450 m SW of the Aragonese Castle in Le Castella at a depth of about 6 m.

It is possible that the sandstone mass containing the flight formed part of old harbour-works.

Another find in these parts consists of the remains of a quarry also at a depth of about 6 m (Fig. 7).

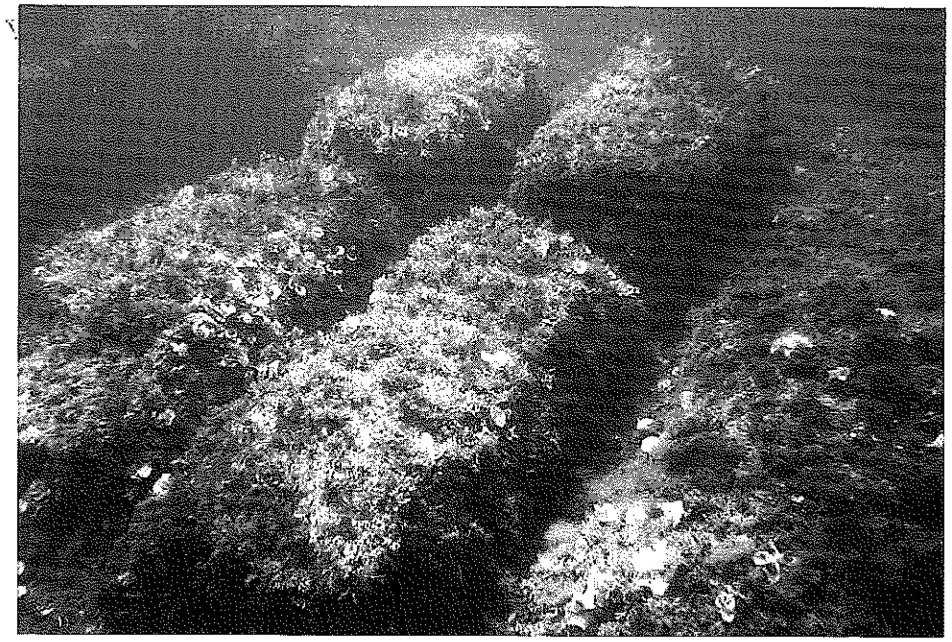

Figure 7. Le Castella. Submerged calcarenitic blocks of an ancient quarry not completely detached by the substratum.

Here there are sandstone blocks already cut and ready to be extracted, similar in all respects to those which occur in the Magna Grecian quarries to the south of Le Castella. Still in the same area, about 450 m WSW of the islet of the Aragonese castle, on a shoal lying at a depth of about 6 m, there is a roadbed formed with flagstones of intrusive and metamorphic rocks, generally somewhat rounded or ellipsoidal, set directly on the basal blue-grey clays (Fig. 8). Rocks of this type do not outcrop in the Crotone area, neither in the proximity of the coast, nor do they comprise offshore bars formed by the sea-currents, which might have transported alluvial deposits in this zone.

The roadbed lies roughly parallel to the coast, running southwards for a hundred or so metres. Numerous fragments of amphorae, tiles and household pottery dating from late-Roman times are found lightly cemented to the elements forming the roadbed (Fig. 8).

These are certainly remains of a settlement and of infrastructure facilities located on islands which old maps show to have existed in the offshore reaches of the Crotone coast. These islands, known as Tyris, Eranusa and Meloessa (Guerricchio, Ronconi 1994), have now disappeared, perhaps due to the action of sliding and collapse phenomena in bygone times induced by marine erosion of the very susceptible clayey deposits.

Figure 8. Roadbed formed of limestone and metamorphic flagstones about 400 m SW of the Aragonese Castle at a depth of around 7 m. The roadbed rests on Quaternary blue-grey clays and extends for a hundred, or so, metres parallel to the coastline on a "shoal", probably the remains of an old islet.

Figure 9 provides a schematic diagram of the mechanism which may have led to the disappearance of the islands once visible off the Crotone coast, especially in the vicinity of Le Castella. As already remarked, erosion of the basal clays caused collapse of the outcropping cap rock which was originally intact or nearly so (Fig. 9a) and was considered to be sound because of its arenaceous nature. However, the lateral spreading which was already occurring (Fig. 9a) led to slides and rockfalls (Fig. 9b) which for a certain time formed islets and dangerous semi-submerged reefs (Fig. 9c). As time passed by, the deteriorating situation led to the formation of "shoals" at a depth of 6-7 m (Fig. 9d).

All the finds described above attest to the existence of a human settlement with man-built structures, harbour-works and quarry sites. The settlement was subsequently invaded by the sea owing to: a) rise in sea-level attributable to glacio-eustatic phenomena (Lisitzin 1974) which is still under way; b) subsidence and/or collapse of what was once dry land. The situation evolved in this manner because of the stratigraphic conditions already outlined, namely the readily erodible Santernian Blue-Grey Clay Formation which provide only weak support for the "competent" late Pleistocene Cemented Sands and Sandstone Formation.

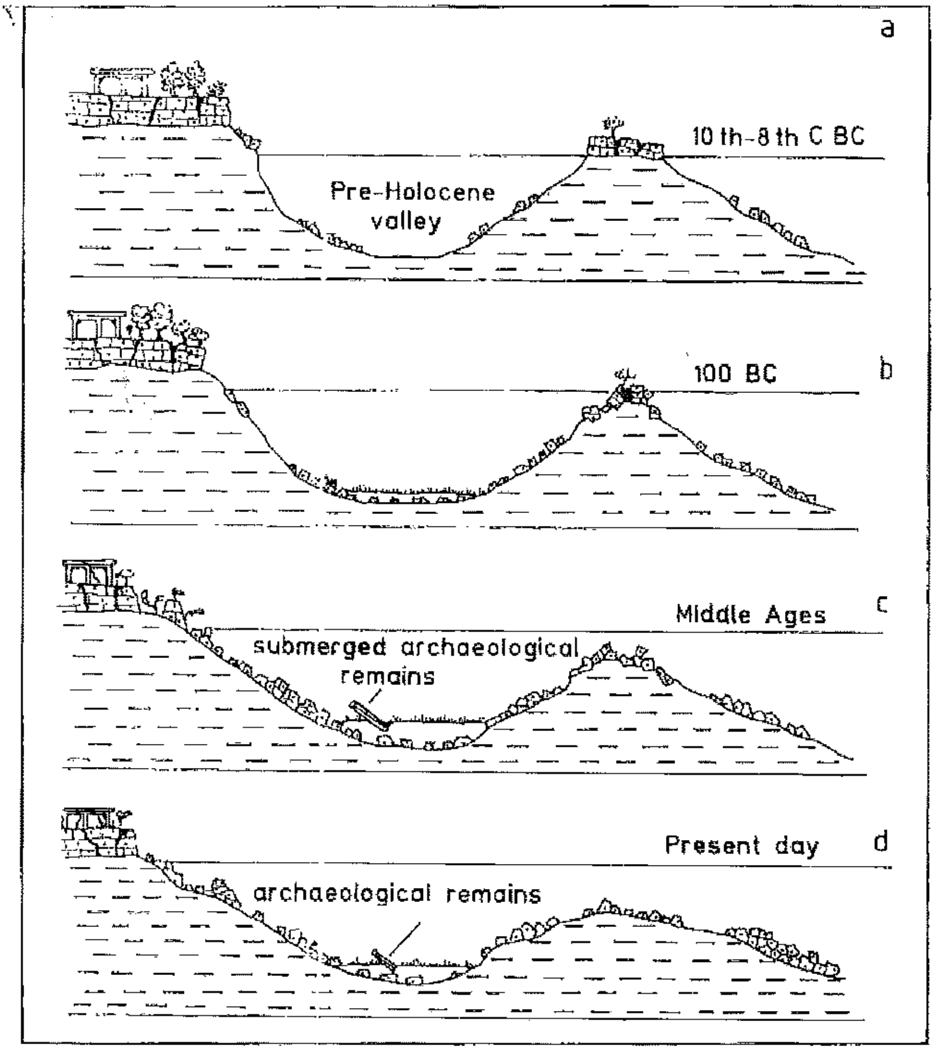

Figure 9. Schematic diagrams showing how the islets that occurred along the Crotone coast in Homeric times gradually disappeared over the centuries

4. CONCLUSIONS

In the coastal strip from Punta Alice to Crotone and Le Castella, where the Plio-Pleistocene Blue-Grey Clays are in continuous outcrop, the main dynamic elements affecting landform are mass-movements ranging in type from landslides *sensu stricto* to deep gravitative deformations, in part due to the relative proximity of the coast strip to the huge Ionian submarine depression.

The mass-movements result in difficult stability problems in numerous towns

and villages both inland (Strongoli, Torre Melissa, Cirò, etc.) and along the coast (Crotone), as well as in certain archaeological and tourist locations (Capo Colonna, Le Castella, etc.). Roads and railways in the coastal strip are also affected by precarious slope stability, communications often being interrupted by mass-movements.

The areas around Cirò Marina, Strongoli Marina and places such as Punta Alice merit diverse considerations. Though not built directly on the Blue-Grey Clay Formation, these locations suffer badly from marine erosion, not least because of the considerable fetch affecting this part of the coast.

However some recent man-built structures may also have accelerated certain processes already of long standing. The construction of a jetty, perpendicular to the windward stretch of coast at Punta Alice, has modified the longshore current regime. Indeed, following the increase in eddy deformations, produced by the particular configuration of the Punta zone, there has been an upsurge in erosive action on the leeward stretch of coast. As a consequence, the shoreline has been cut back by about one hundred metres in recent times, resulting in submersion of a WW2 pillbox the base of which now lies 3.5 m under water.

For the same reason at Cirò Marina, too, retreat of the shoreline has increased. However even in past times, in the days of the original settlement, the dune belt existing to the north and south of the town was eroded. All these geomorphologic actions simulate subsidence phenomena, which could be attributable to various geotechnical aspects. On the contrary these are examples of sea erosion due to particular trend of longshore marine current and to its recent variation due to man works.

Returning to the prevalent morphogenetic phenomenon along the relevant coastal strip, it is apparent that the front of the large landslide masses extending seawards is subject to attack by marine erosion. This simulates retreat of the shoreline as a consequence of subsidence movements but in reality it is frequently the sea which tends to regain its original position now occupied by the large landslide masses.

In this zone, as almost everywhere in the coastal strip, equilibrium is in a difficult or quasi-dynamic state.

In recent decades, while the sea-level has been rising at a rate of only 1.3 mm/year, there has also been a worrying retreat of the shoreline. This is often attributed to the implementation of various civil-works projects such as dam construction, gravel extraction from river beds, watercourse training and catchment basin improvements, consolidation of slopes on which are sited towns and villages, the creation of woods, the gas drilling, etc. As a result there is frequently a tendency to arrive at irrational and absurd conclusions: for instance, to ensure beach restoration, dams should not be built, watercourses should not be trained, landslides should not be stabilized, aggregates should not be extracted from riverbeds, etc. However, it would be ridiculous to apply such a criterion blindly. Everything must be done with reason. It must be borne uppermost in mind that a shoreline is never fixed in time, as is clearly demonstrated by the underwater geoarchaeological investigations conducted in the Crotone region, as well as in Apulia and elsewhere. Hence, settlements and durable structures in the coastal strip must be built at a reasonable distance from the shoreline. If this is not done then very costly and often useless works will be needed to try to protect them from coastal erosion and consequent lowering of coastal strip.

The presence of fixed structures of Magna Grecian and Roman age submerged at various depths has been revealed by the initial results of underwater geoarchaeological investigations in the coastal region, thus confirming the above assertion.

Certainly these finds do not justify the idea that the rise in sea-levels in historic times is solely responsible for the considerable depths at which the fixed structures occur. Due weight must be given to the particular lithological and stratigraphic situation in the Le Castella and Crotonian areas. Here a sandstone cap lies roughly level in the form of a huge "slab" on highly erodible basal clays, which are in direct contact with the sea. Erosion of these clays is responsible for collapse and subsidence of the "slab" together with the masonry structures, flights of harbour steps and quarries founded thereon. This action occurred over the course of time as the sea gradually moved in, eroding the clays and inducing lateral spreads, slides and falls in the overlying "competent" rock slab with consequent detachment of the sandstone blocks which now carpet the seabed so thickly here.

The same mechanism must also have been responsible for the submersion of the islets of Tyris, Eranusa and Meloessa mentioned by Homer, which now occur as "shoals"on the seabed off Le Castella.

Finally, it is evident from the foregoing that underwater geoarchaeological investigations can be of prime importance for the study of subsidence and coastal erosion, often wrongly ascribed solely to the effects of the recent works of man.

REFERENCES

Cantafora L., 1992. *Castella, scoperte isole sprofondate*. Il Crotonese n. 65.

Cotecchia V., Dai Pra G., Magri G., 1974. *Morfogenesi litorale olocenica tra Capo Spulico e Taranto nella prospettiva della protezione costiera.* Geologia Applicata e Idrogeologia, **IX**, Bari, 78-95.

Guerricchio A., Melidoro G. 1975. *Ricerche di Geologia Applicata al l'archeologia della città di Sibari sepolta.* Geologia Applicata e Idrogeologia, **X**, parte 1, Bari, .Guerricchio A., Melidoro G. 1986. *Problematiche di Geologia Applicata lungo la fascia costiera ionica.* ENEA, Convegno su: Evoluzione dei litorali, Policoro-Matera, 1-30, 2 tav.

Guerricchio A. 1987. *L'evoluzione dei litorali*: Tematiche geologico-applicative. Editoriale Bios, Cosenza, 1-54.

Guerricchio A. 1988. *Aspetti geologici sull'evoluzione dei litorali e loro influenza nel campo applicativo.* Geologia Applicata e Idrogeologia, **XXIII**, Bari, 29-78.

Guerricchio A., Guerricchio M., Maruca A., 1993. *Prime osservazioni subacqueee ritrovamento di strutture archeologiche fisse sommerse nella zona di mare antistante la costa di Egnazia (BR-Puglia):* Considerazioni sulle variazioni delle linee di costa in tempi storici. Convegno IRFEA. Cassano all'Ionio (CS), 1-25.

Guerricchio A., Ronconi M.L., 1994. *Geoarcheologia e turismo nell'area erotonese (Calabria Ionica).* Convegno su Ambiente e Turismo - Università della Calabria, Rende (CS), 124-140.

Guerricchio A., Ronconi M.L., 1995. *Osservazioni geomorfolociche finalizzate alla ricerca archeologica dell'antico porto di Crotone (Calabria Ionica).* 2a Giomata Naz. su: Le Scienze della Terra e l'Archeometria. Università di Bologna e Museo Civico di Rovereto, 68-75.

Guerricchio A., Melidoro G., Simeone V., 1996. *Le grandi frane di Petacciato sul versante costiero adriatico (Molise).* Mem. Soc. Geol. It., **51**, 607-632.

Guerricchio A., Ronconi M.L., 1997. *Osservazioni geomorfologiche nella Piana di Sibari e variazioni delle línee di costa storiche nella zona degli scavi archeologia.* I Quaderni dell'Irfea, Ass. Cult. Irfea, Cassano Jonio, 1-25.

Guerricchio A., Guerricchio M., Maruca A., 1997. *Sul presunto antico porto romano di Egnazia (BR).* Centro Editoriale Librario-Università degli Studi della Calabria, Rende (CS), 1-28.

Lisitzin E., 1974. *Sea Level Changes.* Elsevier Scientific Publications, Amsterdam.

Ortolani F., Pagliuca S. 1995. *Climatic variations and crises in the anthropized environment in the Mediterranean Region.* Proc. Geosciences, Archaeology Seminar. The Geol. Survey of Egypt, Special Publ. No. 70.

Schmiedt G., 1972. *Il livello antico del Mar Tirreno.* Testimonianze dei resti archeologici. Ed. Olschki.m

Sovrintendenza Archeologica della Calabria, 1988. *Un secolo di ricerche in Magna Grecia.* Atti del Convegno per gli Studi della Magna Grecia. Taranto 1988.Vlora N.R., 1975. *Considerazioni sulle variazioni delle linee di costa tra Monopoli ed Egnazia.* Bari, 1-45.

SEA LEVEL CHANGE IN THE PO DELTA (N. ITALY): INTERACTION OF GEOLOGICAL DATA ANALYSES WITH MODELLING SIMULATIONS

G. Di Donato, E. Carminati, R. Sabadini and A. Gardi
Dipartimento di Scienze della Terra, Sezione di Geofisica, Via Cicognara 7, 20129 Milano, Italy.

J. X. Mitrovica
Department of Physics, University of Toronto, 60 St. George St., M5S 1A7 Toronto, Canada

Abstract

In this paper we focus on the natural component of vertical motion in the eastern part of the Po plain and in the northern Adriatic Sea (Italy) in relation to sea-level changes affecting the area. In particular we present 'ad hoc' dynamic models, based on realistic geometries and simulating the tectonic mechanisms active in the Po plain region. A sensitivity analysis on a factor forcing the model (the density anomalies within the Adriatic slab) is performed. The model predicted vertical velocities are compared to the tectonic component of vertical velocities inferred from stratigraphic data. We show that the model is a reasonable first order approximation of the tectonics of the central Mediterranean. Moreover we investigate the vertical motions induced by the Pleistocene deglaciation. Vertical velocities due to post glacial rebound (V_{pgr}) are obtained by means of multilayered, spherical Earth models based on PREM, with a compressible, linear, viscoelastic Maxwell rheology. In this work we also report on a new generation of model simulations which explore the influence of fine-scale crustal structure on the rebound predictions. We finally propose a discussion on the influence of the assumed viscosity profile on the modelling results.

Keywords: Po plain, glacial rebound, tectonics, stratigraphic data.

1. INTRODUCTION

The present-day vertical velocity of an area, V_{tot}, with respect to mean sea level is the sum of several factors (e.g., Carminati and Di Donato, 1999):

$$V_{tot}=V_t+V_{sl}+V_c+V_{pgr}+V_a.$$

V_t is the velocity component due to tectonics. V_{sl} and V_c are the components induced by the load of sediments and by sediment compaction respectively. V_{pgr}

is the post glacial rebound component and accounts for the increase of water volume and for the isostatic response to the redistribution of surface loads related to the Pleistocene deglaciation (e.g., Di Donato et al., 1999). The sum of these four factors accounts for the natural component of vertical movements. V_a is the anthropogenic component of vertical motion and is the result of local and global signals.

In this paper we focus on the natural component of vertical motion in the eastern part of the Po plain and in the northern Adriatic Sea in relation to sea-level changes affecting the area. In particular we present 'ad hoc' dynamic models, based on realistic geometries and simulating the tectonic mechanisms active in the Po plain region. A sensitivity analysis on a factor forcing the model (the density anomalies within the Adriatic slab) is performed. The model predicted vertical velocities are compared with the tectonic component of vertical velocities obtained by Carminati and Di Donato (1999). Moreover we investigate the vertical motions induced by the Pleistocene deglaciation. Vertical velocities due to post glacial rebound (V_{pgr}) are obtained by means of multilayered, spherical Earth models based on PREM, with a compressible, linear, viscoelastic Maxwell rheology. In this work we also report on a new generation of model simulations which explore the influence of fine-scale crustal structure on the rebound predictions.

2. TECTONIC COMPONENT OF VERTICAL MOTION

Tectonics affect vertical movements of a region both with surface and subsurface loads (e.g., Beaumont, 1981, Royden, 1993). Typical surface loads are generated by thrust bodies in zones of shortened lithosphere whereas subsurface loads are generally related to density anomalies at depths induced by active geodynamic processes. Negative buoyancy affects, for example, subducting slabs, will be shown in section 2.2. In this section we first analyse the tectonic component of vertical motion for the Po plain area as it can be inferred from geological data and we present the results of numerical models aiming at simulating the tectonics of the area.

2.1 Resolving the tectonic component with stratigraphic data

The geological and the anthropogenic components of vertical motion act on different time scales (millions to thousands years and hundreds to tens of years respectively). This peculiarity has been used by Carminati and Di Donato (1999) in order to separate the different components of vertical motion in the Po plain area. The components due to long term geological processes (V_t,V_{st},V_c) have been calculated from stratigraphic data (commercial wells and seismic lines) utilising a backstripping analysis procedure considering the effects of sediment compaction (Sclater and Christie, 1980). In Fig. 1 we show the vertical velocity field (continuous lines) due to tectonics averaged over the Quaternary obtained by Carminati and Di Donato (1999). In the same picture we show the punctual vertical velocities obtained with the same procedure by Carminati et al. (1999) from offshore wells (black dots).

From Fig. 1 it can be inferred that high subsidence rates (up to 0.8-1 mm/yr) have been induced by tectonics during the Quaternary in the axial part of the Po plain. Maximum rates are approximately aligned along a WNW-ESE trending line, the easternmost tip of this line being coincident with the Po delta. More to the south, in the Adriatic Sea (black dots in Fig. 1), tectonic subsidence occurs with lower rates (up to 0.4-0.5 mm/yr).

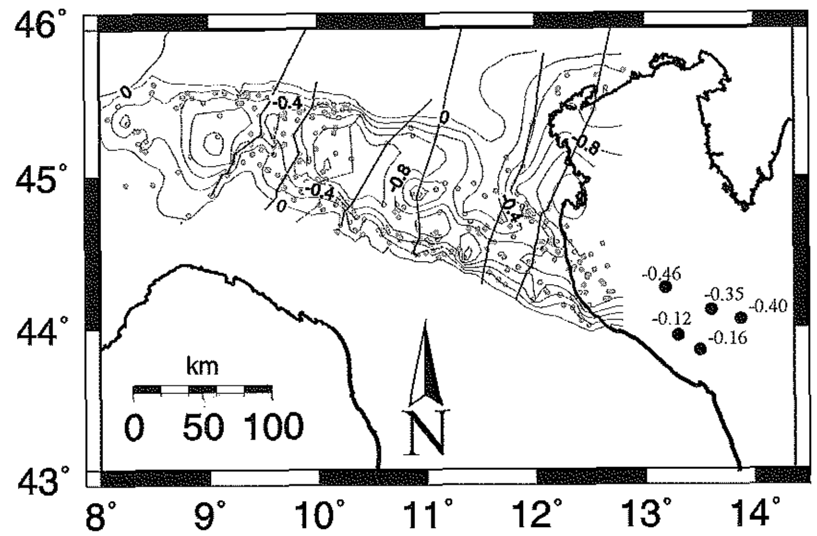

Figure 1. Contours and punctual values of the tectonic component of vertical velocity (in mm/yr) averaged over the Quaternary obtained from stratigraphic data. The grey and black dots indicate the positions of the utilised wells. Redrawn after Carminati and Di Donato (1999) and Carminati et al. (1999).

2.2 Model description

Active tectonic processes in the central Mediterranean, namely Africa-Eurasia convergence and subduction in the southern Tyrrhenian, are modelled by means of finite element solutions in a half-space domain. The models we utilise are similar to those presented by Negredo et al. (1999), and account for the main tectonic and geodynamic features of the area.

The model geometry and boundary conditions are represented in the block diagram of Fig. 2a. The models simulate the subduction of the Adriatic lithosphere underneath the Tyrrhenian lithosphere. The style of subduction changes from south to north. Underneath Calabria, seismological and tomographic studies image a continuous NW-dipping Wadati-Benioff plane down to 500 km depth in the southern Tyrrhenian Sea (Selvaggi and Chiarabba, 1995) which is related to the consumption of oceanic lithosphere. In contrast, a maximum seismicity depth of 90 km has been reported in the northern Apennines and a shallower slab (down to about 200 km) is imaged by tomography (Amato, et al., 1993). The subduction process is associated with the consumption of continental lithosphere. This contrasting style of subduction is considered in our models, which are characterised by a slab reaching a depth of 500 km in their southern and 200 km in their northern portions (Fig. 2a). The model also reproduces the curvature of the subduction hinge along the Apennines.

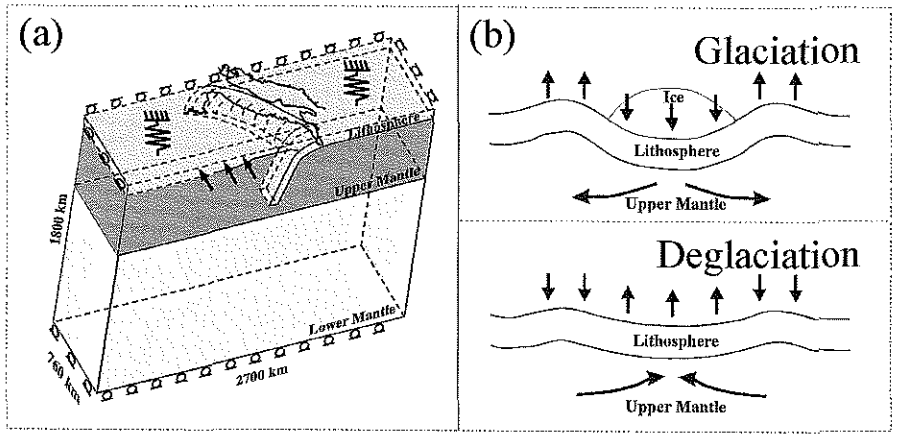

Figure 2. (a) Geometry, materials and boundary conditions of the models simulating the tectonics of the central Mediterranean. (b) Surficial movements and upper mantle flow associated to glaciation and deglaciation processes.

In the model we differentiate crust, lithosphere, upper mantle and lower mantle. We assume a linear viscoelastic Maxwell rheology with viscosities of 10^{24} Pa s for the crust, 5×10^{22} Pa s for the lithospheric mantle, 10^{21} Pa s for the upper mantle and 3×10^{22} Pa s for the lower mantle (Whittaker et al., 1992; Spada al., 1992). The elastic structure is based on the PREM reference model (Dziewonski and Anderson, 1981). We have assumed a Young Modulus of 9×10^{10} Pa for the crust and 1.75×10^{11} Pa for the remaining materials.

The boundary conditions applied at the lithosphere simulate both the continental collision in the Alps (north-south motion is forced to vanish at the northern edge of the model) and the push of the African plate, indicated by the thick arrows directed roughly to the north, in agreement with a recent VLBI solution (Lanotte et al., 1996). The push is simulated with an imposed convergence velocity of 1 cm/yr and constitutes one of the two major loads applied to the model. The second load consists in the density anomalies within the subducting slab due to phase transitions. The density contrasts applied to the Calabrian slab are based on the petrological model of Irifune and Ringwood (1987) and reach maximum values of 400 kg/m^3 at 400 km. Discussion is still open on the density contrast active in the shallower slab subducting underneath the central and northern Apennines. For this reason we perform a sensitivity analysis on this parameter and we present the results of two models, in which the imposed density contrasts are 0 and 80 kg/m^3 respectively.

2.3 Model results

In Fig. 3 we show the vertical velocities obtained for the above described models which account only for the effects of active tectonics. The pattern of vertical motion along the Adriatic coast shows high variability, due to the geometrical complexity of the interaction between the Adriatic and the Tyrrhenian lithospheres (Fig. 2). Active tectonics is responsible for significant rates of vertical motion on the western coasts of the Adriatic Sea. This subsidence is due to the downflexure of the Adriatic plate underneath the overthrusting Apenninic belt. The subduction hinge, displayed as a thick line in Fig. 2a and 3 separates the Tyrrhenian sector of the Italian peninsula to the west and the Adriatic domain to the east. Overthrusting of the Apennines is caused by the push of Africa from the south and by the suction effect induced by the sinking Adriatic slab and is accommodated by the decoupling, on geological time scales, of the western and eastern parts of the peninsula via a megafault.

A closer inspection of Fig. 3 shows that the two models predict quite similar vertical motions for the Adriatic Sea and the eastern coast of Italy. Both the models predict subsidence with low rates (between -0.2 and –0.4 mm/yr) along the Italian coast and the values, obtained for the Po delta, range between -0.2 and –0.3 mm/yr. The two models, on the other hand, differ greatly when the Tyrrhenian domain (west of the subduction hinge) and the central part of the Po plain is considered. Since the aim of this contribution is to constrain vertical motions in the Po delta and in the northern Adriatic Sea, we can conclude that varying greatly the density structure of the subducting slab we do not obtain significant variations of predicted vertical velocities in the area of interest.

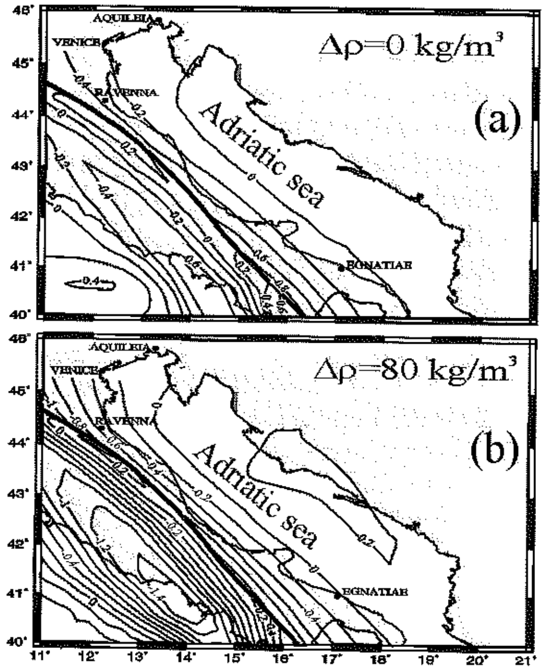

Figure 3. Vertical velocities in mm/yr predicted by two models differing for the density anomaly applied to the slab subducting underneath the central and the northern Apennines. Positive and negative values indicate uplift and subsidence respectively.

3. POST-GLACIAL REBOUND

The redistribution of loads on the Earth's surface due to Pleistocene ice-sheet disintegration drives the glacial isostatic adjustment (henceforth 'GIA'). This is an ongoing global process, although the volume of these ice-sheets has not changed appreciably during the last 4 kyr. In this section we examine present-day sea level changes related to glacial rebound and focus our attention upon this observable in the Adriatic region.

3.1 Model description

A schematic representation of the post-glacial rebound process in the near field of the ancient ice-sheets is shown in Fig. 2b: on the top, the isostatic state is represented; the melting of the ice-sheet, at the bottom, causes the ground to rise within the regions that have lost ice, because of the decrease in surface stress, and subsidence occurs at the periphery of the deglaciation centres. The contribution of

the water coming from the melting of the ice-sheets is evident in the intermediate and far fields (it is the case of the Adriatic Sea) of the ice-sheets where the ocean floor is characterised by a weak subsidence in response to these loads and the continent by a weak uplift due to the motion of viscous material from below the sea regions to beneath the continents (e.g., Clark et al., 1978). The relative sea-level change includes the geoidal change contribution in addition to crustal rebound.

Our predictions incorporate the effects of deglaciation, based on the ICE-3G reconstruction of Tushingham and Peltier (1991), on crustal and sea surface changes in the Adriatic Sea. The sea loading component of the surface load is computed using the gravitationally self-consistent pseudo-spectral algorithm by Mitrovica and Peltier (1991) with a truncation at degree and order 256, so the spatial resolution is sufficient to model sea-level change in small regions.

Our predictions of sea-level variations due to GIA are based on a multilayered, spherically symmetric, self-gravitating Earth model, with a compressible, linear, viscoelastic Maxwell rheology; the elastic and density structure of the model is given by the seismic model PREM (Dziewonski and Anderson, 1981). The employed Earth model has a 80-km elastic lithosphere, an upper mantle viscosity of 5 x 10^{20} Pa s, a lower mantle viscosity of 5 x 10^{21} Pa s and an inviscid core (henceforth model EC, that is, model with an elastic crust). In our post-glacial rebound model we adopt values of lithospheric thickness and viscosity of the upper and lower mantle in agreement with recent studies (Mitrovica and Davis, 1995; Lambeck et al., 1998).

In this work we also report on a new generation of model simulations which predict the influence of fine-scale crustal structure on the rebound process. In particular we consider a 15 km ductile crustal layer of viscosity 10^{21} Pa s between 25 and 40 km depth (henceforth model SC, that is, model with a stratified crust). This choice is in the mid-range of effective lower crustal viscosities calculated by Ter Voorde et al. (1998) for a typical continental lithosphere and stress varying from 0.1 to 1000 MPa. Model SC is a reasonable first approximation of the stratified structure of the Adriatic continental lithosphere.

3.2 Model results

Fig. 4a shows the predicted present-day rates of sea-level change in the Adriatic Sea for the Earth model EC.

In the central Mediterranean the model predicts sea level increase, with rates of 0.5 - 0.6 mm/yr, being due to the subsidence of the sea bottom caused by the water load. The coasts of the Mediterranean Sea are characterised by a weak sea-level fall; rates between 0 and -0.2 mm/yr are obtained in the Adriatic Sea.

The rates of sea-level change have small values in the Adriatic Sea due to two major mechanisms. First of all, the levering effect (e.g., Nakada and Lambeck, 1989), that is, the subsidence of the Mediterranean basin is contoured by the uplift of the surrounding continents; this is due to mantle material presently flowing from the Mediterranean region towards the previously glaciated Fennoscandian area in northern Europe. Therefore, towards the Adriatic coast, the rates of the Mediterranean basin subsidence diminish, reaching values of -0.3, -0.4 mm/yr.

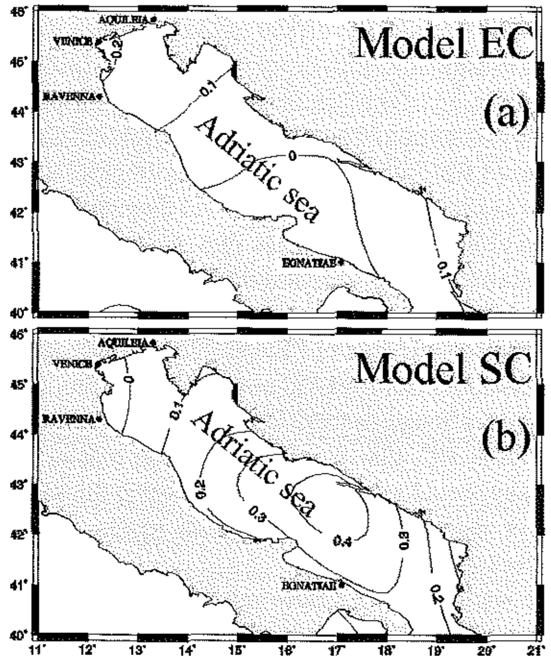

Figure 4. Present-day rates of sea-level change due to GIA in the Adriatic Sea, predicted using (a) Earth model EC and (b) Earth model SC. Positive values indicate sea-level rise and negative values sea-level fall.

Secondly, the sea-level change is not simply given by the solid surface deformation reversed in sign; in fact there is also the contribution of the geoid whose rate of change is about -0.4 mm/yr in the Adriatic area, therefore slightly larger than the rate of solid surface subsidence at the perimeter of the continents. The result is a weak sea level fall in the northern and eastern sector of the Adriatic region as shown in figure 4a. In the far field of the ancient ice-sheets, like in the Adriatic area, the physical cause of the computed present-day drop in sea surface (geoid) is mainly the maintenance of hydrostatic equilibrium by means of a long-wavelength motion of water away from the Mediterranean Sea and towards subsiding oceanic regions at the periphery of previously glaciated areas (Mitrovica and Peltier, 1991).

The internal viscous material and sea water redistribution are dependent on viscoelastic Earth structure. In figure 4b we explore the influence of a ductile layer in the lower crust on the predictions of the rates of sea-level changes, using

model SC. The inclusion of this layer acts to reverse the sign to the velocities in the northern and eastern part of the Adriatic Sea, with values close to zero in Venice and Ravenna and between 0.1 and 0.4 mm/yr along the eastern coasts of the Adriatic Sea. The largest rise in sea level with respect to model EC is predicted in the central Adriatic and is mainly due the increase of the subsidence rate of the sea floor. The cause of the sea-basin behaviour is the reduced flexural rigidity of the crust in model SC: the water load acts to draw viscous mass in the crustal layer from beneath the sea and towards the continents, leading to a partly coupled motion between the lithosphere and the mantle. The net effect is the contours' pattern in figure 4b which reflects the increased power at shorter wavelengths and make the Adriatic Sea to be a self-behaving environment and no longer just an area at the border of the Mediterranean Sea.

4. DISCUSSION

The long term geological processes significantly affect the regional pattern of vertical velocity in the Po plain and in the northern Adriatic area. Long term subsidence rates up to –2.0 mm/yr can be inferred from stratigraphic data for the Po delta region (Carminati and Di Donato,1999). Tectonics accounts for about 50% of the long term geological subsidence, whereas compaction and sediment load account for about 30% and 20%, respectively. Postglacial rebound is an ongoing process active on a shorter time wavelength. A first assessment of the contribution of postglacial rebound in the definition of present-day vertical motions and sea-level variations in the Adriatic region has been presented by Di Donato et al. (1999). The GIA contribution has been evaluated by these authors using analytical models, with an incompressible rheology and they found that sea level is slightly increasing. In the following we discuss the contribution of the modelling presented in sections 2 and 3 to the study of vertical motions induced by tectonics and postglacial rebound.

The models presented in section 2 simulate the geodynamic processes active in the central Mediterranean region. A comparison between the observed (Fig. 1) and predicted (Fig. 3) velocities permits two considerations. The predicted velocities do not vary greatly with respect to the vertical velocities obtained from the wells located in the northern Adriatic Sea (full black circles in Fig. 1). On the contrary, predicted velocities clearly underestimate the velocities obtained from stratigraphic data in the Po delta area. This difference probably indicate that the model, although well suited in order to simulate the geodynamics of the central Mediterranean, is oversimplified in the region of the Po plain. In particular the models do not account for the strong rotation of the thrusts (from NNW-SSE to WNW-ESE) which occur south of the Po delta and the complex crustal and lithospheric structures underneath the Po plain which are the result of the interaction between the Apenninic and the Alpine orogeneses.

The postglacial rebound models presented in section 3 show the sensitivity of sea-level predictions to variations in the crustal structure of the Earth models. The amplitude of GIA signal is dependent on the viscosity model assumed for the upper and lower mantle. In the paper by Di Donato et al. (1999) the models were characterised by an upper mantle viscosity of 10^{21} Pa s and a viscosity increase in the lower mantle of a factor 30, in agreement with long-wavelength geoid modelling (Ricard and Vigny, 1989). In that case, sea-level rise was predicted, with values of 0.3 - 0.4 mm/yr in the northern part of the Adriatic basin. In the work by Carminati and Di Donato (1999) we still utilised the results of an Earth model with an upper mantle viscosity of 10^{21} Pa s and a smaller value of $5x10^{21}$ Pa s for the lower mantle. That model predicted slow sea level increase of 0.15 mm/yr. In the present work we adopt the strategy of choosing viscosities of the upper and lower mantle in agreement with many recent studies (e.g. Lambeck et al., 1998). We also use more realistic Earth models considering the Earth like a compressible body. The calculated fall in sea level with rates of about -0.2 mm/yr in the Po delta region, acts to improve the fitting between the total natural component (calculated as suggested in Carminati and Di Donato (1999) with data. The estimated velocity turns from 1.6 to 1.2 mm/yr in Ravenna and from 1.2 to 0.8 mm/yr in Venice, in better agreement with archaeological data (Flemming, 1992) indicating a sea-level rise of 1.2 and 0.45 mm/yr for the historical towns of Ravenna and Venice, respectively.

We have then explored the influence of a ductile layer in the lower crust on the predictions of the rates of sea-level changes, using Earth model SC. The inclusion of this layer diminishes the velocities in the northern part of the Adriatic Sea, with predicted values close to zero in Venice and Ravenna. The largest rise in sea level with respect to model EC is predicted in the central Adriatic and is mainly caused by the reduced flexural rigidity of the crust in model SC. The use of a compressible Earth model and the differentiation of the crustal structure makes this model to be the one which better accounts for the complexity of the Adriatic region. A test of the GIA velocities predicted by this new generation of Earth models, using data from wells with detailed stratigraphy for the last 10,000 ca years, is the natural follow up to this work and will permit us to better constrain the viscosity profile.

Acknowledgements.

This work was financially supported by the European Space Agency contract *Benefits of High Resolution Earth Gravity and Ice Sheet Elevation Model for Sea Level Change.*

REFERENCES

Amato, A., Alessandrini, B., Cimini, G., Frepoli, A. & Selvaggi, G. (1993) Active and remnant subducted slabs beneath Italy: evidence from seismic tomography and seismicity. *Annali di Geofisica*, 36, 201-214, 1993.

Beaumont, C. (1981) Foreland basins. *Geophys. J. R. astr. Soc.*, 65, 291-329.

Carminati, E. & Di Donato, G. (1999) Separating natural and anthropogenic vertical movements in fast subsiding areas: the Po plain (N. Italy) case, *Geophys. Res. Lett.*, 26, 2291-2294, 1999.

Carminati, E., Giunchi, C., Argnani, A., Sabadini, R. & Fernandez., M. (1999) Plio-Quaternary vertical motion of the Northern Apennines: insights from dynamic modelling. *Tectonics*, 18, 703-718.

Clark, J. A., Farrell, W. E. & Peltier, W. R. (1978) Global changes in postglacial sea level: A numerical calculation. *Quat. Res. N. Y.*, 9, 265-287.

Di Donato, G., Negredo, A.M., Sabadini, R. & Vermeersen, L.L.A. (1999) Multiple processes causing sea-level rise in the central Mediterranean. *Geophys. Res. Lett.*, 26, 1769-1772.

Dziewonski, A.M. & Anderson, D.L. (1981) Preliminary reference Earth model. *Phys. Earth and Planet. Inter.*, 25, 297-356.

Flemming, N.C. (1992) Predictions of relative coastal sea-level change in the Mediterranean based on archaeological, historical and tide-gauge data. In *Climatic Change in the Mediterranean* (ed. by L. Jeftic et al.), Edward Arnold, London, 247-281.

Lambeck, K., Smither, C. & Ekman, M. (1998) Tests of glacial rebound models for Fennoscandinavia based on instrumented sea- and lake-level records. *Geophys. J. Int.*, 135, 375-387.

Lanotte, R., Bianco, G., Fermi, M., Rutigliano, P. & Verdone, G.R. (1996) The CGS VLBI EUR96 geodetic solution, 11th Working Meeting on European VLBI for Geodesy and Astrometry, Onsala, Sweden.

Mitrovica, J. X. & Davis, J. L. (1995) Present day post-glacial sea level change far from the late Pleistocene ice sheets: implications for recent analyses of tide gauge record. *Geophys. Res. Lett.*, 18, 2529-2532.

Mitrovica, J. X. & Peltier, W. R. (1991) On postglacial geoid subsidence over the equatorial oceans. *J. Geophys. Res.*, 96, 20,053-20,071.

Nakada, M. & Lambeck, K. (1989) Late Pleistocene and Holocene sea-level change in the Australian region and mantle rheology. *Geophys. J. Int.*, 96, 497-517.

Ricard, Y. & Vigny, C. (1989) Mantle dynamics with induced plate tectonics, *J. Geophys. Res.*, 94, 17,543- 17,559.

Royden, L.H., (1993) The tectonic expression of slab pull at continental convergent boundaries. *Tectonics*, 12, 303-325.

Sclater, J.G. & Christie, P.A.F. (1980) Continental stretching: an explanation of the post-mid-Cretaceous subsidence of the central North Sea basin , *J. Geophys. Res.*, 85, 3711-3739.

Selvaggi, G. & Chiarabba, C. (1995) Seismicity and P-wave velocity image of the southern Tyrrhenian subduction zone. *Geophys. J. Int.*, 121, 818-826.

Spada, G., Ricard, Y. & Sabadini, R. (1992) Excitation of true polar wander by subduction. *Nature*, 360, 452-454.

Ter Voorde, M., Van Balen, R. T., Bertotti, G. & Cloetingh, S. (1998) The influence of a stratified rheology on the flexural response of the lithosphere to (un)loading by extensional faulting. *Geophys. J. Int.*, 134, 721-735.

Tushingham, A. M. & Peltier, W. R. (1991) ICE-3G: A new global model of late Pleistocene deglaciation based upon geophysical predictions of postglacial relative sea level change. *J. Geophys. Res.*, 96, 4497-4523.

Whittaker, A., Bott, M.H.P. & Waghorn, G.D. (1992) Stresses and Plate Boundary Forces Associated With Subduction Plate Margins. *J. Geophys. Res.*, 97, 11,933-11,944.

LAND SUBSIDENCE - Vol. I
Proceedings of the Sixth International Symposium on Land Subsidence
Ravenna / Italy / 24-29 September 2000

LAND SUBSIDENCE IN ARTIFICIAL ISLANDS DUE TO LIQUEFACTION CAUSED BY THE KOBE EARTHQUAKE IN 1995, JAPAN

Atsushi Kagawa, Kunio Furuno, Takashi Kusuda, Kenzi Satoh, Yutaka Sakai, Kazuo Kamura, Osamu Kazaoka and Masaaki Morisaki
Research Institute of Environmental Geology, Chiba (RIEGC)
3-5-1, Inagekaigan, Mihama-ku, Chiba 261, Japan

Hisashi Nirei
Center for Water Environmental Study, Ibaraki University
1375, Itako, Ibaraki 331-24, Japan

Abstract

The Hyogo-ken Nanbu (Kobe) Earthquake in 1995 resulted in destructive damage to the Kobe and Hanshin areas in the northern margin of the Osaka Bay, West Japan. The earthquake in the coastal reclaimed land areas and the artificial islands caused large land subsidence. In the outer edge of the reclaimed Kobe City islands, many of the quay banks were inclined, subsided and slide into the sea. Maximum subsidence of 470 cm occurred inside the banks due to the outflow of reclaimed materials. In the central region of the islands, the underground lifeline suffered serious damage due to differential subsidence and upward displacement of the piled buildings. Ground sinking and ejection of muddy water caused flooding. These phenomena were caused by large scale Liquefaction - Fluidization with strong ground motion. Liquefaction subsidence is an exceptional event linked to earthquakes and when it occurs it is a big problem for low lying and reclaimed land areas because of the immediate heavy damage caused.

Keywords : liquefaction land subsidence, Kobe Earthquake in 1995, reclaimed land, artificial island.

1. INTRODUCTION

The Hanshin (Osaka to Kobe) area (Fig. 1) was struck by the Hyogo-ken Nanbu (Kobe) Earthquake on the 17 January 1995, the magnitude of which was 7.2 with focal depth down to 14.3 km. Serious damage was distributed over the E-W oriented belt-like zone between Rokko Mountains and Osaka Bay (Figs. 2 and 3). The Hanshin area is constituted by thick sediments lying on granitic bedrock with a step-like configuration along the basin edge. In this area, reclaimed lands have been expanding by overpopulation and industrialization since Edo Era. Characteristics of the damage in artificial lands will be described.

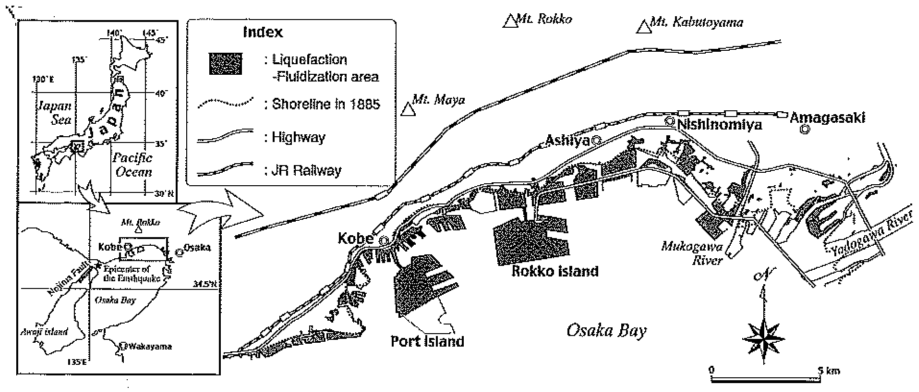

Figure 1. Study area and distributions of the liquefaction-fluidization in the northern part of the Osaka Bay (modified after Kusuda et al., 1995).

2. RECLAIMED LANDS AND ARTIFICIAL ISLANDS

Many cities of the Hanshin area are built on soft sediments deposited in deltaic and lagoonal environments along the foot of the Rokko Mountains. Industrial and urban areas were extended by reclaimed land along the ancient coast. There are two reclaimed islands in Kobe City, called "Port Island" and "Rokko Island" respectively. The reclaimed materials of the islands are composed of boulder-size gravel and coarse grain-size weathered Granite consisting of bad sorting and permeable strata. These strata were until now considered resistible to liquefaction.

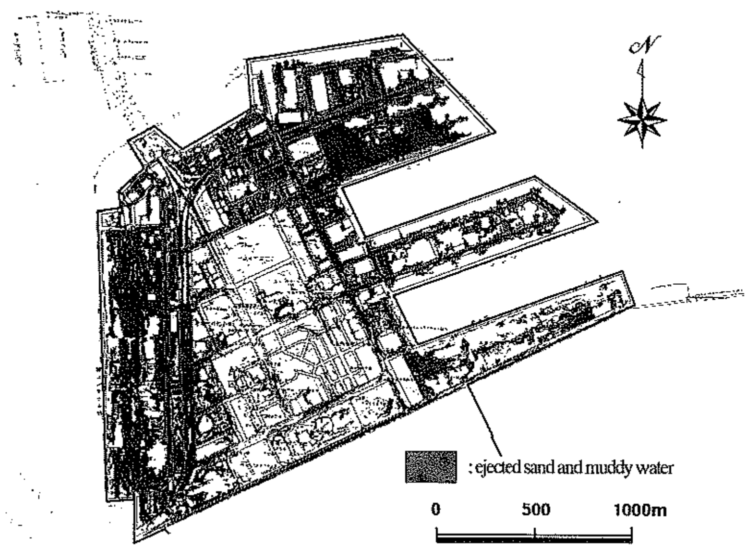

Figure 2. Distribution of ejected sand due to liquefaction in Port Island.

Figure 3. Distribution of ejected sand due to liquefaction in Rokko Island.

3. SUBSIDENCE AND DAMAGE

After dramatic event, most of the harbor facilities in the Kobe port could not be used.

The large-scale land subsidence was observed in the outer edge and in the central part of the islands (Fig. 4 and Fig. 5). In the outer edge of the islands, many of the quay banks were inclined, subsided and slide into the sea. Maximum subsidence inside the banks reached 470 cm. The exposed foundation piles of the buildings were broken and inclined. The outflow of reclaimed materials was taken with a water resistance camera. In the central region of the islands, the water supply pipelines and other underground lifelines used for houses were cut due to differential subsidence and upward displacement of the piled buildings. Most of the newer buildings existing in the central area, guaranteeing a comfortable life, were destroyed. Furthermore, ground sinking and ejection of muddy water caused flooding.

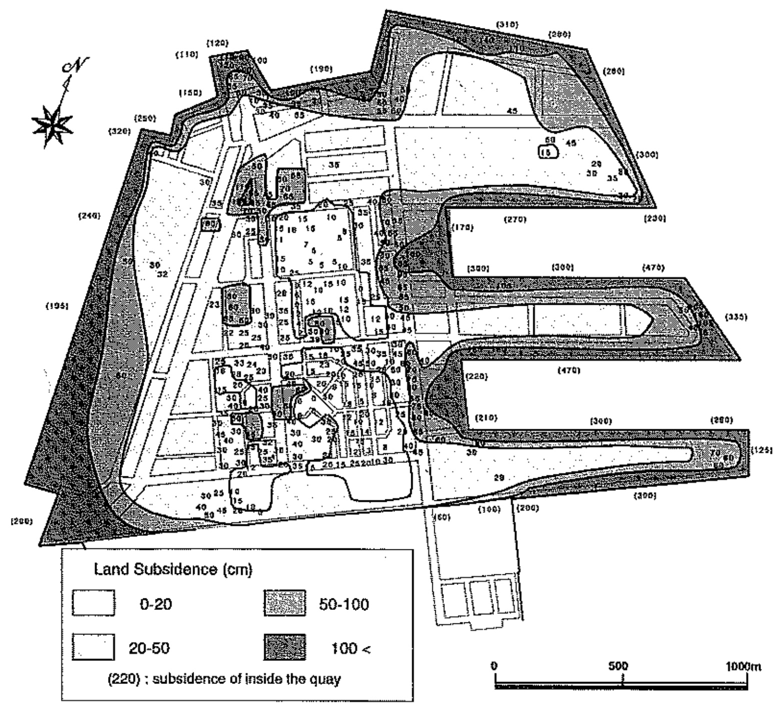

Figure 4. The value of land subsidence in Port island.

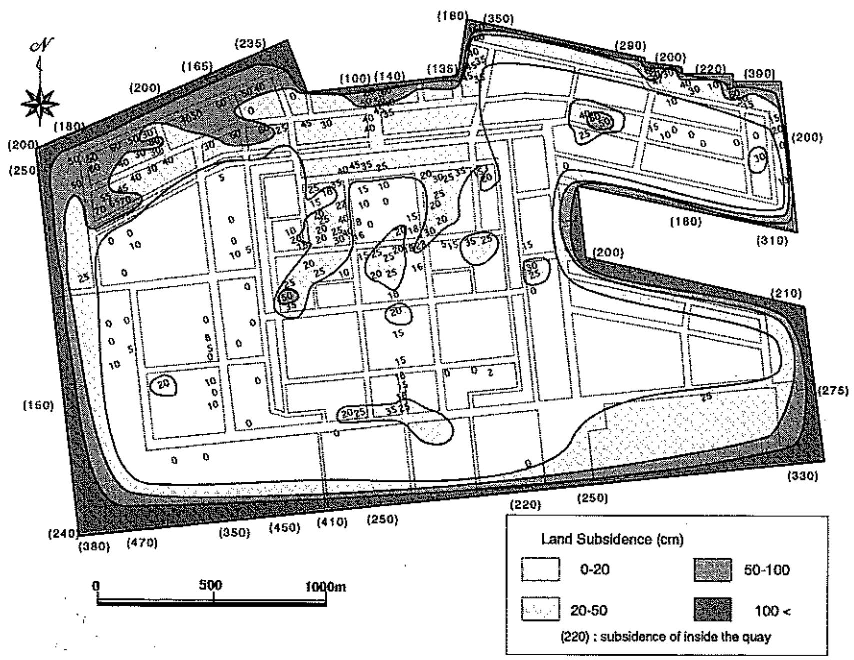

Figure 5. The value of land subsidence in Rokko island.

4. LIQUEFACTION LAND SUBSIDENCE

These phenomena were caused by large scale Liquefaction-Fluidization with strong ground motion. However, damage by strong motion was small at the liquidized area in comparison with the non-liquidized area. It is possible that a long period motion was dominant at the liquidized area. On the contrary, if the long period motion strikes a reclaimed land area, then an increase of the earthquake wave is possible. Even if liquefaction subsidence is an exceptional event, it represents a big problem for low lying and reclaimed land areas because of the immediate and heavy damages it causes. We don't always gain a lot of experience using and making artificial beds, which may demonstrate their weakness during natural hazards as earthquakes.

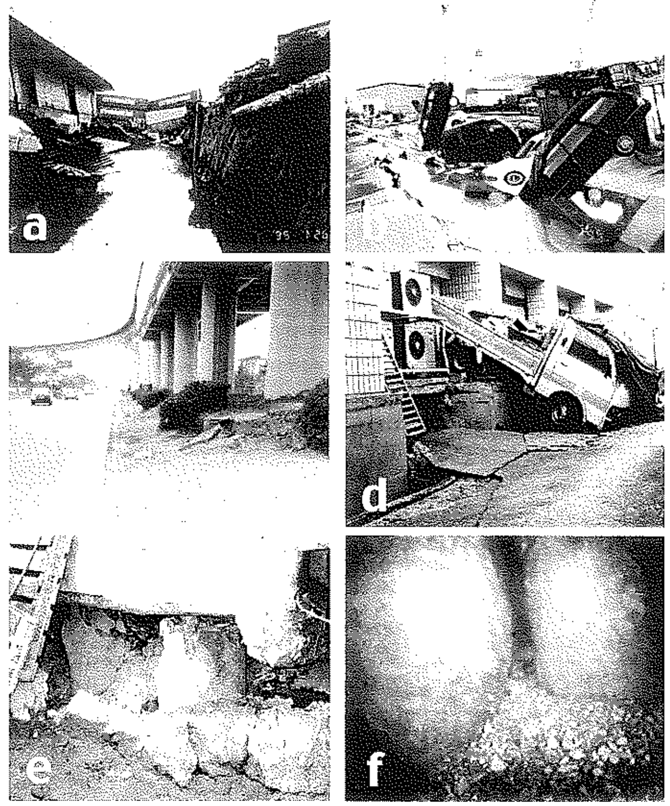

Figure 6. The photographs of the liquefaction land subsidence and the damage.
a : The inside the quay of Port island sank in maximum 470cm.
b : The broken quay and subsided inside where few cars up standing.
c : Upward displacement of the piled railway (Port liner).
d : Upward displacement of the building in the central region of Port island.
e : The exposed foundation piles of the buildings were broken.
f : The jointed part of the quay opens and flow out gravel at depth in 10m (obtained with a water resistance camera).

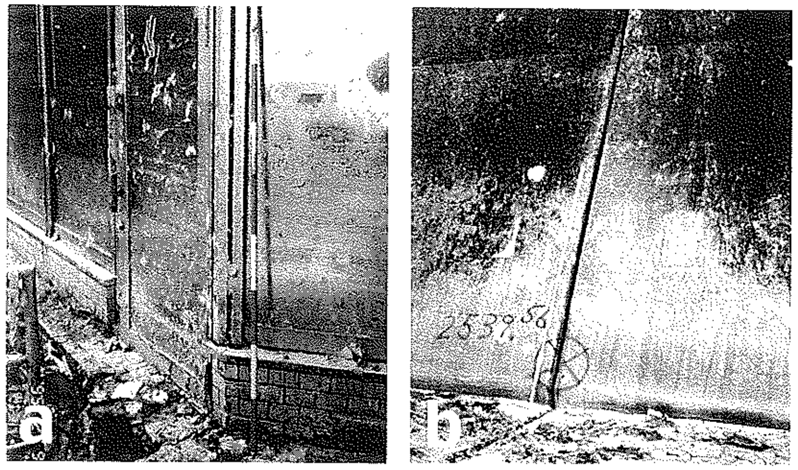

Figure 7. Traces of liquefaction flooding.
a. The muddy water reached a height of 130 cm (see line on the building wall).
b. The trace of the spouted muddy groundwater at the commissure part of the quay.

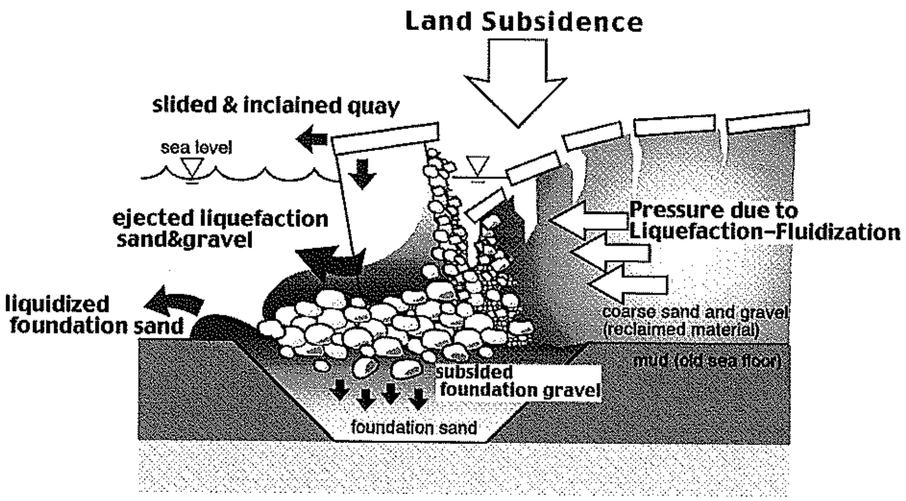

Figure 8. Schematic cross-section of the outer edge of the artificial islands.

REFERENCES

Kagawa, A., Nirei, H., Kusuda, T., Satoh, K., Sakai, Y., Furuno, K., Kamura, K., Kazaoka, O. and Morisaki, M. (1995) Liquefaction-fluidization phenomena due to the 1995 Southern Hyogo Earthquake: Liquefaction-Fluidization in the Artificial Island. In: *The proceedings of the fifth symposium on the Geo-environments and Geo-technics*, The Committee of Environmental Geology, Geological Society of Japan, 13-24. (in Japanese with English abstract)

Kusuda, T., Satoh, K., Furuno, K., Sakai, Y., Kamura, K., Kazaoka, O., Kagawa, A., Morisaki, M., Takanashi, Y., Asao, K., Ishiwata, Y. & Nirei, H. (1995) Geological characteristics and distribution of liquidized-fluidized sites due to the 1995 Southern Hyogo Prefecture Earthquake. In: *The proceedings of symposium on the Great Hanshin-Awaji Earthquake and its geoenvironments*, The Committee of Environmental Geology, Geological Society of Japan, 125-130. (in Japanese with English abstract)

Okada, H., Momikura, Y., Otsuki, K., Takemura, K., Takemura, A. and Nishi, H. (1998) Earthquake and Geological Hazards -The 1995 Hyogo-ken Nanbu Earthquake. Memoirs 51, Geological Society of Japan, 162p. (in Japanese with English abstract).

LAND SUBSIDENCE - Vol. I
Proceedings of the Sixth International Symposium on Land Subsidence
Ravenna / Italy / 24-29 September 2000

SUBSIDENCE PHENOMENA IN THE EVOLUTION OF PONTINA PLAIN, ITALY

Fabio Brunamonte
c/o CNR-Istituto di Ricerca per la Protezione Idrogeologica nel Bacino Padano, Strada delle Cacce, 73 – 10135 Torino, Italy

Sergio Cavelli
Via Spiritiera II trav. 19, Marina di Minturno (LT), Italy

Leonello Serva
National Agency for the Protection of the Environment (ANPA), Via Vitaliano Brancati 48, 00144 Roma, Italy

Alessio Valente
Facoltà di Scienze MM.FF.NN., Università degli Studi del Sannio, Via Port'Arsa 11, 80120, Benevento, Italy

Abstract

By analysing several boreholes, topographic and soil mechanics data, and taking into consideration numerous historical sources, it has been possible to reconstruct the evolution of the Pontina coastal plain. Such a reconstruction has evidenced subsidence phenomena, clearly shown also by the effects on the infrastructures. Because of that, a large area, which at the beginning of the last century was still at a height of some meters above mean se level, has presently been lowered to or below sea level. The maximum subsidence of 5.9 m above m.s.l. observed in the period between 1811 and 1994 is related to the presence of organic sediments (mainly peat), which reach a thickness of over 60 m in some portions of the Quartaccio basin. The consolidation of the peat deposits and the land reclamation activity are considered the causes of subsidence. The interference between natural evolution and reclamation, which took place in the Pontina Plain, represents an emblematic case in the Mediterranean area.

Keywords: Land subsidence, Organic deposits, Hydraulic reclamation, Southern Lazio.

1. INTRODUCTION

Coastal plains are increasingly being regarded as fundamental areas for the socio-economical development of our society. Therefore, they are undergoing changes in their morphological and hydraulic conditions aimed at improving the quality of life.

In the evolution of these plains, however, subsidence phenomena (Cotecchia, 1980; Carbognin, 1985) induced by natural (i.e., tectonics, compaction) and anthropogenic processes (i.e., reclamation) are frequent.

The aim of this work is to understand the processes which occurred in the evolution of the Pontina Plain, where the development of a beach ridge - lagoon system in a particular geomorphological setting was controlled (mainly in the last two centuries) by land reclamation works (Brunamonte et al., 1998).

This understanding has been achieved by means of the reconstruction of the thickness of the peat deposits, as well as through the definition of their physical characteristics, which has been possible by analysing samples obtained by a new borehole drilled purposefully. Land sinking in correspondence of the maximum thickness of peat and the related evolution of man-made drainage processes have also been taken into account.

2. THE PONTINA PLAIN

The Pontina Plain is one of the main coastal plains of the Italian peninsula. It is delimited seaward by the Tyrrhenian Sea and landward by the mesocenozoic carbonate relief of the Lepini-Ausoni mountains (Central Apennines). Heading towards these mountains, the plain gradually reaches the maximum altitude (about 40 m a.s.l.), even if several wide areas lie below sea level.

The plain is characterized by the development of a beach ridge - lagoon system, where prevailing clastic deposits related to littoral and lagoonal environments are present. More specifically, the lagoonal deposits, mostly muds, sometimes calcareous in composition, peats and peat clays, are found near the littoral area, behind beach dune ridges, mainly in the plain lying at the foothill of the Lepini-Ausoni mountains (Fig. 1). Both areas are characterized by a low supply of terrigenous material and very poor drainage.

Furthermore, the issuing of a series of huge springs at the foothill (both single and linear), with an average total flow rate of over 17 mc/s is present. This amount of water mainly flows on the surface, because of the lack of an efficient hydrographic network as well as the already cited presence of depressed areas.

During the interglacial periods, this situation gave origin to the formation of organic deposits, which have played and still play an important role in subsidence processes, likely, accelerated by man's intervention to improve drainage. In fact, since Roman Times, the Pontina plain was subjected to reclamation works mainly aimed at reducing the marshy area in the proximity of the Appian Way (Via Appia); however, later on the condition went back to the original one because of the lack of maintenance following the end of the empire. New significant plans of reclamation were promoted at the end of 18th century and, much more, between 1927 and 1934.

3. PEAT DEPOSITS

The analysis of 469 boreholes, 397 water wells and 50 static penetrometric tests allowed to carry out a detailed reconstruction of the setting of the Pontina plain subsoil, and therefore the distribution of lagoonal deposits.

In the Quartaccio basin, an area (as already mentioned) situated in the vicinity of the karstic springs sheltered by the Lepini Mountains, the organic deposits cover a surface of 139 kmq and can reach a thickness of over 60 m at some sites.

A new, specific borehole (Fig. 1) was drilled in this area in order to define physical characteristics such as density and water content, and to determine the radiometric age of various levels of these organic deposits.

The 31-m deep drilling crossed mainly peat and peat clay deposits, and subordinate fine sandy levels. However, at about 14 m, it shows a substantial change. For instance, the water content, which is over 300-400% in the upper part, decreases to less than 100 % in the lower part. Also the density, which is lower than or close to 10 kN/mc in the upper part, abruptly increases to over 13 kN/mc at the deeper depths, because of consolidation. Primary consolidation takes place rapidly following the dissipation of the interstitial overpressure in a matter of about ten minutes, whereas secondary consolidation, even with modest pressure, proceeds in a matter of weeks.

With regard to the age of these deposits, the deepest sample dated is 21,100 +1660/-1380 yrs B.P., whereas the most surficial one dated is 2,050 +/- 125 yrs B.P. This great thickness of peat, almost continuous in the last 20,000 years, could be considered a rare case for a Mediterranean area located at 41° N latitude.

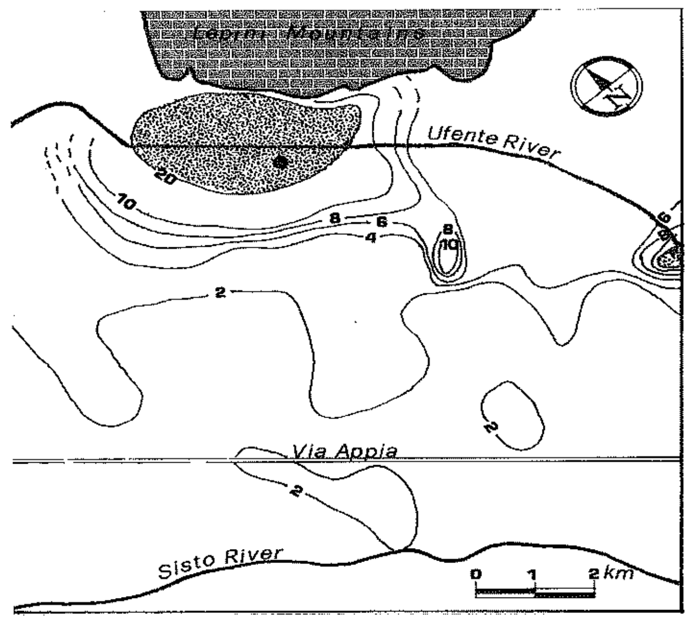

Figure 1. Isopaches (in meters) of the peat deposits. Maximum thickness is coloured in darkish; the black point indicates the new drilling.

4. SUBSIDENCE PHENOMENA

The first studies about subsidence took place in the beginning of the XIX century, as the various reclamation works conducted since the end of XVIII century had proven to be ineffective.

In spite of this, specific surveys have been carried out only during the last decades years (De Vito, 1980). As a matter of fact, the presence of large areas lowered to or below sea level (cf. topographic data) as well as the various effects of yielding in drainage networks and in buildings have stimulated new investigation aimed at reconstructing the subsidence process and recognizing its components (Brunamonte et al., 1998)

4.1 Topographic data

Before the reclamation work of 1927-34 (the so-called "Great Reclamation"), I.G.M. (the official Institute for topographic mapping) carried out detailed topographic surveys and, in particular, it established two high-precision leveling lines. These lines cross the Pontina Plain, and some benchmarks are still preserved. Several benchmarks were utilized again in 1951 by I.G.M. and in 1980 by the University of Rome. Both surveys made evident the presence of a vast area lying below sea level, even larger than the one that had been detected in the previous levelings.

More specifically, in the draining basin of Quartaccio, the most recent geodetic measurements revealed differences of lowering rates ranging between a few tenths of centimeters and over two meters.

4.2 Evidences on man-made activity

During the establishment of the drainage network in the Great Reclamation, twenty-two draining systems (water-scooping machines) were realized. Each system of pumps and tanks, were placed at a definite depth to be efficient.

Between 1930 and 1980, all the characteristic parameters of the water-scooping machines were modified many times in accordance with the variation in depth. The pump heads were increased from 0.3 to 2.6 m. The lowering of the pumping tanks made the extension of the suction pipe necessary.

Between 1950 and 1980 the functioning and capacity of the pumps were increased; nevertheless, a progressive increase in the frequency and serious overflowing of the canals occurred. This indicates a general lowering of the surrounding ground, since the average precipitation in the Plain had decreased in the same period.

The numerous bridges built over the canals were constructed during hydraulic reclamation. They preserve their original framework placed on deep foundations, even if there are some cracks on their shoulders, which are referable to the yielding of the soil. Furthermore on the bridges the surfacing of the foundation plateau, originally under the bottom of the canals, constitutes a barrier for the downflow of the waters. Also the sluices, installed in 1937, necessary to regulate water flow in the canals, show differences in level with respect to the surface of about 0.4 and 0.6 m.

Moreover, at present some buildings built with deep foundation near the drainage system, have their entrance at a height of 1 m above the surface. This isolated situation in Italy is similar to the Florida Everglades case (Stephens et al., 1984).

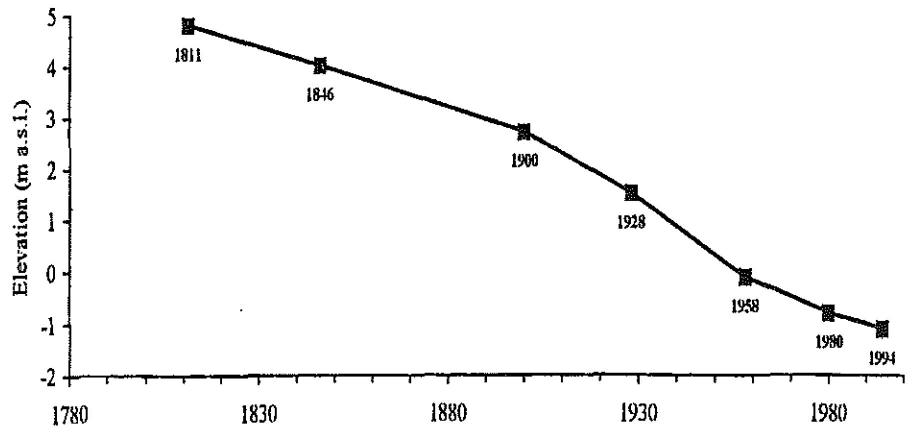

Figure 2. Lowering of the land in the basin of Quartaccio between 1800 and 2000

5. CONCLUSIONS

The analysis of the broad historical and geological documentation, encompassing almost two centuries, has allowed to define both natural and man-induced processes responsible for land subsidence in the Pontina Plain.

The area where the largest subsidence and most significant effects are recorded is in correspondence of the greatest thickness of peat deposits, that is the Quartaccio basin, which is situated at the foothill of the Lepini Mountains. The stacking of these deposits depends on the development of vegetation and the processes of biological oxidation and self-weight consolidation, which in turn reduce the volume of the deposits. The "lost" volume seems to be compensated by the continuous accumulation of new organic matter, but when the production was interrupted or markedly reduced the subsidence phenomena took place. This event could be related to a man-induced process, that is the draining of the surface waters, which directly affected the rate of the natural processes, modifying the deposition and compaction of organic deposits.

The early modifications of the hydraulic and morphological condition of the Pontina Plain in the 19th century caused a settlement rate exceeding 2 cm/yr. The subsequent activation of drainage plants in the early years of the 20th century increased the rate, which reached values of 4 cm/yr. The maximum values - over 5 cm/yr - occurred during the vast land reclamation in the period 1927-1939. More recent measurements show a progressive decrease in settlement of about 3 cm /yr between 1958 and 1994 with rates greater than 2 cm/yr (Fig. 2).

At present, the evolution of the subsidence phenomena caused major problems in large areas of the Pontina Plain, such as: the increase of floods, the decrease of the drainage network efficiency, the modification brought to the drainage plants parameters and the occurrence of damage in several buildings.

REFERENCES

Brunamonte, F., Serangeli, S., & Serva L., (1998) Natural and man-made processes in the subsidence history of the Pontina Plain (Italy). Proc. 8th IAEG, Vancouver, Canada, 21-25 September 1998.

Carbognin, L. (1985) Land subsidence: a worldwide environmental hazard. *Nature and Resources*, XXI, 1, 1-12.

Cotecchia, V. (1980) Review of Subsidence Phenomena in Italy and the World. In: "Hommage a Leon Calambert", 43-72. Ed. Georges Thone, Liège.

De Vito, L. (1980) Studio idraulico delle utilizzazioni delle risorse idriche nel Comprensorio Pontino. 128 pp., Regione Lazio, Rome.

Stephens, J.C., Allen, L.H., & Chen, E. (1984) Organic soil subsidence. In: GSA, *Reviews in Engineering Geology*, Vol. 6, 107-122.

2 Fluid Removal

LAND SUBSIDENCE IN THE EMILIA-ROMAGNA REGION, NORTHERN ITALY

Giuseppe Benedetti and Tiziano Draghetti
Emilia-Romagna Region, Bologna, Italy

Gabriele Bitelli and Marco Unguendoli
DISTART-University of Bologna, Italy

Flavio Bonsignore and Adriano Zavatti
ARPA-Emilia-Romagna Region, Bologna, Italy

Abstract

The Emilia-Romagna Region covers almost all the Southern part of the Po Valley. This zone is affected by strong subsidence, due not only to natural causes but also, and above all, to human activity. Subsidence has been well known for a long time and has been monitored by numerous authorities. These control surveys have, however, been limited to small areas, have been characterised by varying degrees of precision, and have been carried out in different periods using different benchmarks. In an attempt to standardise the historical data and to provide a well-defined space-time reference frame for all future measurements, we have set-up a precise levelling network of about 3000 km connected to all the existing networks. The network was measured in 1999 and allowed us to make interesting comparisons with the past. Connected with this levelling network we have also set-up a GPS network of about 60 points measured with dual frequency instruments and connected to some permanent stations. This GPS network, along with interesting studies on the geoidal undulation in the area, will permit quick and cheaper local control in certain zones. To manage all the data, a dedicated database system has been set-up. The first results appear to indicate that subsidence has accelerated in the western parts of the region but, thanks to legislative action and to the construction of infrastructures, has slowed down in the eastern areas. Monitoring work must therefore continue and must be accompanied by comprehensive actions aimed at reducing withdrawals and optimising water use.

Keywords: land subsidence, levelling, GPS, Emilia-Romagna

1. INTRODUCTION

The land in the Emilia-Romagna region is subject to a natural subsidence process whose rate can be calculated at an average of several millimetres a year, although this varies from area to area. Human activity, however, has accelerated the subsidence caused by natural, geological causes, especially over the last fifty years. The main cause of man-induced land subsidence is over-pumping of groundwater and hydrocarbons. Land subsidence has seriously affected historic monuments, caused a loss in the efficiency of water management systems, accelerated coastline erosion, and increased the probability of flooding in both coastal and inland areas. In the past, remedial actions have been aimed not only at removing the known causes of land subsidence but also at monitoring the geometrical pattern of its distribution. In the nineteen fifties, numerous agencies and local government authorities began setting up networks to monitor subsidence at local level in those areas where its effects were becoming increasingly evident. All these actions, observed in a regional context, however, reveal a great deal of duplications, inconsistencies and flaws which make it extremely difficult to derive an accurate, overall view where the vertical, land surface movements can be observed in a single time period and through a uniform spatial distribution. In 1997, with a view to overcoming these difficulties and producing an up-to-date, uniform picture of land subsidence over the entire plane of Emilia-Romagna, ARPA - Regione Emilia-Romagna, in collaboration with the DISTART Department of the University of Bologna, developed a project for the establishment of a regional land subsidence control network. The network is the result of the interaction of two surveying methods: the conventional surveying method, using spirit levelling lines, and the GPS satellite positioning method. The two methods fulfil different functions since their degree of accuracy and their benchmark distribution differ considerably. In particular, the lower cost and higher speed of the second method make it preferable to obtain information on a limited number of points at great distances from each other but measured at frequent epochs. Both networks are based on the dense net of existing benchmarks in order to optimise and make the most of the earlier experiences that have now been selected and integrated into a project on a regional scale.

The network planning stage was followed by the establishment of the new benchmarks. Two distinct networks were created, differing in terms of both siting and type of benchmark, taking into account the different requirements of the two surveying methods but providing for the altimetric linking of the GPS network to the levelling network. The GPS network consists of 59 benchmarks, of which 12 located in areas considered stable, the network being anchored to the south by the Apennine Mountains and to the north by the Padua and Brescia surrounding areas. The levelling network includes more than 2000 benchmarks distributed over some 2000 kilometres of levelling lines. In particular, there are 6 lines that anchor the network to 6 areas in the Apennine Mountains, considered being stable.

In 1999, thanks to funds from the Emilia-Romagna Region and the Ministry for University Education and Scientific Research, the first survey was performed on the regional network as a whole. Concurrently, surveys were also performed

on other networks to increase the density of the regional network. These other networks included the one set up by the province of Bologna - consisting mostly of the existing benchmarks belonging to the control network of the city of Bologna (1983), to lines of the Reno River Basin Authority (1952) and to other new lines - and levelling lines in the coastal subsidence control network established by Idroser-Regione Emilia-Romagna (1984).

The survey therefore included networks covering a total of more than 3000 km of lines with more than 3000 benchmarks and the altimetric linking of the GPS points (Fig. 1). The levelling measurements were taken over a period of 75 days between the end of August and early November 1999, by 18 operational teams, using only digital automatic levels. At the same time, the DISTART Department of the University of Bologna performed the first measurement of the GPS network using 6 double-frequency receivers and 4 permanent stations.

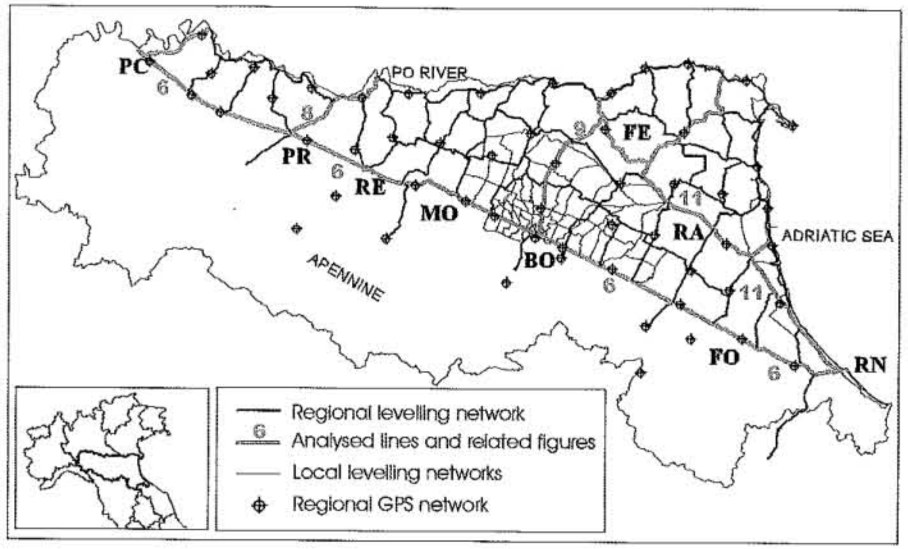

Figure 1. The spirit levelling network and GPS stations surveyed in 1999.

This paper presents the first results of the survey, viewed in particular in relation to two aspects. Firstly, operational and statistical considerations were made in order to perfect the methodologies to be followed in future surveys. Secondly, the data regarding the lowering of the land surface were analysed with particular reference to the lines of the regional network coinciding with the lines of the I.G.M.I. (Istituto Geografico Militare Italiano) and, to a lesser extent, those of the Cities of Bologna and Modena. In comparing the results with the historical data provided by these authorities, no kind of homogenization was necessary. A complete analysis relating to all the existing benchmarks included in the network will require more time than was available for the publication of this paper.

2. THE 1999 SURVEY

2.1 The Levelling Network

The levelling network consists of the regional network extended over the entire Emilia Romagna plane, divided into 44 polygons covering an area of 8609 km2 and including approximately 2000 km of lines with more than 2000 benchmarks. About 70% of these benchmarks existed before this first survey and have therefore been useful in providing a general indication of the changes in land surface movements that have already taken place. In the 1999 survey, besides the regional network, measurements were also taken in other local networks or parts of them, thus increasing the density in the Bologna area and in the areas along the coast. As a result, the network actually observed included 149 polygons consisting of over 3000 km of lines with more than 3000 benchmarks.

2.2 The Altimetric Datum

The levelling network is anchored through 6 open lines to areas, considered to be stable, on the Apennine Mountains. Of these lines, three belong to the national IGM network and three belong to important local networks, namely, Bologna, Modena e Ravenna. The decision to establish different connecting lines was based on two main reasons. Firstly, it will allow future surveys to be made even on part of the network, while still being anchored to a stable point close enough to limit costs and the propagation of errors. Secondly, it satisfies the need to bring all the reference benchmarks used in the past by different authorities into line with each other by assigning to them a height with reference to a single point. The benchmark considered to be the most suitable to be used as reference for the entire network was one near Sasso Marconi (Bologna Apennines). Its barycentric position within the network makes it possible to optimise the error propagation effect. The benchmark, called 025010, belongs to the network of the City of Bologna (SM/2) and has an orthometric height of 226.360 m measured in 1983 – and which remained unchanged in subsequent surveys – with reference to the height of the benchmark I.G.M.I. 5/162" (vertical) measured in 1949. The height of the 5/162" benchmark was confirmed by the I.G.M.I. survey of 1990 when it was measured again. Its stability was further confirmed when the difference between its height and that of the reference benchmark of Castel de' Britti (Bologna Apennines) was subsequently measured and found to have remained unchanged compared to earlier surveys in 1983, 1987 and 1992.

2.3 Checking and Adjustment of the Measurements

The survey was performed using only digital levels. Thanks to this new kind of instrument, work was speeded up and a number of human errors were eliminated, thus allowing a reduction in costs. However, some operational considerations can be made. For instance, it would be useful if these instruments had some means to definitely identify and manage the measurement files. During "a posteriori" testing, in fact, it is possible to know how many measurements were repeated to come within tolerance limits and to check whether the back and forth measurements had been repeated correctly for the out-of-tolerance belts and not simply by making an additional measurement.

Owing to the large amount of data available, the results were analysed statistically, starting from the discrepancies between the forward and backward measurements. Although, the study is still in its early stages, certain considerations can be made. First of all, we examined the absolute values of the discrepancies as a function of the distances (Fig. 2).

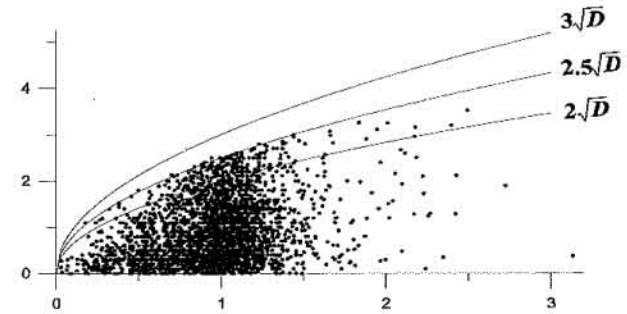

Figure 2. Absolute values of the discrepancies (mm) vs. distances (km).

As can be seen, many of them are within the $2\sqrt{D}$ tolerance, especially for short distances. This leads us to believe that this tolerance is the right one to apply, although it may involve slightly higher costs because of the greater risk of repetition on legs that may be out of tolerance. Measurements are more frequently within the $2\sqrt{D}$ tolerance for distances up to 0.7-0.75 km and this can certainly be attributed to two factors: the first regards the existence of systematic errors, the accumulation of which makes it difficult stay within tolerances for longer lines. The second is a human factor, caused by the tiredness of the persons holding the rods, which may lead to difficulties in keeping the rods perfectly vertical and immobile. Reducing the distances between benchmarks, besides solving the two above mentioned problems, would also lessen the damage created in the event of destruction of or tampering with some of the benchmarks.

We then found the statistical distribution of the normalised residuals calculated as $d = \frac{A+R}{\sqrt{D}}$ (where A and R are the height differences in the forward and backward measurements, and D is the distance in km) and created the histogram shown in Fig. 3 using a step of 0.1 mm. As can be noticed, the distribution well fits a normal curve, with a mean square error of less than a millimetre, but with a non-zero mean value of +0.5 mm. This confirms the existence of a systematic error, which makes the positive height difference increasingly greater than the negative difference. This error has been known for some time and is due to the backward tilt of the rod so that the height difference in the upward measurement is greater than that found in the downward measurement. Although it was known, the error surprised us for its magnitude.

To obviate the error, we proceed as follows:

a) We chose a set of legs (2500) such that the forward measurement was on an upward incline for a half of them and on a downward incline for the other half.

b) We then considered the normalised discrepancy as $d = \frac{|A|-|R|}{\sqrt{D}}$

Again, a normal curve was very well fitted (Fig. 4) with a slightly higher mean square error (higher data spreading) and a zero mean value. This confirms the previous consideration.

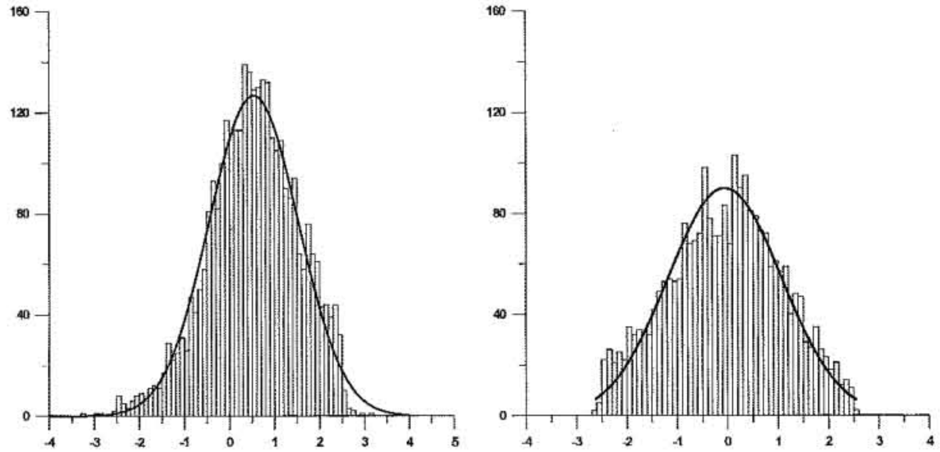

(3) (4)

Figures 3 and 4. Histograms for the distribution of the normalised discrepancies.

It will therefore be necessary to amend the technical specifications to persuade manufacturers to make rod supports more stable (heavier ground plates, special stakes for loose soil, large round headed nails planted in asphalt surfaces, etc.).

Other analyses regarded the influence of light refraction, direction and similar factors but no significant effects were found, mainly because the height differences involved were very small and the sunlight in the season when the measurements were taken (September-October) was already quite weak.

These studies may appear academic but in fact they are very important. The possibility of improving accuracy, even by a little, is for us essential. Thus, although the precision used is more than adequate for large values of land subsidence or for surveys carried out at infrequent intervals, it may become quite inadequate when subsidence is less evident and the surveys are carried out frequently.

After checking that measurements stayed within tolerance limits, we proceeded to calculating the error per kilometre as a function of the discrepancies for the open legs and for the very long East-West and North-South lines. For this, we used the formula:

$$\sigma = \pm \frac{1}{2}\sqrt{\frac{\left[\frac{d^2}{D}\right]}{n}}$$

where n is the number of legs, d is expressed in millimetres and D in kilometres. We found errors of 0.5-0.7 mm/km.

Next, we performed adjustment of the network, first considering only the nodal points and the line height differences as pseudo-observations with a system in 348 equations for 212 unknowns. We thus found the heights of the nodal points and their mean square errors. These varied from a few millimetres for the points close to the reference benchmark to 5-7 mm for the benchmarks furthest away. Lastly, having ascertained the good quality of the measurements, we proceeded to global adjustment of the network using 3180 equations and 3041 unknowns and obtaining the heights of all the points and the mean square error of each, including the points on the reference lines that may be used in future for the partial repetition of the network. The points surveyed included all the GPS vertices and this will enable important studies to be made on the geoidal undulation of the area.

2.4 The GPS Network

For the measurement of the GPS network, we used quite a complex strategy not only because the region includes a number of permanent stations but also because of the presence of some very long baselines necessary to connect the network to at least two stable points in the north.

In other words, we proceeded in cascade fashion, measuring first the framework of the network, with very long sessions (96 hours) involving the permanent stations of Padova, Medicina, Porto Corsini and Modena and another 6 points on the boundary of the network.

Using some of these points as semi-permanent stations and the nearest permanent stations depending on the operations area (so as not to have excessively long baselines), we went on to measure the network as a whole, with sessions of 270 minutes and using the multiple occupation scheme for each point. For the longer baselines, multiple sessions, that is, 540 and 810 minutes, were often used.

Reasoning in terms of independent baselines, we obtained the scheme shown in Fig. 5 with observations taken on more than 160 independent baselines and thus with a redundancy not far from 3, which guarantees a high level of reliability for the results.

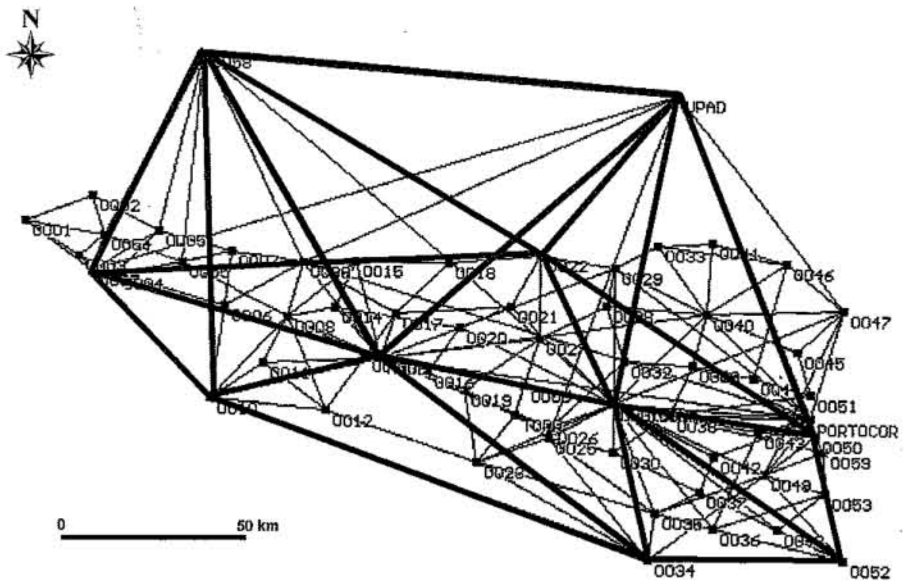

Figure 5. Independent GPS baselines.

According to our usual practice, the computation and adjustment were performed using different methods and different software, not only for Quality Control, but also for the single baselines or multibase-multisession processing. In particular, we used Geotracer, Bernese and even Gipsy for the long baselines.

That is not to say that the results obtained are final. Indeed, having stored the measurement data, it will be possible to recalculate the network if and when programs more sophisticated than those currently used are developed. The adjustment performed proved nonetheless useful to obtain point coordinates for studying the geoid and to ascertain the quality of the measurements. The quality of the measurements met our expectations. The single baseline adjustment, which gives realistic error parameters, provides a degree of accuracy of around one centimetre, which differs little from that obtained using precision levelling for the benchmarks that are furthest away from the origin benchmark.

2.5 Analysis of Land Surface Movements

The analysis of land surface movements at this stage is complicated by the fact that it must be based on a comparison between the measurements taken in 1999 and previous observations often taken over different periods. This report gives only the results of the comparisons made on the lines of the regional network that coincide with the lines of the I.G.M.I. network and with those of the Bologna and Modena city networks – where the latter coincide with the I.G.M.I. lines. No corrective coefficients were used to make the measurements from different surveys uniform with each other, since these surveys were considered to be sufficiently consistent both in terms of altimetric datum and in terms of degree of accuracy. Figures 6 to 17 show the land subsidence rates (in mm/year) calculated on the basis of the different periods according to the lines considered. The most recent period possible is highlighted. Where possible, the latest results are compared with measurements of the previous period, which also varies from area to area but which, in general, relates to the period from 1950-1980/92.

2.5.1 The Via Emilia from Piacenza to Rimini

A single graph showing the changes in land subsidence along the via Emilia, the road which traverses the entire region and has for centuries been a main route for communications between north and south, provides a good overview of land surface movements in the densely populated areas crossed by this road and greatly facilitates the task of comparing the situations in different areas of the region. The period for which the subsidence rate was calculated, that is, 1980/92 to 1999, takes into account the different periods of the surveys carried out prior to 1999 along the lines making up the network of which this road, approximately 280 km long, forms the spine. A more detailed analysis of the different periods to which the subsidence rates calculated refer is given below, area by area. Figure 6 shows that subsidence is more marked in the western provinces. The Bologna area, in particular, holds the unenviable record of the highest subsidence rate, with values up to more than 4 cm/year along the via Emilia in the period 1992-99. In the previous period (1983-1992), however, the rate recorded along the same line had been even higher, with a peak of more than 6 cm/year.

In the period 1985-1999, the Modena area registered maximum rates of more than 1.5 cm/year. In this area, the rate has accelerated slightly, not only compared to the period 1981-85 but also compared to the period 1985-1992. Figure 7a shows the levels calculated for the benchmark of Modena City Hall. The slightly higher rates in the more recent period are noticeable, though not conspicuous. Even higher rates are recorded for the Reggio area from Rubiera to Pieve Modolena, with maximum values around 2.5 cm/year (period 1980-1999). The graph in figure 7b shows the recordings for the benchmark of Pieve Modolena, where in the most recent period the land surface has subsided at a markedly faster rate. Proceeding towards Parma, the values are lower than 1 cm/year, with a few peaks of around 1.5 cm/year at Parma and Roveleto (period 1982/84-1999). Subsidence in the Parma and Piacenza provinces has markedly accelerated compared to the earlier periods 1952/55-1982/84. In fact, the lowering of the land surface in these areas was taking place at close to natural rates, Parma and Roveleto being the only exceptions. That the situation has worsened considerably is confirmed by the observations taken from Piacenza towards Cremona, along the SS.10 road that runs alongside the Po River. Along this line, too, the subsidence process has accelerated considerably: from 0.2-0.5 cm/year in the period 1952-1984 to 0.7-1.1 cm/year in the more recent period 1984-1999.

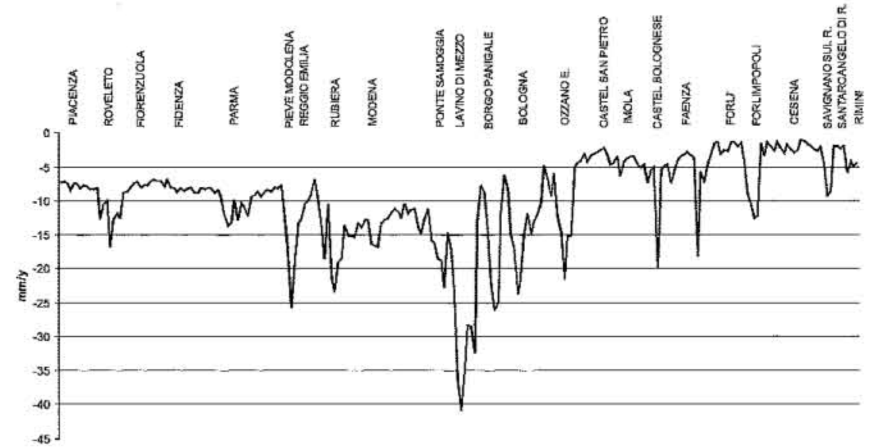

Figure 6. Subsidence rate along Via Emilia (period 1980/92-1999)

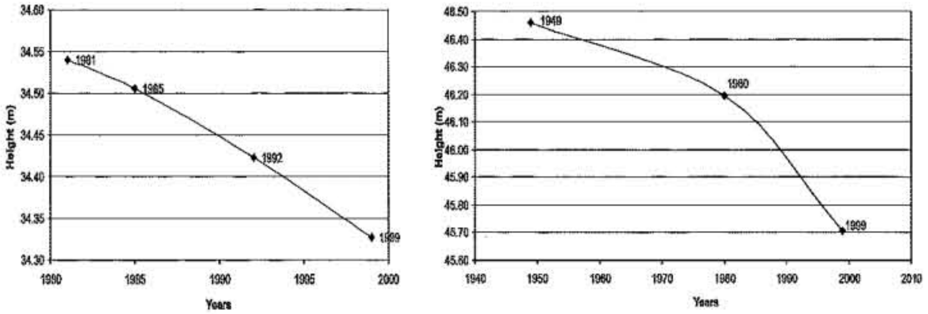

Figure 7. Vertical displacement at benchmark N23 in Modena (a) and at benchmark 17/70'IGM in Pieve Modolena, near Reggio Emilia (b)

Observations along the via Emilia from Bologna towards Rimini show a peak at Ozzano of more than 2 cm/year in the period 1990-99. Although this

peak had already been observed in the earlier periods, the rate here has almost doubled. Other peaks are observed at Castelbolognese and Cosina (Faenza), with measurements of around 2 cm/year in the same period and at Forlimpopoli and Savignano sul Rubicone, with values of about 1 cm/year. Around these critical points, there are large areas of relative stability, with values below 0.5 cm/year, such as at Castel San Pietro, Imola, Cesena, Forlì and Rimini. In these areas, especially Forlì and Rimini, subsidence has in fact slowed down compared to the period 1950-90 during which it ran at the rate of more than 1 cm/year. To sum up, the latest measurements along the via Emilia show that subsidence rates have increased markedly in the areas from Modena to Piacenza, have gone down in the Bologna area – although the latter area is still strongly affected by subsidence – and decreased markedly in the eastern provinces.

2.5.2 From Parma to Luzzara

Along the SS. 62 road from Parma to Luzzara, subsidence during the period 1985-1999 is calculated at around 1.5 cm/year (Fig. 8). It should be noticed that just north of the via Emilia, again at Parma, the subsidence increases from a maximum of 1.3 cm/year on the via Emilia to 1.9 cm/year just north of it. Moving away from Parma, the values recorded are mainly around 1 cm/year or slightly over this, but they rise to several peaks of more than 1.5 cm/year at Sorbolo, Fontana and Tagliata. These values are well above those of the previous period 1953-85 when the lowering was always under 0.5 cm/year and, in many cases, could be ascribed to natural causes.

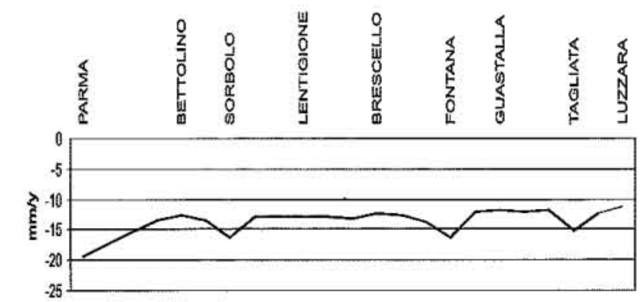

Figure 8. Subsidence rate along SS. 62 from Parma to Luzzara (1985-1999)

2.5.3 From Bologna to Ferrara

Along the SS. 64 road from Bologna to Ferrara, land surface movements vary noticeably from area to area (Fig. 9). Values around 3.5 cm/year in the period

1992-1999 typify the Bologna area from the immediate outskirts north of the city to Castelmaggiore. Values of more than 2.5 cm/year can be observed as far as San Giorgio di Piano, after which subsidence drops to values of around 0.5 cm/year as far as Pontelagoscuro (Po River). A comparison with the previous period 1983-1992, shows that the subsidence process in the Bologna area as far as San Giorgio di Piano, like that along the via Emilia, has slowed down by an average 30%. The process appears to have slowed down even more along almost all of the remainder of the line to Ferrara, while it is increasing by more than 30% from Ferrara to Pontelagoscuro. Figure 10 represents the land subsidence calculated for a benchmark in the worst affected area north of Bologna (Castelmaggiore). In this area, the land subsided at its fastest rate in the seventies, after which lowering slowed but remained practically constant throughout the following period. Altogether, the area has been affected by approximately 3 m of subsidence in the period from 1943 to 1999.

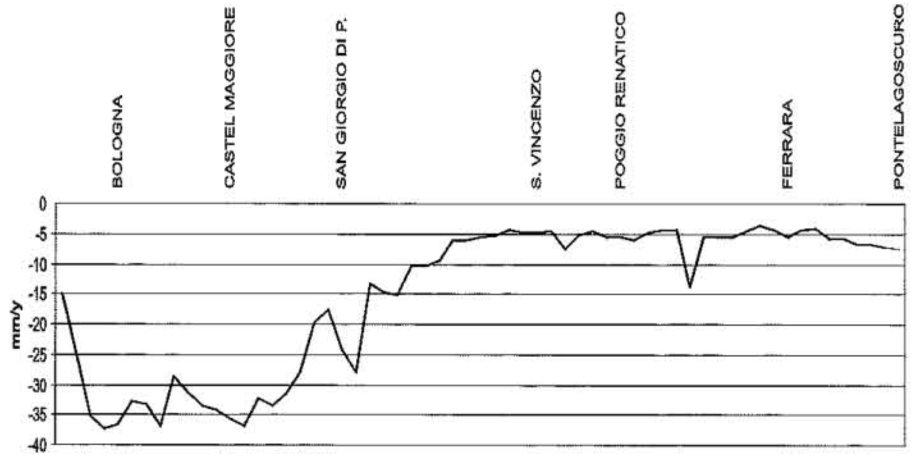

Figure 9. Subsidence rate along the SS. 64 road from Bologna to Ferrara (1992-1999)

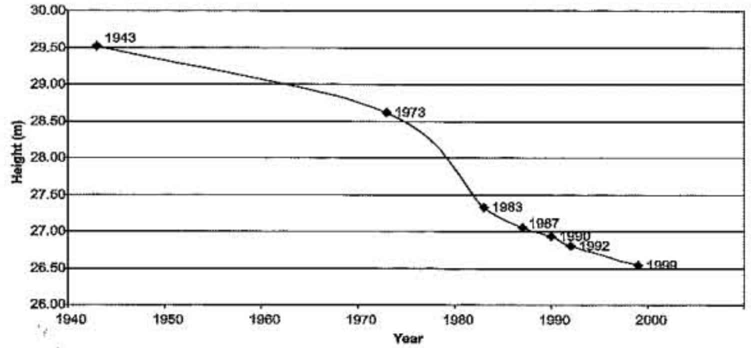

Figure 10. Vertical displacement at benchmark 6/16IGM
at Castelmaggiore, north of Bologna

2.5.4 From Portomaggiore to Ariano Ferrarese

Along the SS. 495 road from Portomaggiore to Ariano Ferrarese (on the Po di Goro), subsidence in the period 1988-1999 gradually increases towards Ariano Ferrarese. From the beginning of the line and as far as Dogato, movements fluctuate around 0.6 cm/year. After that, from Migliaro to Mezzogoro, measurements show lowerings of around 1 cm/year, down to as much as 1.5 cm/year close to the Po di Goro. A comparison with the previous period 1977-1988 reveals that the land is sinking at a gradually increasing rate towards the Po di Goro. The rate in the tract from Codigoro to Ariano Ferrarese has almost doubled.

2.5.5 From Rimini to Ferrara

Along this line, approximately 140 Km long, which traverses the provinces of Rimini, Forlì, Ravenna and Ferrara, the subsidence rates calculated for the period 1990-1999 vary quite considerably (Fig. 11). In the Rimini area, the land is sinking by 0.2 to 0.5 cm/year close to Rimini and by as much as 0.8 cm/year and over at Igea Marina. The Cesena area is affected by fairly extensive subsidence, ranging from a maximum of more than 1 cm/year at Villa Marina to around 0.6 cm/year at Cesenatico. The hinterland of Cervia is affected by rates of around 0.5 cm/year, while another negative peak can be observed further north, at Savio, affected by 1 cm/year. Across the city Ravenna, the subsidence rates fluctuate around 0.6-0.7 cm/year and climb abruptly to more 1.2 cm/year at Taglio Corelli, just north of Alfonsine, remaining at approximately 1 cm/year for another tract of more than 10 km. Proceeding towards Ferrara, the land surface is subsiding at rates ranging from 0.4 to 0.5 cm/year. Comparison with the previous period 1970/77-1999 shows that the subsidence rates have slowed down markedly throughout this part of the region, by as much 80% in the Rimini and Cesena areas, by varying degrees never less than 50% in the Ravenna area and by between 10 and 50% in the Ferrara area. Subsidence in the Ferrara area was much less than in other areas, even in the previous periods, varying between 0.5 and 1 cm/year.

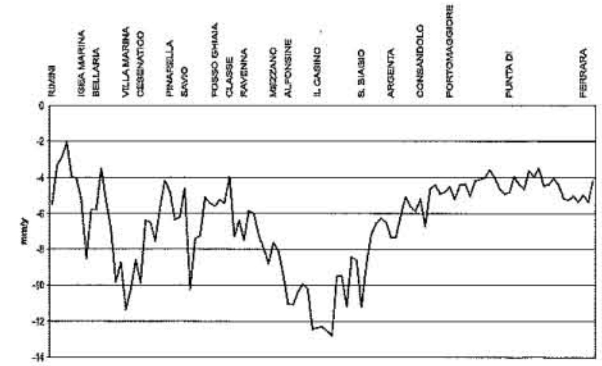

Figure 11. Subsidence rate from Rimini to Ferrara (1990-1999)

From Ravenna to Marina di Ravenna the rates tend to increase towards the coast, passing from about 0.6 cm/year to about 1.2 cm/year. Figure 12a shows a graph of the land subsidence calculated for the benchmark located at the end of this line (Faro di Marina di Ravenna). The graph shows that this benchmark has been affected by approximately 40 cm of subsidence over the last 30 years at a rate that has remained almost constant except during the period 1970-77 when it rose slightly. This fact clearly evidences that the sudden reduction in the subsidence rates in the hinterland of Ravenna does not apply to the Ravenna coastline. The changes in subsidence levels represented by the graph in Figure 12b appear in line with the decreases in subsidence rates mentioned earlier in relation to the Rimini area, where the sudden lowering that took place in the seventies and eighties was followed by an equally sudden slowing down in the nineties, with subsidence approaching values very close to those that can be attributed to the natural lowering of the land surface.

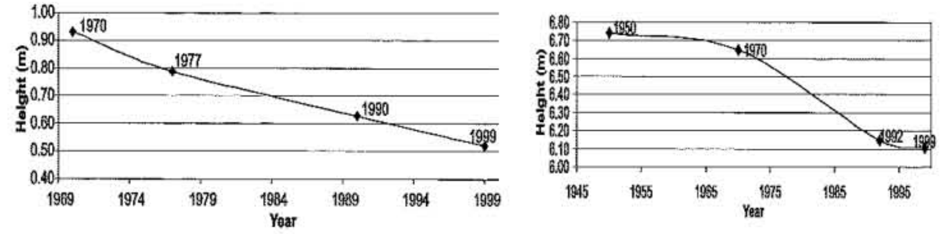

(a) (b)

Figure 12. Vertical displacement at the benchmark 16D1/12IGM, Marina di Ravenna (a) and at the benchmark NOD.34, Rimini (b)

3. CONCLUSIONS

The Emilia-Romagna plain is subject to natural land subsidence caused both by tectonic movements and by the consolidation of the sediments from which the Po Plain was formed. This natural process, whose rate is calculated at around 2 to 3 mm/year in the worst affected areas but which is normally much less than this, is now accompanied by an "artificial" subsidence process which is caused by human activity and whose impact on the land surface has far more serious implications. At the present time, the main cause of land subsidence from human activity is the withdrawal of groundwater, resulting in the lowering of the land surface by several cm a year. The extraction of hydrocarbons from deep geological formations in several parts of the region is another cause of land subsidence from human activity. The impact of hydrocarbon withdrawals in the region, however, are not well documented. The critical situations caused by the lowering of the land surface are added to the rising of the sea level due not only to natural eustasy (approximately 1mm/year) but also to anthropogenic changes in world climate. Having identified the causes of land subsidence from human activity, numerous actions were undertaken to monitor the magnitude and spreading of the subsidence process and also to remove its known causes. Starting from the nineteen fifties, numerous agencies and local government authorities began setting up networks to monitor subsidence at local level in those areas where its effects were becoming increasingly evident. Concurrently, action was taken to govern groundwater withdrawals through legislation (special Law for Ravenna) and infrastructures designed to provide alternative water resources. The Industrial Aqueduct of Ravenna, the Romagna Aqueduct and the Emilia-Romagna Canal are the main examples of these infrastructures. Although these actions, and others at a more local level, have slowed down the subsidence process in certain areas, a number of critical zones remain. In the Bologna area, for example, the rate has decreased slightly but is still very serious (approximately 4 cm/year). The rate has gone up slightly at Modena (more than 1.5 cm/year) and climbed alarmingly in the Reggio area (up to 2.5 cm/year). Subsidence has also worsened in the provinces of Parma and Piacenza (1 cm/year). As a whole, subsidence in the eastern part of the region has slowed down considerably, especially in the coastal areas of Rimini and Cesenatico. The land surface is moving down more slowly in the city of Ravenna, too, (0.6 cm/year), although the city's coastline is still severely affected at the same rate as in the past (more than 1 cm/year). The situation has generally improved in Ferrara province but has worsened in the lower Ferrara Plain towards the Po di Goro (up to 1.5 cm/year). This paper reports the first results of the measurements taken on the regional subsidence control network and will be integrated with other monitoring activities managed by ARPA, especially the regional piezometric control network (Fig. 13), and the surveys of the sea bed along the region's shoreline. However, a full picture of land subsidence in the region will not be possible until the second survey of the network will be performed.

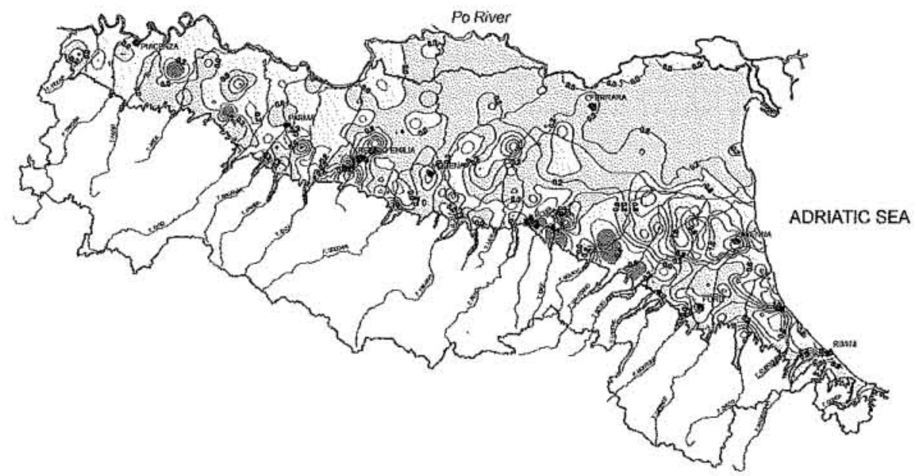

Figure 13. Map of average annual piezometric changes (m) derived from the regional piezometric control network (1976-1998)

These first results, however, do show that actions to reduce groundwater withdrawals have had a beneficial effect in reducing land subsidence. It is therefore essential to develop improved policies for water use. At the same time, it will also be necessary to consolidate actions for the implementation of water conservation measures such as, for example, for recycling industrial waste water, improving the efficiency of mains and irrigation distribution systems and introducing modern methods for reducing water wastage in the home.

Acknowledgements

Scuderi & Associates, Surveyors, for their help during measurement and testing of the network.

REFERENCES

Bitelli G., Bonsignore F., Unguendoli M. (1997) Progetto di una rete per il controllo della subsidenza nella regione Emilia Romagna. *Atti della Conferenza Nazionale ASITA*, Parma, 117-130.

Bitelli G., Bonsignore F., Unguendoli M. (1998) Il controllo della subsidenza nella Valle Padana: Stato dell'arte e sviluppi futuri. *Problemi di geoingegneria: estrazione di fluidi e subsidenza*, G. Brighenti - E. Mesini (eds), Piacenza, Geo-Graph, 19-30.

Bitelli G., Bonsignore F., Unguendoli M. (2000) Levelling and GPS networks for ground subsidence monitoring in the Southern Po Valley. *Journal of Geodynamics*, 30 (3), 355-369.

Bondesan M., Gatti M., Russo P. (1997) Movimenti verticali del suolo nella Pianura Padana orientale desumibili dai dati I.G.M. fino a tutto il 1990. *Bollettino di Geodesia e Scienze Affini*, 56 (2).

Bonsignore F., Draghetti T., (2000) Subsidenza. *Relazione sullo stato dell'ambiente in Emilia-Romagna 1999*, Regione Emilia-Romagna, 299-304.

Chahoud A., Spezzani P., Vincenzi D., Zavatti A. (1999) Ipotesi di metodologie operative per la classificazione quantitativa delle acque sotterranee. *Atti III Convegno Nazionale sulla Protezione e Gestione delle Acque Sotterranee per il Terzo Millennio*, Parma.

Gambolati G. (ed.), (1998) *CENAS - Coastline Evolution of the Upper Adriatic Sea due to Sea Level Rise and Natural and Anthropogenic Land Subsidence.* Kluwer Academic Publishers, Dordrecht.

LAND SUBSIDENCE - Vol. I
Proceedings of the Sixth International Symposium on Land Subsidence
Ravenna / Italy / 24-29 September 2000

LAND AND WATER-RESOURCE DEVELOPMENT ACTIVITIES INCREASE SINKHOLE FREQUENCY IN THE MANTLED KARST REGION OF FLORIDA, USA

A.B. Tihansky
U.S. Geological Survey, 4710 Eisenhower Blvd. Suite B-5, Tampa, FL, 33634, USA

Devin L. Galloway
U.S. Geological Survey, Placer Hall, 6000 J St., Sacramento, CA, 95819, USA

Abstract

Sinkholes are a common, naturally occurring subsidence feature in the mantled karst landscape of west-central Florida. The type and frequency of sinkhole activity is related to the composition and thickness of overburden materials, the degree of dissolution within the underlying carbonate rocks, and local hydrologic conditions. The increasing frequency of sinkholes corresponds to accelerated development of ground-water and land resources. Sinkholes form when the equilibrium between ground-water levels, a buried cavity, and the overlying materials is perturbed. Ground-water pumping, surface loading, surface loading combined with pumping, changes in drainage, construction and development practices all induce sinkholes. Five documented case studies show how human activity and land-use practices induce sinkholes. New regulations that establish critical ground-water levels, reduce ground-water level fluctuations, and provide structures for impounding contaminated surface waters are now used to minimize the detrimental effects of sinkholes.

Keywords: subsidence, sinkholes, ground-water pumping, karst, Florida

1. INTRODUCTION

Sinkholes are a common, naturally occurring geologic feature and a predominant landform in Florida, where they pose hazards to property and the environment. In west-central Florida, the increasing frequency of sinkhole occurrence corresponds to the accelerated development of ground-water and land resources. New sinkholes can cause substantial property damage and structural problems for buildings and roads. Sinkholes also threaten water and environmental resources by draining streams, lakes, and wetlands, and create a direct pathway for a hydrologic link between surface water and ground water (Tihansky, 2000). These pathways can transmit surface waters and surface contaminants that can persistently degrade ground-water resources.

Most of Florida is prone to sinkhole formation because it is underlain by thick carbonate deposits that are susceptible to dissolution by circulating ground water. The vast and complex carbonate aquifers that are Florida's principal fresh-water supply, are some of the most productive in the world. Development of ground-water resources for municipal, industrial and agricultural water supplies creates regional ground-water level declines that may accelerate sinkhole formation and increase susceptibility of the aquifers to contamination from surface drainage. Such interactions between surface-water and ground-water resources in Florida play a critical and complex role in the long-term management of water resources. Geologic and hydrologic features controlling sinkhole development and their related problems have been examined in attempts to better understand subsidence processes in west-central Florida.

2. THE MANTLED KARST OF WEST-CENTRAL FLORIDA

Mantled karst, a subdued gently rolling landscape that develops where solution features in limestone are covered by insoluble deposits, characterizes much of the Florida landscape. The siliciclastic sediments mantle and infill the irregular carbonate surface that has been sculpted by dissolution and weathering processes. The mantled karst of Florida continues to evolve as unconsolidated, insoluble, siliciclastic (sand and clay) deposits settle into the irregular surface and voids within the highly soluble carbonate rocks beneath them. As a result of the depositional history and infilling processes, the sand and clay deposits vary in composition and thickness throughout the State (fig. 1). In west-central Florida, the carbonate units typically are not exposed at land surface but their presence is often indicated by the occurrence of sinkholes and hummocky topography that results when the insoluble overburden subsides into the underlying dissolution features. Sinkhole formation is an important process that continually modifies a mantled karst landscape.

The type and frequency of sinkhole development depends on the extent of limestone dissolution, type and thickness of overburden material, ground-water movement, and other environmental conditions. In west-central Florida there are a number of distinct geomorphic regions that result from differences in the extent of karst development, type and thickness of overburden, and hydrologic conditions (White, 1970; Brooks, 1981).

Limestone dissolution and ground-water flow increase the porosity and permeability of the limestone units, creating a well-developed internal plumbing system. As a result, hydrologic features of the mantled karst landscape include sinkholes, springs, caves, disappearing streams, internally drained basins, and subsurface drainage networks.

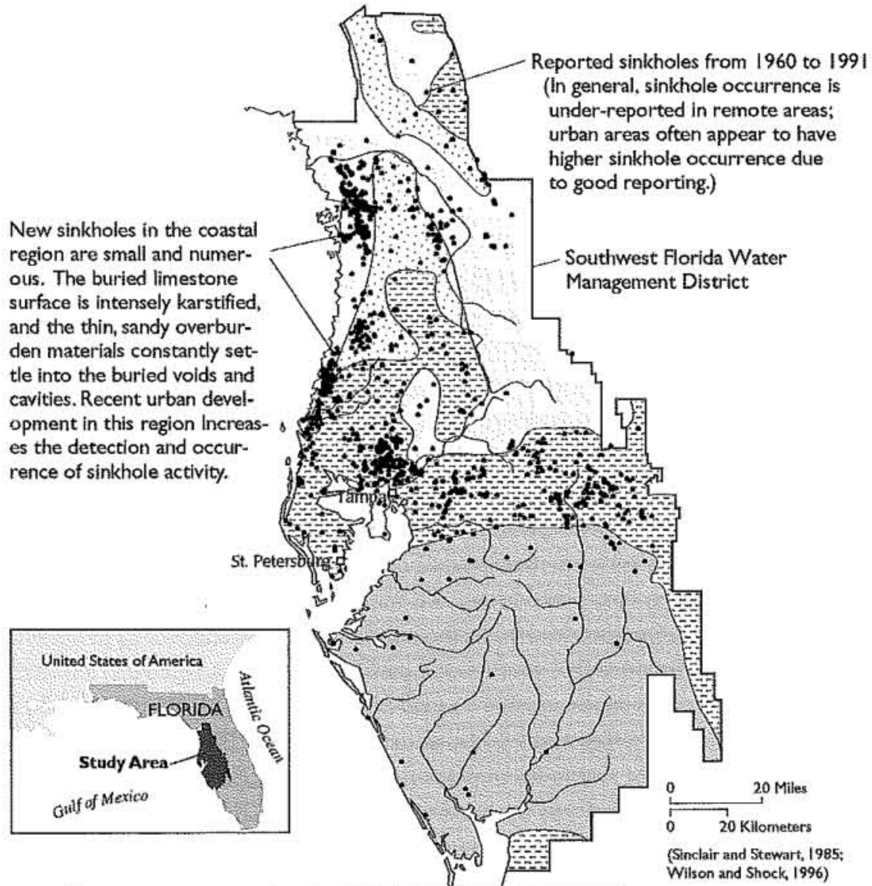

	TYPE AND THICKNESS OF OVERBURDEN	FREQUENCY OF SINKHOLES	TYPE OF SINKHOLES
	Thin; highly permeable	Generally few	Dissolution; cover-subsidence; cover-collapse
	30 to 200 feet thick; permeable sands are dominant	Numerous	Cover-subsidence–occur slowly; cover-collapse–usually induced
	30 to 200 feet thick; more clayey	Very numerous	Cover-collapse–occur abruptly
	Greater than 200 feet	Few	Cover-collapse–large diameter and deep

Figure 1. The type and thickness of overburden materials vary throughout the mantled karst of west-central Florida where they influence the location, type, and frequency of sinkholes.

3. HYDROGEOLOGIC FRAMEWORK

The hydrogeologic framework of west-central Florida consists of three layered aquifer systems. These are the Floridan aquifer system, the intermediate aquifer system or intermediate confining unit, and the surficial aquifer system. These units include both the carbonate units that make up the carbonate platform and the siliciclastic units that form the mantled overburden. The shallowest aquifer system, the surficial aquifer system, generally occurs within the uppermost unconsolidated surficial sand, shell and clay units. The surficial aquifer system ranges from less than 10 to more than 100 ft in thickness throughout west-central Florida. The water table is generally close to land surface, intersecting lowlands, lakes and streams. When sinkholes develop, deposits of the surficial aquifer system commonly fail, infilling cavities below.

In most of west-central Florida, the surficial aquifer system is separated from the Floridan aquifer system by a hydrogeologic unit known as either the intermediate aquifer system or intermediate confining unit, depending upon its local hydraulic properties (Southeastern Geological Society, 1986). The intermediate confining unit retards the exchange of water between the overlying surficial aquifer system and the underlying Floridan aquifer system. Generally, the intermediate confining unit is composed of clay-rich siliciclastic sediments that mantle the carbonate platform. In west-central Florida, these deposits thicken to the south and west, where they include more permeable clastic sediments and interbedded carbonate units and are referred to as the intermediate aquifer system. In northern areas of west-central Florida, where this unit is absent, the surficial aquifer system lies directly above the Floridan aquifer system. The type and frequency of sinkholes that develop is strongly correlated to the sediment composition and thickness of this unit and whether or not it is present (fig. 1).

Figure 2. After removing the overburden materials, this limestone quarry exposed the enlarged dissolution openings characteristic of the buried carbonate rocks of west-central Florida.

The thick carbonate units that constitute the Floridan aquifer system make up one of the most productive aquifer systems in the world. The upper part of this system, the Upper Floridan aquifer, is 500 to more than 1,800 feet thick and is the primary source of spring flow and ground-water withdrawals in west-central Florida. Transmissivities measured in these carbonate units are some of the largest in the world, commonly ranging from 50,000 to 500,000 feet squared per day and near large springs are as much as 13,000,000 feet squared per day (Ryder, 1985). These transmissivity values reflect the presence of enlarged dissolution openings within the carbonate rocks (fig. 2). The presence of extensive karst features and the potential for rapid ground-water movement within these carbonate units ultimately controls subsidence activity observed within the overlying deposits.

4. SINKHOLE TYPES AND MECHANISMS OF OCCURRENCE

Three general types of sinkholes occur in west-central Florida. These are: 1) dissolution sinkholes — depressional features in the limestone surface caused by chemical erosion of limestone, 2) cover-subsidence sinkholes — formed as overburden materials that gradually infill subsurface cavities, and 3) cover-collapse sinkholes — formed when cover materials abruptly fail, falling into subsurface voids or caves.

The mantled karst of west-central Florida has been classified into four distinct zones based on the predominant type of sinkholes (both natural and induced) that occur (Sinclair and Stewart, 1985) (fig. 1). In much of the northern part of the region, a highly permeable, thin (less than 30-feet thick) mantle of sediments overlies the carbonate rock. Rain water rapidly infiltrates the subsurface, dissolving the carbonate rock. Where bare rock is exposed at land surface, dissolution-type sinkholes develop. The dissolution activity occurs over a broad area and on the scale of geologic time, so there is little impact on human activity (Culshaw and Waltham, 1987). Where overburden materials are present, cover-subsidence sinkholes form as overlying sediments settle into dissolution features in the mantled limestone surface.

The overburden materials thicken southward in the region and become less permeable. In areas where the overburden ranges from 30 to 200 feet thick with significant clay content, sinkholes are numerous and generally occur as two types: cover-subsidence and cover-collapse. Where permeable sands are predominant in the overburden sediments, cover-subsidence sinkholes develop gradually as the sands fall into underlying cavities. Where overburden contains more clay, sinkholes are predominantly the cover-collapse type. The more cohesive, less permeable clay-rich deposits deform, postponing failure until the underlying cavity grows too large and the overburden collapses into underlying voids.

In the southern part of the region, overburden materials typically exceed 200 feet in thickness and consist of cohesive sediments interlayered with some carbonate units. Although sinkhole formation is not common under these geologic conditions, where they do occur, they are usually large diameter, deep, cover-collapse type sinkholes.

Though sinkhole types generally correspond to geologic conditions, hydrologic conditions can create optimal conditions for subsidence activity to occur. Local hydrologic conditions such as downward hydraulic head gradients and high recharge rates can accelerate sinkhole occurrence. The potentiometric surface of the Upper Floridan aquifer varies within west-central Florida. In upland regions, where hydraulic heads in the Upper Floridan aquifer are lower than heads in the surficial and intermediate aquifer systems, the potential for downward movement of water and overburden materials is greatest. In these areas ground water moves downward from the surficial aquifer system, recharging the intermediate aquifer system and the Upper Floridan aquifer. Where the intermediate confining unit is present, recharge to the Upper Floridan aquifer may be diminished. However, where the confining unit is predominantly sandy or the unit has been breached by sinkhole collapse, downward movement from the surficial or intermediate aquifer systems to the Upper Floridan aquifer can be greatly accelerated. This downward movement of ground water facilitates the movement of unconsolidated sediments into dissolution features and enhances the formation of sinkholes. Vertical shafts and sand-filled sinkholes can form high permeability pathways through otherwise effective confining units (Brucker and others, 1972; Stewart and Parker, 1992). Additionally, water recharging the Upper Floridan aquifer is chemically aggressive and has the potential to enhance sinkhole formation through increased limestone dissolution.

Along the coastal regions, sinkhole occurrence is rare because these typically are ground-water discharge regions. Artesian conditions exist along much of the west coast of Florida and springs commonly occur where confinement is poor. In the northern area, the Upper Floridan aquifer is exposed at land surface and is highly karstified but the artesian pressure reduces the potential for subsidence activity. Under these hydrologic conditions, ground water has the potential to move upward toward the surficial aquifer. Although sinkholes rarely occur under these conditions, many coastal springs probably functioned as sinkholes when sea level and ground-water levels were lower.

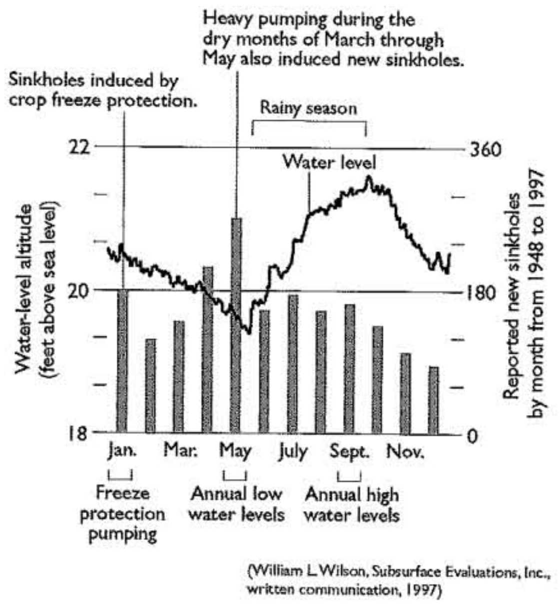

Figure 3. Sinkhole occurrence correlates to ground-water pumping effects and seasonal changes in ground-water levels.

In addition to the geologic framework and hydraulic head gradients, other conditions govern how and when sinkholes occur. Under natural conditions, vertical head gradients vary seasonally. Seasonal changes in ground-water levels reflect the influence of climate and rainfall (fig. 3). At the end of the dry season, typically in May, ground-water levels are near their annual low and at the end of the rainy season, typically in September, they reach their annual high levels. The annual range between the maximum and minimum ground-water levels can be significant. In some areas, the normal vertical head gradient can reverse, especially during prolonged drought or excessive rainfall events. During seasonal low ground-water levels, ground-water flow direction between the surficial aquifer and underlying aquifers can change from upward to downward. A significantly greater number of new sinkholes form during periods when ground-water levels are low (fig. 3).

5. CONDITIONS FOR INDUCED SINKHOLES

Sinkholes can be induced by changes in hydrologic conditions. In areas where sinkhole susceptibility is high, human activity often upsets the tenuous equilibrium that exists between a buried cavity and overburden materials, inducing sinkholes to form. Induced sinkholes are generally cover-collapse type sinkholes and tend to occur abruptly. They are divided conceptually into two types: 1) those resulting from ground-water pumping; and 2) those related to surface loading often associated with construction and development practices (Newton, 1987). Ground-water pumping stresses alter natural conditions in the same way that natural seasonal effects do, but can be more extreme. Extreme short-term pumping periods can cause temporary reversals in head gradients, while long term ground-water pumping can cause sustained ground-water level declines. Sustained water-level declines can induce downward ground-water flow, dewater lakes and wetlands, and cause once-flowing springs to become dry sinkholes. After ground-water pumping stresses are reduced or removed, ambient conditions are usually restored, but these changes can become semi-permanent or permanent if pumping persists over long periods of time, or if confining units are compromised.

Sinkholes caused by construction and development activities are generally associated with modifed drainage and diverted surface water —a common practice of nearly all construction activities. Human-made impoundments used to treat or store industrial process water, sewage effluent, or runoff can cause significant loading at land surface, weaken supporting geologic materials and cause sinkholes. Other construction activities related to induced sinkholes include the erection of structures, well drilling, dewatering, and mining.

6. CASE STUDIES: INDUCED SINKHOLES

There are numerous examples of induced sinkholes in the Florida landscape. Five examples presented here relate to ground-water pumping and surface loading. Four examples of sinkholes induced by ground-water pumping include: (1) the transformation of a spring into a sinkhole associated with long-term regional pumping; (2) sinkholes formed in response to new pumping stresses associated with new well field operations; (3) sinkholes caused by short-term ground-water pumping for crop irrigation; and (4) sinkholes that occurred when a newly-constructed irrigation well was being developed. A fifth example demonstrates how surface loading of ponded water caused sinkholes during a period when natural hydrologic conditions were most conducive to subsidence.

6.1 Kissengen Spring

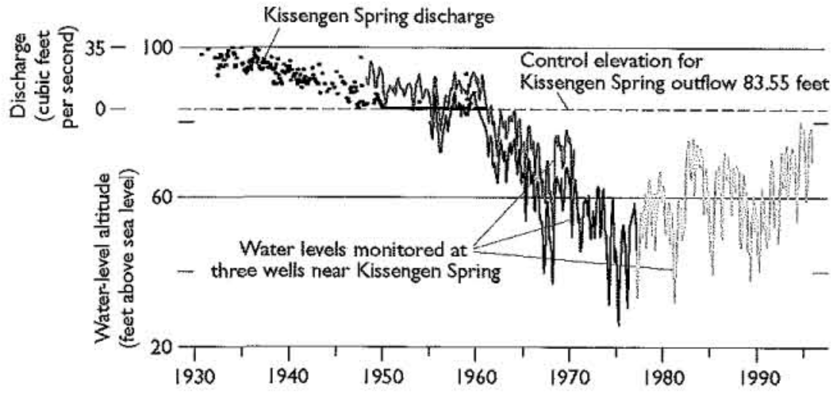

Figure 4. Decreasing ground-water levels due to long-term regional pumping caused Kissengen Spring to stop flowing and reversed the natural hydraulic gradient such that the spring became a sinkhole.

Kissengen Spring, once one of the largest artesian springs on the Florida peninsula, flowed an average of 20 million gallons per day (fig. 4). Ground-water pumping from 1937-1950 in central Florida east of Tampa eventually caused the spring to cease flowing due to regional lowering of ground-water levels (Peek, 1951). Water levels measured at three wells near the spring continued to track the decline after the spring stopped flowing. Continued lowering of water-levels transformed the spring into a sinkhole and provided a direct link between surface and ground-water resources. The spring vent was plugged to prevent ground-water contamination. Reduced pumping in this area more than 40 years after the spring ceased flowing has permitted water levels to recove, but not enough to re-establish spring flow., New sinkholes continue to form in this area during the dry season.

6.2 New well field for public water supply

Sinclair (1982) documented induced sinkholes near a new well field in the Tampa area as operations began and as pumping rates increased. Water levels began to decline when the well-field pumping began in 1963. In 1964, the pumping rate nearly tripled and within 1 month, 64 new sinkholes formed within a 1-mile radius of the well field (fig. 5). Most of the reported sinkholes occurred beyond the well-field boundary and in the vicinity of a well that was pumping at nearly twice the rate of the other wells. Other sinkholes appeared to be randomly distributed, indicating the heterogenous nature of secondary porosity caused by limestone dissolution. Proximity to pumping wells is not always a reliable indicator for predicting the location of induced sinkhole occurrence. In addition to sinkhole development, other effects in neighboring areas included dramatic declines in lake levels and dewatering of wetland areas.

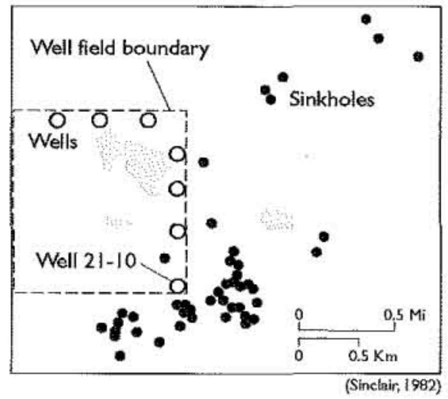

Figure 5. Sinkholes were concentrated near well 21-10 which pumped at the greatest rate.

6.3 Crop freeze protection

Heavy ground-water pumping during a short winter freeze event induced new sinkholes east of Tampa (Bengtsson, 1987). Mild winters are an important growing season for west-central Florida citrus, strawberry and nursery farmers. However, occasional freezing temperatures can result in substantial crop losses. To prevent freeze damage, growers pump warm (about 73O F) ground water from the Upper Florida aquifer and spray it on plants to form an insulating coat of ice. Extended freezes have required intense and prolonged ground-water pumping, causing large drawdowns in the Upper Floridan aquifer and the abrupt appearance of sinkholes. During a

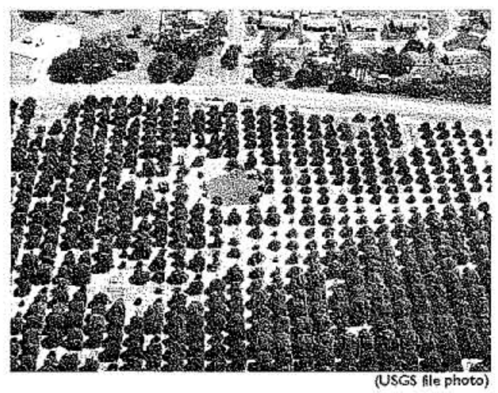

Figure 6. A cover-collapse sinkhole in an orange grove was induced by heavy ground-water withdrawals.

6-day period of record-breaking cold weather in 1977, ground water was pumped at night when temperatures fell below 39 O F. As a result, sinkholes were induced throughout the agricultural area (fig. 6).

The new sinkholes were attributed to the movement of the sandy overburden through a breached clay confining unit into cavities in the limestone below. While these pumping events are short-lived and infrequent, sinkhole occurrences are nearly as high as during dry season conditions when ground-water withdrawals are large (fig. 3).

6.4 New irrigation well

Development of a new irrigation well in February 1998 triggered the formation of more than 700 sinkholes in a 6-hour period. Sinkholes ranged in diameter from 1 foot to more than 150 feet in this unprecedented event (fig. 7). The affected land is located in an upland region near the coast. A 20-foot thick sediment cover composed primarily of sand with little clay is underlain by cavernous limestone bedrock. Because of the high possibility of sinkholes in this region, stability was tested along the margins of paleosinkholes located near the proposed well site to determine if the site had higher than normal risks of sinkhole occurrence. Test borings confirmed the existence of a highly variable limestone surface, typical of the area. Cavities, sudden drill bit drops, and lost circulation of drilling fluid frequently reported during drilling in this area are indicative of significant cavernous porosity in the limestone. While these characteristics are relatively common, only occasionally do they cause trouble during well construction.

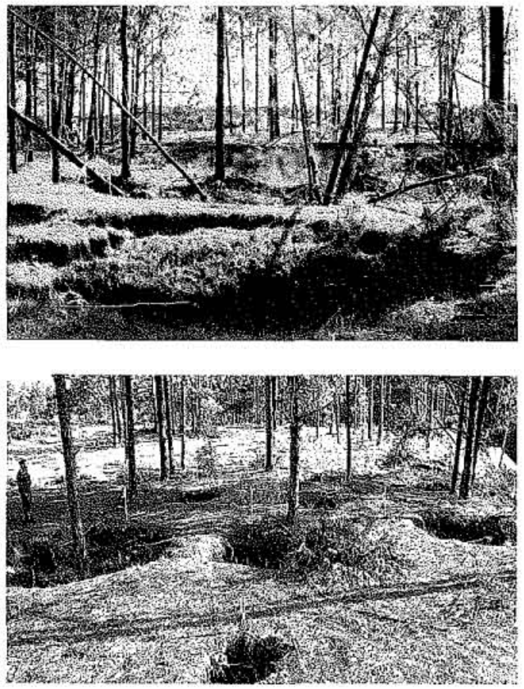

Figure 7. Sediment collapsed and slumped into numerous sinkholes that formed during the development of an irrigation well.

The irrigation well was drilled through 140 feet of limestone into a cavity from 148 to 160 feet where drilling was terminated. Then the well was pumped

to remove any debris that would hamper production capacity. Very shortly after development began, two small sinkholes formed near the drill rig. As these sinkholes expanded, well development was abandoned. Additional new sinkholes of varying sizes began to appear throughout the area even though pumping had stopped. Unconsolidated sand overburden collapsed into numerous cavities. Trees were uprooted and toppled as sediment collapse and slumping ensued. Concentric extensional cracks and crevices formed throughout the 20-acre landscape. The unconsolidated sandy material slumped and caved along the margins of the larger sinkholes as they continued to expand. The first two sinkholes to form eventually expanded to become the largest of the hundreds that formed. They swallowed numerous 60-foot tall pine trees, affected more than 20 acres of forest, and left the well standing on a small bridge of land.

6.5 Ponding of spray effluent (Sewage)

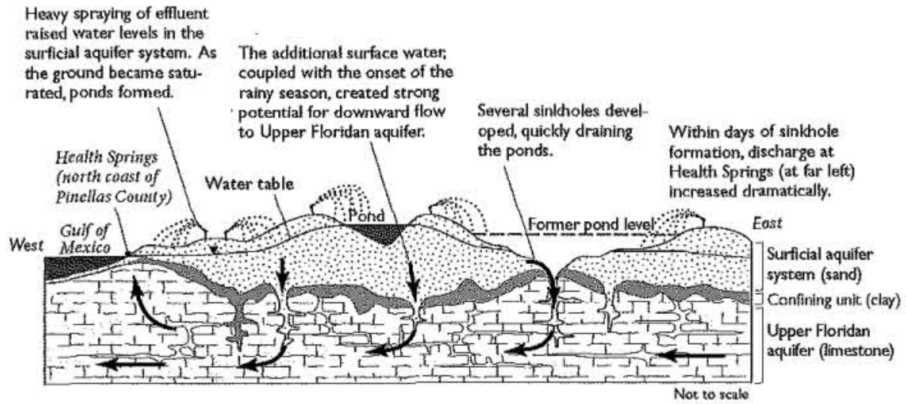

Figure 8. Surface loading in a sinkhole prone area induced a sinkhole to form which drained ponded water directly into the aquifer.

Surface loading at a spray-effluent irrigation facility induced sinkholes in another upland karst region near the coast in west-central Florida in a region where sinkholes are very numerous. In April 1988, several cover-collapse sinkholes developed in an area where sewage effluent from a wastewater treatment plant was sprayed for irrigation. The probable cause of subsidence was an increased load on the sediments at land surface due to natural rainfall and the ponding of waste water from spray irrigation. The 118-acre facility is located on land characterized by internal drainage and partial confinement between the surficial aquifer system and the Upper Floridan aquifer (fig 8). Spray-effluent volume applied in 1988 was equivalent to 290 inches per year, which is nearly 6 times the annual average rainfall for this region (Trommer, 1992). Ponding of spray effluent occurred as the surficial sediments became saturated. The increased weight or load of the pond and saturated sediments likely contributed to the subsidence. At the end of the dry season, when ground-water levels are at their lowest, several cover-collapse sinkholes developed suddenly and drained the pond directly into the aquifer system. Within several days of sinkhole formation, discharge at Health Springs, 2,500 feet down gradient in the ground-water flow path, increased from 2 cubic feet per second to 16 cubic feet per second (Trommer, 1992). Water-quality sampling of the spring during the higher flow detected constituents indicative of the spray effluent. Discharge at Health Springs had returned to the normal rate of 2 cubic feet per second within 2 weeks. A dye tracing test confirmed a preferential ground-water flow path between the upland spray area and the spring (Tihansky and Trommer, 1994). The ground-water velocity based on the arrival time of the dye was about 160 feet per day, or about 250 times greater than estimates of the regional ground-water velocity (0.65 feet per day) in this area. The dye-tracer test demonstrates how sinkholes and enhanced secondary porosity can provide a pathway directly and rapidly linking surface-water to the Upper Floridan aquifer.

7. MINIMIZING IMPACTS OF SINKHOLES

Incidental sinkholes may be a general nuisance with variable and often uncertain economic impacts, but the conditions that contribute to sinkhole formation can affect the quality and availability of ground-water resources. Thus, the creation of widespread conditions conducive to sinkhole formation may have far-reaching consequences beyond land subsidence concerns. Sinkholes are a naturally occurring phenomenon in west-central Florida; however, human activities can accelerate their formation. Land-use changes in rapidly-developing areas are often poorly controlled and include: altering drainage patterns, creating impoundments for surface water, and erecting structures in sinkhole-prone areas. Additionally, rapid population growth generally is accompanied by high demands for water-resource development, which impacts local and regional ground-water levels.

A number of steps are being taken to mitigate sinkhole development. Minimizing declines in ground-water levels has been a constant concern of water-resource managers. The Southwest Florida Water Management District has been working with other water-resources agencies to establish critical minimum levels for ground water within the west-central Florida area. Establishing and maintaining minimum ground-water levels will help to reduce the extreme conditions that induce sinkhole development. Engineering methods to prevent sinkhole damage are becoming standard construction practice (Sowers, 1984). Site assessments using geophysical tools to locate cavities or breaches located beneath planned construction sites help identify areas that may need reinforcement prior to construction. Construction techniques include drilling and driving

pilings into competent limestone for support, injecting cement into subsurface cavities, and constructing reinforced and spread foundations that can span cavities and support the weight of the construction. Compaction by hammering, vibratory rollers, and heavy block drops may be conducted over a site to induce collapse so that these areas of weakness can be reinforced prior to construction.

Land-use planners, resource managers, and actuaries have been able to estimate the probability of sinkhole occurrence and associated risks based on scientific data and insurance claims. The use of scientific information to assess risks and establish insurance rates demonstrates the benefits of understanding the hydrogeologic framework and potential effects of water-resource development. Scientific understanding of subsidence is essential for formulating effective land- and water-resources management strategies (Galloway and others, 2000).

REFERENCES

Bengtsson, T.O., (1987) The hydrologic effects from intense ground-water pumpage in east-central Hillsborough County, Florida. In: Beck, B.F. and Wilson, W.L. eds, (1987) *Karst hydrogeology: engineering and environmental applications:* Proceedings, Univ. Central FL, A.A. Balkema, Boston, 109-114.

Brooks, H.K., (1981) Guide to the physiographic divisions of Florida: Gainesville, Florida Cooperative Extension Service, IFAS, Univ. of FL, 11 p., 1 plate.

Brucker, R.W., Hess, J.W., & White, W.B., (1972) Role of vertical shafts in the movement of ground water in carbonate aquifers, *Ground Water*, **10** (6), 5-13.

Culshaw, M.G. & Waltham, A.C., (1987) Natural and artificial cavities as ground engineering hazards: *Quarterly Journal of Engineering Geology*, **20,** 139-150.

Galloway, D., Jones, D.R., & Ingebritsen, S.E. (2000) Land subsidence in the United States: U.S. G.S. C-1182,177 pp.

Lewelling, B.R., Tihansky, A.B. & Kindinger, J.L. (1998) Assessment of the hydraulic connection between ground water and the Peace River, west central Florida: U.S.G.S. WRI-97-4211, 96 p.

Newton, J.G., (1987) Development of sinkholes resulting from man's activities in the eastern United States: U.S.G.S. C-968, 54 p.

Peek, H.M., (1951) Cessation of flow of Kissengen Spring in Polk County, Florida, in *Water Resource Studies*: FGS RI-7, p. 73-82.

Ryder, P.D., (1985) Hydrology of the Floridan aquifer system in west-central Florida: U.S.G.S. P.P-1403-F, 1 plate, 63 p.

Sinclair, W.C., (1982) Sinkhole development resulting from ground-water development in the Tampa area, Florida: U.S.G.S WRI 81-50, 19 p.

Sinclair, W.C., & Stewart, J.W., (1985) Sinkhole type, development, and distribution in Florida: U.S.G.S. MS-110, 1 plate.

Southeastern Geological Society, (1986) Hydrogeological units of Florida: FGS SP-28, 9 p.

Sowers, G.F., (1984) Correction and protection in limestone terrane. In: Beck, B.F., ed., 1984, *Sinkholes: their geology, engineering and environmental impact*: Proceedings, A.A. Balkema, Boston, 373-378.

Stewart, M. & Parker, J., (1992) Localization and seasonal variation of recharge in a covered karst aquifer system, FL, USA: *International Contributions to Hydrogeology*, **13**, Springer-Verlag,, 443-460.

Tihansky, A.B. & Trommer, J.T. (1994) Rapid ground-water movement and transport of nitrate within a karst aquifer system along the coast of west-central Florida: abs. In: EOS Transactions Sup. AGU, **75**, (16),156.

Tihansky, A.B., (2000) Sinkholes, West-Central Florida—A link between surface water and ground-water. In: Galloway, D., Jones, D.R., & Ingebritsen, S.R., (2000), *Land Subsidence in the United States*: U.S.G.S. C-1182, 123-142.

Trommer, J.T., (1992) Effects of effluent spray irrigation and sludge disposal on ground water in a karst region, northwest Pinellas County, Florida, U.S.G.S. WRI 91-4181, 32 p.

White, W.A., (1970) The geomorphology of the Florida peninsula, Florida Bureau of Geology, B-51, 164 p.

Wilson, W.L. & Shock, E.J., (1996) New sinkhole data spreadsheet manual (v.1.1) Subsurface Evaluations Inc., Tampa, FL, 31 p.

LAND SUBSIDENCE OF PISA PLAIN, ITALY: EXPERIMENTAL RESULTS AND PRELIMINARY MODELLING STUDY

Aristide Rossi and Claudio Calore
Istituto Internazionale per le Ricerche Geotermiche–CNR, Via Alfieri 1, 56010 Ghezzano (Pisa), Italy

Ulisse Pizzi
Consulting Hydrogeologist, Via San Donnino 4, 56100 Pisa, Italy

Abstract

In the Pisa plain a naturally occurring subsidence rate of 0.5-4 mm per year has been inferred from historical and geological data for the last 7000 years. The present, mainly induced, subsidence rate, as determined by precision levelling over the past 30-40 years, is two to five times higher than the natural value, depending on the area, due to groundwater withdrawal and other anthropic activities. Piezometric surveys in wells used to monitor the main aquifer, to a depth of 250 m, contributed substantially to our understanding of the recent behaviour of the groundwater system, which, in the long-term, exhibits an overall lowering trend. The stratigraphic, hydrogeological and geotechnical data available for the Pisa plain have been reviewed and a land subsidence model has been developed to interpret the vertical compaction of the sediments and the degree of land sinking. The results indicate that the lithostratigraphic model of the Pisa plain subsoil, down to a depth of 250 m, is compatible with the observed aquifer drawdown and land subsidence.

Keywords: Pisa plain, land subsidence, drawdown, levelling, modelling

1. OUTLINE OF PISA PLAIN

The Pisa alluvial plain that is confined by the Serchio river (north), Livorno hills (south), Pisan Mounts (east) and Tyrrhenian sea (west) is a part of a Neogenic coastal basin extended between the Pisan Mounts - Apuan Alps ridge to the East and the Meloria submerged ridge to the West. The morphology of the area is almost flat, with an average ground elevation of 2 to 4 m above sea level (a.s.l.). The hydrographic network consists of two main watercourses, the Arno and Serchio rivers, some minor rivers and several large canals that were mainly excavated during the last few centuries. The Pisa plain has been marshland since the end of the Upper Pleistocene; its reclamation was not completed until the first half of the 20th century (Mazzanti, 1994; Fancelli et al., 1986; Della Rocca et al., 1987).

1.1. Geological and hydrogeological setting

From a tectonic point of view the Pisa plain is a sedimentary basin that can be considered an asymmetric graben-like feature shaped by a system of normal faults affecting the pre-Miocene substratum (Fig. 1).

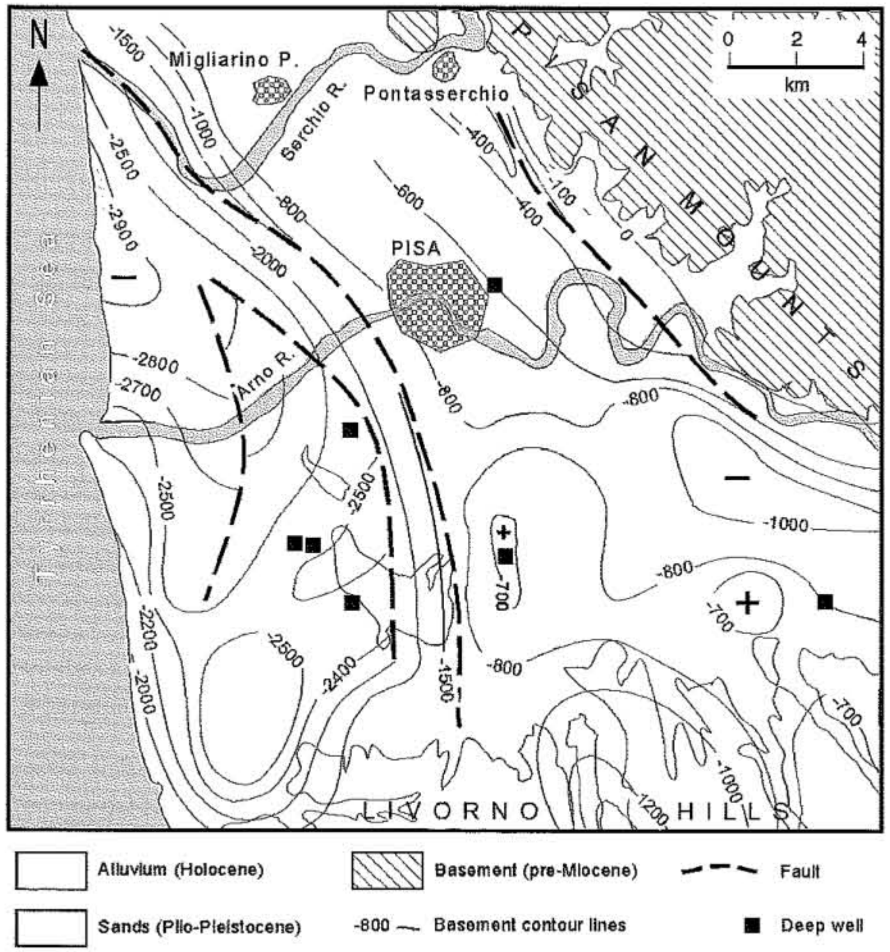

Figure 1. Geological setting of the Pisa plain

The geotectonic aspects of the basin have been investigated by geophysical surveys and deep drillings for both hydrocarbon and geothermal research. The Pisa plain rests on a thick sequence of soft Pliocene and Quaternary unconsolidated sediments down to the pre-Miocene bedrock, about 600 m beneath Pisa town. The Neogenic sequence reaches its maximum thickness of more than 2500 m on the coastal margin of the basin, and is mostly made up of sandy-clayey formations (Mariani and Prato, 1988; Bellani et al., 1995).

Hundreds of water wells and a few deep exploratory wells show the sedimentary sequence of the Pisa plain. Sandy lenses and conglomerates, separated by silty layers, typically occur down to the bedrock; this implies a complicated system of interbedded aquifers and aquitards, typical of an alluvial plain. The main aquifer unit of the groundwater system within the Plio-Quaternary sequence is represented by the formation of conglomerates of the Arno and Serchio rivers, which extends from the eastern border of the area, where it is located at 40 m depth, to the coast, where it occurs at depths ranging from 60 m (South) to about 140 m (North-West and Pisa area). This aquifer is in contact with the permeable formations of the Pisan Mounts and Livorno hills, which represent the two main recharge areas (Fancelli et al., 1986). In the present study it has been assumed that all the pervious formations of the groundwater system are hydraulically interconnected in such a way that, as a whole, they act as a single aquifer.

The geological formations outcropping in and around the Pisa plain area, grouped according to their permeability, are shown in Fig. 2.

1.2. Stratigraphic and hydraulic head data

The basic information on stratigraphic sequences and hydraulic heads in the Pisa plain area have been obtained from data sets and studies performed by the Department of Earth Sciences of Pisa University, from public water companies, water well companies, and Pisa Province water wells archive of the Pisa plain. For more detailed information see Gagliardi and Raggi (1985), Baldacci et al. (1988, 1995), and references therein.

The most recent hydrogeological study was carried out, on behalf of the National Institute of Nuclear Physics, INFN, within the framework of the preliminary investigations for the Virgo Project (Pizzi et al., 1994). The target of this study was the assessment, by numerical simulation, of any land subsidence taking place in the Virgo Project area as a result of long-term groundwater exploitation from the Pisa plain aquifer, south of the Arno river.

A network of 81 piezometric monitoring wells was set up for this study. Four piezometric surveys have been performed and the hydraulic head of the aquifer measured in the wells of the network during the period August 1994 to June 1995. These surveys contributed substantially to our understanding of the recent behaviour of the Pisa plain groundwater system.

In the period 1994-1995, apart from some minor seasonal variations of 1 to 2 m on average, the hydraulic head distribution of the alluvial aquifer shows the characteristic features depicted by the contour lines in Fig. 2. A relative high, supported by the sea-level head and by favourable geomorphologic conditions, has survived in a limited area near to the coast (Rossi and Spandre, 1994). A negative (below sea-level) hydraulic head, extending eastwards to most of the plain,

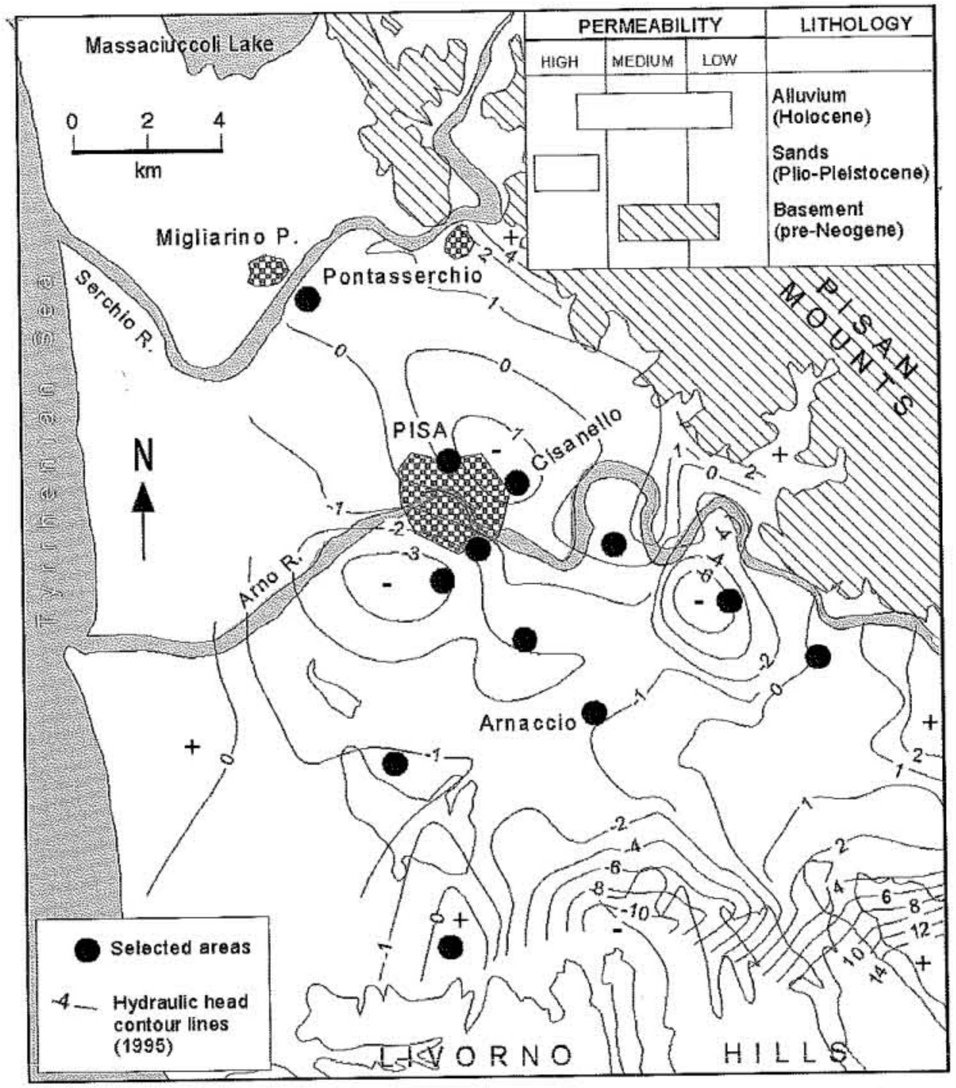

Figure 2. Hydrogeological map, with the areas selected for the subsidence model.

is generally induced by exploitation of the groundwater system. Negative anomalies of the hydraulic head characterize the industrial areas near Pisa. Very negative values of the hydraulic head occur down to 10 m below sea-level, or lower, due to intensive exploitation of well fields 7 km east and 12 km south of Pisa, where the pumping stations of public water companies are located, and extraction rates are of the order of several tenths to a few hundreds litres per second for each field. The hydraulic head remains above sea-level in the south-eastern and north-eastern border zones of the Pisa plain, due to the natural recharge through the Lower Pleistocene permeable outcrops of the Livorno hills, and in correspondence to the Pisan Mount outcrops, through the alluvial fans that are in hydraulical connection with the main aquifer.

1.3. Historical to recent land subsidence data

Historical subsidence values of 2 to 4 mm/y for the last 7000 years in the southern coastal zone near Livorno, and 0.5 mm/y for the Pisa zone have emerged from stratigraphic, radiometric and palynological investigations (Galletti Fancelli, 1978; Barsotti et al., 1974; Romagnoli, 1957). These average values are consistent with a natural compaction of sediments without resorting to neotectonic or anthropogenic phenomena.

Many levelling surveys were carried out during the 20th century by Pisa University, the National Military Geographic Institute, the Government Commission for the Leaning Tower of Pisa, and regional and local authorities.

The studies of land subsidence on Pisa plain carried out by the Institute of Geodesy, Topography and Photogrammetry of Pisa University (Palla et. al., 1976; Palla, 1978) show that the areas with the highest land subsidence values correspond to the industrial or newly developed peripheral belt of Pisa, with a maximum subsidence rate in the Arnaccio area (1,6 cm/y during the period 1976-1984). Levelling data also show negative ground-level variations at a maximum rate of 1 cm/y during the period 1969-1983 for some zones of Pisa (Palla, 1988). This high rate of subsidence can be explained by an unfavourable combination of natural and man-induced effects.

Drainage of surface waters and pumping from aquifers increase the compaction rate of the alluvial layers. The recent intensive urbanization has further jeopardized the unstable foundations of medieval buildings, such as the Leaning Tower of Pisa. The Tower is now undergoing maintenance work to consolidate the structure and foundations.

Subsidence is the surface expression of cumulative subsurface compaction of the sediment cover down to the bedrock. Induced subsidence, however, is commonly caused by the settlement and compaction of sediments due to groundwater exploitation by water wells. The deep pre-Miocene substratum is not exploited at present and not affected by subsidence processes, at least on a century's time-scale.

1.4. Geotechnical data

Many data have been obtained from geotechnical surveys performed within the Pisa town area. Within the framework of the INFN Virgo Project, two geotechnical surveys were also carried out in 1991 and 1994 (Pizzi et al., 1994). Four geotechnical wells were drilled, and several laboratory tests were performed on undisturbed soil samples collected in these wells for the experimental determination of index properties and geotechnical parameters.

For the clay layers, the experimental values of compressibility, α, and of the coefficient of consolidation, C_v, are in the ranges:

α_v = (0.29 – 0.50) 10^{-2} (cm²/kg) in the compression phase
α_s = (1.00 – 4.00) 10^{-4} (cm²/kg) in the swelling phase
C_v = (0.30 – 3.00) 10^{-3} (cm²/s)

The above values have been compared with published data (Gambolati et al., 1974; Helm, 1975; Pizzi and Cappelletti, 1989; Gambolati et al., 1991).

The aquitard clays have been assumed to behave as elasto-plastic materials. The sandy aquifer formations have been assumed to behave as elastic bodies. The compressibility value assumed for these formations is 10^{-4} cm²/kg.

2. NUMERICAL MODEL OF LAND SUBSIDENCE

The land subsidence model we have considered evaluates the vertical compaction of the sediments and the lowering of the ground-level starting from the temporal evolution of the mechanical stress of the sediments. The model is based on the one-dimensional (vertical) Terzaghi's consolidation theory (Terzaghi and Peck, 1967), as improved by Gambolati and Freeze (1973) and Helm (1975, 1976) to take into account the coupling between pore pressure in the plastic materials (clay layers) and hydraulic head in the regional aquifer (sandy layers). This model has been adopted because settlement is mainly due to compaction of the low permeability clay layers, where groundwater flow is nearly vertical.

The temporal evolution of the hydraulic head along the aquitard thickness is computed assuming the aquitard to be homogeneous along the vertical. Considering one-dimensional flow along the aquitard thickness, the following equation is obtained:

$$C_v \frac{\partial^2 h^*}{\partial z^2} = \frac{\partial h^*}{\partial t} \qquad (1)$$

where C_v is the coefficient of consolidation and h^* is the hydraulic head in the aquitard. The initial condition is $h^*(z,t)_{t=0} = h_0$ and the boundary conditions at the top and bottom of the aquitard are $h^*(z,t)_{z=ZTOP} = h$ and $h^*(z,t)_{z=ZBOT} = h$, where and h are the hydraulic head of the adjacent aquifer at t=0 and at t>0, respectively.

The same value of the hydraulic head at the top and the bottom of the aquitard is assumed because, utilising a single-layer scheme for the aquifer, all the water-bearing strata have the same hydraulic head. Moreover, assuming the aquitard to be homogeneous, we can identify the hydrodynamic characteristics of the clays only by considering the coefficient of consolidation C_v, which can easily be determined by laboratory tests or by the well-known correlation in the technical literature.

Stress-strain analysis of a deformable porous media provides the relationships between the displacements of the porous media and the incremental pressure of the fluid. When land subsidence occurs in a large area, horizontal displacements are small compared to vertical ones. Therefore, assuming the horizontal displacements to be negligible, applying the effective stress principle, and considering the incremental stress, with the hypothesis of negligible overburden variation, the following relationship between the incremental pressure, p^e, and the incremental strain in the porous matrix media, ε^e, holds for any point (x,y) of the ground (Huyakorn and Pinder, 1983):

$$\varepsilon^e = \frac{dU_z}{dz} = \alpha p^e = \alpha \rho g \Delta h \qquad (2)$$

where U is the displacement, α is the compressibility of the sediments and ρ is the fluid density.

The temporal evolution of the subsidence in a point (x,y) of the ground is computed by integrating equation (2) along the vertical:

$$\Delta U_z(x,y,t) = \sum_{i=1}^{N} \int_{z_i}^{z_{i+1}} \alpha \rho g \Delta h(x,y,z,t)\, dz \qquad (3)$$

where and are the bottom and the top of the single layer, respectively, and $\Delta h(x,y,z,t)$ is the hydraulic head variation along the vertical of the point (x,y) with respect to an initial condition of equilibrium taken as reference (initial condition of the undisturbed groundwater system).

The Fortran 77 computer code GMTH/SUBSID (Pizzi, 1985), which numerically solves the above equations, has been utilised for simulating the subsidence along the vertical of the stratigraphic sequence, with an assigned hydraulic head of the aquifer vs time, in selected areas of Pisa plain.

3. PRELIMINARY MODELLING STUDY OF THE PISA PLAIN

The main target of this study is the preliminary assessment, by means of numerical simulation, of the land subsidence occurring within the Pisa plain area.

The application of a land subsidence model in an area characterised by a complex succession of aquifer and aquitard layers, such as the Pisa plain, entails the inclusion of a number of parameters that are difficult to evaluate. For each point of the study area, we must determine the thickness and the geotechnical characteristics of each layer within the stratigraphic sequence. Even assuming every layer as homogeneous along the vertical direction, the following data must be known: the thickness b_i and the compressibility a_i, for each aquifer layer; the thickness b_i, the coefficient of consolidation C_{vi}, the compressibility values a_{vi} and a_{si} for each aquitard layer.

Moreover, even assuming that all the pervious formations are hydraulically interconnected in such a way that the whole groundwater system behaves as a single aquifer, the temporal series of the observed hydraulic head of the aquifer are incomplete, and oldest data are generally lacking. This fact results in another shortcoming for the computation. In this case-study the modelling of subsidence may be less effective, also due to small values and low signal to noise ratio of the measured parameters. The hydraulic head trends in the periods not covered by the observations must therefore be inferred by interpolation. A linear interpolation rule has been used in the present study.

Levelling surveys show that land subsidence has definitely occurred in the Pisa plain since the year 1951. For modelling purposes, this date has been assumed as the reference conventional steady-state condition of the undisturbed groundwater system prior to its industrial exploitation, and as the onset of man-induced land subsidence in the Pisa plain. The unobserved original piezometric level of the undisturbed groundwater system in the year 1951 has therefore been considered as an additional parameter in the land subsidence model computation process.

A trial-and-error procedure was followed to calibrate the land subsidence model. The calibration parameters considered in the model are the geotechnical properties of the aquitards and the original value of the hydraulic head of the undisturbed groundwater system. At the onset of the trial process it has been assumed that the initial hydraulic head of the aquifer in the year 1951 was at about the same level of land surface. The stratigraphic data and the compressibility of the aquifer have been considered reliable.

For the preliminary modelling study of land subsidence in the Pisa plain twelve areas have been selected (nine south and three north of the Arno river; Fig. 2), where data on stratigraphy, land subsidence and hydraulic head of the aquifer are coexistent and adequately known. A reasonable fitting between the computed and observed land subsidence over the period 1951-1994 has been reached for each selected area.

3. 1. Land subsidence model of the Arnaccio area

The Arnaccio area, near to the INFN VIRGO Project site, has been chosen as a sample area south of the Arno river (Pizzi et al.,1994).

Levelling surveys show that this area was subjected to high land subsidence rates until the year 1984. In the period 1984-1994, however, a decrease in the land subsidence rate was clearly detected by the last levelling survey (Fig. 3). This event corresponds to the rise in the hydraulic head of the aquifer after the year 1986, which resulted in an increase in pore pressure in the aquitards, thus reducing the compaction process.

The computed land subsidence in the period 1969-1994, apart from an additive constant, representing the land subsidence in the period 1951-1969, fits reasonably well with the observed values (Fig. 3). The computed land subsidence rate strongly decreases after 1984, matching the observed subsidence rate for the period 1984-1994. The calibrated value of the hydraulic head of the aquifer in the year 1951 was 4 m a.s.l.

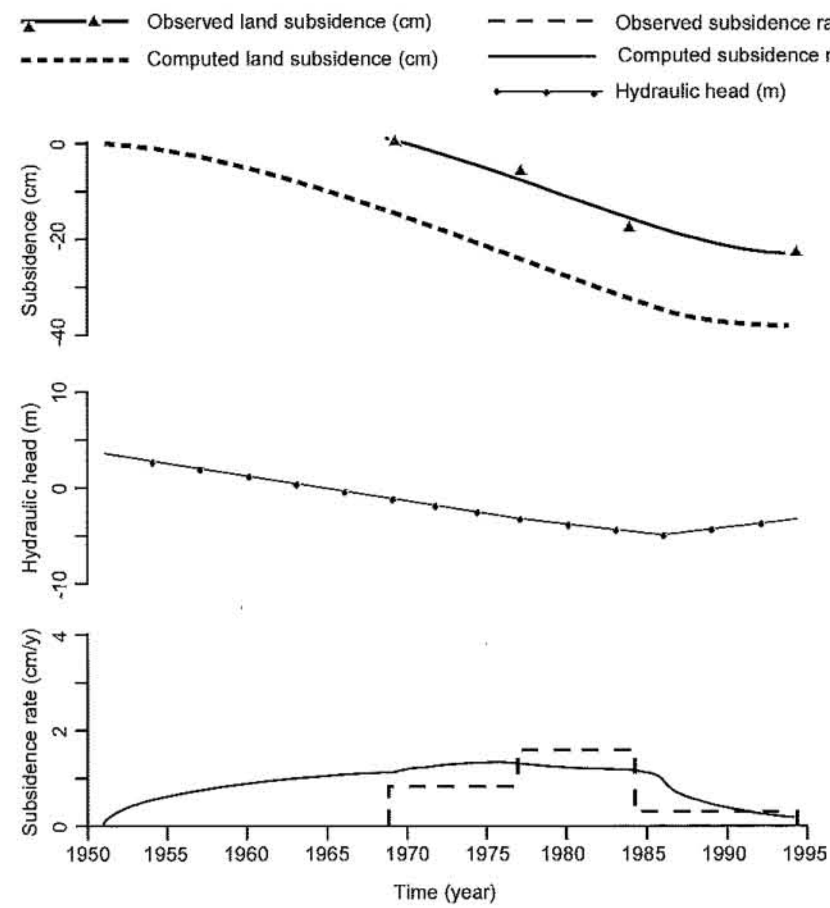

Figure 3. Results of the land subsidence model of the Arnaccio area.

3.2. Land subsidence model of the San Cataldo-Cisanello area

The San Cataldo-Cisanello area has been selected as a sample area north of the Arno river. The stratigraphic sequence of the exploratory well San Cataldo 1, drilled under the CNR-ENEL joint-venture in 1999, has been utilised for this zone. The calibrated value of the hydraulic head of the aquifer in the year 1951 was of 2 m a.s.l..

The model constructed for the period 1951-1999 (Fig. 4) show that the computed land subsidence values fit reasonably well with the observed ones, apart from the additive constant for the period between 1951 and 1969, and the uncertain values of the parameters measured with sporadic field surveys.

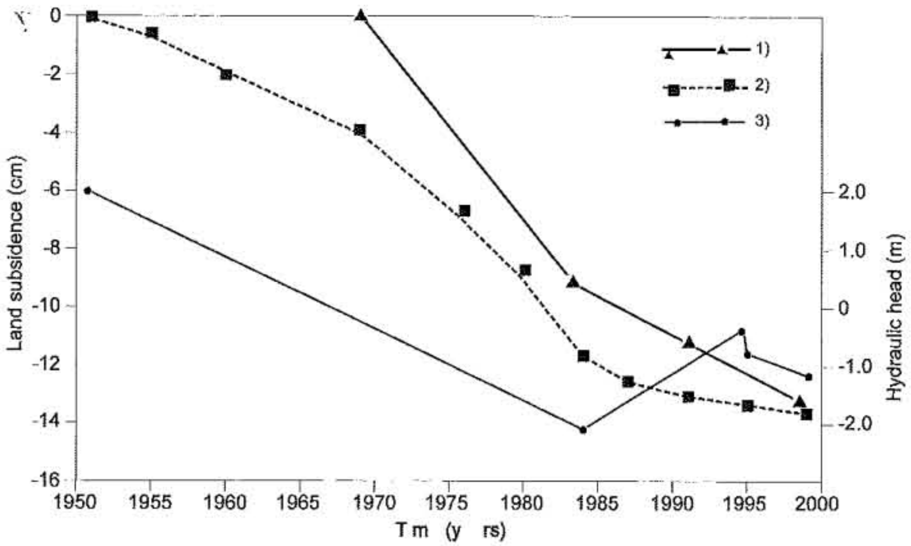

Figure 4. Results of the land subsidence model of the San Cataldo – Cisanello area. 1) observed land subsidence; 2) computed land subsidence; 3) hydraulic head.

4. CONCLUSIONS

A review of a vast historic and recent documentation on geomorphological setting, areal surface resources and human activity has allowed us to reconstruct the distribution of the anthropogenic effects on the Pisa plain from the point of view of subsidence.

The area south of the Arno river, including the so-called "Pisorno" industrial belt of the towns of Pisa and Livorno, show widespread and significative effects of a quite intense anthropic presence, due to widespread surface resource exploitation: surface drainage, groundwater withdrawal for agriculture, industrial and civil use, urbanisation, residual effects of recent reclamation, etc. North of Pisa the anthropogenic effects are less evident. Some positive effects may derive from the Natural Park area of Migliarino-San Rossore. The abundant water reserves of the Arno and Serchio rivers and the large surface water body of Massaciuccoli Lake, north of the study area, may also reduce the impact on groundwater drawdown by supplying surface waters to cope with the growing demand.

Land subsidence and groundwater drawdown have been experimentally documented and interpreted by modelling. In this work an attempt has been made to calibrate the subsidence model using the existing lithostratigraphical data of the Pisa plain subsoil down to 250 m. The results show that the lithostratigraphic reconstruction, based on the available data, is compatible with the observed piezometric decline measured in all the relevant wells and the observed land subsidence.

A groundwater model of the Pisa plain aquifer system is needed, to be used with the subsidence model, in order to more accurately evaluate and forecast the future behaviour of the aquifer and related land subsidence within the Pisa plain, taking into account groundwater abstraction and future needs for civil, industrial and agriculture uses.

Acknowledgements

The authors express their great sorrow at the death of their colleague and friend Prof. Brunetto Palla of the University of Pisa ,who contributed for more than forty years to topographic studies of the subsidence in the Pisa plain.

The authors also wish to thank Prof. G. Bradaschia and the National Institute of Nuclear Physics of Pisa) for providing data from the study of the Pisa plain, south of the Arno river.

REFERENCES

Baldacci, F., Bellini, L., Graziosi, B., Mannocci, C. & Raggi G. (1988) Studio idrogeologico e geomorfologico dei bacini in sinistra dell'Arno e della Pianura Pisana. Unpublished report, Amministrazione Provinciale di Pisa – Dipartimento di Scienze della Terra, Università di Pisa.

Baldacci, F., Bellini, L. & Raggi, G. (1995) Le risorse idriche sotterranee della Pianura Pisana. *Atti della Società Toscana di Scienze Naturali – Memorie*, Serie A, vol. **CI**, 1994, 241-322.

Barsotti, G., Federici, P.R., Giannelli, L., Mazzanti, R. & Salvadorini, G. (1974) Studio del Quaternario livornese con particolare riferimento alla stratigrafia ed alle faune delle formazioni del bacino di carenaggio della Torre del Fanale. *Mem. Soc. Geol. It.*, **13**, 425-495.

Bellani, S., Grassi, S. & Squarci, P. (1995) Geothermal characteristics of the Pisa plain, Italy. *Proc. World Geothermal Congress*, Florence, Italy, v. 5, 1305-1308.

Della Rocca, B., Mazzanti, R. & Pranzini, E. (1987) Studio geomorfologico della pianura di Pisa. *Geogr. Fis. Dinam. Quat.*, **10**, 56-84.

Fancelli, R., Grifoni, R., Mazzanti, R., Menchelli, S., Nencini, C., Pasquinucci, M. & Tozzi, C. (1986) Il contesto geomorfologico. In *Terre e paduli. Reperti, documenti, immagini per la storia di Coltano*, Comune di Pisa, Pontedera, 23-39.

Gagliardi, S. & Raggi, G. (1985) Studio idrogeologico della Pianura Pisana. Unpublished report, Comune di Pisa.

Galletti Fancelli M. L. (1978) Ricerche sulla subsidenza della pianura pisana. Analisi polliniche di sedimenti quaternari della pianura costiera tra Pisa e Livorno. *Boll. Soc. Geol. It.*, **97**, 197-245.

Gambolati, G. & Freeze, R.A. (1973) Mathematical Simulation of the Subsidence of Venice. 1 Theory. *Water Resour. Res.*, **9**(3), 721-733.

Gambolati, G., Gatto, P. & Freeze, R.A. (1974) Mathematical Simulation of the Subsidence of Venice. 2 Results. *Water Resour. Res.*, **10**(3), 563-577.

Gambolati, G., Ricceri, G., Bertoni, W., Brighenti, G. & Vuillermin E. (1991) Mathematical Simulation of the Subsidence of Ravenna. *Water Resour. Res.*, **27**(11), 2899-2918.

Helm, D.C. (1975) One dimensional Simulation of Aquifer System Compaction near Pixley, California. 1 Constant Parameters. *Water Resour. Res.*, **11**, 465-478.

Helm, D.C. (1976) One dimensional Simulation of Aquifer System Compaction near Pixley, California. 2 Stress-Dependent Parameters. *Water Resour. Res.*, **12**, 375-391.

Huyakorn, P.S. & Pinder, G.F. (1983) *Computational Methods in Subsurface Flow*. Academic Press, NY, 473 pp.

Mariani, M. & Prato, R. (1988) I bacini Neogenici costieri del margine tirrenico: approccio sismico-stratigrafico. *Mem. Soc. Geol. It.*, **41,** 519-531.

Mazzanti, R. (1994) La pianura di Pisa e i rilievi contermini. *Mem. Soc. Geogr. It.*, **L**, 491 pp.

Palla, B. (1978) Livellazioni per il controllo della subsidenza nella pianura pisana a Sud dell'Arno e ad Est di Pisa. Comune di Pisa, 73 pp., 1 tav.

Palla, B. (1988) I movimenti verticali del suolo nella città di Pisa e nel territorio circostante. Comune di Pisa, Università di Pisa, 43 pp.

Palla, B., Cetti, T., Poggianti, M., Mengali, E. & Bartolini, A. (1976) I movimenti verticali del suolo nella pianura pisana dopo il 1920 dedotti dal confronto di livellazioni. Comune di Pisa, Provincia di Pisa, 74 pp., 1 tav.

Pizzi, G. (1985) GMTH/SUBSID - Land subsidence numerical model. User's guide. Geomath S.r.l. report, Pisa, 30 pp.

Pizzi, G. & Cappelletti, A. (1989) Modello matematico del fenomeno della subsidenza nel territorio bolognese. In: Idroser S.p.a. "*Studio del fenomeno della subsidenza nel territorio bolognese*", Regione Emilia-Romagna, Bologna, 347 pp., 4 annexes.

Pizzi, G., Pizzi, U., Paolinelli, A., Alvarez, F. & Rossi, S. (1994) Study of the land subsidence of Pisa plain South of the Arno river. Geomath S.r.l. and Geoser s.c.r.l. report for INFN, Virgo Project, 169 pp., and annexes.

Romagnoli, L. (1957) Sondaggi a 200 m di profondità nel Quaternario recente presso Pisa. Studio delle facies attraversate e considerazioni sulla sedimentazione costiera a carattere ciclico. *Bol. Soc. Geol. It.*,**76**(2), 21-35.

Rossi, S. & Spandre, R. (1994) L'intrusione marina nella falda artesiana in ghiaia nel litorale pisano. *Acque sotterranee*, **11**(43), 51-58.

Terzaghi, K. & Peck, R.B. (1967) *Soil Mechanics in Engineering Practice*. John Wiley & Sons, NY.

CHARACTERIZATION OF SHORT- AND LONG-TERM VARIATIONS OF GROUNDWATER LEVEL AND ITS APPLICATION TO NUMERICAL SIMULATION OF LAND SUBSIDENCE

Masayoshi Shimizu
Department of Civil Engineering, Faculty of Engineering, Tottori University
Koyama 4, Tottori, 680-8552 Japan

Abstract

Using the measured data on the groundwater level in the shallow and deep wells in Tottori City, Japan, a method of characterizing the short- and long-term variations is presented. The short-term variation was characterized by Fourier analysis technique and that of the long-term by the moving-averaging method. Also the method of considering their characteristics in numerical simulation using finite element (FE) analysis is described as well as the results of the simulation. Conclusions say that short-term variation characteristics can be well realized by spectral analyses, but they do not affect the simulated settlement unless plastic nature of soils are considered.

Keywords: land subsidence, groundwater, Fourier spectrum, simulation

1. INTRODUCTION

There are many areas of the world in which land subsidence has been caused by groundwater withdrawal. The pore-water pressure decreases in the aquifer from which the groundwater is withdrawn, leading to the increase in the effective stress in the compressible-soil layer close to the aquifer. The pore-water pressure in the aquifer varies with time. The variation depends on the way for withdrawing the groundwater and also on the weather conditions.

For the countermeasure against land subsidence, it would be useful to measure the pore-water pressure of the aquifer, that is practically to measure the water level of the aquifer penetrating through wells. Generally, however, measurements start after evidences of the land subsidence have caused some damage; and usually the data will also be lacking during the period in which pore-water pressure of groundwater decreased so greatly that land subsidence occurred. We will have to estimate the variation of the pore-water pressure, i.e., groundwater level during the period in which we have no data on them.

Figure 1. Locations of observation wells and benchmarks in the area of Tottori City.

The groundwater level varies in a complex way. On the long-term, for example, it varies over a decade and on the short-term such as in a day. The purposes of this study are, first, to establish a way for characterizing the variation of groundwater level and, second, to examine how the short- and long-term variation characteristics will affect the behavior of land subsidence. For these purposes the measured data on the groundwater level of wells in the area of Tottori City, Japan, were analyzed.

This paper presents (1) the behavior of land subsidence and groundwater level variation in Tottori City, (2) a method for separating the long- and short-term variations in the measured data on the groundwater level, and (3) results of the numerical simulation for the land subsidence using some models of groundwater level variation. For the characterization of the groundwater level variation, spectral analyses were conducted; and for the numerical simulation, finite-deformation finite element (FE) technique was used.

2. LAND SUBSIDENCE IN TOTTORI CITY AREA

In the area of Tottori City, Japan, there is a dense net of benchmarks. Figure 1 shows their locations by the symbol ▲. (The figure also shows the locations of the wells for the observation of the groundwater level by ●).

In Figure 2 the accumulated and annual settlements of representative benchmarks located in the northern area of Tottori City are plotted vs time. Their locations can be identified in Figure 1. Although, in the last decade, the annual rate of settlement has become less than 1 cm/year, the subsidence had been so severe that the rate was over 8 cm/year near the benchmark [MC]. Benchmarks located in the southern area of Tottori City started to record subsidence earlier.

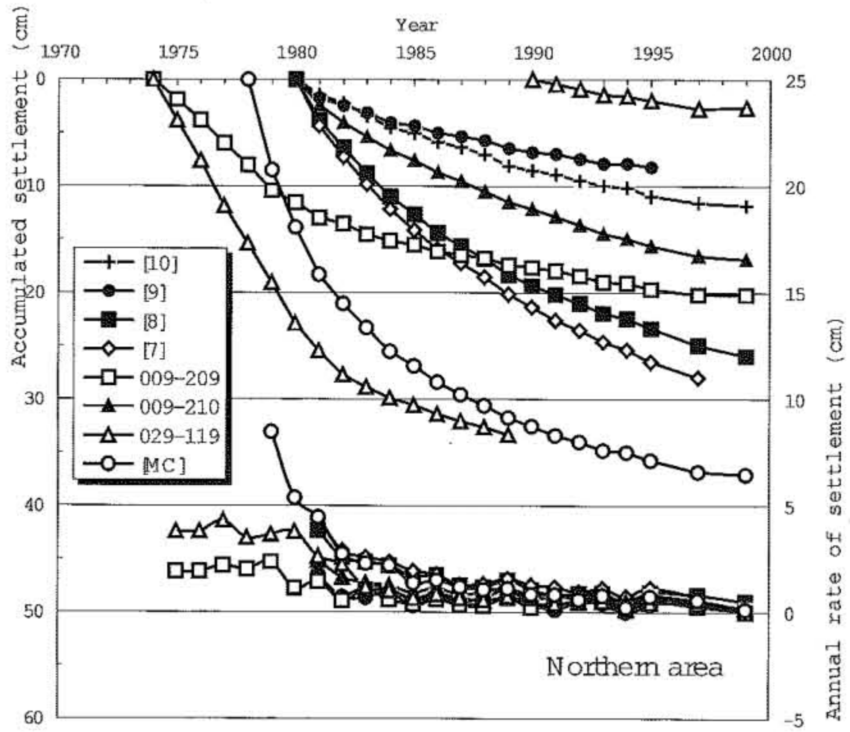

Figure 2. Accumulated and annual settlement of the benchmarks in the northern area of Tottori City.

The subsidence supposedly started to occur around 1964 and is shown in the comparison of the elevation of benchmarks in 1951 and those after 1965 (Shimizu, 1991).

3. GEOLOGICAL FEATURES OF TOTTORI CITY AREA

Figure 3 shows a representative geological cross-section along the line a-a in Figure 1. Table 1 gives a brief description of stratigraphical and geotechnical features of soil layers. Holocene sediments cover a large area along the Sendai River. The upper layer of clay (Uc Layer) is very soft so that the N-value of SPT is lower than 4 and its thickness can reach over 30 m, as at the site near the benchmark No. 7. The land subsidence has resulted from the consolidation of this layer (Shimizu, 1991).

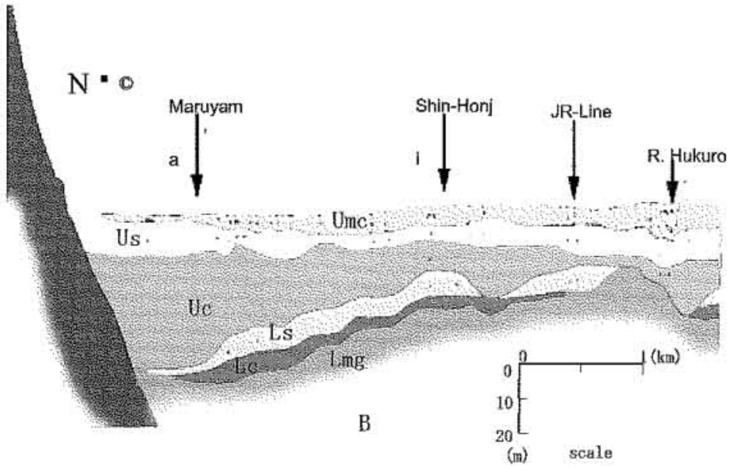

Figure 3. A representative geological section; along the a-a line in Figure 1.

Table 1 Summary of the stratigraphic classification.

Epoch of formation	Layer		Geological and geotechnical features
Holocene	Umc	Surface layer	Including embankment materials with organic matters. N=0 to 3*
	Us	Upper layer of sand	Fluvial sediment.
	Uc	Upper layer of clay	Sediment in transgression; mainly mainly marine sediment. N=0 to 4
Pleistocene	Lc	Lower layer of clay	Marine sediment. N=5 to 15.
	Ls	Lower layer of sand	Marine sediments.
	Lmg	Bottom Layer of sand and gravel	Alluvial fan deposit.
	B	Foundation layer of rock	Igneous or sedimentary rock.

*N is the SPT-N value.

4. VARIATION OF THE GROUNDWATER LEVEL

4.1. System for the observation of groundwater level

The groundwater level has been observed in ten wells at six sites (see Figure 1 and Table 2). A well with strainer(s) made in the upper layer of sand (Us Layer) will be called the shallow well, designated by "1" and one with strainer(s) in the lower layer of sand (Ls Layer) the deep well, designated by "2", hereafter. For example, the well "D-1" and "D-2" are the shallow and deep wells at the site D, respectively.

Table 2: Wells for the observation of the groundwater level.

Site	Well	Type*1	Maximum depth*2	Depths of strainers*2
H	H-1	s	13.0	9.0-12.0
	H-2	d	24.0	19.5-23.0
T	T	d	25.0	17.8-20.8
N	N-1	s	12.0	6.0- 9.0
	N-2	d	29.5	24.0-27.0
D	D-1	s	8.0	7.0- 8.0
	D-2	d	50.0	32.5-35.5 44.0-48.0
S	S-1	s	15.0	10.0-13.0
	S-2	d	25.0	21.0-23.0
G	G	d	45.0	39.0-44.0

*1: 's' stands for shallow wells and 'd' for deep wells.
*2: Meters below the ground level.

The Ministry of Construction works for the measurement of the groundwater level as a national project. The groundwater level at a specified time of each day, read from the record, is the daily level of the ground water. All the data on the daily groundwater level are published every year.

4.2. Outline of the behavior

Fig.4 shows the monthly averaged data on the groundwater level of all the wells. The Tokyo Bay mean sea level (T.P.) is used as the reference elevation. In this figure we can understand the outline of the behavior of the groundwater level as:

1. In all the shallow wells the water level varies in a similar way. The variation is periodic with the amplitude less than 25 cm and the average almost constant

for whole the period. The lowest level is observed in summer every year.

2. The groundwater level in deep wells varies differently between wells. But we see that, as one common feature, except for the well T, the groundwater level rose by about 4 m during the period from April 5, 1978, when the measurement started, to around the year 1984 and since then the long-term variation has become less. The amplitude of variation in the short-term period as long as one year is about 1 m or larger, which is much larger than that of shallow wells.

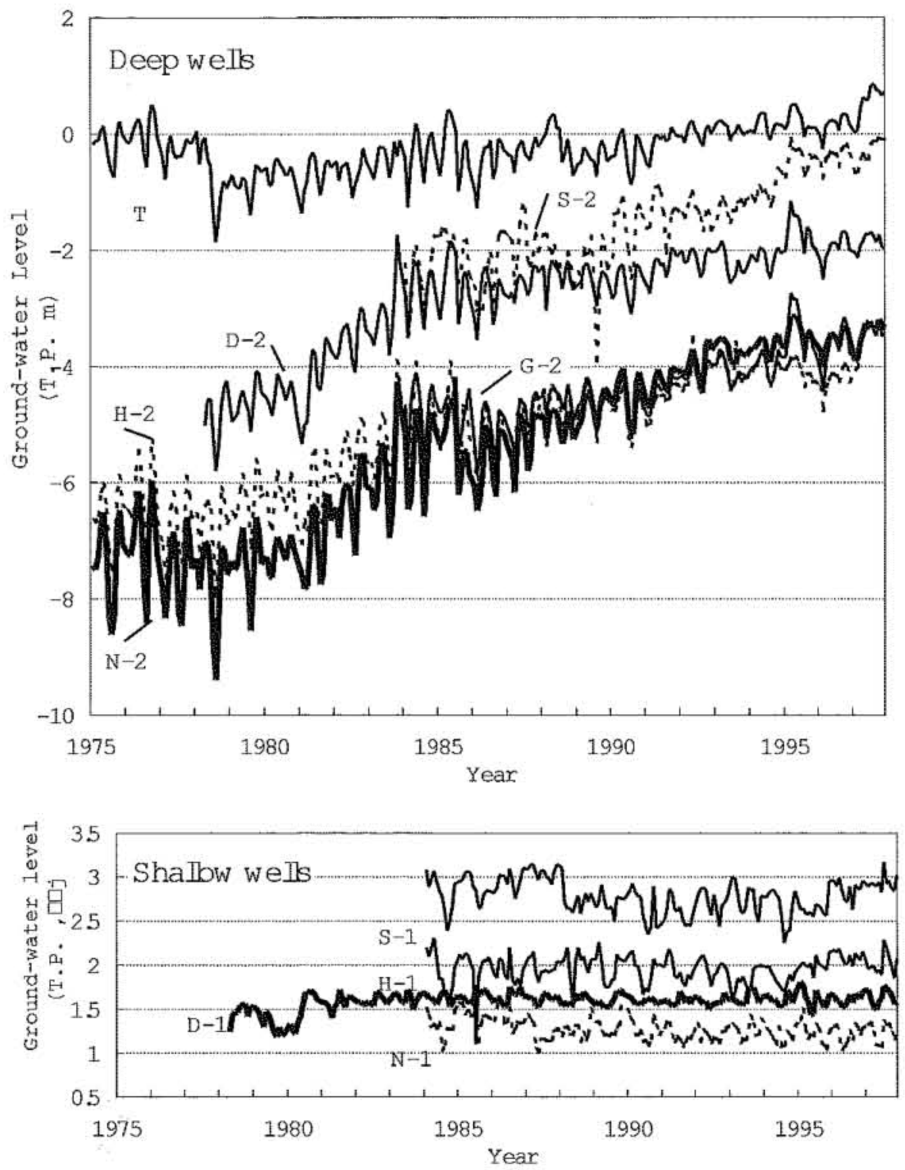

Figure 4. Variations of groundwater level with time; monthly-averaged data.

4.3. Separation of short- and long-term variations

The level of the water surface in a well continuously varies. The data, however, are the sequence of values each of which is the level at a specified time every day, and therefore the data reflect possible variation occurring a day. The data obtained at the site D are exemplified for the explication of the way for separating the variation of the groundwater level in the long-term as in a year or more. The following discussion is valid for the data obtained at sites other than D (Shimizu, 1996).

Figures 5 and 6 show the daily-observed data of the wells D-2 and D-1, respectively, from April 5, 1978 to December 27, 1997. The groundwater level, shown here, varies in the long term with the short-term variations. The amplitude of the long-term variation is much larger than that of the short-term one. We at first try to subtract the component of the long-term variation.

There are two ways of subtracting the long-term variation component: one is to inversely transform after subtracting long-period components from the Fourier spectrum and the other is to take the moving average. The moving-averaging method was used in this study because the long-term variation is not periodic as seen in Figure 5.

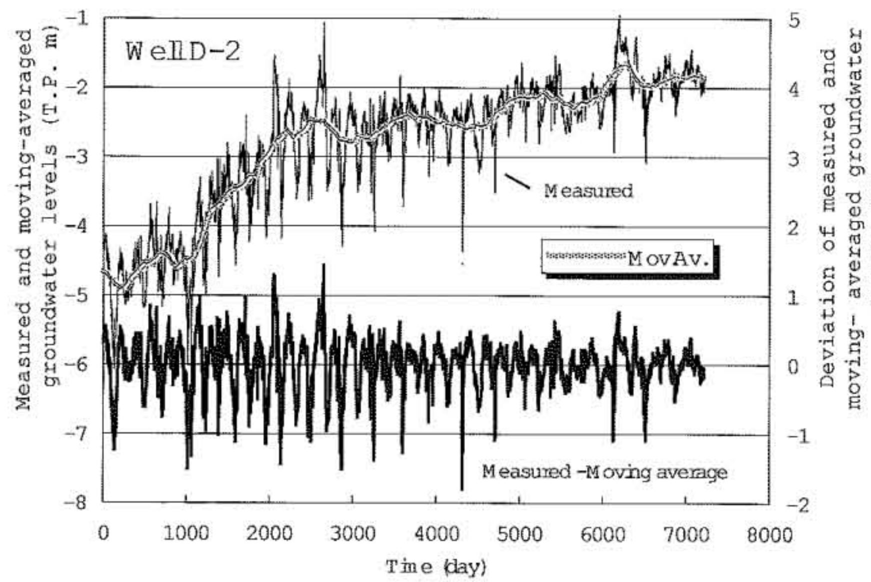

Figure 5. The variation of the groundwater in the deep well D-2 (daily data).

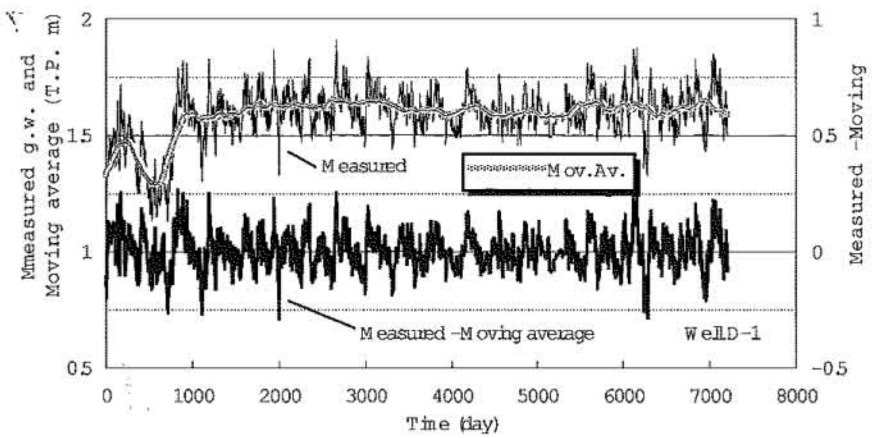

Figure 6. The variation of the groundwater level in the shallow well D-1 (daily data).

According to the theory of spectral analysis, the moving-average with the time duration of L can eliminate the components having the periods of L/n, where n is a positive integer. In other words, the moving-average is composed of the variations having periods longer than L. The results of the case when L=365 days (=one year) are shown in Figures 6 and 7, in which the moving-average is shown by the thick and light curve. The figures also show the difference between the measured data and the moving-average.

In Figure 5 for the deep well D-2, the moving average rose in the period of 2500 days, from the beginning of the observation to around 1984, and since then it has been almost constant. As for the difference of the daily data and the moving-average, which characterizes the variations of periods shorter than 365 days, the behavior seems to be unchanging. In addition, we note that the amplitude of the short-term variations is as large as one to two meters.

In Figure 6 for the shallow well D-1, the moving-average varies periodically a little only in the beginning, later it becomes almost a constant value. The difference between the measured level and the moving average is at most 25cm, which is much smaller than the difference in the deep well.

4.4. Fourier spectra for the short-term variations

Fourier spectra were calculated by the Fourier analysis for the difference between the daily data and the moving-average (Figure 7). As stated above, the spectra characterize the variation of the components having the period T shorter than or equal to 365 days. Because of the many daily data (7210 in this study), the spectra determined with all the data are very complicated. Therefore, to smooth the spectra, continuous running spectra were calculated, each of which consists of data of 2048 (=2^{11}). Fourier spectrum corresponding to a period T was defined as the $XN\Delta t/2$, where X is the amplitude of the Fourier coefficients of the period T, N is the total number of data for an analysis (=2048 in this study) and Δt is the time difference between two data. The spectrum for a period is the one averaged over the total number of running spectra (=5163).

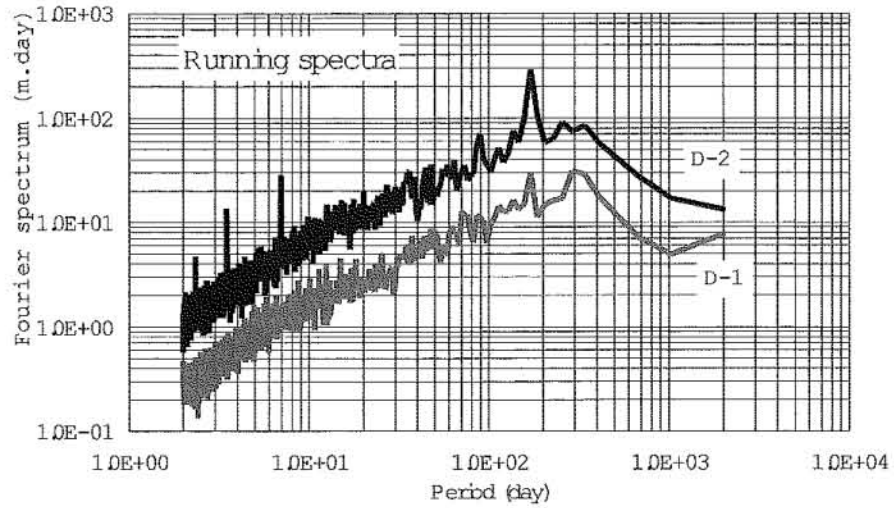

Figure 7. Fourier spectra of the difference in groundwater level between daily data and one-year moving-average.

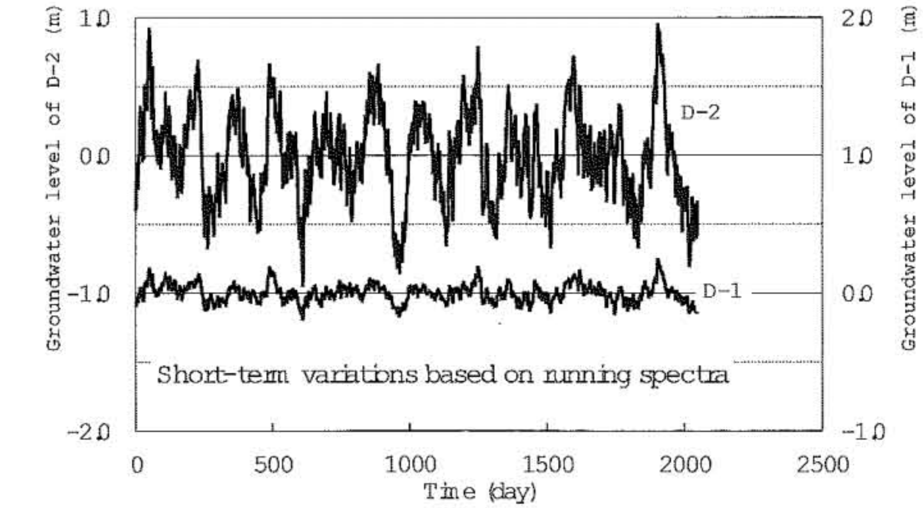

Figure 8 Inverse transformation of the spectra in Figure 7.

The spectra for the groundwater level variation for the deep well D-2 shows clear peaks at T=180 and 7 days. The peak at T=7 days is coincident with the period of the human-life activity with a one-week cycle. The peak at T=180 days seems to reflect the weather conditions. On the other hands, the spectra for the groundwater level in shallow wells has a peak at T=180 days but no peak at T=7 days.

The time variation of the groundwater level was re-evaluated by inverse transformation of the spectra shown in Figure 7. In principle, the inverse transformation yields the actual variation of data. From the view point of the application of the spectra to the FE numerical simulation, phase was deformed using the uniform random numbers. Periodic but random variations were obtained in this way (Figure 8).

5. FINITE ELEMENT ANALYSES OF LAND SUBSIDENCE

The following conditions were assumed (Shimizu, 1991):

1. The consolidation of the upper clay layer (Uc) caused the land subsidence.
2. The land subsidence began to occur on January 1, 1964 when the groundwater level in the lower sand layer (Ls) began to decrease.
3. The groundwater level in Ls Layer was identical to that of the upper sand layer (Us).
4. The groundwater level in Us Layer remained constant both before and after the occurrence of the land subsidence.

Furthermore, a few assumptions were made to model the variation of the groundwater level in Ls Layer before April 5, 1978, when the well observation started, as follows:

5. Characteristics of the short-term variation are unchanged before and after the groundwater level observation and they can be expressed by the inverse transformation of the Fourier spectrum of the difference between the daily data and one-year moving-average.
6. The long-term variation before April 5, 1978 is expressed by the linearly decreasing line.

The model with these assumptions is rather realistic. A more simple model was made that ignores short-term variations, which is designated by the 'linear' model in the following.

The assumed and observed levels of the groundwater were input as the boundary conditions for the pore-water pressure. The constitutive properties of soils in Uc Layer were assessed using the results of oedometer tests on undisturbed samples taken from Uc layer (Shimizu, 1991). Time interval for the calculation was 1/20 day (=72 minutes); the linear change was assumed for the groundwater level during this time interval. The infinitely small deformation was not assumed but finite deformation analyses were made. An iterative calculation was made during the time interval. The detail of the formulation for the finite deformation (FEM) is given in Shimizu (1994; 1996).

Some results of the FE analyses are shown in Figures 9 (a) and (b). Figure 9 (a) shows the models of groundwater level variation and (b) is the corresponding results. The models designated by 'r=1.0' and 'r=1.2' are two types of the realistic model, where r is the coefficient that magnifies the amplitude of the short-term variation. The condition that r=1.0 means the short-term variation is the same as that obtained by the inverse Fourier transformation; and r=1.2 means the variation was magnified by 20%.

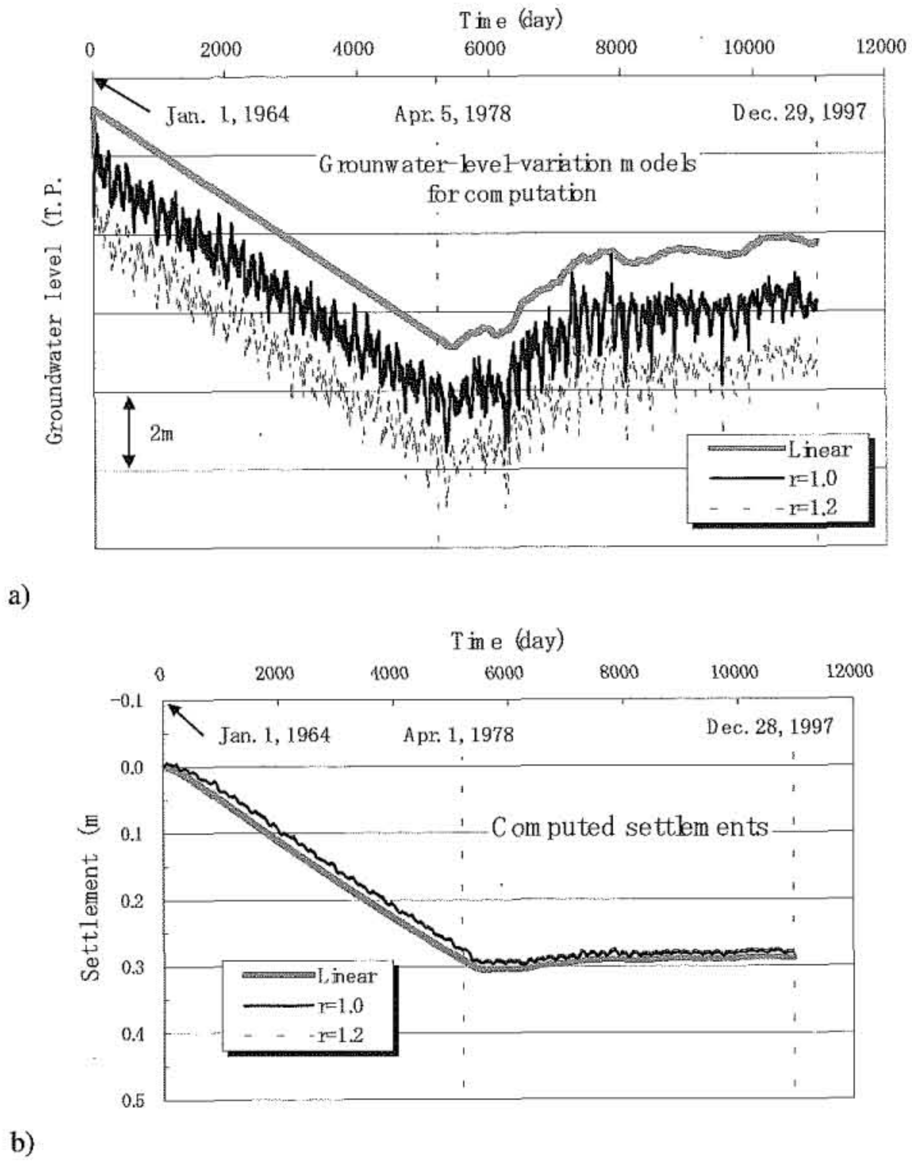

Figure 9. Models of groundwater level variations (a), and results of FE numerical simulation (b).

Figure 9 (b) shows as a conclusion that the behavior of the land subsidence does not depends on the characteristics of the short-term variation. The slight difference in the settlement between the 'linear' model and the 'more realistic' models seems the effects of the variation of the groundwater in Ls Layer at time=0. This conclusion, of course, depends on the assumptions explained above, especially on the constitutive model of the clay in Uc Layer. Viscid nature of soils was not considered in this study where the simplicity is one of purposes, but the consideration of viscid nature is crucial for modeling the behavior of clays under periodic loading conditions.

6. CONCLUSIONS

Using data on the groundwater level measured in the shallow and deep wells in Tottori City, Japan, a method of characterizing the short- and long-term variations was presented. Data characteristics were considered in the finite deformation FE analyses for the land subsidence. Even by considering the short-term variation of the groundwater level, the computed settlement was almost unchanged. The most important reason for this is that plastic nature of soils was not considered in this study.

REFERENCES

Shimizu, M., (1991) Finite element analysis of land subsidence due to the variation of groundwater level, *Proc. of the Fourth Int. Symposium on Land Subsidence,* IAHS Publication No.200, pp.645-654.

Shimizu, M., (1996) Characterization of groundwater variations and its application to the FE analysis of the land subsidence in Tottori Plain (in Japanese), *Reports of the Faculty of Engineering*, Tottori University, Vol.27, No. 1, pp.113-121.

Shimizu, M., (1994) Formulation for finite deformation FE analysis of one-dimensional consolidation of saturated soils, *Reports of the Faculty of Engineering*, Tottori University, Vol.25, pp.187-198.

Shimizu, M., (1996) Application of a large-strain finite element model in predicting land subsidence due to the variation of groundwater levels, *Proc. of Dr. J. F. Poland Memorial Symposium*, Association of Engineering Geologists of USA, pp.239-247.

LAND SUBSIDENCE - Vol. I
Proceedings of the Sixth International Symposium on Land Subsidence
Ravenna / Italy / 24-29 September 2000

GROUNDWATER DRAWDOWN AND LAND SUBSIDENCE IN SOUTH OF ESFAHAN AREA (IRAN)

B. Bahadoran (B.Sc, M.Sc) and R. Ajalloeian (B.Sc, M.Sc, Ph.D)
Department of Geology, University of Esfahan, Iran

Abstract

The subsiding area under study is located just south of Esfahan. The Zayandehrud River flows in the north side of the area. The water table had been controlled for the last three decades. Groundwater movement is mainly toward the north, but during the past few years a kind of reverse movement due to high depletion of aquifer has happened. A group of cracks parallel to a mountain range with a west-east trend almost in the middle of the area has occurred. The study and measurement of crack openings revealed that their rate is almost two centimeters per month. These cracks run through a highway and some residential areas. Based on site investigation and field studies, it can be concluded that some land subsidence is happening throughout the area. The cause of this phenomenon is drawdown of groundwater and ensuing compaction of the aquifer system. It is expected that in case of overloading or continuation of water exploitation, a ground subsidence will happen. It seems that in the case of recharge this phenomenon will be slow down and finally stop.

Keywords: subsidence, groundwater withdrawal, Esfahan (Iran).

1. INTRODUCTION

Subsidence may rank as one of the most widespread ground hazard; therefore it is necessary to carefully assess it at the investigation site, especially in a certain geological environment (Waltham, 1989). In geotechnical and hydraulic engineering, it sometimes becomes necessary to pump water from the ground. This may be for a variety of reasons including: obtaining water supplies, reducing pore water pressures in the ground, or lowering the water table in order to allow construction operations to proceed (Booker et al, 1985).

However, the percolating and pumping of water through the earth material sometimes causes some critical events such as landslides, subsidence and fissures which might cause serious damage in residential areas, farms, and industrial sites. Subsidence at the surface can be regarded as ground movement, which takes place after intensive extraction of groundwater. It is due to the consolidation of sedimentary deposits in which the groundwater is present: consolidation occurs as a result of increasing effective stress. The total overburden pressure in partially saturated or saturated deposits is borne by their granular structure and the pore water (Bell, 1987).

In order to remove pore water from the ground, it is necessary to reduce the pressure in the water in the vicinity of the pump, so there will be in general an increase in the compressive effective stress state. When groundwater extraction leads to a reduction in pore water pressure by draining water from the pores, this means that there is a gradual transfer of stress from the pore water to the granular structure. For instance, if the groundwater level is lowered by 10 cm, this gives rise to a corresponding increase in average effective overburden pressure of about 1 kPa. This increase of effective stress will cause consolidation of the ground and may lead to large-scale subsidence.

The decrease in pore pressure will not occur immediately. After pumping has commenced, the pore pressures will gradually decrease below their initial in-situ values until a steady state distribution is established. Hence the resultant consolidation and surface subsidence will be time dependent. Scott (1979) pointed out that surface subsidence does not occur simultaneously with the extraction of water from an underground reservoir, occurring over a longer period of time than that taken for extraction.

Generally, the amount of subsidence which occurs is governed by the increase in effective pressure, the thickness and compressibility of the deposits involved, the length of time over which the increased loading is applied, and possibly the rate and type of stress applied (Lofgren, 1968). So many of the world's major cities have suffered subsidence self-induced by groundwater pumping that there is an extensive literature of case histories. Subsidence at Tokyo, Osaka and some other Japanese cities has been controlled by reducing pumping (Yamamoto, 1984). Probably the best-known examples of this phenomenon occur in Bangkok, Venice and Mexico City where widespread subsidence has been caused by withdrawal of water from aquifers for industrial and domestic purposes (Booker, 1985). Bell (1994) revealed that subsidence in parts of Mexico City occurred at a rate of 1 mm/day. This was due to the extraction of water from several sand aquifers located in very soft clay of volcanic origin. The aquifers extend under the city from an approximate depth of 50 m below ground surface to well below 500 m. Water has been extracted for over 100 years. A problem that often occurs in practice concerns the pumping of water from an aquifer in a deep layer of homogeneous and isotropic soil. This phenomenon has been observed in different places of Iran, and evidence of subsidence south of Esfahan in central Iran due to withdrawal of water from aquifers has been studied and is described in this paper.

2. LOCATION AND GEOLOGY OF THE AREA

The studied area is located just south of Esfahan, the most famous town in central Iran. The Zayandehrud River flows along the south side of the area.

Geographically, the area is located between 51°40′15″ and 52°5′ East longitude and 32°10′ and 32°25′ North latitude. There are almost 200 square Km of agricultural lands and several residential areas (urban centers). The length of the area is 18 Km, the average width is almost 9 Km, and the average height is 1650 meters.

The oldest sediments, which have outcrop within the area, are Jurassic shale and sandstones. Overlying these rocks, there are 1-2 meters of red sandstone, 3-5 meters of yellow dolomites and more than 100 meters of orbitolina limestones, which belong to Cretaceous and are deposited unconformable on the shales. Dolomites and limestones are folded and their axes are mainly north-south.

3. HYDROGEOLOGICAL STUDY OF THE AREA

Hydrogeological studies have been done extensively through the area for more than 20 years by officials and for almost 3 years by the authors. There are almost 250 wells within the area, which are pumping water from the aquifer for agricultural purposes 24 hours a day. The depth of the wells is mainly between 150-200 meters. Some of them have been selected as observation wells and the periodical measurements have been done for several years.

Due to the information and measurements, the static level of the groundwater within the area during the past 30 years had been too high, almost 18-20 meters from the surface. At the present, the depth of dynamic level is 180-200 meters. Therefore, due to high water pumping during these years, drawdown of the water table is almost 180 meters, which means 6 meters per year. According to the study and measurements, the thickness of the aquifer is 150-200 meters and mainly consists of gravel, sand and clay. Based on monthly measurements of dynamic level, the piezometric maps have been drawn.

Until 5-6 years ago, the direction of groundwater movement had been toward the north and the aquifer drained to the Zayandehrud River. Since almost 5 years ago, a kind of reverse movement due to a high (an over) drawdown of groundwater near Zayandehrud River has happened and some water is recharging the aquifer from Zayandehrud River. The width and depth of this cone of depression is progressing day by day due to a high discharge of groundwater. The hydrodynamic coefficients have been calculated precisely. The porosity coefficient and permeability toward the drainage area becomes lower and lower.

During the last 10 years, several fissures have appeared in the area, with N 50- W 70 strike, a length of almost 10 Km, and a width ranging between 5-50 cm. Fissure openings are differential from 1 to 5 centimeters per year. These fissures pass through a highway, some residential areas [urban centers] and an agricultural area, and have caused some damage every year (figures 1 and 2).

Figure 1. Fissure in the earth

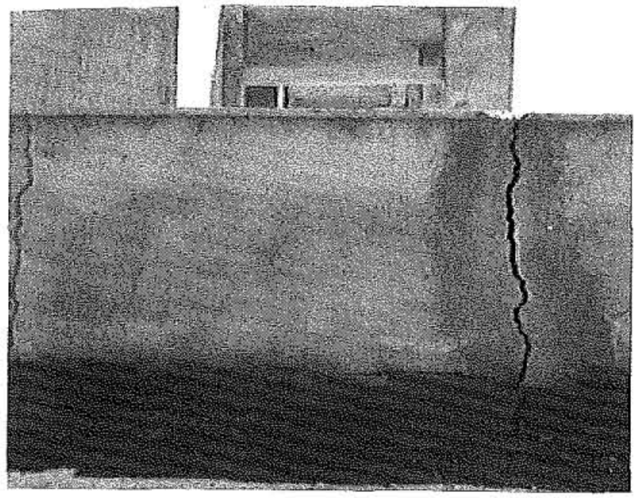

Figure 2. Cracks on the building

4. CONCLUSIVE REMARKS

As a summary, groundwater withdrawal from the aquifer system performed at Esfahan, has caused land subsidence associated with fracturing of the earth material, and cracking the buildings, with considerable amount of damages. It seems that charging the aquifer or at least controlling the recharge is the only way to stop the opening of the fissures. In the case of the continuation of opening, the subsidence will have happened in a vast part of the area. From a geological engineering point of view and because of the compaction of the aquifer system, the disturbance in the equilibrium between grains and water is the main cause of subsidence. Because the weight of the grains after drawdown will increase, the voids will gradually get smaller and some displacement will happen, which causes subsidence through the whole aquifer system. The fissures are the first surface reaction of subsidence. In the case of a continuation of compaction, partial subsidence of the earth or movement and sliding of a land might happen.

REFERENCES

Bell, F.G. (1994), *Fundamentals of Engineering Geology*. Blackie Academic & Professional

Bell, F.G. (1987), *Subsidence, Ground Engineer's Reference Book*. Edited by F.G. Bell, Butterworths and Co. Publishers.

Booker, J.R, Small, J.C. and Carter, J.P. (1985), Prediction of subsidence caused by pumping of groundwater. 21st IAHR Congress, Melbourne, Australia, pp. 130-134.

Lofgren, B.N. (1968), Analysis of stress causing land subsidence, U.S. Geol. Survey, Proc. Paper 600-B, pp. 219-225.

Poland, J.F., Figueroa Vega G., Carbognin L., Johnson A. I., & Yamamoto S. (1994) *Guidebook to studies of land subsidence due to ground-water withdrawal,* Ed. by UNESCO, Paris, France, J.F. Poland Chairman and Editor, 305 p. and Appendices A-E.

Scott, R.F. (1979), Subsidence- a review in evaluation and prediction of subsidence, Ed. by Saxema, S.K., Proc. Conf. ASCE, Gainesville, pp. 1-25.

Waltham, A.C. (1989), *Ground Subsidence*, Blackie & Son Limited.

Yamamoto, S. (1984), Case history no.9.4. Tokyo, Japan. In: Poland, J.F. et al. Op. Cit., pp. 175-184.

RELATIONSHIPS BETWEEN CATASTROPHIC SUBSIDENCE HAZARDS AND GROUNDWATER IN THE VELINO VALLEY (CENTRAL ITALY)

Giuseppe Capelli and Roberto Salvati
Dipartimento Scienze Geologiche, Università Roma Tre, L.go S.Leonardo Murialdo 1, 00146 Roma (Italy) - e-mail: salvati@uniroma3.it

Marco Petitta
Dipartimento di Scienze della Terra, Università "La Sapienza", P.le Aldo Moro 5, 00185 Roma (Italy) – e-mail: petitta@uniroma1.it

Abstract

This paper shows the first results of a study aimed to analyze and define "sinkholes phenomena" both in their trigger and evolution issues. The hydrogeological setting has been taken into account as start up point; S.Vittorino Plain (Velino Valley, Rieti) presents a major groundwater circulation, with a total spring discharge amount up to 25 m^3/s. Catastrophic subsidence phenomena, moving from a karst bedrock, found their trigger issues in: neotectonic activity and seismicity along strike-slip fault sets; fast shallow water seepage in alluvial deposits; hydrochemical and water/rock interaction with deep groundwater and fluid upwelling.

Occurrence of catastrophic subsidence phenomena shows a general scattered time-space distribution. So far, they have been recorded up to thirty sinkholes with different features (shape, dimension, depth, water and gas presence, etc.) in less than six km^2.

Future work will be undertake on the application of a multidisciplinary approach aimed to define sinkhole genesis mode and each issue weight in this phenomena occurrence. The goal is sinkholes conceptual model delineation in this area, to allow an ameliorate land planning which should take into account human needs and protection of environmental resources.

Keywords: catastrophic subsidence, sinkholes, hydrogeology, Velino Valley

1. INTRODUCTION

In the wider range of land subsidence phenomena, cover collapse sinkholes, simply sinkholes, represent a peculiar and not as much studied aspect.

Referred to classical way of land subsidence development, due to ground-fluid removal, sinkhole processes and triggering issues are generally related to fast collapse of surficial terrain strata, induced by the presence of bedrock karst cavities.

Land subsidence phenomena, indeed, are quite often directly induced by human activities, and then preventing actions must involve a review of human activities in subsiding territories. It is intriguingly to point out that to sinkhole formation and development contribute triggering issues due to human activities, as well as natural causes, which could assume at places definitely greater importance.

The effects of such instability phenomena on human activities are, on the other perspective, as heavy as the classical subsidence. In fact, even if real dimensioning of each sinkhole is strongly reduced, if confronted with land subsidence usual extensions of hundreds of Km^2, their occurrence frequency and density in restricted areas lead to a major hazard for human settlements.

Thus, as a matter of fact, the importance of sinkhole phenomena studies must be considered comparable with that of well-known land subsidence development. So far in Italy has not yet been devoted the correct importance to the geological risk related to sinkhole occurrence.

1.1 Short reference to sinkhole phenomena

Sinkhole phenomena general features are represented substantially by a precise geological framework with a fractured and karstified bedrock, overlaid by diversified recent sediments (i.e. gravel, breccia, sands, clays, travertine, volcanic sediments). General conditions involve the presence of a water table able to interact with the bedrock and to induce, then, the karstification and the cavity genesis, leading to the quick collapse of cover and overlain terrain following the increase of tensile stress and deformation in the cavity. The morphologic result is at places represented by a sub-circular small lake or anyhow by a surficial depression, more or less deep, filled with water often connected with the unconfined aquifer (e.g. Tharp, 1999).

Besides the above mentioned features, in many cases the main catastrophic subsidence triggering issue can be traced back to human activities (i.e. water table depletion following heavy exploitation, surficial overloads, heavy trucks movement, etc.) (Nichols, 1998). In as many situations the sinkhole event can be induced directly by natural phenomena (i.e. prolonged rain and stormwater, natural variation of water table, earthquake even of low-grade magnitude).

The case study presented here shows a major hazard induced by the interaction among several natural processes, which leads to a faster evolution and more frequent occurrence of sinkhole phenomena. From the other perspective the studied area has a major vulnerability due to the wide human presence (i.e. several settlements, major communication lines, tourist and services infrastructures).

Thus the studied area represents a so-called "natural laboratory", extremely complex, which could allow a total approach to sinkhole study. A conceptual model delineation, object of the study first step, could be later exported and tested to different geological frameworks. The study second step in this area will aim to a systematic hazard evaluation and human activities related risk.

The presented study, even if it has peculiar features, is set in the general central Apennine geological framework which is the object of a specific join research program between Geological Sciences Department at Rome TRE University and U.T.V.R.A. Department of Latium Regional Government.

2. S.VITTORINO PLAIN HYDROGEOLOGICAL SETTING

S.Vittorino Plain (Fig. 1), located in the northern Latium along the middle Velino River Valley between Rieti and Antrodoco, is a morphological depression that can be defined as an intra-chain basin. It is located in the meeting sector between the Latium-Abruzzi carbonate Apennine (formed by a thick sequence of meso-cenozoic carbonate platform deposits) and the Umbro-Marchean Apennine domain (characterized by coeval carbonate deposits belonging to a transitional-pelagic sequence). The two different depositional environments are bring in contact by a tectonic set called Olevano-Antrodoco (Ancona-Anzio Auct.), which is the result of a compressive tectonic phase aged to later Miocene and linked to Apennine orogenesis (Bigi et al., 1990).

Pleistocene evolution of the area has determined the downthrown of meso-cenozoic carbonate in the S.Vittorino sector, through mainly extensional tectonic phases, with the depression following filling up with alluvial, fluvio-lacustrine and scree deposits. The recent sediment cover, less or absolutely not cemented, which is overlaid by the present Velino River alluvial deposits, shows increasing thickness, from the Plain borders towards its center. Data from geophysical surveys highlight that the major thickness can be supposed to be equal or more than 200 meters. The bedrock is formed, with large confidence, by carbonate deposits belonging to the carbonate platform facies; any borehole has ever drilled the carbonate rockhead in the center of the plain.

The area, besides a high seismicity testified also by recent medium magnitude earthquakes, presents evidences of active tectonic, whose main features highlight the continuity of regional tectonic lines in to the plain itself along typical strikes of Apennine tectonic evolution (Faccenna et al., 1993).

The hydrogeological referring scheme is based mainly on the knowledge acquired during the last twenty years (Boni et al., 1986; Boni et al., 1988; Boni et al., 1995). S.Vittorino area represents the address of important regional aquifers recharged by the carbonate platform domain of Mts. Giano-Nuria-Velino Group (see fig.1).

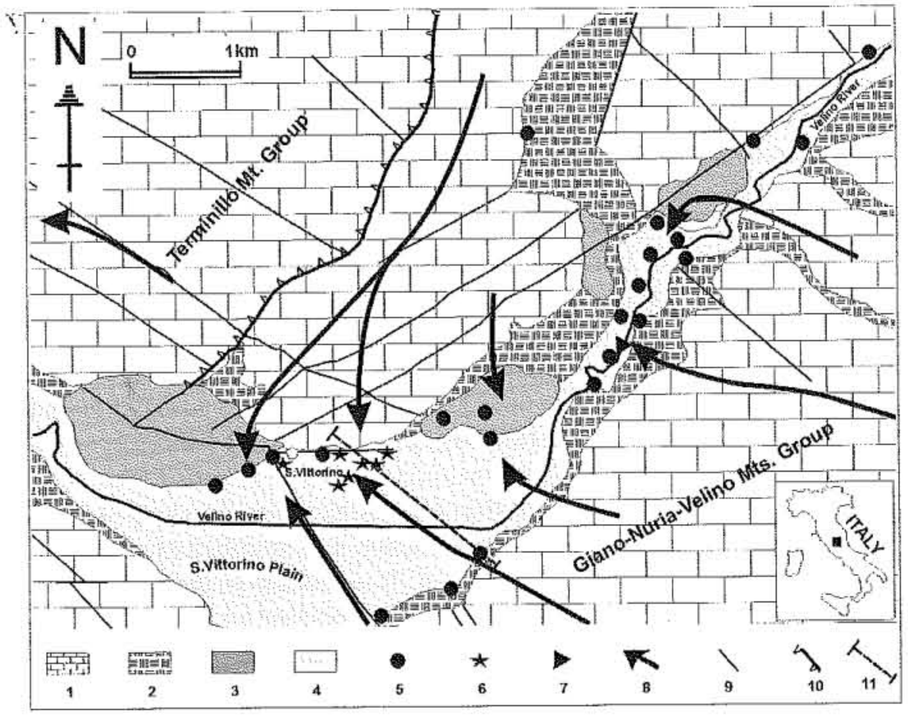

Figure 1. Hydrogeological scheme of S.Vittorino Plain area. 1– Meso-cenozoic karst ridges (transitional pelagic sequence in Mt. Terminillo group and carbonate platform sequence in Giano-Nuria-Velino Mts. group); 2– Scree deposits; 3– Travertine deposits; 4– Alluvial deposits; 5– Spring; 6– Mineral spring; 7– Linear spring; 8– Groundwater flowpaths; 9– Fault; 10– Thrust (triangles show the hangingwall); 11– Cross section (see Fig. 2).
(Redrawn and modified after Boni et al., 1995).

Relevant piedmont springs are located both along the Velino River Valley, mainly linear springs, and on the northern side of S.Vittorino Plain. Spring discharge total amount, inside the Plain sector, is up to 25 m^3/s; this value, adding the groundwater contributions present in the northward proximal sector, lifts up to 30 m^3/s.

Groundwater circulation interests, naturally, the Plain filling up terrain; their permeability has a strong variability following the coarsening and cementing rate. The aquifer coming from the eastern karst ridges is not totally drained by the springs located at the geological contact between carbonate and alluvial deposits, but, even if through terrain with strong permeability contrast, it probably feeds the Velino River alluvial aquifer.

The multilayer aquifer of the Plain is partially drained by the piedmont springs drainage rivers located on the northern side. Following the reclamation works done in the XIX century, the Velino River cuts S.Vittorino Plain in a straightened and suspended channel, enabling thus the groundwater, moving

from S and E, to flow towards the streams located on the northern side. Moreover, the Velino River water can seasonally percolate towards the underlain water table, allowing then the infiltration of surficial water in the aquifer.

Small intake basins mainly recharge the northern side springs but also, as mentioned above, by groundwater flow paths coming from the opposite side of the Plain. Many of these springs show peculiar hydrochemical features (sulphurous and ferrous springs with slight hydrothermal characteristics), induced by a mixing with mostly gaseous fluids upwelling along recent and/or active tectonic lines.

Reassuming, S.Vittorino Plain is place for a major groundwater circulation with flow paths linked to overflow piedmont springs and at places joined to the river bed direct discharge (linear springs). Spring waters are chemically differentiated from point to point following different mixing rates with deep fluids upwelling along recent and active tectonic lines (Fig. 2).

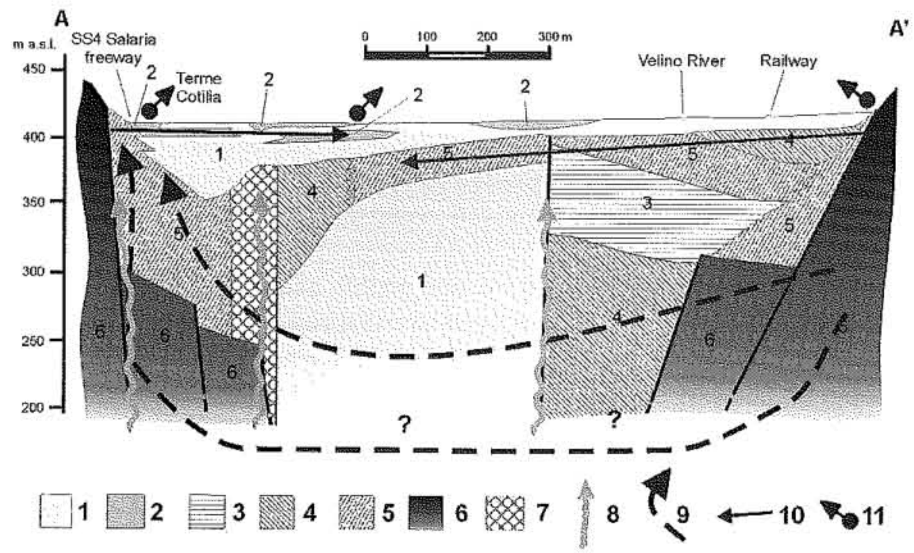

Figure 2. Hydrogeological cross-section (NW-SE, localized in Fig.1), from electric resistivity data interpretation. 1– Clay deposits, low permeability; 2– Travertine seams, high permeability, possible carbonate dissolution; 3– Sand deposits, middle permeability; 4– Gravel deposits, high permeability; 5– Cemented gravel and scree deposits, high permeability, possible carbonate dissolution; 6– Fractured and karst bedrock, high permeability; 7– Shear zone; 8– Deep fluids upwelling flowpaths; 9– Karst groundwater flowpaths; 10– Shallower groundwater flowpaths; 11– Spring. (Boni et al., 1995, modified).

Fundamental issues for the existence of catastrophic subsidence phenomena are, thus, represented by the interaction among:

- the unconfined shallower aquifers, present in the scree and alluvial deposits;

- the complex groundwater flow hydrodynamic;
- the increased aggressiveness of groundwater due to the mixing fluids upwelling.

The reconstruction of the interaction scheme, of its evolution and the drawing up of a conceptual referring model must necessarily start up from multidisciplinary analyses of the available data.

3. SINKHOLES AND GROUNDWATER DATA COLLECTION

The complexity sinkhole phenomena and the high number of variables involved in the process require a multidisciplinary methodological approach coupled with the collection of historical data aimed to implement a complete database. Data processing enables the experimental phases planning about new surveys and further and more detailed analytical elaboration.

Available data collected through out the last 120 years refer to: historical topographic maps, boreholes, geophysical surveys, geological and structural-geological surveys, physical-chemical and chemical data of both spring and sinkhole waters (Bigi et al., 2000). Collected data come partly from the few scientific papers, partly from public and private archives and partly from professional commitment.

Historical data are represented by topographic maps surveyed in the years: 1887, 1907, 1943, 1951, that have been overmapped with the official Latium Region cartography surveyed in 1991. Particular attention has been stressed in the temporal analysis of transformations undergone by some specific anthropic elements (Terni-Sulmona railway and SS4 Salaria freeway), sinkholes location and modification in soil uses. This analysis highlights the continuous transformation undergone by railways track and the modification of river patterns induced by sinkholes occurrence. The SS4 Salaria freeway track instead had not undergone any modification as it is built on the carbonate rocky slope, which borders the plain to north, to testify the stability of this sector in the past. In the last few years some new instability events, referred to sinkhole phenomena, has been recorded though (last event in august 1999).

Sinkhole event chronology (see Tab. 1), reconstructed on historical data, highlights the worsening of sinkhole phenomena occurrence in the last twenty years. The sharp acceleration of new sinkhole recurrence had raised concern and interest with in scientists and local administrators.

Sinkholes in the S.Vittorino Plain present themselves, quite often, as sub-circular depression of surface, whose collapse occurs within few hours, filled with groundwater, located both in the Plain as in the Velino River bank. Their diameter ranges from few meters up to a hundred, with depth up to several tenths of meters. Rarely the instability occurs only through simple land subsidence as in the S.Vittorino church, where the homonym spring is located (mean discharge of 200 l/s).

Table 1. Main features of S.Vittorino Plain sinkholes (ID localization in Fig.4).

N°	*Depth (m)*	*Diam. (m)*	*Event date*	*Notes*
1	2	20	Secular sinking	Repeatedly
2	3	50	Unknown	
3	3	3	July 5th 1993	Backfilled
4	9	80	Secular sinking	Shape settled in 1951
5	7	15	Secular sinking	Saturated since 1913
6	Unknown	15	1986?	
7	Unknown	5	Dec 19th 1986	Following earthquake shock
8	5	3	Dec 19th 1986	Following earthquake shock
9	12	60	Dec 17th 1986	Following earthquake shock
10	Unknown	Unknown	Unknown	
11	Unknown	Unknown	Unknown	
12	3	50	Secular sinking	
13	45	204	Secular sinking	
14	Unknown	130	Secular sinking	
15	Unknown	2	Dec 26th 1902	Between the railway and SS.4
16	Unknown	10	Dec 31st 1900	In the river bed; backfilled
17	Unknown	Unknown	Unknown	backfilled
18	32	18	March 6th 1991	Evident gas emission
19	>15	100	July 27th 1893	Collapsed again in 1915
20	10	10	July 27th 1893	Backfilled
21	10	8	Aug 12th, 13th 1893	Backfilled
22	10	8	Sept 10th 1893	Backfilled
23	33	50	Sept 22nd 1891	Collapsed again in Dec 1902
24	Unknown	5	Nov 25th 1903	In the river bed; backfilled
25	Unknown	5	Nov 25th 1903	In the river bed; backfilled
26	Unknown	8	Nov 25th 1903	In the river bed; backfilled
27	10	102	July 27th 1893	Flowing out water
28	4	27	Feb 1915	
29	Unknown	Unknown	Unknown	

Boreholes and geophysical data concern mainly the Plain eastern sector and they are related to different surveys carried on in different periods with different finalities. The older information is dated at the end of XIX century, when the railway was building up. The more recent surveys highlight the existence of numerous cavities to depth ranging from 10 to 30 meters below surface. Boreholes have investigated the first underground 20-30 meters, with only few exceptions pushed up to 60 meters. The major lateral and vertical variability of quaternary deposits does not allow a detailed reconstruction of stratigraphic sequence, which is formed, in general, by variable coarse deposits from clay to gravel with frequent interbedding of both travertine and scree rock bodies (see Fig.2).

The last years surveys focused the attention on the delineation of already developed cavities above all in correspondence of human settlements and infrastructures; to this aim specific studies of gravimetry and microgravimetry has been undertaken (Ciotoli et al., 2000; Nolasco, 1998).

The structural geology setting reconstruction, regarding, indeed, the relationships between the plain and the surrounding karst ridges, is based also on the surveys carried on by different work groups (i.e. Ciotoli et al., 2000). In this scenario neotectonic activity data have been collected (Faccenna et al., 1993), with the delineation of tectonic patterns that somewhere cut the sedimentary covers.

The hypothesized fault pattern finds out an immediate correspondence with the springs distribution, the groundwater chemical features and sinkholes localization, highlighting in this area a close relationship between active tectonic elements and catastrophic subsidence phenomena (Fig. 3).

In detail the two major sinkhole groupings are localized in the Terme di Cotilia and Micciani sectors, exactly where the railway track has undergone the most important transformations to accommodate the different stability conditions induced by sinkholes occurrences.

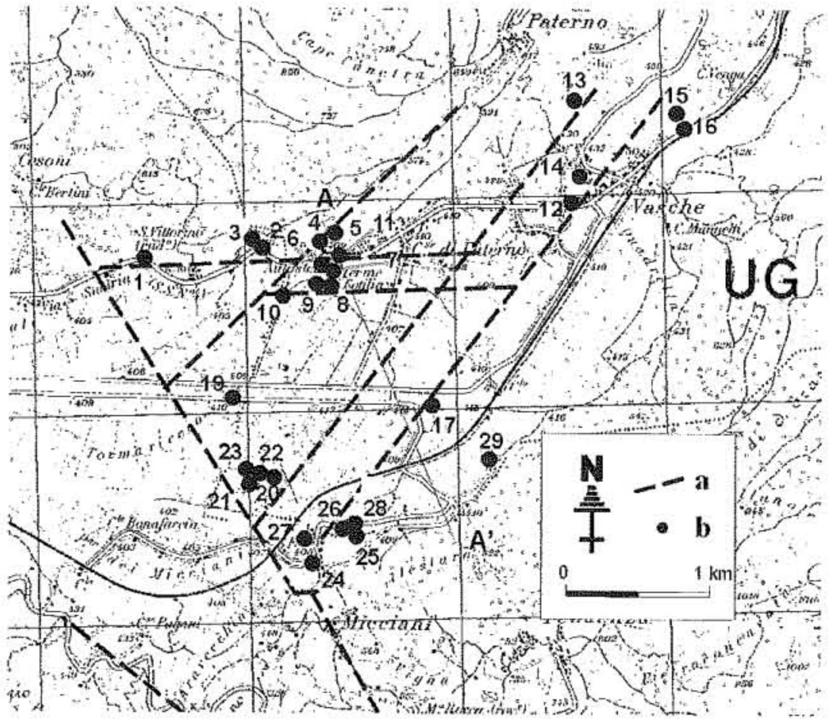

Figure 3. Distribution pattern of neotectonic fault patterns (a) and sinkholes (b). The sinkhole ID is referred to Table 1. A-A': cross-section trace (see Fig. 2).

Hydrochemical data, referred to a century wide temporal interval, were homogenized and re-analyzed in detail. Generally groundwater of S.Vittorino Plain shows calcium-bicarbonate features, typical of carbonate ridges circulation (Dall'Aglio and Campanile, 1996). To this main character is, at places,

superimposed the effect of deep contributions represented in majority by carbon dioxide which has also the role of gas carrier towards H_2S, CH_4, NH_4, He and Rn.

Detailed study on noble gas in the soil focused particularly on He and Rn (Ciotoli et al., 2000) highlighted that maximum values are localized mainly in correspondence of major mineral springs, interested by deep fluids upwelling. Thus groundwater acidity and following aggressiveness toward carbonate rocks are built up by means of H_2CO_3 formation and H_2S and H_2SO_4 oxidation (Dall'Aglio and Campanile, 1996).

This recent study has confirmed that fluids upwelling take place along recent tectonic lines, delineated by means of geophysical surveys and a detailed geological setting reconstruction.

Hydrogeological framework, even if rather detailed, is not yet sufficiently investigated to complete the referring scenario. Hydrogeological circulation model (above described) seems updated, while missing knowledge is mainly due to the scarcity of specific surveys on aquifers and on sinkhole water chemistry.

In progress study presented here is mainly directed to the collection of new knowledge elements in this field. First results given by the undertaken new investigations suggest that groundwater flow-path inside the Plain, coming from SE with main horizontal course, may undergoes sharp velocity variations, following the go-through of heterogeneous sediments which are discontinuous and variables in thickness and give place also to confined aquifers.

The referring scenario is completed by: deep fluids upwelling along tectonic discontinuities, which induces the mixing of different groundwater families; total head difference that characterizes different reservoirs; groundwater flow amount and its velocity. Undoubtedly this scenario supports dissolution phenomena and mechanical erosion in quaternary filling up sediments where consequently sinkhole triggering issues can be generated.

4. CONCEPTUAL MODEL OF INTERACTION BETWEEN SINKHOLES AND GROUNDWATER

From the cognitive scenario above described, it could be hypothesized a possible conceptual model of sinkhole genesis in S.Vittorino Plain and above all a model of running interactions between sinkholes and groundwater.

In this area two different bedrock should be involved in sinkhole genesis. Undoubtedly in the close proximity of Plain borders the bedrock is represented by dowthrown meso-cenozoic carbonate ridges, overlaid by thin layers of recent sediments; depressions and dolines presence located at different elevations along the slopes testify this also.

Regarding the central plain located sinkholes, instead, it would be really difficult to cope their genesis with a carbonate bedrock located at more than 200 meters below surface. Taking into account the stratigraphy of recent deposits, the triggering sinkhole bedrock should be represented by the travertine seams, whose thickness may reach the tenths of meters as for the outcropping travertines, where could take place the carbonate dissolution.

The groundwater flow present in the Plain sediments, and thus in the travertine seams as well, is characterized by a major hydraulic head referred to the wide carbonate ridge, coupled with considerable discharges (more than 25 m^3/s). This situation may induce a greater hydrodynamic pressure inside the karst cavities that are definitely present in the more permeable horizons (i.e. travertines, cemented gravels and gravely-sands).

Furthermore karst fractures and conduits pattern should tend to a rapid enlargement following the increased groundwater aggressiveness, over there where mixing processes with deep upwelling fluids occur. Thus, along tectonic discontinuity trends, karst cavities of considerable extension could be easily induced (Blair et al., 1998).

The deposits overlaying travertines, up to the surface, are definitely incoherent, with variable coarsening and normal or absent consolidation rate. These sediments, thus, trend easily to progressively collapse into the karst cavities contributing to their filling up. Their thickness of some ten meters, by another perspective, is such that it could not enable direct collapses on the surface. The presence of a faster groundwater flow in karst conduits, however, could enable a further erosive action of mechanical type, mobilizing the karst cavities filling up deposits with their consequent moving away in suspension.

In this way, progressive collapses could be induced in the sediments overlaying karst cavities, with upward propagation of deformation and dragging in of shallower cover strata up to the paroxysmal episode of "surficial plug" collapse and sinkhole genesis completing.

According with this possible scheme of evolution, sinkhole filling waters should have hydrochemical and physico-chemical features similar to those of regional groundwater aquifer, circulating in the carbonate ridges, with a possible mixing with Plain shallower waters.

The further evolution of sinkhole, related to its widening, depends from the karst cavity evolution, which influences the static equilibrium of sinkhole itself.

This cycle may then recurs in the same site, following the reactivation of the former karst cavity, or it may migrate in a surrounding position where the joined effect of hydrodynamic flow and groundwater aggressiveness could be focused. Such last model could justify the presence of several collapse points and their reactivation in different times.

We are currently working on the transformation of this evolutive model of sinkhole phenomena from a descriptive conceptual formulation to a quantitative evaluation. At first, the geotechnical model of static equilibrium must be verified

and so far any quantitative datum is available on this item. It still has to be verified the effective mechanical erosion capability of groundwater flowing in karst conduits net. This capability depends on either the sub-horizontal karst conduits dimensions, the water velocity in these conduits or then the available potential energy for solid transport, besides the coarse features of recent top sediments. Programmed analysis will obviously lead in this direction.

5. MANAGEMENT TOOLS: KNOWLEDGE AND PREVENTION

To conclude, the sinkhole problem in S.Vittorino Plain must be firstly faced with specific investigations that could enable to verify, modify and update the progressing conceptual model; the improvement of the strict application of planning tools and preventing rules should immediately follow. The problem is making even more complex by the necessity of finding out the correct equilibrium among environmental values, groundwater exploitation and man-induced changes in pressure (Menotti et al., 1999).

Main difficulties to get this target are due substantially to two different aspects:

- the existence of a territorial management model, heritage of policies adopted in the past decades, based only on building expansion regardless for the environmental values;
- the necessity of basic data collection, by means of scientific and technical researches, whose results would enable the possibility of a territorial and environmental model improvement that could lead then to a sustainable development.

Different studies so far carried on in the area have never found an effective co-ordination that could trespasses the plain collection of data.

The study presented here, currently undertaking, besides the collection of furthermore elements regarding not only the sinkhole phenomena but the other hydrogeological features also, takes particularly into account aquifers on-line monitoring activities and physical-chemical analyses of spring and sinkhole waters. These should support the sinkhole genesis conceptual model improvement , described in the previous paragraph.

With the help of hazard maps that delineate the high density underground cavity areas, it could be performed the draw down of planning tools (vulnerability map, human activities hazard map). For specific problems, such as freeway and railway tracks and infrastructures localization, interventions aiming to reduce the vulnerability and/or the risk shall necessarily be developed.

At the same time, the sinkhole genesis and development model, confronted with similar experiences undertaking in Latium and Tuscany, shall contribute to the general problem solution by means of the application of the same methodology (study, model, rules and intervention) in different areas where catastrophic subsidence phenomena occur.

REFERENCES

Bigi, G., Cosentino, D., Parotto, M., Sartori, R. & Scandone, P. (1990) Structural model of Italy, sheet 4, scale 1/500.000, CNR Italy

Bigi, G., Capelli, G., Mazza, R., Parotto, M., Petitta, M. & Salvati, R. (2000) Strutture di collasso nella Piana di S.Vittorino (Fiume Velino, Lazio): interazione tra circolazione idrica sotterranea e tettonica attiva. Proceedings Congress "Protezione e salvaguardia delle aree di pianura", Ferrara, november 1999, Regione Emilia-Romagna (in press)

Blair, H., Rajaram, R. & Harihar, H. (1998) Influence of aperture variability on dissolution growth of fissures in karts formation. *Water Res. Res.* 34/11

Boni, C., Bono, P. & Capelli, G. (1986) Schema Idrogeologico dell'Italia centrale, scale 1/500.000. *Mem. Soc. Geol.It.* 35, 991-1012

Boni, C., Bono, P. & Capelli, G. (1988) Carta idrogeologica del territorio della Regione Lazio. Regione Lazio e Dipartimento di Scienze della Terra Università di Roma "La Sapienza", scale 1/250.000

Boni, C., Capelli, G. & Petitta, M. (1995) Carta idrogeologica della alta e media valle del fiume Velino. Univ. "La Sapienza", Com. Mont. Velino VI° zona

Ciotoli, G., Di Filippo, M., Nisio, S. & Romagnoli, C. (2000) La piana di S.Vittorino: dati preliminari sugli studi geologici, geomorfologici, geofisici e geochimici. Proceedings VI° Congresso Giovani Ricercatori Geologia Applicata. *Mem.Soc.Geol.It.* (in press)

Dall'Aglio, M. & Campanile, R. (1996) Rinaturalizzazione del bacino del Fiume Tevere alla luce dei peculiari caratteri geochimici del suo bacino. Caratterizzazione geochimica delle acque del bacino del Fiume Velino. Proceedings 4° Seminario International Association for Environmental Design "Rinaturalizzazione fluviale". Roma, March 1996, 78-97

Faccenna, C., Florindo, F., Funiciello, R., & Lombardi, S. (1993) Tectonic setting and sinkhole features: case histories from western Central Italy. *Quaternary Proceedings*, 3, 47-56

Menotti, R.M., Millesimi, F. & Petitta, M. (1999) La Piana di S.Vittorino (Rieti) tra dissesto idrogeologico, valenze ambientali e sviluppo antropico. *Atti dei convegni Lincei*, 154, 327-333

Nichol D. (1998) Sinkholes at Glan Llyn on the A55 North Wales Coast Road, UK. *Engineering Geology*, 50, 101-109

Nolasco F. (1998) La Piana di S.Vittorino. ACEA, 68 pp.

Tharp T. M. (1999) Mechanics of upward propagation of cover-collapse sinkholes. *Engineering Geology*, 52, 23-33

LAND SUBSIDENCE - Vol. I
Proceedings of the Sixth International Symposium on Land Subsidence
Ravenna / Italy / 24-29 September 2000

CASUAL HYDROFRACTURING PROCESS AS A POSSIBLE CAUSE OF LAND SUBSIDENCE

Alexander V. Anikeev
Moscow State University, Geology Faculty, Vorobjovy Gory, 119899, Moscow, Russia

Abstract

The process of spalling and fissuring of a confining bed under the drop of aquifer head due to ground water withdrawal named casual hydrofracturing is described. The analysis of this phenomenon occurring near a single weakened zone lets us derive the failure criterion. Based on some assumptions the formulae available for application in practice are obtained. The physical model tests show the hydrofracturing to result in the collapse of relatively thin aquitards and the entrainment of overlying unbound soils into fissure and karst voids. Small cavities and large regions of spalled rock form within thick weakly permeable strata. The process is accompanied by bending of the upper portions and dilation of overburden. Usually, the confined aquifers composed of carbonate rocks are intensively fissured and karstified. Developing in vicinity of numerous fractures, caves and caverns the hydrofracturing can generate the contact interbeds where clayey rock is qualitatively distinguished from original one. The strain and strength characteristics of the interbeds are much smaller than those of the undisturbed ones. This can be the cause of total high compressibility of impermeable strata and dilated permeable ones. Such a conclusion is supported by field observations in the North-West region of Moscow City (Russia) where some areas of extremely high land subsidence coincide with no areas of karst sinkhole development.

Keywords: hydrofracturing, land subsidence, water head drop, weakened zone

1. INTRODUCTION

Generally, the investigations and estimations of land subsidence induced by ground water withdrawal are based on the analysis of compression and consolidation, i.e. the deformation process of rock, mostly, clayey strata. There are many suggestions how the compressibility of solid grains, water, immobile air, etc. should be considered above the compaction of rock lattice (Land Subsidence, 1995). However, the real values of land subsidence are sometimes much larger than the calculated ones. The purpose of the paper is to discuss the alternative or alternate cause of land subsidence, namely, the destruction of confining beds due to fluid extraction from coarsely porous and fractured aquifers.

2. CASUAL HYDROFRACTURING PHENOMENON AND ITS ANALYSIS

It was found in experiments that a sudden decline of water pressure beneath a weakly permeable bed caused the failure of water saturated clays above even a small cavity. The development of breakdown fractures, spalling and crumbling are observed inside an arch-shaped zone (Fig.1 (a)). Nearly in a trice, the rupture front propagates upward from the bed floor to the surface of equilibrium state. This phenomenon has been named casual hydrofracturing (Anikeev, 1991, 1993) in order to emphasize the difference between this one and that due to premeditated fluid injection into boreholes and mines.

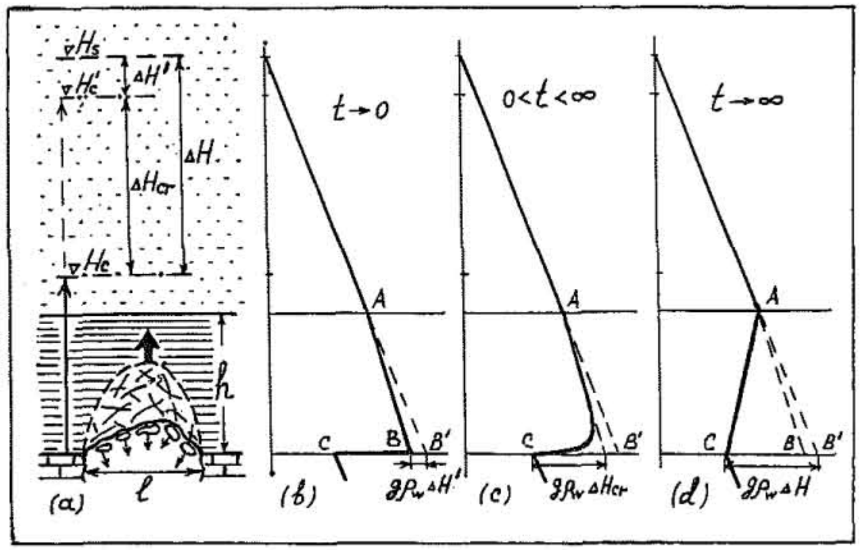

Figure 1. Mechanism of casual hydrofracturing (a), and pore-pressure diagrams at the initial moment (b), intermediate stage of downward seepage (c) and final one (d). H_s: water table; H_c' and H_c: potentiometric level before and after water head decline; l: the span (width or diameter) of an opening at the base of cover deposits; h: the thickness of confining bed; t: time. Big arrow and small ones show respectively the propagation of spalling front and the "shooting" of clay spalls and pieces from the bed floor.

The driving force, which causes the fissuring, results from the difference in hydraulic conductivities of confining layer and aquifer. Generally, the equation for the excess pore pressure inside the layer is written as follows:

$$g\rho_w \Delta H = K_\sigma \sigma_w + K_\tau \tau_w , \qquad (1)$$

where g is the acceleration of gravity; ρ_w is the density of water; ΔH is the magnitude of water head decline; K_σ and K_τ are coefficients, $K_\sigma + K_\tau = 1$, and K_σ / K_τ is the function of time and hydraulic diffusivity; σ_w are the stresses in pore water normal to clay particles, or excess hydrostatic pressure; τ_w are the seepage stresses tangential to the surface of soil grains, hydrodynamic pressure or effective stresses in the theory of aquifer-system compaction (Terzaghi & Peck, 1967; Poland, 1981). In water-saturated rocks with extremely low permeability the shape of the fluid pressure distribution curve is close to that of broken line ABC (Fig.1,b,c) independently on non-steady state percolation or steady state one, i.e. $K_\sigma / K_\tau >> 1$, and equation (1) is rewritten as follows:

$$g\rho_w \Delta H = \sigma_w . \qquad (2)$$

Over a weakened zone (open-joint fissure, cavern, cave, etc.) not balanced by grain-to-grain pressure, the excess hydrostatic stresses cause the spalling of a confining bed long before the dynamic seepage stresses will be exerted on the grains by viscous drag of vertically moving interstitial water (Fig.1,d). Tensile fractures will occur, if the tensile strength T is

$$T \leq \sigma_w - \sigma_{1,2,3} , \qquad (3)$$

where $\sigma_{1,2,3}$ are the main normal stresses in clay solid above an opening. For simplicity the anisotropy of strength properties is neglected now. Though, the tensile strength of any rock is much smaller than its cohesion (C), we shall assume that $T \approx C$. Otherwise, the utilization of failure criterion (3) presents some difficulties in practice, especially for plastic soils. Then, substituting the value of σ_w from (2) into (3) one can write:

$$\Delta H_{cr} = (C + \sigma_{1,2,3}) / g\rho_w , \qquad (4)$$

where ΔH_{cr} is the failure (critical) value of water head decline.

The next obstacle concerns the identifying of the stress state of an aquitard or confining bed in vicinity of an opening with usually unknown dimensions.

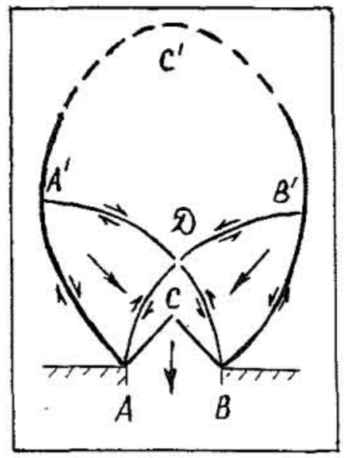

Figure 2. Region of influence of opening AB in rigid base of a soil mass. ACB: falling block or cave-in zone; ADB: relieved arch or zone of decompaction and potential cave-in; AA'D and BB'D: plastic wedges or zone of bearing pressure and potential slippage; DA'C'B': zone of transit from anomalously high and low stresses to lithostatic ones (zone of possible extrusion of spalled solid by downward water flow). Big arrows and small ones show the directions of potential soil flow and those of maximal tangential stresses.

But it is well known that a relieved arch (ADB in Fig.2) forms in rocks over a weakened zone. At the base of the arch stresses can be even tensile ($\sigma_{2,3} < 0$, $\sigma_1 = 0$). Near its top they are compressive ($\sigma_{1,2,3} > 0$), but they are small enough in terms of absolute value. In the first assumption let them be equal to zero inside the zone of low stresses. In other words, we assume that the pressure of overlying rocks acts on wedges AA'D, BB'D (Fig.2), while block ADB is hanging over an opening owing to rock cohesion. Taking into account the second assumption ($\sigma_{1,2,3} = 0$) we obtain the simplest relation between the failure value of water head decline ΔH_{cr} and the standard engineering-geological characteristic of disperse rock C from expression (4):

$$\Delta H_{cr} = C/g\rho_w. \tag{5}$$

Let's examine the scheme of instantaneous propagation of the spalling front from the bed floor to the roof under head reduction from H_c' to H_c (Fig.1, a). Being spalled a clay stratum will be affected by the downward flow of water, and the head difference will wholly manifest itself in the seepage stresses ($K_\sigma / K_\tau <<$ 1, $g\rho_w\Delta H = \tau_w$, Fig.1, d). Before the fracturing, in comparison with water pressure at the top of underlying strata the excess hydrostatic pressure, $(\sigma_w)_z$, changes inside a confining bed. It diminishes from CB=$g\rho_w\Delta H_0$ to DA in Fig. 3, where the unit weight of water is assumed to be unity, and the pressure is expressed in terms of the height of an equivalent column of water for the sake of simplicity. Then, as shown in Fig. 3,

$$\Delta H_z = \Delta H_0 - z + Iz, \tag{6}$$

where $I = dH'/dh$ is hydraulic gradient at the initial stage of steady state percolation ($I = (H_s - H_c')/h = \Delta H'/h$ in Fig. 1, 3), z is a height above the bed floor.

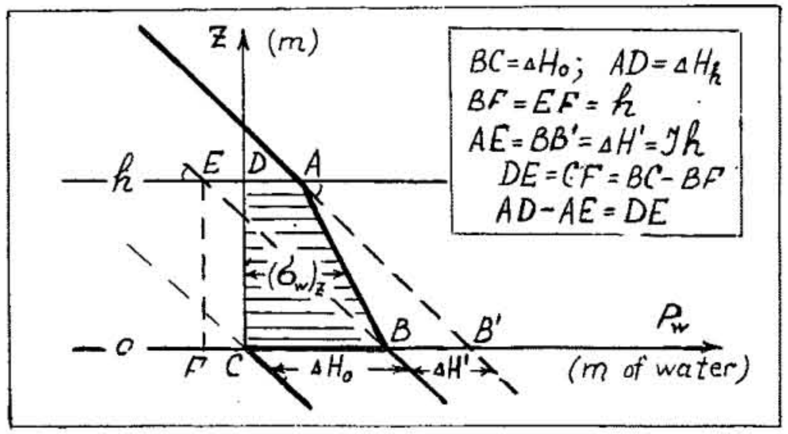

Figure 3. Scheme to determine the critical value of excess pore pressure, (sw)z , in a confining bed with thickness h under a sudden decline of water head, DH0 , in a confined aquifer. Pw : water pressure, in metres of water column.

Substituting $\Delta H_z = \Delta H_h = C/g\rho_w$, $z = h$ and $\Delta H_0 = \Delta H_{cr}$ into (6) we obtain

$$\Delta H_{cr} = C/g\rho_w + h(1 - I), \tag{7}$$

where h is the thickness of an aquitard. Hence, if $I \geq 1$, then $(\Delta H_{cr})_0 \leq C/g\rho_w$, i.e. the condition (5) is more than sufficient for the bed to be spalled entirely. If $0 \leq I < 1$, $C/g\rho_w < (\Delta H_{cr})_0 \leq C/g\rho_w + h$, and where $I < 0$ (the case of upward initial filtration, $H_s < H_c'$ in Fig. 1, a), $(\Delta H_{cr})_0 > C/g\rho_w + h$. In the peculiar but widespread case of initial hydrostatic conditions, $I \cong 0$ ($-0{,}1 < I < 0{,}1$), the hydrofracturing will commence at the layer floor under condition (5), and a confining layer will be disturbed from the floor to the roof (Anikeev, 1991, 1993) under condition (7a):

$$\Delta H_{cr} = C/g\rho_w + h. \tag{7a}$$

3. NEW EXPERIMENTAL DATA AND SOME CONSEQUENCES

Last years, the casual hydrofracturing of thick confining beds was studied in models from water-saturated equivalent materials. The technology of the tests and the theoretical foundation for modelling as well (Anikeev, 1988) are not within the scope of this consideration. It should be noticed only that the experiments consisted in the measured alteration of water pressure beneath the two-layer models and recording of the induced processes. The obtained results (Fig. 4, 5 and Anikeev, 1999) contribute some correctives in the presented conception.

It have been found that the hydrofracturing starts but quickly finishes under the values of water head decrease (ΔH_{ex}) being 2,5 - 3 times smaller than those (ΔH_{cr}) obtained from equations (5), (7). Under these conditions small three-cornered or box-

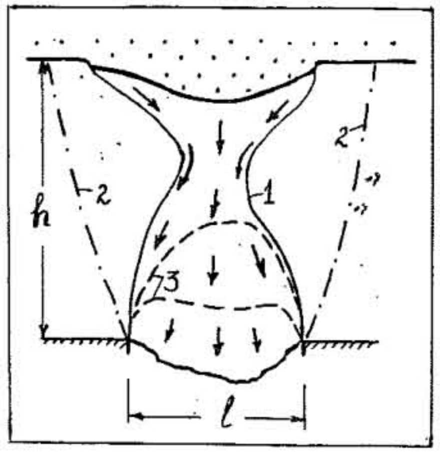

Figure 4. Extrusion zone (1) in the Upper Carboniferous and Upper Jurassic clays joined in a single stratum (h/l = 1,6) in the area of Tuchachevski street in Moscow city (the results of physical model tests). 2, 3: boundaries of open hole and cavity at the final and initial stages of hydrofracturing, respectively. Arrows show the flow of spalled clay solid.

shaped cavity forms at the bed bottom (Fig. 4). Where $\Delta H_{cr} / \Delta H_{ex}$= 1,5 - 2, the spalling leads to the collapse of relatively thin confining beds ($h/l \leq 1,5$). In the thick ones ($h/l >$ 1,5-2,5) it results in the arch-like cavity with the height approximately equal to the opening span (l) in the rigid base (Fig. 4, 5, a). Besides, nearby zone ADB (Fig. 2) clay cohesion may be partially disturbed, and the bed seems to be somewhat crumbled, because further descent of water head pressure causes the downward movement or extrusion of the disintegrated clays similar to unbound soil flow through apertures. These magnitudes of ΔH_{ex} are between those of ΔH_{cr}. At the beginning, the region of extrusion is like vase (Fig. 4), which probably results from the influence of compressed wedges (ADA', BDB' in Fig. 2). Then it becomes wider and parabola-shaped (Fig. 4) or ellipse-like in thicker layers (Fig. 5, a). The crumbling and extrusion of clay is accompanied by the roof bending and the cave-in of the upper portions (Fig. 5, a). The height of the ellipse-like zone of extrusion coinciding with the region of the influence (AA'C'B'B in Fig. 2) is five – seven times as large as the span. If $\Delta H_{ex} > \Delta H_{cr}$, the extrusion continues, the bending increases, new fractures appear, and the old ones dilate (Fig. 5, b). It is possible to make an opening in a thick confining bed (5 in Fig.5, b), but that requires $\Delta H_{ex} >> \Delta H_{cr}$.

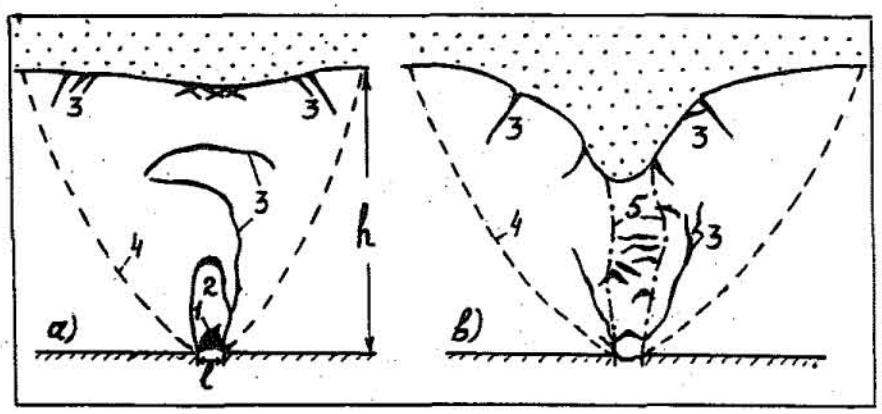

Figure 5. Modelling failure of the Upper Permian clay bed (h/l = 13,5) in an area of Dzerzhinsk City (Russia) at the first (a) and last (b) stages of hydrofracturing. 1: cavity; 2: zone of clay extrusion; 3: breakdown fractures; 4, 5: boundaries of visible deformations and open hole.

Thus, the correspondence between the results of physical model tests and those of calculations is good enough. It is evident that after the fissuring the excess hydrostatic stresses (σ_w) transform to the seepage ones (τ_w), i.e. the transmission ($K_\sigma / K_\tau >> 1 \rightarrow K_\sigma / K_\tau << 1$) takes place in equation (1). That is why, the increase of the water head difference ($\Delta H_{ex} >> \Delta H_{cr}$) is necessary to form the hole in thick aquitards. The discrepancy between ΔH_{ex} and ΔH_{cr} at the beginning of the

fracturing is explained mainly by the first assumption ($T = C$). The experience testify to the correctness of the second assumption ($\sigma_{1,2,3} = 0$) only for the zone of low stresses. Over the relieved arch the compressive stresses prevent from the upward propagation of the spalling front.

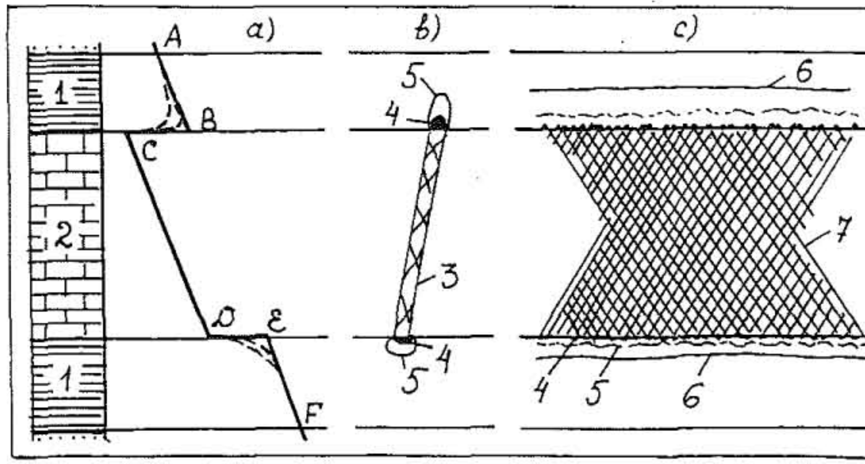

Figure 6. Conceptual model of weak interbed formation under water head reduction. 1: confining bed; 2: confined aquifer; 3: fissure; 4: cavity; 5: zone of crumbling and extrusion; 6: weak interbed; 7: fissure system; ABCDEF: fluid pressure.

Nevertheless, the disturbance of clay cohesion, the partial crumbling and changing of bound soils occur inside the large region near a weakened zone. The confined aquifers composed of soluble rocks such as limestones, dolomites, etc. are usually fissured and karstified. Developing in vicinity of many fractures, caverns and caves casual hydrofracturing process can form the contact interbeds where impermeable rock is qualitatively distinguished from the original one (Fig. 6). The strain and strength characteristics of such interbeds are much smaller than those of the undisturbed rocks. This can be the cause of total high compressibility of clayey strata.

4. CASE OF INDUCED SUBSIDENCE IN MOSCOW CITY (RUSSIA)

There are some areas of anomalously high land subsidence with the average velocity of 3 – 4 mm/year in the North-West region of Moscow city. Commonly, they are connected with the areas of karst sinkhole formation. Somewhere, subsidence development can not be explained from the engineering geological point of view. Such an area, 3,5 km long and 1,5 km wide, is situated along the 1-st Magistralnaya Street (Osipov & Medvedev (eds), 1997, p.263). It coincides with the central part of the pre- Quaternary river entrenchment.

Geologically, in this area the loose covering strata, 42 – 45 m thick, are of Quaternary system, and the basement is composed of Paleozoic strata . From the top to the bottom, the Quaternary sediments are represented by the Middle Pleistocene alluvial sand, glacial loam and clay loam, the Lower-Middle Pleistocene fluvioglacial sand and limnoglacial loamy sand. The Pleistocene deposits overlap the Upper Carboniferous limestones of the Ratmirovskaya Formation with the thickness of 4 – 6 m, and the clays of the Voskresenskaya Form., 7 – 10 m thick. Strongly fractured and karstified the limestones are composed of blocks and fragments with sand filler. The clays characterised by the cohesion of (0,6 – 1,7)10^5 Pa are usually semi-hard plastic and plastic. The Upper and Middle Carboniferous limestones and dolomites (C_2-C_3), lying bellow, are indivisible. Fissured and karstified they have some holes filled with residual colmatage formations of Paleozoic age. The traces of recent karst and large caves have not been encountered.

The upper unconfined aquifer, 2 – 3 m thick, is present within the alluvial sands. The glacial loams serve as an aquitard for the surficial water, and they are the confining bed for the first confined aquifer, which is formed by the Quaternary sands and limestones of the Ratmirovskaya Form. The potentiometric level rises to the height of 2 – 4 m from the loam base. It is 3 – 6 m lower than the water table. The second confined aquifer is found within the (C_2-C_3) deposits. The clays of the Voskresenskaya Form. function as a major separator dividing the ground water from the karst one. The long-continued karst water withdrawal resulted in the decline of the potentiometric level to tens of metres. At the site the difference in elevations between the heads of the confined aquifers was equal to 28 – 35 m in 1989. Since the last eighty years the karst water uptake has been decreased, and the water levels have been reestablishing.

Comparing the critical values of karst-water head decline obtained from formulae (7) with those of the real one (more than 28 – 35 m), we can see that the aquitard of the Voskresenskaya Form. must be entirely disturbed. Really, in the early eighty years the author observed but was not able to explain the local changes in the clay consistency and thickness in the area. For example, it was found that the Upper Carboniferous clays became soft plastic at some sites of the North-West region, they were easily rumpled by hands and had numerous folded folds. At the site, the relatively large thickness of the clay screen and the absence of large karst voids as well prevent from the downward movement of the disintegrated clays and overlying soils. That is why we find no sinkholes in the area. However, the aquitard failure and the alteration of the clay properties can cause the following compaction of the overburden even under hydrostatic conditions.

5. CONCLUSIONS

1. The process of spalling and crumbling of a confining layer or an aquitard over a weakened zone (cave, karst cavity, open-joint fissure, ancient collapse funnel, etc) under water head decrease is named casual hydrofracturing. The analysis of this phenomenon permits to obtain the simplest relations between the failure magnitude of water head decline, the cohesion of relatively impermeable rock, and the thickness of aquiclude, which can be simply used in engineering practice.

2. Both theory and experiments testify to the possibility of partial or complete disturbance of thick clay screens near a single fissure or cavern. Commonly, aquifers composed of carbonate rock are strongly fissured and karstified. Developing in vicinity of many weakened zones the hydrofracturing can form weak interbeds inside clay beds and lead to the dilation of unbound overburden. This can be the cause of extremely high rock compressibility and following subsidence.

3. Taking into account the geological and hydrogeological conditions of the North-West region of Moscow city and the long-term pumpage of the fissure water as well one can consider that it is casual hydrofracturing of the aquitards which have been producing either sinkhole development or land subsidence, as in the case mentioned above.

Acknowledgements

The author is indebted to E. V. Kalinin for the discussion of the obtained results. This research was supported by grant from Russian Ministry of Education.

REFERENCES

Anikeev, A.V., (1988) Conditions of similarity of water saturated model from equivalent materials and rock massif (English translation from Russian, by Allerton Press, Inc.). *Inzhenernaya Geologiya*, No 2, 78-84.

Anikeev, A.V., (1991) Clay collapse over caves and caverns. In: *Geological Hazards*. Proc. of Beijing International Symp. (Beijing, China, October 1991), 336-342.

Anikeev, A.V., (1993) Two forms of destruction of bound soils over cavity (in Russian). *Geoekologiya*, No 2, 115-123.

Anikeev, A.V., (1999) Casual hydrofracturing theory and its application for sinkhole development prediction in the area of Novovoronezh Nuclear Power House-2 (NV NPH-2) Russia. Proc. of the 7-th Multidisciplinary Conf. on Sinkholes and Karst (Harrisburg-Hershey, Pennsylvania, April 1999). Rotterdam, A.A. Balkema, 77-83.

Land subsidence, ed. by F.B.J. Barends, F.J.J. Brower & F.H. Schröder, (1995) Proc. of the 5-th Intern. Symp. (the Hague, October 1995). IAHS Publ., No 234, 492 pp.

Osipov, V.I. & Medvedev, O.P. (eds.-in-chief), (1997) *Moscow: Geology and City* (in Russian). Moscow, Moskovskiye uchebniki i kartografiya, 400 pp.

Poland, J.F., (1981) Subsidence in United States due to Ground-Water Withdrawal. J. of the Irrigation and Drainage Division, ASCE, Vol. 107, No IR2, June, 115-135.

Terzaghi, Karl & Peck, R.B., (1967) *Soil Mechanics in Engineering Practice.* New York, John Wiley and Sons, Inc., 2d ed., 729 pp.

LAND SUBSIDENCE - Vol. I
Proceedings of the Sixth International Symposium on Land Subsidence
Ravenna / Italy / 24-29 September 2000

EVALUATION OF RECENT LAND SUBSIDENCE AND PRESUMPTION OF GEOLOGICAL STRUCTURE IN THE NOBI PLAIN BY GIS

Kenji Daito and Hiroyuki Yamane
Department of Civil Engineering, Daido Institute of Technology
40 Hakusui-cho, Minami-ku, 457-8532 Nagoya Japan

Abstract

In this study, the reason for the enlargement of the area of land subsidence in the Nobi Plain in the period of 1994 was evaluated by using observed data of groundwater level, groundwater withdrawal and ground shrinkage. The Kanie district was selected as the representative area of land subsidence in the Nobi Plain. Land subsidence of the Kanie district was visualized by GIS based on the level of bench marks, groundwater level and thickness of clay strata. From the result of this study, it was realized that changes in bench mark levels and in the lowest groundwater level in a year resemble each other, and that changes of the level of bench marks depended on the thickness of clay strata.

Keywords: water shortage, groundwater withdrawal, land subsidence, groundwater management, GIS

1. INTRODUCTION

Many people have studied land subsidence of the Nobi plain to stop land subsidence (Daito, et al., 1991, Kuwahara, et al., 1976, Sato, et al., 1986 and Ueshita & Daito, 1984). However, an extreme shortage of water in 1994 has enlarged the area of land subsidence in the Nobi Plain. In the summer of 1994, water supply was restricted for a long period of time and over wide area due to the extreme shortage of water. So many enterprisers who usually used surface water turned to use groundwater in this period. The change of observed groundwater level showed this fact. In this period, groundwater level dropped rapidly. It was drawn down near or lower than the safety groundwater level. This safety groundwater level was estimated by one of the authors on an earlier occasion (Daito, et al., 1992). Although the groundwater level in the Nobi Plain was recovered by increased precipitation in September, land subsidence in some districts did not recover.

2. GENERAL CONDITION OF UNUSUAL SHORTAGE OF WATER IN 1994

2.1 Situation of precipitation and the amount of dam storing water

The precipitation at Nagoya Local Meteorological Observatories was 50-70% of normal precipitation in the period from March to June 1994. The amount of storage water in the dams in the Kisogawa water system kept decreasing for this period. Water saving was started at the Makio dam on June 1 and started at the Iwaya dam on June 9. Precipitation became about 30% of the common year in July and August. The Makio dam (available water storage is 68 million m^3), the Iwaya dam (available water storage is 61.9 million m^3), and the Agigawa dam (available water storage is 44 million m^3) had dried up on August 5. However, there was a much rainfall according to the rain front in autumn and typhoon since the middle of September. As a result, the amount of water storage in the dams recovered, and a water saving was eased in October.

2.2 Situation of the amount of groundwater pumping

The amount of groundwater pumping in the entire Owari region increased from July to September in 1994 in comparison with the previous year, though the amount of groundwater pumping in the entire Owari region decreased until June in 1994 in comparison with the previous year. The amount of groundwater pumping after October in 1994 decreased in comparison with the previous year.

2.3 Situation of groundwater level and ground shrinkage

Measurement of the first class bench mark was executed to understand the situation of the land subsidence in the Nobi Plain on November 1 every year. The number of measured bench marks was 1514 points in 1994. When the leveling result was computed, they revealed the generation of land subsidence in the large area shown in Fig. 1. The area subsided more than 2 cm in a year was about 77 km^2. And the area subsided more than 1cm in a year was about 656 km^2.

In the Owari region, the groundwater level and the amount of ground shrinkage are continuously observed in the typical observation wells in each management block of "Owari Regional Groundwater Management System" as shown in Fig.2. The relation between the groundwater level and the amount of ground shrinkage at each management block in 1994 was considered based on these observation results (Daito & Ueshita, 1996). In this paper, the relation between the groundwater level and the amount of ground shrinkage in only the 3rd block is explained.

The situation of the groundwater level and the amount of the ground shrinkage in 1993 and 1994 is shown in Fig. 3 simultaneously. The following is understood from this figure. In 1994, the ground had shrunk when the groundwater level became

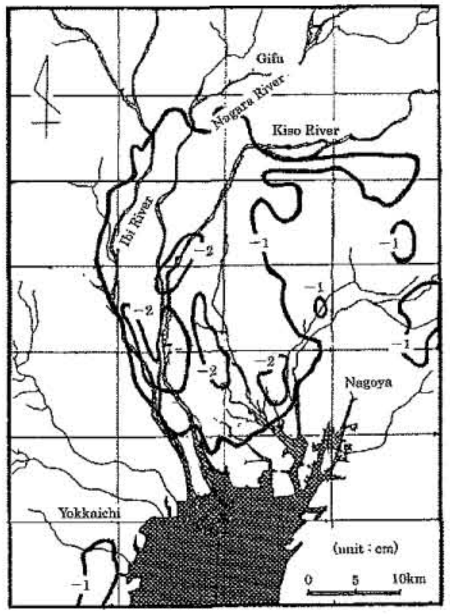

Figure 1. Subsided areas (more than 1 cm/year) in the Nobi Plain from Nov. 1993 to Nov. 1994.

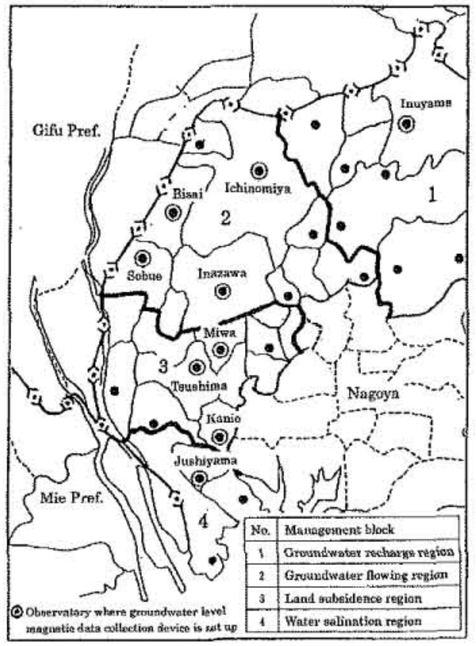

Figure 2. Groundwater management blocks and observatories in the Owari region.

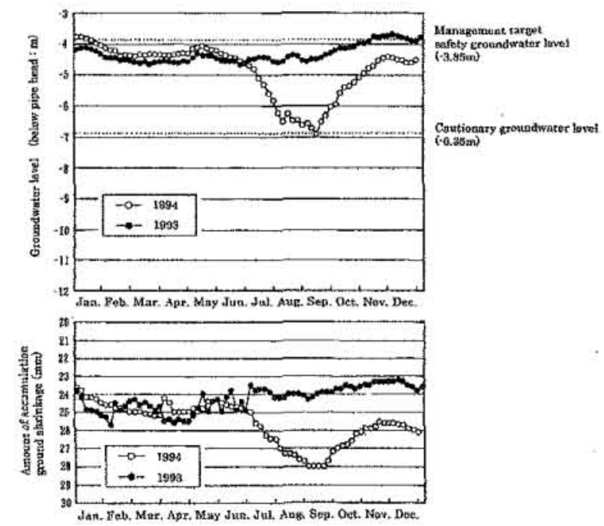

Figure 3. Change of groundwater level and ground shrinkage for a year at the Tsushima observation well (144.5 m in depth) in the 3rd groundwater management block in 1993 and 1994.

lower in summer, and the ground had expanded when the groundwater level became higher. This shows that the ground up to the depth of the 2nd confined aquifer included clay strata was transformed most elastically corresponding to the change in the effective stress, which change was according to the change of the groundwater level of the aquifers. It is speculated that the effective stress, which increased due to lowered groundwater level, was below the consolidation yield stress of the clay strata, and the strata were in a state of the overconsolidation. Minor land subsidence was observed in the 3rd block due to unexpected geological conditions.

3. VISUALIZATION OF LAND SUBSIDENCE BY GIS

3.1 Outline of the research district

Lowering of the confined groundwater level and a distribution of thick clay stratum are thought to be the cause of land subsidence in the Nobi Plain. The Kanie district was selected as a typical subsidence region of the Nobi Plain as shown in Fig. 4. The Kanie district belongs to the 3rd block of "Owari Regional Groundwater Management System". Geo-environmental information in this region, for example, level of the bench mark, groundwater level, and distribution of the thickness of the clay stratum, were arranged to visualize by GIS (Arc View 3.1). An effort was made to clarify the relation among land subsidence, groundwater level, and thickness of the clay stratum based on this geo-environmental information.

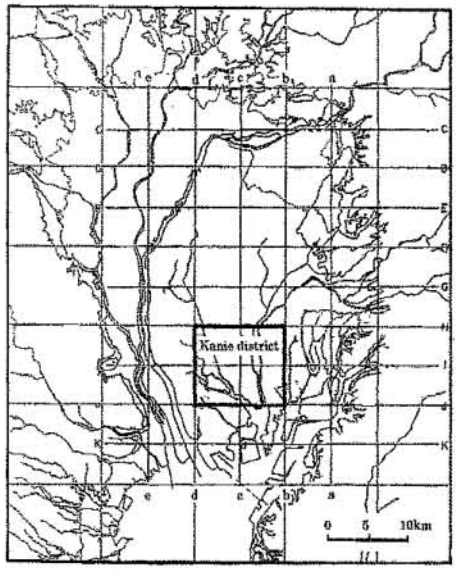

Figure 4. Geological cross section position chart of the Nobi Plain.

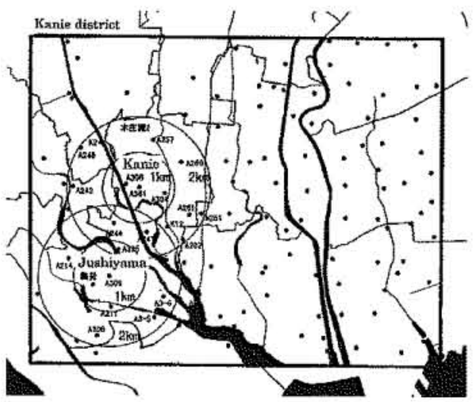

Figure 5. First class bench mark in the range within 2 km in radius from the Kanie and the Jushiyama observatory.

3.2 Relation between the amount of altitude change and groundwater level

The positions of the first class bench marks set up in the Kanie district shown in Fig. 5 were represented by X-Y coordinates to make the land subsidence situation in this district visible. The contour line charts of yearly land subsidence for 1989-1997 were made based on the observation data of each bench mark. Correlation diagram was made to understand the relation between the groundwater level change and land subsidence in the Kanie district based on the level of the bench mark and the yearly lowest groundwater level from 1989 to 1997 at the Kanie observatory (wells are 59 m in depth, 143 m in depth, and 281 m in depth) and at the Jushiyama observatory (wells are 55 m in depth, 163 m in depth, and 307 m in depth).

3.3 Relation between the amount of altitude change and the thickness of clay strata

The boundary depths of the gravel strata and clay strata were measured on the six geological cross sections, which crossed in the Kanie district. The geological cross sections extended east and west in the Nobi Plain were made at intervals of about 10.3 km, and the cross sections extended north and south had been made at intervals of about 8.4 km (Kuwahara, et al., 1976). Each cross section, which belonged to the Kanie district, was divided into 10 zones by 11 points.

Measurement of strata boundaries were made at the top and the bottom of the 1st gravel stratum (G1), the 2nd gravel stratum (G2), the 3rd gravel stratum (G3), and at the top of Tokai strata (Pliocene) at these 11 points. Contour line charts of the boundary surface and the contour line charts of the thickness of the clay stratum were made based on these measurement values.

Correlation diagram of the amount of altitude change and the thickness of the clay stratum at the location of each bench mark, which was within 2 km of the Kanie observatory and the Jushiyama observatory, was made. The correlation diagram of the thickness of clay stratum (C2) between the 1st gravel stratum (G1) and the 2nd gravel stratum (G2) and the amount of altitude change is shown in Fig. 6.

From this figure, it is seen that the thinner the clay stratum, the smaller the amount of the altitude change and thicker the clay stratum, the larger the amount of the altitude change, if the amount of the groundwater level change during the year was almost constant. It is thought that thickness of clay stratum is very significant on the altitude change.

4. CONCLUDING REMARK

Further use of the method using geo-environmental information for large area land subsidence prevention measures should be continued in the future.

Measuring geo-environmental information is necessary for the groundwater management in the Nobi Plain.

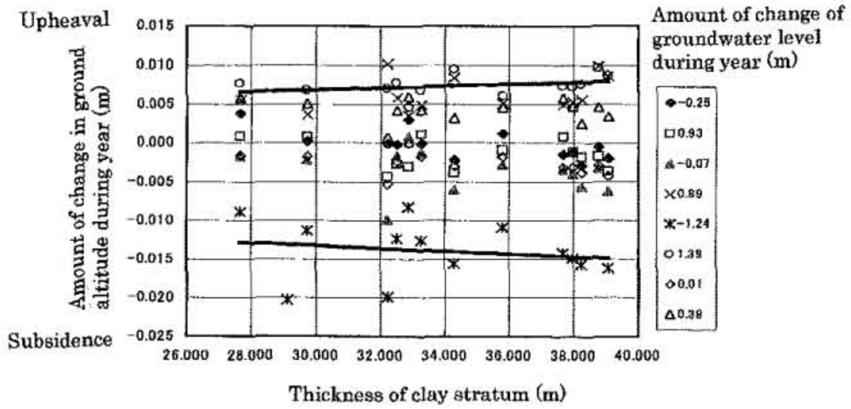

Figure 6. Correlation diagram of the thickness of the clay stratum (C2) and the amount of yearly change of ground altitude at each bench mark which is within a 2 km radius from the Kanie observatory.

Acknowledgements

The authors would like to express their hearty gratitude to the members of Department of Environment, Aich Prefecture and the persons and departments concerned.

REFERENCES

Daito, K., Mizuno, M. & Ueshita, K. (1991) Control of groundwater withdrawal for preventing land subsidence in the Owari Plain, Japan. *Proc. 4th Int. Symp. on Land Subsidence*, IAHS-AISH Publication 200, 533-542.

Daito, K., Amaya, S. & Mukaide, K. (1992) Geo-environmental considerations on use and control of groundwater in coastal alluvial plains. *Journal of groundwater hydrology, JSGH*, **34**(4), 263-282 (in Japanese).

Daito, K. & Ueshita, K. (1996) Extremely shortage of water in 1994 which enlarged area of land subsidence in the Nobi Plain. *Journal of groundwater hydrology, JSGH*, **38**(4), 279-294 (in Japanese).

Kuwahara, T., Ueshita, K. & Iida, K. (1976) Analysis of land subsidence in the Nobi Plain. *Proc. 2nd Int. Symp. on Land Subsidence*, IAHS-AISH Publication 121, 55-64.

Sato, T., Daito, K. & Ueshita, K. (1986) Analysis of land subsidence due to withdrawal of groundwater in the Nobi Plain. *Proc. 3nd Int. Symp. on Land Subsidence*, IAHS-AISH Publication 151, 89-99.

Ueshita, K. & Daito, K. (1984) Land subsidence in Japan, and a case study on the Nobi Plain. *Proc. Int. Symp. on Geotechnical Aspects on Mass and Material Transportation*, 439-460.

ANALYSIS OF SUBSIDENCE IN THE CROTONE AREA ALONG THE IONIAN COAST OF CALABRIA, ITALY

W. Bertoni [1], C. Bratti [1], L. Carbognin [2], C. Cesi [3], G. L. Chierici [4], G. Dossena [5], A. Guerricchio [6], U. La Monica [7], A. La Tegola [6], A. Succetti [5]

[1]*Crotone Municipality Deputy,* [2]*ISDGM-CNR Venezia,* [3]*Italian Geological Survay,* [4]*Bologna University,* [5]*ENI-AGIP Division,* [6]*Calabria University,* [7]*Italian Ministry of Industry*

Abstract

The Ionian coast of Calabria, South Italy, and in particular the coastal area of the province of Crotone, have been subject to subsidence over the centuries. The issue of whether this subsidence has been affected by anthropic activity due, in particular, to the extraction from the 1980's onwards of natural gas from offshore fields close to the coast has been questioned. To investigate this, a "Committee for the Study of Subsidence in the Crotone Area" was set up, operating from 1993 to 1998. After a series of surveys on the geology, geomorphology and hydrogeology of the area, the Committee scheduled and organised annual precision levelling campaigns along a coastal line 340 km long, as well as GPS satellite measurement levellings at the datum points located on 4 natural gas production offshore platforms. On the basis of the studies and levellings carried out, the Committee deemed that there are no existing elements showing that the extraction of gas from the offshore fields close to the area of Crotone have any significant impact on subsidence in the entire Crotone area. This subsidence (9 mm/y) is instead directly correlatable to the gravitational tectonics of the zones, as ascertained historically.

Keywords: land subsidence, Calabria Italy, precision levellings, satellite surveys, natural gas, offshore fields.

1. INTRODUCTION

The Ionian coast of Calabria, and in particular the coastal area of the province of Crotone (Fig. 1), have always been sites of human settlements from the VIII century BC onwards. Crotone was part of Magna Grecia, reaching the height of its splendour in the VI century BC, one reason being the Pythagorus's philosophical-mathematical school, which was established here. In 277 BC Crotone was conquered by Rome and became a Roman colony in the 1st century BC.

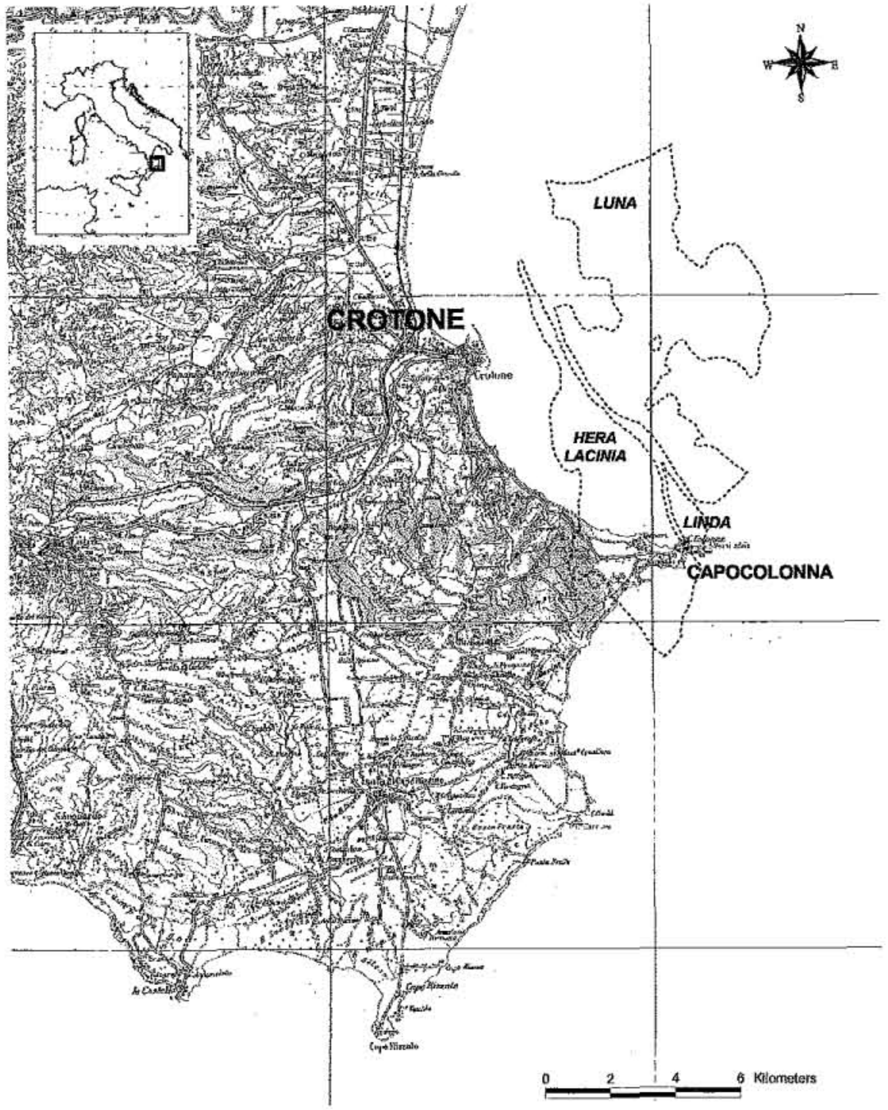

Figure 1. Map of the Crotone area, showing the location of the Luna, Hera Lacinia and Linda natural gas fields.

During the millennium of Greek and Roman rule, important temples, large amphitheaters, splendid villas and a whole range of smaller constructions such as houses, shops, etc were built. The modest ruins discovered during archaeological excavations are all of what is left of this glorious past, while one of the original 24 columns of the Greek temple of Hera Lacinia is the only evidence still standing. This column rises, facing out to sea, on a promontory called Capo Colonna (Fig. 2).

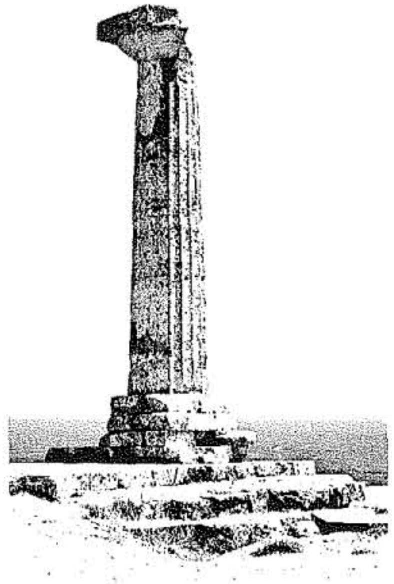

Figure 2. The only column of the Greek sanctuary of Hera-Lacinia (V century BC) still standing on the promontory called Capo Colonna.

The destruction of buildings (not only Greek-Roman) constructed in the Crotone area was due not only to vandalism, but above all to the instability of the surface of the ground (differential subsidence) which has always affected this area. The causes of this subsidence are natural (selective erosion and seismic activity on a regional scale) and anthropic (above all agricultural activities).

From 1975 onwards, besides traditional anthropic activities, natural gas began to be extracted from the deep fields discovered in the Crotone area both onshore and offshore (Fig. 1).

Obviously the local population was highly concerned, fearing that natural gas extraction would accentuate the subsidence, resulting in damage. In such a situation, there is obviously a risk that local public opinion, adopting the well known principle of "*post hoc, ergo propter hoc*"[1], attributes the extraction of natural gas from deep fields as the cause of any subsidence, or worsening of subsidence, and thus as the cause of any damage to material assets or any disturbance to anthropic activities which can be potentially related to subsidence.

The most rational way to clarify the complex mechanism of subsidence in the Crotone area and its environmental effects was to set up a Committee for the study of subsidence in the Crotone area (this report was compiled by the members) and to carry out surveys (discussed herein).

[1] "Event B happened after event A; so, it is certain that event A caused event B".

2. GEOLOGY AND GEOMORPHOLOGY

The geological and geomorphologic framework of the Crotone area (see Fig. 1) is characterised by a coastal plain with a maximum width of approximately 4 km, which gradually thins out southwards to practically disappear close to Capo Colonna, and in the hill area where the old town centre of Crotone stands.

The coastal plain is bounded towards the interior by a range of hills, with a maximum height of 200 m, consisting of mainly shale facies (Cutro shale), belonging to the last Plio-pleistocenic sedimentary sequence, which is transgressive on the crystalline raps dating from the Palaeozoic. Due to the gradual reduction of the coastal plain, the range of hills in the southern part of the territory of Crotone commune extends down to the sea.

The Cutro shales are transgressively overlapped by sediments of a marine terrace sequence with a mainly calcarenite facies, 2-3 m thick maximum, which constitute the topographic termination of the hills.

The areal amplitude of these terraces is highly variable, and affected by the rate at which erosion pushes back the underlying shale slopes.

The hills have many incisions, corresponding to the course of the rivers Esaro and Neto and their main tributaries. Generally speaking, these incisions have a wide valley bottom with a flat morphology or very bland sloping of the bed at the bottom of the hills and are filled with products washed away from the surrounding hill slopes. Besides the geological framework, the geological-structural aspects of the Crotone area itself are of major interest. These consist of series of faults, which displace the Plio-pleistocenic shales, and sedimentary cover of the upper Pleistocene.

The recent age of these faults is confirmed by the conservation, in many cases, of fault scarps despite the mainly loose nature of the displaced sediments.

Two main fault systems can be identified in the Crotone area, trending ENE – WSW and NNE – SSW, with subordinate systems trending E – W, NW – SE, NNW – SSE.

The two main fault systems are tensional and transcurrent respectively, the first dipping SSE and the second subvertical, slightly dipping eastwards.

The above would seem to indicate that the terrain of the Crotone basin, affected by tensional phenomena, is gradually slipping SSE, as proven too by the coast extending in this direction.

Another highly significant geodynamic aspect, which is strictly related to the one above, is the well-known seismic activity of Calabria and the entire Crotone area.

To sum up, the most important morpho-evolutive aspects are:

a. Strong coastal erosion induced by the sea, especially when the winds of the second quadrant blow, due to the major expanse of open sea in the S – SE direction. This aspect is particularly important in the southern part of the Crotone area where the near total absence of the coastal plain means that the erosive action of the sea has a direct effect on the shale formations. This causes rapid coastal retraction and landslide induced phenomena, with effects, which have clearly taken their toll over the centuries on the Magna Grecian buildings at Capo Colonna. Also worth noting are the remains of walls dating from this age, which lie in the sea at the bottom of the headland, ruined centuries before any hydrocarbon production activities began.
b. Proceeding inland, an important factor, which promotes the instability affecting the Crotone area, is the different behaviour of the calcarenite banks compared to that of the shale levels they overlap.
   The calcarenite bank, which is permeable due to the porosity created by diagenetic phenomena and highly fractured, has enabled underground water circulation to develop thus contributing to the deterioration of the bank's mechanical characteristics. The shales which the calcarenites onlap are subject, due to the action of the water flow, to plasticization and solution phenomena which reduce the mechanical characteristics. As a result, the reaction to erosion and the stability of surface terrains are governed by mechanical parameters close to the residual state. These deterioration processes are clearly more active and have a quicker evolution along the coastal part, due to the reasons mentioned in point a.
c. The terrain filling the recently formed valley incisions consists of loose materials with a high shale content, considered "soft" in geomechanical terms, with marked plasticization of the pelitic part.

3. HYDROGEOLOGY

There are two orders of marine terraces directly overlapping the shales in the Crotone area: the first at heights of 15 to 50 m approximately, and the second above a height of 140 m. An aquifer is present in the calcarenites of the first terrace and before the 1950's the water was extracted by agricultural wells to irrigate farming land.

Agricultural reforms passed in the 1950's (which were also responsible for the previous Mediterranean maquis being eliminated) rationalised irrigation techniques. Nowadays, water is obtained from a basin, which lies outside the area and is distributed by a network of canals.

Thus the pre-existing dynamic equilibrium of the aquifer in the first terrace has changed. Prior to the reforms, irrigation water followed a closed cycle (apart from the contribution of infiltrated rain water), where the surplus water which was not absorbed by farm land, or not evaporated, automatically drained back, by gravity, to the aquifer it had been extracted from.

A feedback process therefore existed, helping to attenuate oscillations of the piezometric surface of the aquifer caused by water extraction for irrigation purposes at variable flow rates over time.

With the current "post 1950" technique, the surplus irrigation water which is neither absorbed nor evaporated reaches the aquifer of the first terrace, but water is not extracted from here. Consequently the feedback process no longer exists: instability of the piezometric surface may thus develop, possibly increasing differential subsidence or in any case unsettling buildings as a result of both the increase in interstitial pressure in the terrain and the softening of shales in areas previously above the capillary fringe.

Four isophreatic maps, surveyed in January and April of 1995 and in March (Fig. 3) and June of 1996, show how the water in the first terrace aquifer mainly flows in a SSE direction. The water is discharged into the Ionian Sea along the cliffs: as a result, erosion of the shale banks of the cliffs is accentuated and this in turn increases the instability and induces landslides.

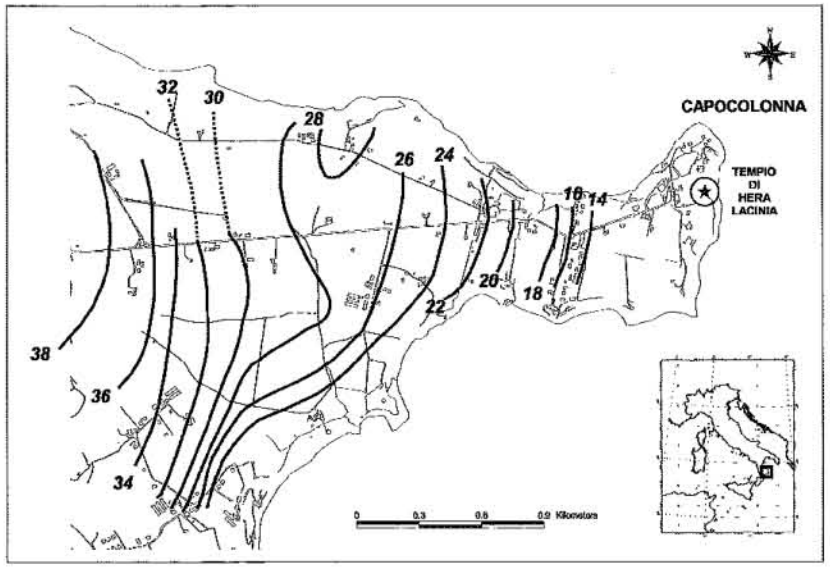

Figure 3. Map of iso-phreatic lines, as resulting from the March 1996 survey in the Crotone area.

4. GAS PRODUCTION FROM FIELDS IN THE CROTONE AREA

Table 1 shows the main characteristics of the 3 gas fields, Luna, Hera Lacinia and Linda, discovered by Agip S.p.A. (now ENI Agip Division) in the Crotone area, from the 1960's onwards.

The gas/water contacts of all three fields are located at 1,700 m below sea level (m.b.s.l.). Their reservoir rocks, with a thickness ranging from 20 m to 150 m, consist of sandstone and conglomerate levels, cut by numerous faults, with interbedding silt and shale. The Luna and Linda fields are entirely offshore, while Hera Lacinia, which is mostly offshore, also extends onshore with its maximum extension at Capo Colonna (Fig. 1).

Initial reservoir pressure at the reference depth of 1,700 m.b.s.l., was 215 kg/cm? for all three fields.

Luna went into production in May 1975, while Hera Lacinia and Linda both went into production in January 1980. Gas production lowered reservoir pressure, which, at 1 January 1999, was 80 kg/cm? for Luna, 135 kg/cm? for Hera Lacinia, and 100 kg/cm? for Linda.

Table 1. Main characteristics of the Luna, Hera Lacinia and Linda fields

	Unit	**Luna**	**Hera Lacinia**	**Linda**
No. pools		1	3	1
Datum depth	m.b.s.l.	1700		
Age		Miocene		
Lithology		Sandstones, conglomerates, silt, shales		
Net pay (min-max)	m	20-150		
Hydrocarbon bearing area	ha	3500	2200	300
Porosity (min-max)	%	15-30		5-14
Permeability	mD	5-1000		0.2-5
Original gas reserves	$G.sm^3$	47.9	8.5	
Starting date of production		May-75	Jan-80	Jan-80
Initial reservoir pressure at 1700 m b.s.l.	kg/cm^2	215		
Gas produced at 1.1.1999	$G.sm^3$	39.23	3.33	0.91
Average reservoir pressure at 1.1.1999	kg/cm^2	80	135	100

5. MONITORING SUBSIDENCE IN THE CROTONE ON- AND OFFSHORE AREA

A geodetic network for the high precision detailed geometric levelling of vertical movements of the terrain along the entire Ionian coast of Calabria, with branches in the Capo Colonna area, was set up (Fig. 4). This network was based

Figure 4. Map of geodetic network for high precision levelling of the terrain in the Crotone area.

on 212 bench marks, overall length 340 km, connected at both ends to two datum points (Soverato and Castrovillari) of the IGM national levelling network which, on the basis of IGM data, had a good stability over time.

The altimetric profiles recorded at each of the 6 levellings carried out in September of 1993, '94, '95, '96, '97 and '98 are shown in Fig. 5 for the coastal sections; Steccato-Capo-Colonna-Crotone overlooking the Luna, Hera Lacinia and Linda fields; Crotone-Cirò; and Cirò-Rossano.

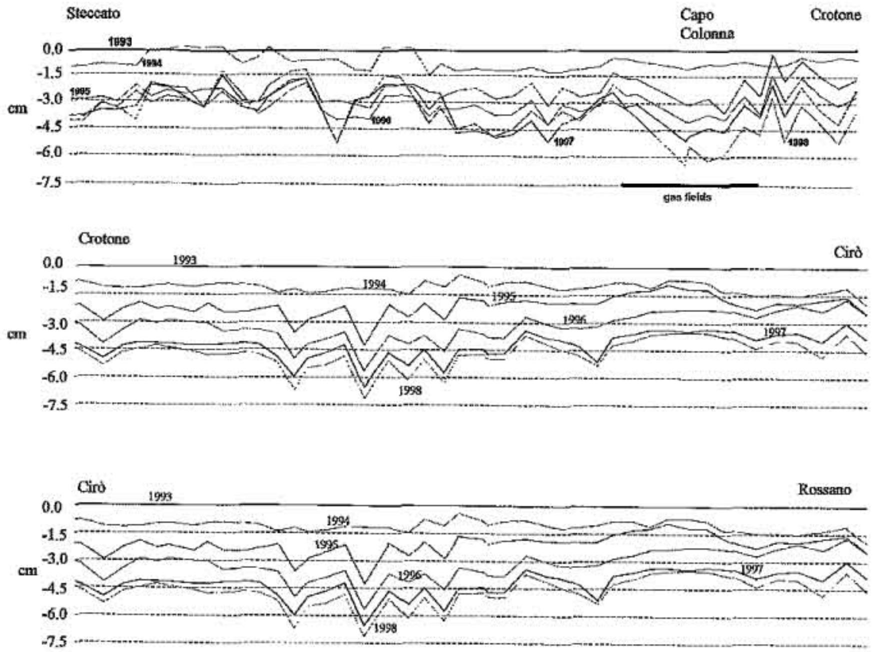

Figure 5. Annual ground elevation between 1993 (base) and 1998 along the levelling lines from Steccato-Capo Colonna-Crotone-Cirò-Rossano.

With reference to the entire levelling line from Soverato to Castrovillari (see fig. 4), the results of the surveys carried out in the 1993-1998 period show that the average land lowering of the coast along these 340 km was of about 45 mm, corresponding to 9mm/y. The detailed representation of the occurred subsidence in figure 5 zooming the local situation (i.e., in the area facing the offshore fields of Luna, Hera Lacinia and Linda[2]) is shows that:

- along the 40 km internal levelling line as well as along the 55 km stretch of coastal line from Steccato to Crotone (see Fig. 4), the average land sinking between 1993 and 1998 was about 45 mm (9mm/y);

[2] As this is closest to, and partly overlying the fields, it should be affected most by gas extraction and the resulting drop in reservoir pressure.

- only along a second survey line, 13 km long, running between Campione and Capo Colonna (see Fig. 4 for exact location) a maximum lowering of 60 mm (12mm/y) was observed at the end of the Cape;
- the two more critical land subsidence values are found between Cirò and Rossano where a peak of 70 mm (14 mm/y) was recorded more than 45 km NNW of the gas field area, and between Rossano and Tor Cerchiara (over 90 km NNW from Crotone) where the highest sinking, equal to 85 mm (17mm/y) occurred.

It is worth mentioning that the average subsidence rate observed in this period is consistent with that resulting from levelling surveys carried out by the ENI-AGIP Division from 1972 to 1991.

As concerns geodynamic offshore monitoring the Committee set up a network for taking GPS satellite measurements. The datum points of this network were located on the offshore platforms of Luna A, Luna B, Hera Lacinia 14 and Hera Lacinia cluster and at two onshore reference bases (Fig.6).

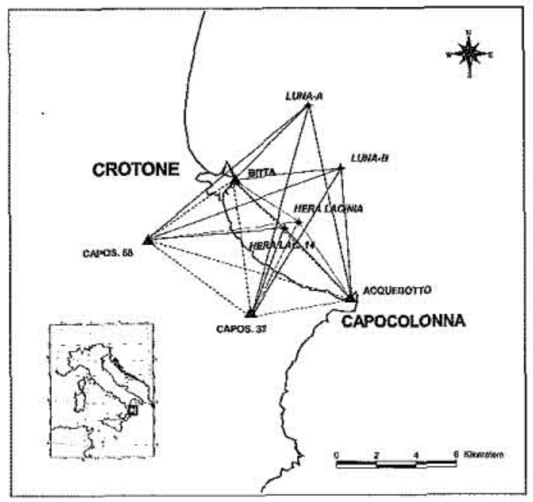

Figure 6. Networks of datum points on the offshore platforms Luna A, Luna B, Hera Lacinia 14, Hera Lacinia cluster, and the onshore datum points 58 and 32 used for GPS satellite survey.

A coastal polygon was then added. This extended from 5 km S of Capo Colonna to 3 km North of the town of Crotone, with the 20 datum points coinciding with the 20 datum points used for onshore precision levellings.

Six Leica System 9500 dual frequency receivers, with a minimum duration of 3 hours (1.5 hours for two sessions), were used at the same time, at each datum point, for the surveys. The static differential method was adopted, because of the moderate length of the bases to measure, which enabled an accuracy rate of ± (1 cm + 1 mm/km of the base).

Seven GPS satellite survey campaigns were conducted: 1 campaign each for the years 1993, 94, 95, 97 and 98, plus two campaigns during 1996. The results are shown in Fig. 7.

The results of the GPS measurements (Fig. 7) basically confirm the trend of the levelling surveys. In fact, the GPS measurements do not increase knowledge about the situation as they are less accurate than the levellings.

In conclusion, on the basis of the data acquired from the surveys it conducted and of levelling surveys 1972-1992 provided by ENI-AGIP Division, it was found that along the entire Ionian coast of Calabria, from Soverato to Castrovillari, extending 340 km, geodynamic behaviour was homogeneous, with an average lowering of 9 mm/year. The Committee also showed that subsidence in the section of coast facing the Luna, Hera Lacinia and Linda fields was not accentuated compared to the regional trend above.

6. ATTEMPT AT MODELLING SUBSIDENCE

The phenomenon is simulated using a numerical model, limiting the study for simplicity's sake to the Hera Lacinia and Linda fields. These fields, which partly extend onshore (Fig. 1) have the most likelihood of causing a subsidence fan detectable by levellings.

The simulated area lies between the UTM co-ordinates 2685000-2733000 East and 4300000-4350000 North (see Fig. 1), reaching a maximum depth of 20 km. All the main structural elements and geological formations of interest were included in the model: the 7 hydrocarbon bearing levels of the Hera Lacinia field and the 2 of the Linda field put into production, as well as the main sub-vertical faults which, present at major depths, rise to the top of the hydrocarbon bearing formations.

Due to the complex nature of the geological structure studied and the limited nature of data available, the behaviour of the faults was approximated using a simple, cautious, linear approach.

The results of subsidence modelling (conducted by Med Ingegneria and concluded in December 1998) should be considered as preliminary. In fact, it has not been possible to use the results, currently being processed, from the new3D seismic survey acquired in the ENI-AGIP area, nor the dynamic reservoir model based on said results. The model therefore provides an initial approximation analysis, which only indicates the magnitude of the maximum lowering values observed at the centre of the field from the start of its development (10 cm), with lower values in the coastal areas of interest to the Committee. At present, on the basis of modelling results, no definitive conclusions can be made.

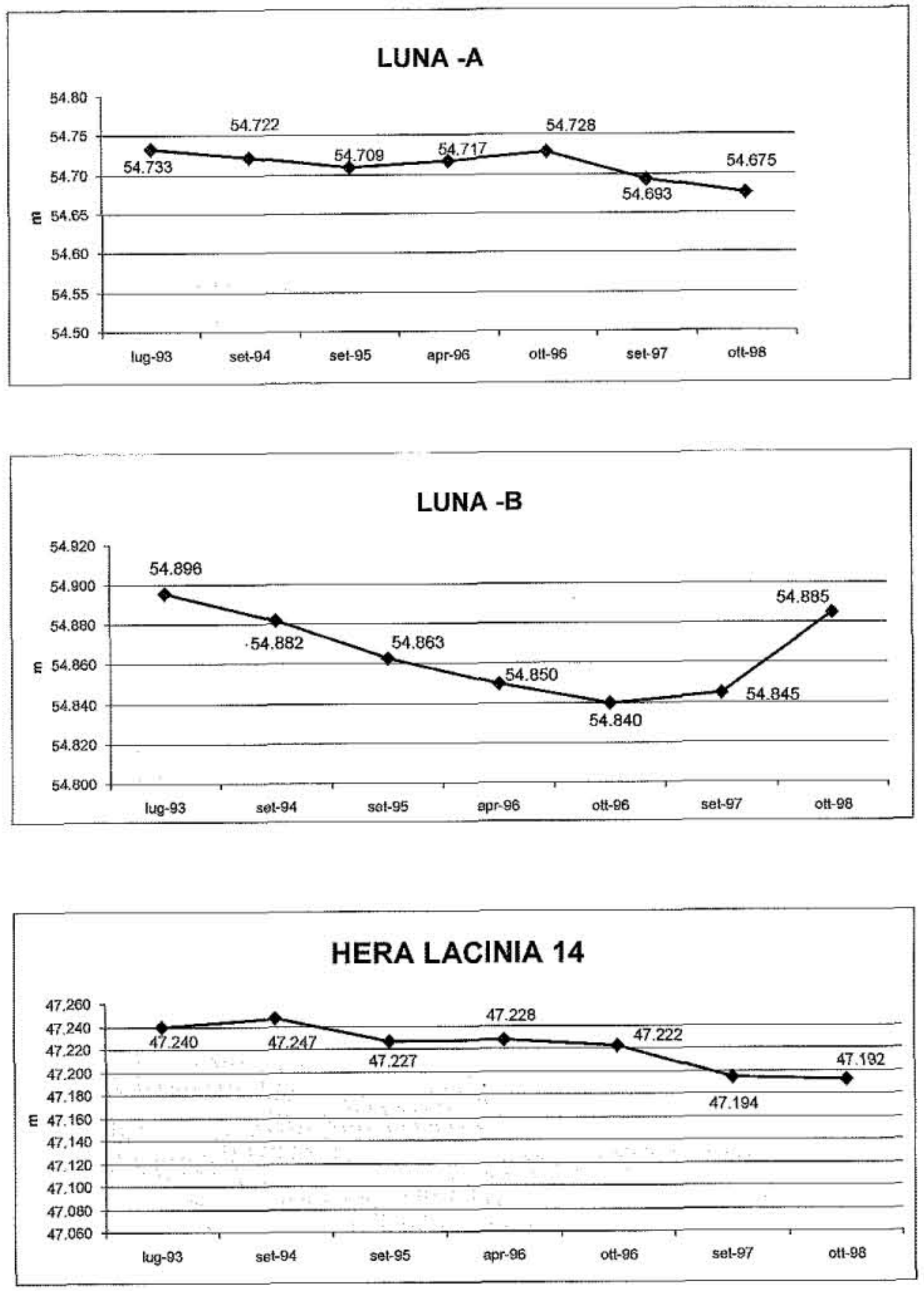

Figure 7. GPS satellite surveys on the Luna A, Luna B and Hera Lacinia 14 offshore platforms. Datum point elevation (meters) vs. time in the period July 1993 – October 1998.

7. CONCLUSIONS

The studies on land subsidence described in this report, are those assessed by the "Committee for the Study of Subsidence in the Crotone Area".

The Committee, through the work of specialised service companies as well, carried out a geological-geotechnical study of the area, a hydrogeological study on the aquifer which is active in the zone, 6 annual precision levelling campaigns along the coastline for 340 km, from Soverato to Castrovillari and 7 GPS satellite survey campaigns in the area of the Luna, Hera Lacinia and Linda offshore fields as well as onshore. ENI-Agip Division furthermore provided the Committee with the data of levelling surveys 1972-1992.

The hypothesis that natural gas extraction from these fields could potentially contribute to subsidence was evaluated in depth, also using a numerical model.

On the basis of the studies carried out and the field surveys conducted over the five year period 1993-1998, the Committee deemed that the subsidence measured along the surveyed coastline is correlatable to the gravitational tectonics of the area, as historically ascertained. There are no existing elements showing that gas extraction from the offshore fields in the Crotone area has any significant impact on the lowering of the terrain in the entire zone and in particular along the Ionian coast in the Crotone area.

LAND SUBSIDENCE - Vol. I
Proceedings of the Sixth International Symposium on Land Subsidence
Ravenna / Italy / 24-29 September 2000

STRUCTURAL DAMAGE BY UNIFORM SUBSIDENCE

Arnold Verruijt and Ronald B.J. Brinkgreve
Delft University of Technology, Delft, The Netherlands

Abstract

It is often assumed that uniform soil subsidence will not lead to structural damage of buildings because the foundation will simply subside together with the soil. In areas in which the groundwater level is close to the soil surface, and mainly controlled by sea level (conditions that prevail in large parts of The Netherlands) a shallow foundation, with its foundation level below the groundwater level, may however lose part of its bearing capacity when the soil level subsides and the groundwater level is maintained at its original level. If the foundation of the structure is loaded non-uniformly, with a variable safety against failure in different parts of the structure, this may lead to non-uniform settlements of the structure, and possible damage.

Keywords: subsidence; gas production; deformations; structural damage.

1. INTRODUCTION

Soil subsidence may be the result of various phenomena, natural or artificial. In the North of the Netherlands soil subsidence occurs because of the extraction of large quantities of natural gas from deep reservoirs. As the upper layers of the soil are very soft, subsidence can also be caused by other phenomena, such as lowering of the groundwater table, oxidation of organic material, loading of the soil by building activities, or traffic vibrations. It is often rather difficult to distinguish between the various forms of soil subsidence, and thus it may be difficult to attribute possible damage to a single cause.

The usual approach in determining the possible cause of structural damage is to investigate the various possible causes of soil subsidence, estimating the amount of damage each of these factors may have caused. For this purpose it is important to establish the geometrical extent of the subsidence of the soil surface. It is usually assumed that structural damage will occur only when the soil subsidence is non-uniform, and that damage is mainly caused by a curvature of the free soil surface, and, to a lesser extent, by a rotation. The large scale of the subsidence bowl caused by the extraction of gas and oil from deep reservoirs (in The Netherlands often at depths of several thousands of meters) in general leads to the conclusion that the shape of the soil subsidence is very uniform. It is then often concluded that such a uniform subsidence can hardly cause any structural damage of structures with dimensions of the order of magnitude of 10 to 50 meters. In reports on the soil subsidence in the provinces of Groningen (Commissie Bodemdaling door Aardgaswinning, 1987) and Friesland (Onderzoekscommissie Bodemdaling Friesland, 1990) structural damage is therefore mainly associated with local effects such as a non-uniform lowering of the groundwater table, in combination with inhomogeneous soil properties or inhomogeneous loading of different parts of a foundation.

A factor that may have been overlooked is the influence of a uniform soil subsidence on the bearing capacity of a shallow foundation if the groundwater table is above the foundation level, and is not directly following the soil surface. In The Netherlands this may happen because groundwater levels are usually prescribed and maintained with respect to a fixed datum, related to sea level. The effect of soil subsidence may then be a relative rise of the groundwater table, and this reduces the bearing capacity of the foundation (Verruijt, 2000). If the actual load on the foundation is close to the maximum value of the bearing capacity such a reduction of the bearing capacity may lead to a vertical deformation of the foundation, of the order of magnitude of the soil subsidence. This phenomenon will occur only in those parts of the foundation that carry the largest loads, so that the result may be that the vertical displacements of the structure are non-homogeneous, possibly causing damage to the structure. The same effect may, of course, also be caused by other forms of groundwater level rise, such as during floods or very heavy rainfall. And the various phenomena may also combine to jointly cause a loss of stability.

An important difference of the effect described above with the classical approach to the analysis of structural damage by soil subsidence is that in this case damage may occur in the case of a completely uniform soil subsidence. Such a uniform subsidence may lead to structural damage if the actual safety margin of the bearing capacity of the foundation is not uniform, and small. In modern structures this is not very likely, as the designer will use a sufficient margin of safety, but in older structures the large safety available when the structure was built may have been reduced considerably by much larger loadings (perhaps due to the weight of modern heavy equipment) than originally foreseen.

In order to estimate the magnitude of the effect a simple example will be considered in the next section. This will be followed by a more general theoretical consideration and a numerical validation of the theory.

2. EXAMPLE

Consider a building with a shallow foundation, at a depth of 1 m in a homogeneous rather soft soil. It is assumed that the initial level of the groundwater table is 0.60 m below soil level, and that the soil strength properties are c = 2 kPa, and φ = 20 degrees. The bearing capacity of the foundation can be determined using Brinch Hansen's generalization (Brinch Hansen, 1970; Craig, 1997) of the

formula originally developed by Prandtl (1970), Keverling Buisman (1940) and Terzaghi (1940). The usual form of this formula for the bearing capacity p of a strip foundation with a centric vertical load is

$$p=cN_c+qN_q+{}^1\!/_2B\gamma'N_\gamma, \qquad (1)$$

where c is the cohesion of the soil, q is the effective load adjacent to the foundation, B is the width of the foundation strip, and γ' is the effective unit weight of the soil. The coefficients N_c, N_q and N_γ are dimensionless coefficients, depending on the friction angle , see Table 1.

φ	N_c	N_q	N_γ
0	5.142	1.000	0.000
5	6.489	1.568	0.099
10	8.345	2.471	0.519
15	10.977	3.941	1.576
20	14.835	6.399	3.930
25	20.721	10.662	9.011
30	30.140	18.401	20.093
35	46.124	33.296	45.228
40	75.313	64.195	106.054

Table 1. Bearing capacity coefficients.

It is assumed that the width B of the foundation strip is 1 meter, that the unit weight of the soil above the groundwater table is 16 kN/m^3, and that the unit weight below the groundwater table is 20 kN/m^3 (so that the effective unit weight γ'=10 kN/m^3). If the level of the groundwater table is 0.60 m below the soil surface and the foundation level is 1.00 m below the soil surface, the effective surcharge is q = 13.6 kPa. In this case the bearing capacity of the foundation is p = 136.4 kPa. In classical soil mechanics this means that for a load below this critical value the deformations will be very small, but for a load exceeding 136.4 kPa the deformations will be very large. In reality the transition will be more gradual, but the limiting value is generally considered as a good approximation of the maximum bearing capacity.

If the groundwater table is raised by 0.20 m (or the soil surface is subsiding by 0.20 m with a groundwater level constant with respect to a fixed datum) the effective surcharge is reduced to q = 12.4 kPa. The bearing capacity then is p = 128.7 kPa, which is about 6 % less than the original value. If the load on the foundation is non-uniform, such that on one part the load is larger than 128.7 kPa, but lower than 136.4 kPa, and on another part the load is lower than 128.7 kPa, the part with the higher load will show large deformations when the groundwater table is raised, whereas the other part will show very small deformations only.

This means that under these conditions there will be unequal settlements of the foundation, possibly resulting in structural damage.

3. GENERALIZATION

In order to predict the magnitude of the additional settlement of a foundation due to a rising groundwater table the Brinch Hansen formula (1) may be reconsidered. It is usually considered that the bearing capacity factors can be expressed into the friction angle φ by formulas of the following form,

$$N_q = (1+\sin\varphi)\exp(\pi\tan\varphi)/(1-\sin\varphi), \tag{2}$$

$$N_c = (N_q-1)\cot\varphi, \tag{3}$$

$$N_\gamma = 2(N_q-1)\tan\varphi, \tag{4}$$

It is assumed that the foundation level is below the groundwater and remains so. If the original depth of the foundation below the soil surface is h and the depth of the groundwater table is d, the effective surcharge is

$$q = d\gamma_d + (h-d)(\gamma_s - \gamma_w), \tag{5}$$

where γ_d is the unit weight of dry soil, γ_s is the unit weight of saturated soil and γ_w is the unit weight of the groundwater. It is now assumed that the subsidence of the soil (relative to the groundwater table) is Δd, so that the depth of the groundwater level below the soil surface becomes d – Δd. It is furthermore assumed that the foundation load is practically equal to the bearing capacity, so that the building is on the verge of failure. This is the extreme case, most unfavorable for the foundation. The depth of the foundation can now be assumed to increase until the bearing capacity is back to its original value. Because the first and the third term in Brinch Hansen's bearing capacity formula are independent of the foundation depth, and the factor N_q also is constant, the settlement of the foundation can be estimated by requiring that the surcharge adjacent to the foundation, before and after the subsidence must be equal. This means that

$$q = d\gamma_d + (h-d)(\gamma_s - \gamma_w) = (d-\Delta d)\gamma_d + (h+\Delta d - d + \Delta d)(\gamma_s - \gamma_w), \tag{6}$$

from which it follows that

$$\frac{\Delta h}{\Delta d} = \frac{\gamma_d + \gamma_w - \gamma_s}{\gamma_s - \gamma_d}. \tag{7}$$

This factor will usually be about 0.5 or 0.6, which means that the additional settlement of the foundation will be of the order of one half of the soil subsidence. This may be unacceptable, especially if the settlement occurs only in part of the foundation. It should be noted that this is the extreme case, with the load on the foundation precisely at the failure limit, so even a very small reduction of the bearing capacity by the rising groundwater table will be the last straw to break the camel's back. It is expected that this situation will occur only in exceptional cases. Most foundations will have a sufficient margin of safety to accommodate the relatively small reduction of the bearing capacity.

4. NUMERICAL SIMULATION

The findings described in the previous sections have been further analysed by means of the finite element method using the program PLAXIS for geotechnical engineering (Brinkgreve and Vermeer, 1998). A 2D-plane strain finite element mesh with about 600 high-order elements (15-node cubic strain triangles) has been used to model the shallow foundation and its surroundings. The reason for using high-order elements is that these are capable of predicting failure loads quite accurately (Sloan and Randolph, 1982). The foundation itself is modelled

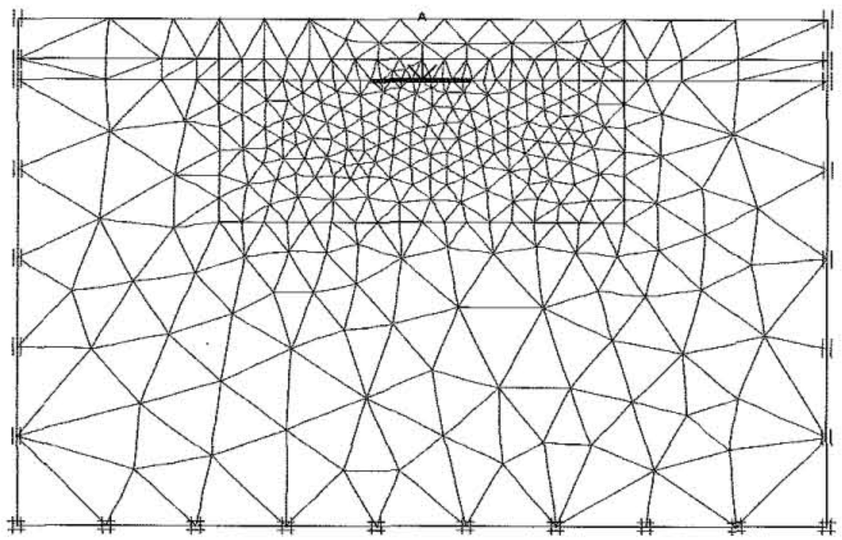

Figure 1. Finite element mesh of foundation model

as a 1 m wide stiff plate, using compatible 5-node Mindlin beam elements. The interaction between the plate and the sub-soil has been considered as rough. A unit point load is placed in the middle of the plate. The actual magnitude of the load is gradually increased in the calculations. In a rectangular area around the plate the mesh is refined, with a further refinement around the plate (see Figure 1). Two positions of the phreatic surface are considered: a lower level at 0.6 m below ground surface, simulating the original position of the phreatic surface, and a higher level at 0.4 m below ground surface, simulating the situation after 0.2 m global settlement of the sub-soil. The boundaries of the model are chosen such that the potential failure mechanism fully fits within the mesh and is not influenced by the boundary conditions. Standard boundary conditions are used, i.e. free vertical displacements and fixed horizontal displacements at the vertical boundaries, a fully fixed bottom and a free surface. Although the situation is plane strain, the stress state is three-dimensional, with three principal stresses σ_1, σ_2, σ_3. A full 3D Mohr-Coulomb model with tension cut-off is used to simulate the behaviour of the soil. Table 1 gives an overview of the model parameters. Since long-term settlement is considered, the behaviour of the soil is considered taken as fully drained. Most of the soil parameters (γ_d, γ_s, φ, c)

Parameter	Symbol	Value	Unit
Unit weight above phreatic line	γ_d	16.0	kN/m^3
Unit weight below phreatic line	γ_s	20.0	kN/m^3
Young's modulus	E	5000	kN/m^2
Poisson's ratio	ν	0.30	-
Friction angle	φ	20.0	°
Cohesion	c	2.0	kN/m^2
Dilatancy angle	ψ	0.0	°

Table 2. Soil parameters.

have been chosen in correspondence with the example described in Section 2. The additional parameters (E, ν, ψ) are chosen arbitrarily, but realistic for this situation. The stiff plate is weightless and is modelled as a linear elastic beam with an arbitrary normal stiffness EA = $1\cdot10^6$ kN/m and a flexural rigidity EI = $1\cdot10^4$ kNm^2/m. For the initial situation, hydrostatic pore pressures are generated beneath the phreatic surface and effective stresses are generated by means of a K_0-procedure, using $K_0 = 1-\sin\varphi = 0.658$.

For the numerical calculations, 4 situations have been considered:

1. Calculation of failure load in the situation with the low phreatic surface.
2. Calculation of failure load in the situation with the high phreatic surface.
3. Calculation of failure load in the situation with the high phreatic surface and the plate 0.1 m deeper.
4. Calculation of failure load in the situation with the high phreatic surface using large deformations.

The first calculation is to determine the actual bearing capacity of the shallow foundation using small strain theory. The second calculation is to determine the decrease in bearing capacity due to a 0.2 m relative increase of the phreatic Surface. The third calculation shows that the decrease in bearing capacity due to an increase in phreatic level is compensated by a deeper positioning of the plate of the order of half the increase in phreatic surface. The fourth calculation (an updated Lagrange analysis) is to show the same effect by simulating the actual penetration of the foundation into the soil using large deformation theory. In the latter calculation, pore water pressures are continuously regenerated in the updated geometry based on the original position of the phreatic surface.

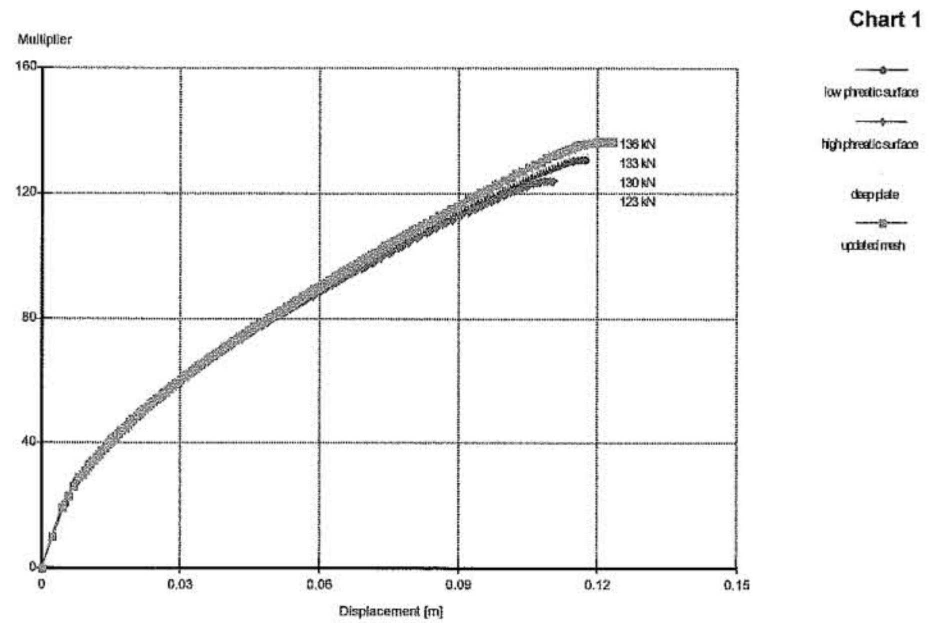

Figure 2. Load-displacement curves of plate centre point.

In all calculations the point load is increased until failure. Failure is defined as the point where the load cannot be further increased while the displacements keep on increasing. Hence, failure is associated with a horizontal end in the load-displacement curve. The load-displacement curves of the plate centre point are plotted for all four calculations in Figure 2, with an indication of the failure loads. Although the failure loads do not differ very much, the differences are clear. A relative change in phreatic level of 0.20 m is seen to result in a reduction of the bearing capacity by somewhat more than 5 %, as indicated by the second calculation. The original bearing capacity can be regained when the plate is positioned at a deeper level. In order to get a similar bearing capacity as the original situation, the deeper position must be in the order of half the change in phreatic level, as indicated by the third and the fourth calculations. This is a confirmation of the approximate computations presented in the previous sections.

Figure 3 shows the shadings of displacement increments from the updated Lagrange analysis. A sudden transition in magnitude gives an indication for a failure mechanism. In this case the failure mechanism is a typical Prandtl-like mechanism around the plate, and it fits quite well in the finite element mesh. The figure also shows the penetration of the plate into the soil, the settlement of the soil above the plate and the relative overburden beside the plate. Although in the other three calculations the failure mechanisms are quite similar to figure 3, they do not show the penetration of the plate, since those calculations are based on small strain theory.

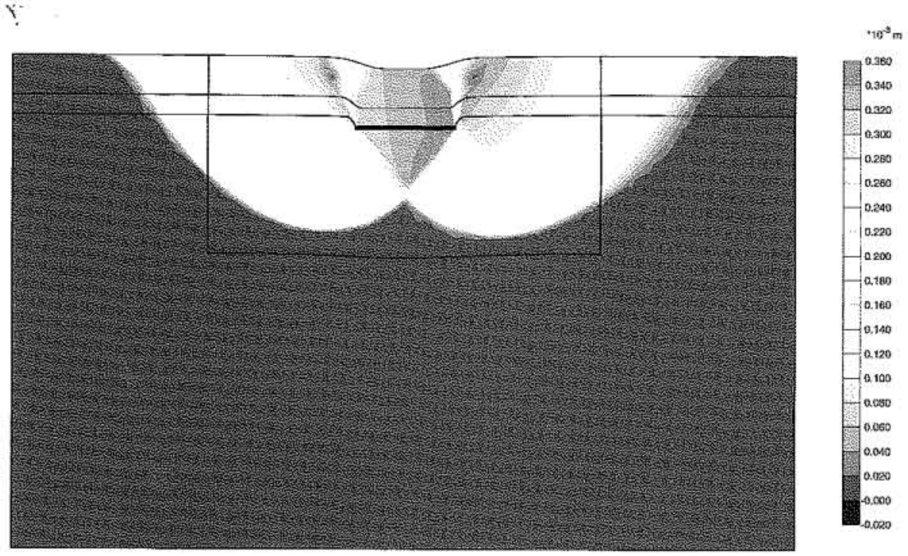

Figure 3. Failure mechanism around foundation in Updated Mesh calculation.

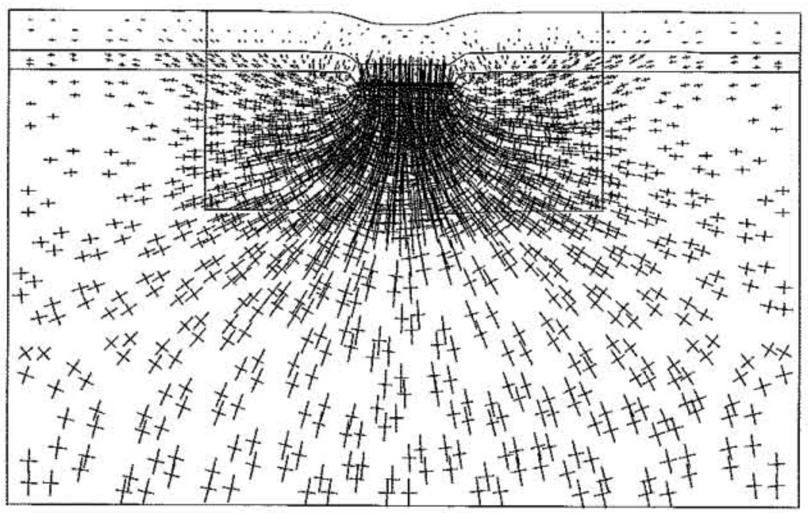

Figure 4. Stress distribution around foundation at failure.

Figure 4 shows the stress distribution around the plate at failure. Along the failure mechanism the stress points are in plastic state according to the Mohr-Coulomb failure criterion. In the area above the plate the stresses are very low. In this area many tension points are found, i.e. stress points where the tension cut-off criterion has been applied.

5. CONCLUSIONS

It has been shown that under certain conditions regarding the level of the groundwater and the distribution and the magnitude of the loads on a shallow foundation, uniform soil subsidence may result in unequal settlements of the foundation, and thus may lead to structural damage.

Numerical simulations confirm the approximate analytical predictions, and they also confirm that a decrease in bearing capacity of a shallow foundation due to a global settlement or a relative increase in phreatic level (δ) can be regained by an extra penetration of the foundation in the order of half the global settlement or increase in phreatic level ($^1/_2\delta$).

REFERENCES

Brinch Hansen, J. (1970) A revised and extended formula for bearing capacity, *Bull. Danish Geotechnical Inst.*, vol. 28, 5-11.

Brinkgreve, R.B.J. & Vermeer, P.A. (1998) *PLAXIS - Finite Element Code for Soil and Rock Analyses*. Balkema, Rotterdam.

Craig, R.F. (1997) *Soil Mechanics*, 6th ed., Spon, London.

Commissie Bodemdaling door Aardgaswinning (1987) Studieresultaten betreffende ongelijkmatige zakkingen in verband met aardgaswinning in de provincie Groningen.

Keverling Buisman, A.S. (1940) *Grondmechanica*, Waltman, Delft.

Onderzoekscommissie Bodemdaling Friesland (1990) Bodemdaling in Friesland.

Prandtl, L. (1920) Über die Härte plastischer Körper, *Nachr. Kgl. Ges. Wiss. Göttingen, Math. Phys. Klasse*, 74-85.

Sloan S.W. & Randolph W.F. (1982) Numerical prediction of collapse loads using finite element methods. *Int. J. Num. Anal. Meth. Geomech.*, vol. 6, 47-76.

Terzaghi, K. (1940) *Theoretical Soil Mechanics*, Wiley, New York.

Verruijt, A. (2000) Schade bij gelijkmatige bodemdaling, *Geotechniek*, vol. 4, 15-18.

THE QUANTIFICATION OF SUBSIDENCE DUE TO GAS-EXTRACTION IN THE NETHERLANDS

Adriaan P.E.M. Houtenbos
NAM Geomatics Department, P.O. Box 28000, 9400 HH Assen, The Netherlands

Abstract

The quantification of subsidence due to gas-extraction in the Netherlands is by no means trivial. The number of benchmarks with continuous height series stretching from before the start of production to the current day is steadily decreasing due to dilapidation of older buildings, while new ones - without heights before the start production - are being established. Available levelling surveys frequently miss a common reference point outside the subsidence bowl. Accumulation of measurement noise in parts of the network furthest away from the reference point occasionally led to false impressions of coherent land rise. Benchmark instabilities due to anthropogenic and natural causes complicate attributing quantified proportions of total subsidence to individual causes. The paper introduces a 7-parameter trend-model for subsidence due to gas-extraction as a function of time and place. This trend model with elliptical contours and a Gaussian profile that deepens linearly with time is found to be consistent with the surveyed height history over 14 gas-reservoirs in the Netherlands to the 5 mm (1 SD) accuracy level. Stochastic modelling of non-gas related subsidence in line with behaviour generally experienced away from gas production areas is shown to provide a practical and verifiable basis for quantitative separation of gas and non-gas effects. Operating directly on observed height-differences the analysis method described is independent of the choice and stability of reference points. There is no summing of height differences to obtain heights and consequently no accumulation of measurement noise. The paper finally identifies a number of economies by exploiting the experimentally established regularity in gas-subsidence in The Netherlands.

Keywords: Land subsidence, levelling, gas-extraction, Netherlands

1. INTRODUCTION

The centuries-old struggle of the Dutch to compete with floods for living space has made subsidence an emotive issue in The Netherlands. Man-made subsidence in general and that caused by gas-extraction in particular has been the focus of public attention in the recent past. Gas reservoirs in the Netherlands occur typically at some 3000 m depth. When gas is produced from the pores of the reservoir rock, pore pressure is reduced and the rock matrix carries more of the weight of the overburden. This causes the rock to compact and the overlying surface to subside. Subsidence in turn affects the utilisation and management of the limited land resource available in The Netherlands. Keeping one's feet dry not being the least of our problems, the effects on water management in polders remain foremost in mind. To manage such interactions typically a prognosis of subsidence is made prior to a production licence being granted. Subsequent levelling surveys serve to monitor subsidence development in time and verify the prognosis.

2. CURRENT PRACTISE

2.1 Data acquisition

Typically subsidence areas are levelled once per centimetre of subsidence in the deepest point. At prevailing subsidence rates of 2 mm to 2 cm per year survey frequencies vary from once a year to once every five years. Smaller subsidence bowls are covered by a pair of profiles at right angles, larger ones by networks with 5 km profile spacing. Benchmark spacing along profiles is approximately 1 km. Levelling surveys are performed to second order MD-RWS (Survey Department of the Ministry of Transport, Public Works and Water Management) specifications resulting in height differences with a precision of 0.6 mm per square root distance in kilometres (1 sd). Hydrostatic levelling is occasionally employed to connect benchmarks in shallow waters offshore. GPS has also been used for this purpose.

2.2 Analysis and reporting

Starting from one or more hopefully stable benchmarks the network of observed height differences is adjusted and heights computed. Subsidence per point at the time of the last survey is subsequently computed by subtracting the similarly computed height before start of production. The resulting point movements are finally contoured and smoothed.

2.3 Experiences and concerns

Over the past half a century NAM acquired a treasure trove of data covering tens of gas fields. The analysis of these data encountered several problems:

- Inconsistent availability of reference benchmarks. Over the years levelling surveys were designed to serve multiple purposes. Coverage and reference points used, varied from one survey to the next. In addition subsidence was sometimes found to extend further than originally expected. This has resulted in survey sets without common stable reference point. In such cases derivation of subsidence by differencing heights with respect to different reference points has introduced biases of up to 2 cm.
- Reference point instability over time. Movement of reference benchmarks in time is hard to detect. Constraining levelling networks to underground benchmarks at published heights has on occasion led to an unlikely conclusion of uplift rather than subsidence.
- Accumulation of measurement noise. As heights are derived by summation of observed height differences observational noise accumulates. Computed heights in the centre of a subsidence bowl at 36 km from the reference benchmark may be up to 1 cm in error. Errors in nearby points strongly correlate, giving a false impression of consistent subsidence or uplift.
- Data gaps. Subsidence due to gas-extraction is derived by subtracting the height measured before the start of production from the height at the last survey. Consequently subsidence can only be computed for benchmarks with observed heights in both the first and last survey. As buildings in which the benchmarks are placed degrade and are replaced the number of benchmarks with heights before production steadily declines. Of the 2000 benchmarks observed in the last survey over the Groningen field only 200 were also observed in the first.
- Subsidence during completion of a network. Occasionally (hydrostatic levelling additions, mega surveys) significant time passes before a survey loop can be closed. Misclosures of up to 1 cm may result if subsidence during the execution of survey is not accounted for.
- Non-gas effects. Apart from gas-extraction there are several other causes of significant benchmark subsidence in the Netherlands. In the period prior to production in the Groningen field between one third and one half of the benchmarks exhibited a subsidence rate in excess of 1 mm per year (Boot 1973). Such non-gas effects are notoriously difficult to separate from total subsidence observed, averaging some 3 mm per year over the NAM fields.
- Subjective contouring. In the absence of a scientific model for the propagation of the above error sources, aesthetic appearance and common sense guided contouring of subsidence derived per benchmark only. The process was consequently vulnerable to the occasional oversight or error of judgement.

3. ADVANCES IN TECHNOLOGY

Quintessential in overcoming problems related to time and distance gaps in the source data is the introduction of a continuous time and space model for subsidence due to gas-extraction. To tackle reference problems derivation of subsidence directly from observed height differences is introduced. In this concept network connection to reference points is no longer essential.

3.1 Continuous time/space gas subsidence trend and trend deviations

Subsidence over producing gas reservoirs in The Netherlands can to a remarkable degree of accuracy be described by a simple trend model:

$$z\{x,y,t\} = \begin{cases} 0 & \text{for } t \le t_0 \\ \dot{z}.(t - t_0).e^{-r^2/2} & \text{for } t_0 < t < t_e \\ \dot{z}.(t_e - t_0).e^{-r^2/2} & \text{for } t \ge t_e \end{cases} \qquad (1)$$

$$\begin{aligned} \text{where } r^2 &= u^2 + v^2 \\ u &= ((x-x_0).\sin\alpha + (y-y_0).\cos\alpha)/a \\ v &= ((x-x_0).\cos\alpha - (y-y_0).\sin\alpha)/b \end{aligned}$$

in which:

z	: computed subsidence trend due to gas extraction
x, y, t	: coordinates and time for which subsidence is to be computed
t_0, t_e	: start and end time of linear subsidence trend
x_0, y_0	: x, y coordinates of the centre of the subsidence bowl
a, b	: distance from the centre of the bowl to the steepest gradient along the long and short axis of subsidence bowl.
α	: bearing of the long axis of the subsidence bowl
$\dot{z}$	: subsidence rate

Characteristic shapes of trend model behaviour in time, contours and profiles are depicted in figure 1a, b and c.

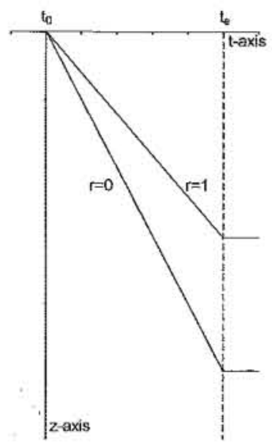

Fig 1.a: Subsidence in time

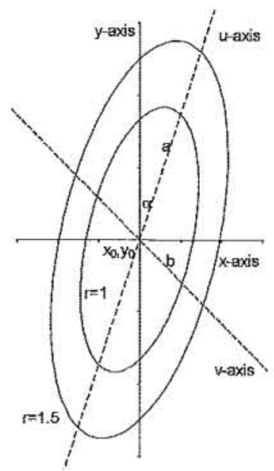

Fig 1.b: Contours

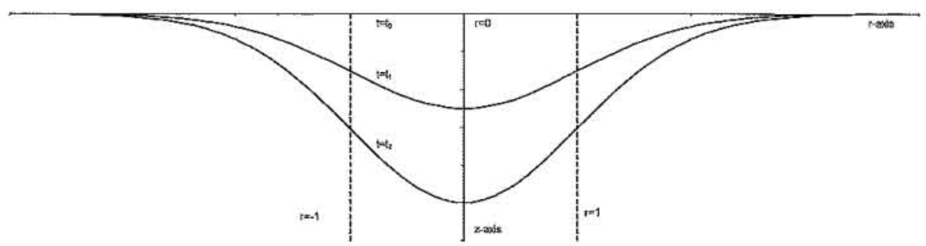

Fig 1.c: Bowl profile

These shapes may seem over-generalized, but first pass assessments have shown a remarkable good fit between observed heights and the model. Standard deviations of height residuals are shown in mm in the sd column of table 1.

Field	sd	t_0	a	b	α	dz/dt	t_e
Ameland	3.7	20-dec-86	2559	2559	0	-18.3	
Annerveen	3.1	25-oct-76	4658	1623	86	-3.6	
Groningen	4.8	17-dec-66	12846	10020	170	-7.7	
Middelie	3.1	28-nov-76	4845	2309	166	-2.1	4-dec-92
Norg	3.6	2-dec-85	6131	2360	130	-5.2	16-okt-95
Roden	3.6	30-jul-77	2965	2386	127	-4.9	
Roswinkel	2.3	4-feb-84	1851	1373	75	-10.2	

Table 1: First pass subsidence trend parameters

Table 2 shows trend-parameter changes as yearly survey campaigns are added to the dataset. A likely explanation for the close trend fit is the smearing effect of the 3 km thick blanket of rock between the reservoir and the surface.

Field	data span	Sd	t_0	x_0	y_0	a	dz/dt
Ameland	'86-'99	3.7	20-dec-86	189942	609562	2559	-18.3
Ameland	'86-'98	3.7	12-jan-87	189957	609578	2573	-18.6
Ameland	'86-'97	3.7	30-jan-87	189988	609541	2575	-18.7
Ameland	'86-'96	3.7	15-feb-87	189998	609700	2598	-19.4

Table 2: Trend parameter response to increasing data span

Although the fit between data and this simple trend model is good enough for most practical purposes, deviations, dz, are further analysed using a stochastic model extension:

$$E\{dz_i\}=(0),\quad D\{dz_i,dz_j\}=\sigma_p^2 z_i z_j.e^{-\left(l_{ij}/L\right)^2} \tag{2}$$

in which:

E{}, D{} : mathematical expectation, dispersion a.k.a. mean and covariance
dz_i, dz_j : trend deviations at x_i, y_i, t_i and x_j y_j t_j respectively
σ_p : sd of trend deviations in percentage of the model value z
z_i, z_j : subsidence trend at coordinates and time i and j respectively
l_{ij} : distance between sample points i and j
L : distance at which correlation is reduced to 38%

As a rule of thumb reservoir compaction at a point at depth d affects subsidence within a circle of radius d above the point. Subsidence trend deviations in nearby points are therefore likely to correlate strongly. Likewise, as variations in the main subsidence drivers, reservoir thickness, compressibility and depletion rate tend to remain constant during production, deviations from the subsidence trend will tend to correlate strongly in time. Ongoing experimentation indicates results to depend on the magnitude of trend deviations rather than correlation between deviations at different times and places. Hence, the exact shape of (2) is of minor importance.

3.2 Non-gas surface dynamics and point noise

Analysis of repeatedly observed height differences over longer periods of time outside gas production areas has demonstrated the presence of significant non-gas related benchmark motion. Such 'autonomous' motion was also noted prior to production out of the Groningen field. A number of benchmarks exhibit clearly anomalous linear behaviour (ALB) with respect to all surrounding points. More often than not such benchmarks are placed in buildings with a poor foundation on relatively compactible Holocene. Such behaviour is detected by a statistical test and modelled as follows:

$$s_i=\begin{cases}\dot{s}_i.(t-t_1) & where\ ALB\ detected\\ 0 & all\ other\ benchmarks\end{cases} \tag{3}$$

in which:

$\dot{s}_i$: the rate of motion
t_1 : the reference time i.e. the time of the first levelling observation

This takes care of the most glaring anomalous behaviour, but leaves the smaller but still significant random motions caused by such things as seasonal

variations in the water table, unaddressed. The deviations from the autonomous motion trend formulated in (3) are therefore separately modelled as:

$$E\begin{Bmatrix}ds_i\\ds_j\end{Bmatrix}=\begin{pmatrix}0\\0\end{pmatrix},\quad D\begin{Bmatrix}ds_i\\ds_j\end{Bmatrix}=\begin{pmatrix}\sigma_s^2(t_i-t_1) & \sigma_s^2(t_i-t_1)\\ \sigma_s^2(t_i-t_1) & \sigma_s^2(t_j-t_1)\end{pmatrix} \tag{4}$$

in which:

ds_i, ds_j : accumulated autonomous motion of the same benchmark at times i and j respectively.
σ_s : sd of autonomous motion (point noise) per square root time period

Analysis of repeatedly observed height differences well away from producing fields in Ameland, Friesland and Groningen resulted in a best fit for point noise of 0.6 mm times the square root of the number of years over which random motion is accumulated:

$$\sigma_s = 0.6\,mm\ per\sqrt{dt_{yrs}} \tag{5}$$

This fits in reasonably well with the MD-RWS classification criterion for stable benchmarks: less than 0.5 mm/yr. Over the average survey interval of 10 years this is equivalent to a tolerable standard deviation of 0.8 mm/$\sqrt{t_{yrs}}$. Point noise exhibits very little area correlation. This is also shown by NAM's shallow compaction monitoring. In this programme compaction in the top 400 m is digitally recorded every day (Wierda 1994). The associated benchmark cluster is levelled twice a year. While the benchmarks within one cluster (<10 m radius) share geological, hydrological and metrological circumstances, subsidence rates vary significantly depending on foundation depth and pressure. Hence no area correlation is postulated in (4).

3.3 Observations and observation noise.

Height differences are predominantly obtained by second order levelling to MD-RWS specifications. The precision can easily be derived from differences between forward and backward levelling and from loop closures in the resulting levelling networks. Various analyses support following a priori value for the average of the forward and backward value of a height difference, observed to second order specification:

$$\sigma_{\Delta h} = 0.6\,mm\ per\sqrt{l_{kms}} \tag{6}$$

in which l is the length of the profile in kilometres. Theoretically observed height differences would just satisfy MD-RWS specifications if their standard deviation would be 0.75mm /$\sqrt{l_{kms}}$.

3.4 Composite observational model for heights

To resolve the model noise elements by least squares adjustment we introduce a pseudo-observation of zero for both the accumulated point noise and the accumulated gas trend deviation at every height we observe. These zero observations are randomly distributed around the actual value of the autonomous motion and trend deviation with variances equal to those listed in (2) and (4) above:

$$E\begin{Bmatrix}\partial s_{it}\\ \partial z_{it}\end{Bmatrix}=\begin{pmatrix}ds_{it}\\ dz_{it}\end{pmatrix},\quad D\begin{Bmatrix}\partial s_{it}\\ \partial z_{it}\end{Bmatrix}=D\begin{Bmatrix}ds_{it}\\ dz_{it}\end{Bmatrix}=\begin{pmatrix}Q_s & 0\\ 0 & Q_z\end{pmatrix} \tag{7}$$

Assuming heights are derived from observations with a variance matrix Q_h the total set of observation equations for least squares solution becomes:

$$E\begin{Bmatrix}h_{it}\\ \partial s_{it}\\ \partial z_{it}\end{Bmatrix}=\begin{pmatrix}h_{i0}+s_{it}+ds_{it}+z_{it}+dz_{it}\\ ds_{it}\\ dz_{it}\end{pmatrix},\quad D\begin{Bmatrix}h_{it}\\ \partial s_{it}\\ \partial z_{it}\end{Bmatrix}=\begin{pmatrix}Q_h & 0 & 0\\ 0 & Q_s & 0\\ 0 & 0 & Q_z\end{pmatrix} \tag{8}$$

The system can further be simplified by row subtraction to:

$$E\{h_{it}-\partial s_{it}-\partial z_{it}\}=h_{i0}+s_{it}+z_{it},\quad D\{h_{it}-\partial s_{it}-\partial z_{it}\}=Q_h+Q_s+Q_z \tag{9}$$

in which:

- h_{it} : height of point i at time t
- ∂s_{it} : zero 'observation' for accumulated autonomous motion
- ∂z_{it} : zero 'observation' for accumulated gas trend deviation
- h_{i0} : height at reference time t_0.
- s_{it} : ALB according to (3). Initially null.
- z_{it} : gas trend according to (1).
- Q_h, Q_s, Q_z : variance matrices of derived heights, autonomous motion (4) and gas trend deviations (2).

While it is possible to resolve the system parameters in this way (Kenselaar/Martens 1999a), significant additional benefits can be derived solving the parameters directly from observed height differences bypassing assumptions regarding the stability of reference benchmarks.

3.5 Composite observational model for height differences

The introduction of a W matrix, differencing heights to obtain height differences (courtesy Delft University of Technology), allows effortless transition of the formulation in terms of heights to that in height differences:

$$\begin{aligned}E\{\Delta h_{ijt}-W.(\partial s_{it}+\partial z_{it})\}&=\\ &=W.(h_{i0}+s_{it}+z_{it})=W.\begin{pmatrix}A_h & A_s & A_z\end{pmatrix}\begin{pmatrix}h_{i0}\\ \dot{s}_i\\ p\end{pmatrix}\\ D\{\Delta h_{ijt}-W.(\partial s_{it}+\partial z_{it})\}&=Q_{\Delta h}+W.(Q_s+Q_z)W^T\end{aligned} \tag{10}$$

in which:

- Δh_{ijt} : height difference between points i and j at time t
- A_h, A_s, A_z : derivatives of the observations w.r.t. null height, autonomous subsidence rate and gas trend parameters respectively.
- $h_{i0}, \dot{s}_i, p$: unknown null height, autonomous subsidence rate and gas trend parameter respectively
- $Q_{\Delta h}$: variance matrices of observed height differences.

Once the null height, ALB and gas-trend parameters are derived from (10) (Kenselaar/Martens 1999b), accumulated random autonomous motion and gas trend deviation can be computed from:

$$\begin{pmatrix}ds_{it}\\ dz_{it}\end{pmatrix}=\begin{pmatrix}Q_s\\ Q_z\end{pmatrix}W^T\left(Q_{\Delta h}+W.(Q_s+Q_z)W^T\right)^{-1}\left(\Delta h_{ijt}-W.(h_{i0}+s_{it}+z_{it})\right) \tag{11}$$

Formula (2) facilitates statistical interpolation of the trend deviation at any point in time and space from the deviations at the data points derived in (11):

$$\begin{aligned}\begin{pmatrix}dz'_1\\ \vdots\\ dz'_n\end{pmatrix}&=\begin{pmatrix}D\{dz_1,dz_1\} & \cdots & D\{dz_1,dz_n\}\\ \vdots & \ddots & \vdots\\ D\{dz_n,dz_1\} & \cdots & D\{dz_n,dz_n\}\end{pmatrix}^{-1}.\begin{pmatrix}dz_1\\ \vdots\\ dz_n\end{pmatrix}\\ dz&=\begin{pmatrix}D\{dz\ ,dz_1\} & \cdots & D\{dz\ ,dz_n\}\end{pmatrix}.\begin{pmatrix}dz'_1\\ \vdots\\ dz'_n\end{pmatrix}\end{aligned} \tag{12}$$

The matrix to be inverted in is the normally singular Q_z. Q_z inversion can be eliminated by combining (12) with (11). Total gas-related subsidence at any point in time and space is finally just a summation away:

$$Z=z+dz \tag{13}$$

3.6 Statistical error testing

To ensure reliable quantification of subsidence a number of data tests are carried out each associated with its own specific action:

- Individual height difference observation error: Remove height difference.
- Point identification error, e.g. levelling rod on incorrect benchmark: Combine 'from-via' and 'via-to' height differences into a new 'from-to' observation bypassing the suspect 'via- benchmark..
- Anomalous linear behaviour: add a rate parameter to be resolved for the anomalously behaving benchmark.
- Excessive point noise, e.g. benchmark disturbed: Increase point noise.
- Excessive epoch noise, e.g. less precise survey: Increase epoch noise.

All tests are computed at every adjustment pass. The test with the largest quotient of test value over tolerance is acted upon. This essential quality control process is developed by the Department of Mathematical Geodesy and Positioning, Faculty of Civil Engineering and Geosciences, Delft University of Technology (Kenselaar/Martens 2000).

3.7 Case study

To demonstrate the various concepts a dataset over the Munnekezijl area comprising 530 height-differences between 137 benchmarks, observed in 7 yearly survey campaigns from '93 till '99, were subjected to analysis. Only 3 of the 137 benchmarks were observed in every campaign, 59 in 5 or more. In the third year parts of two unconnected levelling surveys on either site of the Munnekezijl field were used. The 1993 height of benchmark 6F0052 (in the centre of field) served as reference height. No other reference marker constraints were used. The observational and point noise standard deviations were set to their standard values of 0.6 $mm/\sqrt{l_{kms}}$ and 0.6 $mm/\sqrt{t_{yrs}}$ respectively. Data in the immediate Munnekezijl area were found to fit the trend model with zero trend deviation noise. To still demonstrate trend deviation modelling data coverage was extended to the Grijpskerk area, where subsidence is known to deviate from the Munnekezijl trend, and trend-deviation dispersion was adapted from (2):

$$D\{dz_i, dz_j\} = \sigma_z^2 .(t_i - t_1)\; e^{-\left(\frac{l_{ij}}{L}\right)^2} \quad for\ t_i < t_j \tag{14}$$

in which σ_z is the standard deviation of the gas trend deviations in mm per square root of the accumulation period in years and t_1 is the time of the first levelling. After corrective action for 7 observational errors and anomalous behaviour of 13 isolated benchmarks, observations were consistent with functional and stochastic model at σ_z = 1.5 $mm/\sqrt{t_{yrs}}$, L = 3 kms. Resulting trend parameters together with their precision are given in table 3. The relatively high standard deviations

reflect a low signal to noise ratio. Total subsidence did not exceed 26 mm during survey coverage. Trend deviation (12) and total gas-subsidence (2) in June 1998 are mapped in figure 2.

Field	t_0	x_0	y_0	a	b	α	dz/dt
Munnekezijl	19-nov-95	214634	595728	2259	1573	62	-6.5
sd	141 days	304	221	304	149	11	0.9

Table 3: Trend parameter response to increasing data span

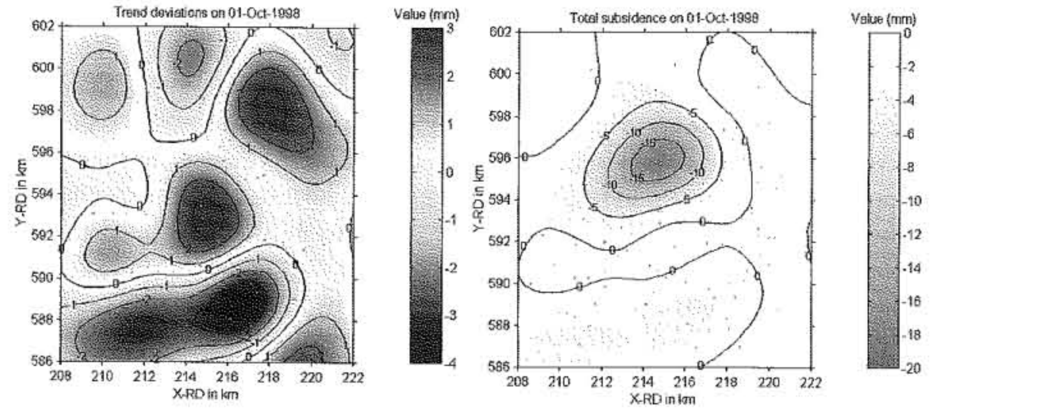

Fig 2: Munnekezijl trend deviations and total gas-subsidence in June 1998.

The effect of production from the Grijpskerk field, for which no a priori subsidence assumptions was made, stands out at the bottom of the picture. Addition of a separate trend parameters set for the Grijpskerk bowl may be expected to reduce deviations from the thus extended trend to the minimal level experienced before extending Munnekezijl data coverage to the Grijpskerk area.

4. CONCLUSIONS

4.1 Comments

- While the ability of the trend model (1) and the quantification methodology (3.5) to overcome practical problems (2.3) is tested and proven in practical use, testing and tuning of collocation (12) and the formal derivation of accuracy (13) is still in progress. The effect of collocation tuning is likely to be an order of magnitude smaller than that of the trend-deviations. As the latter are measured in millimeters this tuning is likely to be more of theoretical than of practical significance.

- For nearly circular bowls (e.g. Ameland) no effective distinction can be made between the length of short and the long axis of the subsidence bowl. To prevent singularity in the solution only one value for the bowl radius R(=a=b) is resolved. The bearing of the long axis is held fixed at zero.
- In case of overlapping subsidence bowls (e.g. Groningen, Annerveen, Roden, Norg) the parameters of a model of type (1) will have to be resolved for each of the bowls. Wherever the subsidence value, z, appears in the formulation, the summation of subsidence for the different bowls should be read instead.

4.2 Problem solving potential

- Inconsistent availability of reference benchmarks is no longer a problem. The analysis operates directly on the deformation measurements themselves and is therefore independent of choice and stability of reference points. As there is no summing of height differences to obtain heights, there is no accumulation of measurement noise.
- The subsidence trend model adopted is continuous in time and space, as is the stochastic trend deviation model. This allows the exploitation of time and spatial correlation to bridge data gaps in the best way possible, i.e. fully 3D. This also lends a great deal of flexibility to the system to utilise data of different types (GPS, hydrostatic), obtained at different times for different purposes.
- The stochastic modelling of non-gas effects in line with behaviour generally experienced away from gas production areas provides a practical and verifiable basis for quantitative separation of gas and non-gas effects. Residuals after removal of the gas trend exhibit very little area consistency. Characteristics in and outside the subsidence bowl are very much the same.
- The margin of error in interpolation of trend deviations between nearby data points in time and space is considerably smaller than that of total subsidence between the far sparser points that were surveyed at the same time. The process described employs the complete historical dataset, requires no human intervention and is therefore considerably less vulnerable to fluke results.

4.3 Further potential

- Advantages of deformation analysis using observed height differences without prior network adjustment and conversion to heights are not restricted to gas production cases. Much sharper detection of observational errors is available by slotting an appropriate subsidence model into (10). To test absence of consistent deformation the model $z = 0$ suffices. Actual deformation will be picked up by the trend-deviation, dz.
- Subsidence is only measurable by changes in height differences over time. Such changes are absent along gas-subsidence contours, largest along radial profiles at crossings with the r=1 contour. Better subsidence quantification can be derived at lower survey costs by designing levelling networks on the basis of this principle.
- Exploiting the experimentally established regularity in gas-subsidence offers further economies. Near future subsidence and its precision can be derived from the continuous trend and trend deviation models. Planning the next survey at the time extrapolation-accuracy exceeds requirements optimises cost-effectiveness.

Acknowledgements

I am greatly indebted to my wife, children, colleagues, employer, D.U.T, SodM and MD-RWS for the time, support and advice necessary to complete this fundamental overhaul of gas-subsidence analysis in the Netherlands

REFERENCES

Boot, R. (1973). *Level control surveys in the Groningen gas field.* In: Verhandelingen Kon. Ned. Geol. Mijnbouwk. Gen. Volume 28.

Wierda, K.J. (1994). *Ondiepe compactie, stage verslag.* Technical University Twente, Faculty of Applied Physics.

Kenselaar, F., M.H.F. Martens (1999a). *Modellering van bodemdaling met een tijd-plaats-model.* Delft University of Technology, Faculty of Civil Engineering and Geosciences, Dept of Mathematical Geodesy and Positioning

Kenselaar, F., M.H.F. Martens (1999b). *Schatting van een tijd-plaats model voor bodemdaling door gaswinning uit gewaterpaste hoogteverschillen.* Delft University of Technology, Faculty of Civil Engineering and Geosciences, Dept of Mathematical Geodesy and Positioning

Kenselaar, F., M.H.F. Martens (2000). *Spatial temporal modelling of land subsidence due to gas extraction.* Delft University of Technology, Faculty of Civil Engineering and Geosciences, Dept of Mathematical Geodesy and Positioning

LAND SUBSIDENCE - Vol. I
Proceedings of the Sixth International Symposium on Land Subsidence
Ravenna / Italy / 24-29 September 2000

COMPACTION OF A POORLY CONSOLIDATED QUARTZ-RICH RESERVOIR SANDSTONE: *EXPERIMENTS FOR THE PROGNOSIS OF COMPACTION DRIVE*

Peter Schutjens
Shell Research (SIEP-RTS), Volmerlaan 6-8, Rijswijk, The Netherlands

Clemens van Dijk, Fons Marcelis, Stefano Pruno
PanTerra Geoconsultants, Veerpolder 5, Warmond, The Netherlands

J. Wesley Martin
TerraTek Inc., Univ. Research Park, Wakara Way, Salt Lake City, USA

Ruud van den Oord
Production Development Oman, Petrophysics OBP/4, Muscat, Oman

Abstract

Fifteen compaction experiments on a poorly consolidated, porous (18 to 35%) quartz-rich reservoir sandstone from Oman revealed that compressibility increased with increasing porosity, increasing grain size and decreasing calcite and feldspar cement. The compressibility under unaxial strain conditions was related to the stress path, with high compressibility being accompanied by high effective radial stress. At low stress/strain, the compaction mechanism was grain rotation/sliding, probably triggered by brittle deformation at grain contacts. Some elastic deformation also occurred. At high strain, intra- and transgranular fracturing was dominant, and time-dependent compaction (creep) and grain size reduction were observed. The creep strain was well described by logarithmic time functions, which gave several tens of millistrain compaction when extrapolated over the duration of the depletion (10 MPa in 10 years). Addition of the extrapolated creep strain to the strain measured during loading predicts a uniaxial reservoir compaction of up to 59 (±14) millistrain and an associated porosity reduction of 3 to 6 porosity units over the target depletion. This high compaction may be an important driving force for hydrocarbon flow towards the wells, but may also induce subsidence and permeability reduction.

Keywords: compaction drive, hydrocarbon reservoir, deformation mechanism

1. INTRODUCTION

Production-induced reservoir compaction is often associated with adverse surface and subsurface deformation such as subsidence and casing failure (see

Barends et al., 1995; Chilingarian et al., 1995, Borchers, 1998). Less well known are its beneficial effects: compaction-induced porosity reduction as a driving force for hydrocarbon flow towards the wellbore ("compaction drive"), and the preferential compaction of porous layers and fault gouge that may delay or prevent water influx (Puig and Schenk, 1984; Espinoza and Mirabal, 1988).

Compaction-drive is expected during the depletion of the Gharif Formation in the Mukhaizna and Thayfut reservoirs in Oman. These are poorly consolidated Permian sandstones and high porosity (18% to 35%) unconsolidated sands with high viscosity oil (14-18° API) in two culminations in a steeply flanked anticlinal structure (Lievaart et al., 1996). With an expected stock-tank oil initially in place (STOIIP) of 3.86 x 10 m^3, Mukhaizna is the third largest oil field in South Oman (Thayfut is only 3.1 10 m^3). However, the thick oil and reservoir structure complicate the reservoir development. The present field development plan relies on compaction as an important drive mechanism for hydrocarbon flow towards the wells, contributing about 9% to the recovery.

A prerequisite for compaction drive is a sufficiently high compaction strain and porosity loss over the targeted depletion, preferably a few porosity units. Low acoustic (wireline log) velocities, poor consolidation and a coarse grain size indicate a high rock compressibility, but its magnitude or dependence on stress cannot be predicted from such observations. What is needed are experimental compaction data (strain, porosity change) and an understanding of the relative importance of different grain scale compaction mechanisms (e.g., elastic, plastic, viscous), which in turn depend on the microstructure of load-bearing detrital grains, grain composition, contact morphology and cement support. We describe such an experimental investigation using Mukhaizna and Thayfut core, compacted under the stress conditions induced by depletion.

2. PREPARATION

2.1 Sample treatment

Fifteen sample batches were drilled from five pieces of preserved core from well Mukhaizna-12 (M1, M4, M7, M8, M10) and three from well Thayfut-7 (T1, T3 and T5)[1], see Table 1. These sandstones were poorly consolidated, with the heavy oil apparently adding to the cohesion of the samples. The material was frozen to -25°C to prevent disintegration. The samples were drilled under "dry" conditions; that is, without adding extra water or using liquid nitrogen[2]. The samples were trimmed, photographed, CT-scanned, encapsulated in a metal gauze sleeve to reduce the risk of sample disintegration, and stored at -25°C.

[1] The Thayfut reservoir is located close to Mukhaizna, and similar in age, composition and texture. Samples from Thayfut and Mukhaizna are indicated by "T" and "M" in Table 1.

[2] First sets of samples were drilled with liquid nitrogen to cool the bit and to remove fine cuttings. This technique was no longer applied when intragranular closed "hairline" cracks were discovered. Batch 4 was drilled with liquid nitrogen; all other samples were drilled "dry".

Three samples from each core piece were cleaned in an azeotropic mixture of chloroform, methanol and water at about 70°C. Toluene flushing at room temperature was also applied. Cleaning took weeks to months, and was stopped when the samples had lost their initial black-brown oil stain. One batch of cleaned samples was resin-impregnated and cut in half along the cylindrical axis for thin section preparation. Another batch was used for helium porosimetry. Grain size distributions were also determined (Table 1).

Table 1. Compaction data for the Mukhaizna and Thayfut reservoirs

Information			Pre-stress					Depletion simulation					Creep		Stress cycling		
sample	porosity (% of bulk vol.)	main grain size fract. (µm, *1)	S_{ax} (MPa)	S_{rad} (MPa)	M_0 (*2)	axial comp. (ms, *3)	radial comp. (ms)	S_{ax} (MPa)	S_{rad} (MPa)	K (*4)	axial comp. (ms)	radial comp. (ms)	duration (hrs)	axial comp. (ms)	axial comp. per 10 MPa of 2nd loading (ms)	ratio 2nd over 1st compaction	inelastic axial comp. (ms) (*5)
Stress path 1	Prestress under uniaxial strain conditions, followed by simulation of depletion under uniaxial strain conditions																
Low-compressibility samples																	
M4c	24	850-1400	10.0	2.8	0.28	7.8	0.0	20.0	7.0	0.43	4.1	0.0	15	0.5	1.7	0.41	7
M8nb	30	210-420	10.0	3.0	0.30	5.5	0.0	20.0	5.7	0.27	6.0	0.0	15	1.8	1.5	0.25	7
T5na	18	105-150	10.0	1.8	0.18	4.0	0.0	20.0	3.8	0.20	1.6	0.0	15	0.2	1.0	0.65	1
									average =	0.30							
High-compressibility samples																	
T1nb	34	420-600	10.0	3.9	0.39	18.4	0.0	19.9	9.7	0.59	27.9	0.0	15	8.6	2.9	0.10	45
T3nb	35	300-420	10.0	1.6	0.16	16.9	0.0	19.7	7.1	0.56	16.0	0.0	16	5.6	2.4	0.15	23
M10na	32	850-1400	10.0	4.5	0.45	25.1	0.0	20.0	11.0	0.65	29.5	0.0	15	9.1	3.2	0.11	57
M7na	29	210-420	10.0	2.4	0.24	17.1	0.0	19.9	7.2	0.48	31.1	0.0	15	3.5	2.4	0.08	41
M1ne	29	150-850 (*1)	10.0	4.4	0.44	34.9	0.0	19.9	11.2	0.69	31.3	0.0	24	15.4	no cycling		65
M1nd	29	150-850 (*1)	9.9	4.4	0.44	38.1	0.0	19.9	12.4	0.80	27.7	0.0	24	23.3	no cycling		71
									average =	0.63							
Stress path 2	Prestress under isotropic increase in stress, followed by simulation of depletion under uniaxial strain conditions																
M12a	n.m.	n.m.	10.1	10.0	0.99	5.3	6.2	16.9	11.3	0.19	7.7	0.0	no creep		no cycling	-	-
M4f	24	850-1400	10.0	9.9	0.99	4.6	12.7	19.9	12.0	0.21	3.7	0.0	15	1.2	2.0	0.54	4
									average =	0.20							
Stress path 3	Prestress under uniaxial strain conditions, followed by simulation of depletion under K = 0.6																
M4e	24	850-1400	10.0	3.2	0.32	6.3	0.0	19.9	9.2	0.60	1.7	1.2	16	0.2	1.1	0.61	3
M7nb	29	210-420	10.0	4.2	0.42	17.1	0.0	19.9	10.1	0.60	5.1	1.4	15	2.5	2.0	0.30	17
M8nc	30	210-420	10.0	2.3	0.23	8.3	0.0	19.9	8.2	0.60	2.8	1.7	15	0.9	1.3	0.40	6
T3nc	35	300-420	10.0	2.1	0.21	18.4	0.0	19.9	8.1	0.61	7.1	3.7	15	6.5	no cycling	-	0
									average =	0.60							

Notes

*1) Measured with a Malvern Particle Sizer at Utrecht University (NL). All samples except M1 had a Gaussian distribution around a peak grain size fraction. The sample from batch 1 shows a bimodal size distribution, peaking at 2 to 8 mm, and at 300 to 400 mm. The reason for this different sorting is unknown. The finer fraction may reflect (coring-induced/enhanced ?) cracking at grain contacts producing fines ("spalling").

*2) $M_0 = \sigma_{rad} / \sigma_{ax} = S_{rad} / S_{ax}$ at pre-production stress state.

*3) Compaction is expressed in strain, which is defined as change in dimension divided by the initial dimension. Compaction is positive strain; Extension is negative strain. Compaction/extension is often given in millistrain (ms), which is strain multiplied by a factor of 1000. It is equivalent to mm/m.

*4) $K = \Delta S_{rad} / \Delta S_{ax}$ describing the stress path during simulation of the depletion-induced increase in effective (= total) stress, see section 2.3.

*5) Defined as difference in sample length before and after compaction, divided by sample length before compaction, and then multiplied by 1000 (to obtain millistrain)

2.2 Composition and microstructure

Quartz is the dominant detrital mineral, although locally high concentrations of feldspar and detrital clay also occur, often in mm-thick clay laminae (Fig. 1a). The other dominant minerals are infiltrated clays, K-feldspar overgrowths and calcite cement, precipitated in this order. The calcite cement is commonly interconnected (*poikilotopic fabric*) and forms mm-size, probably well-consolidated regions (*nodules*); refer to Figure 1b. Minor amounts of kaolinite, pyrite, siderite and quartz overgrowths are also present. Either high concentrations of infiltrated clay or feldspar overgrowths exist: apparently, the earlier clay infiltration inhibited formation of authigenic feldspar, but clays and calcite cement do occur together.

Intergranular macroporosity is generally moderate to abundant, and it is locally absent where the detrital clay content is high. The detrital and infiltrated clays likely contain a high microporosity. Most grains are in point contact in the high-porosity, coarse-grained samples (Fig. 1a and d). Tangential, grain contacts are more abundant in the finer-grained samples (Fig. 1a, central region). Some of the quartz and feldspar grains show open fractures, although some are filled with feldspar or calcite cement, suggesting that brittle deformation and crack healing occurred during diagenesis (Fisher et al., 1999). All samples, except those from batch M1, exhibit a Gaussian distribution around a peak grain size (Table 1). Sample T5 has the smallest grain size, with most grains in the 75 to 210 μm range (Fig. 1a). In most samples, the dominant grain size fraction was in the range 400 μm to 800 μm.

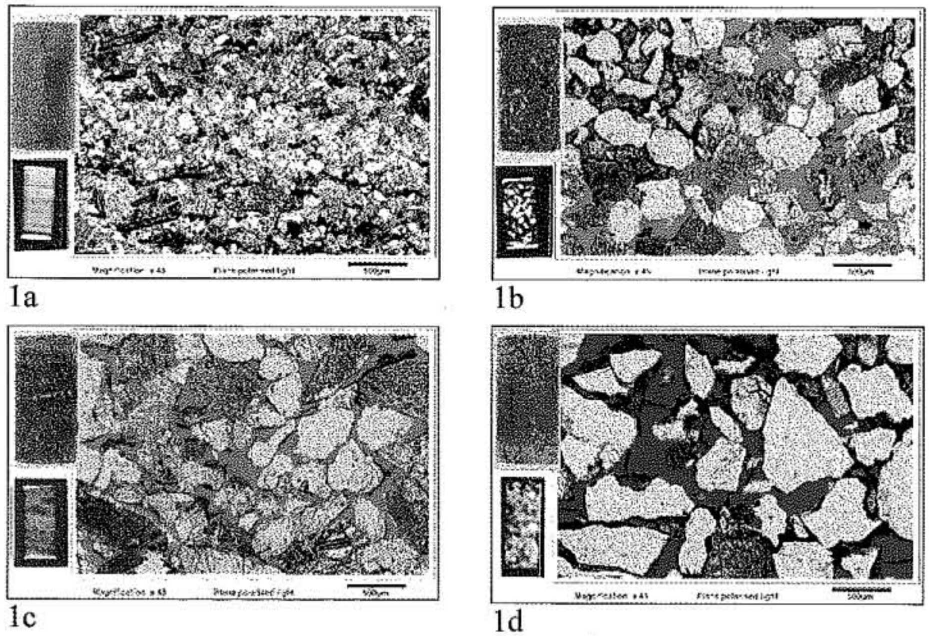

Figure 1 (a-d). Microstructures of Mukhaizna/Thayfut reservoir rock before experimental compaction. Top left inset shows photograph of sample (diameter 2.5 cm), after cleaning from hydrocarbons. Bottom left inset shows CT-scan of cleaned sample. Fig. 1a Batch T5. Detrital mineralogy dominated by fine-grained quartz. Also present are micas and some pyrite. Note tight packing. Extensive cementation with calcite and K-feldspar overgrowths. Fig. 1b Batch M8. Calcite nodules range in size from 1 to 5 mm, enclosing grains and tightly cementing parts of the sample. Some K-feldspar overgrowths are present. Fig. 1c Batch T1. Medium-grained sandstone, mainly quartz, K-feldspar and plagioclase. Clay rims are present around some pores, as well as some finely crystalline kaolinite replacing plagioclase and pyrite. Fig. 1d Batch M4. Very coarse-grained sandstone. Angular grains, mostly in point contact with adjacent grains. No evidence for pressure solution or cementation.

2.3 Stress state and stress path

Before compaction, the initial total vertical stress in Mukhaizna is approximately 20.3 MPa, based on an average reservoir depth of 900 m and assuming an average overburden density of 2.26 g/cm^3. The initial average pore fluid pressure is 10.2 MPa. The initial minimum total horizontal stress is estimated at 14 MPa from fracture-opening pressures in neighbouring fields. This would imply an average horizontal-to-vertical *effective* stress ratio (M_0) before production of about 0.4, and an average horizontal-to-vertical *total* stress ratio before production of approximately 0.7.

Compaction experiments should duplicate the stress path that would be experienced by the reservoir rock during actual depletion (Rhett and Teufel, 1992; Santarelli et al., 1998). Keeping in mind that the depletion-induced reservoir compaction is accompanied by a change in the total (far-field) stress state (Teufel et al., 1991; Hettema et al., 1998), we define the reservoir stress path coefficient K here as:

$$K = \frac{\Delta\sigma_{hor}}{\Delta\sigma_{vert}} = \frac{\Delta S_{hor} - \alpha\Delta P}{\Delta S_{vert} - \alpha\Delta P} = \frac{\dfrac{\Delta S_{hor} - \alpha\Delta P_p}{\Delta P_p}}{\dfrac{\Delta S_{vert} - \alpha\Delta P_p}{\Delta P_p}} = \frac{\gamma_{hor} - 1}{\gamma_{vert} - 1} \quad (1)$$

where σ_{hor} is the effective horizontal stress (assumed to be isotropic), σ_{vert} is the effective vertical stress, S_{hor} is the total horizontal stress, S_{vert} is the total vertical stress, and P_p is the pore fluid pressure. The horizontal stress path coefficient, γ_{hor}, is the change in S_{hor} per unit decrease in P_p. The vertical stress path coefficient, γ_{vert}, is the change in S_{vert} per unit decrease in P_p. Because we expect that the compaction of Mukhaizna and Thayfut is dominated by inelastic strain mechanisms, the Biot-Willis poroelastic coefficient, α, has been assumed to be 1 in the far right-hand term of equation (1), see also Hettema et al. (1998).

Most samples contain high-viscous "thick" oil, which was not removed before compaction. In order to reduce the risk of pore pressure diffusion effects on compaction, all experiments were conducted with the sample drained to atmospheric pressure, and assuming $\Delta P_p = 0$ in the sample. The depletion-induced stress path was applied by independent variation of the total axial and total radial stress, at atmospheric pore pressure, but the same effective stresses (changes) were applied as in the reservoir. For instance, the "virgin stress state" of a reservoir pore pressure of 10 MPa and a total vertical stress of approximately 20 MPa was applied using a pore pressure of 0 MPa and a total vertical stress of about 10 MPa. No pore fluid was added to the samples.

Given the relatively large horizontal extent of Mukhaizna (about 6 x 10 km) compared to its shallow depth (about 900 m), we will assume that γ_{vert} is close to zero (Geertsma, 1973). In that case, equation (1) reduces to:

$$K = 1 - \gamma_{hor} \tag{2}$$

In the absence of information on γ_{hor} in the Mukhaizna and Thayfut reservoirs, three stress paths were applied to systematically investigate the relationship between compaction and stress path coefficient, K. **Stress path 1**: Uniaxial compaction[3] to a total axial stress of 10 MPa (equivalent to the inferred in-situ stress before depletion) followed by uniaxial compaction to a total axial stress of 20 MPa (equivalent to the depletion-induced increase in effective vertical stress). **Stress path 2**: An isotropic increase in stress to 10 MPa was followed by uniaxial compaction to a total axial stress of 20 MPa. **Stress path 3**: Uniaxial compaction to a total axial stress of 10 MPa was followed by compaction to a total axial stress of 20 MPa, while maintaining a constant stress path coefficient K of 0.6.

All experiments were performed at room temperature using a triaxial deformation apparatus with automated control of the total radial (= horizontal) stress and the total axial (= vertical) stress. The axial load rate in all tests was 5 MPa/hr. Compaction was always followed by a period at the constant maximum load (*creep compaction*) and an axial stress cycling in the range 10 to 20 MPa at a rate of 5 MPa/hr, under uniaxial strain or under K = 0.6 conditions.

Thin sections were prepared from several experimentally compacted samples with inelastic (permanent) strains from 1 millistrain (sample T5na) to 71 millistrain (M1nd, Table 1), note that 1 millistrain is 1 mm/m, see footnote 3 to Table 1. Comparison with the microstructure of the non-compacted twin samples revealed the compaction mechanisms in the experiment.

3. RESULTS

3.1 Stress path as a function of compaction

Figure 2 shows the stress path coefficient K, as a function of total axial stress during the pre-stress phase from 0 to 10 MPa, and during the simulation of depletion by increasing the total axial stress from 10 to 20 MPa. The datapoints are average values obtained in experiments done along the same stress path. Large differences in K as a function of stress and stress path were observed.

[3] Uniaxial compaction is defined here as deformation with only axial (i.e., vertical) compaction without radial (i.e., horizontal) deformation.

Uniaxial compaction along stress path 1 was characterised by relatively *low K-values* if the uniaxial compressibility was smaller than 10^{-3}/MPa (low compressibility samples, open squares in Fig. 2). From 0 to 10 MPa, K-values were in the range 0.18 to 0.22 (average of 0.19). From 10 to 20 MPa, K-values gradually increased from approximately 0.21 to 0.54, with the start of a non-linear increase of K with stress at about 16 MPa. In contrast, uniaxial compaction along stress path 1 was characterised by relatively *high K-values* if the uniaxial compressibility was in the range from 10^{-3}/MPa to $3x10^{-3}$/MPa (high compressibility samples, open circles in Fig. 2). At low stresses, the K-values were very similar to those in the low-compressibility samples (about 0.2), but a divergence occurred at about 6 MPa, that is, already during the pre-stressing phase. In the 6 to 10 MPa range, K-values in the high-compressibility samples increased from about 0.25 to about 0.6. From 10 to 20 MPa, the average K-values were in the 0.57 to 0.71 range, and independent of stress.

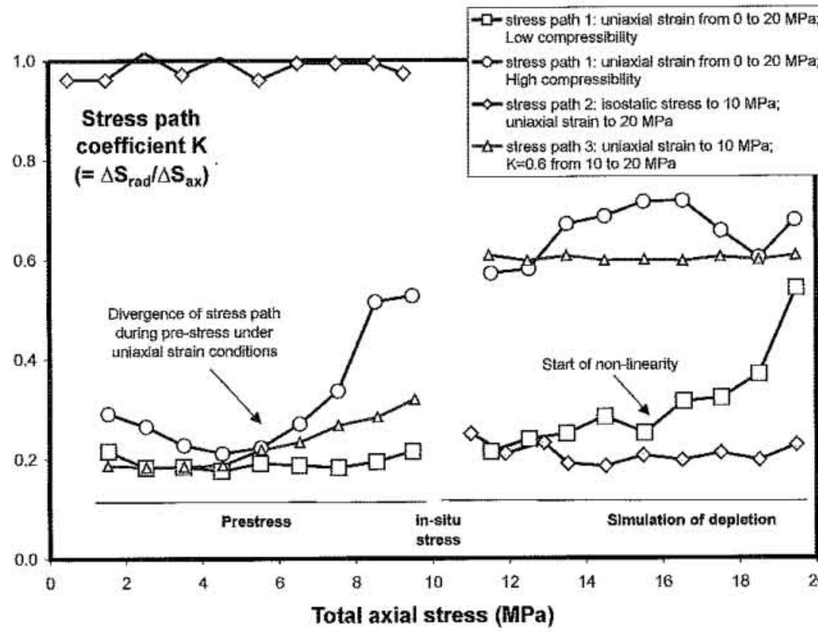

Figure 2. Stress path coefficient K = DSrad/DSax as a function of total axial stress.

Uniaxial compaction along stress path 2 (isostatic pre-stress) occurred with low K-values of approximately 0.2 over the entire 10 to 20 MPa range (Fig. 2, filled rhombs). Compaction along stress path 3 (pre-stressing at uniaxial strain) occurred with a constant pre-set K-value of 0.6. Close inspection of the stress path during the pre-stressing phase revealed a non-linear increase of K with stress, starting at about 5 MPa (Fig. 2, filled triangles).

3.2 and... compaction as a function of stress path

Comparison of the compaction data for three twin samples and one triplet compacted along different stress paths showed that: (a) The pre-stress path exerts a negligible influence on compaction in the range of 10 to 20 MPa, and that (b) uniaxial compaction is two to six times larger than compaction with fixed K = 0.6 (Table 1). However, the volumetric strain is similar because, in tests at K = 0.6, the lower axial compaction is largely balanced by the radial compaction. Since uniaxial compaction is *intuitively* the most likely compaction mode in the Mukhaizna and Thayfut reservoirs, the experimental behavior observed in the stress-path-1 tests is considered in more detail below.

3.3 Stress path 1: Low-compressibility samples

Figures 3(a-c) show the compaction of three samples loaded along stress path 1 which displayed a relatively low compressibility (< 10^{-3}/MPa). The uniaxial compaction during pre-stressing to a total axial stress of 10 MPa (corresponding to the "virgin" effective vertical stress) was non-linear with stress, with compressibility *de*creasing with stress in all samples (Fig. 3a). The compaction during the depletion phase was linear with stress for sample T5na, but non-linear for samples M4c and M8nb, starting at approximately 14 MPa and 16 MPa (indicated by "N" in Fig. 3b), and with compressibility *in*creasing with stress. A compaction of 2 to 6 millistrains was measured, yielding an average compressibility (i.e. slope of curve) of 2×10^{-4}/MPa to 6×10^{-4}/MPa. Compaction creep in the low-compressibility samples was small (Fig. 3c), except for the high creep in sample M8nb in the first two hours. The axial compaction during stress cycling was reversible and in the range of 1.0 to 1.7 millistrain over a 10 MPa change in the total axial stress (Table 1). This is 25 to 65% (average of 44%) of the compaction measured during the first loading.

3.4 Stress path 1: High-compressibility samples

Figures 4(a-c) show the compaction behavior for the six samples loaded along stress path 1, which exhibit a relatively high compressibility. Uniaxial compaction during loading to the virgin stress was non-linear in all samples, except in sample T3nb (Fig. 4a). The uniaxial compressibility *de*creases with stress from 0 to about 4 MPa, is virtually constant up to 6 to 9 MPa, and then starts to *in*crease at higher axial stresses. The start of non-linearity is indicated with capital "N" in Figure 4a, and occurs roughly in the range of 7 to 9 MPa.

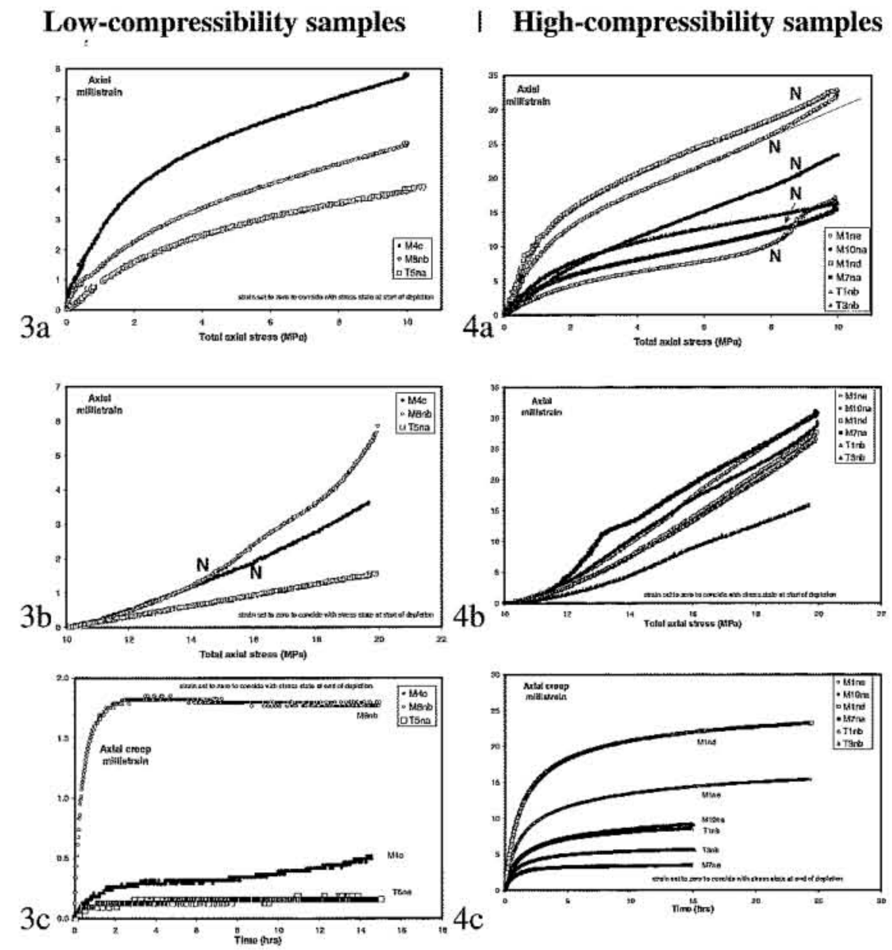

Figure 3(abc). Low-compressibility samples loaded along stress path 1 (uniaxial strain) Fig. 3a: Axial strain versus total axial stress while "pre-stressing" was applied to achieve the inferred in-situ virgin stress conditions. Fig. 3b: Compaction during depletion-induced increase in effective stress. Note non-linearity in two tests (denoted by capital N). Fig. 3c: Creep compaction at a total (= effective) axial stress (σ_{ax}) of 20 MPa, corresponding to the targeted depletion.

Figure 4(abc). High-compressibility samples loaded along stress path 1 (uniaxial strain) Fig. 4a: Compaction during pre-stressing to in-situ stress. Fig. 4b: Compaction during depletion-induced increase in effective stress. Note non-linearity in five tests (capital N) Fig. 4c: Creep compaction at effective stress conditions corresponding to the targeted depletion (σ_{ax} = 20 MPa).

Figure 4b shows the uniaxial compaction from 10 to 20 MPa; the stress range of interest for the Mukhaizna/Thayfut depletion. Except for test T3nb, the trends in the data are similar. Axial strains from 16 to 31 millistrains were measured over the 10 MPa increase in total axial stress. Note the similar, near-linear compaction behavior for five of the six samples for $S_{ax} \approx$ 12 to 20 MPa, with an average axial compressibility of about $3x10^{-3}$/MPa. Despite the similarities in compaction during loading, the creep compaction showed a large spread: over a time-period of 15 to 25 hours, the axial creep strains ranged from approximately 3 millistrain (sample M7na) to 23 millistrain (sample M1nd, Figure 4c). The axial compaction during stress cycling was reversible, with little or no hysteresis, and in the range of 2.4 to 3.2 millistrain over 10 MPa change in total axial stress (Table 1). This is between 8 and 15% (average of 11%) of the compaction measured during the first loading.

3.5 Stress path 1: Average compaction and porosity reduction

Figure 5a shows the average axial compaction behaviour of the low- and high-compressibility samples compacted along stress path 1: vertical lines indicate spread in data. Note the different compaction behavior. At a given stress state, the high-compressibility samples compacted three to six times more than the low-compressibility samples. The low-compressibility samples show a normalised porosity reduction[4] of 0.01 over the 10 MPa increase in total axial stress. The high-compressibility Thayfut and Mukhaizna samples exibit a normalised porosity reduction - computed from the compation data shown in 5a - of about 0.04 and 0.07, respectively, over the 10 MPa increase in total axial stress (Fig. 5b).

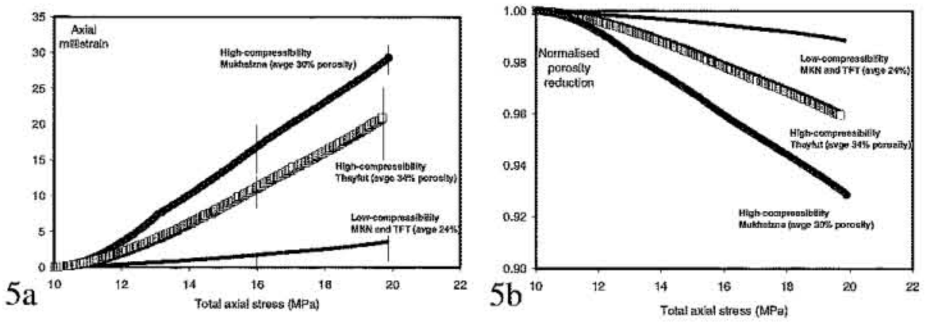

Figure 5. Axial compaction behavior of samples compacted along stress path 1: Average values are shown of the low-compressibility samples (3 samples), and of the high-compressibility Thayfut samples (2 samples) and Mukhaizna samples (4 samples).

[4] The normalised porosity reduction was calculated with the equation

$$\frac{\phi}{\phi_0} = \frac{1}{\phi_0}\left[\frac{V_p - \Delta V_p}{V_b - \Delta V_b}\right] \approx \frac{1}{\phi_0}\left[\frac{V_p - \Delta V_p}{V_b - \Delta V_p}\right] = \frac{1}{\phi_0}\left[\frac{\phi_0 - \varepsilon_b}{1 - \varepsilon_b}\right]$$

assuming the grain compressibility to be very small compared to the bulk rock compressibility (i.e. Biot-Willis coefficient a is 1): a reasonable assumption in cases of high bulk compressibility. The volumetric strain ev is defined as DVb/V b,o, where Vb,o is the initial sample volume.

3.6 Microstructure observations

The main observations can be summarised as follows:

- Samples with an inelastic compaction of less than 10 millistrain (< 1%) showed no (optically visible) change in microstructure. The following microstructural parameters are associated with a low compressibility: A low porosity (< 25%), a strong preferential grain orientation (sample T5na), a relatively high content of calcite cement (see Fig. 1b), a high content of feldspar overgrowths, and a small (fine) grain size (see Fig. 1a).

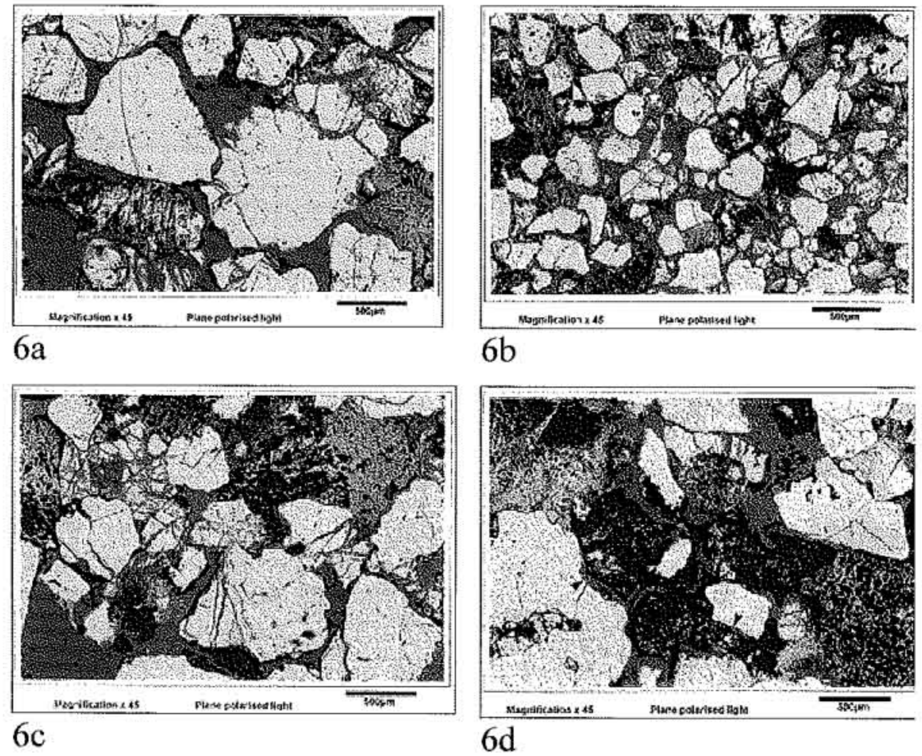

Figure 6(a-d). Microstructures of Mukhaizna/Thayfut reservoir rock after experimental compaction. Fig. 6acd Sample M10na; Compaction under stress (including creep) was 64 millistrain; after unloading 57 millistrain. Fig. 6b Sample M1ne; Compaction under stress was 82 millistrain, after unloading 65 millistrain. There is abundant evidence for brittle deformation, grain rotation and grain sliding, grain size reduction and cement-grain detachment (see Fig. 6d).

- Samples with an inelastic compaction in the 10 to 50 millistrain range show localised zones with fractured grains, as well as zones with no disrupted microstructure. Zones with grain fracturing show a denser packing, probably due to grain sliding and grain rotation. The samples in this group are typically weakly cemented. The one sample with well-developed feldspar overgrowths exhibited the least compaction. Grains encapsulated in calcite cement showed no microcracks.

- Samples with a permanent compaction strain above 50 millistrains had cracks between grains, inside grains and cross-cutting grains, leading to grain size reduction and strong but localised densification (Fig. 6a-c). Grain fracturing apparently reduced the porosity in two ways: by grain sliding and grain rotation, and through grain size reduction, thereby occluding pores with small "chips" from broken grains. Framework reinforcing cements such as calcite or feldspar overgrowths are very rare to absent in these samples. Where present, they are typically detached from the detrital grains (Fig. 6d).

4. INTERPRETATION

4.1 Compaction mechanism

During stress cycling no additional inelastic (permanent) sample deformation occurred. This observation indicates that stress cycling is virtually elastic. Subtraction of the elastic strain from the strain during first loading yields the inelastic strain, which comprises 56% of the total strain in the low-compressibility samples and 89% in the high-compressibility samples (Table 1). At low stress/strain, the inelastic compaction is primarily due to asperity breakage at grain contact points, triggering minor grain rotation and grain sliding. Some brittle or crystal-plastic deformation of clay and (weathered) feldspar may also occur. At high stress/strain, intragranular and transgranular fracturing becomes more important (Figs 6a-d), leading to grain size reduction at high stress/strain. This is very similar to behavior reported by Wong and Baud (1999) and Schutjens et al. (1997, 1998). The start of non-linear compaction may indicate a significant increase in the relative importance of inelastic deformation mechanisms, perhaps indicating that friction at grain contacts is exceeded, or that pervasive cement bond or grain breakage occurs. We think that the rate of time-dependent compaction is controlled by the rate of inter/intra/transgranular microcrack nucleation and propagation (*stress corrosion cracking*, Atkinson, 1987; Critescu and Hunsche, 1997).

Compaction is controlled by textural features: increasing porosity, increasing grain size, and decreasing calcite and feldspar cementation all tend to increase the compressibility, the ratio of inelastic-to-elastic deformation, and probably also the creep rate. In addition, low compressibility rock is characterised by elongated grains with relatively long grain-to-grain contacts compared to the grain diameter, reducing the contact stresses and thus the risk of grain failure.

4.2 Stress path in relation to compaction mechanism

The uniaxial compressibility is closely related to the stress path. Increasing compressibility is accompanied by the development of higher effective radial stress, as manifested by the high K-values (Fig. 2). This effect is probably due to the tendency of high-compressibility samples to expand radially; this has to be counteracted by higher effective radial stresses. Although K-values increase with total axial stress in both the low- and high-compressibility samples, the start of this stress dependence is very different; around 16 MPa and around 6 MPa, respectively. This observation is difficult to explain. Comparison of Figure 2 with Figures 3b and 4a shows that the increase in K-values more

or less coincides with the onset of increasing compressibility, manifested by the non-linearity in the stress-strain relationship (indicated by "N" in these graphs). We suggested above that the non-linearity is associated with an increase in the relative importance of inelastic compaction. Apparently, a yielding or "compaction weakening" occurred, which increased the compressibility, in particular in the high-porosity samples, but did not lead to pervasive pore collapse or strain localisation. The samples continued to compact under increasing stress, with a more or less constant compressibility (Fig. 4b). Our interpretation is that the high-porosity samples yielded *before reaching the inferred virgin in-situ stress state*, at a total axial stress of approximately 7 to 9 MPa (Fig. 4a).

Stresses at interpreted yielding are depicted in Figure 7. The open symbols indicate the in-situ stress states before depletion and after experimental simulation of the depletion. The filled circles and cubes indicate the interpreted yield stress of the high-compressibility and low-compressibility samples, respectively. Note that the yield stress of the high-compressibility samples is lower than the in-situ stress before depletion. The range of experimentally-applied stress paths is too limited to determine the shape of the yield surfaces.

It is not known why the yielding occurs at such low stress levels. Perhaps coring from the reservoir, aging or sampling weakened the rock. Another explanation is that the stress path to the in-situ virgin stress state is not uniaxial strain, or that the in-situ stress state is different from that applied in our tests.

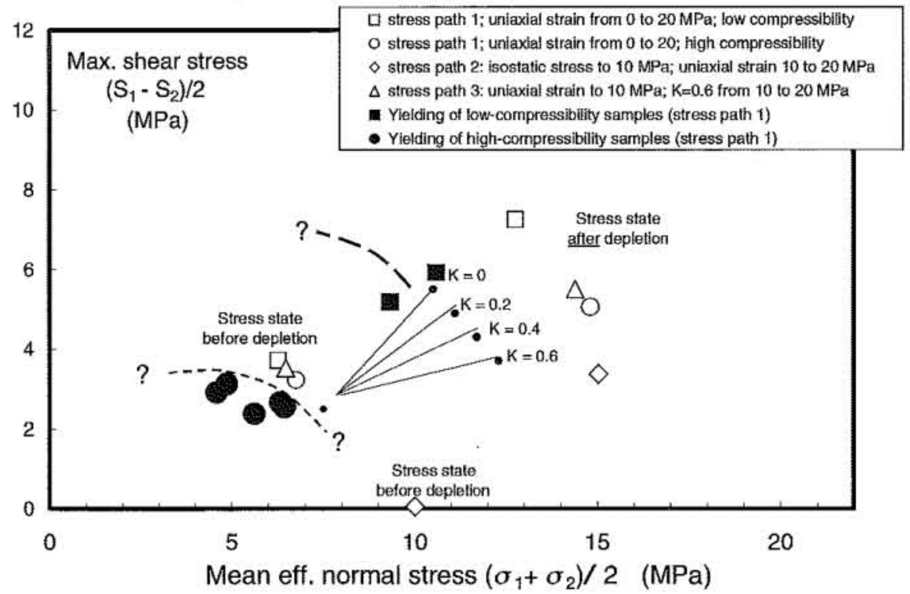

Figure 7. Stress path and yielding. Open symbols indicate stress state at virgin conditions and after depletion. Average values for the different stress paths are shown, connected by (imaginary) stress path vectors K. Filled circles and cubes indicate yield stress of the high-compressibility and the low-compressibility samples, respectively. Note that the yield stress of high-compressibility samples is lower than the virgin stress.

4.3 Compaction creep: Description and extrapolation

Our experiments indicate that compaction in the Mukhaizna and Thayfut samples occurrs by a combination of elastic and inelastic compaction. The inelastic compaction is made up of two components: a *time-independent* component that accounts for the instantaneous inelastic strain, also referred to as plasticity, and a *time-dependent* component referred to as creep. In order to predict compaction as a function of depletion, it is necessary to know the relative contribution of each component. The time-independent strain can be obtained by subtracting the elastic strain from the total strain measured during loading, assuming that the time-dependent inelastic strain component is small during experimental loading (a few hours). As for the creep strain, part of it was measured in the laboratory experiment; However, creep durations in our experiments were only 12 to 25 hours, whereas the 10 MPa depletion in the Mukhaizna and Thayfut reservoirs will take some 10 years. What is needed, therefore, is a method to extrapolate the experimentally-obtained creep strains to the creep strains occuring over this large time span.

We described the creep curves shown in Figure 4c with function where the creep strain is a linear function of the logarithm of the creep time (Eiksund et al., 1995). The input parameters and extrapolations using the Eiksund empirical relation to 10 years are listed in Table 2. Total creep strains of 23, 32 and 43 millistrain are predicted for the low-case based on data from sample M10na, the intermediate-case based on data of sample M1ne, and the high-case based on data of sample M1nd, respectively, see Figure 4c.

Table 2. Extrapolation of the compaction creep

Method based on Eiksund *et al.* (1995)

Case	Experiment	Creep duration (hours)	Measured in experiment (millistrain)	Parameters in Eiksund's (1995) creep model R_0	r	ε_0	Extrapolated to 10 years (millistrain)
Low-case	M10na	15	9	3849	0.63	6.0	23
Average	M1ne	25	15	2346	0.52	10.5	32
High-case	M1nd	25	23	1672	0.43	17.3	43

*) The creep rate was typically determined at about 15 points along the creep curve from the slope of straight line segments between datapoints taken at regular strain-intervals or time-intervals along the creep curve. The inverse of the creep rate (called the time resistance R_t by Eiksund et al.) was then calculated and plotted as a function of creep time. A linear relationship was found in all tests, indicating that this method gives a good description of the experimentally-observed creep.

4.4 Prognosis of depletion-induced porosity reduction

This is done by adding the extrapolated creep strain (accumulating over the 10 years of depletion) to the compaction measured during loading. Only the data gathered from stress-path-1 tests are used. It is assumed that the extrapolated creep strain increases linearly with depletion, i.e., that it is evenly distributed over the effective stress increases from 10 to 20 MPa. This seems reasonable, given the observation that yielding, and thus the strong inelastic compaction, starts just *below* 10 MPa (in the range of 7 to 9 MPa, Fig. 4a). For the strain during depletion-induced loading (i.e. from 10 to 20 MPa in the present tests), average values of 30 and 21 millistrain were taken for Mukhaizna and Thayfut, respectively (Fig. 5a). Low, average, and high-cases were then computed based on the data in Table 2, predicting an axial (vertical) compaction of 53, 62 and 73 millistrain, respectively, during Mukhaizna depletion (Table 3, and Fig. 8a) and 44, 53 and 64 millistrain during Thayfut depletion (Table 3). This result implies that the vertical reservoir compressibility of the high-porosity intervals is in the range of $4x10^{-3}$/MPa to $7x10^{-3}$/MPa, provided that (a) the compaction mode is uniaxial strain, (b) temperature effects on compaction and creep are negligible, and (c) the creep model of Eiksund et al (1995) is valid. The normalised porosity reduction after low-, average-, and high-case creep correction was 0.87, 0.85 and 0.82, respectively, for Mukhaizna, and 0.91, 0.89 and 0.87 (Fig. 8b), respectively, for Thayfut. This corresponds to a reduction of about 3 to 6 porosity units for Mukhaizna and 3 to 5 porosity units for Thayfut.

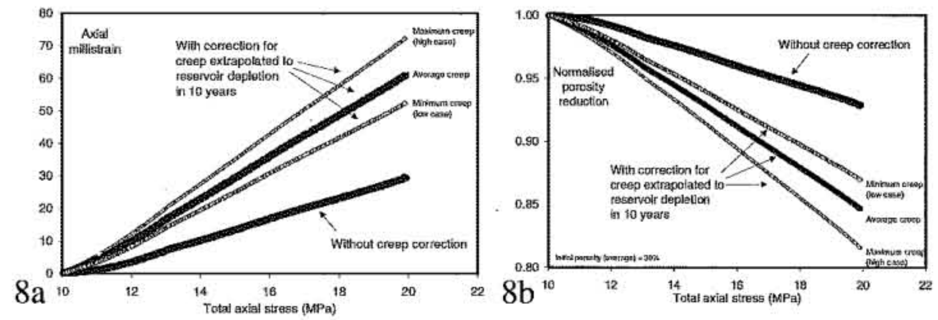

Figure 8. Prediction of axial compaction (Fig. 8a) and porosity reduction (Fig. 8b) for Mukhaizna with and without a correction for the creep compaction.

	Mukhaizna *During loading: 30 ms*		Thayfut *During loading: 21 ms*	
Case	Axial millistrain (= vertical millistrain)	Normalised porosity reduction	Axial millistrain (= vertical millistrain)	Normalised porosity reduction
Low-case	53	0.87	44	0.91
Average	62	0.85	53	0.89
High-case	73	0.82	64	0.87

Table 3. Predicted compaction and porosity reduction during 10 MPa depletion in 10 years

5. CONCLUSIONS, IMPLICATIONS AND RECOMMENDATIONS

- The compressibility of the Mukhaizna and Thayfut sandstone and sands ranges from $2x10^{-4}$/MPa to $3x10^{-3}$/MPa, and increases with increasing porosity, increasing grain size, and decreasing calcite and feldspar cement.
- At low stress and strain levels, the dominant compaction mechanism is grain rotation/sliding, probably triggered by brittle defirmation at grain contacts. High stress/strain behavior is characterised by intra/transgranular fracturing, time-dependent compaction (creep) and grain size reduction. This behavior is accompanied by an increase in compressibility (yielding) and by an increase in the stress path coefficient K, defined as $\Delta S_{hor}/\Delta S_{vert}$.
- Most of the high-porosity samples that were compacted under uniaxial strain conditions yield before reaching the inferred virgin in-situ stress state. After yielding, compaction was linear with stress, and the average compressibility was about $3x10^{-3}$/MPa. It is unknown why yielding occurs at such a relatively low stress. Core damage effects cannot be excluded. The shape of the yield surface and its dependence on porosity should be investigated.
- Comparison of the compaction data obtained along different stress paths showed that: (a) the pre-stress path exerts a negligible influence on compaction in the range of 10 to 20 MPa, and that (b) uniaxial compaction is a factor of two to six times larger than compaction with constant K = 0.6.
- The creep strain can be described by the logarithmic time function proposed by Eiksund et al. (1995). Extrapolation of such empirical relations yields creep strains of several tens of millistrains (i.e., several percent) over the 10 years of depletion. Adding this value to the strain measured during simulated depletion indicates a uniaxial reservoir compaction of up to 59 (± 14) millistrains, and associated porosity reductions of 3 to 6 porosity units.
- Combining the extrapolated creep strain with the experimental data during simulated depletion predicts a vertical reservoir compressibility of the high-porosity intervals in the range of $4x10^{-3}$/MPa to $7x10^{-3}$/MPa, provided the compaction mode is uniaxial strain, temperature effects on creep are small, and the model proposed by Eiksund et al. is valid for Mukhaizna/Thayfut.
- The experiments indicate that the depletion-induced compaction of the Gharif Formation may lead to vertical compaction of 50 to 75 millistrain and a reduction of up to 6 porosity units. This high compaction may act as a driving force for primary hydrocarbon recovery (*compaction drive*).
- The experimental data were used to interpret a well-interference field test, where production was studied as a function of depletion from a small area. The average field compressibility obtained from this independent source was 10^{-3}/MPa. This is a factor of three lower than the average experimental data, suggesting that low-compressibility layers are present in the reservoir.
- The potential consequences of this high compaction are surface subsidence, permeability reduction, and possibly casing damage, particularly if the reservoir compaction has significant vertical variation. In extreme cases, high compaction can also trigger earth tremors. Studies are in progress to address these issues, and also to gain a better understanding of creep. Compaction monitoring devices are being installed in the Mukhaizna field.

Acknowledgements

We thank the Oman Ministery of Oil and Gas and Shell Research (Rijswijk, The Netherlands) for their permission to publish this paper, and SINTEF Petroleum Research (Trondheim, Norway) for the support to present this work.

REFERENCES

Atkinson, B.K. (ed.) (1987) *Fracture mechanics of rock.* Academic Press, London.

Barends, F.B.J., F.J.J. Brouwer & F.H. Schröder, *1995 Land Subsidence: Natural causes, measuring techniques. The Groningen gasfields.* Proceedings of the Fifth International Symposium on Land Subsidence (FISOLS). Balkema, Rotterdam.

Bernabé, Y., Fryer D.T. & Shively, R.M. (1994) Experimental observations of the elastic and inelastic behaviour of porous sandstones. *Geophys. J. Int.* **117**, 403-418.

Borchers, J.W. (ed.) (1998) Land subsidence case studies and current research. *Association of Engineering Geologist Special Publication* **No. 8.**, Proceedings of the Dr. Joseph F. Poland Symposium on Land Subsidence. Star Publishing Company.

Chilingarian, G.V., Donaldson, E.C. and Yen, F.F. (1995) Subsidence due to fluid withdrawal. *Developments in Petroleum Science* **41**, Elsevier Science, Amsterdam.

Critescu, N.D. & Hunsche, U. (1998) *Time effects in rock mechanics*. Wiley & Sons.

Curran, J.H. & M.M. Carroll (1979). Shear stress enhancement of void compaction *J. geophys. Res.*, **84**, 1105.

Eiksund, G., Svanø, G. & Nagel, N.B. (1995) Creep related subsidence caused by oil and gas extraction," (1995) In: *Land Subsidence*, Barends, F.B.J., Brouwer, F.J.J. & Schröder, F.H. (eds), Published by the *IAHS*, N° **234**, 277.

Espinoza, C. & Mirabal M. (1988) Venezuelan experience in simulation of compaction and subsidence associated to oil production. Paper presented at the *4th UNITAR/UNDP Conference on heavy crude and tar sands.*

Fisher, Q.J., Casey, M., Clennell, M.B. & Knipe, R.J. (1999) Mechanical compaction of deeply buried sandstones of the North Sea. *Marine and Petr. Geology* **16**, 606-618.

Geertsma, J. (1973) A basic history of subsidence due to reservoir compaction: The homogeneous case. *Verh. Kon. Geol. Mijnbouwk. Gen.*, **28**, 43-62.

Hettema, M.H.H., Schutjens, P.M.T.M., Verboom B.J.M. & Gussinklo H.J. (1998) Production-induced compaction of sandstone reservoirs: the strong influence of field stress. *SPE* 50630, Paper presented at the EUROPEC Conference, October 1998, The Hague, The Netherlands.

Lievaart, L., Al Hinai K.M., Al Khabori K.J., Van Wunnik J., Masson D., Al-Kindy I.H. & Mul, P.J. (1996) Technology leading the way to Mukhaizna heavy oil development. *SPE* **30242**, 31-40.

Puig, F. and Schenk, L. (1984) Analysis of the performance of the M-6 area of the Ta Juana Field, Venezuela, under primary, steam-soak, and steamdrive conditions. *SPE/DOE*, **12656**.

Rhett, D.W. & Teufel, L.W. (1992) Effect of reservoir stress path on compressibility and permeability of sandstones. *SPE*, **24756**.

Santarelli, F. J., Tronvoll, J., Svennekjær, M, Skeie, H., Hendriksen, R. & Bratli, R.K. (1998) *SPE/ISRM*, **47350**. Proceedings of EUROCK 1998, 203-210.

Schutjens, P.M.T.M. & De Ruig H. (1997). The influence of stress path on compressibility and permeability of an overpressured reservoir sandstone : Some experimental data. *Phys. Chem. Earth* **22**, N° 1-2, p. 97-103.

Schutjens, P.M.T.M., Blanton, T.L., Martin J.W., Lehr B.C. & Baaijens M.N. (1998) Depletion-induced compaction of an overpressured reservoir sandstone: an experimental approach. *SPE/ISRM* **47277**. Proceedings of EUROCK 1998, 53-63.

Teufel, L.W., Rhett D.W., & Farrell, H.E. (1991) Effect of reservoir depletion and pore pressure drawdown on in-situ stress and deformation in the Ekofisk field, North Sea. In: *Roegiers (ed.) Rock Mechanics as a Multidiscipl. Science*, Balkema, 63-72.

Wong, T.-F. & Baud P. (1999) Mechanical compactionof porous sandstone. *Oil & Gas Science and Technology - Rev. IFP*, Vol. **54** (6), 715-727.

3 Solid Extraction

LAND SUBSIDENCE CAUSED BY THE DRAINAGE OF ROCK MASS IN THE LEGNICA - GLOGÓW COPPER BASIN (POLAND)

Janusz Ostrowski and Edward Popiolek
University of Mining and Metallurgy, Chair of the Protection of Mining Areas, Al. A. Mickiewicza 30, 30-059 Kraków (Cracow), Poland

Abstract

In the paper the process of the formation of large area subsidence trough in the area of intensive exploitation of the copper ore deposit in the Legnica-Glogów Copper Basin - Legnicko-Glogowski Okrlg Miedziowy (LGOM) was presented. This trough was formed as a result of bailing an immense amount of underground water during development and exploitation work. In the paper the possibility of forecasting the future development of drainage-cased subsidence trough was also presented.

Keywords: mining, geodetic measurements, rock mass deformation process, indirect influence of mining.

1. INTRODUCTION

Discovered in 1957 in the region of Legnica and Lubin the deposit of copper ore belongs to the largest in the world (about 10% of world copper resources). This deposit is subject to intensive exploitation, which provides about 4% of world production of this important metal.

The deposit of copper ore is situated 400-1500 m under the surface, with an average decline of 3°-5° northeastwards. This is a seam-type deposit of a thickness varying from a few dozens cm to 20 m with about 3,5 m on average.

Preparation and exploitation robots in a deposit demand removing immense amount of water from overlay layers. Over 600 million m^3 of water have been pumped out so far. This resulted in the formation of a large subsidence trough ranging far beyond the borders of exploitation fields. The longer dimension of the trough already exceeds 40 km and the biggest confirmed subsidence approach 0,8 m.

The phenomenon presented in this paper does not cause a direct threat to the buildings in the area. It however causes a range of difficulties in the functioning of surface equipment and has a negative impact on environment.

One has to emphasize that a similar phenomenon, on a smaller scale, can be found in the areas of mineral coal exploitation, where beds are found in similar geological and hydrogeological conditions.

2. THE CHARACTERISTIC OF GEOLOGICAL AND HYDROGEOLOGICAL CONDITIONS

The deposit of copper ores is situated on very hard Triassic and Permian formations There is a several centimetres thick layer of Zechstein, red sandstone and carbonate rocks directly above the bed. Further up, till the surface, there are usually incoherent layers from the Tertiary an Quaternary of a thickness from 300 m up to above 500 m. There are packs of strongly water saturated rocks, separated by impermeable layers. This system of rock layers stimulates a benign course of surface deformation process, caused by the exploitation of the deposit. Immense deposits of water, often lying under a high pressure, cause serious difficulties in mining exploitation.

Within the Legnica-Glogów Copper Basin two main water-bearing complexes are distinguished (Fig. 1):

- Cenozoic – in incoherent formations of Tertiary and Quaternary layers with an inter-granular circulation,
- Triassic and Permian – in dense (porous and chink-shaped) rocks of Bunter Sandstone, Zechstein and Rotligendes rocks with a mainly slit-type circulation.

Both complexes consist of many water-bearing horizons. In a Cenozoic complex, within the Tertiary formation three water-bearing horizons occur: the "undercarbonate", "intercarbonate" and "supercarbonate" one. In the Quaternary formation there are Pleistocene and Holocene water-bearing horizons. In the Triassic-Permian complex the horizons of Rotligendes and Zechstein (limestones and dolomites) occur, which make the Permian formation and horizon of Bunter Sandstone, belonging to Triassic formation.

The water-bearing horizon of "undercarbonate" Tertiary formations stays in direct hydraulic contact not only with the water-bearing Triassic formations, but also - through numerous sedimentation inliers – with the Zechstein limestone and dolomite formations and Rotligendes. The tectonics of a rock mass also plays an important role in forming this link.

Within the mining area of the Legnica-Glogów Copper Basin (LGOM) Quaternary water-bearing formation is separated from older formations by the layer of Pliocene argil from a Poznan series.

Second impermeable layer consists of Miocene argil and separates Tertiary water-bearing horizons – "supercarbonate" and "intercarbonate" ones from the "undercarbonate" horizon and Triassic and Permian formations.

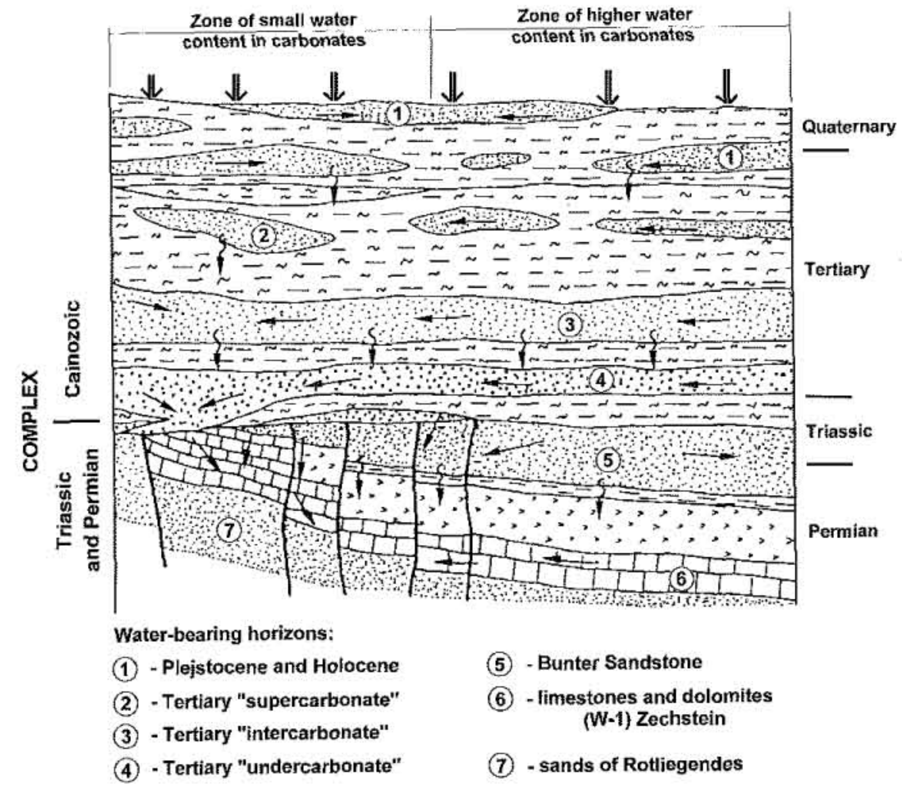

Figure 1. The scheme of the hydrodynamic conditions in Legnica –Glogów Copper Basin

3. GEODETIC OBSERVATIONS OF THE LAND SUBSIDENCE IN THE LGOM

Established in 1959-60 in the area of the Legnica-Glogów Copper Basin (LGOM) network of precise levelling in 1975-1977 was extended and nowadays includes the area of about 2300 km². It consists of levelling traverses 1241 km long and including 78 node marks (Fig. 2).

The accuracy of precise levelling done in the area of LGOM can be characterised in the following ways:

- mean square error of the network measurement (after the levelling) $m_0 = 0.8 – 1.2$ mm/km,
- average value of mean square error of determining the height of the node mark in the latest (1998) series of measurements $m_H = 3.6$ mm,
- average value of mean square error of determining the height of the node mark from earlier measurements, done for many years $m_H = 2.5$ mm.

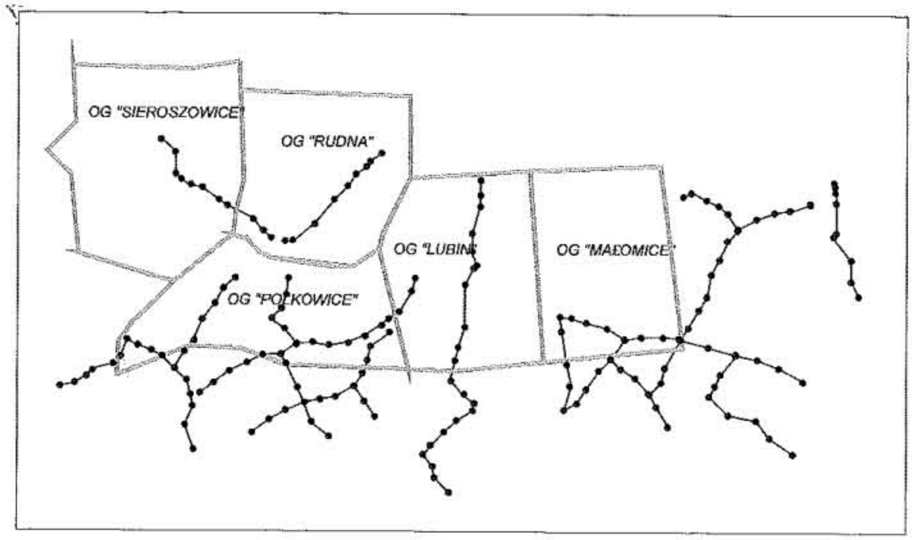

Figure 2. The scheme of the observation network in LGOM

In geodesy there is a rule that changes (in this case changes in height – subsidence) are regarded as certainly existing when the differences are greater or equal triple value of mean square error. According to the results of the observations one can agree that the changes in height equal 10 mm can be treated as those caused by mining exploitation.

4. THE CHARACTERISTICS OF THE DEVELOPMENT OF LARGE AREA SUBSIDENCE TROUGH

The extensiveness of the influence caused by the drainage of the rock mass and resulting from this practical purpose demand making the maps of periodical and permanent subsidence caused by this drainage. These maps have been systematically made (every second year) as the results of height measurements (levelling) in LGOM have been obtained.

As an example in Figure 3 a map of permanent subsidence caused by the drainage of the rock mass is presented.

Comparing and analysing the maps of the subsidence from various periods it can be reviewed how a large surface subsidence trough in the LGOM area developed.

Already in 1973 subsidence trough on a large area was noticed. It shape was an ellipse about 30 km long and about 6-10 km wide towards the dip of the deposit. The bottom of a maximum subsidence of 186 mm was noticed in the Obora village.

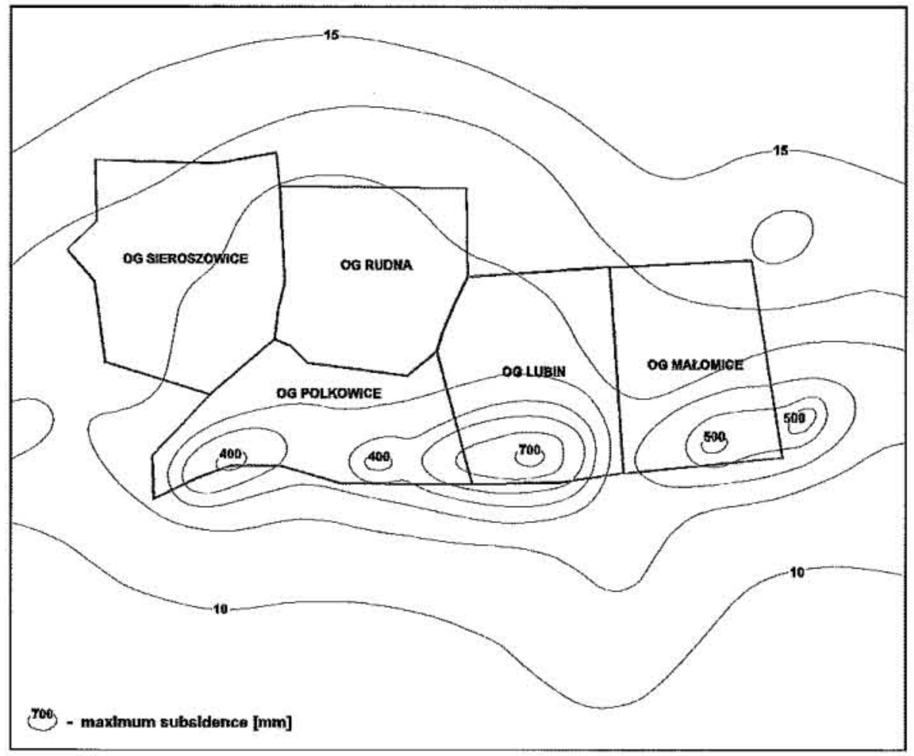

Figure 3. Large surface subsidence trough (state from 1998)

The map of permanent subsidence from 1979 indicates that the trough in the region of Obora village deepened up to 413 mm and a subsidence trough in the area of Niemstów-Osiek was formed. Its maximum subsidence was 194 mm (Table 1).

From the 1985 map of permanent subsidence one can see that maximum subsidence in the central regions of subsidence troughs increased up to 568 mm in Obora and 363 mm in Niemstów-Osiek. There was also a distinct increase of their range southwards.

The map of permanent subsidence from 1990 shows that local subsidence trough deepened up to 650 mm in Obora region and up to 459 mm in Niemstów-Osiek. New local subsidence troughs were also formed in the region of Jldrzychów (with a maximal subsidence of 411 mm) and in Parchów (of a maximal subsidence 177 mm). Before that these troughs could no be distinguished.

Table 1. Maximal (permanent and periodical) land subsidence in a selected areas of LGOM

SUBSIDENCE PERIODICAL													
71-73	73-75	75-77	77-79	79-81	81-83	83-85	85-88	88-90	90-92	92-94	94-96	96-98	REGION
587 2,7	556 4,4	590 9,6	555 4,4	588 2,1	590 7,2	590 65,1	590 68,0	590 49,8	590 32,3	591 73,9	591 90,7	590 30,0	PARCHÓW
530 6,9	530 3,4	530 12,9	530 6,2	530 10,2	530 5,1	530 18,5	530 37,6	530 19,3	530 1,6	530 11,0	530 9,2	530 12,0	POLKOWICE
902 88,3	896 82,8	896 72,1	896 80,9	897 35,3	897 59,3	896 45,1	896 53,4	896 29,5	896 14,8	896 15,5	896 30,5	896 13,0	OBORA
771 12,0	771 10,0	771 19,8	771 11,1	771 7,9	771 36,4	771 163,0	771 87,3	771 31,9	771 13,8	771 13,3	771 21,5	771 16,0	JÊDRZYCHÓW
-	-	-	1004 17,9	1004 36,9	1004 25,8	1004 25,4	1004 32,6	1004 18,0	1004 2,9	1004 2,2	1004 17,5	1004 15,0	ZABORÓW
876 36,8	876 38,3	875 35,7	876 50,8	876 41,4	876 81,2	876 46,3	876 57,2	876 39,0	876 16,8	876 15,5	876 33,2	876 15,0	OSIEK
981 30,8	979 27,2	980 29,8	980 59,7	980 49,6	980 94,0	980 43,9	980 51,7	980 32,0	981 10,0	981 17,0	981 26,4	981 15,0	NIEMSTÓW

SUBSIDENCE PERMANENT														
1971	1973	1975	1977	1979	1981	1983	1985	1988	1990	1992	1994	1996	1998	
589 4,2	590 7,7	589 11,2	591 17,7	589 21,2	589 22,6	589 27,6	588 80,5	588 138,8	588 177,4	588 199,0	588 238,4	588 316,5	588 376,5	PARCHÓW
-	530 8,8	530 12,2	530 25,1	530 31,3	530 41,5	530 46,6	530 65,1	530 102,7	530 122,0	530 123,6	530 134,6	530 143,8	530 155,8	POLKOWICE
902 97,5	902 185,8	902 266,7	896 332,0	896 412,9	902 413,3	896 522,9	896 568,0	896 621,4	896 650,9	896 665,7	896 681,2	896 711,7	896 724,7	OBORA
771 17,7	771 29,7	771 59,5	771 70,6	771 78,5	771 114,9	771 278,0	771 365,3	771 397,2	771 411,0	771 411,0	771 424,3	771 446,8	771 462,8	JÊDRZYCHÓW
-	-	-	1003 20,0	1004 32,9	1004 69,8	1004 95,6	1004 121,0	1004 153,6	1004 171,6	1004 174,5	1004 176,7	1004 194,2	1004 209,2	ZABORÓW
877 28,3	876 71,8	876 110,1	876 143,1	876 193,9	876 235,3	876 316,5	876 362,8	876 420,0	876 459,0	876 475,8	876 491,3	876 524,5	876 539,5	OSIEK
981 34,5	981 65,3	981 92,3	981 120,6	981 178,1	980 225,5	980 319,5	980 363,4	980 415,1	980 448,1	980 456,5	980 470,0	980 494,5	980 504,5	NIEMSTÓW

877 – point number 110,1 – permanent and periodical land subsidence

In the distribution of arising earlier local subsidence troughs did not change dramatically. However a new, previously only slightly marked subsidence trough in the region of Zaborów appeared. Maximum subsidence increased to 94 mm there.

An example of growing permanent subsidence in central regions of local subsidence troughs is presented in figure 4.

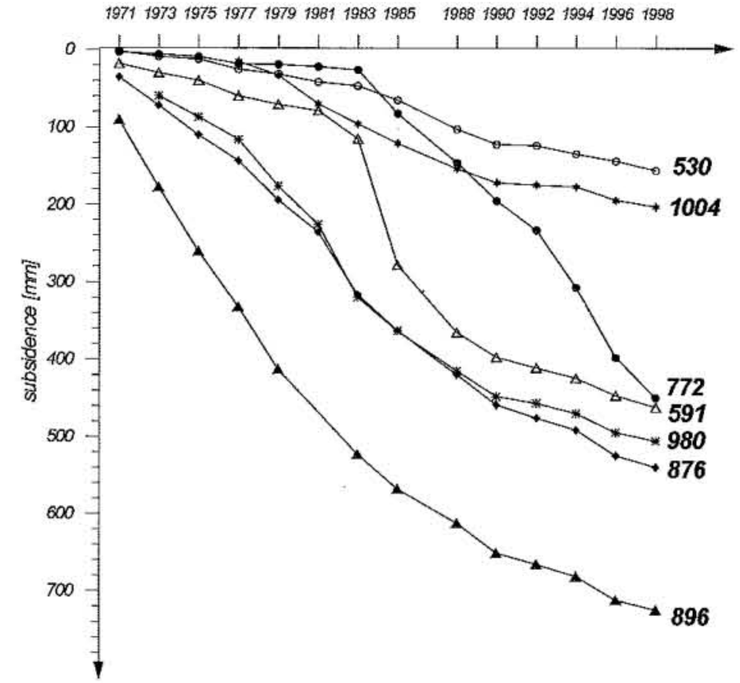

Figure 4. Graphs of the increase of maximal subsidences in local subsidence troughs.

From the analysis of the results of the observations one can draw the conclusion that central node marks of local subsidence troughs, where in 1971-1973 maximum subsidence appeared, in principle did not change their location.

From the map of permanent subsidence (Fig. 3) it results that:

- four among those central node marks, namely: node mark 590 (Parchów region), node mark 771 (Jędrzychów region), node mark 896 (Obora region) and node mark 876 (Osiek region) are situated approximately on a straight line,
- three central node marks, namely: node mark 876 (Osiek region), node mark 980 (Niemstów region) and node mark 1004 (Zaborów region) are also situated approximately on a straight line which makes an angle with the previous one of about 150^0.

The results of the geodetic observations allow to look through the changes of the value of such an important factor as mean annual changes in the height of the observed node marks, thus mean average speed of the increase of drainage caused subsidence.

In the course of the node marks subsidence, the changes of which were registered from the beginning, three stages can be distinguished: initial stage of a very small speed of the subsidence increase (e.g. 1,8 mm/year in the Parchów region); intensive increase of subsidence (e.g. 25 mm/year in the Parchów region); and final stage of the subsidence of a few mm per year. It is important that even in the stage of intensive surface movements the speed of subsidence growth did not exceed 40 mm/year. This means that the process of the formation of large surface subsidence trough is slow and there is no danger resulting from its dynamics.

5. CAUSES AND RESULTS OF THE FORMATION OF A LARGE SURFACE SUBSIDENCE TROUGH

According to the present views on the arising and development of a large surface subsidence trough in the area of LGOM it is assumed that its development is related to the consolidation of the rock mass, resulting from diminishing or eliminating the hydrostatic pressure on the roof of artesian water-bearing horizon.

Within each water-bearing horizon there is a certain stress, caused by the weight of impermeable layers, situated above the roof. Artesian pressure on the impermeable roof of the water-bearing horizon eliminates an effective pressure of overlying layers. Any decrease of artesian pressure caused by the drainage of water, e.g. to post-mining excavations, decreases the force pushing on the roof of water-bearing horizon and results in the increase of the pressure on the rock skeleton of this layer and its consolidation. With limited abilities of side deformations this consolidation can be seen as diminishing the thickness of the layer under stress, which finally causes the subsidence of land subsidence.

The process of subsidence in time and the period necessary for a complete consolidation of rock mass, according to a new balance depends, first of all, on filtration properties of rocks subdued to this process and on the possibilities of draining the "pressed out" water.

The factor that has initiated and still has been shaping the process was first of all many years lasting drainage of the rock mass done by the copper ore mines in LGOM. So far as the result of drainage over 575 mln m^3 of water have been pumped out of the rock mass.

Lasting many years drainage of the rock mass caused far-going changes in the system of natural hydromechanical conditions of respective water-bearing horizons. The symptoms of these changes are deformation of the original shape of piezometric surface and the change in the resources of underground waters effected by the drainage of mines.

Present observations are run on 54 piezometers, which were located mainly in the mining areas, which does not give the opportunity to determine the range

of the drainage taking place. This makes us seek ways of identification of this range, first of all by geodetic methods.

The comparison of the distributions of mean annual depressions with the distribution of mean annual subsidences of node marks on the surface allows to draw a conclusion that there is a connection between these changes.

The confirmation of this connection can be the comparison between the changes in depression registered in piezometer H-6 with the increase of the subsidence of node mark 896 (situated near this piezometer) and the amount of water pumped off the rock mass (Fig. 5). Such a big compliance of the development of depression cone with a development of subsidence trough on the surface of the area can, under certain circumstances, make basis for the forecasting of the development of subsidence trough. Also from the knowledge of the development of subsidence trough one can make the conclusions of the state of the depression cone, which, as it was earlier mentioned, plays a particular role where there are no piezometric measurement.

6. THREAT TO THE AREA SURFACE RESULTING FROM THE PROCESS OF THE DEVELOPMENT OF A LARGE SURFACE SUBSIDENCE TROUGH

Looking at the changes in the surface of the area, caused by drainage, especially Tertiary, "undercarbonate" water-bearing horizon, the newly created and developing large surface subsidence trough should be treated, from the point of view of damage, in the same way as troughs caused by direct impact of mining exploitation.

A characteristic feature of land subsidence caused by the drainage of the rock mass is their very slow increase. Thus the harmfulness of this process for the surface of the area has been very small. In central node marks of local troughs, the average speed of growth is 26.2 mm/year with the maximum value of 40 mm/year. It should however be stressed clearly that in the area of maximal increase of subsidence harmful or even visible changes in the surface area cannot appear.

In the area of intensive drainage subsidence the measurements on observation lines of the sides length equal 48 m were made. This allowed to estimate maximum inclinations and horizontal deformations of the area. These indexes determine the degree of the threat to the area. The observed values did not exceed 0.3 mm/m. Based on this one could conclude that within the developing large surface subsidence trough caused by the drainage system, horizontal deformations or inclinations able to make a threat to the area surface or buildings in the area have not occurred. For the values of these deformation indexes are smaller, even for the objects least resistant to mining-caused impact.

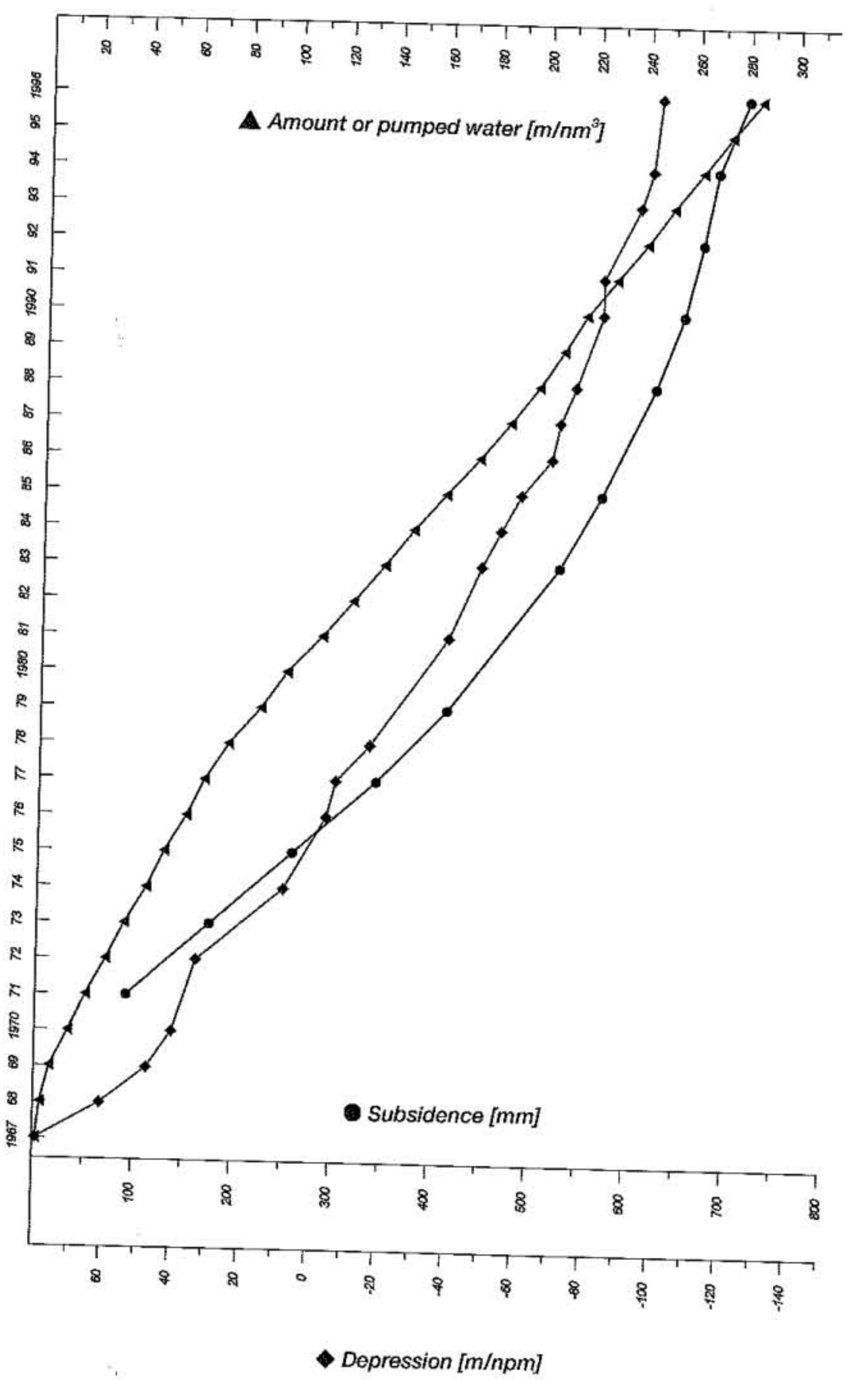

Figure 5. The graph of changes of the depression in H-6 piezometer in the relation to the subsidence of node mark no 896 and the amount of water pumped out the rock mass.

7. FINAL REMARKS

Distinguishing and registering a large surface subsidence trough caused by the rock mass drainage as well as the monitoring of its further development became possible owing to highly precise geodetic measurements (precise levelling of 2^{nd} class), systematically carried out from the time of starting the mining exploitation of copper ores up till now.

High accuracy of geodetic observations allows to assume remote influence of rock mass drainage, where land subsidence is very small. It also makes piezometric observations are carried out.

The results of geodetic observations indicate that the large surface subsidence trough consists of seven local subsidence troughs the central regions of which have not changed their layout since they were first registered.

Systematic geodetic observations carried out in 1965-1998 allow us to state the following:

maximal permanent subsidence in one of local troughs is about 725 mm,

maximal speed of increasing the subsidence in the regions of the biggest changes did not exceed 30 mm/year, i.e. about 0,6 mm/week.

The changes in the surface of the area are characterised by such values of deformation indexes that do not make any threat for this area or buildings located there.

The analysis of the results from geodetic and piezometric observations indicates that there is a tight link between the increase in the subsidence and the amount of water pumped from the rock mass and the changes of the water level in piezometers.

REFERENCES

Collective paper (1996), *Monografia KGHM Polska Miedl S.A. Lubin.*

Knothe, S. (1984) *Prognozowanie wplywów eksploatacji górniczej.* Wydawnictwo, Illsk".

Milewski, M.(1985) Problematyka badal wplywów eksploatacji górniczej na powierzchnil terenu i górotwór w warunkach Legnicko-Glogowskiego Okrlgu Miedziowego. *Materialy II Krajowego Sympozjum nt. „Ochrona powierzchni przed szkodami górniczymi",*

Popiolek, E., Milewski, M., Ostrowski, J.(1997) Usage o wyznaczaniu granic terenu górniczego dla kopall podziemnych warunkach LGOM. *Bezpieczelstwo Pracy i Ochrona lrodowiska w Górnictwie* **5**(33), i **6**(34)

Popiolek, E., Milewski, M., Ostrowski, J.(1994) Zasady wyznaczania filarów ochronnych w Legnicko-Glogowskim Okrlgu Miedziowym. *Rudy i Metale Nielelazne*, **5**,

Popiolek, E. z zespolem (1998) Analiza rozwoju wielkopowierzchniowej niecki obnileniowej terenu na obszarze LGOM wywolanej odwodnieniem warstw trzeciorzldowych i czwartorzldowych wraz z podaniem matematycznego modelu zjawiska w oparciu o wyniki niwelacji precyzyjnej w 1996 r. *Opracowanie Katedry Ochrony Terenów Górniczych AGH Kraków.*

LAND SUBSIDENCE - Vol. I
Proceedings of the Sixth International Symposium on Land Subsidence
Ravenna / Italy / 24-29 September 2000

HALOKINESIS AND SUBSIDENCE IN THE PRICASPIAN BASIN (RUSSIA)

Leonid Anissimov and George Moscowsky
Saratov State University, Astrakhanskaya 83, Saratov 410026, Russia

Vladimir Sinyakov
Volgograd Architecture and Construction Academy, Academicheskaya 1, Volgograd 4000074, Russia

Abstract

The Pricaspian Basin is an area, which has undergone great subsidence during the Paleozoic, Mesozoic and Cenozoic times. These events created the complex basin with sedimentary section to 20000 m thick in the central part including the thick evaporitic deposits. Geological and geomorphologic analysis of subsidence structures in the suprasalt formations has been carried out to assess the dynamics and mechanism of the salt movement and its environment impact. Implication of these data may be useful in planning petroleum production and underground storage facilities.

Keywords: salt structures, subsidence, geomorphology, Pricaspian Basin

1. INTRODUCTION

The study area consists of approximately 600,000 km^2 in the South Volga Region of Russia and Western Kazakhstan. This is a great basin with Permian salt deposits and more than 1000 salt domes around the basin (fig.1). Mobilization of the thick (some thousand meters) evaporitic deposits during salt domes growth enhanced the effect of the tectonic subsidence in the inter-diapiric areas. Another type of subsidence structures has been formed above salt diapirs. These are grabens, which have commonly been interpreted as forming by salt dissolution. Salt-related structures distribution correlate with the topography, hydrographic systems, thickness and parameters of Quaternary sediments.

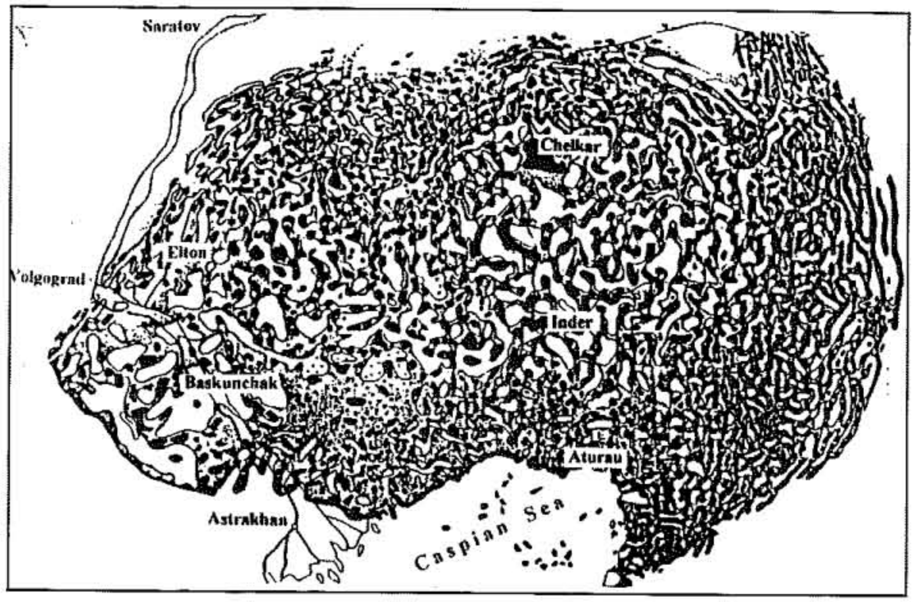

Figure 1. Pricaspian Basin: Salt diapirs distribution.

2. LAND SUBSIDENCE RELATED TO HALOKINESIS

The Kungurian salts were deposited on the floor of an inland sea surrounded by an extensive desert. The overlying Upper Permian and Triassic successions include red beds and marine clastics. Diapirism started during this period as some diapirs reached the surface of the Middle Jurassic unconformity. The next subsiding stage included the Middle and Late Jurassic, Cretaceous and Tertiary periods and it was accompanied by the salt dome growth. The principal part of diapirs reached the pre-Apsheron (N_2) unconformity. The most active diapirs (Baskunchak, Elton, Azgir, Inder) pierced Neogene and Quaternary sediments and created specific landscapes on the surface. These are complex graben structures with a salt lake in the centre and adjoined uplifted sediments.

Baskunchak is the most outstanding structure in the Pricaspian Basin with all the attributes: uplifted sediments (Great Bogdo Hill), salt lake and subsiding fields. Great Bogdo Hill is located in the south of lake and Mesozoic sediments rise is 170 m above the surface of lake. Examination of the diapir growth and related prediapir area subsidence has been carried out on the Baskunchak structure by Pevnev (1968). Position of geodetic network is shown on the map of the Baskunchak zone (fig.2) and the results of leveling on 1951, 1958 and 1961 are shown on fig.3. Modern elevation of Baskunchak dome is 1 mm in a year, calculation of the growth rate shows that the neotectonic movements are more important in comparison with ancient periods. Other salt domes, which have been studied, are characterized by the rise of the same rate during the Quaternary time.

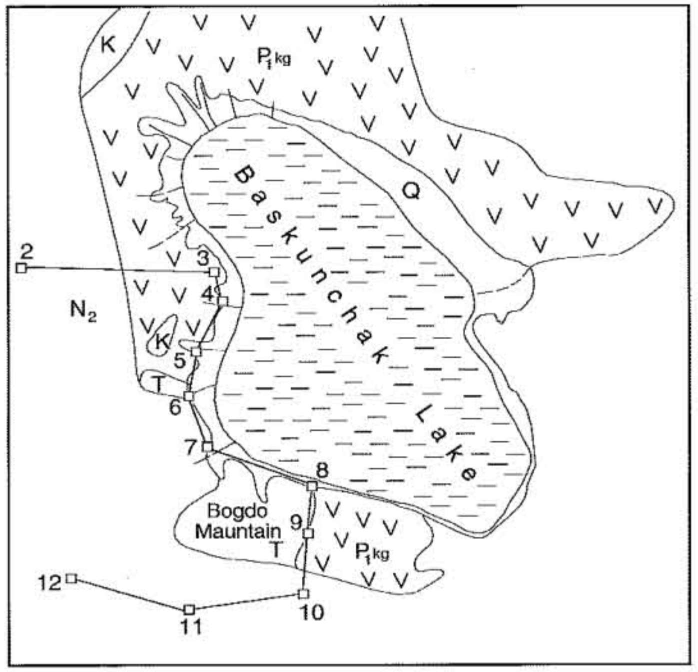

Figure 2. Geological map of the Baskunchak area.

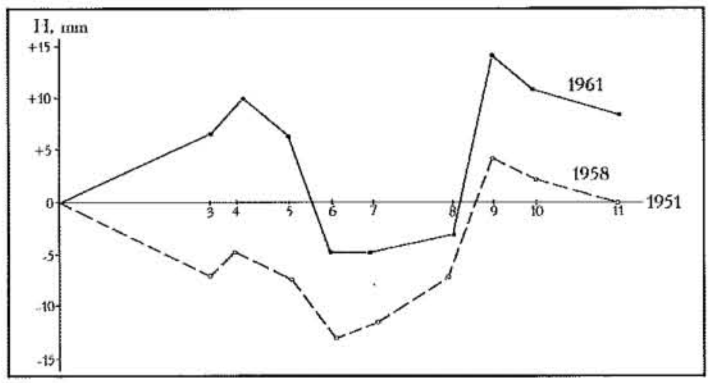

Figure 3. Baskunchak structure: relative position of land surface; Leveling on 1951, 1958, and 1961 (Pevnev,1968).

Baskunchak salt deposits are located on the top of vast salt dome and they have been created by dissolution of Permian salt and sedimentation of salt by solar evaporation. Lake is 10*9 km in size and its area is about 100 km^2.

Secondary salt deposits, which were formed during the Quaternary, are about 400 m in thick. Some clastic layers are included in the salt column proving the humid periods in the life of lake. Salt surface is usually dry but in the wet seasons the lake is covered by brine of 20-25 cm in thick.

There are two extended outcrops of gypsum on the sides of the lake. The extence karstification takes place on the plane especially near the sides of the lake. Karstification of evaporites and the subsidence of the overlying sediments create different geomorphological structures mainly sinkholes. Some of them up to 100 m in diameter and 2-5 m in depth. But fresh sinkholes may be up to 20-25 m in depth.

Salt withdrawal from the interdiapiric zones was accompanied by the great subsidence rate. There are some depressions where salt deposits have been withdrawn completely. The thickness of the Quaternary in these areas can be reached up to 500 m and the thickness of Upper Neogene sediments is up to 3000 m. Assessment of the rate of diapir rise and interdiapiric depression subsidence shows the acceleration of these processes during the geological time for some areas of the Pricaspian Basin. In spite of this fact, the shape of diapirs shows the early stage of halokinesis in the Pricaspian Basin in comparison with the Gulf Coast and German Zechstein Basins.

Grabens above salt domes have usually been interpreted as forming by salt dissolution. Baskunchak case shows that the karstification processes and salt redistribution play very important role for the land subsidence though some authors (Ge and Jackson, 1998) show that most crestal grabens in nature can be explained by tectonic movements and the role of dissolution in deformation around diapirs may be overestimated. In any case subsidence on the salt dome region is more differential in comparison with interdiapiric zones.

3. ENGINEERING GEOLOGY OF SUBSIDING ZONES

The thickness of the Pliocene-Quaternary sediments depends on the position of locality: on the dome or on the interdiapiric area. The thickness of Quaternary clays and sands on the deepest depressions is up to 500 m; in contrast, the thickness of the same sediments decreases to 30-40 m above salt domes. Now subsidence zones are presented geomorphologically by salt lakes, salinas and playas.

Salt domes growth increases the erosion rate. Along the west Volga riverside the elevations of steeps above domes are 6-10 m higher than above interdiapiric depressions. The depth of groundwater level is more above the salt domes and, accordingly, the dryness of vadoze zone is higher as well. The difference of the Quaternary clay parameters above salt domes and interdiapiric depressions is shown on table 1.

Table 1. Geotechnical parameters of the Quaternary clays (average means)

Parameters	Domes	Depressions
Moisture content	0.29	0.40
Density, kg * m^{-3}	1860	1760
Liquid limit	0.56	0.58
Plastic limit	0.28	0.30
Plasticity index	0.28	0.28
Angle of internal friction	19	12
Cohesion, Mpa	0.031	0.036
Swelling pressure, MPa	0.45	0.0
Number of samples	212	193

4. ENGINEERING PROBLEMS

The surface of the Pricaspian Basin consists of lowlands, the surface level varies between +20-30 m on the north to -27 m on the south, near the Caspian Sea coastal zone. Significant variation in the Caspian Sea level occurred during last decades from -26 m (1930) to -29 m (1978) and rising to -27 m at present time. Land subsidence of some decimeters and sea level rise will have serious implications to the environment in the coastal zone of 100 km in width. Two giant hydrocarbon accumulations are situated in this zone and these processes can start on the nearest time.

Tengiz oilfield is located on the north-east part of the Caspian Sea coastal zone with the surface level -23 - -25 m. Oilfield stretches over an area of almost 400 square kilometers with the height of productive zone more than 1500 m. The top of the reservoir is at a depth of 3900 m and the overburden pressure is about 80 MPa. For the recovery the pressure drop to the normal means (40MPa) is in the range of 40 MPa on account of the matrix stress in the carbonate rocks. As a consequence reservoir compaction will develop causing land subsidence to some meters being the largest in the world for such cases. This process may accompanied by salt reactivation, faulting, oil migration to the shallow horizons and surface, seawater flooding.

Astrkhan gas field is located in the south-western part of the Pricaspian Basin, 40-50 km to the north from Astrakhan. The field is approximately 110 km long and 40 km wide with the height of productive zone to 225 m. Astrakhan gas field is currently considered to be largest sour gas field in the world, content of H_2S in gas varies from 16 to 31%. Reactivation of salt and overlying sediments caused by reservoir compaction and land subsidence can have dangerous consequences resulting from the toxic gas migration.

Field development creates some problems with industrial wastes and products storage. Some cavities for liquid hydrocarbon storage have been completed in the different sites of the Pricaspian Basin. Underground nuclear explosions were chosen as a main tool for the cavity construction instead of using leaching process. 15 cavities in salt domes near the Astrakhan gas field were formed by explosion in the period of 1980-1984. Initial cavity sizes range from 50000 m^3 to 70000 m^3, but their volume was decreased to 2000-3000 m^3 in some months. Quick cavern convergence shows the rate of salt movement and mechanical behaviour of the salt mass after the sharp activation of salt rocks by the extremely high temperature (Anissimov & Moscowsky, 1999).

Though the subsidence bowls after having squeezed caverns are relatively small, rendering a maximum subsidence of about 1 cm per 100000 m^3 of cavern volume (Fokker et al., 1995), quick cavern convergence after the sharp activation can promote dangerous processes such as a fault reactivation and earthquakes in geologically anomalous zones. Now some research programs are in planning on the Astrakhan gas field to study the environment impact of field development and accompanying operations.

REFERENCES

Anissimov, L.& Moscowsky, G. (1999) Salt rocks properties of the Pricaspian Basin: Wastes and product storage assessment. Proceedings of the 9th International Congress on Rock Mechanics, G.Vouille, P. Berest (eds.) Balkema, Paris, 33-35.

Fokker, P.A., Urai, J.L., Steeneken, P.V. (1995) Prodution-indiced convergence of solution mined caverns in magnesium salts and associated subsidence. In: Land subsidence. Proceedings of the 5th International Symposium on Land Subsidence. F. Barends, F. Brouwer, F. Schroder (eds.) Balkema / Rotterdam / Brookfield, 281-289.

Ge, H. and Jackson, M. (1998) Physical modeling of structures formed by salt withdrawal: Implication for deformation caused by salt dissolution. AAPG Bulletin, v.82, No 2, 228-250.

Pevnev A.K. 1968. Modern movements of the Earth Surface in the area of the Baskunchak salt structure. Moscow, Nauka. 100 pp. (in Russian).

LAND SUBSIDENCE - Vol. I
Proceedings of the Sixth International Symposium on Land Subsidence
Ravenna / Italy / 24-29 September 2000

SOIL STABILITY AS A CONSEQUENCE OF UNCONTROLLED DISSOLVING DURING SALT DEPOSITS EXPLOITATION

Dragica Stojiljkovic and Snezana Komatina
University of Novi Sad, Agricultural Faculty, Institute for Water Management, Place D.Obradovic 8, 21000 Novi Sad, Yugoslavia
E-mail: dragica@polj.ns.ac.yu
E-mail: komsne@yahoo.com

Abstract

Subsurface exploitation of some raw materials is follow by a series of negative occurrences at the terrain surface, which intensity depends on tectonic, geological and hydrogeological conditions within deposit. Long-term exploration of salt deposits in Tushanj and Tuzla (former Yugoslavia) directed us to conclusion: that soil instability is a cause and consequence of uncontrolled exploitation of natural salt water in the deposit. Mechanism of the source formation and its existence causes hanging - wall degradation (development of fracture-dissolution porosity in stripe marls), as well as soil instability, covering greater area than the area of the salt deposit. The instability is permanent and of low intensity. Lateral development of fracture-dissolution porosity (of so-called salt karst) excludes catastrophic fast settling of the terrain surface in short time intervals.

Key words: salt deposit, stripe marls, dissolution porosity, soil stability

1. INTRODUCTION

Salt deposit in Tuzla town is not known as a world-size interesting deposit for exploitation. That is the only one existent deposit at Balkan exploited by subsurface mining works and drilled wells. Beside salt, coal is also exploited here. Centuries-long extracting of salt and coal is followed by several negative occurrences, as level lowering of artesian aquifer, salt dissolving in the top and bottom of salt layers, soil falling in as well as vertical and horizontal movement at the terrain surface in the urban environment. For salt deposits it is very important to have enough information on Hydrogeology, because each disturbing of natural state causes fast degradation of the salt body and the whole rock mass in the footwall. All present deformations appeared as a result of long-term exploitation are a consequence of dynamics of hydrogeological and engineering-geological processes existing in the Neogene basin, developed because of extraction.

2. METHODS AND EXPLORATION

In the last century for controlled and uncontrolled pumping of salt water, almost 180 wells were drilled. In 1960, because of salt water penetration into subsurface mining works, in order to know more on Hydrogeology of the area, 17 piezometers was put along the edge of the salt deposit, and then, 20 (horizontal, crooked, vertical) boreholes from the pit of Tushanj mine.

At all boreholes, well logging and tracers were used to determine rock porosity. Artesian pressure of all aquifers from series was measured, and water samples collected for chemical, age and isotope analyses, hydrodynamical experiments and regime monitoring were organized. Results of the exploration made reinterpretation of the old geological profiles of the salt deposit possible.

3. GEOLOGICAL-HYDROGEOLOGICAL CHARACTERISTICS OF THE DEPOSIT

Analysis of hydrogeological problems at the fields Hukalo - Trnavac was not adequate in comparison to dynamics of drilling exploratory boreholes from the terrain surface as well as subsurface mining works at the Tushanj field. At the moment of salt-water penetration into mining works, attention was directed to hydrogeological aspects of the deposit. Salt deposit in Tuzla is of sedimentary origin, formed during chemical sedimentation in the lagoon. The deposit is of synclinal type, 0,7 km wide, 2,5 km long and 250-500 m deep. It consists 5 salt series (Fig.1, Fig.2) with minerals-halite, thenardite and anhydrite. Between them, layers of stripped marls and tuffites are present. Only the first series is with smooth synclinal position. The others are with steep slope towards SW, with deepening from the edge of the synclinal to the central parts.

The deposit is very complex because of frequent changing of salt, stripped marls and very intensive interval folding. Hanging-wall of the salt deposit is from Tortonian marls, clay, sands and conglomerates. Footwall was made of the deposit is stripped series-marls, shales and sandstones. As a result of surface water infiltration along the edge and over the dip of layers, salt minerals dissolving and forming lateral equivalents occurred. In other words, salt aquifers with different pressures and NaCl concentration were formed while, the state of salt artesian water equilibrium was present, they were discharging naturally through the springs at the terrain surface. With exploitation, natural state was disturbed. During 100-years long exploitation, lowering of the artesian aquifer pressure and 200 m level lowering happened. By radioactive tracers and pumping tests, changes in porosity of salt series lateral equivalents were determined (Table 1).

Table 1. Changes in porosity and transmissivity of the lateral equivalents.

	Filtration coefficient K (m/s)	Transmissivity T (m/s)
I dissolving zone of halite veins in hanging-wall	$1,33 \times 10^{-6}$ - $2,75 \times 10^{-7}$	$2,34 \times 10^{-5}$ - $4,38 \times 10^{-6}$
II dissolving zone of the first salt series and hanging-wall is underway	$9,67 \times 10^{-6}$ - $1,85 \times 10^{-7}$	$1,62 \times 10^{-4}$ - $1,92 \times 10^{-5}$
III zone of finalized dissolving of the first series and hanging-wall	$1,17 \times 10^{-6}$ - $2,19 \times 10^{-6}$	$1,89 \times 10^{-5}$ - $2,32 \times 10^{-5}$
IV reconsolidation zone	$< 10^{-7}$	$< 10^{-5}$

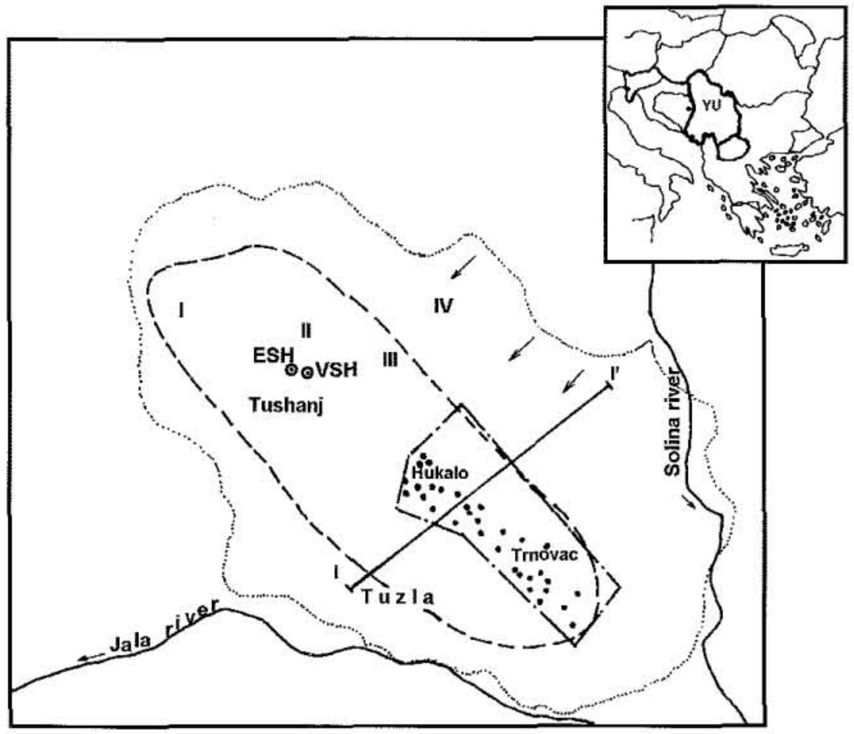

Figure 1. Location of the deposit with exploratory works and Hukalo - Trnovac cross-section.

In Fig. 2., results of the exploration are presented, showing that artesian aquifers are "steeply overlying" the hanging-wall and the youngest salt series. Note that one rock type, in dependence on degradation degree, could be aquifer or aquitard.

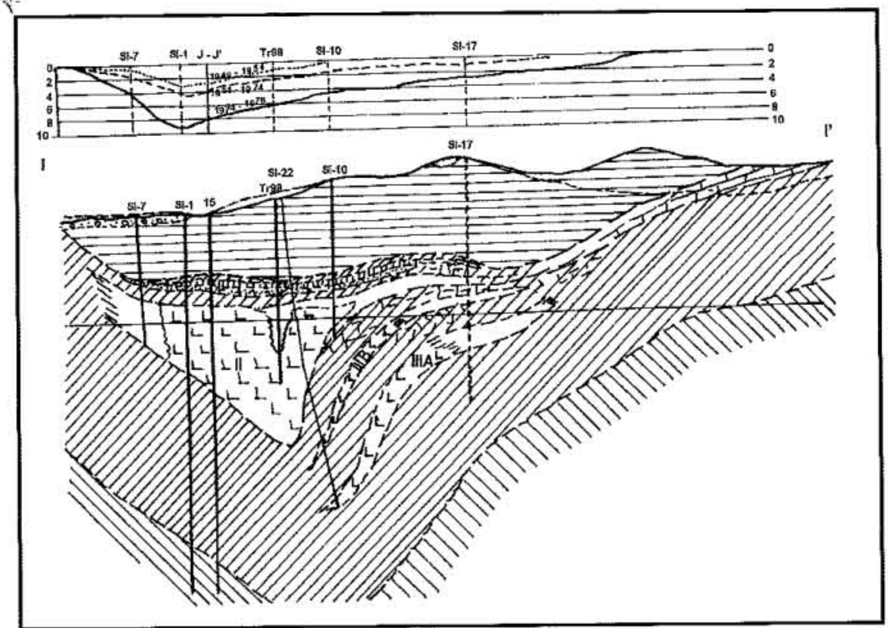

Legend for map and ydrogeological profile:

Alluvial deposit of the Jala river

Salt deposit I-II IIIa IIIb

Marls, clay, sandstone (ca rock)

Anhidrite

Stripe marls

Marly Breccia - products of side salt dissolution and salt water flow

Tufite and salt

Marls, clay, sandstone

Contour of salt deposit

Observation wells, abstraction boreholes

"O" line of the land subsidence

ESH Shaft (export, ventilation) VSH

I I' Trace of the profile

Figure 2. Diagram of soil subsidence intensity along Hukalo - Trnovac profile

4. TERRAIN SUBSIDENCE

Mechanism of the aquifer formed at the contact of salt series with low-mineralized infiltrated water is a main consequence of intensifying uncontrolled exploitation during the last century. However, the presence is determined (Surlan - Stojkovic, 1982) by a series of factors: morphologic, tectonic, geologic, and hydrogeologic, buts, at the same time, making salt water exploitation possible. The hanging-wall falling in, appearing as the soil subsidence at the terrain surface, directly depending on mechanism of forming and existing aquifer with fractured - karst porosity (salt artesian water), as the salt series lateral equivalents.

Temporary measurements of the soil subsidence were made till 1956, followed by organized monitoring from that time at the urban environment. In Fig. 2 soil subsidence during the last 50 years at the cross-section Hukalo - Trnovac around "O" line of subsidence is presented. In Fig. 3, correlation diagram: soil subsidence - exploited salt water quantity during the most intensive uncontrolled exploitation in shown.

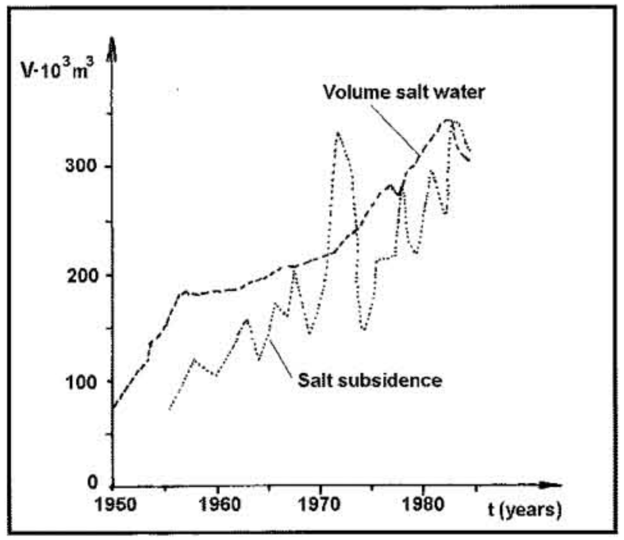

Figure 3. Dependence diagram of soil subsidence and salt exploitation

Subsidence contours are widening to the NW, and rock mass movements are dangerous for the Tushanj mineshaft. It is noticeable that maximal intensity of subsidence is not coinciding with areas of the highest degradation of the salt deposit, but they are shifted for φ angle in direction of the layers dip (Surlan - Stojkovic, 1982), which is 0,60 α (α-dip of layer).

Soil subsidence caused separating two parts of the town: Eastern and Western. In 1982, area of subsidence was over than 500 ha, or 18,5 % of urbanized part of the town subsidence of about 10 m was registered at the central part of the town (for 100 years). From the surface under sliding and subsidence, almost 1000 buildings and structures were destroyed and 15000 inhabitants moved out. Infrastructure objects were significantly destroyed and they are under reconstruction (Djuric and Vujkovic, 1987).

5. CONCLUSION

By the exploration, it was determined that aquifer in the deposit is recharged along salt series lateral equivalents. That is reason why terrain subsidence is of stronger lateral extensity in comparison to that in coal deposit. The only positive side of mechanism of artesian aquifer forming, is in fact that salt series degradation is to lateral sides, and hanging-wall sediments falling is continual, without catastrophic fast terrain subsidence in short time intervals. Stopping with uncontrolled exploitation from the terrain surface by drilled boreholes, and using other methods or new salt deposit "Tetima", smoothing of hydrogeological processes within the salt deposit will occur soon, and also engineering-geological processes at the terrain surface, enabling urban area of the town revitalization.

REFERENCES

Djuric, N. & Vujkovic, M. (1987) Sleganje terena na lezistu kamene soli u Tuzli uslovljeno nekontrolisanom eksploatacijom slanice i njihov uticaj na covekovu okolinu (Soil subsidence at salt deposit Tuzla caused by uncontrolled exploitation of salt water and effects on the environment). Proc. of IX Conf. of Hydrogeologists and Engineering-Geologists of Yugoslavia, Pristina, Vol. 2, 7-13.

Djuric, N. & Vujkovic, M. (1987) Hidrogeološke odlike područja okana rudnika soli Tushanj (Hydrogeological characteristics in area of Tushanj salt mine) Proc. of IX Conf. of Hydrogeologists and Engineering Geologist of Yugoslavia, Pristina, Vol.1, 73-18.

Surlan - Stojkovic, M. (1982) Pukotinsko-karstna izran uslov i posledice eksploatacije prirodnih slanica na sonom lezistu u Tuzli i osnovni uzrok sleganja povrsine terena (Fractured-karst aquifer as a condition and consequence of exploitation natural salt water at the Tuzla salt deposit and main cause of soil subsidence). Proc. of X Conf. of Geologists of Yugoslavia, Budva, Vol. II, 241-253.

SPATIAL ASSESSMENT, MITIGATION AND PREVENTION OF EVAPORITE DISSOLUTION SUBSIDENCE DAMAGE IN THE HISTORICAL CITY OF CALATAYUD, SPAIN

Francisco Gutiérrez and Fernando García-Hermoso
Universidad de Zaragoza, Dpto. de Ciencias de la Tierra, Edificio Geológicas, C. Pedro Cerbuna 12, 50009 Zaragoza, Spain

Anthony H. Cooper
British Geological Survey, Keyworth, Nottingham, NG12 5GG, UK

Abstract

The historically important city of Calatayud in northern Spain is underlain by gypsum and other soluble rocks. The development of the city over the past 14 centuries has been strongly influenced by geohazards including flooding, subsidence and rockfalls. Many of the flooding problems have been mitigated, but evaporite dissolution of the bedrock continually causes subsidence and the collapse of gypsum cliffs overlooking the city. Additional subsidence is caused by the hydrocompaction of gypsiferous silt present in alluvial fan deposits. The city was surveyed for building damage using a classification scheme originally developed to record damage in the British coal mining areas. The damage survey shows that the worst building subsidence is concentrated along the line of the buried channel that drains across the gypsiferous silt alluvial fan. Subsurface drainage is largely responsible for the dissolution and subsidence, but it is also aggravated by leakage from water and sewage service pipes. Damage has also been caused during slow reconstruction by piling over long time intervals. Mitigation measures include the control of water leakage by installing flexible services. Conservation and new developments also require careful reconstruction techniques, especially when piled and minipiled foundations are constructed.

Keywords: dissolution, subsidence, evaporites, gypsum, damage assessment, historical buildings, Spain

1. INTRODUCTION

The historical city of Calatayud, Aragón region (Spain), is situated about 70 km to the south-west of Zaragoza in the bottom of the Jalón River valley. Calatayud is 533m above sea level with 343mm of annual precipitation, an average annual temperature of 12.9°C and a semiarid continental climate. The city was founded by the Muslims in 716 A.D. and currently has a population of about 17,000. Its development, both past and present, have been constrained by the problems caused by evaporite dissolution and subsidence. Much of the inner city comprises ancient historical buildings of immense architectural and cultural worth, and in 1967 it was declared an Historical Monument (SanMiguel, 1995). However, many of the buildings are severely damaged; they are also difficult and expensive to repair. The financial losses in the city are considerable. Modern developments are badly affected by subsidence, which also damages the infrastructure such as drains, water supply and other services. This paper summarises the development of the city, assesses the subsidence damage, the underlying geological and anthropological causes, and looks at some possible remedial measures.

2. GEOLOGICAL SETTING

Calatayud is situated in the Calatayud Graben, a major Neogene intermontane basin in the Iberian Range, developed during the post-orogenic stage of the Alpine Orogen. The basin fill is mainly subhorizontal, Miocene to Lower Pliocene, continental sedimentary rocks grading from alluvial deposits at the margins to lacustrine and palustrine evaporites and carbonates in the centre. Calatayud is situated near the basin depocentre. The Calatayud Gypsum forms an evaporite sequence around 500m thick. About 200m of strata locally crop out comprising mainly rhythmically laminated and nodular gypsum ($CaSO4{\bullet}2H_2O$) with thin interbedded marls (Ortí and Rosell, 1998, 2000). Gypsum forms about 85% of the exposed sequence, but boreholes indicate that highly soluble deposits of halite (Marín, 1932), glauberite ($Na_2Ca[SO_4]_2$) and thenardite (Na_2SO_4) are also present at depth (MYTA, personal communication).

The sedimentary basin fill is transversally cut by the River Jalón valley. This has a broad floodplain, up to 1.6km wide, with alluvial fans at the margins fed from relatively small drainage basins. During its Quaternary evolution, the River Jalón has migrated northwards forming a markedly asymmetrical valley. The north margin is a prominent gypsum escarpment up to 100m high, while the southern flank of the valley has a stepped sequence of nine fluvial terrace levels (excluding the current floodplain) (Gutiérrez, 1995, 1996, 1998).

The interaction of ground and surface water on the highly soluble evaporites has produced karstic features and landforms that have strongly influenced the deposition of the alluvial and terrace deposits described below and which cause active subsidence problems (Gutiérrez, 1998).

3. DISSOLUTION-INDUCED PALEOSUBSIDENCE AND RECENT SUBSIDENCE

Evaporite dissolution and subsidence have operated over a long time in the Calatayud Graben. It occurred synchronously with the filling of the basin (endorheic conditions) and subsequently with the capture of the graben by the external drainage (exorheic conditions) (Gutiérrez, 1996, 1998). Dissolution-induced subsidence affects the Neogene sedimentary basin fill (the intrastratal karst). Subsidence also affects the later Quaternary detrital sediments deposited from the drainage systems that dissected the basin (the mantled or alluvial karst).

South of the Jalón valley, the carbonate and detrital Neogene sequence overlying the evaporites has suffered synsedimentary subsidence caused by karstification of the underlying evaporites. One particular carbonate unit here ranges from 20 to 110m thick and shows cumulative wedge-out systems (Sanz-Rubio et al.,1996). Post-sedimentary karstic subsidence affects two substantial areas where the supra-evaporitic units have subsided more that 200m (Gutiérrez, 1995, 1996, 1998).

Quaternary terraces along the right margin of the River Jalón, and its tributary the River Jiloca, show large amounts of deformation and anomalous thickness changes related to the suballuvial karstification of the soluble bedrock. The karstic subsidence and fluvial deposition were contemporaneous, causing thickness changes from 10m to 100m or more in a single terrace. In addition, the terrace sediments show evidence of brittle and ductile subsidence deformation indicating the formation of palaeosinkholes by collapse and by sagging. Locally these palaeodepressions are filled with palustrine deposits comprising green and grey marls with fresh water faunas. Synsedimentary thickening has also affected the alluvial fan deposits of gypsiferous silt that occur along the valley margins.

Karstification and subsidence are currently active especially in the floodplain. The subsidence produces sinkholes and large closed depressions several hundreds metres across that locally control the river channel's course. The depressed areas are prone to flooding and colonising by phreatophytic and palustrine vegetation. Sinkhole formation is particularly common along unlined irrigation ditches and adjacent areas (Gutiérrez, 1998).

4. THE GEOLOGY BENEATH CALATAYUD CITY

The geology beneath Calatayud City has been deduced from 25 site investigation reports detailing 43 boreholes. The local geology derived from them is:

Made Ground. This anthropogenic deposit of unsorted and unconsolidated rubble is up to 6.5m thick. It is thickest at Plaza del Fuerte, close to the old Rúa channel (see below), which is now the line of the Rúa Street. Some boreholes drilled near to the river showed that the water table is higher than the base of the rubble material suggesting recent subsidence here. Old cellars beneath parts of the city are another anthropogenic feature, and their collapse may cause local subsidence.

Alluvial Fan Deposits. The fan sediments underlie the anthropogenic deposits and are mainly gypsiferous silts with scattered gypsum and limestone clasts. They interfinger with fluvial facies of the Jalon River at depth and wedge out from more than 12m thick in the proximal fan area thinning towards the floodplain.

Fluvial deposits. These underlie the gypsiferous silts in the fan areas and the anthropogenic debris in the floodplain area. They comprise channel gravels with fine-grained floodplain deposits. They also include local palustrine facies deposited in swampy subsiding depressions. The coarse-grained channel facies reaches 4m thick in the proximal fan area beneath the Plaza de España. This suggests that the River Jalón once ran at the scarp foot in the area currently occupied by the alluvial fan and the city. This interpretation is corroborated by historical documents that record the construction of the engineered river channel diversion away from the unstable scarp during the construction of the city (Cos, 1846). Largely because of differential synsedimentary subsidence caused by subsurface bedrock dissolution, the floodplain fluvial deposits range from 7 to 24m thick. Local palustrine facies indicating synsedimentary subsidence are proved by boreholes at the foot of the scarp in the north-eastern part of the city.

Marls and evaporite residues. Poorly consolidated dark grey marls with scattered nodular gypsum particles are present immediately beneath the alluvial sediments. These deposits are a largely insoluble karstic residue that locally reaches more than 9m in thickness.

Calatayud Gypsum. The dark marls and dissolution residues pass down into the unweathered evaporitic Neogene deposits of the Calatayud Gypsum (described above).

5. THE INFLUENCE OF GEOHAZARDS ON THE DEVELOPMENT OF CALATAYUD CITY

Calatayud is located on the left margin of the Jalón river valley, at the foot of an approximately 100m high, nearly vertical, gypsum scarp. The city is positioned partly on an alluvial fan fed by La Rúa and Las Pozas streams, and partly on the River Jalón floodplain. In addition, numerous buildings are also located on the gypsum scarp and the slopes, including cave-houses. Since its foundation by the Muslims in 716 A.D., the urban development of Calatayud has been constrained by several geological hazards including floods, slope movements and subsidence.

The original Muslim settlement was a walled enclave on the gypsum slopes. In contrast, the Jewish and the Mozarabs occupied the flood-prone alluvial fan areas (Cos, 1846; Galindo, 1984). To mitigate this flooding hazard, the runoff of the flash-flood prone La Rúa stream was diverted by the Muslims upstream to an adjacent catchment. This was done by constructing a small dam (the "Sacred Dam") and an artificial channel linking the Rúa stream with El Salto stream, then via the River Ribota to the Jalón (Galindo, 1984). This engineered drainage diverted the runoff from 77% of the catchment (6.3km^2).

After the Christian Reconquest in 1120, Calatayud expanded through the 12th and early 13th centuries. The urban area was on the alluvial fan, where it remained until the early 20th century. The buildings on the distal fan area and on the floodplain were commonly affected by the River Jalón floods (Cos, 1846; Galindo, 1984). The Rúa channel in the alluvial fan was also the main axial city road and flooding here was a constant concern. This was controlled by the construction of the Balsa de Valparaiso Dam in the Rúa channel, close to the basin mouth (Galindo, 1984). This regulates and controls the surface runoff contributed by the 21% of the catchment (1.7km^2) that is downstream of the "Sacred Dam". Presently, the surface flow is diverted through a 1km long tunnel, downstream of the city to the Longia stream. These measures alleviate the flooding and control runoff from 98% of the basin area. In contrast, the Las Pozas stream still causes flooding although it drains a smaller catchment (4.2 km^2). On July 18th 1999, a major storm flood of the Las Pozas stream caused severe damage and financial loss.

Since medieval times, the city plan has scarcely changed. However, many buildings were replaced by more noble structures including 15-16th century Renaissance palaces and 17-18th century religious buildings (Borrás and López-Sanpedro, 1975). In the 19th and 20th centuries, the city expanded towards the floodplain and the opposite side of the valley.

The Jalón River is also a flood hazard; the largest recorded event occurred in May 1956, with a peak discharge over 300m^3/s and flood waters reached 2m deep in the lower parts of the city (Galindo, 1984). These floods have been partially controlled by the construction (1952-1961) of the La Tranquera reservoir. Currently, much of the surface drainage across the alluvial fan and the floodplain is heavily regulated and the flood risk alleviated. However, subsurface flow through the alluvial fan from the Rúa feeder channel causes subsidence that is no longer balanced by alluvial deposition.

Urban development was also restricted by gypsum scarp slope instability, including rock-falls and topples. The most unstable areas are next to large active subsiding depressions formed in the floodplain at the scarp foot. These rockfalls have caused substantial financial losses and one person was killed in 1988. At times, dissolution-induced rock-falls also closed the former Madrid-Barcelona road that is located at the foot of the scarp.

6. BUILDING DAMAGE SURVEY METHOD

In order to appraise the subsidence effects, building damage in 35 hectares of the city was systematically assessed. The buildings varied in age from 12th century to modern, located in different urban growth zones and a wide range of geological settings ranging from proximal fan to river bank. The damage was evaluated by examination of the building façades. A damage category was assigned to each building on a scale of 0-5 based on the *Subsidence Engineers' Handbook* ranking system established by the British National Coal Board (NCB, 1975). This ranking scheme has been usefully applied to evaporite dissolution subsidence studies in the city of Ripon, North Yorkshire, England (Griffin, 1986; Cooper 1998 and references therein).

Peripheral effects (e.g. disruption of service pipes) and damage inside the buildings were not surveyed in our study, so only four levels of damage 0, 3, 4 and 5 were used (Table 1). Thus, level 0 on the map includes damage attributable to levels 1 and 2 in the NCB ranking. This allows categories 1 and 2 to be added later by a more detailed survey, and makes possible direct comparison with other studies that have used this methodology.

Maps of damage levels were produced at a 1:2000 scale, but the results are simplified here for publication (Fig. 1). This map shows the distribution of the subsidence damage as described below and may indicate the causes and controlling factors; it is also potentially useful for zoning subsidence susceptibility. However, occurrence and severity of building damage may depend on numerous factors. These include the age and size of the building, the foundation type and depth, the characteristics of the supporting materials and the building construction quality and materials. By comparison with similar buildings in nearby cities, such as Ateca, built on solid quartzite, it is obvious that building damage in Calatayud is considerably more severe.

Table 1. Ranking of damage categories established by the British National Coal Board and used for the building damage survey in Calatayud. The assessment is based on the features and criteria that shown in bold type.

Class of damage	Description of typical damage
0	**No damage**
1 Very slight or negligible	Hairline cracks in plaster, perhaps isolated slight fracture in the building, **not visible from the outside (this category was not used at Calatayud).**
2 Slight	Several slight fractures showing inside the building. Doors and windows may stick slightly. Repairs to decoration probably necessary. **Not visible from the outside (this category was not used at Calatayud).**
3 Appreciable	**Slight fractures (millimetric) showing on outside of building (or one main fracture). Doors and windows sticking.** Service pipes may fracture.
4 Severe	Service pipes disrupted. **Open fractures (up to 1cm) requiring rebonding and allowing weather into the structure. Window and door frames distorted. Floors sloping noticeably.** Some loss of bearing in beams. If compressive damage, overlapping of roof joints and lifting of brickwork with open horizontal fractures.
5 Veery severe	**As above, but worse (with centimetric cracks), and requiring partial or complete rebuilding.** Roof and floor beams loose bearing and need shoring up. **Windows broken with distortion. Severe slopes on floors. If compressive damage, severe buckling and bulging of the roof and walls.**

7. BUILDING DAMAGE SURVEY RESULTS AND DISTRIBUTION

The map of the subsidence (Fig. 1) shows a triangular area at the foot of the gypsum scarp where severe damage (Level 5) is common. It is cut by Rúa Street that follows the course of the old Rúa channel; here the buildings are the most

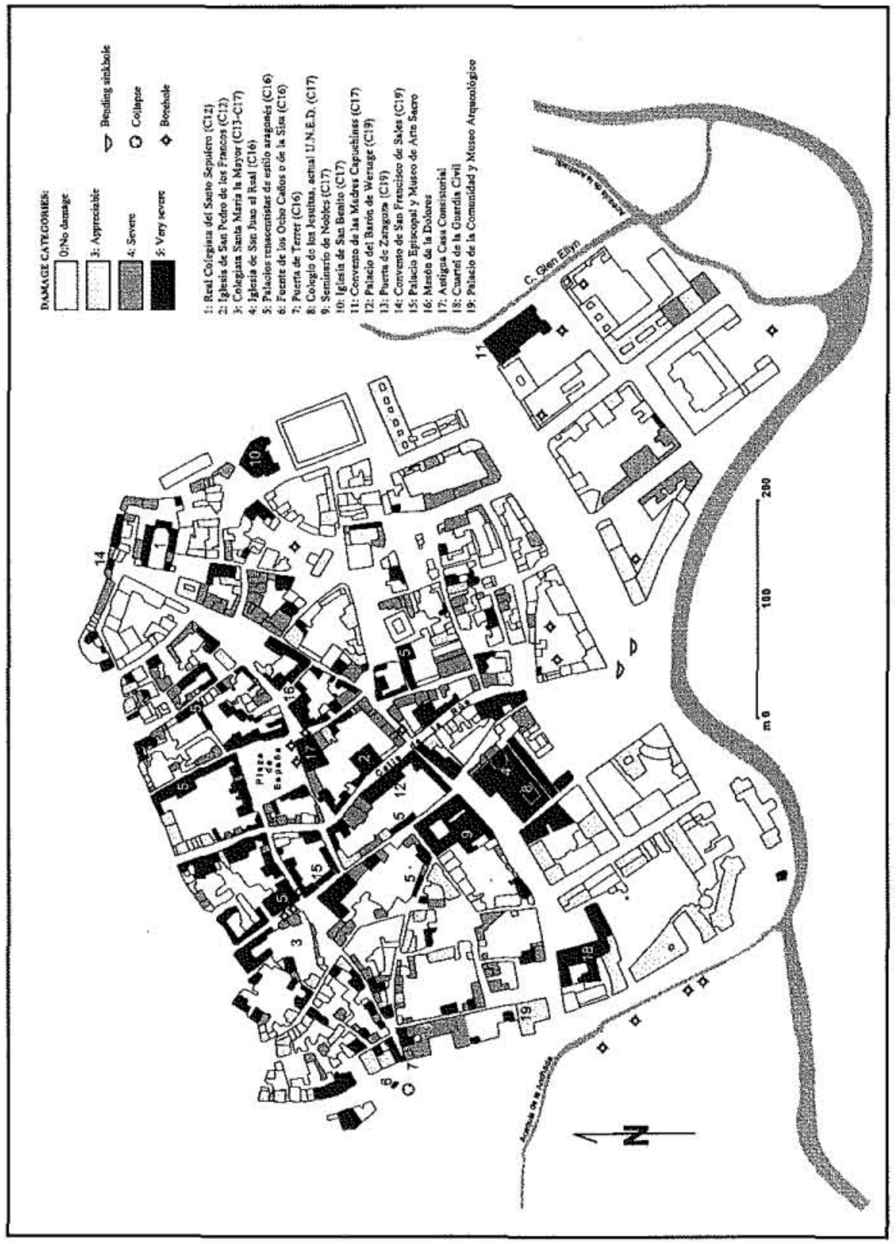

Figure 1. Map showing the distribution of the subsidence damage for the city of Calatayud in northern Spain.

severely damaged. The inner city here is within the 13th Century walled enclave and has numerous churches, monuments and buildings of great historical and aesthetic value with level 5 damage. These include: Iglesia de San Pedro de los Francos (11th -14th C) (Fig. 2); Colegiata de Santa María la Mayor (13th -18th C) (Fig. 3); Iglesia de San Juan el Real and Fundaciones de la Compañía de Jesús (14th C); numerous Aragonian-styled Renaissance palaces (16th C); Seminario de Nobles (17th C); Palacio del Barón de Wersage (19th C); Palacio Episcopal; Museo de Arte Sacro; Mesón de la Dolores and most of the buildings in the Plaza de España, including the abandoned city hall. Here, the majority of the buildings with low damage levels (0 and 3) have been restored or reconstructed. However, some recent buildings less than 20 years old show cracks and slight tilting indicating recent active subsidence.

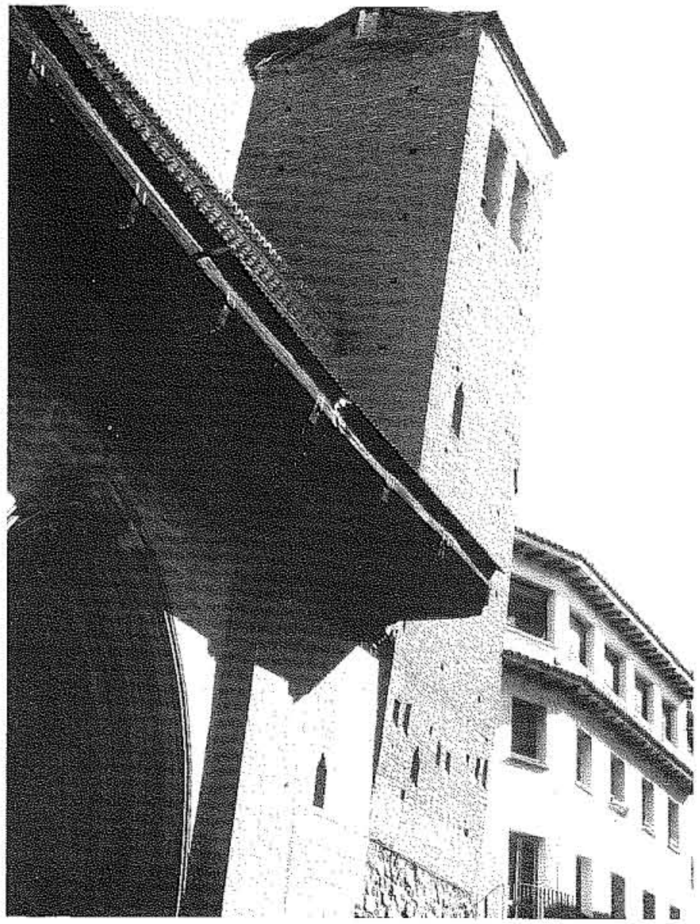

Figure 2. Tilted tower in San Pedro de los Francos Church (11th-14th C).

The area where the damage is most severe lies on the proximal fan and along the medial axis of the alluvial fan coincident with the former Rúa channel. Here the gypsiferous silts reach their maximum thickness.

In the surrounding area, both on the alluvial fan and floodplain, the oldest buildings show less damage than those mentioned above. However monuments with severe damage include: Real Colegiata del Santo Sepulcro (12th C); Fuente de los Ocho Caños o de la Sisa (16th C), where a collapse occurred in April 1995; Puerta de Terrer (16th C); some Renaissance palaces (16th C); Iglesia de San Benito (17th C); Convento de las Madres Capuchinas (17th C); Convento de las Religiosas de San Francisco de Sales (19th C) and Puerta de Zaragoza o de Somajas (19th C).

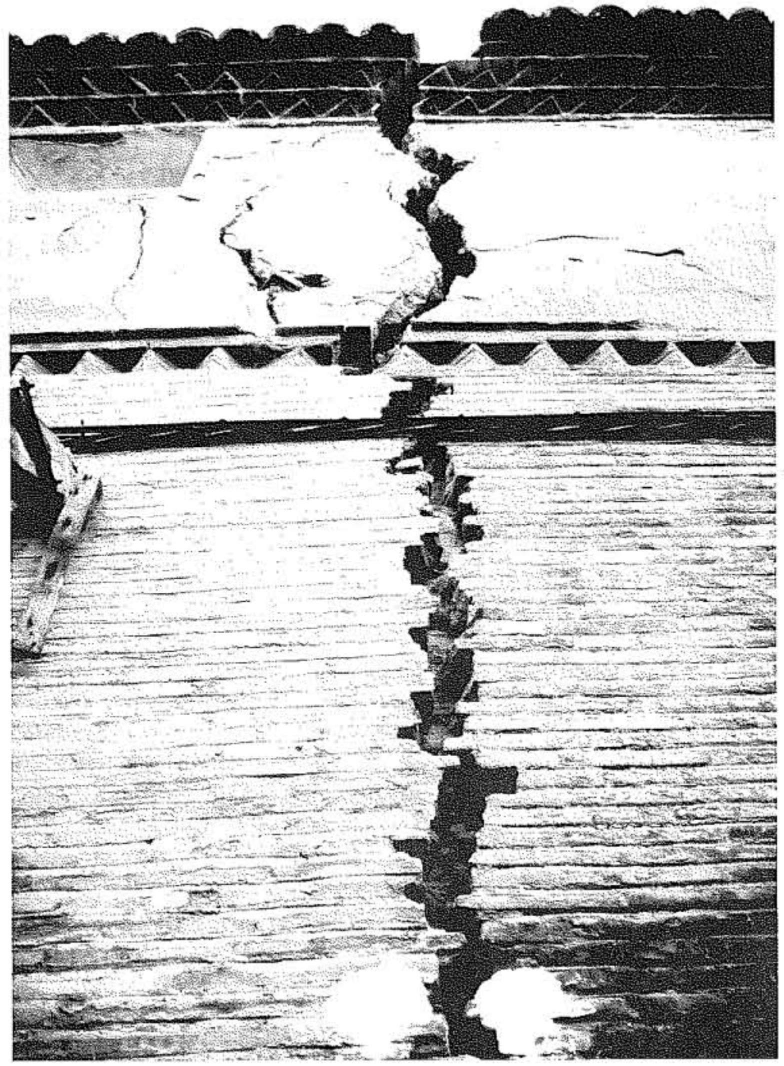

Figure 3. Open fracture in Colegiata de Sta. María la Mayor (13th-18th C).

8. SUBSIDENCE CAUSES AND CONTROLLING FACTORS

The majority of site investigation reports for Calatayud attribute the subsidence damage to hydrocompaction of gypsiferous silts of the alluvial fan, or to the collapse of cellars and anthropogenic rubble. These processes do occur in the Calatayud area, as does sediment consolidation of the alluvial deposits. However, the distribution and nature of the damage in Calatayud suggests that most severe damage is caused by subsidence following the dissolution of the evaporitic substratum. This is concentrated over areas where there is considerable groundwater flow at the bedrock-cover interface and in the upper layers of the evaporite bedrock.

Several factors indicate that evaporite dissolution is the main subsidence-controlling mechanism. Subsidence affects buildings both within and outside of the areas underlain by made ground or gypsiferous silts. Throughout the area sinkholes have revealed considerable cavities, too large to be explained by compaction effects. The presence of dolines with palustrine fill deposits indicate that locally ground subsidence has occurred over a considerable period. Boreholes drilled in the area show that there is a karstic residuum overlying the bedrock indicating evaporite dissolution at this interface. In addition, paleosubsidence features show that evaporite dissolution is the main cause of palaeocollapse and doline formation.

City development aggravates the subsidence effects. Water leakage from supply and sewerage systems has increased gypsum dissolution and subsidence causing considerable damage within Calatayud. In the past, soakaways and septic wells have added to the local infiltration of water and triggered subsidence. Surface runoff still adds to the local groundwater infiltration and may cause localised subsidence; leakage from unlined canals and irrigation ditches can have the same effect. Water abstraction may induce local lowering of the water table and induce subsidence. Ground loading can also trigger subsidence over metastable cavities.

9. PREVENTION AND MITIGATION MEASURES

The losses and problems caused by subsidence in Calatayud are considerable, but they could be reduced by simple cost-effective measures. The most important of these is to minimise the infiltration of water into the ground. This most commonly occurs where water and sewerage pipes are broken. These could be replaced with flexible pipework with telescopic joints (NCB, 1975). The effectiveness of these measures can be monitored by looking at the water balance figures between supply and sewage for the area. Storm water drainage should be treated in a similar manner with lined runoff ditches carrying the water away from the built up area. Water abstraction in the vicinity of Calatayud should be carefully controlled to avoid fluctuations in the water table.

With respect to remedial measures, and new development, considerable care should be exercised when sinking foundation piles or minipiles. Some of the worst damage to historical buildings in Calatayud has been caused by partly underpinning and minipiling buildings (such as the Colegiata de Santa María la Mayor and San Pedro de los Francos) (Figs. 2 and 3). Where the work is unfinished, or has taken place over a considerable time, the buildings have suffered badly from continuing subsidence, especially along the join between the finished and unfinished work. Piling may also open hydrological pathways from the surface to the dissolution prone surface at the top of the gypsum.

Now that the causes and distribution of the subsidence problems have been identified, the next step is to formulate planning control, such as that recorded by Pausktys et al. (1999). Proper planning and control will help to alleviate the worst of the effects and protect the property and heritage of Calatayud.

Acknowledgements

This research was financially supported by projects PMA2093 (CONAI, Diputación General de Aragón) and ENV4-CT97-0603 of the European Community. The authors would like to thank Fernando Munilla and Luis de Blas of Calatayud Council Technical Office for providing maps of the city and geotechnical reports. We would also like to express our gratitude to the companies Entecsa, Arcotecnos and Proyex and to Victor Arqued (C.H.E.) and Captain Pardos Herrer (Regimiento de Pontoneros, Zaragoza) for supplying unpublished reports. Our sincere thanks are offered to the architect Antonio Lorén for his valuable suggestions about architectural aspects, and to Santiago Alberto for help drafting the figure. Dr Bob Addison, Mr Alan Forster and Mr Tim Charsley are thanked for critically appraising the manuscript. AHC publishes with the permission of the Director, British Geological Survey (NERC).

REFERENCES

Borrás, G. & López Sanpedro, G. (1975) *Guía de la ciudad monumental de Calatayud.* Dirección General de Patrimony Artistic y Cultural. Service National de Information Arqueológica y Etnológica. Madrid, 207 pp.

Cooper, A.H. (1998) Subsidence hazards caused by the dissolution of Permian gypsum in England: geology, investigation and remediation. In: *Geohazards in Engineering Geology* (ed. by J.G. Maund & M. Eddleston), Geological Society, London, Engineering Geology Special Publications, **15**, 265-275.

Cos, M. del (1846) *Glorias religiosas de la ciudad de Calatayud.* Centro de Estudios Bilbilitanos, 428 pp.

Galindo, M.C. (1984) *Condiciones de existencia y nivel de vida de Calatayud.* Institución Fernando El Católico. Zaragoza, 82 pp.

Griffin, D.A. (1986) *Geotechnical assesment of subsidence in and around Ripon, North Yorkshire, due to natural solution.* Master Thesis. University of Newcastle upon Tyne, 85 pp. (Unpublished).

Gutiérrez, F. (1995) Synsedimentary and postsedimentary subsidence due to gypsum karstification and derived hazards (Calatayud Graben, Iberian Range, Spain). In: *Land Subsidence, Natural causes, measuring techniques and the Groningen gasfields* (ed. by F.B.J. Barends, F.J.J. Brouwer & F.H. Schröder), Proceedings of the Fifth International Symposium on Land Subsidence. The Hague. Balkema, 47-57.

Gutiérrez, F. (1996) Gypsum karstification induced subsidence: Effects on alluvial systems and derived geohazards (Calatayud Graben, Iberian Range, Spain). *Geomorphology,* **16**, 277-293.

Gutiérrez, F. (1998) *Subsidence phenomena due to evaporite solution in Teruel and Calatayud Neogene Grabens (Iberian Range).* Ph. D. Thesis. University of Zaragoza, 569 pp. (In spanish, unpublished).

Marín, A. (1932) *Boletín de Sondeos.* ITGE. Madird, Vol. 3(1), 29-99.

N.C.B. (1975) *Subsidence Engineers' Handbook.* National Coal Board Mining Department. UK, 111 pp.

Ortí, F. & Rosell, L. (1998) Unidades evaporíticas de la Cuenca de Calatayud (Mioceno inferior-medio, Zaragoza). *Geogaceta,* **23**, 111-114.

Ortí, F. & Rosell, L. (2000) Evaporite systems and diagenetic patterns in the Calatayud Basin (Miocene, central Spain). *Sedimentology.* In press

Pausktys, B., Cooper, A.H. & Arustiene, J. (1999) Planning for gypsum geohazards in Lithuania and England. *Engineering Geology,* **52**, 93-103.

SanMiguel, A. (1995) El Patrimonio arquitectónico de la Comarca de Calatayud. In: *I Jornadas de Recuperación del Patrimonio en la Comarca de Calatayud.* Centro de Estudios Bilbilitanos. Institución Fernando el Católico. Calatayud, 13-21.

Sanz-Rubio E., Hoyos, M., Cañaveras, J.C., Sánchez-Moral, S. & Calvo, J.P. (1996) Caracterización sedimentológica de los sistemas fluviolacustres y tobáceos del Mioceno Superior-Plioceno de la Cuenca de Calatayud (Zaragoza). *Geogaceta,* **20**(2), 277-280.

LAND SUBSIDENCE - Vol. I
Proceedings of the Sixth International Symposium on Land Subsidence
Ravenna / Italy / 24-29 September 2000

SUBSIDENCE RESULTING FROM SOLUTION MINING OF THE BURIANO SALT DEPOSIT, ITALY

Paolo Berry
Dipartimento di Ingegneria Chimica, Mineraria e delle Tecnologie Ambientali, Facoltà di Ingegneria, Università di Bologna

Paolo Squarci
Istituto Internazionale Ricerche Geotermiche, CNR
Pisa

Giovanni Gambini
Solvay Chimica Italia S.p.A.
Rosignano (Livorno)

Abstract

Ninety years of precise levelling and seismic monitoring at the Buriano mine are being presented. The mine exploits a salt deposit by the solution mining method.

The aim of the detailed surveying observations is to understand the character of induced subsidence related to the exploitation of the salt deposit. The objective of seismic monitoring is to predict (both in time and space) the formation of each sink-hole and to detect its development towards the surface.

Surveys concern overlying and surrounding areas of the Buriano district mining activity. Approximately 1500 subsidence observation stations control the response of the ground in the development of subsidence over a large surface (about 6 km^2).

Data collected for the past 90 years provide a complete picture of land deformation and of delayed residual subsidence induced by the extraction of salt. Data analysis by a statistical model reveals that the external safety strip separating the borders of the mining area from civil infrastructures is satisfactorily designed, and that the delayed residual subsidence peters out in sufficiently brief periods of time.

In this area, the sink-holes resulting from solution extraction of salt are about 10-meters in diameter. The occurrence is not very frequent, but can be hazardous to miners. For this reason, a monitoring network set up a few years ago, operates continually to record microquakes caused by the energy released from failure processes induced in the roof rock mass by underground mining. The system facilitates the localization of these events, and permits checking and anticipating of the site zones at risk of collapses.

Finally, continuous monitoring of sink-holes and subsidence enhance management of the land above the mining activity. These will eventually be restored to their previous use and totally revived.

Keywords: solution mining, subsidence, microseismicity, sink-hole, mining panel

1. INTRODUCTION

As from 1912, SOLVAY S.A. exploits the "Buriano", "Casanova" and "Ponte Ginori" (Val di Cecina, Tuscany) salt deposits by a solution mining method.

The Buriano salt deposits are at an average depth ranging from 150 to 350 m below surface and do not exceed a 60 m thickness. They occur as flat lenses arranged on several beds of wide lateral extent and fine thickness.

The deposit contains a volume of salt estimated to be 228 10^6 m^3, corresponding to 40% of the saline series. The mining area covers an extension of about 12 km^2 and just over 3000 brine wells have been drilled thus far. At present the parts North of the Buriano deposit are being mined, while the extension of the mining activities in the areas East of the mine are being planned.

The production of saturated brine (308 g/l) in the 40's was 1 10^6 m^3/year, but at present it is 6 times greater. In just under 70 years the mine has extracted about 32 10^6 m^3 of rock salt, corresponding to 230 10^6 m^3 of saturated brine. The extraction of salt has caused a deactivation equal to approximately 20 10^6 m^3, corresponding to an average subsidence of the Buriano area of 2 m.

The exploitation of salt at the Buriano mine has resulted in a widespread trough-shaped subsidence, which occurs gradually. The morphology of induced depression is also characterized by funnel-shaped holes or sink-holes of varying diameter and depth, and shallow troughs with no stepping of the ground at either side or any appreciable disturbance of the surface.

The extraction of salt by leaching generates large underground openings which are filled by materials falling from the overlying rocks. This is causing a general subsidence of the site, which is a progressively slow phenomenon, but it is also occasionally accompanied by sudden and uncontrolled collapse. The salt exploitation has caused 155 sink-holes over a 70-year period, having a diameter ranging from one meter (30% of the sink-holes) to 45 meters (a few per cent).

On the basis of the results of two precise levelling surveys, aimed to define the regional-scale effects of the geothermal energy exploitation, the areas near Buriano mine appear not affected by subsidence phenomena, in despite of such a long period of mining activity. The two surveys covered the entire Cecina Valley area (Arca et al., 1988) and used benchmarks sited in the Villages of Saline di Volterra and Ponteginori, and along the Road n° 68. The first survey was made in 1923 (the salt extraction began at Buriano mine in 1921) and the second 65 years later. The subsidence between the two surveys was of about a few centimeters.

2. GEOLOGY

The structural and hydrogeological model of the study area can be summarized as follows, beginning with the oldest formations (Squarci, 1999):

- regional basement and tectonic wedges of pre-Paleozoic-Triassic age. These are formations of varying grades of metamorphism and lithology (gneiss, micaschists, phyllites, occasional quartzites); when fractured they form the geothermal reservoir in the nearby Larderello area;
- formations of the Tuscan Series, of Mesozoic age; mainly a carbonate base is overlaid by clayey and sandstone clastic formations of the Cretaceous-Oligocene. The carbonate formations, particularly when they are tectonically thinned out, have a good permeability and also serve as a reservoir in the Larderello geothermal area. In outcrop they act as absorption or recharge areas for the meteoric waters, which penetrate to great depths;
- various allochthonous formations, usually flysch facies, of the Cretaceous-Eocene age, whose predominant clayey-marly nature makes them almost totally impermeable. These formations form the cap rock for the deep hydrological circuit; the geothermal wells that have crossed these formations have met with a very low overall permeability;
- the Neogenic group; this group consists of the evaporitic and "saline series" of the Upper Miocene (Messinian), that are the subject-matter of this study. The Neogenic formations usually have low permeability, and the saline series, with predominant halite by virtue of the fact that it is present (considering the high solubility of halite), suggests that the surrounding formations are more or less impermeable, separating them from the shallow and deep hydrological circuits. The saline series, which belongs to the Lower Messinian evaporitic formations, consists of layers of halite deposits separated by clay, laminitic marl and anhydrite, sandstone and microconglomerates with sulphatic cement components. The saline series is defined as formations between the bottom of the deepest halite deposit and the top of the shallowest. Halite represents about 40% of the total volume of the saline series in the Buriano deposits. As a whole, the natural permeability of the series is fairly low, considering that salt is more or less impermeable (10^{-15} cm/s) and that clay is the predominant component in the intercalated layers (permeability of about 10^{-9} cm/s in compact clay; 2.4 x 10^{-6} cm/s in gypsum clay; 2.3 x 10^{-7} cm/s in sandy clay with gypsum). The

saline series, which was folded during the Upper Messinian, is overlaid transgressively by clayey deposits with gypsum of the Upper Miocene (Upper Messinian evaporites) and by Pliocene clays. Considering the predominance of clayey lithotypes, these formations generally have a low permeability (measured value of 7 x 10^{-9} cm/s in compact clay) and form the cap rock barrier that has preserved the underlying soluble saline deposit for over 5 million years (Squarci, 1999).

3. SOLUTION MINING SYSTEM

Salt exploitation is accomplished by means of a multiple well solution mining system, in separate districts (i.e. panels) of the deposit, covering a variable extension from 0,1 to 0,5 km^2 . So far the mine has mined 21 panels. From 60 to 380 injection and extraction wells are drilled in each one, with a density equal to 1 well for 1455m^2, placed at a distance of 40 – 45 m from one to the other and arranged in a chequered fashion.

Solution mining is initiated near the bottom of a selected water-soluble evaporite sequence by means of a large diameter undercut, a few meters in thickness, obtained using an air "blanket" thereby inhibiting upward dissolution of the salt roof. This initial phase comes to an end when we obtain a coalescence of adjoining single undercuts. Subsequent vertical and lateral cavern development then proceeds in stages, governed by local geologic conditions and consequently, shape, size and extent of solution cavities are usually unknown.

The network of wells extracts about 60% of the salt contained in each panel and generates unstable cavities causing the collapse of the roof rock-mass.

The exploitation is accompanied by normally progressive subsidence, however, a sudden sink-hole occurs occasionally, thereby creating local craters.

The salt saturated (NaCl) brine production is approximately 6 000 000 m^3 per year. To maintain this production requires drilling between 50 and 60 wells per year. The brine produced from Buriano is exported via pipe line to the "Solvay Rosignano" chemical plant. After purification the brine is used for the production of chemical based products (sodium carbonate, sodium bicarbonate and calcium chloride) and through electrolyses, chlorine and chlorine based products are produced.

4. SURVEYING OBSERVATIONS

The Buriano mining subsidence, in relation to the underground salt exploitation, is observed by means of detailed surveying observations at the surface. In the areas on the outside of the mine, monitoring is based on a precise subsidence levelling measuring of the land, with errors less than 2.5 mm/km, using 134 datum points distributed over 27 km. The surface exposed to monitoring with an annual frequency, covers an extension of about 18 km^2 and the measured difference in height is over 60 m.

The mining area with an extension of about 8 km^2 is surveyed on an annual basis with GPS Trimble 4000 ssi, using approximately 1500 datum points, some of which are checked several times in the same measuring campaign.

GPS Trimble works with four or more satellites so as to obtain sufficiently good precision on the inside of the mining area. In fact, with this method we are able to obtain errors less than about 2,5 cm on three axes of X, Y, Z.

The historical series of the survey results indicates that subsidence follows three evolutionary phases (Fig. 1):

- during the realization of the undercut of one panel, subsidences are limited since the external cavities are not too extended and they develop in the deeper part of the deposit;
- during mining of the panel, subsidences are higher and are very well correlated to the quantity of brine produced ;
- having completed the exploitation of the panel, subsidences progressively tend to reach values close to zero.

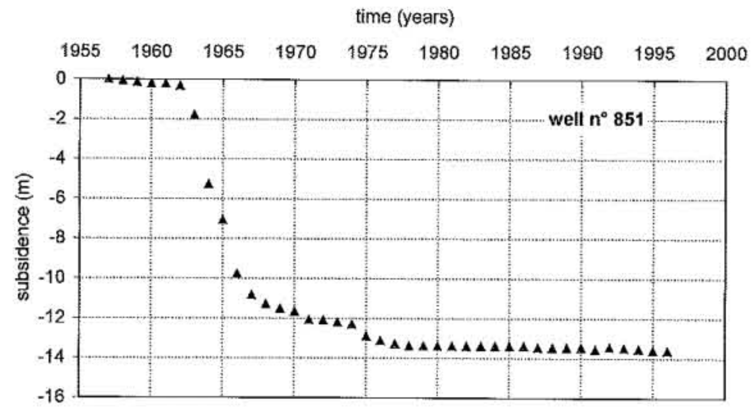

Figure 1. Subsidence development curve vs time.

5. SUBSIDENCE FORMATION AND PREVISION

Fig 2 reveals the interpolation of the total mining subsidence obtained by the detailed surveying as from 1929. The values have been interpolated by both SURFER software of Golden Software Inc. and GEOSWIN. The zero contour line represents the interpolation of subsidence values less than 2 cm. The zero line falls within the limits in which mine management has predicted the effects of the mining activity to be confined.

The analysis of Fig. 2 reveals that subsidence morphology is very irregular. This is to be attributed to irregularities of the:

- thickness and morphology of the deposit (made up of salt lenses accounting for 40 %, having variable dimensions and shapes which are distributed unevenly along the deposit);
- total thickness of the salt (obtained by adding the thickness of lenses along each well axis), that is locally variable within a range of 0 to 100 m;
- thickness of the covering, which is variable from about 60 to 400 m.

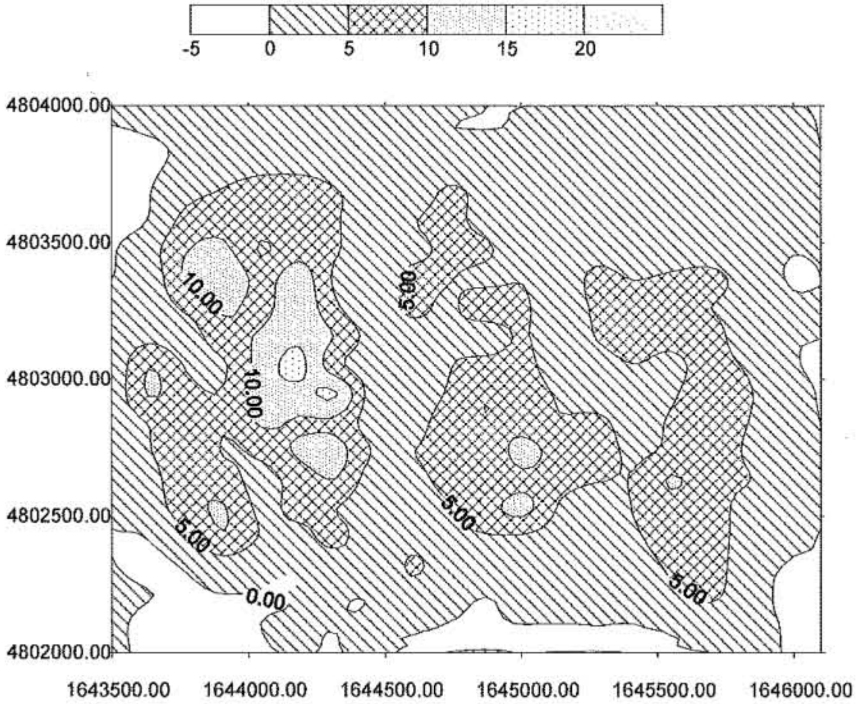

Figure 2. Observed subsidence contour lines

Subsidence is associated with cavities generated by the dissolution of the salt, having shapes and dimensions depending on the above-examined parameters, production speed and engineering requirements in general, that collapse as brine is extracted (Ege, 1984; Ren et al., 1989).

Subsidence values measured along lines orientated according to North – South and East – West directions, and their statistical interpolation, are revealed in the sections containing Figures 3 and 4 by the mobile average method. The sections cover the entire mining extension and provide a clear example of the subsidence characteristics.

In order to better understand how the more significant factors condition the shape and intensity of the Buriano mining subsidence, the underground exploitation of 6 panels has been simulated and the associated effects have been predicted using the focal point method (Whittaker and Reddish, 1989), that is one of the most efficient influence function methods.

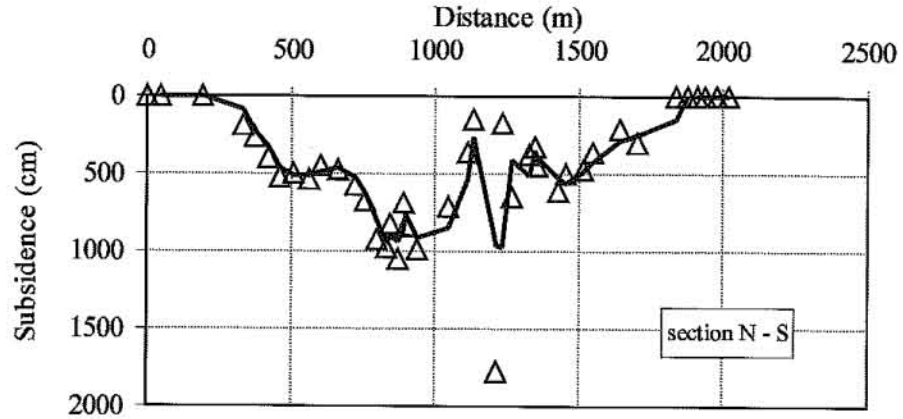

Figure 3. Subsidence in sections directed North – South

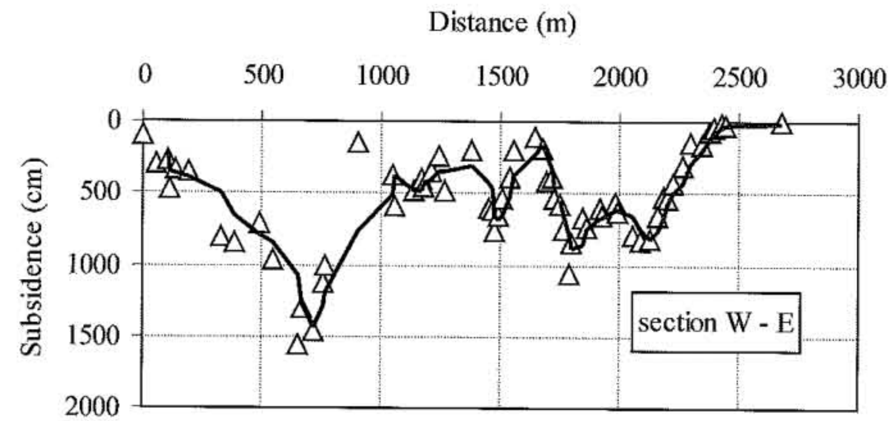

Figure 4. Subsidence in sections directed East – West.

Three of the 6 panels are adjacent to one another and have simulated the exploitation of the South – West corner of the deposit, the other three are also adjacent to one another but are placed in the South – East corner of the deposit.

The 3 panels of the "South – West" model are 50 m wide and 320 m long, while those of the "South – East" model are 135 m wide and 300 m long.

An draw angle has been adopted in the models, subtended between the horizontal line and the line adjoining the extraction edge to the subsidence limit, equal to 45°, on the basis of the experimental values. The values of the strength of the covering, thickness of the deposit and thickness of the salt, attributed to each panel, have been obtained by calculating the statistical average of the data of the panel wells. In each panel, the deposit has been assumed to be made up of an alternation of salt levels and waste, of constant thickness, and not greater than 3 m.

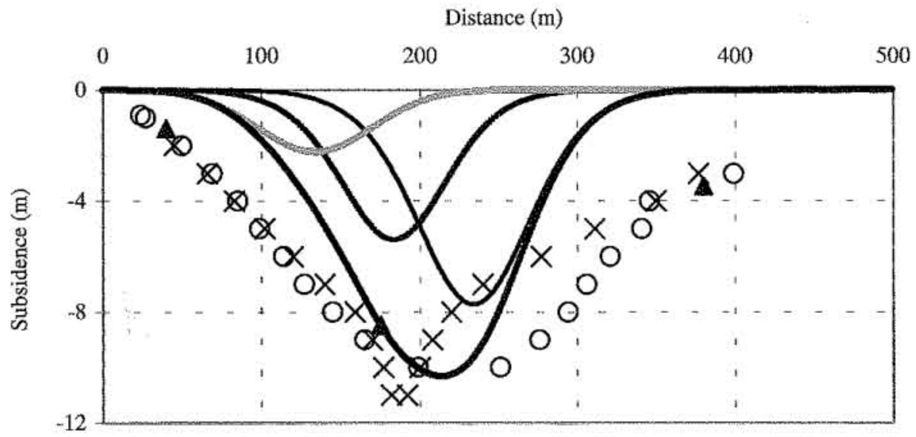

Figure 5. Comparison of influence function method "South – West zone", SURFER and GEOSWIN statistical interpolation and subsidence data values

Fig. 5 reveals the results of the mining simulation to the West and Fig. 6 reveals the mining simulation to the East. Subsidence values obtained by the model are compared with the statistical interpolation curve obtained with SURFER (O) and GEOSWIN (×) and with the measured subsidence data (▲). The total subsidence curve has been obtained by overlapping the effects induced by mining of the three adjacent panels.

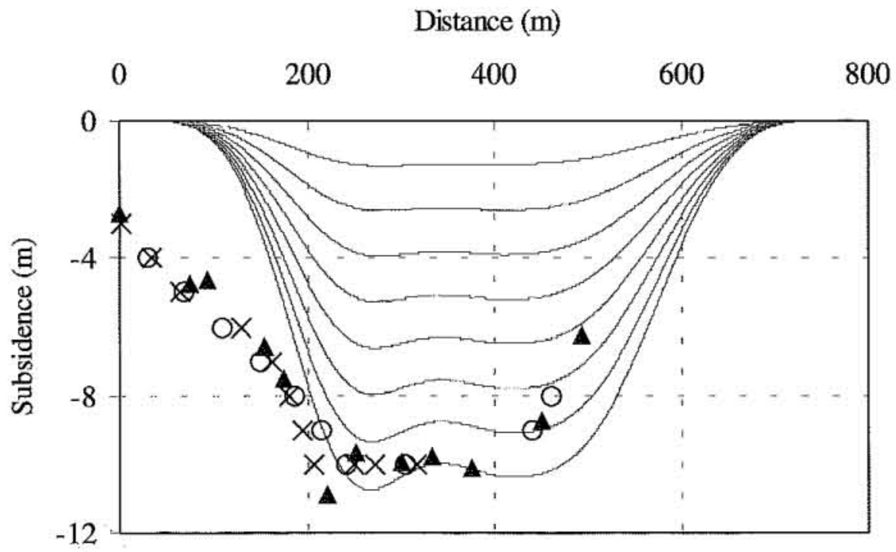

Figure 6. Comparison of influence function method "South – West zone", SURFER and GEOSWIN statistical interpolation and subsidence data values

Simulation with the model is totally satisfactory if we bear in mind that the interpolation curves are obtained by analyzing subsidence values measured in the whole mining area, while the subsidence curves obtained with the models only represent the effects of the dissolution of the salt on the inside of the panels.

The parameters that mainly condition the creation of sinkholes are not yet known with certainty. In fact, the analysis of the strength of the covering and of the salt, and of the geomechanic characteristics of the covering, has not revealed any relationship of dependence between these parameters and the occurrence of sinkholes. Considering that only 60 % is dissolved (mining yield), we can assume that in those zones where the thickness of the salt is greater and the roof of the deposit closer to the surface, shape and dimension of the cavities are discriminated against, and moreover, are not known and certainly vary from zone to zone.

6. DESCRIPTION OF THE SEISMIC MONITORING SYSTEM

The seismic monitoring system is made up of two parts:

- The geophone network
- The acquisition system

The geophone network includes 19 stations, each constituted by 4 vertical geophones hooked up in a series. These sensors are standard geophones. Their natural frequency is 10 Hz which means that the network is not designed to record the low frequency seismic activity related to the general seismology, but rather the local seismicity.

These geophone stations are spread over the whole site covering a surface of 2 x 2.5 km^2, the precise location of each station is susceptible of being moved in accordance with the operations on the site.

Each station is linked to a central acquisition system using multi-conductor cables. The geophone signals are conveyed through the cables by amplification (usual gain 1000 – 2000). When reaching the acquisition system, the signals are low-pass filtered (30 Hz) before the A/D conversion takes place. The A/D conversion and the following steps are then carried out by the SEIS-SCOPE system. This acquisition system is constituted by an IBM compatible PC equipped with a Digital Signal Processing (DSP) board.

The DSP board executes the following tasks:

- A/D conversion on 39 channels;
- Accuracy 12 bytes at a global rate of 80000 samples per second, all channel together;
- Screening of selected channels and conditional detection of a seismic event.

The PC is used to transfer and store those events which have been detected by the board. The transfer is done when activity is occurring and without interruption of the monitoring. The information is then stored on the PC hard disk and ultimately transferred onto magnetic cartridges.

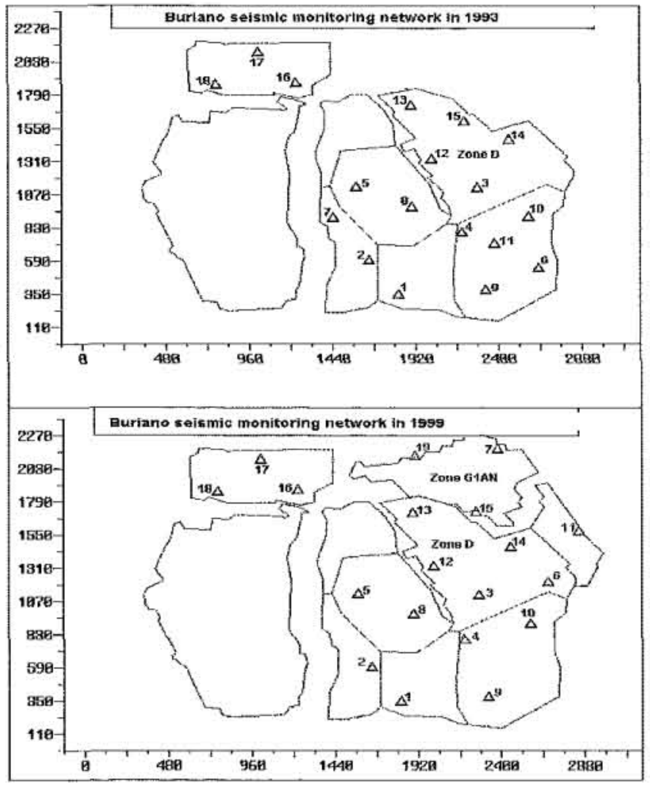

Figure 7. Buriano seismic monitoring networks

The detection algorithm uses a standard STA/LTA criterion applied on three channels. At each time step two counters are updated:
- the STA, which is the short time average of the signal;
- the LTA, which is the long time average of the signal.

When the STA/LTA ratio exceeds a given threshold on more than 3 channels within a given time lag, the detection condition is satisfied and the data transfer is initiated. In order to keep all of the desired information, the signals from all channels are transferred onto a given time window which also includes a pre-trigger period (typically 2 – 6 s).

As mentioned previously, the geophone network is relatively sensitive to ambient noises. This sensitivity to noise leads to the recording of numerous false detections. In order to compress the information volume to be stored and studied, an automatic procedure screens the raw data file in order to discard events which are pure noises, such as 50 Hz oscillation or spiking. This simple procedure carried out automatically every day allows to reduce the volume of the effective data by a factor of two.

The network and its acquisition system are controlled twice a year so as to ensure their efficiency. The response of the monitoring system is checked by generating seismic energy by dropping weights at predefined locations. The signals recorded by the system are then analyzed to check the sensitivity of the network and the accuracy of the localization.

6.1 Data interpretation

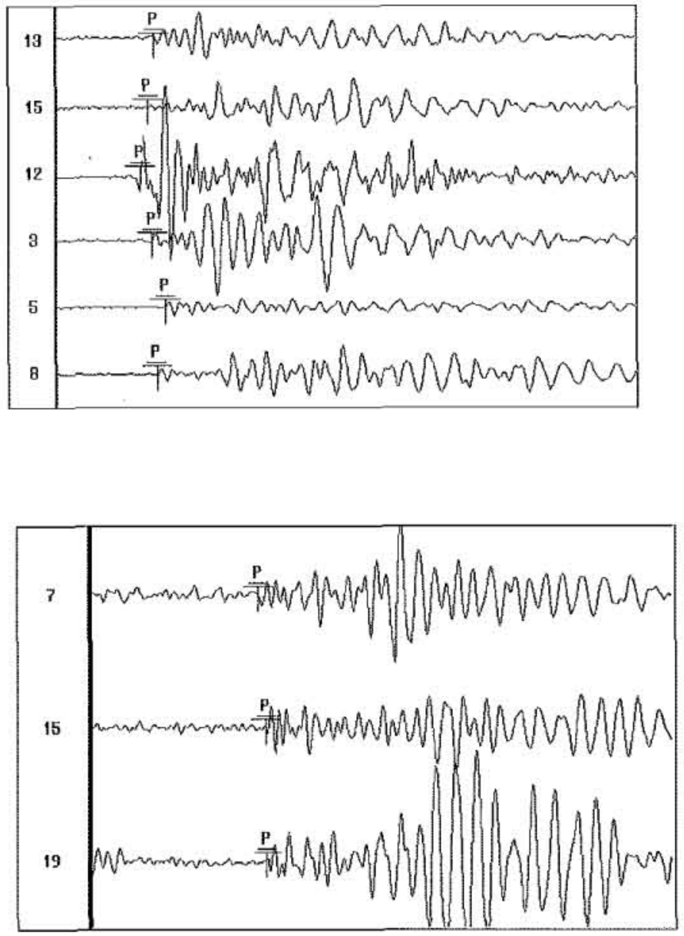

Figure 8. Examples of recorded microseismic events

The interpretation is done in two steps:
- in the short-term, directly in the field in the interest of safety;
- in the long-term, at Geostock with specific interpretation tools, to improve analysis.

Every day before work in the field is actually resumed, all seismicity recorded during the previous day is scrutinized and analyzed. A simple criterion based on the number of events in a given period in each zone is applied. A zone is simply identified by the first three stations which are touched by the event, information of which is provided by the computer.

Several cases are possible:

1. No seismicity, or only a sparse and diffuse seismicity all over the site for 15 days : Authorized access;
2. Growing seismicity in one zone for several days: Restricted access to the area concerned. (Authorized access only on roads, possible access on the field with real time monitoring of the zone with one operator present at the SEIS-SCOPE system);
3. Continuous seismicity for several weeks in one zone: Forbidden access to the area concerned. This zone is classified hazardous;
4. Continuous seismicity for more than 2 months or sudden strong seismicity, in one zone: Collapse in near future.

The seismic activity contains a lot of information which has to be extracted later on by a thorough interpretation using interpretation software.

This interpretation carried out by Geostock is aimed toward:

- the understanding of the seismological framework;
- the understanding of the geotechnical mechanism;
- the possibility of improving the collapse prognosis (improvement of the hazard appraisal in the field using customized criteria, allowing more reliable warning and a more sophisticated plan).

Fig. 8 shows typical examples of the recorded events.

The first task of the interpreter is to classify the events into different families, such as noise, external event, internal event, calibration and so on. Then the event is "picked", which means that each arrival time is determined using an interaction procedure. The "time picking" also allows to determine the real duration of the event, which will be used at a later stage for computing the magnitude.

The different arrival times are used to locate the event in x,y coordinates (epicenter) and also in depth (hypocenter). This location is performed by the computer using a ray-tracing software.

Fig. 9 shows changes in seismicity over a 4-month period.

In addition to these seismicity maps, the seismic activity can be also studied versus time (Fig. 10).

The induced seismicity at Buriano occurs in three distinctly identifiable modes:

1. As a sparse random event
2. In long periods of moderate but concentrated activity
3. In short periods of intense and concentrated activity

Random events are almost always small in magnitude and occur in areas which had previously experienced activity. The frequency of these events is in the order of 1 to 5 events per day. They appear to be associated with general ground subsidence and cannot be used in collapse prediction.

Periods of moderate but continuous activity typically follow sudden and large events. The activity is concentrated within the leaching zone. The frequency of these

events is in the order of 5 to 50 per day. They appear to be associated with cavity leaching or roof falls. According to the seismicity location, these periods can be used to evaluate the depth and extension of the underground failure zone and to classify zones as hazardous, if extension and depth are in the same order (as a thumb rule).

Periods of intense concentrated seismicity are always restricted to short durations in time (1 to 3 days). This kind of activity often occurs at the beginning of a "collapse phenomenon" and always during typical increase of seismicity. The frequency of these events is in the order of 50 to 200 events per day. These periods of activity seem to be related to sudden underground collapse. These periods can be used to locate the major failure front and to identify the potential ground subsidence area within a hazardous zone.

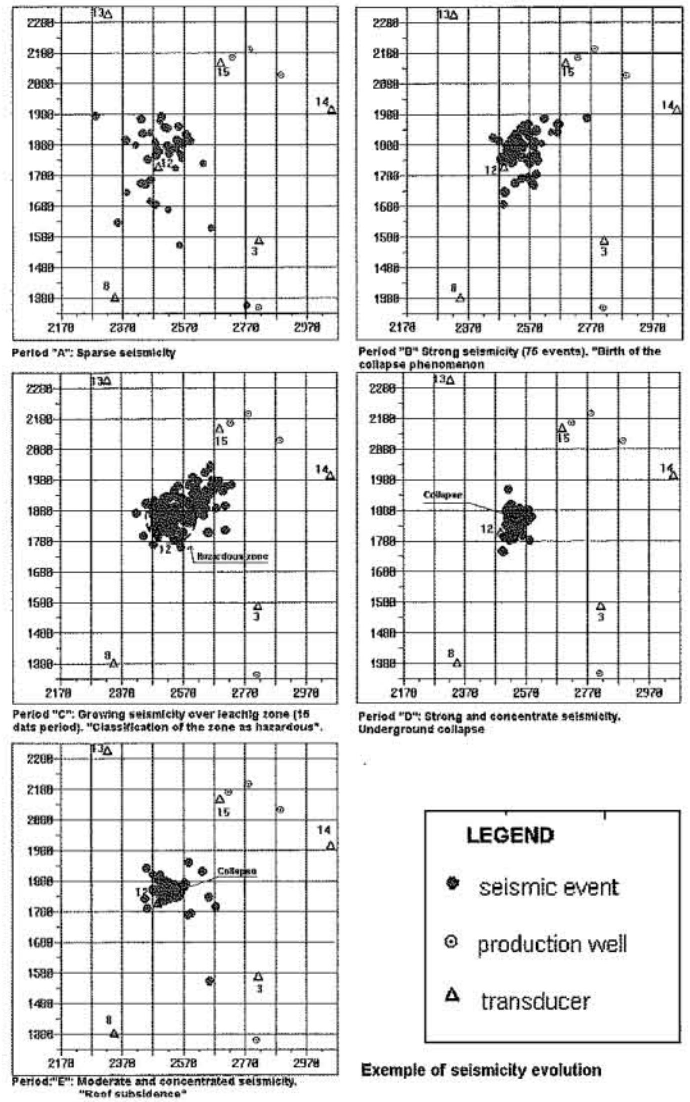

Figure 9. Changes in seismicity over a 4 month period

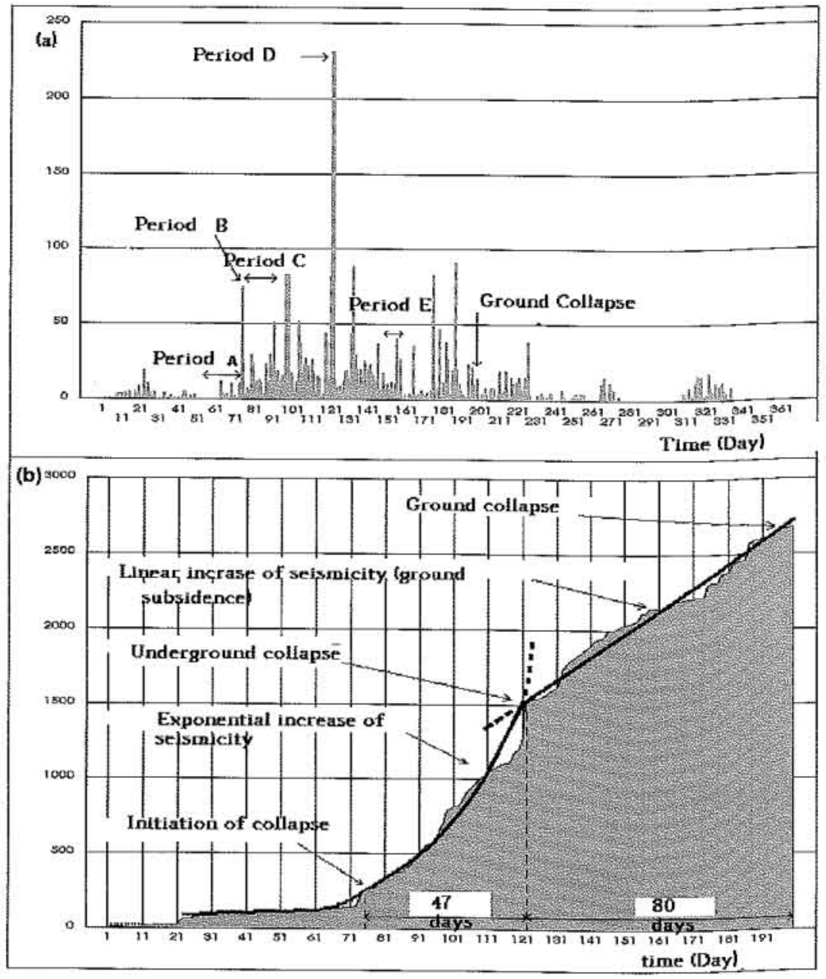

a) Chronograph, time versus seismic activity (Cf Epicenter map)

b) Chronogram, time versus cumulative seismic activity

Figure 10. Time versus seismic activity (a) and time versus cumulative seismic activity (b)

At Buriano, both large and small microseismic events are detectable evidence of rock mass failure induced by salt leaching.

Recognition of concentrated seismic activity location such as "rock mass failure fronts" allows hazardous zones to be clearly and consistently identified and monitored. The identification of a typical seismicity time trend (associated to standard leaching process) is a simple criterion used since 1979 with some success in local ground subsidence prediction. In any event, at safety level this typical trend always allows access to be restricted on a hazardous zone long before ground subsidence. Really accurate time trends must be studied with brine production parameters and geological modeling.

REFERENCES

Arca, S., Geri, G. and Rossi, A. (1988) Controllo altimetrico dell'area boracifera toscana mediante livellazione di precisione. Bollettino di Geodesia e Scienze Affini. I.G.M., 87

Ege, J.R. (1984) Mechanisms of surface subsidence resulting from solution extraction of salt. In "Man induced land subsidence", Ed. Holzer T.L., Reviews in Engineering Geology, Vol. VI; The Geological Soc. of America, 203 – 221.

Ren, G., Reddish, D.J. and Whittaker, B.N. (1987) Mining subsidence and displacement prediction using influence function methods. Mining Science and Technology, 5, 89 – 104.

Squarci, P. Studio geologico, idrogeologico e strutturale dei giacimenti di salgemma della media Val di Cecina. I:I.R.G., C.N.R., Pisa, unpublished report, 0 – 24.

Whittaker, B.N and Reddish, D.J. (1989) Subsidence. Occurrence, prediction and control. Development in Geotechnical Engineering, 56, Elsevier Science Publishers, Amsterdam.0

LAND SUBSIDENCE - Vol. I
Proceedings of the Sixth International Symposium on Land Subsidence
Ravenna / Italy / 24-29 September 2000

GROUND SUBSIDENCE PROBLEMS ASSOCIATED WITH DOLOMITIC LAND GAUTENG PROVINCE, SOUTH AFRICA

Ian de Bruyn and Nicole Trollip
Council for Geoscience, Private Bag X112, 0001, Pretoria, South Africa

Abstract

Significant areas of the densely populated Gauteng Province in South Africa, including most of the gold mining districts of the Far West Rand, are underlain by dolomitic formations. Ground surface instability in the form of sinkholes, dolines (large depressions) and subsidence may occur in such areas. In fact, in the past 40 years 38 people have lost their lives due to sinkhole formation and damage to property has cost hundreds of millions of rands. Both lowering of the groundwater level and the ingress of water into the subsurface are important triggering mechanisms for ground instability. Dewatering associated with mining in the gold bearing reefs of the Far West Rand has resulted in the formation of large numbers of sinkholes and dolines, and has produced widespread differential subsidence.

The risk of sinkhole and subsidence occurrence is greatly increased by development, where disrupted natural surface drainage and leakage from water bearing services can result in the concentrated ingress of water into the subsurface.

A classification system for the evaluation of dolomitic land, based on investigation by means of geophysical surveys and the drilling of boreholes, has enabled such land to be zoned for the purposes of appropriate development.

Keywords: dolomite, sinkholes, subsidence, risk, Gauteng

1. INTRODUCTION

Around 20% of Gauteng Province in South Africa is underlain by dolomitic formations. Significantly, this region includes the cities of Johannesburg and Pretoria, which together form the largest and one of the most rapidly growing urban centres in South Africa, and most of the gold mining districts of the Far West Rand. The units colloquially referred to as dolomite are in fact dolomitic limestones of the Malmani Subgroup, Chuniespoort Group, Transvaal Supergroup, which are early Proterozoic in age. Of the units comprising the subgroup, the Monte Christo and Eccles Formations are rich in chert, which occurs in bands within the dolomite, whilst the Oaktree and Lyttelton Formations are chert poor.

Ground instability in the form of sinkholes, dolines and differential subsidence has occurred on land underlain by dolomite. In the past 40 years, 38 people have lost their lives due to sinkhole formation, damage to property has cost hundreds of millions of rands, and the value of property on dolomitic land has depreciated appreciably. In the area underlain by dolomite, which extends around Johannesburg and Pretoria, the problem has become more notable in recent years because of the great deal of urban and industrial development, and the growth of informal settlements. Development densities may be very high, especially for low cost housing which has in places grown without recognition of the risk posed by dolomite-related ground instability. Site investigations, involving hazard and risk evaluation, are of critical importance in the process of urbanization.

Dewatering associated with mining in the gold bearing reefs of the Far West Rand, which underlie dolomitic formations, has resulted in the formation of sinkholes and dolines, and has produced differential subsidence over significant areas. The risk and incidence of sinkhole formation had been greatly increased with the lowering of the water table in these areas, which had in modern times been relatively free from sinkhole formation. Consequently, it became a matter of urgency that areas at great risk of subsidence and of sinkhole formation be delineated. This has been attempted by means of large scale geophysical surveys (primarily gravity survey, which has been found to be most effective in identifying dolomite bedrock topography), and subsurface investigation by the drilling of large numbers of boreholes.

2. MECHANISMS OF SINKHOLE AND DOLINE FORMATION

The terms "sinkhole" and "doline" are used here for physical description of the instability features, and do not refer to their mechanism of formation. A sinkhole is a steep sided, rapidly occurring feature. These are commonly less than 50 m in diameter, but can be larger, and may appear at the surface without warning. The term "doline" refers to a large, enclosed depression, typically between 30 and 100 m in diameter, which usually forms more gradually. Carbonate rocks commonly are transected by discontinuities which have been subjected to various degrees of dissolution. Ongoing dissolution has with time resulted in characteristic integrated systems of subterranean galleries and caverns in the dolomite. Dolomite bedrock frequently has a highly irregular, karst topography and a pinnacled surface, with varying thicknesses of residual material overlying it. This residual material may contain chert, and ferricrete may have been deposited near the surface. The consistency of the overburden usually deteriorates with depth, and frequently chert gravel layers are underlain by wad, a highly mobilizable (erodible and compressible) manganiferous residual material. Cavities may occur above the bedrock within this material. Natural factors which may influence the formation of sinkhole and dolines include surface topography and drainage, the origin, thickness and character of the overburden (be it transported or residual), the nature and surface expression of the dolomite, the presence and size of voids in the soil mantle and in the dolomite, the depth of the groundwater level and its fluctuation, the presence of wad which may be susceptible to erosion by downward percolating groundwater, and the presence of dykes or sills or covering strata of younger age above the dolomite.

As the solution of carbonate rock is a very slow process, contemporary dissolution is very rarely the cause of ground instability. Most commonly, the downward movement of unconsolidated deposits is responsible for sinkhole and doline formation. Both lowering of the groundwater level and the ingress of water into the subsurface are important triggering mechanisms in subsidence and sinkhole formation. The water table may, for practical purposes, be regarded as the base level of subsurface material mobilization. Where this level is lowered by dewatering, the unconsolidated material thus exposed, which may be in the form of low density, highly compressible wad, is vulnerable to erosion and consolidation by the passage of water. Erosion results in the formation of subsurface cavities and most often leads to sinkhole formation, whereas consolidation leads to surface subsidence.

Ravelling occurs as erosion-enlarged openings extent upwards through the soil (Sowers, 1975). Initially, the soil arches over the openings but, as they are enlarged, a stage is reached at which the soil above the roof can no longer support itself and collapses into the cavity below, resulting in a sinkhole. A number of conditions accelerate the development of cavities in the soil and initiate collapse. The rapid changes in moisture content due to ingress of water at the surface lead to slabbing in clays and flow in sands. A lowering of the groundwater level increases the downward seepage gradient and accelerates downward erosion. Therefore, increased infiltration often initiates failure, particularly when it follows a period when the water table has been lowered. Steeply sloping bedrock promotes subsurface instability in that it allows groundwater to develop higher flow velocities which lead to more effective dissolution and erosion. Pinnacles initially may offer arching support to the residual soil which may result in sinkhole formation upon collapse of the arch. Dolines form as a result of the consolidation of compressible material, frequently due to dewatering, or the premature termination of sinkhole formation. The degree of subsidence which has taken place reflects the thickness, density, and proportion of unconsolidated deposits that have consolidated. Thickness of these deposits varies laterally, thereby giving rise to differential subsidence which, in turn, may cause large fissures to occur at the surface. In fact, the most prominent fissures frequently demarcate the areas of subsidence. The total subsidence has varied from a few centimetres to over 9 m. The time lag between the lowering of the water table and surface subsidence, where observed, has been fairly short.

In ascending stratigraphic order, the Oaktree and Lyttelton Formations are the first and third formations of the Malmani Subgroup. They are poor in chert and richer in manganese oxides, and actual wad formation is thus more prevalent upon the weathering of these units. The chert rich Monte Christo and Eccles Formations (second and fourth in ascending stratigraphic order) have statistically been associated with a higher incidence of sinkhole formation. Up to 1985 the number of sinkholes recorded in the Far West Rand in the Monte Christo and Eccles formations was 524 and 135 respectively, with only 32 recorded in the Lyttelton Formation and 6 in the Oaktree Formation in the same region (Wolmarans, 1996). This has been attributed to the promotion of differential leaching and associated cavity development by the chert content. It is in addition thought that layers of chert within the residual material, which are more competent than the dolomite residuum, facilitate the action of arching over cavities developing within the overburden, thereby allowing for sinkhole formation as opposed to subsidence. Schöning (1996), however noted that up to 1984, in the area South of Pretoria, the most sinkholes had occurred in the Eccles Formation. It was suggested that, because this youngest unit is found closer to Pretoria and had been subjected to the detrimental effects of urban development from an earlier stage, it was indeed likely that more sinkholes would have occurred on the Eccles Formation.

The risk of sinkhole and subsidence occurrence is greatly increased by development, where disrupted natural surface drainage and leakage from water bearing services can result in the concentrated ingress of water into the subsurface. Where overlying material is less permeable, the risk of instability is lower. A high risk of sinkhole or subsidence occurrence exists where erodible, compressible residual soil (wad) overlies dolomite bedrock. Areas at greatest risk of (especially large) sinkhole formation are those overlying scarp zones on the margins of deep palaeo-infilled karst valleys, or in the centre of such valleys that are narrow in width. These are usually reflected as areas of low gravity. Land overlying the margins of igneous bodies or along fault zones is similarly at high risk. Indeed, sinkholes have fallen along faults through even substantial thicknesses of cover rocks of shale and quartzite. Dolomite at shallow depth, that is, occurring at less than 10 m beneath the ground surface, has been associated with the appearance of significant numbers of small sinkholes. For instance, the area south of Pretoria recorded more than 430 events prior to 1997, with over 50 being associated with the heavy rainfall of 1996. The vulnerability of an area overlying shallow dolomite is largely dependent on the presence of erodible and compressible material and the spacing, width and continuity of grykes in the bedrock. The greater the number, width and continuity, the greater the risk. When dolomite is located at depths greater than 10 m, the sinkholes which appear at the surface usually are deeper and have larger diameters. The risk of sinkhole occurrence in areas of shallow dolomite may, in general, be greater, although the hazard itself is less severe. A recent study of the Katorus area south of Johannesburg, for example, indicates a significant number of sinkhole occurrences within this township associated with shallow bedrock conditions. Apparently, 25 sinkholes had developed in the preceding 10 years. The set of subsidence events numbering more than 50, associated with the heavy rains of 1996, had not at the time been added to those figures.

3. A BRIEF ACCOUNT OF INSTABILITY PROBLEMS ON THE FAR WEST RAND

At the time of commencement of large-scale gold mining operations along the Far West Rand prior to and after World War II, the establishment of shaft infrastructure and residential areas was done in accordance with the procedures customary at the time. A few boreholes were drilled to probe for possible cavities close to surface. The area has been affected by extensive faulting. These faults act as conduits which connect groundwater in the dolomite with the underlying gold bearing reefs of the Witwatersrand Supergroup. Accordingly, many mines adopted dewatering techniques to dispose of large amounts of groundwater which entered the mines from above. Several dykes occur in the Far West Rand and divide the area into a number of compartments, with the dykes acting as barriers to groundwater movement. This allowed the gold mines to be dewatered, the groundwater level being lowered within individual compartments. After 1959, phenomena such as slow surface subsidences and linear surface cracks became apparent. All sinkholes developed on mining property prior to dewatering are considered to have formed due to super-saturation and subsurface erosion in the overburden, especially around slimes dams (Wolmarans, 1996). A total of 88 sinkholes was recorded, with 33 formed around Annan Shaft of Doornfontein mine. West Driefontein mine had initiated a dewatering programme from 1956. Ground movements were noticed from 1959, and investigations were still underway when, on 12th December 1962, disaster struck. A huge sinkhole (55 m in diameter) engulfed the three-storey crusher plant resulting in 29 deaths. There was practically no warning, collapse occurring suddenly. The most productive gold mine in South Africa came temporarily to a standstill. The investigations had discovered a fault zone, a gouge-filled fissure some 35 metres in width. A similar phenomenon was observed during an earlier exploratory hole some 20 km east of the site, where drill rods were lowered for 200 m without active drilling being necessary. Less than two years later, in August 1964, two houses and parts of two others disappeared into a sinkhole in Blyvooruitzicht Township with the loss of 5 lives. Lupin Place in Carletonville subsided 7 m over a period of 4 years, resulting in the demolition of 24 houses. In all, several hundred buildings were demolished as a result of water table drawdown in the Venterpost, Bank and Oberholzer compartments between 1960 and 1976.

Consequently, it became a matter of great urgency that areas at great risk of subsidence and sinkhole formation be delineated. During the 1960's, a great deal of time and money was spent on investigating land that had been damaged through dewatering or as a result of other human activities. This was done mainly under the auspices of the State Co-ordinating Technical Committee on sinkholes and subsidences in the Far West Rand (SCTC) which was brought to life in 1964 when it became increasingly evident that the relatively fast drawdown of the watertable was responsible for increasing instability in the groundwater compartments being dewatered. Extensive research was done on the mechanisms responsible for sinkhole and doline formation and methods were sought to predict their occurrence. Various probing techniques were investigated to gain a better understanding of the condition and distribution of the subsurface geology. Gravity surveys were conducted and drilling of large numbers of percussion boreholes was undertaken to calibrate and supplement this work.

4. INVESTIGATION AND CLASSIFICATION OF LAND FOR CONSTRUCTION AND DEVELOPMENT PURPOSES

A fairly well established methodology exists in South Africa for the characterization of dolomitic land[1] in terms of its potential for instability. The current evaluation system, namely the Method of Scenario Supposition, was first described by Buttrick in 1992 and published by Buttrick and van Schalkwyk in 1995. The evaluation is based on the risk of formation of certain-sized sinkholes and is used so that land may be zoned for the purposes of appropriate development. The inherent risk of a site refers to the susceptibility of the dolomite profile to ground instability, based purely on the geological and hydrogeological conditions. It was maintained that the stability characterization of a site requires some hypothesis regarding the likely impact of development on the dolomitic environment during the lifetime of that development. An area may be considered low, medium or high risk respectively where up to 0.01, greater than 0.01 to 0.1, and greater than 0.1 ground movement events are anticipated per hectare within a 20 year period. *Development risk* refers to the likelihood of damage to property, loss of life or financial loss, and is to be considered acceptable or unacceptable. The basic design of a township is a key element in the strategy to minimize the impact of a proposed development. Once the hazard and inherent risk of a site has been established, a type of development can be selected that is appropriate and will result in an acceptable development risk. The stability characterization and evaluation process is constantly in the process of refinement, the most up to date of which is expressed in a new paper by Buttrick *et al.* (in preparation) in which the terms *hazard* and *risk* have been more precisely defined.

A dolomite stability investigation is carried out in order to provide the information on which the evaluation is based. A geophysical exploration most often forms the initial phase of such a ground stability investigation. No reliable geophysical technique exists that can accurately gauge the presence and size of voids in the bedrock or overburden, so the purpose of this phase

[1] The term 'dolomitic land' refers in South Africa to areas underlain directly or at shallow depth (less than100 m) by dolomitic rock. This may therefore include areas where dolomite is covered by younger deposits.

is primarily aimed at determination of the dolomite bedrock topography and thickness and density of overburden. The gravimetric method is the most successful and widely used for this purpose, but other geophysical techniques, such as electromagnetic survey, have been attempted. Seismic refraction is generally not suitable for these purposes in that chert boulders in the overburden produce a scattering effect. In the gravimetric method, readings are taken with a gravimeter at each station of a grid surveyed for the site. The grid spacing is a function of the type of anomaly expected, the depth to the source of the anomaly, and the size of the investigated area. A Bouguer gravity anomaly contour map is then produced, followed by the production of a residual gravity map. The residual field should be adjusted by a constant once drilling information is available so that the map becomes a better representation of depth to dolomite bedrock. Bezuidenhout and Enslin (1969), using the gravimetric method on the Far West Rand, took the zero gravity contour to coincide with the original position of the groundwater level. Hence, positive gravity contours accordingly indicate areas where the bedrock is above the original groundwater level, which are unlikely to have been affected by dewatering. The interpretation of the residual gravity map is then used as the basis for planning the subsequent phase of investigation, in which rotary percussion borehole drilling is carried out. Areas of relatively shallow bedrock are represented as gravity highs, and areas of relatively deep bedrock are represented as gravity lows. Igneous intrusions such as syenite dykes and sills are usually represented as gravity low features. Steep bedrock gradients, often indicative of high risk conditions, are represented by closely-spaced contour lines. Where dolomite is shallow, sudden changes in bedrock topography such as grykes (solution-enlarged vertical joints which form slots in the bedrock) and pinnacles, may have a profound effect on ground stability conditions. These relatively small features, however, are very difficult to identify using the gravity method, and they are often not discovered.

The drilling phase of the investigation is based on the interpretation of the gravity map. The site is divided into zones that are considered likely to have certain characteristics or conditions, and these are then investigated. Rotary percussion boreholes (the most cost-effective and useful drilling technique) are drilled in these zones, on the gravity highs and in the gravity lows, to identify the conditions present within these features. Steep gravity gradients and embayments in gravity gradients are also investigated (the latter may be representative of grykes). It is advisable to drill boreholes so as to provide a fairly good coverage over the area under investigation. Drillholes should be sunk at least 6 m into solid dolomite bedrock. The drilling density is to some degree a function of the site size and purpose of the investigation. Further phases of drilling may be required in order that subsurface conditions may be suitably assessed and risk zones delineated on a map with a degree of confidence. Sample depth (usually taken for every metre drilled), drilling conditions and penetration rates (which depend on the compressor used for the drilling machine), air and sample losses, the addition of any water or foam to facilitate sample recovery, and the groundwater level are recorded during drilling. Holes drilled should subsequently be backfilled properly in order that they do not act as sub-surface conduits for the passage of water. Augering may provide a cost-effective means of gathering additional information. Auger holes may extend several metres in depth. Provided that chert bands can be penetrated and the residuum is somewhat competent, large diameter augering may provide a unique opportunity to observe and sample relatively shallow overburden in a fairly undisturbed state.

A set of generalized evaluation factors is reviewed for the conditions illustrated in the profiles of each of the boreholes drilled, and the risk and size of possible sinkhole formation is determined. These factors are: the presence, nature and position of receptacles (cavities) within the bedrock or overburden; the likely presence of mobilizing agencies (ingress water, groundwater level drawdown, ground vibration); the nature of materials in the blanketing layer; and the maximum potential development space for a sinkhole which takes into account the depth to bedrock, the presence of receptacles for mobilized material, the nature and thickness of the different layers within the overburden, and the position of the groundwater level. The maximum potential development space gives an indication of the size of sinkhole that can be expected to develop. Sinkholes 2 m and less in diameter are considered to be small, and those between 2 and 5 m, 5 and 10 m, and larger than 10 m in diameter are considered medium-sized, large and very large respectively. Risk is described in the context of a dewatering or non-dewatering scenario. If the region has undergone dewatering, the probable effects on ground stability must be assessed. If the region has not been dewatered, the importance of the effects of any future dewatering must be evaluated and stressed. Areas that are characterized as having similar conditions and thus risk for certain sized sinkhole or doline formation are identified as risk zones and classified according to Table 1.

The zonation map produced is merely an indication of possible conditions to be expected over the site based on the point-specific information gained from a number of boreholes. Boundaries should be interpreted and recommendations made conservatively where information in lacking. Types of development appropriate to the risk of ground instability and conditions present are then recommended for each zone according to the guidelines in Table 1. Sites of higher risk are most often not recommended for residential development, but may be considered suitable for certain types of commercial or industrial development. Development should be controlled or regulated so as to reduce risk wherever possible. For residential development, lower densities and lower area of ground coverage are advisable, as this reduces the risk of damage to property or loss of life should a sinkhole occur, and the lower density of water-bearing services required will serve to reduce the risk of sinkhole development.

Characterization: Risk of sinkhole formation					Recommended development type
Risk Class	Small sinkhole	Medium sinkhole	Large sinkhole	Very large sinkhole	
I	Low	Low	Low	Low	All development types at any density.
II	Medium	Low	Low	Low	All development types, including high density, low cost housing.
III	High	Low	Low	Low	Selected residential development. Development at lower density with suitable engineering/precautionary measures. No informal settlements.
IV	Low-Medium	Medium	Low	Low	As above but with exceptionally stringent precautionary measures/ design criteria. No site and service schemes. Consider high-rise development.
V	Low-Medium	Low	Low	Low	High-rise residential structures, gentlemen's estates, commercial or light industrial development. Expensive foundation design and/or earth mattresses necessary. Sealing of surfaces. Water services in sleeves/ducts.
VI	High	High	Medium	Low	Gentlemen's estates (4000 m^2). Commercial or light dry industrial development.
VII	High	High	High	Medium	No residential development. Commercial or light dry industrial development. Parking areas with all surfaces sealed. Park land or nature reserves.
VIII	High	High	High	High	No development. Nature reserves or park land.

Table 1. Instability risk classes and corresponding appropriate development (after Buttrick and van Schalkwyk, 1995)

5. PRECAUTIONARY MEASURES FOR MITIGATION OF DEVELOP-MENT RISK

Over the years, a number of measures have been implemented in development for the mitigation of risk and for the prevention of ground instability occurrence in the future. The scale and number of these measures has grown larger with time and experience, and, whilst the suitable suite of measures to be implemented will be specific to a site, a certain minimum standard now exists for all sites on dolomitic land. Such measures are aimed at either reducing the infiltration of surface water into the subsurface or the prevention of water ingress due to leakage of water bearing services. These measures include, amongst many, the paving of areas around structures in order to render this ground impervious to infiltration, the contouring of land and erection of structures so as to facilitate efficient stormwater drainage, and the correct and timely backfilling of service trenches. In order to prevent leakage from services, these are often constructed of materials such as HDPE (high density polyethylene) or high impact PVC (polyvinylchloride) which offer some flexibility. In addition, these services may be placed either on the surface, or in sleeves or concrete canals which are made easily inspectable for leakage detection.

Certain methods, most particularly those involving the founding of structures, may be considered necessary to prevent the likelihood of damage to these structures.

Engineered soil mattresses can be used to limit total and differential settlement by spreading the loads of structures fairly uniformly beneath the mattress, thereby reducing foundation stress. This may be of particular importance over shallow, pinnacled dolomite bedrock. Where differential settlements of between 10 and 25 mm are expected, split construction similar to that used when building on heaving clays or collapsible sands is to be advised (van der Berg, 1996). On sites where shallow pinnacles and boulders occur, Wagener (1985) suggested that material to a depth of 1m below the tops of pinnacles and large boulders should be removed and replaced with compacted fill, and in some instances the tops of pinnacles should be removed by blasting (although caution is advised, as blasting may disturb the metastable nature of the dolomite residuum). Compacted mattresses of the type mentioned are composed largely of gravel. It is thought that mattresses that are to be constructed merely for the purposes of presenting an impermeable layer for limiting water ingress should be constituted of well compacted fine material in the form of clays and silts. Where they are slightly raised, mattresses also serve to reduce water ingress by diverting it away from the structures concerned. Dynamic consolidation has been used to compact overburden in dolomitic areas. However, especially where chert gravel occurs close to the surface, the overlying material is usually more competent than the material beneath and much of the energy of the compactive effort is expended in the upper layers and the underlying material is left poorly compacted. Concrete raft foundations are often advisable where severe differential settlement or small sinkhole formation is expected. Where pinnacles have been exposed, rafts can be constructed so as to span from pinnacle to pinnacle. The raft may actually bridge smaller sinkholes, and may allow for damaged structures to be evacuated in the event of slightly larger sinkhole formation. Piles should be used in dolomitic areas only when other methods of foundation are not feasible (van den Berg, 1996). Dolomite pinnacles and large boulders can cause piles to deflect and the presence of cavities makes pile installation difficult. The competency of the rock below founding level must in addition be proven. Due to the costs involved, grouting is seldom used in South Africa to treat areas of potential subsidence risk. It is used rather as a remedial measure. Thick grouts, injected at low grouting pressures, have been employed in order to avoid erosion of wad and in an attempt to fill subsurface cavities. Grouting has at times been undertaken from the top down so as to avoid collapse into these cavities, and has been used in a number of instances to protect roads from possible sinkhole development and to arrest subsidence.

6. REGULATION OF RESIDENTIAL DEVELOPMENT ON DOLOMITIC LAND IN SOUTH AFRICA

Under the Housing Consumers Protection Measures Act no. 95 of 1998, the regulation of residential development in South Africa is conducted by the National Home Builders Registration Council (NHBRC). In order to maintain standards and suitable procedure, residential development on dolomitic land must be enrolled with the NHBRC. All investigations for proposed developments undergo evaluation by the Council for Geoscience (formerly the Geological Survey of South Africa) who must affirm that the geological evaluation of risk and recommendations made are suitable. The proposed development is further scrutinized by a panel of consultants, who are suitably experienced in the field of dolomite stability evaluation, prior to provisional enrolment with the NHBRC. Final enrolment is gained upon submittal of a construction report and certification that construction and service installation has been carried out correctly and according to recommendations. In this way, it is attempted to minimize the risk of damage to property and loss of life as a result of unsuitable or poorly conducted development in areas underlain by dolomite. Assessment of industrial and commercial developments by the Council for Geoscience may also be requested at the discretion of local authorities. For the purposes of attempting to ensure the long term stability and safety of development, both individual developments and local authorities must possess a risk management system that must be submitted to the NHBRC. This system should consist of the following elements: an infrastructure maintenance plan including details of the intervals over which routine repair and replacement must take place; a monitoring programme for water bearing services, buildings and infrastructure so that leakage or damages can be timeously detected; an emergency reaction plan and basic remedial strategy in the event of ground instability occurrence; and the maintenance of a database for the recording of routine procedures, instability events and any remedial actions taken. The awareness of property owners concerning the potential risks and the need for timely remediation of poor drainage and damaged services is a key element in the effective maintenance of any risk management system.

7. CONCLUSIONS

Ground surface instability in the form of sinkholes, dolines and subsidence may occur in regions of South Africa that are underlain by dolomitic formations. These regions include significant areas of densely populated Gauteng Province. Both lowering of the ground water level and the ingress of water into the subsurface are important triggering mechanisms in subsidence and sinkhole formation. Where the ground water level has been lowered, the unconsolidated material of the overburden thus exposed, which may be in the form of easily erodible, highly compressible wad, is vulnerable to erosion and consolidation by the passage of water. Erosion results in the formation of subsurface cavities and leads to sinkhole formation, whereas consolidation results in surface subsidence. A classification system for the evaluation of dolomitic land based on the risk of formation of certain-sized sinkholes has enabled land to be characterized for the purposes of appropriate development. Ongoing monitoring and maintenance of water bearing services and the implementation of precautionary measures relating to drainage and infiltration of surface water are regarded as essential in developed areas underlain by dolomite.

REFERENCES

Bezuidenhout, C.A., and Enslin, J.F. (1969) Surface subsidence and sinkholes in the dolomitic area of the Far West Rand, Transvaal, South Africa. In: *Proceedings of the 1st International Symposium on Land Subsidence,* Tokyo, International Association of Hydrological Sciences, UNESCO Publication No. 88, Paris, 482-495.

Buttrick, D.B., and van Schalkwyk, A. (1995) The method of scenario supposition for stability evaluation of sites on dolomitic land in South Africa. In: *Journal of the South African Institute of Civil Engineers, 37,* 9-14.

Schöning, W.L. (1996) Distribution of sinkholes and dolines in the area south of Pretoria. In: *Seminar on the Development of Dolomitic Land,* University of Pretoria, January 1996, 7/1-7/11.

Sowers, G.F. (1975) Failures in Limestone in the Humid Tropics. In: *Proceedings of the American Society of Civil Engineers, Soil Mechanics and Foundations Division, 101,* 771-787.

Van den Berg, J.P. (1996) Construction methods on dolomitic land. In: *Seminar on the Development of Dolomitic Land,* University of Pretoria, January 1996, 11/1-11/18.

Wagener, F. von M. (1985) Dolomites. In: *The Civil Engineer in South Africa, 27,* 395-407.

Wolmarans, J.F. (1996) Sinkholes and Subsidences on the Far West Rand. In: *Seminar on the Development of Dolomitic Land,* University of Pretoria, January 1996, 6/1-6/12.

LAND SUBSIDENCE - Vol. I
Proceedings of the Sixth International Symposium on Land Subsidence
Ravenna / Italy / 24-29 September 2000

SUBSIDENCE EVALUATION DUE TO MINE DEWATERING

Azam Khan and Hamid Nikraz
School of Civil Engineering, Curtin University of Technology, Perth, Western Australia

Abstract

This paper describes the research carried out to evaluate the subsidence associated with dewatering in the Collie Coal Basin. A triaxial test technique has been adapted to evaluate the compaction characteristics of the sandstone aquifer in the Collie Basin. The technique, which allows the strata stress regime to be reproduced by triaxial loading with zero lateral strain, also provides a precise evaluation of lateral stresses and consequently Poisson's ratio under *in situ* conditions.

The paper contains a description of equipment commission, test techniques, results, and the analysis and interpretation of derived data obtained. The testing and evaluation techniques are general in nature and are applicable to field situations in locations where similar weak sandstones occur.

Keywords: land subsidence, stress regime, sandstone, mines

1. INTRODUCTION

The Collie Basin lies nearly 200 km south-southeast of Perth in Western Australia and is 27 km long by 13 km wide, covering an area of approximately 230 km^2 (Figure 1). It contains extensive reserves of good steaming coal, which is currently being mined by both open cut and underground methods.

The Collie Coalfield has a long history of strata control problems. They manifest themselves in the form of localised poor roof control, surface subsidence, slope instability and mine abandonment (due to a sand-slurry inrush). Major sources of these problems include the very extensive, weak, saturated, sandstone aquifers. As a result, underground operations have been limited to room and pillar extraction, presently carried out by continuous miners and road-heading machines. Approximately 30-40% recovery by volume is being achieved by this method.

In order to increase the recovery to approximately 70%, the Wongawilli method of short-wall mining has been introduced. With this method, extensive aquifer dewatering is carried out prior to caving of the immediate roof. However, due to the porous and weak nature of the aquifers, dewatering has the potential to cause subsidence, with a significant risk of environmental instability on a large scale. This is particularly critical adjacent to townsites and industrial complexes. For safe operations and limits to surface subsidence, an engineering design was needed which would control strata deformation wth a high degree of confidence. A better understanding of strata mechanics was needed to achieve this.

The roof dewatering/depressurization procedure involved a combination of in-mine vertical roof drainage holes and conventional dewatering bores constructed from the ground surface above the mining area. A full account of the dewatering strategy may be found at Humphreys et al (1988) and Dundon,P.J et al (1988). Of prime concern is the effect of pore pressure reduction upon strata compaction. To simulate those effects it is necessary to perform tests under triaxial conditions of the same order as experienced *in situ*.

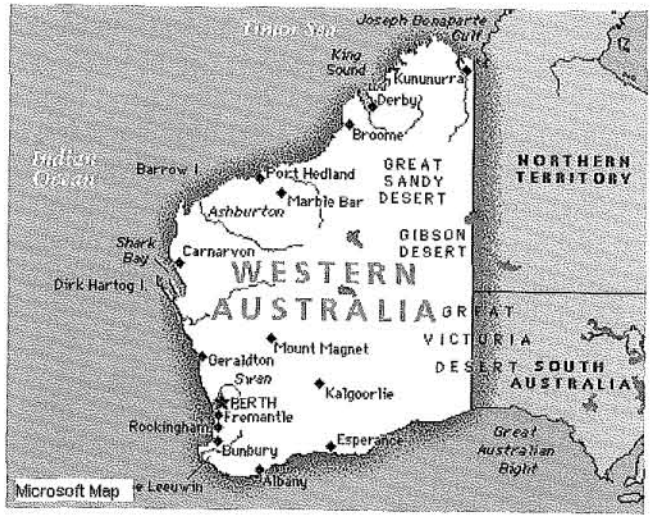

Figure 1. Collie Coal Basin, location and regional geological setting

The pore pressure effect phenomenon is not a new concept. However, investigation of the effect under triaxial conditions is relatively new. Although rock bulk compressibility figures are generally larger for high porosity, simple compressibility porosity correlations do not exist. Furthermore, compressibility data reported for poorly-consolidated sandstone differ greatly. This paper describes the equipment and the techniques and procedures used in carrying out deformation characteristics of poorly-consolidated sandstone in Collie Coal Basin.

2. REGIONAL GEOLOGY AND HYDROLOGY

The Collie Basin is comprised of two unequal lobes in part separated by a fault controlled, basement consists of three sub-basins, the Cardiff, Shotts and Muja. The Collie Basin sediments are mainly cyclic, high-energy fluviatile sandstones with thin gravel and conglomerate lenses. Siltstone and shales occur as

overbank lacustrine or paludal deposits. Coal seams are remarkably uniform in thickness and composition over considerable distances.

The Collie Basin sediments can be described as saturated and weak, and have been altered through weathering or post depositional processes. Lowry, D.C (1976) estimated that the coal measures were composed of 65% sandstone, 25% shale and claystone and 5% coal. The whole Collie Basin can be thought of as an inter-related groundwater system of Permian coal measures bounded by Archaean basement.

Permeable aquifers comprise fine to granular quartzose sandstones with little fines content. Moderately permeable material consists of silty-clayey sandstones. Siltstone represent the low to moderately permeable aquifers whilst mudstone, shale and coal layers form the system aquitards. All coal seams in the deep mines are bounded by aquifers. In some locations aquifers are situated directly above or below the seams, but most areas have aquitard barriers of variable thickness separating the mining seam from neighbouring aquifers (Figure 2).

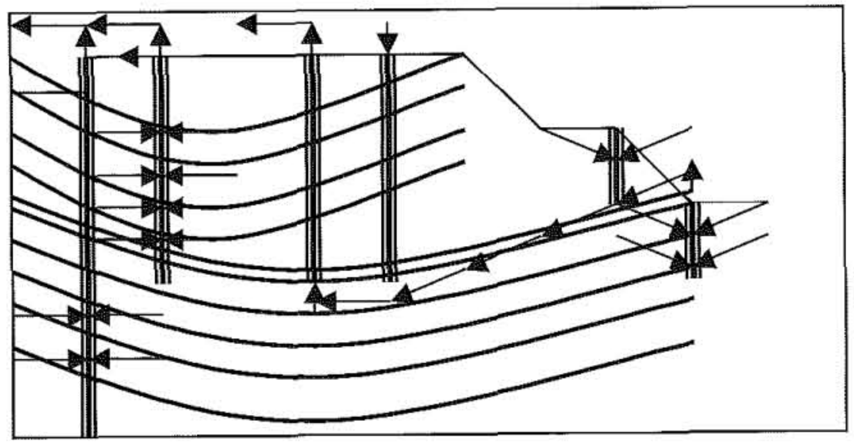

Figure 2. Generalised hydrostratigraphy

3. GEOMECHANICAL PROPERTIES OF THE COAL MEASURES

The geology of the Collie Basin can vary within short intervals, both vertically and laterally. There are also marked variations within the major lithologies (sandstones, shales, siltstones, laminites). Each has a wide range of engineering properties, dependent on past and present geological processes. Table 1 lists typical ranges of compressive strengths, elastic moduli, cohesive strengths and friction-angles for the major lithologies of the collie Coal measures. The table highlights the weak and plastic nature of Collie sediments and also illustrates that coal strengths are in the order of 3-4 times greater than non-coal lithologies. In terms of subsidence, the resistance to movement of non-coals is small, and thus there is the possibility that coal seams will deform differentially and lead to bed separations at coal contact.

4. ROCK MOVEMENTS CAUSED BY DE-WATERING IN POORLY CONSOLIDATED SANDSTONE

Land subsidence is caused by a number of mechanisms including withdrawal of fluid and the collapse of underground openings. This study is concerned with the former. Deformations resulting from equilibrium disturbance of the aquifer rock due to water pressure decline, are either elastic or non-elastic. Elastic deformations are mostly of a negligible extent with respect to both the involved surface subsidence and the reserve of the stored water, being only of importance in respect to the variation of the rate of flow. The extent of the non-elastic deformation are due to compaction or migration of the rock material. The former, depends on the geotechnical characteristics of the rock, and on the extent of the pore pressure reduction. The extent of migration, on the other hand, depends on the pressure gradient (the flow velocity). The compaction may cause regional subsidence, while the migration of the rock particles causes local displacement, both phenomena being dependent upon the characteristics of the aquifer rock and the extent of dewatering.

Several techniques are available for predicting subsidence due to fluid withdrawal, classed by Poland, J.F (1984) into three broad categories : empirical, semi-theoretical and theoretical. Empirical methods essentially plot past subsidence versus time and extrapolate into the future based on a selected curve fitting technique. They suffer from a lack of well documented examples to establish their validity. Semi-theoretical methods link on-going induced subsidence to some other measurable phenomenon in the field. Theoretical techniques require knowledge of the mechanical rock properties, which are either obtained from laboratory tests on core samples or deduced from field observations. Essentially, however, theoretical techniques use equations derived from fundamental laws of physics, such as mass balance.

Geertsma, J (1973, 1966) has shown in a theoretical analysis that reservoirs deform mainly in the vertical direction and that lateral variations may be discarded if the lateral dimensions of the reservoir are large compared with its thickness. For the one-dimensional compaction approximation, the vertical deformation of a prism of the aquifer material can be computed by :

$$\Delta h = C_m \, h \, dP \tag{1}$$

where "Dh" is the change in the prism height, "C_m" is the one-dimensional compaction coefficient, h is the prism height, and "dP" is the change in pore fluid pressure. This approach was adapted by Martin and Serdengecti (1984). They suggest that the best way to obtain values of C_m, which in most cases is the most difficult of the three one-dimensional compaction parameters to determine, is to measure it on core samples in the laboratory.

The one-dimensional compaction coefficient "C_m" of friable sandstones can be measured by different methods :

1. indirect measurement by measuring rock compressibility "C_b" under hydrostatic load and estimating Poisson's ratio of the rock;
2. direct measurement by equipment which simulates the aquifer boundary condition of zero lateral displacement (such as, Oedometer cell test, or a modified triaxial cell test).

Although the triaxial test method is laborious and time consuming, its unique experimental conditions make it essential as they produce aquifer stress quite well. In addition, the triaxial set-up has the advantage that the circumferential pressure needed to prevent lateral stain is measurable. The Poisson's ratio of the rock sample can therefore be determined independently from the ratio of lateral to vertical stress.

5. LABORATORY-DETERMINED COMPRESSIBILITIES

The cores taken from Collie Basin vary markedly in both porosity and grain correlation. Medium to high porosities are found in consolidated and semi-consolidated sections. In addition, the nonhomogeneous appearance of the cores suggest that rock properties vary over short distances. Consequently, compaction is expected to vary considerably with depth, implying that the cores must be sampled systematically at short intervals to obtain a reliable compaction profile. As this involves compaction measurements on a large scale, a simple, rapid, but nevertheless reliable measuring technique must be developed.

The earlier studies by Grassman, F (1951); Biot, M.A (1941); Geertsma, J (1957) and Van der knaap, W (1959) resulted in the theory of pore elasticity. They demonstrated that compaction behaviour depends only on effective frame stress, i.e. the difference between external and internal stresses. Nikraz , H.R (1991) has confirmed that the effective stress theory is applicable to Collie sandstone. Therefore, to stimulate aquifer compaction in a laboratory experiment requires application of the stress difference instead of the actual stresses. Experimentally the most attractive approach is to load the samples externally, keeping the pore water pressure constant and atmospheric.

The triaxial technique which was developed in accordance with this reasoning predicts the compaction behaviour of strata due to dewatering in particular for the weakly cemented Collie sandstone. The technique allows the strata stress regime to be reproduced by triaxial loading with zero lateral strain, and also provides a precise evaluation of lateral stresses and consequently Poisson's ratio under *in situ* stress conditions. The condition of zero lateral strain during triaxial compaction test is achieved by both preventing any volume change in the cell-water system surrounding the specimen and by using the modified piston and top cap. This piston is of the same diameter as the sample, therefore induced the triaxial stress in the sample, but the deviator stress. Because bulk volume change was detected from pore volume changes, the pores of the specimens had to be completely saturated. For the detail of the equipment design see Nikraz, H.R (1991).

The experimental procedure had two stages : (1) the preparatory stage, in which the specimen was brought into an "initial" loading state prior to the test; and (2) the test itself, which further compacted the specimen.

In order to eliminate possible membrane penetration effects during the test and thereby cause errors in test results, the specimens were first loaded hydrostatically to a pressure of 1.25 MPa. The volume change related to this pressure was assumed as a reference point. The axial stress was then measured continuously at a constant rate until the desired axial stress was achieved. The cell pressure was adjusted simultaneously to prevent any lateral strain. However, the maximum axial stress level was confined within cell pressure limitation (maximum cell pressure limited to 12 MPa).

To check the zero lateral strain, the following relationship had to be satisfied:

$$\Delta V = (A\ X)/1000 \qquad \text{(ml)} \qquad (2)$$

where
ΔV = volume change (ml) A = area (mm^2); and X = axial deflection (mm).

To determine the effect of loading history on compaction, the axial stress was released incrementally to approximately 1.5 MPa. Consequently, the confining pressure was adjusted to satisfy equation 2. The loading and unloading were repeated for another two cycles. A total of six tests were made on specimens at strain rate of 2×10^{-4} min^{-1}.

Table 1. Typical mechanical properties of Collie Coal Measures

Lithology	UCS (MPa)	Elastic Modulus (MPa)	Cohesive Strength (MPa)	Friction Angle (Deg.)
Sandstone	5.2	300	0.5	32
Siltstone	4.7	600	0.6	25
Laminite	4.7	700	0.7	25
Shale	7.0	1200	0.8	22
Wyvem Coal	19.8	2000	2.0	42

6. RESULTS ANALYSIS AND INTERPRETATION

Measurements were made on six core samples taken from four locations in the Collie Coal Basin (Table 2). Typical axial stress/uniaxial compaction and lateral stress/uniaxial compactions are shown in Figures 4 and 5 respectively. Similar behaviour was observed in the other five specimens.

The three significant features of the stress/uniaxial compaction curves are their non-linearity, hysteresis and irrecoverable compaction on loading. Microstructural changes, which produced permanent strain, are a likely source of cycling effects. For example, assume that a microstructural element such as an asperity contributes to the elastic response of a rock by separating two grains. If the asperity is crushed subsequently at a high pressure, then later strain curves will be different because of the absence of the asperity. The unloading to atmospheric pressure is believed to have a significant role in stress cycling effects. When cracks are created and asperities crushed, they are probably pinned because of the high confining pressure. However, when the confining pressure is released, the microstructure can deform along new degrees of freedom and thus behave differently when reloaded. Other likely mechanisms, which produced permanent strain, are displacement of fines and clay minerals and frictional sliding on grain contacts Brace, W.F *et al* (1966) and Batzle, M.L *et al* (1980).

The problem of choice of loading cycle for field application has been studied by Knutson and Bohor (1963); Van Kesteren (1973); Mattax *et al*, (1975); and Mess, K.W (1978). For fully undisturbed unloaded core material, compressibility values derived in laboratory tests should be lower than *in situ* values for reservoirs that are not over-consolidated. For over-consolidated reservoirs they could be either too low or too high for *in situ* application, depending on the degree of over-consolidation of the reservoir rock.

Knutson and Bohor (1963) suggest that a reasonable compressibility value may be obtained by averaging values from the first and subsequent cycle. However, from extensive laboratory and *in situ* tests on relatively soft rock, Mattax *et al* (1975), suggest that the first cycle compressibility is the most realistic measure of *in situ* response to changes in effective pressure that occur during reservoir depletion. However, erroneously high values of first cycle compressibility were obtained in the laboratory tests on unconsolidated sands because of systematic experimental error (caused by freezing and thawing of the sample and some grain crushing). It was therefore recommended that about two thirds of the first cycle compressibility be taken as representative of *in situ* compaction.

The uniaxial compaction curves representing the six samples tested are plotted in Figure 6 for the first loading cycles. From the graph in Fig 6 average compaction per unit stress can be calculated for this range. Further, the compaction curves are parabolic thus there is an observed relationship :

$$\varepsilon_1 \ \alpha \ \sqrt{\sigma_1} \qquad (3)$$

where ε_1 = axial strain; and σ_1= axial effective stress.

To demonstrate the observed relationship the axial strains have been replotted against σ_1 (Figure 6). This plot provides strain lines, although it is noted that some points deviate slightly from linearity. By using the linear relationship as shown in Figure 7, the uniaxial compaction coefficient "C_m" may be calculated over the relevant stress interval. Consider the simulation of dewatering operations for a typical specimen such as D156-286. Assuming an average overburden density of 2.5 t/m^3, the initial *in situ* hydrostatic effective stress 7 MPa would increase to 9 MPa to simulate the effects of dewatering. Hence the uniaxial compaction can be calculated by :-

$$C_m = \frac{(\varepsilon_1)_9 - (\varepsilon_1)_7}{9-7} \tag{4}$$

where $(\varepsilon_1)_7$ and $(\varepsilon_1)_9$ are axial strain at hydrostatic effective stresses of 7 and 9 MPa respectively, giving

$$C_m = \frac{(0.288 - 0.277) \times 10^{-2}}{2} \tag{5}$$

The uniaxial compaction coefficient data corresponding to first, second and third loading cycles are plotted as a function of initial porosity in Figure 8. It appears that compaction is greater for the first loading, indicating loading history influences on compaction. However, those correlations serve to assess a reliable average field value of the uniaxial compaction coefficient, which is required for a prediction of field compaction.

In an early study [12], the average porosity obtained from 105 samples tested as 20.77% of bulk volume. Variation in porosity between holes was considered to be minor. This, and the near linear relationship between uniaxial compaction and porosity prompted the acceptance of 20.77% porosity for the determination of an average value of the uniaxial compaction coefficient.

Based on the first loading cycle, Figure 8 indicates a uniaxial compaction coefficient of 3.124×10^{-4} $(MPa)^{-1}$. The effects of stress relief upon sampling are accommodated within this value. However, the second and third loading cycles exhibit elastic compaction characteristics and provide an average value of uniaxial compaction coefficient for the second and subsequent loading cycles of 1.6409×10^{-4} $(MPa)^{-1}$.

The difference between the two values indicates the elastic component of compaction. Considering the strain-hardening and core disturbance arguments one may expect the true compaction to be somewhere in between. In view of the quite small difference between maximum and minimum values, the most practical approach seems to be to take the average as a working value, thus reducing the uncertainty to an acceptable limit. Thus, a mean value of 2.382×10^{-4} $(Mpa)^{-1}$ was used to represent the *in situ* compaction coefficient.

Applying these results to a 12.5 m thick aquifer above the Collieburn No. 2, with an ultimate reduction in pore water pressure of 2.0 MPa could

produce a vertical compaction of :

$$\begin{aligned} \Delta h &= - C_m\, h\, \Delta P \\ &= 2.382 \times 10^{-4} \times 12.5 \times 10^3 \times 2 = 5.96 \text{ mm.} \end{aligned} \tag{6}$$

The Poisson's ratio of the specimens tested can be determined independently using the ratio of lateral to vertical stresses. The ratio of lateral to vertical stresses under isotropic conditions suggested by Teeuw, D (1971) is :

$$\frac{\sigma_h}{\sigma_v} = \left[\frac{\nu}{(1-\nu)}\right]^{1/n} \tag{7}$$

where v is the Poisson's ratio and n is the exponent in relationship of the uniaxial compaction/axial pressure in Figure 3. The exponent reflects the deformation of the contact points and/or contact areas between grains Brandt. H (1955). According to Hertz's theory Timoshenko, S and Goodier, J.N (1951), for perfect spheres n = 2.3, while for linear elastic media such as non-porous quartz and steel, n = 1.

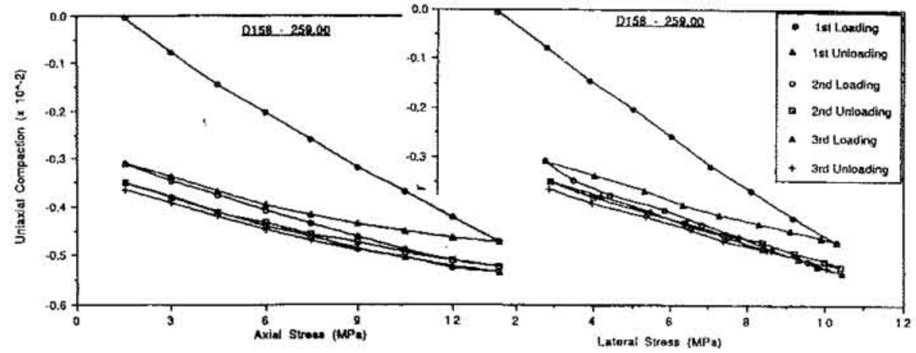

Figure 3. Typical axial and lateral stress-strain with three loading cycles

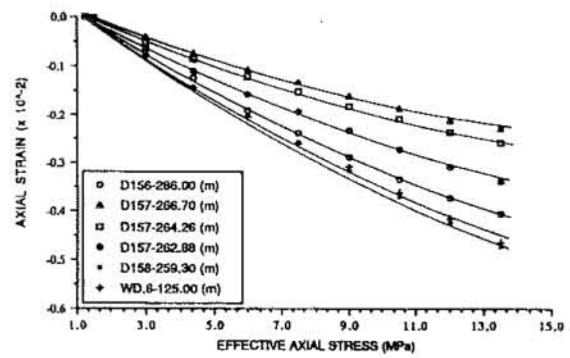

Figure 4. Axial strain and effective axial stress for first loading

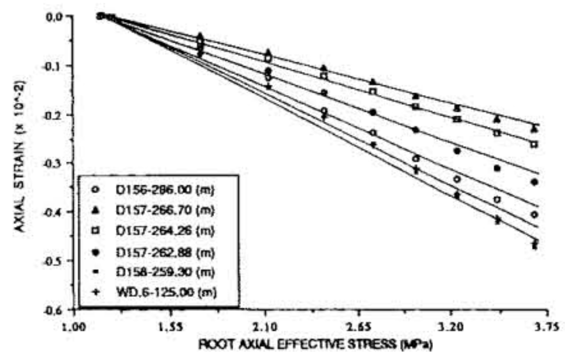

Figure 5. Relationship between axial strain and root of effective axial stress for first loading

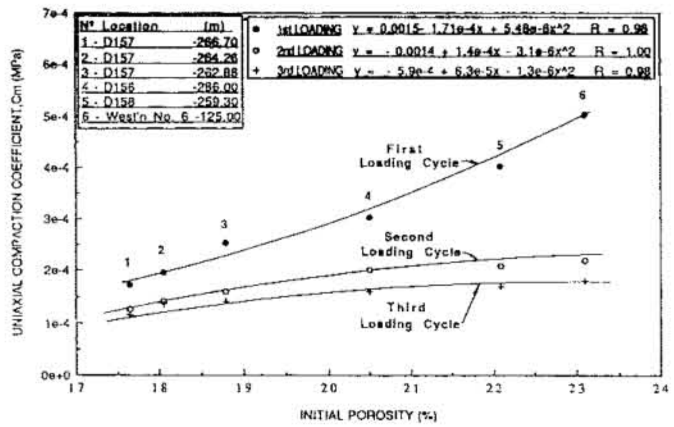

Figure 6. Relationship between uniaxial compaction coefficient and initial porosity for first, second and third loading

The values of n for the specimen tested range from 0.869 to 0.982. This range is higher than the value of 0.677 for spheres and indicates flatter contact surfaces.

Table 2. Sandstone properties

Sample Number	Location	Depth (m)	UCS (MPa)	Initial Porosity (%)	Permeability (10^{-8} m/s)
1	D156	286.00	3.351	20.50	36.22
2	D157	262.88	5.895	17.65	18.33
3	D157	264.26	5.201	18.05	20.62
4	D157	266.70	4.783	18.78	21.64
5	D158	259.30	3.481	22.09	34.07
6	Western 6	125.00	2.311	23.10	41.31

7. CONCLUSION

Special purpose-designed triaxial testing equipment has been designed, tested and commissioned. A series of uniaxial compaction tests were performed for laboratory determination of compressibilities and *in situ* behaviour of the Collie sandstone. The following conclusions are drawn.

Whilst recognizing the early stages of development of subsidence prediction, some deformation has been postulated based on laboratory observations. *In situ* monitoring of strata deformation will be required for verification of the actual deformation mechanisms at work. It has been observed that the uniaxial compression of Collie sandstone is characterised by significant non-linearity, hysteresis and an irrecoverable strain on unloading.

Uniaxial compaction curves have been presented for the sandstone aquifer in the Collie Basin. It was found that the uniaxial compaction curves were parabolic over the major part of the stress range. This yielded the expression :

$$\varepsilon_1 \; a \; \sqrt{s_1{}'} \tag{8}$$

A good correlation was found to exist between the uniaxial compaction coefficient and porosity. The correlation was quantified by regression analysis. Considering the different compaction behaviour of the specimens in the first and subsequent loading cycles, an average value for uniaxial compaction coefficient equal to 2.382 x 10^{-4} $(MPa)^{-1}$ was obtained for an average porosity of 20.77%.

REFERENCES

Batzle, M.L., Simmonds, G., and Siegfried, R.W. (1980). Microcrack Closures in Rocks Under Stress: Direct Observation. *Jnl Geophys*. Res. 85, pp 7072-7090.

Boit, M.A. (1941), General Theory of Three-dimensional Consolidated. *Jnl App. Phys* 12, 2, pp 155-162.

Brace, W.F., Paulding, B.W., and Scholz, C. (1966). Dilatancy in the Fracture of Crystalline Rocks, *J. Geophys*, Res. Vol. 71, No. 16, pp 3939-3958.

Brandt, H. (1955). A Study on the Speed of Sound in Porous Granular Media, *Jnl. App. Phys*. March, Vol. 22, p479.

Dundon, P.J., Humphreys, D., and Hebblewhite, B. (1988). Roof Depressurisation for Total Extraction Mining Trials, Collie Basin, Western Australia. *3rd International Mine Water Congress, Melbourne, Australia*, pp 743-752.

Geetsma, J. (1957), The Effect of Fluid Pressure Decline on Volumetric Changes of Porous Rock, Trans, *AIME, Vol.* 210, pp 331-430.

Geertsma, J. (1966). Problems of Rock Mechanics in Petroleum Production Engineering, proceedings, *First Congress of the International Society of Rock Mechanics*, Lisbon, Vol. 1, pp 584-594.

Geertsma, J. (1973). Land subsidence above compacting oil and gas reservoirs, Jnl *of Petroleum Technology*, Vol. 25, pp 734-744.

Grassman, F. (1951), "Uber die Elastizitat Poroser Medien", *Vierteljahrschrift der Naturforschenden Gesellschaft* in Zurich, 96, 1, Sec. 1-51.

Humphreys, D. and Hebblewhite, B.K. (1988). Introduction of Total Extraction Mining in Conjunction with Strata Dewatering at Collie, Western Australia. *The Coal Journal, Australian Journal of Coal Mining Technology and Research, No. 19*, pp 45-56.

Knutson, C.F. and Bohor, B.F. (1963). Reservoir Rock Behaviour under Moderate Confining Pressure, Rock Mechanics, Proceedings, *5th Rock Mechanics Symp*. University of Minnesota, Macmillan, New York.

Lowry, D.C. (1976). Tectronic History of the Collie Basin, Western Australia, Geol. Soc. *Australia Jnl,* Vol. 23, pp 95-104.

Martin J.C. and Serdengecti, S. (1984). Subsidence over oil and gas fields. In Holzer, T.L. (ed), Man-induced Land Subsidence, *Rev. Engng Geology VI*, The Geological Soc. of America, pp 23-34.

Mattax, C.C., McKinley, R.M. and Clothier, A.T. (1975). Core Analysis of Unconsolidated and Friable Sands, *Jnl of Pet.* Techn., p. 1423.

Mess, K.W. (1978). On the Interpretation of Core Compaction Behaviour. Surendra, K.S. (ed) Evaluation and Prediction of Subsidence, publ. by *American Society of Civil Engineers*, pp 76-91.

Nikraz, H.R. (1991). Laboratory Evaluation of the Geotechnical Design Characteristics of the Sandstone Aquifer in the Collie Basin, *PhD Thesis*, Curtin University of Technology, p. 317.

Poland, J.F.; G. Figueroa-Vega; L. Carbognin, A. I. Johnson & S. Yamamoto (1984). *Guidebook to studies of land subsidence due to ground-water withdrawal,* J.F. Poland Chairman and Editor, UNESCO, Paris, France, p. 305 and Appendixes.

Teeuw, D. (1971). Prediction of formation compaction from laboratory compressibility data. *SPE Journal*, 1193), pp 263-271.

Timoshenko, S and Goodier, J N (1951), *Theory of Elasticity*, McGraw-Hill Book Co Inc., New York

Ven Kesteren, J. (1973). Estimate of Compaction Data Representative of the Groningen Field, *Verhandelingen Mijnbouwkundig Genootschap*, Vol. 28, pp 33-42.

4 Remedies - Decision Making

COMPARISON AND ANALYSIS FOR THE EFFECTS OF CONSTRUCTION ENGINEERING AND WATER RESOURCES DEVELOPMENT ON SHANGHAI LAND SUBSIDENCE

Weihua Shi
Shanghai Institute of Geological Survey, Lingshi Rd. No.930, Shanghai, 200072, P.R. of China

Rongze Jiang
Shanghai Municipal Engineering Research Institute, Jianguo Rd. No.609, Shanghai, 200031, P.R. of China

Weimin Yie
Tongji University, Geotechnique Department, Siping Rd. No. 1239, Shanghai, 200092, P.R. of China

Abstract

According to the distribution of land subsidence in the past ten years and site measured data, different kinds of engineering construction have been summed up and analyzed. In addition, the ground water exploitation has been compared quantitatively in the aspect of causing land subsidence and the municipal engineering construction has played an important role in land subsidence.

Keywords: construction engineering, land subsidence, ground water resources, aquifer, compressive layer

1. INTRODUCTION OF SHANGHAI LAND SUBSIDENCE

Land subsidence in Shanghai is considered to be a kind of environmental geological disaster and has been regarded seriously by people since 1950. The land subsidence in Shanghai approximately experienced four stages: the first stage, from 1921 to 1965, the ground settled severely and the average settlement reached 39.1 mm per year; the second stage, from 1966 to 1971, the land subsidence was efficiently controlled and the ground rebounded 18.1 mm; the third stage, from 1972 to 1990, the ground settled slowly and the average settlement was 2.3 mm per year; the fourth stage, since 1991, the ground settlement has been accelerated evidently, and the average settlement in the center city area reached 12.6 mm per year from 1991 to 1998. According to the research on water level, exploited water amount, irrigated water amount, pore water pressure and measured data of layered settlement, it is known that the direct and main reasons causing land subsidence is exploitation of ground water. Ground water exploitation and irrigation are important factors producing ground settlement, and the depressions were distributed unequally because the ground water is exploited and irrigated unequally. Exploitation of deep ground water and continual engineering construction are the main reasons for acceleration the land subsidence in recent years.

2. SETTLEMENT PRODUCED BY ENGINEERING CONSTRUCTION

The influence of city construction on ground settlement can be summed up in the following ways:

2.1 The strip or rectangular loads on half-infinity elastomer surface

Stress caused by construction in soil decreased with the depth and distance away from the load imposed surface, the stress affected area in soil is about one to two times the width of the load foundation (Fig.1). According to the analysis of Shanghai multilayer structure building settlement, it related to the property of the soil within the scope of compressed layers. The larger the thickness of schlick, the greater the soil compresses. The abstract settlement of multilayer buildings is usually less than 30 mm and the settlement of ground surface is usually from several centimeters to tens of centimeters within the area of one time that of the building's foundation width.

There will be large settlement if the embankment height is over 2.5 m and the settlement is mostly larger than 40 cm in Shanghai. The shape of the embankment bottom is like a basin and the settlement is large in the middle and small at the edge (Fig. 2). The embankment also produced settlement in the nearby area, usually there will be several to tens of centimeters within a distance of 50 m from the center of the embankment. In freeway and arterial road engineering many of the embankments are higher than 5 m and the ground surface settlement is large along the embankment.

2.2 Excavation and unload engineering in half infinity elastomer surface

Research has indicated that the amount of soil deformation around the foundation pit produced by excavation is associated with many facts, like the dimension, excavation depth, timbering and time limit of the excavations, etc. The excavation depth of a foundation pit usually exceeds ten meters in Shanghai and the main settlements appear within a range three to four times the depth of the foundation pit. In timbered excavations the largest settlement can be controlled within 2 to 3 centimeters and there will be only several millimeters in the far distance.

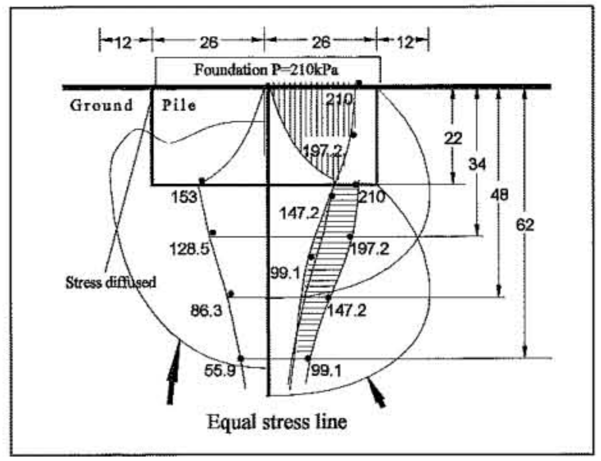

Figure 1. Vertical stress analysis of pile and natural ground under strip load

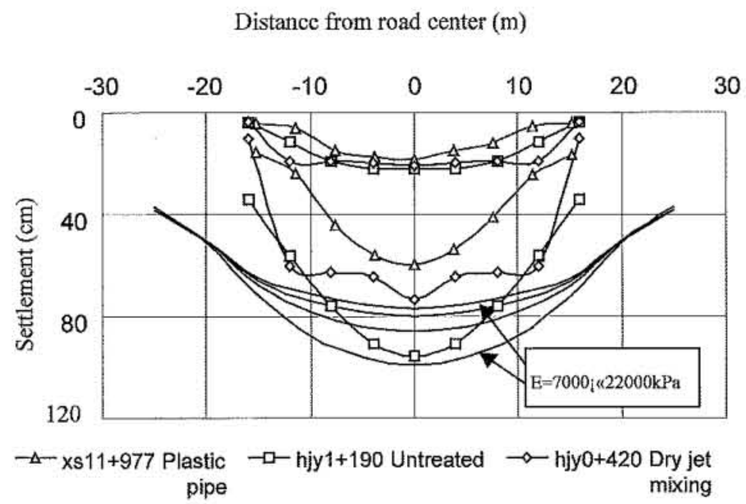

Figure 2. Transect settlement distribution under strip load and different soil treatment condition.

In open excavation or river dredging, the soil on a slope will deform in horizontal and vertical directions, and the vertical deformation rate is usually bigger than the horizontal. Research work illustrating that the slope soil first produces little elasticity deformation, usually zero to four centimeters, then it creeps slowly. This usually lasts 100 days, then the slope soil creeps more steadily and lasts longer. It is illustrated by means of surveying that excavations deeper than 13 m will produce 30 centimeters of the creep deformation and this certainly produces surface settlement in surrounding areas.

2.3 Pumping drainage engineering

Lowering of ground water level will make the soil produce compression deformation, which can affect the soil from 30 to 80 meters from the ground surface. According to experience of ground water lowering by pumping in Shanghai, the ground surface settles 2 to 3 centimeters when the water level drops to 3.5 m in the pump well. If using the ejector well point system and the tube water level descends 10 to 15 m, the ground surface settles 9 centimeters in a distance of 12 m away from the well point and the largest settlement can reach 13 cm. Thus, well point pumping method can cause large settlement.

2.4 Shield driving works and tunneling

In shield driving engineering the ground surface upheaves along the tunnel axis in front of the shield machine just the same distance as the depth of the shield. After the shield has passed, the ground surface gradually settles down. The settlement differs largely from each other according to different shield methods. For example, the crushing shield of completely closed chest can produce great upheaval when it is pushed, and it leaves large hollows on the ground surface which can be as deep as 1 m. If using an air pressure shield, or a partial extrusion shield, the settlement of ground surface can be controlled within 5 to 10 centimeters. The shield also produces ground deformation in a lateral way, which is like the shape of the soil wreck wedge. It can affect as deep as 60 to 75 m.

2.5 Cycle dynamic loads and impact loads produced ground surface settlements

Dynamic loads, such as sinking piles and dynamic compaction, etc, disturb soils in a definite range, raise pore water pressure to evanesce and make soil consolidate. Dynamic loads usually affect the sandy soils, make the sandy soil liquefy and cause the surface to sink. On the other hand, sinking piles or dynamic compaction usually make ground upheave.

The soil produced permanent deformation by cycle load action relates to the energy of the impact dynamic load and the weight of the cycle dynamic load. If the strain caused by stress wave is less than 10^{-5}, the soil is in a state of elasticity and no permanent deformation will be produced. If the strain is larger than 10^{-5}, the soil is in an elastic-plastic state, and after a definite number of loading actions the diaphysis curve secant modulus decreases and permanent deformation appears. According to the in situ data measured of a dynamic compaction works, the ground surface acceleration is 0.1g which is equivalent to 7 degrees of seismic intensity, and the ground can produce 2 centimeters settlement under this condition according to the Shanghai seismic zoning.

2.6 Rheologic phenomena under building structure loads

The mucky soil of shallow ground in Shanghai, the first and the second compression layer, has the property of high compression and rheology. Compared with other clayey and sandy soils, it needs longer time to consolidate and produce larger secondary consolidation settlement under additional stress. The amount of rheology is related to the stress condition in soil. The larger the vertical stress and the difference between the vertical and horizontal stress, the larger the rheology. According to the analysis of the high embankment settlement data measured in the last ten years for the Hujia freeway in Shanghai, secondary settlements represent ten percent of the total ground settlement.

3. COMPARISON WITH CONSTRUCTION AND GROUNDWATER EXPLOITATION PRODUCED SETTLEMENTS

In the following paragraphs, in situ observed settlement data of recent years in land subsidence and construction in Shanghai are compared as obtained by means of land subsidence monitoring pole and telescoping tube settlement gauges.

Since the 1980s, ground water exploitation planning has been regulated and the fourth aquifer was the greatest exploited in the city area of Shanghai (Table 1), and the compression deformation under 150 meters was greatly increased in relation to the ground surface settlement. From the relationship of soil deformation distribution along with depth under high embankments in municipal road constructions, it can be found that most of the soil deformation takes place in the ground 20 meters under the surface (Table 2, Fig. 3).

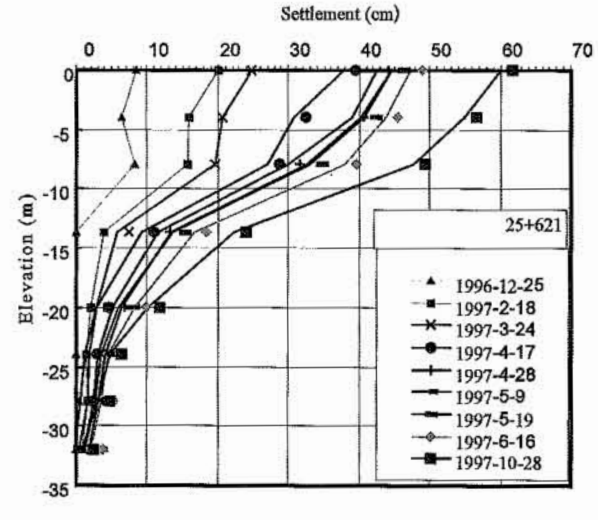

Figure 3. Curve of settlement in layers under high embankment.

Progressive land subsidence in Shanghai is mainly due to exploiting ground water. The ground water level depressions due to the exploitation of ground water relate correspondingly to the land settlement depressions. Before 1968 exploitation of ground water was restricted to the shallow parts of the second and the third aquifers. Because the hydraulic relationship exists between the shallow aquifers and the first, the second, and the third compression layers are normally consolidated, the lowering of ground water level increases the additional stress in soil and produces large compression deformations. Thus, the land subsidence has been serious before 1960 in Shanghai. After the adjustment of the exploitation plan, ground water of the fourth and the fifth deep aquifers, was mainly exploited instead of the shallow aquifers. Although the amount of exploited ground water increased greatly, the settlement of the ground did not increase much. This is because the same fall of ground water level will cause smaller compression deformation in deep soil, but larger compression deformation in shallow soil.

Table 1. Relationship between deformation in different layers of soil and amount of land subsidence

Depth (m)	layers	1981-1985 Sum. (mm)	1981-1985 Average (mm)	1981-1985 Percent (%)	1986-1990 Sum. (mm)	1986-1990 Average (mm)	1986-1990 Pércent (%)	1991-1998 Sum. (mm)	1991-1998 Average (mm)	1991-1998 Percent (%)
Surface		15.85	3.17		23.95	4.79		95.92	11.99	
0-25	1,2 CL	7.06		44	7.81	1.56	33	12.14	1.52	13
25-75	1A,3CL	3.56	0.71	23	6.46	1.29	27	26.67	3.34	28
75-150	2,3A	1.71	0.34	11	1.41	0.28	6	10.22	1.27	10.6
150-300	4A,	3.51	0.71	22	8.27	1.66	34	46.89	5.86	48.4

Note: CL: express compression layer A: express aquifer

Table 2. Comparison with deformation under different soil treatment condition

		Soil treatment methods					
		Untreated(sand drain, plastic drainage pipe)		Dry jet mixing pile		Waste steel dreg pile	
		CD (mm)	Percent (%)	CD (mm)	Percent (%)	CD (mm)	Percent (%)
Total settle.(mm)		103.1		97.1		99.1	
Depth sections	0? 5m	41	40	9.7	10	24.1	24
	5? 10m	30.8	30	16.8	17	35.7	36
	10? 15m	18.5	18	37	38	17.9	18
	15? 20m	8.1	7	18.4	19	10.7	11
	>20m	4.7	**5**	**15.2**	**16**	**10.7**	**11**

Note: CD: express compression deformation.

Municipal constructions are the main reasons for changes in the shallow soil stress conditions. According to Shanghai construction and geologic properties, the first and second compression layers have much of a rheologic property. The rheology can only happen when the stress balance is destroyed and municipal constructions can produce rheologic deformations. From the amount of the settlement, we can see that construction-produced settlement is large and the measured settlement observed by layer settlement pole is less, but data measured from the pole in the construction affected area is larger. Following the development of Shanghai municipal construction, the shallow soil deformation plays an important role in land subsidence. In the crowded building construction area, where all buildings have shallow foundations, the total ground surface settlement is large, and the post settlement within two or three years after their construction can reach 10 to 20 centimeters. The several recent years of research work illustrated that settlement caused by engineering construction results in 30 percent of the total ground surface settlement.

To reduce the effect of engineering construction on land subsidence, the following control measures must be taken. First, avoid lowering of the ground water level; second, reduce the disturbance of construction to ground soil; third, make the most of using deep foundations to convey the building load to the deeper part of soil; fourth, avoid constructing buildings too close to one another to reduce their joint effects.

4. CONCLUSION

Construction-produced settlements have had a large part in the land subsidence in Shanghai in the last decades. Compared with the land subsidence caused by ground water exploitation, the construction mainly affects the first and the second shallow compressible layers, which are the softest of the Shanghai ground soil with low strength and large rheologic properties. So, construction-produced ground surface settlements play a more and more important role in the total land subsidence environment and should bring about more attention by the government officials.

Acknowledgements

Thanks to those who have given their support and advice for this paper.

REFERENCES

Exploration Research Report on Land Subsidence in Shanghai (1962-1976), Shanghai Geological Bureau, 1979.2.

Liuyi, Xianlin Z., Guifu W., Qingde H. (1998) The situation of land subsidence and countermeasures in Shanghai for recent years, *The Chinese Journal of Geological Hazard and Control*, Vol. 9, 13-17.

Rongze J. (1998) Classification of soft ground under embankment in Shanghai and analysis on settlement property, *Shanghai Highway* (supplement), 33-42.

LAND SUBSIDENCE - Vol. I
Proceedings of the Sixth International Symposium on Land Subsidence
Ravenna / Italy / 24-29 September 2000

A SEMI-EMPIRICAL METHOD FOR THE PREDICTION OF SUBSIDENCE IN MULTI-SEAM COAL MINES

P.P. Bahuguna
Assistant Professor, Department of Mining Engineering,
Indian School of Mines, Dhanbad (India)

Abstract

Subsidence Prediction in coal mines with single seam extraction has been widely investigated in the different parts of the world. In case of multi-seam coal mines there is not enough field database from case histories to develop a reliable empirical method for the prediction of subsidence. The present paper describes a method developed on the basis of additional data generated by numerical modelling of subsidence for a variety of situations in multi-seam coal mines. The present studies involve the analysis of the influence of various subsidences contributing factors. The qualitative data so generated have been incorporated to supplement the available field data, which led to the development of a semi-empirical method for the prediction of subsidence in multi-seam coal mines.

Keywords: mine subsidence, numerical modelling, multi-seam coal mines

1. INTRODUCTION

A number of methods depending on local considerations have been developed in different parts of the world for the prediction of subsidence in single seam coal mines. It was possible because a good number of case histories were available from field for single seam coal mines to build up a good database. Subsidence prediction in multi-seam coal mines is a more complex problem because more factors influence the mechanism of subsidence in such situations. Unfortunately there is not enough data base available from case histories from multi-seam coal mines.

It is possible to calibrate a numerical model of mine subsidence with the help of available field data and then to generate additional data from the model for a variety of situations. In the present studies the qualitative data generated from numerical modelling have been used to supplement the available field data for the development of a semi-empirical method of subsidence prediction in multi-seam coal mines in India.

2. PARAMETRIC STUDIES

The present work is the extension of a semi-empirical method developed by the author (Bahuguna, 1998) for the prediction of subsidence in single seam coal mines. The numerical modelling was carried out by using Displacement Discontinuity Method (Sinha, 1979) which is a sub-variation of Boundary Element Method. The overburden rockmass was treated as a homogenous, transversely anisotropic and elastic medium. The material properties of overburden rockmass as well as that of the coal seam were obtained from back analysis so as to produce the known displacements from the case histories for such situations. The model was 'calibrated' with the help of the available field data. The results were then obtained from the model by varying the various subsidence contributing factors.

The various subsidence contributing parameters identified and analysed earlier (Bahuguna et. al, 1993) for single seam coal mines are : -

1. Dimensions of the panel - Length , width and depth of the panel and thickness of the seam,
2. Extraction percentage,
3. Composition and condition of overburden rockmass,
4. Method of goaf treatment,
5. Dip of the seam, and
6. Time after the extraction of coal.

Besides the above parameters, the following factors also contribute to subsidence in multi-seam coal mines (Bahuguna, 1997) :-

1. Number of seams extracted and thickness of each seam,
2. Depth and parting between the seams,
3. Extraction ratio in each seam,
4. Dimensions of extraction in each seam,
5. Relative positions of different seams , and
6. Physico-mechanical properties of each seam and the overburden .

2.1 Parametric studies for single seam workings

1. The maximum possible subsidence, S_{max} does not exceed 0.95 times the seam thickness for the cases of caving as goaf support and 0.1 times for hydraulic sand stowing in Indian coalfields. Therefore the effect of goaf support, g_f may be taken as 0.95 and 0.1 respectively for such cases.

2. The effect of partial extraction, e_f in board-and-pillar mine working is to reduce the magnitude of subsidence. A factor for partial extraction may be taken as equal to $(ER)^k$ where ER is the extraction ratio and k is a constant which may be taken as equal to 1 for ordinary coal seam and 2 for hard coal seams.

3. Subsidence is less for inclined coal seam than the horizontal ones. A factor of $cos\ \alpha$ may be taken as effect of dip where α is the angle of dip.

4. The magnitude of subsidence is also influenced by the composition and condition of overburden rockmass. The presence of hard rock layers in the overburden causes reduction in the subsidence and the discontinuities and disturbances in those layers have an opposite effect. A factor for the effect of overburden rock mass, R_f can be estimated from Table - 1 and the plots given in Figure 1.

Table 1. Classification of Overburden rockmass

Rockmass Classification	G/E_v	Description
Competent	0.07 - 0.38	Massive rockmass with few planes weakness
Undisturbed	0.03 - 0.07	No previous mining but few natural discontinuities
Partially disturbed rockmass	0.016 - 0.03	Parting between the mined seams more than 5 times the seam thickness or cases with no previous mining but many natural discontinuities
Disturbed rockmass	0.0005- 0.016	Parting between the mined seams not more than 5 times the seam thickness and many discontinuities
Highly disturbed rockmass	< 0.005	Highly fragmented rockmass with repetitive workings or having very thick seams mined in descending slicing

5. Subsidence increases with the increase in width-by-depth (w/d) ratio or length-by-depth (l/d) ratio till critical dimensions are reached. The effect of this factor is given by the following equation.

$$w' = [\ 1 - e^{-n(w/d)}\ ]^2 \tag{1}$$

$$l' = [\ 1 - e^{-n\ (l/d)}\ ]^2 \tag{2}$$

Where w' and l' are the effects of w/d ratio and l/d ratio respectively. The value of constant n varies from 2.5 to 3.5 for different areas but may be taken equal to 3 as an average.

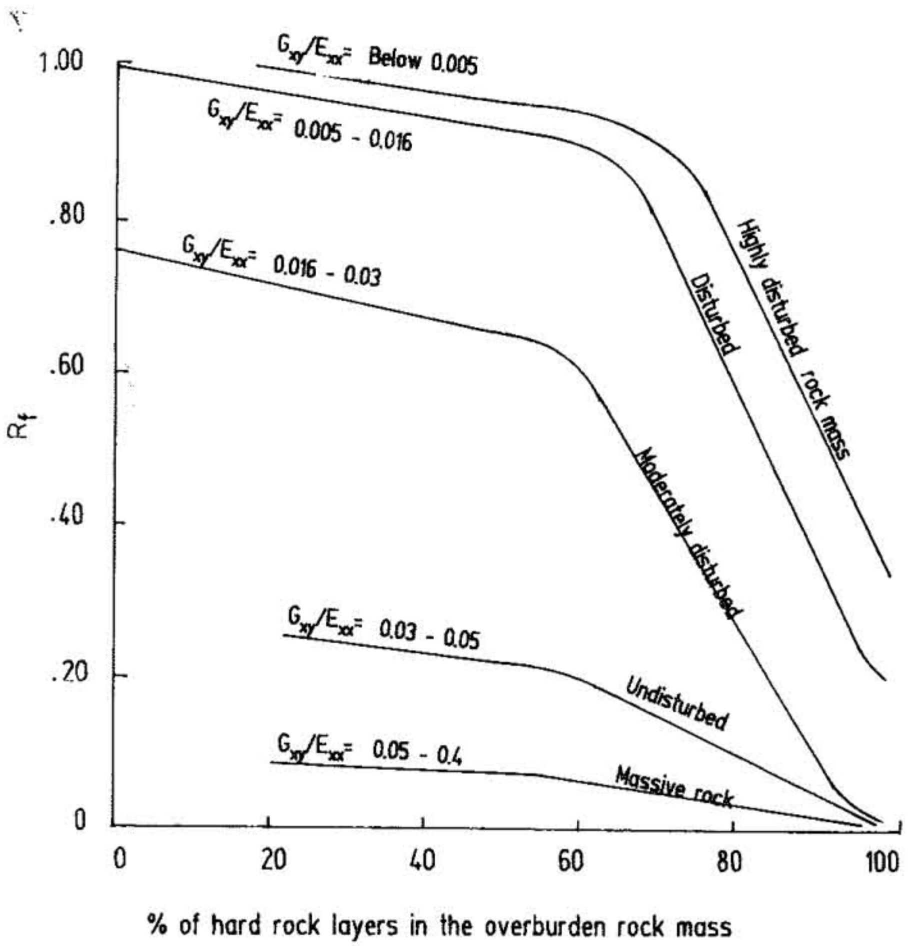

Figure 1. Value of factor Rf for different composition and condition of rockmass

6. The maximum possible subsidence S_{max}, therefore is given by the following equation :

$$S_{max} = m.\ g_f\ .\ e_f\ .\ R_f.t\ .\ \cos \propto \quad (3)$$

Where,

m = Seam thickness,
g_f = Goaf treatment factor,
e_f = Extraction factor,
R_f = Rock factor,
$\propto$ = Angle of dip of the seam, and
t = time factor which is equal to 1 for finished subsidence.

7. The maximum subsidence, S_o in a panel of sub-critical dimension is given by the following equation.

$$S_o = S_{max}.\ w'.\ l' \quad (4)$$

8. Subsidence S_i at any point i at a distance of x_i from a point under going maximum subsidence S_o, (at or near the centre of the panel) is given by following equations :-

For sub-critical area,

$$S_i = S_o\left[e^{-M\left(\frac{x_i}{2r+x_i}\right)^2}\right] \quad (5)$$

or, for critical area,

$$S_i = S_{max}\left[e^{-M\left(\frac{x_i}{2r+x_i}\right)^2}\right] \quad (6)$$

Where, M is a proportionality constant and r is the radius of critical extraction area. The value of M can be obtained from Figure 2.

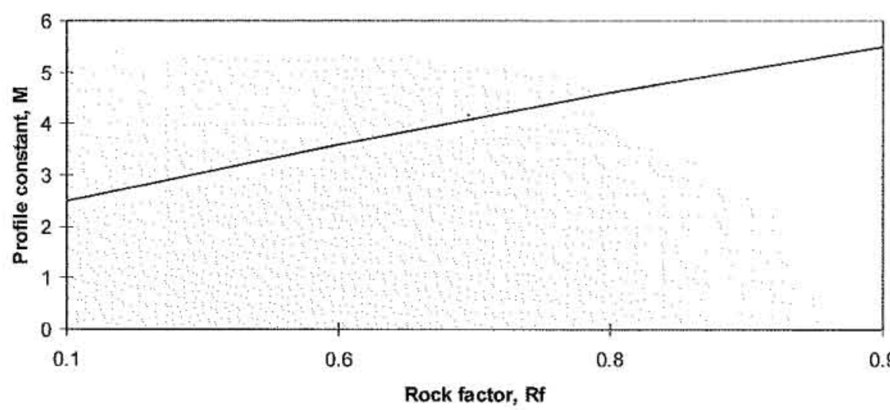

Figure 2. Relationship between Roch Factor Rf and Profile constant M

2.2 Parametric studies for multi-seam workings

1. The maximum subsidence is directly proportional to the thickness of the seams, but as the number of worked seams increase the overburden rock mass gets more and more disturbed increasing the proportionality constant also.

2. As the depth and parting between the seams increases the magnitude of subsidence decreases (Fig. 3).

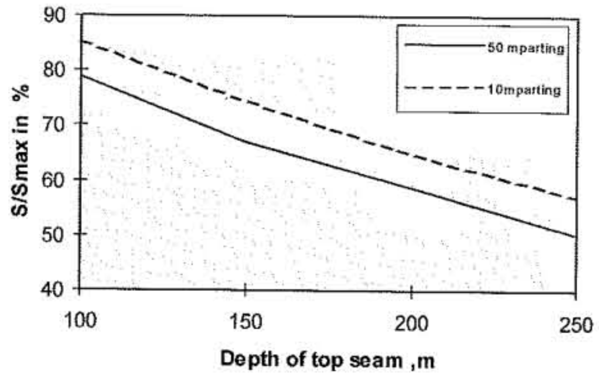

Figure 3. Relationship of subsidence with depth and parting of seams

3. The magnitude of subsidence also depends on the relative positions of workings in different seams. The profiles of subsidence due to each seam may first be plotted individually with the help of eqs. (5) or (6) and then the combined effect can be obtained by adding the individual values at different points and multiplying the result with a factor N for number of seams (Fig. 4).

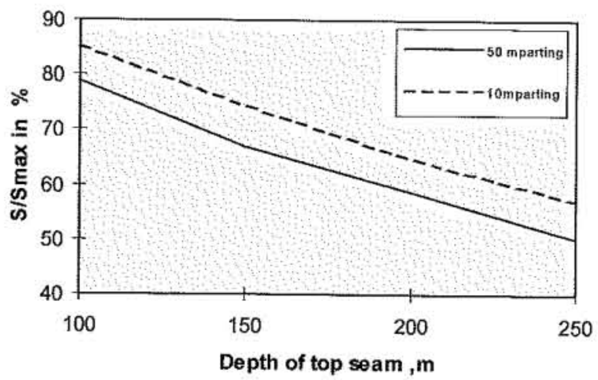

Figure 4. Relationship of width/depth ratio to Proportionality constant N

Therefore, the subsidence due to all seams can be obtained as given below :-

$$S = N \,.\, (S_1 + S_2 + S_3 + \ldots) \qquad (7)$$

3. CONCLUSIONS

The objective of these studies was to obtain a relationship between the subsidence occurring due to the extraction of single seam and the combined effect of such working or worked individual seams at different depths. Based on the subsidence obtained for each seam the combined effect of all seams has been obtained by establishing an empirical relationship for a given coal mine area.

REFERENCES

Bahuguna, P.P., (1998) A Semi- empirical method for the prediction of mine subsidence and associated parameters in Indian coalmines, *J. Rock Mechanics and Tunnelling Technology,* Vol.4, No.1, pp. 43 - 69.

Bahuguna, P.P., (1997) Subsidence studies by numerical modelling in multi-seam coalmines, *Proc. X Intl. Cong. Intl Soc. for Mine Surveying,* Nov. 2-6 ,1997, Fremantle, W. Australia, pp. 679-684.

Bahuguna, P.P., Singh, B., Srivastava A.M.C. and Saxena N. C., (1993), Semi empirical method for the calculation of maximum subsidence in coal mines, *Geol. & Geotech. l Engineering,* Vol. ii, pp. 249-*261*.

Sinha, K.P., (1979) Displacement discontinuity technique for analysing stresses and displacements due to mining in seam deposits, *Ph. D. thesis, Univ. of Minnesota,* 311p.

INTERVENTIONS TO SAFEGUARD THE ENVIRONMENT OF THE VENICE LAGOON (ITALY) AGAINST THE EFFECTS OF LAND ELEVATION LOSS

Laura Carbognin
Istituto per lo Studio della Dinamica delle Grandi Masse – CNR, San Polo 1364, 30125 Venezia, Italy

Giovanni Cecconi and Viviana Ardone
Consorzio Venezia Nuova, San Marco 2803, 30124 Venezia, Italy

Abstract

The first part of the paper presents an analysis of the environmental problems of Venice in relation to the overall 23 cm loss in land elevation occurred with respect to mean sea level since the turn of the century.

The physical structure of the city is characterised by the presence of historic buildings – some of which were constructed more than five centuries ago – in contact with the water and with ground levels only some ten centimetres above normal high tide level.

The loss in elevation has brought about an increase in flooding events, as well as triggering erosion and other hydraulic processes, which have accelerated the structural deterioration of the city, which now requires ever more frequent restorative interventions. The disappearance of the wetlands and the narrowing of the shores, respectively, have left the lagoon basin and the coastal strip more vulnerable, aggravating the destructive action of sea storms along the littoral.

The second part of the paper describes the safeguard measures already implemented or currently under way, such as the creation and/or the nourishment of beaches, the restoration of sand dunes, the reconstruction and protection of the wetlands, the local defence works in the historic city and other lagoon centres, as well as a major project involving temporary closure of the three inlets to guard against exceptional floodings in the lagoon.

These interventions are also particularly well suited to protect the city and lagoon of Venice in future against the effects of a possible sea level rise due to subsidence and eustacy.

Keywords: subsidence, eustacy, flooding, flood barriers.

1. INTRODUCTION

The situation in Venice has been the subject of studies for decades, and is known all over the world not so much for the magnitude of subsidence recorded here, but for the unique nature of the city and the lagoon and for the significance of the drop in elevation for the conservation and indeed the very survival of Venice, in as much as Venice lives in the water.

Extending for a surface area of approximately 550 km² the lagoon of Venice is around 50 km long and ranges between 8 and 14 km in width (Fig. 1). The conservation of this coastal area has always been rendered more complex by the low ground surface height above mean sea level of the historic city and the other landmasses emerging from the lagoon.

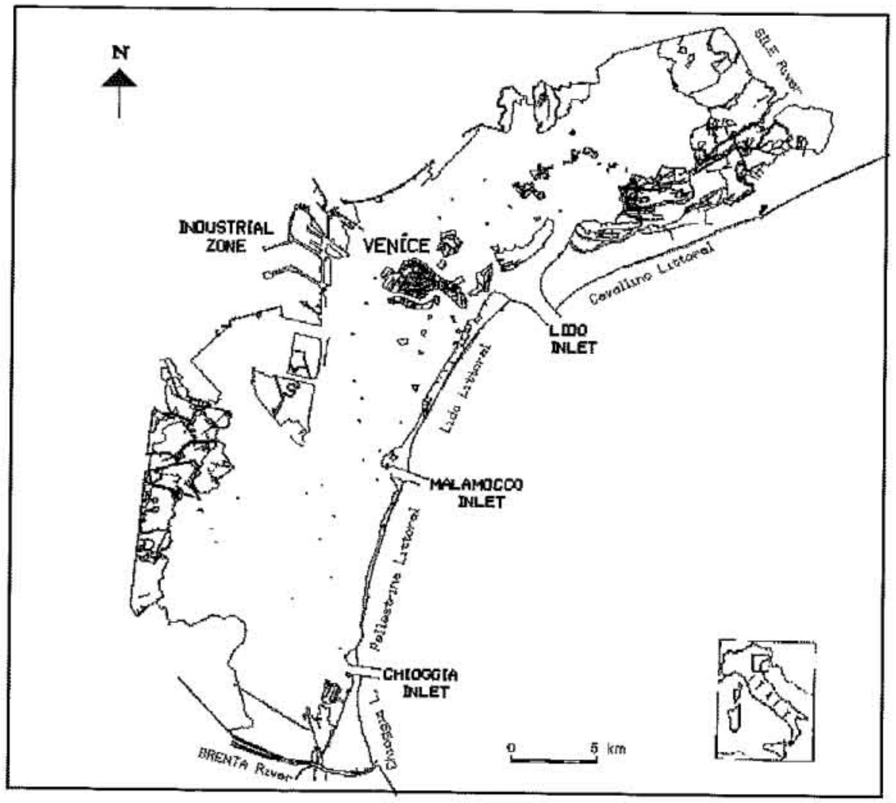

Figure 1. The lagoon of Venice.

Particularly significant is the 23 cm relative loss in land elevation, which has taken place over the last 100 years. In other words, the level of the sea has risen by 23 cm with respect to the ground level. Three factors have contributed to this relative loss (Gatto P. & Carbognin L., 1981) which today remains substantially unchanged: geological subsidence, anthropogenic subsidence and sea level rise due to eustacy.

The relative loss in land elevation has altered the relationship between land and water, contributing to:

- an intensification of the *acqua alta* phenomenon (a local idiom meaning flooding), both in the frequency and degree;
- an increase in wave action and lagoon currents across the main channels, leading to erosion of the lagoon floor, the silting up of channels and changes in the habitat of flora and fauna on the bed of the lagoon;
- greater fragility of the littoral - which provide a tenuous bulwark defending the entire lagoon against the destructive attacks of the sea - and a higher risk of flooding from overtopping.

This paper presents the information available on subsidence and eustacy, and on the safeguard measures currently implemented throughout the lagoon territory by the Venice Water Authority (Magistrato alle Acque di Venezia, (MAV) through Consorzio Venezia Nuova (CVN).

2. ANALYSIS OF THE DATA

2.1 Subsidence and eustacy

Geological subsidence, anthropogenic subsidence and eustacy, the three factors noted earlier as responsible for the 23 cm drop in relative elevation (referred to mean sea level) can be described briefly as follows:

- Geological subsidence, differentiated in time and space, has taken place in the area of Venice over a period of millennia (since the birth of the lagoon). For a number of reasons, the average rate of 1.3 mm/y corresponding to the natural period of evolution, fell over recent centuries reaching the current figures of approximately 0.4 mm/y in the area of the lagoon which includes the city of Venice, and its closest hinterland (0-0.5mm/y) (Gatto P. & Carbognin L., 1981; Bortolami et al., 1985; Carbognin et al., 1995b). On the contrary a certain sinking at the furthermost northern and southern boundary areas and along stretches of the coastline is still in progress due to greater compaction of recent deposits in these areas which are part of the delta formations of the Bacchiglione-Brenta Rivers to the south and of the Sile-Piave rivers to the north (Carbognin et al., 1995a; 1995b).
- Anthropogenic subsidence is the result of progressive and intensive depletion of the six artesian aquifers which succeed each other to a depth of approximately 320 m. Groundwater exploitation, which began in the 1930s with the first industrial installations, grew with post-war industrial development to reach a peak (together with the subsidence it caused) between 1950-1970. Following drastic measures to curtail artesian consumption, the ensuing subsidence slowed down, coming to a stop in 1973 (Carbognin L. et al., 1976; 1981).

Of particular significance is the regional survey carried out in 1993 along identical lines to previous survey carried out in 1973, confirming the arrest of subsidence, as a widespread phenomenon resulting from intensive groundwater withdrawals. The survey also confirmed the stability of both the zones in mainland, Venice and its surroundings. The subsidence rates (1-2 mm/y) recorded along the coastline and at the furthermost northern and southern boundaries can be attributed to different local situations and to the more active consolidation process in progress in these areas, as above mentioned.

- Eustacy is widely known to be the result of variations in the mass and volume of oceans due to the effect of climatic changes. In historic times, global climatic fluctuations have been noted over long periods (on a scale of centuries) which have obviously also affected the Adriatic Sea and the lagoon of Venice. The evolutionary period of the coastal strip of the Northern Adriatic was characterised by a very warm phase during the Middle Ages ("Medieval Climatic Optimum") followed by a relatively cold phase ("Little Ice Age") ending in the mid-1800s, during which the sea level rise was estimated at 0.3-0.5 mm/y. Alternating cold-wet and hot-dry cycles lasting for decades (from around 15 to 30 years: Brükner's cycles) have been noted since 1700 among the large scale climatic sequences of significance at a regional level. In fact, episodes of higher rainfall, violent sea-storms and the advance of alpine glaciers are linked to the cold-wet cycles whereas periods of positive sea and weather condition are noted during the hot-dry phases (Brükner E., 1890; Veggiani A., 1987).

The most reliable estimate of the rise in sea level in the Upper Adriatic Sea over the last 100 years is provided by a study performed on a century-long historic series of tide-gauge measurements recorded between 1896-1993 at Venice and Trieste (Carbognin L., & Taroni G., 1996). From an analysis of the entire period, and excluding subsidence, a constant and linear growth rate for eustacy was calculated at 1.3 mm/y. The extent of the historic series used in the study was sufficient to average the internal short period climatic variation. However, it should be noted that the most severe flooding events of the last 50 years were recorded during a cold-wet climatic cycle in the 1960s. A reduction in the number of flooding events was noted during the next hot-dry cycle, which began in the 1970s. The 1990s brought a new cold-wet cycle and a return to more frequent sea storms along the entire littoral of the Northern Adriatic and an increase in the frequency of flooding in Venice. Finally, it should be borne in mind that although the rising rate for sea level of 1.3 mm/y may be considered representative for the entire century, tide-gauges in Venice and Trieste showed the phenomenon of eustacy to be in steadiness between 1970 and 1993.

Thus the figure of 23 cm, calculated in 1981 as corresponding to the overall relative loss in ground surface height, is confirmed to be valid still today.

In any case, both the land elevation (regional and in the lagoon) and the level of the Adriatic Sea are the subject of continuous and increasingly accurate monitoring.

2.2. The present situation

Conditions similar to those, which may be expected as a result of climatic change over the next 100 years, are already being experienced throughout the territory of the lagoon of Venice. The 23 cm relative sea level rise has brought about a more than seven-fold increase in the frequency of flooding events (Fig. 2) to the great inconvenience of the population and with enormous damage to the urban heritage. Populated areas are submerged today, which at the turn of the century were unaffected by flooding in the city (Fig. 3).

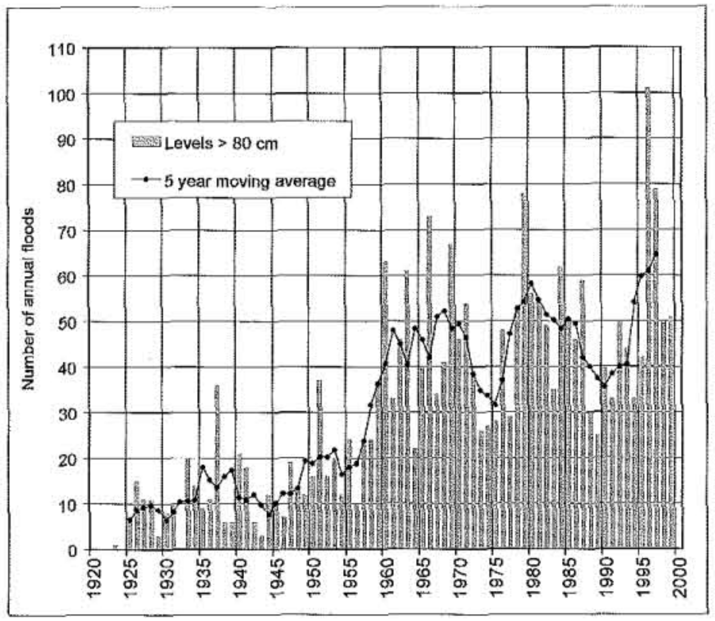

Figure 2. The increase in the number of high water events (in excess of 80 cm) since the turn of the century.

In 1966, exceptional high tide conditions arose contemporaneously with a sea storm; the severe storm surge of 4th November flooded the city with over a metre of water for a whole day; the entire coastline was affected and the historic *murazzi*[1], constructed in the 17^{th} century to protect the populated areas which lay behind them, were overtopped by the sea and collapsed in a number places causing extreme damage. Today, the 1966 event, which in 1800 had a probability of occurring once every 1000 years, has a return period of approximately 150 years.

[1] Murazzi : sea wall, 5.5 m above sea level at the summit and protected at the base by rock armour, resting on the lagoon bed at a depth of approximately three metres.

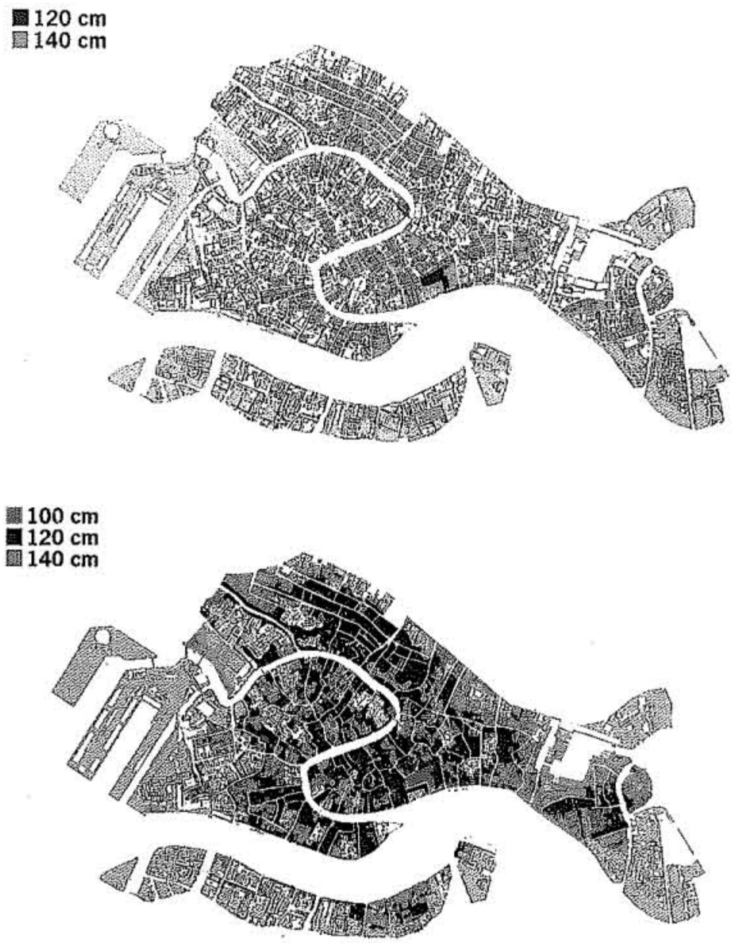

Figure 3. Flooding in Venice. The situation at the turn of the century and today.

2.3. Future scenarios

Reasonable forecasts of possible sea level rise during the next century must be provided in order to assess the efficiency of safeguard measures in the lagoon of Venice.

It is well known that the international scientific community is not in agreement over the conclusions concerning future tendencies linked to climatic change. The understandable uncertainties surrounding climatic models lead scientists to propose scenarios, which predict trends rather than univocal estimates forecasting the rise in sea level. The numerous theories to be put forward include estimates of an average rise in sea level of between 10 and 20 centimetres over the next century (Mörner, 1995) and, conversely, a far more pessimistic view of future climatic variations and the ensuing rise in

average sea level on a global scale (Alley et al., 1998). Among the authoritative contributions on the subject, we refer to a study carried out in 1995 by the Intergovernmental Panel on Climatic Change (IPCC). The Panel's report, IPCC-SAR'95 (which is currently undergoing revision to incorporate new and updated hypotheses on climate) presents numerous scenarios of rising sea levels over the next 100 years. From a very wide range with a lower limit of 13 cm and an upper limit of 94 cm, the most probable mean values in 2100 will be comprised between 27 a 49 cm. The estimate of 49 cm corresponds to a scenario of increased emissions of greenhouse gases, IS92a ("business as usual", in other words), and was obtained using the model officially adopted in SAR'95. However, elsewhere in SAR'95 – in Chapter 7 of Volume II (IPCC, 1995) – the figure of 27 cm is reported to be the best estimate since it was obtained using a more evolved model which takes into account phenomena of retroaction.

With due consideration for the uncertainties regarding prospective scenarios, and having assessed the history of the region, three scenarios of rising sea levels over the next century at Venice were seen reasonably to provide the indications essential to the planning of defence works in the city and the lagoon (Fig. 4):

Scenario A (optimistic): taking into account the fact, noted above, that no significant trend towards rising sea levels has been recorded between 1970 and 1993, it can be assumed that in future the only factor to cause a "rise" in sea level will be natural subsidence at a rate of 4 cm/century. Under this scenario, in 2100 approximately 70 *acqua alta* events over 80 cm could be expected each year.

Scenario B (realistic): taking into account the fact that, on average, sea level in the Adriatic has risen by 11 cm over the last century, it can be assumed that this trend will continue throughout the next century in addition to subsidence as described in scenario A (4 cm/century + 11 cm/century = 15 cm/century). Under this scenario, in 2100 approximately 180 flooding events over 80 cm could be expected each year.

Scenario C (pessimistic): taking into account the possibility of a further rise in sea level due to climatic variations resulting from increased greenhouse gas emissions into the atmosphere, but considering also that the estimates given in IPCC - SAR '95 are somewhat uncertain and may vary according to the model used, two median scenarios were examined. In the first case (scenario C1), a 27 cm rise in sea level in addition to subsidence rates of 4 cm/century, will result in an overall rise in sea level 240% greater than in the past; in the second case, (scenario C2), a 49 cm rise in sea level in addition to subsidence rates of 4 cm/century, will result in a rise in sea level 430% greater than in the past.

Even considering the less severe Scenario C1, in 2100 as many as 400 events of *acqua alta* over 80 cm could be expected each year.

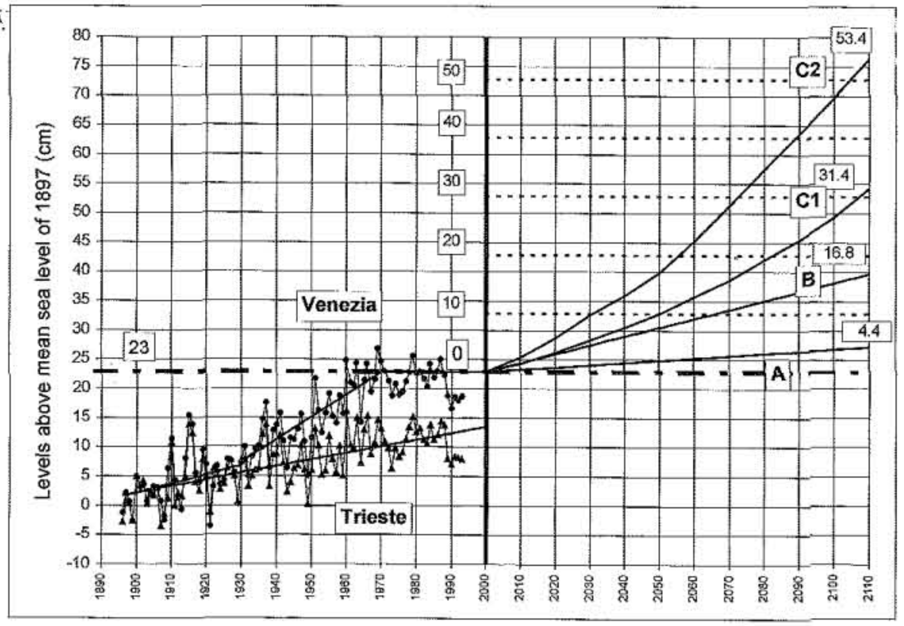

Figure 4. Scenarios of rising sea levels in Venice, compared with levels recorded over the last century in Venice and Trieste (the lines indicating historic trends are drawn from Carbognin and Taroni, 1996).

3. SAFEGUARD INTERVENTIONS IN THE VENICE LAGOON

After the disastrous event of 4 November 1966, which brought home the precariousness of the entire lagoon basin, the need became all the more urgent for safeguard interventions in the lagoon and in the unique and precious city of Venice (Cecconi et al., 1999).

These interventions, regulated by four Special Laws (1973, 1984, 1991, 1992), were shown to be indispensable, even excluding the hypothesis of a rise in sea level due to the effect of climatic changes; however, if a sea level rise were to occur during the course of the next century without having completed safeguard interventions, the damage to the territory and to the historic patrimony would far exceed those experienced to date, because of the exponential increase in the frequency of flooding and the related damage.

The State, through the Venice Water Authority and Consorzio Venezia Nuova, has already elaborated a unitary plan of intervention, and numerous projects have already been completed (MAV-CVN, 1992a). The safeguard works foreseen in the plan of interventions summarised in Tab. 1, cover the entire range of problems relating to Venice, and include measures which, to some extent, go beyond the scope of this paper.

Table 1. General plan of interventions with current status of implementation (updated at 30.06.1999).

INTERVENTIONS	NOTES
REINFORCEMENT OF BREAKWATERS	Reinforcement work has been carried out on the 6 breakwaters at the inlets, for a total of 10 km.
SHORELINE DEFENCE WORKS	The fortification of 39.5 km of the coastal strip provides a safeguard against flooding for events with a return period of 300 years.
LOCAL FLOODING DEFENCE WORKS Smaller populated centres (960 ha) Historic town centres (23 ha) Waterfront reconstruction (53 km)	Passive defence works against more frequent flooding, to a level of 100 cm in the historic town centre of Venice and 150 cm in the minor populated centres of the lagoon.
ENVIRONMENTAL INTERVENTIONS	
Recovery of the lagoon morphology Channel re-profiling and maintenance (9 million m^3; 59 km) Construction and reinforcement of *wetlands* (390 ha) Raising of lagoon floor (to contrast erosion from wave action; 630,000 m^3) Phanerogam plantations (6 modules) Arrest of erosion on 7 smaller islands Reinforcement of the lagoon embankments (8 km)	The *wetlands* consist of *mudflats* and *salt marshes*: the mudflats are areas in the shallows which emerge under certain tide conditions; the salt marshes are the areas situated at an elevation comprised within the tidal excursion range (between 0 and +60 cm). The planned interventions are aimed at withstanding the tendency towards erosion, triggering at the same time mechanisms of retroaction, which would determine an improvement in the quality of the water and the environment.
Improvement of the environment Clearing of four dumps Embankments – industrial channels (7 km) Dredging – industrial channels (92,000 m^3) Raising of lagoon floor (capping; 90,000 m^3) Construction of an area for phyto-purification	
EXCLUSION OF OIL-TANKER TRAFFIC Working design (completed)-	Reduction of the risk of serious accidents in the lagoon, using alternative methods for the supply of oil products.
OPENING OF THE FISH FARMS Working design completed Pilot project – 1 fish farm opened under varying conditions	Assessment of the environmental effects of reopening the fish farms along the mainland shore of the lagoon. Three more fish farms are expected to be opened.
INTERNAL NAVIGATIONAL AIDS Illuminated route along the Oil-Tanker Channel (12 km)	Navigational aids have been installed, allowing the safe transit of shipping at night and in fog conditions.
MOVABLE BARRIERS AT THE THREE INLETS Propaedeutic study; REA design; Preliminary design; Environmental Impact Study	The preliminary design and the Environmental Impact Study have been completed, as have the in-depth studies requested by the Inter-ministerial Committee before its decision on the authorisation of the final design.

3.1. Protection of the littoral

The Venetian littoral is a narrow strip of land separating the lagoon from the sea and defending the former against the destructive action of the latter. It extends for a total length of approximately 50 km, broken by three inlets. These openings, which allow the exchange of water between the sea and the lagoon, divide the Venetian coastline into four sections: Chioggia (with the Sottomarina and Isola Verde beaches), Pellestrina, Lido and Cavallino (see Fig. 1). Prior to the interventions, some sections of the shoreline were only a few metres wide. Elsewhere, as in the case of Pellestrina, the beach did not exist at all, having been replaced by the *murazzi* sea walls. The conservation of the whole of the lagoon basin is clearly linked to the physical integrity of the shorelines, which have been deeply compromised by subsidence and other man-made interventions leading to a reduction in littoral sand feeding. Thus the coastal strip has been the subject of intensive restorative measures. Mathematical and physical models were used to determine the choice of defence interventions, assessing the effects of the works on longshore sediment transport, on the propagation of wave action, and on water circulation.

Works began in 1994 with the defence measures at the Cavallino, Pellestrina, Sottomarina and Isola Verde shorelines and will be completed within the next year (MAV-CVN, 1992b).

The solution adopted, which consists of replenishing the shorelines, will protect the entire Venetian coastline against exceptional events such as that which took place in November 1966, without the risk of inundation caused by the collapse of embankments or sea walls: the qualities of resilience inherent in this kind of shoreline reconstruction can counter the effects of possible climatic change. The ample safety reserves available with this method to face the variability of meteo-marine events are much higher than those afforded by solutions involving rock armour defence works.

The most radical intervention was implemented at Pellestrina where the defence system extended for the entire stretch of coast[2]: a new beach was created, approximately 30 m wide and protected by transversal breakwaters connected by an underwater barrier ("cell" system) (Fig. 5a and 5b). The beach was constructed with sand dredged from an area at sea, around 20 km off the Malamocco inlet and approximately 20 m deep.

[2] The populated centres along the coast are now protected against events combining wave action and high waters with a return period of approximately 300 years, e.g. offshore wave action with a significant wave height of 5.3 m combined with a 1.5 m above mean sea level flooding event.

a)

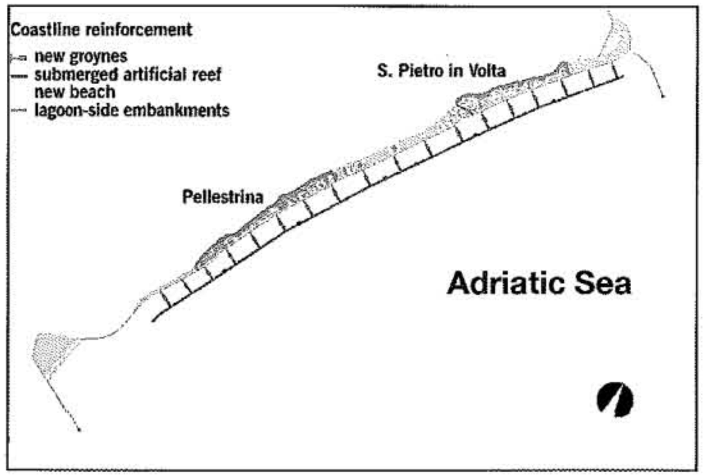

b)

Figure 5. a) Plan of intervention along the Pellestrina shoreline; b) The Pellestrina shoreline before and after the works.

3.2. Morphological and environmental recovery

The interventions for the safeguard of the lagoon territory consist mainly in re-employing dredged sediment for the reconstruction of wetlands (see table 1) in the lagoon. The surface area of these wetlands in the lagoon today has been more than halved with respect to 1900 as a result of erosion caused by wave action and a high rate of subsidence, uncompensated by sediment transported by rivers and the sea.

A large proportion of morphological deterioration will be eliminated over the next 10 years[3], with the reconstruction of salt marshes in the lagoon and the protection of the lagoon floor and natural salt marsh perimeters from wave action.

Besides the reconstruction of mud flats and salt marshes, other safeguard interventions in the lagoon territory are aimed at contrasting erosion of the lagoon floor. Plans are currently being elaborated for interventions to raise shallows subject to erosion using sand dredged at sea, in an effort to stabilise the bed of the lagoon, improving habitability and reducing wave action along the perimeters of the bordering salt marshes.

3.3. Local defence works and the barriers at the lagoon inlets

A system integrating local defence works in the town centres and movable barriers at the lagoon inlets for temporary closure of the lagoon during storm surges has been elaborated as a safeguard against flooding.

Local defence works involve "raising" the lower urban areas permanently and compatibly with the architectural conditions and habitability: some degree of movable ground elevation can thus be obtained with local defence, optimising the operation of the barriers at the inlets. These works include raising waterfronts, foundations and more generally, the paving in those areas most seriously effected by flooding. Indeed the intervention typology presents different characteristics according to the area concerned: the urban centres along the littoral are protected against tides even over 150 cm, whereas the architectural value of the structures in the historic centres within the lagoon allow a rise in elevation only of up to 100 cm in Venice and 120 cm in Chioggia.

The movable barrier project (MAV-CVN, 1992c; 1997) is the final and crucial element of a "grand design" which aims to maintain water levels acceptable for the lagoon ecosystem and to avoid the deterioration of the town patrimony as a result of overly frequent exceptional flooding events.

[3] The salt marshes are a valuable element of the lagoon territory which help contain eroded and transported sediment within the lagoon, which would otherwise be deposited in the channels or lost at sea.

The solution adopted envisages the temporary closure of all three inlets in the event of flooding over 100 cm, by means of a movable formation of oscillating buoyant flap gates, housed (when not in use) in purpose-built recesses on the bed of the lagoon (Fig. 6). The gates are 20 m wide, but vary in height and thickness according to the depth of the inlet channel. The barriers have been designed to withstand a 2m difference between seaward and lagoon water levels when in operation.

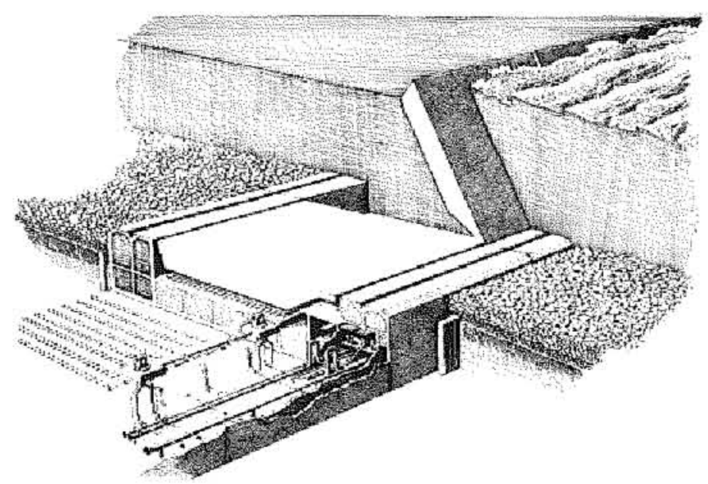

Figure 6. Vertical section of a gate formation showing the gate operation systems in the foreground, and a non-operational gate (filled with water and lying in the its housing) and an operational gate (filled with air) in the background.

Combining the barriers and the local defence works it will be possible to isolate the lagoon temporarily from the sea[4], avoiding both the direct and immediate damage resulting from *acqua alta* (the inconvenience of the population and the induced socio-economic costs) and the indirect damage arising from the need for more frequent maintenance of urban heritage. In fact, the exceptional flooding episodes give rise to a number of clear risk factors, such as the direct attack of wave action against the masonry facades of the buildings leading to the danger of collapse due to the horizontal pressure of the water, or the increased capillary action of salt water along the masonry with the ensuing crystallisation of salt and disintegration of the mortar and masonry (Cecconi G., 1997).

[4] Under current sea level conditions, 12 barrier closures would be expected each year for a duration of approximately 3 hours each.

4. CONCLUDING REMARKS

Over the last century, the relative sea level in Venice has risen by 23 cm due to the effects of subsidence and eustacy. This apparently modest figure has become of crucial importance to Venice, with its singular relationship with the water within a complex lagoon basin. In fact, the increasing frequency of flooding can be ascribed to this 23 cm loss of elevation, as can the onset of processes of erosion within the lagoon and the greater precariousness of the coastal strip. Furthermore, one can say that the Lagoon is already experiencing (at least in part) the effects of the predicted deterioration in climatic conditions, associated with the risk of a global rise in sea level.

On one hand, important steps are being taken to monitor sea levels for any abnormal rise over the next decade, including continuous and increasingly accurate high-precision surveys of bench marks along the coast, the installation of permanent GPS stations and the study and comparison of tide-gauge measurements in the lagoon with those recorded at other stations around the Mediterranean Sea.

On the other hand, the Venice Water Authority has designed interventions to protect the entire lagoon environment, taking into account the occurred and the forecastable relative land elevation loss and the high variability of meteorological-marine events so as to attenuate and contrast the combined effects of these processes. Solutions such as replenishment of the coastline and the reconstruction of stretches of beaches, sand dunes and salt marshes (which are able to adapt to withstand extreme conditions with limited damage) have been incorporated in the design of these interventions.

Under present sea level conditions the conservation of the historic and architectural heritage of Venice is already deeply compromised by the acqua alta phenomenon: the final approval and construction of the movable barriers at the inlets for the regulation of flooding events, would not only eliminate the socio-economic damage caused by acqua alta, but would also allow the preservation of the historic buildings in Venice.

REFERENCES

Alley R.B. et al. (1998) Comment in "Forum about AGU", EOS, Transactions, American Geophysical Union, 79, 15, 188.

Bortolami G., Carbognin L., & Gatto P. (1985). The natural subsidence in the lagoon of Venice, Italy, in *"Land subsidence"* (Proc. 3rd Int. Symp. on Land subsidence, Venice, 1984) Publ. IAHS 151, 777-785.

Brückner E (1890). Klimaschwqnkungen seit 1700 nebest Bemerkungen uber die Klimaschwankungen der Diluvialzeit, *Geographisce abbandlungen*, B IV, H2, Wien, 153-184.

Carbognin L., Gatto P., Mozzi G., Gambolati G., & Ricceri G. (1976). New trend in the subsidence of Venice, in *"Land Subsidence"* Pubbl. IAHS N° 121, Proc 2nd Int. Symp. On Land Subsidence, Anaheim, Ca., USA, 65-81.

Carbognin L., Gatto P., Mozzi G. (1981). La riduzione altimetrica del territorio veneziano e le sue cause. *Rapporti e Studi*, VIII, Ist. Veneto SS.LL..AA, 55-83.

Carbognin L., Marabini F., & Tosi L. (1995a). Land Subsidence and Degradation of the Venice Littoral Zone (Italy), in *"Land Subsidence"* Publ. IAHS 234, Proc. 5th Int. Symp. on Land Subsidence, the Hague, The Netherlands, 391-402.

Carbognin L., Teatini P., & Tosi L. (1995b). Analysis of actual land subsidence in Venice and its hinterland (Italy), *Land Subsidence*, Barends, Brouwer & Schröder (eds.), 129-138.

Carbognin L., & Taroni G. (1996). Eustatismo a Venezia e Trieste nell'ultimo secolo. *Atti dell'Istituto Veneto di Scienze Lettere ed Arti*, Tomo CLIV - Classe di Sc. Fis. Mat. e Nat., pg. 281-298.

Cecconi G. (1997). Venezia e il problema delle acque alte. Il rischio di danno al patrimonio urbano a causa della crescita relativa del livello del mare. Consorzio Venezia Nuova, *Quaderni Trimestrali N. 2-97 (Aprile –Giugno 1997)*, Venezia.

Cecconi G., & Ardone V. (1999). La protezione dell'ambiente lagunare e costiero veneziano. *Atti della XVII Giornata sull'Ambiente* "Venezia: città a rischio", Accademia Nazionale dei Lincei (in stampa).

Gatto P., & Carbognin L. (1981) The lagoon of Venice – Natural environmental trend and man-induced modification. *Hydrological Sciences Bulletin*, 26/4/12, 379-391.

IPCC, Climate Change (1995). The Science of Climate Change, Summary for policymakers and technical summary of the working group I report. *Cambridge University Press*, New York.

MAV - CVN (1992a). Progetto di massima degli interventi per il recupero morfologico della laguna.

MAV - CVN (1992b). Progetto di massima dei litorali veneti.

MAV - CVN (1992c). Progetto di Massima degli interventi alle bocche lagunari per la regolazione dei flussi di marea.

MAV - CVN (1997). Studio di Impatto Ambientale (SIA) del progetto di massima delle opere mobili alle bocche di porto.

Veggiani A. (1987). Le fluttuazioni del clima dal XVIII al XX secolo. I cicli di Brückner, *Torricelliana*, 37, Faenza, 107-155.

PREVENTIVE MEASURES FOR SHANGHAI LAND SUBSIDENCE AND THEIR EFFECTS (CHINA)

Liu, Yi
Shanghai Institute of Geological Survey, 930, Lingshi RD, Shanghai (200072), P. R. of China

Abstract

Shanghai has become a model city to prevent and control land subsidence in China. The history of Shanghai land subsidence can be divided into two different periods, namely a rapidly sinking period from 1921 to 1965 and slowly sinking one from 1966 to 1995. Since the 1920's Shanghai, affected by land subsidence, has suffered tidal inundating, rainstorm waterlogging, block of navigation under bridge, damage of infrastructure and change of morphology. Based on these, the following eight preventive measures have been adopted since 1956: construction of a flood-control wall, setting up drainage stations, decreasing the pumping of groundwater, artificially recharging groundwater, adjusting pumping of aquifers, making annual planning of pumping and recharging of groundwater, monitoring and carrying out research in land subsidence, and working out the laws to prevent land subsidence. Nowadays, not only the tidal inundation has been stopped but also the amount of the ground being waterlogged during rainstorms has been greatly reduced and the amount of subsidence has been controlled efficiently. From 1966 to 1995, the sinking magnitude in the downtown area was only 116 mm, and it only accounted for 6.6% of the sinking magnitude between 1921 and 1965, reaching an ideal effect with a minimum subsiding amount to exchange maximum pumping volume of groundwater resources.

Keywords: land subsidence, preventive measures, effect, Shanghai.

1. INTRODUCTION

Land subsidence in the plain has occurred in more than 45 cities or locals (Duan Yonghou, 1998), of which Shanghai is the earliest one in China. Early in 1921, land subsidence was discovered in the Shanghai downtown area by leveling. Since the 1920's, the area of Shanghai affected by this problem has suffered tidal inundating, rainstorm waterlogging, block of navigation under bridges, damage of infrastructure and change of morphology et al. Since 1956, Shanghai has adopted a series of preventive measures such as construction of a flood-control wall, setting up drainage stations and systems, decreasing the pumping of groundwater, artificially recharging groundwater, adjusting pumping of aquifers, monitoring and carrying out research in land subsidence, making annual planning of pumping and recharging of groundwater and working out the laws to prevent land subsidence. These measures not only efficiently controlled Shanghai land subsidence between 1966 and 1995 but also made its damage decreased to a minimum degree. At the same time, groundwater resources were fully utilized. Shanghai has become a model city to prevent and control land subsidence in the plain and obtained precious experience for other cities or locals in China.

2. AN OUTLINE OF SHANGHAI LAND SUBSIDENCE HISTORY

From 1921 to 1995, the total average sinking magnitude in Shanghai downtown area was 1807 mm, and its corresponding rate was 24 mm/a. According to its rates over years, Shanghai land subsidence history can be divided into two different periods, namely a rapidly sinking period from 1921 to 1965 and a slowly sinking period from 1966 to 1995(the land subsidence was controlled). During the first period, the total average sinking amount in the downtown area was 1691 mm and its rate was 38 mm/a. During the second period, it was only 116 mm and its rate was 4 mm/a. The precedent can be further divided into apparently sinking stage (1921 to 1948), fast sinking stage (1949 to 1956), severely sinking stage (1957 to 1961) and mitigatively sinking stage (1962 to 1965). The latter can be further divided into slightly rebounding stage (1966 to 1971), slightly sinking stage (1972 to 1989) and growing sinking stage (1990 to 1995)(Liu Yi et al, 1998).

3. DAMAGES FROM LAND SUBSIDENCE

3.1. Tidal inundating

Eight tidal inundation, in which six were during the rapidly sinking period and other two were during the slowly sinking period, have taken place in Shanghai. But the tidal inundating on July 25, 1949 is the most serious one of them. Although this tide was lower than the previous three tides, the most part of the downtown area was inundated with a water depth of 0.2 to 2.0m in this time so that 11,768 rooms of house buildings were damaged.

3.2. Rainstorm waterlogging

During a rainstorm, the low-lying land caused by subsiding is usually waterlogged. After 1949,every rainstorm during storm surge waterlogged severely on roads in the downtown area. But since the 1980's, a general rainstorm has also waterlogged the roads. For example, between 1981 and 1994, all 22 rainstorms that happened in the downtown area waterlogged on the ground.

3.3. Block of navigation under bridge

Suzhou creek is one of the important water transport routes. When the tide is more than 4 m, then the net space under bridge is not close enough to 2.5 m and the navigation under bridge will be blocked.

3.4 Other damages

Land subsidence is responsible for other damages such as wharves along the river being lowered, buildings and well pipes rising above the ground level, bench marks losing stability, river bed sinking and morphology being changed (sunken low-lying land formatting).

3.5. Economic loss of land subsidence

Economic loss due to Shanghai land subsidence includes the cost of constructing a flood-control wall along the Huangpu and Suzhou rivers, navigation loss on Suzhou creek, the loss of port and wharf sinking and other loss (Wang Yong and Zhuo Hua, 1993).

4. PREVENTIVE MEASURES FOR LAND SUBSIDENCE

Since 1956, a series of preventive measures have been adopted to stop land subsidence in Shanghai. They are generalized as the following eight aspects.

4.1. Construction of a flood-control wall

There was no flood-control wall before 1956. A flood-control wall was constructed along the Huangpu and Suzhou rivers in Shanghai downtown area starting in 1956. Up to the end of 1998, the wall had been elevated and consolidated four times, and its gross length was 208 km.

4.2. Setting up drainage stations

Since 1956, municipal drainage stations have been set up in Shanghai downtown area. Up to the end of 1996, 161 drainage stations had been set up and their gross drainage ability reached $969 m^3/s$ in their reserved area of $230 km^2$.

4.3. Decreasing the pumping of underground water

This measure to control the pumping volume of underground water in the downtown area decreased the use from 110 million m^3 in 1963 to about 11-12 million m^3 between 1964 and 1995. As a result the ground water level has increased to control land subsidence.

4.4. Artificially recharging water into the ground

Starting in the winter of 1965, a measure was used to recharge water during winter and pump it during summer and then to recharge during summer and pump it during winter. From 1965 to 1995, the gross recharging volume of groundwater was 598 million m^3 (annually about 20 million m^3).

4.5. Adjusting pumping of aquifers

Because the specific unit deformation value (a value that a certain soil layer with a unit thickness is deformed by changing of a unit head of groundwater) of deep soil layers is greater than that of shallow soil layers, pumping groundwater from the 4th and 5th aquifers with an equal volume can produce a lesser land sinking amount instead of pumping it from the 2nd and 3rd aquifers to control land subsidence. The pumping volume from the 4th and 5th aquifers accounted for 73.2% between 1980 and 1995(it accounted for only 28.7% in 1965).

4.6. Developing annual planning of pumping and recharging of groundwater

Starting in 1966, annual planning has been maintained to the present. Based on evaluating the operated results of the last planning and making the next years goal to control land subsidence, this annual planning is determined by repeated running of a groundwater flow mathematical model incorporated with land subsidence to find an optimal planning of pumping and recharging of groundwater. This planning is put into effect after the municipal government ratifies it.

4.7. Monitoring and carrying out research in land subsidence

By leveling, Shanghai land subsidence was discovered in 1921 and became serious between 1952 and 1960. Since 1965, the Grade I and Grade II leveling have been carried out respectively at the end of winter recharging and at the end of summer pumping in the downtown and suburban areas. Groundwater fluctuations, including pumping volume, level and its quality, have been monitored since 1965. About 17 groups of extensometers were set up to monitor the deformations of various soil layers from 1962 to 1995. A series of results on Shanghai land subsidence investigation and research were obtained between 1962 and 1995.

4.8. Working out the laws to prevent land subsidence

In June 1963, "Shanghai Deep Well Regulation" was issued by the local government to control land subsidence.

5. PREVENTIVE EFFECTS FOR SHANGHAI LAND SUBSIDENCE

5.1. The flood-control wall has played a great role in preventing the tidal inundating in the downtown area.

Firstly, conventional tides have not inundated the area since 1956. Secondly, no inundation caused by storm surge tide has taken place in the area since the 1980's. For example, the record tide of 5.72 m caused by storm surge didn't inundate in the area on Aug. 18,1997.

5.2. The drainage stations alleviated the degree of rainstorm waterlogging in the downtown area

Theoretically, the existing stations can drain water off up to 300 mm per day. A rainstorm over 300 mm happened only one time, on Aug 9, 1985, from 1981 to 1994, but the volume of rainstorm that could cause waterlogging was usually less than 300 mm and even less than 100 mm. Considering unblockage of surface drainage, distribution of drainage stations and degree of rainstorm concentration, it is evident that the existing drainage stations can not eliminate the waterlogging problem in the low-lying area caused by land subsidence. But they can greatly mitigate the disastrous degree in depth, limitation and time of waterlogging.

5.3. Effect of decreasing pumping was striking in the initial stage of controlling land subsidence

Between 1963 and 1968, when groundwater levels rose rapidly with decreasing pumping, the annual land sinking amount decreased sequentially and the land even rebounded. But after 1970, the groundwater levels didn't continue to rise and land appeared to sink slightly at a rate of less than 5mm/yr.

5.4. Effect of artificially recharging groundwater was outstanding and of long-term to curb land subsidence

Main recharging aquifers were the 2nd and 3rd ones in the beginning year of 1966. This recharging volume of only 3.37 million m^3 made groundwater levels rise largely and land rebound with a rate of 6.3 mm/yr. After 1967, the annual recharging volume increased yearly, and groundwater levels sustainably rose from –10m to about –1.5m between 1970 and 1995. Land sank 0 to 5 mm annually. After 1990, because pumping volume increased largely in the suburbs and suburban counties but recharging volume didn't, groundwater levels developed a lowering trend and increasingly sank as a result.

5.5. Adjusting pumping aquifers had a good effect in curbing land subsidence relatively

The 4th and 5th aquifers gradually became the main pumping ones after 1972. The pumping in the two aquifers was estimated to have decreased land subsidence of about 5 mm/yr between 1969 and 1990.

5.6. Monitoring and carrying out research in land subsidence is a scientific basis of preventing it

Land subsidence would not have been discovered without leveling. If no improved monitoring network of land subsidence had been set up and monitored for a long-term, there wouldn't have been some further research on Shanghai land subsidence and its scientific countermeasures wouldn't have been developed. So the monitoring and studying is a scientific basis of preventing it.

5.7. It was learned that a control management in groundwater utilization and land subsidence has reached an ideal effect that is with minimum subsiding amount in exchange for maximum pumping amount of groundwater resources.

The reason for average sinking amount to 1.69 m in the rapidly sinking period was without an united planning and management in groundwater pumping. An annual planning of groundwater pumping and recharging was made every year from 1966. Apparently, this annual planning has played a key role to make Shanghai land subsidence only 116 mm in the slowly sinking period. At the same time, the gross pumping volume of groundwater in 1994 reached 154 million m^3 which accounted for 75.9% of the maximum annual pumping volume between 1921 and 1965.

5.8. Legal measures ensured the preventive measures made in effect extensively

The "Shanghai Temporal Regulation of Wharf Management and Flood-control Wall along Suzhou Creek" was issued in 1963. Shanghai Regulation of Constructing Management of Flood-control Wall Consolidation Engineering" was issued in 1989. The "Shanghai Regulation of Flood-control Wall Protection along HuaÝngpu River" was issued in 1996. These laws ensured construction of the Shanghai flood-control wall system, which basically resulted in no tidal inundation occurring in the downtown area since 1980's.

The "Shanghai Regulation of Deep Well Management" issued in 1963 promoted decreasing of groundwater pumping and in effect makes artificial recharge of groundwater and spread of annual planning of pumping and recharging.

6. CONCLUSION

The average land sinking was only 116 mm(about 4 mm/yr) in Shanghai downtown area between 1966 and 1995, indicating that Shanghai has greatly controlled land subsidence. At the same time, groundwater resources have fully been utilized in Shanghai. Tidal inundating has been efficiently eliminated since 1980's. The degree of rainstorm waterlogging on ground has been alleviated. But the navigation being blocked has not been solved efficiently, and the low-lying area caused by land subsidence will develop at a little degree in future.

REFERENCES

Duan Yonghou (1998) Research status on land subsidence development in the 21st century of China, *Chinese Journal of Geological Hazard and Control,* No. 2, Vol. 9, 5.

Liu Yi et al. (1998) The situation of land subsidence and countermeasures in Shanghai for recent years, *Chinese Journal of Geological Hazard and Control,* No. 2, Vol. 9, 5.

Wang Yong and Zhuo Hua (1993) An assessment of economic loss of Shanghai land subsidence, *Journal of Natural Disasters (in Chinese),* No. 1, Vol. 2, 1.

LAND SUBSIDENCE - Vol. I
Proceedings of the Sixth International Symposium on Land Subsidence
Ravenna / Italy / 24-29 September 2000

MANAGEMENT OF THE ENVIRONMENTAL RESOURCES OF THE KANTO GROUNDWATER BASIN IN JAPAN -LAND SUBSIDENCE AND MONITORING SYSTEM-

Kunio Furuno, Atsushi Kagawa and Takashi Kusuda
Research Institute of Environmental Geology, Chiba (RIEGC)
3-5-1, Inagekaigan, Miham-ku Chiba, 261-0005 Japan

Hisashi Nirei
Center for Water Environmental Study, Ibaraki University
1375, Itako, Ibaraki 331-24,Japan

Abstract

Kanto plain is called Kanto groundwater basin. Groundwater level and land subsidence are monitored by about 500 monitoring wells and almost 5000 bench marks respectively. The groundwater level fell to its lowest in the early 1970s. Then regulations were strictly adhered to in the southern Kanto in the 1970s. Consequently, the recovery of the groundwater level was recognized according to the control of the pumping. Groundwater resources can be used meanwhile the health condition of the groundwater basin is examined by periodical health checks. Monitoring system is important for the sustainable use of groundwater.

Keywords: land subsidence, Kanto groundwater basin, levellings, monitoring well.

1. INTRODUCTION

The Kanto plain is situated at the junction between one of Japan's island arcs and Izu-Ogasawara island arc. The Kanto plain is also called "the Kanto fore-arc submarine basin" or "the Kanto paleo-submarine basin", based on surrounding geological and physiographical features such as Nasu Volcanic Zone, Fuji Volcanic Zone, Japan trench and Izu-Ogasawara trench (Nirei et al., 1990)

Over 38 million people live on the Kanto plain, which includes the Tokyo metropolis. The waterfront area around Tokyo Bay mostly includes both alluvium and reclaimed areas and is densely covered with houses and factories. Sediments of the Kanto basin are 2,500-3,000 m thick and are of Miocene to Holocene age. The basin is also called the Kanto groundwater basin from the standpoint of the production of groundwater, natural gas and iodine. Uncontrolled use of land and resources has caused many environmental problems, such as land subsidence, floods caused by urbanization, slope failure, geo-pollution (sedimentary strata pollution, groundwater pollution and air pollution), waste disposal, liquefaction, earthquake disasters and so on.

To ensure effective use of environmental resources without causing environmental problems, a monitoring system for their management and land use has been developed. The system includes about 500 self-recording observation wells, almost 5,000 bench marks (leveled every year), a seismic observatory array, and so on. These monitoring networks are one of the largest in the world. Especially the system to monitor the behaviors of land subsidence and groundwater is one of the most important of environmental management systems in the Kanto basin.

Over-pumping of the groundwater resulted in a serious land subsidence problem in various areas, especially in alluvial plains so that it was inevitable to control the groundwater use to solve the problem (Aihara et al., 1969). Consequently, systematic observations of pumping up volumes, groundwater level changes and land subsidence records for the effective groundwater use have been carried out for preventing the land subsidence from a geological point of view (Research Committee for Land subsidence Prevention in Southern Kanto District, 1974).

Observations have succeeded in preventing land subsidence so far in various areas, especially in the Kanto groundwater basin, which is the largest groundwater basin where the longest records of the observations in Japan exist (Inaba, 1969).

2. KANTO GROUNDWATER BASIN AND UNDERGROUND FLUID RESOURCES

The Kanto paleo-submarine basin has been intensively studied for surface geology including tephrochronology, subsurface geology with deep drilling, magnetostratigraphy, foraminiferal and pollen analyses and fission track dating. The basement rocks of the basin distribute at 3,000-2,500 m below the surface. The basement outcrops on the surface at areas surrounding the basin, i.e. the Kanto and Tsukuba mountains.

The Kanto paleo-submarine basin can be called the Kanto groundwater basin from the standpoint of the distribution and the fluidity of the underground fluid resources (Nirei and Furuno, 1986). The bottom of the groundwater basin corresponds to the base of Kanto tectonic basin, which is situated at 3,000-2,500 m below the surface. The sediments of the Kazusa subgroundwater basin contains brine groundwater including natural gas and iodine (Fig. 1). The equivalent layer of the of the Kazusa Group that extended to the western and northern part of the Kanto plain is composed of alternating beds of coarse- to fine-grained deposits suitable for groundwater.

The lower part of the Shimosa subgroundwater basin contains groundwater colored with humid material from the northern to the central part of the Boso peninsula, and the colored groundwater is unsuitable for drinking. In the upper part of the Shimosa subgroundwater basin, most of the aquifers contain freshwater; this basin had the largest pumpage volume of water in the Kanto groundwater basin. However, the more the pumping up volume is increased, the lower the groundwater level becomes in the Shimosa upper subgroundwater basin. The lowering of the groundwater level in the alluvial deposits has also induced a sinking in ground surface. It is now widely confirmed that the amount of ground subsidence is affected by the thickness of alluvial deposits (Nirei et al., 1979).

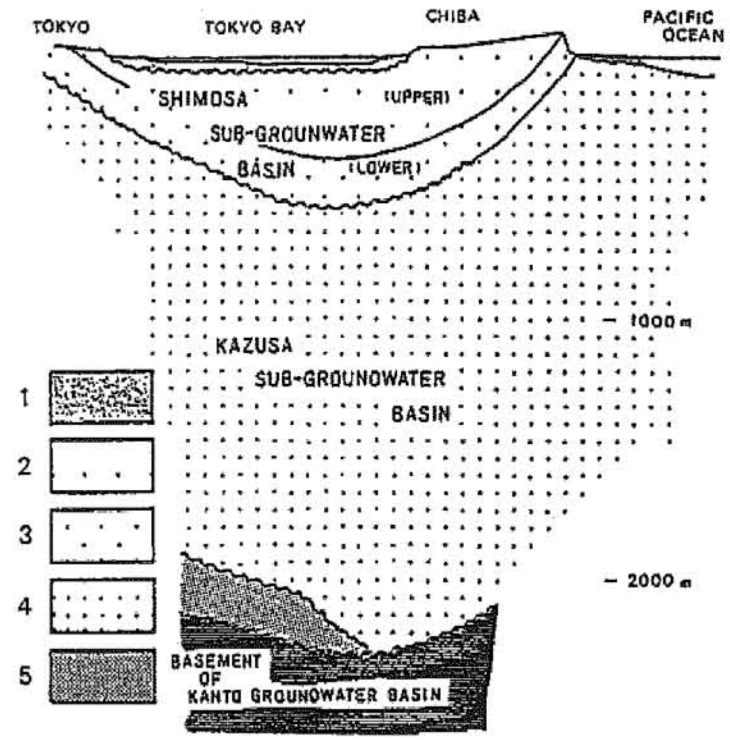

Figure. 1. Schematic section of the Kanto groundwater basin. 1: Alluvial deposits, 2:Upper part of the Shimosa Group, 3:Lower part of the Shimosa Group, 4: Kazusa Group, 5:Miura Group

3. STATUS OF UNDERGROUND FLUID RESOURCE USE

Natural gas and groundwater have been produced as the underground fluid resources in the Kanto groundwater basin. The former is mainly derived from the Kazusa subgroundwater basin. Annual production of natural gas was 52×10^7 Nm^3 in 1980, and 45×10^7 Nm^3 in 1984. The natural gas produced from the Kazusa subgroundwater basin was contained in fossil sea water of the Kazusa group. Accordingly, it was inevitable to pump up the fossil sea water when exploiting natural gas, frequently causing a land subsidence problem. Therefore, the pumping is now limited to the area of hills and the Pacific coast in the southern Kanto, a considerable distance from the metropolitan area.

Recently, the groundwater is mainly pumped up at the marginal area of the Shimosa lower subgroundwater basin and the upper Shimosa subgroundwater basin. Annual pumped volume was 3,363,248 m^3/day in 1978 and 3,328782 m^3/day in 1981 (Prefectoral Governors Committee for Land subsidence Prevention in Kanto District, 1983). These data were obtained in the limited area where reporting of pumped volume is required for groundwater users by regulation for land subsidence prevention. This area covers about half of the Kanto groundwater basin. Consequently, the actual pumping volume is estimated to have been twice as much as the aforementioned values. The groundwater has been used for (1) aqueducts, (2) industries, (3) agriculture (4) buildings and (5) other uses. The used volume generally increases as aqueducts, industries and so on increase. However the used volume shows a little difference based on each autonomy on the Kanto groundwater basin and the scale of the volume used by the agriculture and the building is different at each Prefectoral government. The volume of other uses is the smallest amount of the total volume pumped. The fact that the aqueducts make up the largest amount of the ground water use may be the consequence of the concept that groundwater use is necessary for the benefit of the inhabitants (Shibasaki, 1976, and Research Group for Water Balance, 1976).

4. CONTROL OF PUMPED VOLUME AND CHANGE OF GROUNDWATER LEVEL AND LAND SUBSIDENCE

Each local self-governing body has attempted to regulate the pumping volume of the groundwater in order to prevent land subsidence. For example, users are required to report the pumping volume compulsorily. Criteria of depth and diameter of discharge pipes were set up (Prefectoral Governors Committee for Land subsidence Prevention in Kanto District, 1983).

An agreement to control the pumping of fossil sea water containing natural gas was also made between the Chiba prefecture administration and each gas production company.

The condition of groundwater levels in the whole Kanto groundwater basin has recently been clarified. The number of observation wells was 375 in total as of 1982 (Furuno et al., 1983) and 459 as of 1991 (Fig. 2). The amount of land subsidence has been measured by yearly precise leveling. The number of benchmarks attained 4,880 and the total length of the leveling, 7363.6 km as of 1983, 4945 benchmarks and 7387.6 km as of 1986. The scale of monitoring system for the groundwater basin management is one the largest in the world. The groundwater management in the Shimosa subgroundwater basin is described below.

Figure 2. Distribution of monitoring wells in the Kanto groundwater basin. 1: Alluvial deposits, 2: Upper part of the Shimosa Group, 3: Lower part of Shimosa Group, 4:Kazusa Group, 5: Boundary between lower part and upper part of the Shimosa Group, 6: Tokyo Bay Unconformity, 7: Naganuma Unconformity, 8: Kurotaki Unconformity, 9: Pre-Kazusa Group, 10: monitoring well.

4.1. Control of Groundwater Over-pumping

In the Keihin industrial zone (coastal zone of Tokyo, Yokohama and Kawasaki) located in the southwestern part of the Kanto groundwater basin, the land subsidence caused by over-pumping of groundwater was recognized as early as in the 1940s. As a result, industrial aqueducts were established to replace the groundwater pumping from the coastal zone of Kawasaki and Yokohama. In the industrial zone, the pumping was controlled in the 1950s by regulations on the depth of wells and the diameter of discharge pipes. In the industrial zone of Tokyo and its suburbs, the pumping volume was controlled in the 1960s by two laws concerning industrial usage of water and pumping at building sites. However, groundwater users, especially industries, often loosely applied the countermeasures for land subsidence.

In the 1970s, with the rapid growth of the Japanese economy, environmental problems combined with land subsidence has been recognized as one of the important problems. In such a social background, not only the national government enacted the strict criteria for the regulation concerning the industrial water and the pumping up law for building use, but also the Prefectoral governments (Tokyo Metropolis, Chiba Prefecture, Kanagawa Prefecture, Saitama Prefecture, Yokohama City and Kawasaki City) in the southern part of the groundwater basin strictly applied these regulations. As a result, the groundwater level recovered and the land subsidence stopped gradually. However, excessive regulations produce another problem in some areas.

4.2. Change of Groundwater Level

It was in the early 1960s that the groundwater level fell to 30 m below sea level in the Keihin industrial zone, and 60 m below sea level in the coastal industrial zone of Tokyo metropolis. Later, the recovery of the water level was monitored according to the pumping up control.

In the 1970s the regulations were strictly adhered to in the southern Kanto groundwater basin. Accordingly, in the years from 1975 to 1980, the water level recovered 30 m to 40 m in the area where groundwater level had lowered. Thus the ground level showed a recovering tendency in the whole area (Fig.3 and 4).

In recent years, in the central to northern part of the Kanto groundwater basin, the water level has shown a lowering tendency again. The area where groundwater level dropped 20m to 30 m below sea level has expanded. In other words, a center of groundwater depression moved up to the northern part because the pumping control in the southern Kanto groundwater basin is applied strictly. The water level is not so low as the former 60 m but 20 m below sea level, and such area has spread out.

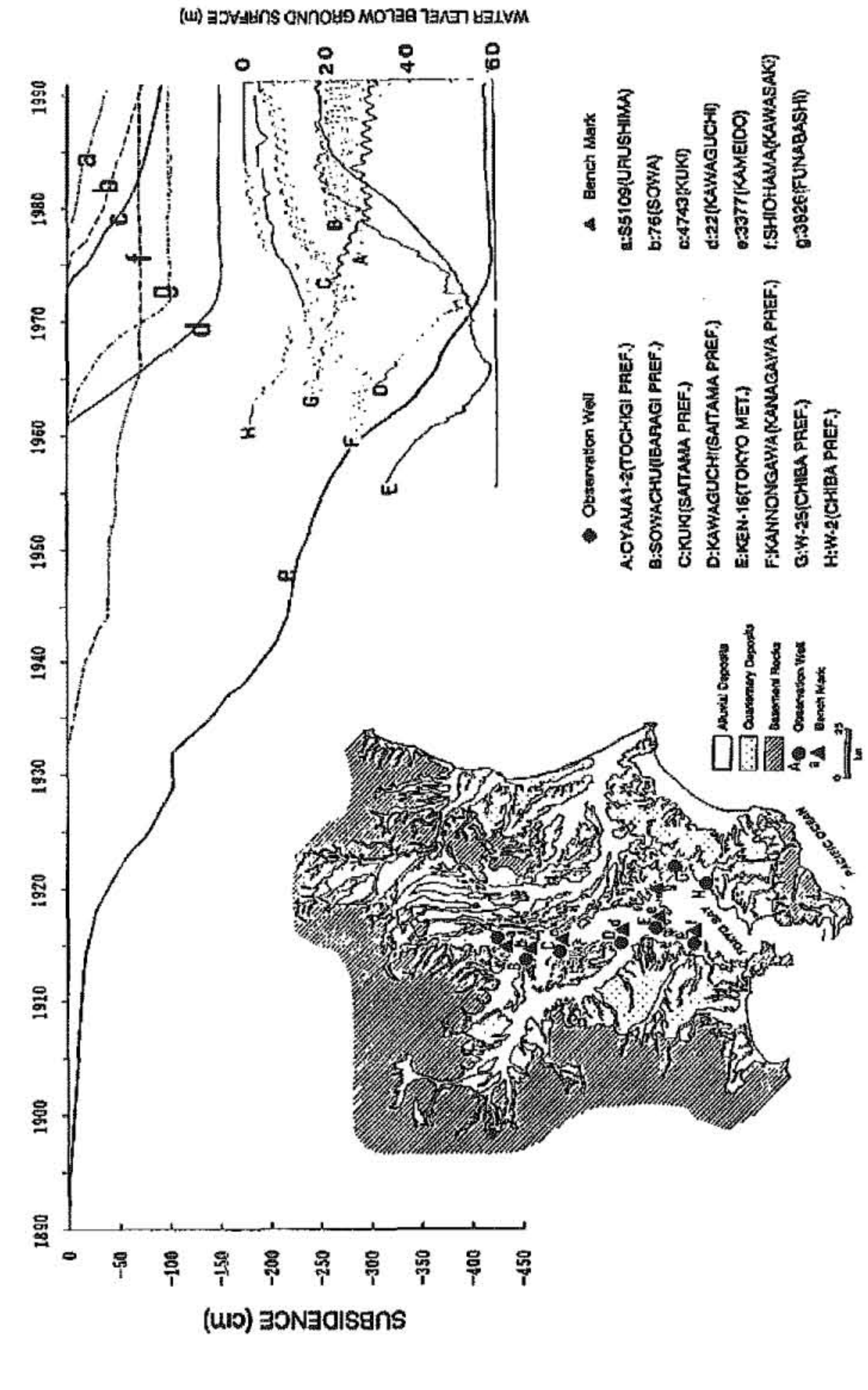

Figure 3. Historical change of the land subsidence values and groundwater level in the Kanto groundwater basin.

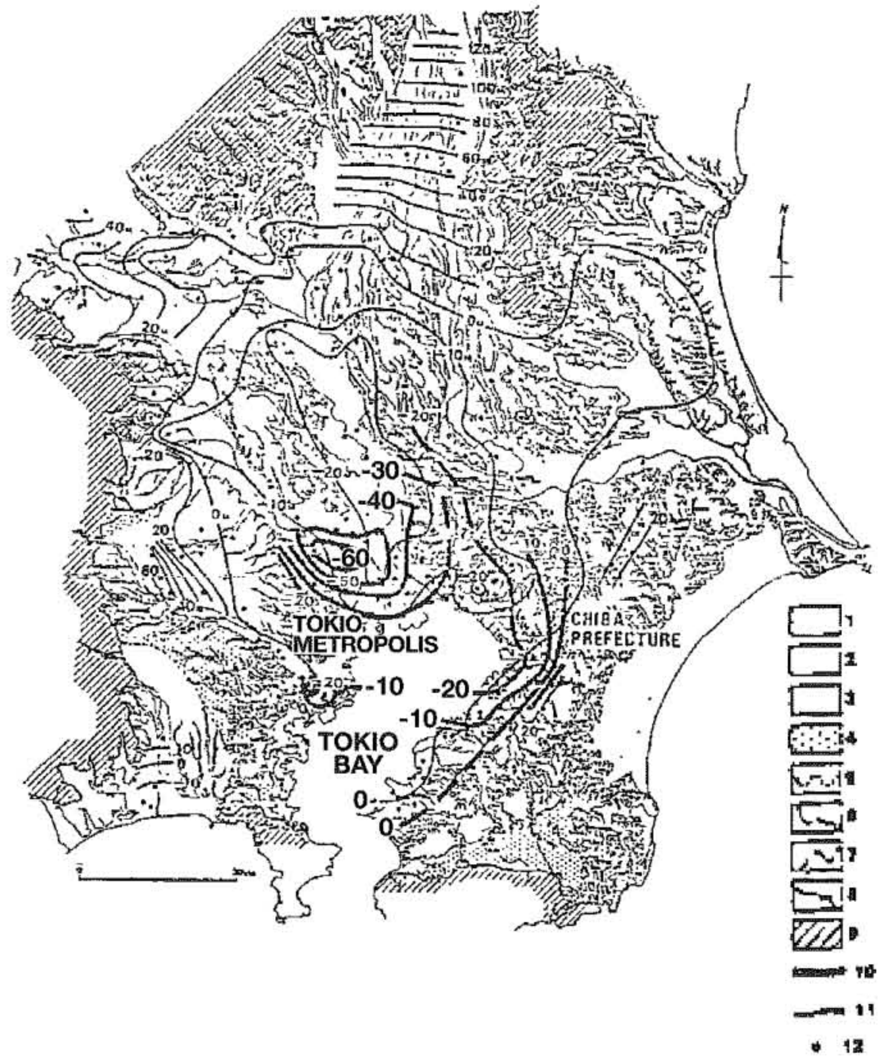

Figure 4. Confined groundwater level in the Kanto groundwater basin (especially the Shimosa subgroundwater basin). 1: Alluvial deposits, 2: Upper part of the Shimosa Group, 3: Lower part of Shimosa Group, 4:Kazusa Group, 5: Boundary between lower part and upper part of the Shimosa Group, 6: Tokyo Bay Unconformity, 7: Naganuma Unconformity, 8: Kurotaki Unconformity, 9: Pre-Kazusa Group, 10: Contour line of confined groundwater level in 1971, 11:Counter line of confined groundwater level in 1984, 12: monitoring well of groundwater.

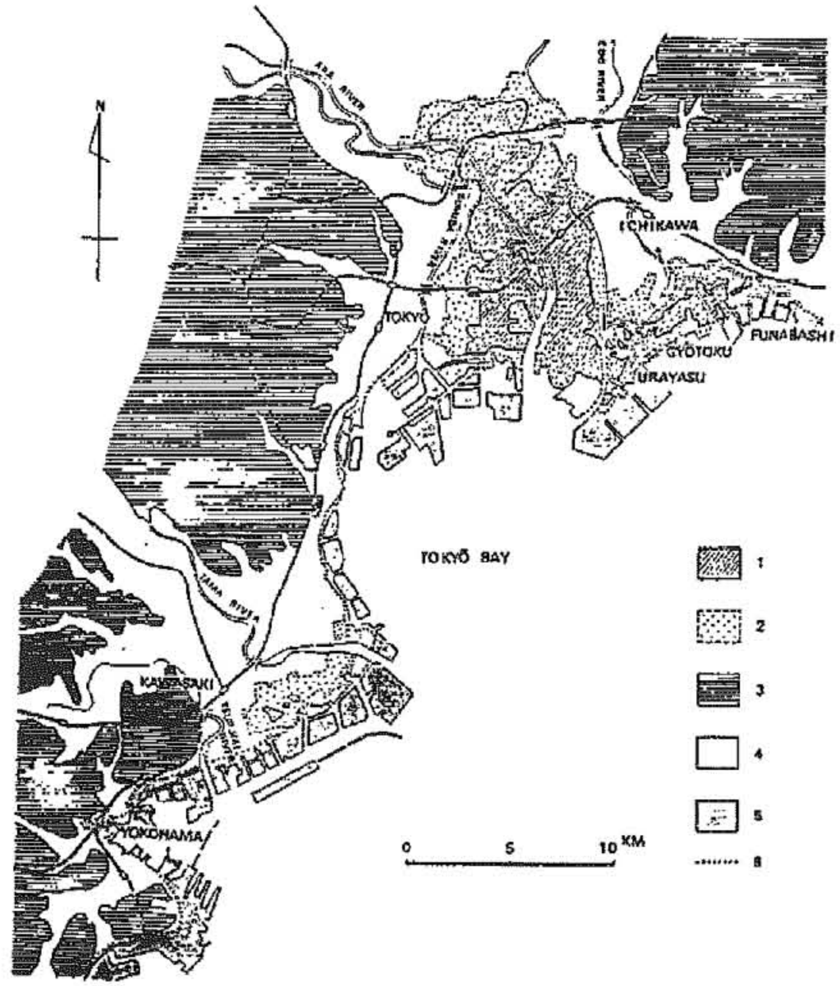

Figure 5. Area changed to marine environmental potentially by land subsidence in Tokyo and its suburbs. 1: Area showing lower ground level than mean sea level of Tokyo Bay (T.P.), 2: Area showing lower ground level than high water ordinary spring tide of Tokyo Bay, 4: Alluvial plain higher than 0.93m(T.P.), 5: Reclaimed land after the early 191s, 6: Old shore line of the early 1910s (Nirei et al., 1979).

4.3. Change of Land Subsidence

The land surface has been sinking to below sea level in the downtown Tokyo area (Shitamachi) for mixed industrial and residential groundwater uses since 1910s. Coincidentally, the areas showing ground level lower than mean sea level and high water level of ordinary spring tide of Tokyo Bay were widely scattered (Fig. 5). Recently, however, these phenomena have been recognized in alluvial area not only in Shitamachi of Tokyo, but also in suburbs of Tokyo such as

Kawasaki in Kanagawa Prefecture, Funabashi, Gyotoku and Urayasu on western Chiba Prefecture. This land subsidence has been stabilized by the regulation of the pumping. The land subsidence was stopped in certain areas and the ground surface slightly rebounded by the recover of the groundwater level (Fig.4). On the other hand, in the area from the central to the northern part of the Kanto groundwater basin, land subsidence has begun to sink as a result of over-pumping. This means that the land subsidence area is moving northward.

5. CONCLUSIONS

For the purpose of effective use of groundwater and preventing of land subsidence, simulation model analysis based on their relation have been done on several dozen examples (Research Group for Water Balance, 1976; Shibasaki, 1981; Kamata, 1983). These simulation analyses are prerequisite for calculation of the appropriate pumping up volume without causing any land subsidence. It is also necessary to establish a more effective monitoring system for continuous observation of the pumping of groundwater and the changes in groundwater level and land subsidence, and to decide the pumping volume in consideration of the change of the groundwater level and the ground movement with the law of dynamic equilibrium between man and nature due to the relation among human groups. In other words, the groundwater resources can be used while the health condition of the groundwater basin is examined by periodical health checks. This idea is in the implementation stage and making a good progress (Nirei, et al., 1979).

Acknowledgements

We sincerely appreciate the members of Research Institute of Environmental Geology, Chiba (RIEGC) and the staff of the local governments of the Kanto district who developed the monitoring system and continued to record land subsidence and groundwater level.

REFERENCES

Aihara, S., Ugata, H., Miyazawa, K., & Tanaka, U. (1969) Problems on groundwater control in Japan. *Land Subsidence* 2, IAHS-UNESCO, 635-644.

Furuno, K., Nemoto, K., Takanashi, Y., Yada, T., Takizawa, H., Oshima, K., Saotome., W., & Nirei, H. (1983) The monitoring of land subsidence and groundwater head in the Kanto groundwater basin. *Bull. Chiba Pref. Res. Inst. Envir. Pollut.*, 15, 99-108.

Inaba,Y., Abe, I., Iwasaki, S., Endo, T., & Kaido, R. (1969) Reviews of land subsidence researches in Tokyo. *Land Subsidence,* Proc. 1st Int. Symp. on Land Subsidence, Tokyo, Japan, Publ. IAHS No.121, 80-86.

Kamata, A., 1983. Development of Groundwater simulation models. *Memoir Geol. Soci., Japan,* No. 25, 463-472.

Nirei. H., & Kunio F. (1986) Development of Quaternary Resources and Environmental Protection, -Status of underground fluid resources use in the Kanto groundwater basin-, Recent Progress of Quaternary Research in Japan, National Committee for Quaternary Research in Japan, Vol.11, *Quaternary Research*, 71-80.

Nirei, H., Kusuda., T., Suzuki, K., Kamura, K., Furuno, K., Hara, Y., Satoh K., & Kazaoka. O. (1990) The 1987 East Off Chiba Prefecture Earthquake and It's Hazards. *Mem. Geol. Soc. Japan,* No. 35, 31-46.

Nirei, H., Yada, T., Hara, Y., Furuno, K., Adachi, I., & Nakamura, M. (1979) Artificial ground movement in the south Kanto district. *Quaternary Research*, 17, 287-298 (in Japanese with English abstract).

Prefectoral Governors' Committee for Land Subsidence Prevention Kanto District (1983) Report of groundwater volume pumping up. 228 pp. (in Japanese).

Research Group for Water Balance (1976) Groundwater basin management. Tokai Univ. Press, Tokyo, 242 pp. (in Japanese).

Research Committee on Land Subsidence in Southern Kanto District (1974) Report of research on land subsidence in Southern Kanto District. 297 pp. (in Japanese).

Shibasaki, T. (1976) Carrying capacity of groundwater development and conservation. *Groundwater basin management*, Tokai Univ. Press, Tokyo, p. 47-75 (in Japanese).

Shibasaki, T. (1981) Groundwater basin management and land subsidence control. *Recent Proc., Natural Sci. Japan*, Science Council of Japan, No. 6, p. 256-267.

LAND SUBSIDENCE
LEGAL AFFAIRS AGAINST TECHNICAL KNOW HOW

Frans B. J. Barends
Director Scientific Affairs, GeoDelft, P.O. Box 69, 2600 AB DELFT, Netherlands;
Professor in Mechanics of Porous Media, Civil Eng. Faculty, TUDELFT, Netherlands

Abstract

The land surface moves very slowly or very rapidly due to natural and human processes, felt and noticed as vibration, inundation and property damage that may take serious proportion. Regional surface hydrological systems and water management becomes malfunctioning. Water defense systems of low land areas lose safety margins. City sewerage systems may stop operating properly. Unique monumental buildings show signs of enhanced deterioration. With respect to damage claims it is essential that direct and indirect causes can be quantified with sufficient accuracy from a technical and scientific point of view. Laws and jurisprudence provide the legal frame within which damage claims are accepted. There is, however, a discrepancy between scientific insight and legal rules or public opinion. Sometimes so great that common sense is lost, which is a frustration to all parties involved. The article is devoted to enlighten reasons that cause this situation and suggests ways to improvement.

Keywords: land subsidence, damage claim, law, property, jurisprudence

1. APPEARANCE AND CAUSES OF LAND SUBSIDENCE

Land subsidence as a natural process is as old as the separation between land and sea was a fact in the world's history of existence. Man induced land subsidence took place only the last century, accelerated with the years by the rapid increase of the use of ground water and of oil and gas. Land subsidence by the underground withdrawal of fluids or the extraction of solids through mining or underground building, in fact, a subtle irreversible phenomenon at relative large scale and slow rate, becomes evident when surface drainage stagnates, pipelines crack, cables break, sewer runs the wrong direction, canals do not function properly, groundwater regimes have to be adjusted, and buildings and foundations may be damaged. At present, more than 100 notorious subsidence areas are known, some of which with a surface lowering of more then 10 meter, mostly along coasts and in deltas, usually with a dense population and intensive industrial development, protected against water surges by extensive and expensive systems of dikes, flood walls and pumping systems. In those areas subsidence may cause extremely expensive damage to the infrastructure.

Industrials and local governments, as well as engineers and scientists in charge of maintaining and developing industrial complexes, urban growth, water supply systems and natural territories need to know about the potential hazards, costs, and the socio-environmental impacts due to land subsidence, in order to design sustainably and prevent damage by subsidence on the long term. When damage occurs in a subsiding area, it is the same person or institution to blame and to hold responsible for the repair costs, when the cause is proved to be the induced subsidence. Here is ample place for vivid disputes often fought out before the court. Other causes could be involved, such as draught, natural shrinkage and oxidation, changing (natural) habitation, groundwater changes – in some urban areas the groundwater withdrawal has stopped and the corresponding groundwater level rise will jeopardize cellars and tunnels in due time – road and dike improvement, traffic and temporary construction sites.

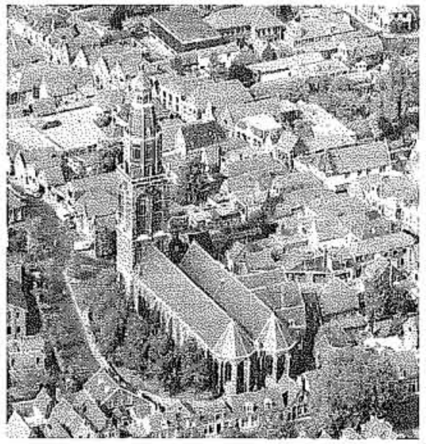

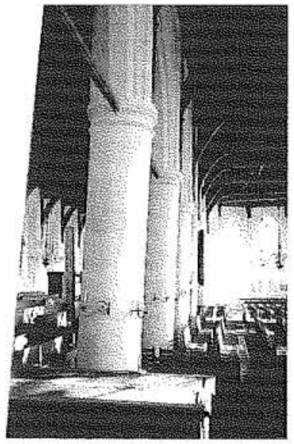

Figure 1. Top monument Zuyder Church at Enkhuizen, Netherlands. The ship distorted since the Zuydersee Barrier dam was built.

A major improvement in the Dutch coastal defenses came in 1932, when the Afsluitdijk (Zuydersea Barrier Dam) was built, linking the coasts of the provinces of North Holland and Friesland. This dike shortened the 1900-km coastline to 1300 km. Since then, many decennia later, several old monuments suffered considerable and costly damage due to induced geohydrological changes that promoted differential settlements.

Effects may become apparent only afterwards, sometimes long after the culprit can be appointed.

2. LAWS, DAMAGE LIABILITY AND INSURABILITY

2.1. Property and liability

In general, somebody who is owner of a piece of land, has diction over the subsoil up the earth center, and diction over the space above until the border of the atmosphere. In many countries limitations to this diction are posed by law. The use of space above and underneath is admitted to others, if so high or so low that the owner has no interest to resist against. Since ores are usually so deep, the landowner above has no diction. However, the ownership of unexploited ores is not always settled legally. The old laws, dating a century ago and more, provide a concession for coal mining on land giving ownership for ever even if not won, but at sea only after winning. New mining laws dictate the ownership of unexploited ores to the State. The State can allow for mining, by giving mining concessions. This situation indicates the importance with regard to legislation of the liability of mining damage to landowners above subsiding areas.

2.2. Subsidence damage

Fluid withdrawal or solid extraction may have unpleasant consequences for landowners above, by subsidence and earthquakes. It is just and fair when the State will provide arrangements for this hindrance, as the State limited the ownership. Damage should be passed on to the culprit. Yet, for a proper damage claim little to nothing was settled in laws, and much is solved by jurisprudence.

In Europe national mining laws and jurisprudence refer to the Napoleon's mining law of 1810 that ordains liability at unlawful acts, like in Germany (1865), France (1901), Russia (1903), Netherlands (1920), Italy (1927), Romania (1929), and United Kingdom (1939). Coal mining exploitation companies in the Netherlands and Belgium, have settled many claims, hundreds of millions of dollars, to owners of damaged buildings. Sometimes damage occurred after 30 years or more. Since 1920, damage claims had to be settled only in few cases by court.

With regard to solid extraction mining recent laws, for example the Bundesberggesetz in Germany (1982), the Code Minier in France (1994), and the Mineralstoffgesetz in Austria (1975), the civil right with regard to mining damage is covered. Mining causality of damage claims has to be disproved by the licensee. Moreover, the State should remains (partly) liable when, long after the (ex)licensee stopped to exist. This vision is based on the fact that mining is an act of expropriation (admitted limiting ownership) of those who live above.

In the new laws, a clear distinction is made with regard to mining gas and oil.[1] Many coal mines in Western Europe are now closed. At present, old abandoned mine shafts are becoming submerged. The environmental effects are closely observed, as damage is expected. In Germany coal mining companies owe most of the territory, probably to keep damage costs in house.

A new mining law is in preparation in the Netherlands, covering fluid and solid mining activities and the causal relation between damage and mining, as the fact that proof, usually for the demanding party, is particularly difficult by the complexity of the process and the weak legal position of a private house owner with building damage. The dispute is about turning the burden of proof and about financial guarantees for the long term. A notorious example is the sudden collapse of an abandoned salt mining cavity, appearing in some minutes with a roaring growl, leaving a pond in a farmer's house garden.

Figure 2. A sinkhole caused in 1991 by collapse of a salt mining cavity abandoned in 1920. Emmen, Netherlands.

[1] Bundesberggesetz: Bergbau und Grundbesitz, Haftung fur Bergschaden (11-11-1982), IV Inhalt der gesetzlichen Bergschadensvermutung, pag 866: (...) *Bei der Bergschadensvermutung handelt es sich aber nur um den Bereich, auf den die untertägigen Betriebsteile des Bergbaubetriebes einwirken, in denen Steinkohle, Salze oder andere Bodenschätze untertägig aufgesucht oder gewonnen werden. Dazu gehört nicht die Erdöl- und Erdgasaufsuchung und –gewinnung mit Hilfe von Bohrlöchern. Das ergibt sich eindeutig aus der in §122 Nr. 3 RegE 1977 getroffen unterscheidung (...).* Mineralrogstoffgesetz (BGB1.I, 38, 1-01-1999): § 153 (Abschnit III), pag 373: *(1) Als Bergbaugebiete gelten Grundstücke und Grundstücksteile innerhalb der Begrenzungen von Grubenmaßen und Überscharen, Speicher- unde Gewinningsfeldern mit Aunahme jener auf Vorkommen von Kohlwsserstoffen, sowie Grundstücke und Grundstückteile, auf die sich ein genehmigter Gewinnungsbetriebsplan für grundeigene mineralische Rohstoffe bezoeht und (...).*

2.3. Insurability

An entrepreneur can insure unlawful acts and liability risk. Acts of God (*forces majeures*) fall beyond this category, and land and building owners can insure against such events. Sometimes, such risks cannot be insured. The statement of acts of God depends on the following criteria: (1) external (2) unforeseen (3) uncontrollable (4) unavoidable. The former two are objective, the latter two subjective, since they depend on the conduct of the entrepreneur. In case of damage he should clarify to have done all he could to limit the controllable and avoidable. The statement that the type of event related to a specific damage claim involves therefore legal, juridical and technical aspects.

There is normally no insurance for damage caused by mining. Mining companies - often the State has interests – are usually large monopolies that take special arrangements to cover liability risks, like the installation of a damage guarantee fund and independent consultancy for corresponding damage claims. With regard to damage by water extraction from upper aquifers, liability not only with regard to damage to the infrastructure but also to natural habitat is covered by specific groundwater laws.

The insurability of damage caused by building activities, such as excavations and tunneling, is limited to external and unforeseen collapse of structural elements, damage due to leakage is judged unavoidable and is normally not insurable. Here, the proof is not for the demander, but for the originator. The discussion focuses on the designer, the controller/consultant or the contractor/entrepreneur, and since unavoidable damage is usually complex and proper information is usually incomplete, impartial expert consultants are required to clarify the (technical) true cause and – what is even more difficult – explain it in a legal context. Here, is a special role for the expert. An illustrative example is the development of building techniques of large infrastructural projects, such as underground waterway crossings by tunnels in the Netherlands. Large dewatering systems, usually insufficient, for immense building pits have damaged the environment by vast pasture and orchard parching, differential settlements of roads, bridges and buildings, and other geohydrological effects. The damage costs were unacceptable, and only partly foreseen. The environmental damage caused by building activities is elucidated by two tunnel projects, the Vlake Tunnel and the Princes-Margriet Tunnel. At present about 45 such tunnels are built and they form key connections in a modern road and railway network. Building without causing damage to the environment in the soft soil conditions in the Netherlands seems just impossible. However, limiting damage by prediction of unavoidable effects and adequate anticipation is possible.

The building technique was therefore adapted to the cut-and-cover method and immersion-caisson method, and damage was significantly restricted, but still around 10% of the total building cost. At present proper countermeasures are required for such as legal limitation of the pumping discharge, by injection and freezing methods, deepwalls and sheetpilings, and as an alternative the tunnel-boring method. Moreover, the (risk) liability for these large projects, put in the hands of the contractor by the modern design-and-construct contracts, invokes a predetermined quality control playing a prominent role in the building process, involving all parties.

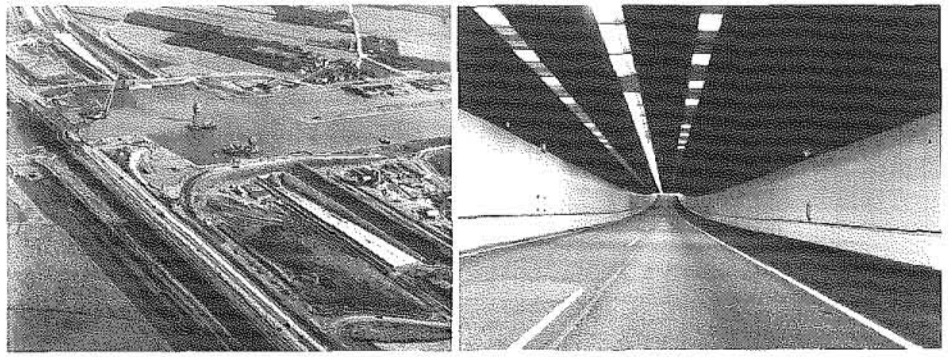

Figure 3. A building site (immersion-caisson method and a completed tunnel

	Vlake Tunnel, 1975 on land: open drained pit off land: sinking caissons	P.Margriet Tunnel, 1977 on land: open drained pit off land: sinking caissons
geohydrology	deep sandy aquifer thin top layer of clay	multi-aquifer system intermediate clay layers
pumping test	T = 335 m²/day λ = 100 to 1600 m Q = 750 m³/hr	prognosis 32 wells Q = 1880 m³/hr
used drainage system	11 deepwells (37 m-NAP) well radius 250 mm	48 wells (17 m-NAP) Q = 2400 m³/hr
damage costs	(NGL)	(NGL)
- building repair	3.204.000	4.120.000
- agriculture		2.260.000
- guidance	588.000	590.000
- investigation	346.000	170.000
- taxation	331.000	116.000
- sundries	250.000	590.000
- administration	250.000	180.000
total	4.722.000	7.946.000
damage/total cost	10 %	12 %
damage evaluation	aquifer inhomogeneity time variation (weather)	extremely dry summers peat erosion (pastures) damage gas/water pipes

3. THE ROLE OF THE TECHNICAL EXPERT

The role of the technical expert in the damage claims is yet marginal. Listening to experts is, when done, usually with suspicion, as the audience has different interests. There is no objection against a close cooperation between the expert and any party involved, but the price is loss of independence and impartiality. Specialists do have usually certain apathy for simplifying technical information towards the public. They seem to believe in the battle for individual existence, i.e. prestige and status, and they forget that a battle for being understood is equally essential, particularly for the court.

The technical expert should know the state of the art, refrain from speculation, restricts himself to quantification of effects in a technical sense, and pay a great effort in the way to communicate his findings with all parties involved. The first step is to define the essential questions to be answered. The court sometimes provides these questions. Next, collecting data. Sometimes data is hold back, seemingly by accident. Essential information, obtained by putting data in the context, may be invisible at first sight. Then, a site inspection and an official discussion with each party separately will complete the available information. One should not inspire any suggestion about a possible outcome. The main work is the analysis and conception of the answers to the specific questions asked. The concept report could be discussed with, preferably, another impartial expert.

The report containing the findings of the expert is different from a normal consulting report that contains, in sequence, introduction, problem definition, approach, application, validation and conclusion. In stead, a damage report starts, after a short introduction, directly with the final conclusion, in terms of a firm and clear statement, the words of which are carefully chosen. Next, this statement is worked out in details, step by step, as much in detail as required. Proofs of the details are given with complete references, in fact, well retrievable.

4. SOME CASES

The various aspects of a proper technical consultancy in case of a damage claim related to induced land subsidence will be outlined on the basis of several cases. Because a damage claim has always to do with appointing a culprit or a losing party, emotions are involved. The description of the cases is therefore kept short, just to serve an educational purpose. In the presentation a more complete insight is presented.

CASE 1. A private house owner noticed his house being damaged by either drainage for building activities or for sewerage repair. Before the activities started the owner had photographed his house, and could therefore show the damage cause and originator. The responsible parties, contractor and municipality, could not agree about either part of damage. An expert was asked. No technical data was available! How to find a proper technical consistent answer, is the crux. The outcome, to which parties committed beforehand, was yet a frustration for both.

CASE 2. The abutment of a large high road bridge crossing a main river is creeping and settling. The oil mining company, exploiting a reservoir at 3000 m depth at the location, was appointed the culprit. A proper investigation showed a surprising and embarrassing result. The case was dismissed.

CASE 3. Seismic exploration of the subsoil for mining purposes involves explosions at the surface. A farmer was convinced that due to these activities the geohydrological situation of his land was altered and he claimed compensation for disappointing crops. Two experts looked at the case, a geohydrologist and an agriculture specialist. The case was technically clear and proven, but a tactic move gave adventure to the odd party.

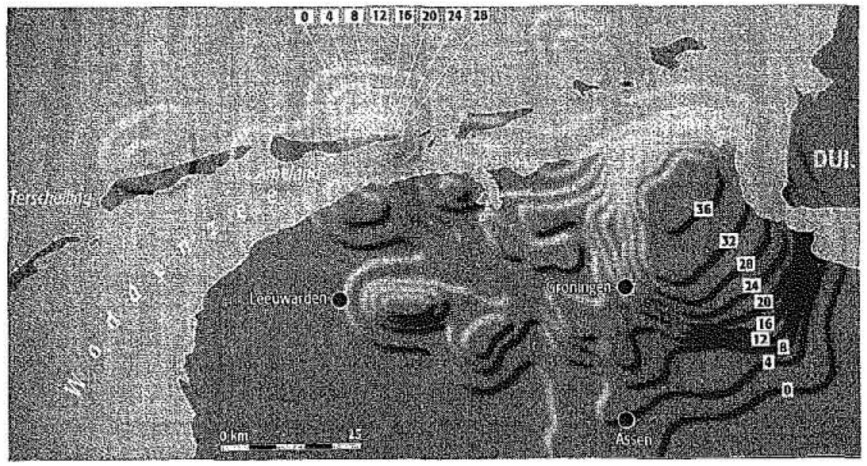

Figure 5. Predicted land subsidence in the North of the Netherlands. (deVolkskrant, Source: NAM, 1999)

CASE 4. A public debate about exploitation of gas from deep reservoirs under a nature reserve, Waddenzee in the north of the Netherlands, gave rise to significant deformation of scientific and political arguments, enhanced by the media and press. Emotional aspects disturbed a proper debate. Experts could do little to nothing, except losing their status and temper.

LAND SUBSIDENCE - Vol. I
Proceedings of the Sixth International Symposium on Land Subsidence
Ravenna / Italy / 24-29 September 2000

SOCIAL DECISION MAKING AND LAND SUBSIDENCE

R. Allan Freeze
R. Allan Freeze Engineering, White Rock, BC, Canada

Abstract

This review paper uses the concepts of decision analysis to lay out a framework for the assessment of land subsidence problems. It emphasizes the need for integrated consideration of the technical, social, economic, legal, and political issues. The ultimate goal is a negotiated settlement of land-subsidence conflicts among adversarial stakeholders.

Keywords: Land subsidence, decision analysis, risk-cost-benefit analysis.

1. INTRODUCTION

The occurrence of land subsidence has become a serious problem at many locations around the world. At these sites, which are primarily urban, and often coastal, decisions with respect to preventive or remedial strategies take place in a complex decision-making milieu that depends on the results of technical analysis, but is heavily influenced by social, economic, legal, and political issues. There are many stakeholders, and adversarial conflicts often arise during the decision-making process. Cooperation is required across a wide suite of government agencies, including those responsible for water management, land-use planning, industrial development, and environmental protection.

This review paper uses the concepts of decision analysis to lay out a more holistic framework of land subsidence than is usually attempted. It indicates the types of decisions that are faced by the various decision-makers and stakeholders, and identifies the benefits, costs, and risks that drive their political actions. The paper is *not* a blueprint for any specific strategy for coping with land subsidence. Rather, it is intended as a template for the comparison of alternative strategies, especially when such strategies attempt to integrate both technical actions and social policies.

This paper is somewhat unconventional in format. The primary contribution lies in the twenty-one tables that appear at the end. The text is very brief and is designed simply to serve as a roadmap through the tables, which are hopefully more-or-less self-explanatory. The paper is organized into five sections that treat (1) the causes and impacts of land subsidence, (2) the available strategies for coping with subsidence, (3) the decision-analysis framework, (4) examples of the economic costs and risks associated with land subsidence, and (5) pathways and roadblocks to social consensus in multiple-stakeholder scenarios.

2. CAUSES AND IMPACTS OF LAND SUBSIDENCE

Table 1 summarizes the recognized causes of land subsidence, both natural and anthropogenic. One can differentiate between cases of rapid local subsidence, and long-term regional subsidence. The former can occur naturally as collapse features in karst and salt terrain, or anthropogenically as a result of subsurface mining. The latter can occur naturally due to sediment compaction, or anthropogenically due to the withdrawal of fluids from the subsurface. Table 2 addresses the relative importance of some of these mechanisms. Table 2a indicates that at coastal sites where the observed rate of relative subsidence can be ascribed to a combination of natural sediment compaction, sea-level rise, and subsidence due to fluid withdrawal, the latter mechanism is usually responsible for as much as 90% of the total. Table 2b indicates that at sites where both oil-and-gas withdrawal and groundwater withdrawal have occurred simultaneously, the latter is usually the primary mechanism. Table 3 lists thirty-two locations from around the world where land subsidence has been documented and described in the literature. The great majority are the result of groundwater withdrawals. Table 3 also indicates that many of the most serious cases of land subsidence lie in coastal environments. In view of these findings, this paper emphasizes long-term, regional, anthropogenic subsidence due to the withdrawal of groundwater at sites in coastal environments.

Table 4 summarizes the environmental and engineering impacts of land subsidence in inland and coastal environments. Structural damage to engineered structures such as buildings, roads, bridges, dams, pipelines, railways, and canals, is likely to occur in either environment. Coastal environments may suffer added impacts due to temporary flooding, permanent inundation, loss of coastal land and ecological habitat, and damage to harbors, ports, and other coastal facilities.

The remedial costs associated with these impacts can be enormous. But then so too are the benefits associated with groundwater production. And so too might be the costs of actions designed to prevent such impacts. Social decisions are needed. Is it possible to develop politically-acceptable preventive strategies? If so, who will bear the costs of these preventive strategies? How will their costs compare with remedial costs if the subsidence were left unchecked? How does society determine an optimal integrated strategy for water-supply management, land use, and hazard protection?

3. STRATEGIES FOR COPING WITH LAND SUBSIDENCE DUE TO GROUNDWATER WITHDRAWAL

The preventive strategies summarized on Tables 5 through 8 are divided into those that are primarily technical in nature, and those that are primarily socioeconomic. The technical strategies are further divided into those that deal with assessment and prediction, and those that lead to damage prevention. The socioeconomic strategies are further divided into those that would be needed to exert effective control on groundwater pumping, and those that rely on land-use planning. In preparation for the later economic arguments, perusal of these tables should be accompanied by some thought as to what each of the elements of the various preventive strategies might cost.

Assessment of alternative strategies for coping with land subsidence due to groundwater withdrawal requires a level of technical support that allows for a cause-effect analysis of a wide range of pumping and land-use scenarios, with output in a form that is suitable for socioeconomic decision-making. Table 5 outlines the various steps in a program of technical assessment and prediction, from vulnerability mapping and field monitoring, through the development, calibration, and application of a coupled model of groundwater flow and land subsidence. The work of Gambolati et al (1991, 1999) near Ravenna, Italy provides a classic example of technical modeling in the service of socioeconomic goals. In that work, an interuniversity research team carried out studies with the support and cooperation of local, regional, and national government agencies. They used a quasi-coupled numerical groundwater/land-subsidence model to produce maps of projected flooded area along the Romagna coastline at various future dates under optimistic and pessimistic land-subsidence scenarios. The results were also used to support the partitioning of responsibility for observed subsidence between onshore groundwater pumping and offshore gas production.

Table 6 summarizes a variety of damage-prevention strategies. Most of them (pumping controls, flood protection works, and canal redesign, for example) have a strong technical component that would require careful engineering design. Each strategy might include many alternative design configurations, and each one would come with its own benefits, costs and risks. The consideration of alternative design configurations would be part of the overall decision process, and some of the design parameters highlighted in the right-hand column of the table (pumping rate, or seawall height, or canal freeboard, for example) would be decision variables in the decision process.

The issues are not wholly technical, however. Each damage-prevention strategy also comes with an associated set of socioeconomic issues that influence its economic, legal, or political feasibility. If we look first at a groundwater-control strategy, Table 7 outlines some of the possible management policies that might be put in place by a groundwater-management authority to exert the necessary control on groundwater withdrawals. They include specified pumping limits, permits, fees, taxes, metering, and enforcement activities. Again, each policy has its own costs and benefits. The issues listed in the right-hand column of Table 7 identify some of the socioeconomic decision variables that would come to the fore. The underlying message is that land subsidence must be included as a driver in the development of groundwater management strategies along with the other more usual drivers such as water-table declines, saltwater intrusion, or avoidance of contamination.

Table 8 lists some of the alternative management policies that could be put in place as part of a land-use-planning approach to damage prevention. They make use of regulatory instruments such as land-use plans, zoning restrictions, and building codes. The underlying message here is that land subsidence must be included as a driver in land-use planning along with the other more usual drivers such as earthquake protection, flood protection, or protection of ecological habitat.

There are many precedents for management policies of the type outlined above. Table 9 lists several precedents from North America involving restrictions on groundwater withdrawals from aquifers. Table 10 identifies some management strategies used for control of groundwater contamination in the USA that might be transferable to the land- subsidence milieu.

4. A DECISION-ANALYSIS FRAMEWORK

Table 11 provides a list of the various stakeholders who might wish to be heard in the course of negotiations leading to the development of management policies for the prevention of land subsidence due to groundwater withdrawals. Table 12 provides examples of the types of decisions that might be faced by several of them. Some of the decisions are technical; some are socioeconomic. In each case only two alternatives are listed, but in reality many alternatives would likely be under consideration. Each stakeholder works toward his own objective. For private individuals or companies, the objective is likely to be to maximize profit or minimize economic loss. For public agencies, the objective ought to be to meet the mandates of their enabling legislation, which was hopefully designed to maximize social benefit or minimize social cost.

Table 13 outlines a very general objective function that could in principle be used by any of the stakeholders to assess the alternatives. The quantitative value of the objective function, Z_j, for each alternative, j, is given by the sum of the discounted stream of benefits, $B_j(t)$, minus costs, $C_j(t)$, minus risks, $R_j(t)$, over a time horizon, T. The risks are defined as the probability of failing to meet design objectives, $PF_j(t)$, times the costs associated with such a failure, $CF_j(t)$. The $CF_j(t)$ term is sometimes called the risk cost. All the technical input from a site goes into the estimate of $PF_j(t)$. All the other terms in the objective function have a socioeconomic basis.

Every stakeholder will likely have a different objective, a different discount rate, a different time horizon, a different definition of failure, and different benefits, costs, and risk costs. The method of calculation is common to all stakeholders, but the results are particular to each one. Each stakeholder could use the decision framework in one of two ways: either to aid in making a decision over which they have total control; or to develop a ranked preference vector of alternatives for use in negotiations with the other stakeholders.

Table 14 summarizes the benefits, costs, and risk costs for three of the identified stakeholders: a corporate groundwater purveyor, a private party that is impacted by the subsidence, and a government land-use planning agency. This table provides a more detailed idea of the types of economic data that are required for the assessment of each alternative management strategy, including both its technical and socioeconomic components.

5. COSTS AND RISKS ASSOCIATED WITH LAND SUBSIDENCE

Table 15 provides some estimates of the costs associated with land subsidence, taken from the literature. All costs have been converted to net present values in Year 2000 $US, using an historical price index and published currency conversion tables. The first two categories on the table (actual past damages, and predicted future damages) represent estimates of the risk costs, $CF_j(t)$. The third category (proposed future damage prevention activities) provides estimates of the direct costs, $C_j(t)$. The numbers are very large in both cases. Estimates of the risk costs run from $120 million to $1.78 billion. The total annual losses that can be ascribed to land subsidence in the USA are estimated at $500 million per year. The values given by Broadus (1996) for the Bengal Delta, Bangladesh, and the Nile Delta, Egypt, represent a significant percentage of the GNPs for each of those countries.

Estimates of the direct costs for massive public works designed to prevent subsidence (or the flooding events enhanced by subsidence) run as high as $32.5 billion.

There is some evidence in the literature (as summarized in the final section of Table 15) that the risk costs associated with legal claims may not be as large as some stakeholders fear. In the most pertinent case (Carpenter and Bradley, 1986), plaintiffs in Galveston TX were not able to convince the courts that observed land subsidence was caused by groundwater pumping, and their suit was unsuccessful.

Table 16 provides an example of a risk calculation taken from the literature (CENAS, 1997). The risks are those associated with flooded land caused by land subsidence near Ravenna, Italy. In order to avoid the impacts of inflation and economic cycles on the numbers, the risks have been normalized on a scale from R=0 to R=100. The output is in the form of normalized risk maps for various land-subsidence scenarios and flood-event return periods.

Table 17 provides two examples of risk-cost-benefit calculations carried out in a decision-making framework. The first involves a decision between the no-action alternative and a controlled-pumping alternative to address subsidence impacts in Shanghai, China (Hua et al, 1993). The second involves a decision between four alternative remedial policies to address the impacts of land subsidence over mine workings in the West Midlands, England (Whittaker and Reddish, 1989; Brook, 1991).

The decision-analysis framework provides a rational context for assessment, but it too has its shortcomings. Table 18 summarizes some of the issues and difficulties associated with the application of decision analysis to social decision-making.

6. WORKING TOWARD CONSENSUS

There are many difficulties that can arise in trying to reach a consensus in multiple-stakeholder scenarios of the type that arise in the negotiation of land subsidence strategies. Table 19 identifies some of the sources of adversarial conflict, and the possible role of conflict analysis as an aid to multiple-stakeholder negotiation.

As noted on Table 20, the main roadblocks to consensus lie in the interpretive differences that can arise between the parties due to the unavoidable presence of uncertainty in the technical analyses, and the temptations toward social bias in the negotiation process.

Lastly, it must be recognized that government policy decisions cannot create wealth; they simply transfer wealth from one economic sector (or stakeholder) to another. The top half of Table 21 provides an example of the economic transfer that resulted from a groundwater management decision made by the Edwards Aquifer Authority in Texas (McCarl et al, 1999). The promise of a positive transfer or the fear of a negative transfer can lead to a spirited adversarial climate in negotiating sessions.

Sometimes it is not wealth that is transferred but power. The lower half of Table 21 summarizes the sad result of an interagency power struggle over land subsidence issues in Bangkok, Thailand.

Table 1. Causes of land subsidence

Type	*Result*	*Cause*
Natural	• Compaction of surficial soils.	• Hydrocompaction of dry soils on initial wetting. • Compaction of organic soils on drainage.
	• Rapid local subsidence.	• Sinkholes in karst terrain. • Collapse features over salt.
	• Long-term regional subsidence.	• Compaction of basin sediments. • Tectonic influences.
Anthropogenic	• Rapid local subsidence due to subsurface mining.	• Collapse of underground coal mines, salt mines, limestone mines. • Impact of engineered underground openings such as tunnels.
	• Long-term regional subsidence due to withdrawal of fluids.	• Groundwater withdrawals. • Oil and gas production. • Geothermal development. • Mine dewatering.
Mitigating Factor	• Long-term regional impact on coastal environments.	• Sea-level rise due to global warming.

Table 2. Relative importance of causes of land subsidence

(a) Natural vs anthropogenic: Rates of relative subsidence (cm/year)

	Sea-level rise	*Natural sediment compaction*	*Subsidence due to fluid withdrawal*
Shangai, China (Hua et al, 1993)	0.10	0.04	0.32 – 0.45
Ravenna/Po Delta, Italy (Carbognin et al. 2000; Gambolati et al. 1999)	0.13	0.20 - 0.40	1.00 - 4.00
Global ranges[1]	0.00 – 0.50	0.00 – 0.50	0.00 – 10.00
Representative percentages	5%	5%	90%

[1]Rates concerning sea level rise refer to future tendencies

(b) Groundwater withdrawal vs oil-and-gas withdrawal

	Groundwater withdrawal	*Oil-and-gas withdrawal*
Ravenna/Po Delta, Italy (Gambolati et al, 1991)	Primary cause, regional influence, 1.30 m maximum	Secondary cause, restricted influence, 0.65 m maximum
Houston/Galveston, TX, USA (Holzer and Bluntzer, 1984)	Primary mechanism	Small contribution

Table 3. Inland and coastal subsidence environments

	Inland Environment	Coastal Environment
Hydrocompaction	Riverside County, USA	
Mining	Katowice Province, Poland West Midlands, England Appalachia, USA	
Oil-and-gas Production		Lake Maracaibo, Venezuela
Oil-and-gas Production and Groundwater Withdrawal		Ravenna/Po Delta, Italy Niigata, Japan Houston/Galveston, USA Wilmington/Long Beach, USA
Groundwater Withdrawal	Mexico City, Mexico Kanto Basin, Japan Kerman Province, Iran Bologna, Italy Utrecht, The Netherlands Santa Clara Valley, USA San Joaquin Valley, USA Las Vegas, USA El Paso, USA Eloy/Phoenix, USA	Venice, Italy Bangkok, Thailand Shanghai, China Taipei Basin, Taiwan Osaka, Japan Tokyo, Japan Hanoi, Vietnam Jakarta, Indonesia Thessaloniki, Greece
Geothermal Development	Wairakei, New Zealand Abano Terme, Italy	
Natural Sediment Compaction		Nile Delta, Egypt Bengal Delta, Bangladesh

Table 4. Impacts of land subsidence

	Impacts Experienced in both Inland and Coastal Environments	Additional Impacts Experienced in Coastal Environments
Environmental Impacts	• Differential land settlement. • Earth fissures, sinkholes, collapse features.	• Permanent inundation and loss of coastal lands. • More frequent flooding events due to storms, seiches, and high tides. • Loss of lagoonal ecosystems and habitat. • Saltwater intrusion into freshwater estuaries and aquifers. • Soil salinization.
Impacts to Engineered Structures	• Structural damage to buildings. • Alignment damage to lifts and sensitive machinery in buildings. • Damage to roads, bridges, culverts, and dams. • Buckling and shearing of pipelines and railways. • Loss of design gradients in canals, drains, water mains, and sewers. • Protusion, buckling and shearing of well casings for water supply wells and oil-and-gas production.	• Water damage from flooding events. • Structural damage to port and harbor facilities. • Structural damage to coastal protection works: seawalls, dikes, embankments, levees.

Table 5. Technical strategies for coping with land subsidence due to groundwater withdrawal: assessment and prediction

Phase	Activity	Issues
Assessment	• Vulnerability mapping.	• Availability of conceptual geologic model of area.
	• Monitoring: - Land elevations. - Water levels.	• Data collection protocols, chain of custody. • GIS data storage, retrieval, and interpretation.
Prediction	• Model development: - Hydrogeologic model. - Land subsidence model.	• Selection of appropriate model: - Analytical or numerical. - 2D or 3D. - Coupled or decoupled.
	• Model calibration.	• Availability of data: **- Calibration parameters: hydrogeologic properties.** - Calibration targets: land elevations, water levels.
	• Model application: - Range of scenarios. - Output suitable for socioeconomic decision-making.	• Coping with uncertainty: - In hydrogeologic data. - In future scenarios.

Table 6. Technical strategies for coping with land subsidence due to groundwater withdrawal: damage prevention

Phase	Activity	Issues
Damage Prevention: General	• Reduce pumping. • Resite pumping. • Repressure aquifers through artificial recharge.	• Determination of optimal pumping rates and locations. • Provision of alternative water supplies to users affected by reduced pumping. • Identification of source of recharge water (imported water, treated wastewater, captured runoff); selection of method of recharge (injection, spreading).
Damage Prevention: Coastal	• Flood protection: levees, seawalls, and dikes; drainage works and pumping stations; coastal polders.	• Determination of optimal locations, lengths, and heights of levees; pumping capacities of pumping stations; location, size, and dike heights for polders.
Damage Prevention: Urban	• Relocation of endangered buildings and facilities.	• Identification of endangered buildings; determination of acceptable alternative locations.
Damage Prevention: Canals	• Relocate canals to avoid subsiding areas. • Additional freeboard, reinforced concrete, more closely spaced check structures.	• Uncertainty in future gradients. • Selection of new canal route. • Determination of optimal freeboard heights.

Table 7. Socioeconomic strategies for coping with land subsidence due to groundwater withdrawal: management policies for groundwater control

Phase	Activity	Issues
Management Policies: Reduced Pumping	• Development of regional water-supply strategy.	• Optimal conjunctive use of groundwater and surface water. • Inclusion of land subsidence as driver in groundwater management strategy along with other drivers such as: - Water-table declines. - Saltwater intrusion. - Pump-and-treat control of existing contaminant plumes.
	• Establishment of regional groundwater management authority with power to control pumpage through: - Groundwater withdrawal permits. - Collection of permit fees and/or taxes on groundwater use. - Metering and direct control of pumping rates. - Enforcement of regulations through legal action.	• Development of political consensus to establish management authority with sufficient power to attain goals. • Optimization of water pricing structure to create desired use patterns. • Source of funding for administration of management authority. • Development of proper mix of economic and legal incentives and penalties. • Apportionment and recovery of costs of alternative water supplies.
Management Policies: Enhanced Recharge	• Inclusion of enhanced recharge in regional water management strategy.	• Apportionment and recovery of costs of recharge program.

Table 8. Socioeconomic strategies for coping with land subsidence due to groundwater withdrawals: management policies for land-use planning

Phase	Activities	Issues
Management Policies: Land-Use Planning	• Development of regional land-use plan.	• Inclusion of land subsidence as driver in land-use planning strategy along with other drivers such as: - Earthquake hazards. - Flooding hazards. - Protection of ecological habitat. - Minimization of service costs.
	• Resiting: - Pumping wells. - Endangered buildings and facilities.	• Apportionment of costs of resiting.
	• Zoning: - Groundwater-use exclusion zones. - Construction restrictions in subsiding areas. - Setback provisions from earth fissures, collapse zones.	• Compensation for landowners harmed by zoning decisions. • Generation of litigation.
Management Policies: Building Codes	• Guidelines for construction in areas of land subsidence.	• Gaining cooperation of construction industry. • Development of economic or legal incentives and penalties for meeting or not meeting guidelines. • Source of funding for enforcement of guidelines.

Table 9. Precedents from North America for management policy of controlled pumping

Location	*Reason for Controlled Pumping*	*Method*
Ville Mercier, PQ, Canada	To prevent health effects from drinking groundwater contaminated with organic chemicals from local waste-management site.	Provincial legislation establishing groundwater-use exclusion zone.
Sierra Vista, AZ, USA	To prevent decline in regional groundwater discharge to river valley which could lead to ecological damage to National Conservation Area.	Voluntary agreement between federal agencies, City of Sierra Vista, and private water companies, under threat of litigation from environmental groups.
San Fernando Valley, CA, USA	To ensure that groundwater withdrawals do not exceed aquifer safe yield, and to limit migration of contaminant plumes.	State-legislated Watermaster with legal authority to ensure safe yield not exceeded. Voluntary cooperation between Watermaster and USEPA to remediate contaminated aquifers.
Edwards Aquifer, TX, USA	To ensure that springflows from the aquifer will be maintained at rates that will sustain adequate streamflow for downstream ecological health and recreational use.	State legislation establishing groundwater management authority with mandate to reduce pumping to specific legislated rate.
Santa Clara Valley, CA, USA	To ensure that groundwater withdrawals do not exceed safe yield, to prevent saltwater intrusion, and to prevent land subsidence.	State legislated Water District with power to establish safe yield and allocate groundwater pumping rights. Overpumpers pay tax; underpumpers receive rebates.
Galveston, TX, USA	To prevent land subsidence.	State legislation establishing Coastal Subsidence District with power to regulate pumping.

Table 10. Precedents for land subsidence management strategies gleaned from management strategies used for the control of groundwater contamination in the USA

Objective	*Groundwater Contamination Management Strategy*	*Possible Land Subsidence Management Strategy*
Remediation of Historical Chemical Contamination from Industrial Plants and Waste Management Facilities	• Tax on chemical industry to feed a cleanup "Superfund". • Identification of contaminated sites, and "Potentially Responsible Parties" (PRPs) for each contaminated site. • Cost of remediation of contaminated sites paid from the Superfund, and from cost recovery from the PRPs achieved through voluntary assumption of cleanup costs, negotiation, and/or litigation. • Legal liability provisions that are "retroactive" and "joint-and-several".	• Tax on industries responsible for land subsidence. • Identification of parties responsible for specific cases of land subsidence. • Recovery of costs of damage prevention measures from responsible parties. • Development of strong liability doctrines for cases of land subsidence.
Prevention of Contamination from New Waste Management Facilities	• Legislated design standards. • Legislated system of facility permits. • Strong enforcement and heavy penalties for non-compliance with standards and permit conditions.	• Use of economic and legal incentives and penalties to promote policies that lead to reduced subsidence. • Enforcement of building codes to minimize impacts of subsidence.
Protection of Water-Supply Wells and Groundwater Aquifers	• Wellhead protection programs. • Capture-zone protection programs. • Recharge-area protection. • Sole-source aquifer programs.	• Controls on pumping. • Zoning and land-use measures to minimize impacts of land subsidence.

Table 11. Socioeconomic decision-making in the presence of land subsidence due to groundwater withdrawals: a list of the stakeholders

Category of Stakeholder	Stakeholders
Groundwater Pumpers	• Privately-owned water-supply companies. • Publicly-owned municipal water-supply systems. • Industrial users who provide their own supply. • Agricultural users who provide their own supply.
Groundwater Users Served by Private or Public Water Supply Systems	• Domestic users. • Industrial users. • Agricultural users.
Government Regulatory Authorities	• Water management authorities. • Land-use planning agencies. • Zoning commissions. • Building Code agencies. • Industrial development agencies. • Environmental impact agencies.
Parties Directly Impacted by Subsiding Lands	• Landowners and property developers of subsiding lands. • Residents of subsiding lands.
Parties Indirectly Impacted by Subsiding Lands	• Insurance companies holding liability policies and damage policies of landowners, developers, and residents of subsiding lands. • Environmentalists and environmental lobby groups.

Table 12. Examples of decisions faced by stakeholders in areas of land subsidence

Stakeholder	Objective	Alternative A	Alternative B
Private Water-Supply Company	Maximize profit.	Keep pumping at current rates at current locations; pay added taxes and/or fines; face possible litigation from regulatory agencies or parties impacted by land subsidence.	Reduce pumping rates at current locations; pay for development of alternate water supplies for current client base (new wells at more favorable locations, alternative sources, added conveyance costs).
Water Management Authority	Meet goals of enabling legislation at minimum cost.	Set maximum pumping rate for a particular wellfield at Q_1.	Set maximum pumping rate for a particular wellfield at Q_2.
		Set tax on groundwater use at \$X/litre.	Set tax on groundwater use at \$Y/litre.
		Set fine for noncompliance at \$X/day.	Set fine for noncompliance at \$Y/day.
		Apportion budget at X_1% administration, Y_1% enforcement.	Apportion budget at X_2% administration, Y_2% enforcement.
Land-Use Planning Agency in Coastal Environment	Maximize social benefit; minimize social cost.	Allow continued subsidence; pay for new or improved coastal seawall system to protect coastal land.	Set policies that will lead to reduced pumping; establish government compensation program to help affected water producers.
		If Alternative A selected, design coastal seawall height at X metres.	If Alternative A selected, design coastal seawall height at Y metres.
Landowner of Undeveloped Coastal Subsiding Land	Maximize return (or minimize loss) on property investment.	Try to sell land to government for more appropriate coastal land use (eg. parkland, ecological preserve)	Identify PRPs of land subsidence; sue them for lost property value.

Table 13. Decision analysis for a single stakeholder

Objective	Choose between a finite number of alternative courses of action.
Objective Function	Maximize Z_j over alternatives j = 1, ... J, where: $$Z_j = \{1/(1+d)^t\} \sum_{t=0}^{T} [\, B_j(t) - C_j(t) - R_j(t) \,]$$
Definition of Terms	Z_j = objective function for alternative j [$] = net present value (NPV) of all benefits, capital costs, operational costs, and risk costs d = discount rate [decimal fraction] T = time horizon [years] $B_j(t)$ = benefits of alternative j in year t [$] $C_j(t)$ = capital costs and operational costs of alternative j in year T [$] $R_j(t)$ = risk costs of alternative j in year t [$] $= CF_j(t) \bullet PF_j(t)$ $CF_j(t)$ = cost associated with failure of alternative j in year t [$] $PF_j(t)$ = probability of failure of alternative j in year t [$]
Technical Input	$PF_j(t)$
Socioeconomic Input	$B_j(t)$, $C_j(t)$, $CF_j(t)$, d, T

Table 14. Land subsidence due to groundwater withdrawals: examples of benefits, costs, and risk costs

Decision Maker	*Benefits*	*Capital Costs and Operational Costs*	*Risk Costs Associated with Land Subsidence*
Ground-water Pumper	• Income generated from sale of water.	• Cost of wellfield, pumping, and delivery system.	• Taxes or fines from government regulatory authority. • Litigation from parties impacted by subsiding lands. • Cost of resiting wellfield, or finding alternative supply.
Parties Impacted by Subsiding Lands	• Compensation received from government regulatory authority. • Settlements from litigation.	• Cost of technical consulting. • Cost of lobbying for compensation • Cost of litigation.	• Remedial costs. • Cost of resiting facilities. • Decreased property values. • Psychological costs.
Govern-ment Land-Use Planning Agency	• Social benefits associated with land-use management policies (total economic value to industry, agriculture, tourism, etc.)	• Cost of construction and operation of public damage prevention works (if any).	• Social costs associated with failure of management policies (total economic loss due to physical damage, loss of agricultural production, impact on tourist industry, etc.)
	• Income from permits, taxes, and fines. • Settlements from litigation.	• Cost of administering management policies. • Cost of litigation.	• Cost of compensation of impacted parties.

Table 15. Estimates of costs associated with land subsidence (all costs converted to year 2000 $ US, using us department of labor historical consumer price index, and published currency conversion tables).

Type of Cost	Site	Reference	Details	NPV
Actual past damages	Long Beach, CA, USA	Poland/ Davis (1969)	Flood damage, structural damage.	$500 million
	San Joaquin Valley, CA, USA	Proko-povich (1986)	Rehabilitation of existing canals, design modification of new canals.	$120 million
	Bangkok, Thailand	Sabhasri/ Suwarnarat (1996)	Flood damage.	$160 million/ event
	Katowice Province, Poland	Liszkowski (1991)	Structural damage, property loss, due to mining subsidence.	$0.5 million/ year
	USA	National Research Council (1991)	Total annual loss.	$500 million/ year
Predicted future damages if no damage-prevention activities undertaken)	Shanghai, China	Hua et al (1993)	Flood damage due to overtopping of protective flood-control wall.	$1.78 billion/ event
	Bengal Delta, Bangladesh	Broadus (1996)	Loss of coastal land by year 2050 due to 144 cm natural land subsidence.	$550 million
	Nile Delta, Egypt	Broadus (1996)	Loss of coastal land by year 2050 due to 144 cm natural land subsidence.	$320 million
	Marker-waard, The Netherland	Caree and Hulsbergen (1986)	Construction damage (70%), legal costs (15%), government administrative costs (15%)	$508 million

Table 15. *Continue.*

Type of Cost	Site	Reference	Details	NPV
Proposed future damage prevention activities	Bangkok, Thailand	Sabhasri/ Suwarnarat (1996)	Dikes, canal improvements, pump stations.	$297 million capital costs + $10 million/ year operating costs
	Pennsyl-vania, USA	Gray/Bruhn (1984)	Stabilization of 400,000 acres urban land above abandoned mines.	$32.5 billion
	The Nether-lands	De Ronde (1996)	Direct shoreline protection (60%), water management (30%), harbors, locks, and bridges (10%)	$5.8 billion
Actual past legal claims	Riverside County, CA, USA	Corwin et al (1991), Shlemon (1995)	Plaintiffs: over 200 homeowners on land impacted by fissures perhaps caused by land subsidence due to groundwater pumping. Defendants: land developers, home builders, geotechnical consultants, permit agencies.	Claim: $50 million Settlement: $10 million
	Galveston Bay, TX, USA	Carpenter/ Bradley (1986)	Plaintiffs: owners of subsiding land. Defendants: groundwater pumping company.	Claim: Not specified. Settlement: $0

Table 16. Example of risk calculation: Ravenna/Po Delta, Italy (CENAS, 1997)

Definition of Risk	R(t) = PF(T,t) • CF(T) [$]
Definition of Terms	PF(T,t) = probability that flood event of return period, T, will occur once during a specified time interval, t [decimal fraction] CF(T) = cost associated with flood event of given return period, T = E(T) • V(h) E(T) = economic value of land flooded by event of return period, T (based on historical flood analysis and land-use mapping) [$] V(h) = vulnerability of flooded land to damage (assumed proportional to floodwater elevation, h, where h is in turn controlled by amount of land subsidence) [decimal fraction]
Output	Normalized risk maps (R = 0 → 100) for a variety of scenarios
Scenarios	• Specified time intervals: to Year 2050, to Year 2100 • Flood event return periods: 1, 10, 100 years • Land-subsidence scenarios: optimistic, pessimistic (as determined by predictions of subsidence from a quasi-coupled numerical groundwater/land-subsidence model)

Table 17. Examples of risk-cost-benefit calculations
(All costs converted to Year 2000 $US, using US Department of Labor historical consumer price index, and published currency conversion tables.)

SHANGHAI, CHINA (Hua et al, 1993)
Decision-maker: Government disaster-prevention authority.
Objective function: Social risk-cost minimization.
Background: An existing flood-control wall is to be reinforced and raised to an elevation of 6.9 m for a distance of 100 km along the banks of the Huangpu River. The probability of overtopping the wall during high-tide/storm events depends in part on the rate of future land subsidence.
Alternative land-subsidence policies:
(A) No action with respect to land subsidence, which continues to occur at a rate of 0.32-0.45 cm/year.
(B) Total control of land subsidence through tightly-enforced pumping/recharge policies.

	Alternative A	*Alternative B*
Capital costs of raising and reinforcing flood control wall to elevation 6.9 m	$219 million	$219 million
Capital costs of establishing land-subsidence control program	0	$223 million
Annual costs of maintaining flood control wall	$0.2 million	$0.2 million
Annual costs of land-subsidence control program	0	$0.32 million
Probability of flooding in a given year	0.005	0
Remedial costs per flood event	$1.78 billion	0

If we make the simplifying assumption that the appropriate discount rate equals the inflation rate, then Alternative B is superior to Alternative A for all time horizons exceeding about 25 years.

Table 17. *Continue.*

WEST MIDLANDS, ENGLAND (Whitaker and Reddish, 1989; Brook, 1991)
Decision –maker: Government authority. Objective function: Social benefit-cost-risk maximization. Background: Land subsidence has occurred over abandoned limestone mines in an 486 ha area with a population of 9000 and property values estimated at $247 million. There is a probability of "some" damage to 31% of the buildings in the impacted area, and a probability of "appreciable, severe, or very severe" damage to 1% of the buildings. Solving the problem would lead to an estimated 11% increase in property values in the impacted area. Alternative remedial policies: (A) Relocation of surface development. (B) Infilling of one large mine considered to be most significant. (C) Inducing controlled subsidence at the same mine. (D) Compensation to affected parties for damage repair.

	Alternative A	Alternative B	Alternative C	Alternative D
Benefits: increase in property values	0	$27 million	$27 million	$27 million (or less?)
Costs: remedial costs	$27-32 million	$35 million	$15-17 million	0
Risks: compensation costs	0	0	0	$5.0-7.5 million

Alternative D selected.

Table 18. Issues and difficulties associated with the application of decision analysis to decisions involving land subsidence

Feature	Issues and Difficulties
Appropriateness of decision-analysis framework	• Ethical appropriateness of trying to fit all aspects of decision-making into an economic framework. • Political acceptance of results.
Objective function	• Suitability of the maximum utility framework. There are many other possibilities (eg. minimize maximum loss).
Non-economic entities	• How to place an economic value on the protection of human life, health, well-being, and freedom from stress. • How to put an economic value on the protection of coastal lands, ecological habitat, and human recreational land-use.
Discount rate	• How to define an appropriate discount rate for the calculation of the net present value of future risk costs: market interest rate, social discount rate, or zero discount rate.*
Cross-sector and intergenerational equity	• How to ensure that the economic sectors that get the benefits of water and oil production also bear the costs of any land subsidence that is generated. • How to ensure that the liabilities associated with land subsidence are not transferred to future generations.
Multiple stakeholders	• Decision analysis may be appropriate for a single decision-maker, but it does not provide a framework for integrating the preferences of multiple stakeholders with diverse interests. • Multiple-stakeholder scenarios are zero-sum games, that often lead to conflict, which if not resolved, can lead to management gridlock.

* See Broadus (1996), for example, where it is shown that the impact of coastal flooding from 92.4 cm subsidence by year 2075 in Galveston, TX, USA, would have a net present value of $555 million at a discount rate of 3%, but only $10 million at a discount rate of 10%.

Table 19. Reaching consensus in multiple stakeholder scenarios

Aspect	Issues and Methods
Decision-making environment	• Cooperative. • Adversarial.
Sources of adversarial conflict	• Over facts. • Over assumptions. • Over interpretations. • Over values. • Over biases. • Over personalities.
Differences between parties in an adversarial decision-making environment	• Different and often conflicting objectives. • Different perceptions of the economic value of the benefits and costs associated with the available alternative courses of action. • Different perceptions of the inherent uncertainties, the probabilities of failure, the consequences of failure, and the risk costs associated with the available alternative courses of action. • Different assumptions with respect to discount rates and time horizons. • Different value systems with respect to environmental protection, intergenerational equity, acceptable risk, appropriateness of governmental intervention in the marketplace, etc.
Approaches to multiple-stakeholder decision-making	• Imposed powerbroking by most powerful party. • Negotiation with or without mediation. • Negotiation with binding arbitration. • Adversarial litigation in the courts.
Multiple-stakeholder extension of decision analysis	• Conflict Analysis: Each party uses a decision-analysis framework to set up a preference vector that ranks the available alternative courses of action from most-acceptable to least-acceptable. A mediator helps parties search for "stable" compromise solutions among the many preference vectors.
Roadblocks to consensus	• Technical uncertainty. • Social bias.

Table 20. Roadblocks to consensus

(a) Some sources of technical uncertainty

Data	Over the accuracy of measurements.
	Over the representativeness of measurements.
	Over the worth of additional data.
Interpretation of the Data	Interpretation of geological environment.
	Interpretation of groundwater flow system.
	Interpretation of extent of land subsidence.
Physical Processes	Nature of coupling between groundwater flow and land subsidence.
Performance of Engineered Remediation	Effectiveness of controlled pumping and/or aquifer repressuring in controlling land subsidence.

(b) Examples of social bias

Cognitive Bias: negotiator's conscious beliefs do not reflect available information	Anchoring: insufficient adjustment of initial estimates in light of new information.
	Personal bias: tendency to weight an event that has personal significance too heavily.
Motivational Bias: negotiator's statements and conscious beliefs are inconsistent	Management bias: interpretations biased toward client's wishes.
	Group dynamics bias: the desire to please a dominant leader.
	Personal benefit bias: due to personal reward structure.
	Conservative bias: err on the safe side.
Bias due to Values	Utilitarian: maximizes sum of individual costs and benefits.
	Egalitarian: desire to protect the least well-off in society.
	Libertarian: emphasis on individual rights.
Bias due to Personality Conflict	

Table 21. Complexities of multiple stakeholder scenarios

Issue	Details
Zero-Sum Effect (Transfer of wealth from one economic sector to another by policy decisions) ***Example: Edwards Aquifer, TX, USA (McCarl et al, 1999)***	• Texas Senate Bill 1477 established Edwards Aquifer Authority (EAA) to manage groundwater in aquifer. • Bill was passed in response to lobbying from environmentalists to maintain historical springflows at several large springs that discharge from the aquifer in order to protect endangered species; and from recreational users who wish to maintain downstream streamflow for fishing and other recreational use. • EAA mandated to apportion remaining safe yield between agricultural users, municipal users, and industrial users. Apportionment has resulted in 18.7% reduction in total agricultural income. • Economic studies show that springflow maintenance is economically justifiable only if it has value greater than $1.1 million per year. • Zero-sum result: Texas Bill 1477 has transferred wealth from farmers to environmentalists and recreational users.
Management Gridlock ***Example: Bangkok, Thailand (Bangkok Post, 14/02/99)***	• Flooding events are exacerbated by land subsidence. • Damage estimates: $160 million per event. • Previous policies aimed at reducing groundwater pumping have been ineffective because the cost of alternative water supplies for industrial users is six times that of pumped groundwater. • Mineral Resources Department (MRD) of the Industry Department has proposed to spend $135 million on 50 injection stations to arrest land subsidence. • Office of Environmental Policy and Planning of the Science, Technology and Environment Ministry opposes MRD plan without further studies. • Provincial Waterworks Authority (PWA) has proposed that industrial users within its service area be prohibited from pumping groundwater, and forced to use its higher-priced water. • Federation of Thai Industries opposes PWA plan. • Result has been interagency gridlock and no action.

REFERENCES

The references have been divided into two groups. The first group comprises the general sources, primarily in the form of symposia proceedings. These books include many case histories that treat the amount and extent of subsidence at various sites around the world, the causes and mechanisms of subsidence, the impacts of subsidence, and the strategies used for prevention and remediation. The second group highlights specific research papers of interest. Many of the references from both groups are cited directly on specific tables. Those that are not cited individually were used to develop Tables 1, 3, 4, 6, 7, 8, 11, and 14.

GENERAL SOURCES

Barends, F.B.J., F.J.J. Brouwer and F.H. Schroder, editors (1995) *Land Subsidence,* Proceedings Fifth International Symposium on Land Subsidence, The Hague, The Netherlands, IAHS Publication No. 234.

Borchers, J.W., editor, (1998) *Land Subsidence Case Studies and Current Research*, Proceedings of the Dr. Joseph F. Poland Symposium on Land Subsidence, Association of Engineering Geologists, Special Publication No. 8.

Carbognin L. (1985) Land Subsidence: a worldwide environmental hazard. *Nature and Resouces,* XXI, 1, 1-12.

Chilingarian, G.V., E.C. Donaldson and T.F. Yen, Editors (1995) *Subsidence Due to Fluid Withdrawal*, Elsevier.

Johnson, A.I., Editor (1977) *Land Subsidence*, Proceedings Second International Symposium on Land Subsidence, Anaheim, California, IAHS Publication No. 121.

Johnson, A.I., Editor (1991) *Land Subsidence,* Proceedings Fourth International Symposium on Land Subsidence, Houston, Texas, IAHS Publication No. 200.

Johnson, A.I., L. Carbognin and L. Ubertini, Editors (1986) *Land Subsidence*, Proceedings Third International Symposium on Land Subsidence, Venice, Italy, IAHS Publication No. 151.

Holzer, T.L., Editor (1984) *Man-Induced Land Subsidence*, Geological Society of America, Reviews in Engineering Geology, **6**.

Milliman, J.D. and B.U. Haq, Editors (1996) *Sea-Level Rise and Coastal Subsidence: Causes, Consequences, and Strategies*, Kluwer Academic Publishers.

Poland, J.F. and G.H. Davis (1969) Land Subsidence Due to Withdrawal of Fluids, Geological Society of America, *Reviews in Engineering Geology*, **2**, 187-269.

Poland, J.F., Figueroa Vega G., Carbognin L., Johnson A. I., & Yamamoto S. (1994) *Guidebook to studies of land subsidence due to ground-water withdrawal,* Ed. by *UNESCO,* Paris, France, J.F. Poland Chairman and Editor, 305 p. and Appendices A-E.

Saxena, S.K., editor (1979) *Evaluation and Prediction of Subsidence*, Proceedings International Conference on Evaluation and Prediction of Subsidence, Pensacola Beach, Florida, American Society of Civil Engineers.

Tison, L.J., editor (1970) *Land Subsidence*, Proceedings First International Symposium on Land Subsidence, Tokyo, Japan, IAHS Publication No. 88.

Waltham, A.C. (1989) *Ground Subsidence*, Chapman and Hall.

Whittaker, B.N. and D.J. Reddish (1989) *Subsidence: Occurrence, Prediction and Control*, Elsevier.

RESEARCH PAPERS

Broadus, J.M. (1996) Economizing human responses to subsidence and rising sea level, in *Sea-Level Rise and Coastal Subsidence: Causes, Consequences, and Strategies*, edited by J.D. Milliman and B.U. Haq, 313-325.

Brook, D. (1991) Abandoned limestone mines in the West Midlands of England: A strategy for action, in *Land Subsidence*, IAHS Publication 200, 215-222.

Carbognin L., Cecconi G. & Ardone V. (2000) Interventions to safeguard the environment of the Venice Lagoon (Italy) against the effects of land elevation loss, in *Land Subsidence,* Vol. I, Proc. Sixth Int. Symp. on Land Subsidence, Ravenna, Italy, Eds. L. Carbognin et al., 304-324.

Caree, G.J. and J.G. Hulsbergen (1986) A method for estimating building damage in subsiding areas, in *Land Subsidence*, IAHS Publication 151, 907-914.

Carpenter, M.C. and M.D. Bradley (1986) Legal perspectives on subsidence caused by groundwater withdrawal in Texas, California and Arizona, USA, in *Land Subsidence*, IAHS Publication 151, 817-829.

Commission of the European Communities Directorate (CENAS) (1997) *Study on the Coastline Evolution of the Eastern Po Plain due to Sea Level Change Caused by Climate Variation and to Natural and Anthropic Subsidence, 345 pp.*

Corwin, E.J., S.C. Alhadeff, S.P. Oggel and R.J. Shlemon (1991) Earth fissures, urbanization and litigation, A case study from the Temecula area, southwestern Riverside County, California, in *Land Subsidence*, IAHS Publication 200, 291-299.

de Ronde, J.G. (1996) Man-made projects and relative sea-level rise, in *Sea-Level Rise and Coastal Subsidence: Causes, Consequences, and Strategies*, edited by J.D. Milliman and B.U. Haq, 327-342.

Gambolati, G., G. Ricceri, W. Bertoni, G. Brighenti and E Vuillermin (1991) Mathematical simulation of the subsidence of Ravenna, *Water Resources Research,* **27**, 2899-2918.

Gambolati, G., P. Teatini, L. Tomasi and M. Gonella (1999) Coastline regression of the Ravenna region, Italy, due to natural and anthropogenic land subsidence and sea level rise, *Water Resources Research*, **35**, 163-184.

Gray, R.E. and R.W. Bruhn (1984) Coal mine subsidence – eastern United States, Geological Society of America, *Reviews in Engineering Geology*, **6**, 123-149.

Henley, A.T. (1986) Land subsidence in a California county: The legal issues, in *Land Subsidence*, IAHS Publication 151, 853-862.

Holzer, T.L. and R.L. Bluntzer (1984) Land subsidence near oil and gas fields, Houston, Texas, *Ground Water,* **22**, 450.

Hua, Z., L. Tiezhu and L. Xinhong (1993) Economic benefit-risk assessment of controlling land subsidence in Shanghai, *Environmental Geology,* **21**, 208-211.

Liszkowski, J. (1991) Engineering and environmental impacts caused by land subsidence due to subsurface extraction of solid raw materials from Poland, in *Land Subsidence*, IAHS Publication 200, 369-377.

McCarl, B.A., C.R. Dillon, K.O. Keplinger and R.L. Williams (1999) Limiting pumping from the Edwards Aquifer: An economic investigation of proposals, water markets, and springflow guarantees, *Water Resources Research*, **35**, 1257-1268.

Prokopovich, N.P. (1986) Economic impact of subsidence on water conveyance in California's San Joaquin Valley, USA, in *Land Subsidence*, IAHS Publication 151, 795-803.

Sabhasri, S. and K. Suwarnarat (1996) Impact of sea level rise on flood control in Bangkok and vicinity, in *Sea-Level Rise and Coastal Subsidence: Causes, Consequences, and Strategies*, edited by J.D. Milliman and B.U. Haq, 343-356.

Sandoval, J.P. and S.R. Bartlett (1991) Land subsidence and earth fissuring in the Central Arizona Project, in *Land Subsidence,* IAHS Publication No. 200, 249-260.

Sato, K. and N.V. Hoang (1995) Recent countermeasures for land subsidence and groundwater resources in Japan, in *Land Subsidence,* IAHS Publication 234, 471-479.

Shlemon, R.J. (1995) Groundwater rise and hydrocollapse: technical and political implications of "Special Geologic Report Zones" in Riverside County, California, USA, in *Land Subsidence,* IAHS Publication 234, 481-485.

Snelting, H. and A.J. van Bruchem (1986) The role of land subsidence and damage to buildings in the selection of suitable sites for groundwater extraction, in *Land Subsidence*, IAHS Publication 151, 767-776.

U.S. National Research Council (1991) *Mitigating Losses from Land Subsidence in the United States*, National Academy Press, 58 pp.

Yokel, F.Y. (1979) Guidelines for housing construction in mine subsidence areas, in *Evaluation and Prediction of Subsidence*, edited by S.K. Saxena, 129-139.

ISBN 88-87222-06-1

LAND SUBSIDENCE

Vol. II

PROCEEDINGS OF THE SIXTH INTERNATIONAL SYMPOSIUM ON LAND SUBSIDENCE
RAVENNA / ITALIA / 24 - 29 SEPTEMBER 2000

LAND SUBSIDENCE

Vol. II

Measuring and Monitoring
Theory and Modeling

Edited by

LAURA CARBOGNIN
GIUSEPPE GAMBOLATI
A. IVAN JOHNSON

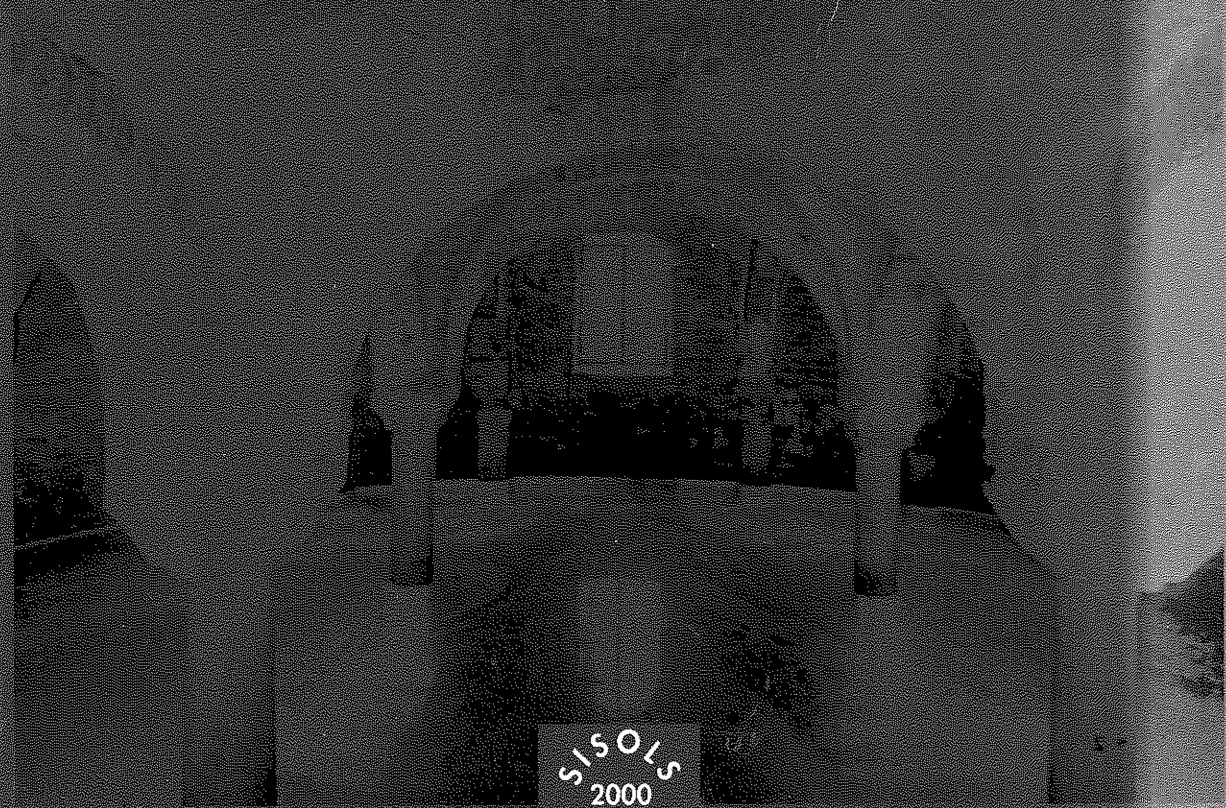

SISOLS 2000

PROCEEDINGS OF THE SIXTH INTERNATIONAL SYMPOSIUM ON LAND SUBSIDENCE

RAVENNA / ITALIA / 24 - 29 SEPTEMBER 2000

LAND SUBSIDENCE

Vol. II

Measuring and Monitoring
Theory and Modeling

Edited by

LAURA CARBOGNIN
National Research Council, ISDGM, Venezia, ITALY

GIUSEPPE GAMBOLATI
University of Padova, DMMMSA, Padova, ITALY

A. IVAN JOHNSON
Arvada CO, USA

C. N. R.
National Group for the Pretection Against Hydrogeologic Catastrophies provided financial sponsorship for this publication.

Cover:
Ravenna, the Crypt of San Francesco's Church flooded.

The camera-ready copy for the papers was prepared by the authors and improved and completed at the C.N.R., - Istituto per lo Studio della Dinamica delle Grandi Masse (by Laura Carbognin and Jane Frankenfield Zanin), S. Polo 1364, 30125 Venice, Italy. Neverthless, in some cases, it was difficult to improve the quality of figures submitted by authors.

Printed by
"La Garangola", Via Montona, 4 - 35137 Padova, Italy
ISBN 88-87222-06-1

In honor of many years of research in land subsidence and very active participation in the UNESCO-IHP Working Group on Land Subsidence, this proceedings volume is dedicated to Doctor Laura Carbognin

This dedication provides high praise and Working Group recognition to Laura Carbognin for her long and dedicated participation in research, teaching, and writing about the subject of land subsidence during her activities with the UNESCO - IHP Working Group on Land Subsidence as well as during her position with the National Research Council of Italy (CNR).
Although the First International Symposium on Land Subsidence was convened in 1969, The UNESCO - IHP Working Group on Land Subsidence was not formally established until 1974 as one of the objectives of UNESCO's International Hydrological program (IHP-I). At that time Doctor Laura Carbognin was selected as a member of that Working Group and remained active in its affairs ever since. She assisted with the organization of all five UNESCO -sponsored subsidence symposia, and was local organizer of the Third edition convened in 1984 in Venice, and co-editor of the proceedings volume (published as IAHS Publication No. 151) resulting from that symposium. Laura also chaired this Sixth Symposium (SISOLS 2000) and is senior editor of the resulting proceedings.
Up to now Laura Carbognin has served for 31 years on the staff of the CNR at the Istituto per lo Studio della Dinamica delle Grandi Masse (ISDGM), where she joined the research staff in 1970 to work in the field of geostatistics. Presently, in the ambit of CNR, she is Director of Research.
During her career Laura had the responsibility for research concerning the understanding of environmental problems mainly related to land subsidence and coastal processes, especially for the lagoon of Venice and the North Adriatic Sea. Studies she and her colleagues performed, the first in Italy, on the subsidence in Venice and Ravenna, and on the environmental impact of this process, are of primary importance and of international interest. Within the framework of the ISDGM research activity, Laura has been involved in scientific studies concerning geomorphology, micropaleontology, water pollution, flooding and eustacy. In particular, the study on sea level rise made through a series of statistical analyses, partly original, has permitted definition of the eustatic trend for the last century, filtering out the influence of land subsidence during its occurrence.
For her innovating statistical approaches to environmental problems, she has received international recognition in the book "Italian Contributors to the Methodology of Statistics", 1987. In addition to her research career, she has dedicated herself to training young scientists specializing in land subsidence studies, teaching courses and organizing national and international schools.
Laura Carbognin has been a prolific author of papers and reports, many of which have been on the subject of land subsidence.
In recognition of her scientific accomplishments, and because of her devoted participation and achievements in the activities of the UNESCO - IHP Working Group on Land Subsidence and its sponsored symposia, this proceedings volume resulting from the SISOLS 2000 of Ravenna, Italy is dedicated with great respect and appreciation to Laura Carbognin.

A. Ivan Johnson
Chairman, UNESCO-IHP W.G. on Land Subsidence

The Organizing Committee would like to express their appreciation to the many people who gave their time, effort and knowledge to produce a successful programme and enjoyable field trip.

The collaboration of the Scientific Advisory Board and the Local Working Committee is gratefully acknowledged.

Special thanks go to Mrs. Jane Frankenfield Zanin who provided the technical scientific secretarial job needed for the symposium and invaluable assistance in the publication of this proceedings volume.

The Editors would also like to express their thanks for the sponsorship and endorsement provided for the symposium by the following organizations and companies.

Sponsoring Organizations:

UNESCO

CNR (National Research Council of Italy)

ANPA (National Agency for the Protection of the Environment)

ARPA (Emilia Romagna Regional Agency for the Protection of the Environment)

ASSOMINERARIA

CVN (Consorzio Venezia Nuova)

Emilia-Romagna Regional Government

ENI-Agip

GNDCI (National Group for the Protection against Hydrogeologic Catastrophes)

IHP (International Hydrological Programme)

MED-Ingegneria

Municipality of Ravenna

NGC (Netherlands Geodetic Commission)

Romagna Acque

Solvay Chimica Italia S.p.A.

University of Ferrara

University of Padova

Endorsing Organizations:

IAHS / ICGW (International Association of Hydrological Sciences / International Commission on Ground Water)

AGID (Association of Geoscientists for International Development)

IAH (International Association of Hydrogeologists)

ISSMGE (International Society for Soil Mechanics and Geotechnical Engineering)

Ministry of Industry, Trade, and Handicraft of Italy

Ministry of the Environment of Italy

Organizing Committee

Laura Carbognin - Symposium Chairman
National Research Council, ISDGM, Venezia, Italy

Giuseppe Gambolati - Symposium Co-chairman
University of Padova, DMMMSA, Padova, Italy

A. Ivan Johnson, Chairman, UNESCO Working Group
Arvada, CO, USA

Scientific Advisory Board

James W. Borchers, U.S. Geological Survey, Sacramento, CA (USA)

Frans B.J. Barends, Delft Geotechnics, Delft, The Netherlands

Gianluigi Chierici, University of Bologna, Bologna, Italy

German E. Figueroa Vega, Coordinacion General de Los Proyectos de Abastecimiento de Agua Potable y Saneamiento del Valle de México, Mexico D.F.

Donald Helm, Morgan State University, Baltimore, MD, USA

Keith Prince, U.S. Geological Survey, Menlo Park, CA, USA

Francis Riley, U.S. Geological Survey, Menlo Park, CA, USA

Abdin M.A. Salih, Hydrological Sciences & Ecology, UNESCO, Cairo, Egypt

Andras Szollosi-Nagy, Director, Division of Water Resources, UNESCO, Paris, France

Local Working Committee

Alice Aureli, Division of Water Resources, UNESCO, Paris, France

Werther Bertoni, Geological Survey, Municipality of Ravenna, Ravenna, Italy

Giovanni Brighenti, University of Bologna, Bologna, Italy

Roberto D'Amico, ENI-Agip, Ravenna, Italy

Giancarlo Dossena, Assomineraria, Roma, Italy

Marco Gonella, MED-Ingegneria, Ferrara, Italy

Francesco Marabini, CNR-IGM, Bologna, Italy

Raffaele Pignone, Geological Survey, Emilia-Romagna Region, Bologna, Italy

Paolo Russo, University of Ferrara, Ferrara, Italy

Leonello Serva, ANPA, Roma, Italy

Pietro Teatini, University of Padova, Padova, Italy

Luigi Tosi, CNR-ISDGM, Venezia, Italy

Lucio Ubertini, Chairman, IHP National Committee, Perugia, Italy

Adriano Zavatti, ARPA, Bologna, Italy

Scientific Secretariat

Mrs. Jane Frankenfield Zanin, CNR-ISDGM, Venezia, Italy

CONTENTS

Vol. II

1 Measuring and Monitoring

2 Theory and Modeling

Vol. I

1 Geological Issues

2 Fluid removal

3 Solid extraction

4 Remedies - Decision Making

Preface

Since the 1950s, there has been an ever increasing global awareness of problems related to the sinking of the land surface. The efforts by the scientific community were directed toward furthering the understanding and knowledge on both natural and anthropogenic causes, field and lab measurements, mechanisms, prediction techniques, effects and remedial measures. In the course of time, man realized that he could no longer follow a "use and discard" philosophy with underground resources. As a result, a need for a consistent policy of rational management of underground resources became evident. The seriousness of land subsidence was recognized by the United Nations Educational, Scientific and Cultural Organization (UNESCO) in 1969, when this problem was first included for study under the International Hydrological Decade (IHD), and later the International Hydrological Programme (IHP). This resulted in the organization of six International Symposia on Land Subsidence jointly sponsored by UNESCO, the International Association of Hydrological Sciences (IAHS), and other International and National Organizations that were held in 1969; 1976; 1984; 1991; 1995; and the Sixth International Symposium on Land Subsidence (SISOLS) in Ravenna, Italy in 2000.

SISOLS 2000 aimed to gather together members of the Scientific Community to review the advances achieved in the field of land subsidence, to present new research ideas, to exchange experiences, and to discuss a *sustainable approach* to land subsidence, intended to seek a compromise between the use of natural resources and mitigating negative effects caused by their exploitation. Issues include: the sustainable development of subsurface resources which may induce land subsidence, distinguishing natural subsidence from the anthropogenic one, predicting potential hot spots, in particular those located in coastal and low-lying flat areas, new monitoring techniques and advanced computer models to control and predict land subsidence phenomena. It is now recognized that decisions with respect to preventive or remedial land-subsidence strategies take place in a complex decision-making milieu in which there are many potentially-adversarial stakeholders. Negotiated settlements among these stakeholders depend on the results of technical analysis, but are heavily influenced by social, economic, legal, and political issues. The SISOLS 2000 program highlights the need for the integration of social policies that address resource management, land-use planning, industrial development, hazard mitigation, and environmental protection.

From the large number of contributions received, 68 have been selected and published in two separate proceeding volumes as follows:

Symposium topic	*Proceedings volume*
Geological issues	Volume I
Fluid removal	Volume I
Solid extraction	Volume I
Remedies - decision making	Volume I
Measuring and monitoring	Volume II
Theory and modeling	Volume II

The symposium was hosted by the Municipality of Ravenna at the beautiful Alighieri Theater inaugurated in 1852 in commemoration of the famous Italian poet Dante Alighieri (1265-1321) who is buried in Ravenna.

The one-day technical-environmental excursion to the Po Delta area, the largest expansion of land sinking in Italy, gave participants a chance to see and to visit one of the many beautiful natural reserves of Italy rich in flora and avifauna. The ENI-Agip Division contributed to making the trip possible through its sponsorship.

On Thursday afternoon, September 28, many representatives from local, regional, national and private agencies participated in the Round Table on problems connected with land subsidence problems in Italy.

Laura Carbognin
Symposium Chairman, National Research Council of Italy (CNR), Venezia, Italy

Giuseppe Gambolati
Symposium Co-chairman, University of Padova, Padova, Italy

A. Ivan Johnson
Chairman, UNSECO/IHP W.G. on Land Subsidence, Arvada, CO, USA

September, 2000

1 Measuring and Monitoring

TOWARDS A RECONCILIATION BETWEEN LABORATORY AND IN-SITU MEASUREMENTS OF SOIL AND ROCK COMPRESSIBILITY

G. Cassiani[1] and C. Zoccatelli[2]
[1]*Department of Environmental Science, Lancaster University, UK*
[2]*Eni, Divisione Agip, Milan, Italy*

Abstract

Soil and rock compressibility is the chief parameter governing compaction of sediments under changes in their stress state, induced for instance by fluid withdrawal. All modelling efforts aimed at predicting compaction, and the consequent surface subsidence, invariably face the question of what is the value of compressibility of the depleted reservoirs, let alone values of elastic and plastic moduli of the over-burden, side-burden and under-burden. Two pathways are available for measuring this parameter, namely: (a) laboratory measurements, via oedometric and/or triaxial tests; and (b) in-situ measurements, using the radioactive markers technique. In the authors' experience, the data derived by both techniques are often found to differ by orders of magnitude, especially in the case of unconsolidated sediments. This is a clear problem for the prediction of compaction and subsidence. Laboratory measurements provide evidence of the characteristics of the sediments before the actual pressure depletion takes place. In this regard, they are fundamental. However, laboratory measurements have a consistent tendency at overestimating soil compressibility, if compared to the evidence from in-situ measurements. Bridging this conceptual and practical gap is not an easy task. In this paper, new evidence from careful laboratory experiments, in situ measurements and subsidence simulation is brought together to show how the apparent inconsistencies are progressively resolved in a unitary explanatory framework.

Keywords: oedometric measurements, triaxial measurements, soil compressibility, radioactive markers, ageing, finite element models.

1. INTRODUCTION

The control of subsidence caused by fluid extraction has been one of the key environmental priorities for the Italian oil industry over the past thirty years. Subsidence prediction is an essential step in any sound technical or industrial procedure aimed at controlling this phenomenon. Other fundamental steps involve monitoring of actual subsidence, and prevention, e.g. by water injection, whenever feasible and necessary. In particular, modelling is the only tool that can provide answers in terms of future behaviour of gas fields planned for new development. As such, this tool has been extensively used [e.g., Geertsma and van Opstal, 1973; Gambolati et al., 1999]. However, models are effective only if footed on a solid experimental basis. Subsidence models are no exception. In particular, such models are strongly dependent on the degree of knowledge regarding the deformation characteristics of the soil or rock under changing stress conditions.

In general, the deformation characteristics of soils and rocks for subsidence prediction are described in terms of uniaxial compressibility or C_m [Geertsma, 1973]. This parameter is a measurement of the compaction of a specimen under vertical stress and impeded lateral deformation. Such condition is deemed to be the prevalent one in the case of hydrocarbon reservoirs [Gambolati et al., 1999]. This corresponds also to the typical experimental setup of an oedometric test. For this reason, oedometers have been largely used to measure C_m in the laboratory [e.g., Teeuw, 1971].

It has been observed for some time [Pottgens and Brouwner, 1991] that in-situ compressibility values, obtained with the so-called radioactive marker technique [De Loos, 1973], may substantially differ from values measured in the laboratory for the same kind of material and, apparently, under the same stress conditions. This discrepancy has appeared even more evident in the case of loose, albeit deep, sediments such as the ones found in the North Adriatic basin [Cassiani and Zoccatelli, 2000]. Evidence suggests that in-situ and laboratory experiments may bear results that differ by an order of magnitude or more, being the in-situ behaviour much stiffer than observed in the laboratory. This strong discrepancy has caused substantial disagreement among researchers and practical problems for those faced with the dilemma of which data set to choose as a basis for predictive simulations. A possible way of dealing with this uncertainty is by stochastic simulations [Cassiani and Zoccatelli, 2000]. While more and more evidence has been collected over the past few years, clearly showing that in-situ experiments offer the best available estimate of actual soil compressibility, the problem of having reliable compressibility values for new development areas, where no in-situ experiment is yet possible, still remains.

The objective of this paper is to show how increasing field evidence, modelling analysis of gas producing fields, and novel laboratory techniques and procedures, all concur towards a more unitary framework of interpretation and estimation of soil compressibility. The analysis will be particularly focused on the gas fields operated by ENI-Agip in the Adriatic offshore and the Eastern Po River Plain.

2. TRADITIONAL LABORATORY MEASUREMENTS

Well-established techniques for the measurement of soil compressibility comprise oedometric and triaxial tests. Oedometers have been widely used because simple to operate and deemed to reproduce the stress path considered predominant in deep hydrocarbon reservoir, i.e. vertical compaction with negligible lateral expansion. Similar tests have been run by ENI-Agip for over thirty years on material obtained from drilling cores, yielding a fairly large database of information about the compressibility values of deep soils in the Adriatic offshore as well as the Eastern Po River Plain. All such compressibility values, albeit decreasing with depth, lie in the range of $5x10^{-5}$ bar^{-1} to $1x10^{-3}bar^{-1}$ (see Figure 3 below), with mean values around $1x10^{-4}$ bar^{-1}. In theory, for sediments in a state of normal consolidation, i.e. that are in the maximum state of stress ever experienced, only virgin loading oedometric compressibilities shall be used. However, such values are sometimes so high that re-loading compressibilities has been often used instead, albeit theoretically applicable only to over-consolidated sediments. Experience has shown that all such values, obtained in the laboratory, can lead to a large overestimation of actual subsidence, as measured in the field over existing gas field that have been in production for tens of years. Subsidence measurement onshore and offshore is not an easy task, also because of interference with other, often predominant, causes of compaction – such as water extraction for agricultural or drinking use. Consequently, only the introduction of in-situ compaction measuring techniques that rely on the positioning of radioactive markers in deep wells has offered a viable alternative to classic oedometric measurements, and has consistently shown that laboratory values are largely overestimated.

3. IN SITU MEASUREMENTS: RADIOACTIVE MARKER DATA

The technique of radioactive markers for in-situ measurement of deep sediment compaction has been used for more than 25 years [De Loos, 1973] in areas or situations where compaction and subsidence raised concern regarding environmental [Mobach and Gussinklo, 1994] or operational (Ekofisk) problems. The technique is based on subsequent measurements of vertical distance between radioactive bullets previously shot in the wall of a newly drilled well. As hydrocarbon production continuous and depletion takes place, a slight compaction can usually be measured. The method precision is deemed to range around 1 mm for the 10.5 m average vertical distance between two markers. Tens of markers are usually positioned in each well, covering a thickness of several hundred metres.

ENI-Agip has adopted this methodology in early 1990s. To date, six deep wells have been equipped with radioactive markers, five of them in the Adriatic offshore. Meaningful measurements require that a certain amount of pressure drop takes place. Consequently, some time has to elapse after marker installation before results can be obtained. Only some of the earliest equipped wells have as yet produced measurements, notably Amelia 21 and Barbara 101 (Figure 1). The latest survey on Amelia 21 has been run in November 1999, and results have only recently been available.

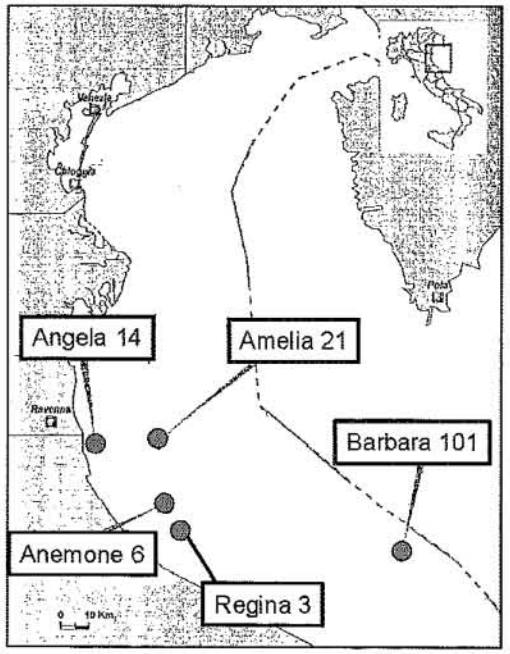

Figure 1. Location of wells with radioactive markers in the Adriatic offshore

The analysis of compaction data from radioactive markers can be coupled with pressure history information to yield estimates of rock compressibility, generally in terms of C_m:

$$C_m = \frac{1}{\Delta p}\frac{\Delta H}{H} \tag{1}$$

where H is the original vertical distance between a couple of markers, ΔH is its variation over a given time interval, and Δp is the corresponding pressure variation over the same time. The values of C_m obtained for individual intervals of well Amelia 21 are shown in Figure 2. Note that intervals with larger pressure drop show a smaller scatter. This result is expected, since it can be easily shown that the standard deviation (σ_m) of C_m is inversely proportional to Δp:

$$\sigma_m = \sqrt{\sigma_m^2} = \frac{1}{\Delta p}\sqrt{E\left[\left(\frac{H_2}{H_1^2}dH_1 - dH_2 - \frac{1}{\Delta p}\frac{H_1 - H_2}{H_1}d(\Delta p)\right)^2\right]} \tag{2}$$

where H_1 and H_2 are the interval lengths before and after depletion, dH_1, dH_2 and $d(\Delta p)$ are the errors in measuring the respective quantities, and $E[.]$ is the expected value operator. Note also that, by virtue of (2), as Δp increases, σ_m is even less sensitive to errors in Δp (the sensitivity decreases with Δp^2) than to errors in interval length.

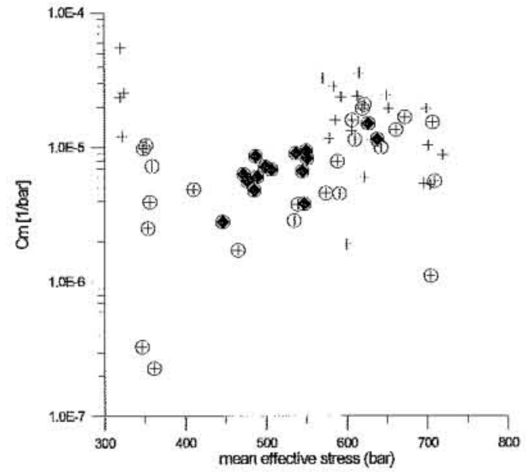

Figure 2. C_m from individual marker intervals in Amelia 21 well:
+ represent all intervals with consistent compaction/depletion signs;
O represent intervals with pressure drop larger than 30 bar;
● represent intervals with pressure drop larger than 100 bar

In all cases, the C_m values obtained from radioactive markers are substantially lower than the corresponding values measured in oedometric tests. A comparison is shown in Figure 3, where results from markers in well Barbara 101 are also displayed.

The calculation of one value of C_m for each 10.5 m interval can lead to inconsistent results. Some intervals in the series may show expansions rather than compaction, even though the pressure in the corresponding layer might have decreased. A possible reason is that the nominal precision of 1 mm might indeed be slightly overestimated [Mobach and Gussinklo, 1994] and not all intervals reach a compaction large enough to be significantly above the actual precision. Another hypothesis is that local expansion might occur as a result of mechanical-fluid-dynamic coupling [e.g., Hsieh, 1995]. Both possible phenomena are much less significant if intervals are grouped and C_m is computed in an averaged way over larger intervals. These intervals have larger overall compaction, thus eliminating the problem of reduced precision. In addition, local coupling effects cannot hold over intervals many tens or hundred of metres thick.

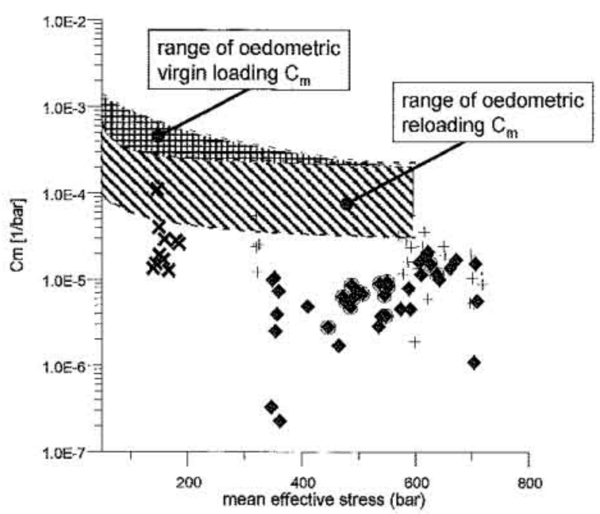

Figure 3. A comparison between C_m values from in-situ markers and the range of C_m values obtained via oedometric tests from all available samples of deep Adriatic and East Po Plain sediments. ✖ are C_m values from marker measurements in well Barbara 101; other symbols are as in Figure 2.

Marker interval averaging can be conducted by averaging the pressure drop in each interval, and expressing the "effective" uniaxial compressibility coefficient as:

$$C_m^{eff} = \frac{N}{\sum_{i=1}^{N} \Delta p_i} \frac{\sum_{i=1}^{N} \Delta H_i}{\sum_{i=1}^{N} H_i} \tag{3}$$

where N is the number of contiguous intervals considered, H_i is the individual interval original length, and ΔH_i is its variation. In fact, by rearranging equation (3), C_m^{eff} can be expressed as the weighted average of C_m computed for individual intervals, where the weights are the pressure drops in each interval:

$$C_m^{eff} = \sum_{i=1}^{N} C_m^i \frac{\Delta p_i}{\sum_{i=1}^{N} \Delta p_i} \tag{4}$$

This formulation therefore weights more the contribution from intervals that have higher depletion, consistently with the sensitivity equation (2).

The impact of errors in individual interval length and pressure measurements has been assessed by drawing random samples from the probability distributions of individual quantities and combining the resulting values into equation (3). All distributions have been assumed Gaussian. The standard deviation of interval lengths is obtained from the radioactive marker surveys as the same interval is repeatedly measured (up to 45 times). The standard deviation of pressure measurements has been assumed equal to 1 bar. The resulting distributions of C_m^{eff} values over the whole monitored interval, for different choices of initial and final survey on the well Amelia 21 are shown in Figure 4. The distributions are fairly narrow and have a mean consistently close to $1 \div 2 \times 10^{-5}$ bar^{-1}. Note that the mean of oedometric C_m values for the same range of effective stress would be around 1×10^{-4} bar^{-1} for reloading C_m and 4×10^{-4} bar^{-1} for virgin loading C_m. The resulting C_m^{eff} distributions are fairly Gaussian themselves.

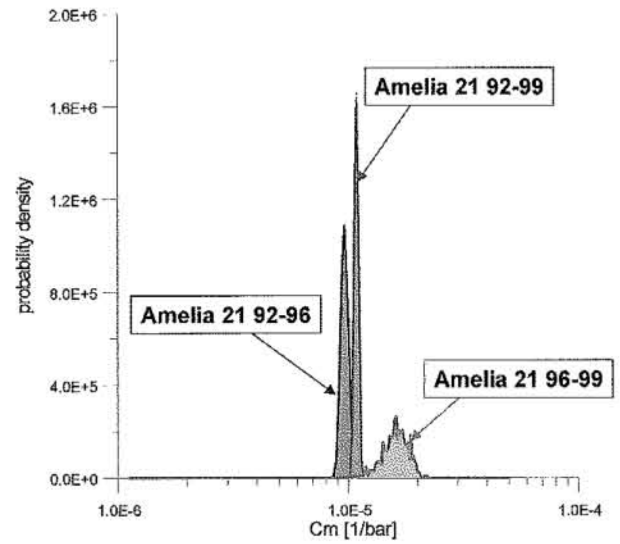

Figure 4. Monte Carlo probability distributions of C_m^{eff} calculated over the whole monitored interval for well Amelia 21; the three distributions refer each to a different choice of the first and second marker survey (1992-1996, 1996-1999 or 1992-1999).

The same Monte Carlo approach can be applied also to individual marker intervals. While the spread is of course larger, the mean value is again centred around $1 \div 2 \times 10^{-5}$ bar^{-1}. The spread also decreases as Δp increases, along the lines of equation (2), leaving a pronounced peak around the mean value (Figure 5).

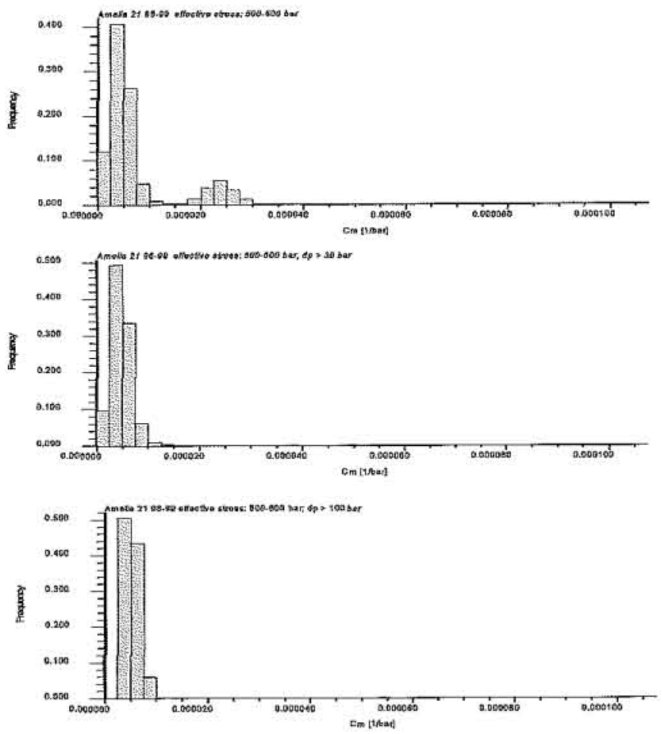

Figure 5. Monte Carlo probability distribution of C_m calculated for the 500-600 bar effective stress range, for well Amelia 21.

4. EVIDENCE FROM SUBSIDENCE MODELLING: THE BARBARA FIELD

The results from radioactive markers clearly show that in-situ uniaxial compressibility is substantially lower than predicted from laboratory experiment (Figure 3). For the Barbara field, the largest of all shallow gas fields in the Adriatic offshore, having most producing layers in the range of 1000 m to 1500 m depth and a net pay about 400 m thick, in-situ C_m ranges between $2x10^{-5}$ and $5x10^{-5}$ bar^{-1}. Oedometric C_m from the same field range between $1x10^{-4}$ to $5x10^{-3}$ bar^{-1} (Figure 6). The field is located approximately 60 km from the coast, in a North-East direction from the city of Ancona (Figure 1). The field has been producing since early 1980s a considerable portion of the gas extracted in all the Italian fields. Numerical modelling of subsidence caused by the Barbara field has been undertaken with the aim of (i) evaluating how the choice of compressibility values might affect the level of predicted subsidence , and (ii) analysing whether evidence from modelling could support further the hypothesis that in-situ compressibility values are a better representation of reality. Modelling has included the simulation of geo-mechanical compaction as well as propagation of pressure disturbance in the aquifer surrounding the field. Full details of this study are available in Palozzo et al. [2000].

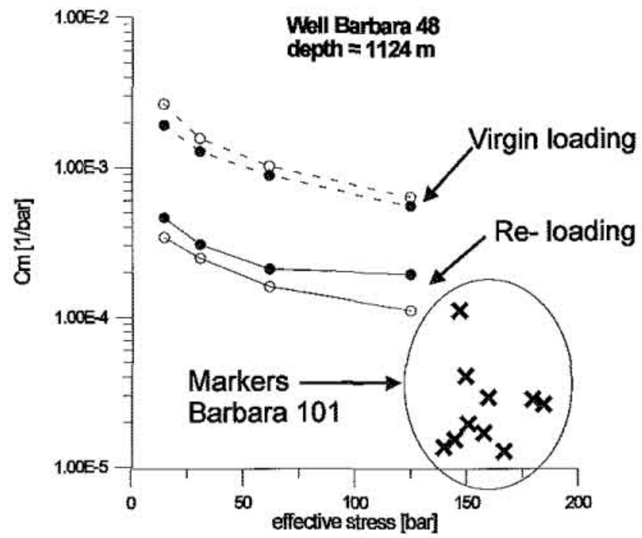

Figure 6. Laboratory and in-situ C_m values for the Barbara gas field.

One of the most revealing features of the modelling exercise has been the calibrated simulation of aquifer depletion (Figure 7). Data on aquifer pressure has been available at selected points in space and for particular moments in time. As described by Palozzo et al. [2000], such data has been successfully used for a calibration of soil compressibility, in that such compressibility affects not only the deformation of the porous medium, but also its hydraulic storing capacity, and consequently its pressure history. Results from this calibration are summarised in Figure 8.

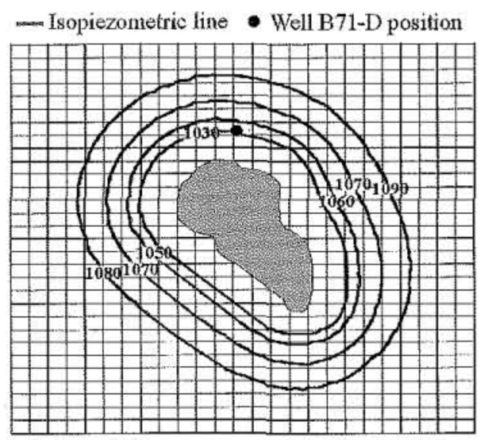

Figure 7. Barbara field simulation: an example of aquifer parameter calibration.

Figure 8 shows that it was possible to reproduce the pressure history of the aquifer, as well as of the gas reservoir, with C_m values fully compatible with the ones measured with the radioactive marker technique.

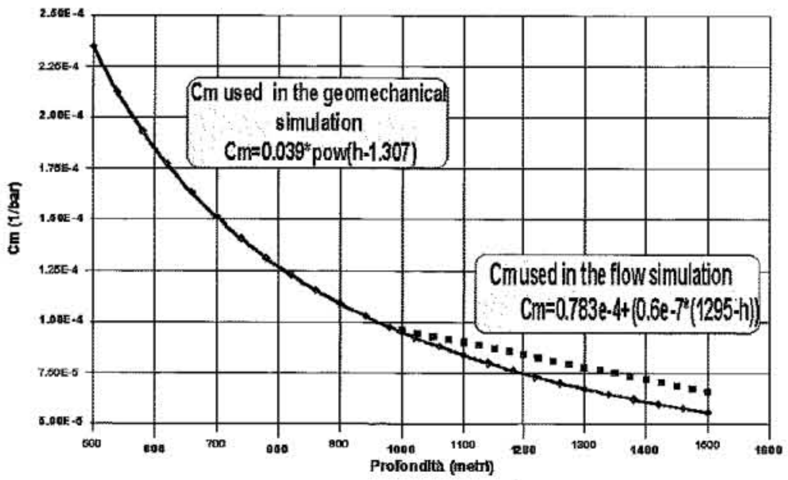

Figure 8. Barbara field simulation: C_m values used in geo-mechanical and fluid-dynamics simulations.

In addition, subsidence levels simulated with the finite element model using in-situ C_m values are also compatible with evidence from GPS monitoring, being the maximum simulated subsidence value equal to about 80 cm in 17 years. This value is within the range of sea tide value (about 1.5 meter) and therefore likely to pass unnoticed.

5. NEW LABORATORY TECHNIQUES: THE EFFECT OF AGEING

All evidence clearly supports the hypothesis that in-situ measurements yield the correct C_m value, while classical laboratory experiments substantially overestimate it, at least in the case of deep unconsolidated sediments. The specimens collected for laboratory testing must therefore be "disturbed". However, the nature and level of this disturbance is only starting to be analysed. Novel laboratory experiments have been designed and carried out for ENI-Agip and are fully described in Hueckel et al. [2000], with the aim of demonstrating that "ageing" effects are responsible for the enhanced stiffness of sediments under in-situ conditions. Ageing is a phenomenon that manifests itself when a specimen is left at a constant level of stress – generally the in-situ stress – and under this condition undergoes a time-dependent deformation, named secondary compression. In this process, the soil develops a certain amount of strain. When loaded subsequently above the in-situ effective stress, as in the case of gas or oil extraction, the material exhibits a much higher "*apparent* pre-compression stress", and also a much lower compressibility, over certain stress range. Experiments have been undertaken to verify if, and in the positive case, to what extent, the above described effects develop also in sediments of North Adriatic, at depths pertinent to oil/gas extraction. Two distinctly different materials were used. One, from well Dalia 1, is predominantly sandy clay, and the samples used in the tests come from the depth of 1210 m. The other, from well TEA 1, is a clayey material, from a depth of 3270 m. The *in situ* effective vertical stresses were established for DALIA 1 as equal to 12.6 MPa, whereas for TEA 1 as 35.04 MPa. Oedometric tests with moderate duration (14 days) ageing were performed. An example of the results is shown in Figure 9. The deformability was reduced by nearly 40 %, when compared to traditional tests with monotonic loading. That leads to a proportional (~40%) reduction of subsidence prediction according to 1-D, linear compression theory. Larger compressibility reductions might be possible under longer ageing conditions, e.g. during geological times. The "aged" micro-structure is effectively destroyed during coring and sampling. An even stiffer behaviour was observed during tests in high pressure triaxial cells equipped with non-contact small-strain sensors.

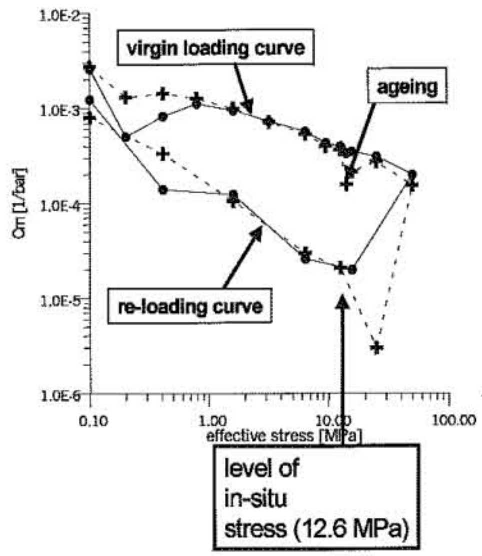

Figure 9a. the ageing effect during oedometric tests on a sample from well Dalia 1 – Adriatic offshore; ● indicate experiment with no ageing; ✚ indicate experiment with ageing.

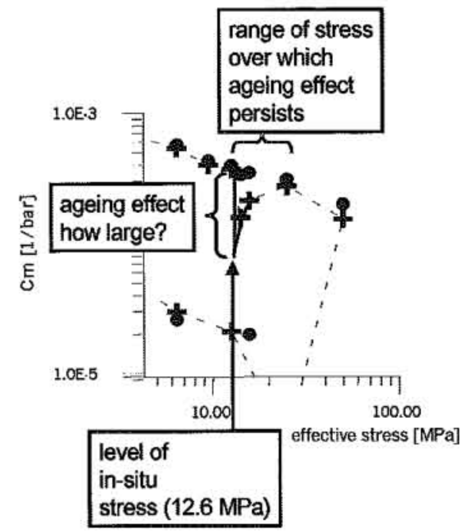

Figure 9b. a zoomed image of Figure 9a around the in-situ stress value, showing the effect of ageing, possibly moving virgin C_m to values closer to reloading C_m.

6. CONCLUSIONS

This paper presents a wide range of data about deep unconsolidated sediment compressibility under gas extraction. This information comes from in-situ measurement, modelling analysis of producing gas fields and novel laboratory measurements. All evidence consistently show that in-situ marker measurements provide the most reliable compressibility values. Such values are also consistent with independent evidence coming from inversion of aquifer pressure history coming from a major gas field in the Adriatic offshore. More accurate laboratory measurements also start to demonstrate that the discrepancy previously observed between laboratory and field data is attributable to the disturbance caused by coring and sampling on the "aged" microstructure of the unconsolidated sediments.

Acknowledgements

The authors acknowledge ENI-Agip for the permission granted to publish the results of this study. All laboratory experiments were performed at ISMES, Bergamo, Italy.

REFERENCES

Cassiani, G. & Zoccatelli, C. (2000) Subsidence Risk in Venice and Nearby Areas, Italy, owing to Offshore Gas Fields: a Stochastic Analysis, in press, *Environmental and Engineering Geoscience Journal.*

De Loos, J.M. (1973) In-situ compaction measurements in Groningen observation wells, *Verhandelingen Kon. Ned. Geol. Mijnbouwk. Gen.*, 28, 79-104.

Gambolati, G., Teatini, P. & Tomasi, L. (1999) Stress-strain analysis in productive gas/oil reservoirs, *International Journal for Numerical and Analytical Methods in Geomechanics*, 23(13), 1495-1519.

Geertsma, J. (1973) A basic theory of subsidence due to reservoir compaction: the homogeneous case, *Verhandelingen Kon. Ned. Geol. Mijnbouwk. Gen.*, 28, 43-62.

Geertsma, J. & Van Opstal, G. (1973) A numerical technique for prediction subsidence above compacting reservoir, based on nucleus of strain concept, *Ned. Geol.*, Vol. 28.

Hsieh, P.A. (1995) Deformation-induced changes in hydraulic head during groundwater withdrawal, Ground Water.

Hueckel, T., Tao, F., Cassiani, G. & Pellegrino, A. (2000) Sediment compressibility evolving during aging: Experiments and reactive plasticity model. In *Land Subsidence*, Vol. II Proc. Sixth Int. Symp. on Land Subsidence, Ravenna, Italy, Sept. 2000, Eds. L. Carbognin et al., 31-44.

Mobach, E. & Gussinklo, H.J. (1994) In-situ reservoir compaction monitoring in the Groningen field, Proceedings Eurock'94, Balkema, Rotterdam.

Palozzo, W., Cassiani, G., Brighenti, G. & Zoccatelli, C. (2000) Three Dimensional Simulation of Subsidence caused by gas production in the Barbara Gas Field and Comparison with Field Data. In *Land Subsidence*, Vol. II Proc. Sixth Int. Symp. on Land Subsidence, Ravenna, Italy, Sept. 2000, Eds. L. Carbognin et al., 397-408.

Pottgens J.J.E. & Browner, F.J.J. (1991) Land Subsidence due to Gas Extraction in the Northern Part of the Netherlands, *Land Subsidence*, Proceeding of the Houston Symposium, Pub. No. 200, 99-108.

Teeuw, D. (1971) Prediction of Formation Compaction from Laboratory Compressibility Data, SPE Journal, Trans. AIME 251, 263-271.

RESERVOIR COMPACTION: A PARAMETRIC STUDY ON IN-SITU MEASUREMENTS

Giovanni Brighenti, Paolo Macini and Ezio Mesini
University of Bologna, Viale del Risorgimento 2, 40136 Bologna, Italy

Abstract

The research is devoted to evaluate the effectiveness of *in-situ* measurements, and particularly the ones performed by extensometers and radioactive markers. To this purpose, a parametric study has been performed by means of a finite element model: the effects of the casing on formation compaction measured in the vicinity of the borehole have been evaluated. Near-borehole deformations have been compared to the ones simulated at larger radial distance, where the formation is not disturbed. Results show that the presence of a casing around a wellbore causes perturbations of the deformations in the vicinity of the borehole. In particular, compaction in the vicinity of the borehole is lesser than the one of the undisturbed formation. Moreover, the possible effects of formation precompression in production wells are considered, for the evaluation of the effects induced by using production wells as measuring sites.

Keywords: land subsidence, *in-situ* measurements, compressibility

1. INTRODUCTION

Measurement of subsoil and reservoir compaction can be useful to quantify subsidence. In some cases it is possible to have information on the evolution of subsidence vs. time, providing valuable indications to undertake possible actions of environmental protection. Generally, measurement techniques of subsoil and reservoir compaction due to underground fluid withdrawal can be divided into two groups. The first one is based on laboratory estimation of the mechanical properties of cored samples, performing stress and strain tests. The second one relies on *in-situ* measurement of soil sinking (subsidence), and/or on *in-situ* measurement of thickness reduction of underground layers (compaction). From both methods it is possible to derive an estimation of uniaxial rock compressibility coefficient (C_m), necessary as input data for mathematical modelling, the most powerful tool to simulate the behaviour of land sinking phenomena. So far, it is common practice in subsidence modelling is to utilise compressibility estimations derived from laboratory measurements, being *in-situ* measurements not yet so much developed and fully reliable.

The comparison between lab and *in-situ* measured C_m evidences that there can be significant differences, even of one order of magnitude. So, it is evident that subsidence estimation obtained by means of mathematical modelling can significantly differ in the two cases. This occurrence is confirmed as well by field measurements performed at Groningen gas reservoir (The Netherlands) and from studies on several Adriatic offshore gas fields (Italy). In particular, C_m values derived from *in-situ* measurements at Groningen are about one-third of those measured in laboratory (NAM, 1995). These data, used as input in mathematical modelling, fit adequately the subsidence values measured by precision levelling. Different compressibility values have been found also in recent studies on Adriatic offshore gas fields, where laboratory calculated C_m's are higher than the ones estimated *in-situ*.

In this scenario, one can remind that even the most accurate laboratory measurements can be affected by errors due to: a) sample disturbance during coring operation; b) damages due to handling, storage, transportation and laboratory preparation; c) uncertainties on *in-situ* stress field, from which the sample has been removed; d) difficulties to take into account the viscous component of the measured deformation during the relatively short timeframe of laboratory measurements (Brighenti et al., 1998). Moreover, regardless to the fact that a small number of sampled cores might not be representative of studies at regional scale, lab measurements are performed on small samples (of the order of some centimetres), which cannot give information on the presence of macro-discontinuities, overlooking completely their effects. Notwithstanding these limitations, lab measurements are vital in providing direct information on the mechanical properties of the samples.

In-situ measurement techniques (which allow also for the evaluation of C_m in reservoir conditions) can be divided into two main types; both are aimed to evaluate the distance variation between two or more points.

The first one was mainly developed for geotechnical applications (Dunnicliffs and Green, 1988), and measures the distance variation between one point at the surface and one or more points inside a well. The equipment (also known as cable or bar extensometer) is fixed permanently inside a dedicated well, and can be used to a depth of some hundreds of metres (usually, less than 1000 m). The description of the technique and instrumentation can be found in Poland (1984), Mobach and Gussinklo (1994), Brighenti et al. (1998) and enclosed references.

The second one, which can be run also inside deep wells (up to some thousands of metres), measures the distance variation between two or more reference points by running into the well (not necessarily a dedicated well) a specially equipped wireline tool. The reference points are located along the well by means of markers fixed in correspondence of the layers under compaction. Among these measurements, Radioactive Marker Technique (RMT) is nowadays the most utilised one (Bevilacqua et al., 1999, De Kock et al., 1998). RMT is based on the placement of low-emission radioactive bullets (the markers) along the wellbore, straddled between the formations under depletion. The position of each marker is determined by specialised wireline gamma ray logs (Macini and Mesini, 1998), which are run at regular time intervals to monitor the possible distance variation between each pair of markers, allowing for the detection of compaction phenomena.

A common feature of both extensometers and RMT is that measurements are necessarily performed in the vicinity of the wellbore. This paper reports a parametric study that takes into account the presence of a steel casing and the past production history on the compaction due to fluid withdrawal of a layer in the vicinity of a borehole. The study has been carried out by means of a finite element numerical model.

2. CONSIDERATIONS ON POSSIBLE CAUSES OF ERRORS

Basically, the precision of *in-situ* measurements depends on the technique adopted and on the accuracy of the investigations. Nonetheless, additional sources of errors, by now not so much discussed and experienced, can be induced by: a) the presence of a casing to protect the borehole (usually, a steel casing); b) the type of cementation between the casing and the borehole; c) the possible precompression of the formations around the borehole.

In-situ measurements investigate only the "actual" behaviour of the formations (*i.e.*, the one at the time of the measurement, influenced by the "history" of the loading cycle), and cannot provide information about the deformation of the material as stresses vary. This is a restrictive factor, since mechanical properties of most rocks are highly dependent on applied stresses. This kind of behaviour can be predicted only by using laboratory measurements. To this regard, it is worthy to remind the case of some North Sea carbonate reservoirs, such as Ekofisk (Smiths et al., 1988, Johnson et al., 1989), where a significant compaction of highly porous intervals happened when the effective vertical stress exceeded a threshold value, causing the collapse of the porous medium.

In-situ measurements are designed to evaluate underground compaction caused by pore pressure decline (*i.e.*, by increasing the effective stress). Undoubtedly, measurements performed inside a cased borehole are influenced by the presence of the casing, usually characterised by a rigidity quite different than the one of the adjacent formations. The different mechanical properties and behaviour of the casing and the formation may cause local perturbations of deformations around the borehole. For example, it is well known the effect of foundation piles, which are partially bound to the formation by friction. In case of underground compaction, the pile induces a lesser compaction around its circumference, in correspondence of the layer subjected to compaction, and transmit stresses to the formation underneath (Lambe and Whitman, 1979).

As for as wells utilised for underground fluid production, it is important to remind the presence of cement between the casing and the borehole. Cement thickness and its mechanical properties may vary along the wellbore, introducing further complication to assess the deformation of the bulk structure (*i.e.*, the cylinder consisting of formation, cement and casing). In case of *in-situ* measurements by extensometers, some of these problems can be reduced by an appropriate design of the well completion (Brighenti et al., 1999a).

RMT requires that a marker must be positioned not too deep inside the formation (in order to avoid difficulties for its detection, being marker strength quite low), and not too shallow, in order to avoid its removal by casing centralizers. Again, RMT measures the deformation of a portion of formation located in close proximity of the borehole. This portion can be affected by the local perturbation induced by the presence of materials characterised by different rigidity. This phenomenon is of paramount importance, particularly when measurements are run inside a well which has been formerly used (or is still used) as a production well. In fact, it is well known that most of pressure drawdown occurs in the proximity of a producing well, eventually inducing most of the compaction around the well itself. In this case, the compaction rate of the formation gradually increases toward the borehole, and permanently affects its mechanical properties. The present study investigates also this possible cause of errors.

3. PARAMETRIC STUDY

The parametric study has been performed by means of a three-dimensional finite element model characterised by radial symmetry (Brighenti et al., 1999b). The medium under investigation has been supposed linearly elastic, and therefore superposition effects have been taken into account. The porous medium has been discretised by annular finite elements with triangular cross-sections: a mesh of 727 nodes and 1369 elements (Fig. 1) has been used. The numerical model makes use of the "frontal technique" to solve the linear system (Irons, 1970), and can provide stresses and strain field associated to the nodal points of the mesh. The precision of the model has been assessed by comparing its solutions with those provided by Geertsma (1973) and Van Opstal (1974). In both cases, the accuracy was proven satisfactory.

The study has been performed considering a well of external radius r_0, with or without casing, drilled inside a homogeneous formation where a layer of thickness $h = 10\ r_0$ and radius $r = 150\ r_0$ undergoes a uniform pore pressure drawdown $\Delta p_0 = 10$ MPa. A preliminary study of the mesh sensitivity in radial direction proved that the value $r = 150\ r_0$ can be considered as infinite.

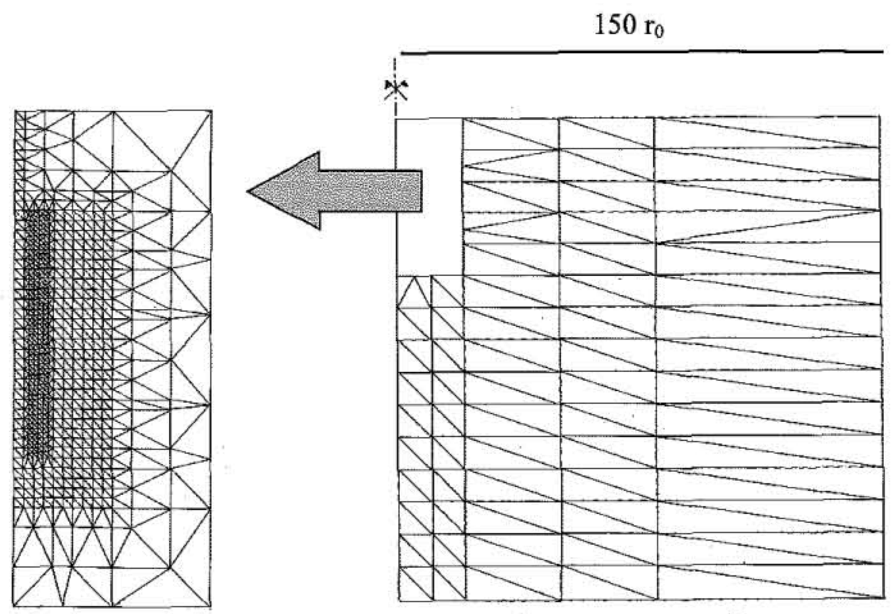

Figure 1. Global view (right) and window (left) of a vertical cross-section of the three-dimensional axial symmetric finite element mesh used by the model.

As it has been previously stated, the model considers the case of a material characterised by linear elasticity. For this particular case, the elastic modulus has been calculated from the oedometric C_m coefficients by means of the relationship:

$$E_0 = \frac{1}{C_m}\frac{(1-2\nu)(1+\nu)}{1-\nu} \qquad (1)$$

The study of the deformations induced by pore pressure drawdown was performed by replacing the casing of the well with an equivalent solid cylinder characterised by a Young's modulus E_t which determines the same vertical deformation, when subjected to the same axial load (Fig. 2). In the same figure, E_0 indicates Young's modulus of the undisturbed formation. The study took into account the mechanical behaviour of both loose and cemented formations. Concerning loose or weakly consolidated formations, the study was based on the average oedometric C_m values calculated by lab measurements performed on samples from wells drilled in Ravenna area (Italy). Two sets of samples have been utilised: the first one cored at depths ranging from 100 to 500 m (Comune di Ravenna, 1988), typical of water bearing formations exploited for fresh water production. The second one cored at depths ranging from 1000 to 4000 m, in correspondence of loose or weakly cemented gas bearing formations (sand, silt and clay). Concerning cemented formations, the study was based on the well-known mechanical properties of the consolidated sandstone of Groningen gas field (NAM, 1995). By comparing the mechanical behaviour of Ravenna and Groningen formations with the one of a cylinder equivalent to a steel casing of 20 cm diameter and 1 cm thickness, assuming a Poisson's coefficient $\nu = 0.25$, the ratio E_t/E_0 ranges between 10^3 and 10 (from 100 to 4000 m depth, respectively) for the formations of Ravenna, and ranges between 1 and 5 for the formations of Groningen.

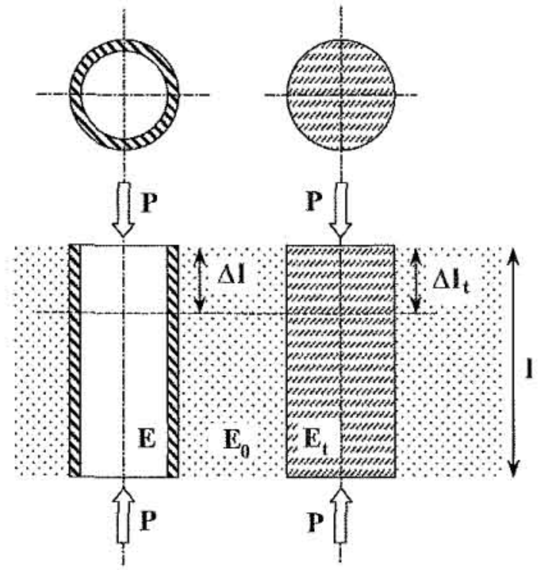

Figure 2. Concept of equivalent cylinder: the numerical simulation considered a solid cylinder (right) equivalent to the actual casing (left).

Considering all the above hypotheses, it has been calculated the relative compaction ($\Delta h/\Delta h_0$) as a function of the dimensionless coordinates r/r_0, z/r_0, and of the elastic modulus of casing and formation. Δh_0 and Δh represent the thickness variation of the layer in case of open hole and cased hole, respectively. An additional hypothesis is the continuity of deformations between the casing and the formation (*i.e.*, there is no shift between casing, cement and formation).

The parametric study assumes different values of the ratio between the elastic modulus of the casing and the formation. In particular, the cases $E_t/E_0 = 1$, 10, 10^2, 10^3, 10^4 (where the last one can be representative of an infinitely rigid casing), have been evaluated. The particular case of a casing set at different depths in front of the formation under depletion has been assumed as well. At last, it has been studied the effect of local perturbations induced by the presence of formations characterised by different rigidity (*i.e.*, the consolidation that can be present around producing wells due to pressure drawdown).

4. RESULTS

The first case considered a homogeneous formation and a fully cased hole, where $E_t/E_0 = 10^2$. Figure 3 (left) reports a qualitative illustration of the deformations resulting from the depletion. In particular, here are highlighted the lines representing soil surface, top and bottom of the formation under depletion. Before depletion, all the lines are parallel.

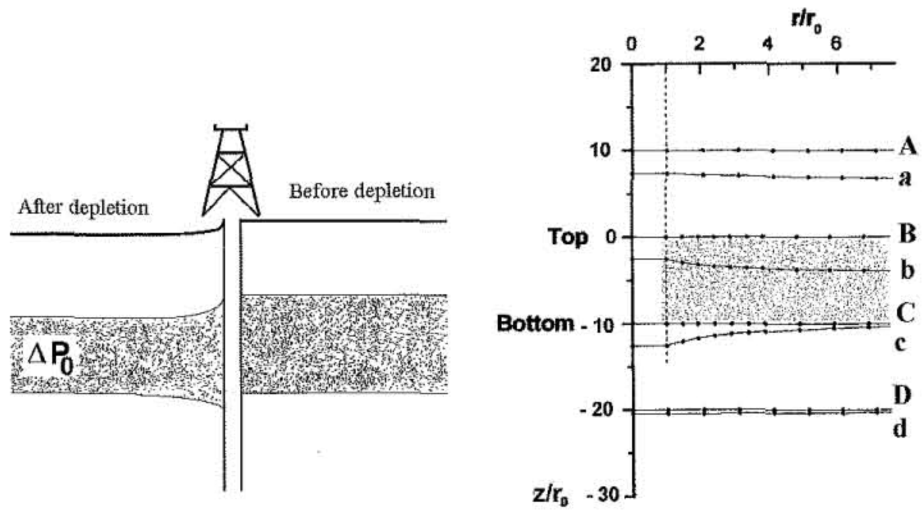

Figure 3. Left: deformations resulting from the depletion of an underground formation. Right: elastic deformation around the wellbore (not in scale).

Figure 3 (right) reports the elastic deformation around the wellbore, function of r/r_0, in correspondence of the ordinates $z/r_0 = +10$, $z/r_0 = 0$ (top), $z/r_0 = -10$ (bottom) and $z/r_0 = -20$. The deformations are amplified. In particular, the straight lines B and C represent top and bottom of the layer subjected to compaction before depletion, while the curved lines b and c represent the deformation of the same after depletion. The compaction of the layer is not uniform, due to the presence of a rigid casing. The top of the layer undergoes a lesser deformation in the vicinity of the borehole (drag effect), while the bottom shows a contrary behaviour (pile effect).

Table 1 reports the relative compaction $\Delta h/\Delta h_0$ of the above case, calculated in the vicinity of the borehole (for $r/r_0 < 10$). Four different rigidity ratios have been considered: $E_t/E_0 = 10$, 10^2, 10^3, 10^4. In general, the compaction in the close proximity of the borehole is lesser than the one at larger radial distances. The effect is practically negligible for $r > 10\ r_0$. As the rigidity ratio of the casing increases, the effect is amplified.

Table 1. Relative compaction around the wellbore, function of dimensionless radius, calculated for the ratios E_t/E_0=10, 10^2, 10^3, 10^4. The well is fully cased.

r/r_0	$\Delta h/\Delta h_0$ ($E_t/E_0 = 10$)	$\Delta h/\Delta h_0$ ($E_t/E_0 = 10^2$)	$\Delta h/\Delta h_0$ ($E_t/E_0 = 10^3$)	$\Delta h/\Delta h_0$ ($E_t/E_0 = 10^4$)
1	0,718	0,279	0,044	0,005
1,5	0,801	0,447	0,250	0,217
2	0,853	0,558	0,389	0,361
2,5	0,888	0,637	0,489	0,465
3	0,909	0,695	0,565	0,544
6	0,960	0,861	0,794	0,784
10	0,985	0,943	0,910	0,903

The presence of a casing can induce significant errors, particularly in unconsolidated or loose formations. Figure 4 reports the relative compaction of a homogeneous formation at distance $r = 2r_0$ and $r = 1,5\ r_0$, as a function of the rigidity ratio E_t/E_0. These radial distances are typical of measurements performed by RMT.

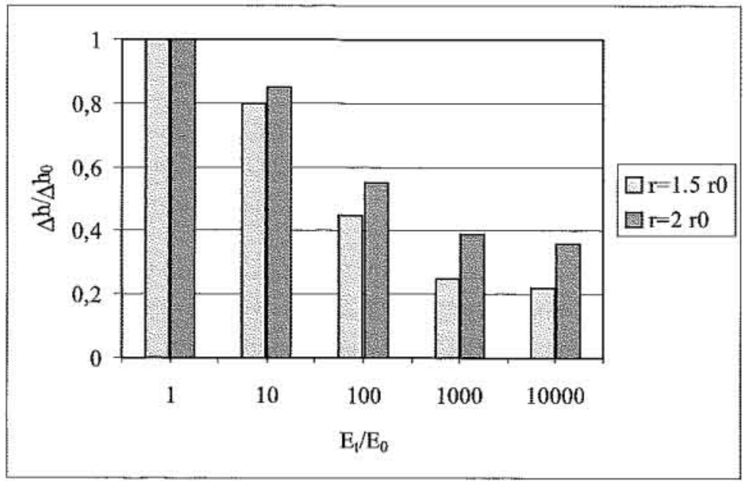

Figure 4. Relative compaction at distance $r = 1.5r_0$ (left bar) and $r = 2r_0$ (right bar), for a homogeneous formation.

Successively, it has been investigated the influence of a casing set at different depths in front of the formation under depletion (useful for the evaluation of errors connected with *in-situ* measurements by extensometers). Several cases have been considered, in which the setting depth varies between 10 r_0 above and 10 r_0 below the formation under depletion. It has been noticed that the presence of the casing is relevant only when it is set between the top and the bottom of the depleted formation. Also in this case, the presence of a rigid casing induces a lesser compaction around the borehole (with respect to the one at larger radial distance). In particular, Figure 5 reports the relative compaction, as a function of r/r_0, for the two cases $E_t/E_0 = 10^2$, 10^4, when the casing is set at the top and at the bottom of the formation under depletion. The effect of a casing set at the top of the formation is practically negligible.

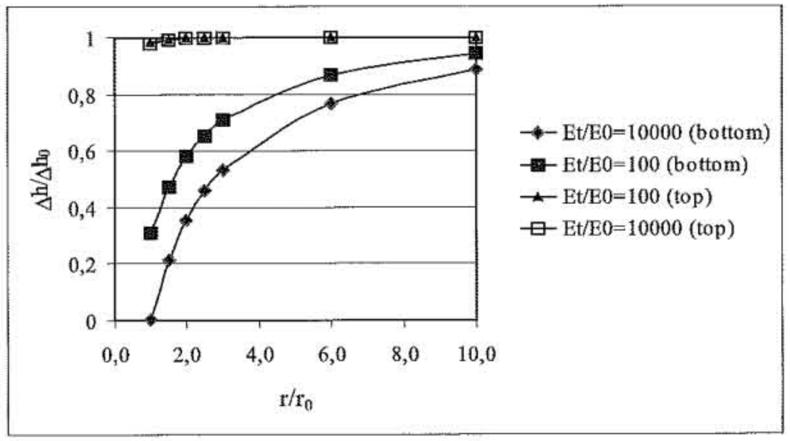

Figure 5. Relative compaction for the two cases $E_t/E_0 = 10^2$, 10^4; the casing is set at the top and at the bottom of the formation under depletion.

Finally, the study investigated the possible errors associated with *in-situ* measurements performed inside production wells. During production, the pressure drawdown in the vicinity of the wellbore is the highest. Subsequently, the pressure builds up when production is stopped. Thus, the formation in proximity of the wellbore undergoes a precompression higher than in the rest of the reservoir, changing its mechanical properties, and particularly the compressibility coefficient C_m. To evaluate the precompression rate, the mechanical properties of a sample cored in Ravenna area at a depth of about 1000 m have been considered. Then, the pressure drop profile of a radial filter for the steady flow of an uncompressible fluid was assumed. Pressure drawdown in the proximity of the wellbore was supposed to range from 10 MPa (at $r = r_0$) to 0 MPa (at $r = 20\ r_0$). Once production is stopped, pressure builds up to the initial value. The sample under investigation is characterised by a qualitative oedometric curve reported in Figure 6.

In particular, when pressure builds up (σ_{ez} decreases) the sample under investigation follows the unloading curve B–D. When production starts again, the sample undergoes the loading curve D–B–C. In this way, the C_m associated to the first loading cycle (curve A–C) is different to the one associated also with the second loading cycle (curve D–B–C), being C_m the angular coefficient of the tangent at each point of the curve. In particular, the mean value of C_m of a layer that was subjected to a second loading cycle (typically in the vicinity of the wellbore) is lesser than the one of a layer subjected only to a first loading cycle. Clearly, this reflects on the value of Young's modulus E.

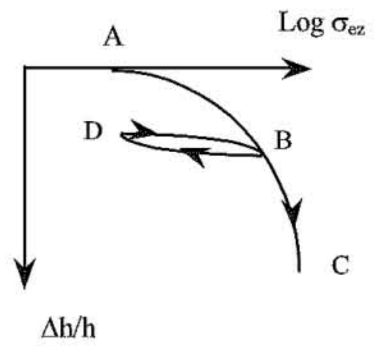

Figure 6. Qualitative oedometric curve of a sample from Ravenna area. Accordingly with Terzaghi's law, $\sigma_{ez} = \sigma_z - p$, where σ_{ez} = effective vertical stress, σ_z = overburden pressure, p = pore pressure.

Figure 7 reports the final results of the above estimation, derived by means of the oedometric curve of the above sample, calculated in correspondence of the simulated pressure drop around the wellbore.

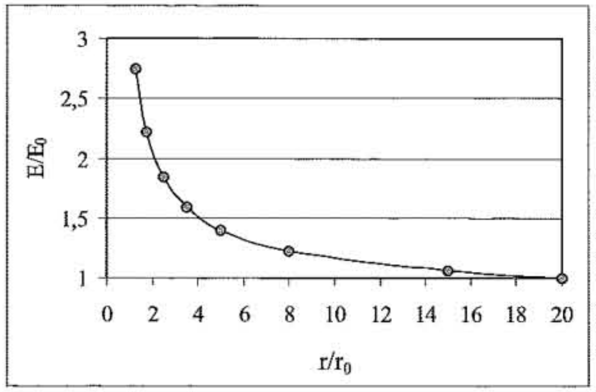

Figure 7. Average rigidity ratio E/E_0 function of r/r_0. E_0 is Young's modulus of the original formation, while E is the one of the precompressed formation.

Within these hypotheses, it has been simulated the relative compaction of a depleted layer in function of the dimensionless radius, for an open hole and for the rigidity ratios $E_t/E_0 = 10^2, 10^4$. Results are plotted in Figure 8.

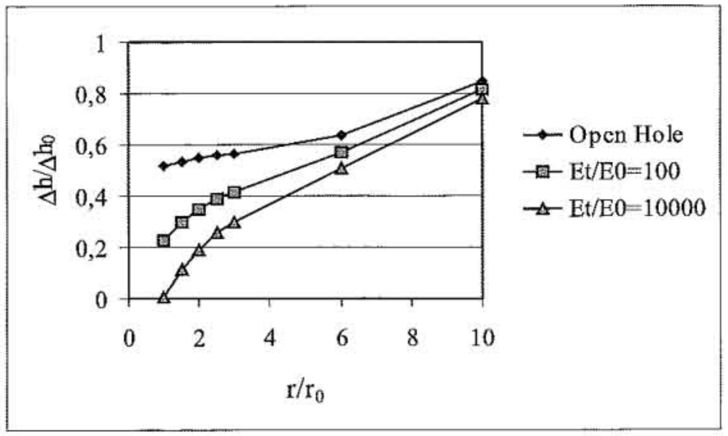

Figure 8. Relative compaction of a layer for an open hole and for a cased hole with rigidity ratios $E_t/E_0 = 10^2, 10^4$. The formation is assumed to be precompressed as reported in Figure 7.

5. CONCLUSIONS

Results of the simulation via mathematical modelling show that the presence of a casing around a wellbore causes perturbations of the deformation (*i.e.*, of the relative compaction) in the vicinity of the borehole. In particular, the relative compaction around a cased hole is lesser than the one of the undisturbed formation. These perturbations are much more evident in the close vicinity of the borehole (for $r < 10\ r_0$), and in the case of loose or unconsolidated formations (clay, silt and sand), characterised by a rigidity much lesser than the one of steel casing. These considerations are less evident in consolidated formations (cemented sandstone, limestone, dolomite), whose rigidity is comparable to the one of the casing.

Measuring reservoir compaction by means of *in-situ* techniques, performed inside cased holes, might not be representative of the compaction in the undisturbed zone, especially when the formation is loose or unconsolidated. In fact, *in-situ* measurements estimate the deformations in the close vicinity of the borehole. This can be critical when RMT is adopted, as markers are positioned not too deep inside the formation (typically, of the order of one well radius). As for extensometers, the practice of setting the casing a few metres above the anchoring point seems not sufficient to fix the problem, unless the casing is set at the top of the formation under depletion.

The study investigated also the case of the perturbation of the elastic deformation around production wells, where the formation is precompressed. Results pointed out that the relative compaction around the borehole is lesser than the one of the undisturbed formation.

REFERENCES

Bevilacqua, N., Cassiani, G., Macini, P., & Mesini, E. (1999) Compaction monitoring in Adriatic gas fields, *Proc. "New methods and technologies in petroleum geology, drilling, reserv. and gas engineering"*, 103-112, Krakow.

Brighenti, G., Macini, P. & Mesini, E. (1998) Subsidence in Northern Italy: compaction measurements of water-gas bearing formations. *Proc. 8th IAEG Congress*, Vancouver.

Brighenti, G., Macini, P., & Mesini, E. (1999a) Determinazione del compattamento del sottosuolo in aree soggette a subsidenza: misure su campioni ed in situ. *Progetto IRIS – Proposte di linee guida per la caratterizzazione, il controllo e la bonifica di siti inquinati.* CNR – Progetto strategico ambiente e territorio, BIOS, Cosenza.

Brighenti, G., Falsini, F., Macini, P., & Mesini, E. (1999b) Monitoraggio *in situ* del compattamento del sottosuolo conseguente all'estrazione di fluidi: possibili cause d'errore. *Proc. XX Conv. Naz. Geotecnica,* 379-385, Parma.

Comune di Ravenna (1988) *Commissione per lo studio della subsidenza: risultati degli studi.* Ravenna, 147 pp.

De Kock, A.J., Johnson, T.J., Hagiwara, T., Zea H.A., & Santa, F. (1998) Gulf of Mexico Subsidence Monitoring Project with New Formation-Compaction Monitoring Tool, *SPE Drilling & Compl.*, **13 (4)**, 223-230.

Dunnicliff, J., & Green, G. E. (1988) *Geotechnical instrumentation for monitoring field performance.* John Wiley & Sons, New York.

Geerstma, J. (1973) Land subsidence above compacting oil and gas reservoirs. *J. Petr. Tech.*, **22**, 734-731.

Irons, B.M. (1970) A frontal solution program for finite-element analysis. *Int. Journ. Num. Methods in Eng.*, **2**, 5-32.

Johnson, J.P., Rhett, D.W., & Siemers, W.T. (1989) Rock mechanics of the Ekofisk reservoir in the evaluation of subsidence. *J. Petr. Tech.*, **41**, 709-716.

Lambe, T. W., & Whitman, R. V. (1979). *Soil Mechanics.* John Wiley & Sons, New York, 553 pp.

Macini, P., & Mesini, E. (1998) *Alla ricerca dell'energia: metodi di indagine per la valutazione delle georisorse fluide.* CLUEB, Bologna, 410 pp.

Mobach, E., & Gussinklo, H.J. (1994) In-situ reservoir compaction monitoring in the Groningen field. *EUROCK'94*, Delft, 535-547.

NAM (1995) *Subsidence caused by Natural Gas Production: Summary of 1995 Groningen Subsidence Prognosis.* NAM report nr. 27600, Assen.

Poland, J.F., Figueroa Vega G., Carbognin L., Johnson A. I., & Yamamoto S. (1984) *Guidebook to studies of land subsidence due to groundwater withdrawal.* ed. by *UNESCO*, Paris, France, J.F. Poland Chairman and Editor, 305 p. and Appendices A-E.

Smiths, R.M.M, de Waal, J.A., & van Kooten, J.F.C. (1988) Prediction of abrupt reservoir compaction and surface subsidence caused by pore collapse in carbonates. *SPE Form. Eval.*, **3**, 340-346.

Van Opstal, G. (1974) The effect of base-rock rigidity on subsidence due to reservoir compaction. *3rd Int. Congr. ISRM,* Denver, 1102-1111.

SEDIMENT COMPRESSIBILITY EVOLVING DURING AGING: EXPERIMENTS AND REACTIVE PLASTICITY MODEL

T. Hueckel[1], Fan Tao[1], G. Cassiani[2] and A. Pellegrino[3]
[1]- *Duke University, Civil and Environmental Engineering Dept., Durham, NC 27708, USA;*
[2]- *Department of Environmental Science, Lancaster University, Lancaster, UK*
[3]- *ENI, Divisione Agip, Milan, Italy*

Abstract

In situ stiffness and apparent maximum preconsolidation stress of almost any soil are notoriously higher from those determined on the basis of laboratory tests. Classical explanation for the difference is the sample damage during coring. This paper seeks to verify experimentally whether the effect occurs in deep marine sediments, and it espouses an alternative explanation. This explanation suggests possible unaccounted changes occurring in sediments *in situ* when subjected to secondary compression for geological scale time periods. For North Adriatic sediments tested, only two weeks of aging during secondary compression produced a notable increase in stiffness and in the apparent maximum preconsolidation stress. The paper presents the results from aging tests on sandy and clayey sediments. It appears that there is about 40% decrease of compressibility of sediment after even moderate duration of the aging episode. Characterization of the whole process is attempted via four parameters. A key parameter is a limited stress range in which the decrease of compressibility persists. In the mathematical model the sediment develops a secondary microstructure through reactions of local dissolution/precipitation of less stable minerals. The secondary structure may reach a significant stiffness and compressive strength contributing to a higher overall *in situ* strength, but over a limited stress range. The mechanical behavior of the composite is described as that of a mixture of the superimposed continua deforming simultaneously.

Keywords: subsidence, sediments, aging, chemo-plasticity

1. INTRODUCTION

Despite advances in modeling of the deformational behavior of fluid-saturated porous solids, predictions of the actual subsidence based on numerical models tend to overestimate the surface displacement. For instance, a simulation of subsidence at Grøningen through Geertsma and van Opstal's (1973) model lead to four times higher maximum subsidence values than those observed. More recent non-linear models based on a separation of the horizontal flow in aquifers and the vertical 1-D Terzaghi consolidation within aquitards with back-calibrated empirical relationships for variable porosity, variable vertical permeability and specific storage (Rivera et al., 1991;), lead to the results much closer to those measured. Models of Wilmington subsidence based on a calibrated linear-elastic or Cam-clay based cap soil models accurately predicts the subsidence, but overestimate by a factor of three the horizontal extent of subsidence bowl (Kosloff et al., 1980). By the very nature of the back-calibration and forward projection in a non-linear domain such empirical approaches become less reliable when extrapolated and applied to conditions different from those used in the calibration, as emphasized by Rivera et al. (1991).

In conclusion, the state of the art in modeling and prediction of subsidence is less than satisfactory. A model user is currently presented with a choice between the theoretically consistent models that are based on the laboratory tests, but often yield results different from the field data, and the empirical models that are site-calibrated, but offer a limited confidence range in time and loading conditions. The interpretation of the results becomes even more complicated in the presence of natural compaction of fresh sediments contributing to overall subsidence (Carbognin et al., 1995) or a sea level rise (Gambolati et al., 1999). There is a clear need to both re-examine the physical and mathematical basis of the models, and to investigate a possible bias in experimental techniques and interpretation.

This paper examines a possible contribution to the above discrepancy between laboratory based predictions and field measurements attributed to the effect of the secondary compression on sediment stiffness and apparent preconsolidation stress, or in brief aging. Experimental results are presented.

2. BACKGROUND INFORMATION

The effect of aging has been recognized for long time and been attributed to diverse physical phenomenon collectively called aging or structuration (Leonards and Altschaeffl, 1964, Schmertmann, 1991, Zeevaert, 1983). While traditionally linked to clays, aging is also known to occur in sands, sandstones, and clayey sands (Schmertmann, 1991). However, no systematic analysis of it was attempted (except for Schmertmann 's (1991) Terzaghi lecture) nor have understanding of many its possible implications been reached. To briefly describe the nature of the phenomenon consider a natural sediment loaded in laboratory in 1-D strain conditions (in oedometer) up to its *in situ* stress and allowed to reach the end of primary consolidation, that is a state of normal consolidation. Subsequently, assume that the sediment is subjected to a secondary compression, at constant load for a long period of time, corresponding to a period of geological process of compaction. During the secondary compression soil develops certain strain. When loaded subsequently over an effective stress increment, as in the case of gas or oil extraction, the material exhibits a much higher "*apparent* precompression stress", and also a much lower compressibility, over certain stress range. However, upon a significant further loading, the compressibility tends to return back to the values, equal to or slightly higher than typical of normally consolidated clay. The phenomenon seems to be so universal to prompt Schmertmann (1991) in his Terzaghi lecture to wonder "...whether a natural clay, aging at a constant vertical effective stress ...ever exists in a truly normally consolidated state ".

The actual physico-chemical processes leading to the overall process of aging are not exactly known. Earlier hypotheses and some experiments (Mitchell and Solymer (1984), Denisov & Reltov (1961)) suggested that dissolution of some minerals in the primary structure (silica in the case of sand, and montmorillonite in the case of clays), which is known to be facilitated by inter-granular stress concentration, may contribute to an initial weakening and deformation of sediment. A subsequent change in electrolytic properties of the pore liquid (gel formation) may in turn contribute either to building a secondary structure onto the primary structure through formation of a rigid structure of sand bonded by silica acid gel film on particle surface caused by precipitation of silica from solution or suspension and acting as a cementing agent between them (Mitchell and Solymer, 1984 or in the pore liquid, turning it into a stress carrying suspension, flocculate or gel.

3. LABORATORY AGING OF NORTH ADRIATIC SEDIMENTS AND ITS EFFECT ON COMPRESSIBILITY

Experiments have been undertaken to verify if, and in the positive case, to what extent, the above described effects develop also in sediments of North Adriatic, at depths pertinent to oil/gas extraction. Two distinctly different materials were used, DALIA 1, and TEA 1 , the former being is predominantly sandy clay, and the samples used in the tests come from the depth of 1210 m. TEA 1 is predominantly clayey material, and that used in the tests comes from the depth of 3270m. The *in situ* effective vertical stresses were established for DALIA 1 as equal to 12.6 MPa, whereas for TEA 1 as 35.04 MPa. The main set of tests are oedometric tests performed on undisturbed material. They consist in one monotonic, incremental loading test, and one aging test with monotonic loading to the stress equal that *in situ* , of 12.6 MPa for Dalia 1, and 35.04 MPa MPa for Tea 1, followed by a pause of a constant loading of duration of 14 days, followed then by resumption of the monotonic loading. It is obviously realized that such test does not reproduce exactly the loading history of the actual sediments.

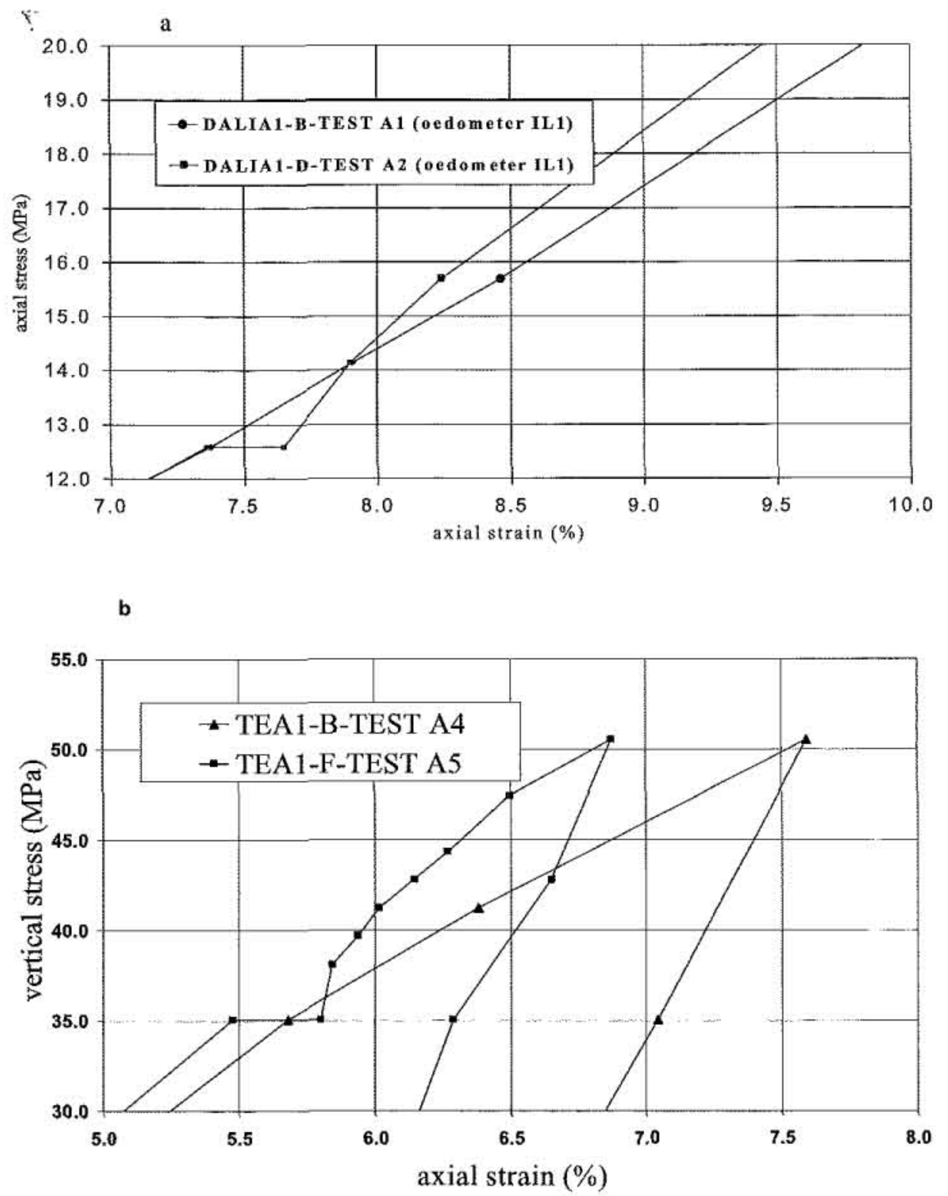

Figure 1 a and b. Axial stress-strain representation of oedometer test results above the in situ stress on undisturbed specimens of Dalia 1 (a), and Tea 1 (b) sediments.

The actual process is presumably composed of a series of loading episodes due to deposition of new alluvia and of secondary compression between them. The results for undisturbed sediments, both sandy (Dalia 1) and clayey (Tea 1) are shown in Fig. 1a and b.

Four principal characteristic aspects of the post-aging behavior were identified (see Fig. 2, in circled callouts), which are crucial for the subsidence prediction. These are: (i) decrease in incremental compressibility moduli in the post-aging stress excess range; (ii) relative reduction in strain in the post-aging stress excess range; (iii) a stress excess range affected by (i), (iv) strain gain during the aging period. The first three characteristics affect directly the numerical prediction of subsidence , the fourth one may be a factor in the experimental determination of the three former ones. There is another important characteristics of the post-aging behavior, which is (v) the total post-aging stress excess or total strain reduction range, defined as the total range in which stress is above the comparable stress, and strain is below that in reference monotonic tests. However, the values were not measured in the performed tests, because they were much higher than expected, and resulted to be outside the test range.

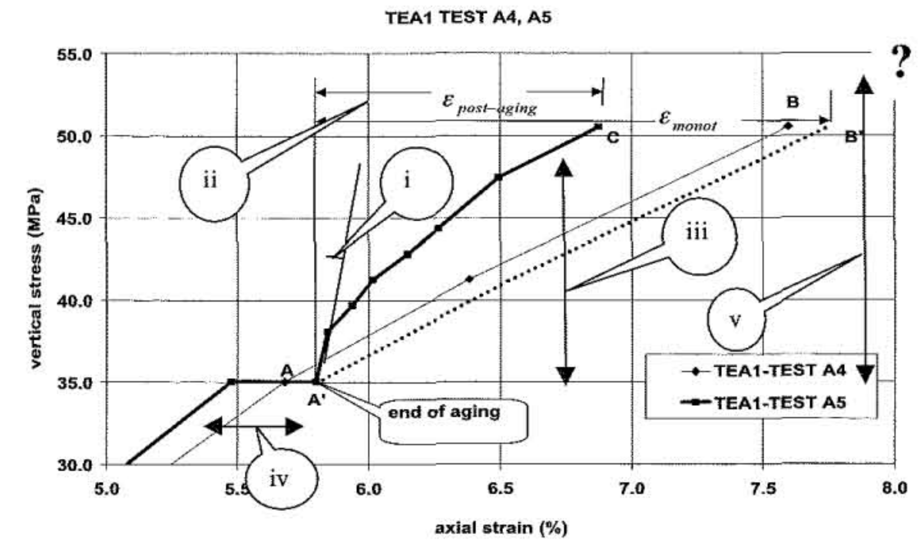

Figure 2. Cleyey sediment Tea 1. Response, A' C, to loading above the in situ stress of a 14 day aged, sample A5, and that, AB, of an un-aged material, test A4; A' B' is obtained by a parallel shifting of the curve, AB, from a monotonic loading.

The above characteristics (i) and (ii) of the post-aging behavior, both expressing the decrease in deformability have a different connotation. The decrease in the incremental moduli expresses a local effect, which is stress dependent. The strain reduction is an integrated effect and gives a global measure of the aging impact, over certain stress range above the aging stress level. The standardized stress excess value corresponds to the value at which the incrementakmoduli decrease falls to zero. The stress range is defined as that in which the incremental compressibility moduli are lower than in the reference tests, as opposed to the total stress range (v) where the stress value is above that in monotonic stress.

Deformability in oedometric tests is measured in terms of incrementally variable moduli either of compressibility index, C_c for a law expressing void ratio change as a function of a logarithmic measure of the axial stress component, with the uniaxial compressibility coefficient c_M, defined as

$$C_c = \frac{e_1 - e_2}{\log(\frac{\sigma_2}{\sigma_1})} \quad \text{or} \quad c_M = \frac{\varepsilon_2 - \varepsilon_1}{\sigma_2 - \sigma_1} \qquad \text{(1 a and b)}$$

calculated with a backward finite difference step.

To convey the sense of the effects of aging numerically, relative (normalized) values calculated for the four characteristics discussed above are summarized in Table 1, in terms of the average values below.

Table 1. Aging test highlights

material and sample type (all undisturbed)	relative reduction in incremental uniaxial compressibility modulus, c_M (i)	relative strain reduction due to aging (ii)	stress excess range affected by aging (iii)	ratio of strain gain to total strain at aging onset (iv)
avg. of DALIA	49.4% (&)	38.0%	12.0%*	2.1%
avg. of TEA	69.9% (#)	44.0%	45.0%	5.5%
avg. of all undist.	**59. 6%**	**41. 0%**	28.5%	3.8%

(&) at 112% of the aging stress
(#) at 116.6% of aging stress

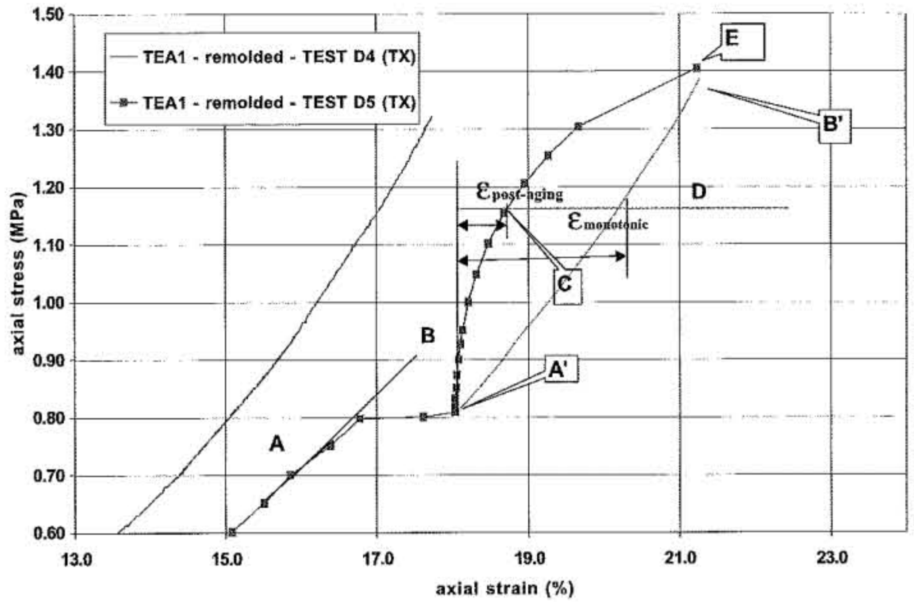

Figure 3 Remolded clayey samples TEA1- D4 and D5. Monotonic and aging test in triaxial apparatus simulating oedometric stress path. A'B' is a projection of the monotonic curve AB.

In generic terms, the clayey sediment TEA has shown a more pronounced effect of aging than the sandy sediment DALIA. However, characteristically, sandy and clayey sediments show a very similar range of relative strain reduction, even if other characteristics differ between the two types of sediments.

Because of a limited supply, and natural inhomogeneity of undisturbed sediments, additional tests were conducted on remolded compacted materials, where a fictitious *in situ* stress of 0.8 MPa was chosen for the aging stress level. Oedometric test results for remolded clayey material TEA 1 are shown in Fig. 3. In general for remolded materials, the numerical order of the observed aging effects in terms of normalized values is very close to those obtained from the tests on the undisturbed specimens. The most outstanding difference was observed in terms of the deformability immediately after the onset of post-aging loading, which in the remolded material is extremely low (20 times less than in monotonic tests, in terms of moduli in one test for DALIA1, and about 10 times for TEA1).

A single most important value in the summary Table 1 is the average 41% reduction in sediment deformation (at the standardized stress excess value) prediction if (14-day) aging is taken into account. In other words, deformation of the aged sediments is 60% of the non-aged sediments) in laboratory testing. Locally, at one specific stress value a nearly 60% reduction in incremental compressibility moduli may be expected, for details see Hueckel and Tao (1999).

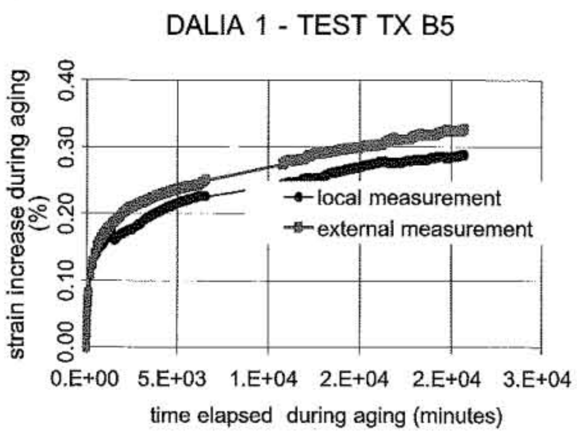

Figure 6. Strain development during aging effect in remolded material at stress of 0.82 MPa

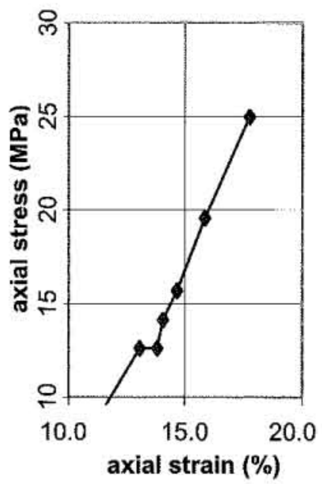

Figure 7. Seven month aging test E4 (detail) on Dalia 1

However, in the context of subsidence two additional concerns need to be addressed. First, the phenomena of aging and the associated secondary compression might be expected to occur also after the end of extraction. The secondary compression would then annihilate the benefit of the decreased of deformability due to "first aging ". However, it appears that this is not the case and that sediments have the memory of their previous aging episodes. Tests performed on remolded Dalia B8 and B10 samples show that when aging is repeated at the same stress level after a cycle of partial unloading, the amount of strain during "second aging " is up to more than one order of magnitude lower than during the "first aging ". The rate of straining over the first two hours in both cases was respectively, $2.11\text{x}10^{-6}$ [1/min] vs $1.073\text{x}10^{-5}$ [1/min]. For B10 for first 16 minutes of aging at much lower stress (0.5 MPa) the rates were $1.125\text{x}10^{-5}$ [1/min] and $4.91\text{x}10^{-5}$ [1/min], respectively. It is thus clear that aging has an irreversible and cumulative effect.

The second issue is that of the duration of aging episode. Figure 5 shows the time function of strain during aging in test on remolded specimen B6. It is clear that the rate of straining changes significantly after 24 hours, but it is also clear that the rate does not decrease significantly after 14 days. However, the material stiffening seems to occur much faster. Two accidental, short duration, aging episodes were characterized by a significant decrease in deformability (75% reduction of the uniaxial compressibility modulus). However, the stress range affected by the short-term aging is very small, 5% of the aging stress level, against 28%, for a longer term aging.

To further explore the effect of aging duration, a 3- and 7-month aging episode effects on compressibility were tested on Dalia1 specimens. The most prominent observation is that there is relatively little difference between 3, 7 month test and two week test. The biggest difference (see Fig. 7) is in the strain developed during aging during 7 months is 0.759%, against 0.165% in test A2 and 0.210% in test C1, (both with a 14 day aging). As for compressibility, the decrease in compressibility modulus over 7 month is from 4.61x10 -4 cm^2 /kg to 1.935x10 -4 cm^2 /kg, that is 57.9%, against analogous decrease for 14 –day tests A2 and C1, of 49.4% and 54%, respectively. Thus, it appears that some effects in aging are more time dependent than other .

The observed reduction in compressibility in the post-aging stress range leads to a proportional (~40%) reduction of subsidence prediction according to 1-D, linear compression theory. Therefore, it may be argued that since subsidence is preceded *in situ* by an extensive aging process, and the response of the sediment should be characterized by the post-aging moduli, as resulting from the proposed experimental procedure.

4. AN OUTLINE OF A MODEL OF THE AGING SEDIMENT WITH EVOLVING SECONDARY STRUCTURE.

In this Section we shall outline a framework for a model of the aging sediment with an evolving secondary structure, following the original hypothesis by Mitchell and Solymer (1984). It is assumed that in the aging conditions soil develops a secondary microstructure through physico-chemical reactions of local dissolution/precipitation of some less stable minerals. In this model the initial (primary) structure consist exclusively of a system of grains. At constant *in situ* stress linked to overburden, a state of compressive strain may be increased during dissolution over an irreversible strain of the primary structure, linked to its "chemical softening ' (Hueckel et al., 1999) in analogy to thermal softening. Further during aging the dissolved silica (or other mineral dissolved) precipitates onto this primary structure forming a secondary structure. This secondary material structure remains unstressed and unstrained if the two processes are sequential.

Any additional compressive stress is distributed between the two components, because the two materials now deform jointly. Thus, it is an increment is a sum of the rates of the partial stresses, or a weighed sum of the specific partial stresses in the constituents

$$\dot{\sigma}_{ij} = \dot{\sigma}_{ij}^{(I)} + \dot{\sigma}_{ij}^{(II)} = \dot{\sigma}_{ij}^{(1)}\alpha + (1-\alpha)\dot{\sigma}_{ij}^{(2)} \tag{2}$$

The partial stress components $\sigma^{(I)}$ and $\sigma^{(II)}$ are total stresses carried by the individual fractions, whereas $\sigma^{(1)}$ and $\sigma^{(2)}$ are specific partial stresses occurring in the material of each fraction. In a simplest option coefficient α, $0 < \alpha < 1$ is related to the fractions of the two materials in the total volume of solids, considered as constant. Before reaching the aging stress σ_{ag}, the load is carried by the only constituent, i.e. primary material (1). After completion of the aging episode, two materials partake in the stress transmission, and the total stress now reads:

$$\sigma = \sigma_{ag} + \alpha\sigma_{ag}\,exp(\frac{e_a - e}{K_3^{(1)}}) + (1-\alpha)\sigma_j^{(2)}\left[1 + exp(\frac{e_j^{(2)} - e}{K_{j+1}^{(2)}})\right];\ for\ e_j^{(2)} > e > e_{j+1}^{(2)} \tag{3}$$

where $j = 0, 1, 2$ ...are number of nodal points of the beginning of each segment. The superscripts *(1) and (2)* refer to primary and secondary material, respectively . Note that material *(1)* is characterized only by one segment above the *in situ* stress, σ_{ag}. $K\,i^{(l)}$ denotes piecewise modulus, for the segment i - $i+1$, whereas $\sigma_i^{(l)}$ denote stress values at the initial node of the segment. The aging strain, and the corresponding decrease in void ratio of Δe_a are taken directly from the experiments. The numerical parameters used for the simulation are listed in Table 2. The material parameters for the primary material were identified on the basis of the pre-aging phase behavior.

Table 2. Model parameters to simulate post- aging behavior of DALIA-A2

Material	σ_0*	σ_1	σ_2	σ_3	K_1	K_2	K_3	K_4
1	0.1	4.0	12.59	-	0.014	0.06	0.178	-
2	0.1	3.9	7.2	27.0	0.0009	0.0101	0.0305	0.055

*: stress unit, MPa; e_0=0.5 9; α = 0.629

It may be seen that the specific partial stress difference in the secondary material is higher than the corresponding partial stress difference in the primary material. Note however, that the global partial stress in material (1) is its "initial " aging stress, (12.59 MPa) plus the stress difference, or 19.07 MPa. Thus it is larger than that in the secondary material up to the strain of about 0.03. The above results suggest that the secondary structure play a vital role in decreasing sediment compressibility. From the engineering point of view, it is the load above the in situ stress that is important. In carrying this load the role of the secondary material is more important than that of the primary material. Thus, understanding of its strength is crucial for the prediction of the stress range in which the decreased compressibility occurs.

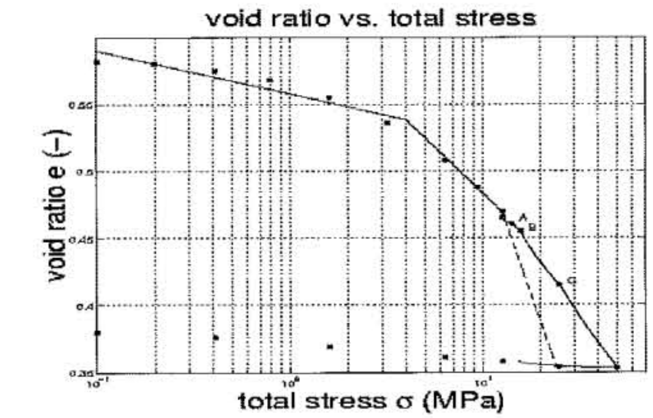

Figure 8a. Aging of DALIA-A2

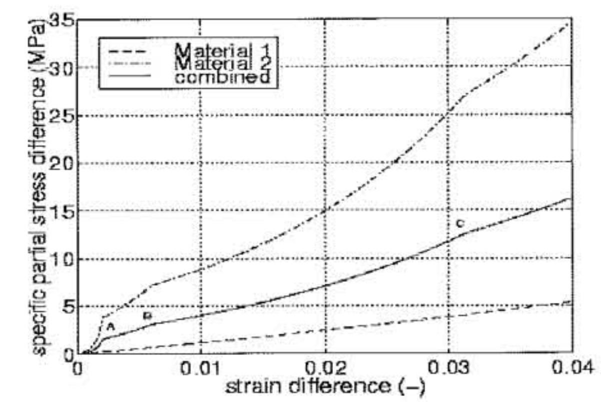

Figure 8b. DALIA-A2: specific partial stress difference

5. CONCLUSIONS

Experiments performed on undisturbed clayey and sandy sediments subject to a moderate duration aging (14 days) at the *in situ* stress level respond to a further loading with a deformability reduced nearly 40 %, when compared to those tested in a traditional way with monotonic loading. That leads to a proportional (~40%) reduction of subsidence prediction according to 1-D, linear compression theory. This effect occurs in a stress range in excess to the *in situ* stress of 12% to 45% of the *in situ* stress value. It is argued that subsidence is preceded *in situ* by the extensive aging process, and thus its response could be characterized by the post- aging moduli. Clearly, the above tests constitute only an exploratory effort, and further tests are needed prior to proposing a new industrial practice.

Acknowledgment

Experiments were executed at ISMES, Bergamo, Italy.

REFERENCES

Carbognin L., Tosi L. & Teatini P. (1995) Analysis of actual land subsidence in Venice and its hinterland (Italy). In: *Land Subsidence - Proc. 5th Int. Symp. on Land Subsidence*, Eds.: B. J. Barends, J. J. Brouwer and F. H. Schröder, Balkema, Rotterdam, 129 - 137.

Gambolati G., Teatini P., Tomasi L., & Gonella M. (1999), Coastline regression of the Romagna region, Italy, due to natural and anthropogenic land subsidence and sea level rise , *Water Resourses. Res.* **35** (1) 163-184,

Geertsma J. & van Opstal, (1973) A numerical technique for predicting subsidence above compacting reservoir compaction based on the nucleous of strain concept, *Verhandl. Konigl. Nederl. Geolog. Mijnbouwk*, Gen. Vol., **28**, 63 -78.

Hueckel T. & F. Tao (1999) Reduced compressibility of aged sediments subject to oil/gas exploitation induced subsidence, Fin. Report, Duke U., for Agip, v. 1, p.86

T. Hueckel, F. Tao, G. Cassiani & A. Pellegrino, (1999) Reactive plasticity for geological materials with a double structure evolving during aging, *in Constitutive Laws for Engineering Materials,* R.C. Picu and E. Krempl, eds ., 383 –387.

Kosloff, D., R.F. Scott & Scranton, 1980, Finite element simulation of Wilmington oil field subsidence: Non-linear modeling, *Tectonophys.*, **70**, 159-183.

Leonards, G.A. & Altschaefl, A.G., 1964, Compressibility of clay, *J. of Soil Mechanics and Foundations Division, ASCE* , **SM5**, 133-155

Mitchell, J.K. & Z.V. Solymer, (1984). Time dependent strength gain in freshly deposited or densified sand, *J. Geotech. Engineering,* **110** (11), 1559-1576

Rivera, A., Ledoux E. & G. de Marsily, (1991), Non-linear modeling of groundwater flow and total subsidence of the Mexico City aquifer aquitard system. In: *Land Subsidence* , IAHS Publ., 200, 45-58

Schmertmann , J.H. (1991). "The mechanical aging of soils ", *J. Geot. Eng.* , **117**, 9

LAND SUBSIDENCE - Vol. II
Proceedings of the Sixth International Symposium on Land Subsidence
Ravenna / Italy / 24-29 September 2000

COMPACTION MONITORING FROM RADIOACTIVE MARKER TECHNIQUE

Paolo Macini and Ezio Mesini
University of Bologna, Viale del Risorgimento 2, 40136 Bologna, Italy

Abstract

The study reports the fundamentals of Radioactive Marker Technique (RMT) for the estimation of reservoir rock compaction. RMT is based on the placement of low-emission radioactive bullets (markers) along the wellbore. The measurement of the distance variation between two markers, within an appropriate timeframe, allows for the monitoring of compaction phenomena, especially in unconsolidated reservoirs. This technique seems suitable to provide good estimations of uniaxial compressibility coefficients to perform subsidence modelling. Finally the study reports some applications of RMT in the Adriatic Sea, The Netherlands, North Sea and Gulf of Mexico. In some field examples, RMT-derived uniaxial compressibility coefficients match with sufficient precision with the ones calculated from the surface subsidence actually observed over the field.

Keywords: subsidence, compaction, *in-situ* measurements, markers.

1. INTRODUCTION

Production of underground fluids is often associated with compaction of the reservoir rocks, which can be transmitted to the surface through the overburden of the formations above. Formation compaction is an issue of great concern and uncertainty in unconsolidated reservoirs: in fact, it can reduce formation porosity and permeability, influencing the reservoir fluids production, the final recovery (Macini and Mesini, 1998), and hence the economy of the field. Apart from the estimation of the magnitude of the compaction drive vs. secondary recovery project (e.g., waterflood), it is believed that the pressure depletion and the associated compaction may cause fracture closure, affecting recovery efficiency and well productivity. Moreover, compaction may induce casing deformation, either in the producing zone or in the overburden, creating operational problems to the well.

Formation compaction of onshore reservoirs should be carefully monitored, due to possible environment impairments induced by subsidence phenomena. This is true also for offshore reservoirs, where compaction can influence coastal territories (especially when reservoirs are located nearby the coastline), and can induce subsidence of the sea floor, leading to severe safety problems for production platforms.

The monitoring of compaction phenomena due to fluid withdrawal can be studied by matching land subsidence values, predicted by mathematical modelling (Evangelisti and Poggi, 1970; Geertsma, 1973; Gambolati et al., 1991, *etc.*), and field data obtained by GPS and geodetic measurements (Fourmaintraux et al., 1994). The application of modelling requires the availability of reservoir geometrical data, production history data and uniaxial compressibility coefficient C_m. At present, there is a considerable gap between the quality of simulations achieved by the more and more sophisticated mathematical models and the much lower quality of geomechanical measurements that are necessary as input data. A correct study requires that the quality of the model be comparable to the one of its input data. Thus, in order to improve the studies of subsidence, it is vital to enhance measurements of the mechanical properties of the formations under investigation. In particular, the estimation of C_m is critical for the precision of the models. The measurement of C_m still concerns researchers, for both the intrinsic type of techniques, and the statistic validity of sampled points, connected with the possibility to characterise large volumes of formation by relatively few measurements.

C_m can be evaluated by both *in-situ* and laboratory measurements (Brighenti et al., 1998). Laboratory measurements investigate the behaviour of the material in a wide range of stress conditions. However, these measurements, performed on centimetric samples, cannot give information on macro-discontinuities, and often it is very difficult to take into account the influence of damages induced by coring operations (Holt et al., 1994). Experimental simulations (Netland et al., 1996) have proven that for relatively unconsolidated formations, laboratory measurements are likely to overestimate the initial compaction rate significantly. Amongst the *in-situ* measurements, Radioactive Marker Technique (RMT) is the most developed method to measure the compaction of deep formations. Moreover, this technique allows also for the evaluation of C_m in reservoir conditions. To this purpose, it is a good practice to perform measurements in front of homogeneous sections, avoiding measurements inside of thin clay and sand interbeddings, or straddled between formations with large differences in pore pressure.

This paper reports the fundamentals of RMT, and its applications for the compaction monitoring of oil and gas fields. In particular, the research examines the compaction monitoring programme started in the Adriatic Sea, the well-studied case of Groningen gas field (The Netherlands), and other offshore North Sea and Gulf of Mexico applications.

2. RADIOACTIVE MARKER TECHNIQUE (RMT)

RMT was originally designed to monitor the subsidence of the Champion oil field offshore Brunei (Schmitt, 1996), and then successfully applied to the Groningen gas field and to the Ekofisk field in the North Sea (Mobach and Gussinklo, 1994; Menghini, 1989). RMT is based on the placement of low-emission radioactive bullets (markers) in the formations under depletion, using tools similar to those used for casing perforation (Fig. 1). In order to evaluate the possible compaction in the very early stage of production, the markers should be implemented before casing operations. The position of each marker can be determined by specialised wireline Gamma Ray (GR) logs, which are run at regular time intervals to estimate the possible temporal changes in the distance between the markers. In fact, moving a set of radioactivity detectors at a constant speed results in a correlation of the count rate vs. time, which can be transformed in distance.

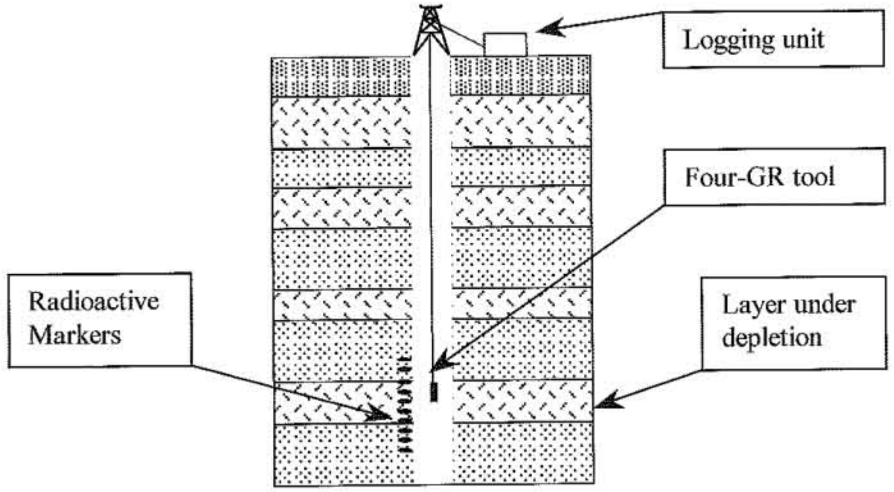

Figure 1. Schematic of Radioactive Marker Technique

RMT adopts a marker spacing of the order of 10 m, a distance dictated by the geometry of the logging tool. The markers are characterised by a radioactive source (Cs^{137} or Co^{60}, which have a relatively long half-time, about 5 years) contained inside a bullet-shaped steel case. Source strength ranges between 150 and 300 μCurie (usually, 150 μCurie in 8" holes and 300 μCurie in 12-1/4" holes). However, some applications were made with sources of lesser strength, from 5 to 10 μCurie (Green, 1991; De Kock et al., 1998), which were proven to be not adequate to the expected length of the monitoring programme (5 to 10 years). In order to avoid problems of environmental contamination, the radioactive source is sealed inside a leak-proof steel container, inserted into the hardened steel body of the bullet. The bullets, similar to the ones used for casing perforation, are shot by means of a bullet gun perforator, utilising a small charge (usually, 5 to 20 g), variable accordingly to the formation properties and borehole conditions. The selection of the correct amount of explosive is very important for the effectiveness of the measurements. In fact, the marker must be implemented not too deep inside the formation (in order to avoid difficulties for its detection, being the GR response too weak to measure), and not too shallow, in order to avoid a possible dislodging by centralizers when casing is set.

The critical stage of RMT can be split into two major points: 1) the detection of markers position, and 2) the measurement of relative distances between each pair of adjacent markers. The location of each marker can be calculated by utilising several methods, either based on numerical techniques, or on the physical principles of GR measurements.

As for the numerical techniques, the simplest one is the "peak method", which locates the marker at the depth where the GR count rate takes the peak value. The "midpoint method" is based on the location of two depths, above and below a peak, identified where the GR count rate reaches a fixed threshold value; the marker location is then calculated as the mid-point of the depth interval. The "area method" relies on the calculation of the area under the count rate curve above the threshold between two depths; the marker location is calculated as the point, which determines half of the area in the depth interval. The "inflection-point method" is based on the calculation of inflection points on the GR peak flanks; the marker location is assumed to be at the intersection of the tangents drawn through the inflection points. One more approach is the "slope method", which locates the peak as the intersection point of two straight lines which fit the two sides of the GR curve.

A method based on a physical response derives by modelling the signal to a point-like GR source (marker). It has found that the GR count rate at a detector can be represented by an attenuating Lorentzian distribution (De Kock et al., 1998), that allows to determine the marker's vertical location by fitting the GR count rates to the distribution. In addition, the Lorentzian fit enables one to determine the marker's lateral location (D) from the width of GR count rate. The estimation of D, together with its temporal change, may be used in identifying horizontal stress-pressure gradient in the formation. Moreover, the evaluation of the lateral location is paramount to correctly estimate the vertical compaction of the layer under depletion. In fact, the presence of a casing causes perturbations of the deformation in the vicinity of the borehole (Brighenti et al., 2000). In particular, the deformation around a cased hole is less than the one of the undisturbed formation. These perturbations are much more evident in proximity of the borehole ($D < 10$ well radii), and, *a fortiori*, for unconsolidated formations, characterised by a rigidity much less than the one of steel casing.

As far as the measurement of the relative distance between each pair of adjacent markers is concerned, it is useful to consider that, in theory, it is possible to measure the distance between each pair of adjacent markers by a single GR detector run in the hole by a wireline tool. In practice, this kind of measurement induces errors larger than the quantity under investigation; in fact, the absolute precision of a cable-based measurement, due to cable stretch, "*yo-yo*" and stick-and-slip motion, is not adequate to evaluate the compaction of a relatively short interval of formation, especially in highly deviated wells. To avoid

these errors, the most recent tools utilise four GR detectors, positioned on a rigid measurement base, whose length is approximately equal to the distance between each pair of adjacent markers. Theoretically, two detectors are enough for a correct measurement, but it is preferred to have data redundancy for the interpretation. Being the distance between the detectors precisely known (approximately equal to the distance between each pair of adjacent markers), during the measurement the wireline cable shifts a very short distance, limiting the errors due to cable movement registration. Considering the number of detectors, the spacing, and the distance between the recorded GR peaks, it is possible to derive simple relationships for the calculation of the distance between two adjacent markers (Fig. 2).

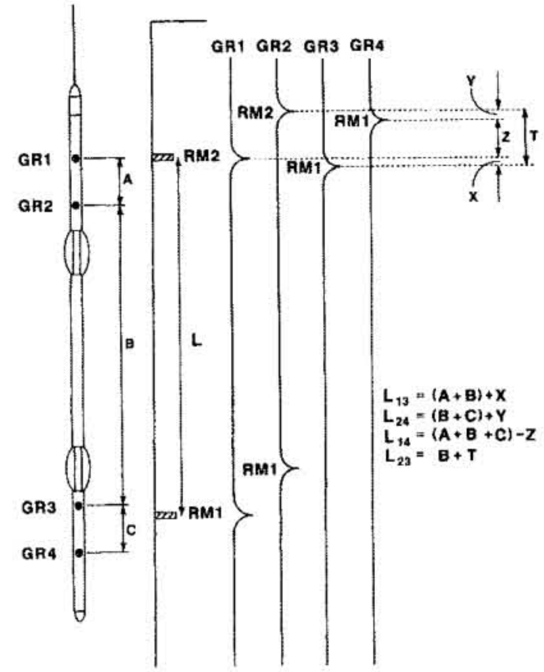

Figure 2. Theoretical log of a four detectors tool (curves GR1, GR2, GR3, GR4), recorded in front of two markers (RM1, RM2) (from Menghini, 1989).

The more the distance between two markers equals the distance between the detectors, the more is the accuracy of the measurement. Usually, the rigid measurement base (*i.e.*, the tool, whose thermal deformation can be precisely calculated) features two pairs of detectors, positioned at 9 and 12 m from each other. The tool is also equipped with a precision thermometer, to record temperature variations, and with a three-axes accelerometer, to correct for the tool movement in case of variation of the logging speed during the run ("*yo-yo*" and stick-and-slip motion). The calibration of the measurement base is of paramount importance: usually, it is performed by means of a precision reference base, a bar made with low deformation materials (*e.g.*, *Invar*), which mounts four GR sources, whose distance is known within a precision of 10^{-2} mm. With a four detector tool, the distance between two markers can be measured four times during a single logging pass. The standard practice is to run three passes, giving 12 individual and independent measurements of the distance. Logging speed ranges from 1.5 to 3 $m \cdot min^{-1}$, while data are collected at 0.1 inches intervals. Particular situations (*e.g.*, logging inside a production tubing, *etc.*) may require a reduced logging speed (1 $m \cdot min^{-1}$).

Figure 3 reports the influence of logging speed variation on the quality and shape of the GR peaks, which can negatively affect the final log interpretation.

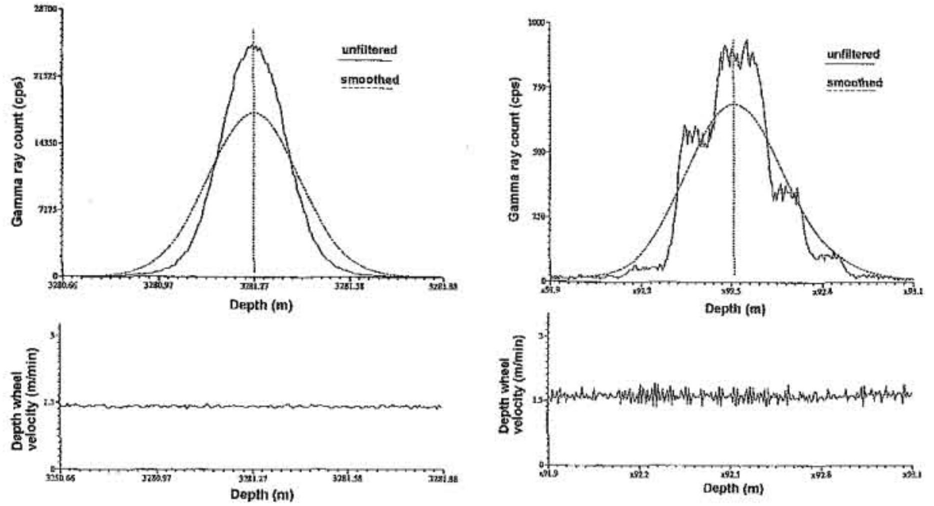

Figure 3. Left: filtered and smoothed registration of GR signal (above); the logging speed is fairly constant (below). Right: the same, when the logging speed is not constant (below), because of overpulls during the run.

The log output does not permit any kind of quick interpretation on site: however, it allows for the control of the correct data acquisition. The log interpretation is usually performed by a computing centre, where it is possible evaluate the distance between each pair of adjacent markers. Spacings with the higher standard deviation are discarded and, after the application of the necessary log corrections, it is obtained the "true" spacing and its closure, calculated from the average of the single values, which represents the actual distance between two adjacent markers. The attainable precision is of the order of 10^{-4}, that is 1 mm/10 m (Schlumberger, 1994; Pemper et al., 1996), but probably less, about $3 \cdot 10^{-4}$ (De Kock et al., 1998, Ramirez and Zubillaga, 1987).

3. APPLICATIONS IN THE ADRIATIC SEA

In 1992, a campaign to control formation compaction due to gas production has been started in the Adriatic Sea, where five offshore fields were instrumented with radioactive markers. Marker position is determined by FSMT (*Formation Subsidence Monitoring Tool*, Schlumberger) and CMI (*Compaction Monitoring Instrument*, Baker Atlas). In order to improve data quality, and to have information about log repeatability before the reservoir depletion, it is common practice to run a control survey after the well completion. Marker spacing has been periodically surveyed every 1 or 2 years, depending on the reservoir depressurisation. During the measurements it is also recorded the static reservoir pressure for each interval, which is necessary for the estimation of C_m. At the end of 1999, at least 11 surveys have been run in the Adriatic Sea.

From the measurements, C_m has been determined for each single layer, where a pressure decline occurred. In particular, in order to minimise the effects of random errors, C_m has been determined as a mean value calculated over a variable number of adjacent layers, and not as an absolute value associated to each single layer (Bevilacqua et al., 1999). Considering N + 1 markers (*i.e.*, N intervals), and the generic interval i (i = 1, ..., N) of initial thickness H_i, assuming that for a pressure drop ΔP_i the i-th interval be subjected to a thickness variation ΔH_i, it is possible to define the mean effective uniaxial compressibility C_m as follows:

$$C_m = \frac{1}{\Delta P} \sum_{i=1}^{N} \Delta H_i \Big/ \sum_{i=1}^{N} H_i \qquad (1)$$

where: ΔP = mean effective pore pressure drop of the interval considered.

The value of C_m depends on the definition of ΔP, that is the mean depressurisation of the interval of formation considered. This definition is quite arbitrary, and thus it is necessary to establish an assumption. The simplest one is to calculate ΔP as the mean depressurisation weighted by the thickness of each interval between the markers. With this hypothesis, it can be derived that C_m represents a weighted mean of the C_m^i of each interval, the weight being the pressure drop of each interval; thus, eq. (1) can be rewritten as:

$$C_m = \sum_{i=1}^{N} C_m^i \Delta P_i \Big/ \sum_{i=1}^{N} \Delta P_i \qquad (2)$$

In this way, C_m is more influenced by the intervals where the depressurisation is larger. This result agrees with the fact that the larger the depressurisation, the smaller the uncertainty associated with C_m, being the standard deviation of C_m^i the inverse of the depressurisation ΔP_i by which it is calculated.

The calculation of C_m by the analysis described above, are plotted in Figure 4 (Bevilacqua et al., 1999; Palozzo, 1999). Here are reported also the histograms of C_m values obtained by lab oedometric tests, on cores taken from several wells of Adriatic offshore. Results show that C_m values obtained by RMT are smaller than the ones obtained with laboratory oedometric tests. The difference is about one order of magnitude, by comparing the second loading cycle, and even more, by comparing the first loading cycle. However, a large data scattering was observed, as well as a high variability of the associated standard deviation. It is thus necessary to acquire much more experience before RMT can be used to predict land subsidence in the Adriatic gas fields (Baù et al., 1999).

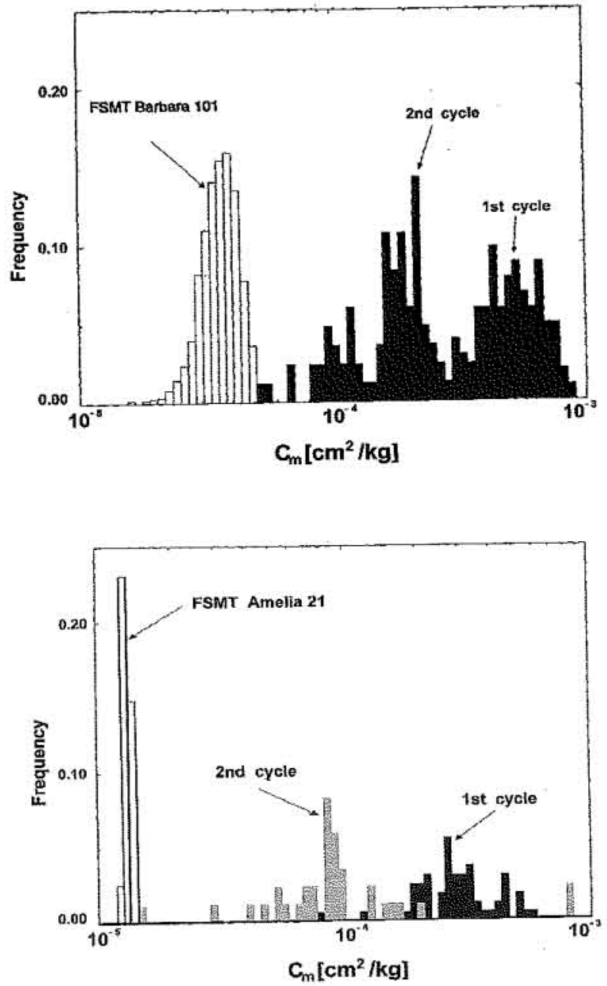

Figure 4. Markers-derived Cm's for well Amelia 21 (below) and Barbara 101 (above). It is possible to compare the values calculated by the log (FSMT) with the ones obtained by laboratory oedometric measurements (1st and 2nd cycle).

4. OTHER APPLICATIONS

Formation compaction in Groningen gas field is monitored since the start of production (1964). Eight wells, spread across the field, were dedicated to *in-situ* compaction measurements. RMT was initiated in 1967 (De Loos, 1973), and in 1982 the four detector monitoring tool (FSMT) was introduced. The application of this technique is quite unique for this field, as it is normally used to monitor compaction in unconsolidated reservoirs. Here the reservoir rocks are so competent, that the target resolution is very close to the instrument resolution. In practice, it has been proven difficult to obtain the required accuracy that is of the order of 1 mm/10 m (Mobach and Gussinklo, 1994). The pressure decline during the measurement period is on average 120 bar.

Over the years, much effort has been put into improving the accuracy and reliability of the measurements, improvement on tools as well as on interpretation techniques. In 1993-94, part of the surveys have been re-interpreted, using a new marker position algorithm, and a selection mechanism has been developed to identify statistically significantly deviating data. As a result, in all but one well could the C_m be obtained. The study has shown that the measurements can be used to determine the total compaction of the reservoir, but the accuracy of the measurement is not adequate to determine the compaction of individual intervals. The *in-situ* measured C_m matches with the one as inferred from the surface subsidence over the field, measured by levelling (Fig. 5). It is believed that a better calibration procedure could reduce the effect of systematic errors. The best way would be to calibrate the distance between the detectors in a way where the tool remains stationary (Schmitt, 1996; NAM, 1995). In this way, errors caused by movement of the instrument can be avoided.

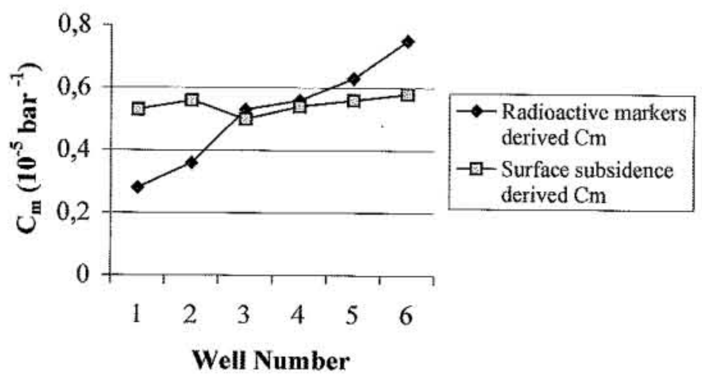

Figure 5. Comparison between surface-subsidence-derived C_m's and RMT-derived C_m's (rearranged from Mobach and Gussinklo, 1994).

The Ekofisk field was discovered in 1969, but only in 1984 a vast subsidence phenomenon was discovered, through measurements from fixed platform references to mean sea level (Menghini, 1989). The first compaction monitoring programme was based on the analysis of open- and cased-hole neutron logging surveys. Because of the scarcely accurate methods of mechanical depth-measurements, and of non-distinct formation signatures in some wells, the results of this campaign were only rough estimates. The accuracy was of the same order of magnitude as the compaction rate, about 60 cm per year. In 1985 a compaction monitoring programme began with the installation of radioactive markers of 100 to 150 μCurie strength. Numerous technical problems were encountered in this field, mainly related to the presence of directional wells, tubing diameter, weak formations, hole washouts, *etc.* After the solution of these problems, a survey (run six month later the base log) produced accurate measurements. Compaction rate for the reservoir was calculated to be 55 ± 10 cm per year. The conclusion from the first part of the monitoring campaign indicated that compaction could be accurately measured at time intervals as small as every 3 to 4 months. So far, it seems that no estimation of C_m have been published for this field.

RMT baseline logs were collected successfully in four wells in a deepwater development field of Gulf of Mexico (De Kock et al., 1998). In particular, FCMT (*Formation Compaction Monitoring Tool*, Halliburton) was run in 1996-97. The log results will be used as a baseline log in future compaction monitoring. All the wells were cased in producing zones, and markers were not shot into the formation. In this application, four 10 μCurie Cs^{137} sources were implemented on the outside wall of each casing. Expected accuracy, already tested in a laboratory facility, is about $3\cdot10^{-4}$. In this application, it is interesting to acknowledge the use of a new algorithm to determine the vertical and the lateral location of the marker. The GR detector response has been modelled with a Lorentzian distribution. In this case, considering the source placed near the detector, the GR count may be further approximated by a simpler Lorentzian distribution:

$$I(z) = A\frac{1}{(z-z_0)^2 + D^2} + B \qquad (3)$$

where: z and z_0 = vertical location of the detector and of the source, respectively, D = lateral distance between the source and the logging tool axis, A = source strength, B = background, I(z) = signal intensity.

5. CONCLUSIONS

RMT seems to represent a promising technique for monitoring the compaction of geological formations and for estimating the uniaxial compressibility

C_m in reservoir conditions. At present, the technique is much more reliable in unconsolidated formations, where the compaction rate is higher than the intrinsic precision of the measurement: in general, it has been proven really difficult to reach the expected accuracy of a few mm per 10 m. Measurement precision is influenced by irregular speed of both tool and depth wheel, by marker signal strength, by tool calibration and by number of log passes. Possible improvements of RMT could be obtained on one hand by using a different measurement technique, e.g. with the tool performing the survey stationary across the marker (even though this technique seems to be too much time-consuming). On the other hand, further possible developments could be found in the implementation of new numerical algorithms to locate the marker position, to determine the distance between a pair of marker, and, possibly, to evaluate the marker lateral location.

In the case of unconsolidated formation and in presence of a cased hole, RMT compaction measurements can be seriously influenced by the lateral location of the markers, since the vertical compaction measured in proximity of the borehole might not be representative of the one measured in the undisturbed zone.

RMT-derived C_m's in some of the field applications examined in this study seem in good agreement with the compressibility inferred from the measured surface subsidence from levellings. For the Adriatic Sea, C_m's from laboratory measurement are overestimated with respect of the ones from RMT. However, it still seems to be a good practice to perform laboratory and *in-situ* measurements, and to compare these results with those obtained from high precision levellings.

REFERENCES

Baù, D., Gambolati, G., & Teatini, P. (1999) Statistical analysis of in situ compaction measurements for anthropogenic land subsidence prediction in the Northern Adriatic basin. *Proc. 5th Conf. Int. Ass. Mathematical Geology*, Vol. I, Trondheim, 299-304.

Bevilacqua, N., Cassiani, G., Macini, P., & Mesini, E. (1999) Compaction monitoring in Adriatic gas fields. *Proc. 10th International Scientific and Technical Conference "New Methods and Technologies in Petroleum Geology, Drilling, Reservoir and Gas Engineering"*, Krakow, 103-112.

Brighenti, G., Macini, P., & Mesini, E. (2000) Measuring reservoir compaction: a study on in-situ techniques. In *Land Subsidence*, Vol. II Proc. Sixth Int. Symp. on Land Subsidence, Ravenna, Italy, Sept. 2000, Eds. L. Carbognin et al., 17-29.

De Kock, A.J., Johnson, T.J., Hagiwara, T., Zea, H.A., & Santa, F. (1998) Gulf of Mexico subsidence monitoring project with a new formation-compaction monitoring tool. *SPE Drilling. & Compl.*, **13**, 223-230.

De Loos, J.M. (1973) In situ compaction measurements in Groningen observation wells. *Verhandelingen Kon. Ned. Geol. Mijnbouwk. Gen.*, **28**, 79-104.

Evangelisti, G., & Poggi, B. (1970) Sopra i fenomeni di deformazione dei terreni da variazioni della pressione di strato. *Mem. Acc. Sci. Ist. Bologna,* **II,** 6, 1-124.

Fourmaintraux, D.M., Flouzat, M., Boutéca, M.J., & Kasser, M. (1994) Improved subsidence monitoring methods. *Paper SPE/ISRM 28095, Proc. Eurock '94*, Delft, 549-556.

Gambolati, G., Ricceri, G., Bertoni, W., Brighenti, G., & Vuillermin, E. (1991) Mathematical simulation of the subsidence of Ravenna. *Water Resources Research,* **27** (11), 2899-2918.

Geertsma, J. (1973) Land subsidence above compacting oil and gas reservoirs. *J. Petr. Tech.*, **25**, 734-744.

Green, D.E. (1991) Subsidence monitoring in the Gulf Coast. *Paper SPE 22884, Proc. 66th SPE/ATCE*, Dallas, 665-678.

Holt, R.M., Brignoli, M., Fjaer, E., Unander, T.E., & Kenter, C. J. (1994) Core damage effects on compaction behaviour. *Paper SPE/ISRM 28027, Proc. Eurock '94*, Delft, 55-62.

Macini, P., & Mesini, E. (1998) Static and dynamic reservoir rock compressibility at high pressure. *Paper SPE 49549, Proc. 8th Adipec (Abu Dhabi Petroleum Conference)*, Abu Dhabi, 813-820.

Menghini, M.L. (1989) Compaction monitoring in the Ekofisk area chalk fields. *J. Petr. Tech.*, **41** (7), 735-739.

Mobach, E., & Gussinklo, H.J. (1994) In-situ reservoir compaction monitoring in the Groningen field. *Paper SPE/ISRM 28094, Proc. Eurock '94*, Delft, 535-547.

NAM (1995) Subsidence caused by natural gas production: summary of 1995 Groningen subsidence prognosis. *NAM report nr. 27600*, Assen, 28 pp.

Netland, S.O., Knapstad, B., & Holt, R.M. (1996) Estimation of in situ compaction modulus from tidal response in well test data. *Paper SPE 36821, Proc. European Petroleum Conf.*, Milan, 81-87.

Palozzo, W. (1999) Studio modellistico di subsidenza nel campo a gas offshore "Barbara". *MS Thesis*, University of Bologna, 210 pp.

Pemper, R., Ahmad, I., Brewer, J., & Gold, R. (1996) Development of a compaction monitoring measurement system. *Proc. 17th SPWLA European Symp.*, Amsterdam.

Ramirez, M.O., & Zubillaga, J.I. (1987) Applications of well logging for compaction and subsidence studies in the Orinoco oil belt, Venezuela. *SPE Paper 16773, Proc. 62nd SPE/ATCE*, Dallas.

Schlumberger (1994) Formation subsidence monitoring. *Internal report.*

Schmitt, T. (1996) The measurement of the subsidence of geological formations with position sensitive detectors. Application to the oil fields. *Proc. 5th European Union Hydrocarbon Symp.*, Edinburgh, 1028-1061.

PORE COMPRESSIBILITY UNDER UNIAXIAL STRAIN

Robert W. Zimmerman
T. H. Huxley School of Environment, Earth Sciences and Engineering,
Imperial College of Science, Technology and Medicine, London SW7 2BP, UK

Abstract

A derivation is given of the pore volume compressibility coefficient of a poroelastic rock under conditions of uniaxial strain. For most reservoir-type rocks, the uniaxial pore volume compressibility is only about half of the hydrostatic pore volume compressibility. This expression for uniaxial pore volume compressibility compares well with some previously measured values on Berea sandstone.

Keywords: poroelasticity, pore compressibility, compaction, uniaxial strain

1. INTRODUCTION

When reservoirs compact due to the withdrawal of water or liquid hydrocarbons, the pore volume decreases, and the entire reservoir compacts. Traditionally, this compaction is assumed to occur under conditions of uniaxial strain, which is to say it is assumed that no deformation occurs in the horizontal plane. (Recently, some research has been done under the assumption that the reservoirs are bounded laterally by faults that are at their limiting equilibrium condition (Addis et al., 1998); this model leads to different conclusions than does the uniaxial strain assumption.) As laboratory compressibility data are most easily obtained under hydrostatic conditions, it is often desired to convert these hydrostatic compressibilities to uniaxial compressibilities. The relationship between uniaxial compressibility and hydrostatic compressibility is well known for elastic materials. This relationship was extended to linearly *poroelastic* materials by Geertsma (1966). However, the relationship between uniaxial *pore* compressibility and hydrostatic pore compressibility has not received much study. In this paper the constitutive equations of linear poroelasticity will be briefly reviewed, and then used to derive an expression for the uniaxial pore compressibility. Finally, comparison will be made with some laboratory data from the literature.

2. LINEAR POROELASTIC CONSTITUTIVE EQUATIONS

A porous rock has both a macroscopic bulk volume, and a pore volume. Changes in each of these volumes will depend on both the macroscopic "confining pressure", and the pore pressure. Four porous rock compressibility coefficients can therefore be defined, as follows (Zimmerman, 1991):

$$C_{bc} = \frac{-1}{V_b}\left(\frac{\partial V_b}{\partial P_c}\right)_{P_p}, \quad C_{bp} = \frac{1}{V_b}\left(\frac{\partial V_b}{\partial P_p}\right)_{P_c}, \tag{1}$$

$$C_{pc} = \frac{-1}{V_p}\left(\frac{\partial V_p}{\partial P_c}\right)_{P_p}, \quad C_{pp} = \frac{1}{V_p}\left(\frac{\partial V_p}{\partial P_p}\right)_{P_c}. \tag{2}$$

where V_b is the macroscopic bulk volume, V_p is the pore volume, P_p is the pore pressure, and P_c is the confining pressure, which is also equal to the mean normal stress. The two volumes are related by $V_b - V_p = V_m$, where V_m is the volume of the rock matrix; the porosity is given by $\phi = V_p / V_b$.
The bulk and pore strain increments can be expressed in terms of the porous rock compressibilities as follows:

$$d\varepsilon_b = \frac{-dV_b}{V_b} = C_{bc}dP_c - C_{bp}dP_p \ , \tag{3}$$

$$d\varepsilon_p = \frac{-dV_p}{V_p} = C_{pc}dP_c - C_{pp}dP_p \ , \tag{4}$$

where, to simplify the subsequent derivations, the "compression is positive" convention is used for the both bulk *and* the pore strains. If the mineral grains are assumed to be microscopically homogeneous, then use of simple superposition arguments shows that the four porous rock compressibilities are related to one another by (Geertsma, 1957; Zimmerman, 1991)

$$C_{bc} = C_{bp} + C_m \ , \tag{5}$$

$$C_{pc} = C_{pp} + C_m \ , \tag{6}$$

$$C_{bp} = \phi C_{pc} \ , \tag{7}$$

where C_m is the compressibility of the rock matrix material (i.e., the mineral grains).

The more general linear constitutive equations of isotropic poroelasticity that apply under non-hydrostatic loading are derived by starting with Hooke's law for an isotropic, non-porous elastic material (Jaeger and Cook, 1979):

$$\varepsilon_{xx} = \frac{1}{2G}\left[\tau_{xx} - \frac{\nu}{(1+\nu)}(\tau_{xx}+\tau_{yy}+\tau_{zz})\right] , \tag{8}$$

$$\varepsilon_{yy} = \frac{1}{2G}\left[\tau_{yy} - \frac{\nu}{(1+\nu)}(\tau_{xx}+\tau_{yy}+\tau_{zz})\right] , \tag{9}$$

$$\varepsilon_{zz} = \frac{1}{2G}\left[\tau_{zz} - \frac{\nu}{(1+\nu)}(\tau_{xx}+\tau_{yy}+\tau_{zz})\right] , \tag{10}$$

$$\varepsilon_{xy} = 2G/\tau_{xy}, \quad \varepsilon_{xz} = 2G/\tau_{xz}, \quad \varepsilon_{yz} = 2G/\tau_{yz} \ . \tag{11}$$

If a porous rock is macroscopically isotropic, a pore pressure increment will lead to equal extensions along each of three mutually orthogonal directions, but within the context of a linear theory cannot cause any shear strains. The total bulk volumetric strain resulting from an applied pore pressure is $-C_{bp}P_p$, so the coefficient that relates each macroscopic longitudinal strain to the pore pressure must be $-C_{bp}/3$. Hence, a term $-C_{bp}P_p/3$ must be added to each of the longitudinal strains, yielding (Biot, 1941; Detournay and Cheng, 1993; Zimmerman, 2000)

$$\varepsilon_{xx} = \frac{1}{2G}\left[\tau_{xx} - \frac{\nu}{(1+\nu)}(\tau_{xx}+\tau_{yy}+\tau_{zz})\right] - \frac{C_{bp}}{3}P_p \ , \tag{12}$$

$$\varepsilon_{yy} = \frac{1}{2G}\left[\tau_{yy} - \frac{\nu}{(1+\nu)}(\tau_{xx}+\tau_{yy}+\tau_{zz})\right] - \frac{C_{bp}}{3}P_p \ , \tag{13}$$

$$\varepsilon_{zz} = \frac{1}{2G}\left[\tau_{zz} - \frac{\nu}{(1+\nu)}(\tau_{xx}+\tau_{yy}+\tau_{zz})\right] - \frac{C_{bp}}{3}P_p \ , \tag{14}$$

whereas the shear strains remain unaffected by the pore pressure. Recalling from equation (5) that $C_{bp} = C_{bc} - C_m$, where C_m is the compressibility of the matrix, and noting that $C_{bc} = 1/K_{bc} = 1/K$, where K is the macroscopic bulk modulus, the pore pressure terms in the above equations can be written as $-\alpha P_p/3K$, where the Biot coefficient α is defined by

$$\alpha = 1 - \frac{C_m}{C_{bc}} = 1 - \frac{K_{bc}}{K_m} = 1 - \frac{K}{K_m} \ . \tag{15}$$

The equations for the stresses in terms of the strains are found by inverting equations (12-14) with the aid of equation (15). The result can be written as

$$\tau_{xx} - \alpha P_p = 2G\varepsilon_{xx} + \lambda(\varepsilon_{xx}+\varepsilon_{yy}+\varepsilon_{zz}) \ , \tag{16}$$

$$\tau_{yy} - \alpha P_p = 2G\varepsilon_{yy} + \lambda(\varepsilon_{xx}+\varepsilon_{yy}+\varepsilon_{zz}) \ , \tag{17}$$

$$\tau_{zz} - \alpha P_p = 2G\varepsilon_{zz} + \lambda(\varepsilon_{xx}+\varepsilon_{yy}+\varepsilon_{zz}) \ , \tag{18}$$

$$\tau_{xy} = 2G\varepsilon_{xy}, \tau_{xz} = 2G\varepsilon_{xz}, \tau_{yz} = 2G\varepsilon_{yz} \ . \tag{19}$$

where $\lambda = 2G\nu/(1-2\nu)$ is the Lamé parameter.

3. UNIAXIAL COMPACTION COEFFICIENT

When a reservoir compacts, it is usually assumed that this compaction occurs under conditions of zero lateral strain (Fjaer et al., 1992). The coefficient that relates the vertical strain to the vertical stress, under conditions of zero lateral strain, is called the uniaxial compressibility coefficient, C_{uni}. For a non-porous rock, the uniaxial compressibility can be found from eq. (18) by setting $\alpha = 0$ and $\varepsilon_{xx} = \varepsilon_{yy} = 0$, to arrive at

$$C_{uni} = \left(\frac{\partial \varepsilon_{zz}}{\partial \tau_{zz}}\right)_{\varepsilon_{xx},\varepsilon_{yy}} = \frac{1}{\lambda+2G} = \frac{(1+\nu)}{3(1-\nu)K} = \frac{(1+\nu)}{3(1-\nu)}C_{bc}, \tag{20}$$

where the subscripts on the partial derivative indicates those parameters that are held constant.

This uniaxial compaction coefficient may be relevant to compaction occurring over a geological time span, due to continued deposition of sediments. Of more relevance to the problem of subsidence is the deformation that is caused by withdrawal of fluid from a reservoir, with the lateral strains and vertical stress held constant. The relevant compaction coefficient in this case is found directly from eq. (18) to be (Geertsma, 1966)

$$C_{uni,p} = -\left(\frac{\partial \varepsilon_{zz}}{\partial P_p}\right)_{\varepsilon_{xx},\varepsilon_{yy},\tau_{zz}} = \frac{(1+\nu)}{3(1-\nu)}\alpha C_{bc} \ . \tag{21}$$

4. UNIAXIAL PORE COMPRESSIBILITY

The pore volume compressibility is defined in eq. (2) under the condition of a hydrostatic stress increment. A more meaningful pore compressibility for a reservoir subject to fluid withdrawal is that which is defined under conditions of uniaxial strain:

$$C_{pp}^{uni} = -\left(\frac{\partial \varepsilon_p}{\partial P_p}\right)_{\varepsilon_{xx},\varepsilon_{yy},\tau_{zz}} \ . \tag{22}$$

The relationship between this coefficient and other poroelastic coefficients can be found by dividing both sides of equation (4) by the pore pressure increment, under conditions of uniaxial strain:

$$C_{pp}^{uni} = -\left(\frac{\partial \varepsilon_p}{\partial P_p}\right)_{\varepsilon_{xx},\varepsilon_{yy},\tau_{zz}} = C_{pp} - C_{pc}\left(\frac{\partial P_c}{\partial P_p}\right)_{\varepsilon_{xx},\varepsilon_{yy},\tau_{zz}} \ . \tag{23}$$

The derivative of the confining stress (i.e., the mean normal macroscopic stress) with respect to pore pressure, under uniaxial strain conditions, can be found as follows. Setting $\varepsilon_{xx} = \varepsilon_{yy} = \tau_{zz} = 0$ in eq. (18) yields

$$-\alpha P_p = (\lambda + 2G)\varepsilon_{zz} \ . \tag{24}$$

Adding eqs. (16) and (17) under uniaxial strain conditions yields

$$\tau_{xx} + \tau_{yy} = 2\alpha P_p + 2\lambda\varepsilon_{zz} \ . \tag{25}$$

Eliminating between eqs. (24) and (25) yields

$$\tau_{xx} + \tau_{yy} = \frac{4G}{\lambda+2G}\alpha P_p = \frac{2(1-2\nu)}{(1-\nu)}\alpha P_p \ . \tag{26}$$

But $P^c = (\tau^{xx} + \tau^{yy} + \tau^{zz})/3$, so eq. (26) shows that

$$\left(\frac{\partial P_c}{\partial P_p}\right)_{\varepsilon_{xx},\varepsilon_{yy},\tau_{zz}} = \frac{2(1-2\nu)\alpha}{3(1-\nu)} \ . \tag{27}$$

3

Hence, from eq. (23),

$$C_{pp}^{uni} = C_{pp}^{hydro} - \frac{2(1-2\nu)\alpha}{3(1-\nu)}C_{pc} \ . \tag{28}$$

The uniaxial pore compressibility is therefore less than the hydrostatic pore compressibility, reflecting the additional stiffness imparted by the lateral constraints.

In the idealised limiting case of "incompressible grains", $C_m \to 0$, so $C_{pc} = C_{pp}$ by eq. (6), and by eq. (15); eq. (28) then reduces to

$$C_{pp}^{uni} = \frac{(1+\nu)}{3(1-\nu)}C_{pp}^{hydro} \ . \tag{29}$$

According to Raaen (1993), this relation is commonly used, although it now appears to be only an approximation to the more precise relation, (29). For a reservoir with incompressible grains, the ratio of uniaxial to hydrostatic pore compressibility is identical to the ratio of uniaxial to hydrostatic bulk compressibility, as given by eq. (21) with $\alpha = 1$. This is to be expected, since if the grains are incompressible, the change in the bulk volume must *exactly* reflect the change in pore volume.

The pore compressibility is usually an order of magnitude greater than the grain compressibility (Laurent et al., 1993), in which cases C_{pc} can be replaced by C_{pp} in eq. (28) to yield

$$C_{pp}^{uni} = \left[1 - \frac{2(1-2\nu)\alpha}{3(1-\nu)}\right]C_{pp}^{hydro} \ . \tag{30}$$

Numerical magnitudes of the compressibility ratio can be seen in Table 1. The porosities, Poisson ratios and Biot parameters are taken from Detournay and Cheng (1993). The last two columns show the ratio of uniaxial to hydrostatic pore compressibility, as calculated by eq. (30) and by the commonly-used simplified relation, eq. (29).

Table 1. Ratio of uniaxial to hydrostatic pore compressibility.

Rock	ϕ	ν	α	eq. (29)	eq. (30)
Ruhr sandstone	.02	.12	.65	.42	.63
Berea sandstone	.19	.20	.79	.50	.61
Weber sandstone	.06	.15	.64	.45	.65
Ohio sandstone	.19	.18	.74	.48	.61
Boise sandstone	.26	.15	.85	.45	.53
Pecos sandstone	.20	.16	.83	.46	.55

Measurement of C_{pp} requires careful calibration to account for the expansion of the pore fluid as the pore pressure is changed; for this reason, measurements of C_{pp} are rarely attempted. Instead, it is common to measure the coefficient C_{pc}, and to assume that $C_{pc} \approx C_{pp}$ (Andersen, 1988). Although these two coefficients are usually nearly equal, the data of Laurent et al. (1993) on several limestones show that they may differ by as much as 15%.

The "uniaxial" analogue of the coefficient C_{pc} is

$$C_{pc}^{uni} = \left(\frac{\partial \varepsilon_p}{\partial \tau_{zz}}\right)_{\varepsilon_{xx},\varepsilon_{xx},P_p} , \qquad (31)$$

which, from eq. (4), can be expressed as

$$C_{pc}^{uni} = C_{pc}\left(\frac{\partial P_c}{\partial \tau_{zz}}\right)_{\varepsilon_{xx},\varepsilon_{xx},P_p} - C_{pp}\left(\frac{\partial P_p}{\partial \tau_{zz}}\right)_{\varepsilon_{xx},\varepsilon_{xx},P_p} . \qquad (32)$$

The second derivative term on the right is zero, by definition, and the first derivative term can be found from eqs. (16-18) to be

$$\left(\frac{\partial P_c}{\partial \tau_{zz}}\right)_{\varepsilon_{xx},\varepsilon_{yy},P_p} = \frac{(1+\nu)}{3(1-\nu)} , \qquad (33)$$

in which case eq. (32) becomes

$$C_{pc}^{uni} = \frac{(1+\nu)}{3(1-\nu)} C_{pc}^{hydro} . \qquad (34)$$

The ratio of the uniaxial to the hydrostatic values of C_{pc} agrees with the corresponding ratio for C_{pp} given by eq. (29). However, whereas eq. (29) only

applies in the limit of incompressible grains, eq. (34) holds for finite values of the grain compressibility. In general, the relation between uniaxial and hydrostatic pore compressibilities is not the same for C_{pp} as for C_{pc}.

5. COMPARISON WITH EXPERIMENTAL DATA

Andersen (1988) measured both C_{pc}^{hydro} and C_{pc}^{uni} on a Berea sandstone that had a Poisson ratio of 0.22. The pore pressure was maintained at atmospheric pressure throughout the test. His pore volume data are shown in Fig. 1, along with fitted curves of the form (Zimmerman, 1991)

$$\varepsilon_p = A + BP_c + C\exp(-P_c / P^*) . \qquad (35)$$

The constant A should in principle be equal to $-C$, but is allowed to vary independently to account for the fact that the "zero strain" point in Andersen's data was chosen arbitrarily; its value has no effect on the computed compressibilities. These data show that the compressibilities decrease with stress, as is usually the case for sandstones. This is in contrast with the preceding linear poroelastic analysis, which assumed that the elastic coefficients were constant. Nevertheless, it seems reasonable to interpret equations such as (34) in an incremental sense.

Fig. 2 shows the hydrostatic and uniaxial pore compressibilities, as computed by differentiating the fitted pressure-pore strain relationships. Also shown is the uniaxial pore compressibility curve that has been predicted from the hydrostatic curve using eq. (34). The agreement is reasonable, particularly considering the inherent inaccuracies in "numerically differentiating" the pore strain data to arrive at the compressibilities.

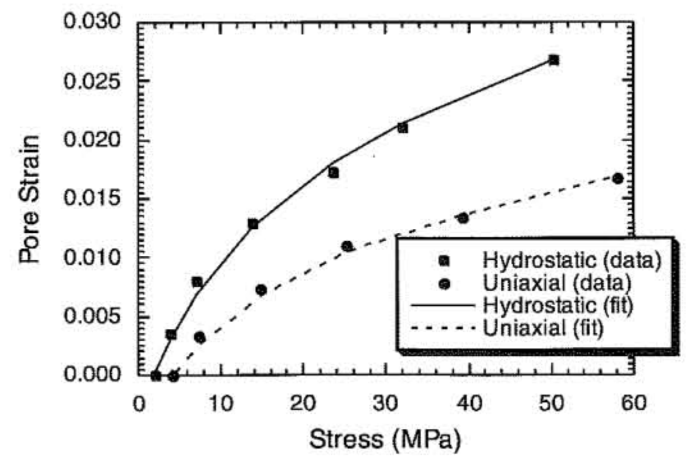

Figure 1. Pore strain of a Berea sandstone (after Andersen, 1988).

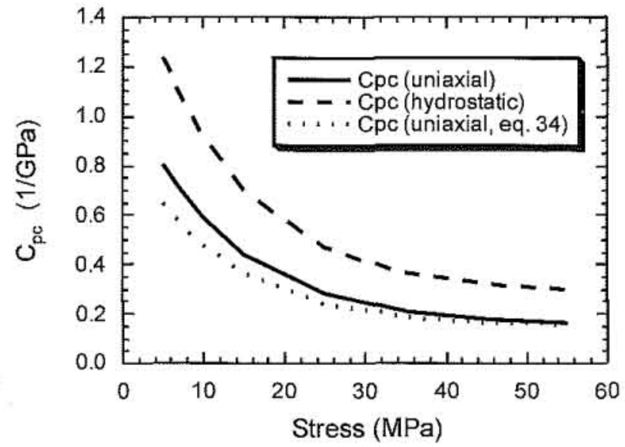

Figure 2. Pore compressibilities of Berea sandstone (see text for explanation).

It would be interesting to compare uniaxial and hydrostatic measurements of the pore compressibilities with respect to changes in the pore pressure, so as to test eq. (30), but such data do not yet seem to be available.

6. CONCLUSIONS

Relationships have been presented to relate the pore compressibilities as measured under hydrostatic conditions to those that would pertain under uniaxial strain conditions. For the pore compressibility with respect to confining stress, the relationship has been tested against some data from the literature on Berea sandstone. Uniaxial strain data does not yet seem to be available for the pore compressibility with respect to changes in pore pressure, which would seem to be the coefficient most directly applicable to subsidence predictions.

REFERENCES

Addis, M. A., N. C. Last & N. A. Yassir (1996) Estimation of horizontal stresses at depth in faulted regions and their relationship to pore pressure variations. *SPE Form. Eval.* **12**, 11-18.

Andersen, M. A. (1988) Predicting reservoir-condition PV compressibility from hydrostatic-stress laboratory data. *SPE Reserv. Eng.*, **3**, 1078-1082.

Biot, M. A. (1941) General theory of three-dimensional consolidation. *J. Appl. Phys.*, **12**, 155-164.

Detournay, E. & Cheng, A. H.-D. (1993) Fundamentals of poroelasticity. In: *Comprehensive Rock Engineering*, J. A. Hudson, ed., Pergamon, Oxford, pp. 113-171.

Fjær, E., Holt, R. M., Horsrud, P., Raaen, A. M. & Risnes, R. (1992) *Petroleum Related Rock Mechanics*, Elsevier, Amsterdam, 338 pp.

Geertsma, J. (1957) The effect of fluid decline on volumetric changes of porous rocks. *Pet. Trans. AIME*, **210**, 331-340.

Geertsma, J. (1966) Problems of rock mechanics in petroleum production engineering. In *Proc. 1st Cong. Int. Soc. Rock Mech.*, Lisbon, 25 September - 1 October 1966: 585-594. Lisbon: Nat. Lab. Civil. Eng.

Jaeger, J. C. & Cook, N. G. W. (1979) *Fundamentals of Rock Mechanics*, 3rd ed. Chapman & Hall, London, 593 pp.

Laurent, J., Bouteca, M. J., Sarda, J.-P. & Bary, D. (1993) Pore-pressure influence in the poroelastic behavior of rocks: experimental studies and results. *SPE Form. Eval.*, **9**, 117-122.

Raaen, A. M. (1993) Pore volume compressibility under uniaxial strain conditions from Biot-Gassmann theory. In *15th Eur. Form. Eval. Symp.*, 5-7 May 1993: 1-9. Stavanger: Norw. Form. Eval. Soc.

Zimmerman, R. W. (1991) *Compressibility of Sandstones*. Elsevier, Amsterdam, 173 pp.

Zimmerman, R. W. (2000) Coupling in poroelasticity and thermoelasticity, *Int. J. Rock Mech.*, **37**, 000-000.

MEASURING SUBSIDENCE WITH SAR INTERFEROMETRY: APPLICATIONS OF THE PERMANENT SCATTERERS TECHNIQUE

A. Ferretti, C. Prati, and F. Rocca
Politecnico di Milano, Dipartimento di Elettronica ed Informazione,
Piazza Leonardo da Vinci 32, Milano. Email: rocca@elet.polimi.it

Abstract

Differential SAR interferometry is a recent and powerful tool to measure small motions of the terrain; the available measurements start from 1991, date of launch of the European satellite ERS-1. The spatial resolution is about 20X20m and the temporal resolution is a pass every 35 days. Most of the earth surface has been monitored systematically first by ERS-1, then by ERS-2 (launched in 1995) and it will be with the satellite ENVISAT to be launched in 2000, thus creating long and consistent series of data. In urban areas and where exposed rocks are visible, it is possible to identify numerous back scatterers that do not change their signature with time (the Permanent Scatterers) and therefore can be used as natural monuments to estimate the progressive motion of the terrain. The precision of the measurement is a small fraction of a wavelength (5.6 cm) and millimetric motions are appreciable with good reliability. The atmospheric contribution is rather smooth spatially and independent from take to take, so that it can be identified and removed from the data using a proper processing, provided that the density of the PS is high enough as it happens in urban areas. Then, it is possible to obtain maps of subsidence with very high spatial sampling rate (more than 20 PS/km^2, in urban areas) and high quality. After a short description of the possibilities and limits of this technique, the paper will present results in Paris (France); results in Ancona, Camaiore, Pomona (US) have been discussed in other papers.

Keywords: SAR interferometry, subsidence maps, Paris (France)

1. INTRODUCTION

The Synthetic Aperture Radar is a microwave imaging system of the earth surface [4]. It has cloud-penetrating capabilities because it uses microwaves. It has day/night operational capabilities because it is an active system. Finally, in its "interferometric configuration", it allows accurate measurements of the radiation travel path because it is coherent. Measurement of travel path variations as a function of the satellite position and time of acquisition allow to generate Digital Elevation Maps (DEM) and to measure centimetric surface deformation of the terrain. A SAR imaging system from satellite (as ERS-1 and ERS-2) is sketched in figure 1. A satellite carries a radar with the antenna pointed to the earth surface in the plane perpendicular to the orbit (the inclination of the antenna with respect to the Nadir is called off-Nadir angle and usually ranges between 20 and 50 deg. (21 deg. for ERS-1 and ERS-2) for the available systems.

Currently operational satellite SAR systems work at C band – 5.3GHz (the European ERS, the Canadian Radarsat, and the US Shuttle missions), L band - 1.2GHz (the Japanese J-ERS), and X band – 10GHz (the German-Italian X-SAR on the shuttle missions). In the case of ERS, the illuminated area on the ground (antenna footprint) is about 5km in the along-track direction (also said azimuth direction) and about 100km in the across-track direction (also said ground range direction). The direction along the Line of Sight (LOS) is usually called slant-range direction. The antenna footprint moves at the satellite speed (about 7500m/s for ERS) along its orbit (a quasi-polar orbit for ERS-1 and ERS-2 that crosses the equator with an angle of 9 deg. at an elevation of about 800km). It forms a 100km wide strip on the earth surface with the capability of imaging a 450km long strip every minute.

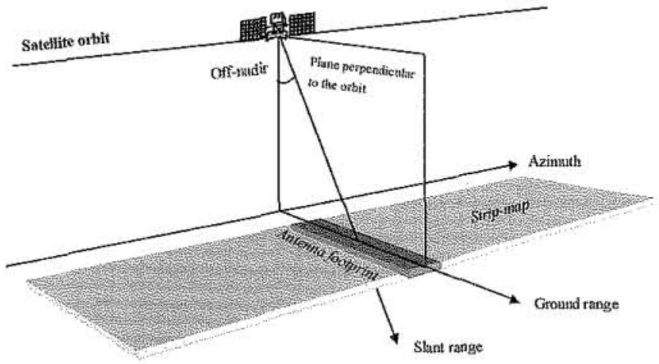

Figure 1. Description of a SAR system from satellite

2. COMPLEX SAR IMAGES

A digital SAR image can be seen as a mosaic (i.e. a two-dimensional array formed by columns and rows) of small picture elements (pixels). A small area (resolution cell) of the earth surface is associated to each pixel. Each pixel carries amplitude and phase information (i.e. a complex number) of the microwave field back-scattered by all the scatterers (rocks, vegetation, building etc) within the correspondent resolution cell projected on the ground (see next section on SAR resolution cell projection on the ground). Different columns of the image are associated to different azimuth locations whereas different rows indicate different slant range locations (see figure 1). Location and dimension of the resolution cell in azimuth and slant-range coordinates depend only on the SAR system characteristics. In the ERS-1 and ERS-2 case the SAR resolution cell dimension is about 5 meters in azimuth and about 9.5 meters in slant-range. The distance between adjacent cells is about 4 meters in azimuth and about 8 meters in slant range (SAR resolution cells are thus slightly overlapped both in azimuth and slant-range).

The detected SAR image

The detected SAR image contains a measurement of the amplitude of the radiation backscattered toward the radar by the objects (scatterers) contained in each SAR resolution cell. This amplitude depends more on the roughness than on the chemical composition of the scatterers on the terrain. Typically, exposed rocks and urban areas show strong amplitude whereas smooth flat surfaces (like quiet water basins) show low amplitude since the radiation is mainly mirrored away from the radar. The detected SAR image is generally visualized by means of gray scale levels as shown in the example of figure 2. Bright pixels correspond to areas of strong backscattered radiation (e.g. urban areas), whereas dark pixels correspond to low backscattered radiation (e.g. quiet water basin).

The phase SAR image

The radiation transmitted from the radar has to reach the scatterers on the ground and then to come back to the radar in order to form the SAR image (two ways travel distance). Scatterers at different distances from the radar (different slant range) introduce a different delay between transmission and reception of the radiation. Due to the almost pure sinusoidal nature of the transmitted signal, this delay is equivalent to a phase change between transmitted and received signals. The phase change is thus proportional to the two ways travel distance of the radiation divided by the transmitted wavelength.

However, due to the periodic nature of the signal, travel distances that differ by an integer multiple of the wavelength introduce exactly the same phase change. In other words the phase of the SAR signal is a measure of just the last fraction of the two ways travel distance smaller than the transmitted wavelength. In practice, due to huge ratio between the resolution cell dimension (in the order of a few meters) and wavelength (~5.6 cm for ERS), the phase of a single SAR image looks random passing from one pixel to another and it is of no practical utility.

3. SAR INTERFEROMETRY

A satellite based SAR can observe the same area from slightly different looking angles. It can be done simultaneously (two radar should be mounted on the same platform, as in the recent NASA/DLR/ASI survey SRTM) or at different times by exploiting repeated orbits. The latter is the case of ERS-1 and ERS-2. In that case, time intervals between observations of 1, 35 or a multiple of 35 days are available. The distance between the two satellites in the plane perpendicular to the orbit is called "interferometer baseline" and its projection perpendicular to the slant range is called "perpendicular baseline".

The SAR interferogram is generated by cross-multiplying pixel by pixel the first SAR image times the second one complex conjugated. Thus, the interferogram amplitude is the amplitude of the first image times that of the second one, whereas its phase (called interferometric phase) is the phase difference between the two images.

Figure 2. ERS SAR detected image of Milano (Italy). The image size is about 25 km in ground range (vertical) and 25 km in azimuth (horizontal). Bright pixels correspond to areas of strong backscattered radiation (e.g. buildings), whereas dark pixels correspond to low backscattered radiation (e.g. quiet water basin).

3.1 Terrain altitude measurement through the interferometric phase

Let us suppose to have only one dominant point scatterer that does not change in time in each ground resolution cell. Then the interferogram phase would depend on the travel path difference only since the phase of the scatterers is cancelled by the difference. The **variation** of the travel path difference Δr that results passing from one resolution cell to another has a simple expression (an approximation that holds for small baselines and resolution cells not too far apart) that depends on a few geometric parameters shown in figure 3:

1- the perpendicular baseline B_n
2- the radar-target distance **R**
3- the displacement between the resolution cells along the perpendicular to the slant range q_s.

The following approximated expression of Δr holds:

$$\Delta r = 2\frac{B_n q_s}{R}$$

The interferometric phase variation has thus the following expression (where λ is the SAR wavelength):

$$\Delta\varphi = \frac{2\pi\Delta r}{\lambda} = \frac{4\pi}{\lambda}\frac{B_n q_s}{R}$$

The altitude of ambiguity is defined as the altitude difference q_a that generates an interferometric phase change of two-pi after interferogram flattening. The altitude of ambiguity is inversely proportional to the perpendicular baseline:

$$q_a = \frac{\lambda\, R \sin\theta}{2B_n}$$

In the ERS case with λ=5.6 cm, θ =23 deg., R=850 km the following expression holds:

$$q_a \approx \frac{9300}{B_n} \text{ meters}$$

As an example, if a 100 meters perpendicular baseline is used, a two-pi change of the interferometric phase corresponds to an altitude difference of about 93 meters. In principle, the higher is the baseline the more accurate is the altitude measurement since the phase noise (see next section) is equivalent to a smaller altitude noise.

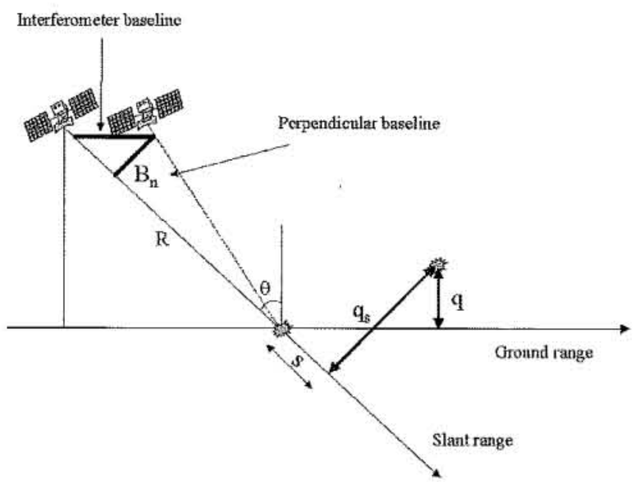

Figure 3. Geometric parameters of a satellite interferometric SAR system.

3.2 Phase unwrapping and DEM generation

The flattened interferogram provides just a measurement of the relative terrain altitude that is ambiguous. The phase variation between two points on the flattened interferogram provides a measurement of the actual altitude variation plus an integer number of altitude of ambiguity (equivalent to an integer number of 2^ phase cycles). The process that allows to add to the interferometric fringes the correct number of altitude of ambiguity is called phase unwrapping. There are several well-known phase unwrapping techniques that are not discussed here. However it should be noted here that usually phase unwrapping does not have a unique solution and "a priori" information should be exploited to get the right solution [1].

Once the interferometric phases are unwrapped, an elevation map in SAR coordinates is obtained. As an example, the flattened interferogram and the relative DEM of Mt. Etna (Sicily – Italy) obtained through phase unwrapping and resampling are shown in figures 4, 5.

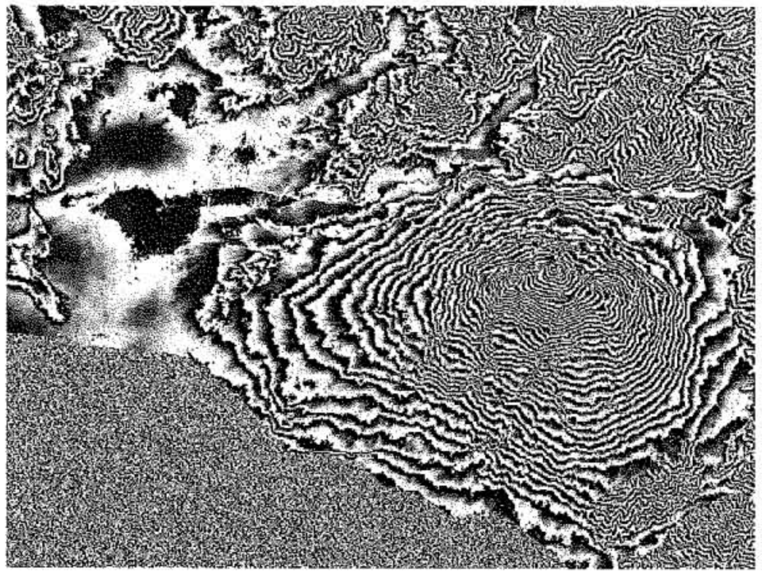

Figure 4. Flattened interferogram of Mt. Etna generated from ERS tandem pairs. The perpendicular baseline of 115 meters generates an altitude of ambiguity of about 82 meters.

Figure 5. Perspective view of Mt. Etna as seen from North-East. The estimated vertical accuracy is better than 10 meters.

3.3 Terrain motion measurement through the interferometric phase

Let us now suppose that some of the point scatterers on the ground slightly change their relative position in the time interval between two SAR observations (as, for example, in case of subsidence, landslide, earthquake ...). In such cases the following additive phase term, independent of the baseline, appears in the interferometric phase, where **d** is the relative scatterer displacement projected on the slant range direction.

$$\Delta\varphi_d = \frac{4\pi}{\lambda} d$$

It is thus evident that after interferogram flattening, the interferometric phase contains both altitude and motion components:

$$\Delta\varphi = \frac{4\pi}{\lambda}\frac{B_n q}{R\sin\theta} + \frac{4\pi}{\lambda} d$$

Moreover, if a digital elevation model (DEM) is available, the altitude contribution can be subtracted from the interferometric phase (generating the so-called differential interferogram) and the terrain motion component can be measured [6]. In the ERS case with λ=5.6 cm and assuming a perpendicular baseline of 150 m (a rather usual value), the following expression holds:

From this example it appears that the sensitivity of SAR interferometry to terrain motion is much larger than that to the altitude difference. A 2.8cm motion component in the slant range direction would generate a 2π interferometric phase variation. As an example, the map of the terrain deformation in Paris that occurred from 1992 to 1999, is shown in figure 6.

It should be pointed out that there are many different ways to get a differential interferogram:

1. With a single interferometric pair (two SAR images) and baseline close to zero: the interferometric phase contains the motion contribution only (see equation (2)). No other processing steps are required.
2. With a single interferometric pair (two SAR images) and baseline different from zero: the interferometric phase contains both altitude and motion contributions (see equation (2)).

The altitude component has to be removed using a priori information or a Digital elevation model obtained from the data themselves.

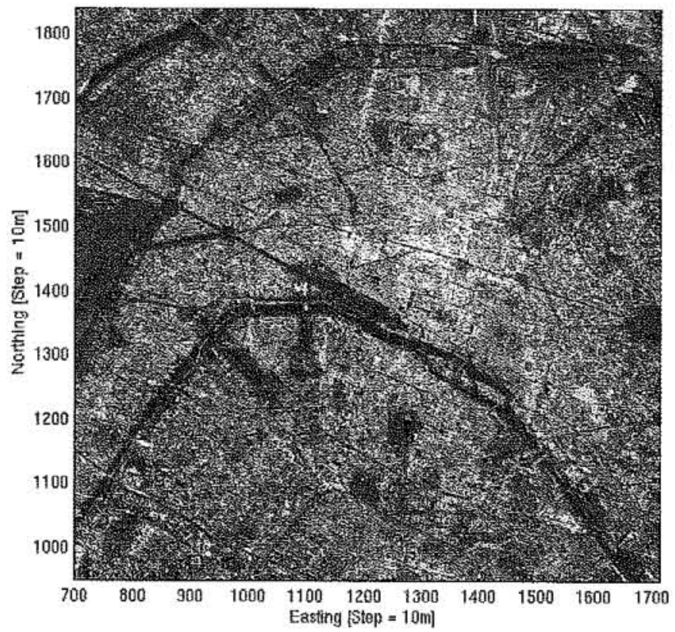

Figure 6. The map of the terrain deformation in Paris that occurred between 1992 and 1999. The map has been generated by means of ERS interferometric images. Blue-green colors show stable areas whereas areas subsiding with 4 mm/year rate are shown in red.

3.4 The atmospheric contribution to the interferometric phase

When two interferometric SAR images are not simultaneous, the radiation travel path can be affected differently by the atmosphere. In particular, different

atmospheric humidity, temperature and pressure between the two takes have a visible consequence on the interferometric phase (Atmospheric Phase Screen: APS) [7]. This effect is usually confined within a two-pi peak to peak interferometric phase change along the image with a smooth spatial variability (from a few hundreds meters to a few kilometers). The effect of such a contribution impacts both on altitude (especially in case of small baselines) and terrain deformation measurements.

As an example, the atmospheric phase contribution to the ERS interferogram generated on Paris is shown in figure 7. Here the turbulence effect has been superimposed to the detected image of Paris.

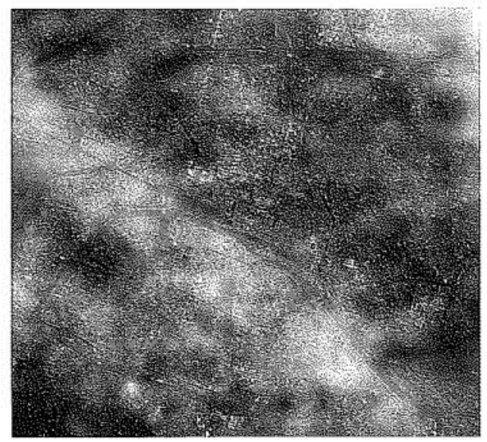

Figure 7. An example of atmospheric phase contribution to the ERS interferogram generated on Paris.

3.5 Phase noise sources

Three main contributions to the phase noise should be taken into consideration:

1. *Phase noise due to temporal change of the scatterers*. As an example, in the case of water basin or densely vegetated areas, the scatterers change totally after a few milliseconds, whereas exposed rocks or urban areas remain stable even after years. Of course, there are also the intermediate situations where the interferometric phase is still useful even if corrupted by change noise.
2. *Phase noise due to the different looking angle*. The speckle changes due to the different combination of the elementary echoes even if the scatterers do not change in time. The most important consequence of this effect is that there exists a critical baseline over which the interferometric phase is pure noise. In the ERS case, the critical baseline for horizontal terrain is about 1150 meters.
3. *Phase noise due to volume scattering*. The critical baseline reduces in case of *volume scattering* when the elementary scatterers are not disposed on a plane surface but occupy a volume (e.g. the branches of a tree).

3.6 Coherence maps

The phase noise can be estimated from the interferometric SAR pair by means of the local coherence L. The local coherence is the cross-correlation coefficient of the SAR image pair estimated on a small window (a few pixels in range and azimuth), once all the deterministic phase components (mainly due to the terrain elevation) are compensated. The coherence map of the scene is then formed computing its absolute value on a moving window that covers the whole SAR image. The coherence value ranges from 0 (the interferometric phase is just noise) up to 1 (absence of phase noise).

4. THE PERMANENT SCATTERERS

Stable natural reflectors (Permanent Scatterers) can be identified from long temporal series of interferometric data [2,3]. They can be used in urban areas, like Paris or Pomona [6] showing subsidence effects. Two animations relative to the estimated displacement field in Pomona since June 1992 are available on our web site: http://www-dsp.elet.polimi.it/andrea/www/sar/pomona.htm.

One of the main difficulties encountered in Differential SAR interferometry applications is due to temporal and geometric decorrelation. We have been able to identify single pixels (the PS's) coherent over long time intervals and for wide look-angle variations. This allows one to use all ERS acquisitions relative to an area of interest. In fact when the dimension of the PS is smaller than the resolution cell, the coherence is good (the speckle is the same) even for image pairs taken with baselines larger than the decorrelation one. Then, on those pixels, sub-meter DEM accuracy and millimetric terrain motion detection can be achieved, even if the coherence is low in the surrounding areas. Reliable elevation and deformation measurements can then be obtained on this subset of image pixels that can be used as a "natural" GPS network.

5. RESULTS

An interesting case of subsidence, already studied using differential interferometry and other techniques, is found in Paris. Sixty-four ERS images were available. All were resampled on the same master and 60 interferograms were obtained. After the initial selection of the PS set (about 3 PS/km2 were identified), phase increments between each PS and all the others less than 1 km apart were estimated. The range of normal baselines is about +/- 1100 m, while the maximum temporal baseline is more than 6 years. If a PS had a LOS velocity of, say, 2 cm/yr and a residual elevation difference of 5 m with respect to a neighboring scatterer, considered as a reference, its phase variations as a function of time and baseline would be a 2D sinusoid. If now we accept, temporarily, the hypothesis of constant LOS velocity of each pixel, then using a periodogram we can estimate both the residual elevation and the LOS velocity difference of the pixels. This operation was carried out for all PS pairs less than 1km apart, thus removing the effects of the residual elevation with respect to the average DEM and of the LOS velocity and estimating the unwrapped phase values. After estimation of both elevation and mean velocity of the targets, time series analysis of the phase residues in correspondence of each PS was carried out. The target is to identify possible non-linear motion contributions. For each PS we carried out a temporal smoothing using a triangular filter (300 days long) and we removed the low pass component. Phase residuals were then spatially filtered using a moving average on a 2x2 km window. APS's were then interpolated on the original regular grid and removed from each datum. It should be noted that each APS is actually the difference of the atmospheric component of the slave image and the APS of the master acquisition. Averaging the 60 APS's it was possible to get an estimation of the master contribution and then of each single contribution. After APS removal it is possible to estimate not only the mean velocity field of the area but a displacement field as a function of time, possibly interpolating the displacement maps on a regular temporal grid. In figure 8 we report an example of non-linear motion of one pixel in Paris located in the area of Gare St. Lazaire where works for the construction of a new metro line created subsidence and heave.

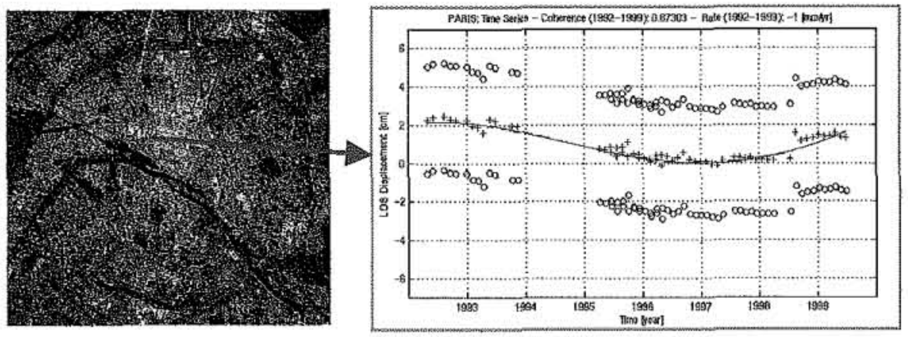

Figure 8. An example of non-linear motion of one pixel in Paris located in the area between P. de la Concorde (red star) of Gare St. Lazaire (blue star) where works for the construction of a new metro line created subsidence and heave.

The validation and an experimental estimates of the accuracy of the results have been carried out by cross-correlating the dilation of the metallic building of La Cite des Sciences with the temperatures in Paris. The result is shown in figure 9. The cross-correlation coefficient is 0.92 showing that the accuracy of our measurements is better than 1mm.

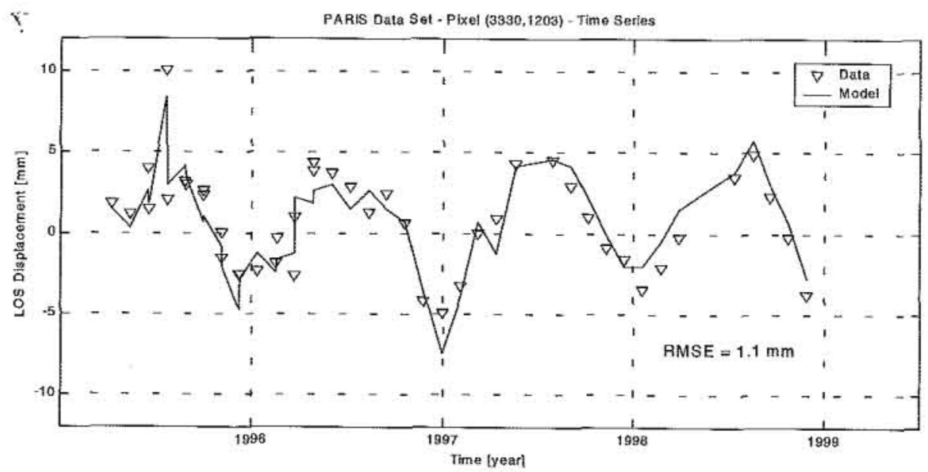

Figure 9. Dilation of the metallic building of La Cite des Sciences measured by means of the PS technique (triangles) superimposed to the temperatures in Paris (solid line).

6. CONCLUSIONS

We have shown that in urban areas Permanent Scatterers exist that allow to generate interferograms on a sparse grid, even if the time lapse between takes is many years long. The density of the PS's, small enough to have sufficient phase stability with respect to the baseline, was seen to be sufficient in urban areas to be able to estimate the atmospheric disturbance (the APS) with a sufficient spatial resolution. Then, the estimated APS can be removed from the interferometric phase, improving the DEM estimates and improving the estimate of the pixel motion. The long time lapse observations made available by this technique allow to estimate long term pixel motion with an accuracy that was previously attainable using optical techniques only.

REFERENCES

[1] Ferretti, A., Prati, C. & Rocca, F. (1999) Multibaseline InSAR DEM Reconstruction: the Wavelet Approach, *IEEE Trans. Geosci. Remote Sensing,* **37** (2), pp. 705-715.

[2] Ferretti, A., Prati, C. & Rocca, F. (1999) Permanent Scatterers in SAR Interferometry, in *IEEE Trans. Geosci. Remote Sensing (in press).*

[3] Ferretti, A., Prati, C. & Rocca, F. (1999) Non-linear Subsidence Rate Estimation Using Permanent Scatterers in Differential SAR Interferometry, in *IEEE Trans. Geosci. Remote Sensing (in press).*

[4] Franceschetti, G. & Lanari, R. (1999) Synthetic Aperture Radar Processing, *CRC Press*, Boca Raton.

[5] Gambolati, G., Ricceri, G., Bertoni, W., Brighenti, G. & Vuillermin, E. (1991) Mathematical Simulation of the Subsidence of Ravenna," *Water Resour. Res.*, **27** (11), No. 11, pp. 2899-2918.

[6] Peltzer, G. Monitoring Ground Subsidence, http://www.esrin.esa.it/esrin/eos/mon2.html

[7] Williams, S., Bock Y., & Pang, P. (1998) Integrated satellite interferometry: Tropospheric noise, GPS estimates and implications for interferometric synthetic aperture radar products, *J. Geophys. Res.*, **103**, B11, pp. 27.051-27.067.

LAND-SURFACE SUBSIDENCE AND ITS CONTROL IN THE HOUSTON-GALVESTON REGION, TEXAS, 1906-1995

R.K. Gabrysch, *Consulting Engineer*

Ronald J. Neighbors, General Manager
Harris-Galveston Coastal Subsidence District, 1660 West Bay Area Blvd., Friendswood, Texas 77546

Abstract

Large amounts of groundwater have been withdrawn from the Chicot and Evangeline Aquifers in the Houston-Galveston region of Texas. The withdrawals for municipal and agricultural uses began in the late 1800's. Withdrawals for industrial use began after the opening of the Houston Ship Channel in 1915. The rate of pumpage grew slowly until about the late 1930's and then rapidly in the early 1940's. These withdrawals caused declines in the potentiometric surface of about 70 m in the Chicot Aquifer and about 91 m in the Evangeline Aquifer between 1943 and 1977. Water-level declines from beginning of pumpage have caused as much as 3.0 m of subsidence in southeastern Harris County.

The Harris-Galveston Coastal Subsidence District was created by the state of Texas in 1975 to stop subsidence leading to flooding. Water from Lake Livingston became available to the coastal area in late 1976 and surface water became the primary source in southeast Harris County. In 1976, groundwater withdrawal in Harris and Galveston Counties was 20.0 cubic m/sec; in 1987, withdrawal was 15.5 cubic m/sec and, in 1994, withdrawal was 14.0 cubic m/sec. Withdrawals were decreased in Galveston County and southeastern Harris County. The 1999 District Plan calls for decreases in withdrawals in the inland part of the region.

The decreases in groundwater withdrawal resulted in rises in the potentiometric surfaces of the Chicot and Evangeline Aquifers of about 48.8 m and 54.9 m in southeastern Harris County by 1995. As a result, the rate of subsidence decreased dramatically. No subsidence occurred in southeastern Harris County between 1987 and 1995. Subsidence in northern Harris County continues and, in part of the area, has accelerated. Between 1978 and 1995, as much as 1.1 m of subsidence occurred.

Historically, regional subsidence was determined by using conventional spirit leveling. Beginning in 1973, site-specific subsidence was measured by borehole extensometers. In 1987, a network of benchmarks was established to use the Global Positioning System (GPS) for height determinations. In 1994, a program to evaluate the use of trailer mounted receivers to collect

GPS data intermittently at specially set benchmarks was initiated and is providing satisfactory data.

Keywords: land-surface subsidence, Houston, Texas, extensometer, groundwater.

1. INTRODUCTION

Land-surface subsidence associated with the lowering of water levels resulting from groundwater development is evident in many parts of the world. One important location where subsidence became critical was the Houston-Galveston region of Texas. The region consists of Harris, Galveston, and parts of surrounding counties and is located on a low sloping coastal plain adjacent to the Gulf of Mexico.

The region is important both nationally and internationally. Harris County, where a majority of Houston's citizens reside, is the third most populous county in the United States; Houston is the fourth largest city in the nation. The port of Houston, an inland port located about 70 kilometers (km) from the Gulf of Mexico, is the second largest port in the United States in total and foreign tonnage. It ranks eight worldwide. The region contains the world's largest petrochemical complex and is a very significant producer of agricultural products, such as rice, corn, soybeans, and beef cattle. Galveston Island, located 65 km southeast of Houston, also contains a deep-water port and is a recreational center.

Water for municipal and agricultural needs had been met by groundwater withdrawals from the late 1800's until 1954 when water from Lake Houston became available. In 1954, Houston was the largest city in the United States using groundwater exclusively for public supply. Withdrawals of groundwater for industrial use began after the opening of the Houston Ship Channel in 1915.

Land-surface subsidence resulting from the withdrawals of groundwater and lowering of artesian pressure caused serious problems in the region, especially in the low-lying areas along Galveston Bay and the Gulf of Mexico, which have been further subjected to inundation by tidal waters. There are numerous growth faults that dip to the southeast as well as faults associated with salt domes in the region. Since the 1930's, activation of dormant geological faults and acceleration of the movement of active faults have been observed. Later studies showed a relation between water-level declines and fault movement (Holzer and Gabrysch, 1987).

2. AQUIFERS

The groundwater system is composed of lenticular deposits of sand and clay. The medium to fine-grained sand lenses are generally connected laterally, but the vertical connection is tortuous. Because of the vertical connection, the system is termed "leaky". The pressure in the sands is greater than atmosphere, and therefore the system is artesian.

This system has been divided into two major aquifers that are used in Harris and Galveston counties, the Chicot and Evangeline, and an underlying confining unit, the Burkeville. The Burkeville is a massive (60 m to 120 m thick) predominantly clay unit with some thin lenses of sand mostly near the outcrop. Below the Burkeville, an aquifer composed of fine-grained sand, the Jasper, contains fresh water in the extreme northern part of Harris County, but only two wells produce water from the aquifer in the county. The Jasper aquifer is a principal aquifer in adjacent Montgomery County.

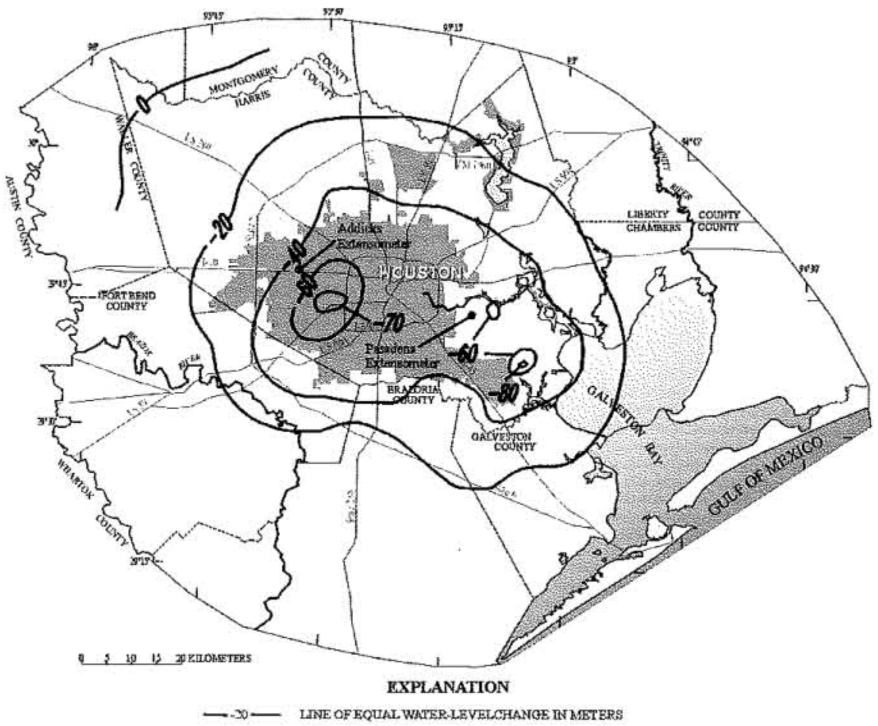

Figure 1. Water-Level Changes in Wells in the Chicot Aquifer, 1943-77.

3. GROUNDWATER WITHDRAWALS

The withdrawal of groundwater for all uses in the region increased gradually from about 0.1 cubic m/sec in 1890 to about 4.4 cubic m/sec in 1937 and then rapidly increased to 22.6 cubic m/sec in 1976. The Harris-Galveston Coastal Subsidence District was created by the Texas Legislature in 1975 to regulate the production of groundwater and thereby end subsidence leading to flooding. Because of the District's efforts and the availability of an alternate source of water, pumpage of groundwater was reduced to about 17.6 cubic m/sec in 1987 and about 16.5 cubic m/sec in 1995.

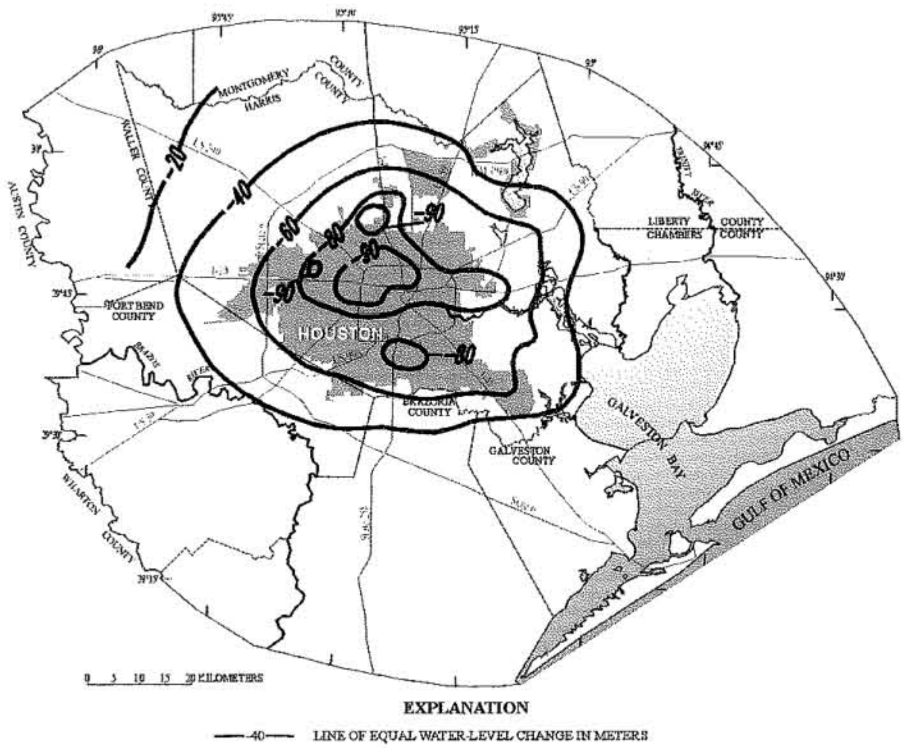

Figure 2. Water-Level Changes in Wells in the Evangeline Aquifer, 1943-77.

4. CHANGES IN THE POTENTIOMETRIC SURFACES

Before the beginning of large-scale withdrawals, the potentiometric surfaces of the two aquifers were much higher than land surface. Groundwater development has caused large declines in the potentiometric surfaces of the Chicot and Evangeline Aquifers. Very few water-level measurements are available for the early days of groundwater development. Much better records of depth to water in wells are available since 1943 when water level declines were greatest.

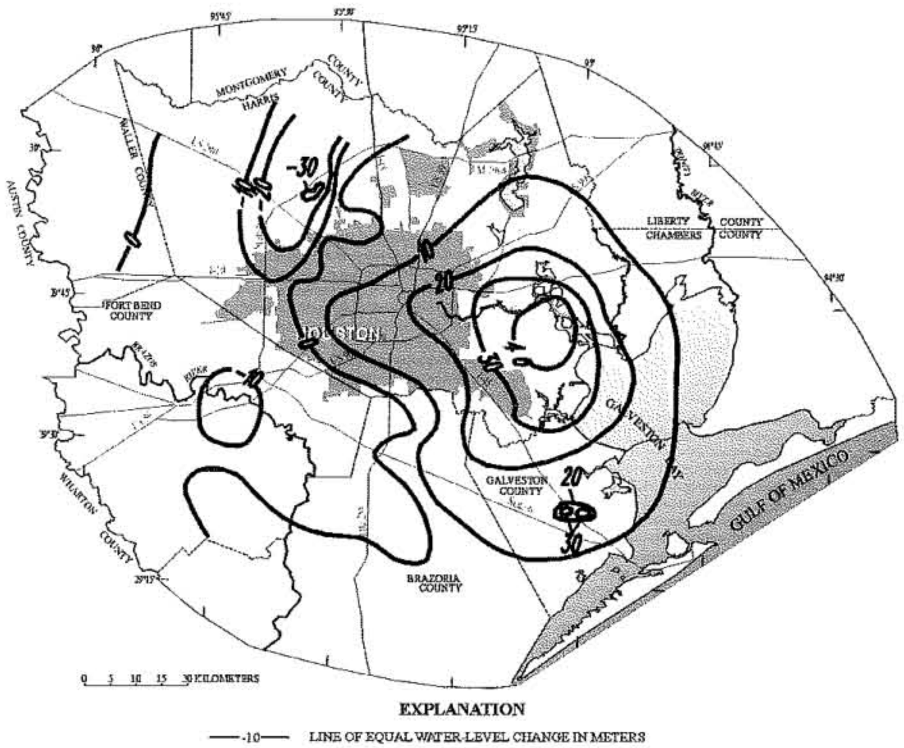

Figure 3. Water-Level Changes in Wells in the Chicot Aquifer, 1977-95 (After Kasmarek et al, 1995).

Figures 1 and 2 show water level changes for the Chicot and Evangeline aquifers during the period 1943-77. The maximum decline in the potentiometric surface of the Chicot aquifer was more than 70 m. The maximum decline in the potentiometric surface of the Evangeline aquifer was more than 91 m. After the decreases in groundwater withdrawals began in late 1976, water levels began to rise in the central and eastern parts of Harris County while they continued to decline in the northern and western parts of the region. Figures 3 and 4 show the changes in water levels in wells in the Chicot and Evangeline aquifers during the 1977-95 period. Water levels rose

48.8 m in wells in the Chicot aquifer and about 54.9 m in wells in the Evangeline aquifer because of the decreases in pumpage. Meanwhile, the potentiometric surfaces of the Chicot and Evangeline aquifers declined as much as 30 m and 75 m due to increases in pumpage in the northern and western parts of Harris County.

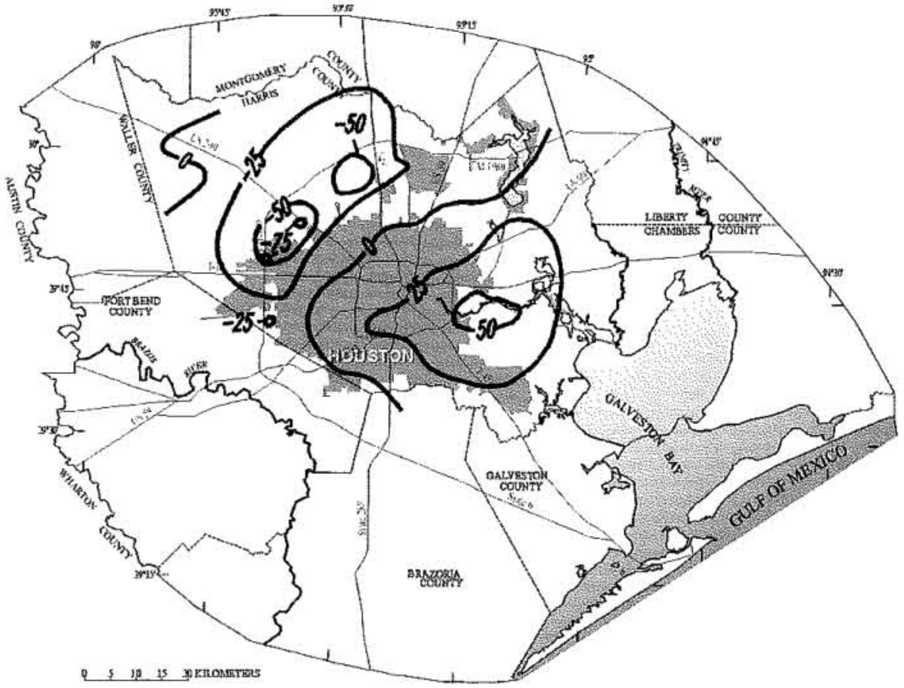

EXPLANATION

—-25— LINE OF EQUAL WATER-LEVEL CHANGE IN METERS

Figure 4. Water-Level Changes in Wells in the Evangeline Aquifer, 1977-95 (After Kasmarek et al, 1995).

5. SUBSIDENCE

Historically, subsidence was measured using conventional spirit leveling. A single line of benchmarks across the region was established in 1906 by the United States Coast and Geodetic Survey, (USCGS). Other lines were established in 1918, 1932-33 and 1935-36. The comprehensive network of benchmarks in existence in 1995 was established in 1943. Because of the limited

amount of elevation data available before 1943, subsidence for the 1906-43 period can only be estimated. In southeastern Harris County estimated subsidence for the 1906-43 period was about 0.3 m. A localized area of subsidence also occurred in southern Galveston County where there was about 0.5 m loss of elevation. Due to the lack of level data before 1943 and because most pumpage and lowering of the potentiometric surfaces causing subsidence did not occur until the late 1930's and early 1940's; the 1943 comprehensive elevation data is often used as the base for subsidence determinations.

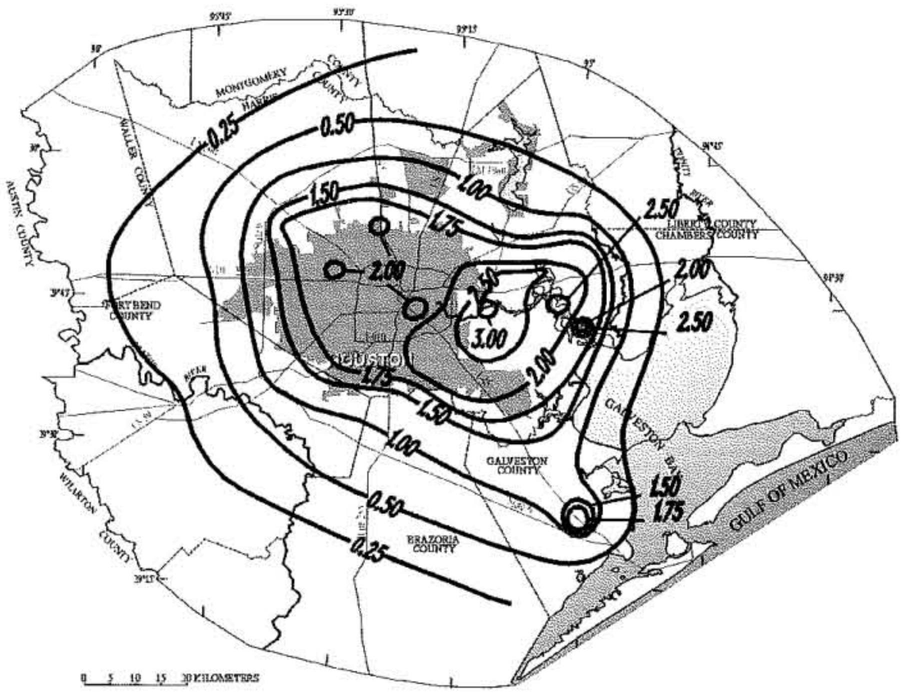

EXPLANATION

—0.50— LINE OF EQUAL LAND-SURFACE SUBSIDENCE, IN METERS

Figure 5. Approximate Land-Surface Subsidence, 1906-95.

Figure 5 shows the approximate subsidence for the 1906-95 period. The pattern of subsidence is circular and uniform; the maximum subsidence of 3.0 m occurred in the Houston Ship Channel area of eastern Harris County.

After the change in groundwater withdrawal (decrease in Galveston County and in the southeastern part of Harris County and increase in north and western Harris County) the rates and magnitude of subsidence changed. The rate of subsidence in the center of the area, decreased dramatically. Between 1943 and 1978, subsidence was about 2.7 m. Between 1978 and 1987, subsidence was about 8 cm. No subsidence occurred in this area of maximum rise in potentiometric surface between 1987 and 1995.

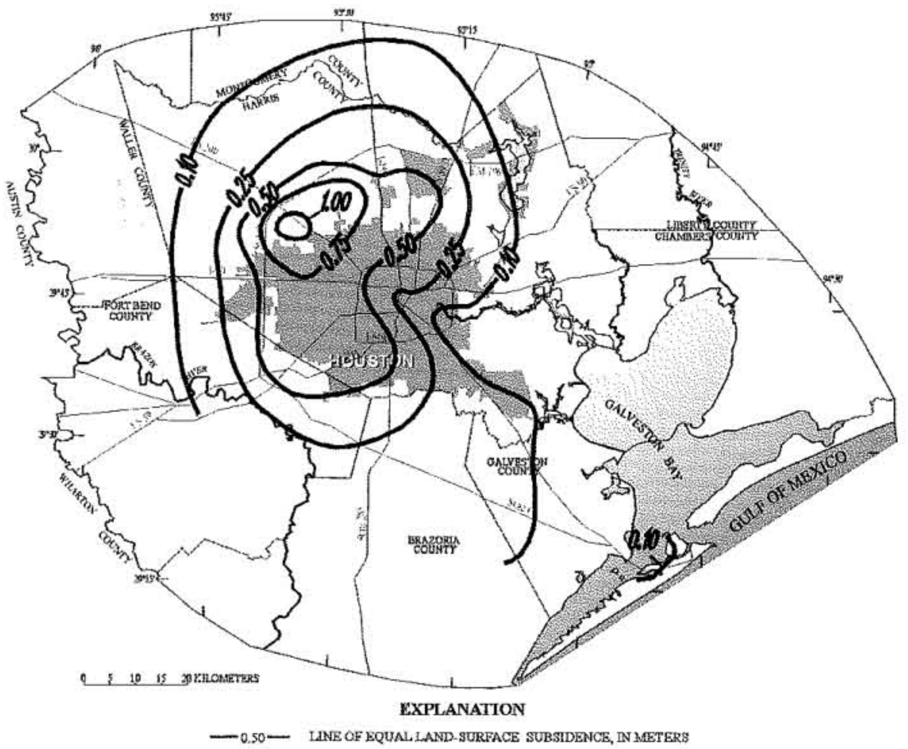

Figure 6. Approximate Land-Surface Subsidence, 1978-95.

During the 1978-95 period (Figure 6) the area of maximum subsidence shifted to the western part of Harris County where 1.1 m was determined. Less than 0.1 m of subsidence occurred in eastern Harris County and in Galveston County during the same period. A good description of the most current conditions is shown by Figure 7, which shows a map of subsidence that occurred during 1987-95. A maximum of about 0.5 m of subsidence occurred in the near western part of Harris County, and no subsidence occurred in Galveston County and southeastern Harris County.

Continuous records of changes in elevation at Pasadena, the center of the bowl of subsidence from 1906 to 1995, and at Addicks on the near western side of Houston are presented by the graphs of Figure 8. The record at the Pasadena site shows a slight rise in the land surface during the 1987-1995 period, while the record at the Addicks site shows continuing subsidence. Locations for the two extensometers are shown on Figure 1.

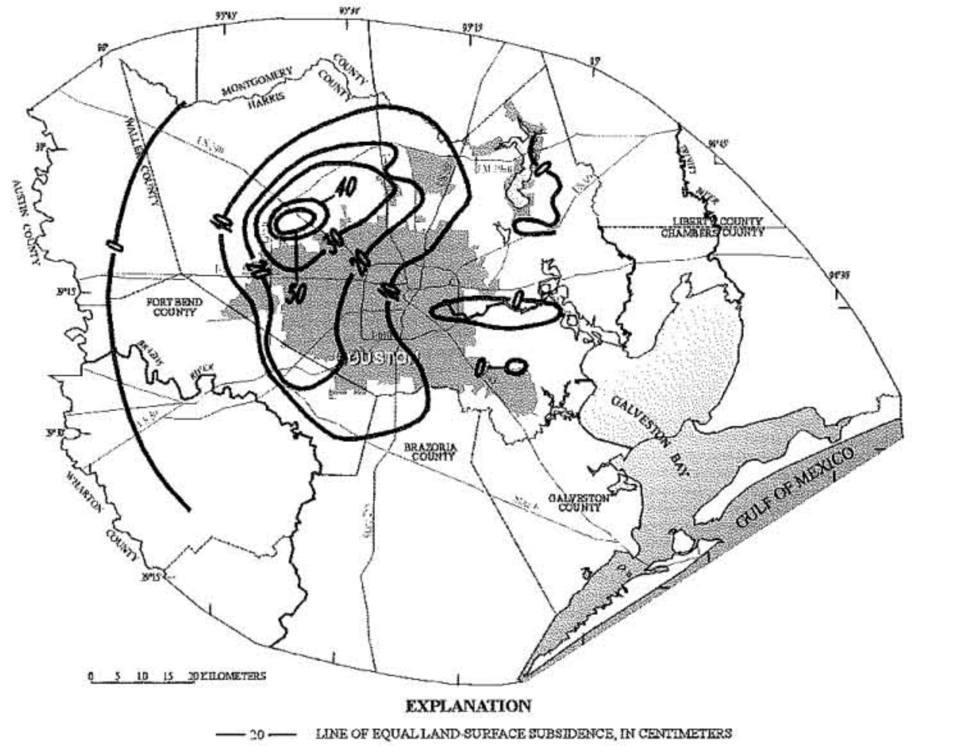

Figure 7. Approximate Land-Surface Subsidence, 1987-95.

6. CONTROL OF SUBSIDENCE

Public awareness of subsidence and its detrimental effects led to the creation of the Harris-Galveston Coastal Subsidence District by the Texas Legislature in 1975. Fortunately, the City of Houston had planned and constructed Lake Livingston on the Trinity River, about 72 kilometers northeast of Houston. The reservoir was built to supply water especially to industrial users along the Houston Ship Channel. Although this alternate source of water was available, the City of Houston and the groundwater using industries were at an impasse concerning contractual agreements. Under the Subsidence District's first plan, emphasis was placed on Galveston County and that part of Harris County generally less than 10 m in elevation. Under the plan, the Subsidence District was able to assist in the negotiation of the contracts. The conversion from groundwater to surface water began in late 1976.

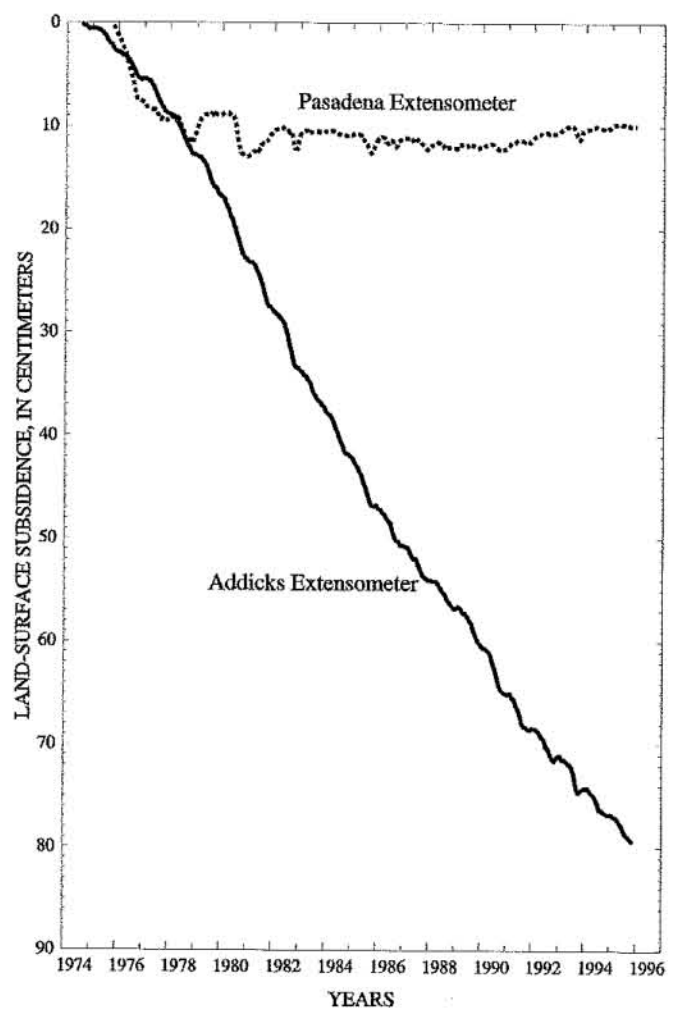

Figure 8. Land-Surface Subsidence at the Pasadena and Addicks Sites, Using Borehole Extensometers.

After creation of the Subsidence District, data collection and analyses intensified. Using a groundwater model and a subsidence model adapted from the U.S. Geological Survey and modified for the Houston Region, the District began an analysis of groundwater withdrawal and water level declines for various scenarios for the region and made site-specific subsidence predictions. The second District plan was adopted in 1985. It divided Harris and Galveston Counties into eight areas with planned conversion to surface water in relation to percent of usage within a specified period. In 1992, another plan was adopted based on detailed re-analysis of regional population and water demand growth. The two

counties were then divided into seven regulatory areas. The plan adopted in 1999 divides the District into three regulatory areas generally reflecting areas that have converted to surface water versus areas that have not converted. The 1999 plan is based on the most current data and models, studies of water demand, water level changes, and historical subsidence.

7. METHODS OF SUBSIDENCE MEASUREMENT

First and second order conventional leveling was used to obtain ellipsoidal heights for regional appraisal of subsidence before 1995. The Global Positioning System (GPS) was used to obtain geodial heights in 1995. A few short lines of spirit levels were run in 1995 to supplement the GPS data and aid in modeling the geoid. Geodial heights were converted to ellipsoidal heights for determination of subsidence for the 1987-95 period. Additionally, 14 borehole extensometers have been installed at 11 sites by the United States Geological Survey (USGS) using its own funds and in cooperation with the U. S. Army Corps of Engineers, the Texas Department of Highways and Public Transportation, and the Harris-Galveston Coastal Subsidence District. Six of the extensometers are installed at the base of the aquifers being pumped and measure total subsidence. The remaining extensometers were designed to collect compaction data for different depth intervals. Three of the extensometers are Continuous Operating Recording Stations (CORS), one of which is in the national network being established by the National Geodetic Survey (NGS) formerly the USCGS. The latest innovation is the development of a trailer mounted GPS receiver, termed Port-A-Measure (PAM). The PAM was designed and built under a cooperative research program between the Subsidence District and the NGS. The PAMs occupy preselected sites in Harris and Fort Bend Counties. At each site, a permanent GPS antenna mount consisting of a sleaved pipe set in concrete at a depth of about 6 m and extending to about 3 m above land surface has been installed. The PAMs gather and store GPS data continuously for a period of one week at each site. Thus, the GPS data collected provides somewhat of a continuous record of subsidence at a site. The District has five PAMs and 12 sites in operation. Ultimately, the network will contain 20 sites. Data collected through the early part of 1999 agrees quite favorably with the stable (CORS) marks. Data collected from the PAMs will be used with the extensometer data and periodic regional GPS data to evaluate subsidence.

8. CONCLUSION

The valuable groundwater resources in the Houston region have prompted tremendous growth in agriculture, industry, and population. Development of groundwater has caused declines in potentiometric levels of the Chicot and

Evangeline aquifers which has resulted in as much as 3.0 m of subsidence of the land surface in the low-lying coastal plain. Because of the detrimental effects of subsidence, the Texas Legislature created the Harris-Galveston Coastal Subsidence District in 1975. Due to the regulation of the withdrawals of groundwater, subsidence has ceased in the most critical area of the region. However, subsidence continues in the inland part of the region. A District Plan based on the latest measurements and modeling technology was adopted in 1999, which directs the groundwater users in the inland part of the region to convert to an alternate source of water according to a definite schedule.

REFERENCES

Gabrysch, R.K. (1982) Ground-Water Withdrawals and Land-Surface Subsidence in the Houston-Galveston Region, Texas, 1906-80: *United States Geological Survey Open –File Report 82-571,* 68p.

Holzer, T. L. & Gabrysch, R. K. (1987) Effects of Water-Level Recoveries on Fault Creep, Houston, Texas, *Ground Water,* **25** (4), July-August 1987, p. 392-397.

Kasmarek, M. C., Coplin L.S. & Santos H. X. (1995) Water-Level Altitudes 1995, Water-Level Changes 1977-95 and 1994-95 and, Compaction 1973-94 in the Chicot and Evangeline Aquifers, Houston-Galveston Region, Texas: *U.S. Geological Survey Open-File Report 95-182,* 8 sheets.

Neighbors, R. J. & Thompson R. E. (1984) Subsidence in the Houston Galveston Area of Texas: Proceedings of the *Third International Symposium on Land Subsidence,* Venice, Italy, March 19-25, 1984, p. 785-793.

LAND SUBSIDENCE - Vol. II
Proceedings of the Sixth International Symposium on Land Subsidence
Ravenna / Italy / 24-29 September 2000

DIFFERENTIAL SAR INTERFEROMETRY FOR LAND SUBSIDENCE MONITORING: METHODOLOGY AND EXAMPLES

Urs Wegmüller and Tazio Strozzi
Gamma Remote Sensing, Thunstrasse 130, 3074 Muri BE, Switzerland

Luigi Tosi
Istituto per lo Studio della Dinamica delle Grandi Masse, CNR, 30125 Venezia, Italy

Abstract

In recent years significant progress was achieved in SAR interferometry. In this paper we report on the potential of differential SAR interferometry to map land subsidence. After a presentation of the methodology the focus will be on feasibility demonstration and accuracy assessment. The theoretical considerations are verified with the selected cases Ruhrgebiet, Mexico City, Bologna, and Euganean Geothermal Basin, representing fast (*m/year*) to slow (*mm/year*) deformation velocities.

The accuracy of the generated deformation maps, the huge SAR data archive starting in 1991, the expected continued availability of new data, and the maturity of the required processing techniques, lead to the conclusion that differential SAR interferometry has a very high potential for operational mapping of land subsidence.

Keywords: subsidence, SAR interferometry, interferogram stacking, accuracy assessment.

1. INTRODUCTION

The potential of differential Synthetic Aperture Radar (SAR) interferometry to map coherent displacement at *cm* to *mm* resolution resulted in spectacular new results for geophysical sciences. Earthquake displacement (Massonnet et al., 1993), volcano deformation (Massonnet et al., 1995), glacier dynamics (Goldstein et al., 1993), and land subsidence (Strozzi et al., 1999a, 1999b, Wegmüller et al., 1999) were mapped. The required data are provided by the space-borne SAR sensors on the ERS-1, ERS-2, Radarsat, and JERS satellites. The planned follow-on sensors on ENVISAT and ALOS will guarantee the availability of appropriate data into the future.

The objectives of this contribution are the presentation of the SAR interferometric methodology and the assessment of its performance. A special focus will be on the interferogram stacking technique, a combination of multiple interferograms, which allows to reduce the error introduced by atmospheric distortions, the main error source in SAR interferometry.

2. DIFFERENTIAL SAR INTERFEROMETRY

Until recently, the phase in SAR imagery was not considered since it is uniformly distributed in the interval $[-\pi,\pi]$ for rough surfaces. However, two images acquired from almost the identical aspect angle have almost the same identical speckle. Under such conditions the phase difference ϕ is related to the imaging path length difference

$$\phi = -\frac{4\pi}{\lambda}(|r_2| - |r_1|) \quad , \tag{1}$$

where λ is the radar signal wavelength. The phase is determined as the argument of the normalized interferogram, γ, defined as the normalized complex correlation coefficient of the complex backscatter intensities s_1 and s_2 at positions $\boldsymbol{r_1}$ and $\boldsymbol{r_2}$

$$\gamma = \frac{\langle s_2 s_1 {}^*\rangle}{\sqrt{\langle s_1 s_1 {}^*\rangle\langle s_2 s_2 {}^*\rangle}} \quad , \tag{2}$$

with the brackets $\langle x\rangle$ standing for the ensemble average of x. The variance of the estimate of the interferometric phase ϕ is reduced by coherent averaging over statistically independent samples. The degree of coherence, a measure of the phase noise, is defined as the magnitude of the normalized interferogram $\gamma = |\gamma|$.

The interferometric imaging geometry formed by two passes of a radar sensor separated by the baseline B is shown in Fig. 1. The interferometric phase is sensitive to both surface topography and coherent displacement along the look vector occurring between the acquisition of the interferometric image pair. Inhomogeneous propagation delay and phase noise are the main error sources. The unwrapped interferometric phase ϕ_{unw} can be expressed as a sum of a topographic term ϕ_{topo}, a displacement term ϕ_{disp}, a path delay term ϕ_{path}, and a phase noise (or decorrelation) term ϕ_{noise}:

$$\phi_{unw} = \phi_{topo} + \phi_{disp} + \phi_{path} + \phi_{noise} \quad . \tag{3}$$

The phase to height sensitivity,

$$\delta\phi_{topo} = \frac{4\pi}{\lambda}\frac{B_\perp}{r\cdot\cos\theta}\delta h \quad , \tag{4}$$

with the wavelength, λ, the baseline component perpendicular to the look vector, $B_\perp$, the incidence angle, θ, and the slant range, r, characterizes the topographic

term. Knowing the baseline geometry and ϕ_{topo} allows to calculated the exact look angle and together with the orbit information the position of the scatter elements allowing to derive the surface topography.

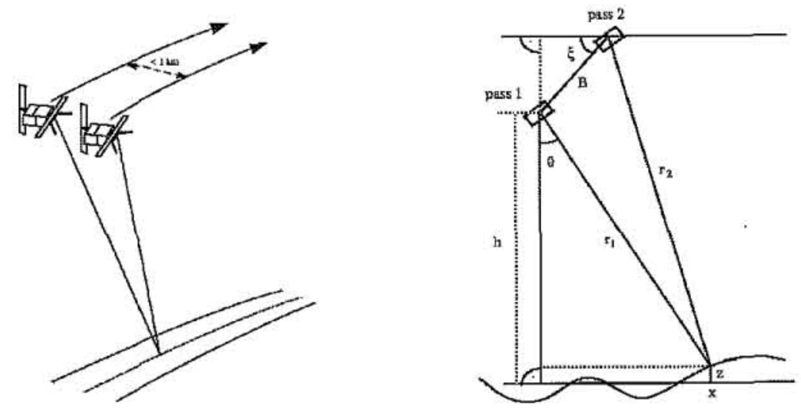

Figure 1. Interferometric imaging geometry showing the two passes with range vectors $\boldsymbol{r_1}$ and $\boldsymbol{r_2}$ to the resolution element. The look angle of the radar is θ. The baseline B is tilted at an angle ξ measured relative to horizontal.

The displacement term, ϕ_{disp}, is related to the *coherent* displacement of the scattering centers along the radar look vector, r_{disp}:

$$\phi_{disp} = 2kr_{disp} \quad , \tag{5}$$

where k is the wave number. In this context *coherent* means that the same displacement is observed for adjacent scatter elements. Under the assumption of exclusively vertical displacement Equation 5 can be converted to

$$\phi_{disp} = \frac{2kr_{sub}}{\cos\theta} \quad , \tag{6}$$

where r_{sub} is the vertical displacement. The sensitivity of ϕ_{disp} to surface deformation is very high. In the case of ERS, for example, 2π displacement phase corresponds to only 2.7 *cm* displacement along the look vector or 3 *cm* of vertical subsidence. Vertical subsidence can usually be assumed in the case of ground water extraction. In the case of mining induced subsidence, on the other hand, the observed geometry of the ground movement is more complicated. Even a combination of SAR data acquired in ascending and descending mode does not allow to resolve the complete three dimensional displacement vector field, without use of additional information.

The path delay term ϕ_{path} is the result of spatial inhomogeneity in the atmospheric conditions (mainly water vapor content). *(see Section 3)*

The decorrelation term ϕ_{noise} is caused by random (or incoherent) displacement of the scattering centers and by SAR signal noise. Multi-looking and filtering of the interferogram allow to reduce the phase noise. The main difficulty with high phase noise is not so much the statistical error introduced in the estimation of ϕ_{topo} and ϕ_{disp} but resulting phase unwrapping problems. Ideally, the phase noise and the phase difference between adjacent pixels are both much smaller than π. In reality this is often not the case, especially for areas with a low coherence and rugged topography. The coherence of ERS Tandem pairs (1 day acquisition time interval) is very low for open water and forest and higher for most other classes. For a 35 day time interval the coherence is still quite high over sparsely vegetated terrain. For acquisition intervals longer than one year the areas with higher coherence levels are further reduced mainly to urban and sub-urban areas.

The basic idea of the differential interferometric approach is to separate the effects of surface topography and coherent displacement, allowing to retrieve differential displacement maps (Wegmüller and Strozzi, 1998a, Wegmüller and Strozzi, 1998b). This goal is achieved by subtracting the topography related phase, ϕ_{topo} , which is either calculated based on a available Digital Elevation Model (DEM) or estimated from an independent interferogram with a short acquisition interval, such as an ERS Tandem pair. In many cases the use of a DEM turns out to be more robust and operational. The phase unwrapping required in the multi-pass approach is often difficult to resolve and far from operational for low coherence areas, especially in rugged terrain. In addition, gaps in the unwrapped topographic phase for areas of too low coherence may be present, depending on the phase unwrapping method used. Because of the scaling of the topographic phase with the perpendicular baseline component (Equation 4) the accuracy of baseline estimation is very important. At present we use various estimation methods based on the orbits data, the registration offsets, and the fringe rate of the interferogram. The error in a displacement measurement resulting from inaccurate baseline increases with the size of the area investigated.

Data processing related aspects, which influence the robustness and operationality of the application as well as the accuracy of the result, include phase filtering, phase unwrapping, geocoding, and the averaging scheme for multiple results. More details on the processing chain used for the generation of the results presented in this paper are found in Wegmüller and Strozzi, 1998b.

3. ACCURACY CONSIDERATIONS AND INTERFEROGRAM STACKING TECHNIQUE

The path delay term ϕ_{path} of Equation 3 is the result of spatial heterogeneity of the atmospheric (mainly water vapor content) and ionospheric conditions.

These so-called *'atmospheric distortions'* are the main error source of SAR interferometry. As a relatively strong atmospheric distortion we consider a phase error of $\pi/2$. This relatively high error value is not just motivated by a rather conservative assessment of the accuracy, but also to achieve a more robust and operational technique. High atmospheric errors can often be identified by its specific shape, by cross-comparison of multiple interferograms, or possibly based on meteorological data. It is not clear, though, how to best integrate such tests in an operational processing chain.

For the ERS SAR configuration an atmospheric distortion of $\pi/2$ results in an error of approximately 0.75 *cm* in the estimation of a vertical displacement. To obtain reliable displacement values with SAR interferometry the subsidence signal should dominate over the error terms. To keep the expected error in the order of 5% of the maximum displacement the displacement phase term should be 20 times the assumed atmospheric distortion, i.e. 10π , or about 15 *cm* of vertical subsidence. With this in mind, we preferably select an interferogram with 3 or more years acquisition interval to map a subsidence velocity of 5 *cm/year*. To map higher subsidence velocities shorter intervals are preferred, allowing a better temporal resolution of the subsidence history. In addition, the coherence is higher for shorter time intervals allowing a more complete spatial coverage. To map slow subsidence, longer intervals are required. The intervals cannot be freely extended because of the limited mission duration. In addition, the use of very long intervals introduces excessive temporal decorrelation, which precludes interpretation of data except for urban areas. Furthermore, the temporal resolution of the monitoring is reduced.

An approach to improve the ratio between the subsidence signal and the atmospheric phase error is the stacking of multiple interferograms. Under the assumption of a stationary process the subsidence term adds up linearly, i.e. the addition of the unwrapped phases of two interferograms with one and two years acquisition intervals results in an unwrapped phase covering an effective time interval of 3 years. For the error term, on the other hand, we can assume statistical independence between independent interferograms resulting in an increase with the square root of the number of pairs. The relative subsidence velocity estimation error is calculated as

$$\frac{\Delta r_{sub}}{r_{sub}} = \frac{\sqrt{n} \cdot E}{v \cdot \sum t_i} \quad , \tag{7}$$

with n the number of independent interferograms used, E the absolute error estimate for a single interferogram, v the subsidence velocity, and Σt_i the cumulative time interval. Equation 7 can be used to determine the cumulative time required to map a certain subsidence velocity with a predefined expected relative estimation error (see Figure 2 for ERS SAR data). The potential of the interferogram stacking technique is demonstrated by the fact that the stacking of more than 10 independent interferograms allowing to reach a cumulative time interval of more than 20 years results in an expected subsidence velocity estimation error below 1 *mm/year*. Such stacking is indeed possible thanks to the immense ERS data archive. The condition, that the estimation accuracy can be expected to improve if an additional interferogram is added to a stack of n interferograms,

$$\frac{t_{n+1}}{\sum_n t_i} \geq \frac{\sqrt{n+1}}{\sqrt{n}} - 1 \quad , \tag{8}$$

depends only on the relative increase of the cumulative time and the number of independent interferograms in the stack.

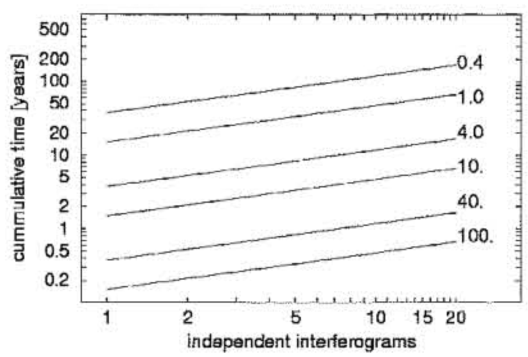

Figure 2. Quality assurance plot used in ERS data selection for interferogram stacking as calculated for an atmospheric distortion of $\pi/2$. For the selected subsidence velocities, 0.4 *cm/year*, 1.0 *cm/year*, 4.0 *cm/year*, 10.0 *cm/year*, 40.0 *cm/year*, and 100 *cm/year* the lines indicate the cumulative time required to achieve with the indicated number of independent interferograms a relative estimation error of 5%.

4. EXAMPLES

Four sites characterized by different displacement velocities were selected to investigate the performance of differential SAR interferometry for land subsidence monitoring: the Ruhrgebiet (Germany), Mexico City (Mexico), Bologna (Italy), and the Euganean Geothermal Basin (Italy). In the case of Bologna the subsidence was first estimated using single interferograms with acquisition time intervals of more than three years. In a second phase the feasibility of an annual subsidence monitoring was investigated using the interferogram stacking technique. The approximate subsidence velocities, the monitoring interval selected, the number of interferograms used and the expected estimation error are summarized in Table 1. In the following the results achieved for the four sites will be summarized.

Table 1. Subsidence velocities for the selected sites. In all cases SAR data of the European Remote Sensing Satellites ERS-1 and ERS-2 were used.

	Velocities *[cm/year]*	Monitoring interval	Interferograms / Cumulative time	Expected accuracy[1] *[cm/year]*
Ruhrgebiet (Germany)	0 - 200	1 month	1 / 1 month	9.0
Mexico City (Mexico)	0 - 40	3 months	1 / 3 months	3.0
Bologna (Italy)	0 - 4	4 years	3 / 9 years	0.15
Bologna (Italy)	0 - 4	1 year	6 / 4 years	0.5
Euganean Geothermal Basin (Italy)	0 - 0.4	5 years	10 / 20 years	0.1

[1] as calculated for an atmospheric distortion of $\pi/2$. No other errors considered.

4.1 Ruhrgebiet

Coal mining causes significant surface movement in the German Ruhrgebiet. Due to legal requirements the mining companies are obliged to assess the environmental impact of the excavations. Surface deformation caused by mining is a very dynamic process with high spatial and temporal variability. For mining areas with high subsidence velocities, interferometric pairs with acquisition intervals of only one or a few 35 day repeat cycles are preferred. Subsidence maps of different time intervals clearly indicate the progress in the sub-surface coal excavation. Figure 3 shows an example of a typical deformation cone observed for areas of active excavation. The colors indicate the deformation along the SAR observation direction. One color cycle corresponds to a displacement of 2.7 *cm* during the 35 days time interval. Vertical subsidence cannot be assumed in this case of mining induced deformation. The white color indicates areas of low coherence where the phase could not be unwrapped. Detailed studies and a validation with excavation plans are ongoing.

4.2 Mexico City

Mexico City is built on highly compressible clays and by reason of strong groundwater extraction a total subsidence of more than nine meters has been of the interferogram stacking technique is demonstrated by the fact that the stacking of more than 10 independent interferograms allowing to reach a cumulative time interval of more than 20 years results in an expected subsidence velocity estimation error below 1 *mm/year*. Such stacking is indeed possible thanks to the immense ERS data archive. The condition, that the estimation accuracy can be expected to improve if an additional interferogram is added to a stack of n interferograms,

$$\frac{t_{n+1}}{\sum_n t_i} \geq \frac{\sqrt{n+1}}{\sqrt{n}} - 1 \quad , \tag{8}$$

depends only on the relative increase of the cumulative time and the number of independent interferograms in the stack.

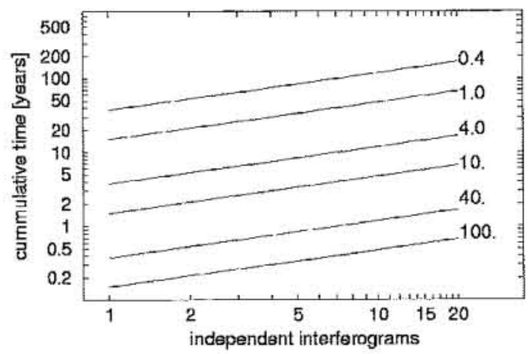

Figure 2. Quality assurance plot used in ERS data selection for interferogram stacking as calculated for an atmospheric distortion of $\pi/2$. For the selected subsidence velocities, 0.4 *cm/year*, 1.0 *cm/year*, 4.0 *cm/year*, 10.0 *cm/year*, 40.0 *cm/year*, and 100 *cm/year* the lines indicate the cumulative time required to achieve with the indicated number of independent interferograms a relative estimation error of 5%.

4. EXAMPLES

Four sites characterized by different displacement velocities were selected to investigate the performance of differential SAR interferometry for land subsidence monitoring: the Ruhrgebiet (Germany), Mexico City (Mexico), Bologna (Italy), and the Euganean Geothermal Basin (Italy). In the case of Bologna the subsidence was first estimated using single interferograms with acquisition time intervals of more than three years. In a second phase the feasibility of an annual subsidence monitoring was investigated using the interferogram stacking technique. The approximate subsidence velocities, the monitoring interval selected, the number of interferograms used and the expected estimation error are summarized in Table 1. In the following the results achieved for the four sites will be summarized.

Table 1. Subsidence velocities for the selected sites. In all cases SAR data of the European Remote Sensing Satellites ERS-1 and ERS-2 were used.

	Velocities *[cm/year]*	Monitorin g interval	Interferogram s / Cumulative time	Expected accuracy[1] *[cm/year]*
Ruhrgebiet (Germany)	0 - 200	1 month	1 / 1 month	9.0
Mexico City (Mexico)	0 - 40	3 months	1 / 3 months	3.0
Bologna (Italy)	0 - 4	4 years	3 / 9 years	0.15
Bologna (Italy)	0 - 4	1 year	6 / 4 years	0.5
Euganean Geothermal Basin (Italy)	0 - 0.4	5 years	10 / 20 years	0.1

[1] as calculated for an atmospheric distortion of $\pi/2$. No other errors considered.

4.1 Ruhrgebiet

Coal mining causes significant surface movement in the German Ruhrgebiet. Due to legal requirements the mining companies are obliged to assess the environmental impact of the excavations. Surface deformation caused by mining is a very dynamic process with high spatial and temporal variability. For mining areas with high subsidence velocities, interferometric pairs with acquisition intervals of only one or a few 35 day repeat cycles are preferred. Subsidence maps of different time intervals clearly indicate the progress in the sub-surface coal excavation. Figure 3 shows an example of a typical deformation cone observed for areas of active excavation. The colors indicate the deformation along the SAR observation direction. One color cycle corresponds to a displacement of 2.7 *cm* during the 35 days time interval. Vertical subsidence cannot be assumed in this case of mining induced deformation. The white color indicates areas of low coherence where the phase could not be unwrapped. Detailed studies and a validation with excavation plans are ongoing.

4.2 Mexico City

Mexico City is built on highly compressible clays and by reason of strong groundwater extraction a total subsidence of more than nine meters has been observed over the last century. The selection of ERS data to map subsidence at Mexico City is strongly restricted by the relatively few acquisitions found in the archive. From the available data acquisitions, three independent differential interferograms, one in ascending and two in descending mode, were selected. The subsidence maps derived from the three independent interferograms are consistent. For the period January 1996 – May 1996 (Figure 4) the observed maximum subsidence velocities are about 40cm/year, in general agreement with those reported in the literature and derived form levelling surveys and theoretical models. For a more detailed description of this case see Strozzi and Wegmüller, 1999a.

4.3 Bologna

At Bologna, Italy, the subsiding area is large with maximum subsidence velocities of 6 to 8 *cm/year* and characteristic spatial gradients of the vertical movement. Levelling surveys are being conducted at intervals of several years. We decided to use this case to investigate the potential of differential SAR interferometry because of the large science community involved in this case and the available reference data which can be used for validation purposes. A more detailed discussion of the interferometric investigation is given by Strozzi et al. (2000). Here, the focus is on the evaluation of the performance of the technique.

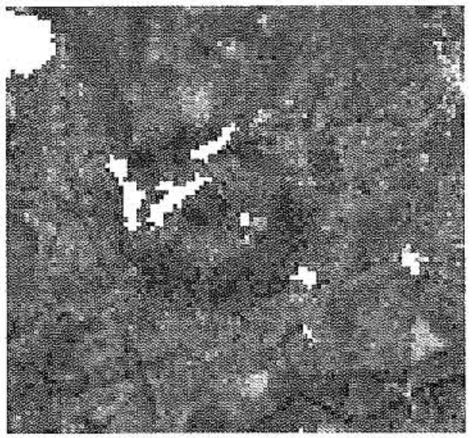

Figure 3. Ruhrgebiet: deformation map for active coal excavation site. The image width is 2.5 *km*. The color scale is defined in the text. For the image brightness the backscattering coefficient is used.

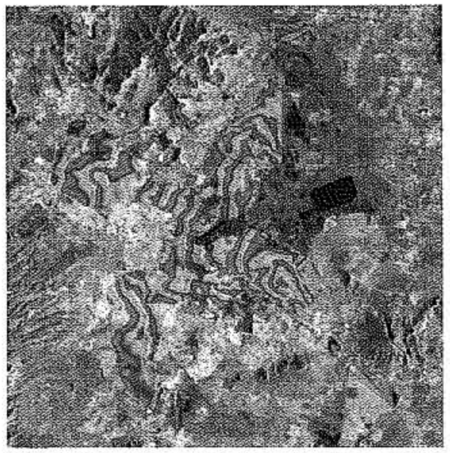

Figure 4. Mexico City: interferometric subsidence map derived from the ERS pair 29-Dec-1995 / 16-May-1996. Subsidence velocity per color cycle: 5 *cm/year*. For the image brightness the backscattering coefficient is used.

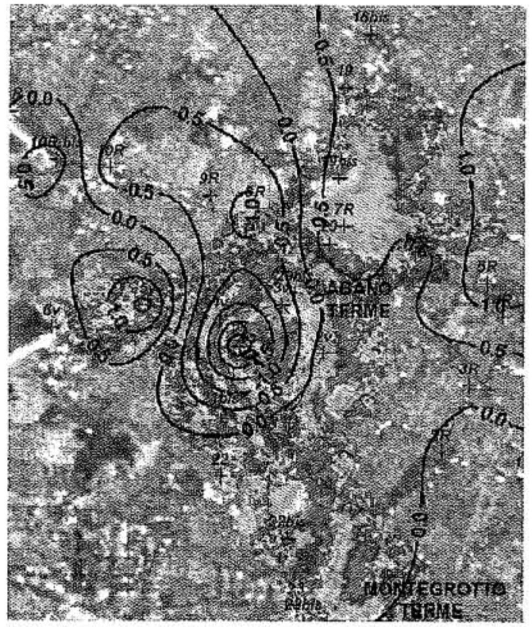

Figure 5. Vertical ground movements (in *mm/year)* from levelling surveys in 1991 and 1995 in the urban areas of Abano and Montegrotto Terme (data from Comune di Abano Terme and Regione del Veneto) superposed to the interferometric displacement velocity map for the interval 1992 to 1996. Also shown are the position of the levelling lines and benchmarks.

In a first step three long-time ERS interferometric pairs were selected (Wegmüller at al., 1999). Cross-comparison of the three resulting subsidence maps was used as an immediate quality check, confirming good consistency between the results. In a next step interferogram stacking was applied. The resulting interferometry based subsidence map was then validated with levelling data. For the urban area of Bologna the absolute values and the shapes of the contour lines of the interferometric subsidence map are in good agreement with those derived from levelling surveys. The quantitative validation, nevertheless, indicated a systematic offset between the subsidence velocity values determined from levelling surveys (period 1987-1992) and SAR interferometry (period 1992-1996). This difference can be explained by the different observation time period, indicating a decrease of the subsidence velocity. To confirm this interpretation more recent levelling data with a better correspondence to the time interval covered with SAR interferometry will be used for the validation as soon as such data will become available.

The hypothesis of the temporal decrease of the subsidence velocity at Bologna raised our interest in a better temporal resolution of the subsidence monitoring. To investigate the feasibility of an annual monitoring with differential SAR interferometry we produced subsidence maps for the time periods 1992-1993 and 1997-1998 applying the interferogram stacking technique with 6 and 7 interferograms, respectively, and cumulative time intervals of more than four years. The comparison of the two subsidence maps confirmed the decrease of the subsidence activity in Bologna during the last decade. The 1992-1993 map was validated with the 1987-1992 levelling surveys (Strozzi et al., 2000), confirming the expected feasibility of an annual subsidence monitoring. Up to present the 1997-1998 result could not be validated.

4.4 Euganean Geothermal Basin

Land subsidence of the Euganean Geothermal Basin, Italy, is related to the geothermal groundwater withdrawal. Precision levelling surveys conducted for the Commune di Abano Terme and the Regione del Veneto indicate maximum subsidence rates of 1 *cm/year* for the period up to 1991. After 1991 the subsidence velocity decreased as a consequence of a regulation of the groundwater withdrawal. In our investigation this case is used to analyze the feasibility of differential interferometric monitoring of slow subsidence velocities.

To map the expected low sub-*cm/year* subsidence velocity 10 interferograms in the time span 1992 to 1996 were selected. Interferogram stacking was used to generate a single subsidence map with a cumulative time interval of more than 20 years, allowing to reduce the expected velocity estimation error caused by atmospheric phase distortions to approximately 1 *mm/year*, a level which is significantly below the expected subsidence level of several *mm/year*.

The resulting interferometric deformation map shows a clear subsidence over Abano Terme with a maximum velocity of 4 *mm/year*, in agreement with the results of the last levelling surveys performed in 1991 and 1995 (Figure 5). The correspondence of the results of the two different surveying techniques is high, as confirmed by a direct quantitative validation of the interferometry based subsidence values along the levelling lines, an example of which is shown in Figure 6. For 17 points where we had values available from both surveying techniques the average difference of the vertical displacement velocity values was 0.2 mm/year with a standard deviation of 1.0 *mm/year*. The minimum and maximum differences were –1.5 *mm/year* and +2.2 *mm/year*, respectively. This result confirms the expected high accuracy achieved with the interferogram stacking technique. A more detailed description of this case was given by Strozzi et al., 1999.

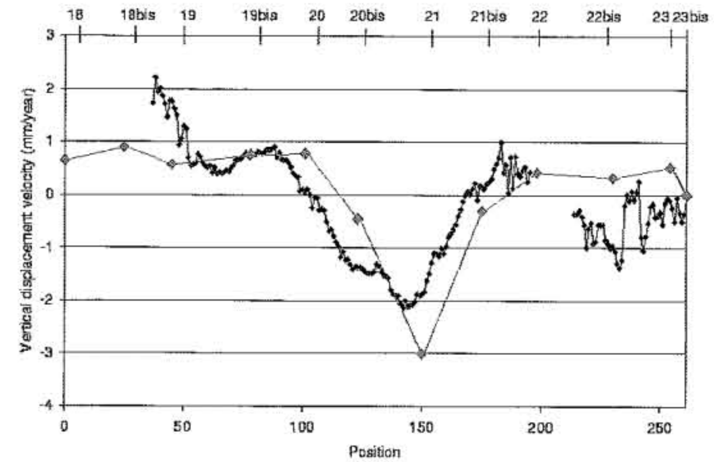

Figure 6. Profiles of the vertical displacement velocity from SAR interferometry (black line, period 1992-1996) and levelling surveys (gray line, period 1991-1995, data from Comune di Abano Terme and Regione del Veneto) along the levelling line Abano Terme – Montegrotto Terme (yellow line in Figure 5).

5. CONCLUSIONS

The feasibility of surface deformation mapping with ERS differential SAR interferometry was confirmed for a wide range of deformation velocities ranging from *m/year* (Ruhrgebiet, Mexico City) to *cm/year* (Bologna) and *mm/year* (Eugenean Geothermal Basin).

Data availability was found to be a limiting factor in the case of Mexico City. For the investigated European sites, on the other hand, a large number of ERS acquisition are available, allowing to optimize the data selection with respect to acquisition dates and interferometric baselines. For the planned future missions with SAR sensors which can be operated in a variety of modes (ENVISAT, ALOS) this means that the robustness and operationality of the subsidence application relies very much on the selection of a single interferometric mode for most of the time.

As demonstrated for the Euganean Geothermal Basin the interferogram stacking technique allows to reduce the errors caused by atmospheric distortions to a low level making the measurement of slow deformation velocities in the *mm/year* range feasible. The technique also allows to increase the temporal resolution of the monitoring, as demonstrated with the annual monitoring of the subsidence for Bologna.

The main limitations of the interferometric technique are the temporal decorrelation of the signal, which leads to an incomplete coverage with deformation information, with gaps mainly in forested and agricultural areas, and the well known problems of the SAR imaging geometry in areas of rugged topography, such as layover and radar shadow.

The interferometric technique was found to be fast, as demonstrated by the fact that we are still waiting for the levelling data to validate the latest Bologna results, and cost effective.

Considering the high quality of the results achieved for the investigated sites, the huge SAR data archive starting in 1991, the expected continued availability of new SAR data, and the maturity of the required data processing techniques, we conclude that differential SAR interferometry has a very high potential for operational mapping of land subsidence.

The complementarity of the interferometric technique with levelling surveys and GPS measurements suggests that the most effective monitoring strategy will be an integration of the different techniques.

Acknowledgments

This work was supported by the ESA Data User Program (DUP). The Italian National Geologic Survey is acknowledged for the DEM.

REFERENCES

Massonnet D., M. Rossi, C. Carmona, F. Adragna, G. Peltzer, K. Feigl & T. Rabaute (1993), The displacement field of the Landers earthquake mapped by SAR interferometry, *Nature*, **364** (6433) pp. 138-142.

Massonnet, D., P. Briole & A. Arnaud (1995) Deflation of Mount Etna monitored by spaceborne radar interferometry, *Nature*, **375**, pp. 567-570.

Goldstein R.M., R. Engelhardt, B. Kamb & R. Frolich (1993), Satallite Radar Interferometry for Monitoring Ice Sheet Motion: Application to an Antarctic Ice Stream, *Science,* **262**, pp. 1525-1530, 3-dec-1993.

Strozzi T. & U. Wegmüller (1999a), Land Subsidence in Mexico City Mapped by ERS Differential SAR Interferometry, *Proc. IGARSS'99*, Hamburg, 28 June - 2 July.

Strozzi T., L. Tosi, L. Carbognin, U. Wegmüller & A. Galgaro (1999b), Monitoring Land Subsidence in the Euganean Geothermal Basin with Differential SAR Interferometry, *Proc. Fringe'99*, Liège (B).

Strozzi T., U. Wegmüller & G. Bitelli (2000), Differential SAR interferometry for land subsidence mapping in Bologna, *Proc. SISOLS'2000*, Ravenna, Italy, 25-29 September.

Wegmüller U. & T. Strozzi (1998a), Characterization of differential interferometry approaches, EUSAR'98, 25-27 May, Friedrichshafen, Germany, *VDE-Verlag, ISBN 3-8007-2359-X*, pp. 237-240.

Wegmüller U. & T. Strozzi, (1998b), SAR interferometric and differential interferometric processing chain. *Proc. of IGARSS'98*, Seattle, USA.

Wegmüller U. & T. Strozzi (1999), Validation of ERS Differential SAR Interferometry for Land Subsidence Mapping: the Bologna Case Study, *Proc. IGARSS'99*, Hamburg, 28 June - 2 July.

APPLICATION OF GPS TO EVALUATE LAND SUBSIDENCE IN IRAN

S. Morteza Mousavi and M. Hesham El Naggar
Geotechnical Research Centre, University of Western Ontario, London, Ontario

Abolfazl Shamsai
Civil Engineering Department, Sharif University of Technology, Tehran, Iran

Abstract

Groundwater withdrawal is one of the most important causes of land subsidence all over the world that has caused extremely expensive damages to buildings, walls, roads, railroads, pipelines and casings of the water wells. One example for subsiding areas is Rafsanjan plain, which has had the most subsidence in Iran. A necessary step to perform a proper analysis for land subsidence is to obtain accurate measurements of actual subsidence at certain intervals. In this paper, the latest situation of land subsidence in Rafsanjan plain as well as the geological, hydrogeological conditions and groundwater utilization are explained. Finally the results of two successive measurements carried out recently as the first attempt in Iran to monitor land subsidence by using GPS (Global Positioning System) are presented and discussed.

Keywords: land subsidence, groundwater, GPS, Iran

1. INTRODUCTION

Land subsidence induces very serious economic and social problems, which unfortunately appears much later after than commencement of the subsidence event and when most damages are irreversible.

The increasing exploitation of groundwater, especially in basins filled with unconsolidated alluvial, lacustrine, or shallow marine deposits, has as one of its consequences the sinking or settlement of the land. The occurrence of major land subsidence due to the withdrawal of groundwater is relatively common in highly developed areas (Poland, 1982).

2. USE OF GPS FOR GROUND SUBSIDENCE MONITORING

Conventional surveying techniques have been used to measure the subsidence. However this procedure is both expensive and time consuming, especially if done properly using a matrix of permanent bench marks that are monitored on a periodic basis

The operational deployment of GPS (the Global Positioning System) by the U.S. Department of Defense now makes it possible to perform subsidence monitoring much more efficiently and at reduced costs, compared to the conventional surveying techniques. Furthermore the GPS approach can be integrated with a conventional bench mark system allowing substantial cost and timesaving to be realized.

The GPS consists of the constellation of orbiting satellites that continuously transmit radio navigation signals. The satellites are launched and maintained by the U.S. Department of Defense, and the radio signals are made available free of charge (Ender and Chilingarian, 1995).

GPS provides an important technological advancement for monitoring land subsidence. The accuracy of measurement using GPS is within 5-8 mm. This accuracy is considered to be satisfactory given that land subsidence is usually in the order of ten millimeters or more. Meanwhile monitoring can be done with fewer expenses and in less time. Using this method, direct sight line between constant bench marks is not necessary so that much flexibility appears in using the system.

3. RAFSANJAN PLAIN

3.1 General

Rafsanjan subbasin, located near central Iran, with a general elevation between 1400-1500 meters above sea level, has a total area of 10905 square kilometers. This area includes 4636 square kilometers plains and 6269 kilometers mountains (Figure 1). This subbasin is roughly rectangular in shape. The main agricultural product of the area is pistachio, and many wells have been drilled to develop the agricultural lands for this product.

In general, alluvial materials deposited in the Rafsanjan basin consist of heterogeneous unconsolidated mixture of clay, silt, sand and gravel, which locally contain cobble, salt, and gypsum (GSI, 1972, 1981, 1992). These materials are graded from coarser to finer grains as the distance increases from their sources in the surrounding mountains.

Land subsidence due to groundwater has been reported in the whole area of Rafsanjan plain in Iran, which causes serious obstacles to agricultural development, and urban areas. The ground surface in this area has been subsided up to .90 m. The rate of subsidence recently is about 50 to 150 mm. for decline of about one meter in groundwater level, causing extremely expensive damages.

Unfortunately until 1999, there had not been any systematic instrumentation for measuring ground level changes. The only available information had been from farmers who have to cut the casings of their wells every year.

In Iran, RWO in every province is responsible for surface and groundwater management. Rafsanjan area is under the responsibility of RWO in Kerman province and its office in Rafsanjan City. Many field and laboratory works have been done by RWO in this plain.

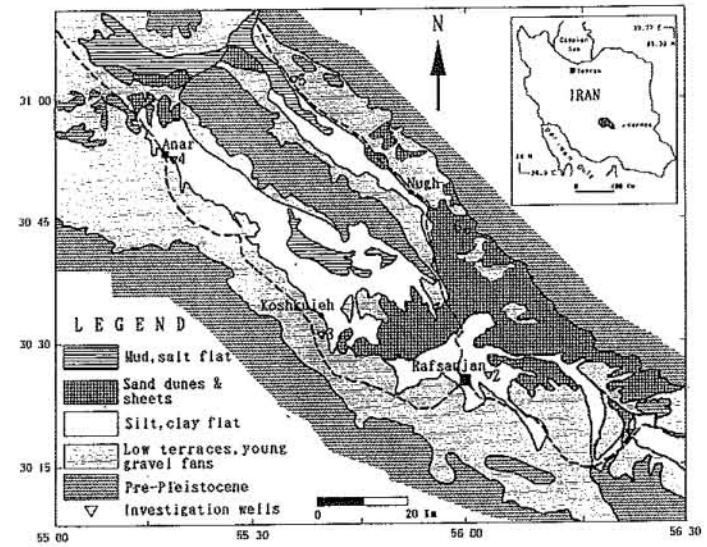

Figure 1. Geological and location map of Rafsanjan plain

3.2 Groundwater utilization

Drilling of deep wells by using boring machine in Rafsanjan plain, started since 1953. The number of wells increased between 1969 and 1999 and accelerated with draughts in 1971 and 1979 Total number of wells has increased from 209 to 1798 in the period of 1969 to 1999 (Table 1).

Table 1. Total discharge of groundwater in Rafsanjan plain.

Year	1969	1976	1981	1986	1989	1993	1996	1999
Disch.(mm^3)	149	425	713	686	760	799	821	839
No. of wells	209	1032	1503	1478	1539	1621	1719	1798

On the basis of the last count of the wells, the numbers of drinking, agricultural and industrial wells have been 151, 1526 and 121 respectively, or 8.4%, 84.9% and 6.7% of the total number of the wells (Table 2). The number of wells has been continuously increased because of increasing needs of farmers.

The consumption of groundwater in Rafsanjan plain increased about six times since 1969 to 1999 (Table 1). Groundwater has been consumed about 8.22 percent for drinking, 90.69 percent for agricultural and 1.09 percent for industrial purposes (Table 2).

Table 2. Use of groundwater in Rafsanjan plain (1999)

Use	Discharge (mm^3)	No. of wells	Percent
Drinking	69	151	8.4
Agricultural	760.9	1526	84.9
Industrial	9.1	121	6.7

4. MONITORING

Considering the vast area of Rafsanjan plain, actually more than 100 GPS stations were needed to be established at the plain, but due to the financial limitation, through first stage of monitoring program, 35 stations could be established. Establishment of more GPS stations in the next stages of monitoring program is scheduled. The network of GPS stations was designed considering the pattern of distribution of groundwater wells and also decline of groundwater level in past years.

Two successive measurements were done on August 1998 and April 1999. Further details can be found in Mousavi, 1999. Continuing of the monitoring in a regular periodic manner is scheduled. The resulted data are summarized.

5. RESULTS

Overdraft of groundwater to meet the drinking, agricultural and industrial needs in Rafsanjan plain of Iran has declined the groundwater level by a total of about 25 meters, causing land subsidence. The isodecline contours (Figure 3) generally correspond with well locations (Figure 2).

Considering the results, the decline of groundwater has been the major cause of land subsidence in Rafsanjan plain, but it has not been the only cause. Other factors such as tectonic and dissolving of salts into the groundwater have been effective. This is consistent with the former reports (Nikdel, 1992).

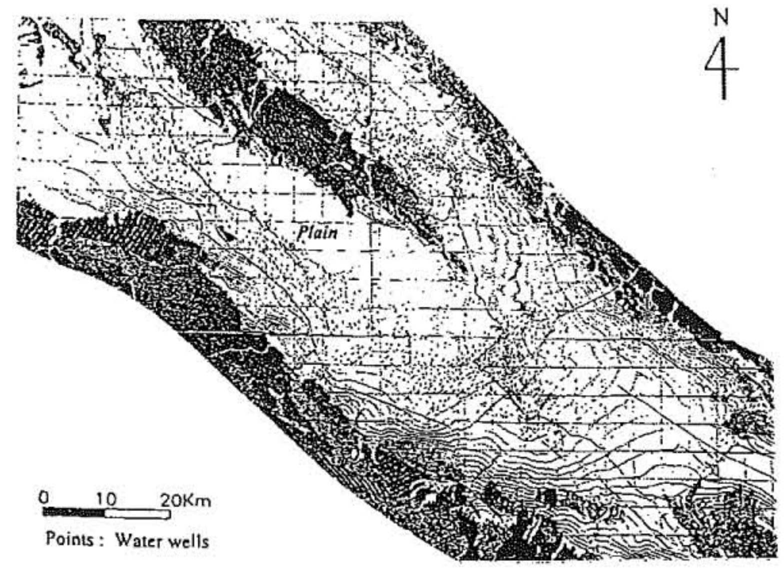

Figure 2. Water wells in Rafsanjan plain

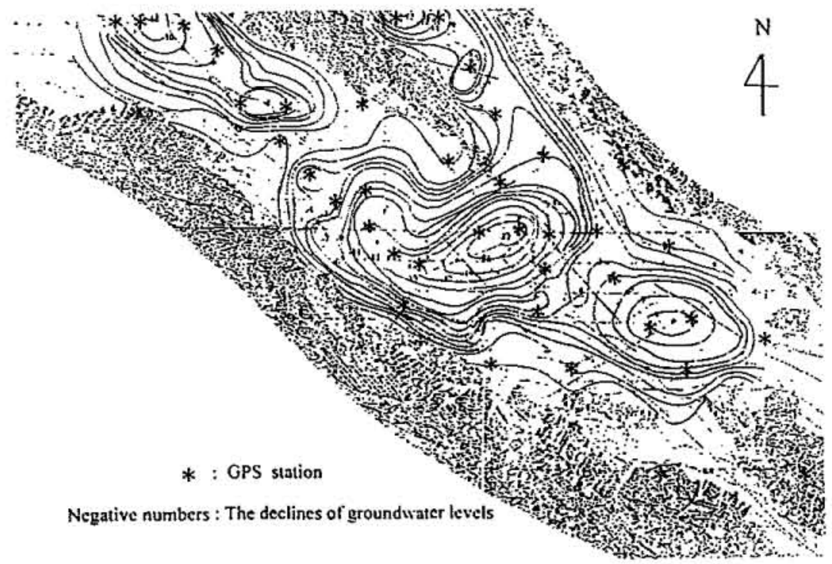

Figure 3. Isodeclines of groundwater Level and GPS stations

During the 8 months interval between two successive measurements, the most decline of groundwater level has been about 1m. At the same time, different points have subsided from less than 10 mm to about 80 mm. land subsidence near Rafsanjan City has been about 40 mm. The preliminary analysis of the results suggests that the magnitude of the land subsidence is approximately 10% of the magnitude of the decline in groundwater level.

6. Acknowledgements

This paper is based on a part of Mousavi's Ph. D. thesis, which has been done under supervision of Professor Shamsai at Sharif University of Technology, Tehran, Iran. The authors would like to express their gratitude to Professors Abbas Afshar, S. Mohsen Haeri and Mashalah Khamehchian of "Science and Technology", "Sharif" and "Tarbiat-e-Modares" Universities, Tehran, Iran, who have been of great help while the research was being done.
The authors would also like to thank KRWO (Kerman Regional Water Organization), "Rafsanjan Irrigation Office", and Microgeodesy Department of Mahab-e-Ghods Company in Tehran for their support and great help in supplying the major portion of the data, assisting field investigation, and performing the first GPS measurement of land subsidence in Iran.

7. REFERENCES

Endres B. & Chilingarian, G. V. (1995) Use of the Global Positioning System (GPS) for ground subsidence monitoring. *Subsidence due to fluid withdrawal*, Elsevier, 453-457.

Geological survey of Iran (GSI) (1972) *1:1250000 geological map series*, Yazd sheet, Iran.

Geological survey of Iran (GSI) (1981) *1:250000 geological map series*, Anar sheet, Iran.

Geological survey of Iran (GSI) (1992) *1:250000 geological map series*, Rafsanjan sheet, Iran.

Mousavi, S. M. (1999) The analysis of mutual effects between hydraulic parameters and land subsidence due to groundwater withdrawal, *Ph. D. thesis*, Civil Engineering Department, Sharif University of Technology, Tehran, Iran.

Nikdel, E. (1989) Mechanism of land subsidence due to groundwater withdrawal and tectonic movements in Rafsanjan plain, *professional report (in Persian)*, RWO, Iran.

Poland, J. F., Figueroa Vega G., Carbognin L., Johnson A. I., & Yamamoto S. (1994) *Guidebook to studies of land subsidence due to ground-water withdrawal*, Ed. by UNESCO, Paris, France, J. F. Poland Chairman and Editor, 305 p and Appendices A-E.

LAND SUBSIDENCE - Vol. II
Proceedings of the Sixth International Symposium on Land Subsidence
Ravenna / Italy / 24-29 September 2000

THE ISES PROJECT SUBSIDENCE MONITORING OF THE CATCHMENT BASIN SOUTH OF THE VENICE LAGOON (ITALY)

Luigi Tosi and Laura Carbognin
Istituto per lo Studio della Dinamica delle Grandi Masse – CNR
San Polo 1364, 30125 Venezia, Italy

Pietro Teatini
Dept. of Mathematical Methods and Models for Scientific Applications (DMMMSA)
University of Padova, Via Belzoni 7, 35131 Padova, Italy

Roberto Rosselli
Magistrato Alle Acque - Consorzio Venezia Nuova – Servizio Informativo
Campo S. Stefano 2949, 30124 Venezia, Italy

Giuseppe Gasparetto Stori
Consorzio di Bonifica Adige Bacchiglione
Via Scrovegni 29, 35131 Padova, Italy

Abstract

The catchment located south of the Venice Lagoon experienced during the last century a general land settlement owing to groundwater pumping, oxidation of organically rich soils enhanced by agricultural activities, and natural sediment compaction. High land subsidence rates (2-4 cm/year) have been estimated in the area comprised between the lagoon edge and the Adige River and located between two leveling lines of the Italian national network (IGM lines n° 7 and n∞ 19). Only a partial knowledge on the behavior of land elevation is available in this region. To overcome this lack of information, a new fine leveling and GPS network has been established in the area within the *ISES* Project funded by National/Local water and administrative Authorities. The first field measurement carried out in 1999 have produced as a major result an accurate knowledge of the geoid height in this part of the Po River plain and has pointed out the stability of the area located along the lagoon boundaries during the six-year period from 1993 to now.

Keywords: leveling, GPS, southern Venetian catchment, land subsidence.

1. INTRODUCTION

The regulation of groundwater exploitations from the Venetian multiaquifer system started in 1970 induced a very fast recovery of the piezometric levels along with a remarkable slowing down of the ensuing subsidence definitely ascertained in 1973 (Carbognin *et al.*, 1976). A high precision leveling survey carried out in 1993 confirmed the arrest of the anthropogenic subsidence in Venice and its surroundings, and concurred to evaluate the natural subsidence rates for the Venetian region (Carbognin *et al.*, 1995a; 1995b). Results of the 1993 survey have also shown that land subsidence is still in progress with a 1-2 mm/year rate in the southern and northern lagoonal areas and in the nearby mainland. The littoral and lagoon extremities are subject to the consolidation process of the recent river delta progradations caused by the fluvial sedimentary loads and to the residual compaction of the highly compressible marine-lagoonal Holocene clayey and silty layers.

The mainland and the lagoon margins, that before this century were wetlands (salt and fresh water marshes and swamps), are now reclaimed areas intensively used for agricultural activities and characterized by highly organic soils. Subsidence of coastal lowlands with these environmental features is mainly caused by the loss of organic matter due to peat oxidation (Rojstaczer and Deverel, 1995; Deverel and Rojstaczer, 1996).

Land subsidence has increased the vulnerability and the geological hazard of these areas, a large portion of which lies below the mean sea level, and are crossed by watercourses whose water level is above the surrounding ground surface. River flooding, riverbank stability, and intrusion of seawater in the aquifer system are the main hydrogeological problems. In particular, the loss in elevation has increased the requirement of pumping to maintain the subsiding lands free of inundation with a consequent increase of the saltwater intrusion in the coastal aquifer and river systems. Moreover, land settlement has contributed to deteriorating of the littoral sectors with a general coastline regression and an increment of the sea bottom slope close to the shoreline (Carbognin *et al.*, 1995a).

ISES, *i.e.*, Saltwater Intrusion and Land Subsidence, is a project started in 1999 to accurately quantify and control saltwater intrusion and land settlement in the basin south of the Venice Lagoon (Figure 1). The project is supported by the Public Agencies that manage this part of the Veneto Region. ISES has instituted in 1999 a new fine leveling and GPS network connected to the more stable Euganean Hills to measure the vertical movement of this area. The network configuration, with the superimposition of a traditional leveling and a GPS network (with one GPS benchmark every 5 leveling benchmarks), has been planned so that in the future every Local Agency will be able to independently control its territory within an homogenous framework.

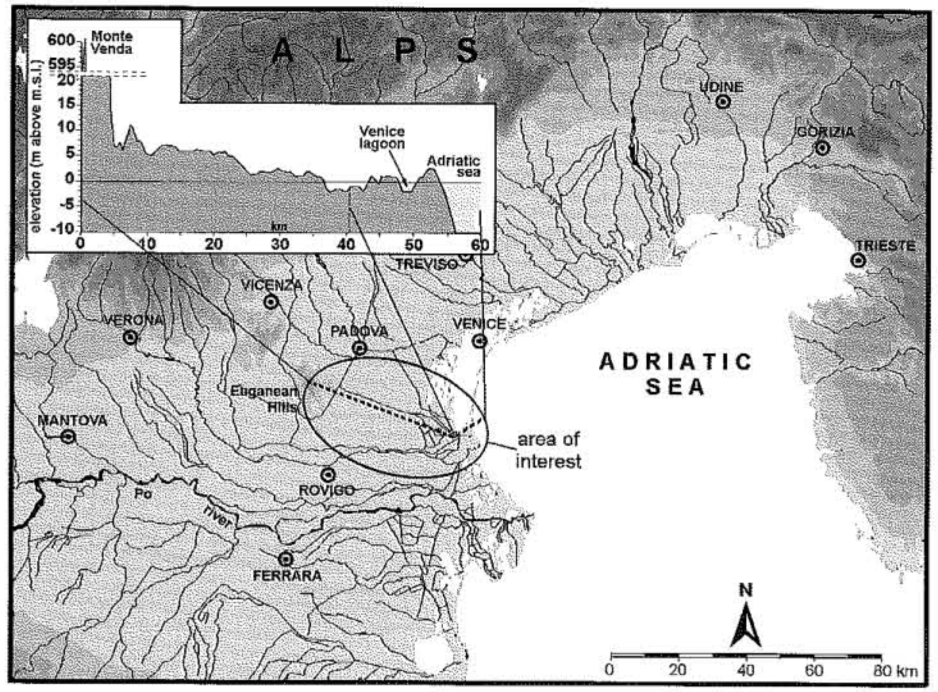

Figure 1. Location of the area of interest in the Eastern Po plain with a vertical cross section showing the elevation above the mean sea level.

After a short overview on the historical subsidence measurements performed in the study area, the present work describes the main characteristics of the new ISES controlling network and gives some preliminary results obtained at the end of the first field measurements.

2. OVERVIEW ON LAND SETTLEMENT MEASUREMENTS IN THE STUDY AREA

Ground vertical movements in the central-southern part of the Veneto Region have been measured with sufficient accuracy and reliability since the end of the previous century with different National and Local Agencies involved in the monitoring effort. However, leveling surveys have been carried out only along the east and west boundaries of the study area (*i.e.*, along the coast and the lagoon edges, and in the Euganean area and along the National Route 16 "Adriatica" connecting Padova and Rovigo, respectively), usually assuming as reference stable position a benchmark located in Treviso some 20 km north of Venice (Figure 1).

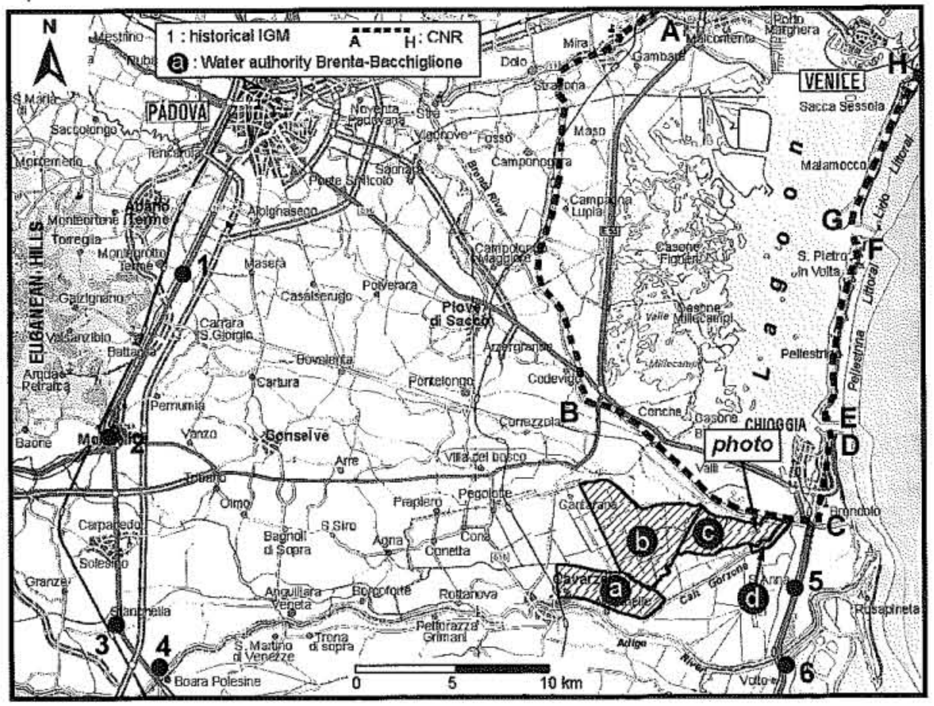

Figure 2. Locations in the study area where land subsidence measurements have been carried out in the past.

The first IGM (Military Geographic Institute) leveling was made in 1884/87-1897 in a number of reference points of the national topographic network, and other surveys followed in 1942/47-1951 and every 5-10 years during the last half century (Salvioni, 1957; Bondesan *et al.*, 1997). Unfortunately, most of the 1884/87-1897 network benchmarks were missing and only six reference points, shown in Figure 2, were leveled in the following surveys. Their subsidence rates are presented in Table 1. Higher rates occurred from 1970 to 1986 at point 1 due to thermal water exploitation from the Euganean basin (Gottardi *et al.*, 1995), and from 1950 to 1970 at positions 6 and 5 (to a lesser extent) for their closeness to the Po River delta where a huge amount of gas-bearing water was pumped during that period (Caputo *et al.*, 1970).

Periodic leveling measurements were carried out during the last 30 years in the Venice Lagoon and its hinterland by the CNR (National Research Council) (Carbognin *et al.*, 1976; 1994). The available information is summarized in Figure 3. Figure 3a shows the changes in land-surface elevation along the leveling line A-C of Figure 2 (from Mestre surrounding the lagoon towards the South)

assuming the IGM 1951 as reference survey. The first leveling for the entire littoral strip was carried out in 1968 (Figure 3b), and only for the Lido littoral a previous measurement (in 1961) is available. Inspection of Figure 3 reveals the higher subsidence rate during the period 1960-1970 due to groundwater withdrawal at Porto Marghera for industrial use, at Lido for tourism needs, and in the Chioggia-Brondolo area for the superimposition of several causes such as a higher natural compaction rate, sediment loss due to oxidation and water pumping for drinking and agricultural purposes. The subsidence peak pointed out by all the measurements between points B and C (Figure 3a) is anomalous and its causes are currently under investigation.
Besides the National Agencies, also the Local Water Management Authorities ("Consorzi di bonifica") have established during the last century few leveling networks to control major hydraulic structures such as watercourse embankments and pumping stations. Leveling surveys were carried out in 1916, 1929, 1935, 1941, and 1965 in the area comprised between the lagoon and the Adige River (Consorzio di Bonifica Adige-Bacchiglione, 1996), but their results are difficult to use and compare because different and unstable reference benchmarks were adopted. Nevertheless, since the area has experienced a high rate of land subsidence mainly related to peat oxidation, as it is supported by the evidences of the disastrously lowering of the territory (Figure 4), these data are useful for a qualitative analysis. This is done by comparing the local leveling output with the ground elevation of the 1983 Regional Topographic Map (scale 1:10000) obtained by aerial photogrammetry. The average subsidence rate obtained for the 4 sub-basins shown in Figure 2 is given in Table 2. Due to the inaccuracy introduced in the elevation assessment, the error associated to the Table 2 values can be estimated in ±1 cm/year.

Table 1. Subsidence rate (cm/year) at the IGM benchmarks of Figure 2.

	Point			
Period	1	2	3	4
1884-1947	0.5	0.3	0.4	0.4
1947-1970	0.7	0.0	0.2	1.0
1970-1986	1.6	0.1	0.0	0.1

	Point	
Period	5	6
1897-1951	0.5	0.7
1951-1956	1.1	9.3
1956-1958	1.7	16.3
1958-1970	1.3	3.7
1970-1977	0.7	0.6
1977-1988	0.4	0.5

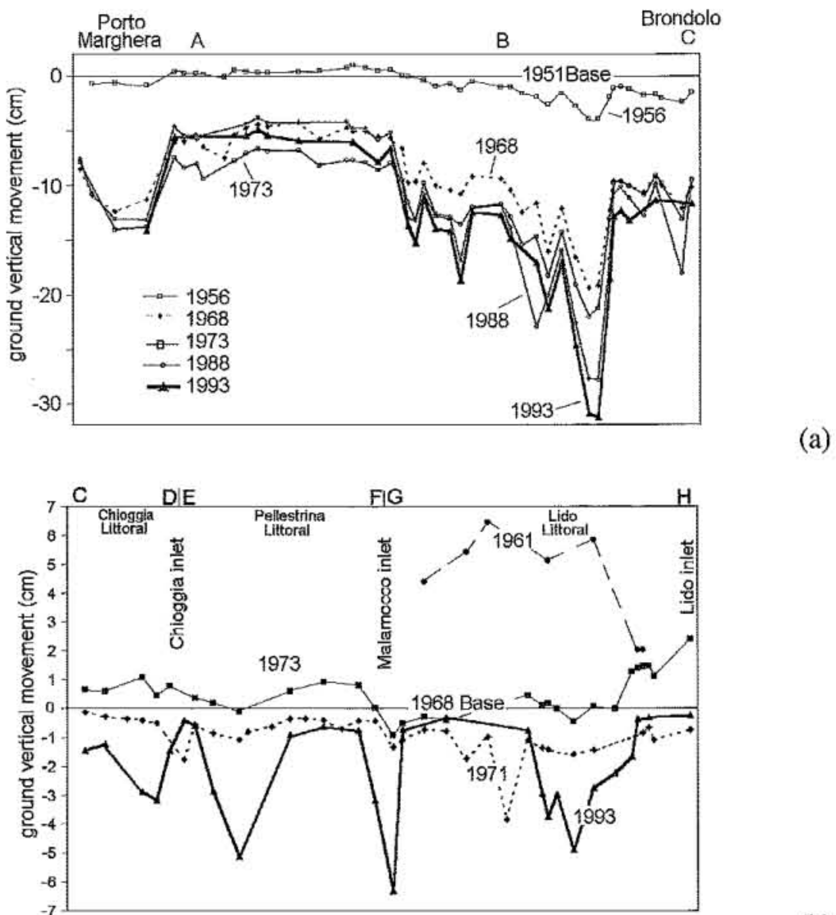

Figure 3. Ground vertical movement obtained from IGM/CNR leveling surveys (a) along the south-western boundary of the Venice Lagoon (dashed line A-C, Figure 2) and (b) along the Chioggia, Pellestrina, and Lido littorals (dashed line C-H, Figure 2).

Table 2. Average land subsidence rate in the 4 sub-basins shown in Figure 2 estimated from the Regional Topographic Map and the leveling surveys carried out by the Local Water Management Authorities (after Consorzio di Bonifica Adige-Bacchiglione (1996)).

Zone	Leveling survey (year)	Land subsidence rate (cm/year) up to 1983
a	1935	1.9
b	1965	2.7
c	1929	2.6
d	1941	3.5

Figure 4. An old bridge constructed in the Twenties whose foundation protrudes about 150 cm owing to land subsidence caused by peat oxidation and groundwater exploitation. In the background, the newer bridge today in use reveals a subsidence of about 50 cm during the last 30 years. The location of the photo is given in Figure 2.

3. ISES LEVELING NETWORK

The ISES Project has established during the 1999 a new refined leveling network in the eastern part of the Po Plain comprised between the Venice Lagoon and the Adige River with the purpose of efficiently controlling the vertical movements of this area where, aforementioned, precise leveling measurements have been carried out in the past only along its boundaries (Figure 2).

The area covered by the network (Figure 5) extends between the alignment Lova - Piove di Sacco - Pontelongo in the north-west direction and the conclusive part of the Adige River southward, and is bounded eastward by the Adriatic coastline from the Adige mouth to Chioggia and the Venice Lagoon. This low-lying area is connected to the southeastern part of the Euganean Hills through the lines that from Pontelongo and Borgoforte reach Battaglia Terme. This latter is linked to Monte Venda and to the thermal resort area of Galzignano, Abano, and Montegrotto where stable reference marks on rock of the Veneto Region are located. Moreover, new benchmarks have been instituted in the lagoonal areas of Valle di Millecampi, Conche, Valli, and along the CNR monitoring lines of Pellestrina and Lido littorals. The existing benchmarks of IGM, CNR, Veneto Region and Consorzio di Bonifica Adige Bacchiglione have been included in the network.

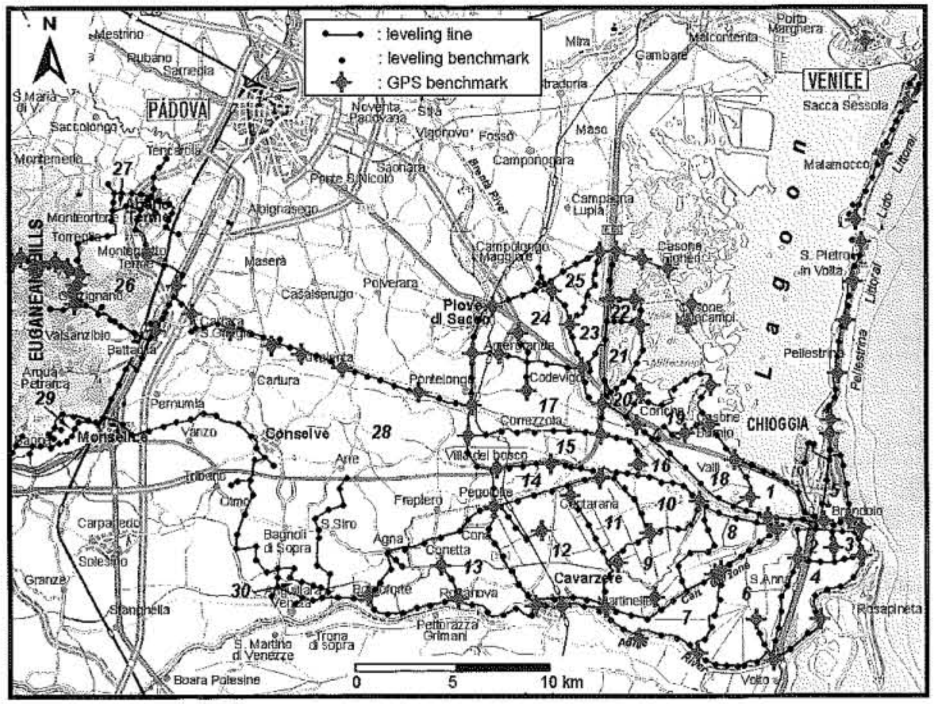

Figure 5. The ISES leveling network and GPS benchmarks.

Table 3. Length of the polygons of the ISES leveling networks. Polygon numeration is given in Figure 5.

Polygon	Length (km)	Polygon	Length (km)
1	19.523	16	29.527
2	9.941	17	24.762
3	10.023	18	17.104
4	23.031	19	18.750
5	12.078	20	10.146
6	33.412	21	17.367
7	30.321	22	7.190
8	22.035	23	18.837
9	25.650	24	19.044
10	20.057	25	13.634
11	16.323	26	27.144
12	24.588	27	7.806
13	34.122	28	80.602
14	16.533	29	8.594
15	27.677	30	9.305

3.1. Geometric leveling network

A total amount of 568 benchmarks, 346 of new installation, have been connected by a leveling network about 522 km long. The network is composed of 42 lines forming 30 closed polygons (Figure 5 and Table 3), with the distance between benchmarks along the different routes averaging 900 m.

The lines have been located along the road and watercourse networks, with a benchmark always placed in the nodal positions, *i.e.*, where two lines or more concur, and in the center of polygons ("*centrimaglia*").

The first leveling of the entire network has been carried out in 1999 in accordance with the guidelines issued by IGM relating to measurement methods and tolerance for high accuracy leveling survey.

3.2. Global Positioning System network

The GPS network is composed of 93 benchmarks with an optimal ratio of 1/5 between the GPS and geometric measurement points. All the nodal and the "*centrimaglia*" benchmarks have been used as GPS stations, and a number of benchmarks have been located on the stable Euganean Hills to be used in the future as reference positions for different and hence more checkable and reliable survey schemes.

GPS measurements has been performed in 1999 following the FGCC (Federal Geodetic Control Committee) guidelines that prescribe for the AA (high precision) GPS network the triple occupation of 80% of the network benchmarks. The DGPS (Differential GPS) technique has been implemented using as reference point the IGM'95 benchmark of Arzergrande (Figure 5) which is located in a quite central position of the study area, and whose WGS-84 coordinates and height are available. The survey has been carried out connecting the benchmarks by a number of intersecting and redundant baselines (Figure 6) and considering as points of strategic relevance few nodal or "*centrimaglia*" benchmarks with an optimal visibility. These benchmarks have been used as reference points for local sub-networks, each of them characterized by short baselines of similar length, and connected by longer baselines measured by dual frequency receivers with prolonged observing sessions. During the survey of the Lido and Pellestrina littorals, the ISES benchmarks have also been connected to the permanent GPS station of the Italian Space Agency located in Venice. The target accuracy of one part per million has been reached with excellent repeatibility using both broadcast and precise ephemeris.

4. PRELIMINARY RESULTS

Since the ISES leveling and GPS networks have been established in 1999 and only the first reference measurement has been carried out, only preliminary results are currently available.

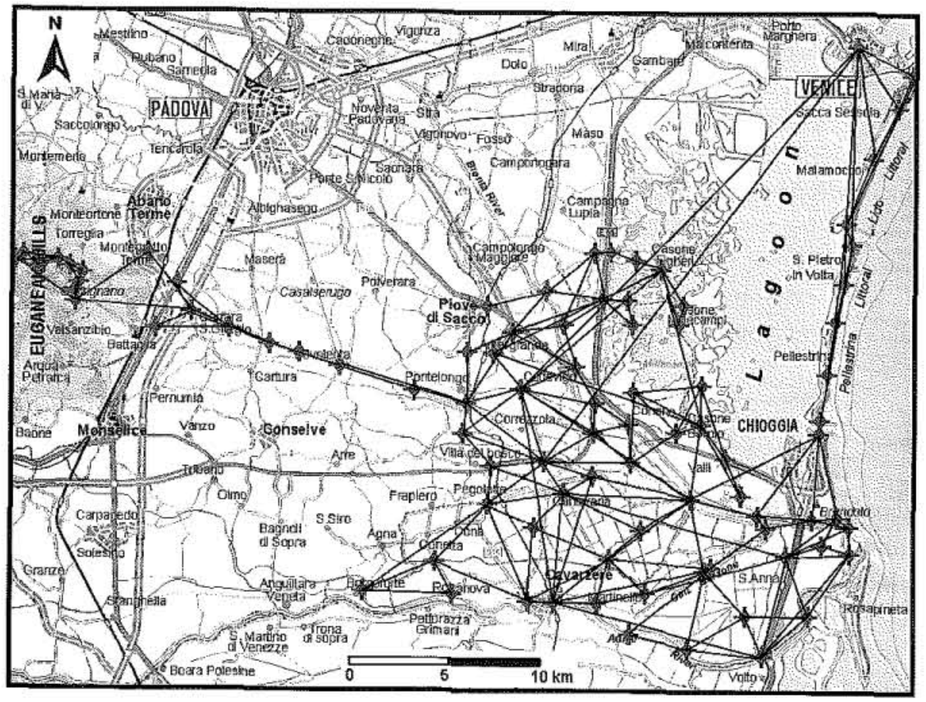

Figure 6. Sketch of the baselines measured during the 1999 GPS survey of the ISES network.

4.1. Geoid height in the ISES area

A result that the first leveling and GPS surveys have made available is a more accurate geoid undulation (or height) N in the ISES area than that given in the literature (Caporali *et al.*, 1989; Barzaghi *et al.*, 1996; Barbarella *et al.*, 1998). The difference between the WGS-84 ellipsoid altitude measured by GPS and the topographical altitude (with respect to the elevation reference of the IGM network, *i.e.*, the mean sea level at the Genoa tidal gauge in 1942) provided by leveling has been computed for all the 93 GPS benchmarks of the ISES network.

For the central part of the study area, where the zone benchmark distribution is homogenous, a local model of the geoid undulation has been computed interpolating the scattered data by the quadratic function:

$$N(x,y) = 39.9315 - 0.0305302 \cdot x + 0.101398 \cdot y - 0.00029785 \cdot xy + \\ + 0.000403801 \cdot x^2 - 0.00045003 \cdot y^2$$

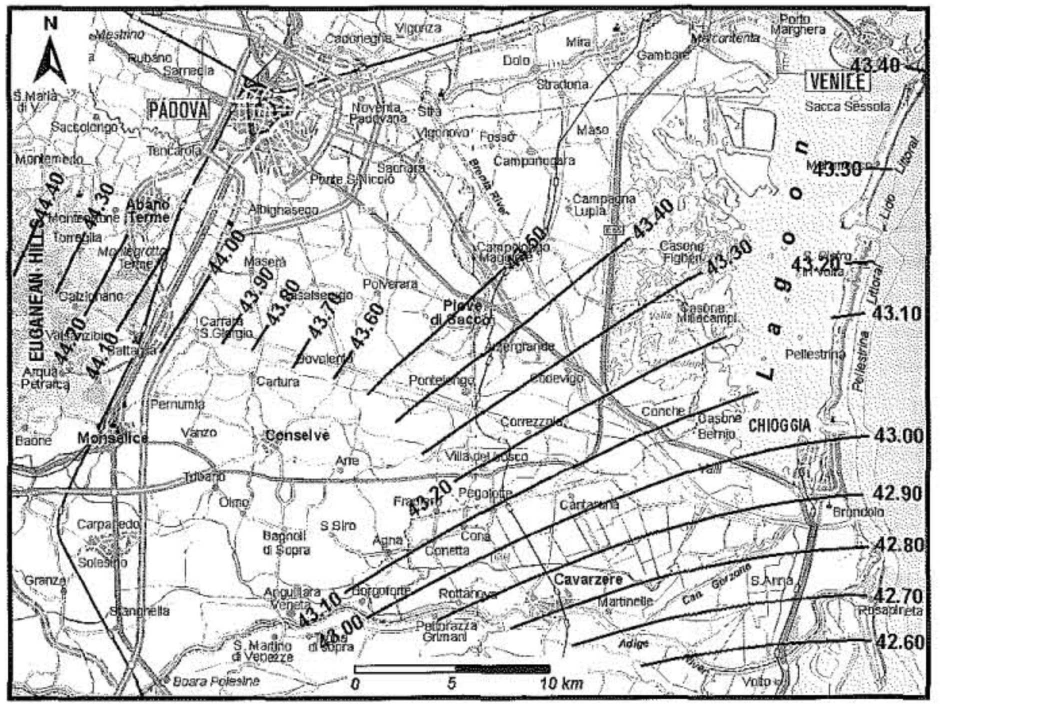

Figure 7. Geoid undulation (m) in the area covered by the ISES Project.

where $[N]$=m, and x and y are the east and north Gauss-Boaga (East fuse, $[x,y]$=km) coordinates of the generic point, decreased by the constants X=2250 km and Y=4950 km, respectively. The high accuracy of this model is confirmed by the low residuals in the measured positions, always less than 2 cm in modulus. A contour line map of the above model is given in Figure 7, where the geoid height directly obtained by the measurements along the littoral strips and the line connecting the lagoon mainland to the Euganean Hills is also shown.

4.2. Actual land subsidence of the Venice Lagoon boundary

The ISES network has been connected within a project funded by the Venice Water Authority, Consorzio Venezia Nuova, to the IGM/CNR leveling lines surrounding the lagoon and reaching a stable area at the Alpine foothills north of Treviso.

Comparative plots of the leveling profiles of the lagoon boundary from Porto Marghera to Brondolo and of the littoral strips are given in Figure 8. Except for a sector between positions B and C (Figure 2), the vertical movement rate of the lagoon boundary is less than 0.3 cm/year (Figure 8a) and the overall line (A-C) shows a surprisingly similar behavior with the 1951-1956 profile given in Figure 3a. Inspection of Figure 8b reveals more stability of the littoral strips than in the past (Carbognin *et al.*, 1995a), with altimetrical movement lower than 1 cm. In particular, the Chioggia littoral seems stable, while the Pellestrina littoral shows positive and negative movements in the lagoonal and sea side, respectively. These oscillations could be related to the huge restoration works carried out both along the sea shore and, to a lesser measure, the lagoon shore during the last 10 years. The movement of the central zone of the Lido littoral confirms the settlement trend pointed out in 1993 (Figure 3b).

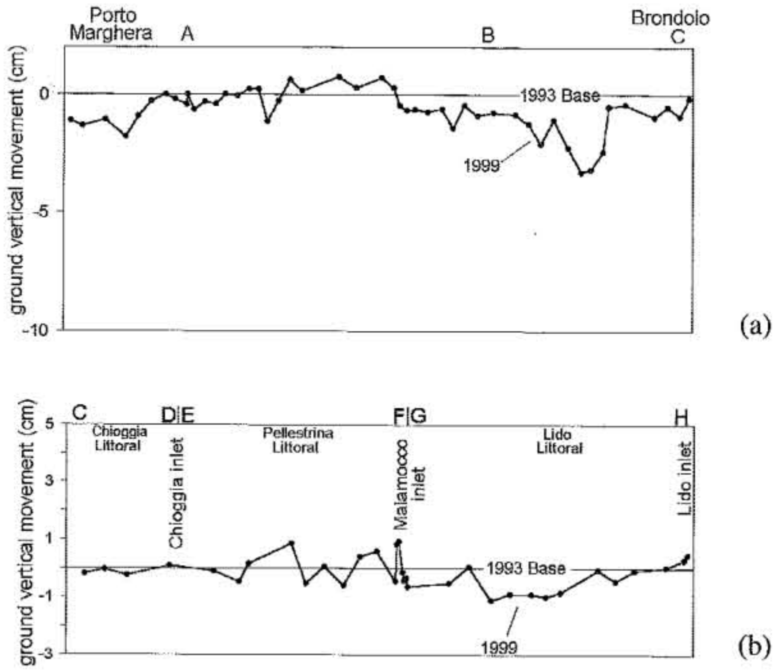

Figure 8. Ground vertical movement between 1993 and 1999 (a) along the south-western boundary of the Venice Lagoon (dashed line A-C, Figure 2) and (b) along the Chioggia, Pellestrina, and Lido littorals (dashed line C-H, Figure 2).

5. CONCLUDING REMARKS

From the knowledge about land settlement in the overall region of Venice and its hinterland, it clearly emerged that the southern and northern lagoon extremities are the more precarious areas. In particular, the most serious condition presently exists in the catchment between the lagoon and the Adige River where the loss in ground elevation has increased the hydrogeological hazard (saltwater intrusion, river bank stability, river overflow). This zone is generally below mean sea level and problems related to agricultural activities and ensuing socio-economic damages have become more and more serious.

In 1999, the three-year, ISES Project was started with the aim of improving the monitoring of land subsidence and saltwater intrusion in this part of the Po plain by the institution of *ad hoc* networks. To address the demand of the Local Authorities a new refined leveling and GPS network has been established and connected to the more stable area of the Euganean Hills. The network is 568 km long and is composed of 522 benchmarks, 93 of which are used for GPS measurement.

The first geodetic survey carried out in the second half of 1999 constitutes the reference base for the feature leveling and GPS measures in the overall area. Comparison with the 1993 survey along the leveling IGM/CNR routes already existing around the Venice Lagoon has provide a first partial estimate of the present land subsidence rate. Moreover, as preliminary result, a very accurate reconstruction of the geoid undulation has been performed using GPS and leveling output.

Acknowledgments

Authors wish to express their acknowledgment to the Consorzi di bonifica Adige-Bacchiglione, Bacchiglione-Brenta, Delta Po-Adige, the Consorzio Venezia Nuova (Servizio Informativo), Magistrato alle Acque per la Laguna di Venezia, Comune di Chioggia, Provincia di Padova and Provincia di Venezia which support the ISES Project. Particular thanks go to Mrs Jane Frankenfield Zanin for her help in the editing.

REFERENCES

Barbarella, M., Bianco, A., Carella, P., & Fiani, M. (1998) Ondulazione sperimentale e prevista lungo la costa della Penisola Italiana. *Rivista del Dipartimento del Territorio*, **1**, 25-42.

Barzaghi, R., Brovelli, M. A., Sona, G., Manzino, A., Sanso' F., & Sguerso, D. (1996) The new Italian Quasi-Geoid: ITALGEO95. *Bollettino di Geodesia e Scienze Affini*, n.1/96.

Bondesan, M., Gatti, M., & Russo, P. (1997) Movimenti verticali del suolo nella Pianura Padana orientale desumibili dai dati I.G.M. fino a tutto il 1990. *Bollettino di Geodesia e Scienze Affini*, **LVI**(2), 141-172.

Caporali, A., Dallaporta, G., Marzari, F., Rusconi, A., Curiotto, S., Facchinelli, F., & Zambon, G. (1989) Rete geodetica GPS in territorio veneziano. In: *3° Conv. Nazionale AIT.*

Caputo, M., Pieri, L., & Unguendoli, M. (1970) Geometric investigation of the subsidence in the Po delta. *Bollettino di Geofisica Teor. e Appl.*, **XIII**(47), 187-207.

Carbognin, L., Gatto, P., Mozzi, G., Gambolati, G., & Ricceri, G. (1976) New trend in the subsidence of Venice. In: *Land Subsidence – Proc. II Int. Symp. on Land Subsidence,* IAHS Publ. No. 121, 65-81.

Carbognin, L., Marabini, F., Taroni, G., Teatini, P., & Tosi, L. (1994) *Altimetria recente del comprensorio lagunare Veneziano. Un'analisi critica.* Technical Report n. 193, 32pp., CNR-ISDGM, Venezia.

Carbognin, L., Marabini, F., & Tosi, L. (1995a) Land subsidence and degradation of the Venice littoral zone, Italy. In: *Land Subsidence - Proc. V Int. Symp. on Land Subsidence* (ed. by: F. B. J. Barends *et al.*,) , IAHS Publ. No. 234, 391-402.

Carbognin, L., Tosi, L., & Teatini, P. (1995b). Analysis of actual land subsidence in Venice and its hinterland (Italy). In: *Land Subsidence - Proc. V Int. Symp. on Land Subsidence* (ed. by: F. B. J. Barends *et al.*,) , A. A. Balkema, Rotterdam, 129-137.

Consorzio di Bonifica Adige-Bacchiglione (1996) *Studio del fenomeno della subsidenza nei bacini Orientale, Zennare, Punta Gorzone e Foresto Centrale, ricadenti nel comprensorio consorziale.* Relazione Tecnica, 37pp.

Deverel, S. J., & Rojstaczer, S. (1996) Subsidence of agricultural lands in the Sacramento – San Joaquin Delta, California: Role of aqueous and gaseous carbon fluxes. *Water Resour. Res.*, **32**(8), 2359-2367.

Gottardi, G., Previatello, P., & Simonini, P. (1995) An extensive investigation of land subsidence in the Euganean geothermal basin, Italy. In: *Land Subsidence - Proc. V Int. Symp. on Land Subsidence* (ed. by: F. B. J. Barends *et al.*,) , IAHS Publ. No. 234, 21-30.

Rojstaczer, S., & Deverel, S. J. (1995) Land subsidence in drained histosols and highly organic mineral soils of California. *Soil Science Society of America Journal*, **59**, 1162-1167.

Salvioni, G.(1957) I movimenti del suolo nell'Italia centro-settentrionale. Dati preliminari dedotti dalla comparazione di livellazioni. *Bollettino di Geodesia e Scienze Affini,* **XVI**(3), 325-366.

LAND SUBSIDENCE IN LAS VEGAS, NEVADA, USA: NEW GEODETIC DATA REVEAL LOCALIZED SPATIAL PATTERNS, STRUCTURAL CONTROLS, AND REDUCED RATES

John W. Bell[1], Falk Amelung[2], and Alan R. Ramelli[1]
[1]*Nevada Bureau of Mines and Geology, University of Nevada, Reno*
Reno, Nevada, USA 89557
[2]*HIGP/SOEST, University of Hawaii, Honolulu, Hawaii, USA 96822*

Abstract

Conventional leveling and campaign GPS surveys together with synthetic aperture radar interferometry (InSAR) mapping provide new insights into the spatial distribution and rates of land subsidence in Las Vegas, Nevada since 1991. Detailed spatial mapping of subsidence by InSAR shows that subsidence is much more localized than suggested by previous conventional leveling data, and that the movement is strongly controlled by the location of Quaternary faults which cut the basin floor. Four localized subsidence bowls are now recognized with each bowl spatially controlled by faults. A revised subsidence map for the period 1963-1998 has been developed based on the new spatial data. Seven second-order level lines established across geologic faults in 1978 were resurveyed in 1991 and 1997, and a GPS network established in 1990 was resurveyed in 1998. The results of the surveys combined with the InSAR data for 1992-97 indicate that subsidence rates have decreased in comparison to pre-1991 rates by between 40-80%. The reduction in the subsidence rate is attributed to an artificial recharge program initiated in 1990.

Keywords: land subsidence, geodetic data, spatial patterns.

1. INTRODUCTION

Las Vegas has been one of the fastest growing metropolitan areas in the USA during the last 10 years with a population that exceeded 1.3 million people in 1999, an increase of more than 60 % since 1990. Las Vegas is located in southern Nevada, within a 1300 km^2 alluvial valley that receives between 12-20 cm/yr of average annual precipitation. Land subsidence in Las Vegas Valley is primarily related to groundwater withdrawals which have annually exceeded natural recharge since the 1960's, and the long term effects have included depressurization of the confined aquifer system, regional decline of water levels, the development of earth fissures, and subsidence.

2. LAND SUBSIDENCE HISTORY

Groundwater in Las Vegas Valley is withdrawn by pumping and artesian flow from a principal zone of confined and semi-confined aquifers lying at depths of 200-300 m. Groundwater withdrawals began in 1905; in 1946, Maxey and Jameson (1948) concluded that annual withdrawals had begun to exceed the annual recharge to the aquifers and found that measurable subsidence was occurring.

By the mid-1960's, a subsidence bowl with a maximum depth of 0.75 m had formed over an area of about 500 km^2 in the central portion of Las Vegas Valley. By 1980, the affected area had doubled to more than 1000 km^2, the central subsidence bowl had deepened to 1.5 m, and two additional localized subsidence bowls each having more than 75 cm of movement formed in the northwestern and south-central portions of the valley (Bell, 1981). A compilation of leveling data through 1987 subsequently showed that the three localized bowls were continuing to subside and that the northwest bowl had as much as 1.52 m of subsidence (Bell, 1991; Bell and Price, 1991).

2.1 Groundwater withdrawals and water level declines

Maxey and Jameson (1948) estimated that the annual natural recharge to the groundwater system in Las Vegas Valley is between 31-43 hm^3/yr. A recent study by Donovan and Katzer (2000) suggests, however, that the natural recharge is on the order of 61 hm^3/yr. Beginning in the mid-1950's, groundwater withdrawals increased from about 50 hm^3/yr to an all-time peak of 108 hm^3/yr in the late 1960's. Total pumpage declined to about 86 hm^3/yr beginning in 1972, after a water importation program was begun that brought water from the Colorado River directly into the valley, and annual pumpage has remained at about the same level through the present.

An artificial recharge program was initiated in 1990 by the Las Vegas Valley Water District in which imported Colorado River water was pumped into the groundwater reservoir during the winter non-pumping season. The annual amount of artificial recharge has ranged between 12-30 hm^3/yr, and it reached a peak in 1998 at 34 hm^3/yr.

Due to the continued overdrafting of the groundwater reservoir since the 1960's, water levels have declined throughout the valley. A comparison of 1990 water levels with pre-development levels showed a decline of more than 90 m in some portions of the valley (Burbey, 1995). Since the implementation of the artificial recharge program in 1990, the long-term declines have been largely arrested, and water levels have risen in some parts of the valley by as much as 15 m.

2.2 Subsidence maps

Previous maps showing subsidence have been based on conventional leveling of first-order benchmarks established in 1935 and 1963 by the National Geodetic

Survey. A first-order level survey of 75 of these first-order benchmarks in 1980 provided a detailed subsidence map for the period 1963-1980 (Bell, 1981). Using second- and third-order leveling data provided by city and county level surveys, the most recent maps (Fig. 1) were developed showing subsidence for the period 1963-1987 (Bell, 1991; Bell and Price, 1991; Bell and Helm, 1998). The map was based on only 28 benchmarks owing to the loss of many of the original benchmarks through urban development.

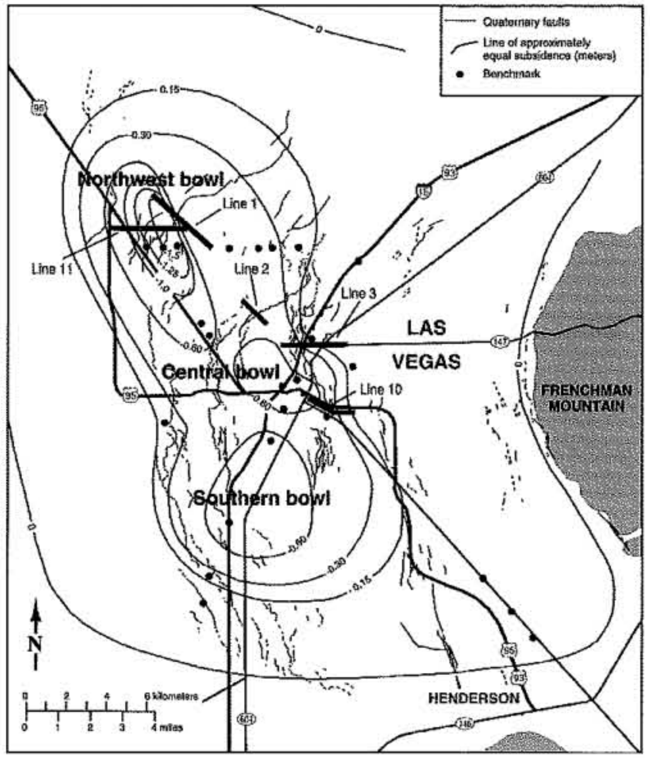

Figure 1. Subsidence map for 1963-1987 (Bell and Price, 1991) based on conventional leveling of 28 benchmarks. Contours for the three bowls were drawn based on interpolation of values without consideration of geologic controls.

The subsidence contour maps were developed by conventional interpolation of elevation change values between surveyed benchmarks. The 28 benchmarks are distributed sparsely throughout the valley, and the elevation changes were assumed to be uniformly distributed around the localized bowls in the central, south-central, and northwestern portions of the valley. The pattern of subsidence surrounding the northwest bowl was adjusted to account for a sharp gradient on the east side of the bowl determined from conventional leveling along Line 1 (Fig.1). This line is further discussed in the section below.

2.3 Level lines across geologic faults

The floor of Las Vegas Valley is cut by Quaternary faults which each offset the basin fill sediments by 30 m or more (Fig. 1). In 1978 a series of 1.5- to 4-km-long, second-order level lines was established across selected faults in order to determine whether the faults were potential sites for differential movement induced by subsidence. The lines were re-surveyed annually until 1989; surveys were later conducted in 1991 and 1997.

The results of the leveling between 1978 and 1999 for selected lines are illustrated in Fig. 2. Line 1 extended across the Eglington fault in the northwest part of the valley; it was leveled annually until 1985 when it was destroyed by development, and the total change measured was 36 cm. The differential elevation changes were found to lie coincident with the fault, providing the basis for the sharp subsidence gradient shown in Fig. 1.

Line 2 is located across a compound set of faults occurring between the Northwest and Central subsidence bowls. For the period 1978-1997, the elevation changes show a consistent but irregular pattern of relative displacement of as much as 30 cm down to the northwest.

Lines 3 and 10 are located along a set of faults on the eastern edge of the central subsidence bowl. Both lines show similar patterns of displacement across the faults with as much as 30 cm of movement down-to-the-west toward the Central subsidence bowl.

Line 11 was established in 1991 to replace Line 1 and to monitor movement across the Eglington fault. The line was resurveyed in 1997 and 1999.

3. 1998 INSAR STUDY

The European Space Agency (ESA) has been acquiring 56-mm wave length synthetic aperture radar (SAR) images since 1992. Two SAR images are combined to form an interferogram. The phase differences of the reflected radar signals provide information about the displacements of all ground objects imaged by the radar, as well as information about the topography and atmospheric water vapor. One cycle of phase change (one color fringe) represents 28 mm in radar line-of-sight (range) displacements between observations. The accuracy of the measurements is normally on the order of 2-4 mm in arid environments such as the Nevada region.

We used interferometric synthetic aperture radar (InSAR) to obtain spatially detailed maps of subsidence occurring in Las Vegas Valley between 1992-1997 (Amelung et al., 1999). Four differential interferograms were developed for different time intervals during this period; the composite interferogram map of subsidence for the period is shown in Fig. 3.

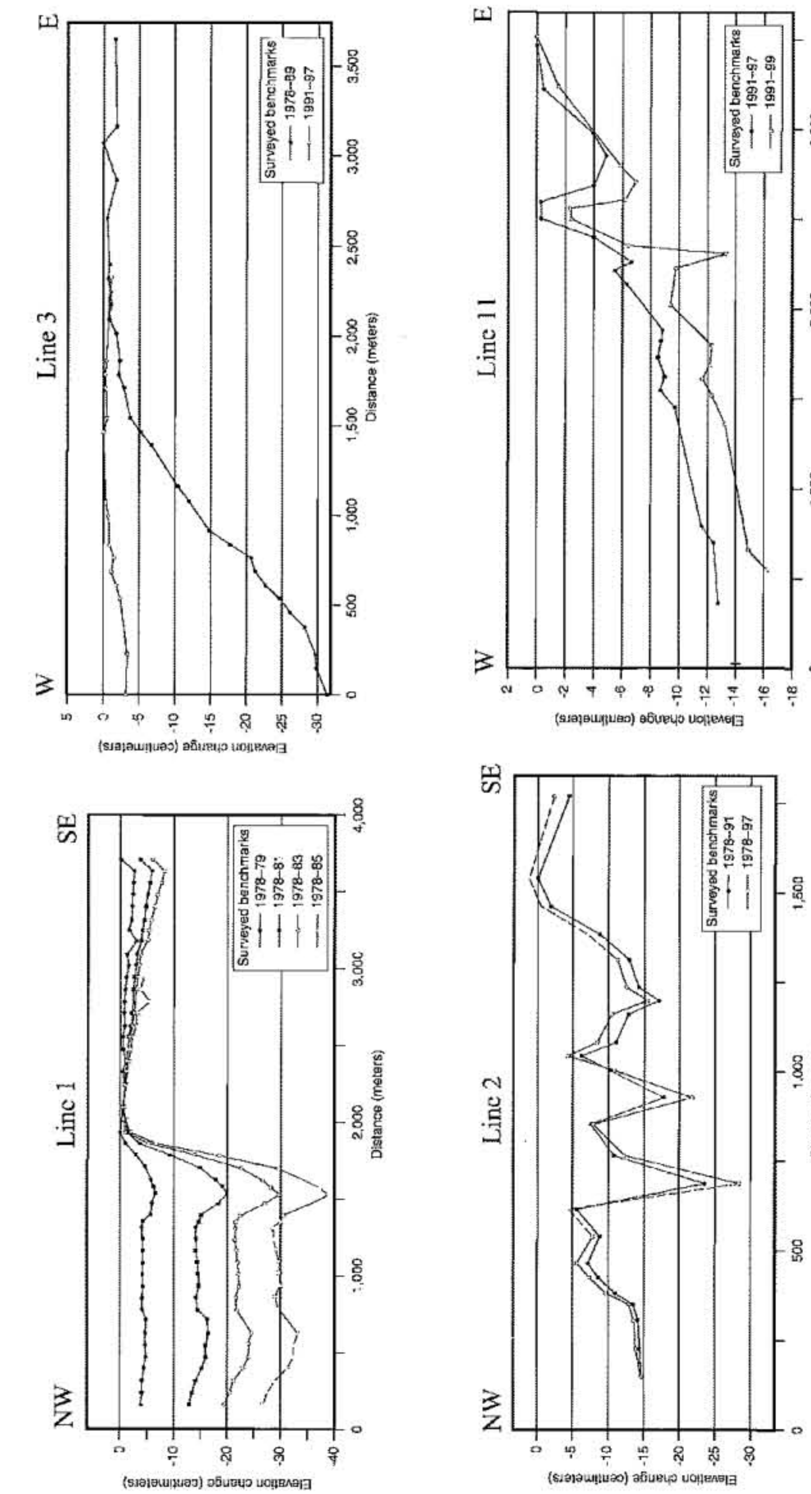

Figure 2. Results of second-order leveling along lines 1, 2, 3, and 11 between 1978-1999. The lines all lie across east-southeast-dipping Quaternary faults, and the upthrown (footwall) blocks of all four lines are moving down in response to the localized subsidence bowls.

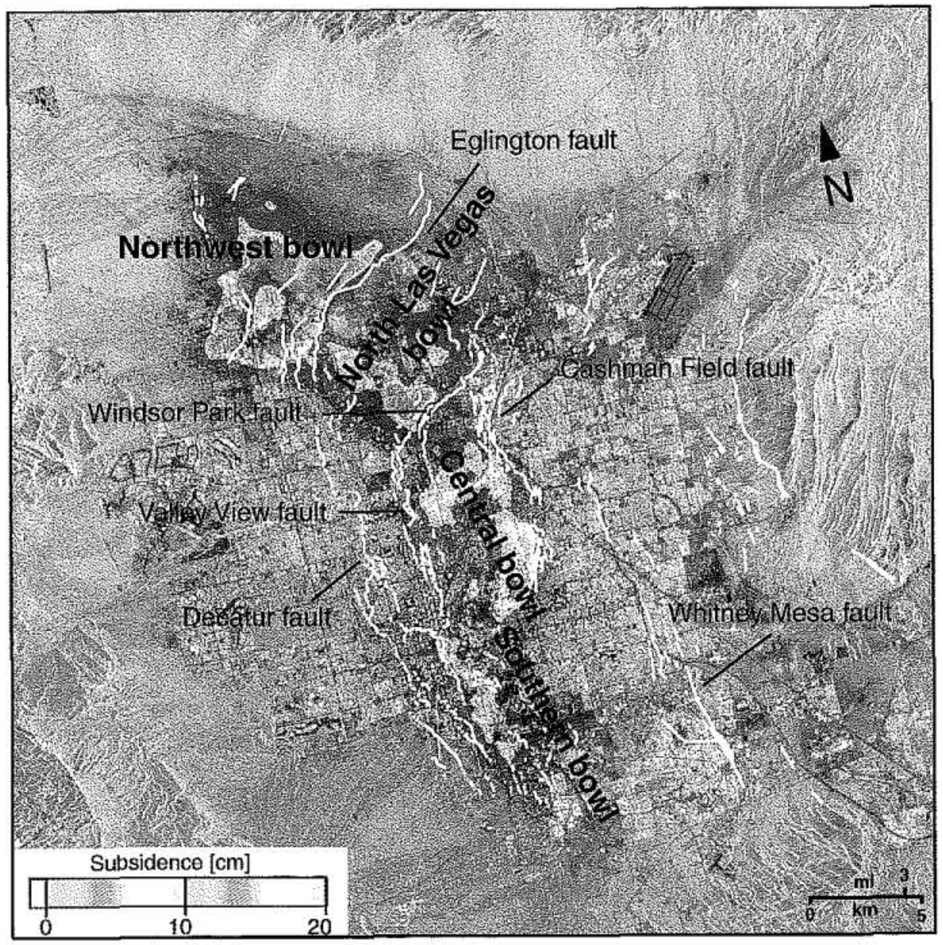

Figure 3. InSAR map of subsidence in Las Vegas Valley between April, 1992 and December, 1997 based on a composite of three SAR interferograms covering the periods April, 1992-November, 1993; November, 1993-February, 1996; and January, 1996-December, 1997. InSAR values are displayed as 10 cm color cycles. The base is the radar image of Las Vegas Valley. The Northwest bowl shows nearly two complete cycles (19 cm). The four recognized localized subsidence bowls are bounded by several prominent faults (shown in white) which are acting as subsidence barriers. See Amelung et al. (1999) for a detailed discussion of the study.

3.1 Structural Control of Subsidence Revealed by InSAR

The 1992-1997 InSAR map reveals for the first time that subsidence in Las Vegas Valley is occurring in a series of elongated, localized bowls strongly controlled by the location of the geologic faults which cut the basin fill. Four principal localized bowls are now recognized. The Northwest bowl is a prominent,

triangular-shaped, bowl that is sharply bounded by the Eglington fault. The North Las Vegas bowl consists of several coalescing bowls bounded by the Windsor Park fault. The Central bowl is an elongated, north-south-trending zone bounded on the east by the Cashman Field fault and on the west by the Valley View fault. The Southern bowl extends to the south of the Central bowl and is bounded on the west by the Valley View and Decatur fault zones.

The Northwest bowl exhibits 19 cm of subsidence, the maximum amount of subsidence for the 1992-97 period measured from the InSAR map. The other bowls exhibit subsidence ranging between 5-15 cm for the same period. Several small areas of uplift were also detected by the InSAR map, including a area near Whitney Mesa exhibiting about 1 cm of uplift.

The InSAR results clearly demonstrate that the spatial pattern of land subsidence in Las Vegas Valley is controlled by the geologic faults to a much larger degree than shown on previous maps (Fig. 1; Bell and Price, 1991). In particular, the Eglington fault, and to a lesser degree the Windsor Park fault, appear to form subsidence barriers with nearly all of the movement restricted to the northwest sides of the faults. In both cases, subsidence is occurring on the geologic footwall (upthrown) side of these southeast-dipping faults, consistent with the results of conventional leveling on Lines 1, 2 and 11 (Fig. 2). Based on subsurface geologic data, no significant differences are seen in hydrologic properties of the sediments across the faults. This relation is likely related to preferential dewatering and depressurization of the footwall blocks by heavy pumping in nearby areas, but the geohydrologic relations responsible for the subsidence barriers are poorly understood.

The Central subsidence bowl is a structural graben formed between the Valley View fault and the Cashman Field fault. Line 4 crosses the Valley View fault (Fig. 3, 4), and the results of leveling between 1991-1997 indicate that as much as 6 cm of down-to-the east movement occurred. Lines 3 and 10 (Fig. 2) both extend across the Cashman Field fault, and they show more than 30 cm of down-to-the-west movement for the 1978-1997 period. As indicated by both the INSAR map and the level line results, the subsidence graben is forming in the footwall of the Cashman Field fault.

The InSAR results were found to be consistent with the results of the 1991-1997 level surveys. As discussed in Amelung et al. (1999), results of leveling on lines 4, 10, and 11 were compared to InSAR subsidence values taken along the same transect lines. The leveling and InSAR data cover slightly different time periods, but the results indicate the patterns and magnitudes of movement are closely similar.

4. GPS SURVEYS

In 1990 a Global Positioning System (GPS) network was established throughout Las Vegas Valley to replace the conventional benchmark network which was being destroyed by urban development. The 1990 survey was conducted using a combination of static and kinematic observations, a methodology believed at that time to be adequate for detecting subsidence of several centimeters or greater. In 1998, the entire network was resurveyed using static and rapid static methodologies and upgraded P-code geodetic receivers. Based on the results of the 1998 survey, it was found that the kinematic methodology used in the 1990 survey had generated large uncertainties in measured heights, and the 1990 data were considered to contain only limited baseline data. The best results were obtained from comparisons of 1990 and 1998 ellipsoid heights for about 20 stations in the northern half of the valley where subsidence ranging between 0-10 cm was measured.

In order to test the accuracy of 1998 survey data, 1998 orthometric heights on several stable benchmarks were compared to published first-order level heights for the same benchmarks. Ellipsoid heights derived from the 1998 GPS observations were converted to orthometric heights using GEOID 99, a geoid model developed by the National Geodetic Survey. The calculated orthometric heights were then compared to the first-order level heights for the stable benchmarks and found to be within 1 cm of the published elevations.

The first-order level heights were established in 1963 and they form the baseline for most subsidence maps produced for Las Vegas Valley. The previous map (Fig. 1) was based on the most recent level survey of these benchmarks in 1986-87 compared to 1963. The 1998 GPS orthometric heights provide additional data for determining the cumulative subsidence occurring in the valley since 1963. The largest elevation change measured by the 1963-1998 GPS study was 1.42 m near the center of the Northwest bowl.

Selected stations surveyed in the Northwest bowl in 1998 were resurveyed in 1999 to document continuing movement of the bowl. The largest change for this one-year period was 3.5 cm on a station near the center of the bowl.

5. REVISED SUBSIDENCE MAP FOR LAS VEGAS VALLEY

Based on the new patterns revealed by the 1992-97 InSAR map, a revised subsidence map for the period 1963-98 has been produced (Fig. 4) that incorporates 1998 GPS measurements. As noted earlier, the previous 1963-1987 map was based on conventional interpolation of elevation changes between surveyed benchmarks without regard to geologic control. On the revised map, the spatial patterns of the subsidence contours have been redrawn to more closely reflect the pattern shown by the spatial detail of the InSAR map, while at the same time remaining consistent with the location and magnitude of measured geodetic change on individual benchmarks.

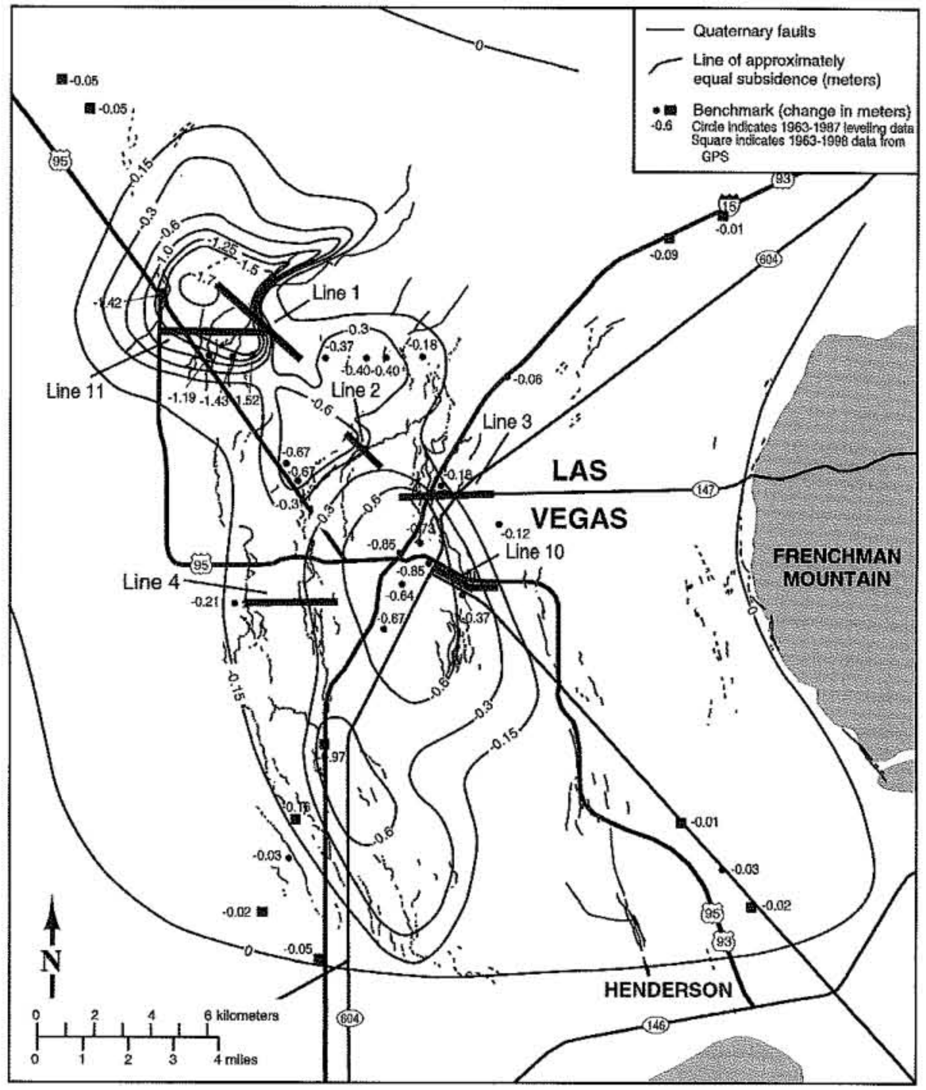

Figure 4. Revised map showing subsidence for the period 1963-1998 based on incorporation of spatial patterns revealed on InSAR map (Fig. 3) and on the results of leveling and GPS surveys between 1978-1998. The contour gradients surrounding the localized subsidence bowls have been redrawn to more closely reflect the influence of geologic structure, with the faults forming the boundaries to the bowls. The original conventional survey points are shown together with GPS data determined from a comparison of the 1998 survey to 1963 benchmark elevations.

6. COMPARISON OF SUBSIDENCE RATES

A significant reduction in the rate of subsidence is evident in a comparison of level line results for the 1978-1991 and 1991-1997 periods (Fig. 5). The rate of subsidence in the most active Northwest bowl was more than 50 mm/yr based on the 1978-1985 leveling for Line 1. Conventional leveling of first-order benchmarks in the Northwest bowl also showed that the long-term (1963-1987) rate was more than 50 mm/yr (Bell and Price, 1991). The InSAR study showed, however, that the rate along this line had declined to about 33 mm/yr, a reduction of about 40%. Amelung et al. (1999) further concluded that the rate of movement along the line 1 transect may have locally decreased to 15-20 mm/yr in recent years based on a comparison of 1996-1997 interferograms.

The most substantial reductions in subsidence rates have occurred in the Central subsidence bowl where rates have declined by as much as 80%. Lines 3 and 10 both indicate that subsidence rates in the 1978-1997 period remained consistently at between 25-30 mm/yr. The 1991-1997 leveling results show that these rates have declined to about 5 mm/yr on both lines.

Line 11 leveling (Fig. 2) and GPS measurements suggest that subsidence rates have remained relatively unchanged at about 2-3 cm/yr since 1991. The 1991-1997 leveling showed more than 14 cm of subsidence along the line; the 1997-1999 survey showed a maximum subsidence of 3.5 cm. These results are consistent with the subsidence measured by the 1998-1999 GPS survey in this area that showed a maximum of 3.5 cm. These results indicate that although the subsidence rate has declined in the Northwest bowl since 1991, the rate now appears relatively stable at several centimeters per year and indicates that the Northwest bowl is still actively subsiding.

7. CONCLUSIONS

The combined results of conventional leveling together with the new spatial detail provided by InSAR indicate that subsidence in Las Vegas Valley is occurring in a series of four localized bowls which are strongly controlled by the existing geologic structure. Previous subsidence maps were based on conventional interpolation contouring of benchmark data without regard for structural controls. These new data allow a revised subsidence map for the period 1963-1998 to be drawn for the area that incorporates the conventional leveling, InSAR, and GPS data for the entire period.

A comparison of subsidence rates determined from level line, InSAR, and GPS results indicates that rates have declined between 40-80% since 1991 (Fig. 5). The greatest reduction has occurred in the Central subsidence bowl where the rate has declined from 25-30 mm/yr to about 5 mm/yr. The rates in the most active Northwest bowl have declined, but remain stable at about 25-30 mm/yr.

The reduction in subsidence rates is attributed to the effects of an artificial recharge program initiated by the Las Vegas Valley Water District in the early 1990's. Although the total volume of groundwater pumpage in Las Vegas Valley has remained constant at 73-86 hm^3/yr since the late 1970's, large volumes of

imported Colorado River water have been used to recharge the groundwater reservoir during the winter season. Beginning in 1990, more than 12 hm^3/yr have been pumped into the groundwater reservoir using existing municipal wells throughout the valley. The annual recharge reached a peak of 34 hm^3/yr in 1998, producing a net withdrawal of about 52 hm^3/yr, a volume close to the newly revised natural recharge estimates of Donovan and Katzer (2000). The long-term effect of this extensive recharge program has been a general rise in water levels, particularly in the central part of the valley where water levels have risen as much as 20 m since 1990 (Las Vegas Valley Water District, 1998), and a corresponding reduction in the rate of subsidence. The only part of the valley where water levels have continued to decline is in the Northwest bowl, where water levels dropped as much 6 m between 1990-1998, a relation that is consistent with the continuing, albeit reduced, subsidence measured in the Northwest bowl.

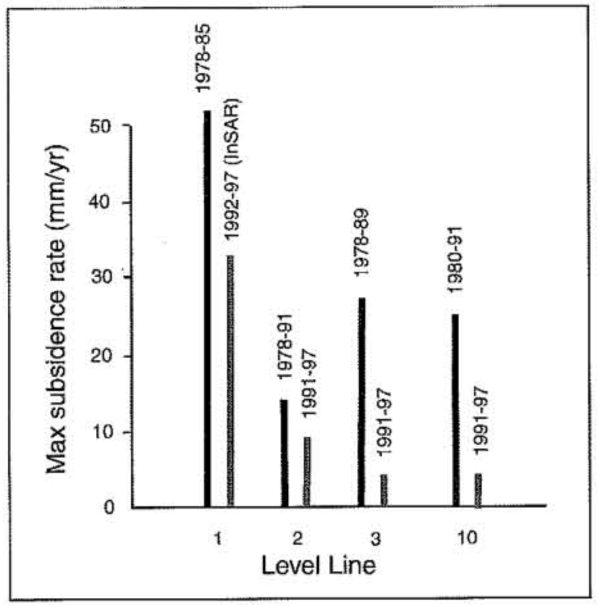

Figure 5. Comparison of pre-1991 maximum subsidence rates measured from level lines across faults with rates measured during the 1991-1997 period. Line 1 is compared with InSAR values along the same transect. The comparison shows that rates have decreased significantly, particularly along Lines 3 and 10 in the Central subsidence bowl.

Acknowledgments

This research was supported by the Las Vegas Valley Water District and the Southern Nevada Water Authority.

REFERENCES

Amelung, F., Galloway, D.L., Bell, J.W., Zebker, H.A., & Laczniak, R.J. (1999) Sensing the ups and downs of Las Vegas: InSAR reveals structural control of land subsidence and aquifer-system deformation. *Geology*, **27** (6), p. 483-486.

Bell, J.W. (1981) Subsidence in Las Vegas Valley. *Nevada Bureau of Mines and Geology Bulletin 95*, 81 pp.

Bell, J.W. (1991) Elevation changes associated with subsidence in Las Vegas Valley, Nevada. In: A.I. Johnson, ed., *Land Subsidence* (Proceedings of the Fourth International Symposium on Land Subsidence), p. 473-481.

Bell, J.W., & Price, J.G. (1991) Subsidence in Las Vegas Valley 1980-91. *Nevada Bureau of Mines and Geology Open-file Report 93-5*, 182 pp.

Bell, J.W., & Helm, D.C. (1998) Ground cracks on Quaternary faults in Nevada: hydraulic and tectonic. In: J.W. Borchers, ed., *Land Subsidence Case Studies and Current Research* (Proceedings of the Dr. Joseph F. Poland Symposium), Star Publishing Company, p. 165-173.

Burbey, T.J. (1995) Pumpage and water-level change in the principal aquifer of Las Vegas Valley, Nevada, 1980-90. *U.S. Geological Survey Water-Resources Information Report 34*, 224 pp.

Donovan, D.J., & Katzer, T. (2000) Hydrologic implications of greater ground-water recharge to Las Vegas Valley, Nevada. *American Water Resources Journal* (in press).

Las Vegas Valley Water District (1998) Las Vegas Valley Water District Artificial Recharge Project, 1998 Year end Report: Unpublished report, 128 pp.

Maxey, G.B., & Jameson, C.H. (1948) Geology and water resources of Las Vegas, Pahrump, and Indian Springs Valleys, Clark and Nye Counties: Nevada State Engineer, Water Resources Bulletin 5, 128 pp.

LAND SUBSIDENCE - Vol. II
Proceedings of the Sixth International Symposium on Land Subsidence
Ravenna / Italy / 24-29 September 2000

GPS MEASUREMENT OF GEOTECTONIC RECENT MOVEMENTS IN EAST SLOVAKIA

Vladimír Sedlák
Technical University, Department of Geodesy and Geophysics,
Park Komenského 19, SK-043 84 Košice, Slovakia

Abstract

The paper deals with the coordinate transformation procedures of the observed *GPS* (*Global Positioning System*) data from *WGS-84* (*World Geodetic System 1984*) into the national geodetic grid datum *S-UTCN* (*System of United Trigonometric Cadaster Network*) and *Baa* (*the Baltic Sea after adjustment*). *GPS* measurements are situated in the geodetic monitoring network in the Košice-Valley for a purpose of deformation surveying geotectonic recent movements in the East-Slovak region. Adjustment with constraints and free adjustment are applied at determining coordinates of the geodetic network points. Coordinate transformation from *WGS-84* into *S-UTCN* is realised by means of using the 7-element Helmert transformation with using three identical points.

Keywords: GPS, 3D transformation, geotectonic movements, East Slovakia

1. Introduction

The *GPS* measurements are realised on points of the geodetic network (*GN*) localised in the Košice-Valley (Slovakia) (Fig. 1). The aim of these measurements is determining recent geotectonic movements in the urban agglomeration of Košice-city (Sedlak et al., 1998). 3D coordinates of the network points determined from satellite navigation present a realisation result of the solved scientific project at the Department of Geodesy and Geophysics of the Technical University of Košice since 1997.

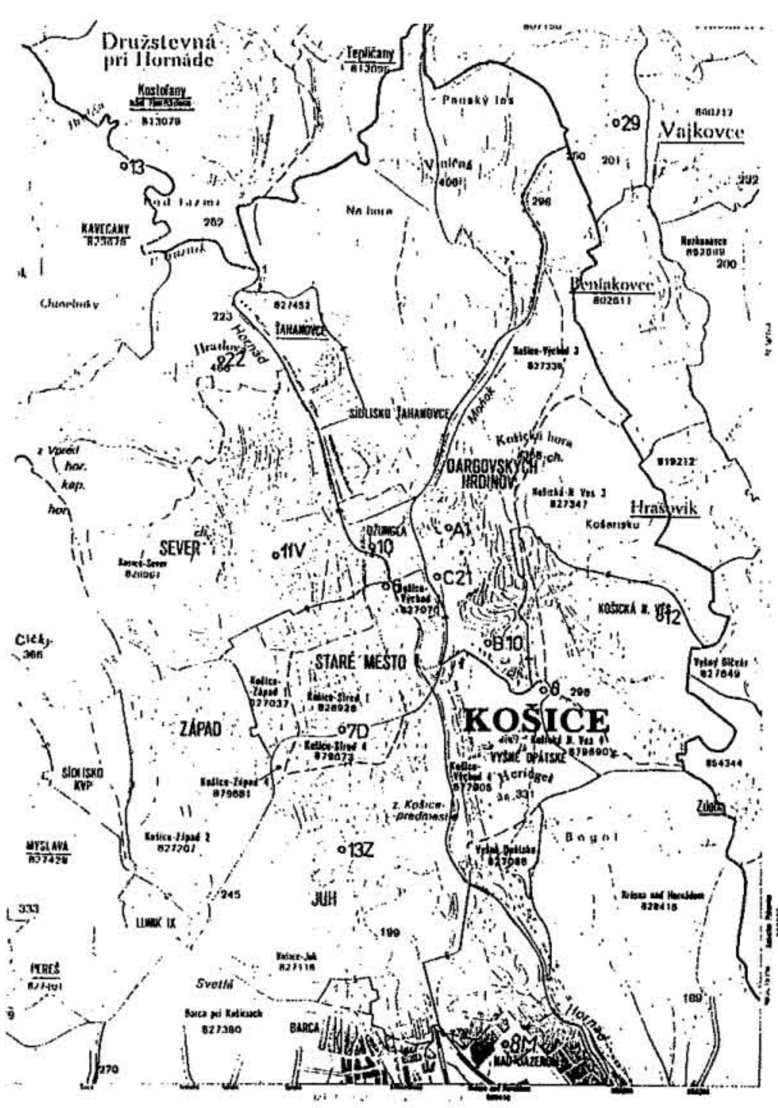

Figure 1. Positioning the Košice-Valley GN (1:100 000).

2. GPS MEASUREMENTS IN THE KOŠICE-VALLEY

GPS measurements are periodically realised twice a year (spring and autumn). Altogether, 17 points of *GN* are measured by means of using the *GPS* static method. A priority of the chosen static method for our measurements is above all a high accuracy in determining point positions which is conditioned by longer period of measurement on a determined point (cca 45 minutes)

(Hofmann-Wellenholf et al., 1993; Seeber, 1993; Leick 1995). The determined *GN* points are solved by double *GPS* vector technology always regarding two reference points, i.e., three *GPS* receivers are used for measurements. These points are placed so that the territories in which some geotectonic movements are presupposed according to geologists. The main tectonic fault in the Košice-Valley, according to which two expressive geological faults of the Earth ground blocks should move, is assumed in the north-south direction along the river Hornád. The secondary tectonic faults of smaller extent are in the direction perpendicular to the Hornad fault, i.e. in the east-west direction. These secondary tectonic faults are mutually parallel (Jacko, 1997).

Three double-frequency *GPS* receivers Sokkia GRS 2100 were used to measurement. Adjustment of observed data was realised by the firm software Prism ver 2.1 Sokkia. Coordinates of all points in *GN* were transformed from *WGS-84* into a plane coordinate system *S-UTCN,* which is obligatory coordinate system for realisation of geodetic works in Slovakia. The non-linear rotary matrix method was applied to the adjustment (Melicher and Flassik, 1998). After transformation, the coordinates were consecutively adjusted by an adjustment with constraints.

3. COORDINATE TRANSFORMATION OF THE GN POINTS FROM WGS-84 INTO S-UTCN

System *NAVSTAR GPS* uses *WGS-84* with the purpose of expressing the position anywhere in the earth and space. The reality that the *GPS* system determines a position in global dimensions is its priority. However, the disadvantage for surveying is its limitation in a plane rectangular system that is our national geodetic grid *S-UTCN* (system *S*).

3.1. Transformation of coordinates from WGS-84 into a topocentric horizontal system

The coordinate axes $(X, Y, Z)_{WGS\text{-}84}$ with an origin in the centre of ellipsoid create the system $S_{WGS\text{-}84}$ (Fig. 2). The coordinate axes X'', Y'', Z'' create the topocentric horizontal coordinate system S'' (Melicher and Flassik, 1998; Hurčíková, 1998). Its origin lies in the point *D*. Point *D* is one point belonging to points of a local network. This point is situated approximately in its centre. To assume that the geodetic horizon in *D* is a parallel plane to *S-UTCN* is only possible in a case of local *GN* with a small dimension (if distances between network points are not longer than some units of kilometres). Table 1 presents coordinates of the point *D*. Axes X'' and Y'', which lie in a geodetic horizon of the point *D*, while the axis X'' is oriented into the south branch of a meridian. The axis $+Z''$ lies in a normal line and is directed into the geodetic zenith and the axis $+Y''$ creates with the mentioned axes a left-hand system.

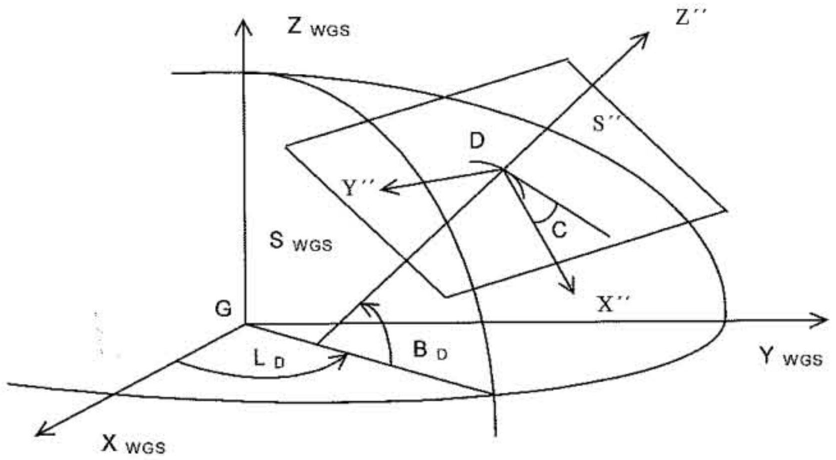

Figure 2. $S_{WGS\text{-}84}$ and S''.

Table 1. Coordinates of the point *D* in *WGS-84* and *S-UTCN*.

	WGS-84 [m]	*S-UTCN* [m]
X	3 927 761.7721	1 237 997.5879
Y	1 528 741.4010	262 066.5466
Z	4 771 351.2319	212.0736

Ellipsoid latitude	φ_D = 48° 44´ 7.12´´
Ellipsoid longitude	λ_D = 21° 16´ 21.22´´
Meridian convergence	C = 2° 39´ 42.89´´

Transformation of coordinates from the system $S_{WGS\text{-}84}$ into the system S'' is a possible according to the following equation

$$\begin{bmatrix} X \\ Y \\ Z \end{bmatrix}_{S''} = \begin{bmatrix} 1 & 0 & 0 \\ 0 & -1 & 0 \\ 0 & 0 & 1 \end{bmatrix} \mathbf{R}_Y(90° - \varphi_D)\,\mathbf{R}_Z(\lambda_D) \begin{bmatrix} X - X_D \\ Y - Y_D \\ Z - Z_D \end{bmatrix} \qquad (1)$$

where index *D* means that the tangent point is considered, φ_D,(λ_D) is ellipsoidal geocentric latitude, (longitude) of point *D*, $\mathbf{R}_Y$ ($90° - \varphi_D$), $\mathbf{R}_Z(\lambda_D)$ are non-linear rotation matrices according to the following equations (Melicher et al., 1993)

$$\mathbf{R}_Y(90° \text{-} \varphi_D) = \begin{bmatrix} \cos(90° - \varphi_D) & 0 & -\sin(90° - \varphi_D) \\ 0 & 1 & 0 \\ \sin(90° - \varphi_D) & 0 & \cos(90° - \varphi_D) \end{bmatrix} \qquad (2)$$

$$\mathbf{R}_Z(\lambda_D) = \begin{bmatrix} \cos(\lambda_D) & \sin(\lambda_D) & 0 \\ -\sin(\lambda_D) & \cos(\lambda_D) & 0 \\ 0 & 0 & 1 \end{bmatrix} \qquad (3)$$

The coordinates of the *GN* points in *WGS-84* are obtained by a convenient adjustment of measurements, which were realised by the system *NAVSTAR GPS*. The right-hand system is changed into left-hand which is preferred in geodesy. This change can be reached by multiplying a diagonal matrix with the diagonal (*1, -1, 1*). The point *D* has the coordinates $(X, Y, Z)^T = (0, 0, 0)^T$ in the system S''.

The system S'' is also possible to obtain by using the following equation

$$\begin{bmatrix} X \\ Y \\ Z \end{bmatrix}_{S''} = \begin{bmatrix} 1 & 0 & 0 \\ 0 & -1 & 0 \\ 0 & 0 & 1 \end{bmatrix} \mathbf{R}_Y(90° \text{-} \varphi_D)\mathbf{R}_Z(\lambda_D) \begin{bmatrix} X \\ Y \\ Z \end{bmatrix}_{WGS-84} + \begin{bmatrix} -\Delta X \\ 0 \\ -\Delta Z \end{bmatrix} \qquad (4)$$

where ΔX is distance of the normal from the centre of the ellipsoid, ΔZ is a displacement of the plane *XY* into the point *D* in the normal direction.

In the sense of Figure 3, the quantities ΔX and ΔZ are derived according the equations

$$\begin{aligned} \Delta X &= N(\varphi_D)\, e^2 \sin\varphi_D \cos\varphi_D, \\ \Delta Z &= N(\varphi_D) - \Delta X tg\varphi_D + H_D, \end{aligned} \qquad (5)$$

where $A(\varphi_D)$ is the transverse radius of curvature in the point *D*, *e* is the numerical eccentricity, H_D is the ellipsoid height of the point *D*.

A transition between the local and the commonly used national system should be the simplest in their contact point for a purpose of using the state network. It means that the coordinates of the local network should not much differ from *S-UTCN*. It can be reached by turning the system S'' in the point *D* about the meridian convergence *C* (Fig. 2) of *S-UTCN* and by displacement of the origin of the system S'' round the rectangular coordinates X_D, Y_D in *S-UTCN*. The mentioned transformation is expressed by the following equation

$$\begin{bmatrix} X \\ Y \\ Z \end{bmatrix}_{S'} = \mathbf{R}_3(-C) \begin{bmatrix} X \\ Y \\ Z \end{bmatrix}_{S''} + \begin{bmatrix} X_D \\ Y_D \\ h_D \end{bmatrix}_{S-UTCN,Baa} \qquad (6)$$

where $R_3(-C)$ is the rotation matrix determined by the equation

$$\mathbf{R}_3(-C)=\begin{bmatrix}\cos(-C) & \sin(-C) & 0\\ -\sin(-C) & \cos(-C) & 0\\ 0 & 0 & 1\end{bmatrix} \tag{7}$$

and h_D is the over-sea level height of the point D in the Baltic sea elevation system after adjustment (*Baa.*).

In this way we obtained the topocentric horizontal coordinate system whose the coordinate axes X', Y' lie in the geocentric horizon of the point of normal intersection of the point D with the geoid. Because the point D has the coordinates $(0,0,0)^T$ in the system S'', then this point will obtain identical coordinates with the coordinates in *S-UTCN* by adding the vector $(x_D, y_D, h_D)^T_{S\text{-}UTCN}$.

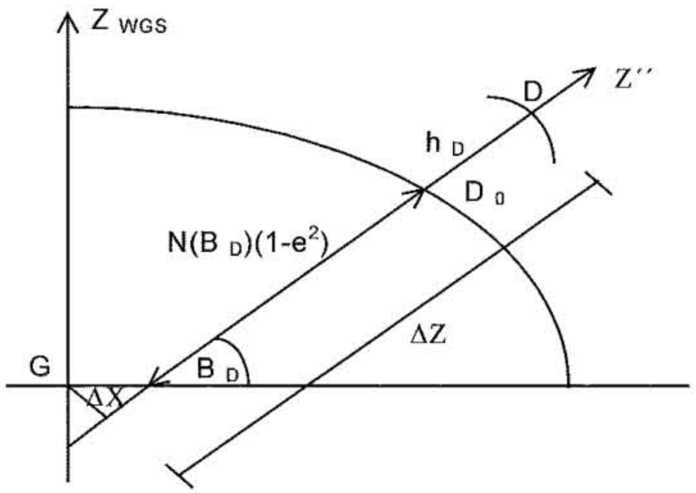

Figure 3. Transformation from the geocentric into the topocentric system.

3.2. Transformation of coordinates into the local coordinate system

It is not possible to calculate directly the values of elements which would harmonise with the values measured in a terrain using the coordinates of points in the system S'. These coordinates are influenced by the Earth curvature and also by a relative difference in elevation of point over the horizon plane. Regarding to a network dimension, we can substitute the ellipsoid by the reference sphere whose radius is equal to the mean radius of the Earth curvature R in the point D according to the equation

$$R=\sqrt{M(\varphi_D)N(\varphi_D)} \tag{8}$$

where M is the meridian and N the transversal radius of curvature of the ellipsoid, which are described by the following equations (Mervart and Cimbalník, 1997)

$$M(\varphi_D)=\frac{a(1-e^2)}{(1-e^2\sin^2(\varphi_D))^{3/2}} \tag{9}$$

$$N(\varphi_D)=\frac{a}{(1-e^2\sin^2(\varphi_D))^{1/2}} \tag{10}$$

where a and e^2 are the constants of the used ellipsoid (the semimajor axis and square of the 1st numerical eccentricity) (the Bessel ellipsoid).

An influence of the difference of elevation is possible to eliminate if the coordinates X', Y' are reduced into the intersection of the normal with the tangent plane, or with the basic plane. The reduction from a relative difference of elevation is possible to influence significantly by moving the geodetic horizon into the basic plane of *GN* in the height z_0. This height equals to approximate mean elevation value in which geodetic measurements are realised. The reduction of the coordinates X', Y' of the *GN* points in the system S' into the intersection of the normal with the basic plane equals to a gnomic projection which regarding to the network dimension is considered a conform projection.

The presented method has several priorities. Above all, it is the fact that a high relative accuracy in determining point positions by means of using *NAVSTAR GPS* technology is not lost. Similarly a measurement on one identical point is only enough instead of three identical points, by that a transmission of some errors at the transformation can be reduced. Reductions from elevation and cartographic distortion are needed in *S-UTCN* where only reduction from a relative height or elevation is considered in some local system. This reduction is also minimised by a convenient choice of transformation parameters (Melicher and Flassik, 1998).

3.3. Adjustment with constraints of 2D geodetic network

Geodetic networks can be adjusted by two ways. If we consider datum parameters as absolutely accurate and we do not include them into an adjustment process, the adjustment with constraints is considered in this case. In fact that datum parameters are also determined with a concrete accuracy that has an influence on an accuracy of adjustment parameters except for measurement accuracy. In this case a network can be adjusted by a free adjustment with consideration of datum parameters (Hefty and Husar, 1994;

Mervart, 1994). Regarding the applied confinement adjustment in the Kosice-Valley GN a theoretic procedure of this adjustment is presented, which is the most convenient for our national geodetic grid *S-UTCN*.

The least mean square method (*LMSM*) is chosen as an estimate principle, and the inverse solution is chosen as a mathematical principle, which is a standard procedure in an adjustment of *GN*. After adjustment the position and form of *GN* are changed but the datum point positions are not changed (datum points are considered as absolutely accurate). This fact is presented so that the configuration matrix ***A*** and also the matrix ***N*** of *GN* will be regular; the rank of matrices $h(A)=k$, $h(N)=k$, where k is a number of determined parameters. For the adjustment the following four vectors and matrices are necessary to be:

$$\underset{k,1}{C^{o}}$$

is the vector of approximate coordinates of the network points which are calculated from measured quantities and approximate coordinates of the reference points, instead of the coordinates obtained after transformation;

$$\underset{n,1}{l^{o}}$$

is the vector of approximate values of measured observations which are calculated from the approximate coordinates of the *GN* points on a base of the model equations (i.e. common mathematical equations for calculation of geodetic elements, for example lengths, angles, etc.);

$$\underset{n,k}{A}$$

is the configuration matrix of *GN*. Terms of this matrix are determined by partial derivatives of the model equations ***L*** according to the studied parameters. For a check it is possible to spread this matrix for the datum (object) points too, by this way we can get a global configuration matrix. A sum of the terms in a row of the constructed matrix must be equaled to zero. However, we only consider a submatrix containing the determined points at calculations, where n is a number of measurements and k is a number of the determined parameters;

$$\underset{n,n}{Q_{l}}$$

is the cofactor matrix of the measured quantities.
It is the matrix in which cofactors of the measured quantities are occurred. These cofactors can be calculated according to the equation

$$q_{l_i} = \frac{\sigma_i^2}{\sigma_o^2} \qquad (11)$$

where is the standard deviation of measurement, while the variance factor (a priori variance factor) is determined by the equation

$$\sigma_o^2 = \frac{\sum_{i=1}^{n} \sigma_i^2}{n} \qquad (12)$$

Solving equations of the estimate statistic model by means of using *MSM* we will get the following the linear equation

$$A^T Q_l^{-1} A \, d\hat{C} - A^T Q_l^{-1} dl = 0, \qquad (13)$$

where $dl=l-l^o$ is the vector of reduced observations, while l is the vector of the observed quantities and l^o is the vector of the approximate values of the measured quantities.

If we indicate $N=A^T Q_l^{-1} A$ and $n = A^T Q_l^{-1} dl$, we will get the following equation for the vector of the adjusted coordinate complements $d\hat{C}$

$$\begin{aligned} d\hat{C} &= N^{-1} n \\ d\hat{C} &= (A^T Q_l^{-1} A)^{-1} A^T Q_l^{-1} dl \end{aligned} \qquad (14)$$

Table 2. The adjusted coordinates of the GN points in S-UTCN.

	Autumn 1997			*Autumn 1999*		
Point	*S-UTCN* *X*	*Y*	*Baa.* *H*	*S-UTCN* *X*	*Y*	*Baa* *H*
	[m]		[m]	[m]		[m]
29	1 232 352.445	258 830.025	219.398	1 232 352.460	258 830.011	219.387
6	1 237 997.593	262 066.532	212.081	1 237 997.607	262 066.533	212.071
10	1 237 549.022	262 319.756	210.528	1 237 549.025	262 319.768	210.549
22	1 234 955.179	264 129.685	466.150	1 234 955.166	264 129.693	466.169
8H	1 239 477.294	260 026.978	315.799	1 239 477.301	260 026.970	315.814
A1	1 237 378.648	261 318.594	255.320	1 237 378.669	261 318.575	255.351
B10	1 238 862.613	260 850.840	281.508	1 238 862.590	260 850.819	281.547
C21	1 238 055.052	261 451.563	219.404	1 238 055.060	261 451.555	219.385
7D	1 239 951.154	262 718.114	229.253	1 239 951.172	262 718.096	229.212
11V	1 237 635.842	263 468.497	223.750	1 237 635.806	263 468.471	223.707
KN1	1 238 654.533	258 910.911	283.878	1 238 654.548	258 910.925	283.899
KN2	1 238 719.094	258 712.611	297.412	1 238 719.070	258 712.627	297.425
KN3	1 238 720.158	259 175.751	292.020	1 238 720.164	259 175.759	291.991
KN4	1 239 037.024	259 050.728	281.639	1 239 037.035	259 050.739	281.604
KN5	1 238 850.984	258 802.450	271.850	1 238 850.973	258 802.435	271.867

After adding $d\hat{C}$ to the vector of the approximate coordinates of points we will obtain the adjusted coordinates $\hat{C}$ of points (Table 2) according to the equation

$$\hat{C} = C^{o} + d\hat{C}. \tag{15}$$

The quality of the adjusted network is universally characterised by two matrices:

- the cofactor matrix of the estimates $Q_{\hat{C}}$ of coordinates

$$Q_{\hat{C}} = (A^{T}\ Q_{l}^{-1}\ A)^{-1} = N^{1}, \tag{16}$$

- the covariance matrix of the estimates $\Sigma_{\hat{C}}$ of coordinates

$$\Sigma_{\hat{C}} = s_{0}^{2}\ Q_{\hat{C}}, \tag{17}$$

$$\Sigma_{\hat{C}} = \begin{bmatrix} \sigma^{2}_{\hat{X}_1} & \sigma^{2}_{\hat{X}\hat{Y}_1} & & & \\ \sigma^{2}_{\hat{Y}\hat{X}_1} & \sigma^{2}_{\hat{Y}_1} & & & \\ & & \ddots & & \\ & & & \sigma^{2}_{\hat{X}_k} & \\ & & & & \sigma^{2}_{\hat{Y}_k} \end{bmatrix} \tag{18}$$

where s_0^2 is empirical variance factor determined by the equation

$$s_0^2 = \frac{\mathbf{v}^{T}\ \mathbf{Q}_{l}^{-1}\ \mathbf{v}}{n-k} \tag{19}$$

in which a numerator expresses the quadratic form of corrections Ω and a denominator expresses the number of superfluous measurements (redundantion of a network). A presumption of better quality of *GN* will increase together with increasing the difference *n-k*. The vector of corrections v is determined by the equation

$$v = A\ \ d\hat{C} - dl \tag{20}$$

The covariance estimates of the coordinates are situated on a diagonal of the covariance matrix in a direction of individual axes. The adjusted values of the measured terms $\hat{l} = l + v$ are also determined in a frame of an adjustment.

Deformation vector $\boldsymbol{d}$ was estimated by a simple way, i.e. algebraic calculations in rectangular triangles in the plane of *S-UTCN*. Position deformation vector presents deformations in a plane of *X,Y* axes and height deformation vector

presents deformations (subsidences) in the Baltic sea level system as a difference between the heights on the *GN* points. Table 3 presents the deformation vectors with standard deviations of the *GN* points. Because all deformation vectors are in limits of the error circles, we did not presuppose any recent geotectonic movements in the Košice-Valley.

Table 3. The deformation vector $\boldsymbol{d}$ and standard deviations of the *GN* points.

Point	Position $\boldsymbol{d}$ (X ,Y) [m]	Height $\boldsymbol{d}$ (H) [m]	σ_X [mm]	σ_Y [mm]
29	0.024	0.011	5.308	6.698
6	0.014	0.010	4.965	6.842
10	0.012	- 0.021	4.924	7.204
22	0.015	- 0.019	4.970	7.081
8H	0.031	- 0.015	6.187	6.098
A1	0.020	- 0.031	5.104	6.975
B10	0.026	- 0.039	5.682	5.974
C21	0.044	0.019	5.129	6.450
7D	0.021	0.041	4.951	7.548
11V	0.028	0.043	8.221	7.538
KN1	0.011	- 0.021	6.669	5.444
KN2	0.012	- 0.013	5.955	6.078
KN3	0.010	0.029	6.561	5.224
KN4	0.016	0.035	5.991	6.107
KN5	0.017	- 0.017	5.808	6.232

4. CONCLUSIONS

The results of measurements by *GPS* technology confirm a typical event of using this satellite measurement in *GN* with a spread application in geodesy. The applied static method of *GPS* measurements shows on a high accuracy of satellite measurements which is also acceptable for some other geodetic measurements, for example: a deformation surveying the earth surface and engineering structures. The reached results of the presented transformation procedures refer to the adaptability of transformations from *WGS-84* into the national geodetic grid *S-UTCN* and *Baa*. The chosen confinement adjustment by means of using the Gauss-Markov model is demonstrated as the most suitable mathematical model in an adjustment of *GN* in the Kosice-Valley locality (Hurèikova, 1998). The presupposed possible recent geotectonic movements in the direction of north-south along the Hornád River are not confirmed.

Acknowledgements

The paper followed out from the research Project No. 1/4008/97. The research was financially supported by the *Ministry of Education* of Slovakia.

REFERENCES

Hefty, J. & Husár, L. (1994) Družicová geodézia, Globálny polohový systém, (in Slovak language). Slovak Tech. Univ. Bratislava.

Hofmann-Wellenhoff, B., et al. (1993) *GPS Theory and Practice.* Springer-Verlag, Wien-New York, 1993.

Hurčíková, V. (1998) Určenie 3D súradníc v národnej geodetickej sústave bodov geodetickej siete v Košickej kotline-východ GPS technológiou, (in Slovak language). Diploma thesis, Tech. Univ. Košice.

Jacko, S. (1997) Polystadiálny vývoj SZ-JV zlomov pri východnom okraji integríd Západných Karpát, (in Slovak language). In: *9. Inter. Mine Conf.*, (ed. by Stroffek), Tech. Univ. Košice, 15-18.

Leick, A. (1995) *GPS Satellite Surveying.* John Wiley - Interscience Publication 2nd Edition, New York.

Melicher, J. & Flassik, T. (1998) Transformácia súradníc WGS-84 do lokálneho súradnicového systému pomocou nelinearizovaných rotaèných matíc, (in Slovak language). *Geodetický a kartografický obzor*, **44/86**(2), 25-29.

Melicher, J., Fixel, J. & Kabelac, J. (1993) Geodetická astronómia a základy kozmickej geodézie, (in Slovak language). Alfa, Bratislava.

Mervart, L. (1994) Globálny polohový systém, (in Czech language). Czech Tech. Univ. Prague.

Mervart, L. & Cimbalník, M. (1997) Vyšší geodézie 2. Czech Tech. Univ. Prague.

Sedlák, V., Kunák,L., Sütti,J., Kovaniè,L., Havlice,K., Šadera, M., Gašinec, J. & Jacko, S. (1998) Deformaèné modelovanie geotektonických recentných pohybov vo východoslovenskom regióne, (in Slovak language). Research report, Tech. Univ. Košice.

Seeber, G. (1993) Satellite Geodesy, Foundation, Methods and Applications. W de G, Berlin.

VERTICAL CRUSTAL MOTIONS AND MEAN SEA LEVEL: AN EXPERIMENT IN THE EASTERN PO PLAIN

S. Zerbini (1), B. Richter (2), M. Negusini (1), D. Simon (2), C. Romagnoli (3), F. Domenichini (1)
(1) Dipartimento di Fisica, Università di Bologna, Viale Berti Pichat 8, 40127 Bologna,Italy, zerbini@astbo1.bo.cnr.it;
(2) Bundesamt fuer Kartographie und Geodaesie, Richard-Strauss Allee 11, Frankfurt am Main, Germany;
(3) Dip. di Scienze della Terra e Geologico Ambientali, Università di Bologna, Piazza di Porta San Donato 1, 40127 Italy.

Abstract

Continuous GPS observations are being performed since 3.5 years at Medicina and Porto Corsini stations in the eastern Po Plain. At Medicina also continuous observations of the gravity field are being performed by means of a superconducting gravimeter. Environmental parameters are also being collected at both stations. At Porto Corsini, located on the Adriatic coast near the city of Ravenna, a tide gauge of the Italian national network is operational. To accurately measure and understand vertical crustal motions at tide gauge stations is of major importance in order to properly determine sea level fluctuations. While at Porto Corsini a subsidence rate of -7.8±0.2 mm/yr was identified, at Medicina the available data series did not show any significant linear trend which could be attributed to land subsidence. This is confirmed by the gravity series behavior.

The analysis of about 9 years (1990-1998) of the Porto Corsini tide gauge data indicates a sea level trend for the North Adriatic of +21.4±2.2 mm/yr. By accounting for the vertical rate provided by the GPS observations, the true sea level variation turns out 13.6±2.2 mm/yr, in excellent agreement with the rate (14.7±3.2 mm/yr) estimated, for the northern Adriatic, from six years (1993-1998) of Topex satellite radar altimeter data.

Keywords: subsidence, height fluctuations, sea level variations.

1. INTRODUCTION

One of the main objectives of the European Union SELF II project (Sea Level Fluctuations in the Mediterranean: interactions with climate processes and vertical crustal movements) was the improvement of the long-term monitoring of sea level variability by applying the most advanced geodetic techniques, including satellite altimetry (Zerbini et al., 2000a; Zerbini et al., 2000b). However, in order to understand true sea level variations from the analysis of tide gauge time series, the knowledge of the vertical crustal movements of the Tide Gauge Benchmarks (TGBM) is required to an accuracy of one mm/yr or better (Carter 1994). Nowadays, space geodesy provides the means to monitor, in a global reference system, horizontal as well as vertical velocities of stations on the Earth's surface to a high degree of accuracy. Global Positioning System (GPS) measurements can be used for TGBMs fixing thus unifying the tide gauge network. Fixing the TGBMs at the few millimeters level of accuracy is necessary in order to be able to separate sea level variations from vertical crustal movements and potential changes, which may originate from different phenomena. Recent developments in the field of GPS, including the fact that GPS is now providing station coordinates on a global scale at the 1 cm level on a daily basis, and the realization and operation of the International GPS Service for Geodynamics (IGS) making available to the scientific community precise GPS orbits and Earth rotation parameters, indicate that this system can be reliably used to determine vertical crustal movements of the TGBMs in the International Terrestrial Reference System (ITRS) (Blewitt, 1994). To achieve the required level of accuracy, permanent occupations of tide gauge stations by means of GPS systems shall be implemented. According to the recommendations of major international bodies (Carter, 1994), absolute gravity measurements should also be performed at tide gauge stations in order to provide an assessment of height variations through a completely independent observing system. The sea level trend obtained from tide gauge observations corrected for vertical crustal motion can then be compared to the sea level trend deduced from satellite altimetry observations. These are, in fact, absolute sea level measurements related through the satellite orbit to the Earth's center of mass.

In the framework of the activities of the SELF II project, in July 1996 two permanent GPS receivers were installed at Medicina, a fundamental station of the space geodesy network, and at Porto Corsini on the Adriatic coast near Ravenna (Fig. 1). At Porto Corsini the GPS receiver is located in the proximity of the tide gauge belonging to the Italian tide gauge network. At Medicina, in October 1996, also a superconducting gravimeter (SG) has been installed to monitor the variations of the gravity field continuously. The SG is being periodically controlled by means of absolute gravity measurements (AG). The combination of the relative (SG) and absolute measurements fully exploits the potential of the two techniques by making use of the sub-μGal resolution of the SG and of the long-term stability of the AG.

At both stations relevant meteorological parameters such as air pressure, temperature, relative humidity and precipitation data are also collected on a continuous basis. In addition, at Medicina continuous observations of water table are being recorded and the atmospheric information obtained by 12-hour radio sonde balloon launches are also collected.

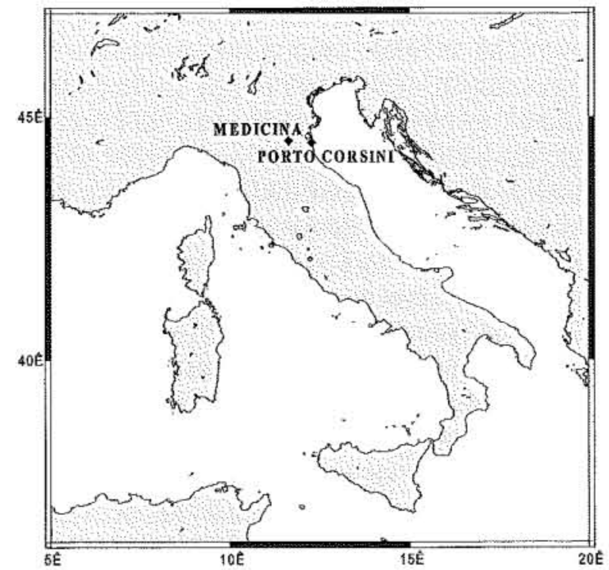

Figure 1. Locations of the Medicina and Porto Corsini stations.

2. GEOLOGIC AND CLIMATIC FRAMEWORK

The Southeastern Po Plain represents a sediment-filled foredeep, where a huge sedimentary deposition (more than 5000 m of thickness) occurred during the Plio-Pleistocene. North-east verging Apennine fronts, in the form of arcuate thrust belts buried in the Po Plain subsurface, are sealed by Upper Pliocene to Quaternary marginal marine and alluvial sediments (Pieri and Groppi, 1981). The thickness of the alluvial deposits in the Plain reflects the structural setting of the underlying features, being high at the southern and eastern margin. Differential subsidence is thus linked to the inherited control of buried tectonic structures, which is present at both local and regional scale, and to sediment compaction. Natural average subsidence rates for the coastal tract of the Plain, where the base of the Quaternary lies close to 2000 m of depth, have been included between a minimum of 0.75 mm/yr (inland Porto Corsini) and 1.1 mm/yr (in correspondence of gas fields in the offshore) for the Late Pleistocene (last 125 kyr; Astorri and Venturini, 1997). Subsidence rates for the Holocene (last 6,000 yr), obtained through radiocarbon dating of material recovered from borings in the Venetian area, have been estimated as 1-1.5 mm/yr (Fontes and Bortolami, 1973; Gatto & Carbognin, 1981), while for the last 2 kyr and the recent times, the average subsidence trend in the Ravenna area (about 10 km inland with respect to Porto Corsini) has been estimated as 2-2.5 mm/yr on the basis of historical-archaeological and stratigraphical data (Roncuzzi, 1992; Gambolati et al., 1991; Gambolati and Teatini, 1997). The natural, long-term subsidence has been greatly enhanced, in the second half of this century, by anthropogenic factors (such as the ones connected to overpumping of water and gas from the underground). Altimetric data, collected for the years 1950s to 1980s in the area onshore Porto Corsini, showed a land lowering of more than 100 cm, with average subsidence rates up to 3-4 cm/yr, reaching values of 6-7 cm/yr in the 1970s (Bertoni et al., 1988). More recent leveling indicate for Marina di Ravenna-Porto Corsini an average subsidence rate of 1.74 cm/yr for the 1984-93 interval (Idroser, 1996) and of about 1 cm/yr for the period 1992-99 (Unguendoli, personal communication); this noticeable decrease in the man-induced subsidence is related to the adoption of groundwater control policies since the beginning of the 80's and the consequent reduction in water withdrawal.

Though spatially rather close to each other (about 50 km), the two sites of Medicina and Porto Corsini show different surficial litho-stratigraphical characters and microclimatic conditions, and this has to be considered in relation to the occurrence of environmental-induced effects in the GPS and gravity signals.

The Medicina station is located in a low-lying sector of the middle-lower Po Plain, where the surficial sedimentary sequences are mostly fine-grained and interbedded with sandy lenticular bodies only locally, i.e. in correspondence of the fluvial drainage of Apennine provenance flowing and laterally migrating in the Plain. Clayey deposits, which predominate in the first 18-20 meters of the ground, are generally characterized by low permeability values and high water retention. Their typical behavior, in relation to the water content, is represented by the alternation of shrinkage and swelling following, with some delay, the different degree of evapotranspiration or humidity and responsible for volumetric changes of the soil, for re-arrangements in its fabric and for changes in its secondary permeability.

Medicina has a humid/sub-humid climate (average annual rainfalls = 650-800 mm/yr; high degree of humidity also during summer season) and is characterized by limited hydric insufficiency during summer. Monthly average temperature is minimum in January and maximum in July. A shallow unconfined (phreatic) aquifer is present very close to the topographic surface in this sector of the Plain. The water table, continuously monitored during the experiment, lies within the first 2 meters of the ground. It is mainly fed by infiltration of meteoric water and by losses in the hydrogeological surficial system, represented by both the natural drainage and by the widely extended artificial network due to the most recent hydraulic reclamation of the Plain.

Porto Corsini is located on the present-day coastal belt of the easternmost Po Plain. It belongs to the sub-humid to sub-arid climate zone, where hydric surplus is limited or absent (average annual precipitation < 500-600 mm/yr). Local effects from the littoral breeze may induce a better developed mixing of the air close to the coastal surface, with lower temperature and humidity gradients. The lithological and stratigraphical framework of the surficial deposits in the area reflects the progressive basinward shift in the shoreline position which occurred after the maximum marine ingression (which was reached here about 5 kyr B.P., when the shoreline was located a few tens of km landward of the present-day position). Porto Corsini lies on coarse-textured soils of the coastal plain belt (well sorted beach-ridge sands interbedded with finer-grained alluvial, lagoonal and shallow marine sediments, Amorosi et al., 1999), with high permeability and general low water retention. The relatively shallow depth (1-2 meters) of the water table of the surficial phreatic aquifer (that lies in the upper 25-35 m and is mainly composed of coastal sands) induces in the soil hydromorphic characters, i.e. conditions of hydric saturation (Regione Emilia Romagna, 1994).

3. VERTICAL MOVEMENTS

GPS daily heights are computed for both the Porto Corsini and Medicina stations. The height series are relevant, at present, to a period of 3.5 years (July 1996-December 1999). The GPS data analysis is performed by means of the well-known Bernese package, version 4.0 (Rothacher and Mervart, 1996). For a description of the adopted data analysis procedure we refer to Zerbini et al. (2000a and 2000b). Figure 2 shows, for the two stations, the height time series. In the upper plot (a) the Medicina data are displayed, while the lower graph (b) illustrates the Porto Corsini results. It is clear that the behavior, as regards the subsidence rate, is quite different for the two stations. At Porto Corsini, a significant negative linear trend equal to -7.8±0.2 mm/yr was detected. This is quite in good agreement with the results of high precision leveling measurements performed in the area during the last decade (Unguendoli, personal communication). The Medicina results, to the contrary, do not exhibit any significant linear trend over the available time period. This is confirmed by the results of the analysis of the gravity data, as it will be shown in the following. By removing the detected linear trend from the Porto Corsini data, the residual series of Figure 3 exhibit periodicities, which are similar to those present in the Medicina height series, though they are different in amplitude.

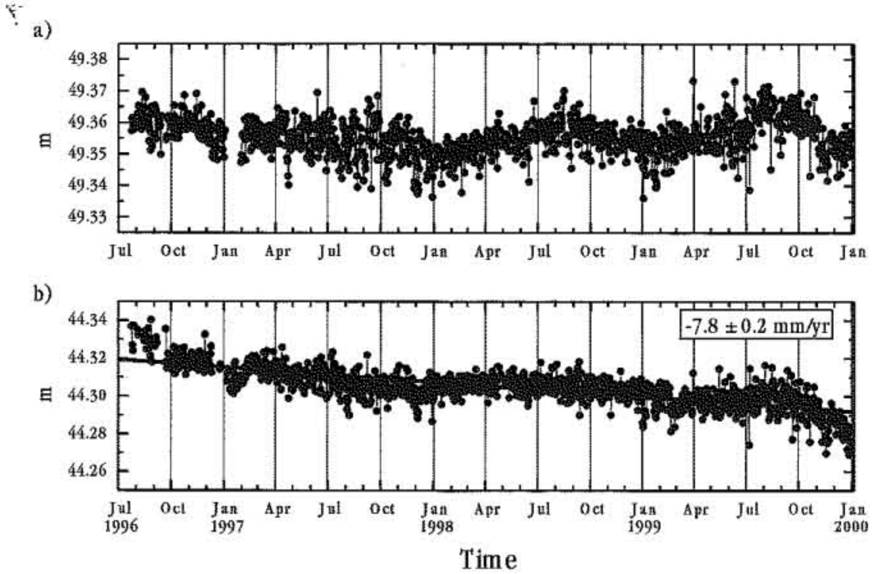

Figure 2. a) Medicina GPS daily heights; b) Porto Corsini GPS daily heights and linear trend estimated by linear interpolation of the daily heights.

The most relevant are the annual (4.5 mm for Medicina and 3.3 mm for Porto Corsini) and semi-annual fluctuations. A significant contributor to these fluctuations is, most likely, the loading effect induced by atmospheric pressure.

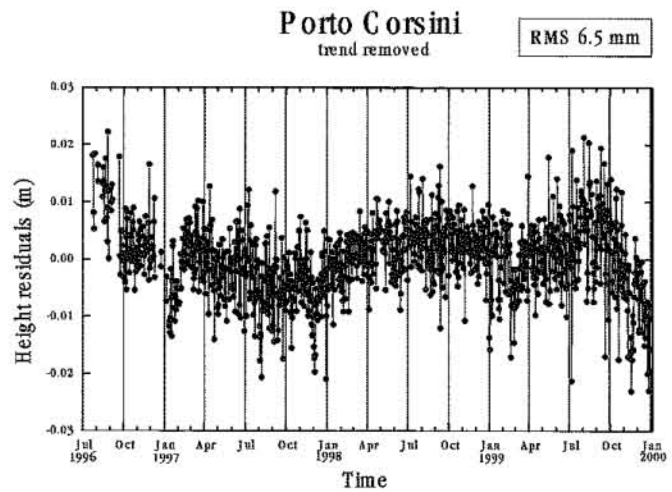

Figure 3. Height residuals for the Porto Corsini station after removal of the linear trend. The rms of the series is about 7 mm, which can be considered a reliable estimate of the error to be associated to the height daily solutions.

This effect can be modeled by means of the simple Rabbel and Zschau model (1985) based on local and regional pressure data. The amplitude of these annual waves turns out to be in the order of 1.3 mm with maxima occurring at the end of January-beginning of February, corresponding to minima in the stations' height. The amplitude of the semiannual component is 0.7 mm for Porto Corsini and 1.1 mm for Medicina. Other potential contributors to the observed fluctuations are the loading effects induced by the ocean and surficial groundwater. A more specific discussion on this topic is given in Zerbini et al. (2000b). The observed height fluctuations are a relevant signal, which must be interpreted and removed form the data series, in order to allow a correct determination of the long-term trend which, otherwise, could be in error of as much as 1-to-2 mm/yr.

Figure 4 illustrates the SG data series. Continuous monitoring of vertical height and gravity changes allows the separation of the gravity potential signal due to the mass redistribution from the geometric signal due to height changes.

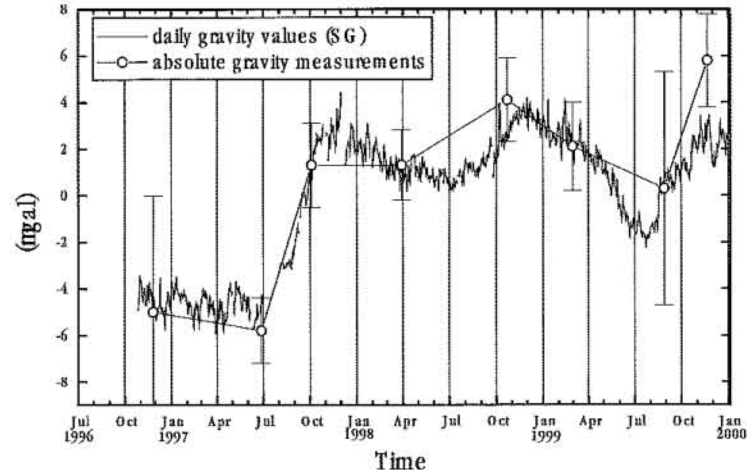

Figure 4. Daily gravity time series (SG) and AG measurements at Medicina.

If one leaves out the sharp increase in gravity occurring in the period July-September 1997, the remaining series shows a marked seasonal signal comparable in amplitude to that observed in the Medicina GPS heights. The remarkable increase in gravity, which is confirmed also by the absolute measurements (open circles in Fig. 4), can be explained partly by the concomitant decrease in height observed in Medicina and partly by a mass increase occurring mainly during the month of September 1997 prior to the beginning of the Central Italy seismic crisis (Umbria). This finding is described in Zerbini et al. (2000a). As pointed out previously, the gravity series (excluding the sharp increase mentioned above) do not present any significant linear trend, which could be attributed to land subsidence over the time period of the recorded data.

4. SEA LEVEL DATA

The data of the Porto Corsini tide gauge have been digitized from the paper records, for the period 1990-1999, in order to obtain hourly values for the sea level elevation. Work is in progress to digitize and process the whole available set of data (starting from 1936). Figure 5 shows the daily sea level means computed from the hourly data. On June 20, 1998 a new tide gauge has been installed and the old one removed. Unfortunately, there is no overlap between the old and new data series. For this reason, in our estimates, only the data from the old tide gauge till June 1998 are considered.

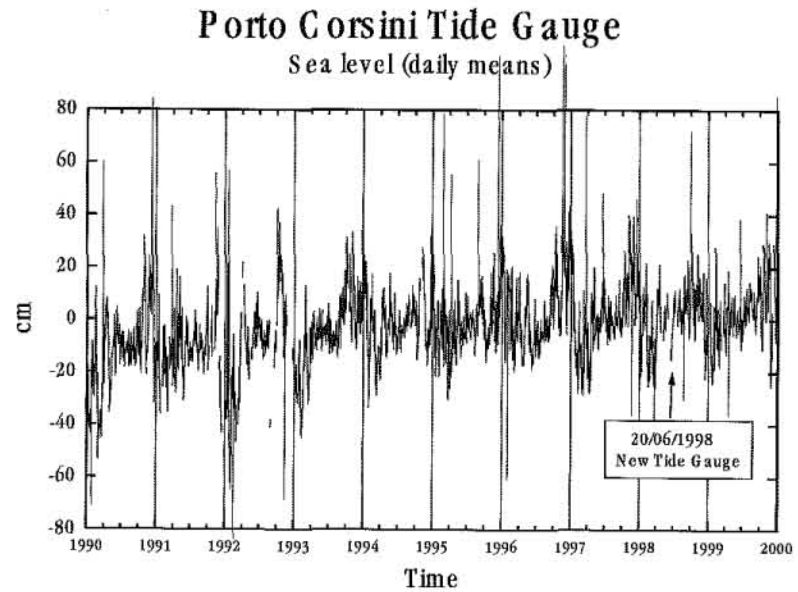

Figure 5. Daily means of sea level data from the Porto Corsini tide gauge from 1990 to 1999.

For the interval 1993-98, sea level height measurements obtained through the Topex/Poseidon satellite altimetry mission are also available. An important result of this mission is the measurement of seasonal and interannual variations in the global mean sea level with a precision better than 1 mm/yr (Cazenave et al., 1998; Minster et al., 1999). Moreover, altimetry observations allow the geographical mapping of the mean sea level drift, evidencing the spatial pattern of the temporal variability of the sea level. In the Mediterranean, a strong annual cycle of 8 cm amplitude and maxima occurring in early October is clearly recognizable, although it shows a non homogeneous geographical distribution, partly reflecting the main circulation features within the basin. Large intra-seasonal fluctuations dominate the residual (annual signal removed) sea level time series. These fluctuations are highly correlated with averaged surface pressure variations suggesting that at time scales of 100-200 days the Mediterranean sea level changes mainly as a result of atmospheric perturbations (Cazenave et al., 2000).

Figure 6 shows, in the upper part, the weekly means of the Porto Corsini tide gauge data corrected for the inverted barometer (IB) effect. In the lower graph of Figure 6, also an annual and a semiannual wave have been subtracted from the sea level weekly means. By taking into consideration these 8.5 years of tide gauge data, the residual sea level series provide a linear drift of 21.4±2.2 mm/yr.

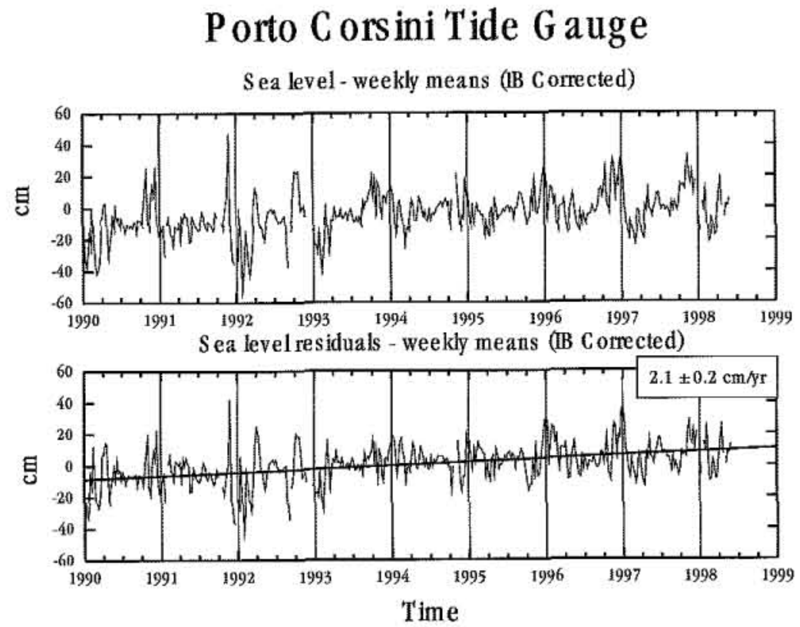

Figure 6. The upper plot shows the sea level weekly means for the Porto Corsini tide gauge corrected for IB; in the lower plot the residual data series after removal of an annual and a semi-annual wave are displayed. The linear trend over the 1990-1998.5 time interval is shown.

By accounting for the vertical rate at Porto Corsini, as determined by continuous GPS measurements (-7.8±0.2 mm/yr), the sea level rate obtained from the tide gauge observations turns out to be 13.6±2.2 mm/yr, in excellent agreement with the estimate obtained for the northern Adriatic by Cazenave et al. (2000) from the analysis of the Topex data in the time interval 1993-98. Table 1 summarizes the tide gauge, GPS and Topex results.

Table 1. Sea level rate at Porto Corsini from tide gauge data corrected for vertical crustal motion and from Topex satellite altimetry data.

	Rate (mm/yr)	Time scales
Tide Gauge data 1990-1998.5	21.4±2.2	8.5 years
GPS vertical rate	-7.8±0.2	3.5 years
Topex Northern Adriatic (Cazenave et al., 2000)	14.7±3.2	6 years

5. CONCLUSIONS

The results obtained so far clearly indicate the importance of using a multiple technique approach (GPS/gravity/tide gauges and satellite altimetry) in the study of sea level variability. Sea level variations in response to climate change/fluctuations seem to occur at different space and temporal scales. Recent developments have highlighted the concept that global warming induced sea-level change will not be globally uniform. Predictions from Atmosphere-Ocean General Circulation Models (AOGCM), though still with a relevant degree of uncertainty, indicate that local sea level changes could be higher or lower by a factor of two than the global average. For the past decade, satellite altimetry has detected a global mean sea level rise of about 2 mm/yr (Cazenave et al., 1998). However, very strong positive or negative (i.e., rising or falling sea level) regional variations, amounting to 10 times the global mean in some areas, have been observed. These latter effects are particularly important in highly populated coastal areas; combined with regional subsidence, these regional sea level variations determine the long-term fate and short-term inundation vulnerability of coastal areas.

Space geodetic techniques such as GPS, if used in a continuous mode, have demonstrated the capability to observe vertical motions of the Earth's crust to a high level of accuracy. Simultaneous observations performed by means of a completely independent system (gravity measurements) have proved the capability of the combined observational strategy to determine height variations of a few millimeters per year with sub-millimeter accuracy, provided that periodic signals of environmental origin are removed from the data.

Sea level variations/fluctuations in the order of a few millimeters per year shall be identified unambiguously, if a proper understanding of the interactions between the different components of the Earth's system shall be achieved. This is most important for climate change predictions and impact assessment.

Acknowledgments

This work has been developed under contract ENV4-CT95-0087 from the Commission of the European Union in the framework of the Environment and Climate Programme, Contract ARS-96-50 from the Italian Space Agency and jointly financed by MURST 1998.

REFERENCES

Amorosi A., Colalongo M.L., Pasini G., & Preti D. (1999) Sedimentary response to Late Quaternary sea-level changes in the Romagna coastal plain (Northern Italy). *Sedimentology,* 46-1, in press.

Astorri M. & Venturini S., (1997) Preliminary data on stratigraphy and natural subsidence in Quaternary in the areas of Ravenna and Venice. *Abstracts Meeting on Environmental Geology*, IAS-SEPM, Venice, October 27-29, 1997.

Bertoni W., Brighenti G., Gambolati G., Gatto P., Ricceri G. & Vuillermin F., (1988) Risultati degli studi e delle ricerche sulla subsidenza di Ravenna. Comune di Ravenna, 147 pp.

Blewitt G., (1994) The Global Positioning System. In Report of the Surrey Workshop of the IAPSO Tide Gauge Bench Mark Fixing Committee, W.E. Carter Ed., Deacon Laboratory, Godalming, Surrey, United Kingdom, December 13-15, 1993, *NOAA Technical Report NOSOES0006*, 17-26.

Carter, W. E. (Ed.), (1994) Report of the Surrey Workshop of the IAPSO Tide Gauge Benchmark Fixing Committee. Deacon Laboratory, Godalming, Surrey, United Kingdom, December 13-15, 1993, *NOAA Technical Report NOSOES0006.*

Cazenave A., Dominh K., Gennero M.C., & Ferret B., (1998) Global Mean Sea Level Changes Observed from Topex-Poseidon and ERS-1, *Physics and Chemistry of the Earth,* **23**, 1069-1075.

Cazenave A., Mercier F., Dominh K., Bonnefond P., & Exertier P. (2000) Sea level changes in the Mediterranean and Black Seas, *Global and Planet. Change, (submitted).*

Fontes J.C.H. & Bortolami G., (1973) Subsidence of the Venice area during the past 40,000 years. *Nature,* **244**, h.5415, 339-341.

Gambolati G., Ricceri G., Bertoni W., Brighenti G., & Vuillermin E., (1991) Mathematical simulation of the subsidence of Ravenna. *Water Resources Res.*, **27** (11), 2899-2918.

Gambolati G. & Teatini P., (1997). Natural subsidence of the Upper Adriatic Sea Basin. In: "CENAS: Study on the coastline evolution of the Eastern Po Plain due to sea-level change caused by climate variation and to natural and anthropic subsidence". Environment Programme 1990-94. Padova, settembre 1997, pp.105-134.

Gatto P., & Carbognin L. (1981) The Lagoon of Venice. Natural environmental trend and man-induced modification. *Hydr. Sc. Bull.*, **26**, (4), 379-391.

Idroser - Regione Emilia Romagna, (1996) Progetto di piano per la difesa dal mare e la riqualificazione ambientale del litorale della Regione Emilia-Romagna.

Minster J.F., Cazenave A., Serafini V., Mercier F., Gennero M.C., & Rogel P. (1999) Annual cycle in mean sea level from Topex-Poseidon and ERS-1: inferences on the global hydrological cycle, *Global and Planetary Change*, **20**, 57-66.

NCEP http://www.cdc.noaa.gov/

Pieri M. & Groppi G., (1981) Subsurface geological structure of the Po Plain, Italy. Publ. N. 414, Progetto Finalizzato Geodinamica, Italian National Council of Research, 23 pp.

Rabbel W. & Zschau, J. (1985) Static deformations and gravity changes at the earth's surface due to atmospheric loading, *J. Geophys.*, **56**, 81-99.

Regione Emilia Romagna, (1994) I suoli dell'Emilia Romagna. Note illustrative. Servizio Cartografico Regione E.R., Bologna, 383 pp.

Roncuzzi A., (1992) Topografia di Ravenna antica: le mura. *Bollettino della Camera di C.C.A.R.B.*, **XXXIX**, 691-742.

Rothacher M., & Mervart L. (eds.) (1996) Bernese GPS software version 4.0, Astronomical Institute – University of Bern, 417 pp.

Zerbini S., Richter B., Negusini M., Simon D., Schwahn W., Domenichini F. & Romagnoli C. (2000a) Height and gravity variations by continuous GPS, gravity and environmental parameter observations in the southern Po Plain near Bologna, Italy, *GRL, (submitted).*

Zerbini S., Richter B., Negusini M., Simon D., Schwahn W., Domenichini F. & Romagnoli C. (2000b) High-precision monitoring of vertical ground deformation for the study of sea level variability, *Global and Planet. Change, (submitted).*

LAND SUBSIDENCE - Vol. II
Proceedings of the Sixth International Symposium on Land Subsidence
Ravenna / Italy / 24-29 September 2000

MULTIMEDIA GIS DATA IN THE STUDY OF LAND SUBSIDENCE

Marco Gatti and Alberto Pellegrinelli
Department of Engineering - University of Ferrara
via Saragat 1, 44100 Ferrara.
E-mail: mgatti@ing.unife.it, apellegrinelli@ing.unife.it

Abstract

In this paper, we describe the characteristics of a Multimedia Geographic Information System devised for the study of land subsidence in the Po River valley. The database, the data input procedures and the procedures of interrogation of the files are structured within the Microsoft Access 97® environment. The interrogations are viewed within the ArcView® GIS environment. In the System, we have stored data deriving from levelling measurements performed in the Po Valley from 1950 to 1993. At present, the System can be available to only one user. However, its sharing by several users, connected in a local network and in the Intranet/Internet environment, is in the planning stage.

Keywords: geodetic database, GIS data, Po Valley, Internet.

1. INTRODUCTION

Land subsidence is quantified by means of repeated geometric levelling measurements of permanent benchmarks. The levelling campaigns performed in the last fifty years in territories subject to subsidence have produced a huge quantity of geometric data and technical information. Before the data can be used in the study of subsidence, they must be stored and managed in a modern computerized support system. The introduction of geodetic databases and the automatic procedures of data acquisition and processing have permitted the correlation of this information; thus we now have knowledge of some aspects of the phenomenon, which were difficult to identify a short time ago. A database for the management and use of levelling data has been devised for the study of subsidence in the eastern Po Valley (Gatti and Russo, 1995). In this database, we have stored the information from levelling campaigns performed from 1950 to the present by the Italian Military Geographic Institute (IGMI) and by the Land Registry Office. This database has recently been modified and expanded by the addition of information deriving from levelling campaigns performed by other public and private institutions. Moreover, the database has been connected to a commercial GIS software to permit the immediate viewing of the interrogations on a monitor and to produce thematic maps of the subsidence phenomena. In this way, we have created a Geographic Information System (GIS) whose future use will allow us to obtain the information necessary to study subsidence in the Po Valley with scientific rigor. In the present paper, we illustrate:

- the structure of the database;
- the input procedures and the procedures of interrogation of the data;
- the connection with the GIS environment.

In addition, we provide some examples of thematic maps that can be produced with the Information System. Finally, we present a plan for the sharing of the System in a local network and in an Intranet/Internet environment, with the aim of making it available to external users for input, consultation and modification of the data.

2. THE DATABASE

The present work originated from the experience of one of the authors in the creation of a database for the study of subsidence in the eastern Po Valley (Gatti and Russo, 1995). That database contained the information from levelling campaigns conducted by the Italian Military Geographic Institute (IGMI) and by the Cadastral Office from 1950 to 1990. The same database was used to represent the "Vertical movements of the ground" on the Geomorphological Map of the Po Valley (Bondesan et al., 1997).

With the aim of extending the study of land subsidence to the remaining parts of the Po Valley, the database has been expanded with information from geometric levelling campaigns performed by other agencies in the entire territory of the Po Valley. Thus the information presently stored in the database derives from levelling campaigns performed by the IGMI, the Cadastral Office and AGIP in the eastern and western parts of the Po Valley, by IDROSER along the coast of Romagna, by the municipalities of Ravenna, Bologna and Modena, by the Reclamation Consortiums of Ferrara and Ravenna, by the Regional Agency for Agricultural Development of Emilia Romagna, by the Magistrato per il Po along the axis of the Po River, from Parma to its mouth, etc. The collection and combination of data from different sources compelled us to revise the structure of the first database. The definitive conceptual model of the database is represented in Figure 1, while its physical structure (chief fields) is reported in Figure 2.

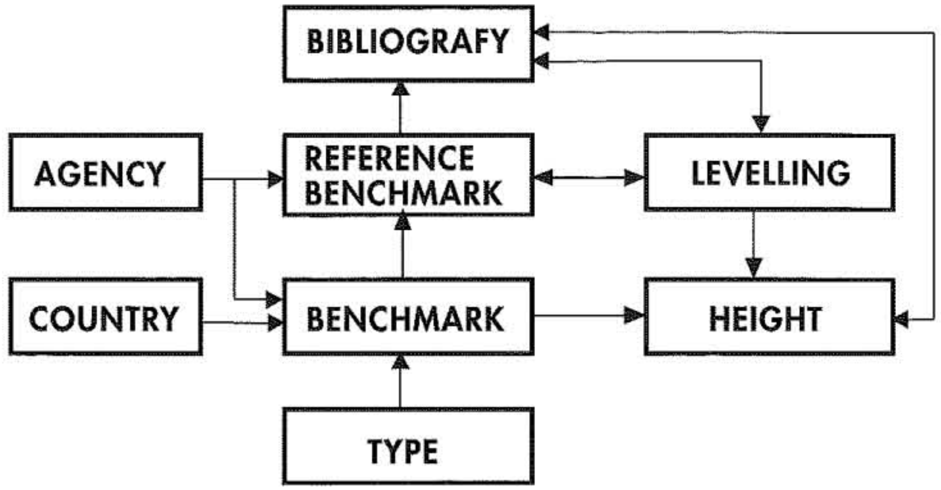

Figure 1. The conceptual model of the database and the "relational" charts.

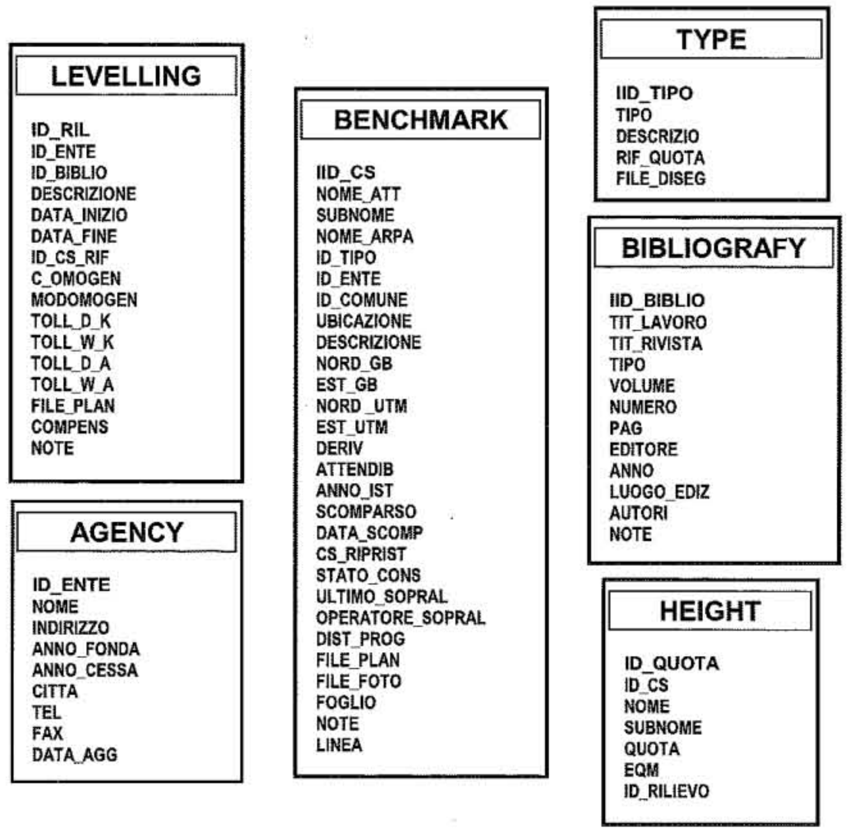

Figure 2. The physical structure of the database.

The database was created in the Microsoft Access 97 environment. From the numerous relational databases on the market, we chose MS Access 97 for the following reasons:

- its widespread availability;
- the possibility of importing data in numerous formats;
- the possibility of performing automatic controls of the validity of the data;
- the possibility of creating user interface screens;
- the possibility of performing simple (mono-table) or complex (multi-table) interrogations.

In addition, Access 97 allows the use of a programming language (Visual Basic for applications) to create automatic search and calculation procedures which can be personalized for the user.

At the end of the input operations, the database contained 3550 benchmarks, with a strong density in the areas of Ferrara and Ravenna, and a total of about 10000 heights. When the database program is started, the initial screen illustrated in Figure 3 appears. As can be observed, the database was planned with the precise aim of maintaining the consultation of the files separate from the updating procedure. This agrees with the common practice for databases of distinguishing between the users who may only consult the data and those who instead administer the system and can access the files for updating by the introduction of a personal identification number.

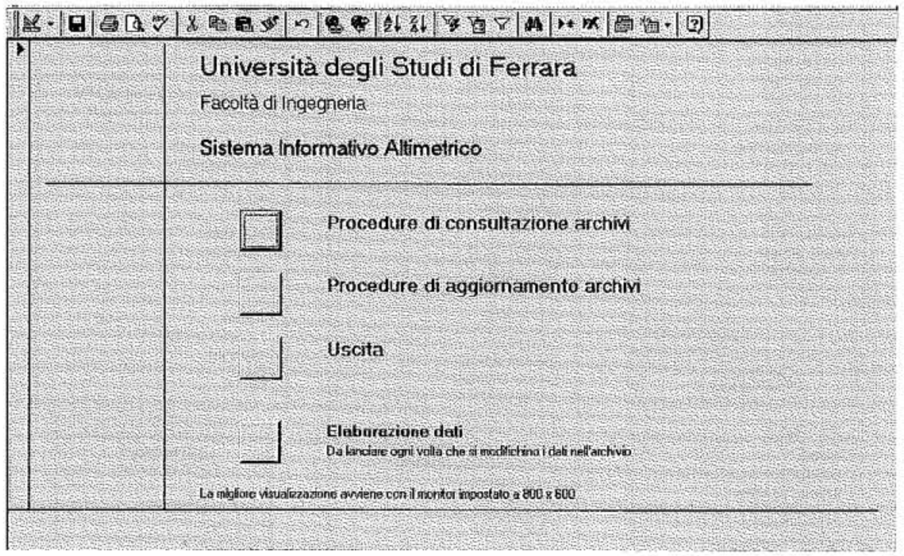

Figure 3. Startup screen of the database.

The "Procedure of updating the files" allows the introduction of new data or the modification of existing data relative to the tables: "benchmarks", "heights", "levellings" and "bibliography". In each case, to introduce new data or to modify existing data, it is necessary to proceed by means of a search screen (Figure 4) which performs a "query" on the basis of the "name" and "subname" of the benchmark and/or of its coordinates. This query is useful both to search for an already stored benchmark and to introduce a new one. It allows the user to verify that the new information is not already present in the file. For this search, it is necessary to type in a pair of cartographic coordinates and a capture radius (100 m is the default). The query searches for and highlights all the benchmarks located within the circular area with the pair of coordinates at its center and with a radius equal to the selected capture radius.

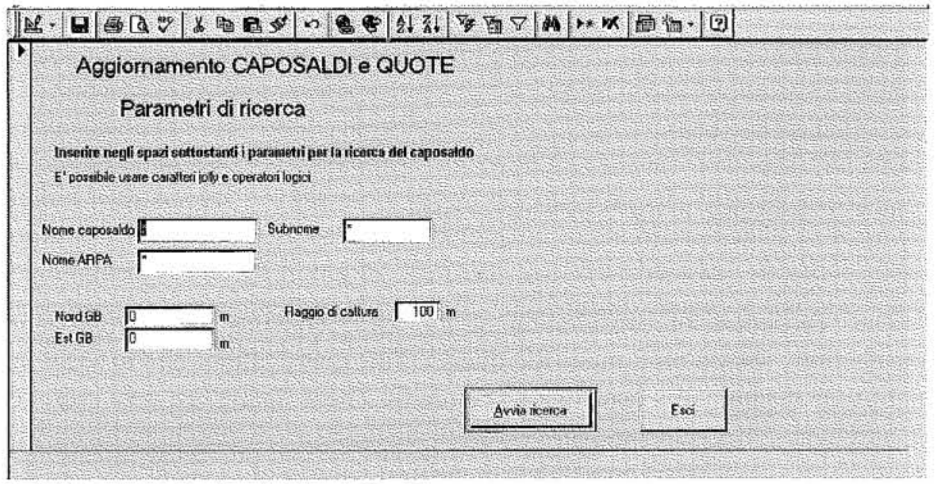

Figure 4. The start of the updating procedure proceeds by means of a search screen which allows one to recall the data to be modified, as well as to verify that a benchmark is not already in the file.

The "Procedure of consultation of the files" allows only consultation of the tables: "benchmarks", "heights", "levellings" and "bibliography". As in the procedure of updating, the consultation takes place by means of an initial search screen in which the user can introduce the name of the benchmark, the subname or its coordinates with an appropriate capture radius. The result of a consultation for benchmarks is shown in Figure 5.

Using the "Access" commands, it is possible to perform simple interrogations such as:

1. all the benchmarks that belong to the same levelling line;
2. all the horizontal benchmarks located within the same municipality;
3. etc.

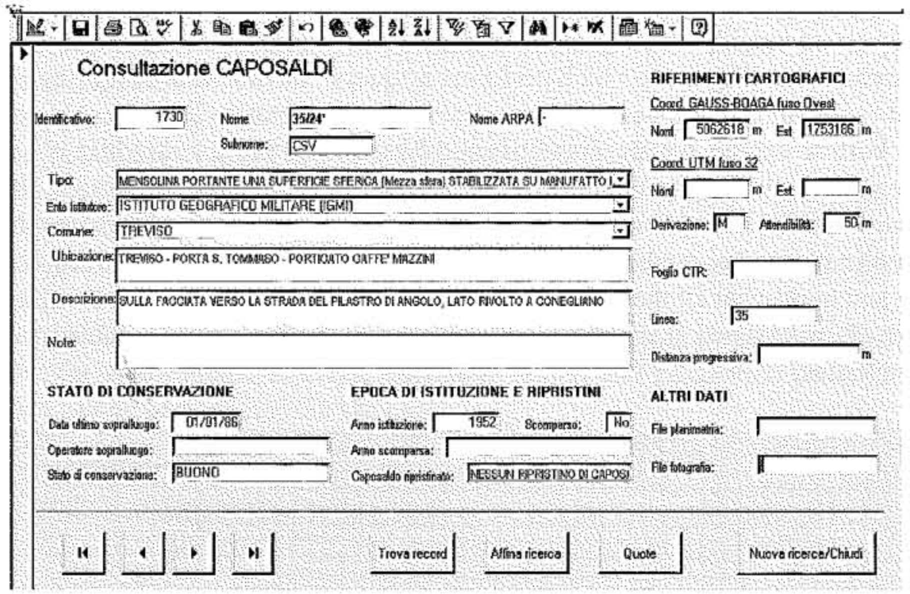

Figure 5. Consultation of the "benchmarks" table.

The "Procedure of consultation of the files" contains the "Height-Time Consultation" (based on a multi-file query). This query allows one to view the height-time diagram of a benchmark (Figure 6). These figures are very useful in the editing phase: an increasing trend of the height-time diagram of a benchmark almost always indicates a gross error in the introduction of the data.

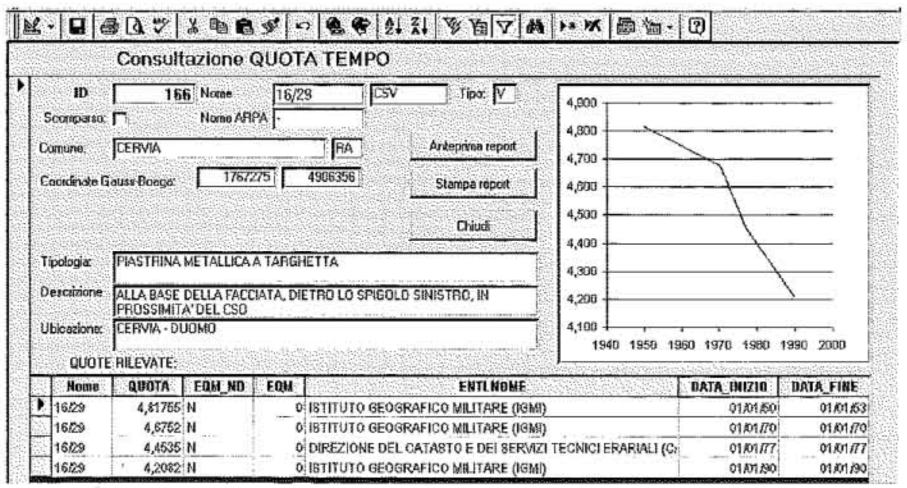

Figure 6. Height-time diagram of a stored benchmark.

3. THE INFORMATION SYSTEM

To allow rapid viewing of the interrogations, the database is connected to GIS software. Within the ambit of "user friendly" GIS, we chose the ArcView release 3.1 system. However, with this GIS (as with most systems of this category), it is not possible to make multi-file queries without first building ad hoc tables for each interrogation. This involves a redundancy of the data. Thus we adopted the following solution:

- maintain the database in the Access 97 platform;
- connect the Access file to the ArcView GIS.

ArcView can be connected to an external database through the ODBC driver; this driver makes it possible to create a DSN (Date Source Name), i.e. a source of data made available for other applications. Thus, with both applications open (Access and ArcView), it is possible to perform the interrogations in Access 97 and view the results in ArcView by means of a simple "refresh" of the table connected to the video page of ArcView. This allows one to maintain the consultation of the files with ArcView separate from the database managed and administered with Access 97. Figure 7 shows the result in ArcView of a query performed in Access 97: "Benchmarks belonging to the Municipality of Ravenna" (highlighted in black). It can be seen that the "Benchmarks" vectorial entities have been superimposed on a geo-referenced raster image of the map (scale 1:250000) of the Region of Emilia-Romagna.

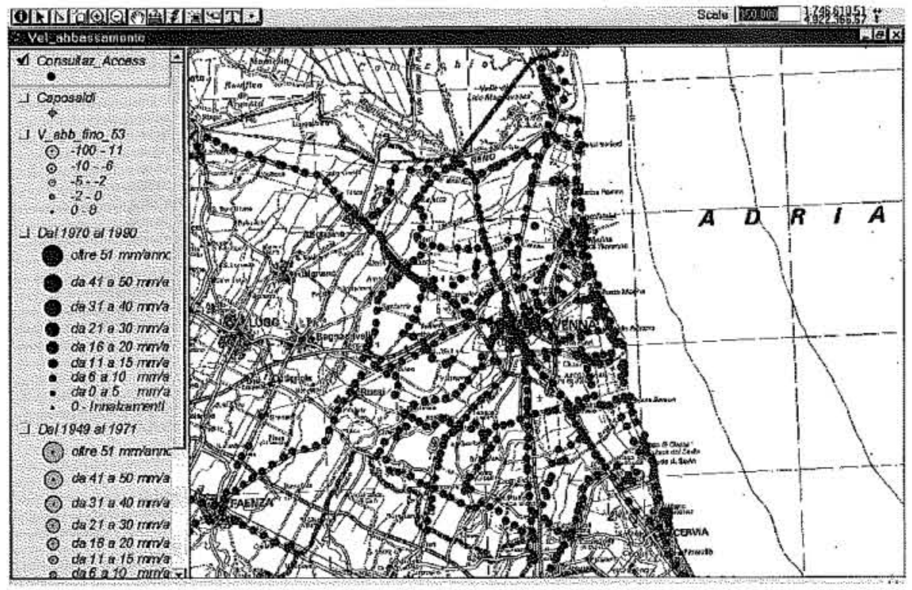

Figure 7. Viewing in ArcView of the Access query "Benchmarks belonging to the Municipality of Ravenna".

With the ArcView software, we subsequently created a series of thematic maps, resulting from some of the many analyses that can be performed on the available data. For example, we calculated the speed of lowering of the benchmarks in a given period of time. The choice of the time intervals was based on an analysis of the periods of the measurements present in the database and on the currently available information about the speed of subsidence. The selected periods were: up to 1953; from 1953 to 1971; and from 1971 to 1990. For each period, we selected the benchmarks with at least two height values in the file (there can be even three or more values within a given period). With these data, we calculated the least squares regression line; the speed of lowering was assumed to be the value of the angular coefficient of the regression line. At this point, the data for the speed of lowering of the benchmarks were used to create extremely interesting thematic maps in ArcView (one for each time period). The maps for the period 1971-90 are shown in Figure 8: in the figure, the benchmarks are represented by circles whose diameters are proportional to the speed of lowering.

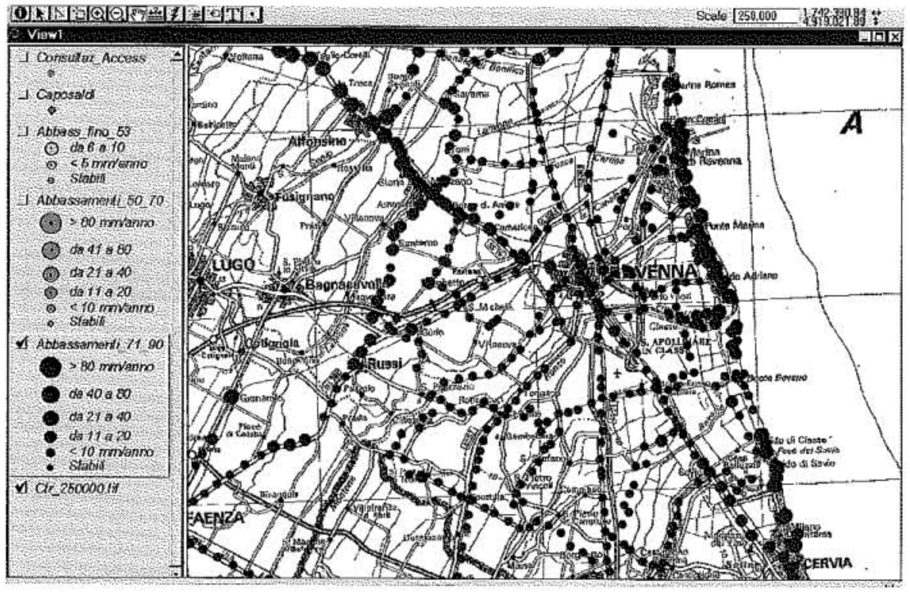

Figure 8. Thematic maps created with ArcView. "Speed of lowering in the period 1971-90"; the benchmarks are represented by circles whose diameters are proportional to the speed of lowering.

4. MULTIMEDIA PLAN FOR THE INFORMATION SYSTEM

The multimedia plan for the Information System foresees the possibility of sharing the system as a resource in a local network and in an Intranet/Internet

(WWW) environment. In this way, it will be possible to access the Information System from the outside to consult some of the main interrogations and processing performed with the system.

The plan involves an interaction between an HTTP server and the GIS according to the "off line" scheme (Fortunati et al., 1998), i.e. the data available to the external user will be present on an HTTP server (Figure 9). The data will first be prepared in the GIS environment and then translated for the Internet environment.

The external user will interrogate the HTTP server without interacting directly with the geographic server containing the real Information System. In this way, there will not be a dynamic interaction between the System and the outside. The external user is thus limited to performing a minimum number of actions decided a priori. However, there will be:

a) an advantage with regard to the preservation and security of the data, essential in the case of access to information that is reserved and protected by copyright laws;
b) a decrease of the waiting times for consultation of the System.

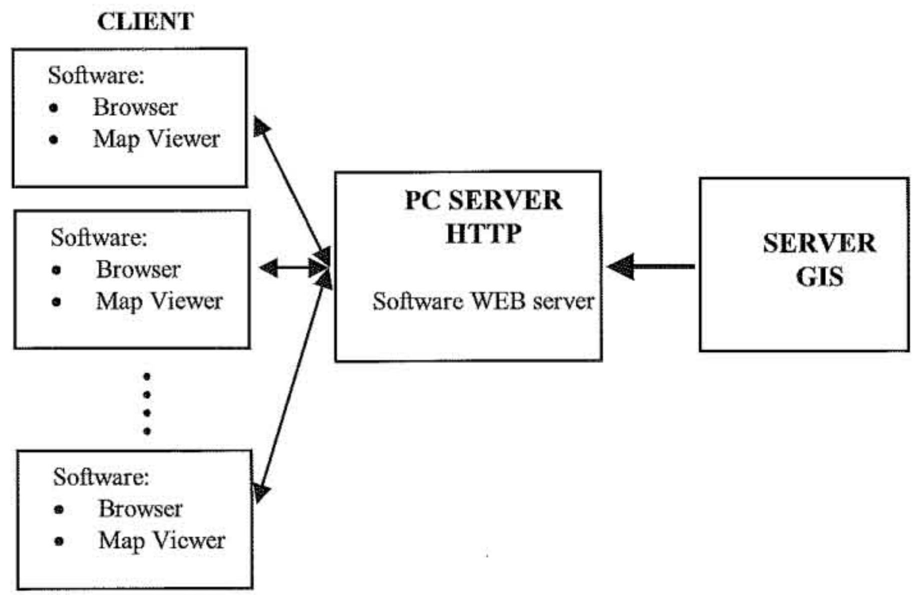

Figure 9. Scheme of the Multimedia Information System.

Moreover, in the first phase of the multimedia plan, the data that can be consulted by external users will be limited to:

- the height-time diagrams of the benchmarks present in the database;
- the thematic maps created with the Information System;
- the metadata;

In conclusion, the phases of the multimedia plan will be:
1. creation of a database, thematic maps and metadata to be shared in a network;
2. their input to an HTTP server system of the Department of Engineering, University of Ferrara;
3. consultation from the outside via Internet using a standard WEB browser.

Acknowledgments

The authors thank:
- the Regional Agency for Prevention and the Environment of Emilia Romagna and the Municipality of Ravenna for providing us with part of the material used for the construction of the database;
- Dr. Luca Leonelli for his collaboration in the creation of the Information System.

REFERENCES

Bondesan M., Gatti M., & Russo P. (1997) Carta Altimetrica e dei Movimenti Verticali del Suolo, Ministero dell'Università e della Ricerca Scientifica e Tecnologica. Editore SELCA, Firenze, 1997.

Fortunati L., Cresci G., & Demontis R., (1998) La distribuzione via rete dell'informazione geografica, in *Atti del 2° Convegno Nazionale ASITA*, Bolzano, 1998, volume 2, pp. 51-56.

Gatti M., & Russo P. (1995) Land subsidence in Po river valley. In: *Land Subsidence,* Proc. 5th Int. Symp. on Land Subsidence, (ed. by B.J. Barends et al.), A.A. Balkema, pp. 149-157.

LAND SUBSIDENCE - Vol. II
Proceedings of the Sixth International Symposium on Land Subsidence
Ravenna / Italy / 24-29 September 2000

FIRST RESULTS OF SUBSIDENCE MEASUREMENTS WITH THE WIDE-ANGLE AIRBORNE LASER RANGING SYSTEM

Olivier Bock
CNAM / Ecole Supérieure des Géomètres et Topographes, Le Mans, France

Christian Thom and Michel Kasser
IGN / Lab. d'Optoélectronique et de Microinformatique, Saint-Mandé, France
IGN / Laboratoire de Recherche en Géodésie, Saint-Mandé, France

Abstract

The first aircraft experiment with the Wide-Angle Airborne Laser Ranging System has been conducted in May 1998 over a small network of 1 km², equipped with 64 retroreflectors. The ranging system was operated from the French research aircraft ARAT at an altitude of 1 km, during two 4-hour flights. The paper describes the data processing method and presents the first results from this experiment. A precision of 2 cm in differential vertical coordinates has been achieved from two sets of 3000 distance measurements. This moderate precision is mainly due to severe data sorting for outliers in the distance measurements. These arose from the strong overlap of reflected echoes, a result of the high retroreflector density. In addition, the overall number of measurements was relatively small. However, the results are consistent with simulations and a posteriori covariance. Higher precision is predicted for future experiments, after the instrumental link budget will be improved.

Keywords: laser ranging, relative height measurement, aircraft experiment.

1. INTRODUCTION

A new geodesy technique has been developed at the Institut Géographique National (IGN), France, for the quick (a few hours) and accurate (a few millimeters) monitoring of land subsidence in networks covering areas of 1–100 km², with a number of benchmarks of between 50 and 400 (Bock et al. 1995, 1998a). Specifically, the technique might be useful for surveying land subsidence due to fluid withdrawal or solid extraction (Fourmaintraux, 1994). Such measurements would considerably add to the understanding and numerical modeling of compaction owing to mineral extraction (Dingwen, 1989, Bertoni *et al.*, 1995) and possibly estimating the spatial extension of reservoirs, in order to increase hydrocarbon field production (Bouteca, 1990).

The technique is also intended to measure geodynamic processes producing small vertical displacements, such as tectonic motion, volcano deflation and geological instability. The magnitude of these deformations is between the 0.1 mm and 10 cm for periods between days and years (Christodoulidis et al., 1985).

This technique is based on the measurement of simultaneous pseudo ranges (PRs) between an aircraft and ground-based benchmarks (cube-corner retroreflectors, CCRs), which allow for the adjustment of both benchmark and aircraft coordinates, according to the multilateration principle (Seeber, 1993). These measurements are achieved by laser ranging, based on a specific instrument, the Wide-Angle Airborne Laser Ranging System (WA-ALRS), see Figure 1. This principle has been inspired from airborne and spaceborne geoscience laser ranging systems, though their instrumental implementations were quite different (Kahn, 1980, 1982; Cohen, 1987). The specificity of the WA-ALRS is to use a widely divergent laser beam, producing a large beam pattern on the ground (Bock et al. 1999a). For any laser pulse transmitted by the laser, several CCRs provide thus echoes which are recorded by the system (see upper right angle of Figure 1).

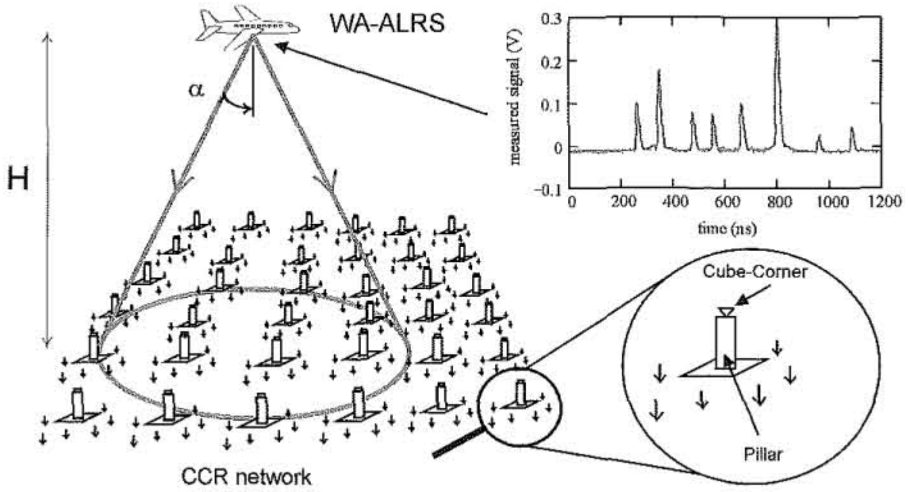

Figure 1. View of the WA-ALRS operated over a network of CCRs.

The technique has been first assessed in a ground-based experiment, in 1995. There, uncertainties in relative radial coordinates as low as 1 mm have been achieved (Bock et al. 1998a, 1999a). These results were consistent with a covariance analysis from both experimental data and numerical simulations, taking the specificity of the experiment into account.

Numerical simulations have been performed, for assessing the ultimate accuracy in aircraft experiments (Bock, 1999b). It has been shown that the accuracy can be optimized, to the first order, as a function of instrument performance, the number of laser shots and the network size. Laser beam divergence, aircraft altitude and CCR density were only second order parameters, provided the number of echoes per laser shot was of 10–20. An accuracy in the vertical of about 1 mm has then been predicted, assuming a signal to noise ratio (SNR) of 50 at nadir, an aircraft altitude of h = 10 km, a laser beam divergence of $\alpha = 20°$, a network size of A_{Net} = 10 × 10 km², with N_{CCR} = 100 CCRs and a number of measurements per CCR of $N_{Meas/CCR} = 5\times10^3$.

The first aircraft experiment has been conducted in 1998 with the aim of validating the aforementioned simulation predictions and further assess the accuracy of the technique.

The specific configuration of this experiment is described in section 2. Estimation algorithms for the processing of these data are outlined in section 3. Results are given and discussed in section 4, in terms of positioning accuracy achieved between two complete surveys of the network. Finally, in section 5, the possibilities for improving the technique for future test experiments and / or field experiments is addressed.

2. AIRCRAFT EXPERIMENT DESCRIPTION

The first aircraft experiment has been conducted over the air base of Crucey, France. For this experiment, it was decided to install between 6×6 and 10×10 CCRs over the 1-km² area available for the network. The separation between CCRs, Δx , was thus necessarily small and likely to lead to many echo superposition in the measured signal (see Figure 3). For reducing this effect, the photodetector and amplifier have been modified to diminish the overall impulse response of the detection stage, see (Bock et al. 1998b).

The instrument's SNR was also much below the above-mentioned ideal configuration of SNR = 50, h = 10 km and α = 20 °. The SNR of the modified detection stage was estimated to be about 30 at h = 1 km and α = 20 °. This imposed thus a rather low flight altitude. Additionally, α is limited, in practice, to ~ 25 °. It is difficult to achieve a stronger divergence while maintaining a reasonable beam diameter at the exit of the optics, which is required for keeping the detector within the diameter of the return beam pattern (~ 12 cm for a 6-cm diameter CCR).

The network size, instrument SNR and response time being fixed, parameters h, α and Δx had to be optimized before the experiment for achieving the highest positioning precision in the vertical component, σ_z. This precision is difficult to predict from system parameters alone. The optimization was thus performed by numerical simulations according to the methodology presented in (Bock 1999b). The results of the optimization suggested configurations around h = 1–1.5 km, α = 15–20°, and Δx = 150–175 m, assuming outlier-test thresholds of $t_{\Delta R}$ = 2 m, $t_{J/N} = \infty$ and t_{SD} = 0.3 m (see section 3 for the definition of these thresholds).

The actual experiment has been conducted over a network of 8×8 CCRs of 6-cm diameter, with a separation of Δx = 150 m. A priori CCR positions have been surveyed by kinematic-type GPS with an accuracy of ~5 cm. Two 4-hour flights have been conducted with the Avion de Recherche Atmosphérique et de Télédétection (ARAT), the French aircraft for atmospheric research and remote sensing of CNES/IGN/INSU. Each flight was composed of 5 series of 6 parallel legs oriented in two perpendicular directions (see Figure 2a). The aircraft's trajectory was measured by D-GPS with single-frequency receivers (Sercel NR-103), but its attitude was not measured. The positioning error of trajectography-type GPS can be modeled by a ~5 cm random component and a ~1 m short term bias (see Bock et al. 1998a).

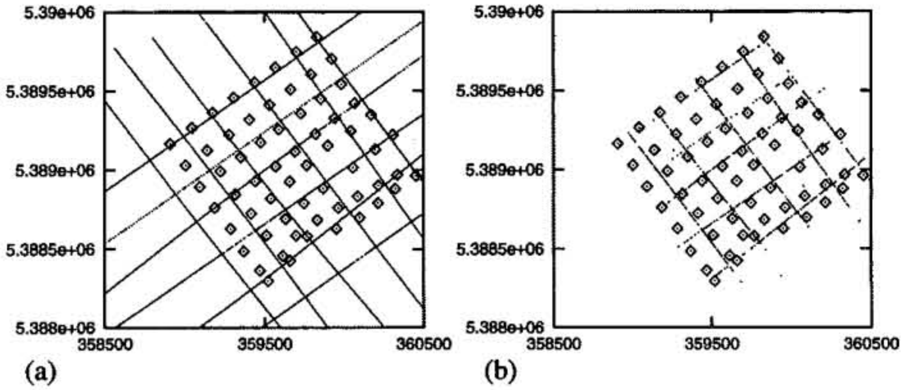

Figure 2. View of the aircraft trajectory over the network (diamonds represent CCRs). (a) for all the laser shots during 12 flight legs, (b) for only the laser shots retained after data sorting.

The focal point of the transmitted laser beam was located some 10 m toward the tail of the aircraft and 2 m beneath. This offset was corrected in the a priori data processing, assuming the aircraft was in uniform translation during data acquisition. However, small accelerations and steering of the aircraft introduced some uncertainty on the location of the focal point due to attitude changes. As we shall see, this will a have some consequence on the parametrization and convergence of estimation algorithms. This effect will be referred to as the attitude effect in the following.

The two flights have been made with legs at h = 1- and 1.3-km altitudes (above ground level) and α = 15 - 20 ° laser beam divergences. Data have been collected during 3 hours for each flight. Typical signals achieved in this experiment are shown in Figure 3. Unfortunately, most of the measurements produced superimposed echoes. This effect, combined with the attitude effect, implied the implementation of the robust deconvolution algorithm described in section 3.

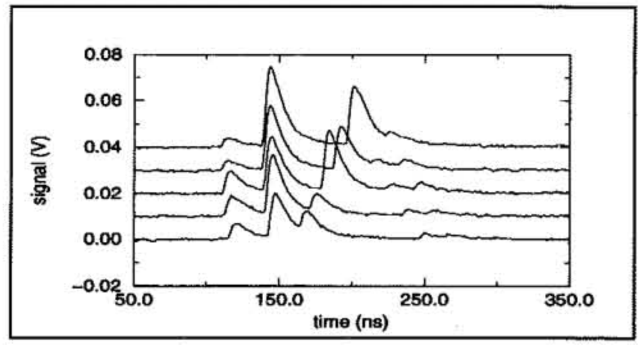

Figure 3. Consecutive signals, at = 1 km and = 20 °, offset by 10 mV each, for clarity.

3. ESTIMATION ALGORITHMS

3.1 Signal deconvolution

With the WA-ALRS, for any laser shot (LS), the incoming signal is composed of echoes (optical pulses) with amplitudes a_i and pseudo times of flight, $\tau i + \tau_0$, where τ_0 is a random pseudo-range offset (PRO) and subscript i refers to a particular CCR. The optical signal is converted into an electrical signal in which the pulse waveform is assumed known. The signal is measured with an additive electronic noise and a low-frequency background signal (due to Rayleigh and Mie back-scattering), which is simply modeled by an offset and a slope, z_0 and z_1, respectively.

The digital signal, **x**, is modeled by **f(p)**, where **p** is the vector of parameters for the model, composed of all τ_i and a_i, with $i = 1,\ldots,N_{CCR}$, τ_0 , z_0 and z_1 . The model also includes an a priori correction for the optical path delay, calculated from measurements of atmospheric pressure both at the aircraft and the ground. This latter correction is, however, not critical since only differential times of flight need be corrected (Bock et al. 1999b).

The solution for **p** is obtained by minimizing the misfit function

$$J(\mathbf{p})=[\mathbf{x}-\mathbf{f}(\mathbf{p})]^T \mathbf{C}_{nn}^{-1}[\mathbf{x}-\mathbf{f}(\mathbf{p})]+[\mathbf{p}-\mathbf{p}_0]^T \mathbf{C}_{pp}^{(prior)^{-1}}[\mathbf{p}-\mathbf{p}_0] \quad (2)$$

where $\mathbf{C}_{nn} = \mathbf{I}\sigma^2_n$ is the covariance matrix associated to the noise, with σ^2_n its variance and **I** the identity matrix, $\mathbf{p}_0$ an a priori solution for **p** and $\mathbf{C}_{pp}^{(prior)}$ its covariance matrix. Pseudo-ranges are calculated from $\hat{\mathbf{p}}$, the solution for **p** , by $\rho_i = (\hat{\tau}_i + \hat{\tau}_0) \times c/2$, where c is the speed of light in vacuum.

Since **f(p)** is not linear in **p** , and the uncertainty in $\mathbf{p}_0$ is relatively high, as discussed in section 2, an iterative quasi-Newton method is implemented as a non-linear algorithm for the minimization of the misfit function (Tarantola 1987). The convergence of the algorithm is checked by the condition $J(\mathbf{p}_{k+1}) < J(\mathbf{p}_k)$, and a relaxation coefficient is applied when necessary. At each step, the solution is calculated by a Cholesky method.

The variable $J(\mathbf{p})$ theoretically follows a χ^2 distribution with a number of degrees of freedom equal to the number of samples, N, in the digital signal. For $N = 10^3$, $J(\mathbf{p})$ tends toward a Gaussian distribution, with mean $\mu_J = N$ and standard deviation $\sigma_J = \sqrt{2N}$. Hence, a second convergence test can be performed by rejecting signals for which $J(\mathbf{p}) / \mu_J > t_{J/N}$, where $t_{J/N}$ is a threshold to be adjusted.

3.2 Outlier detection tests

Data sorting is a critical step, during which outliers in PR estimates are detected before these estimates are used for solving the multilateration problem. Outliers are mainly due to pulse superimposition in the signal which arise when echoes from different CCRs are coincident on the detector. Several tests have been described in (Bock et al. 1998a) for the detection of outliers, which had to be refined for processing the present data.

For each laser shot, the a posteriori covariance matrix for $\mathbf{p}$, $\mathbf{C}_{pp}^{(post)}$, is evaluated. From this matrix, the ranging accuracy, $\sigma_{p,i}$, and the degree of correlation between echoes, $\gamma_{i,j}$, are estimated. PRs verifying $\sigma_{p,i} \leq \tau_\sigma$, $\gamma_{i,j} \leq t_\gamma$ and $a_i \leq t_a$ are considered as valid. Typical values for these thresholds are $t_\sigma = 10$ cm, $t_\gamma = 40$ % and $t_a = 3 \times \sigma_n$.

Since outliers are most probable when echoes are nearly coincident, a test is made on their closeness. For each laser shot, the differences in distance between the reference point in the aircraft and CCRs, ΔR_i, are evaluated. PR estimates for which $\Delta R < t_{\Delta R}$ are rejected. Typically, $t_{\Delta R} = 1$–3 m.

Laser shots for which the number of PR estimates having passed the previous tests, $N_{Meas/LS}$, is below $t_{Meas/LS}$ are rejected. These contribute only weakly to the estimation of CCR coordinates. Typically, $t_{Meas/LS} = 3$ or 4.

An additional test is performed in which the standard deviation (SD) in a priori PR residuals (difference between measured an a priori values for ρi), is evaluated. When SD is above a threshold, t_{SD}, the laser shot is rejected. Typically, $t_{SD} = 0.1$–0.3 m.

3.3 Coordinate estimation

The coordinate estimation algorithm has been extensively described in (Bock et al. 1998a; Bock 1999b). Only small modifications have been brought to that

algorithm. They were mainly the adjunction of one offset parameter in aircraft coordinates per leg, and an overall offset in PR data (discussed in section 3.1). These parameters are well constrained since individual legs contain up to 300 PR measurements.

In order to take the attitude effect into account, the a priori uncertainty, $\sigma_{\mathrm{V}}^{(prior)}$, in aircraft coordinates, $\mathbf{V}_j$, has simply been increased. Numerical simulations showed that this effect could be compensated with $\sigma_{\mathrm{V}}^{(prior)} = 0.25$ m, while the use of $\sigma_{\mathrm{V}}^{(prior)} = 5$ cm, as in previous experiments, would produce biases in CCR coordinates of 10–15 cm.

Numerical simulations based on the experimental data, after outlier detection (illustrated in Figure 2b), have shown that X and Y components of CCRs were not well constrained, due to the relatively small values for $N_{Meas/LS}$. Consequently, these components were fixed ($\sigma_{\mathrm{X}}^{(prior)} = \sigma_{\mathrm{Y}}^{(prior)} = 0.1$ mm). This procedure is, in fact, not very restrictive for the assessment of the technique since the goal is to achieve accurate estimates of vertical coordinates. The positioning accuracy in Z predicted from these numerical simulations was $\sigma_Z = 2$ cm for $N_{Meas} = 1.2 \times 10^3$, with $\sigma_{\mathrm{Z}}^{(prior)} = 5$ cm, $t_{\Delta R} = 1$ m, $t_{J/N} = 1.3$ and $t_{SD} = 1$ m.

4. RESULTS

For the processing of the experimental data, a priori uncertainties have been fixed to the values given in section 3.3. Additionally, the mean and random errors in aircraft position are set to $\sigma_{\mathrm{W_0}}^{(prior)} = 3$ m and $\sigma_{\mathrm{V}}^{(prior)} = 0.25$ m, respectively, and uncertainty in PRO to $\sigma_{\mathrm{b_0}}^{(prior)} = 0.5$ m. The four CCRs at the corners of the network were also fixed ($\sigma_{\mathrm{Z}}^{(prior)} = 0.1$ mm) for defining a reference frame in which the solutions from different surveys could be compared.

Data sorting thresholds $t_{\Delta R}$, $t_{J/N}$ and t_{SD} have been adjusted by trial, in order to achieve consistency between the theoretical accuracy in differential Z, $\sigma_{\Delta Z}$, and the observed RMS $\hat{\sigma}_{\Delta Z}$, along with a mean error $\hat{\mu}_{\Delta Z} \approx 0$. The two solutions of the differential have been obtained each from a one-flight data set. The threshold on N_{Meas} was $t_{Meas/LS} = 3$.

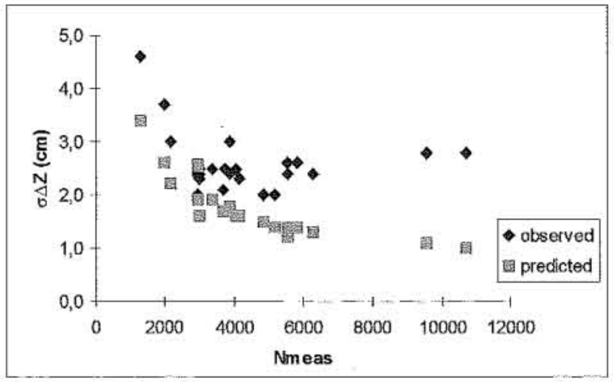

Figure 4. Observed RMS and theoretical accuracy in relative Z coordinates, obtained from two flights, for different data sorting thresholds.

Figure 4 shows the positioning accuracy as a function of the average N_{Meas} over the two flights. Each point corresponds to one particular combination of data sorting thresholds $t_{\Delta R}$, $t_{J/N}$ and t_{SD}. One can see that in most cases, $\hat{\sigma}_{\Delta Z} > \sigma_{\Delta Z}$. Starting on the right end of the figure, where $N_{Meas} \sim 11{,}000$, and scanning to region where $N_{Meas} \sim 3000$, one can see that $\hat{\sigma}_{\Delta Z}$ remains roughly constant. This behavior is characteristic of outlier rejection. Around $N_{Meas} \sim 3000$, $\hat{\sigma}_{\Delta Z} \approx \sigma_{\Delta Z}$ and $\hat{\mu}_{\Delta Z} \approx 0$ (see Table 1), where the best threshold parameterization seems attained. For the cases where $N_{Meas} < 3000$, $\hat{\sigma}_{\Delta Z}$ is again greater than $\sigma_{\Delta Z}$, but there it is suspected that the problem becomes ill-conditioned (too few measurements available).

Table 1 gives more details of results achieved for some of the data sorting threshold combinations of Figure 4. One can see that in most cases where $\hat{\sigma}_{\Delta Z} > \sigma_{\Delta Z}$, $\hat{\mu}_{\Delta Z} \neq 0$. The mean number of measurements per laser shot and per CCR are relatively small. As a consequence, the positioning accuracy was only at the one-cm level, and aircraft trajectory offsets and PRO were only determined on the decimeter level.

Table 1. Average results in differential Z coordinates, from two flights, as a function of data sorting thresholds.

$t_{\Delta R}$, $t_{J/N}$, t_{SD}	$\overline{N}_{Meas/LS}$	$\overline{N}_{Meas}$	$\overline{N}_{Meas/CCR}$	$\hat{\mu}_{\Delta Z}$	$\hat{\sigma}_{\Delta Z}$	$\overline{\sigma}_{\Delta Z}$
1.0 m, ∞, 0.3 m	5.4	10700	167	1.0 cm	3.1 cm	1.1 cm
1.0 m, 1.33, 0.3 m	5.4	3300	52	0.1 cm	5.3 cm	2.5 cm
1.0 m, ∞, 0.1 m	5.4	5500	86	0.6 cm	2.4 cm	1.4 cm
1.5 m, 1.33, 0.3 m	4.8	2200	34	-0.1 cm	4.7 cm	2.9 cm
1.5 m, ∞, 0.1 m	4.8	5200	81	0.6 cm	2.0 cm	1.4 cm
2.0 m, 2.0, 0.3 m	4.2	3800	59	0.7 cm	3.2 cm	1.8 cm
2.0 m, 4.0, 0.2 m	4.2	5800	91	1.2 cm	2.6 cm	1.2 cm
2.0 m, ∞, 0.1 m	4.2	4100	64	0.3 cm	2.3 cm	1.6 cm
2.5 m, ∞, 0.2 m	3.8	4100	64	-0.3 cm	2.6 cm	1.6 cm
2.5 m, ∞, 0.15 m	3.8	3700	58	0.0 cm	2.1 cm	1.7 cm
2.5 m, ∞, 0.1 m	3.8	3000	47	0.1 cm	2.1 cm	1.9 cm

The best results have been obtained with $t_{\Delta R} = 2.5$ m, $t_{J/N} = \infty$ (no test) and $t_{SD} = 0.1$ m. The values for these parameters show that the best outlier test is achieved by detecting high standard deviations in a priori PR residuals ($t_{SD} = 0.1$ m) and nearly coincident echoes ($t_{\Delta R} = 2.5$ m). This reveals that though the deconvolution algorithm has been modified, it does not allow for the separation of echoes closer than 2.5 m. The fact that the test on J/N was not necessary ($t_{J/N} = \infty$) can be explained by the effectiveness of the two other tests and the need for maximizing the data set for achieving a high positioning accuracy. However, the number of measurements was still relatively small ($\overline{N_{Meas/LS}} = 3.8$ and $\overline{N_{Meas/CCR}} = 47$). The positioning accuracy was thus of ~ 2 cm on differential vertical coordinates.

A normality test has also been performed on the histogram of weighted coordinate differences, $\Delta Z / \sigma_{\Delta Z}$. It was fairly Gaussian, with a mean value of 0.08 and a standard deviation of 1.2 (see Figure 5). Hence, it can be concluded that no outliers remained in this sorted data set.

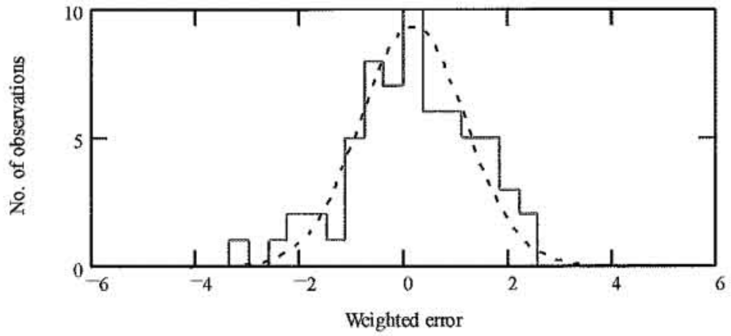

Figure 5. Histogram of weighted coordinate differences (solid line) vs. zero-mean, unity-variance, Gaussian distribution (dashed line).

5. DISCUSSION

The moderate vertical positioning accuracy (1.4 cm in single shot) achieved in this aircraft experiment is mainly a result of possible estimation algorithm limitations, and certainly of the severe data sorting for outliers. Outliers were suspected as a result of a high uncertainty in aircraft coordinates, a small CCR separation and a low SNR.

Further improvement of estimation algorithms might be obtained by the combination of both estimation procedures (pseudo-ranges and coordinates). This should improve the convergence of the signal deconvolution and limit the CCR misidentification since updated CCR and aircraft coordinates would be used for the calculation of a priori times of flight. In that case, assuming that the threshold parameterization of row # 1 in Table 1 would be appropriate, the positioning accuracy would be increased to $\overline{\sigma_{\Delta Z}} = 1.1$ cm in differential vertical coordinates, or $\overline{\sigma_Z} = 7.8$ mm in single shot.

A reduction of the a priori uncertainty in aircraft coordinates might be achieved by a reduction of the distance between the GPS antenna and the laser-beam focal point onboard the aircraft, or measuring the aircraft attitude with an inertial measurement unit. These recommendations should be followed for future experiments. Hence, setting $\sigma_V^{(prior)} = 0.05$ m in row # 11 would lead to $\overline{\sigma_{AZ}} = 1.6$ cm, i.e. an improvement of about 16 %. In addition, processing D-GPS data in kinematic mode might also allow for a reduction in $\sigma_V^{(prior)}$.

As concerns the configuration of the experiment, especially the CCR separation, it was concluded from numerical simulations that the actual configuration was nearly optimal. However, these numerical simulations predicted a slightly better positioning accuracy than achieved here: 4.3 mm vs. 7.3 mm for $N_{Meas} = 14200$. This small discrepancy reveals that the simulated SNR was slightly overestimated (by a factor of about 1.7) with respect to the actual SNR of the instrument.

Improvement of the SNR is the only way for reaching the goal of millimeter positioning with the WA-ALRS. A promising solution is presently investigated, based on the use of a large-area avalanche photodiode (Advanced Photonix Inc.) followed by a transimpedance amplifier. It seems that the SNR might be increased by a factor of 20–25, while the response-time would be only slightly modified. This would permit to achieve the 1-mm accuracy expected for the technique. The design of a new detection stage should be finalized during spring 2000. A second aircraft experiment is already planned for summer 2000, as a final validation of the technique.

The next application of the technique will be with subsidence monitoring of the Piton de la Fournaise volcano in the French island of La Réunion, during the 2001-2002 period. Other applications like surveying of land subsidence due to fluid withdrawal or solid extraction are still of high consideration. Therefore, partners are welcome for defining demonstration experiments.

REFERENCES

Bertoni, W., Brighenti, G., Gambolati, G., Ricceri, G., & Vuillermin, F. (1995) Land subsidence due to gas production in the on- and off-shore natural gas fields of the Ravenna area, Italy. In: *Land Subsidence* (ed. by F. B. J. Barends, F. J. J. Brouwer & F. H. Schröder), Proc. 5th Int. Symp. on Land Subsidence, The Hague, The Netherlands, IAHS publ. N. 234, 13-20.

Bock, O., Thom, C., Kasser, M., & Fourmaintraux, D. (1995) Development of a new airborne laser subsidence measurement system, aiming at mm-accuracy. In: *Land Subsidence* Proc. 5th Int. Symp. on Land Subsidence (ed. by F. B. J. Barends, F. J. J. Brouwer & F. H. Schröder), Balkema, 113-122.

Bock, O., Thom, C., Kasser, M., & Pelon, J. (1998a) Study of a wide angle laser ranging system for relative positioning of ground-based benchmarks with millimeter accuracy. *J. Geod.*, **72**(7/8), 442-459.

Bock, O., Kasser, M., & Thom, C., (1998b) First aircraft experiment with the WA-ALRS. In: *Proceedings of the 11th International Workshop on Laser Ranging Instrumentation* (ed. by W. Schlüter, U. Schreiber & R. Dassing) Bundesamtes für Kartographie und Geodäsie, Franckfurt, 1999, 761-767.

Bock, O., Thom, C., Kasser, M., & Pelon, J. (1999a) Multilateration with the wide angle laser ranging system: ranging performance and first ground-based validation experiment. *IEEE Trans. Geosci. Remote Sensing*, **37**(2), 739-747.

Bock, O. (1999b) Multilateration with the wide-angle airborne laser ranging system: positioning precision and atmospheric effects. *Appl. Opt.*, **38**(15), 3343-3359.

Bouteca, M.J., Fourmaintraux, D., & Meimon, Y. (1990) In situ measurements and numerical modeling of the reservoir compacting and surface subsidence. In: *Proceedings of the European Oil and Gas Conference* (ed. by G. Imafiso, M. Frias, J..M Bentgen), Graham and Totman, 127-135.

Christodoulidis, D.C., Smith, D.E., Kolenkiewicz, R., Klosko, S.M., Torrence, M.H., & Dunn, P.J. (1985) Observing tectonic plate motions and deformations from satellite laser ranging. *J. Geophys. Res.*, **90**, 9249-9263.

Cohen, S.C., Degnan, J.J., Bufton, J.L., Garvin, J.B., & Abshire J.B. (1987) The geoscience laser altimetry/ranging system. *IEEE Trans Geosci Remote Sensing*, **25**, 581-592.

Dingwen, L. (1989) Some general problems of the interpretation of geodetic deformation data. In: *Proceedings of the IAG: Global and regional geodynamics* (ed. by P. Vyskocil, C. Reigber & P.A. Cross), Springer, 369-375.

Fourmaintraux, D., Flouzat, M., Bouteca, M.J., & Kasser, M. (1994) Improved subsidence monitoring methods. In: *International Symposium of the SPE-ISRM, Eurock'94*. Balkema, 549-556.

Seeber, G. (1993) *Satellite geodesy : foundations, methods and applications*. De Gruyter, 531 pp.

Tarantola, A. (1987) *Inverse problem theory. Methods for data fitting and model parameters estimation.* Elsevier, 613 pp.

DIFFERENTIAL SAR INTERFEROMETRY FOR LAND SUBSIDENCE MAPPING IN BOLOGNA

Tazio Strozzi and Urs Wegmüller
Gamma Remote Sensing, Thunstrasse 130, 3074 Muri BE, Switzerland

Gabriele Bitelli
DISTART, University of Bologna, Viale Risorgimento 2, 40136 Bologna, Italy

Abstract

This paper reports on the application of differential SAR interferometry to the monitoring of land subsidence in Bologna. Two time series of ERS SAR data from May 1992 to July 1993 and from June 1997 to August 1998, respectively, are analyzed. The comparison of the two subsidence maps shows a decrease of the subsidence velocity from 1992-1993 to 1997-1998. The validation of the subsidence map of 1992-1993 with leveling surveys performed in 1987 and 1992 demonstrates the high accuracy of this new remote-sensing technique. Our investigations allow us to conclude that for the mapping of land subsidence in Bologna ERS differential SAR interferometry presents complementary characteristics to levelling surveys and GPS with regard to cost effectiveness, resolution and accuracy.

Keywords: land subsidence, differential SAR interferometry, Bologna

1. INTRODUCTION

At present, Bologna is one of the most remarkable cases of urban land subsidence in Italy with regard to the extent of the subsiding area and to the velocity of the vertical displacement (Folloni et al., 1996). Land subsidence is induced by ground-water exploitation. The subsidence rate varies in space, with maximum values of 6 to 8 cm/year in the time period from 1983 to 1992. Also the gradient of the movements shows variations in absolute value and direction in some precise areas. One of these sharp gradients is found in the historical center of the city, where damages produced by differential foundations sinking have been detected in several buildings. Considering these negative effects regular monitoring of land subsidence is required. Traditionally, subsidence is measured with levelling surveys. Recently, satellite-based techniques have increased the number of the available measurement methods: GPS's allow the measurement of subsidence in few significant points (Bitelli et al., 2000); differential SAR interferometry is suitable for a monitoring over urban and sparsely vegetated areas (Strozzi and Wegmüller, 1999; Strozzi et al., 1999; Wegmüller et al., 1999). The increasing number of surveying techniques requires a best strategy for their integration in order to perform an accurate, rational and cost effective monitoring.

The question of a convenient use of differential SAR interferometry for land subsidence mapping is addressed in Bologna using time series of Synthetic Aperture Radar (SAR) data of the European remote sensing satellites ERS-1 and ERS-2. The SAR data were used to generate subsidence maps that were examined in terms of spatial resolution, vertical accuracy and temporal frequency. The technical capability of differential SAR interferometry for land subsidence mapping in Bologna was compared to that of levelling surveys and GPS measurements in order to define the characteristics of a monitoring service in which these three surveying techniques are best integrated.

2. ERS SAR DATA AND PROCESSING

Two sets of ERS SAR data were considered: the first one includes six images from May 1992 to July 1993; the second one six scenes from June 1997 to August 1998. With these data sets two independent subsidence maps for the time periods 1992-1993 and 1997-1998 were generated and compared. With both data sets interferograms with very short spatial baselines were selected in order to maximize the coherence over urban areas.

The main processing steps included SAR processing, interferometric processing, subtraction of topographic phase term using 2-pass differential interferometry, adaptive filtering, phase unwrapping, stacking of multiple results in order to reduce atmospheric disturbance, quality control, conversion of the unwrapped phase to vertical displacement per time, geocoding and presentation of the results (Wegmüller and Strozzi, 1998). The stacking of the interferograms was completed taking into account the different time-intervals. An area close to the Appennini by the "Facoltà di Ingegneria" was used as stable reference.

3. LAND SUBSIDENCE IN BOLOGNA IN 1992-1993 AND 1997-1998

Two land subsidence maps of Bologna for the time periods May 1992 – July 1993 and June 1997 – August 1998 were completed and are shown in Figures 1 and 2, respectively. The pixel size of the geocoded products is 25 m. Contour lines of the subsidence velocity are superimposed to a SAR backscattering intensity image. The interpretation of the two figures suggests that the subsidence velocity decreased from 1992-1993 to 1997-1998. In particular to the north of Bologna, where subsidence is more important, the subsidence velocity decreased from maximal values of 5-6 cm/year in 1992-1993 to maximal values of 3 cm/year in 1997-1998. The decrease of the subsidence activity can be attributed to the regulation of the ground-water extraction. The general shape of the subsidence velocity, on the other hand, remained the same and thus the zones that suffer from a strong gradient of the subsidence velocity did not change.

4. VALIDATION WITH LEVELLING SURVEYS

The performance of differential SAR interferometry for land subsidence mapping in Bologna was validated with available levelling data. The current levelling network was established in 1983 by the city and university of Bologna and extends over around 460 km^2, with 455 benchmarks distributed along 375 km (Folloni et al., 1996). The density of the bench marks increases in the direction of the historical center, where the average distance between consecutive points is on the order of 250 m. Leveling surveys were performed in 1983, 1987, 1992 and 1999. Contour lines of subsidence during the time intervals between two levelling surveys were made by interpolation. Figure 3 shows a map of the vertical ground movements between 1983 and 1987 in the area around Bologna. The form of the gradient of the subsidence in Figure 3 is very similar to the one observed in Figures 1 and 2.

Unfortunately the new levelling data of 1999 were not yet available at the time of publication. Therefore, we could only compare the SAR subsidence map of 1992-1993 with the levelling surveys of 1987 and 1992. A statistical analysis was made in order to quantify the difference between the two measurements: for 179 points spread over the urban area of Bologna the subsidence velocities determined from levelling surveys (1987-1992) were on average 0.4 cm/year higher than those derived from SAR interferometry (1992-1993) with a standard deviation of 0.9 cm/year and minimum and maximum differences of –3.7 and +2.6 cm/year, respectively. The small standard deviation of 0.9 cm/year between the two methods indicates a good performance of differential SAR interferometry for subsidence mapping. The systematic bias between the two data sets can be explained by the different time period, indicating a decrease of the subsidence velocity. This conclusion is confirmed by a more detailed comparison performed along three levelling lines in the historical center of Bologna (see Figure 4). The profiles of Figure 5 indicate similar behaviors of the two measuring techniques with smaller velocities for the SAR data.

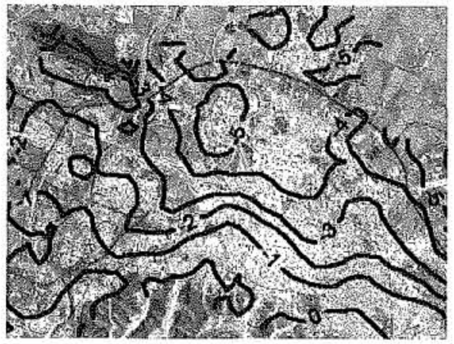

Figure 1. Land subsidence velocity (in cm/year) in the urban area of Bologna for the time period 1992-1993.

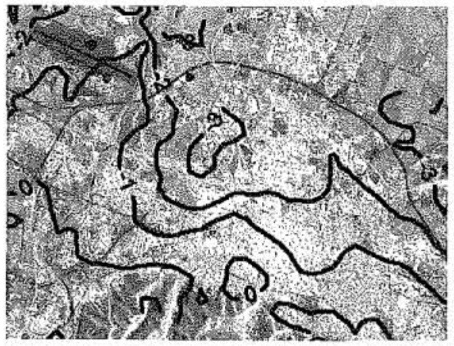

Figure 2. Land subsidence velocity (in cm/year) in the urban area of Bologna for the time period 1997-1998.

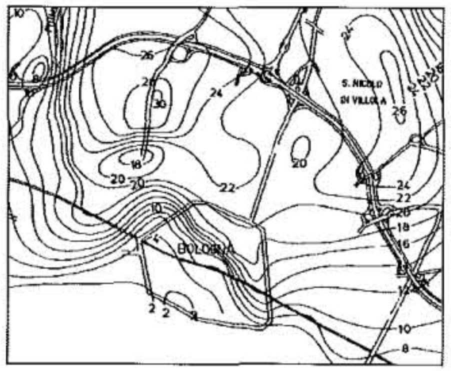

Figure 3. Map of the vertical ground movements from two levelling surveys in 1983 and 1987 in the urban area of Bologna (Barbarella et al., 1990).

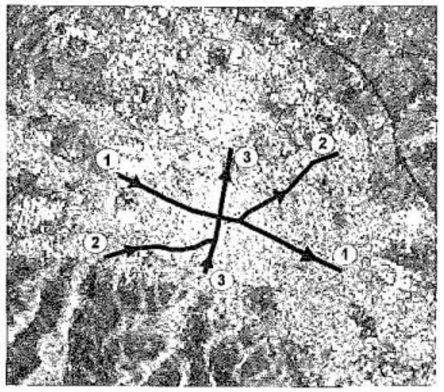

Figure 4. Levelling lines selected for the comparison of the subsidence velocities derived from SAR interferometry and levelling surveys.

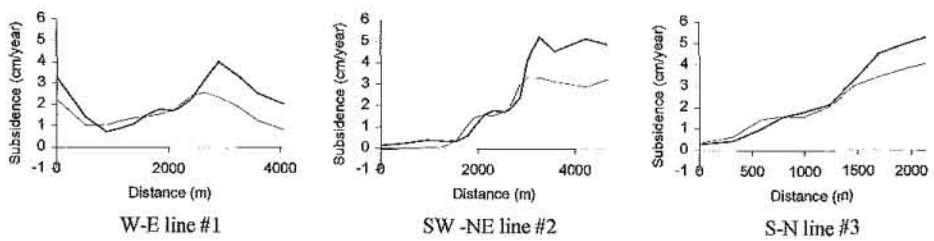

Figure 5. Profiles of the subsidence velocities determined from ERS SAR interferometry (period 1992-1993, normal line) and levelling surveys (period 1987-1992, bold line) along the three levelling lines shown in Figure 4.

5. SUBSIDENCE MONITORING SERVICE IN BOLOGNA

The results achieved from 12 ERS SAR scenes (six for each of the two time periods 1992-1993 and 1997-1998) demonstrate that the interferogram stacking technique reduces errors caused by atmospheric phase distortions and allows the generation of land subsidence maps with an accuracy of less than 1 cm/year and a spatial resolution of 25x25 m. The benefit of using SAR data over the urban area of Bologna is therefore evident. In Table 1 we summarize the characteristics of ERS differential SAR interferometry, levelling surveys and GPS for the mapping of land subsidence in Bologna with regard to spatial resolution, accuracy and cost.

Table 1. Comparison of the characteristics of differential SAR interferometry, levelling surveys and GPS for land subsidence mapping in Bologna.

	ERS SAR	Levelling	GPS
Spatial resolution	25 m	> 250 m	~10 km
Characteristics	urban areas	levelling lines	few points
Temporal frequency	1 year	'83 / '87 / '92 / '99	2-3 years
Accuracy	< 1 cm/year	1 mm / 1 km of line	1-2 cm
Reference point	Facoltà di Ingegneria	Sasso Marconi	Sasso Marconi, Castel de Britti, Facoltà di Ingegneria
Cost	26'000 EURO	~ 200 EURO / km	≥ 500 EURO / pt.

The best spatial resolution is found with differential SAR interferometry, but information is available only over urban areas. Levelling lines, on the other hand, cover the whole territory but the average distance between consecutive benchmarks is on the order of 250 m. Finally, GPS stations allow to detect ground movements in few significant points.

Precise levelling surveys give the best accuracy: the error is on the order of 1 mm for 1 km of line. Since the reference benchmark, i.e. the one considered stable, is very close to Bologna, the error of the subsidence map derived from levelling surveys is very small. The measurement accuracy of GPS for height movement detection is on the order of 1 to 2 cm, depending also on the technique adopted. In differential SAR interferometry the main source of inaccuracy is related to atmospheric path-delay inhomogeneities. However, stacking of multiple results reduces the error in Bologna below 1 cm/year.

The cost to repeat the measurement of a complete levelling network is high, in particular over urban areas. Therefore complete levelling surveys cannot be repeated often. With GPS it is time and cost effective to repeat the measurements every 2-3 years. Finally, with differential interferometry it is feasible to set up a cost-effective monitoring service on an annual basis.

In conclusion, the best way to investigate the regional subsidence process is an integrated survey. The integrated survey improves the qualitative and quantitative analysis of the vertical displacements. The use of differential SAR interferometry and GPS measurements allows the investigation of the critical areas in quasi real time permitting to follow the evolution the displacements.

Acknowledgments

This work was supported by the ESA Data User Program (DUP). The Italian National Geologic Survey is acknowledged for the DEM.

REFERENCES

Barbarella, M., Pieri, L., & Russo, P. (1990) Studio dell'abbassamento del suolo nel territorio bolognese mediante livallazioni ripetute: analisi dei movimenti e considerazioni statistiche. *INARCOS*, **506**, 1-19.

Bitelli, G., Bonsignore, F., & Unguendoli, M. (2000) Levelling and GPS networks for ground subsidence monitoring in the Southern Po Valley. *Journal of Geodynamics*, **30-3**, 355-369.

Folloni, G., Russo, P., & Radicioni, F. (1996) La subsidenza del territorio bolognese dal 1983 al 1993. *INARCOS*, **571**, 400-413.

Strozzi, T., & Wegmüller, U. (1999) Land Subsidence in Mexico City Mapped by ERS Differential SAR Interferometry. *Proceedings of IGARSS'99*, Hamburg, Germany.

Strozzi, T., Tosi, L., Carbognin, L., Wegmüller, U., & Galgaro, A. (1999) Monitoring Land Subsidence in the Euganean Geothermal Basin with Differential SAR Interferometry. *Proceedings of FRINGE'99*, Liege, Belgium.

Wegmüller, U., & Strozzi, T. (1998) SAR interferometric and differential interferometric processing chain. *Proceedings of IGARSS'98*, Seattle, USA.

Wegmüller, U., Strozzi, T., Wiesmann, A., & Werner, C. (1999) Land Subsidence Mapping with ERS Interferometry: Evaluation of Maturity and Operational Readiness. *Proceedings of FRINGE'99*, Liege, Belgium

LAND SUBSIDENCE - Vol. II
Proceedings of the Sixth International Symposium on Land Subsidence
Ravenna / Italy / 24-29 September 2000

SUBSIDENCE IN THE EASTERN PO PLAIN (ITALY)

Marco Bondesan (*), Marco Gatti (**) & Paolo Russo (**)
(*) Dipartimento di Scienze Geologiche e Paleontologiche,
Università degli Studi di Ferrara, Via Ercole I d'Este 32, 44100 Ferrara (Italy)
(**) Dipartimento di Ingegneria,
Università degli Studi di Ferrara, Via Saragat 1, 44100 Ferrara (Italy)

Abstract

The study was carried out in the eastern part of the Po plain, which is the area most affected by both natural and artificial subsidence. The data utilized derive from various high precision levellings carried out by the Istituto Geografico Militare (I.G.M.) and the Italian Cadastre. The results of levellings are analyzed and interpreted. A coincidence between rapid rates of subsidence, including artificial subsidence, and the greater thickness of Quaternary sediments is pointed out.

Keywords: subsidence, I.G.M., Italy, levelling, Po Plain, Quaternary

1. INTRODUCTION

Levelling has been undertaken periodically in the eastern Po Plain since the end of the 19th century. The Italian first order levelling network (Nuova Rete Altimetrica Fondamentale) carried out by the Istituto Geografico Militare (I.G.M.) is particularly important for two reasons. The first is the updating and standardisation of the heights of the existing bench marks. The network in fact constitutes the vertical datum according to which all the other lines and networks in the plain are regulated. Periodic surveys do not only make it possible to update the reference bench marks of the individual local networks, but they also provide important indications for the comparison of bench marks in different networks or those measured in different periods. The second important result is that it makes possible the quantification of ground movement over a much larger area. Since the survey, made between 1943 and 1956 in the eastern Po Plain, the national levelling network has furnished data of great interest on the movements which took place in the first half of the century (Salvioni, 1957; Arca & Beretta, 1985). Subsequent levelling carried out between 1968 and 1973 not only confirmed some previously-known artificial subsidence, but also registered new examples. The surveys carried out by the Italian Cadastre between 1974 and 1977 also produced fundamentally important information. It is therefore clear that the recent series of measurements carried out by the I.G.M. in the eastern Po Plain between

1986 and 1992 were destined to arouse the interest of scientists and workers in the area. In this article the results of the study of the ground movements, which have taken place in the second half of the twentieth century, together with some interpretative notes on the observed phenomena, are presented.

2. LEVELLING INVESTIGATIONS

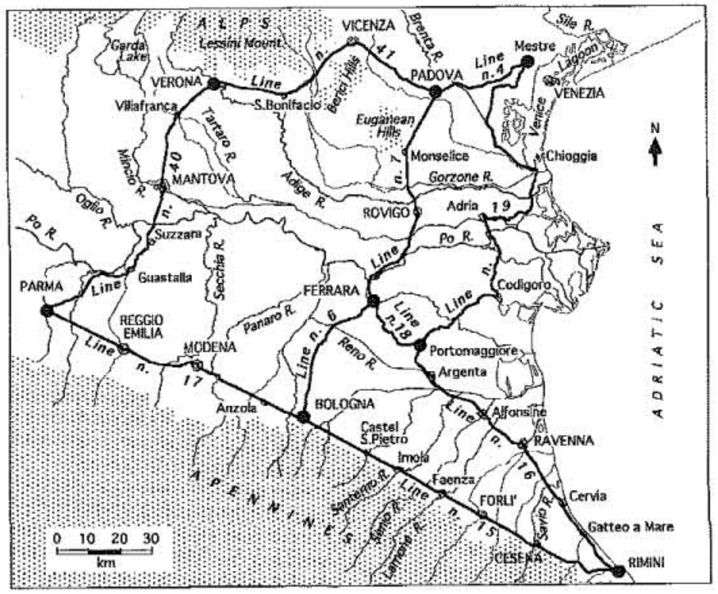

Figure 1. Levelling lines analyzed, in the I.G.M. first order levelling network; (in figs. 2, 3 and 4, the graphs that show the subsidence which has occurred are drawn from left to right, following the south-north component of the orientation of the single levelling lines).

The graphs in Figures 2, 3 and 4 show the vertical ground movements which have taken place since the I.G.M. measurements for the "Nuova Rete Altimetrica Fondamentale" (late 1940s and 1950s) (Fig. 1) and the subsequent levellings up to and including 1990.

For each line only the levellings for the largest number of bench marks have been graphed. Only the levellings of the I.G.M. are of this type, therefore the levellings of the Cadastre were not shown in the graphs. Each graph includes only the bench marks which were measured in all of the different I.G.M. levellings presented. The first levelling is shown conventionally by a straight line, and for each bench mark the height change with respect to the preceding levelling is shown.

In the graphs of lines 4, 40 and 41, along which the movements have only been very slight, the vertical scale has been expanded.

3. INTERPRETATION OF THE RESULTS

With regard to the subsidence registered between the 1950s and the 1970s, interpretations can be made which incorporate data from levellings carried out by other agencies and on specific local networks.

For the area between the rivers Po and Adige and the area to the south-west of the Po river, it has been possible to demonstrate that the subsidence is mainly the result of the extraction of water containing methane from the Quaternary strata between 1938 and 1964, which resulted in notable lowering of the piezometric surfaces (Caputo *et al.*, 1970; Barbujani, 1973; Mazzalai *et al.*, 1978; Borgia *et al.*, 1982); the marked subsidence, which took place here in the 1970s, also seems to have been caused by these activities (Bondesan *et al.*, 1986, 1990). The rates recorded in the most recent surveys are decidedly lower in this area, although in general they are still higher than those attributable to natural subsidence.

For the Ravenna area, the subsidence is mainly due to the intensive extraction of underground water for uses connected with industry, tourism and agriculture, especially in the 1960s and 1970s, and to a lesser extent to the extraction of methane from deep formations (Carbognin *et al.*, 1978; Bertoni *et al.*, 1987); in these areas marked lowering of the piezometric surfaces has also been recorded. The subsidence in the coastal plain between Ravenna and Rimini was mainly induced by the extraction of underground water for uses connected with tourism. Subsequently the area has been served with surface water brought by new canals and aqueducts. The latest I.G.M. levellings again registered marked subsidence in various zones, once again probably due to the effects of water extraction and other causes related to recent urban and industrial developments, although in general the phenomenon is diminishing; this reduction is also demonstrated by the recent surveys carried out by another society: Idroser (Regione Emilia Romagna, 1994a).

In the areas near Bologna and Modena as well, subsidence observed from previous levelling has been primarily attributed to excessive exploitation of ground water (Arca & Cardini, 1977; Pieri & Russo, 1977, 1978, 1980, 1984; Barbarella *et al.*, 1990). Lowering of the piezometric surfaces was found here as well, and analogous phenomena were recorded in the 1970s near Ferrara and in various tracts along line 15. The most recent levellings show that the rate of subsidence has since then increased in all these areas, especially near Bologna, in Modena and to the east of Forlì. In general these are areas where there has been, in recent times, an expansion of urban and industrial areas accompanied by the extraction of water from the subsoil (Regione Emilia Romagna, 1994b).

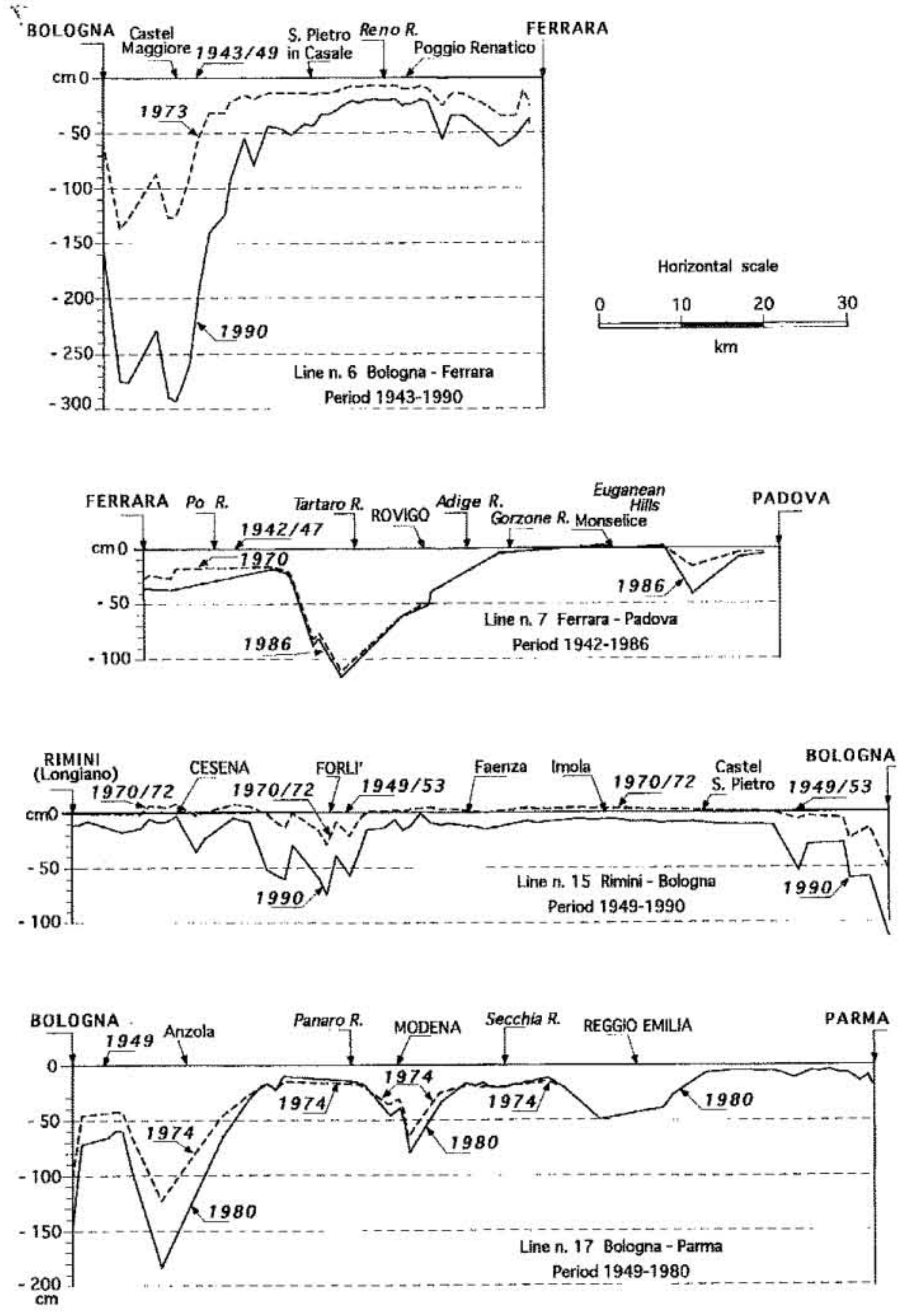

Figure 2. Ground movements in the second half of this century along the I.G.M. levelling lines n. 6, 7, 15 and 17 (see Fig. 1).

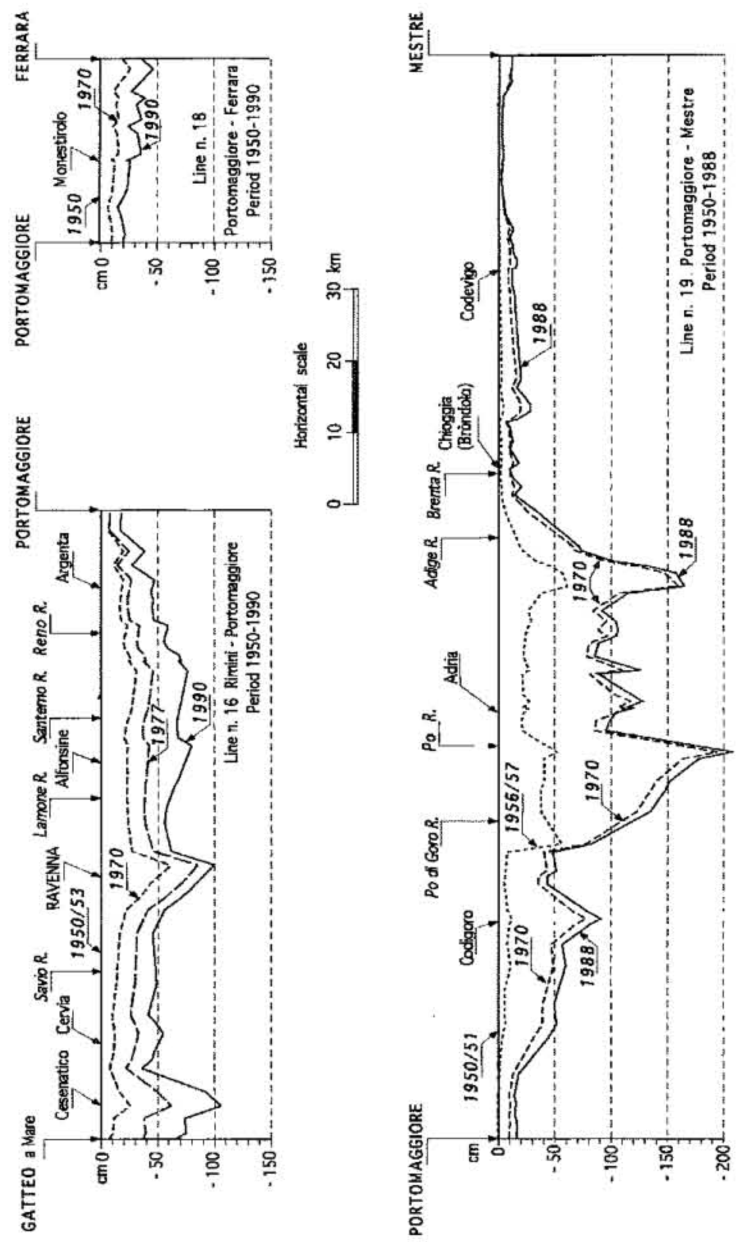

Figure 3. Ground movements in the second half of this century along the I.G.M. levelling lines n. 16, 18 and 19 (see Fig. 1).

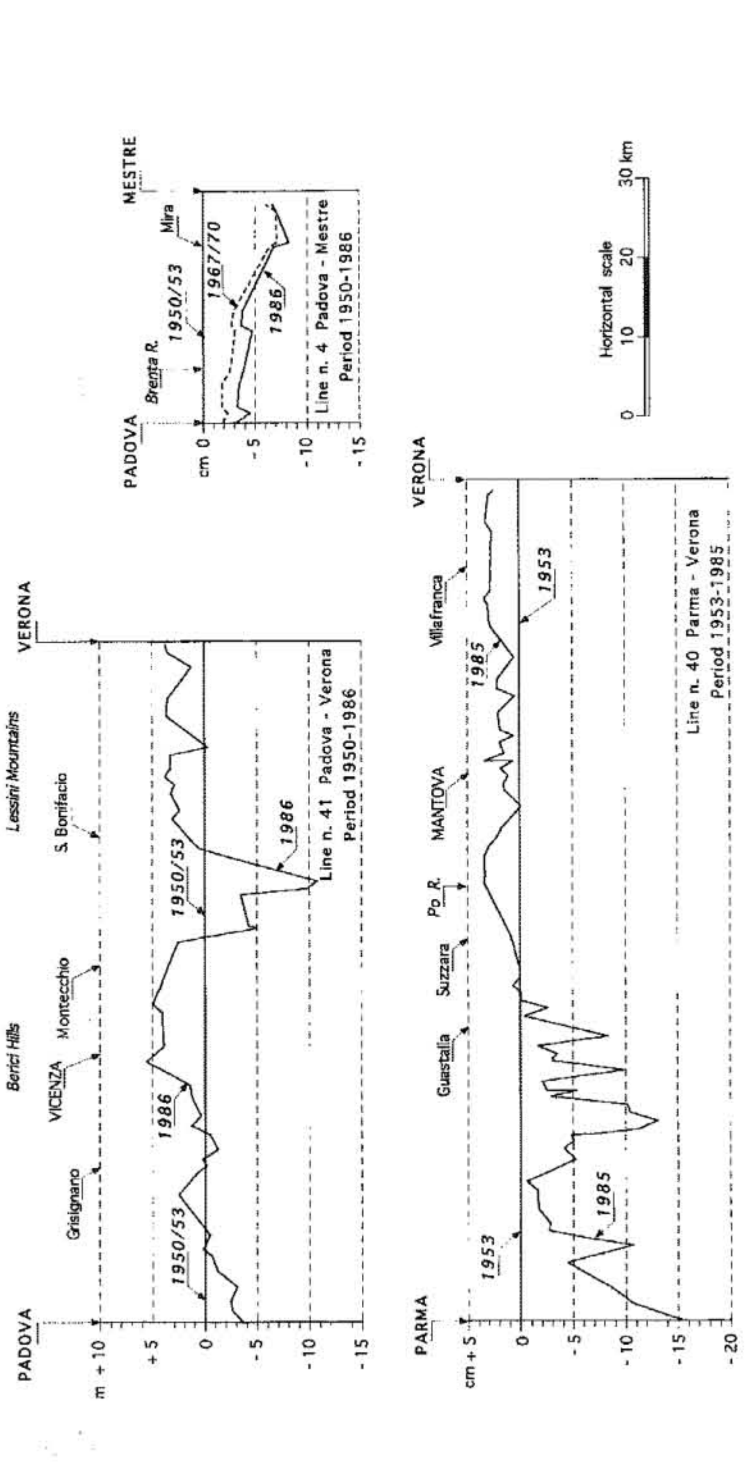

Figure 4. Ground movements in the second half of this century along the I.G.M. levelling lines n. 4, 40 and 41 (see Fig. 1); the vertical scale has been expanded with respect to the other graphs.

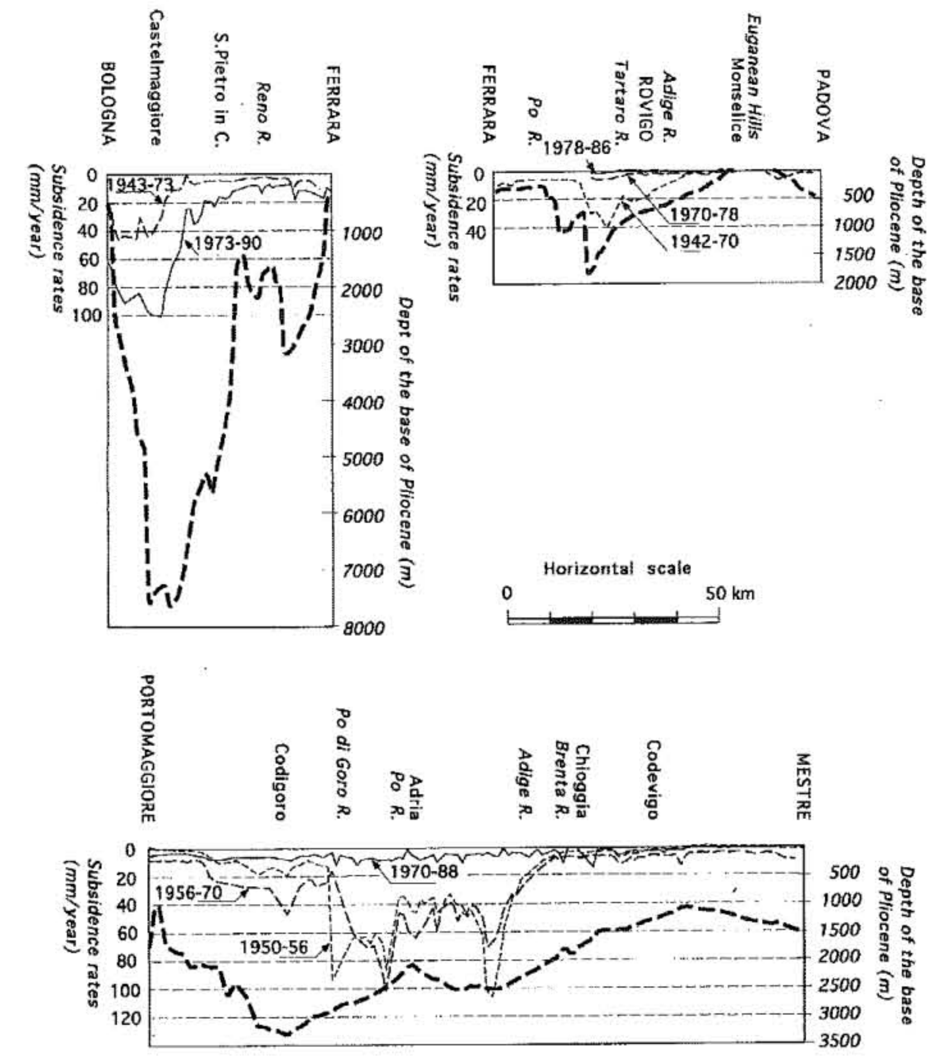

Figure 5. Depth of the base of Pliocene and Quaternary sediments and subsidence rates along the I.G.M. levelling lines n. 6, 7 and 19.

The subsidence of the Venice hinterland has also been attributed to exploitation of deep ground water primarily for industrial use (Caputo et al., 1972; Carbognin et al., 1976, 1995). Extraction here has now been strictly limited, and in fact the most recent levellings show a considerable reduction in subsidence. Although subsidence has never been very great in this area, it has nevertheless been very important, given the vulnerability of the area.

3.1 Correlation between the rate of subsidence and the depth of the base of Pliocene and Quaternary sediments

Along some levelling lines (e.g. lines 6, 16 and 19), one can observe a certain similarity between the pattern of the highest speeds of subsidence and the form of the basal surface of the Plio-Quaternary sedimentation (fig. 5). Since it is unlikely that this is a mere coincidence, the phenomenon deserves further discussion. This spatial distribution is understandable for natural subsidence. However, natural subsidence has always exhibited much lower speeds than those occurring in this situation have. Hence we are dealing with artificial subsidence.

Moreover, the investigations indicate that the territories and periods for which this coincidence is observable are characterized by marked withdrawals of groundwater from various depths.

Therefore, the phenomenon appears to be attributable mainly to the compaction of the highest sediments of the Plio-Quaternary series. Although a map of the distribution of these sediments is not currently available, it has been possible to observe, by means of core samples, that particularly coarse and permeable materials were deposited in the areas of structural depression during the periods characterized by continental sedimentation, i.e. in the late Quaternary. In fact, it is obvious that rivers were very often present in these zones, also as a result of the marked natural subsidence that occurred there. These sedimentary bodies are the sites of strong aquifers, which have recently been subject to excessive exploitation.

An interpretation of the phenomenon within this context is possible for the area of Emilia by means of a comparison of the above-mentioned speeds of subsidence with the thickness of the aquifers currently most exploited. In a study conducted by the Region of Emilia-Romagna (1999), the ground-water reserves of this sector of the plain were grouped into three large aquifers: the first, rechargeable, from the surface to 400 m depth; the second, non-rechargeable, between 400 and 600 m depth; and the third, slowly rechargeable, between 500 and 700 m depth.

In the comparison, there is an evident coincidence between the lowering in the coastal band between Ravenna and Rimini and the 1° aquifer. At Ravenna, where the groundwater has been withdrawn from greater depths, there is a marked coincidence between the greatest lowering and the geometry of the 2° aquifer. Other particularly subsiding zones coincide with areas of great thickness of several aquifers. In particular, the zone north of Bologna, the site of recent intense exploitation of groundwater and of strong lowerings, coincides with the 1° and 3° aquifers, while the area south of Ferrara, where the withdrawals have been less intense, coincides with the 1° and 2° aquifers (obviously the subsidence related to the deepest withdrawals is small).

With regard to the area north of the Po, it is especially interesting to observe along line 6, between the Po River and the city of Rovigo, a coincidence between the pattern of the pre-Pliocene surface, the zone that experienced withdrawals of methane-producing waters from the Quaternary between 1938 and 1964, and the speeds of lowering in the period 1942-70.

Therefore, it is very likely that the coincidences reported here, which however should be confirmed by further observations, are of the indirect type: the deep structural pattern would have influenced the pattern and nature of subsequent sedimentation, favoring the formation of very thick and currently very exploited layers.

4. CONCLUSIONS

The present study has made it possible to compare homogeneous data over a long period and over a very large area. This has enabled us to update the picture which emerged from the levellings carried out up to the 1970s; at the same time it has been possible to investigate the causes underlying the observed movements.

Comparing the data for the 1970s with the most recent data, it has been shown that the rates of subsidence recorded between the rivers Po and Adige, and in particular in the area around the Po delta have markedly diminished: here the positive consequences of halting (since 1964) the extraction of water containing methane from shallow strata have been clearly demonstrated.

Our comparisons have also made it possible to ascertain a reduction in the high rate of subsidence which had been recorded in the Venice hinterland and in the coastal plain between Rimini and Ravenna, where the main cause was in fact the excessive extraction of ground water for industrial and agricultural purposes. These needs have clearly been satisfied by the construction of new aqueducts and new irrigation canals.

Nonetheless the groundwater withdrawal is still seems to be the main cause behind the artificial subsidence in the eastern Po Plain. It is this factor which is responsible for the high and steadily increasing rates of subsidence recorded at Bologna and in the surrounding area, at Modena, between Forlì and Cesena and in other areas, especially to the south of the Po: in general in these areas there has recently been substantial urban development with, in particular, the arrival of new small and medium-sized industrial plants.

It is still necessary to explain various cases of subsidence, and especially those recorded during the latest levellings, in areas where there has been no exploitation of the ground water. This is especially the case of the agricultural land situated in the coastal depressions or located nearby; despite the reduction in the rate of subsidence, rates have been recorded which are higher than the natural rates in the areas where water containing methane was extracted; it is however unlikely that this is only the residual effect of such activities, which ceased 30 years ago.

This research has also enabled us to highlight a frequent coincidence between high rates of subsidence and greater thickness of Quaternary sediments. From the studies carried out it has been shown that the areas and periods for which this coincidence was observed are characterised by considerable drainage of ground water: the phenomenon is therefore mainly related to a concatenation of various factors, such as the different lithology of the material deposited in the structurally more depressed area, the thickness and extent of the aquifers (which are often intercommunicating), and the reduction in strata pressure caused by water exploitations.

Acknowledgments

Research carried out using MURST 40% funds: La risposta dei processi geomorfologici alle variazioni ambientali (Prof. M. Bondesan), Po Plain: new regional geomorphological themes (Prof. GB Castiglioni); C.N.R. Venetian Lagoon System Project (Prof. M. Bondesan).

REFERENCES

Arca, S. & Beretta, G.P. (1985) Prima sintesi geodetico-geologica sui movimenti verticali del suolo nell'Italia Settentrionale (1897-1957), *Bollettino di Geodesia e Scienze Affini,* **44**, 2, pp. 125-156.

Arca, S. & Cardini, A. (1977) Analisi degli spostamenti verticali del suolo nella città di Bologna *Bollettino di Geodesia e Scienze Affini,* **36**, 4, pp. 439-450.

Barbarella, M., Pieri, L., & Russo, P. (1990) Studio dell abbassamento del suolo nel territorio bolognese mediante livellazioni ripetute: analisi dei movimenti e considerazioni statistiche *Inarcos,* 506, Bologna, pp. 1-19.

Barbujani, E. (1973) Evoluzione recente del delta del Po, *Annali Università di Ferrara,* suppl. 1, Ferrara, pp. 29-54.

Bertoni, W., Brighenti, G., Gambolati, G., Gatto, P., Ricceri, G., & Vuillermin F. (1987) *Risultati degli Studi e delle Ricerche sulla subsidenza a Ravenna.* Comune di Ravenna, pp. 1-145.

Bondesan, M., Castiglioni, G.B., Elmi, C., Gabbianelli, G., Marocco, R., Pirazzoli, P.A., & Tomasin, A. (1995) Coastal areas at risk from surges and sea-level rise in northeastern Italy, *Journal of Coastal Research,* 11, 4, Florida, USA, pp. 1355-1379.

Bondesan, M., Gatti, M., & Russo, P. (1997) Movimenti verticali del suolo nella Pianura Padana orientale desumibili dai dati I.G.M. fino a tutto il 1990 *Bollettino di Geodesia e Scienze Affini*, **56**, 2, pp. 141-172.

Bondesan, M., Minarelli, A., & Russo, P. (1986) Studio dei movimenti verticali del suolo nella provincia di Ferrara *Studi idrogeologici sulla Pianura Padana,* 2, Clup, Milano, pp. 1-31.

Bondesan, M., Minarelli, A., & Russo, P. (1990) Analisi dei movimenti verticali del suolo avvenuti nel periodo 1970-1978 lungo l'asta del Po a est di Polesella e nel delta, In (AA.VV.) *PO AcquAgricolturAmbiente, 2, L'alveo e il Delta,* Soc. Ed. Il Mulino, Bologna, pp. 385-404.

Borgia, G., Brighenti, G., & Vitali, D. (1982) La coltivazione dei pozzi metaniferi del bacino polesano e ferrarese. Esame critico della vicenda *Inarcos,* 425, Bologna, pp. 13-23.

Caputo, M., Pieri, L., & Unguendoli, M. (1970) Geometric investigation of the subsidence in the Po delta *Bollettino di Geofisica Teorica e Applicata,* 47, Udine, pp. 187-207.

Caputo, M., Folloni, G., Gubellini, A., Pieri, L., & Unguendoli, M. (1972) Survey and geometric analysis of the phenomena of subsidence in the region of Venice and its hinterland *Rivista Italiana di Geofisica,* **21** (1 -2), pp. 19-26.

Carbognin, L., Gatto, P., Mozzi, G., & Gambolati, G. (1978) Land subsidence of Ravenna and its similarities with the Venice case. *Evaluation and Prediction of Subsidence,* J.K. Saxena ed., A.S.C.E., New York, pp. 254-266.

Carbognin, L., Gatto, P., Mozzi, G., Gambolati, G. Ricceri, G. (1976) New trend in the subsidence of Venice. In: *Land Subsidence - Proc. II Int. Symp. on Land Subsidence*, IAHS Publ. No 121, 65-81.

Carbognin L., Tosi, L., & Teatini, P. (1995). Analysis of actual land subsidence in Venice and its hinterland (Italy). In: *Land Subsidence - Proc. V Int. Symp. on Land Subsidence* (ed. by: F. B. J. Barends *et al.*,), A. A. Balkema, Rotterdam, 129-137.

I.G.M. (1971) *Relazione sui lavori di livellazione geometrica di alta precisione eseguiti nel 1970 dall'I.G.M. nelle zone della Laguna Veneta e del Delta Padano.* Comitato per lo studio dei provvedimenti a difesa della città di Venezia, pp. 1-170.

Mazzalai, P., Ricceri, G., & Schrefler, B. (1978) Studio della subsidenza nel delta padano, *Atti Conv. Problemi della subsidenza nella politica e difesa del Territorio,* Comune di Pisa, Comune di Ravenna, Reg. Emilia Romagna, Reg. Toscana, Pisa, 4, pp. 50-57.

Pieri, L., & Russo, P. (1977) Studio del fenomeno di abbassamento del suolo in atto nella zona di Bologna *Bollettino di Geodesia e Scienze Affini*, **36**, 3, pp. 365-388.

Pieri, L., & Russo, P. (1978) Nuovi contributi allo studio di abbassamento del suolo in atto nella zona di Bologna *Atti Conv. Problemi della subsidenza nella politica e difesa del Territorio*, Comune di Pisa, Comune di Ravenna, Regione Emilia Romagna, Regione Toscana, Pisa, 5, pp. 3-24.

Pieri, L., & Russo, P. (1980) Abbassamento del suolo nella zona di Bologna: considerazioni sulle probabili cause e sulla metodologia per lo studio del fenomeno *Collana di orientamenti geomorfologici ed agronomico-forestali, MTB 6*, Regione Emilia Romagna, Pitagora Ed., Bologna, pp. 1-43.

Pieri, L., & Russo, P. (1984) The survey of soil vertical movements in the region of Bologna *Proc. 3° Int. Symp. on Land Subsidence*, Venice, I.A.H.S., 151, pp. 1-11.

Regione Emilia Romagna (1994a) *Piano progettuale per la difesa della costa adriatica; aggiornamento e integrazione.* Idroser, Bologna, pp. 1-276.

Regione Emilia Romagna (1994b) *Sistematizzazione dei dati ambientali relativi al territorio regionale soggetto a subsidenza (Legge 845/80)*, Idroser, Bologna, pp. 1-111.

Regione Emilia Romagna, Eni Agip (1998) *Riserve idriche sotterranee della Regione Emilia-Romagna*, Selca, Firenze, pp. 1-119.

Salvioni, G. (1957) I movimenti del suolo nell'Italia centro-settentrionale. Dati preliminari dedotti dalla comparazione di livellazioni *Bollettino di Geodesia e Scienze Affini*, **16**, 3, pp. 325-366.

LAND SUBSIDENCE - Vol. II
Proceedings of the Sixth International Symposium on Land Subsidence
Ravenna / Italy / 24-29 September 2000

CURRENT STATUS OF LAND SUBSIDENCE IN TAIWAN

Chih-Hsi Liu, Fu-Li Tu, Chen-Tair Huang, Shoung Ouyang
Energy and Resources Laboratories, Industrial Technology Research Institute, Bldg. 24, 195-6 Sec. 4, Chung- Hsing Road, Chutung, Hsinchu, Taiwan, R.O.C

Kuo-Chyang Chang, Ming-Chien Tsai
Water Resources Bureau, Ministry of Economic Affairs
10F, 41-3, Sec. 3, Hsin-Yi Road, Taipei, 106 Taiwan, R.O.C.

Abstract

Land subsidence in Taiwan has increased over the past four decades owing to heavy withdrawal of groundwater, resulting in flooding, poor drainage, sea-water intrusion, and lower pumping efficiency in low-lying coastal areas. This article reviews land subsidence in Taiwan, including its underlying factors, monitoring activities, trend predicting, and remedial measures.

Land subsidence in Taiwan has been described by leveling surveys and field monitoring wells. The most recent data revealed that the subsiding area is 697 km^2. Although the maximum cumulative subsidence of 3.12 m occurred in Pingtung County in southern Taiwan between 1972 and 1999, the maximum average rate was 14.3 cm/year in Changhua County in central Taiwan.

A one-dimension model (COMPAC) was used to simulate the subsidence in Changhua County. Simulation results indicate that, under current groundwater pumping rates, the predicted subsidence rate will be around 8 cm/year by 2005.

The Taiwan governmental agency that governs water resources has promulgated a prevention and contingency strategy since 1996 to mitigate land subsidence. Fifteen action items have been taken in re-planning landuse, industrial reform, groundwater control, and education in areas that are subjected to land subsidence. The plan has so far reduced subsiding areas by 40% as of 1999.

Keyword: land subsidence, monitoring, predicting, remedial measures

1. INTRODUCTION

Due to the rapid growth of economic development, groundwater has been overused for the past several decades in Taiwan, and subsequently resulted in severe subsidence in the overpumping areas. The Taipei Basin was the first major subsidence area, where the phenomenon has been mitigated and stopped by reducing the groundwater withdrawal. However, the western and southwestern parts of Taiwan, became the focus areas in terms of land subsidence, after Taipei

Basin. Figure 1 depicts the current land subsidence areas in Taiwan. The total subsiding area is 697 km², scattered in the coastal areas of Changhua, Yunlin, Chiayi, Tainan, Kaohsiung, and Pingtung Counties. Although the maximum cumulative subsidence of 3.12 m occurred in Pingtung County in the southern Taiwan between 1972 and 1999, the current maximum subsiding rate was 14.3 cm/year in Changhua County in the central western Taiwan.

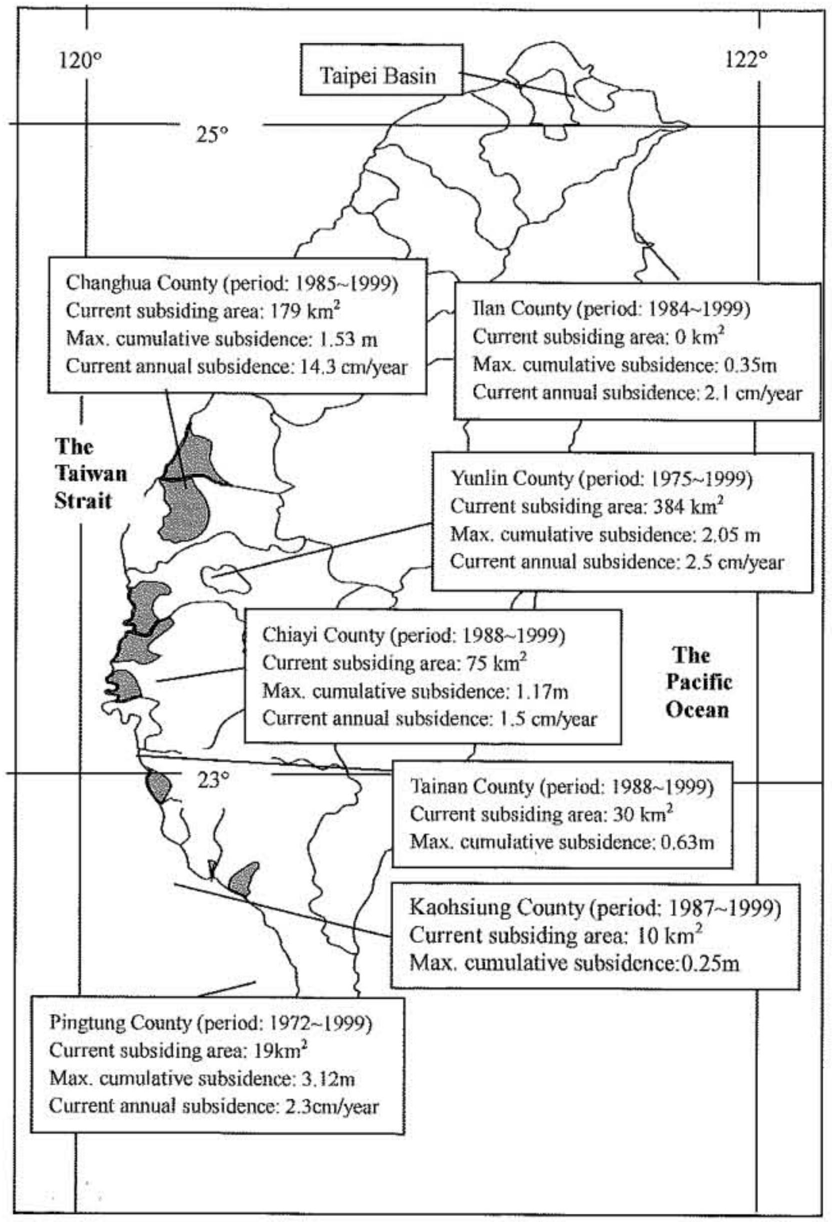

Figure 1. The current status of land subsidence in Taiwan.

2. HYDROGEOLOGY

Around 28% of Taiwan's area is composed of Quaternary sediments and terrace materials. These soils usually have good potential for groundwater storage, but land subsidence is often accompanied by the overpumping of this groundwater. In Taiwan, there are nine major potential groundwater regions (Water Resources Planning Commission, 1986, also see Table 1), five of them have encountered land subsidence problems in the past two decades.

Table 1. The total area and subsidence affected area of the groundwater potential regions in Taiwan.

Regions	Groundwater potential	Total area(km²)	Subsidence affected area(km²)
1.Taipei Basin	Good	380	252
2.Taoyuan Chungli Terrace	Fair	1,090	-
3.Hsinchu Miaoli Coastal Area	Fair	900	-
4.Taichung Area	Good	1,180	-
5.Choshui River Alluvial Fan	Excellent	1,800	400
6.Chianan Plain	Fair	2,520	250
7.Pingtung Plain	Excellent	1,130	105
8.Lanyang Plain	Good	400	50
9.Hualien-Taitung Valley	Good	930	-

As shown in Table 1, the Choushui Alluvial Fan is the most important area of groundwater potential in western Taiwan, and is also the largest subsiding region. The Choushui Alluvial Fan area represents the reference case study to better illustrate the mechanism and the distribution of land subsidence in Taiwan.

Figure 2 is the conceptual hydrogeological profile of Choushui Alluvial Fan. The layers are composed of gravel, sand, silt and clay. The gravel and coarse sand are concentrated near the upstream area of the fan, forming an excellent unconfined aquifer. The fine sand, silt and clay are deposited in the middle and downstream of the fan, developing an aquifer-aquitard system (Kester and Ouyang, 1996). Illite and chlorite are the major clay minerals found in the deposits (Yuan et al., 1996). As known, gravel and coarse sand deposits have better groundwater storage capacity than fine sand and silt. If intensive groundwater withdrawal occurred, the coastal area (downstream of alluvial fan) is more affected by land subsidence than the inland area (upstream).

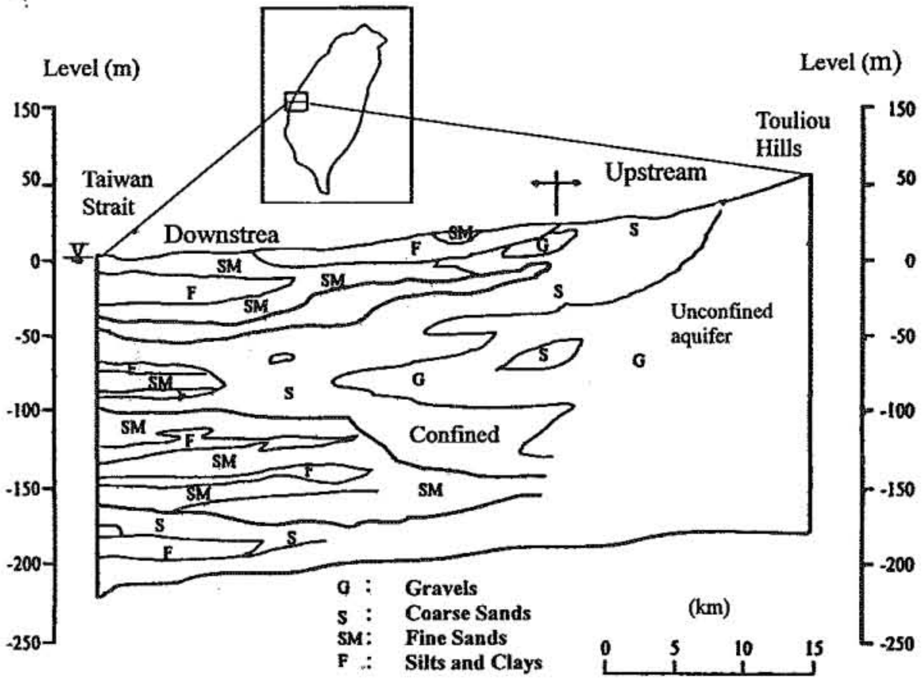

Figure 2. The conceptual hydrogeological profile of Choushui Alluvial Fan. (Modified from Liann C. Kester and Shoung Ouyang, 1996)

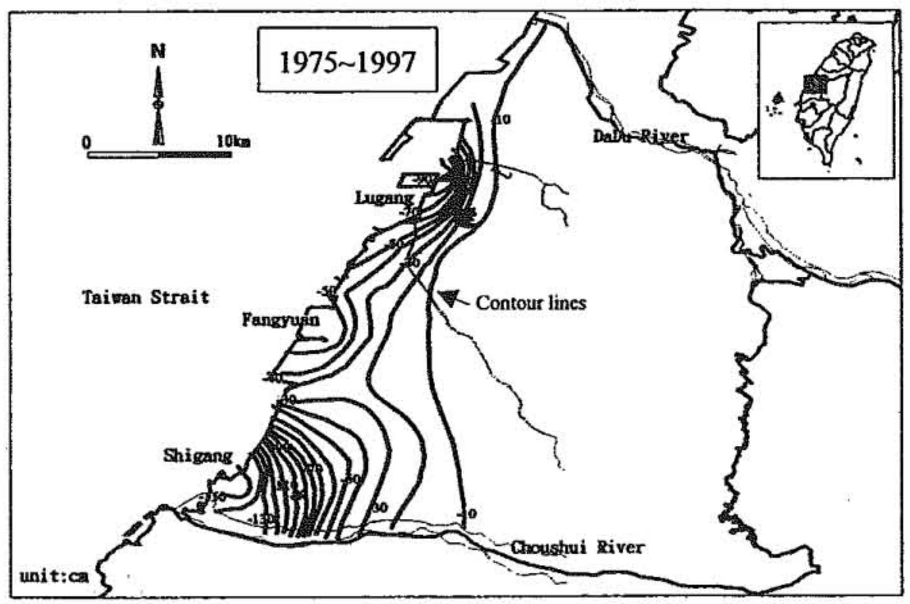

Figure 3. Land subsidence contour lines at the coast of Changhua County. (Modified from Taiwan Provincial Water Conservancy Department, 1998)

3. INVESTIGATION

Leveling survey has been utilized to investigate land subsidence in Taiwan since the late 1950's. The leveling data were used to evaluate the rate and area of subsidence. Figure 3 depicts the subsidence contours based on the leveling data of Changhua County from 1975 to 1997 (Taiwan Provincial Water Conservancy Department, 1998). The center of subsidence is located at the Shigang Village where the most significant subsidence was surveyed in Taiwan up till now.

In addition to levelings, thirty monitoring wells of four types were installed in the coastal areas of Taiwan (ERL,1999)

Table 2 indicates the monitored subsiding rate and depth range of significant compaction and consolidation. The results indicate that Changhua County is the hot-spot area of land subsidence at present, with the subsiding rate of 12~14 cm/year. The Yunlin, Chiayi and Pingtung Counties are areas of fair subsidence, the subsiding rate ranging from 1.5 to 5.0cm/year. The land subsidence in Ilan County appears to be quiescent, with a rate below 0.5cm/year. Excluding the Ilan County, in the other subsiding areas the major compaction occurred at depths between 60 m to 300 m.

Table 2. The results of field wells monitoring

county	Annual subsidence	Depth range where major compaction occurred
Ilan	~0.5cm	NA
Changhua	12.0~14.0cm	60~180m
Yunlin	2.0~4.0cm	100~300m
Chiayi	2.5~5.0cm	160~280m
Pingtung	1.5~3.0cm	70~180m

4. PREDICTION

COMPAC model (Helm, 1984; 1987) was used to simulate land subsidence in the Choushui Alluvial Fan (across Yunlin and Changhua Counties) and the Pingtung Plain (in Pingtung County). The Terzaghi one-dimensional consolidation theory was applied to calculate the settlement of soils in the model. The prediction parameters include SSF(the skeletal specific storage of permeable aquifer material), PRM(the hydraulic conductivity), SP(the nonrecoverable skeletal specific storage), and SE (the recoverable skeletal specific storage).The parameters were obtained by curve fitting to the historical data of subsidence and groundwater level records. To optimize the parameters, the deviation of curve fitting was controlled within 2 cm.

Using these parameters and assuming that the future groundwater level fluctuation will remain in the same range as that of the previous five years, the predicted subsidence of each site is between 5 and 43 cm by 2005. The most significant subsidence predicted will occur in the Shigang Village of Changhua County totaling 43 cm from 2000 to 2004. In Fig. 4 the predicted subsidence and groundwater level up to 2004 are reported.

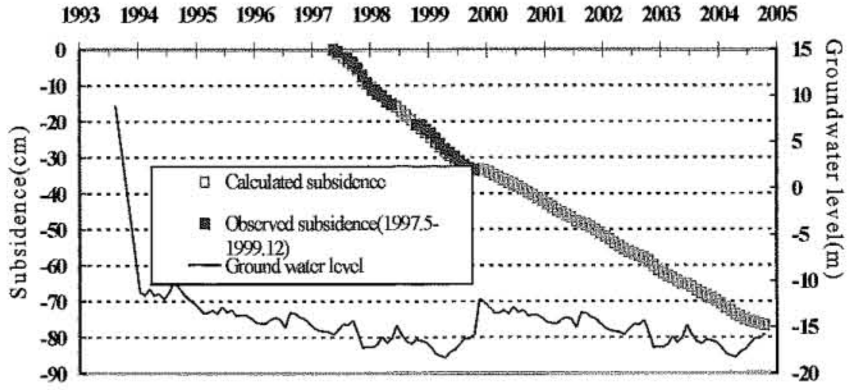

Figure 4. Predicted results of the Shigang Village in Changhua County

5. REMEDIAL MEASURES

Land subsidence has caused serious impact on the local economic growth, community development, and environment in Taiwan. The induced loss and cost associate with the subsidence problem has reached multibillions of dollars over the past four decades. In order to prevent the land subsidence getting worse, a prevention and contingency plan has been promulgated since 1996 by the Central and Provincial Government (MOEA,1998). In the plan, there are fifteen action items covering the aspects of landuse replanning, industrial reform, groundwater control , and social education in the land subsidence areas. Figure 5 depicts the structure and content of the plan. After several year's devotion and efforts, a preliminary success has been witnessed. The subsiding area had been reduced from 1057 km^2 to 697 km^2 during the period of 1996 to 1999.

6. CONCLUSION AND RECOMMENDATION

Taiwan has struggled with land subsidence for four decades. Since 1996, the Government of Taiwan has initiated a subsidence prevention and contingency plan to mitigate the problem and to minimize the associated damage. Although the subsidence rate is still conspicuous in the Changhua County, in the other areas it appears to have decreased in recent years. The prevention and contingency plan will be to further enhance remedial effect on the land subsidence.

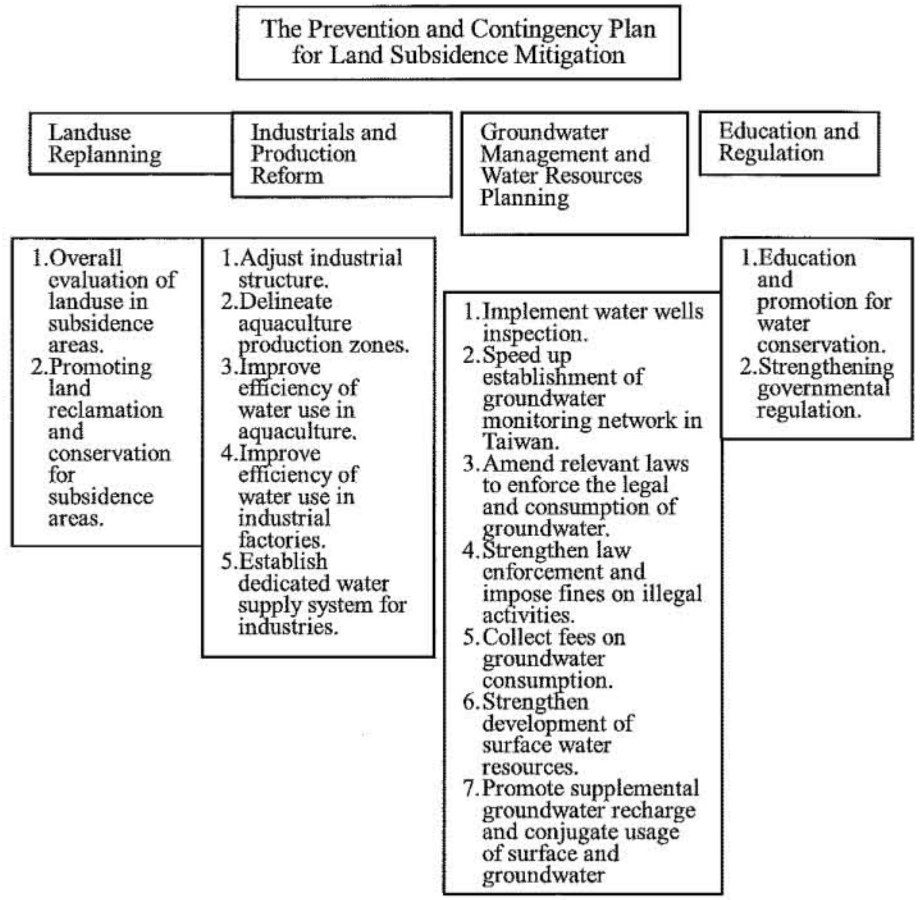

Figure 5. The structure of land subsidence prevention and reclamation plan

Besides the existed works, the advance study would be implemented in future.

Parallel to the undertaking of the plan, the following studies are recommended:

a. Advancement of surveying and monitoring technologies, for example, applying GPS to improve land survey technique, and applying INSAR for regional subsidence monitoring.
b. Identification of major groundwater recharges in or adjacent to the subsiding regions. Initiating a groundwater recharge pilot project to study the mitigating effect on the subsidence.
c. Precautionary studies of the impact of land subsidence on major public works, such as the construction of high-speed rail across subsidence areas.

Acknowledgment

The major investigation funded by the Water Resources Bureau, Ministry of Economical Affairs of Taiwan. The authors wish to express thanks to Dr. Hsiang-Kueen Hsu and Mr. Shao-Hsing King for their support and guidance, and also thanks to Dr. Donald C. Helm for instructing us to use the COMPAC program.

REFERENCES

ERL, Energy and Resources Laboratories, ITRI. (1999) Leveling survey and Instrument monitoring in subsidence areas of Taiwan, Final Report, Sponsored by Water Resources Bureau, 4-1~4-99.

Helm, D.C. (1984) Latrobe Valley subsidence predictions, The modelling of ground water withohawal, Joint report of the Fuel Dept. and the Design, Engineering, and Environmental Dept., State Electricity Commission of Victoria, Melbourne, Australia. Vol.1 & Vol. 2.

Helm, D.C. (1987) Prediction of subsidence due to groundwater withdrawal in the Latrobe Valley, Australia, Proceedings 6th International society for rock mechanics, 125-129.

Kester, Liann C. & Ouyang, Shoung (1996) Analysis of groundwater and water balance in Yunlin County, Proceeding of Groundwater and Hydrogeology Conference in Choushui Alluvial Fan, 181-206, Taipei, Taiwan

MOEA, Ministry of Economical Affairs and Council of Agriculture (1998) Land subsidence prevention and reclamation plan, 24p, Taiwan.

Taiwan Provincial Water Conservancy Department (1998) The report of land subsidence leveling survey in the coastal area of Changhua, 195p.

Water Resources Planning Commission, Taiwan, (1986) Groundwater Development in Taiwan, 1-16.

Yuan, P. B., Teng, L. S., & Lin, S. B. (1996) Characteristics and distribution of sediments in the Choushui Alluvial Plain, Proceeding of Groundwater and Hydrogeology Conference in Choushui Alluvial Fan, 43-54. Taipei, Taiwan.

LAND SUBSIDENCE - Vol. II
Proceedings of the Sixth International Symposium on Land Subsidence
Ravenna / Italy / 24-29 September 2000

WIDE-AREA PRECISION SURVEYING OF LAND SUBSIDENCE FROM SPACE USING RADAR INTERFEROMETRY

Mark Haynes
NPA Group, Crockham Park, Edenbridge, Kent TN8 6SR, United Kingdom
Tel: +44-(0)1732-865023; E-mail: markh@npagroup.co.uk

Abstract

The NPA Group has developed a fully operational radar interferometry facility, and through this offers a complete service for mapping and monitoring land subsidence, as well as other ground displacements such as earthquakes.

Radar interferometry (or *InSAR*) surveying offers several advantages over conventional methods for mapping subsidence. Standard techniques, such as line levelling and extensometers, rely on some prior knowledge of a subsidence-prone region, such as location and extents. In contrast, InSAR requires no such information to survey the Earth's surface and to detect previously unidentified zones of subsidence. Such detection, as well as monitoring of known, active areas, is accomplished by comprehensive scanning across a 100 km square image swath as a standard coverage, in a matter of a day at the most of processing and analysis. Surveying an area of this magnitude for land displacements could not be contemplated by a conventional ground survey team; even if it were envisaged, the survey resource and time costs would be prohibitively expensive. InSAR also quantifies the areal extents and rates of motion of subsiding regions and, in contrast with ground surveys that produce discrete point samples, InSAR analysis presents a continuous deformation field to assist, for example, with geophysical modelling of surface displacement phenomena. InSAR is not limited to mapping currently active sites of subsidence but can also study historical events, since the archive of radar imagery stretches back almost a decade.

Keywords: subsidence mapping, InSAR, radar interferometry

1. INTRODUCTION

Using SAR (i.e. ground imaging radar) instruments aboard orbiting satellites, the technique of SAR interferometry can be employed to detect and measure ground motion on the Earth's surface, to a magnitude less than the radar sensors' wavelengths, i.e. to a sub-centimetric level. After several years of research and development programs, the NPA Group, a satellite mapping company based in Edenbridge, England, has combined InSAR techniques together with state-of-the-art radar processing technology and skilled data interpretation, value-adding and data merging to provide a fully operational ground displacement mapping and monitoring service. NPA undertakes this subsidence and earthquake surveying service on behalf of earth scientists, government agencies, risk management, mining, surveying, civil engineering and water companies.

NPA has also mapped a large number of surface movement phenomena worldwide, under contract to the European Space Agency, the European Centre for Earth Observation and other agencies. Projects have included a year-long subsidence detection and mapping program in a great number of sites around the world, most of them in important urban areas and many where large-scale subsidence was hitherto undetected or unquantified (for further details on projects, see the *Radar Interferometry* section at *http://www.npagroup.com*).

The company is active in developing and enhancing this technology with new techniques applied to mapping subsidence and seismic motion (Haynes, 1999a, Haynes, 1999b). In collaboration with geodesy and geophysics researchers, we have reported on recent and past earthquakes analysed with InSAR (e.g. Wright *et al.*, 1999a, Wright *et al.*, 1999b), as well as on some of our numerous InSAR subsidence case studies (Haynes *et al.*, 1997, Sato & Haynes, 1998). The purpose of this article is to present a selection of subsidence results, derived from our InSAR mapping facility, of interest to those concerned with the detection, surveying and monitoring of land surface sinking.

2. INSAR SUBSIDENCE MAPPING

The technique of SAR interferometry is now well established and will not be covered here in detail. The present article is concerned with operational, differential SAR interferometry for ground displacement mapping, and for a recent, general introduction of issues on this particular aspect, see Haynes (1999a) for example.

In summary, from the satellite orbit acquisition geometry and the physical parameters of the radar instrument, each distinct fringe cycle in a differential interferogram represents 28 mm of movement, in the line-of-sight of the SAR sensor, during the period between the dates of the two radar acquisitions. Moreover, portions of incomplete cycles represent corresponding fractions of this 28-mm unit. Hence by phase unwrapping, or by summation of complete 28-mm fringes plus any incomplete fringe portions, one can establish the maximum displacement, with respect to the SAR sensor, of ground points within the innermost fringe relative to stable ground beyond the fringe group.

One of the results of NPA's interferometric subsidence study over Houston, Texas is illustrated in Figure 1, which we undertook on behalf of the Harris-Galveston Coastal Subsidence District. Analysis revealed a pattern of subsidence on a large scale over this area, occurring at a rate of at least 40-50 mm per year (relative to the reference contour). The overall surface subsidence pattern and its magnitude appear to be consistent with (sparse) extensometer surveys undertaken by the US National Geodetic Survey.

Figure 1. Red contours of subsidence in 1.1-inch (28-mm) intervals relative to yellow reference contour, in a 26-month period over central and west Houston, Texas, overlaid on an ERS radar intensity image. Contours interpreted from colour-coded differential interferogram (inset); dashed contours are for guidance only and correspond to regions where fringes degenerate into poorer coherence. *Copyright: NPA Group 1999, ESA 1993/96. (Reproduced with kind permission from Harris-Galveston Coastal Subsidence District).*

The inset of Figure 2 shows a differential interferogram over Stoke-on-Trent, England. The fringes represent recent ground movement over a period of almost 2½ years. InSAR analysis found that the centre of Stoke subsided by some 8 cm over this period, with subsidence extending about 5 km East-West and 10 km North-South, as shown by the movement contours in Figure 2. On this evidence, a ground survey team from a major UK civil engineering company validated this finding using GPS methods (as shown along the yellow path). GPS results were shown to be in agreement with the subsidence trend, as detected by our InSAR work (Haynes *et al.*, 1997). Subsidence of this magnitude has been attributed to the collapse of the underground coal workings beneath the area.

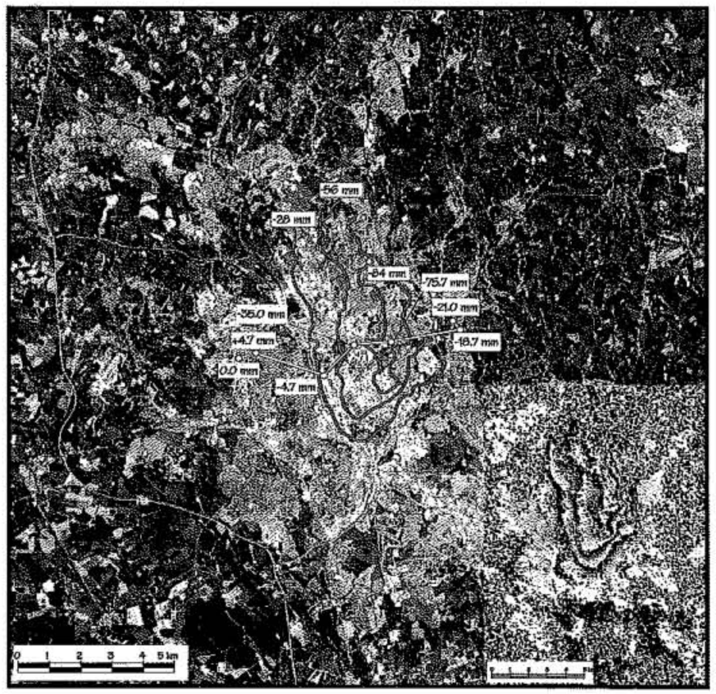

Figure 2. Red contours of displacement in 28-mm increments derived from the differential interferogram (inset) and superimposed on a Landsat TM image centred on Stoke-on-Trent, UK. The transect path along which GPS measurements were made is shown in yellow with corresponding displacement readings. (*Interferogram image copyright: NPA Group 1997, ESA 1993/95, WS Atkins Consultants Ltd 1997*).

Figure 3 shows two regions in the very centre of Tucson, the smaller exhibiting subsidence of 6 cm and the larger 9 cm over a period of almost 4 years, resulting from groundwater withdrawal. Detecting and mapping the extents and scale of subsidence activity in urban areas is of vital use to city planners' and civil engineers' development projects, as well as to the water authorities to assist them with mitigation plans.

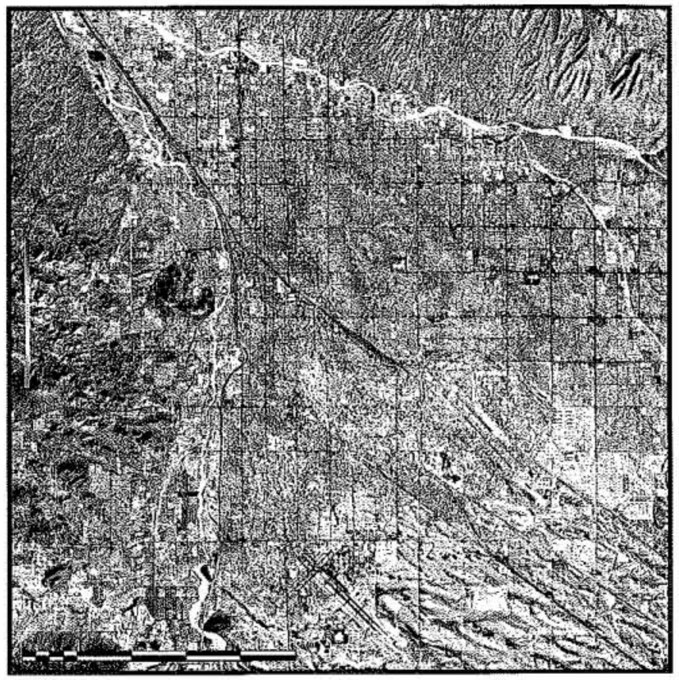

Figure 3. Colour-coded extract of differential interferogram, showing subsidence in Tucson, Arizona, fused with a Landsat TM/SPOT PAN optical merge. (*Interferogram image copyright: NPA Group 1998, ESA 1993/97. SPOT image copyright: CNES 1993*).

3. CONCLUSION

InSAR offers an effective alternative to conventional wide-area displacement mapping methods, and can be applied to a variety of ground motions and locations. As well as providing surface areal extents and an estimate of rates of surface movement, differential interferograms provide a continuous deformation field to assist with geophysical modelling and analysis of ground motion phenomena. A growing archive of SAR data stretches back to 1991 for ESA's ERS-1 and ERS-2 satellites, and continuity of InSAR data is assured with forthcoming satellite launches, such as ESA's ENVISAT platform.

NPA's InSAR displacement mapping service is routinely undertaken for a variety of customers worldwide, who need to determine rapidly and efficiently whether their region of interest is undergoing large-scale subsidence or uplift, and if so, to what magnitudes and areal extents. (This mapping facility also extends to other ground motion phenomena, such as earthquakes). Subsidence-prone regions can be pinpointed within typical 10,000 km² coverage areas in a matter of days. Interferometric results are analysed together with all the characteristics of a given area such as the geology, and may be combined with other data and presented as displacement and other map visualisations.

Acknowledgements

NPA would like to thank the European Space Agency and the British National Space Centre for enabling this work, and is grateful to its many collaborators and associates, including the UK Defence Evaluation and Research Agency, Phoenix Systems, WS Atkins Consultants Ltd and the University of Oxford's Department of Earth Sciences. We are also grateful to Harris-Galveston Coastal Subsidence District for their kind permission to present some of our results of the Houston interferometric study that they commissioned.

REFERENCES

Haynes, M. (1999) New Developments in Wide-Area Precision Surveying from Space, *Mapping Awareness,* **13** (10), pp. 40-43.

Haynes, M. (1999) Corner reflector aspects of the SNAP program: Demonstrating the utility of differential SAR interferometry for the assessment of earthquake risk, *FRINGE '99, Second International Workshop on ERS SAR Interferometry, Advancing ERS SAR Interferometry from Applications towards Operations*, 10-12 November 1999, Liège, Belgium.

Haynes, M., Capes, R., Lawrence, G., Smith A., Shilston, D. & Nicholls, G. (1997) Major urban subsidence mapped by differential SAR interferometry, *Proceedings of the Third ERS Symposium on Space at the service of our Environment*, Vol. 1, pp. 573-577, Florence, Italy, 14 –21 March 1997.

Sato, I. & Haynes, M. (1998), ESA/SAR Interferogram and Land Subsidence in the Southern Kanto Plain, *Abstract for Geological Survey Seminar, No. 257: Research on global environment*, pp. 83-88, 4 December 1998.

Wright, T.J., Parsons, B.E., Jackson, J.A., Haynes, M., Fielding, E.J., England, P.C., & Clarke, P.J. (1999) Source parameters of the 1 October 1995 Dinar (Turkey) earthquake from SAR interferometry and seismic bodywave modelling, *Earth and Planetary Science Letters,* **172** (1-2), pp. 23-37.

Wright, T., England, P., Fielding, E., Haynes, M. & Parsons, B. (1999) Source Parameters of the 17 August 1999 Izmit Earthquake From SAR Interferometry, *Proceedings of the American Geophysical Union Fall Meeting*, San Francisco, December 13-17, 1999.

LAND SUBSIDENCE - Vol. II
Proceedings of the Sixth International Symposium on Land Subsidence
Ravenna / Italy / 24-29 September 2000

GIS FOR LAND SUBSIDENCE EVALUATION IN NORTHERN KANTO PLAIN, JAPAN

Satoshi Murakami and Kazuya Yasuhara
Department of Urban and Civil Engineering, Ibaraki University, Nakanarusawa 4-12-1,Hitachi, Ibaraki, 316-8511, Japan

Fumiko Murata
Japan Regional Development Corporation, Kasumigaseki 3-8-1,Chiyoda, Tokyo, Japan

Abstract

Nearly 80% of land subsidence due to groundwater pumping in Japan takes place in the Northern Kanto region. It is important to estimate potential damage caused by land subsidence and to visualize this on a map over a wide area such as the Northern Kanto Plain, Japan. This paper describes the present situation and future prediction of land subsidence in this area and the evaluation of damage potential caused by land subsidence using a Geographical Information System (GIS). A simplified method for predicting future trends using observed settlements has been proposed and the applicability of the model has been verified by comparing the predicted and measured results at 1,282 points over the area. Using GIS, the present and future land subsidence has been visualized on a map. In addition, the occurrence of damage caused by land subsidence for each site can be assessed by means of a map based on a database consisting of a combination of predicted land subsidence and existing regional information.

Keywords : land subsidence, groundwater pumping, visualization, geographical information system (GIS), Northern Kanto Plain.

1. INTRODUCTION

Nearly 80% of land subsidence due to groundwater pumping in Japan takes place in the Northern Kanto Plain whose bordered area covers the five prefectures as shown in Fig. 1, Saitama, Gunma, Tochigi, Ibaraki and Chiba. According to recent subsidence records, the average amount of subsidence in this area due to groundwater pumping for agricultural, industrial, and drinking purposes has been approximately 5cm every year although the situation is different depending on the prefecture. The amount of land subsidence and its variation with time are normally evaluated by adopting one-dimensional consolidation theory which is modified to take into account the variation in live loads due to seasonal changes in groundwater level. To achieve this and in particular, to prevent disasters to the infrastructure and to regulate groundwater pumping, we need a great deal of information on geotechnical properties from field and laboratory investigations over the whole area under consideration. However, this is not practical from the viewpoint of expense and time. To overcome this difficulty, a simplified method is proposed which is capable of forecasting the future time-settlement relations based upon the information presently available, regarding settlements due to groundwater pumping. This method can be used even where the soil profiles are unknown although the soil parameters are necessary for conventional settlement calculations.

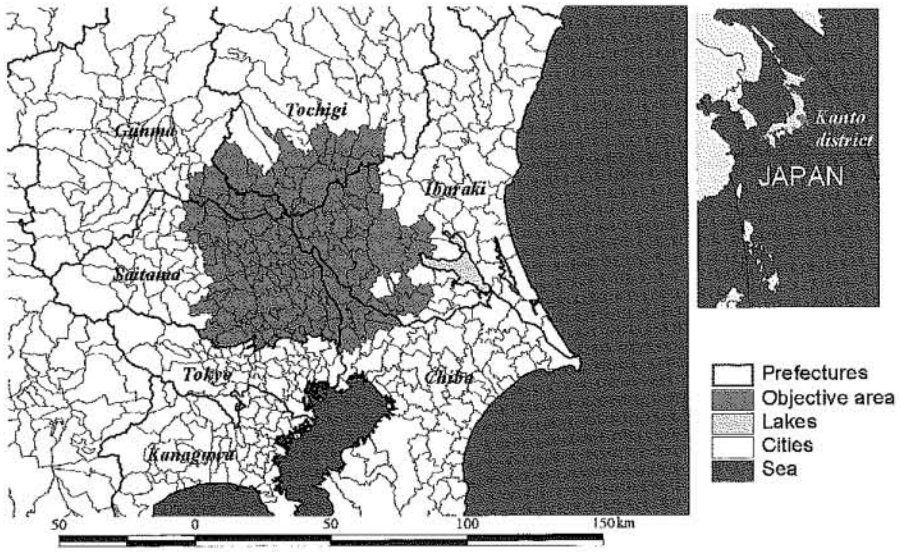

Figure 1. Objective area for land subsidence.

2. A SIMPLIFIED PROCEDURE

Strictly speaking, the solution of one-dimensional consolidation theory cannot be directly applied to land subsidence due to groundwater pumping. However, as a first approximation, it is here assumed that using the solution of Terzaghi's theory for one-dimensional consolidation of clayey soils, settlements due to groundwater pumping can be simply expressed as (see Appendix):

$$S = S_{po}[1 - \exp(-C_R t)] \qquad (1)$$

where S_{po} is the residual settlement expected from the present time until the termination of subsidence under the assumption that the groundwater variation is kept the same as observed at the present time, and C_R is a parameter corresponding to settlement strain rate. These are given by:

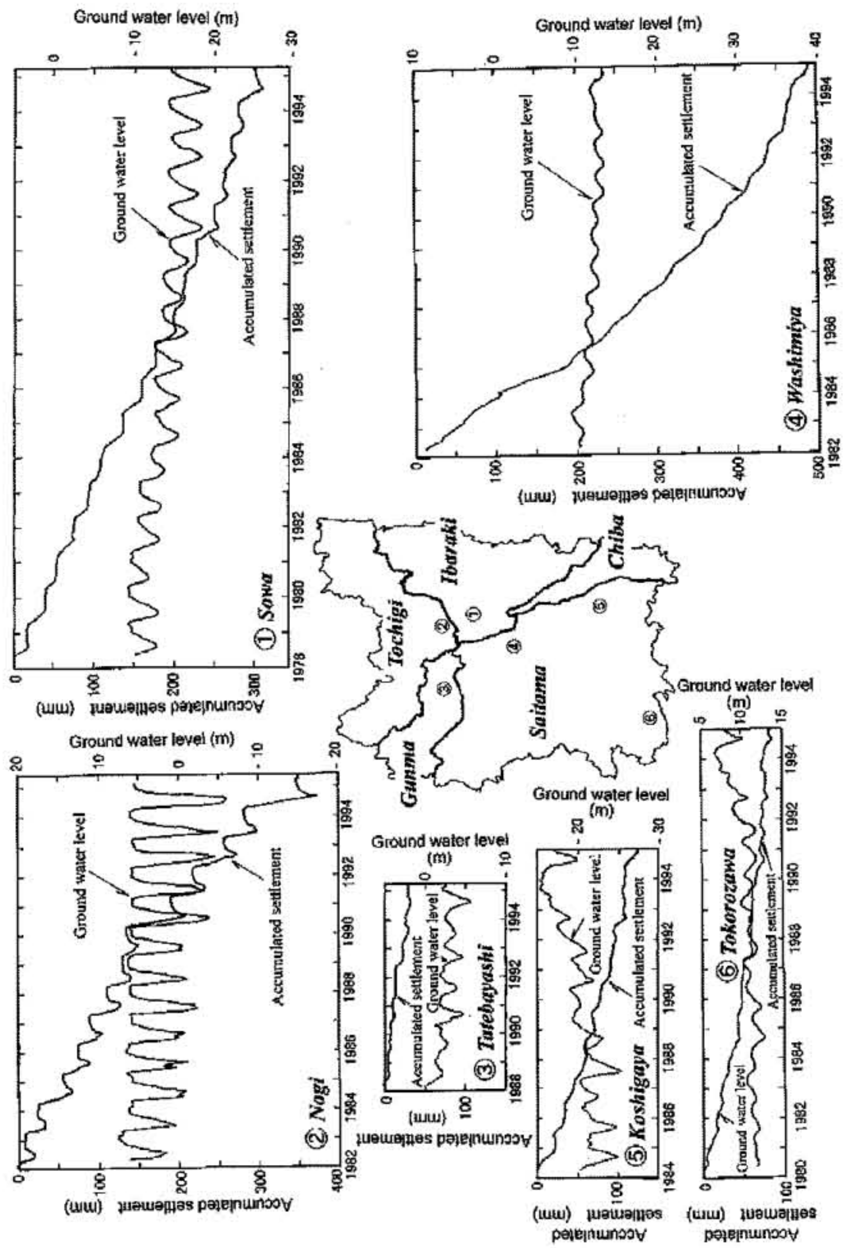

Figure 2. Variations of settlement and ground water level with elapsed time.

$$S_{po} = S_{r,f} = (8/\pi^2)\exp(-T_{vo}/4) \quad (2a)$$

$$C_R = T_{vi}/t_i = 4c_v/H_d^2 \quad (2b)$$

where $S_{r,f}$ is total residual settlement, T_{vo}, T_{vi} are time factors at the starting time to measure settlement and the arbitrary time during subsidence, t_i is an arbitrary time during subsidence, c_v is coefficient of consolidation, and H_d is the maximum length of drainage path for the clay layer.

If instead of such soil parameters as c_v, H and T_v two parameters, S_{po} and C_R, denoted by Eqs. (2a)and (2b) can be determined by using a statistical analysis of previously observed settlement records, the amount of settlement and settlement versus elapsed time relations can be obtained using the "non-linear least squares method".

3. APPLICATION OF THE METHOD PROPOSED

Applicability of the method proposed above is illustrated by comparing the calculated settlements with those observed. The two parameters $S_{p,o}$ and C_R were determined by a statistical analysis of land subsidence settlement-time records from 1970 until 1990 at 1,282 locations in the Northern Kanto plain in Japan covering the five prefectures: Tochigi, Gunma, Saitama, Chiba and Ibaraki. Typical variations of settlements and groundwater level with time for several locations are shown in Fig. 2. It was found that the variation of groundwater level and amount of settlements with elapsed time depends on each location. One of the characteristic features in Fig. 2 is that observed fluctuations in settlements followed seasonal changes in groundwater level.

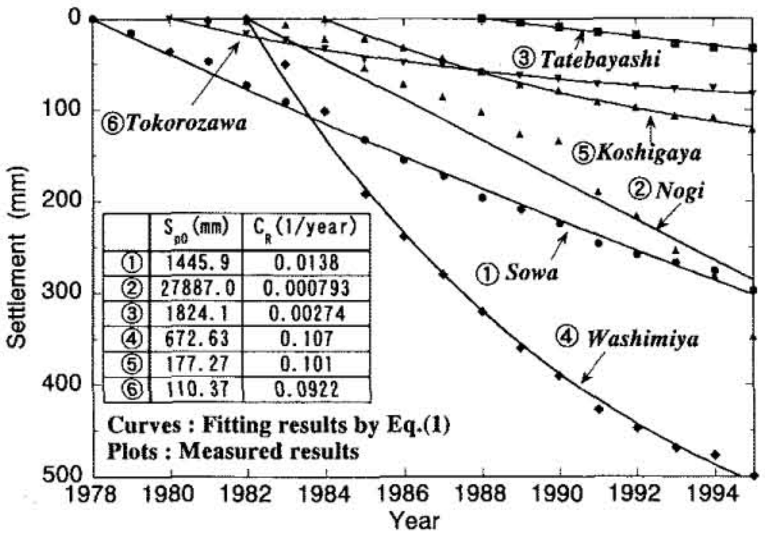

	S_{p0} (mm)	C_R (1/year)
①	1445.9	0.0138
②	27887.0	0.000793
③	1824.1	0.00274
④	672.63	0.107
⑤	177.27	0.101
⑥	110.37	0.0922

Figure 3. Comparison for observed and calculated settlement versus time relations.

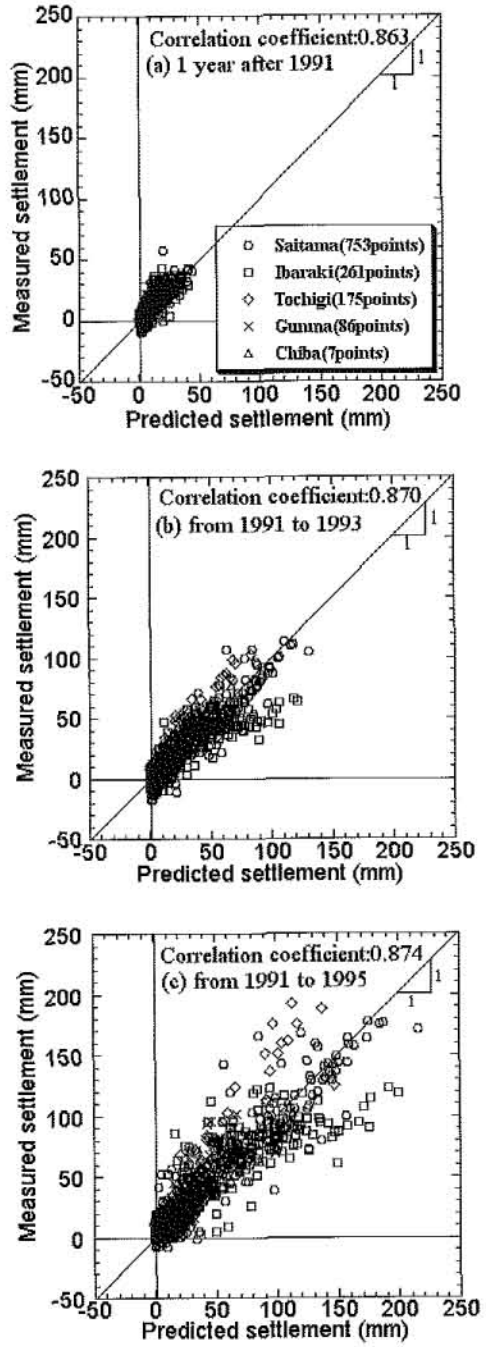

Figure 4. Comparison between predicted and measured settlements.

The procedure described in the Chapter 2 was applied to the previously observed settlements versus time records accumulated in the Northern Kanto district for approximately the last twenty years. The typical examples of observed and calculated settlement versus time relations for records from 1970 to 1995 are shown in Fig. 3. The relations of total observed and predicted settlements are given in Fig. 4 corresponding to the same period as used in Fig. 3. The comparisons in Fig. 3 and Fig. 4 are in fairly good agreement with each other.

4. FUTURE SETTLEMENT PREDICTION AND ITS REPRESENTATION USING GIS

Following the above-mentioned procedure for predicting land subsidence settlements using the previously observed field records at total of 1,282 locations, the future prediction of settlements was conducted for the next 5 years from 1998 to 2002. The results are represented and illustrated in Fig.5 as a hazard map of land subsidence in the Northern Kanto plain using a Geographical Information System (GIS). It is predicted that severe settlements will probably accumulate in some areas if the groundwater is pumped with continuous variations in groundwater level, although there is a tendency for gradually decreasing settlements in most areas in the Northern Kanto plain. Considering that there is possibility of big earthquakes occurring in this area, it is also suggested that through further investigation the potential for disastrous land subsidence from anticipated earthquakes could be demonstrated using a hazard map developed using GIS.

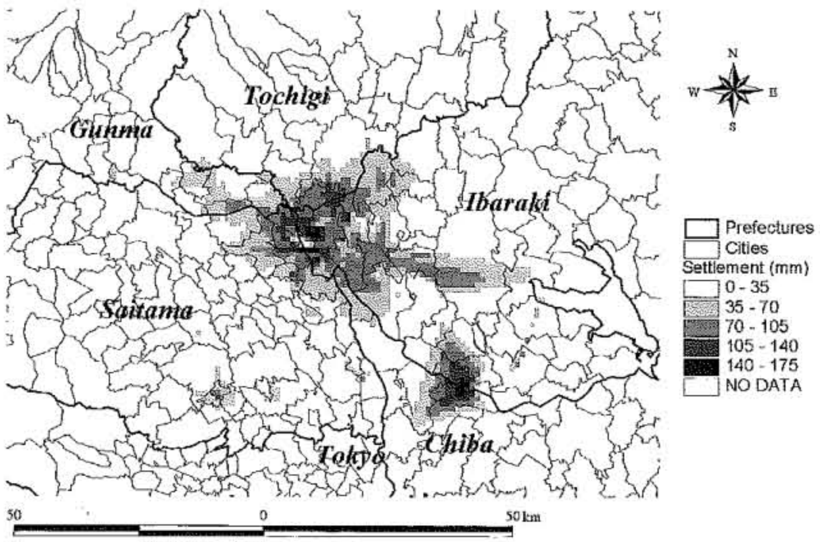

Figure 5. Map of land subsidence in the Northern Kanto Plain using GIS (1998-2002).

5. ESTIMATION OF DAMEGE POTENTIAL CAUSED BY LAND SUBSIDENCE

Damage caused by land subsidence is different for each site in the objective area because the characteristics of the sites are different. For example, water supply for irrigation deteriorates in agricultural areas. Bearing capacity of structures on piled foundations declines and underground lifelines are broken in industrial and business areas. Therefore, it is necessary to consider the characteristics of the sites for estimating the possible damage caused by land subsidence.

Damage potential D_p at a site expresses the summation of the products of the degree of damage D_i and the weighting w_i as is given by:

$$D_p = \Sigma\, w_i D_i \qquad (3)$$

For simplicity, D_i is assumed to be given by the following equations:

$$D_i = d_i / d_{max} \qquad (4a)$$

Where d_i and d_{max} are:

$$d_i = A_i\, S \qquad (4b)$$

$$d_{max} = \max \{ d_i \} \qquad (4c)$$

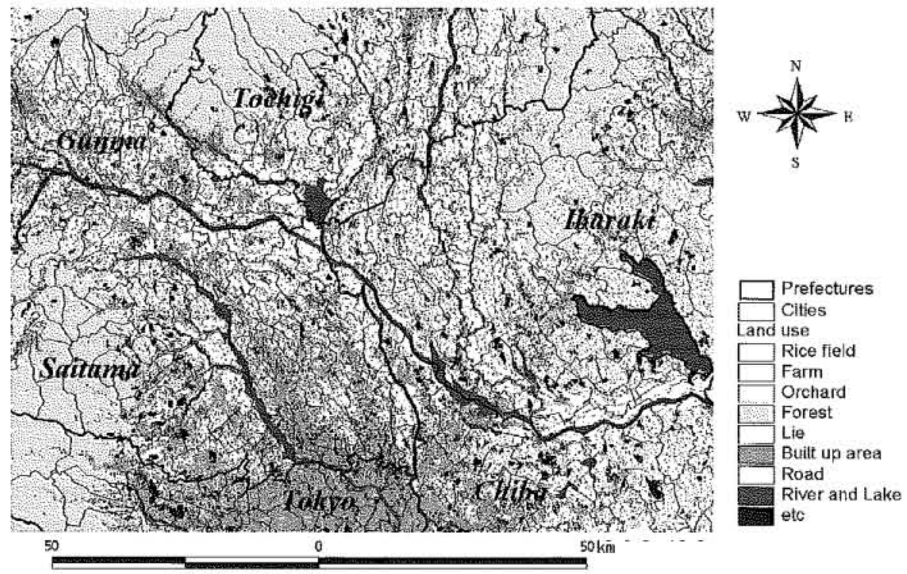

Figure 6. Land use map in the Northern Kanto Plain.

In Eq. (4b) A_i is the damage area and S is the future settlement in a site, and d_{max} is the maximum value of d_i in the objective area.

Using the above, we have tried to draw a damage potential map. The built up areas and rice fields obtained from a database of existing regional information, shown in Fig. 6, were used as the damage area A_i and the predicted settlements, from Fig. 5, were used as the future settlement S. The weighting w_i was assumed to be 1.0. The results are presented in Fig. 7. The occurrence of damage caused by land subsidence for each site can be specified by means of this map rather than a mere future settlement map.

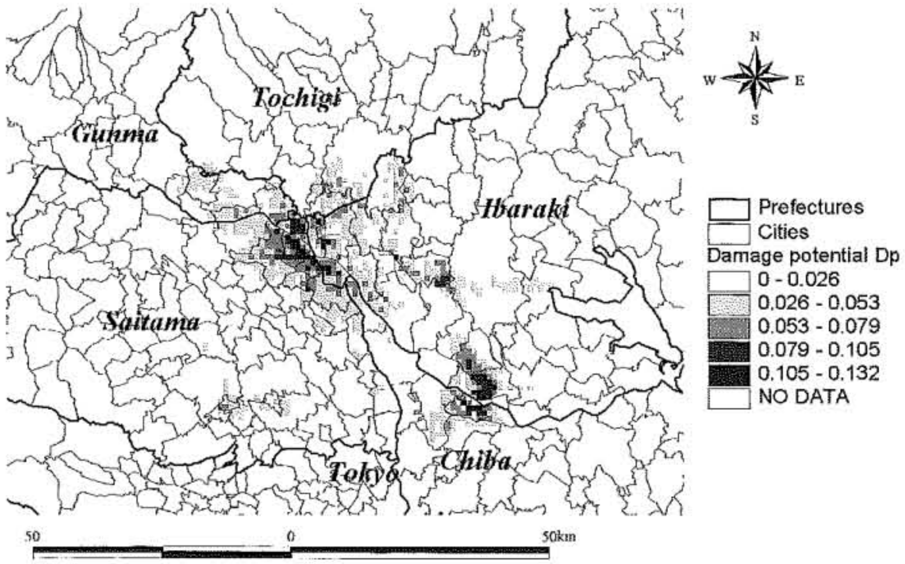

Figure 7. Damage potential map by land subsidence.

6. CONCLUSIONS

The results in this study are summarized as follows :

1) It is recognized that the land subsidence in the Northern Kanto Plain is caused by seasonal changes in the groundwater level due to the groundwater pumping.
2) A simplified method for predicting future trends using observed settlements has been proposed and the applicability of the model has been verified by comparing the predicted and measured results at 1,282 points over the area. Using GIS, future land subsidence has been visualized on a hazard map.
3) In addition, the occurrence of damage caused by land subsidence for each site can be assessed by means of a hazard map based on a database consisting of a combination of predicted land subsidence and existing regional information.

REFERENCES

Murakami, S., Yasuhara, K., Noguchi, N. & Hinoki, Y. (1997) *Journal of the Faculty of Engineering, Ibaraki University,* **45**, 65-72, (in Japanese)

Murakami, S., Yasuhara, K., & Murata, F. (1998): Land subsidence prediction using Geographical Information System (GIS), *Proc. Int. Symp. Lowland Technology*, 1, 507 - 512, Saga, Japan.

Appendix : Derivation of Eq. (1)

If land subsidence would approximately be governed by the one dimensional consolidation theory, the general solution for the both drainage ends is given by:

$$U = 1 - \frac{4}{\pi^2}\sum_{n=0}^{\infty}\frac{1}{a_n^2}\exp(-a_n^2 T_V) \quad \text{(A.1)}$$

When we consider the interval in two time factors of T_{vo} and T_{vi}, as shown in Fig. A1, the difference, δU, in degree of consolidation yields:

$$\delta U_i = U_i - U_0 = \sum_{n=0}^{\infty}\{\frac{2}{a_n^2}\exp(-a_n^2 T_{V0}) - \frac{2}{a_n^2}\exp(-a_n^2 T_{vi})\} \quad \text{(A.2)}$$

In the above equation, by replacing $T_{vi} - T_{vo}$ as δT_v and then neglecting the difference in inherent values after the second order of the solution of the consolidation theory, Eq. (A.2) leads to:

$$\delta U_i = \frac{8}{\pi^2}\exp(-\frac{T_{v0}}{4})\{1-\exp(-\frac{\delta T_{vi}}{4})\} \quad \text{(A.3)}$$

By referring to Fig. A2, Eq. (A3) can be rewritten as:

$$\delta Si = S_{PO}\{1-\exp(-C_R \delta t_i)\} \quad \text{(A.4)}$$

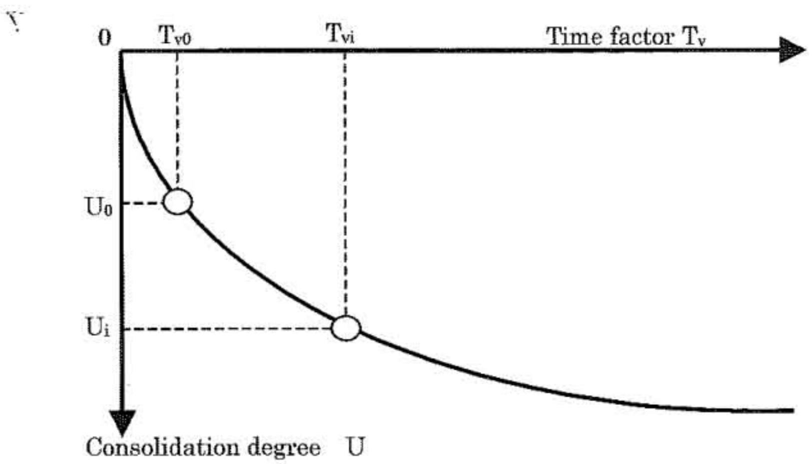

Figure A1. Degree of consolidation versus time factor curve.

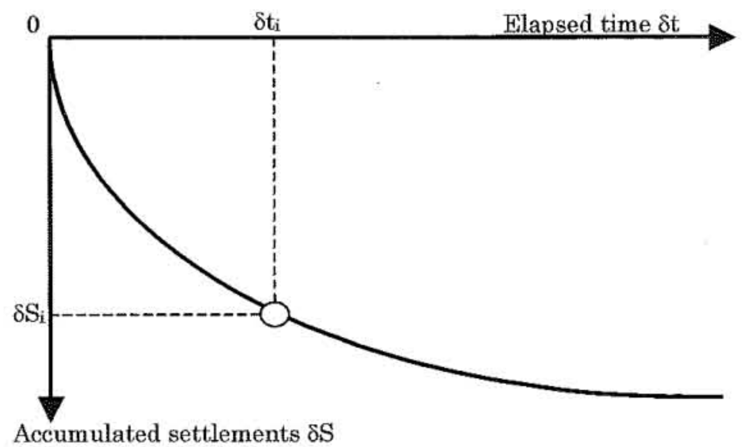

Figure A2. Settlement versus elapsed time curve.

LAND SUBSIDENCE - Vol. II
Proceedings of the Sixth International Symposium on Land Subsidence
Ravenna / Italy / 24-29 September 2000

MAPPING RECOVERABLE AQUIFER-SYSTEM DEFORMATION AND LAND SUBSIDENCE IN SANTA CLARA VALLEY, CALIFORNIA, USA, USING SPACE-BORNE SYNTHETIC APERTURE RADAR

Devin L. Galloway
U.S. Geological Survey, Placer Hall, 6000 J St., Sacramento, CA USA

Roland Bürgmann
Department of Geology, University of California, Berkeley, CA USA

Eric Fielding
Jet Propulsion Laboratory, Pasadena, CA USA

Falk Amelung
Hawaii Institute of Geophysics and Planetology, University of Hawaii, Honolulu, HI USA

Randell J. Laczniak
U.S. Geological Survey, Las Vegas, NV USA

Abstract

Interferometric Synthetic Aperture Radar (InSAR) is a powerful tool that exploits differences in reflected radar signals acquired at different times in order to measure deformation of the Earth's crust at an unprecedented level of spatial detail and a high degree of measurement resolution. Radar scenes obtained from satellites were used to map local- and regional-scale uplift and subsidence attributed to elastic deformation of the aquifer system in Santa Clara Valley, USA. InSAR displacement maps (interferograms)es reveal patterns of seasonal elastic uplift and subsidence (as much as 40 mm) superposed on longer-term uplift in Santa Clara Valley and on a declining rate of subsidence in Las Vegas Valley. The longer-term changes are a result of artificial recharge programsdistricts. The patterns of displacement are related to ground-water-level changes, as well as the trace of the Silver Creek fault zone. The influence of the fault zone on displacements suggests that the fault zone juxtaposes sedimentary sections of contrasting time-consolidation characteristics, or impedes lateral ground-water flow. Stress/strain analysis of paired time series of ground-water levels and InSAR derived displacements are used to compute elastic storage coefficient values. InSAR dramatically improves capabilities for detecting and monitoring subsidence, and provides new insights into the heterogeneity and properties of aquifer systems.

Keywords: subsidence mapping, aquifer-system deformation, InSAR, interferometry, synthetic aperture radar

1. INTRODUCTION

Interferometric Synthetic Aperture Radar (InSAR) is a powerful technology that exploits differences in reflected radar signals acquired at different times to measure active deformation of the Earth's crust. The technology provides displacement maps at an unprecedented level of spatial detail (pixel resolution on the order of 10s of m) and a high degree of measurement resolution (~ 5 mm). InSAR has been applied previously to investigate earthquakes, volcanoes, and land subsidence related to poro-elastic and -inelastic deformation (Massonnet et al., 1997; Fielding et al., 1998; Galloway et al., 1998; Amelung et al., 1999). Table 1 summarizes spatial and resolution characteristics of methods used to measure subsidence caused by the compaction of aquifer systems.

Table 1. Measurement characteristics of methods used to measure subsidence caused by aquifer-system compaction (modified from Galloway et al., 2000).

Method	Component Displacement	Resolution[1] millimeters	Spatial Density[2] samples/survey
Spirit level	Vertical	1-10	10-100 (*l*,*n*)[3]
Geodimeter	Horizontal	1	10-100 (*l*,*n*)[3]
Borehole extensometer	Vertical	.01-.1	1-3 (*p*)[3]
Horizontal extensometer: Tape	Horizontal	.3	1-10 (*l*)[3]
Invar wire	Horizontal	.001	1 (*l*)[3]
Quartz tube	Horizontal	.0001	1 (*l*)[3]
GPS	Vertical	20	10-100 (*n*)[3]
	Horizontal	5	
InSAR	Range	5-10	.1-10 x 10^6 (*pixels*)[3]

[1]Measurement resolution in millimeters, generally attainable under good conditions
[2]Number of measurements generally attainable under good conditions to define the spatial extent of land subsidence at the scale of the survey
[3]Survey scale in order of increasing spatial density: *p*=point, *l*=line, *n*=network, *pixels*=picture elements

Land subsidence attributed to the compaction of aquifer systems caused by ground-water pumping is a global problem and the single largest cause of subsidence in the USA (National Research Council, 1991). Favorable radiometric conditions in the urbanized Santa Clara Valley and elsewhere, especially in the arid western USA have led to the successful application of InSAR to mapping aquifer-system compaction and subsidence in alluvial basins hosting non-agricultural land-uses including the Antelope Valley in California (Galloway et al., 1998) and Las Vegas Valley (Amelung et al., 1999) in Nevada. One abbreviated case study is presented — Santa Clara Valley, California (Fig. 1A), where InSAR was applied to investigate elastic deformation of the aquifer systems attributed to seasonal changes in ground-water levels caused by ground-water pumping.

2. APPROACH

Differential interferograms were developed using synthetic aperture radar (SAR) scenes (Track 70, Frame 2853) acquired for Santa Clara Valley by European Remote Sensing satellites. Using a two-pass method (e.g. Massonnet et al., 1993) three SAR scenes were combined to form two "change" interferograms with temporal baselines of 210 days, January 4, 1997 to August 2, 1997 (Orbits 8942, 11948), and 1,774 days, September 23, 1992 to August 2, 1997 (Orbits 6227, 11948). The phase component of the "change" interferograms contains information not only about the coherent displacements of all scatterers imaged by the radar, but also topography. The topographic component was removed using a topographic interferogram simulated from a 30-m digital elevation model (DEM) of the study area. The full resolution differential interferogramss were translated from the geometry of the radar to cartographic coordinates. The coherent phase component of the resulting differential interferograms represents range (line-of-sight) displacements, mapped modulo 28 mm (one-half the wavelength of the C-band radar), for the period covered by the interferogram. The interferograms were processed using the DIAPASON software system developed by the *Centre National D'Etudes Spatiales, Agence Francaise De L'Espace.*

The interferograms were unwrapped and resampled, resulting in a relatively smoothed, georeferenced displacement surface at a pixel size of 30 m x 30 m. The displacement surface represents the spatially continuous line-of-sight displacements. These were scaled to compute an equivalent vertical displacement assuming all deformation was vertical. The interferograms were interpreted using available hydrogeologic information, including contemporaneous ground-water levels, aquifer-system compaction measured by borehole extensometers, and geodetic surveys.

3. SUBSIDENCE AND REBOUND IN THE SANTA CLARA VALLEY, CALIFORNIA

The Santa Clara Valley was the first area in the USA where land subsidence due to ground-water withdrawal was recognized (Tolman and Poland, 1940). From 1934 to 1967 subsidence ranged from 0.5 to 1.5 m under the bay and its tidelands to more than 2 m in much of San Jose and Santa Clara (Fig. 1A). The maximum detected subsidence during this period, nearly 5 m, occurred in San Jose. The Santa Clara Valley was also the first area where, in the mid-1960s, effective remedial action was undertaken to mitigate subsidence. By 1969 rapid subsidence had been arrested by the importation and recharge of surface water. Through the late 1980s only a small amount of residual aquifer-system compaction and subsidence occurred (Poland and Ireland, 1988). Since then, no inelastic compaction (permanent subsidence) has been detected by annual leveling surveys and continuous-recording borehole extensometers. Since 1965 water levels in the confined aquifer system have recovered as much as 70 m, and presently stand near their predevelopment levels in many areas. These longer-term changes are chiefly a result of artificial recharge programs operated by the Santa Clara Valley Water District.

Seasonal elastic (recoverable) displacements (uplift and subsidence) measured by extensometers in Santa Clara Valley occur in response to seasonal variations in ground-water levels. Presently, as much as 30 mm of seasonal displacement is measured in San Jose in response to about a 20 m variation in ground-water levels (written communication, B. Ahmadi, Santa Clara Valley Water District, 1999). The summer 1992 to summer 1997 interferogram (not shown here) revealed small magnitude (5-10 mm) generalized uplift occurring throughout the valley floor. Seasonal elastic displacements were detected in the winter 1997 to summer 1997 interferogram.

The 1997 interferogram is shown in Figure 1B, and contours of subsidence measured on the interferogram are shown in Figure 1C. The period covered by the interferogram, January to August, excludes most of the seasonal recovery of ground-water levels that typically occurs between October and December, and includes nearly all of the seasonal drawdown period, April to September. More than 100 km^2 of seasonal, recoverable subsidence in excess of 10 mm is observed in the central part of the valley. The maximum detected subsidence is about 40 mm in San Jose. The shape of the seasonal area of recoverable subsidence is similar to the shape of the historically measured subsidence bowl (Fig. 1A). Some uplift occurs along the margins of the valley; about 15 mm of uplift is observed east of the Silver Creek fault zone. The uplift may be related to recharge (artificial and natural) from percolation ponds and streams draining the surrounding ranges. The spatially detailed, high resolution displacements measured in the elastic range of deformation suggests that detailed maps of the elastic storage coefficients

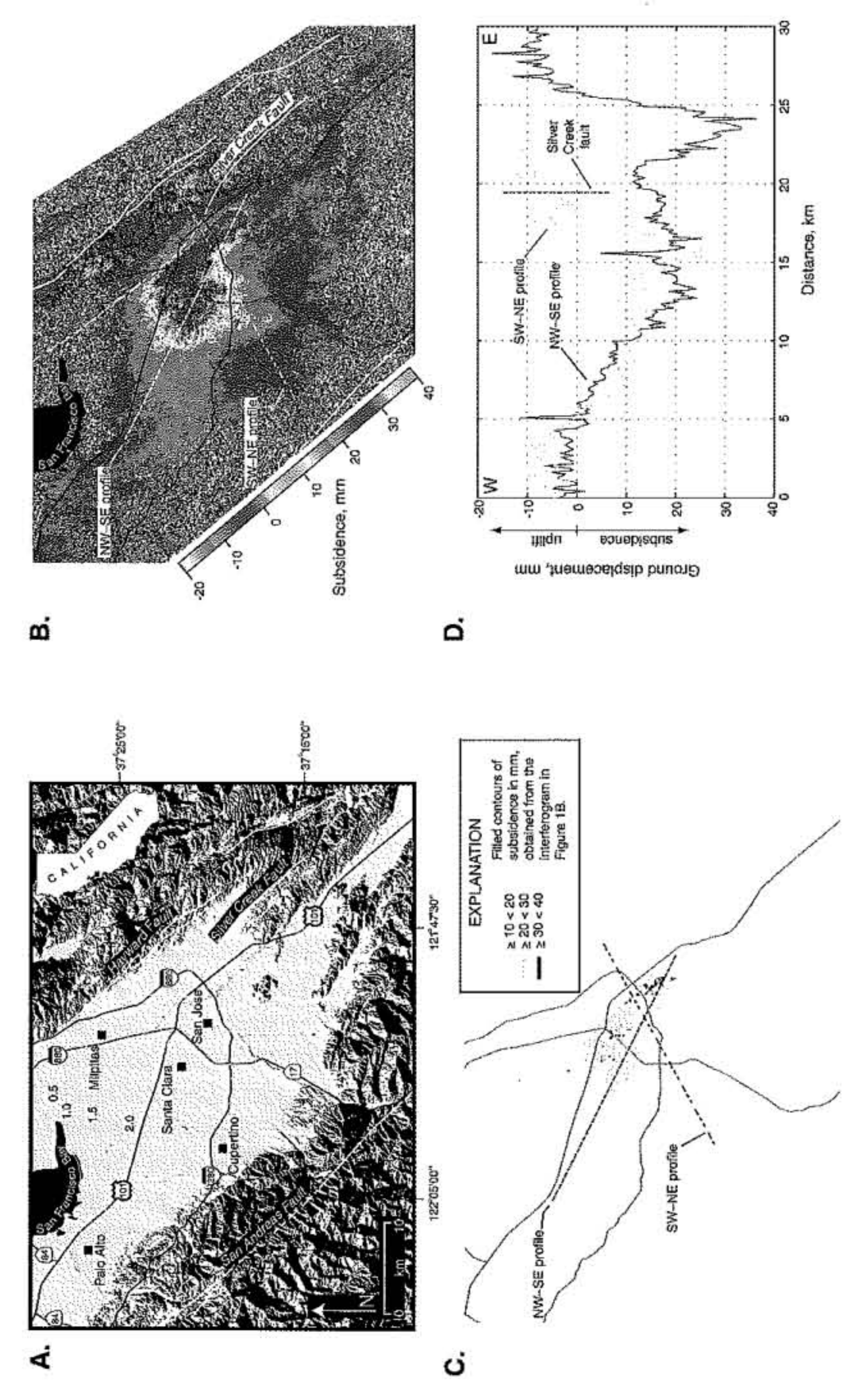

Figure 1. Santa Clara Valley subsidence. **A.** Location map showing historical subsidence; **B.** Interferogram (1/4/97-8/2/97) showing pattern of reversible subsidence and uplift; **C.** Contoured interferogram showing reversible subsidence; **D.** Interferometrically-derived ground displacements measured from profiles.

could be developed. Synchronous, seasonal water-level change maps and interferograms could provide stress/strain information to compute skeletal elastic storage coefficients at the scale of pixels using methods employed for analyzing displacements at borehole extensometer sites (Riley, 1969).

The northeastern boundary of the seasonal subsidence pattern is linear and subparallel to the trace of an inferred northwesterly extension of the buried Silver Creek fault zone. Two profiles taken from the interferogram (Fig. 1D) reveal steep gradients of ground displacements at or near this boundary, as high as 30 mm in 1.5 km (2×10^{-5} km/km). Recent seismic reflection/refraction surveys, undertaken as a result of the interferogram, confirm the presence of buried faults at this boundary (written communication, R. Catchings, U.S. Geological Survey, 2000). Larger summer water-level declines occur west of the fault zone and may explain the larger subsidence magnitudes measured there compared to east of the fault zone. The linear shape of the displacement surface near this boundary suggests that, 1) the fault zone juxtaposes sedimentary sections of contrasting time-consolidation characteristics (stress history, compressibility, sediment thickness, and vertical hydraulic conductivity); or, 2) lateral ground-water flow across the fault zone is impeded; or both. More detailed hydrogeologic information in this area is needed to resolve the controlling factors.

4. CONCLUSIONS

Mapping programs are recognized as a critical element in efforts to identify and manage subsidence problems (National Research Council, 1991). InSAR can provide deformation maps of Santa Clara Valley and other areas at an unprecedented level of spatial detail and a high degree of measurement resolution. The interferograms reveal patterns of seasonal elastic uplift and subsidence (as much as 40 mm) superposed on longer-term uplift. These longer-term changes are chiefly a result of artificial recharge programs operated by the Santa Clara Valley Water District. Since 1965 water levels in the confined aquifer system have recovered as much as 70 m, and presently stand near their predevelopment levels in many areas. The patterns of displacement are related to the seasonal and longer-term patterns of ground-water-level changes as well as the trace of the Silver Creek fault zone. The influence of the fault zone on displacement patterns suggests that, the fault zone juxtaposes sedimentary sections of contrasting time-consolidation characteristics, or impedes lateral ground-water flow.

InSAR not only dramatically improves capabilities for detecting and monitoring subsidence, but also provides new insights into the poroelastic properties and heterogeneity of aquifer systems. The spatially detailed, high measurement resolution of displacement in the elastic range of deformation suggests that detailed maps of the elastic storage coefficients could be developed. Favorable radiometric conditions in the urbanized Santa Clara Valley and elsewhere, especially in the arid western USA have led to the successful application of InSAR to mapping aquifer-system compaction and subsidence in alluvial basins hosting non-agricultural land-uses, including the Antelope Valley in California (Galloway et al., 1998) and Las Vegas Valley (Amelung et al., 1999) in Nevada.

Acknowledgements

Radar data for this study was obtained from the European Space Agency, distributed through Eurimage Corporation and Radarsat International for purposes of research and development. This work was supported by NASA, Goddard Space Flight Center (agreement no. S-10156-X). The Santa Clara Valley Water District provided geodetic and hydrogeologic data.

REFERENCES

Amelung, F., Galloway, D.L., Bell, J.W., Zebker, H.A., & Laczniak, R.J. (1999) Sensing the ups and downs of Las Vegas: InSAR reveals structural control of land subsidence and aquifer-system deformation, *Geology*, **27**(6), 483-486.

Fielding, E.J., Blom, R.G., & Goldstein, R.M. (1998) Rapid subsidence over oil fields measured by SAR interferometry, *Geophys. Res. Lett.*, **25**, 3215-3218.

Galloway, D.L., Hudnut, K.W., Ingebritsen, S.E., Phillips, S.P., Peltzer, G., Rogez, F., & Rosen, P.A. (1998) Detection of aquifer system compaction and land subsidence using interferometric synthetic aperture radar, Antelope Valley, Mojave Desert, California, *Water Resour. Res.*, **34**(10), 2573-2585.

Galloway, D.L., Jones, D.R., & Ingebritsen, S.E., eds. (2000) Land subsidence in the United States, *U.S. Geol. Surv. Circ.* 1182, 177 pp.

Massonnet, D., Rossi, M., Carmona, C., Adragna, F., Peltzer, G., Feigl, K., & Rabaute, T. (1993) The displacement field of the Landers earthquake mapped by radar interferometry, *Nature*, **364**, 138-142.

Massonnet, D., Holzer, T., & Vadon, H. (1997) Land subsidence caused by the East Mesa geothermal field, California, observed using SAR interferometry, *Geophys. Res. Lett.*, **24**(8), 901-904.

National Research Council (1991) Mitigating losses from land subsidence in the United States, Nat. Acad. Press, Washington, D. C., 58 pp.

Poland, J.F., & Ireland, R.L. (1988) Land subsidence in the Santa Clara Valley, California, as of 1982, *U.S. Geol. Surv. Prof. Pap.*, 497-F, 61 pp.

Riley, F.S. (1969) Analysis of borehole extensometer data from central California, *in* Land subsidence, v. 2, Tison, L.K. ed., *Int. Assoc. Sci. Hydrol.*, **89**, 423-431.

Tolman, C.F., & Poland, J.F. (1940) Ground-water, salt-water infiltration, and ground-surface recession in Santa Clara Valley, Santa Clara County, California, *American Geophys. Union Trans.*, pt. 1, 23-24.

LAND SUBSIDENCE - Vol. II
Proceedings of the Sixth International Symposium on Land Subsidence
Ravenna / Italy / 24-29 September 2000

STATISTICAL ANALYSIS OF BENCHMARK STABILITY PRIOR TO NATURAL GAS EXTRACTION IN A HOLOCENE CLAY AND PEAT AREA, PROVINCE OF FRIESLAND, THE NETHERLANDS

Cheung, G., M.A. Grima, P.M. Maurenbrecher[1] and F. Schokking[2]

[1] *TU-Delft Faculty of Civil Engineering and Geosciences, P.O. Box 5028, NL-2600 AD DELFT*

[2] *GeoConsult bv, P.O. Box 2296, NL-2002 CG HAARLEM, The Netherlands*

Abstract

Benchmarks attached to civil structures are used for monitoring of land subsidence above natural gas extractions. Many of the structures are founded on compressible clay and peat layers. Autonomous vertical velocities of the benchmarks (- 6.75 to + 1.75 mm/year), mainly related to excessive lowering of polder water levels, which cause the oxidation of peat, give a component in measured bruto height differences between successive surveys, which has to be eliminated, to reach the true land subsidence value.

Statistical K-means cluster analysis was found suitable to classify the data set of historical vertical velocities of the benchmarks, prior to the start of the natural gas extraction. The optimum number of clusters appeared to be three, with clay thickness as the leading parameter and to be the most important factor in the process causing the vertical velocities. The other parameters used in the analysis were peat thickness and polder water levels. Not enough data was available on foundation conditions to be used in the analysis, although from the interpretation of cluster results the generally known foundation conditions in the area could be reasoned.

If validated with data sets of similar areas and further developed, the described method may serve as a basis for selecting benchmarks with an acceptable confidence level of autonomous historic vertical velocities, to be used in surveys for land subsidence measurement.

Keywords: land subsidence, monitoring, benchmarks, settlement, autonomous vertical velocities, statistics, distribution

1. INTRODUCTION

Research of the stability of benchmarks used in monitoring land subsidence related to natural gas extraction in the north of The Netherlands was carried out by GeoConsult for the Nederlandse Aardolie Maatschappij (NAM). This study comprised investigation of land subsidence related to excessive polder water level lowering in an area of compressible Holocene clay and peat layers, and an analysis of the vertical movement of benchmarks founded in these deposits, described in terms of the geological, hydrological and foundation parameters. This latter part of the study was carried out by GeoConsult in co-operation with TU-Delft, Faculty of Civil Engineering and Geosciences, by using statistical methods.

The autonomous vertical velocity of benchmarks mounted on constructions can be caused by many internal (structural) and external influences. The latter can be related to applied changes to the stress on the foundation, such as from an added floor to a building or related to movements of the foundation itself: settlements or differential settlements. If buildings are founded on the firm

Pleistocene layers the settlements (or sometimes rises) are related to deeper geological processes: compaction of aquifers, compaction of deeper clay layers, tectonic movements or movement of salt layers or structures (salt squeeze and halokinesis). Structures founded in the compressible Holocene clay and peat layers, may undergo settlements resulting from subsidence of these layers, related to excessive lowering of polder water levels, inducing oxidation of peat, hydrodynamic settlement and soil shrinkage (Schothorst, 1979; Schokking, 1995). Also the water extraction by trees in dry summers, additional loads by placed embankments or roads can cause additional stress on the soil and resulting settlement or differential settlement. The rotting of wooden piles where ground water tables are lowered can also induce settlements.

As many of the above described phenomena can influence the autonomous vertical velocities, besides the noise attached to the geodetic measurements, a method was looked for, which would point at the leading influence(s) on the settlement processes. Statistical techniques such as spatial correlation, multiple regression, principal component analysis, discriminant analysis and cluster analysis were thought to possibly aim at solutions to connect geological, hydrological and foundation engineering parameters to a data set of measured historical vertical velocities.

The above mentioned statistical methods were applied to the data set by trial and error to show in the end, that the K-means cluster analysis gave the most satisfying results. Although only giving an indication of a possible procedure to use in future, the adopted method may serve if validated on other data sets and developed further, as a means to select benchmarks with an acceptable autonomous vertical velocity to be used in monitoring of land subsidence.

The authors are thankful to NAM, allowing publication of the research by GeoConsult and TUDelft and the data used in it.

2. BENCHMARK STABILITY

Land subsidence resulting from the extraction of natural gas is anticipated to occur in the first quarter of the century above reservoirs in the north east of the

Province of Friesland (Fig1). A major part of the reservoirs is situated in areas where Holocene clay and peat layers occur near the surface (Fig 2a and b). The lowering of polder water levels, with the aim to keep the land as dry as practically possible for agricultural purposes, results in considerable subsidence of the surface, with rates generally varying from approximately 2 to 6 mm/year. The processes which are involved in the surface subsidence are, in order of significance: oxidation of peat, consolidation, resulting from increase in effective stresses and shrinkage of peat (Schothorst, 1979; Schokking, 1995). Where peat is covered by clay it has been found, that there is decrease in the land subsidence with an increase in the thickness of the clay.

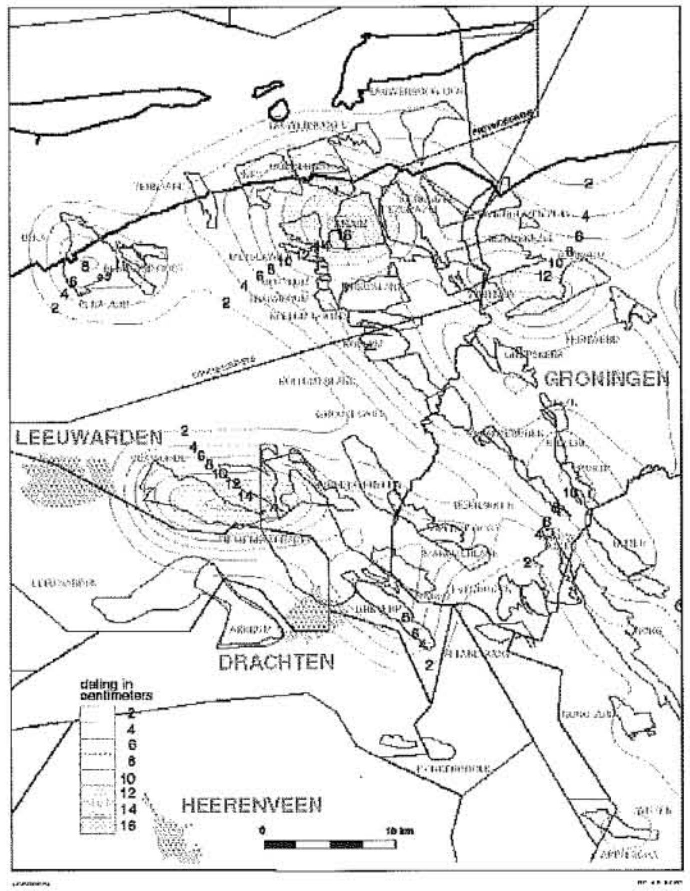

Figure 1. Land subsidence resulting from natural gas extraction. Prognosis Friesland 2025 (NAM, 1998).

The measurement of the land subsidence related to the gas extraction is hampered as a large number of benchmarks mounted on structures (i.e. buildings, bridges etc.) whose foundations are on the soft clay and peat layers, exhibit autonomous velocities. The foundations are only partly related to the rates of surface subsidence resulting from the lowering of polder water levels. The vertical velocity of structures in the clay and peat may differ from the subsidence rates of the free field as near to and beneath the structures hydrological and geotechnical conditions can be quite different (Hannink, 1984). Benchmarks connected to structures with foundations in the firm granular Pleistocene layers below the clay and peat layers, show lower autonomous velocities of up to approximately 1 mm/year.

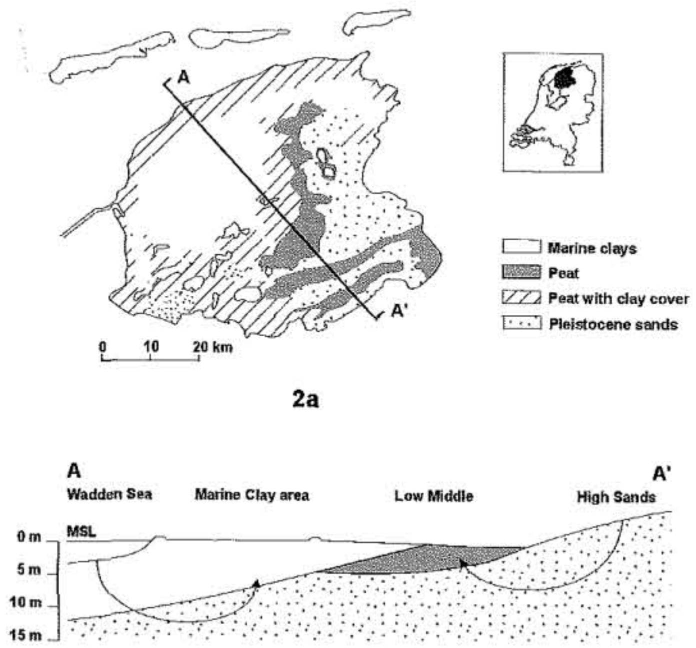

Figure 2 Geological map and cross section of the Province of Friesland (after Schokking, 1995).

To be able to use the benchmarks with a given autonomous velocity for the measurement of the land subsidence above the reservoirs, it appeared important to assess the parameters which influence the general patterns of the vertical velocities of the structures on which the benchmarks are mounted. This is to be able to increase the confidence level of the velocities. Only parameters occurring with a regional distribution were considered appropriate to be used in such an assessment. These are the distribution of clay and peat layers and surface water levels which are considered to be the parameters having an influence of the rate of subsidence of the free field surface and the foundation types of the structures.

3. AVAILABLE DATA SETS

For this study several data sets were obtained from the archives of the Province of Friesland and of NAM. The data were processed and interpreted for use in a suitable numerical format in statistical analysis.

3.1. Vertical velocities of benchmarks

The geodetic data from which the vertical velocities are derived have been obtained from the Netherlands Ordnance Survey records stretching from surveys carried out from the end of the 19th century until the start of gas extraction in the early 1970. The velocities were established for each benchmark by linear regression analysis with the method of square roots, using at least three successive epochs. Verification of the data was done by discarding data with a standard deviation of the regression line of > 0.8 mm and by visual recognition of inconsistent trends. The whole population of velocities ranges from – 6.75 mm/year to + 1.75 mm/year. The frequency distribution of the vertical velocities shows several distinctive sub- populations of which the origin is unclear at first sight, although the most prominent subpopulation appears to indicate benchmarks mounted on constructions with foundations in the firm Pleistocene layers (Fig. 3). The average of these velocities lies around zero, with positive and negative deviations, which may be caused by several geodetic related phenomena (e.g. geodetic noise, measurement faults, non-compatibility of successive surveys) and geological phenomena, such as natural land subsidence from compaction of deeper layers, resulting in the subsidence of underground benchmarks of the basal network, and the halokinesis of salt.

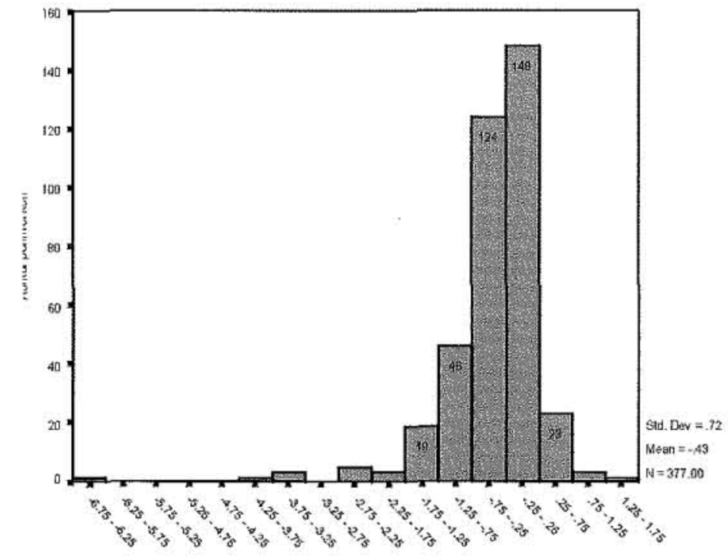

Figure 3. Frequency distribution of vertical velocities.

3.2. Holocene clay and peat distribution

The distribution of the thickness of the clay and peat layers deposited during the Holocene on the Pleistocene surface could be established from a database of average thicknesses based on approximately 9 boreholes for each km^2. Clay and peat isopachs were made from this data using spatial correlation with the method of inverse distance (Fig. 7). Most important general patterns are an increase in thickness of the clay layer (up till approx. 4 m) which covers the underlying peat in northerly and westerly directions, and a thinning out of the peat in the same directions. In the north occur thicker clays (up till 10 m) which are infillings in marine inlets.

3.3. Polder surface water levels

The level of the surface water in polders which are underlain by peat have a strong relationship with the with the rate of surface subsidence resulting from the oxidation of peat. The water levels are from a database set up by the Province of Friesland containing the present day surface waterlevels maintained by the Waterboards within the province.

3.4. Foundation conditions

The data on foundations were found to be particularly scarce, which was searched for in the archives of municipalities of north Friesland region. Only very few actual data on foundation conditions of the structures on which the benchmarks are attached could be obtained. The generally known types of foundations in the area of study are described below.

Most of the older constructions, built before 1950, have pad or strip foundations either on Pleistocene firm sands, on peat or on clay covering the peat (Fig. 4a). Where the peat occurs at the surface the material is generally highly compressed and the foundations are in fact resting on the Pleistocene. The same holds true for pad or strip foundations on relatively thin clay layers underlain by thin layers of peat. Where clay and peat layers are thicker these layers can carry the load, which is then distributed more within the clay layers. Also tapered wooden friction piles, ending within thicker clay layers have been used in the past (Fig 4c). Present day foundations are often made by using prefabricated concrete piles driven into the firm Pleistocene sands (Fig 4b).

4. METHOD DEVELOPMENT

The purpose of the project was to find a relationship between the benchmark velocities and the local geological parameters. These parameters are clay thickness, peat thickness, water level and foundation types and conditions. Although the foundation types are generally known, as described above, in most specific benchmark locations they are not known. For that reason the foundation type and loading cannot, unfortunately, be used as a parameter in the analysis.

Spatial correlation methods could not be used as the benchmark velocities are very dependent on local geotechnical and hydrological conditions and on foundation types, which was also recognised in earlier studies (Hoefnagels et al., 1995). Further there is the difference in the velocity of subsidence in the free field, and that of structures in geologically similar areas.

Since there was a relatively large amount of benchmark velocity data available , multivariate data analysis was examined. Multivariate methods examine the influence of changes, which occur in a number of variables. Finding a relationship with the geology can be complex for similar reasons as for the spatial correlation techniques. These influencing factors are impossible to isolate and to be studied individually. It is often the case that the relative importance of one of the possible important variables can not be determined. The best strategy is frequently to study as many factors of a problem as possible first. This usually helps identify the major influencing factors.

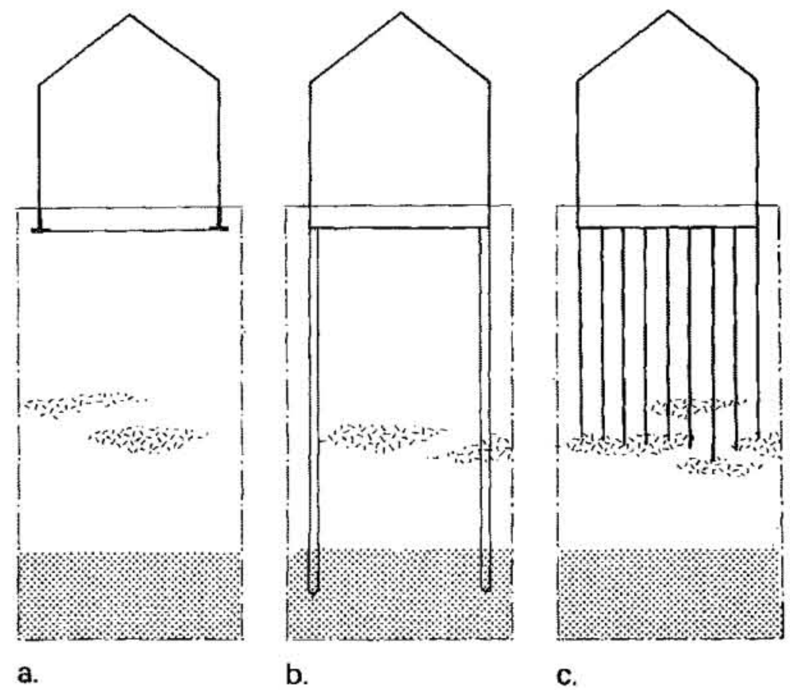

Figure 4. Common foundation types in the Province of Friesland (a) Pad or strip foundation (b) Concrete piles in firm layer (c) Wooden tapered friction piles in clay layer (after Commissie Bodemdaling door Aardgaswinning, 1987).

The methods that were studied are:

(1) Multiple regression
(2) Principal component analysis
(3) Cluster analysis
(4) Discriminant analysis

(1) Multiple regression analysis showed that there was no linear relationship between the dependent benchmark velocity and the independent geological parameters.
(2) Principal component analysis also did not provide a solution because of the low number of available variables. Principal component analysis is specially developed to determine the most important parameters of the data. The analysis can be regarded, indirectly, as a variable reducing technique.
(3) Cluster analysis enables zonation of the data. Clustering algorithms divides the data in distinct groups. Discriminant function analysis (4) would have been a good technique to apply after clustering, if the data had been normally distributed. This method involves putting objects in predetermined groups with a discriminant function.

Since cluster analysis was not limited by such factors as data population or distribution restrictions and appeared to produce good results, this method was adopted in the method procedure.

To validate hypotheses derived from interpretation of the clustered data research was done of the foundation types and specific conditions. A few structures had records on their foundations that were found in the municipal archives.

5. CLUSTER ANALYSIS

The data distribution when plotted as a distribution curve (Fig. 3) showed small groups as outliers to largely normally distributed data from –2.75 to +1.75 mm/yr centred slightly asymmetrically peak data at nominal settlement velocities of between –0.25 to +0.25 mm/yr. The distribution relative to the settlement velocities suggests the possibility of splitting the data set into different subgroups such as the outliers, and into at least two further zones within the large population in the normally distributed histogram relative to sinking and rising velocities. To accomplish this, data clustering methods were examined.

The goal of data clustering is to distil a data set into different classes or groups. This method originates from data analysis and pattern recognition (Bezdek, 1981). Generally speaking clustering methods can be divided into two categories – hierarchical clustering and non-hierarchical clustering. The approach adopted in the current paper is the non-hierarchical one.

Within the non-hierarchical category various clustering algorithms have been introduced such as the K-means method, the fuzzy C-means method, the Mountain method, and the subtractive clustering method (Bezdek, 1981).

There are two ways of partitioning a data set into different clusters - a hard clustering approach such as the K-means method and a soft clustering approach such as the Fuzzy C-means method. When the hard partition approach is used, each data point belongs to one cluster only. When a soft clustering approach is used (i.e. fuzzy clustering), each data point belongs to more than one cluster at the same time with a corresponding degree of membership. This seems to be of great help in defining transition zones.

Clusters are formed by means of a similarity measure such as the Euclidean distance, the diagonal distance or the Mahalanobis distance. The Euclidean distance induces hyper-spherical clusters, while both the diagonal distance and the Mahalanobis distance induce hyper-ellipsoidal clusters (Bezdek 1981).

Two important aspects of concern with data clustering methods are the determination of the optimum number of clusters in the data set and the influence of the data distribution on the derived clusters. When there is a high concentration of data points in a specific part of the data space, the data clustering algorithm tends to find more clusters in that region, yet those clusters essentially capture the same information. To overcome these problems, two approaches can be employed - cluster validity measures, and compatible cluster merging. Another important aspect, which plays a key role in data clustering, is the normalisation of the data. Some clustering algorithms such as the K-means method for example are influenced by data normalisation, while others are not, (Alvarez Grima and Babu?ka, 1999).

5.1 K-means cluster analysis

The method used in this paper is the K-means method. The algorithm is provided in Appendix A. The K-means method partitions a data set into ***c*** groups (clusters), and finds a cluster centre in each group such that a cost function measure is minimised. The K-means method is inherently iterative, and no guarantee can be made that it will converge to an optimum solution. Furthermore, the performance of the K-means method depends on the initial position of the cluster centres.

Important steps in the cluster analysis were:

1. Initially all the benchmarks were chosen as objects, then those which appeared to be outliers were excluded.
2. The cluster variables such as vertical velocities, water levels, thicknesses of clay and peat were chosen to be used in the cluster analysis.
3. A similarity measure assuming larger values as two objects become more similar, was chosen as a classification criterium.
4. Initially a number of clusters of five was chosen, which by iteration reduced to three.

6. INTERPRETATION OF CLUSTER RESULTS

The plot of the cluster results (Fig. 5 and 6) show that the basis for the classification has been the clay thickness. The peat thickness appears to give no correlation.

Also the geographical distribution of cluster results (Fig. 7) gives an indication of the spread of the velocity data related to distribution and thickness of the main geological units.

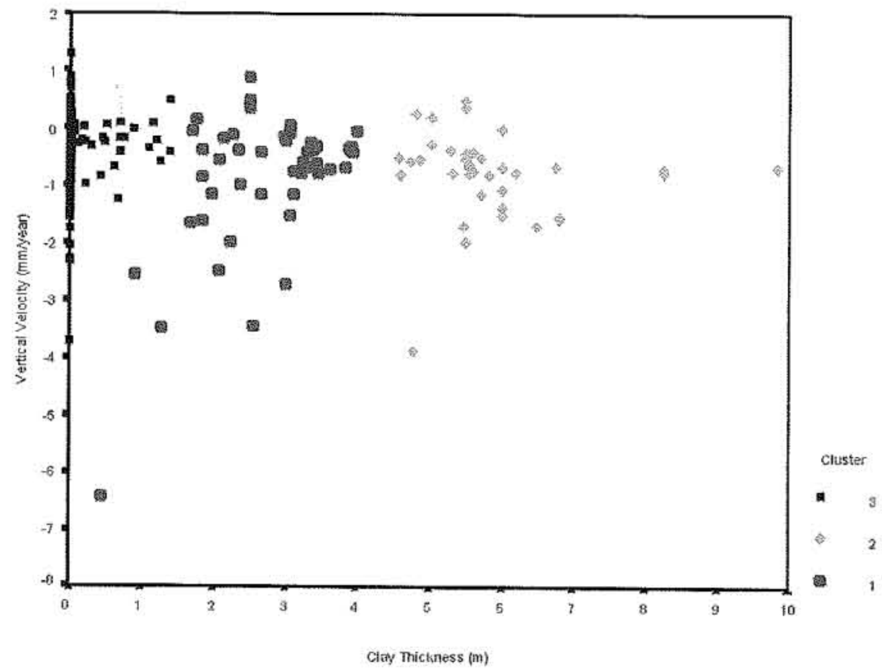

Figure 5. Results of K-means clustering, vertical benchmark velocity vs. clay thickness

The major part of the benchmarks (Cluster 3) are mounted on structures with pad or strip foundations placed on to the Pleistocene sands. Foundations underlain with peat layers of up to 1.75 m in thickness – measured in the free field – are present, fall within this cluster. These foundations have comparable vertical velocities. This appears to indicate, that the peat has been fully compacted by the foundation pressures so that the structure follows the movement of the Pleistocene. In some cases piles founded on the Pleistocene have been used. However, most structures have a pad or strip foundation. In the areas where these above phenomena occur, there is quite a difference in velocity of the land surface in the free field and under building and civil engineering structures.

In areas of peat with a covering clay layer of approximately 1.5 to 4.0 m (Cluster 1) again, for a large number of the benchmarks, the vertical velocity falls

in the same range as that for the foundations on the Pleistocene. Similar arguments for the compaction of the peat layers can be applied, in this instance, for the peat under the clay layers.

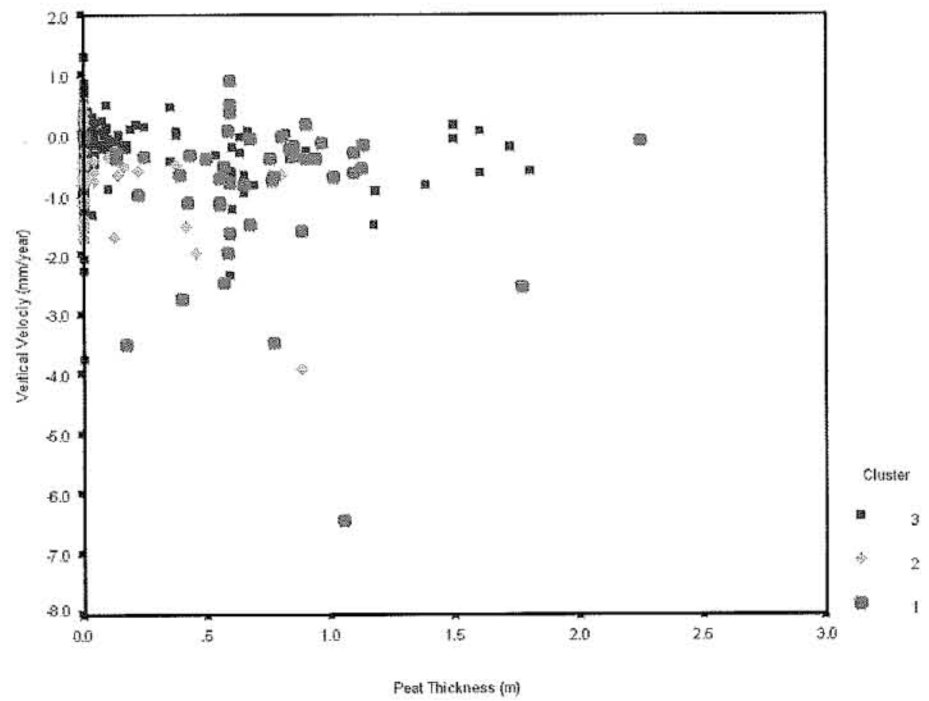

Figure 6. Results of K-means clustering, vertical benchmark velocity vs peat thickness

In addition there are several benchmarks whose vertical velocity falls outside the bandwidth of the benchmarks on structures with foundations on the Pleistocene. These indicate decreasing vertical velocity with a corresponding increase in clay thickness. The structures with shallow foundations on or in the clay follow the oxidation of the peat, albeit with lower velocities, than those which can be expected with comparable clay thicknesses in the free field. The velocities for structures are estimated at a factor 0.20 to 0.25 smaller than the free field for similar geological profile. There is the possibility that this relationship applies to within the zone of vertical velocities of structures on the Pleistocene with velocities as low as approximately 0.50 mm/year. This corresponds to velocities based on consolidation models for comparable clay and peat thicknesses.

For clay thicknesses > 4.0 m (Cluster 2), in the north and the west of the investigation area, where peat is very thin or absent a large number of benchmarks shows a velocity picture comparable to that of the structures founded on the Pleistocene. Below this bandwidth again larger velocities are found which

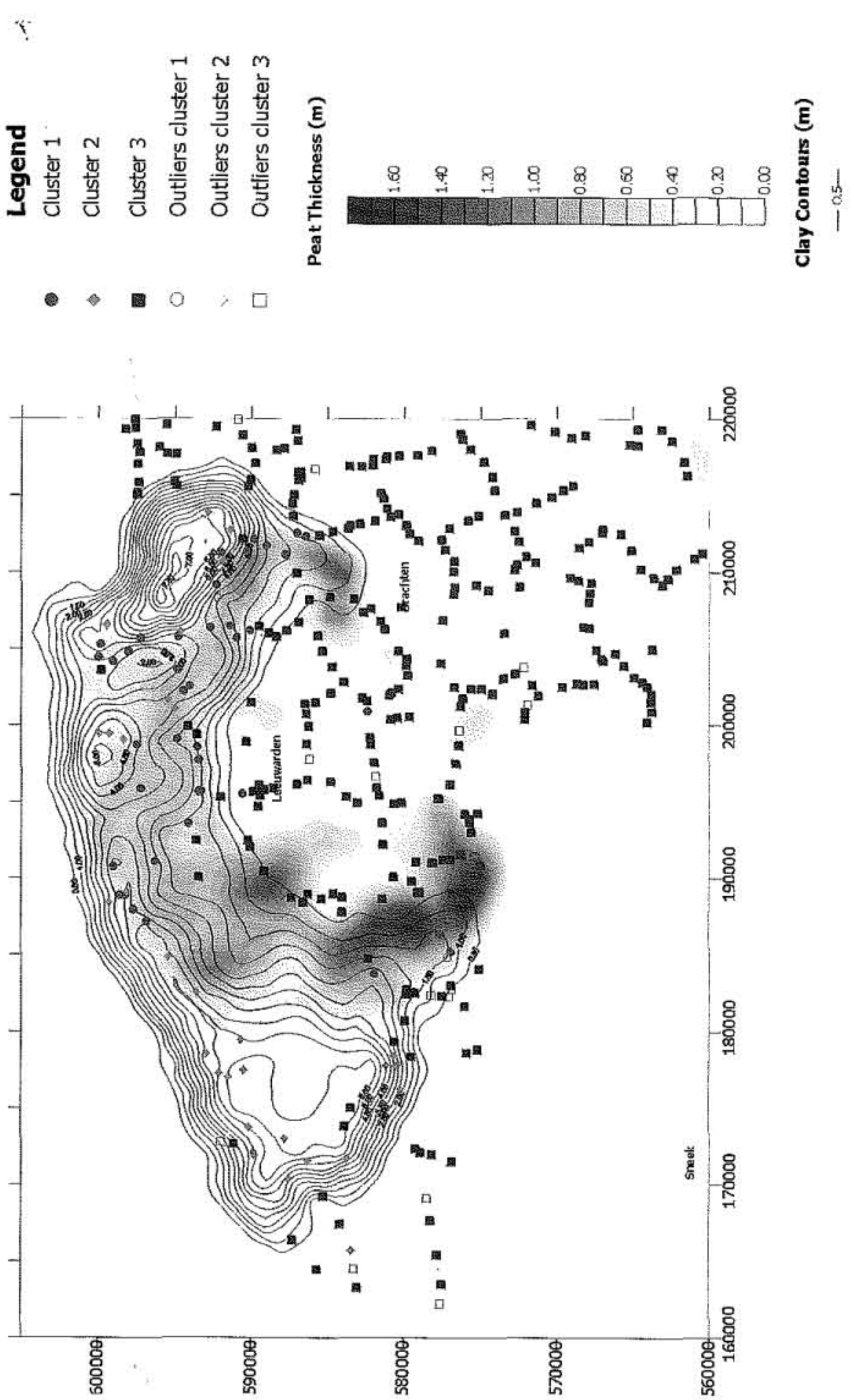

Figure 7. Map with distribution and thicknesses of Holocene clay and peat layers with locations of clustered benchmarks.

increase proportionally with the thickness of the clay layer. Consolidation of the clay resulting from an increase in effective stress, induced by a lowering of the surface water levels is, probably, the governing process. Strip and pad foundations are then associated with the lower velocities. The larger vertical velocities can also result from foundations which have friction piles subjected to negative skin friction caused by consolidation of the clay layers.

It is very remarkable, that the clustering results in a subdivision of the clay thickness below and above 4 m, which is the maximum thickness of the covering clay layer, the approximate limit for the occurrence of peat and also for the possible progress of the oxidation process. Finally, one can conclude, that the clay thickness is the overall governing parameter for the vertical velocity for structures whose foundations are not directly or indirectly connected to the Pleistocene.

There appeared to be no relationship between the surface water levels and the vertical velocities. This is, in contrast with the findings for the velocity of the surface in the free field. The difference between the behaviour of the soil layers under structures and the free field is that the hydrological conditions around and near structures can differ dramatically from that of the surface water in the polders.

7. CONCLUSIONS AND DISCUSSION

The statistical K-means clustering analysis can be used to classify vertical velocity data of benchmarks in compressible Holocene deposits based on the clay thickness as the leading parameter. Other parameters used in the cluster analysis, the peat thickness and near-surface groundwater levels appears to have no influence on the rate of the subsidence process.

The clustering results can be explained in terms of foundation type of the structures on which the benchmarks are secured. The actual foundation conditions of only a few benchmarks could be found in archives. General conditions are known and these can be recognised by reasoning from the cluster results.

Many of the foundations (approx. 91.5 % of the total population, 345/377) show similar vertical velocities as those of benchmarks mounted on structures having strip or pile foundations on the firm Pleistocene layers and with values up to – 1.25 mm/year.

Benchmarks mounted on structures founded on clay layers of 1.5 to 4.0 m in thickness show vertical velocities of up to – 2.50 mm/year (only about 1.3% of the total population, 5/377), with a decrease in vertical velocity with increasing clay thickness.

Benchmarks mounted on structures founded on clay layers of 4.0 to 7.0 m in thickness show vertical velocities of up to – 2.0 mm/year. These are probably due to negative skin friction on piles ending in the clay layers (only 1.9% of the total population, 7/377). There appears to be a slightly increasing trend of the vertical velocity with an increase in clay thickness.

This method adopted for the first time to this type of problem appears to give an increased level of confidence in interpreting the historic autonomous vertical velocities of the benchmarks. The velocities in the clustered results indicate the foundation behaviour of structures on which the benchmarks are mounted.

If validated with data sets of similar areas and further developed, the described method may serve as a basis for selecting benchmarks with an acceptable confidence level of historic autonomous vertical velocities, to be used in surveys for land subsidence measurement.

REFERENCES

Alvarez Grima, M. & R. Babuška (1999) Fuzzy model for the prediction of unconfined compressive strength of rock samples. *Int. Jour. Rock Mechanics & Mining Science,* **36,** 339-349.

Bezdek, J.C. (1981) Pattern recognition with fuzzy objective function algorithms Plenum press, 256 pp.

Commissie Bodemdaling door Aardgaswinning, (1987) Studieresultaten betreffende ongelijkmatige zakkingen in verband met aardgaswinning in de Provincie Groningen.

Hannink, G. (1984) Onderzoek in Noord-Holland naar de geotechnische aspecten van de aanleg van de Markerwaard; LGM-mededelingen nr. 89.

Hoefnagels, A.A., P.M. Maurenbrecher, & F. Schokking (1995) Long-term movements of benchmarks in the Groningen area preceding hydrcarbon extraction; *Proceedings Fifth International Symposium on Landsubsidence,* The Hague, the Netherlands, Oct. 1995.

NAM (1998) Bodemdalingprognose door aardgaswinning, Provincie Friesland, Status Rapport 1998 en Prognose tot Eindsituatie; *Nederlandse Aardolie Maatschappij bv,* Rapport n. 199806000350.

Schokking, F. (1989) Zettinggevoeligheid kaart Provincie Friesland; RGD Rapportnr. (Settlement map of the Province of Friesland) RGD-Report BP 10696.

Schokking, F. (1995) Prediction of long-term landsubsidence in drained peat areas in the Province of Friesland, RGD-Report 10981.

Schothorst (1979) Maaivelddalingen door peilverlagingen in het westelijk veenweidegebied, *Waterschapsbelangen,* 64, 7

APPENDIX A

This K-means algorithm assigns an object to a cluster with the nearest centre (mean). This process can be described in three steps:

1. Specify the number of clusters. Each cluster will have a centre (mean).

2. Each object in the database will be assigned to a cluster with the closest centre. The Euclidean distance is used as a dissimilarity measure for the data. The distance between two items is defined as the square root of the sum of the squared differences in values for each variable.
   The Euclidean distance between two p-dimensional objects x = [*x1,x2,....,xp*] and y = [*y1,y2,...,yp*] is:

$$d(x,y)=\sqrt{(x1-y1)^2+(x2-y2)^2+.....+(xp-yp)^2}$$

3. Step 2 is repeated until each object is assigned to a cluster. At the end of the iteration all of thecentres will be recalculated.
   The iteration in step 3 continues until the solution converges. Finally each object will be assigned to the cluster with the nearest centre.

2 Theory and Modeling

EVALUATION OF SUBSIDENCE AND SKELETAL SPECIFIC STORAGE FROM STRESS-STRAIN HYSTERESIS LOOPS USING ONE- AND THREE-DIMENSIONAL DEFORMATION MODELS

Thomas J. Burbey
Dept. of Geological Sciences, Virginia Tech, Blacksburg, VA 24060, USA

Abstract

Extensometer data are inherently three dimensional in scope, yet historically these data have been used in conjunction with hydrograph data to calculate the skeletal specific storage values of aquifer systems in which vertical strain is assumed. Stress-strain hysteresis loops produced from extensometer and hydrograph data of cyclically pumped aquifers have allowed for estimation of both the inelastic and elastic specific storage values of confining units. Numerical simulations involving vertical strain (Interbed Storage model with Modflow) and volume strain (Biot model) were used to generate hypothetical hysteresis loops for a cyclically pumped confined aquifer overlain by a thick compressible clay confining unit. Simulation results indicate that (1) the presence of a thick confining layer with delayed drainage can create hysteresis loops that reflect a system experiencing inelastic compression with elastic recovery, (2) the assumption of purely vertical compression tends to overestimate subsidence and skeletal specific storage, particularly near the wellbore, and (3) skeletal specific storage estimates from the Biot model reflect the presence of horizontal strain and deformation.

Keywords: subsidence, numerical models, stress, strain

1. INTRODUCTION

The use of extensometers for measuring total compaction of heavily pumped compressible aquifer systems has been employed for over 50 years (Poland, and Davis,1969; Poland and others, 1975). In aquifer systems where pumping is cyclic, total compaction records can be used in conjunction with hydrograph data to produce stress-strain diagrams. These diagrams often result in hysteresis loops that allow for the evaluation of storage properties of the aquifer system and individual units of the system (see for example Riley, 1969, 1984; Hanson, 1989; and Cleveland et al., 1992). In aquifer systems with thick confining layers, the dissipation of pore pressures within the clay lags behind that of the aquifer. This time lag, or delay in equilibration, between the confining unit and aquifer is believed to be represented in the "width" of the hysteresis loop produced in the stress-strain diagram (Riley, 1984).

In this study the mechanisms responsible for the shape of the hysteresis loops are evaluated numerically. These mechanisms are difficult to evaluate with field data alone because of the paucity of extensometers and monitoring wells in the field at any study site, and the general limitation of knowledge of the specific aquifer properties. Furthermore, perhaps of greatest concern and a central focus of this study has to do with the fundamental assumption applied to all extensometer data. In every case where extensometers have been used, it has been assumed that the compaction associated with a change in effective stress occurs only in the vertical direction. That is, horizontal strain within the aquifer or confining units is assumed negligible, or the evaluation of its contribution has been intractable and hence ignored. If horizontal strain is occurring, then the extensometer record does indeed include such information. If the contribution of horizontal strain imposed by the increase in effective stress is significant, then the assumption of zero-horizontal strain may lead to significant errors in the evaluation total subsidence and perhaps skeletal specific storage.

Burbey (1999) has determined both in the field and in theoretical developments, that horizontal deformation can be important even in systems with thick clay confining units. The purpose of this study is to evaluate the mechanisms influencing the shape of the hysteresis loops, evaluate any errors in allowing only vertical compaction, and determine if the hysteresis loops may contain information about possible horizontal deformation.

2. SUBSIDENCE MODELING

Until recently, most numerical models developed to simulate compaction or total subsidence have been one-dimensional in scope. That is, horizontal strain has been assumed to be negligible, and hence not considered. (e.g. Gambolati and Freeze, 1973; Helm, 1975; Prudic and Williamson, 1984; Leake, 1990; Leake and Prudic, 1991). In addition, these models assume that no change in total stress takes place during the simulation process. As a result, any change in pore-water pressure, , is equal and opposite to changes in effective stress, . In converting pore-water pressure to hydraulic head, the expression for effective stress becomes

$$\Delta\sigma' = \rho_w g \Delta h \qquad (1)$$

where is the density of water, g is the gravitational constant, and is the incremental change in hydraulic head. In assuming only vertical strain, an increase in effective stress results in a linear incremental increase in vertical compression through the constant elastic skeletal specific storage, S_{ske}, given by the relation

$$\Delta b = -\Delta h S_{ske} b_o \qquad (2)$$

where is the compaction within the unit being measured, and is the original thickness of the unit of concern. In general the compacting unit is either a confining unit, multiple interbeds, or an entire aquifer system. The assumption here is that the compacting unit represents the same interval over which the change in hydraulic head is measured. In equation (2) S_{ske} can be replaced with an inelastic skeletal specific storage, S_{skv}, where the inelastic storage term is applied to fine-grained sediments that undergo an effective stress (reduction in head) in excess of any previous maximum stress level (Leake and Prudic, 1991). When stress levels are below the previous past maximum value, equation (2) is used with the elastic component of skeletal specific storage. The compaction obtained from equation (2) during inelastic compression is approximate because virgin compaction tends to be proportional to the increase in logarithm of effective stress (Jorgenson, 1980). Leake and Prudic (1991) discuss the simulated over-prediction in total compaction that may occur if the change in effective stress during any single time step is large. In simulations used in this investigation, time steps are incrementally increased from an initial step of several seconds. Hence, the error in assuming a linear approximation is small.

The IBS (InterBed Storage) package is used (Leake and Prudic, 1991) with Modflow (McDonald and Harbaugh, 1988) in this study to obtain subsidence and hydraulic head information for simulations involving purely vertical compaction or deformation. Results from these simulations are compared with displacement and hydraulic head data from an axisymmetric Biot code (Hsieh, 1996) that has both hydraulic head and granular displacement as the dependent variables. Furthermore, both horizontal and vertical deformation are assumed. The form of Biot's coupled equations (Burbey, 1999) used here can be expressed as

$$(G+\lambda)\nabla(\nabla \cdot \mathbf{u}) + \nabla^2 \mathbf{u} = \rho_w g \nabla h \text{ and} \qquad (3a)$$

$$K\nabla^2 h = \frac{\partial}{\partial t}(\nabla \cdot \mathbf{u}), \qquad (3b)$$

where G is the shear modulus, K is the hydraulic conductivity, $\mathbf{u}$ is a vector representing the displacement field of solids, and is one of Lame's constants expressed in terms of the shear Modulus, G, and Poisson's ratio, , as . The vertical component of displacement , u_z, is calculated numerically from equation (3) and can be compared directly with the cumulative compaction (total subsidence) obtained from simulation of the IBS model (equation 2) at the top of the aquifer system. Burbey and Helm (1999) and Burbey (1999) have shown that a relation can be made between the elastic constants of equation (3) and the skeletal specific storage for volumetric aquifer compression as

$$S_{sk} = \rho_w g \left[\frac{3(1-2\nu)}{2G(1+\nu)} \right] \tag{4}$$

Two elastic constants are used to define the skeletal specific storage in volumetric strain problems and therefore more than one set of values for G and will yield the same value of S_{sk}. Because of the narrow range of acceptable values for (typically between 0.1 and 0.5 for unconsolidated deposits), this does not preclude the direct application of equation (4) for comparison with the skeletal specific storage used in the IBS model.

3. HYPOTHETICAL MODEL DESIGN AND PARAMETERS

A hypothetical model was designed for the purpose of evaluating how hydraulic head and subsidence data are affected under cyclic pumping conditions where vertical and volume strain and deformation conditions are imposed. The conceptual model considered for this investigation is shown in Figure 1. A 50m-thick confining unit separates a 10m-thick overlying unconfined aquifer from a 50m-thick underlying confined aquifer. One model layer was used to simulate each of the two aquifers, 10 model layers (each 5 m thick) were used to simulate the confining layer. The purpose of the thick confining layer is to evaluate how the dissipation of excess pore-water pressure within the confining unit may affect the extensometer record over time. Radial flow conditions are assumed and the distant boundary is 20,000 m from the pumping well and does not affect the simulation results in the vicinity of the well. A no-flow and zero-traction boundary condition is imposed on the distant boundary. At the wellbore water is free to move into the well, but the wellbore inhibits horizontal displacement from occurring. However, in the vertical direction the well bore is traction free, meaning that vertical displacement can occur freely along the wellbore. The bottom of the model is represented as a no-flow boundary and a zero-vertical displacement boundary. In the horizontal direction the bottom is traction free. The water table is a free-water surface and represents a zero-total load surface and is free to deform.

Water was cyclically pumped from the confined aquifer. Five stress periods, each 100-days long, were used to simulate cyclic pumping. Pumping was simulated at a constant rate of 2,000 m³/d during the first, third, and fifth stress periods, while no pumping was simulated during the second and fourth stress periods. In this way elastic recovery of both the aquifers and confining unit could be monitored during non-pumping periods. Table 1 lists the aquifer parameters used for simulations with both the IBS and Biot models.

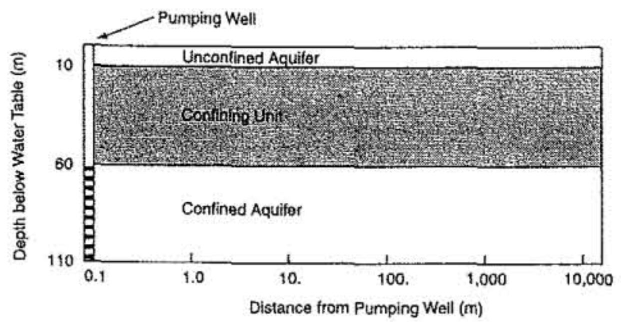

Figure 1. Conceptual model used for all simulations.

Table 1. Aquifer properties assigned to IBS and Biot model simulations.

Aquifer Property	IBS Model	Biot Model
Aquifers		
Hydraulic conductivity, K_h, K_v (m/d)	5.0	5.0
Skeletal specific storage, S_{ske}, S_{skv} (m^{-1})	1.0x10^{-5}	----
Shear modulus, G (N/m^2)	----	1.176x10^8
Poisson's ratio n, (dimensionless)	----	.25
Specific Yield[a] (dimensionless)	.20	----
Confining Unit		
Horizontal hydraulic conductivity, K_h (m/d)	.05	.05
Vertical hydraulic conductivity, K_v (m/d)	.05	.05
Inelastic skeletal specific storage, S_{skv} (m^{-1})	5.0x10^{-3}	----
Elastic skeletal specific storage, S_{ske} (m^{-1})	5.0x10^{-4}	----
Shear Modulus, G_e [b] (N/m^2)	----	9.046x10^6
Shear Modulus, G_v (N/m^2)	----	1.789x10^6
Poisson's ratio, n_v (dimensionless)	----	.15
Poisson's ratio, n_e (dimensionless)	----	.30

[a] Unconfined aquifer only
[b] Subscripts on shear modulus and Poisson's ratio refer to values that correspond to the elastic or inelastic skeletal specific storage values used for IBS model.

4. HYSTERESIS UNDER VERTICAL STRAIN CONDITIONS

Riley (1969) proposed a method whereby hysteresis loops representing stress (measured as drawdown) plotted against strain (measured as total subsidence) for cyclically pumped aquifers could be evaluated to estimate the elastic and inelastic skeletal specific storage values of the aquifer system. The inverse of the slope produced by the recompression loops and the inverse slope produced from the portion of the curve adjoining the loops can be used to estimate the values of both elastic and inelastic specific storage of the compressible units according to the relation established by Riley (1969)

$$S_{sk} = \frac{\Delta b}{b(\Delta h)} \tag{5}$$

where S_{sk} is either inelastic or elastic specific storage depending on which slope is being estimated. These estimated values of specific storage are often attributed to the confining unit because of their high degree of compressibility relative to the aquifer. In general, extensometer data measure the compressibility of the confining unit, but the hydraulic head data are often measured within the aquifer. At any point in time, the pore-water pressures of these two units may be quite different, yet these sets of data are plotted together on stress-strain diagrams.

Figure 2 shows the recovery response (stress period 2) after the confined aquifer had been pumped for 100 days assuming one-dimensional strain (IBS model) and assuming only one elastic constant for the skeletal specific storage (S_{skv}). The time constant, representing the time required for 93 percent of the excess pore water to dissipate (Riley, 1969), can be expressed as

$$\tau = \frac{S_{skv}(b_o)^2}{K_v} \tag{6}$$

where a singly draining confining unit is assumed. According to equation (6) 250 days would be required for the pore-water pressure to dissipate. This value appears reasonable based on the head configurations shown in Figure 2. If S_{ske} is used in place of S_{skv} in equation 6, the time required for dissipation of pore pressures in the confining unit would decrease by an order of magnitude to 25 days. These time lags can create hysteresis effects even without implementing both elastic and inelastic specific storage values.

For the one-dimensional strain case (IBS model), numerous simulations were run to evaluate the factors that influence the shape of the hysteresis loops. Although Riley (1969, 1984) pointed out that the value of the time constant affected the width of the loops, no research has been done to determine how various aquifer parameters affecting the time constant ultimately affect the shape of the hysteresis loops. Furthermore, it has been unclear whether equation (5) could be effectively used to evaluate the values of the specific storage constants for all types of aquifer parameters in this one-dimensional setting.

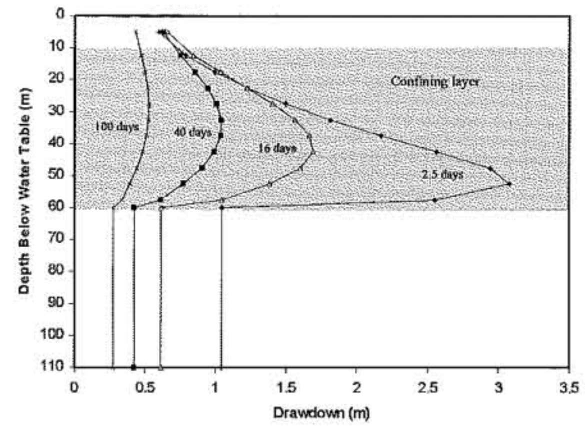

Figure 2. Simulated lines of equal head during recovery period for IBS model using inelastic specific storage value listed in Table 1.

Hypothetical simulations reveal that the width of the hysteresis loop during recovery and recompression prior to excess of past maximum effective stress is affected by (at least) four factors:

1. The relative difference between the elastic and inelastic specific storage values of the confining (and compacting) unit. Figure 3 shows three sets of simulated loops selected at a distance of 150 m from the pumped well. The first (a) uses parameter values listed in Table 1. In (b) the elastic specific storage was increased by a factor of two. In (c) the elastic specific storage was increased to be equal to that of the inelastic specific storage. The result shown in Figure 3C indicates that even when values of S_{ske} are equal to those of S_{skv}, the recovery loop does not retrace the compression loop as it does in a homogeneous isotropic system. Hysteresis in the presence of a confining layer (with delayed drainage) can mimic a homogeneous isotropic aquifer system with different inelastic and elastic constants.

2. The proximity of the extensometer to the pumped well. Rarely are multiple extensometers available for evaluation of a single aquifer system. However, for these hypothetical simulations, simulation data were evaluated at distances from 1, 150, and 1,000 m from the pumped well. Simulation results indicate that as the distance to the pumped well increases, the relative change in pore pressures becomes less and therefore the response within the confining unit is also reduced, resulting in hysteresis loops that become thinner with increasing distance from the well.

3. The length of the recovery period relative to the pumping period. In general, the longer the recovery the greater the dissipation of excess pore water from the confining unit, which results in wider loops.

4. The vertical hydraulic conductivity of the confining unit. As the value of K_v of the confining unit approaches the larger hydraulic conductivity of the underlying pumped confined aquifer, the loops become markedly narrower. The narrow loops are the result of a greatly increased elastic recovery within the confining unit and a smaller time constant according to equation (6).

The factors affecting the length of the hysteresis loop include (1) the difference in hydraulic conductivity between the confined aquifer and the confining unit, and (2) the length of the recovery cycle.

One important observation that can be made regarding all simulations is that applying equation (5) to the simulated stress-strain diagrams resulted in calculated values of elastic and inelastic specific storage that close to those used in the model simulations for the confining unit. This is particularly noteworthy considering the hydraulic heads used in the results were those from the confined aquifer and that the time lag in several simulations was quite large. The large time lag indicates that the heads within the confining unit do not accurately reflect those of the confined aquifer. Nonetheless, the specific storage values calculated using equation (5) were all well within a factor of 2 of the actual values used in the model simulations. However, in each case the estimated values from equation (5) were larger than the simulated values.

5. ANALYSIS OF HYSTERESIS LOOPS-VOLUME STRAIN CONDITION

Unconsolidated aquifer systems that undergo increased effective stress due to pumping experience vertical and horizontal strain. That is, the assumption of zero horizontal strain as described above may be too limiting for proper evaluation of total subsidence and skeletal specific storage. If horizontal strain is significant then it must be addressed when analyzing the extensometer record, because the data recorded from extensometers reflect volume strain and three-dimensional displacement of the aquifer system.

For aquifer parameters listed in Table 1, Figure 4 shows simulated hydraulic head (a) and vertical displacement (b) at the top of the system (total subsidence) using the Biot and IBS models. Results indicate that although head values match well for both the one and three-dimensional displacement models, the total subsidence is significantly different inside a distance of 500m from the pumped well.

The large differences in simulated subsidence do not require the simulation of large amounts of horizontal strain. In fact in no instance during the first 100 days of pumping does horizontal deformation exceed 10 mm, more than an order of magnitude less than the vertical deformation at the wellbore; an expected result for a thick clay-rich confining unit. The largest horizontal deformation occurs within the confining unit where compressibilities are high. The magnitude of horizontal deformation is a function of the pumping rate, the time since the start of pumping, and hydraulic diffusivity, K_v/S_{sk} (Helm, 1996; Burbey and Helm, 1999).

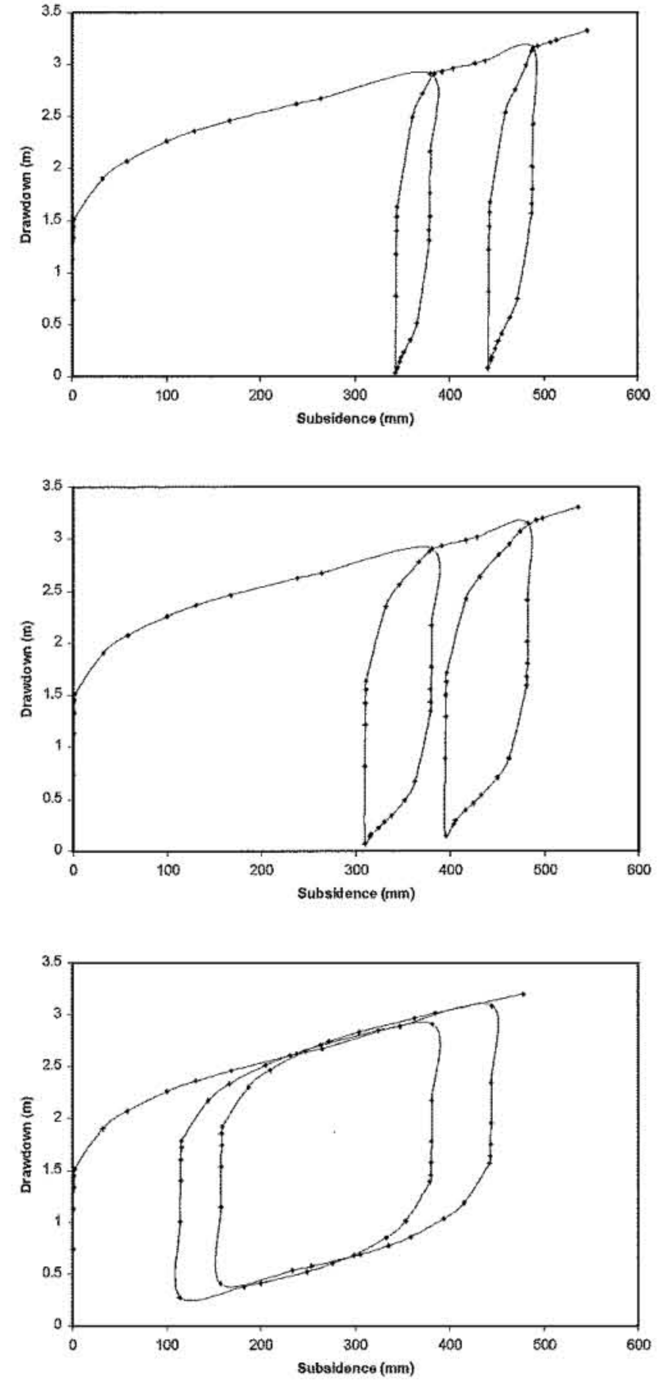

Figure 3. Simulated stess-strain hysteresis loops from IBS model using aquifer properties and (a) skeletal specific storage values from table 1, (b) $S_{ske} = 1x10^{-3}$ / m and (c) $S_{ske} = 5x10^{-3}$ (equal to S_{skv}). Plots generated from data 150 m from pumped well.

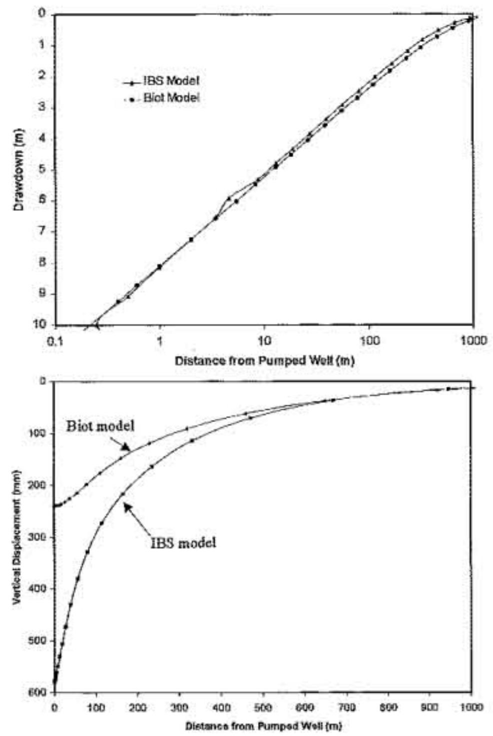

Figure 4. Simulated (a) heads and (b) subsidence using Biot and IBS models as a function of distance from the pumped well using aquifer values from Table 1 for the first stess period (pumping).

If the simulated vertical deformation at the top of the aquifer system (shown in Figure 4b) represents the correct or measured value, then using the IBS model for this magnitude of subsidence would require that the simulated elastic and inelastic skeletal specific storage of the confining unit be reduced by an amount proportional to the distance (position in the radial direction representing the location of the extensometer) from the pumped well at which the measurement is made. For example, at 1m from the pumped well, the reduction in specific storage required for the IBS model to match the subsidence predicted by the Biot model would be about 40 percent. This percentage would decrease as the distance from the pumped well is increased. Thus, in field situations where extensometer data are available at different radii from the pumped well, the estimated skeletal specific storage values from hysteresis loops would increase as the distance from the pumped well increased if one-dimensional subsidence models are used.

Hysteresis loops developed from simulations using the Biot model are similar in shape to those developed from the IBS model. However, in applying equation (5)

to estimate the skeletal specific storage value of the confining unit, the estimates obtained from the slopes of the plots are less than the simulated value and therefore are also less than the estimates obtained from the IBS model. Furthermore, the estimated value decreases as the distance from the pumped well increases. For the IBS model, estimates of skeletal specific storage from hysteresis loops did not change as a function of distance. These differences can be explained by the presence of horizontal strain and deformation. Equation (5) assumes all strain and deformation is vertical and therefore using this equation to estimate skeletal specific storage would tend to result in an underestimation of the actual value (as evidenced here). Finally, the decrease in estimated skeletal specific storage as a function of distance is due to the fact that at the wellbore all the strain is vertical (horizontal movement is inhibited by the wellbore), but as one moves outward from the pumped well, the contribution of storage from horizontal strain increases. Further research needs to be done to determine if the actual storage contribution from horizontal strain can be estimated.

REFERENCES

Burbey, T.J. & Helm, D.C., (1999) Modeling three-dimensional deformation in response to pumping of unconsolidated aquifers. *Environmental and Engineering Geoscience,* **2**(3), 199-212.

Burbey, T.J., (1999) Effects of horizontal strain in estimating specific storage and compaction in confined and leaky aquifer systems. *Hydrogeology Journal*, **7**(6), 521-532.

Cleveland, T.G., Bravo, R., & Rogers, J.R., (1992) Storage coefficients and vertical hydraulic conductivities in aquitards using extensometer and hydrograph data. *Ground Water*, **30**(5), 701-708.

Gambolati, G., & Freeze, R.A., (1973) Mathematical simulation of the subsidence of Venice, 1, Theory. *Water Resources Res.*, **9**, 721-733.

Hanson, R.T., (1989) Aquifer-system compaction, Tucson Basin and Avra Valley, Arizona. *U.S. Geol. Surv. Water-Resources Invest. Report* 88-4172, 69 pp.

Helm, D.C., (1996) Horizontal aquifer movement in a Theis-Thiem confined aquifer. *Ground Water*, **30**(4), 953-964.

Helm, D.C., (1975) One-dimensional simulation of aquifer-system compaction near Pixley, California, 1. Constant parameters. *Water Resources Res.*, **11,** 465-478.

Hsieh, P.A., (1996) Deformation-induced changes in hydraulic head during ground-water withdrawal. *Ground Water*, **34**(6), 1082-1089.

Jorgenson, D.G., (1980) Relationships between basic soils-engineering equations and basic ground-water flow equations. *U.S. Geol. Surv. Water-Supply Paper* 2064, 40 pp.

Leake, S.A., & Prudic, D.E., (1991) Documentation of a computer program to simulate aquifer-system compaction using the modular finite-difference ground-water flow model. *U.S. Geol. Surv. Techniques of Water Resour. Invest. Book 6, Ch A2*, 68 pp.

Leake, S.A., (1990) Interbed storage changes and compaction in models of regional groundwater flow. *Water Resour. Res.*, **26**, 1939-1950.

McDonald, M.G., & Harbaugh, A.W., (1988) A modular three-dimensional finite-difference ground-water flow model. *U.S. Geol. Surv. Techniques of Water Resour. Invest. Book 6, Chap. A1*, 586 pp.

Poland, J.F., & Davis, G.H., (1965) Land subsidence due to withdrawal of fluids. *in* Varnes, D.J., and Kiersch, G., eds., *Geol. Soc. of Am., Reviews in Engineering Geology*, **2**, 187-269.

Poland, J.F., Lofgren, B.E., Ireland, R.L., & Pugh, R.G., (1975) Land subsidence in the San Joaquin Valley as of 1972. *U.S. Geological Survey Prof. Paper* 437-H, 78 pp.

Prudic, D.E., & Williamson, A.K., (1984) Evaluation of a technique for simulating a compacting aquifer system in the Central Valley of California, USA. *in Land Subsidence*. Proceedings of the Third Inter. Symp. On Land Subsidence, Venice, Italy, Publ. IAHS n° 151, 53-63.

Riley, F.S., (1969) Analysis of borehole extensometer data from central California. *in* Tison, L.J., ed., *Land Subsidence*, Tokyo, Inter. Assoc. of Scientific Hydrology Pub. 89, **2**, 423-431.

Riley, F.S., (1984) Developments in borehole extensometry. *In Land Subsidence*. Proceedings of the Third Inter. Symp. On Land Subsidence, Venice, Italy, Publ. IAHS n° 151, 169-186, Wallingford, England.

LAND SUBSIDENCE - Vol. II
Proceedings of the Sixth International Symposium on Land Subsidence
Ravenna / Italy / 24-29 September 2000

CAPILLARY EFFECTS IN RESERVOIR COMPACTION AND SURFACE SUBSIDENCE

Bernard A. Schrefler and Luciano Simoni
University of Padua, Dept. Construction and Transportation Engineering
Via Marzolo 9, 35131 Padova, Italy

H.W. Zhang
Dept. of Engineering Mechanics
Dalian University of Technology, P. R. China

Abstract

The paper analyses the capillary effects and structural collapse in the development of subsidence occurring above gas fields. An elasto-plastic constitutive model is presented, able to reproduce in a concise manner the basic features of the behaviour of unsaturated porous media, especially collapse-related phenomena. The presented material model is validated against a laboratory test, which demonstrates its effectiveness. It is then introduced into a general numerical model for studying surface subsidence phenomena, which is here summarised and then applied to the analysis of an ideal gas reservoir.

Keywords: capillary effects, plasticity, surface subsidence.

1. INTRODUCTION

Numerical models have been widely used in the past to analyse the mechanical behaviour of exploited gas reservoirs and forecast surface subsidence. These models however did not prove to be very realistic for long periods of time and the real behaviour has not been completely fitted. The main deficiency exhibited by numerical models is certainly the inability to represent the ongoing subsidence after depletion of the wells, which has been recorded in several occasions. This is the reduced effect at the surface of compaction of gas bearing strata, the deformation of which is hence more pronounced and continuing for several years even when gas extraction is stopped.

A sophisticated technique allows careful monitoring of the deformational behaviour of the mineralised zones by means of down-hole measurements of the position of radioactive markers (Schoonbeek, 1976). The corresponding compaction coefficients differ substantially from those obtained from laboratory tests. In the literature all these phenomena have been justified by different reasons, but we interpret the observed behaviour within a unique material model which is summarised in the following. Possible scenarios associated with gas extraction are then examined using a framework of this type.

Three typical phases of gas field development are considered: 1) initial phase in which gas pressure in the reservoir decreases due to gas extraction; 2) steady state phase in which gas withdrawal continues, but at a constant gas pressure; 3) final phase in which gas extraction is stopped and gas and water pressures recover. In all three cases the degree of saturation increases as water comes in to occupy the space left by the gas. Therefore there will be a continuous suction reduction throughout the whole process of gas extraction and pressure recovery. This provides a sound explanation for continuing surface settlements when reservoir pore pressures stabilise and for additional settlements occurring even after the end of gas production. Conventional subsidence models fail to simulate this settlement behaviour. Capillary effects also explain the lower rock compressibility observed in gas bearing strata as compared to the values obtained in the laboratory from fully saturated samples. Up to now the only explanation put forward for this was damage of the samples.

First of all, we summarise the elasto-plastic material model, which explicitly accounts for capillary effect. A more detailed presentation can be found in (Schrefler and Simoni, 2000).

2. THE ELASTO-PLASTIC MATERIAL MODEL

The elasto-plastic model is defined in the space (p', q, s) of the mean stress p', the deviatoric stress q, invariants of Bishop's stress, and suction s. The latter is combination of total stress σ_{ij} and pressure acting on the solid, represented by a weighted average of water and gas pressure. As weighting function, water saturation S_r is here assumed, hence the stress measure takes the form

$$\sigma'_{ij} = \sigma_{ij} - \left[S_r p_w + (1 - S_r) p_g\right]\delta_{ij} = \sigma_{ij} - \left[p_g - S_r s\right]\delta_{ij} \tag{1}$$

with soil suction s defined as

$$s = p_g - p_w \tag{2}$$

Soil suction and water saturation may be mutually related by means of the following relationship (Alonso et al., 1990)

$$S_r = 1 - m\, tanh(ls) \tag{3}$$

where m and l are material parameters (S_r=1-m represents *irreducible saturation*, i.e. the limiting value of S_r as suction approaches infinity). In Eq. (1), parameter S_r represents a phenomenological measure of the capillary effects, through its experimental relationship with suction. Bishop's stress definition recovers the Terzaghi's effective stress definition, usually assumed in fully saturated soil mechanics, when saturation equals one, hence the consistency condition between stress measures is guaranteed.

From Eq. (1) it results that changes in Bishop's stress may be induced by changes in total stress but also by changes in gas pressure, suction and saturation. The model is defined in a generalised plasticity frame, in which loading-unloading direction vector and the direction vector defining the plastic flow are directly assumed, without definition of the yield and potential surfaces. From these vectors, we obtain by integration the yield surface f and the potential surface g which are ellipses (Delage and Graham, 1996) represented by

$$f \equiv q^2 + M_f^2 p'^2 - M_f^2 p' p'_f = 0 \tag{4}$$

$$g \equiv q^2 + M_g^2 p'^2 - M_g^2 p' p'_g = 0 \tag{5}$$

The material parameters M_g and M_f represent the slope of the critical state line and the slope of the zero dilatancy line in the plane (p', q, 0) respectively and are dependent on suction in partially saturated problems (Laloui et al, 1997, for M_f). Parameters p_f and p_g are integration constants which determine the size of the surface but have no influence in defining the respective normals. Even though Eqs. (4)-(5) are formally the same as for fully saturated materials (Pastor et al., 1990), they must be assumed in (p', q, s) space, when dealing with partially saturated problems (see Figure 1). In addition to the aforementioned dependence of M_g and M_f on suction, also parameters p_g and p_f depend on suction, as suggested by experimental evidence (Fredlund et al., 1978). Further assumptions for f and g are however possible, for instance they may coincide, which results in associative plasticity.

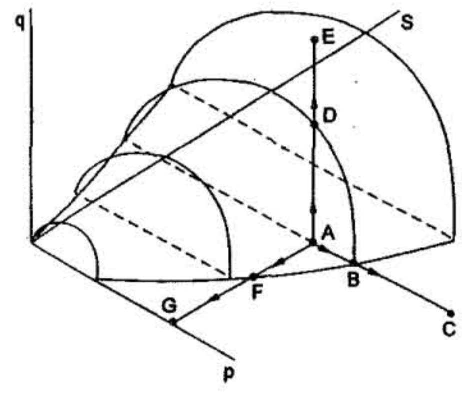

Figure 1. Yield surface in (p, q, s) space for partially saturated problems.

Three different loading paths are depicted in Figure 1 starting from point A inside the elastic domain: A-B-C and A-D-E are the usual isotropic and deviatoric paths, which are elastic inside the yield surface, then present a hardening part. Transformation A-F-G is the hydric-path, which involves changes in saturation only: wetting from point A would initially produce elastic expansion (swelling) before yielding at F and plastic compression (or collapse) in the part F-G. (Escario and Sáez, 1973).

Following the critical state models, the total volumetric strain (recoverable and not) associated with the change in the hydrostatic component of Bishop's stress tensor p' can be linearised as

$$d\varepsilon_v = \frac{\lambda(s)}{v_0}\frac{d p'}{p'} \tag{6}$$

For the soil compressibility $\lambda(s)$ a dependence on suction is assumed of the type

$$\lambda(s) = \frac{\lambda(0)}{1+as} \tag{7}$$

where $\lambda(0)$ is the compressibility of the saturated sample and a a material parameter. Similar dependence on suction is assumed for the elastic part of the volumetric strain and elastic compressibility coefficient $\kappa(s)$. Some authors (e.g. Laloui et al., 1997) assume the elastic modulus κ independent of suction. This is however in contrast with the results of (Brignoli et al., 1995) and probably depends on the range of applied forces, larger for rock type materials.

This dependence of soil stiffness on suction comply with the laboratory experiences in which unsaturated specimens exhibit a lower volume change than saturated ones when e.g. subjected to the same increment of vertical stress. Further, when the unsaturated samples are soaked and hence saturated, the soil exhibits a significant volumetric strain under constant stress.

The enlargement of the region of the elastic behaviour due to stress increments depends on plastic hardening. The hierarchical structure of the generalised plasticity allows to choose a hardening parameter of the type

$$H = H_0\, p'\, H_w \left(H_v + H_f\right) \tag{8}$$

In eq. (8) the term H_0 depends on the material characteristics in fully saturated conditions whereas H_w is related to partially saturated behaviour. These coefficient are respectively assumed as

$$H_0 = \frac{1+e_0}{\lambda(0)-\kappa(0)}, \qquad H_w = 1+as \tag{9}$$

being e_0 the initial void ratio. H_f is the stress path dependent term and H_v represents the effects of the deviatoric strain hardening. For the structure of these coefficient we refer to (Simoni and Schrefler, 2000). The model represented by Eq. (8) can be further enhanced to account for memory effects and plastic unloading by introducing additive or multiplicative terms.
Once the dependence on suction of the plastic modulus has been defined, we have to introduce the same effects in the yield and potential surface equations (Eqs. 4 and 5). Experimental observations show that parameter p_f is increasing with suction (Fredlund et al., 1978). Given the initial yield stress for saturated conditions, the dependence of p_f on suction is assumed as

$$p_f = p'_{y_i}(s) = p'_{y0_i} + is \tag{10}$$

Parameter i has to be determined by interpolation of experimental data to obtain an increasing function of suction when water saturation is less than one.

The same variation with suction can be assumed for the parameter p_g, which means that yield and potential surfaces expand with the same law when suction is increasing. This is suggested by the possibility to assume associative plasticity, in which case $f=g$.

The applicability of this mathematical model requires the determination of ten material parameters by using experimental data. This has been performed for a laboratory test, which is discussed in the next section.

3. APPLICATION TO AN OEDOMETRIC TEST

The material model previously summarised is applied within a identification method (Simoni and Schrefler, 2000) to a laboratory experiment performed at IKU Petroleum Research, Trondheim (Papamichos and Schei, 1998, Papamichos et al., 1998) on behalf of AGIP (Italian National Petroleum Company). It deals with a silty consolidated sandstone sample extracted from a gas bearing formation in the Northern Adriatic basin at a depth of 3400 m. Effective porosity, *in situ* water saturation and irreducible saturation of the material were independently obtained, then the specimen underwent an oedometric test. The loading was scheduled as follows: the sample at *in situ* saturation (0.38-0.45) is firstly stressed with an initial hydrostatic phase presenting σ_r-rate equal to 0.01 MPa/s until σ_r=0.5 MPa. This is followed by an uniaxial phase with σ_z-rate of 0.004 MPa/s until σ_z reaches 35 MPa; the sample is then hold at constant stress level and water is injected for 25 hours until full saturation is attained. During this period of time, volumetric changes of the specimen are recorded, as during the phases of stress changes. Once the full saturation is reached, a second uniaxial phase, at constant water content, with stress rate of 0.004 MPa/s till about 110 MPa is performed. The test includes also unloading cycles to determine the elastic behaviour and recoverable deformation. The water injection test (hydric-path) simulates the behaviour of the gas reservoir rock during artificial water injection or during the flooding associated to gas extraction. For this reason the axial stress level at which the sample is injected is representative of the vertical stress in reservoir conditions. In lack of other information, we assume that gas pressure during the test maintains the same value (reference or zero pressure).

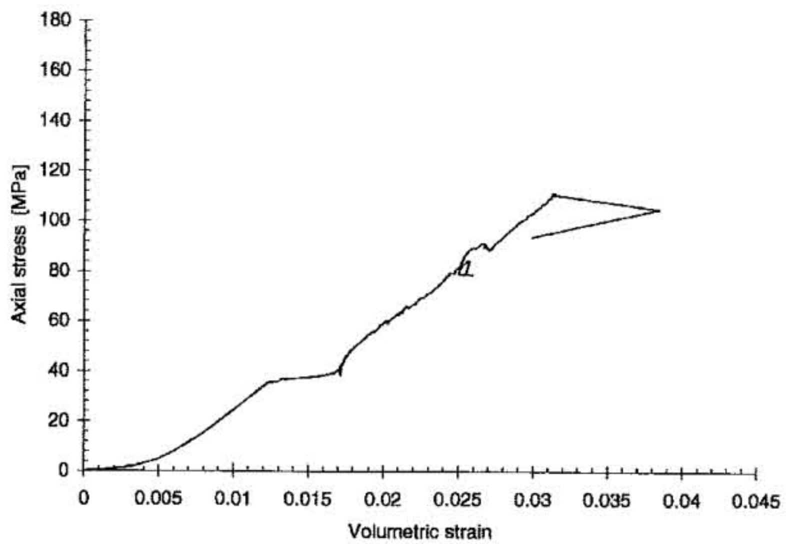

Figure 2. Oedometric test with water injection: axial stress vs. volumetric strain. (redrawn from Papamichos and Schei, 1998).

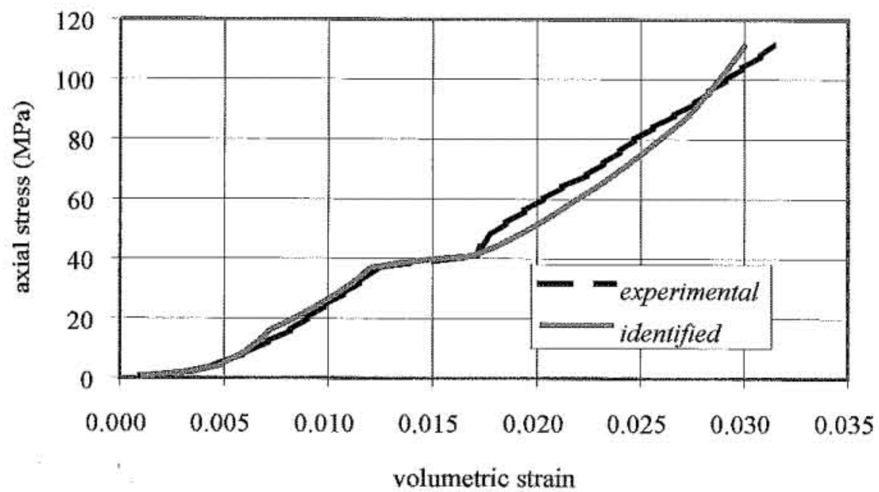

Figure 3. Idealised lab response and material model response.

Table 1. Identified material data.

l	m	a	$\lambda(0)$	i	p_f	$\kappa(0)$	β_0	β_1	η_f
0.8506	4.8166	2.5654	0.0296	1.5019	16.484	0.0046	1.0839	1.8487	2.9793

Figure 2 shows axial stress vs. volumetric strain as results from the experiment. For identification purposes, the experimental curves are slightly changed by eliminating the unloading reloading cycles. Also the experimental response has been slightly idealised by assuming 30 points, inclusive of the initial known conditions, as shown in Figure 3 together with the model response. The agreement is very satisfactory, in particular for the increase of volumetric strain caused by water injection. Table 1 presents the pertinent material data.

From Fig. 3, it may be noted that only by assuming a stress definition similar to eq. (1) it is possible to obtain a large strain effect associated with water saturation only, when assuming (nearly constant) total stress. Possible creep behaviour of the material has not been investigated, even if suggested by Papamichos et al. (1998). On the other hand, for reservoir sands it was excluded by Gertsma and Van Opstal (1973).

4. THE COMPLETE MATHEMATICAL MODEL FOR RESERVOIR ANALYSIS

A gas reservoir of the type investigated in this paper contains gaseous and liquid phases at the same time and within it pressure gradients are possible. As a consequence, the pressure measurements usually performed can not represent what happens in the whole reservoir. Moreover the reservoirs are in hydraulic continuity with the confining aquifers and aquitards. A complete mathematical model to simulate the mechanical behaviour within such a multiphase system certainly needs a mass balance equation for all present fluids together with momentum balance equations for fluids and the mixture. All these equations are coupled owing that they have to represent the overall behaviour of the system, which is the result of the interactions between the fluids and the solid. The mathematical model is hence composed of (Lewis and Schrefler, 1998)

- an equilibrium equation for the multiphase mixture (solid + water + gas) of the type

$$\sigma_{ij,i} + \rho g_j = 0 \tag{11}$$

where σ_{ij} is the total stress tensor (as in eq. 1), ρ the density of the mixture (solid plus fluids), g_j the gravity acceleration vector;

• a mass balance equation for water inside and outside the reservoir in the form

$$\left(\frac{\alpha - n}{K_s} S_w^2 + \frac{nS_w}{K_w}\right)\frac{\partial p_w}{\partial t} + \frac{\alpha - n}{K_s} S_w S_g \frac{\partial p_g}{\partial t} + \alpha S_w v_{i,i}^s + \left(\frac{\alpha - n}{K_s} p_w S_w - \frac{\alpha - n}{K_s} p_g S_w + n\right)\frac{\partial S_w}{\partial t} + \left[\frac{k_{ij} k_{rw}}{\mu_w}\left(-p_{w,j} + \rho_w g_j\right)\right]_{,i} = 0 \tag{12}$$

where α is Biot's coefficient, n the porosity, K_s and K_w the bulk moduli for solid and liquid phases respectively, S_g the gas saturation, the velocity vector of the solid phase, k_{ij} the absolute permeability tensor of the medium, k_{rw} the relative permeability, μ_w the dynamic viscosity and ρ_w the density of water.

• a mass balance equation for gas inside the reservoir in the form

$$\frac{\alpha - n}{K_s} S_w S_g \frac{\partial p_w}{\partial t} + \frac{\alpha - n}{K_s} S_g^2 \frac{\partial p_g}{\partial t} + \alpha S_g v_{i,i}^s - \left(n + \frac{\alpha - n}{K_s} S_g \left(p_g - p_w\right)\right)\frac{\partial S_w}{\partial t} + \frac{nS_g}{\rho_g}\frac{\partial}{\partial t}\left(\frac{p_g M_g}{\theta R}\right) + \left[\frac{k_{ij} k_{rg}}{\mu_g}\left(-p_{g,j} + \rho_g g_j\right)\right]_{,i} = 0 \tag{13}$$

where ρ_w the density of gas, M_g the molar mass of gas, R the universal gas constant, θ the absolute temperature, k_{rg} the relative permeability and μ_g the dynamic viscosity of gas. Mass balance equation for gas refers to reservoir conditions, but can be written at standard conditions, as usual in reservoir engineering, by introducing the formation volume factor.

All the governing equations are solved at the same time to obtain the flow, compaction and subsidence data.

The model is completed by a constitutive relation for solid mechanical behaviour relating the effective stress , still defined by eq. (1), and the adopted strain measure. In general, for small displacement gradients, it can be written in incremental form as

$$d\sigma'_{ij} = D_{ijkl}\left(d\varepsilon_{kl} - d\varepsilon_{kl}^{p} - d\varepsilon_{kl}^{0}\right) \tag{14}$$

ε_{ij} being the infinitesimal total strain tensor, the plastic strain and the strain component not related to stress (e.g. caused by temperature changes). D_{ijkl} is the fourth order tensor

$$D_{ijkl} = D_{ijkl}\left(\varepsilon_{kl}, \sigma'_{ij}, s \ldots\right) \tag{15}$$

which for the material at reservoir level is assumed to be also dependent on capillary pressure s, as explained in the section on elasto-plastic behaviour. Constant

absolute permeabilities are assumed, as is usual in subsidence problems, whereas relative permeabilities vary with the degree of saturation.

We now perform a numerical simulation of a well-documented model reservoir, which hence represents an interesting validation tests for the presented numerical models.

5. A CASE STUDY

For our investigations on subsidence analysis above gas fields we use a hypothetical reservoir (Figure 4), which has already been studied in (Evangelisti and Poggi, 1970) and, with an additional clay layer, in (Lewis and Schrefler, 1998). Production and gas pressure histories are those of a real reservoir. From the physical point of view, gas production and gas pressure decline are certainly linked, hence in the numerical simulation we should obtain similar results by fixing gas outflow or gas pressure history, the free parameter representing a check for the correctness of the formulation. Figure 5 presents gas production histories used as input and those obtained as output when imposing two different pressure histories. These, during the exploitation time, are the same as the recorded one and differ after 25 years: one assumes a free reservoir pressure, the second maintain the pressure value of the end of extraction (Figure 6). As can be seen, the results compare reasonably well.

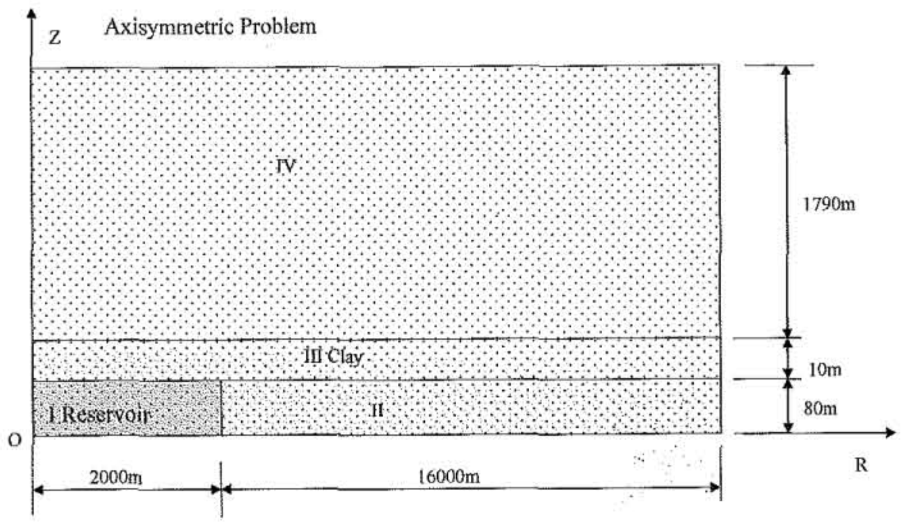

Figure 4. Geometry of the reservoir.

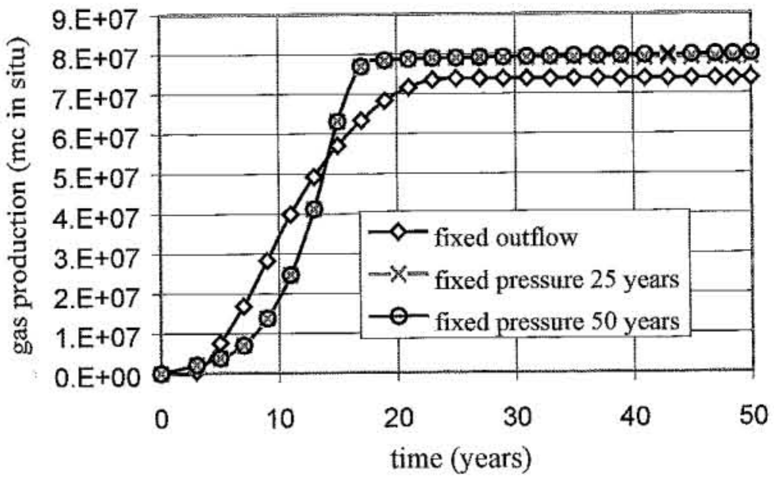

Figure 5. In situ gas production histories for different numerical simulations.

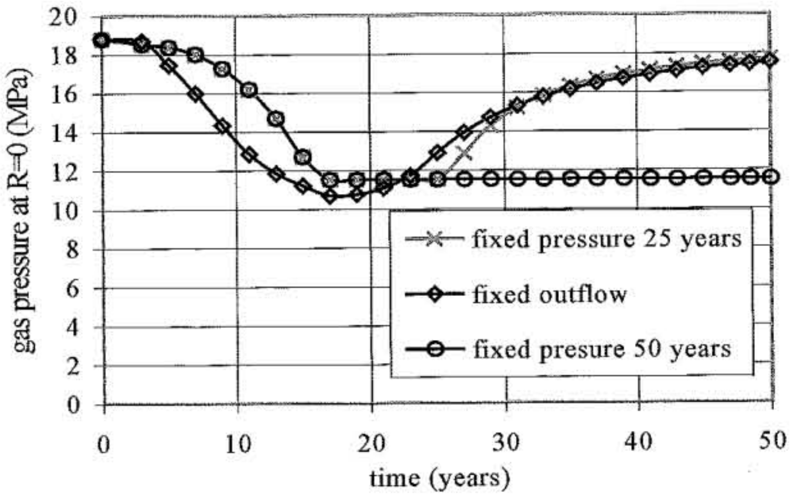

Figure 6. Gas pressure histories on the symmetry axis for different numerical simulations.

It may also be argued that at depletion of the wells the flow fields still present gradients which require pressure changes, fluxes of fluids and solid deformation developing for some time after the end of gas extraction. Figure 7 shows reservoir saturation history, which lasts for 50 years, the double than the assumed period of exploitation. Hence, when introducing in the numerical simulation pressure histories, usual recordings limited to the exploitation period are insufficient for the complete subsidence history determination. In the present paper the missing information is completed by either fixing the pressure at a constant value, or by letting the pressure completely free after 25 years (Figure 6).

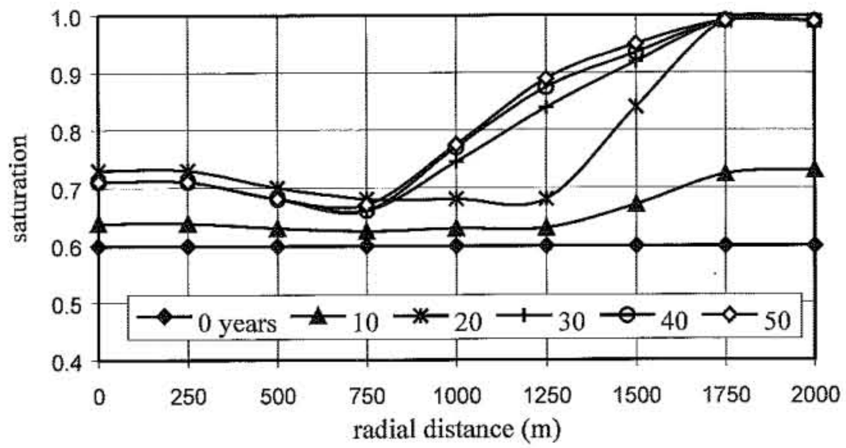

Figure 7.- Saturation versus radial distance at different times

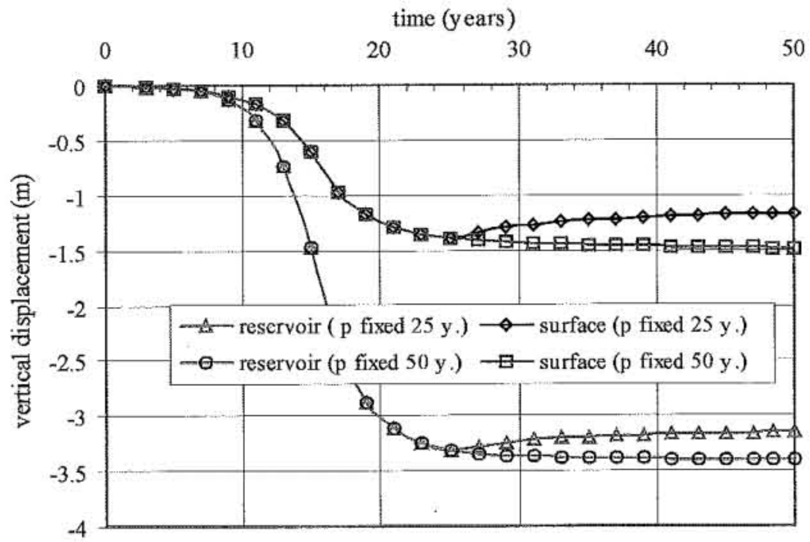

Figure 8. Maximum vertical displacements at the top of the reservoir and at the surface for two different length of applied pressure conditions

The effects of the aforementioned assumptions on maximum vertical displacements on the top of the reservoir and at the surface can be seen in Figure 8. To the pressure recovery phase corresponds a recovery in vertical displacement, limited in strength owing that the behaviour is essentially plastic. On the other hand, for constant pressure the subsidence continues.

6. CONCLUSIONS

The paper summarises an elasto-plastic model, which accounts for capillary effects. This model allows to represent well a laboratory test on flooding of a sample of gas reservoir rock. It is hence introduced in a general mathematical model for subsidence due to water and gas extraction from underground. An ideal case study is eventually presented and discussed.

Acknowledgements

This research was partially supported by the Italian Ministry of University and Scientific and Technological Research (Grant MURST ex 60%) and (Cofinanziamento MURST 9808160821_003).

We thank AGIP (Italian National Petroleum Company), S. Donato Milanese for allowing us to use data concerning saturation experiments carried out for AGIP by IKU Petroleum Research, Trondheim.

REFERENCES

Alonso E.E., Gens A. & Josa A. (1990) A constitutive model for partially saturated soils, *Géotechnique*, **40**, 405-430.

Brignoli M., Santarelli F.J. & Papamichos E. (1995) Capillary effects in sedimentary rocks: Application to reservoir water-flooding, *Rock Mechanics*, Proc. 35th U.S. Symposium, Eds. J.J.K. Daemen - R.A. Schltz, Balkema, Rotterdam, 619-625.

Delage P. & Graham J. (1996) Mechanical behaviour of unsaturated soils: Understanding the behaviour of unsaturated soils requires reliable conceptual models, *Unsaturated soils*, Alonso E.E. and Delage P. (eds.), Balkema, Rotterdam, 1223-1256.

Escario, V. & Sáez, J. (1973) Measurement of the properties of swelling and collapsing soils under controlled suction, Proc. 3rd I.C.E.S., Haifa, 195-200

Evangelisti, G. & Poggi B. (1970) Sopra i fenomeni di deformazione dei terreni da variazione di strato, *Atti Acc. delle Scienze dell'Istituto di Bologna*, Serie II, 6, 1-124.

Fredlund D.G., Morgenstern N.R., & Widger R.A. (1978) The shear strength of unsaturated soils, *Can. Geotech. J.*, **15**, 313-321.

Gertsma J. & Van Opstal G. (1973) A numerical technique for predicting subsidence above compacting reservoirs, based on the nucleus of strain concept, Verhandelingen Kon. *Ned. Geol. Mijnbouwk. Gen.*, **28**, 63-78.

Laloui L., Geiser F., Vulliet L., Li X.L., Bolle A. & Charlier R. (1997) Characterization of the mechanical behaviour of an unsaturated sandy silt, Proc XIVth Int. Conf. On *Soil Mechanics and Foundation Engineering*, Hamburg, 347-350.

Lewis R.W. & Schrefler B.A. (1998) *The Finite Element Method in the Deformation and Consolidation of Porous Media*, Wiley, Chichester.

Papamichos, E. & Schei, G. (1998) Characterization of Adriatic soft weak sediments for subsidence studies, IKU Petroleum Research, Trondheim, Norway, Report No. 33.0693.00/01/01/98.

Papamichos, E., Brignoli, M. & Schei, G. (1998) Compaction in soft weak rocks due to water flooding, *Proc. SPE/ISRM Eurock*, 411-417.

Pastor M., Zienkiewicz O.C. & Chan A.H.C. (1990) Generalised plasticity and the modelling of soil behaviour. *Int. J. Numer. Anal. Methods Geomech.*, **14**, 151-190.

Schoonbeek J.B. (1976) Land subsidence as a result of natural gas extraction in the province of Groningen, *Proc. Society of Petroleum Engineers of AIME*, Preprint.

Schrefler B.A. & L. Simoni (2000) An Elastoplastic Constitutive Model for Partially Saturated Soils. In: Handbook of Material Behavior, *Nonlinear Models and Properties*. J. Lemaitre (ed.), Academic Press, San Diego (California).

Simoni L. & Schrefler B. (2000) A. Parameter identification for a suction dependent plasticity model. Part II: Application to problems of reservoir engineering. Submitted for publication.

TIDE INDUCED SUBSIDENCE IN THE SUPERFICIAL SOIL DEPOSITS IN THE VENICE LAGOON

Luigi Belloni and Simone Venturini
Technital S.p.A. – Consulting Engineers – via Cattaneo n. 20, 37121 Verona - Italy

Alfredo Caielli
Magistrato alle Acque – Rialto – Venezia - Italy

Abstract

During the tide period in the Venice lagoon the pore pressure diffusion with depth is limited by the permeability of the surface layers and their specific storage. Therefore for the equilibrium of the total vertical stress, effective stresses are induced in the soil. The piezometric measurements made down to almost 50 m below sea level and the theoretical analysis with a FEM model show that the soil is under the effect of repeated loading. The relevant literature contains evidence that soils, particularly sandy soil, under repeated loading continue to accumulate permanent deformations, irrespective of the number of load cycles. The problem will be to define the threshold tide amplitude and the depth where stress increments could still be significant.

From a very preliminary analysis of available data there are at least 10 events in a year and 100 m of foundation soil may contribute to the settlement. In order to have a better estimate of the above phenomenon and its consequences on the lagoon subsidence, more research is needed on the effect of cyclic loading on the superficial soil.

Keywords: tide, cyclic loading, pore pressure, lagoon subsidence.

1. INTRODUCTION

The Adriatic Sea enters the Venice lagoon through three mouths, one of which was extensively investigated in 1995 for the design of the mobile gates, see Fig. 1. The investigation reached almost 100 m depth below sea level. The geotechnical profile was then defined on the base of in situ and laboratory tests.

One of the boreholes was then instrumented with three piezometers in order to monitor the pore pressure induced by the tide. The recording lasted three months, providing the variation of the pore pressure as a function of the tide excursion.

The analysis of these experimental data show that effective stresses do change with depth and therefore the soil undergoes a cycle loading which will contribute to the subsidence of the lagoon.

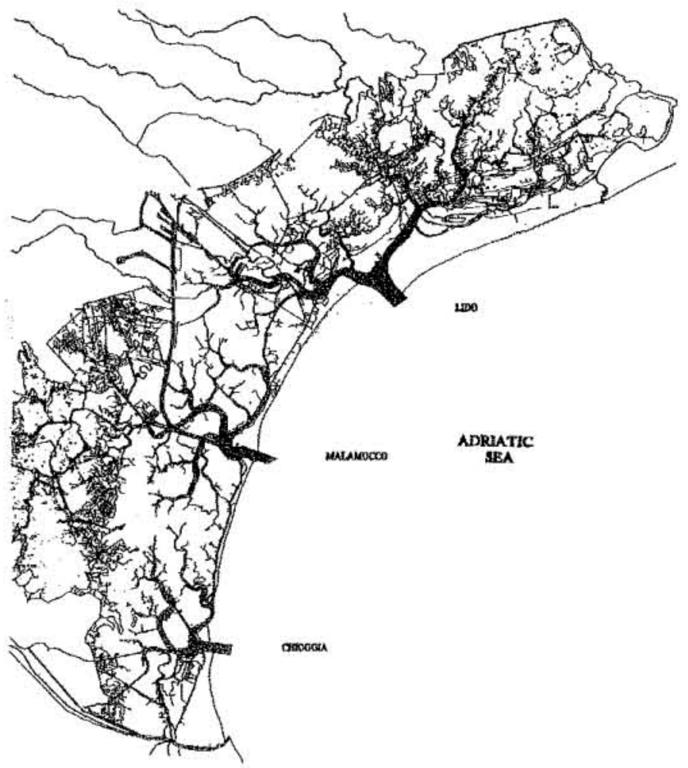

Figure 1. Location map.

2. STRATIGRAPHY

The soil stratigraphy is presented in Table 1, together with the geotechnical characteristics of the different layers. It is composed of a series of layers from clayey soil to sand, which has been deposited in a transitional environment: on a beach subjected to the wave energy or in the nearby lagoon, depending on the position of the sea level in relation to that of the land (Belloni et al., 1997).

Organic matter and gas are present in the soil, particularly in the upper layers. Gas however is dissolved into water, so that the soil can be considered fully saturated at the in situ water pressure.

Table 1. Soil stratigraphy at Malamocco.

Layer	Description	Depth below sea level (m)		E (MPa)		e_0	n	γ (kN/m^3)
		From	to	Dynamic	Static			
A	1	5.35	12.76	105	7.76	1.00	0.50	1.85
B'	2	12.76	17.32	132	19.05	0.80	0.44	2.00
B	3	17.32	20.88	190	13.05	0.85	0.46	1.90
C	4	20.88	24.5	225	19.50	1.00	0.50	1.80
D	5	24.5	42.18	335	35.90	0.80	0.44	1.85
E	6	42.18	48.96	436	30.20	0.90	0.47	1.82
E'	7	48.96	54.49	480	67.64	0.80	0.44	1.80
E	8	54.49	77	580	45.70	1.10	0.52	1.80
F	9	77	86	676	28.20	0.80	0.44	1.90
G	10	86	91	725	60.25	0.85	0.46	1.85
H	11	91	100	800	29.52	0.75	0.43	1.92

Description of the layers
1. fine sand with silt
2. overconsolidated clay
3. NC and OL layers of silty clay, some layers of sandy silt
4. fine sand with some silt
5. clayey silt with thin layers of silty sand
6. sand
7. sand including layers of clayey silt
8. sand
9. clayey silt
10. fine silty sand
11. silty clay

The meaning of the symbols in Table 1 are the following:

E= deformation modulus, e_0 = void ratio, n = porosity, γ = bulk density

3. PIEZOMETER INSTALLATION

Three piezometers were installed in the borehole and the depths of the sensors are the following below sea level:

PZ1 = -12 m; PZ2 = - 20 m; PZ3 = - 45 m.

With reference to the stratigraphy, PZ1 monitored the sandy layer A, PZ2 the clayey layer B and PZ3 the sandy layer E.

Before installation the piezometers were tested in the laboratory, with the following results, as in Table 2:

Table 2. Piezometers sensitivity

Piezometer	Max pressure (bar)	Maximum error	
		bar	cm of water
PZ1	1.5	0.001	1
PZ2	4.5	0.0025	2.5
PZ3	5.0	0.0031	3.1

4. PIEZOMETRIC DATA INTERPRETATION

In Fig. 2 a sample of the recorded data is plotted together with the tide.

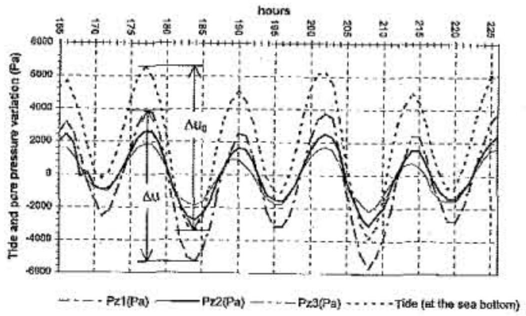

Figure 2. Tide and piezometric readings – a sample recorded in April 1995.

As it can be observed neither the tide nor the piezometer readings are symmetrical with respect to the mean sea level (0.00). However, there is no phase lag between them. The attenuation of the tide with depth, as measured by the piezometers, was evaluated using the double amplitude of the signal, and is therefore defined as: attenuation $\alpha = \Delta u / \Delta u_0$, where Δu = double piezometric amplitude, Δu_0 = double tide amplitude.

The average values of α obtained over the registration period for the three piezometers are plotted in Fig. 3, with the interpolated attenuation function.

Since the pore pressure is attenuated with depth and is less than the total load applied by the tide at the sea bottom, it follows that effective stresses do vary with depth.

5. THE MATHEMATICAL MODEL

The problem of pore pressure distribution in the soil below the sea bottom has been the object of many papers in recent years. Generally solutions are available under the load condition imposed by storm waves (Madsen (1978), Okusa (1985) and for an homogenous half space.

In the present case, considering that the soil is stratified and the load is represented by the tide, no general closed form solutions are available and it has been necessary to employ a finite element model SEFTRANS (1996), which solves only the transient flow equation, therefore pore pressure is evaluated but not the corresponding changes in effective stresses. The governing equation is:

$$\nabla^2 h = \frac{S_s}{K}\frac{\partial h}{\partial t} \ ,$$

where the specific storage S_s is given by: $S_s = \rho \cdot g \cdot (\alpha + n\beta)$, K = soil permeability, ρ = mass per unit volume, g = acceleration of gravity, n = soil porosity, α $=1 / E$ compressibility of the soil skeleton, β = compressibility of water.

A simplified tide has been used with period T=12 hours, consisting of a rectangular pulse with amplitude A = ± 1 m, which nevertheless can provide some insight. By trial and error the values of K and S_s were determined so that the SEFTRANS attenuation curve fit the experimental points, see Fig. 3.

With reference to the geotechnical characteristics of the soils reported in Table 1, the following comments can be made:

- the values of determined are in agreement with the dynamic moduli of the soils;
- the soil is saturated;
- the coefficients of permeability are fully in agreement with those determined for the sandy layers, but one order of magnitude higher than those of the clayey soil as determined from the coefficient of consolidation.

The difference may be due to the frequent presence of thin layers of sand and silt in the clayey layers.

6. CYCLIC LOADING IN THE FOUNDATION SOIL

The pore pressure recorded at the piezometers and the results from the FEM model both lead to the conclusion that under the total load induced by tide the foundation soil undergoes a cyclic loading of the effective stresses, which may cause vertical settlements.

The effective cyclic vertical stresses at depth z approximately will be given at time t by: $\sigma'_z = \sigma_z - u = \sigma_z \cdot (1-\alpha)$ where σ_z = total load imposed by the tide = $\Delta u_0 / 2$, Δu_0 = tide double amplitude.

The σ'_x component is probably equal to σ'_z but of opposite sign (Madsen, 1978; Okusa, 1985), therefore the soil element is subjected to a quasi-isotropic cyclic stress.

There is evidence in literature that plastic deformation is accelerated with the number of cycles (Li et al, 1996; Uzan, 1998).

It will also be noted that at the beginning of a cyclic loading the axial deformation is much higher and then becomes progressively smaller. This means that, if the cyclic loading stops for a given time and then starts again, the incremental axial deformation at reloading could be higher than that accumulated between the last two cycles before stopping the load.

Tides are irregular in amplitude, duration and symmetry about mean sea level. Exceptional events do occur, with amplitude of more than 1 m and a period longer than 12 hours. These events have a frequency of 1 or 0.1 in a year.

If in 100 years the number of representative events in one year is 10, the soil undergoes 1000 cycles at an average deviator stress of 5 kPa.

The corresponding plastic deformation (Li et al, 1996), can be of the order of = 0.05% and the vertical settlement for a 100 m layer can be in the order 5 cm in 100 years.

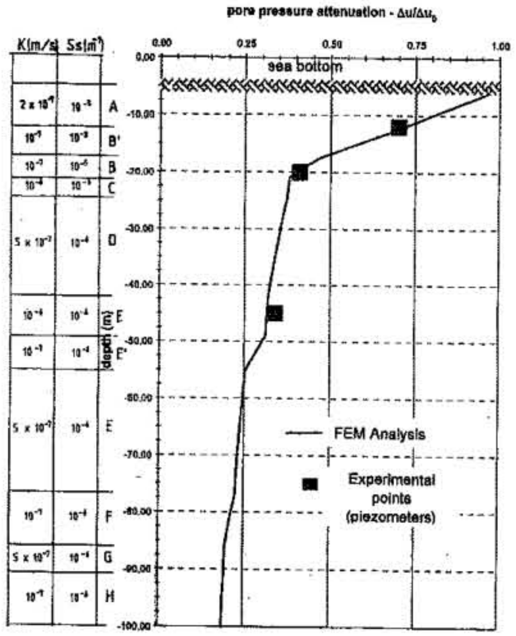

Fig. 3. Pore pressure attenuation evaluated with the finite element model.

REFERENCES

Belloni L., Caielli A. (1997) "Origine dei sedimenti a Malamocco", *Atti dell'Istituto Veneto di Scienze, Lettere ed Arti,* Tomo CLV (1996 – 1997)

Madsen O.S. (1978) "Wave induced pore pressures and effective stresses in a porous bed", *Geotechnique* **28**, n. 4

Okusa S. (1985) "Wave induced stresses in unsatured submarine sediments", *Geotechnique* **35**, n. 4

Li D., Selig T. (1996) "Cumulative plastic deformation for fine grained subgrade soils", *ASCE GT*, December 1996

Uzan J. (1999) "Granular material characterisation for mechanistic pavement design", *ASCE J. Of Transp.* Eng. March/April 1999

SEFTRANS (1996) Simple and Efficient Flow and TRANSport model, ver. 6.20 (1996) by Oxford Geotechnica International (UK) Ltd.

MODELLING REGIONAL AND LOCAL SURFACE SUBSIDENCE DUE TO COMPACTION OF UNCONSOLIDATED SEDIMENTS

G. de Lange [1], G.B.M. Brand [2], A.J.Th. de Bruijne [2], E.J. de Min [2], M.J. Ringelberg [2]

[1] *Nederlands Instituut voor Toegepaste Geowetenschappen, Afd. Geo-infrastructuur, Section Geomechanical Research, PO box 6012, 2600 JA Delft, The Netherlands*

[2] *Directoraat-Generaal Rijkswaterstaat, Meetkundige Dienst, Afd. Advies en Onderzoek Plaatsbepaling, PO box 5023, 2600 GA Delft, The Netherlands*

Abstract

The composition of the unconsolidated subsurface of the western and northern part of The Netherlands is complex and heterogeneous. This results in a heterogeneous pattern of surface subsidence.

A geomechanical model is proposed which translates the lithology into geostatistically derived subsidence parameters and applied to a pilot study area. Historical records of ground and surface water levels provide the input for the hydrodynamically driven portion of compaction.

The models are compared with geodetical survey data. These data comprise the levelling time series of the national grid of surface benchmarks and of the deep-rooted NAP (national datum)-bench marks.

The problems and geostatistical solutions to irregularities in the data are described for a peat meadow area in the vicinity of Amsterdam. The area was recently covered with airborne laser altimetry. The merits of this method are analysed. Also the developments in the use of satellite-borne interferometric SAR (Synthetic Aperture Radar) are described.

A calibrated model of the surface subsidence can help in predicting future land subsidence, having implications on flooding prevention measures, land use and infrastructure.

Keywords subsidence, water management, InSAR

1. INTRODUCTION

The prediction of surface subsidence is of great importance in order to take decisions on environmental planning in The Netherlands and on the maintenance and adjustments of its large works of infrastructure, such as dikes and polders. These works are built to last for at least 50 years and surface subsidence is one of the factors that determine their capacity. Dutch authorities on water management, national (Rijkswaterstaat) as well as regional and local, can benefit much from improved prognosis of expected surface subsidence. Therefore, the aim is to achieve an improved prediction map of surface subsidence in The Netherlands.

The main causes of subsidence in The Netherlands are consolidation of the Holocene cover and oxidation of peat layers as a result of artificial lowering of freatic levels. In some areas (Groningen) oil and gas extraction is another important human cause of subsidence. Natural causes are glacial rebound, tectonics and compaction of Tertiary clays. Especially in strongly subsiding peat meadow areas, surface subsidence is a hot item. Despite a lot of debate in the past years, little is known about the actual deformations. There is a big lack of measurement data; in fact, height information from old maps is now being used for analysis.

Up till now, the quality of the surface subsidence predictions in The Netherlands is generally not satisfying. In order to improve this, we investigated a small test area in the North Western part of the country, called Waterlanden, cf. figure 1.

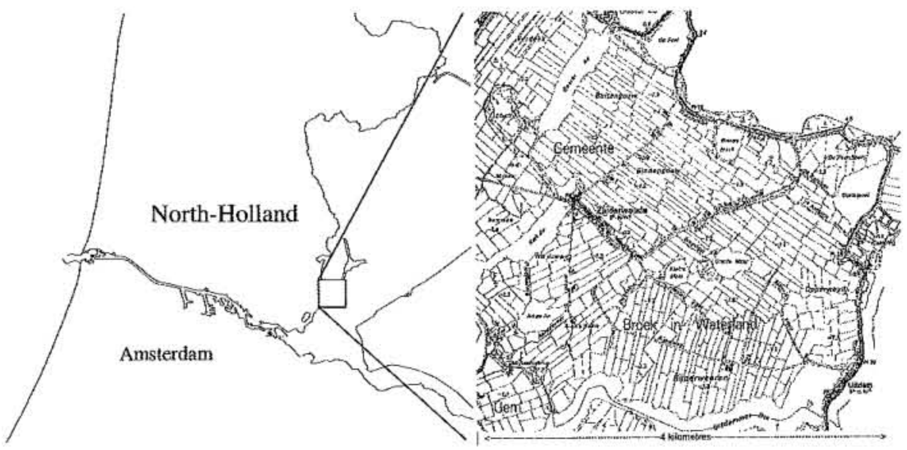

Figure 1. Location of test area Waterlanden near Amsterdam.

Here, we have 4 series of height measurements (from 4 different epochs) in this clearly subsiding area. This means that we were able to confront our geological prediction model with these data in order to improve this model. In the end, the improved model should cover the whole of The Netherlands or at least those areas of interest. The aim is to achieve a better modelling from both the measurements (precision of 1 cm over 10 years) and geological input; next, we want to use these models to predict surface subsidence for the next 50 years with cm-accuracy.

First, the ingredients of the study are discussed: the geological model and its underlying ideas, the height measurements, and the methods used to confront the geological model with the measurements. Secondly, we present the results of the confrontation and discuss the outcome by comparison. Thirdly, we give an outlook to possibilities for application of future measuring techniques, such as InSAR and laser altimetry; these can improve the prediction of surface subsidence. Finally, conclusions and recommendations are presented.

2. APPROACH

2.1 Engineering geological model

As only surface levelling data are considered in the study, the layers which are included in the geological model are limited to the Holocene cover on top of the Pleistocene sand substratum. The surface levelling is related to the height reference system (NAP), which has its base in the Pleistocene. The dynamic behaviour of the national datum surface is subject of a separate study [Kooi, 1998]. The horizontal variation in the relatively small area is not big. The Holocene succession in the area can be generalised as follows:

- Lower unit of peat and clay
- Sandy tidal flat deposits
- Upper clay unit
- Holland peat unit
- Clay cover

The thickness of these layers varies slightly over the area as can be seen in an east-west projection (about 3 km long) of all available bore holes, see figure 2.

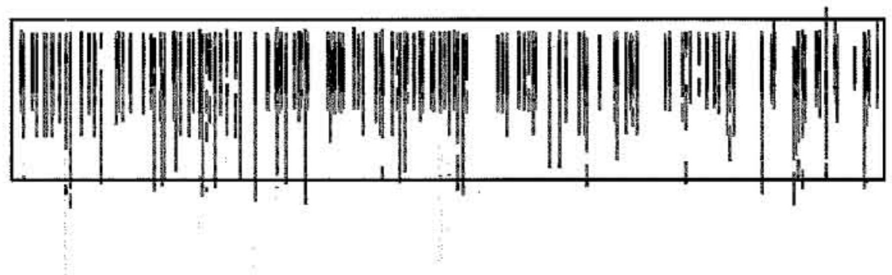

Figure 2. Projection of bore holes. The upper and lower boundaries of the box represent the reference datum NAP and NAP-12m respectively. Black = peat, Dark grey = clay, Light grey = Sand

Because most available bore holes do not penetrate the Pleistocene-Holocene interface, an arbitrary bottom for the model had to be chosen. This is represented by the average depth of the interface. For the subsidence calculations the missing interval in the bore holes was assumed to be consisting of clay. Besides some cone penetration tests only few geomechanical data are available for the area, which were collected in the 70s for the land reforms and the studies of the effects of the planned reclamation of the Markerwaard. The parameters necessary for the subsidence calculations were correlated with the lithological descriptions on the basis of these data. Furthermore correlations were used based on a geotechnical database of a larger area covering the entire province of North-Holland and the representative values given in The Netherlands Standard NEN 6740 [NEN, 1991].

Most one-dimensional calculation methods use the Terzaghi formula in some way to calculate surface subsidence. Based on experience in The Netherlands the adapted formula derived by Koppejan [Koppejan,1948] is considered more useful for small load increment effects, such as associated with lowering of the freatic water level. Also, all consolidation parameters pertaining to the present area are represented in the Koppejan coefficients. Therefore the Koppejan formula is used in our subsidence calculations. Its simplicity makes it very well suited to incorporate in a regional database manipulation.

Even in such a small area the variation in boundary conditions justifies subdivision into smaller units. The boundary conditions pertaining to the surface subsidence analysis are:

- Lateral variation of peat thickness
- Lateral variation of cover layer thickness
- Different freatic levels

The outer boundary of the area is determined by the outer boundary of surface level measurements. The area was subdivided into smaller polygons. The boundaries of the polygons were determined by the areas of equal freatic level and by the geology. In order to incorporate the geology in the subdivision the subsidence susceptibility was used as a direct expression of the subbottom profile. By calculating the subsidence of the entire area for a uniform freatic lowering, a pattern emerges which can be used to subdivide the area in subunits of "equal" susceptibility.

2.2 Groundwater history

Data pertaining to the history of the level of the freatic surface is diffuse. The level is dictated by the surface water authorities. This level is not always maintained by the landowners for different reasons. In some properties the level is lower to counteract storm-runup in the north-east due to the prevailing south-westerly winds. In other places the level is lowered to enable the grow of crops. Although the location of these areas is known, the exact

amount of lowering and the start time is not recorded. The freatic levels as dictated by the authorities is as follows:

Source	Year (Period)	Waterlevel	
		NAP-...metre	AP-...metre
Annals	1650		1.05
Annals	1896		1.30
Edict	1957	1.43	
	1967	1.43	
Pumping records	1976-1980	1.49	
Edict	1982-1983	1.49	
Pumping records	1994-1998	1.53	
Edict	1998	1.53	

In the 70-ties a plan was made to reform the landownership. This meant the reshuffeling of scattered ownership into more manageble larger properties. A part of this plan was also to create larger areas for crop growth by lowering the freatic surface. Lowering in the designated areas started in May 1994.

2.3 Classification of the areas

In order to account for the geological variability, the area was subdivided into two sub-units. The subdividion was overlain by the subdivision according to the recent surface water regime. The regime is characterized by four different water levels:

- the general level of NAP - 1.53m
- the block level of NAP - 1.96m
- the intermediate block level of NAP - 1.75m

This results in six classes. Figure 3 explains the classification of the areas in the Waterlanden area; next, table 1 shows the criteria upon which the classification was made.

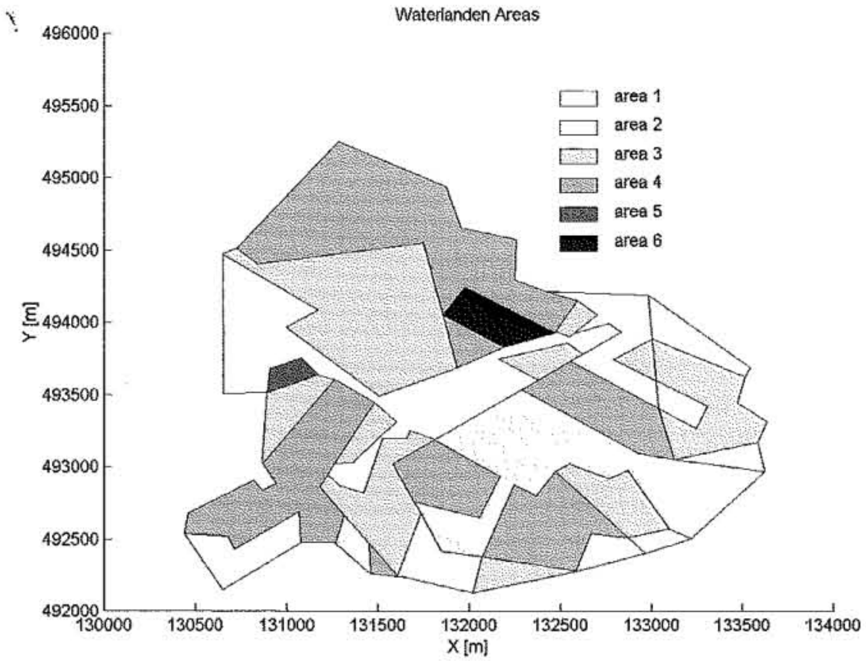

Figure 3. The classification of the areas.

Table 1. Criteria for classification of areas.

Area Class	Definition	No. of boreholes
1	Less susceptible, small freatic lowering	29
2	More susceptible, small freatic lowering	49
3	Less susceptible, large lowering 36	
4	More susceptible, large freatic lowering	38
5	Less susceptible, moderate freatic lowering	none
6	More susceptible, moderate freatic lowering	4

Due to lack of data Area 5 was not analysed.

2.4 Calculation of subsidence

The compaction was calculated for the last two epochs of surface water level adjustment of the area:

Epoch	Year	Level adjustment
1	1976 - 20 May 1994	NAP-1,43m - NAP-1.49
2	20 May 1994 - 1998	NAP-1.49 - NAP-1.53 NAP-1.49 - NAP-1.75 NAP-1.49 - NAP-1.96

The calculations were performed in a ACCESS/EXCEL environment coupled to the DINO borehole database of NITG-TNO. Using the geomechanical parameters gathered from the available reports a correlation between soil type, geological setting and depth allows automatic attribution of the relevant parameters to the individual soil profiles. The compaction behaviour with time was calculated for each borehole using the modified Koppejan formula which takes into account the development with time of the consolidation degree for the hydrodynamic part. The secondary consolidation was allowed to continue. Because the soil profile has experienced greater loadings due to groundwater lowering the compaction coefficients for load levels lower than the preconsolidation pressure were used. From groundwater level records in deep boreholes in and surrounding the area it was concluded that the piezometric level of the upper aquifer underlying the compressible profile remains constant over the considered epochs at NAP-2.2m. This piezometric level was fixed at the base of the profile. Because the average lowering of the freatic level is less than the lowering in the surface water in the ditches and canals the lowering applied in the computations was reduced empirically.

2.5 Surface level measurement data

In the Waterlanden area height data is available from the epochs 1964, 1978, 1995 and 1997. This offers the possibility to carry out a calculation of the average surface subsidence of (certain parts of) the area. The precision of an average surface level both depends on the point noise of the observations, which is the independent part of the standard deviation, and on systematic error(s), which is the part of the standard deviation which has correlation to other data points or even may remain constant for a whole area. Within this spatially correlated part of the errors two types of error have been taken into account: seasonal height variations, cf. [Beuving, 1996] and [Schothorst, 1979], and inaccuracies in the connection to the height reference system bench marks (NAP), cf. [Spierenburg, 1995]. The influence of terrain variations on the calculated average surface levels is supposed to be relatively small because of the relatively large number of height values involved.

Below some background information is given which is important for the quality description of the data sets. As the whole area is covering about 560 hectare or ha (i.e. 1400 acres) and because 5 or 6 height reference system bench marks are used in it, the area which has data correlation is estimated at 100 ha (250 acres).

- 1964: these height data were collected in the summer and obtained by levelling. The heights are rounded off to dm's (to the next integer) and the data density is about one point per ha. Taking into account the effects of rounding, the point noise of the data is estimated at 6 cm. The part of the standard deviation due to systematic errors has been assessed at 3 cm per 100 ha and 1 cm for the whole area.
- 1978: this data set was also obtained by levelling and was collected in spring. The heights are in cm and the density is approximately 3 points per ha. The point noise is estimated at 5 cm. Unfortunately this data set turned out to be not very reliable: obviously an error has been made in connecting a part (approximately one third) of the observations to the reference height system (NAP), resulting in a systematic error of approximately 9 cm for that part. After making a correction for that error the remaining systematic errors are estimated at 4 cm per 100 ha (correlated) and 1 cm for the whole area.
- 1995: this data was obtained by GPS observations and collected in spring. Data density is 1 point per ha and the point noise is assessed to be 4 cm. The part of the standard deviation due to systematic errors has been assessed at 2 cm per 100 ha and 1 cm for the whole area.
- 1997: the data of this epoch was obtained by laser altimetry and collected in spring. The data was gridded in a 25 m grid. The point noise of the gridded data points can be estimated at 10 cm. Area dependent (correlated) errors are the flight strip error, this error is estimated at 5 cm and is valid for areas up to 5 ha (strip length 120 m and width 400 m), and the drift error which is assessed at 4 cm and is valid for single flight strips of 400 m width. The constant error valid for the whole area is assessed at 1 cm.

Table 2 summarises the types of error for different correlation areas. The months noted represent the centre of the measurement period that usually lasts several months. Point noise is denoted as "pn". Error types "corr1" and "corr2" consist of errors that are correlated over areas of various size; these errors are more or less averaged out in the computation of the average surface level. Error type "const" is affecting the whole measured area in the same way.

Table 2. Error types for different correlation areas.

	1964 (August)	**1978 (May)**	**1995 (April)**	**1997 (April)**
σ_{pn} (cm)	6	5	4	10
σ_{corr1} (cm)	3 (100 ha)	4 (100 ha)	2 (100 ha)	5 (5 ha)
σ_{corr2} (cm)	--	--	--	4 (400 m strips)
σ_{const} (cm)	1	1	1	1

The number of height observations for the six areas as introduced in 2.2 in the 4 epochs is shown in Table 3.

Table 3. Number of height observations.

	1964	**1978**	**1995**	**1997**
Area 1	94	233	96	1674
Area 2	99	239	103	1538
Area 3	163	426	207	2659
Area 4	193	580	271	3174
Area 5	5	15	6	56
Area 6	13	26	18	183

On the basis of the above mentioned information, the precision of the mean surface level height for the six areas can be calculated with the formula

$$\sigma_{area} = \sqrt{\frac{\sigma^2_{pn}}{n} + \frac{\sigma^2_{corr1}}{r} + \frac{\sigma^2_{corr2}}{s} + \sigma^2_{const}} \qquad (1)$$

where n is the number of points in the area, r is the surface ratio of the area in question divided by the area where a certain kind of correlation is valid (with a minimum value of 1) and s is the number of flight strips which is supposed to be in consideration for a certain area.

Table 4 presents the calculated standard deviations of average surface levels.

Table 4. Calculated standard deviations.

	1964	**1978**	**1995**	**1997**
σ_{area1} (cm)	1.8	2.1	1.4	2.3
σ_{area2} (cm)	1.8	2.1	1.4	2.3
σ_{area3} (cm)	1.7	2.1	1.4	2.3
σ_{area4} (cm)	1.7	2.1	1.4	2.3
σ_{area5} (cm)	3.6	2.6	2.4	4.8
σ_{area6} (cm)	2.6	2.4	2.0	4.0

It appears that the precision of the average surface levels is mainly determined by the systematic errors; the influence of the point noise is practically negligible, since we have a large number of measurements. The precision of the laser altimetry data set of 1997 is worse than the levelling data, although much more points have been measured.

As the areas 5 and 6 are relatively small in comparison with the other areas, the influence of the terrain height variations might not be negligible; for that reason these two areas are further left out of consideration.

3. RESULTS

3.1 Confrontation

The confrontation of the predictions from the geological model and the measured surface levels forms the core of the results. In figures 4-7 the predictions from the geological model are confronted with the measured surface levels. In the error bars the precision (standard deviation) of both is shown. The areas 5 and 6 are left out of consideration as mentioned in the previous section.

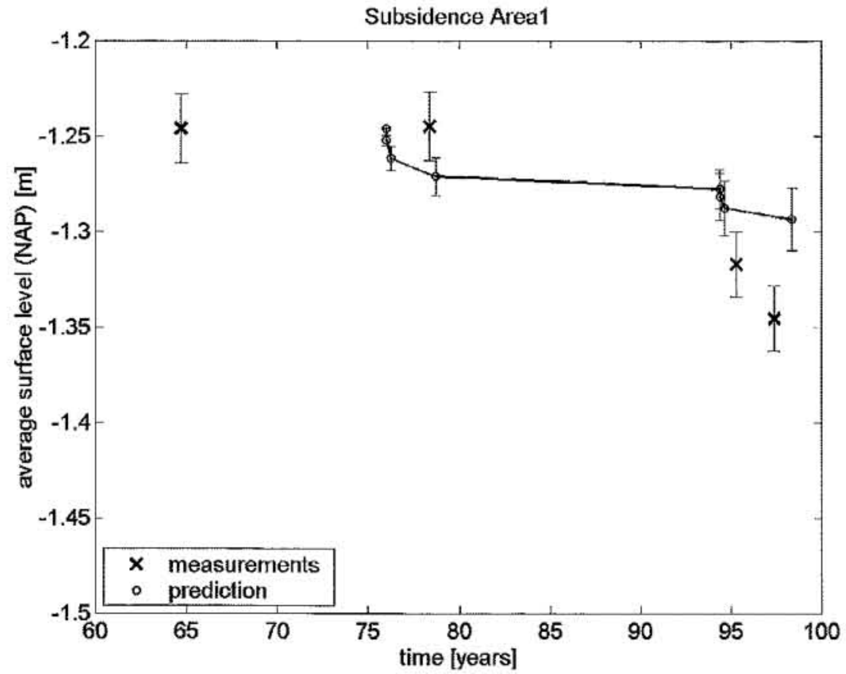

Figure 4. Confrontation of model and measurements in area 1.

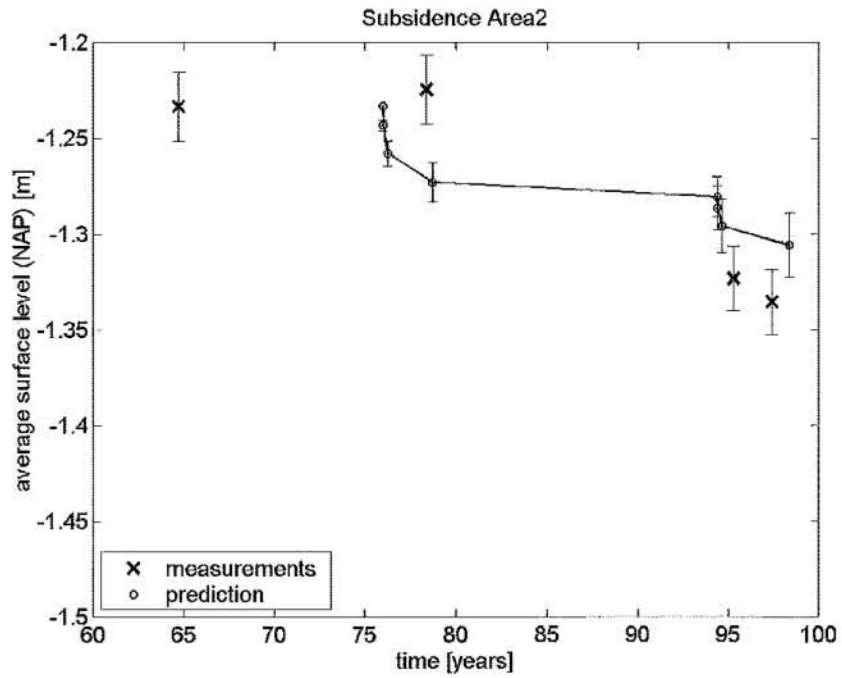

Figure 5. Confrontation of model and measurements in area 2.

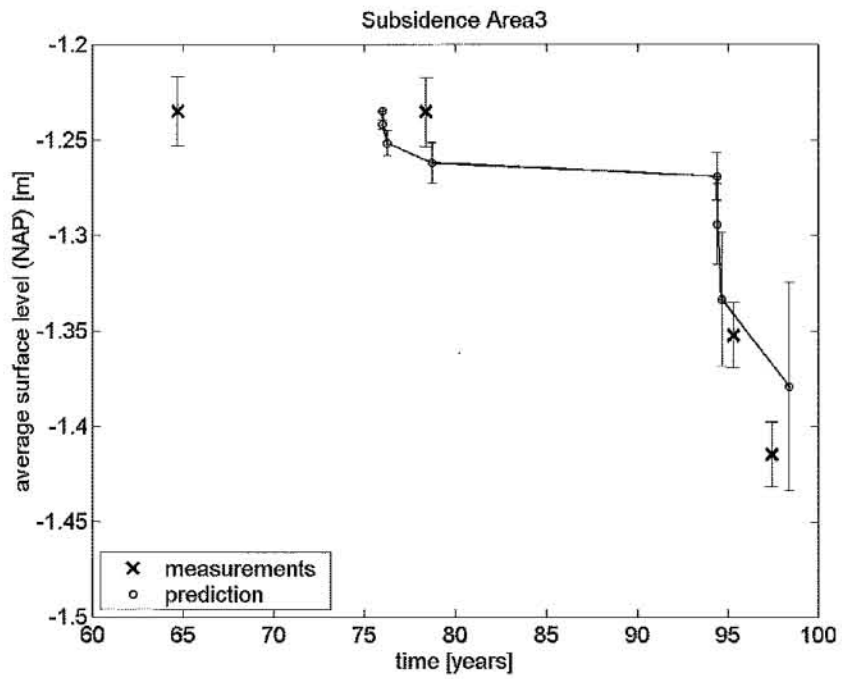

Figure 6. Confrontation of model and measurements in area 3.

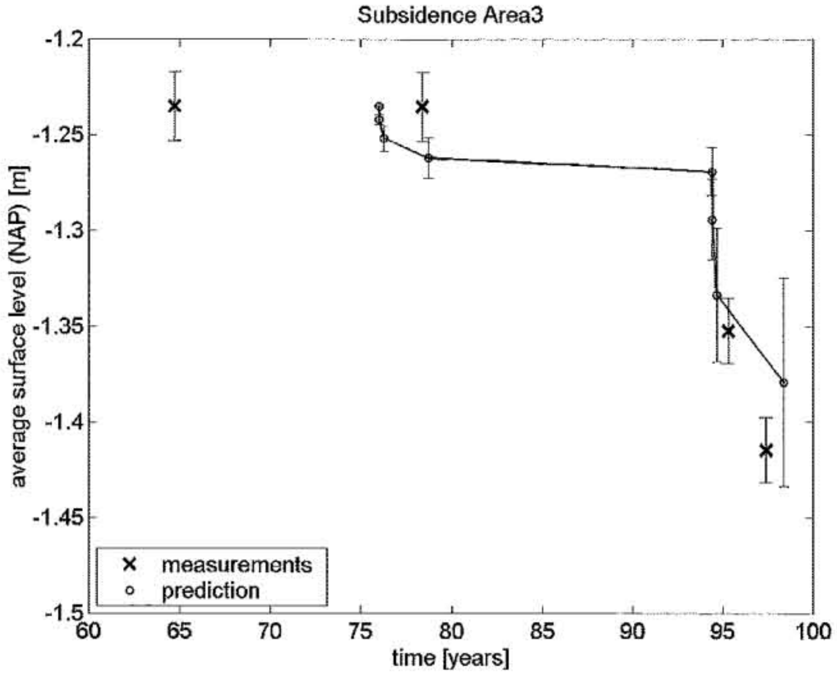

Figure 7. Confrontation of model and measurements in area 4.

The predictions are computed as subsidence relative to 1976. In this year the first lowering of the freatic level is known. Computations are made on 10, 100 and 1000 days after the time of lowering and on the time just before the next lowering. The standard deviations of the predictions are computed relative to their starting time of 1976. These standard deviations are exclusively based on the lithological variability in the investigated area. The relative error resulting from the generalization of the geomechanical parameters is represented by a standard deviation of 30% of the computed compaction of the individual soil profiles, corresponding to a 90% reliability cf. (Hannink). In the figures above, the predictions are converted to NAP heights by fixing the start level to the start of the measured surface levels (1964).

The average surface level measurements are plotted as separate points. Connecting these points would give a false picture of the actual situation in the area. The computation of the standard deviations of the measurements is comprehensively described in the previous section.

3.2 Discussion

Several things can be said when looking at the figures (when we speak of significance, we refer to a phenomenon that exceeds the standard deviation at least once; this is of course a somewhat subjective measure):

1. The effect of the freatic lowering in 1976 does not show in the surface level measurements of 1978 (except perhaps for area 4). Of course, the sampling of the data in time (epoch) is of great influence on the results: a possible phenomenon occurring in between two samplings/epochs can not be discovered, resulting in an erroneous appearance of the subsidence.
2. In all areas except Area 4 the measured subsidence is greater than the computed compaction. The residual gap can be attributed to the effects of shrinkage and oxidisation of the peat above the freatic level. The latter phenomenon was also described in the borehole logs. Studies made in the area for the land reform (cf. Heidemij) indicate that for this degree of freatic lowering a combined effect of 3 to 6 cm can be expected, which is equal to the residual difference between the measured and computed trends. Part of the residual can also be attributed to the fact that the 1964 levelling was done in the summer, resulting in a lower surface level relative to the spring measurements of the subsequent data sets.
3. When comparing the results for areas 1 and 3 and for areas 2 and 4, both cases exhibiting different freatic lowering with equal susceptibility, the differences in the height data are clearly significant. Thus, here the model prediction is satisfied.
4. Next, we compare the results for areas 1 and 2; both exhibit small freatic lowering. The differences in the height data are certainly not significant, even though the susceptibility of area 2 is considered to be larger than area 1. The differences in the model predictions are also not significant.
5. Next, we compare the results for areas 3 and 4; both exhibit fairly large freatic lowering. The differences in the height data are certainly not significant, even though the susceptibility of area 4 is considered to be larger than area 3. The differences in the model predictions are just about significant. Probably the subdivision in susceptibility is biased by the lower borehole density. This is also indicated by the relatively large standard deviations for the calculated compaction in Area 3.
6. One must not forget that the point noise of the height measurements may be non-white: a different systematic error in each epoch (e.g. caused by different surveyors) directly influences the results.

4. OUTLOOK TO FUTURE MEASUREMENT TECHNIQUES

Levelling is an expensive and time-consuming technique for collecting information on height changes to improve and calibrate the subsidence models. Therefore, we are looking for other techniques to collect this information.

One important new technique is interferometric radar (InSAR). This technique has proven to be able to detect mm-changes over a time period of several months. However, this was done using C-band satellite InSAR, which is not suitable for the improvement of subsidence models. The wavelength is too small to give coherent images over long time periods, and the resolution is too low. Therefore, the Survey Department of Rijkswaterstaat is focusing on L-band airborne InSAR for this application. The wavelength is longer, which decreases the precision, but might yield sufficient coherence in time. The use of an airborne system implies that a better resolution can be obtained, and, what is even more important, that observations can be done at the best time to measure. Until now, atmospheric disturbances are the major drawback of using (satellite) InSAR. By using a plane, you can wait for good circumstances to do the measurements. At present, there are no airborne L-band systems operational yet, but a few institutes/companies are working on such systems. We intend to start tests when they come available.

Another relatively new technique for height determination is laser altimetry, also performed from aircraft. Our experience with this technique is that errors from GPS and INS (Inertial Navigation System) can amount to dm-level, which means that the data can not directly be used for subsidence determination (see also the used 1997 data set in 2.5). However, the errors are mainly of systematic character, hence the addition of (terrestrial) reference data may increase the precision to cm-level. Studies on this problem are going on.

5. CONCLUSIONS AND RECOMMENDATIONS

In the investigated area the available levelling and laser altimetry measurements can be used to make some refinements on geological prediction models, especially the prediction of peat oxidisation. The present model appears to be in statistical agreement with the measured subsidence. The relatively low density of boreholes seems to result in an oversimplification of the geological model.

The most important factors that limit the precision of surface level measurements are seasonal variations and inaccuracies in the connection to the height reference system. Point noise is of less influence. Most of it can be averaged out. Laser altimetry is the least precise measurement technique because of certain specific systematic errors.

Before using the improved prediction model in other areas it is recommended to check the general validity of the model by comparing the results with measurements in some other test areas.

With respect to the aim to realise surface subsidence predictions with cm accuracy it must be clear that this is not possible with the present state of measurement techniques. For this we should put our hope on improved results with interferometric radar (InSAR) in the future. Another possible improvement might be found in the laser altimetry technique with the addition of (terrestrial) reference data.

Acknowledgements

Authors express their gratitude to Remco Groen of Waterschap "De Waterlanden" for permission to use their water level data and Rijkswaterstaat and the Ministry of Economic Affairs for the funding of this project.

REFERENCES

Beuving, J. & van den Akker J.J.H. (1996) Maaiveldsdaling van veengrasland bij twee slootpeilen in de polder Zegvelderbroek, Vijfentwintig jaar zakkingen op het ROC Zegveld, Staring Centrum, Instituut voor Onderzoek van het Landelijk Gebied, SC-DLO rapport 377, Wageningen, 1996.

Hannink, G. (1984) Onderzoek in Noord-Holland naar de geotechnische aspecten van de aanleg van de Markerwaard, LGM Mededelingen, deel XXII nr. 3 (nr. 89) pp. 1-69

Heidemij Nederland (1978) Landinrichtingsproject "Waterland" rapportnr. 645-78/3, pp. 1-70

Kooi, H., Johnston P., Lambeck K., & Smither C. (1998) Geological causes of recent (~100 yr) vertical land movement in the Netherlands, *Tectonophysics* (299)4, pp. 297-316.

Koppejan, A.W. (1948) A formula combining the Terzaghi load-compression relationship and the Buisman secular time effect, Proc. 2nd Int. Conf. Soil Mechs. and Found. Engng., Part 3, Rotterdam.

NEN 6740 (1991) Nederlandse Norm, Geotechniek, Basiseisen en belastingen, Nederlands Normalisatie Instituut, Delft.

Schothorst, C.J. (1979) Subsidence of low moor peat soils in the Western Netherlands, *Geoderma,* **17**, 265-291, 1977.

Spierenburg, S.E.J. (1995) Modelling uncertainty components of surface level and land subsidence, *Land Subsidence*, Proceedings of the Fifth International Symposium on Land Subsidence, 207-213, The Hague, 16-20 October 1995, Eds Barends, F.B.J. et al., A.A. Balkema, Rotterdam.

LAND SUBSIDENCE - Vol. II
Proceedings of the Sixth International Symposium on Land Subsidence
Ravenna / Italy / 24-29 September 2000

SIMULATION OF LAND SUBSIDENCE IN A GLACIAL AQUIFER SYSTEM ABOVE A SALT MINE COLLAPSE IN NEW YORK, USA

Richard M. Yager
United States Geological Survey, 30 Brown Rd, Ithaca, New York 14850

Abstract

The bedrock ceiling in parts of the Retsof salt mine in the Genesee Valley in western New York collapsed in March and April 1994, and water from overlying glacial aquifers began to flow into the mine at rates of as much as 1,300 L/s. Water-level declines within the aquifer system and the accompanying increase in effective stress caused compression of fine-grained sediments in two confining layers. By February 1996, as much as 24 cm of land subsidence was measured 1 km south of the mine.

One-dimensional, transient simulations were conducted with MODFLOW and the ISB1 package to represent vertical fluid flow and sediment compression in the confining layers at two locations—one near a borehole instrumented with pressure transducers and a second at a survey monument. Vertical hydraulic conductivity and specific storage of the confining layers were estimated through nonlinear regression from observations of pore pressure and subsidence. Computed fluid pressure changes were in close agreement with measured pressures, and the maximum computed subsidence at the survey monument was about 6 percent less than that observed. About 92 percent of the computed subsidence was the result of compression in the lower confining layer, of which 90 percent was attributed to inelastic compaction.

Estimated values of vertical hydraulic conductivity and specific storage of confining-layer sediments were incorporated into a three-dimensional, ground-water-flow model calibrated with MODFLOWP to measured water-level declines in wells and estimated ground-water discharges to the salt mine. The computed subsidence in February 1996 along a survey transect compared favorably with the measured subsidence. As much as 3 cm of the simulated subsidence had occurred by February 1996 over a 41-km^2 area that extended 8 km north and 11 km south of the collapse area.

Keywords: land subsidence, simulation, nonlinear regression, mine collapse

1. INTRODUCTION

Land subsidence in the the United States has been associated with both localized collapses into mined cavities (Ege, 1984, Autin, 1984; Neal, 1995) and regional withdrawals of subsurface fluids. Although some land subsidence has resulted from production and subsequent compaction of hydrocarbon reservoirs, subsidence related to ground-water withdrawals is much more widespread. Compaction of fine-grained sediments within pumped aquifer systems has resulted in subsidence of over 8 m near both Houston, Texas (Holzer, 1984) and in the San Joaquin Valley, California (Poland et al, 1975). Ground-water flow models developed to simulate land subsidence in these areas are described in Carr et al (1985; Texas) and Williamson et al (1989; California).

The 1994 collapse and flooding of a salt mine near Retsof, New York (Fig. 1) caused land subsidence resulting from both collapses into the mined cavity and the rapid compaction of sediments in the overlying aquifer system in response to water-level drawdown. The salt mine, which had been in operation since 1885, was sealed after the mine became completely flooded in January 1996. Subsidence rates of over 15 cm/yr during a 20-mo period were attributed to sediment compaction, comparable to the subsidence rates measured in Texas (10 cm/yr) and California (20 cm/yr) over several decades. Comprehensive monitoring of this catastrophic event provided a unique opportunity to simulate the response of an aquifer system to rapid drawdowns initiated by a mine collapse, and thereby estimate the mechanical and hydraulic properties of overlying aquifers and confining layers.

1.1 Hydrogeologic Setting

The glacial aquifer system within the Genesee Valley consists of three aquifers separated by two confining layers and underlain by water-bearing zones in bedrock (Fig. 2). The glacial aquifers are hydraulically connected at the edges of the confining layers near the bedrock valley walls. The uppermost (unconfined) aquifer consists of alluvial sediments 6 to 18 m thick; a middle confined aquifer consists of glaciofluvial sand and gravel 3 to 5 m thick, and a lower aquifer consists of glaciofluvial sand and gravel about 7.5 m thick overlying the bedrock valley floor. The upper and middle aquifers are separated by an upper confining layer of lacustrine sediments and till as much as 75 m thick, and the middle and lower aquifers are separated by a lower confining layer of undifferentiated glaciolacustrine sediments as much as 75 m thick.

1.2 Effects of Mine Collapse

The effects of the mine collapse and subsequent flooding included (1) land subsidence, (2) severe water-level declines, (3) changes in ground-water quality and (4) exsolution of natural gas. The effects of the mine collapse on the aquifer system are described in Yager et al (in press). Possible causes and effects of the collapses are discussed by Gowan et al (1999) and Nieto and Young (1998).

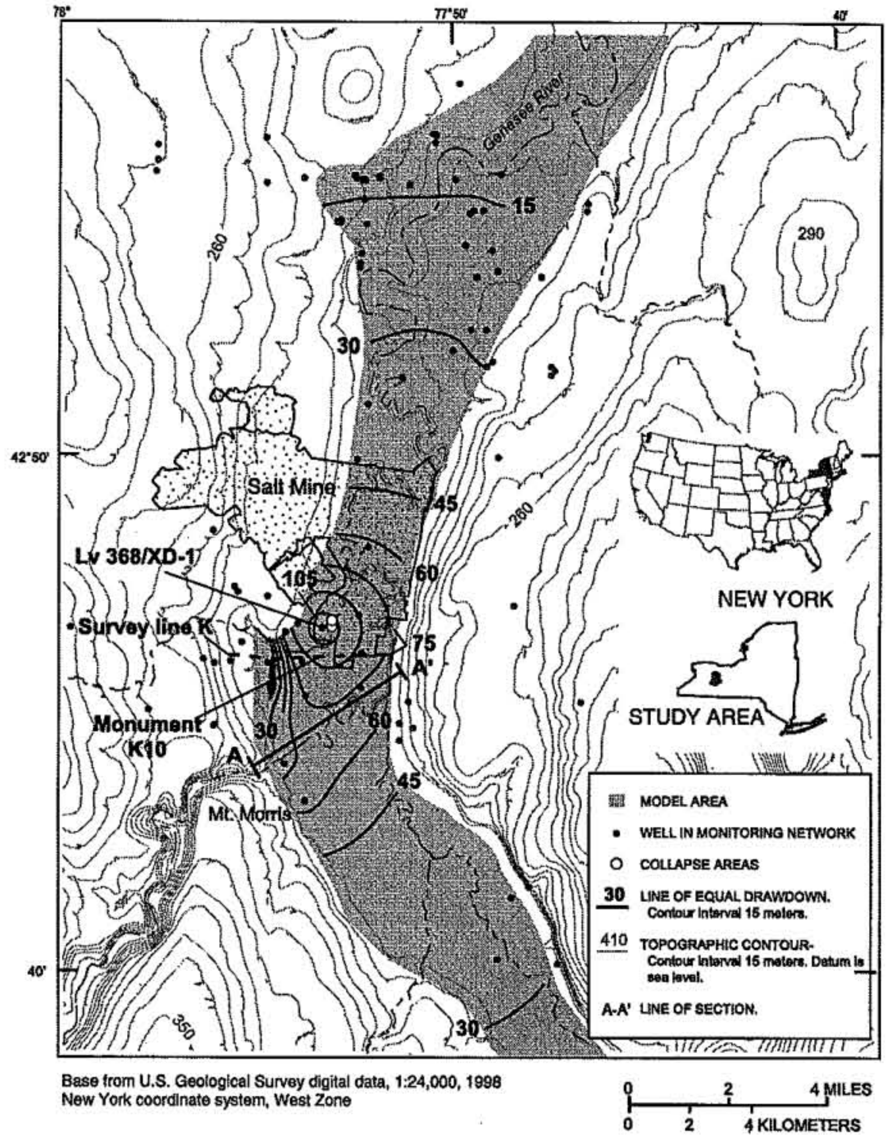

Figure 1. Extent of mined area, site of collapse and distribution of drawdown in lower aquifer in January, 1996 in response to mine flooding

The collapses in the mine allowed water to cascade into the mine from the lower aquifer at the bedrock surface, which is 150 m lower than the natural outlet at the north end of the Genesee Valley. Water levels in the lower aquifer had dropped as much as 120 m by January 1996 when the mine was completely flooded and several wells screened in the middle aquifer went dry. Drawdowns of 15 to 40 m were recorded at wells 10 km north and south of the collapse area (Fig. 1). Water levels in the collapse area had recovered 90 m (75 percent) about 2 years after drainage to the mine had ceased.

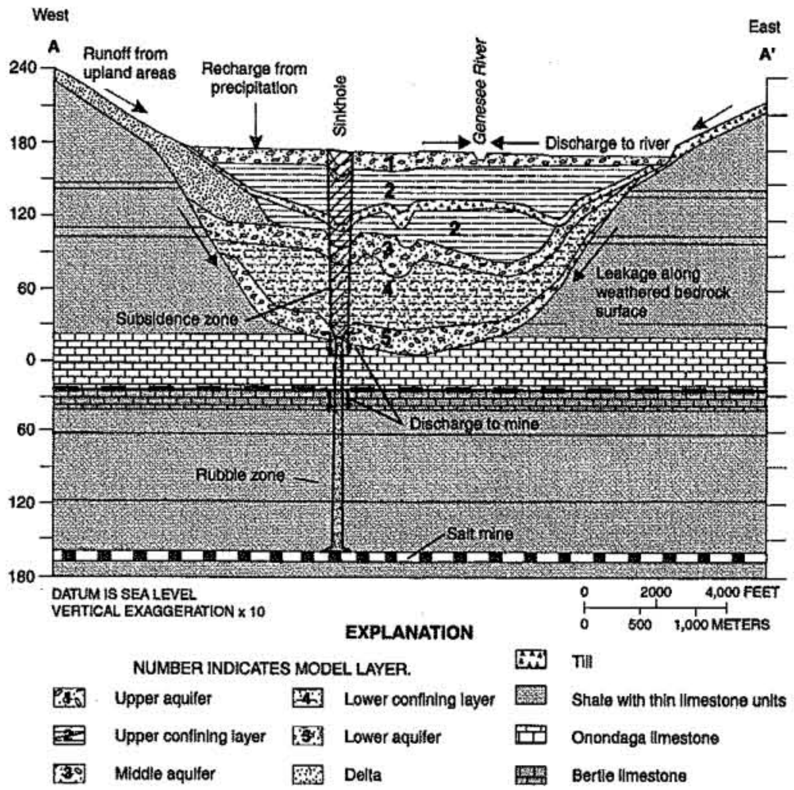

Figure 2. Generalized section showing aquifers and confining layers in the Genesee Valley (line of section shown in Fig. 1).

Collapse of the overlying rock and sediment propagated from the mine to land surface, leaving two 90-m-diameter sinkholes as much as 21 m deep that damaged nearby structures. Subsidence ranged from 24 cm or less south of the mined area to as much 5 m over the uncollapsed mined area. The subsidence south of the mine is attributed to compression of fine-grained sediments in the confining layers, while most of the subsidence over the mine was caused by closure of the mine cavity, a process that was accelerated by the dissolution of the salt pillars by water that flooded the mine.

Consolidation curves for lower confining-layer sediments indicated that the stress resulting from water-level declines after the mine collapse corresponded to the transition from the elastic to the inelastic stress range (Yager et al, in press). The increased stress in the upper confining layer was not much greater than the ambient stress because relatively little drawdown

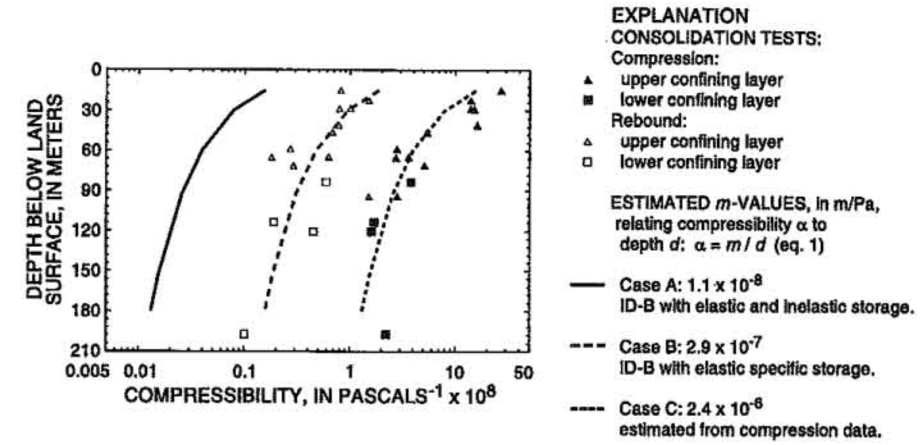

Figure 3. Relation of compressibility to depth as derived from consolidation curves of confining-layer sediments in Genesee Valley aquifer system.

occurred in the upper confining layer. Compressibility α of confining layer sediments under ambient stress was computed from consolidation curves for 15 samples of confining-layer sediments (Alpha Geoscience, 1996). Compressibility generally declined with increasing effective stress at increasing burial depths d, as expected from empirical relations given in Neuzil (1986). The relation of compressibility to depth is

$$\alpha = \frac{m}{d} \tag{1}$$

where m = constant (m/Pa). An m-value of 2.4 x 10^{-6} m/Pa gives the compressibility values computed from consolidation curves during compression with a correlation coefficient (r^2) of 0.94 (Fig. 3, case C).

2. SIMULATION OF GROUND-WATER FLOW

Ground-water flow within the aquifer system was simulated by a three-dimensional (3D) model using MODFLOWP to represent flow conditions before and after the mine collapse (Yager et al, in press). Hydraulic heads computed by steady-state simulation representing conditions prior to the mine collapse provided initial conditions for a transient-state simulation representing drainage from the aquifer system to the mine (March 1994 through December 1995) and recovery of water-levels after the mine completely filled (January 1996 through August 1996).

2.1 Model design and calibration

The three aquifers and two confining layers within the aquifer system (Fig. 2) were represented by five model layers. Recharge to the unconfined aquifer (model layer 1) was represented by a constant-flow boundary at land surface with larger rates specified along valley walls to account for recharge from upland runoff. The contact between the aquifer system and the shale bedrock at the valley wall was represented by a no-flow boundary. Vertical leakage through permeable deposits and (or) bedrock fractures along the valley wall was represented by hydraulic connections between adjacent model layers.

In transient-state simulations, constant-head boundaries were specified at the two collapse sites in the lower aquifer (model layer 5) to represent drainage from the aquifer system to the mine from March 1994 through December 1995. Six parameters were estimated through transient-state simulations from 354 water-level measurements recorded in 51 wells, and two estimates of ground-water discharge to the mine in March and September 1994 (Table 1).

2.2 Simulated Response of Aquifers

The computed distribution of drawdown in January 1996 was similar to the measured distribution, and the standard error in heads was 10 m. Computed drawdowns near the collapse area (123 m) were overpredicted by less than 3 m, and the predicted change in drawdown with time was in close agreement with measured drawdowns at individual wells (Fig. 4). Drawdowns 10 km to the north (10 m) and 12 km to the south (15 m) were generally underpredicted by about 5 m and 18 m, respectively.

Computed discharges to the mine in April 1994 (570 L/s) were 100 percent greater than the values estimated from the observed rate of mine flooding, and computed discharges to the mine in September 1994 (790 L/s) were 40 percent less than the values estimated. The computed water budget indicated that ground water released from storage provided 73 percent of the water discharged to the mine, and that most of the inflow was from storage in the lower aquifer (58 percent). The estimated volume of water discharged to the mine (2.8×10^{10} L) was only 55 to 60 percent of the estimated mine volume because drawdowns were underpredicted south of the mine.

Values of specific storage S_s estimated for the middle and lower aquifers (2.3×10^{-4} m^{-1} and 9.5×10^{-4} m^{-1}, respectively) were much larger than the range of values (2.3×10^{-6} m^{-1} to 7×10^{-6} m^{-1}) estimated for other sand and gravel aquifers from extensometer data (Riley, 1998). Assigning a lower value of specific storage greatly increased model error (Fig. 4), however, and no combination of the remaining parameter values was found through non-

Table 1. Optimum parameter values estimated for confined aquifer system (model layers 2 through 5) through nonlinear regression in transient-state simulation, and their approximate confidence intervals at 95-percent level.

Variable	Value	Approximate individual confidence interval	Coefficient of variation (percent)[a]
Hydraulic conductivity, m/d			
middle aquifer	1.1	.4 - 3.4	30
lower aquifer	91	55 - 150	26
Vertical hydraulic conductivity of lower confining layer, m/d			
collapse area	8×10^{-3}	7×10^{-5} - .94	37
remainder of layer	3.7×10^{-4}	1.2×10^{-4} - 9.7×10^{-4}	4
Specific storage, m^{-1}			
middle aquifer	2.3×10^{-4}	4.3×10^{-5} - $1.2. \times 10^{-3}$	5
lower aquifer	9.5×10^{-4}	4.6×10^{-4} – $2. \times 10^{-3}$	3

a Coefficient of variation on log-transformed parameter.

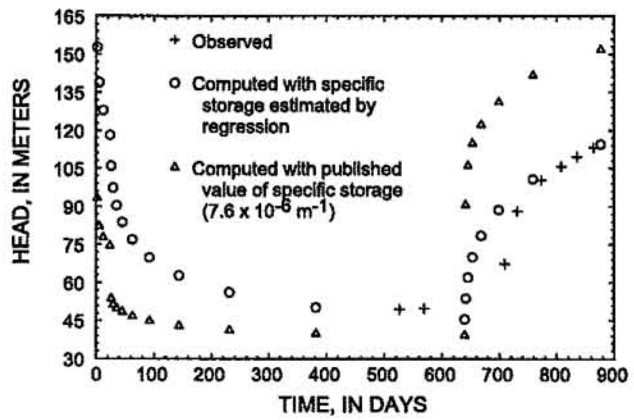

Figure 4. Water levels predicted from two alternative values of S_s and measured in the lower aquifer at well Lv368 near the collapse area.

linear regression that provided an acceptable match to the measured water levels. The larger values of specific storage estimated by the regression probably resulted from gas exsolution. Releases of methane from several wells suggest that gas was present as a free phase over a wide area during water-level declines. The gas partially dewatered the confined aquifers, releasing water from storage. The effect of gas exsolution on specific storage in the Genesee Valley aquifers is discussed in Yager et al (in press).

3. SIMULATION OF LAND SUBSIDENCE

Two 1-dimensional (1D) models were developed with MODFLOW with the interbed-storage package IBS1 to estimate hydraulic properties of the confining layers from observations of (1) pore pressure near the collapse area, and (2) land subsidence 850 m south of the collapse area. Estimates of hydraulic values derived from calibration of the two 1D models were then substituted in the 3D model described earlier to depict the spatial distribution of land subsidence.

Two pressure transducers were installed in September 1995 in borehole XD1 (Fig. 1) within the upper confining layer at a depth of 66 m, about 30 m above the top of the middle aquifer. The transducers were placed within a saturated sand pack, and the borehole was sealed to land surface with an expansive grout to isolate the monitored interval from atmospheric pressure (Alpha Geoscience, 1996). Land-surface altitudes were surveyed along survey line K (Fig. 8) from September 1994 through July 1996 (K. Cox, Akzo Nobel Salt, written commun., January 1997).

3.1 Model Design and Calibration

Model 1D-A for borehole XD-1 represented only the upper confining layer and used a column of 257 cells 30-cm thick. Model 1D-B for survey monument K10 represented both the upper and lower confining layers with a column of 446 cells 30-cm thick. Aquifer boundaries in both models were assigned hydraulic heads generated from transient-state simulations with the 3D model. Subsidence resulting from compression of the confining layers was computed as the sum of the volume of water released from storage.

The confining layers in each 1D model were assigned values of vertical hydraulic conductivity K_v and specific storage S_s. The K_v value for the upper confining layer in both models was obtained through the nonlinear regression method described below, and the K_v value for the lower confining layer (model 1D-B) was fixed at the value estimated from the 3D model (3.7×10^{-4} m/d). The S_s values assigned to both confining layers were chosen to represent both elastic and inelastic compression. Values of elastic storage $S_{se}(i)$ were computed for each cell i using compressibility values α from eqn. 1 with the depth below land surface d_i and an m-value estimated by nonlinear regression. Inelastic storage values $S_{sin}(i)$ were specified to be either 30 or 50 times greater than $S_{se}(i)$ values on the basis of published values (Riley, 1998). The magnitude of stress (preconsolidation head H_{pc}) at which the transition from elastic to inelastic storage occurred was also estimated in the regression.

A nonlinear regression method (PEST; Doherty et al, 1994) estimated three parameters (K_v, m, and H_{pc}) in both 1D models using eight observations of pressure at borehole XD-1 (model 1D-A) and four observations of subsidence at monument K10 (model 1D-B). Weights were assigned to the pressure and subsidence observations to account for differences in the measurement ranges (pressure: 123 to 132 m; subsidence 5.5 to 24 cm). Parameters were estimated through a 12.4-year transient-state simulation representing postcollapse conditions.

Table 2. Parameter values estimated for confining layers in one-dimensional models 1D-A (borehole XD-1) and 1D-B (monument K10), approximate confidence intervals at 95-percent level, and mean values specified in 3D model.

Variable	Value estimated in 1D models	Approximate individual confidence interval	Mean values specified in 3D model
Aquifer property			
Vertical hydraulic conductivity, m/d			
upper confining layer	2.1×10^{-6}	1.3×10^{-6} - 3.4×10^{-6}	3.0×10^{-6}
lower confining layer	3.7×10^{-4} [a]		3.7×10^{-4}
Mean elastic specific storage, m^{-1}			
upper confining layer	7.5×10^{-6}	4.6×10^{-6} - 1.3×10^{-5}	7.2×10^{-5} [b]
lower confining layer	3.6×10^{-6}	2.6×10^{-6}- 5.6×10^{-6}	2.6×10^{-5} [b]
Preconsolidation head, m	125	110 - 140	
Subsidence at monument K10, cm	Model 1D-B	Measured subsidence	3D Model
Upper confining layer	1.8	--	1.5
Lower confining layer	20.4	--	15.2
Total at monument K10	22.2	23.8	16.7

a Fixed value in regression.
b Estimated in regression with one-dimensional models, case B.

The K_v-value for the upper confining layer estimated by the PEST regression was close to that specified in the 3D model (Table 2). Mean elastic specific-storage values for the upper and lower confining layers agree with that estimated for a confining layer of glacial drift in Anchorage, Alaska (7.5×10^{-6} m^{-1}) from extensometer measurements during an aquifer test (Nelson, 1982). The preconsolidation head of 125 m corresponds to a prior loading of about 46 m of water at land surface and indicates that the confining-layer sediments are overconsolidated; this result is consistent with the presence of till in the upper confining layer that was probably deposited during a temporary glacial advance. Specifying values of inelastic storage that were either 30 or 50 times the S_{se}-values resulted in little difference in model error.

3.2 Simulated Response of Confining Layers

Computed pressure changes in the upper confining layer (model 1D-A) were in close agreement with pressures measured in borehole XD1 during drainage of the confined aquifer system and the subsequent recovery once the mine was flooded in January 1996 (Fig. 5). The maximum residual was about 1.5 m, and the mean error was 0.64 m, less than 2 percent of the computed 44-m drawdown.

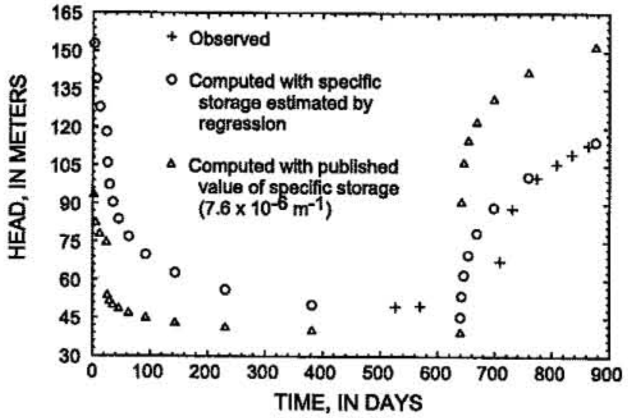

Figure 5. Pressures in upper confining layer near collapse area as computed by one-dimensional model 1D-A and measured at borehole XD-1.

The predicted subsidence at monument K10 (model 1D-B) closely matched the observed subsidence, and the maximum simulated subsidence (22 cm) was about 6 percent less than that observed (24 cm) (Fig. 6). About 90 percent of the simulated compression was inelastic, nonrecoverable compaction. The consistent downward trend in subsidence measurements along the K survey line from February 1995 through January 1996 suggests that the measurements were relatively accurate, but whether the land surface rebounded slightly once water levels began to recover in January 1996, as simulated in the model, is difficult to discern because the measured values have wide scatter.

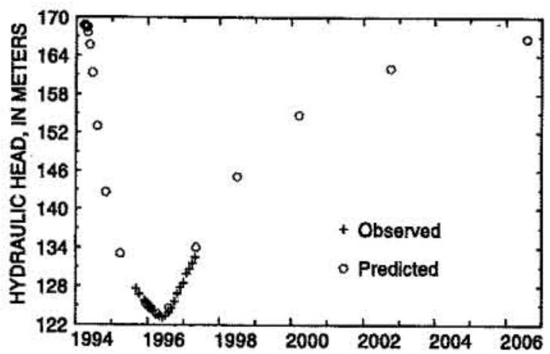

Figure 6. Subsidence computed by one-dimensional model 1D-B and measured land subsidence at monument K10, 850 m south of collapse area.

Elastic compressibility values computed from the m value of 1.1 x 10^{-8} m/Pa estimated by the regression (case A, Fig. 3) were about 1 order of magnitude less than those calculated for confining layer sediments during the rebound phase of the consolidation tests. Model sensitivity to specific storage was investigated in two alternative regressions in which the observed subsidence was assumed to result solely from elastic compression. The mean S_{se} values obtained in these regressions were larger than those computed in case A, which represented both elastic and inelastic compression. Results of the two alternative regressions matched the pressure response observed at borehole XD-1 (model 1D-A) equally well, however, because estimated K_v-values were larger also than in case A, so that the vertical hydraulic diffusivity (K_v/S_s) was unchanged.

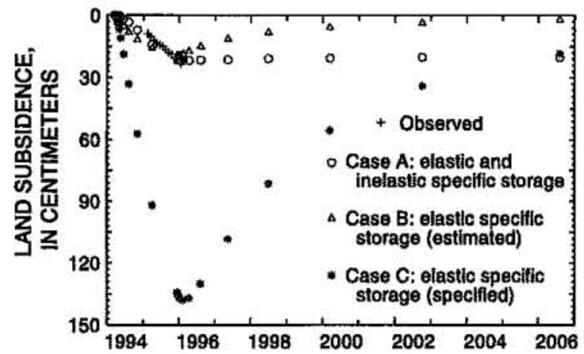

Figure 7. Land subsidence measured at monument K10 and predicted by model 1D-B in three alternative regressions.

Case B, with the estimated m value of 2.9 x 10^{-7} m/Pa, yielded a maximum subsidence of 20 cm at monument K10—about 85 percent of the measured value, and elastic compressibilities matched reasonably well the values calculated for the rebound phase of consolidation tests. This case indicates that the compressed sediments would expand elastically, causing the land surface to rebound after water levels had begun to recover—a result that is clearly unrealistic (Figs. 6 and 7). Case C, with a specified m value of 2.4 x 10^{-6} m/Pa estimated from the compression phase of consolidation tests, resulted in a maximum subsidence of 1.5 m, about 6 times greater than the measured value (Fig. 7).

3.4 Spatial Distribution of Simulated Subsidence

The 1D models indicate that land subsidence south of the mine was the result of both elastic and inelastic compression, but the program MODFLOWP, which was used to construct the 3D model, allows only one storage value for each model cell. The S_s-values specified in 3D model for the upper and lower confining layers (3.3 x 10^{-5} m^{-1} and 1.6 x 10^{-5} m^{-1}, respectively) are close to the mean S_{se}-values computed by case B in which elastic compression was assumed. In that regression, the close match between computed and maximum subsidence at monument K10 indicates that an approximate value for the volume of water released from storage in the confining layers can be obtained from a single S_s value. Values of K_v and S_s estimated assuming elastic compression (case B) were therefore incorporated into the 3D model to compute the spatial distribution of subsidence when water-level drawdown was a maximum. The subsidence at each cell was calculated as the sum of the volume of water released from storage in each confining layer (model layers 2 and 4), divided by the cell area.

The maximum subsidence at monument K10 as computed by the 3D model (17 cm, Table 2) is about 70 percent of that observed (24 cm). The cumulative subsidence in February 1996 along survey line K as computed by the 3D model was reasonably consistent with the measured subsidence (Fig. 8), although offset 900 m to the east. The 900-m discrepancy in the location of maximum subsidence along survey line K suggests that the confining-layer thickness specified in the 3D model does not accurately represent the actual thickness of fine-grained confining-layer sediments.

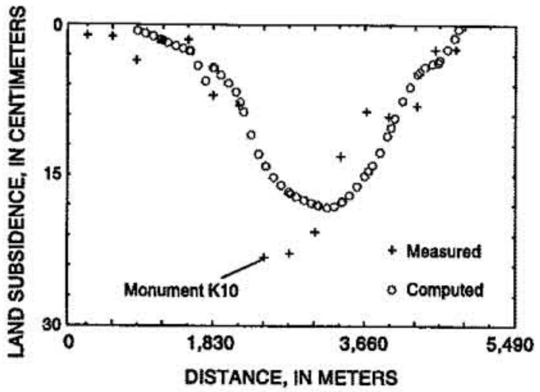

Figure 8. Land subsidence along survey line K as measured in February 1996 and as computed by three-dimensional model.

The 3D model indicates that as much as 3 cm of subsidence had occurred by February 1996 over an area covering about 41 km^2 that extended 8 km north, and 11 km south, of the collapse area (Fig. 9) and that as much as 15 cm of subsidence occurred over an area covering about 3.6 km^2. Simulated subsidence closely matched the measured subsidence in Mt. Morris, 5 km south of the collapse, where as much as 9 cm of subsidence was measured. Subsidence was greatest near the collapse area and in the center of the Genesee Valley, where deposits of fine-grained sediments are thickest.

4. CONCLUSIONS

Specific storage was estimated for confining layer sediments through simulation of pressure and subsidence at two locations near a salt mine collapse where severe water-level drawdowns resulted from mine flooding. One-dimensional simulations indicated that land subsidence resulted mainly from inelastic compaction, but an alternative simulation indicated that the maximum subsidence could be computed considering solely elastic storage. This elastic storage value was incorporated into a 3D flow model in which the confining layers were represented by single model layers. The subsidence computed from the volume of water released from storage in the confining layers agreed reasonably well with measured subsidence, suggesting that the 3D model could be used to simulate the distribution of the maximum subsidence resulting from mine flooding. Estimated elastic-compressibility values were about 1 order of magnitude less than those calculated for confining-layer sediments during the rebound phase of the consolidation tests, suggesting that values derived from consolidation tests do not accurately represent the actual compressibilities under field conditions.

Acknowledgements

This study was conducted in cooperation with the Livingston County Department of Health. Measurements of water levels, pore pressures and subsidence were provided by Akzo Nobel Salt, Inc.

References

Alpha Geoscience (1996) Geologic and hydrogeologic investigation of the Genesee River valley, Albany, N.Y., Alpha Geoscience, 31 p.

Autin, W. J. (1984) Geologic significance of land subsidence at Jefferson Island, Louisiana, *Trans.-Gulf Coast Assoc. of Geological Soc.*, v. 34, p. 293-309.

Carr, J.E., Meyer, W.R., Sandeen, W.M, & McLane, I.R. (1985) Digital models of simulation of ground-water hydrology of the Chicot and Evangeline aquifers along the gulf coast of Texas, Texas Dept. of Water Res. Rept. 289, 101 p.

Doherty, J., Brebber, L., & Whyte, P. (1994) PEST—Model-independent parameter estimation, Ipswich, Australia, Watermark Computing, 135 p.

Ege, J. R. (1984) Mechanisms of surface subsidence resulting from solution extraction of salt, in Holzer, T. L. (ed.), Man induced land subsidence, *Rev. in Engr. Geo.*, **6**, p. 201-221.

Gowan, S. W., Trader, S. M., & Van Sambeek, L. L. (1999) An apparent brine pool associated with anomalous closure patterns and the eventual failure of the Retsof Salt Mine, *Soln. Mining Res. Inst. Fall Mtg*, Encinitas, Ca, p. 241-272.

Holzer, T. L. (1984) Ground failure induced by ground-water withdrawal from unconsolidated sediment, in Man induced land subsidence, Holzer, T. L. (ed.), *Rev. in Engr. Geo.*, **6**, p. 67-122.

Neal, J. T. (1995) Origin, diagnostics and mitigation of a salt dissolution sinkhole at the U. S. strategic petroleum reserve storage site, Weeks Island, Louisiana, Sandia National Laboratory, Albequerque, N.M., 10 p.

Nelson, G. L. (1982) Vertical movement of ground water under the Merrill field landfill, Anchorage, Alaska, U.S. Geol. Survey Open-File Rept. 82-1016, 24 p.

Neuzil, C. E. (1986) Groundwater flow in low-permeability environments, *Water Resources Research,* **22**, (8) p. 1163-1195.

Nieto, A. S., & Young, R. A. (1998) Retsof Salt Mine collapse and aquifer dewatering, Genesee Valley, Livingston County, New York, in *Land subsidence*, Proc. of the Dr. J. F. Poland Symp. on land subsidence, Borchers, J. W., (ed.), Belmont Ca., Star Publishing Co., p. 309-325.

Poland, J.F., Lofgren, B.E., Ireland, R.L., & Pugh, R.G. (1975) Land subsidence in the San Joaquin Valley, Ca, U.S. Geol. Survey Prof. Paper 437-H, 78 p.

Riley, F. S. (1998) Mechanics of aquifer systems—the scientific legacy of Joseph F. Poland, in *Land subsidence*, Proc. of the Dr. J. F. Poland Symp. on land subsidence, Borchers, J. W., (ed.), Belmont, Ca., Star Publishing Co., p. 13-27.

Williamson, A.R., Prudic, D.E., & Swain, L.A. (1989) Ground-water flow in the Central Valley, California, U.S. Geol. Survey Prof. Paper 1401-D, 127 p.

Yager, R. M., Miller, T. S., & Kappel, W. M., in press, Simulated effects of a 1994 salt-mine collapse on ground-water flow and land subsidence in a glacial aquifer system, New York, U. S. Geol. Survey Prof. Paper

LAND SUBSIDENCE - Vol. II
Proceedings of the Sixth International Symposium on Land Subsidence
Ravenna / Italy / 24-29 September 2000

A NONLINEAR VISCOUS MODEL FOR AQUIFER COMPRESSION ASSOCIATED WITH ASR APPLICATIONS

Jiang Li and Donald C. Helm
Morgan State University, 5200 Perring Parkway, Baltimore, MD 21251-0001, USA

Abstract

Compression of confining beds and the resulting land subsidence can be caused by periodic withdrawal and injection of water from or into the adjacent aquifers. A nonlinear viscous model is applied for the first time to reach an analytic solution of the one-dimensional case. A conceptual sandwich model is assumed and calculated. The potential risk of aquifer system deformation due to aquifer storage and recovery (ASR) technology can be estimated based on the results of calculations.

A governing equation expressed directly in terms of displacement is employed to describe one-dimensional vertical compression and expansion. A sinusoidal function changing with time is assumed at the boundaries to simulate changes in stresses that are induced by hydraulic head fluctuations due to the ASR activity. The two aquifers (one above the confining bed and the other beneath) can mathematically be pumped independently of each other. The results from the analytic solution can be utilized to estimate and predict potential risk of recoverable land subsidence due to applications of the ASR technology.

Keywords: land subsidence, aquifers storage and recovery (ASR), deformation.

1. INTRODUCTION

In order to meet the demand of water supply or to improve water quality, the technology of aquifer storage and recovery (ASR) has been widely employed in the United States (e.g., Texas, New Mexico, Nevada, Arizona, California, Florida, etc.). For example, more than forty sites or locations are using ASR technology in thirteen states, and more than a dozen new sites or locations are applying for permits to use the ASR technology in the field (Pyne, et al, 1995). The purposes of using the ASR technology are various. For instance, in Florida, the ASR method is used indirectly to improve the water quality of contaminated surface water (i.e., aquifers used as filters), while in Los Angeles, California, the ASR method is applied to impede sea water intrusion by injecting lightly treated sea water into aquifers. In Texas, ASR technology is employed to improve water quality and to remove harmful byproducts of disinfectants by recharging aquifers with treated wastewater.

Contrastingly, aquifers in Nevada are employed as buffers through utilization of ASR approaches so that groundwater can meet high demand in summers. In other words, surface water is recharged into aquifers in the winters and is discharge from aquifers in the summers. It is evident that ASR activity causes the fluctuation of hydraulic head. Changes in hydraulic head in turn cause land subsidence because changes in hydraulic head changes effective stress within the aquifer system through the principle of effective stress (Terzaghi, 1943). Effective stress fluctuations control the skeletal displacement field and cause deformation of the aquifer system. Eventually, any accumulated compression of an aquifer system due to groundwater withdrawal is reflected at the land surface as land subsidence (Poland, et al, 1975).

The present paper is a first attempt to find an analytic solution of the displacement field based on a nonlinear viscous constitutive relation. This constitutive relation, called poroviscosity, accounts for both primary and secondary consolidation. The governing equation in terms of skeletal displacement for a vertical one-dimensional problem is introduced with specific boundary conditions. At the boundaries, an assumption of cyclic variations in effective stress is applied due to periodic pore water pressure variations. Accordingly, the boundary conditions are related directly to the strain of the soil skeleton based on this nonlinear viscous model (Li and Helm, 1995). In contrast, traditionally, a linear poroelastic model is usually adopted for simplicity in modeling land subsidence. Risk assessment of subsidence based on the analytical solution has been included. As a result, general guidance for applications of the pumping-injection technology to multiple aquifer systems can be offered.

2. A NONLINEAR VISCOUS RELATION IN ONE DIMENSION

If saturated sedimentary material is assumed to behave a nonlinear viscous flow, one has the following expression:

$$\sigma = \mathbf{D}\dot{\varepsilon} \tag{1}$$

where ε denotes the structural infinitesimal strain which is as symmetric second order tensor that can be defined as **Lu** where **L** is a matrix for definition of strain and **u** is the displacement field of the solid phase. The dot represents a total derivative with respect to time. **D** is a fourth order tensor of viscosity for the constitutive law and is usually defined as a function of stress, strain, rate of stress and strain, time, space and temperature. For isotropic and isothermal material, **D** has only 2 independent parameters and can be expressed in the following form:

$$\mathbf{D} = (\kappa - 2\mu/3)\delta\delta + \mu(\delta\delta + \delta\delta) \tag{2}$$

where κ and μ are nonlinear viscous parameters and are assumed to have an exponential relation with strain invariants (Li and Helm, 1995 and 1998). δ is the Kronecker delta. In the present paper, the bulk viscous parameter κ is assumed to equal $\kappa = \kappa_0 \exp(\Delta\, J_1 A_1)$ for saturated sedimentary material where the first strain invariant J_1 equals $\mathrm{tr}\varepsilon$ ($\mathrm{tr}\varepsilon$ denotes the trace of strain tensor ε). Similarly, shear viscosity term μ is expressed as $\mu = \mu_0 \exp[\Delta\, J^D_2 A_2]$ where J^D_2 is the second deviatoric strain invariant, equals $0.5\varepsilon^D\varepsilon^D$ where ε^D denotes the deviatoric strain. A_1 and A_2 are constants and Δ denotes increment. If one assumes relation (1) is valid for the one dimensional case, in the present paper (1) may be expressed by:

$$\sigma_z = D_z\dot{\varepsilon}_z = [D_{z0}\exp(A_z\varepsilon_z)]\dot{\varepsilon}_z \tag{3}$$

where D_z denotes nonlinear one dimensional viscosity and equals $D_{z0}\exp(A_z\varepsilon_z)$. The subscripts z and 0 denote the dimension z and the initial value at $t = t_0$. Equation (3) is the original expression introduced by Helm (1998). Thus, the incremental stress-strain-time relation that results from (3) is:

$$\varepsilon_z(t) = (1/A_z)\ln[(A_z/D_{z0})\int_0^t \sigma_z(t)dt + 1] \tag{4}$$

If the effective stress is assumed to change with time in sinusoidal and linear functions [i.e., $f_1(t) = \sigma_m\sin(\omega t)$ and $f_2(t) = at$] induced by the fluctuations and linear changes in hydraulic head, then (4) becomes:

$$\varepsilon_z(t) = 1/A_z\{\ln[(1 + A_z\sigma_m/\omega D_{0z}) - (A_z\sigma_m/\omega D_{0z})\cos(\omega t)] + \ln(1 + aA_zt^2/2D_{0z}) \tag{5}$$

where ω stands for the angular frequency, t is time, a is the slope of the linear function, and σ_m denotes the magnitude of the sinusoidal stress function. Relation (5) will be applied to the boundary of a sandwich model that is described later.

3. THE GOVERNING EQUATION FOR ONE DIMENSIONAL SUBSIDENCE

The governing equation for aquifer motion with consideration of viscous drag force due to pore water flow is given as (Li and Helm, 1995 and 1998):

$$c_1\ddot{\mathbf{u}} + \dot{\mathbf{u}} + \mathbf{c}_2\nabla(\mathbf{DL}\dot{\mathbf{u}}) = \mathbf{R} \tag{6}$$

where two dots indicate the second derivative with result to time. The right-hand side vector **R** is defined by:

$$\mathbf{R} = c_3\mathbf{b} + c_4\dot{\mathbf{q}}^b + \mathbf{q}^b + c_5 \tag{7}$$

where coefficients c_i (i=1...5) are parameters of governing equation (6). The vectors **b** and $\mathbf{q}^b$ denote the body force and the bulk flux [$\mathbf{q}^b \equiv n\mathbf{v}^w + (1-n)\mathbf{v}^s$] where $\mathbf{v}^w$ and $\mathbf{v}^s$ are velocities of pore water and solid, and n denotes porosity. The divergence of $\mathbf{q}^b$ can be reduced to zero by invoking the incompressibility conditions of solid grain and pore fluid (i.e., the divergence of the second and third terms on the right-hand side of (7) become zero due to $\nabla\cdot\mathbf{q}^b = 0$). In this paper, for one dimensional subsidence, all acceleration terms, (i.e., $\mathbf{a}^w$, $\mathbf{a}^s$, and their difference

$\mathbf{a}^r$) are assumed to be small when compared to the terms of velocities (i.e., $\mathbf{v}^w$, $\mathbf{v}^s$, and their difference $\mathbf{v}^r$). Equation (6) thereby simplifies to(Li and Helm, 1995):

$$\dot{\mathbf{u}} + \gamma_w^{-1}\mathbf{K}\nabla(\mathbf{DL}\dot{\mathbf{u}}) = \mathrm{B} \tag{8}$$

where **B** () is reduced from **R**, and ρ^* [$=(1-n)(\rho_s - \rho_w)$] denotes the submerged density of the solid phase (or effective density), **K**, a matrix, stands for the hydraulic conductivity and γ_w is the unit weight of water. If one further assumes such a condition and notes the fact of (Li and Helm, 1995), for the one-dimensional case (6) becomes:

$$\partial u_z / \partial t - c_v \partial^2 u_z / \partial z^2 = B \tag{9}$$

where c_v is a new consolidation coefficient that is defined as $c_v = (K_z A_z \sigma_z / \gamma_w)$. For simplicity, in the present paper c_v is assumed to be a constant, namely the product of $K_z \sigma_z$ does not change very much in both time and space though individually they are not constants. One may note the change in sign of the second term in (9) which is due to the sign convention.

4. AN ANALYTICAL SOLUTION FOR A CASE OF ASR APPLICATION

A model of two aquifers with two assumed wells for withdrawal and injection of water is drawn in Figure. 1:

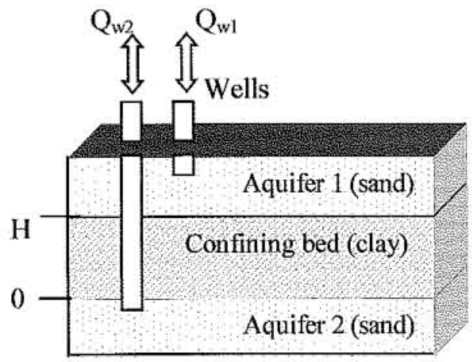

Figure 1. A diagram for an aquifer system

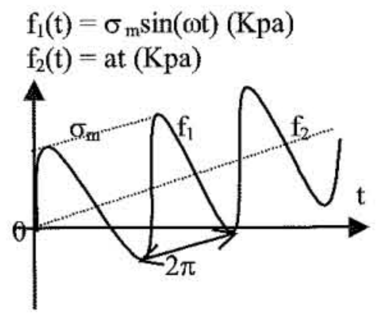

Figure 2. A diagram for function f(t)

In Figure 1, the two wells are located in the top aquifer (sand) and the bottom aquifer (sand). They pump and inject water from or into each aquifer independently of each other with pumping-injecting rates Q_{w1} and Q_{w2}.

If one assumes: 1) that the hydraulic separator between the two aquifers is poroviscous; 2) that the fluctuation of effective stress induced by pore water pressure within each aquifer approximately changes as a sinusoidal

function (see Fig.2); 3) that the effective stress principle holds; 4) that total stresses within the boundary layers do not change very much with time, then governing equation (9) written in terms of displacement u is applicable for a one-dimensional vertical subsidence, initial and boundary conditions based on the stress-strain relation (5) as well as the model shown in Figure 1 give the following set of equations:

$$\partial u / \partial t - c_v \partial^2 u / \partial z^2 = B/2 \tag{10}$$

$$u(z,0) = 0, \quad 0 \le z \le H \tag{11}$$

$$\partial u / \partial z = \varepsilon(H,t), \quad z = H \tag{12a}$$

$$\partial u / \partial z = \varepsilon(0,t), \quad z = 0 \tag{12b}$$

where z is the coordinate in the vertical direction, H stands for the thickness of the clay layer in Figure 1 and B is a function of time and space (Helm, 1987). The term ωt_0 in (12b) represents the lag of phase in time within the second aquifer on the bottom. For convenience, the subscript z is dropped in the set of equations (10), (11) and (12). Boundary conditions $\varepsilon(H, t)$ and $\varepsilon(0, t)$ are related to loading functions f_1 and f_2 in Figure 2, and are defined as $\varepsilon(H, t) = 1/A\{\ln[Aa_1t^2/2D_0+1] + \ln[(1+A\sigma_{m1}/\omega D_0) - (A\sigma_{m1}/\omega D_0)\cos\omega_1 t]\}$and $\varepsilon(0, t) = 1/A\{\ln[Aa_2t^2/2D_0+1] + \ln[(1+A\sigma_{m2}/\omega D_0) - (A\sigma_{m2}/\omega D_0)\cos\omega_2(t-t_0)]\}$. The parameter a is the slope of the loading function f_2 that linearly decreases or increases with time in Figure 2. The parameter a is associated with the slope of the average mean water pressure that linearly decreases or increases with time in Figure 2. The cases of long-term recharge larger than ($a < 0$), less than ($a > 0$) and equal to ($a = 0$) long-term discharge within an aquifer system can be analyzed. Subscripts 1 and 2 denote the upper and lower aquifers respectively. For convenience of finding the analytic solution, the term B in (9) is changed to B/2 in (10).

If one takes the Laplace transform (Spiegle, 1965) of all terms in governing equation (10), and the initial and boundary conditions (11) and (12), one has the following expressions in the Laplace transform space:

$$su^*(z,s) - u(z,0) = c_v \partial u^*(z,s)/\partial z^2 + B/2s \tag{13}$$

$$u(z,0) = 0, \quad 0 \le z \le H \tag{14}$$

$$\partial u^*(H,s)/\partial z = \varepsilon^*(H,s), \quad (z = H) \tag{15a}$$

$$\partial u^*(0,s)/\partial z = \varepsilon^*(0,s), \quad (z = 0), \tag{15b}$$

where u^* and ε^* represent the Laplace transforms of u and ε, and s is the Laplace transform parameter. The term B is assumed to be constant so (10) can be represented by equation (13). Keeping initial condition (14) in mind and solving equation (13) for u^* with an assumption that B is not a function of z, one finds the solution in Laplace transform space to be:

$$u^* = C_1 \cosh[(\frac{s}{c_v})^{1/2} z] + C_2 \sinh[(\frac{s}{c_v})^{1/2} z] + \frac{B}{s^2} \qquad (16)$$

where C_1 and C_2 are constant coefficients. With help of initial and boundary conditions (14) and (15a), C_1 and C_2 are found to be:

$$C_{11} = -\frac{B}{2s^2} \qquad (17a)$$

$$C_{12} = [\varepsilon(H,s) + \frac{B}{2s^2}\sqrt{\frac{s}{c_v}} \sinh(\sqrt{\frac{s}{c_v}}H)] / \sqrt{\frac{s}{c_v}} \cosh(\sqrt{\frac{s}{c_v}}H) \qquad (17b)$$

Similarly, applying initial and boundary conditions (14) and (15b), one has:

$$C_{21} = -[\frac{B}{2s^2}\sqrt{\frac{s}{c_v}} + \varepsilon(0,s)\sinh(\sqrt{\frac{s}{c_v}}H)] / \sqrt{\frac{s}{c_v}} \cosh(\sqrt{\frac{s}{c_v}}H) \qquad (18a)$$

$$C_{22} = \varepsilon(0,s)\sqrt{\frac{c_v}{s}} \qquad (18b)$$

where the first subscript (i.e., 1 and 2) denotes coefficients C_1 ad C_2 from the first and second sets of equation. Substituting equations (17) and (18) into (16), one obtains the superposed expression (16):

$$\begin{aligned} u^* = \frac{B}{s^2} + \frac{B}{2s^2}\{\cosh[\sqrt{\frac{s}{c_v}}(H-z)] / \cosh(\sqrt{\frac{s}{c_v}}H) + \cosh(\sqrt{\frac{s}{c_v}}z) / \cosh(\sqrt{\frac{s}{c_v}}H)\} \\ + \varepsilon(H,s)\sinh(\sqrt{\frac{s}{c_v}}z) / \sqrt{\frac{s}{c_v}}\cosh(\sqrt{\frac{s}{c_v}}H) + \varepsilon(0,s)\sinh[\sqrt{\frac{s}{c_v}}(H-z)] / \sqrt{\frac{s}{c_v}}\cosh(\sqrt{\frac{s}{c_v}}H). \end{aligned} \qquad (19)$$

In order to find the analytical solution with a complete mathematical description (10)-(12), boundary condition related to the stress-strain-time expression (5) can be written in an alternative form, namely

$$\varepsilon(t) = \frac{1}{A}\{\ln b - \sum_{n=1}^{\infty}(-1)^n[(d/b)^n \cos^n(\omega t) + (c^n/A)t^{2n}]/n\} \qquad (20a)$$

where d_i, b_i, and c_i (i =1, 2) are constants, and equal $A\sigma_{mi}/D_0\omega_i$, and $(A\sigma_{mi}/D_0\omega_i + 1)$, and $aA/2D_0$ respectively. The term $\cos^n(\omega t)$ can itself be expressed in the form:

$$\cos^n(\omega t) = \begin{cases} \frac{1}{2^{2n-1}}[\sum_{k=0}^{n-1} C_{2n}^k \cos(2n-2k)\omega t + \frac{1}{2}C_{2n}^n], & (when\ n\ is\ even), \\ \frac{1}{2^{2n}}\sum_{k=0}^{n} C_{2n+1}^k \cos(2n-2k+1)\omega t, & (when\ n\ is\ odd). \end{cases} \qquad (20b)$$

Relation (20a) will be applied to finding an analytical solution in a later discussion.

Taking the inverse Laplace transform of each term in (19), one can write the solution as a function of non-dimensional variables T and Z with six parts:

$$u(Z,T) = u_I + u_{II} + u_{III} + u_{IV} + u_V + u_{VI}. \qquad (21)$$

The variables Z and T are defined as normalized space Z (= z/H) and non-dimensional time T (= tc_v/H^2). The six components of the solution (u_i, i = I…VI) are given by the following expressions:

$$u_I = \begin{cases} b_0 \sum_{i=1}^{\infty}\left(\frac{-d_1}{b_1}\right)^i \{\frac{1}{i2^{2i}}\sum_{k=o}^{i} C_{2i+1}^k \sum_{n=1}^{\infty}\frac{(-1)^{n-1} - \sin MZ[\cos(\varpi_1^{2i+1}T - \phi_1) - \cos\phi_1 e^{-M^2T})]}{\sqrt{(\varpi_1^{2i+1})^2 + M^4}}\}, \\ b_0 \sum_{i=1}^{\infty}\left(\frac{-d_1}{b_1}\right)^i \{\frac{1}{i2^{2i-1}}[\sum_{k=o}^{i-1} C_{2i}^k \sum_{n=1}^{\infty}\frac{(-1)^{n-1} - \sin MZ[\cos(\varpi_1^{2i}T - \phi_1) - \cos\phi_1 e^{-M^2T})]}{\sqrt{(\varpi_1^{2i})^2 + M^4}} \end{cases}$$
$$+ C_{2i}^i (\sum_{n=1}^{\infty}\frac{(-1)^{n-1} - \sin MZ(1 - e^{-M^2T})}{M^2})]\}, \qquad (22a)$$

$$u_{II} = \begin{cases} b_0 \sum_{i=1}^{\infty}\left(\frac{-d_2}{b_2}\right)^i \{\frac{1}{i2^{2i}}\sum_{k=o}^{i-1} C_{2i+1}^k \sum_{n=1}^{\infty}\frac{(-1)^{n-1}\sin M(1-Z)[\cos(\varpi_2^{2i+1}\Delta T - \phi_2) - \cos(\varpi_2^{2i+1}T_0 + \phi_2)e^{-M^2T})]}{\sqrt{(\varpi_2^{2i+1})^2 + M^4}}\} \\ b_0 \sum_{i=1}^{\infty}\left(\frac{-d_2}{b_2}\right)^i \{\frac{1}{i2^{2i-1}}[\sum_{k=o}^{i-1} C_{2i}^k \sum_{n=1}^{\infty}\frac{(-1)^{n-1}\sin M(1-Z)[\cos(\varpi_2^{2i+1}\Delta T - \phi_2) - \cos(\varpi_2^{2i+1}T_0 + \phi_2)e^{-M^2T})]}{\sqrt{(\varpi_2^{2i})^2 + M^4}}) \end{cases}$$
$$+ C_{2i}^i \sum_{n=1}^{\infty}\frac{(-1)^{n-1}\sin M(1-Z)(1 - e^{-M^2T})}{M^2}]\}, \qquad (22b)$$

$$u_{III} = \frac{2c_v}{HA^2}\sum_{n=1}^{\infty}\frac{(-c_1)^n}{n}\sum_{j=1}^{\infty}(-1)^{j-1}(\frac{H^2}{c_v})^{2n+1}\sin M_j Z \sum_{k=0}^{2n}\frac{(-1)^k (T)^{2n-k} 2n!}{(M_j^2)^{k+1}(2n-k)!} - \frac{e^{-M_j^2T}(-1)^{2n}2n!}{(M_j^2)^{2n+1}}] \qquad (22c)$$

$$u_{IV} = \frac{2c_v}{HA^2}[\sum_{n=1}^{\infty}\frac{(-c_2)^n}{n}\sum_{j=1}^{\infty}(-1)^{j-1}(\frac{H^2}{c_v})^{2n+1}\sin M_j(1-Z)\sum_{k=0}^{2n}\frac{(-1)^k (T)^{2n-k} 2n!}{(M_j^2)^{k+1}(2n-k)!} - \frac{e^{-M_j^2T}(-1)^{2n}2n!}{(M_j^2)^{2n+1}}] \qquad (22d)$$

$$u_V = b_0\{\sum_{n=1}^{\infty}(-1)^{n-1}[\ln(b_2)\sin M(1-Z) - \ln(b_1)\sin MZ](1 - e^{-M^2T})/M^2\} \qquad (22e)$$

$$u_{VI} = BH^2/C_v\{T + \sum_{n=1}^{\infty}(-1)^{n-1}\{\cos[M(1-Z) - \cos MZ\}[T/M - (1 - e^{-M^2T})/M^3]\} \qquad (22f)$$

in which components of u_I and u_{II} have two solutions respectively for cases of odd and even integers n in (20b); $b_0 = 2H/A$; ΔT (= $T - T_0$) is incremental non-dimensional time; T_0 represents the initial T; M, a parameter, defined as functions of $(2n-1)\pi/2$; coefficients ϕ_i (i = 1, 2) and ϖ_j (j = 1, 2) are defined as follows:

$$\varpi_j^{2i} = 2(i-k)\omega_j H^2 / c_v, \; (j=1,2) \tag{23a}$$

$$\varpi_j^{2i+1} = [2(i-k)+1]\omega_j H^2 / c_v, \; (j=1,2) \tag{23b}$$

$$\phi_i = \tan^{-1}(M^2/\varpi_i), (i=1,2) \tag{24}$$

The superscripts 2i and 2i+1 represent even and odd integers. In the above formulas, one should keep it in mind that ϕ is a function of n due to the definition of M [= (2n-1)π/2].

Based on the solution [i.e., (21) and (22)], it is not difficult to find the strain field by taking the derivative with respect to space z, namely:

$$\varepsilon(Z,T) = \varepsilon_{I} + \varepsilon_{II} + \varepsilon_{III} + \varepsilon_{IV} + \varepsilon_{V} + \varepsilon_{VI} \tag{25}$$

where ε_i (i = I...VI) are found from (11) to be:

$$\varepsilon_I = \begin{cases} b_0 \sum_{i=1}^{\infty}\left(\frac{-d_1}{b_1}\right)^i \{\frac{1}{i2^{2i}} \sum_{k=o}^{i} C_{2i+1}^k \sum_{n=1}^{\infty} \frac{(-1)^{n-1} - M\cos MZ[\cos(\varpi_1^{2i+1}T-\phi_1)-\cos\phi_1 e^{-M^2T})]}{\sqrt{(\varpi_1^{2i+1})^2+M^4}}\}, \\ b_0 \sum_{i=1}^{\infty}\left(\frac{-d_1}{b_1}\right)^i \{\frac{1}{i2^{2i-1}}[\sum_{k=o}^{i-1} C_{2i}^k \sum_{n=1}^{\infty} \frac{(-1)^{n-1} - M\cos MZ[\cos(\varpi_1^{2i}T-\phi_1)-\cos\phi_1 e^{-M^2T})]}{\sqrt{(\varpi_1^{2i})^2+M^4}} \end{cases}$$
$$+C_{2i}^i (\sum_{n=1}^{\infty} \frac{(-1)^{n-1} - \cos MZ(1-e^{-M^2T})}{M})]\}, \tag{26a}$$

$$\varepsilon_{II} = \begin{cases} b_0 \sum_{i=1}^{\infty}\left(\frac{-d_2}{b_2}\right)^i \{\frac{1}{i2^{2i}} \sum_{k=o}^{i-1} C_{2i+1}^k \sum_{n=1}^{\infty} \frac{(-1)^n M\cos M(1-Z)[\cos(\varpi_2^{2i+1}\Delta T-\phi_2)-\cos(\varpi_2^{2i+1}T_0+\phi_2)e^{-M^2T})]}{\sqrt{(\varpi_2^{2i+1})^2+M^4}}\} \\ b_0 \sum_{i=1}^{\infty}\left(\frac{-d_2}{b_2}\right)^i \{\frac{1}{i2^{2i-1}}[\sum_{k=o}^{i-1} C_{2i}^k \sum_{n=1}^{\infty} \frac{(-1)^n M\cos M(1-Z)[\cos(\varpi_2^{2i+1}\Delta T-\phi_2)-\cos(\varpi_2^{2i+1}T_0+\phi_2)e^{-M^2T})]}{\sqrt{(\varpi_2^{2i})^2+M^4}}) \end{cases}$$
$$+C_{2i}^i \sum_{n=1}^{\infty} \frac{(-1)^n \cos M(1-Z)(1-e^{-M^2T})}{M}]\}, \tag{26b}$$

$$\varepsilon_{III} = \frac{2c_v}{HA^2} \sum_{n=1}^{\infty} \frac{(-c_1)^n}{n} \sum_{j=1}^{\infty} (-1)^{j-1} (\frac{H^2}{c_v})^{2n+1} M_j \cos M_j Z \sum_{k=0}^{2n} [\frac{(-1)^k (T)^{2n-k} 2n!}{(M_j^2)^{k+1}(2n-k)!} - \frac{e^{-M_j^2 T}(-1)^{2n} 2n!}{(M_j^2)^{2n+1}}] \tag{26c}$$

$$\varepsilon_{IV} = \frac{2c_v}{HA^2} \sum_{n=1}^{\infty} \frac{(-c_2)^n}{n} \sum_{j=1}^{\infty} (-1)^{j} (\frac{H^2}{c_v})^{2n+1} M_j \cos M_j (1-Z) \sum_{k=0}^{2n} [\frac{(-1)^k (T)^{2n-k} 2n!}{(M_j^2)^{k+1}(2n-k)!} - \frac{e^{-M_j^2 T}(-1)^{2n} 2n!}{(M_j^2)^{2n+1}}] \tag{26d}$$

$$\varepsilon_V = b_0 \{\sum_{n=1}^{\infty} (-1)^n [\ln(b_1)\cos(MZ) + \ln(b_2)\cos M(1-Z)](1-e^{-M^2T})/M\} \tag{26e}$$

$$\varepsilon_{VI} = BH^2/C_v \{\sum_{n=1}^{\infty} (-1)^{n-1} [\sin M(1-Z) + \sin MZ][T-(1-e^{-M^2T})/M^2] \tag{26f}$$

where $\varepsilon = \partial u/\partial z$. Local strain ε at a depth Z of interest should not be confused with accumulated deformation between two depths, Z and Z0. From (21), the accumulated deformation can be calculated from the difference $u(Z, T) - u(Z_0, T)$, where Z_0 can be any element elevation at which no displacement (or no vertical movement) is occurring mathematically and hence serves as a specified datum, say at Z=0. In order to estimate the impact of pumping-injecting water within aquifers, some simplified cases based the above solution are discussed in the next section.

5. DISCUSSION OF THE SOLUTION

From equations (21) and (22), one can see that the present poroviscous analytic solution is similar to the analytical solution with an assumption of poroelastic material (Li and Helm, 1998). It comprises three parts, namely, periodic variation, exponential reduction and nonlinear change with nondimensional time T.

Components u_I and u_{II} of the solution change exponentially and periodically with time. If one assumes that pumping and injecting water in the upper and lower aquifers start simultaneously with the same period, namely, $\varpi_1 = \varpi_2 = \varpi$ and $\varpi\, T_0 = 0$, then relative displacement with a maximum value at Z = H results from u_I and u_{II} [i.e., (22a) and (22b)] from the following expression [assuming n = odd number in (20b), $d_1/b_1 = d_2/b_2 = d/b$, and $u(Z_0, t) = u(0, t)$ at a datum Z = 0]:

$$u_I + u_{II} = \sum_{i=1}^{\infty}\left(\frac{-d}{b}\right)^i \frac{b_0}{i2^{2i}} \sum_{k=0}^{i} C_{2i+1}^k \sum_{n=1}^{\infty} \frac{(-1)^{n-1}[\sin M(1-Z) - \sin MZ - \sin M][\cos(\varpi T-\phi)-\cos\phi e^{-M^2T})]}{\sqrt{(\varpi)^2+M^4}} \tag{27}$$

where ϕ is defined in the same form as (1) except for $\varpi_i = \varpi$. If one assumes the pumping-injecting activity in both the upper and lower sandy layers has the same period but different phase, say a phase-lag π, namely, $\varpi_1 = \varpi_2 = \varpi$ and $\varpi\, T_0 = \pi$, then relative displacement may be produced from the relation:

$$u_I + u_{II} = \sum_{i=1}^{\infty}\left(\frac{d}{b}\right)^i \frac{b_0}{i2^{2i}} \sum_{k=0}^{i} C_{2i+1}^k \sum_{n=1}^{\infty} \frac{(-1)^{n-1}[\sin M(1-Z) + \sin MZ - \sin M][\cos(\varpi T-\phi)-\cos\phi e^{-M^2T})]}{\sqrt{(\varpi)^2+M^4}} \tag{28}$$

The maximum relative displacement from (28) (at Z = 1/2) is only half of that from (27). This means that one can reduce the potential displacement by controlling the pumping-injecting activities with a proper phase-lag between the upper and lower sandy areas. From (27) It is evident that pumping-injection in a single aquifer also causes a half of the maximum displacement Z = 1.

Displacement components u_{III} and u_{IV} caused by the linear loading function change nonlinearly with time, and represent in this paper nonrecoverable displacement. The component u_V (22e) does not change periodically but exponentially with time though the parameter b (= $1+ A\sigma_m/D_{02}\omega$) which is related to parameters of periodic loading at boundaries (e.g., σ_m and ω). Thus, u_V contributes recoverable and non-recoverable deformation to the total deformation (21) under cyclic loading. One may note that if b_1 and b_2 approximately equal a unit value, the displacement component u_V can be reduced, this means that in order to reduce risk of vertical subsidence, small ratios of $\sigma_{m1}A_1/D_{01}\omega_1$ and $\sigma_{m2}A_2/D_{02}\omega_2$ can be controlled by pumping-injection parameters such as discharge-recharge magnitudes and cycles and their ratio (i.e., σ_m/ω). The term u_{VI} in (22f) comprising both linear and exponential changes with time also expresses both recoverable and non-recoverable deformation. The component u_{VI} can be simplified when the ratio BH/c_v or B is negligibly small as discussed by Helm (1987). Relative displacement of u_{III}, u_{IV} u_V, and u_{VI} can be found in the same way for (27) and (28).

It is apparent that if the pumping-injecting activity takes place in a single aquifer only (i.e., either the top or the bottom aquifers, but not both), one may be not able to reduce the sinusoidal component of displacement in (22a) and (22b).

6. CONCLUSIONS

In brief, the following conclusions can be drawn. First, a one-dimensional analytic solution has been found. This analytic solution is based on a model featured by a two-aquifer sandwich pattern. Boundary conditions are set according to the sinusoidal pumping-injecting activity at the interfaces of two sand and one clay layers. Second, the constitutive relation of nonlinear poroviscosity has been introduced. This relation assumes the compressible layer can behave as a non-Newtonian flow. Third, the solution of the displacement field comprises three components, namely, alternating fluctuation, exponential reduction and nonlinear variation with time. Fourth, the solution has been based on some special assumptions. Based on the model in Figure 1, the following factors may affect deformation of the clay layer (compressible bed)

1) The phase-lag ϖT_0 of the pumping and injecting activities between the upper and lower aquifers may reduce the risk of deformation. When the phase-lag equals π, the potential risk of net compression may be reduced when compared to the case without a phase-lag (i.e., $\varpi T_0 = 0$),
2) Similarity of pumping-injecting periods of the upper and lower aquifers. When $\varpi T_0 = 0$ is considered Identical periods (i.e., $\omega_1 = \omega_2$) may reduce the top the potential displacement of the clay layer relative to the base.
3) Negligibly small ratio of $\sigma_m A/D_0\omega$ related to parameters b and d (e.g., a small pumping magnitude and a lager pumping frequency ω) may reduce risk of subsidence.

4) Negligibly small parameter c associated with $aA/2D_0$, (e.g., s small loading slope of f_2) may reduce risk of subsidence, especially for a long term.
5) Negligible small ratio of BH^2/c_v, (e.g., small bulk flow), may reduce risk of subsidence.

Finally, pumping-injecting water in two or more aquifers (e.g., the sandwich model: s-c-s in Figure 1 or multiple sandwich models: s-c-s-c-s) has a better chance, when compared to the case of pumping-injecting in a single aquifer, to control the displacement of the top of the clay layer.

It should be pointed out that in order to allow an analytic approach [i.e., equations (10), (11) and (12)], some factors are not been taken into account in the present paper. For instance, the effect of stress history (e.g., current stress status related to over, under and normally consolidated states) of sedimentary material is not considered. These factors, however, can be considered by using a numerical approach as was done by Helm (1975). The dynamic behavior of clay under cyclic loading will be considered in the future.

Acknowledgement

Writing this paper is supported by the research project funded by the National Aeronautics and Space Administration (NASA). The authors gratefully acknowledge this support.

REFERENCES

Gersevanov, N. M. (1934) The foundation of dynamics of soils (in Russian), Leningrad: Stroiizdat

Helm, D.C. (1975) One-dimensional simulation of aquifer system compaction near Pixley, Calif., 1: constant parameters. *Wat Resour. Res.* 11 (3), 465-478.

Helm, D.C. (1987) Three-dimensional consolidation theory in terms of the velocity of solids. *Geotechnique* 37(3), 369-392.

Helm, D.C. (1998) Poroviscosity, *in* Borchers, J. (ed.) Land Subsidence Case Histories and Current Research: *Proceedings of the Dr. Joseph F. Poland Symposium on Land Subsidence*, AEG Special Publication No. 8, p. 395-406.

Li, J. & Helm, D.C. (1995) A general formulation for aquifer deformation under dynamic and viscous conditions, in *Land Subsidence*, Proc. Fifth Int. Symp. on Land Subsidence The Hague, The Netherlands, Oct. 1995, IAHS Publ. N. 234, Barends F.B.J., F.J.J. Brouwer & F.H. Schröder Eds., p. 323-332.

Li,J & Helm D.C. (1998) An analytic solution for subsidence due to pumping and injecting activity, *Proceedings of the Eighth Congress IAEG*, Vancouver, Canada, Vol. 4, pp. 2381-2386.

Poland, J. F., Lofgren, B.E., Ireland, R.L. & Pugh, R. G. (1975) *Land subsidence In the San Joaquin Valley, California, as of 1972.* USGS Professional Paper 437-H.

Pyne G., Singer P. C. & Miller. C. T. (1995) Miller, Aquifer Storage Recovery of Treated Drink Water, Research Report published by AWWA Research Foundation and American Water Work Association.

Spiegle, M. R. (1965) *Theory and problems of Laplace transforms.* New York, Schaum.

Terzaghi, K. (1943) *Theoretical soil mechanics.* New York, Wiley, 510 p.

LAND SUBSIDENCE - Vol. II
Proceedings of the Sixth International Symposium on Land Subsidence
Ravenna / Italy / 24-29 September 2000

A NONLINEAR ELASTIC SOLUTION FOR SUBSIDENCE DUE TO ASR APPLICATIONS TO MUTLI-AQUIFER SYSTEMS

Jiang Li
Morgan State University, 5200 Perring Parkway, Baltimore, MD 21251-0001,USA

Abstract

Land subsidence due to the net compression of one or more semi-pervious clay beds can be caused by the application of aquifer storage and recovery (ASR) technology. ASR periodically withdraws and injects of water from or into adjacent aquifers for various purposes. In order to estimate the potential risk of aquifer system deformation in response to an injecting-pumping scheme, an analytic solution for the one-dimensional case (a sandwich model) is solved. The solution is analyzed along a cross-section of an idealized compressible semi-pervious layer. A governing equation expressed directly in terms of displacement (Helm, 1987) is invoked. The saturated aquifer system is assumed to behave like nonlinear poroelastic material. The two idealized aquifers (one above the modeled semi-confining bed and the other beneath) can be pumped independently of each other. Results from the analytic solution are applied to estimate and predict potential risk of land subsidence due to groundwater withdrawal and injection and to provide a first-estimate type of guideline for applications of aquifer storage and recover.

Keywords: Land subsidence, nonlinear elasticity, aquifer storage and recovery

1. INTRODUCTION

In order to meet water supply demand and improve water quality, the technology of aquifer storage and recovery (ASR) is being more and more widely used throughout the United States (e.g., Texas, New Mexico, Nevada, Arizona, California, and Florida). In 1983, only three operational sites in United States were involved in ASR technology. By 1994 (Pyne, 1995), more than forty sites or locations in thirteen states were using ASR technology. Today, ASR technology is even more popular. Currently, more than a dozen new sites are applying for permits to use the ASR technology in the field. The purposes for using ASR technology are many. For instance, in Florida, the ASR method is used to improve the quality of contaminated surface water (i.e., aquifers are used as filters). In Los Angeles, the ASR method helps to impede seawater intrusion by injecting lightly treated seawater into aquifers. In Texas, ASR technology helps to improve water quality and remove harmful byproducts of disinfectants by recharging aquifers with treated wastewater. Subsequently, clean water is discharged from aquifers and used for water supply. By contrast, in Las Vegas, Nevada, aquifers are used to store water through application of the ASR approach. In order to meet the high demand of water during the summer months, surface water is injected into aquifers during wintertime and then withdrawn from aquifers in the dry summer season. In Texas and Arizona, a similar approach is adopted for water management. The only difference is that surface water is injected into aquifers during the summer monsoon season and discharged from aquifers during the dry wintertime.

ASR activities induce fluctuations of hydraulic head. Changes in hydraulic head can in turn cause land subsidence. This is because changes in hydraulic head cause changes in pore water pressure that are directly related to changes in effective stress on an aquifer's skeletal frame through the principle of effective stress (Terzaghi, 1943). Effective stress fluctuations control the deformation of any aquifer system (Helm, 1972). Due to groundwater withdrawal, the accumulated compression of an aquifer system eventually manifests itself at the land surface as land subsidence (Poland et al, 1975, Poland 1984). In the present paper, potential risk of land subsidence due to pumping and injecting water into two aquifers on opposite sides of a compressible confining bed is examined. For the one-dimensional case, an analytic solution for the displacement field of the confining bed is presented. Boundary conditions on the compressible layer (say, clay) are given in terms of displacement or strain.

Nonlinear poroelastic behavior is assumed in this paper for the porous structure of the clay separator. A governing equation in terms of aquifer displacement (Helm, 1987) for the one-dimensional problem is used with specified boundary conditions. At the boundaries, an assumption of both sinusoidal and linear variations of pore water pressure with respect to time is made. Based on the principle of effective stress, the boundary conditions are related to boundary strain of the soil skeleton. The sinusoidal component of pore water pressure fluctuation is meant to simulate the situation of pumping and/or injecting water into an aquifer at regular intervals. At the same time the average mean of the fluctuating pore water pressure is assumed to decrease or increase linearly with time or to be constant. Thus, the case of the long-term recharge into the two aquifers can be less than, more than or equal to the overall long-term discharge from the aquifers. A simple model is assumed in the following section.

2. ANALYTIC SOLUTION

A conceptual model of two aquifers with two assumed wells for withdrawal and injection of water is drawn in Figure 1:

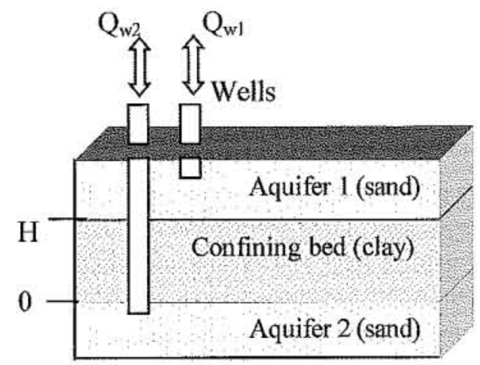

Figure 1. A diagram for an aquifer system

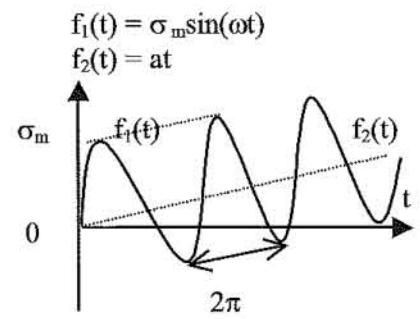

Figure 2. A diagram for function f(t)

In Figure 1, one well is located in the top aquifer (sand) and the other is located in the bottom aquifer (sand). They pump and inject water from or into each aquifer independently of each other at pumping-injecting rates Q_{w1} and Q_{w2}. The pattern of pumping and injecting water from or into aquifers is assumed to be a sinusoidal function shown in Figure 2.

In Figure 2, functions f_1 and f_2 are loading functions that change sinusoidally and linearly at the interface between sand and clay layers. The term σ_m with a unit of kg/ms^2 (Kpa) denotes the amplitude of pore water pressure, the coefficient a with a unit of kg/ms^3 (Kpa/s) stands for the slope of the linear loading function, t is time and ω is angular frequency that is introduced for sinusoidal fluctuation of water pressures due to pumping-injecting water into or from each of the two aquifers.

If one assumes that the compressible bed (clay) behaves as nonlinear poroelastic material, a nonlinear relation of stress versus strain under periodic, and linear plus periodic loadings are illustrated in Figures 3a and 3b.

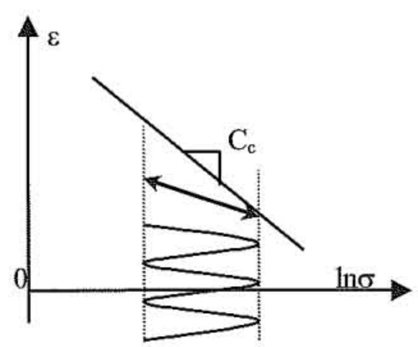

Figure 3a. Periodic loading without a linear trend.

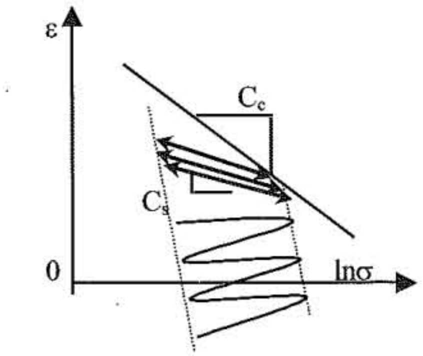

Figure 3b. Periodic loading with a linear trend.

Parameters C_c and C_s in Figure 3b denote slopes of virgin and swelling curves of consolidation. If one assumes: that the hydraulic separator between the two aquifers is nonlinear poroelastic shown in Figure 3; that the fluctuation of pore water pressure within each aquifer approximately changes as a sinusoidal function, and that the average mean of water pressure changes linearly; that the effective stress principle holds; that total stresses within the boundary layers do not change very much with time, then a governing equation written in terms of displacement u of the skeleton frame (Helm, 1987) is applicable for the one-dimensional vertical case. Based on loading at both the upper and lower boundary and initial conditions shown in Figure 1, the conceptual model can be mathematically described by the following set of equations.

$$\partial u / \partial t - c_v \partial^2 u / \partial^2 z = B / 2 \quad (1a)$$

$$u(0,z) = 0, \quad 0 \le z \le H \quad (1b)$$

$$\partial u(H,t) / \partial z = \varepsilon_1(t), \quad z = H \quad (1c)$$

$$\partial u(0,t) / \partial z = \varepsilon_2(t), \quad z = 0 \quad (1d)$$

where t is time, c_v (= $K/\gamma_w m_v$) is the consolidation coefficient of the clay layer that is assumed to be a constant though conductivity K and coefficient of volume compressibility m_v are individually not constant (Makasa, 1965), z is the coordinate in the vertical direction, H stands for the thickness of the clay layer in Figure 1, and B is a function of time and space (Helm, 1987). The functions $\varepsilon_1(t)$ and $\varepsilon_2(t)$ related to loading functions f_1 and f_2 in Figure 2 are defined as $\varepsilon_1(t) = -\{C_c \ln[a_1 t/\sigma_0+1] + C_s \ln(\sigma_{m1} \sin\omega_1 t/\sigma_0+1)\}$ and $\varepsilon_2(t) = -\{C_c \ln(a_2 t/\sigma_0+1) + C_s \ln[\sigma_{m2} \sin\omega_2(t-t_0)/\sigma_0+1]\}$. The term σ_0 represents current effective stress within the clay layer. Subscripts 1 and 2 denote the upper and lower aquifers respectively. The parameter a is related to the slope of the average mean water pressure that linearly decreases or increases with time in Figure 2. The cases of long-term recharge larger than ($a < 0$), less than ($a > 0$) and equal to ($a = 0$) long-term discharge within an aquifer system can be analyzed. If one assumes the compressible clay is nonlinear poroelastic, it is not difficult for one to find the facts: 1) that for the case of $a > 0$, C_s is less than C_c since the index C_c represents the slope of the virgin curve of consolidation, and the index C_s represents the slope of the loading-unloading curve of consolidation, and 2) that for the case of $0 \ge a$, C_s equals C_c since both C_s and C_c are slopes of the loading-unloading curve of consolidation (e.g., overconsolidated material).

Keeping the initial condition [i.e., (1b)] in mind and solving Equation (1a) for displacement with an assumption of a constant B, one finds the solution in Laplace transform space to be:

$$u^* = C_1 \cosh\left(\sqrt{\frac{s}{c_v}} z\right) + C_2 \sinh\left(\sqrt{\frac{s}{c_v}} z\right) + B/2s^2 \quad (2)$$

where u^* is displacement in Laplace transform space, C_1 and C_2 are constant coefficients. With help of boundary conditions [i.e., (1b) and (1c)], C_1 and C_2 for the first set of equations are found to be:

$$C_{11} = -B/2s^2 \quad (3a)$$

$$C_{12} = [\varepsilon_1(s) + \frac{B}{2s^2}\sqrt{\frac{s}{c_v}} \sinh\sqrt{\frac{s}{c_v}}H] / [\sqrt{\frac{s}{c_v}} \cosh(\sqrt{\frac{s}{c_v}}H)] \quad (3b)$$

where the first subscript of constants C stands for a designated set of equations. The value 1, for example, stands for the first set. With boundary conditions (1b) and (1d), the constants of C for the second set of equations are found to be:

$$C_{21} = -[\frac{B}{2s^2}\sqrt{\frac{s}{c_v}} + \varepsilon_2(H,s)\sinh(\sqrt{\frac{s}{c_v}}H)] / \sqrt{\frac{s}{c_v}} \cosh(\sqrt{\frac{s}{c_v}}H) \quad (4a)$$

$$C_{22} = \varepsilon_2(H,s)\sqrt{\frac{c_v}{s}} \quad (4b)$$

Substituting constants (3a) and (3b) into (2) for u_1^* and substituting (4a) and (4b) into (2) for u_2^*, one can find the sum of solutions u_1^* and u_2^* (i.e., $u_1^* + u_2^*$), in Laplace space to be as follows:

$$\begin{aligned} u^* = & \frac{B}{s^2} + \frac{B}{2s^2}\{\cosh[\sqrt{\frac{s}{c_v}}(H-z)]/\cosh(\sqrt{\frac{s}{c_v}}H) + \cosh(\sqrt{\frac{s}{c_v}}z)/\cosh(\sqrt{\frac{s}{c_v}}H)\} + \\ & \varepsilon_1(s)\sinh(\sqrt{\frac{s}{c_v}}z)/\sqrt{\frac{s}{c_v}}\cosh(\sqrt{\frac{s}{c_v}}H) + \varepsilon_2(s)\sinh[\sqrt{\frac{s}{c_v}}(H-z)]/\sqrt{\frac{s}{c_v}}\cosh(\sqrt{\frac{s}{c_v}}H) \end{aligned} \quad (5)$$

Taking the inverse Laplace transform of each term in (5), the solution can be written as a function of non-dimensional variables T and Z with five parts:

$$u(Z,T) = u_1 + u_2 + u_3 + u_4 + u_5 \quad (6)$$

The variables Z and T are defined as normalized space ($Z = z/H$) and non-dimensional time ($T = tc_v/H^2$). The five components of the solution (u_i, i = 1…5) are given by the following expressions:

$$u_1 = R_1 \sum_{n=1}^{\infty} \frac{(-a_1)^n}{n(\sigma_0)^n} \sum_{j=1}^{\infty} (-1)^{j-1} \left(\frac{H^2}{c_v}\right)^{n+1} \sin M_j Z \sum_{k=0}^{n} \left[\frac{(-1)^k (T)^{n-k} n!}{(M_j^2)^{k+1}(n-k)!} - \frac{e^{-M_j^2 T}(-1)^n n!}{(M_j^2)^{n+1}}\right] \quad (7)$$

$$u_2 = R_1 \sum_{n=1}^{\infty} \frac{(-a_2)^n}{n(\sigma_0)^n} \sum_{j=1}^{\infty} (-1)^{j-1} (\frac{H^2}{c_v})^{n+1} \sin M_j (1-Z) \sum_{k=0}^{n} [\frac{(-1)^k (T)^{n-k} n!}{(M_j^2)^{k+1} (n-k)!} - \frac{e^{-M_j^2 T} (-1)^n n!}{(M_j^2)^{n+1}}] \quad (8)$$

$$u_3 = -R_2 \sum_{n=1}^{\infty} \frac{(-\sigma_{m1})^n}{n(\sigma_0)^n} \sum_{j=1}^{\infty} (-1)^{j-1} \sin M_j Z \{ [\sum_{k=0}^{(n-2)/2} \frac{\sin^{n-(2k+1)}(\varpi_1 T) \sin(\varpi_1 T - \phi_{n-2k})}{\sqrt{(n-2k)\varpi_1^2 + M_j^4}} \\ \prod_{i=0}^{k} \frac{(n-2i+2)(n-2i+1)\varpi_1^2}{(n-2i+2)^2 \varpi_1^2 + M_j^4} + (1 - e^{-M^2 T} \frac{H^2}{C_v}) \prod_{i=1}^{n/2} \frac{(n-2i+2)(n-2i+1)\varpi_1^2}{(n-2i+2)^2 \varpi_1^2 + M_j^4}]\} \quad (9)$$

$$u_4 = -R_2 \sum_{n=1}^{\infty} \frac{(-\sigma_{m2})^n}{n(\sigma_0)^n} \sum_{j=1}^{\infty} (-1)^{j-1} \sin M_j (1-Z) \{ [\sum_{k=0}^{(n-2)/2} \frac{\sin^{n-(2k+1)}(\varpi_2 \Delta T) \sin(\varpi_2 T_0 - \phi_{n-2k})}{\sqrt{(n-2k)\varpi_2^2 + M_j^4}} \\ \prod_{i=0}^{k} \frac{(n-2i+2)(n-2i+1)\varpi_2^2}{(n-2i+2)^2 \varpi_2^2 + M_j^4} + (1 - e^{-M_j^2 T} \frac{H^2}{C_v}) \prod_{i=1}^{n/2} \frac{(n-2i+2)(n-2i+1)\varpi_2^2}{(n-2i+2)^2 \varpi_2^2 + M_j^4}]\} \quad (10)$$

$$u_5 = R_3 \{ T + \sum_{n=1}^{\infty} (-1)^{n-1} \{ \cos[M(1-Z)] + \cos MZ \} [T/M - (1 - e^{-M^2 T})/M^3] \} \quad (11)$$

in which $\Pi_{k=0}$ is defined to be unit, ΔT (= T - T_0) is incremental non-dimensional time, T_0 represents the initial T and M is a parameter defined as a function of n by (2n-1)π/2 respectively, coefficients R_i (i = 1…3), ϕ_{1i} (i = 1, 2) and ϖ_i (i = 1, 2) are defined as follows:

$$R_1 = 2c_v C_c / H \quad (12)$$

$$R_2 = 2C_s H^3 / c_v \quad (13)$$

$$R_3 = BH^2 / c_v \quad (14)$$

in which ϖ and ϕ^i are given by:

$$\varpi_i = \omega_i H^2 / c_v, (i = 1,2) \quad (15)$$

$$\phi_i = \tan^{-1}(\varpi_i / M^2), (i = 1,2) \quad (16)$$

In the above formulas, one should keep it in mind that M and ϕ are functions of n.

Based on the solution [i.e., (10) and (11)], it is not difficult to find the strain field by taking the derivative with respect to normalized space Z, namely:

$$\varepsilon(Z,T) = \varepsilon_1 + \varepsilon_2 + \varepsilon_3 + \varepsilon_4 + \varepsilon_5 \quad (17)$$

where ε_i (i = 1...5) are:

$$\varepsilon_1 = R_1 \sum_{n=1}^{\infty} \frac{(-a_1)^n}{n(\sigma_0)^n} \sum_{j=1}^{\infty} (-1)^{j-1} (\frac{H^2}{c_v})^{n+1} M_j \cos M_j Z \sum_{k=0}^{n} [\frac{(-1)^k (T)^{n-k} n!}{(M_j^2)^{k+1} (n-k)!} - \frac{e^{-M_j^2 T} (-1)^n n!}{(M_j^2)^{n+1}}] \quad (18a)$$

$$\varepsilon_2 = R_1 \sum_{n=1}^{\infty} \frac{(-a_2)^n}{n(\sigma_0)^n} \sum_{j=1}^{\infty} (-1)^{j} (\frac{H^2}{c_v})^{n+1} M_j \cos M_j (1-Z) \sum_{k=0}^{n} [\frac{(-1)^k (T)^{n-k} n!}{(M_j^2)^{k+1} (n-k)!} - \frac{e^{-M_j^2 T} (-1)^n n!}{(M_j^2)^{n+1}}] \quad (18b)$$

$$\varepsilon_3 = -R_2 \sum_{n=1}^{\infty} \frac{(-\sigma_{m1})^n}{n(\sigma_0)^n} \sum_{j=1}^{\infty} (-1)^{j-1} M_j \cos M_j Z \{ [\sum_{k=0}^{(n-2)/2} \frac{\sin^{n-(2k+1)}(\varpi_1 T) \sin(\varpi_1 T - \phi_{n-2k})}{\sqrt{(n-2k)\varpi_1^2 + M_j^4}} \\ \prod_{i=0}^{k} \frac{(n-2i+2)(n-2i+1)\varpi_1^2}{(n-2i+2)^2 \varpi_1^2 + M_j^4} + (1 - e^{-M^2 T} \frac{H^2}{C_v}) \prod_{i=1}^{n/2} \frac{(n-2i+2)(n-2i+1)\varpi_1^2}{(n-2i+2)^2 \varpi_1^2 + M_j^4}]\} \quad (18c)$$

$$\varepsilon_4 = -R_2 \sum_{n=1}^{\infty} \frac{(-\sigma_{m2})^n}{n(\sigma_0)^n} \sum_{j=1}^{\infty} (-1)^{j} M_j \cos M_j (1-Z) \{ [\sum_{k=0}^{(n-2)/2} \frac{\sin^{n-(2k+1)}(\varpi_2 \Delta T) \sin(\varpi_2 T_0 - \phi_{n-2k})}{\sqrt{(n-2k)\varpi_2^2 + M_j^4}} \\ \prod_{i=0}^{k} \frac{(n-2i+2)(n-2i+1)\varpi_2^2}{(n-2i+2)^2 \varpi_2^2 + M_j^4} + (1 - e^{-M_j^2 T} \frac{H^2}{C_v}) \prod_{i=1}^{n/2} \frac{(n-2i+2)(n-2i+1)\varpi_2^2}{(n-2i+2)^2 \varpi_2^2 + M_j^4}]\} \quad (18d)$$

$$\varepsilon_5 = R_3 \sum_{n=1}^{\infty} (-1)^{n-1} \{ \sin M(1-Z) - \sin MZ \} [T/M - (1 - e^{-M^2 T})/M^2] \quad (18e)$$

From solution (6), the accumulated deformation can be calculated from the difference u(Z, T) - u(Z_0, T), where Z_0 can be any elevation at which no displacement (or no vertical movement) is assumed to be occurring, say, a point that serves as a datum. For example, one can choose a convenient datum to lie at the base of the clay bed, namely at z = 0. Solving (6) for Z at the specified Z_0 (= 0) and then subtracting the result from an independent solution of (6) for nonzero Z yields the accumulated displacement between the two elevations. This subtraction process simply translates the origin of the zero-displacement coordinate to a datum of interest. This coordinate translation is not done in the present paper.

In order to estimate the impact of pumping-injecting water within aquifers, the solution and analysis of some simplified cases are discussed in the next section.

3. DISCUSSION AND ANALYSIS OF THE SOLUTION

From Equations (6) for displacement and (17) for strain, one can see the analytic solution comprises three parts, namely, periodic variation, exponential reduction and nonlinear change with time. It is apparent that the periodic component of displacement as a function of time is caused by the cyclic pumping-injecting activity. The exponential reduction is related to the consolidation process of soil mechanics that results from the dissipation of excessive pore water pressure due to consolidation that is expressed mathematically by Terzaghi's one-dimensional solution (1943). The nonlinear and linear changes in displacement with time are associated with linear loading function f_2 and the bulk flow parameter B. The parameter B represents a possible background vertical flow rate through the system. Displacement components u_1 and u_2 caused by the linear loading function change nonlinearly with time, and represent in this paper nonrecoverable displacement. From (7) and (8), components u_1 and u_2 can be reduced using a small slope (i.e., parameter a). Component u_5 in (11) related to the constant vertical bulk flow changes both linearly and exponentially with time. Thus, u_5 contributes recoverable and non-recoverable deformation to total deformation (6). Component u_5 can be simplified when the ratio BH/c_v or B is negligibly small as discussed by Helm (1987). Components u_3 and u_4 induced by the sinusoidal function change with time, and represent in this paper recoverable displacement. To reduce risk of subsidence, small ratios of σ_m/σ_0 can be controlled by pumping-injection activity (i.e., discharge-recharge magnitude). The phase leg of pumping-injection between the two aquifers in Figure 1 plays a role in inducing subsidence in multiple aquifer systems. For example, if one chooses Z = 0 and assumes u(0, t) = 0 and the phase leg $\varpi T_0 = 0$ with $\varpi_1 = \varpi_2 = \varpi$, then the maximum value (at Z = 1) of relative displacement for components u_3 and u_4 is:

$$u_3+u_4=-R_2\sum_{n=1}^{\infty}\frac{(-\sigma_m)^n}{n(\sigma_0)^n}\sum_{j=1}^{\infty}(-1)^{j-1}2\sin M_jZ\{[\sum_{k=0}^{(n-2)/2}\frac{\sin^{n-(2k+1)}(\varpi T)\sin(\varpi T-\phi_{n-2k})}{\sqrt{(n-2k)\varpi^2+M_j^4}}$$
$$\prod_{i=0}^{k}\frac{(n-2i+2)(n-2i+1)\varpi^2}{(n-2i+2)^2\varpi^2+M_j^4}+(1-e^{-M^2T}\frac{H^2}{C_v})\prod_{i=1}^{n/2}\frac{(n-2i+2)(n-2i+1)\varpi^2}{(n-2i+2)^2\varpi^2+M_j^4}]\} \tag{19}$$

When the phase leg equals zero (i.e., $\varpi T^0 = 0$), the sum of u^3 and u^4 becomes:

$$u_3+u_4=R_2\sum_{n=1}^{\infty}\frac{(-\sigma_m)^n}{n(\sigma_0)^n}\sum_{j=1}^{\infty}(-1)^{j-1}2\sin M_j/2-\sin M_jZ\{[\sum_{k=0}^{(n-2)/2}\frac{\sin^{n-(2k+1)}(\varpi T)\sin(\varpi T-\phi_{n-2k})}{\sqrt{(n-2k)\varpi^2+M_j^4}}$$
$$\prod_{i=0}^{k}\frac{(n-2i+2)(n-2i+1)\varpi^2}{(n-2i+2)^2\varpi^2+M_j^4}+(1-e^{-M^2T}\frac{H^2}{C_v})\prod_{i=1}^{n/2}\frac{(n-2i+2)(n-2i+1)\varpi^2}{(n-2i+2)^2\varpi^2+M_j^4}]\} \tag{20}$$

It is not difficult to find that fact the maximum value (at Z = 1) of subsidence in (19) will be twice of that (at Z = 0.5) in (20). Relative displacement for other components such as u_1, u_2 and u_5 can be found in the same way for u_3 and u_4.

In order to compare the linear elastic solution to the nonlinear one, the analytic solution for two cases are drawn in the following figures:

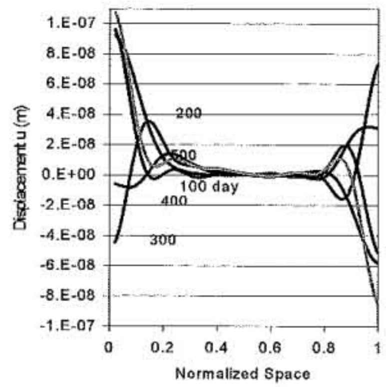

Figure 4a. u vs. Z for a nonlinear elastic model with time (100-500 days).

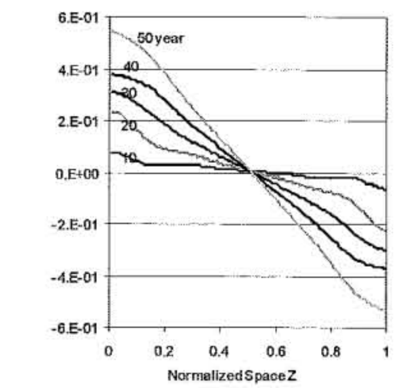

Figure 4b. u vs. Z for a nonlinear elastic model with time (10-50 years).

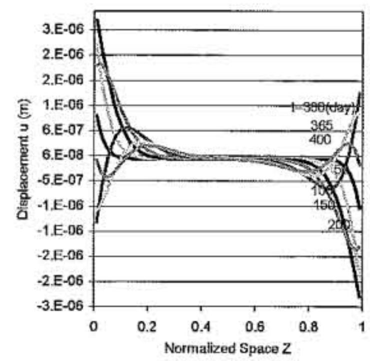

Figure 5a. u vs. Z for a linear elastic model with time (100-500 days).

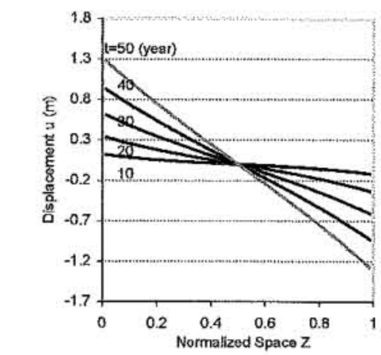

Figure 5b. u vs. Z for a linear elastic model with time (10-50 years).

The main parameter used to draw Figure 4 and 5 are listed the following table:

	H m	C_v m^2/day	B m/day	a/σ_0, a/E_a	σ_m/σ_0, σ_m/E_p	f1=f2 1/day	Cs, Cc
Nonlinear	5	0.001	0	2.3E-5	0.02	2.8E-3	0.5,0.83
Linear	5	0.001	0	2.3E-5	0.02	2.8E-3	na

If one compares Figures 4 with Figure 5, one can find that both linear and nonlinear solutions have a similar pattern for short and long terms. Namely, for a short period of time (Figures 4a and 5a), displacement at the upper and low boundaries changes with time periodically. During a short period of time, the total displacement is dominated by the component caused by sinusoidal loading function f_1. In contrast, for a long term (Figure 4b and 5b), displacement is dominated by the component of displacement related to the linear loading function f_2. Displacement changes linearly along the cross-section of the compressible clay layer. From the results shown in Figures 4 and 5, the main difference between linear and nonlinear models is that the linear elastic model gives larger deformation when one compare to that produced by the nonlinear elastic model. For the linear model, the linear loading function can cause infinite deformation with increase of time. This is not realistic. For the nonlinear model, however, deformation increases much slower than that predicted by linear model because of the relation of ε versus $\ln\sigma$. The subsidence can be better predicted by the nonlinear elastic solution.

4. CONCLUSIONS

In brief, the following conclusions can be drawn. First, a one-dimensional analytic solution has been found. This analytic solution is based on a concept model featured by a two-aquifer sandwich pattern. Boundary conditions are set according to the sinusoidal pumping-injecting activity at the interfaces of two sand layers and one clay layer. Second, the analytical solution is found based on the assumption of nonlinear elasticity for the compressible bed. Third, the solution of the displacement field is composed of three components, namely, periodic fluctuation, exponential decay and nonlinear variation with time. Each component of the displacement solution is illustrated and discussed in turns. According to the model shown in Figure 1, the following factors may affect the total cumulative displacement u and relative displacement along the cross-section of the clay layer (compressible bed): 1)The phase-lag ϖT_0 of the pumping and injecting activities between the upper and lower aquifers. When the phase-lag ϖT_0 equals π, the potential risk of deformation may be reduced when compared to a case without a phase-lag (i.e., $\varpi T_0 = 0$); 2) Negligibly small values of a_1 and a_2. Namely, if discharge-recharge is well balanced in aquifers and the slope for long-term change in the mean hydraulic head is negligibly small, risk of subsidence due to components u_1 and u_2 can decrease; 3) Opposite values of a_1 and a_2. This suggests that if the slope for linear changes in the mean hydraulic head is positive in one aquifer and negative in the other aquifer, the risk of the total displacement of the compressible bed can be possibly reduced; 4) Relatively small values of σ_m and the ratio of σ_m/σ_0. This means that if fluctuations of hydraulic head (i.e., periodic loading amplitude) are properly controlled, subsidence due to components u_3 and u_4 can be reduced; 5) Similarity of pumping-injecting parameters within the upper and lower aquifers such as periods, amplitudes and loading rates. When pumping-injecting activity is properly controlled, identical parameters within the overlying and underlying aquifers allow the potential displacement of the clay layer to be minimized; 6). Controlled pumping-injecting of water within two or more aquifers (e.g., the sandwich model: s-c-s in Figure 1 or multiple sandwich model: s-c-s-c-s) has better chance, when compared to the case of pumping-injecting in a single aquifer, to reduce the displacement. Finally, nonlinear elastic model can give more realistic results for prediction during a long term.

REFERENCES

Gersevanov, N. M. (1934) The foundation of dynamics of soils(in Russian). Leningrad: Stroiizdat

Helm, D.C. (1972) Simulation of aquitard compaction due to changes in stress. *Trans. Am. Geophys. Un.* **53** (11), 979.

Helm, D.C. (1975) One-dimensional simulation of aquifer system compaction near Pixley, Calif., 1: constant parameters. *Wat Resour. Res.* **11** (3), 465-478.

Helm, D.C. (1976) One-dimensional simulation of aquifer system compaction near Pixley, Calif., 2: stress-dependent parameters. *Wat Resour. Res.* **12** (3), 375-4391.

Helm, D.C. (1987) Three-dimensional consolidation theory in terms of the velocity of solids. *Geotechnique* **37** (3), 369-392.

Makasa, M. (1965) The consolidation of soft clay- A new consolidation theory and its application, in *Civil Eng.* in Japan, Jpn. Soc. of Eng., Tokyo, 21-26

Poland, J.F. Figueroa Vega G., Carbognin L., Johnson A. I., & Yamamoto S. (1994) *Guidebook to studies of land subsidence due to ground-water withdrawal,* Ed. by UNESCO, Paris, France, J. F. Poland Chairman and Editor, 305 p. and Appendices A-E.

Poland, J. F., Lofgren, B.E., Ireland, R.L. Pugh, R. G. (1975) Land subsidence In the San Joaquin Valley, California, as of 1972. USGS Professional Paper 437-H

Pyne G., Singer, P. C. and Miller, C. T. (1995) Miller, Aquifer Storage Recovery of Treated Drink Water, Research Report published by AWWA Research Foundation and American Water Work Association.

Spiegle, M. R. (1965) *Theory and Problems of Laplace Transforms*. New York, Schaum.

Terzaghi, K. (1943) *Theoretical Soil Mechanics*. New York, Wiley, 510 p.

LAND SUBSIDENCE - Vol. II
Proceedings of the Sixth International Symposium on Land Subsidence
Ravenna / Italy / 24-29 September 2000

MODELING RESIDUAL AQUIFER-SYSTEM COMPACTION: CONSTRAINING THE VERTICAL HYDRAULIC DIFFUSIVITY OF THICK AQUITARDS

Michelle Sneed[1], Michael T. Pavelko[2], and Devin L. Galloway[3]
[1]*California State University Foundation, U.S. Geological Survey, Placer Hall, 6000 J Street, Sacramento, CA 95819-6129*
[2]*U.S. Geological Survey, 6770 South Paradise Road, Las Vegas, NV 89119*
[3]*U.S. Geological Survey, Placer Hall, 6000 J Street, Sacramento, CA 95819-6129*

Abstract

One-dimensional (vertical) delayed drainage and resultant residual compaction of thick aquitards were simulated using the computer program MODFLOW-96. The modeling technique focused on aquitard hydraulic diffusivity, discretization of aquitards, and aquifer-system stresses that can cause compaction. The preliminary model results for a case study in Las Vegas, Nevada, USA, indicate that aquitard hydraulic diffusivity estimated from field studies, stress-strain analyses, and laboratory analyses were inaccurate.

The model uses different diffusivity values for the elastic and inelastic ranges of stress. Aquitards are finely discretized to better represent the highly nonlinear, vertical pore-fluid pressure gradients associated with delayed drainage to allow for a slower propagation of pore-fluid pressure and to more accurately simulate the timing of residual compaction. Ground-water levels are specified as the transient stresses that cause aquifer-system compaction. The model is calibrated to estimated and measured compaction.

Vertical hydraulic-diffusivity estimates for thick aquitards were refined during model calibration. Initial estimates of vertical hydraulic diffusivity for thick aquitards at the Las Vegas, Nevada site ranged from about 50 to 500 m^2/d; preliminary model results indicate a value of about 2.2×10^{-2} m^2/d. The refined property estimates may be useful for regional modeling efforts and to aid groundwater managers seeking a long-term balance between ground-water use and potential land subsidence.

Keywords: land subsidence, model, residual compaction, diffusivity

1. INTRODUCTION

Aquifer-system compaction, and resultant land subsidence, caused by ground-water withdrawals is a global problem that has caused hundreds of millions of dollars worth of damage in the United States (Galloway et al. 2000). To best mitigate this type of subsidence, accurate knowledge of the hydraulic properties of susceptible aquifer systems is needed. In an aquifer system, the hydraulic properties of coarse-grained sediments (aquifers) generally are easily measured or calculated from field tests. Most land subsidence, however, is caused by drainage and compaction of aquitards. Numerical models of land subsidence are more sensitive to aquitard hydraulic properties, which are more difficult and costly to obtain from field tests. Consequently, values of aquitard hydraulic properties used in numerical models often are estimated from the scarce information available or from values obtained from time-intensive model-calibration techniques.

To improve the estimates of aquitard properties, a numerical, one-dimensional (vertical) aquifer-system-compaction model was developed for a site in Las Vegas, Nevada, USA. To increase the accuracy of the aquifer-system-compaction simulations, the modeling technique focused on assigning a detailed aquifer-system stress history, discretizing time and space, and constraining the vertical hydraulic diffusivity of aquitards. The model simulates the timing and magnitude of measured deformation and accounts for delayed drainage and residual compaction. One-dimensional model-derived values of vertical hydraulic diffusivity can be used in regional models of ground-water flow and aquifer-system compaction to optimize ground-water use and to help mitigate land subsidence.

2. MECHANICS OF LAND SUBSIDENCE

Land subsidence caused by aquifer-system compaction is attributed mainly to the permanent compaction of aquitards as pore-fluid pressures in the aquitards slowly equilibrate with lower pore-fluid pressures in adjacent aquifers. This concept, known as the aquitard-drainage model, is based on two fundamental principles of aquifer-system mechanics: the principle of effective stress and the theory of one-dimensional hydrodynamic soil consolidation (Terzaghi, 1925; 1943). Aquifer-system stresses and vertical hydraulic diffusivity of aquitards are important properties involved in these principles. For this paper, the terms pore-fluid pressure, hydraulic head, head, and water level represent aquifer-system stresses.

2.1 Principle of Effective Stress

The effective stress in an aquifer system is the difference between the downward geostatic load of overlying sediments and the supporting pore-fluid pressure. Assuming a constant geostatic load, a change in pore-fluid pressure is balanced by an equivalent change in effective stress (Terzaghi, 1925). Accordingly, as pore-fluid pressures decrease, effective stress will increase and cause some degree of compression of the aquifer-system skeleton.

The preconsolidation stress of an aquifer system is the previous maximum effective stress and often is represented by the previous lowest hydraulic head (Riley, 1969). When the effective stress exceeds the preconsolidation stress, compression of aquitards is unrecoverable (inelastic) and termed compaction. Deformation (compaction or expansion) that occurs when the effective stress is less than the preconsolidation stress is recoverable (elastic). Inelastic deformation of the coarse-grained aquifers is negligible (Hanson, 1989).

When aquifer-system stresses are in the inelastic range, it is useful to determine separate specific-storage values for aquifers and aquitards because aquitard compressibility (and therefore specific storage) typically is several orders of magnitude larger than aquifer compressibility (Hanson, 1989). The specific storage of an aquifer system is adequately separated into three components: the inelastic and elastic specific storage of aquitards and the elastic specific storage of aquifers.

2.2 Theory of Hydrodynamic Consolidation

The theory of hydrodynamic soil consolidation (Terzaghi, 1925) accounts for the time delay involved in aquitard drainage and the resultant residual compaction. For a given decrease in aquifer-system hydraulic head, pore-fluid pressures in aquifers equilibrate more rapidly than in less diffusive aquitards. Water is slowly released from aquitards into adjacent aquifers, resulting in a pore-pressure imbalance (gradient) between aquifers and aquitards. Aquitards will continue to release water until pore-fluid pressures equilibrate. Residual compaction is the compaction that occurs in aquitards while they are equilibrating to pore-fluid pressure in adjacent aquifers. The thickness and vertical hydraulic diffusivity of an aquitard determine the rate and duration of equilibration with adjacent aquifers and, thus, residual compaction.

The time constant of an aquitard is the time required to attain about 93 percent of the ultimate compaction following a given stress increase (Riley, 1969). Ultimate compaction is the total compaction that would occur if a given increase in stress were maintained until pore pressures equilibrated. The time constant is directly proportional to the square of the drainage-path length and inversely proportional to the vertical hydraulic diffusivity of an aquitard (Riley, 1969; Ireland et al. 1984).

3. STRESS-STRAIN ANALYSIS

Elastic and inelastic storage coefficients can be estimated using an established graphical method (Riley, 1969). The method involves plotting stress (hydraulic head) on the y-axis and strain (compaction) on the x-axis. Riley (1969) showed that for aquifer systems where pressure equilibration can occur rapidly between aquifers and aquitards, the inverse slopes of the predominant linear trends in the compaction-head trajectories represent measures of the skeletal storage coefficients. A modified approach to the Riley (1969) method involves attempting to isolate, on a seasonal basis, the elastic and inelastic components of the measured, mixed response of the aquifer system. A detailed discussion of this modified method can be found in Sneed and Galloway (2000).

4. MODELING TECHNIQUE

A transient, one-dimensional (vertical), numerical model of aquitard drainage was developed to simulate vertical aquifer-system deformation caused by water-level variations and to refine estimates of hydraulic properties that control deformation. The model uses the computer program MODFLOW-96 (Harbaugh and McDonald, 1996), with the Flow and Head Boundary (FHB1) (Leake and Lilly, 1997) and Interbed Storage (IBS1) (Leake and Prudic, 1991) packages. In addition to MODFLOW-96, a computer code for universal inverse modeling (UCODE) (Poeter and Hill, 1998) was used for parameter estimation of the vertical hydraulic diffusivity of aquitards.

The temporal and spatial discretization of the model domain, the assignment of detailed transient stresses using estimated or measured water levels, and the assignment of preconsolidation heads and inelastic and elastic specific-storage values allow the model to simulate delayed drainage and residual compaction.

4.1 Temporal and Spatial Discretization

MODFLOW-96 discretizes time with stress periods, which are subdivided into time steps. Time-step intervals are used when calculating the volumetric exchange of water within, into, or out of the model domain. For this modeling technique, time-step intervals are relatively large when water-level variations are relatively small and available water-level measurements are sparse. Time-step intervals are smaller when aquifer-system hydraulic heads undergo larger (seasonal) and more frequent (daily) changes. The smaller time steps aid in the simulation of delayed drainage in aquitards, a relationship described later in this section.

MODFLOW-96 spatially discretizes the model into layers, rows, and columns, which typically are associated with volume; in a one-dimensional (vertical) model, however, they are associated with thickness. The modeling technique uses a single layer with one row and many columns (Fig. 1). This one-layer, columnwise arrangement in the numerical model effectively translates the aquifer system from one-dimensional vertical to one-dimensional horizontal. This adaptation (Leake and Prudic, 1991) was used to make use of the layerwise formatting of MODFLOW-96 for data input and output, while preserving the accurate simulation of the vertical flow and deformation processes. Thicknesses were specified according to sediment type.

IBS1 is limited by the assumption that all adjacent cells are in equilibrium at the end of each time step: residual compaction cannot be simulated in a single cell. To account for this assumption and to accurately represent the slow propagation of heads through aquitards, the model domain was discretized into many thin model cells and the model time steps were kept small. Assigning small thickness and diffusivity values to a group of adjacent cells representing a single aquitard allows specified aquifer heads to propagate into aquitards one cell at a time, rather than throughout the entire aquitard, for each time step. This methodology also allows for a more detailed simulation of hydraulic heads throughout the aquitards, which can have highly nonlinear hydraulic gradients across their thickness because of their small diffusivity. The resulting model grid is a vertical column with variably spaced layers that generally are thicker for aquifers than for aquitards.

4.2 Initial and Boundary Conditions and Stresses

Initial conditions for the model included hydraulic heads and preconsolidation stresses (heads); these conditions were based on assumed predevelopment steady-state head profiles and assumed head values throughout the vertical profile, respectively.

The boundary conditions and stresses (heads) assigned to model cells are critical features of the model that allow realistic stress histories to be used. The cell representing the deepest point in the vertical section is designated as a no-flow cell to prevent water from entering or exiting the system. At least one cell in each aquifer is designated as a specified-head cell. FHB1 enables the head of specified-head cells to change with time as prescribed by the user. Consequently, because there are no other stresses introduced to the model, the variations in head at the specified-head cells are responsible for all ground-water flow that occurs in the model and, thus, the resulting aquifer-system compaction. The relatively high vertical hydraulic conductivity of aquifers ensures that, for each time step, heads in all cells representing an aquifer will be equal to the specified-head value assigned in FHB1 for the aquifer. All other model cells are designated as variable-head cells.

5. LAS VEGAS, NEVADA

Las Vegas Valley is the fastest growing metropolitan area in the United States. Since the 1950s, annual ground-water withdrawals have exceeded natural recharge. In the late 1800s, several springs flowed in the valley and most wells were artesian. Today, there are no springs and, locally, water levels are more than

100 meters (m) below land surface. A result of these ground-water-level declines has been widespread aquifer-system compaction, accompanied by nearly 2 m of land subsidence in some areas.

In 1994, the U.S. Geological Survey installed a 244-m borehole extensometer and three piezometers to monitor land subsidence and ground-water levels in Las Vegas. Geophysical and lithologic logs of the extensometer borehole indicate that there are three aquifers confined by three aquitards (Fig. 1).

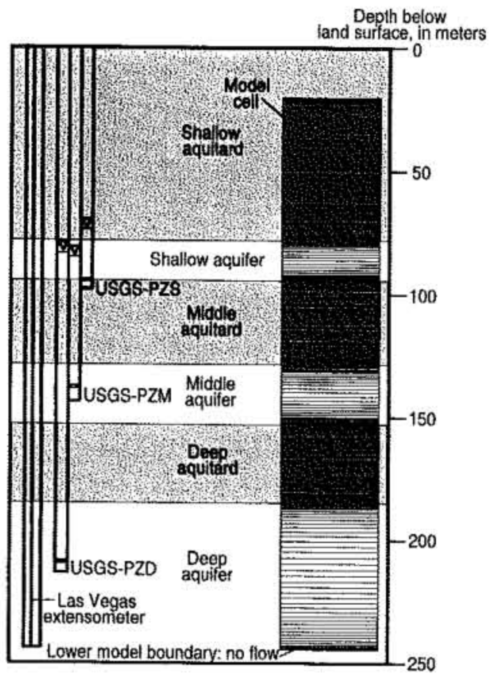

Figure 1. Conceptual model and model grid for the Las Vegas, Nevada, monitoring site.

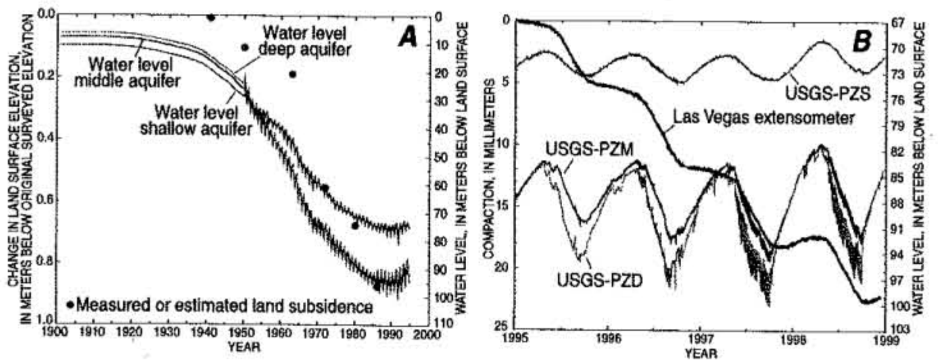

Figure 2. Ground-water-level and land-subsidence data for the Las Vegas, Nevada, monitoring site. A, The historical period, 1901-95. B, The recent period, 1995-99.

Each piezometer at the site is screened within one of the aquifers (Fig. 1), which are affected by nearby production and artificial-recharge wells. In Las Vegas, ground water is pumped from about May to September and the aquifer system is artificially recharged during the rest of the year. Consequently, water levels in the deep aquifer (piezometer USGS-PZD) annually fluctuate as much as 19 m (Fig. 2B). When water levels are declining, compaction occurs at a rate of about 1 millimeter (mm) per month; when water levels are recovering, compaction either nearly stops or reverses, depending on the amount of artificial recharge (Fig. 2B).

From 1995 to 1999, nearly 23 mm of compaction was measured at the extensometer (Fig. 2B). During this period, ground-water levels in the piezometers fluctuated seasonally according to ground-water use, but the annual mean water levels did not change significantly (Fig. 2B).

5.1 Stress-Strain Analysis

The stress-strain analysis of the measurements shown in Figure 2B yielded an aquifer-system elastic specific-storage estimate of about 2.8×10^{-6} m^{-1} and an aquitard inelastic specific-storage estimate of about 4.1×10^{-6} m^{-1}. The two specific-storage values are similar because the derivation relies on nearly instantaneous deformation associated with water-level fluctuations. At the Las Vegas site, the effect of delayed drainage of the aquitards and residual compaction dominated the compaction signal, masking some or all of the elastic rebound, which compromised the analysis. Using literature-derived ranges of vertical hydraulic conductivity values for aquitards (from about 2.1×10^{-4} meters per day (m/d) to 2.1×10^{-3} m/d) and the inelastic specific storage value derived from the stress-strain analysis, vertical hydraulic diffusivity values ranged from about 50 to 500 square meters per day (m^2/d).

5.2 Numerical Model

The aquifer system at the extensometer borehole is represented with 245 model cells ranging from about 0.3 to 2 m in thickness (Fig. 1). Aquifer-system compaction was simulated from 1901 to 1999, with two distinct periods of temporal discretization. From 1901 to 1995, the historical period, 1-year stress periods with 1-month time steps were used; from 1995 to 1999, the recent period, 50-day stress periods with 3-hour time steps were used. Transient stresses were represented by estimated water levels for the historical period (Fig. 2A) and by continuously measured water-level data for the recent period (Fig. 2B). Initial preconsolidation heads were deduced from the paired ground-water-level and historical land-subsidence time series (Fig.

2A). Initial values for the vertical hydraulic diffusivity of aquitards were obtained from literature and the stress-strain analysis.

5.3 Parameter Estimation

UCODE was used to assist in calibration by estimating the inelastic specific storage and vertical hydraulic conductivity of aquitards. UCODE iteratively runs MODFLOW-96 using statistically refined hydraulic parameter estimates for each model run. UCODE estimated parameters based on the statistical comparison between simulated and measured compaction values. This iterative process derives a statistically validated combination of hydraulic parameters that will accurately simulate measured compaction.

5.4 Simulations

The model simulates estimated land subsidence for the historical period (Fig. 2A) and the continuously measured compaction data for the recent period (Fig. 2B). Aquitard hydraulic parameters were adjusted in the model to obtain the best match between simulated and measured aquifer-system compaction and land subsidence. In addition to providing estimates of aquitard hydraulic properties, the model results provide information on the aquitard head gradients and the relative contribution of individual aquitards to total aquifer-system compaction. Time constants were calculated on the basis of model-derived aquitard properties.

Total simulated compaction compares well to measured or estimated land subsidence to 1986 (the last year land surveys were done), with the simulated compaction being slightly overestimated (Fig. 3A). Simulated compaction for the recent period compares well with measured compaction (Fig. 3B).

Model results indicate that the elastic specific storage of the aquifer system is about 2.5×10^{-6} m^{-1}. For aquitards, the inelastic specific storage is about 2.0×10^{-4} m^{-1} and the vertical hydraulic conductivity is about 4.4×10^{-6} m/d, which corresponds to a vertical hydraulic diffusivity value of about 2.2×10^{-2} m^2/d. Time constants for the shallow, middle, and deep aquitards are about 435, 35, and 27 years, respectively. The time constant of the shallow aquitard is significantly larger because it is the thickest aquitard and because it drains downward only, whereas the other aquitards drain upward and downward.

Model-derived profiles of aquitard heads indicate that by 1960, residual pore-fluid pressures were large (Fig. 3C). Although pore-pressure gradients in the aquitards remained nonlinear at the end of the simulated time, the gradients had decreased, indicating that aquitards are slowly equilibrating with adjacent aquifers (Fig. 3C). The simulations indicate that most of the measured compaction (recent period) is residual compaction occurring in the aquitards.

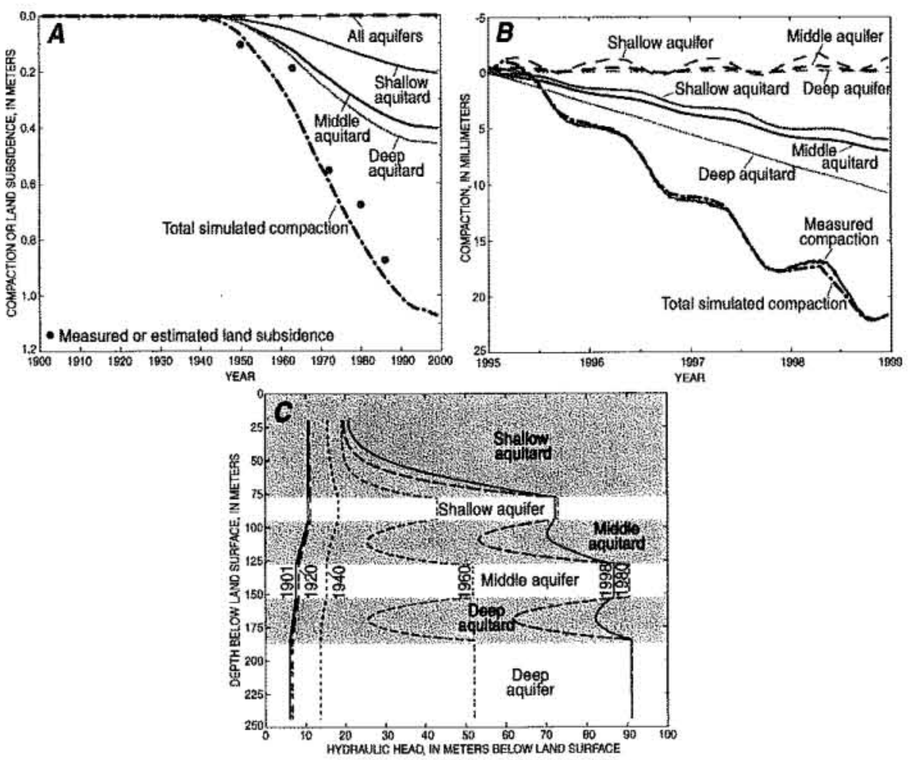

Figure 3. Las Vegas, Nevada, case study. A, Measured and simulated compaction for the period 1901-99. B, Measured and simulated compaction for the period 1995-99. C, Simulated hydraulic-head profiles for selected years.

6. CONCLUSIONS

A transient, one-dimensional, numerical model was developed to simulate delayed drainage and residual compaction of the aquitards in the aquifer system at a site in Las Vegas, Nevada, USA. The fine-scaled spatial discretization of aquifer system properties and temporal discretization of observed stresses allowed for detailed analyses of aquitard properties, aquitard-head profiles, and residual compaction. Because of the difficulty and cost of making reliable field measurements of these aquitard properties, many past studies have relied on inaccurate data obtained from indirect field measurements, laboratory studies, or studies of other areas. The modeling technique used for this study provides a method to obtain site-specific hydraulic properties for aquitards using standard field measurements and established computer codes.

The preliminary model results indicated that inelastic specific-storage estimates derived from the stress-strain analysis were too low by at least one order of magnitude and therefore inaccurate. Model results also were used to quantify storage values for each aquifer-system component, as opposed to the averaged aquifer-system storage values that resulted from the stress-strain analysis. The model results also indicated that the initial literature-derived estimates for vertical hydraulic-conductivity values for aquitards were too large to accurately simulate measured compaction.

The model-derived hydraulic-property values are refined estimates of the true values and will be useful in other hydrologic investigations. The model results emphasize the importance of the long-term management of ground-water resources; although aquifer-system stresses during the recent period have remained relatively stable compared with historical declines, aquifer-system compaction, mainly in the form of residual compaction, continues. Management of ground water can help mitigate potential aquifer-system compaction and resultant land subsidence, and improvements in the accuracies of aquitard property estimates can assist in the optimal management of ground-water and land resources.

7. REFERENCES

Galloway, D.L., Jones, D.R., & Ingebritsen, S.E., eds., (2000) Land subsidence in the United States: U.S. Geological Survey Circular 1182, 177 p.

Hanson, R.T., (1989) Aquifer-System Compaction, Tucson Basin and Avra Valley, Arizona: U.S. Geological Survey Water-Resources Investigations Report 88-4172, 69 p.

Harbaugh, A.W., & McDonald, M.G., (1996) User's documentation for MODFLOW-96, an update to the U.S. Geological Survey modular finite-difference ground-water flow model: U.S. Geological Survey Open-File Report 96-485, 56 p.

Ireland R.L., Poland, J.F., & Riley, F.S., (1984) Land subsidence in the San Joaquin Valley, California, as of 1980: U.S. Geological Survey Professional Paper 437-I, 93 p.

Leake, S.A., & Prudic, D.E., (1991) Documentation of a computer program to simulate aquifer-system compaction using the modular finite-difference ground-water flow model, U.S. Geological Survey Techniques of Water Resources Investigations, book 6, chap. A2, 68 p.

Leake, S.A., & Lilly, M.R., (1997) Documentation of a computer program (FHB1) for assignment of transient specified-flow and specified-head boundaries in applications of the modular finite-difference ground-water flow model (MODFLOW): U.S. Geological Survey Open-File Report 97-571, 50 p.

Poeter, E.P. & Hill, M.C., (1998) Documentation of UCODE, A Computer Code for Universal Inverse Modeling, U.S. Geological Survey Water Resources Investigation Report 98-4080, 116 p.

Riley, F.S., (1969) Analysis of borehole extensometer data from central California, In Tison, L.J., ed., *Land Subsidence*, International Association of Hydrological Sciences Publication 89, v. 2, p. 423-431.

Sneed, M., & Galloway, D.L., (2000) Aquifer-system compaction and land subsidence: measurements, analyses, and simulations— the Holly site, Edwards Air Force Base, Antelope Valley, California: U.S. Geological Survey Water-Resources Investigation Report 00-4015, *in press*.

Terzaghi, K. (1925) Principles of soil mechanics: IV; settlement and consolidation of clay, *Erdbaummechanic*, **95**, (3) 874-878.

Terzaghi, K. (1943) *Theoretical soil mechanics*, New York, Wiley, 510 p.

A 3-D COUPLED MODEL WITH CONSIDERATION OF RHEOLOGICAL PROPERTIES

Xiao-yun Gu
Institute of Mechanics, Chinese Academy of Sciences, Beijing 100080, China

Qi-quan Ran
Research Institute of Petroleum Exploration and Development, CNPC, Beijing 100083, China

Abstract

In this paper a 3-D coupled model with consideration of rheological properties is established. The aquifer-aquitard system is treated as a whole 3-D body. Sands and clays have the same geotechnical parameters, but with different values. 3-D flow is considered. Creep rate is involved in the stress-strain relationship. The coupling effect between flow and deformation is reflected by the k-e relationship. Basic assumptions and equations are given in the paper. Numerical solution is conducted by using finite difference method. The model is checked by the computation for Shanghai area of 8000 km^2. The model can be used for predicting subsidence as well as for selecting effective countermeasures.

Keywords: land subsidence, 3-D model, groundwater withdrawal, rheological property, countermeasures

1. INTRODUCTION

For computing land subsidence by groundwater withdrawal the classical approach for quasi-3D model is usually adopted. Flow is assumed to be 2D (horizontal) in the aquifers, and 1D (vertical) in the aquitards. However, actually, within the aquifer-aquitard system overlying the bedrock, as shown in Fig. 1, the hydrodynamic characteristics is changing continuously. Particularly, within the sand layers, the vertical flow not only comes from the neighboring clay layers, and also can not be ignored in the vicinity of area a in Fig.1, where different aquifers are connecting. Thus, 3-D flow should be considered. The aquifer-aquitard system is treated as a 3-D body. Sands and clays possess the same geotechnical parameters, such as void ratio, permeability, compressibility, etc., but with different values. The volume change of the soil element equals to the net flow quantity, which depends on the soil permeability. It means permeability determines void ratio change, and then void ratio affects permeability reversely.

So, the water flow through the soil pores and the soil deformation are coupled each other. Furthermore, since in deltaic regions the aquitards often consist of very soft clay, the rheological properties should be considered. On the basis of the above points, a 3-D coupled model with consideration of rheological properties is established.

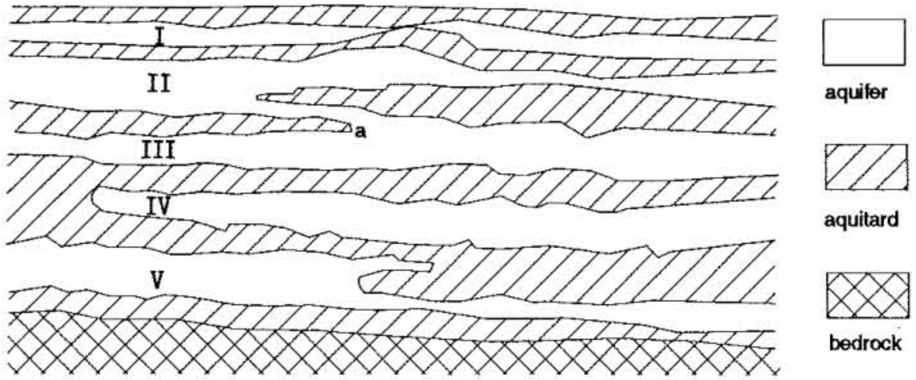

Figure 1. Scheme of aquifer-aquitard system.

2. MATHEMATICAL MODEL

2.1. Basic assumptions

(1) The aquifer-aquitard system above the bedrock is treated as a whole 3-D body. Sand and clay layers in the system have the same geotechnical parameters, but with different values.
(2) The flow is 3-D, the effect of gravity to the soil strata is considered, and Darcy's law is satisfied.
(3) Soils within the 3-D body are saturated, heterogeneous and anisotropic.
(4) Total stress is unchanged. The absolute change of the pore water pressure induced by water level change equals to the effective stress change.
(5) Water and soil grains are incompressible. The compressibility of soil skeleton is represented by m_{vc} under lowering of water level, and under arising of water level.
(6) Horizontal displacements are neglected.
(7) The rheological property, i.e. secondary consolidation under constant effective stress, of the soft clays is considered.
(8) The coupling effect between flow and deformation is involved.

2.2. Differential equation of flow

For the 3-D body, a soil element is divided. Since the soil is saturated and the compressibility of water and soil gains is ignored, the volume change of the soil element $\partial V / \partial t$ equals to the net flow from the element:

$$\frac{\partial V}{\partial t} = -\left(\frac{\partial v_x}{\partial x} + \frac{\partial v_y}{\partial y} + \frac{\partial v_z}{\partial z}\right) dxdydz \tag{1}$$

where v_x, v_y, v_z are the flow velocity in the direction x,y,z respectively.

The volume change of the soil element can be expressed by the void ratio change:

$$\frac{\partial V}{\partial t} = \frac{dxdydz}{1+e}\frac{\partial e}{\partial t} \tag{2}$$

Let (1)=(2), the following equation is obtained:

$$\frac{1}{1+e}\frac{\partial e}{\partial t} = -\frac{\partial v_x}{\partial x} - \frac{\partial v_y}{\partial y} - \frac{\partial v_z}{\partial z} \tag{3}$$

The Darcy's law with consideration of gravity is expressed as follows:

$$v_x = -\frac{k_x}{\gamma_w}\left(\frac{\partial p}{\partial x} - \gamma_w \frac{\partial D}{\partial x}\right) \qquad v_y = -\frac{k_y}{\gamma_w}\left(\frac{\partial p}{\partial y} - \gamma_w \frac{\partial D}{\partial y}\right)$$
$$v_z = -\frac{k_z}{\gamma_w}\left(\frac{\partial p}{\partial z} - \gamma_w \frac{\partial D}{\partial z}\right) \tag{4}$$

where k_x, k_y, k_z are the coefficient of permeability in the direction x, y, z respectively, γ_w is the unit weight of ground water, p the pore water pressure, D the relative depth with respect to a fixed reference level.

Substituting eq.(4) into eq.(3), and in case of multi-well pumping and recharging, eq.(5) is obtained:

$$\frac{\partial}{\partial x}\left[\frac{k_x}{\gamma_w}\left(\frac{\partial p}{\partial x} - \gamma_w \frac{\partial D}{\partial x}\right)\right] + \frac{\partial}{\partial y}\left[\frac{k_y}{\gamma_w}\left(\frac{\partial p}{\partial y} - \gamma_w \frac{\partial D}{\partial y}\right)\right]$$
$$+ \frac{\partial}{\partial z}\left[\frac{k_z}{\gamma_w}\left(\frac{\partial p}{\partial z} - \gamma_w \frac{\partial D}{\partial z}\right)\right] + q = \frac{1}{1+e}\frac{\partial e}{\partial t} \tag{5}$$

where q is the flow rate of pumping or recharging per unit volume.

The pore water pressures are related to the water levels as follows:

$$L = \frac{P}{\gamma_w} - z + H \tag{6}$$

where L is the groundwater level relative to the sea level, z the depth of the investigating point from the ground level, H the distance between ground level to the sea level.

2.3. Stress- strain relationship of soils

In case of considering the rheological property, the void ratio change should include the change caused by the effective stress change and the change with constant effective stress (Gu et al., 1995):

$$\frac{\partial e}{\partial t} = \frac{\partial e}{\partial p'}\frac{\partial p'}{\partial t} + \left[\frac{\partial e}{\partial t}\right]_c \tag{7}$$

$\frac{\partial e}{\partial p'}$ and the creep rate $\left[\frac{\partial e}{\partial t}\right]_c$ are determined by the following eqs.

$$-\frac{\partial e}{\partial p'} = \frac{ae}{p'} \quad (p_0' \le p' \le p_c') \tag{8a}$$

$$-\frac{\partial e}{\partial p'} = \frac{be}{p'} \quad (p' > p_c') \tag{8b}$$

$$-\left[\frac{\partial e}{\partial t}\right]_c = \frac{ce}{t_1}\left(\frac{e}{e_c}\right)^{1/c}\left(\frac{p'}{p_c'}\right)^{b/c} \tag{8c}$$

where $e_c = e_0\left(p'/p_c\right)^{-a}$, $a = m_{vs}(1+e_0)p'/e_1$, $b = m_{vc}(1+e_0)p'/e_1$,

$c = 0.434\,c_\alpha/e_1$, $t_1 = H^2/c_v$, e^1 is the void ratio at p'_0.

In the light of effective stress principle, eq. (7) can be written in the following form:

$$\frac{\partial e}{\partial t} = -\frac{\partial e}{\partial p'}\frac{\partial p}{\partial t} + \left(\frac{\partial e}{\partial t}\right)_c \tag{9}$$

For sand layers, $\left[\frac{\partial e}{\partial t}\right]_c = 0$.

2.4. Relationship between void ratio and permeability

The coupling effect between flow and deformation is reflected by the relationship between void ratio and permeability. Lambe and Whitman (1979) pointed out, the linear correlation between k and $\frac{e^3}{1+e}$ is good for sands, but not for clays. They suggested using linear e - log k correlation for clays. But the figure they cite from Michael and Lin shows that for kaolinite with water as permeate, the correlation between k and $\frac{e^3}{1+e}$ is not far from a straight line. Therefore, the linear k - $\frac{e^3}{1+e}$ relationship is adopted here. When the soil is consolidating from the initial state (e_0, k_0) to the current state (e,k) , the permeability ratio can be expressed as follows:

$$\frac{k}{k_0} = \left(\frac{e}{e_0}\right)^3\left(\frac{1+e_0}{1+e}\right) \tag{10}$$

2.5. Equation for computing subsidence

In case without horizontal displacements, subsidence is computed by the void ratio change:

$$S = \frac{\Delta e}{1+e_0}H \tag{11}$$

2.6. Initial and boundary conditions

Initial condition is the given pore water pressure distribution at a time selected as the beginning of the computing process (t=0). It can be written as:

$$p(x,y,z)\big|_{t=0}=p_e(x,y,z) \tag{12}$$

Boundary conditions can be expressed in two forms: pressure boundary p_G, i.e. pore water pressure of x,y,z on the boundary G at time t ,

$$p_G=f_p(x,y,z,t) \tag{13}$$

and flow quantity boundary

$$\left.\frac{\partial p}{\partial n}\right|_G=f_q(x,y,z,t) \tag{14}$$

If the whole system above the bedrock is computed, the lower boundary condition will be very simple: $\frac{\partial p}{\partial z}=0$.

3. NUMERICAL SOLUTION

The mathematical model is solved by the finite difference method.
Eqs.(5) and (9) are incorporated into a new equation:

$$\frac{1+e}{\gamma_w}\left\{\frac{\partial}{\partial x}\left[k_x\left(\frac{\partial p}{\partial x}-\gamma_w\frac{\partial D}{\partial x}\right)\right]+\frac{\partial}{\partial y}\left[k_y\left(\frac{\partial p}{\partial y}-\gamma_w\frac{\partial D}{\partial y}\right)\right]+\frac{\partial}{\partial z}\left[k_z\left(\frac{\partial p}{\partial z}-\gamma_w\frac{\partial D}{\partial z}\right)\right]\right\}+q=\frac{\partial e}{\partial p'}\frac{\partial p}{\partial t}+\left(\frac{\partial e}{\partial t}\right)_c \tag{15}$$

After conducting the difference discretization of the equation and performing the necessary algebraic manipulation, the pore water pressure or water level are solved implicitly. Then the void ratio, coefficient of permeability, and subsidence are solved explicitly. The solution sequence is shown in Fig.2.

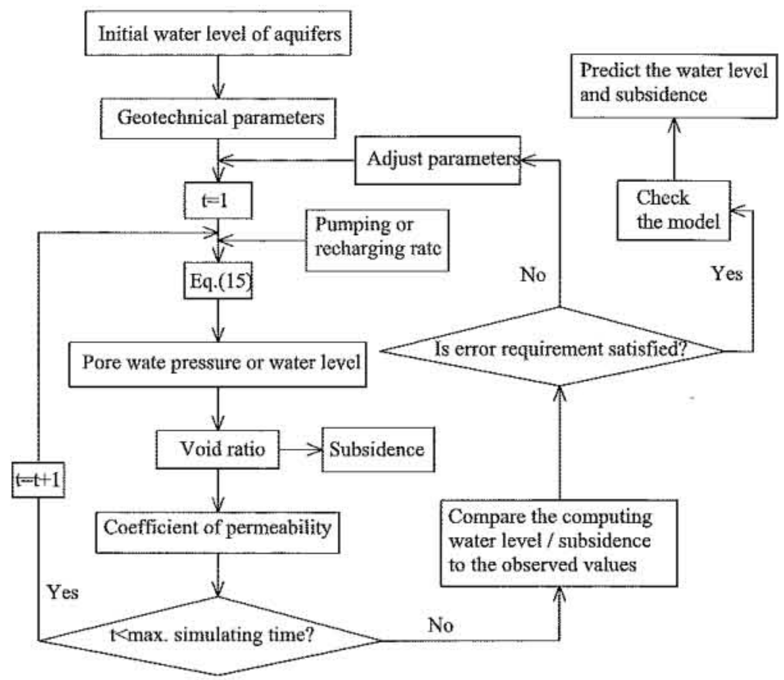

Figure 2. Flow chart for numerical solution.

4. MODEL CHECKING

The mathematical model is checked by the computation for Shanghai with area of 8000 Km². Horizontally, the area is divided into 70×80 grids (see Fig.3). The bedrock in Shanghai locates at the depth about 300 m. However, due to lack of available data, the computation is made for the upper strata of 100 m thick. Vertically, soil layers are subdivided into 14 sublayers (see Table 1). So totally there are 70×80×14 grids. The lower boundary is affected by the water level change of the II aquifer, so the flow boundary is used.

Table 1. Vertical distribution of soil layers.

Nomenclature of soil layers	Number of sublayers
Superficial layer	1
Silty sand layer	1
I soft clay layer	3
II soft clay layer	3
Hard clay layer	1
I aquifer (sand layer)	1
III soft clay layer	3
II aquifer (sand layer)	1

In order to check the mathematical model, the computation period is artificially divided into two stages: fitting stage and checking stage.

The fitting stage lasts 12 years, from Dec.30, 1980 to Dec.30, 1992. For fitting stage, the input geotechnical parameters are provided by some internal reports. By fitting the computing data to the water levels of the observing wells, pore water pressures of the piezometers, and subsidence values from the stratification benchmarks, the parameters are finally defined.

At the checking stage, the computation is conducted by regarding water levels on Dec.30, 1992 as initial condition and using the parameters defined above. The results show good agreement between computing and observed data. It verifies the model has been checked.

5. PREDICTION AND SELECTION OF COUNTERMEASURES

By using the checked model, the subsidence prediction can be made.

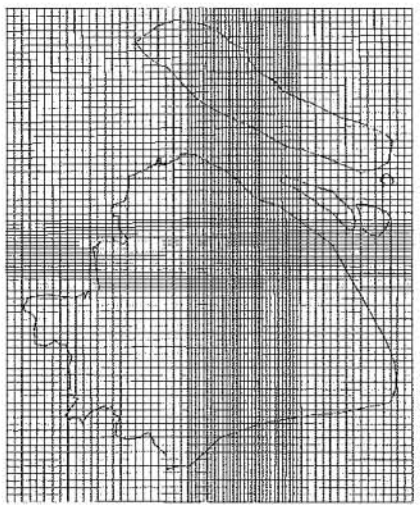

Figure 3. Division of grids in the horizontal plane.

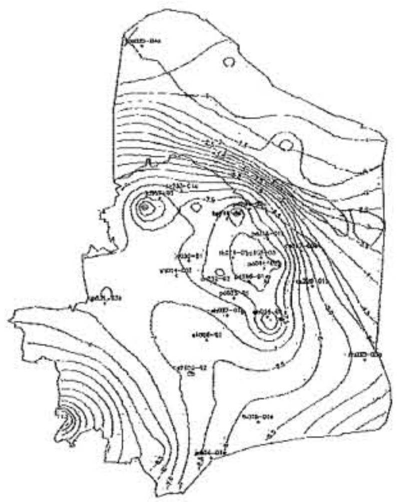

Figure 4. Predictive map of water level distribution.

Furthermore, groundwater is a kind of natural wealth of human being. We can not control subsidence only by reducing the pumping amount or increasing the recharging amount. Gu et al. (1991) had pointed out, determination of the most effective recharging program as to its implementing time, depth, frequency and intensity deserves careful considerations. The established model has just the advantage of fulfilling this requirement.

For this purpose the predictive computation is made for the future 10 years with several pumping-recharging programs, maintaining the water supply amount unchanged.

(1) Program A: The same as 1996's pumping-recharging program. The predictive map of water level distribution by the end of 2010 is shown in Fig.4.
(2) Program B: Adjusting the areal distribution. Water supply in the area of water level depressions in Fig.4 is reduced. As a result subsidence in these areas is lessened.
(3) Program C: Changing the characteristics of water level fluctuation.

According to Gu & Xu (1997), the smaller period of cyclic loading in consolidation tests can reduce the deformation to some extent. So computation for different characteristics of water level fluctuation is conducted. Commonly, the water level change is yearly periodical, as shown by the dash line in Fig.5. By adjusting the monthly pumping or recharging amount, water level change can possess two peaks (Fig.5a) or several peaks (Fig.5b) per year. Compare to program A, the decrease of subsidence per year amounts to 0.1-0.4 mm and 0.1-0.5 mm respectively.

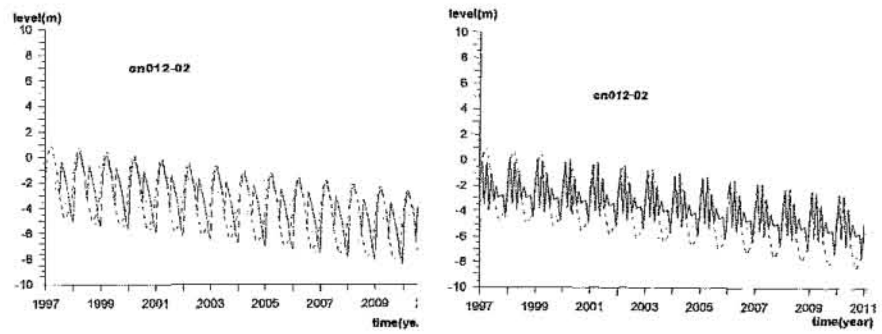

Figure 5. Water level change of II aquifer for program C.

(4) Program D: Recharging water into the shallow aquifer.

The observed data have shown that the deformation of I and II soft clay layers constitutes a significant position in the total subsidence. While recharging water into the II aquifer doesn't make the pore pressure rising in I and II soft layers. The question whether recharging water into I aquifer is effective has been raised. The predictive computation is made with program D1 and D2.

Program D1: Equal distribution of the recharging amount for the I and II aquifers , with unchanged total recharging amount. The computation results in Fig.6 show that program D1 is unfavorable .

Program D2: Recharging water into I aquifer with unchanged recharging amount into II aquifer. The recharging amount into I aquifer equals to 1/5 of II aquifers. Compare to the results for program A, the water level amplitude of I aquifer is larger, and the central line of the water level is upper (see Fig.7), thus some decrease of deformation takes place.

The computation of program D indicates, whether recharging water into the shallow aquifer is effective, depends on the distribution of recharging amount between different aquifers, because hydraulic connection exists between different aquifers.

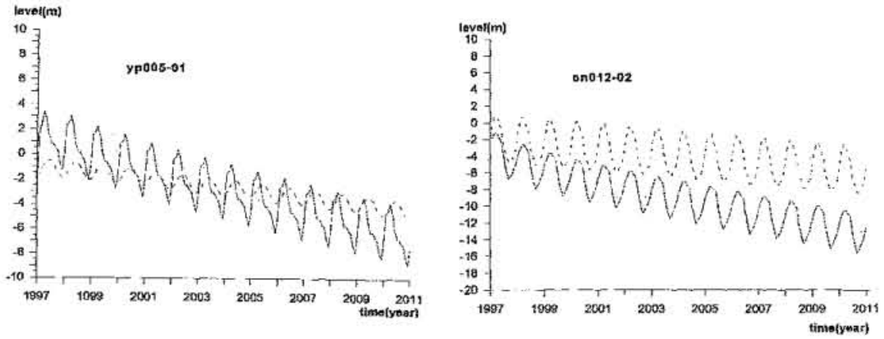

Figure 6. Comparison between Levels for programs D1 & A.

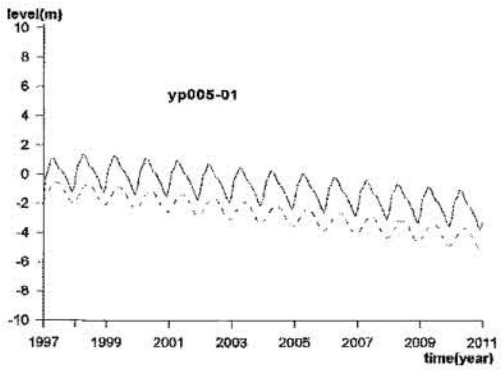

Figure 7. Water level of I aquifer for program D2.

The above predictive computations illustrate the principles of selecting effective countermeasures. Of course, to realize the countermeasures depends on many other social and economic factors as well.

6. CONCLUSIONS

(1) In order to more closely reflect the real geological conditions, a 3-D coupled model with consideration of rheological properties is established.

(2) On basis of assumptions of 3-D Darcy's flow, heterogeneity and homogeneity of soils, constant value of total stress, compressibility of water and soil grains, rheological properties of soft clays, and coupling effect between flow and deformation, basic equations are set up. The initial and boundary conditions are given.

(3) The numerical solution is conducted by using finite difference method. Water level of pore water pressure is solved implicitly first, and then void ratio, coefficient of permeability and subsidence are computed explicitly.

(4) The model is checked by the computation for Shanghai area of 8000 km^2.

(5) The predictive computation is made for the future 10 years with different pumping-recharging programs. The model serves as a powerful tool for selecting effective countermeasures.

Acknowledgements

The geologic data was provided by the Shanghai Geological Bureau .

REFERENCES

Gu X.Y., Tsien S.I., Huang H.C. & Liu Y. (1991) Analysis of Shanghai land subsidence. In: *Land subsidence* (ed. by A.I. Johnson), IAHS 200, 603-612.

Gu X.Y., Xu D.N. & Deng W. (1995) A computing model based on cyclic consolidation tests. In: *Land subsidence*. Proc. Fifth Int. Symp. on Land Subsidence (ed. by F.B.J. Barends, et al), IAHS 234, 295-303 Publ. No.

Gu X.Y. & Xu D.N. (1997) Consolidation behavior of Shanghai clay under cyclic loading. In: *Proceedings of 14th International Conference on Soil Mechanics and Foundation Engineering* , 115-118.

Lambe T.W. & Whitman R.V. (1979) *Soil Mechanics, SI Version*. John Wiley & Sons., 553pp.

TIME-SPACE GROUND SUBSIDENCE PREDICTION DETERMINED BY VOLUME EXTRACTION FROM THE ROCK MASS

Ryszard Hejmanowski
University of Mining and Metallurgy, Department of Mine Surveying and Environmental Engineering, al. Mickiewicza 30, 30059 Krakow, Poland

Anton Sroka
Technical University - Bergakademie Freiberg, Department of Mine Surveying and Geodesy, Agricolastrasse 1., 09599 Freiberg, Germany

Abstract

The underground exploitation of mineral and fossil fuel deposits in the solid, liquid or gaseous form leads to the disturbance of the existing equilibrium in the rock mass. The tendency of the rock mass to achieve a new, even a mere temporary equilibrium state is manifested also with movements of the ground surface. These movements, or deformations, depending on their magnitude and their course in time, can affect the ground infrastructure, like building structures, communications networks, gas and water-pipe networks, sewerage systems and the lakes, very adversely. In order to increase the efficiency of preventive actions it is necessary to accurately foresee these deformations *a priori*, among others, on the basis of a planned course of the exploitation both in time and in space. The Litwiniszyn theory of stochastic movements completed with the solution of the time problem will be presented in the paper. Typical applications in the coal, ore, salt mining and the exploitation of oil and natural gas will be discussed.

Keywords: land subsidence, mathematical model, underground exploitation

1. INTRODUCTION

The surface deformations caused by mineral ore extraction have been calculated in a number of European countries based on the geometrical-integral theories. Originally, they were meant for predicting of deformations over horizontal and relatively shallow coal beds. These theories started in the early 20th century as a result of observations of ground subsidence over the exploitation fields (usually backfilled) (Keinhorst, 1925; Bals, 1931; Knothe, 1953; Kochmański, 1959). Despite the highly idealised assumptions and significant changes in the conditions of deep extraction, these theories have been used for subsidence predicting in a number of countries up to day. The simplicity and relatively high accuracy of the theories (sufficient to meet the practical requirements) make them especially attractive. This mainly applies to the theories operating the function of influence in the form of a suitably parameterised function of Gauss normal distribution. Knothe's theory, being a special case of Litwiniszyn theory of stochastic formation, belongs to this group of theories (Litwiniszyn, 1956).

2. MATHEMATICAL MODELING OF SUBSIDENCE IN TIME

To calculate the ground subsidence over the exploited deposit it is necessary to have a possibly accurate description of causes of subsidence and the ways of its propagation through the rock mass layers (stochastic character of the rock mass assumed) (Fig. 1). In the case of solid ores extraction, we have to do with

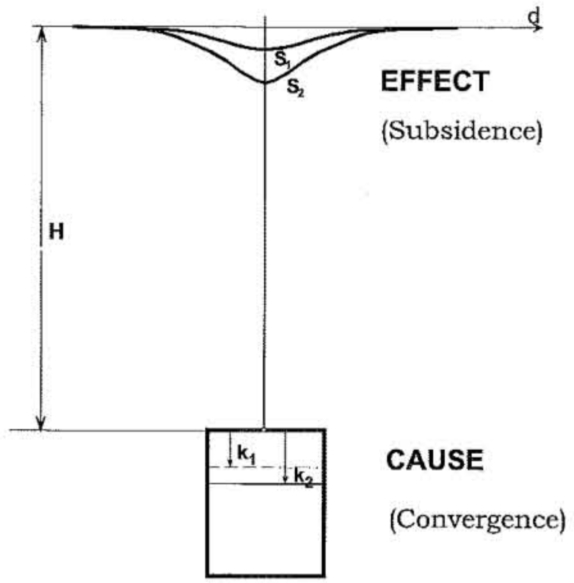

Figure 1. Basic cause-effect relation

the narrowing of the past-exploitation space, further called "convergence" or "compaction" (for porous deposits). When analysing the deposit element, this parameters will be treated volumetrically (convergence of a certain volume of past extraction working). Bearing in mind the development of the deformation process in time, the general formula for subsidence of a point of surface under the influence of a selected elementary part of deposit can be written by the following general formula (1):

$$S(t,d) = \frac{M(t)}{r^2} \cdot \exp\left(-\pi \frac{d^2}{r^2}\right) \tag{1}$$

where:

r - Knothe's theory parameter (the other parameter, a - extraction coefficient),
t - time calculated from the termination of deposit element extraction, on the assumption that it was extracted in one instance,
d - horizontal distance between the point and the deposit element,
$M(t)$ - volume of elementary depression.

The relation between the volume of the extracted element V and the volume of the elementary depression $M(t)$ is defined in the literature by a logarithmic function (Sroka A., 1984) or function (2). This function was made on the assumption that volume convergence of elementary working in time can be described by an exponential function, whereas the delaying influence of the rock mass can be modeled according to the equation used by Knothe for describing the course of subsidence of a point in time (Sroka et al., 1987).

$$M(t) = a \cdot V \cdot \left(1 + \frac{c}{\xi - c} \cdot \exp(-\xi \cdot t) - \frac{\xi}{\xi - c} \cdot \exp(-c \cdot t)\right) \tag{2}$$

where:

a - the volume of depression to the volume of depleted deposit element ratio,
V - volume of depleted deposit element,
ξ - relative rate of volumetric convergence (ξ = 0.01 year $^{-1}$, i.e. the rate of volumetric convergence is 1% of the actual volume per year),
c - time factor for the overburden zone, describes the delaying influence of the rock mass [year $^{-1}$].

3. EXAMPLES FOR THE SUBSIDENCE PREDICTION ON SOME MINERAL DEPOSITS

Having assumed such a model of a function of time with two parameters, let us characterize the deformation process for ***salt cavity*** exploitation.

The magnitude of ground subsidence over slim salt cavities is mainly modifiedby lateral convergence. This process takes place radially, as shown in Fig. 2.

The subsidence on the surface can be described by the following formula:

$$S(d,t) = S_{\max}(t) \cdot \exp\left(-\pi \frac{d^2}{\bar{r}^2}\right) \tag{3}$$

where:

$\bar{r} = \sqrt{r_o \cdot r_u}$,

r_o - radius of main influences of the cavity roof,
r_u - radius of main influences of the cavity bottom,

$S_{max}(t)$ - maximum subsidence depending on the assumed geometrical model of convergence (Haupt et al., 1983).

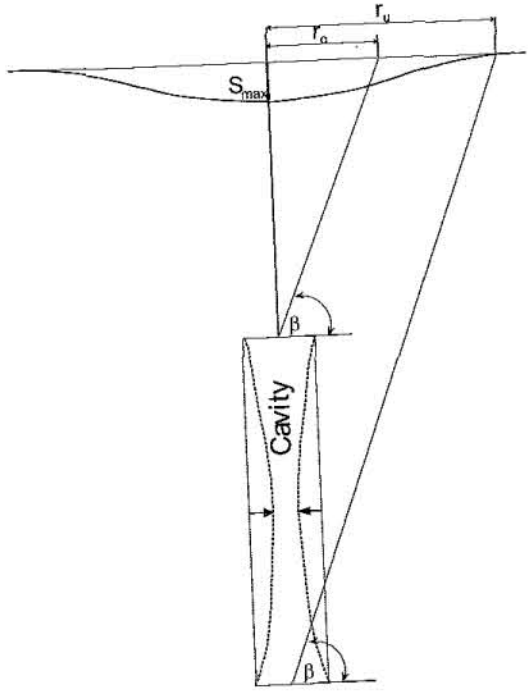

Figure 2. Depression over salt cavity

Based on the presented model, the subsidences over the field of 33 salt cavities were predicted. For the results see Fig. 3 (Sroka, 1984).

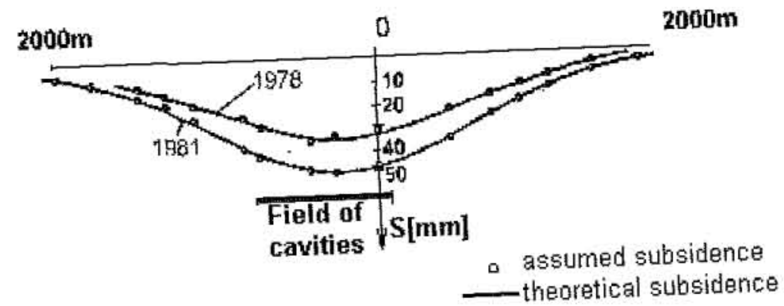

Figure 3. List of assumed and calculated values of subsidence over a field of salt cavities

Knothe's theory can be also applied for the calculation of subsidences over a ***room-and-pillar*** exploitation if the solution for a deposit element was assumed

(1). In such a case it is possible to describe the two-parameter time model (2) in a great detail, accounting for the development of the convergence process exactly in the region of excavations. The matching of the theoretical and measured depression in the region of copper ore extraction in three spans of time, has been presented in Fig. 4.

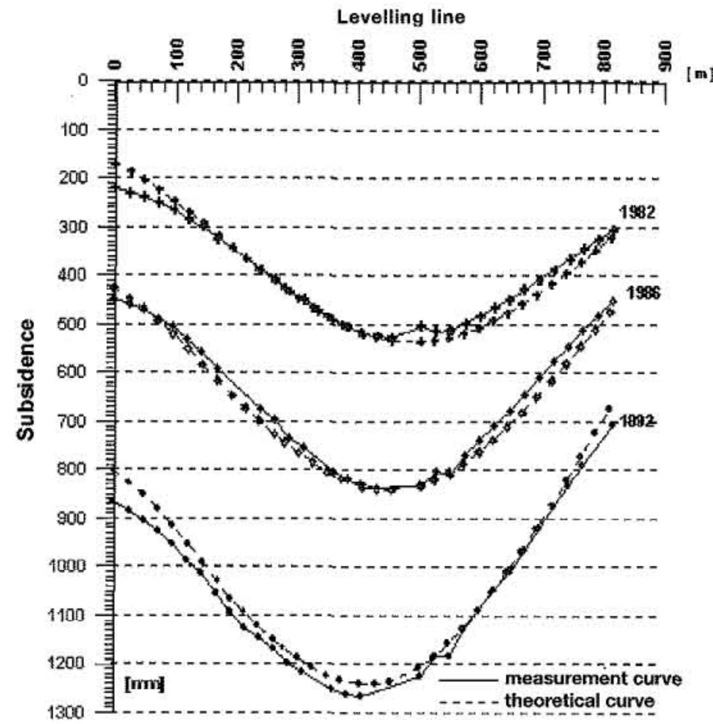

Figure 4. Depression over a room-and-pillar copper ore excavation

The calculations for the first case (as in Fig. 4) were based on the relation (1), for the assessed values of Knothe's theory parameters and time parameters. The time factor for the workings area (ξ) depends on the strength of safety pillars and possible the backfilling. As mentioned earlier, it describes the relative rate of roof convergence. Having discretized the deposit in the form of elements it is possible to account for the variability of attributes of the analysed deposit (distribution of thickness, depth, system of pillars and volumetric convergence of workings), and also for extraction technology modelling (direction of extraction and time) in the calculation method. This often suffices to obtain an almost complete matching of the model and actual mining-geologic conditions. Needless to say how much it affects the accuracy of the deformation prognosis.

The last of the presented applications of Knothe's theory is the prediction of ground subsidence over ***oil and gas fields***. This problem also affects the issues typical of deformations accompanying gas stores in porous geologic basins, underground gas removal from coal beds and underground water withdrawal.

The calculation algorithm bases on deposits discretisation and ascribing of local parameters (i.e. co-ordinates, thickness, original formation pressure, formation pressure in time „t", etc.) to each of the deposit elements (Hejmanowski, 1993; 1995) (Fig. 5).

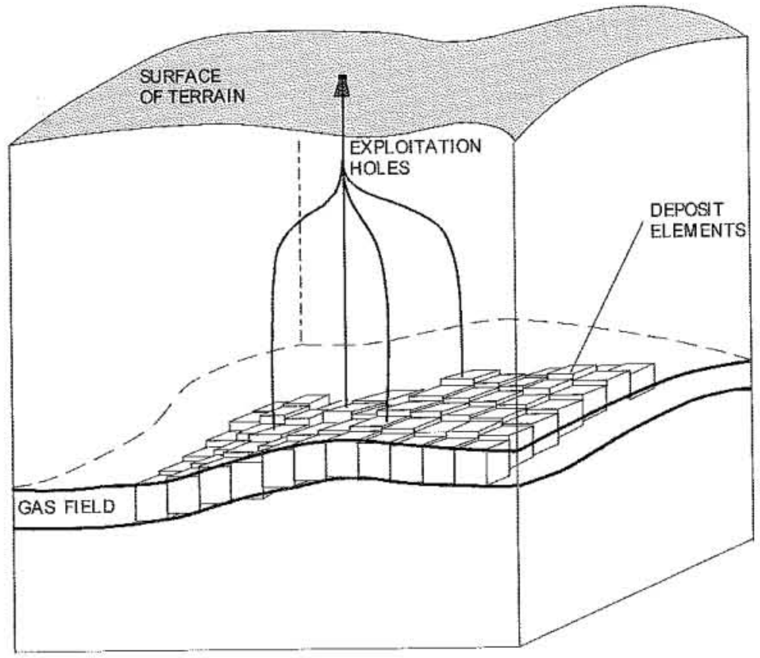

Figure 5. Discretisation of an exemplary gas field

Subsidence caused by the drop of pore pressure in the deposit element can be calculated from the formula:

$$S(d,t) = \frac{a \cdot \Delta M(t) \cdot L^2}{r^2} \cdot \exp\left(-\pi \frac{d^2}{r^2}\right) \tag{4}$$

where:

$$\Delta M(t) = c_m \left(p_0 - p_i(t)\right) \cdot M \tag{5}$$

$\Delta M(t)$ - compaction,
a - coefficient of volume losses in the process of rock mass deformation,
L - length of the edge of the deposit element's base,

c_m - compressibility factor of porous formation rock,
p_0 - original formation pressure,
$p_i(t)$ - formation pressure in the i-th element in moment t,
M - original thickness of the reservoir.

The result of calculations for a stage of subsidence prognosis for one of the European gas fields has been presented in Fig. 6. The calculation method based on Knothe's theory has been presented in its simplest form.

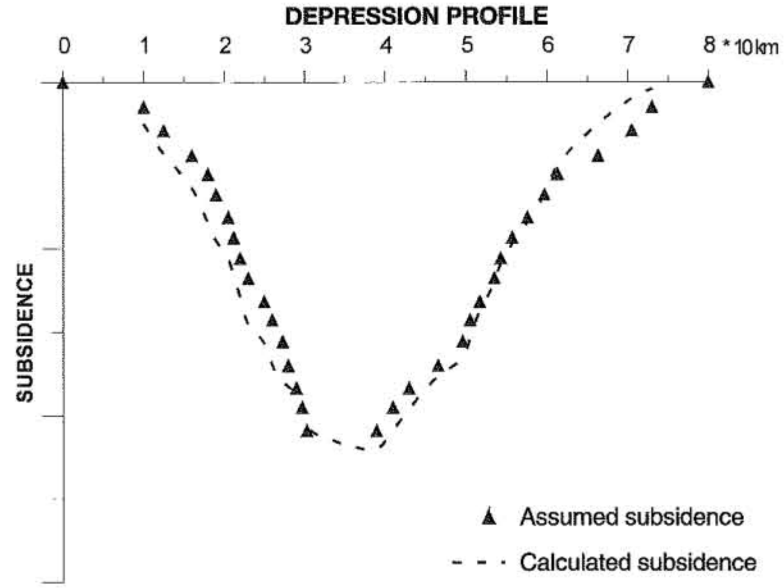

Figure 6. Comparison of predicted and calculated depressions for a gas field

4. SUMMARY

The three applications of Knothe's theory presented in the paper do not exhaust the existing possibilities. The aim of the paper is to show that it is possible to calculate subsidences for complex formations with the use of a relatively simple calculation method. This method employs two parameters (a and β) and time coefficients (ξ, c), where one describes the course of convergence, and so, the source of deformation, and the other one - the course of deformation through the rock mass layers.

The importance of the description of both components (cause of deformation and transition function) constitutes the essence of the approach. Satisfactory results can only be obtained via an accurate and correct characteristic of the source of deformation.

As practical experience shows the application of the time model for this purpose allows one to reach the reliable results of prognoses of surface deformations.

Acknowledgements

The research was financially supported by the State Committee for Scientific Research, Project N° 9 T12A 042 16 (1999-2001).

REFERENCES

Bals R. (1931) Beitrag zur Frage der Vorausberechnung bergbaulicher Senkungen, *Mitt. aus dem Markscheidewesen.* Nr 42/43, 98/111.

Haupt W., Sroka A., & Schober F. (1983) Die Wirkung verschiedener Konvergenzmodelle für zylinderformige Kavernen auf die übertägige Senkungsbewegung. *Das Markscheidewesen*, 90(1983), Nr 1.

Hejmanowski R. (1993) Zur Vorausberechnung förderbedingter Bodensenkungen über Erdöl- und Erdgaslagerstätten. *Doctor's thesis, Technical University Clausthal*, Clausthal-Zellerfeld.

Hejmanowski R. (1995) Prediction of surface subsidence due to oil- or gasfield development in *Land Subsidence* Proceedings of the Fifth International Symposium on Land Subsidence FISOLS'95 (ed. by F.B.J. Barends, F.J.J. Brouwer, F.H. Schröder), The Hague, Netherlands, 16-20 October 1995, 291-300.

Keinhorst H. (1925) Die Berechnung der Bodensenkungen im Emschergebiet. *Festschrift 25 Jahre Emschergenossenschaft*, Essen, 347/50.

Knothe S. (1953) Równanie ostatecznie wykształconej niecki osiadania. *Archiwum Górnictwa i Hutnictwa*, tom 1, z.1, 1953. (Equation of a finally developed depression. In: *Mining and Metallurgy Archives*, Col. 1, Bull. 1).

Kochmański T. (1959) Integral-Theorie der Bodenbewegungen unter Einwirkung des Abbaus. *Freiberge Forschungshefte.* A 118, 36/58.

Litwiniszyn J. (1956) Application of the equation of stochastic process to mechanics of loose bodies. *Archiwum Mechaniki Stosowanej, Vol.8*, Krakow, Poland.

Sroka A. (1984) Abschätzung einiger zeitlicher Prozesse im Gebirge. *Schriftenreihe Lagerstättenerfassung und -darstellung Bodenbewegungen und Bergschäden, Ingenieurvermessung.* Kolloquium Leoben 15/16.11.1984.

Sroka A., Schober F., Sroka T. (1987) Ogólne zaleznoœci miedzy wybrana objetoscia pustki poeksploatacyjnej a objetoœcia niecki osiadania z uwzglednieniem funkcji czasu. *Ochrona Terenów Górniczych*, nr 79/1, Katowice. (General relations between a selected volume of past-extraction voids and volume of depression, accounting for the function of time. In: *Mining Terrain's Protection*, no. 79/1, Katowice).

LAND SUBSIDENCE - Vol. II
Proceedings of the Sixth International Symposium on Land Subsidence
Ravenna / Italy / 24-29 September 2000

MATHEMATICAL MODELLING OF SUBSIDENCE AT AND AROUND BOLOGNA (NORTHERN ITALY)

Franco Francavilla
Università di Bologna, Dipartimento di Scienze della Terra e Geologico-Ambientali, Via Zamboni 67, 40126 Bologna, Italy

Rinaldo Genevois and Roberta Paretini
Università di Padova, Dipartimento di Geologia, Paleontologia e Geofisica, Via Giotto 1, 35137 Padova, Italy

Abstract

Considerable land lowering has occurred throughout the area of the city of Bologna (Northern Italy), due to intensive exploitation of groundwater since the 1950s. The rate of lowering, which differs from area to area, is still quite fast. The aim of the present work - presented here in the form of poster - was to undertake mathematical modelling in order to predict the future development of this phenomenon, and involves careful reconstruction of subsoil lithology, determination of the physico-mechanical features of fine-grained materials, and measurements of water table oscillations over time. Modelling was carried out using a finite differences code (FLAC) on two stratigraphic sections of particular interest, and supplied results which could be compared with land settlement measured directly by means of precision topographic surveys.

Keywords: subsidence, soil mechanics, mathematical modelling, Bologna.

1. INTRODUCTION

The phenomenon of subsidence due to water pumping has been extensively studied in the past (e.g.: Gambolati and Freeze, 1973; Gatto and Carbognin, 1981; Poland, 1981; Lewis and Schrefler, 1998).

Current subsidence in the area of the city of Bologna, although it undergoes natural subsidence of about 2 mm/year, is without doubt mainly due to groundwater pumping. Reduced pore pressures cause an increase in effective stress, with consequent settling of compressible soil layers.

Systematic exploitation of groundwater for civil and industrial use began in the 1950s and, since then, has caused considerable soil settlement, especially in the plain area north of Bologna. The city centre is now in a particularly critical position between the practically stable foothills and the flatter area subject to maximum subsidence.

Surveys carried out between 1970 and 1983 in two peripheral areas west and north of Bologna, on the sides of the large fan of the river Reno, revealed maximum overall settlement of almost 2.5 m, with average rates of 15-16 cm/year. However, more recent measurements have recorded a reduction in rate, maximum subsidence now being estimated at about 8 cm/year (Borgia et al., 1995).

2. SUBSOIL LITHOLOGY

Many data have revealed the highly complex soil lithology of the study area, prevailing gravel and clay mainly alternating with smaller quantities of sands.

The main features of the study area (Figure 1) are clear-cut: the fan of the river Reno, the interfan area, and the fan of the river Savena.

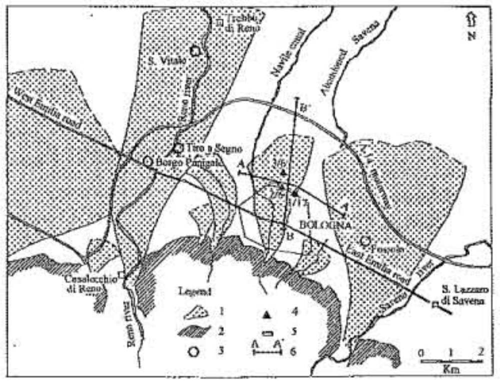

Figure 1. Location of study area. 1) Fans; 2) margin of foothills; 3) water management centres; 4) benchmarks; 5) railway station; 6) cross-sections. (From Elmi et al., 1984, modified).

The Reno fan is long and narrow, indicating that the river remained more or less in the same position for a long period of time. The fan contains very thick layers of gravel, which may be found even at the northern end of the study area.

The Savena fan is wide and splayed open, showing that this watercourse underwent many natural or artificial diversions over time. Its gravel layers are less thick, sometimes sandy, and with little lateral continuity.

The interfan area, which includes the city centre of Bologna, is composed of sometimes very thick clay layers. The few gravelly-sandy deposits found at great depth are attributed to the fans of minor watercourses or to diversions of the two main rivers.

3. PHYSICO-MECHANICAL CHARACTERISTICS

Of particular interest is geotechnical characterization of fine-grained materials, since these are responsible for almost all settling.

According to the Casagrande Plasticity Map, the 98 samples examined here are mainly classified as inorganic clays of medium and high plasticity.

Mean values and relative standard deviations of the main physical and mechanical features are shown in Table 1. The volumetric compressibility coefficient (m_v, m^2/MN) was calculated around the value of effective vertical pressure in situ.

Table 1. Geotechnical characteristics of fine-grained materials.

	Mean	S.D.	N° of tests
γ (KN/m^3)	19.45	0.65	300
w (%)	27.9	5.0	300
m_v (m^2/MN)	0.14	0.05	21
c_{uu} (KN/m^2)	98	46	48
c' (KN/m^2)	26.2	16.2	19
φ' (°)	23.7	2.2	19

4. WATER TABLE OSCILLATIONS

Until the early years of the 20th century, it is presumed that the water table was everywhere at a maximum depth of about 4 m from ground level. Later, above all when the main aqueduct management centres were set up (Figure 1), the piezometric level steadily fell, in ways varying from place to place, until it reached a maximum depth of about 70 m from ground level.

In the late 1980s, water table lowering in the Savena fan was attenuated and, in the case of the river Reno, even reversed. However, the piezometric level was generally always lower in the western sector of the study area, certainly due to the greater quantities of water pumped by the water management centres of Borgo Panigale, Tiro a Segno and S. Vitale.

In the interfan area a series of more or less impermeable layers separate a deep aquifer from a superficial one which, over time, has maintained a constant piezometric level (about -4 m) thanks to feedwaters coming directly from the foothills.

The trend of the piezometric level of the deep aquifer in the interfan area generally follows that of the aquifer in the fan nearer to it. The deep aquifer is therefore probably connected with that of the two fans.

5. MATHEMATICAL MODELLING OF SUBSIDENCE

Mathematical modelling of subsidence was carried out by means of a finite differences code (Fast Lagrangian Analysis of Continua, FLAC) on the basis of two particularly significant cross-sections (Figure 1).

The years considered for modelling are 1900, 1970-1986 and 1990, the latter taken as a symbolic date of piezometric levels stable to infinity. Analysis was uncoupled, i.e., flow and mechanical deformations were treated separately for the sake of simplicity.

Analytical results for transversal section A-A', which crosses the interfan area approximately following the railway line, gave a maximum lowering value of 2.63 m, due exclusively to groundwater pumping (Figure 2).

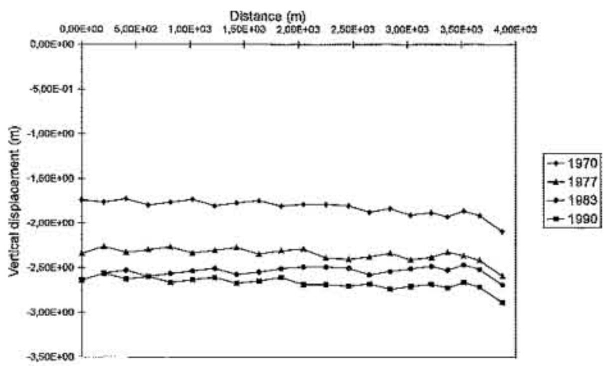

Figure 2. Settlements calculated along section A-A'.

The longitudinal section (B-B') in the interfan area, crossing the city centre, gave a maximum lowering value of 2.25 m at the point where it intersects section A-A' (Figure 3).

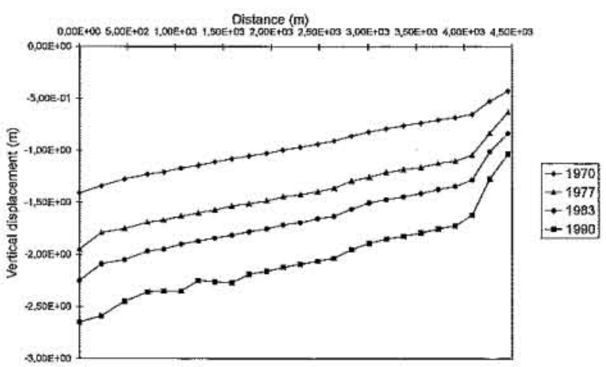

Figure 3. Settlements calculated along section B-B'.

Figure 4 shows settling trends measured topographically, starting from 1950, at three benchmarks near the railway station (1/17, 2/6, 3/6), together with trends calculated numerically at the two nearest points of the analysed sections.

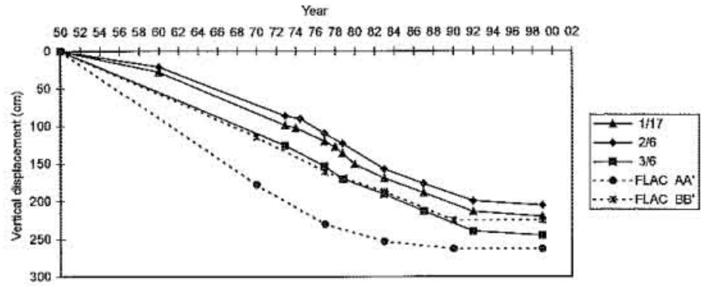

Figure 4. Settling trends measured experimentally (1/17, 2/6, 3/6) and calculated numerically (FLAC AA' - FLAC BB').

The difference between the two FLAC curves is due to the differing spatial distribution of the hydraulic load and stratigraphy of the two sections. It should not be forgotten that the model is a continuum and that all points are also influenced by the lowering of nearby points. However, only for section A-A' is there reliable distribution of water pressure in the subsoil; for section B-B' available data are not sufficient to exactly define the piezometric level and its trends in time. Moreover, the model is only two-dimensional and thus does not take into account the three-dimensional complexity of the actual lithological and hydraulic situation.

Results show that settling trends over time in the longitudinal section fit measured values quite well; higher values (not exceeding 15%) are found in the transversal section.

It must also be recalled that the benchmarks were only measured from the 1950s onwards, while FLAC analysis begins with the year 1900. During mathematical modelling, consolidation was taken to 100% year by year, whereas it is in fact constantly delayed with respect to water table lowering. In addition, FLAC settling values are to be added to natural subsidence of about 2 mm/year.

6. CONCLUSIVE CONSIDERATIONS

Mathematical modelling of subsidence in the Bologna area, carried out until now, allows the following considerations to be made:

1. great difficulties are found in reconstructing the stratigraphic setting;
2. available data do not include data representing the trend of the piezometric surface from the late 1980s onwards;
3. numerical modelling must take into account true consolidation trends, so that coupled analyses must be carried out;

4, better representation could be obtained with three-dimensional coupled analyses.

In spite of these difficulties and limitations, the results obtained are quite satisfactory. Mathematical modelling may be applied as a valid instrument, not only for studying the phenomenon, but also for proper planning of future exploitation of groundwater's, by means of simulations of varying intensities and methods of pumping.

The preparation of a three-dimensional mathematical model, together obviously with improvements to the two-dimensional model presented here, will certainly contribute to further steps towards 'sustainable development', for the collective benefit of all.

REFERENCES

Borgia, G.C., Brighenti, G. & Mesini, E. (1995) Subsidenza della Pianura Padano-Veneta da produzione di fluidi dal sottosuolo. Parte II: Case histoires (Subsidence in the Po-Venetian Plain due to fluid withdrawal. Part II: Case histories). In: *Acque sotterranee*, **1**, 55-70.

Elmi, C., Bergonzoni, A., Massa, T. & Montaletti, V., with the contribution of Baratella, P.L. & Ronchi, A. (1984) Il territorio di pianura del Comune di Bologna: aspetti geologici e geotecnici (The plain area of the municipality of Bologna: geological and geotechnical aspects), *Giornale di Geologia*, **46** (2), 127-152.

Gambolati, G. & Freeze, R.A. (1973) Mathematical simulation of the subsidence of Venice, 1, Theory, *Water Resources Research*, **9**, 33-721.

Gatto, P. & Carbognin, L. (1981) The lagoon of Venice: natural environmental trend and man-induced modification, *Hydr. Sci. Bull.*, **26** (4), 91-379.

Lewis, R.W. & Schrefler B.A. (1998) *The Finite Element Method in the Static and Dynamic Deformation and Consolidation of Porous Media*. Wiley Ed., Chichester, 492 pp.

Poland, J.F. (1981) Subsidence in United States due to groundwater withdrawal. In: *J. Irr. Drain Div. ASCE*, 107 (IR2), 35-115.

LAND SUBSIDENCE - Vol. II
Proceedings of the Sixth International Symposium on Land Subsidence
Ravenna / Italy / 24-29 September 2000

SPATIAL TEMPORAL MODELLING OF LAND SUBSIDENCE DUE TO GAS EXTRACTION

Frank Kenselaar and Marcel Martens
Delft University of Technology, Department of Mathematical Geodesy and Positioning, Thijsseweg 11, 2629 JA Delft, The Netherlands.

Abstract

In this paper land subsidence due to gas extraction is modelled by a continuous spatial temporal trend function. This approach is an answer to the increasing complications in the monitoring of the Groningen gas field, when based on deformation analysis per benchmark, using heights resulting from connected levelling networks. The subsidence model is determined by an extensive stepwise estimation and testing procedure, combining data screening and fine-tuning of both the functional and stochastic model. This procedure is demonstrated on five epochs of levelling data, monitoring subsidence above a small isolated gas field. Moreover, first computations are presented to study the optimal design of the levelling measurements, when employing the qualities of the continuous spatial temporal model.

Keywords: land subsidence, modelling, testing procedure, measurement design

1. LAND SUBSIDENCE ABOVE THE GRONINGEN GAS FIELD

Since 1964 gas is extracted in the Northeast of the Netherlands. The Groningen gas field is one of the largest gas fields in the world, stretching over an area of 900 square kilometers with initial gas reserves of 2900 billion cubic meters. Later on smaller adjacent fields were explored. The gas production results in reservoir compaction and consequently surface subsidence. To date, a maximum subsidence of 23 centimeters has been established. The Groningen case is described extensively, e.g. in several papers in the proceedings of the previous Fifth International Symposium On Land Subsidence (Barends et al., 1995).

Since the start of the production the subsidence is monitored with great care by levelling and GPS networks and compaction measurements. By now, about 25 epochs of levelling networks have been measured and processed. In cooperation with the Nederlandse Aardolie Maatschappij (NAM), the gas producing company, a deformation analysis strategy was developed by Delft University of Technology (DUT) to optimize the processing of the levelling data. This strategy consists of the following steps:

1. *Single epoch analysis* in order to screen the data of each levelling network.
2. *Stability analysis* of the benchmarks.
3. *Kinematic deformation analysis* by modelling a 1-dimensional polynomial subsidence curve per benchmark.

In each step the optimal model was found by an iterative procedure of least-squares adjustment, hypothesis testing and variance component estimation. An overview of this analysis procedure was given in (de Heus et al., 1995).

During the years the area of subsidence has grown. Larger networks were necessary and the search for stable reference points became the most difficult part of the deformation analysis procedure. Half way the nineties NAM and DUT cooperated in a project to use GPS height measurements as an additional tool for the deformation analysis. Although it is known that the accuracy of GPS height measurements still can not compete with levelling, it is a relative efficient method to bridge longer distances (Krijnen and de Heus, 1995; de Heus et al., 1999).

Moreover, years of accurate height data processing have shown that in a country like the Netherlands, with its soft soil, even benchmarks far outside the gas production area can hardly be assumed stable due to natural surface changes and man made causes like salt and water extraction. This is seriously complicating high precision subsidence analysis based on benchmark heights resulting from connected levelling networks. In order to handle these problems a further cooperation between NAM and DUT started at the end of 1998. Research was following a new approach based on two basic concepts that were suggested by NAM (Houtenbos, 2000):

1. In order to exploit the smooth behavior of the subsidence caused by gas extraction, both in space and time, a *continuous spatial temporal trend function* is used to model the subsidence bowl above a gas field, at least as a first approximation at the centimeter level.
2. Instead of using benchmark heights obtained from connected levelling networks, the subsidence analysis is based on the *original levelled spatial height differences*. In this way relative deformation analysis can be performed without the assumption of stable reference benchmarks.

In this paper we will describe the estimation and testing procedure of the spatial temporal subsidence model and demonstrate it for a small gas field. A first study is carried out towards the optimal design in space and time of the levelling measurements and the potential of the approach for further development and research is discussed.

2. A SPATIAL TEMPORAL SUBSIDENCE MODEL

In a continuous spatial temporal subsidence model the land subsidence in time in each point is described as a function of its positional coordinates (x_i,

y_i), the time-lag ($t - t_0$) since the beginning of subsidence and parameters describing the subsidence:

$$z_{i,t} = f(x_i, y_i, t - t_0, par) \qquad \text{for} \qquad t_0 < t < t_{\text{end}}\,. \tag{1}$$

The model used here assumes in each point a *constant subsidence velocity*, exponentially descending with the *ellipsoidal distance* to the center of the subsidence bowl:

$$z_{i,t} = s.(t - t_0).e^{-\frac{1}{2}(u_i^2 + v_i^2)} \qquad \text{for} \qquad t_0 < t < t_{\text{end}} \tag{2}$$

with $u_i = \dfrac{(x_i - x_0)\sin\alpha + (y_i - y_0)\cos\alpha}{a}$, $v_i = \dfrac{(x_i - x_0)\cos\alpha - (y_i - y_0)\sin\alpha}{b}$,

where t_0 is the time of the beginning of subsidence, s is the linear subsidence velocity in the center of the bowl, x_0 and y_0 mark the position of the center and a, b and α describe the shape of the subsidence ellipse, i.e. the length of the long and short axes to the point of inflection and the orientation.

This model is described in more detail in (Houtenbos, 2000). In principle the parameters can be estimated from observed heights, height differences between points and height differences in time. The time of the beginning of the subsidence t_0 can only be estimated if height data is available before gas production. Otherwise it should be constrained on an a priori value. The model is primarily based on the experienced behavior of benchmarks. For a single gas field such a simple and smooth model fits the geodetic data quite well, mainly because of the great depth of the gas layer (3 km). The parameters have no direct geophysical interpretation.

The parameters of the subsidence bowl are presently determined from observed height differences by an iterative least squares estimation of a linearized model of observation equations. For a levelled height difference between two benchmarks, the *observation equation* reads

$$\underline{h}_{ij,t} = -H_{i,0} + H_{j,0} + z_{i,t} - z_{j,t} + \underline{e}_{ij,t}\,, \tag{3}$$

with $h_{ij,t}$ the levelled height difference between benchmarks i and j at epoch time t, $H_{i,0}$ the initial height of benchmark i before the beginning of subsidence, $z_{i,t}$ the subsidence of benchmark i since the beginning of subsidence, according to model (2) and $e_{ij,t}$ a stochastic error.

The stochastic error consists of several noise components. Presently the stochastic model accounts for:

- *Measurement noise*. The levelling measurements are assumed uncorrelated, with a standard deviation increasing with the length of the trajectory, e.g. 0.7 mm/√km.
- *Point noise*, in order to account for the small benchmark instabilities due to other causes than gas production. This is described by a standard deviation per benchmark, increasing with the time lag since the first epoch of measurements, with an initial value of 0.6 mm/√year. This stochastic model induces time correlation between the benchmark heights at several epochs.
- *Model noise*. Since the spatial temporal subsidence model is only considered a good first approximation of the land subsidence above a gas field, remaining local and temporal discrepancies are accounted for in the stochastic model. First computations were based on a scaled unit matrix per epoch for the model noise. Further analysis of the remaining signal after removing the estimated trend model should result in a better knowledge of the model noise. Both spatial and temporal correlation can be expected.

Based on observation equations (3) and the assumptions made on the stochastic model, the *linearized model of observation equations* for the levelled height differences in a network at epoch time t can be written as

$$E\{\Delta \underline{h}_t\} = W_t (P_t \quad Z_t)\begin{pmatrix}\Delta H_0 \\ \Delta p\end{pmatrix}; \quad D\{\Delta \underline{h}_t\} = Q_{w_t} + W_t (Q_{p_t} + Q_{m_t}) W_t^T \tag{4}$$

with Δh_t the vector of m_t linearized levelled height differences in the levelling network at epoch time t, matrix W_t relating levelled height differences and benchmark heights at epoch time t (the levelling network matrix), P_t a permutation matrix selecting the n_t benchmarks occupied at epoch time t from the complete set of n benchmarks, coefficient matrix Z_t containing the partial derivatives of equations (2) to the 7 unknown parameters, ΔH_0 the vector of n linearized initial benchmark heights and Δp the vector of 7 linearized parameters describing the subsidence bowl. Variance matrices Qw_t , Qp_t and Qm_t respectively describe the measurement, point and model noise at epoch time t.

In the complete model the levelling networks at all epochs are taken into account in one integrated adjustment. From formulation (4) it can clearly be seen that the estimation of the subsidence model from levelled height differences combines the adjustment of the individual free levelling networks and the actual estimation of the spatial temporal model subsidence parameters. To solve this model only for one randomly chosen benchmark the initial height needs to be constrained. This choice influences the estimation of the initial heights by a translation, not the subsidence model itself.

3. THE ESTIMATION AND TESTING PROCEDURE

The subsidence analysis is based on determination of the optimal subsidence bowl fitting through the levelling data in a *stepwise procedure* of *iterative least-squares estimation, hypothesis testing* and *variance component estimation*. In each step, after iterative least-squares estimation of the subsidence model, the model and data – the null hypothesis (H_0) – is tested against a large number of alternative hypotheses (H_a), each specifying a model adaptation or possible error(s). The alternative hypotheses are specified as a linear extension of the null hypothesis with q additional error components, q being the dimension of the test:

$$H_0: \; E\{\underline{y}\} = A.x \quad \text{versus} \quad H_a: \; E\{\underline{y}\} = A.x + C.\nabla \tag{5}$$

with, in case of our subsidence model: y the vector of $\sum m_t$ levelling observations, $A.x$ the linearized model of observation equations with vector x containing n+7 unknown initial benchmark heights and parameters of the subsidence bowl and $C.\nabla$ a linear(ized) model extension with vector ∇ containing q unknown possible errors.

The *test quantity* for testing the null hypothesis against a specific alternative hypothesis can be computed from the adjustment results of the null hypothesis and the matrix C, specifying the alternative hypothesis under study:

$$\underline{T}_q = \hat{\underline{e}} Q_y^{-1} C (C^T Q_y^{-1} Q_{\hat{e}} Q_y^{-1} C)^{-1} C^T Q_y^{-1} \hat{\underline{e}}, \tag{6}$$

with and the least-squares residuals under the null hypothesis and the corresponding covariance matrix. Assuming the observations obey a normal distribution, this test quantity is Chi-squared distributed with q degrees of freedom. Thus, with a level of significance α the null hypothesis is rejected in favor of the alternative hypothesis if $T_q > \chi^2_\alpha(q)$.

Before making any further inferences a so called *overall model test* of the null hypothesis is computed, as a general check whether the data fits the subsidence model within the tolerances as specified in the stochastic model. This test quantity can easily be computed as the length of the vector of least squares residuals. The dimension of the test equals the redundancy of the model:

$$\underline{T}_q = \hat{\underline{e}} Q_y^{-1} \hat{\underline{e}} \sim \chi^2(q) \quad \text{with} \quad q = \sum_t m_t - (n - 1 + 7). \tag{7}$$

As long as the overall model test is rejected, identification of the most likely error is supported by specifying various alternative hypotheses. The most significant error is identified by the largest rejected test quantity. Since tests of different dimension can not be compared straightforwardly, actually the quotients of test quantity and critical value are compared (). The largest rejected test quotient points to the most likely error in the null hypothesis and requires specific adaptations in the model or data set. After adaptation of the null hypothesis for this error the estimation and testing procedure is repeated.

Presently the null hypothesis is tested against the following alternative hypotheses:

- Observational errors in the levelling data (*observation test*). By so called datasnooping a possible error is tested in each of the observations. Implying $\sum m_t$ 1-dimensional tests. In case an observation test has the largest rejected test quotient the levelled height difference is excluded from the data set.
- Identification errors (*identification test*). For each benchmark a deviation from the subsidence model in a single epoch is tested. Implying $\sum n_t$ 1-dimensional tests. When marked as the most likely error, the benchmark is excluded from the data set in the identified epoch. In this case a new observation is formed, excluding the rejected benchmark but still using all the levelling data.
- Deviating behavior of a benchmark (*point test*). For each benchmark an unspecified deviation in all epochs from the subsidence model is tested. Implying n tests with a dimension equal to the number of epochs the benchmark is occupied, minus one. In case a point test has the largest test quotient the benchmark is excluded from the data set in all epochs.
- Autonomous linear behaviour of a benchmark (*ALB test*). Each benchmark is tested for a linear velocity of subsidence, deviating from the subsidence model. Implying n 1-dimensional tests. In case a test for ALB has the largest rejected test quotient the model is extended with an additional linear subsidence velocity for this benchmark.
- Deviating epoch of levelling data (*epoch test*). It is tested whether a complete epoch is deviating from the subsidence model. Implying a number of tests equal to the number of epochs with dimension n_t. Since it is not very realistic to exclude a complete epoch from the data set, in case an epoch test has the largest rejected test quotient, further investigation is necessary. Rejection of the epoch test could e.g. be caused by remaining systematic errors in the levelling network or the model assumption of constant subsidence velocity fails. It could also be a reason for adaptation of the stochastic model.
- In case the *overall model test* has the largest rejected test quotient the data and model just do not match, without a specific alternative hypothesis indicating the problem. Further investigation is necessary. For example too optimistic assumptions have been made for the stochastic model.

Also in earlier studies (Verhoef and de Heus, 1995) such a stepwise estimation and testing procedure has proven to be very useful for combined data screening and kinematic deformation modelling. In successive steps multiple errors will be identified and both the functional and stochastic model can be refined.

4. EXAMPLE: THE ROSWINKEL DATA SET

The estimation of the subsidence bowl and the hypothesis testing analysis procedure has been implemented in software. First computations were performed on the so-called *Roswinkel gas field*. This is a small isolated gas field south of the Groningen area. Five epochs of levelling networks were measured in 1980, 1985, 1990, 1994 and 1997, the first one before gas production in 1983 (see Figure 1). Note that the individual levelling networks have very low redundancy. Free network adjustment of the individual epochs will yield little information about the data quality. Therefore, the standard deviation of the measurement noise was initially set at a standard value of 0.7 mm/√km for all networks. Moreover, the first four networks are extended to the south while the last one is only extended to the north, thus complicating the search for stable reference points, available in all epochs. Therefore, straightforward adjustment of all levelling data by integration in a continuous spatial temporal subsidence model could support the data analysis.

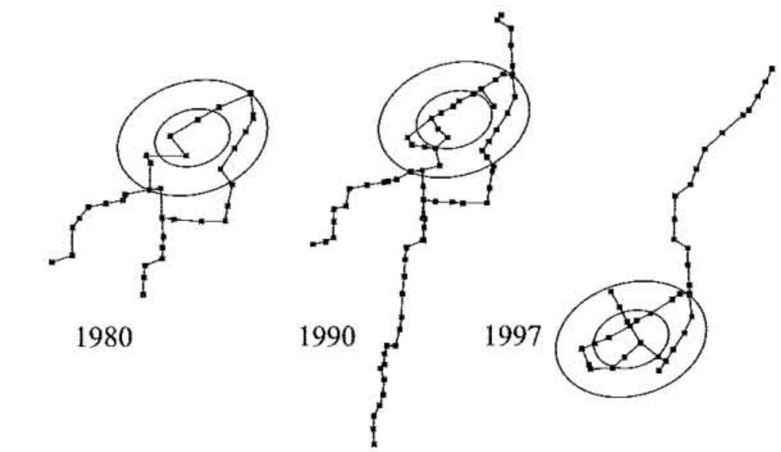

Figure 1. The Roswinkel dataset, epoch networks 1980, 1990 and 1997.

In this paper we briefly discuss *two analysis computation variants*, both initially assuming measurement noise only, point and model noise were a priori set to zero. In the stepwise estimation and testing procedure successive model adaptations were undertaken based on evaluating the alternative hypothesis with the largest rejected test quotient, until either the overall model test or one of the epoch tests resulted in the largest test quotient. It was then concluded that the data would not fit the subsidence model, within relaxation for measurement noise only. The stochastic model was extended by either:

A. Accounting for *point noise* with a standard deviation of 0.6 mm/√year.

B. Accounting for *model noise* with a standard deviation of 1.0 mm.

In Table 1 a summary is given of the successive test results and model adaptation in the stepwise procedure.

Table 1. Summary of successive test results and model adaptations.

Step	Alternative hypothesis with largest test quotient (actual largest test quotient between brackets)	Model adaptation
1	ALB point no. 18A0090 (57.14)	additional velocity term
2	ALB point no. 18A0006 (27.43)	additional velocity term
3	point test no. hp0650 (26.57)	point excluded from data set
4	ALB point no. 18A0089 (10.97)	additional velocity term
5	epoch test network 1980 (5.78)	variant A or B
	Variant A: extension of stochastic model for point noise, σ = 0.6 mm/√year	
6A	observ. test 18C0095 – 18C0152 in 1994 (1.67)	observation excluded from data set
7A	epoch test network 1980 (1.08)	meas. noise 1980 σ = 0.8 mm/√km
8A	largest test quotient is 0.98 (overall model test)	accept model
	Variant B: extension of stochastic model for model noise, σ = 1.0 mm	
6B	observ. test 18C0095 – 18C0152 in 1994 (2.03)	observation excluded from data set
7B	epoch test 1980 (1.56)	meas. noise 1980 σ = 0.8 mm/√km
8B	observ. test 18C0097 – 18C0095 in 1980 (1.41)	observation excluded from data set
9B	largest test quotient is 1.05 (epoch test 1994)	accept model

The redundancy of the accepted model is 134 for variant A (225 observed height differences, 81 unknown initial benchmark heights, 7 unknown parameters of the subsidence bowl and 3 individual benchmark velocities) and one lower for variant B. In case the hypothesis of autonomous linear behavior (ALB) of a benchmark is accepted it is assumed that the subsidence velocity of such a benchmark significantly deviates from the general velocity of the trend model. The model is extended with an additional velocity parameter for this benchmark. As an example, the estimated velocity for benchmark 18A0090 is 1.3 mm/year lower than according to the subsidence model. In step 7 epoch 1980 is pointed as problematic, without identification of specific errors. It was decided to increase the measurement precision of this epoch network to σ = 0.8 mm/√km.

In Table 2 the *estimated parameters of the subsidence bowl* are presented for both variant A (point noise σ = 0.6 mm/√year) and B (model noise σ = 1.0 mm). The differences, caused by the chosen stochastic model and one extra excluded observation in variant B, fall within the standard deviation.

Table 2. Estimated parameters of the subsidence bowl.

Parameter	Variant A		Variant B	
	value	σ	value	σ
Subsidence velocity (mm/year)	-10.1	0.2	-10.4	0.2
Beginning of subsidence (days)	Feb 13, 1984	80	Mar 6, 1984	78
X-position center of bowl (m)	266341	49	266365	37
Y-position center of bowl (m)	539502	34	539493	25
Half long axis subsidence bowl (m)	1863	50	1848	40
Half short axis subsidence bowl (m)	1358	52	1317	39
Orientation of subsidence ellipse (gon)	82.4	3.5	81.7	2.5

5. OPTIMIZATION OF THE LEVELLING MEASUREMENTS

The analysis of the Roswinkel data set gave first insight in the very promising possibilities of the continuous spatial temporal subsidence model and the stepwise estimation and testing procedure. It showed the possibility for high accuracy monitoring of land subsidence with low redundancy levelling networks and without the difficult connection to stable reference points.

In order to gather more experience into the estimability of the subsidence bowl from levelled height differences, some *design studies* were carried out to optimize the measurement setup and the frequency of the levelling networks. A single subsidence bowl is assumed, nearly three times larger than Roswinkel, with the following characteristics:

- subsidence velocity in center of bowl: -10.0 mm/year
- long and short axes of the ellipse: 5000 and 3500 m
- argument of the long axis: 80 gon
- measurement noise standard deviation: 0.7 mm/√km
- point noise standard deviation: 0.6 mm/√year
- zero model noise.

Five types of levelling networks were analyzed (see Figure 2), measured in five epochs with 4-year interval. The beginning of subsidence is taken halfway the first and second epoch.

A. *Network A* is a regular grid of levelling lines with about 3 km point distances. Within the area of two times the axes of the subsidence bowl, points were added halfway the levelling trajectories. Such a dense and regular network will probably yield best results, but is also very expensive to measure and maintain. In this study it serves as a reference for more efficient network designs.

B. *Network B* is equal to A, but without the point densification in the central area, in order to show the influence of point density.

C. *Network C* is formed by two crossing levelling lines, following the axes of the ellipse.
D. *Network D* is analogous to C, but with the orientation of the levelling lines about 50 gon different from the axes.
E. *Network E* consists of six unconnected short levelling lines, more or less radial from the center of the subsidence bowl.

With about 40 km of levelling, networks C, D and E are considerable more efficient than A and B (250 km of levelling). It may be clear that the precision and reliability of the estimation from C, D and E will not match A and B. Question is whether the quality will still be good enough. It is important to note that the precision and reliability figures of the design computations are valid under the assumption that the model is correct, implying that if we would have real data it can be described by the subsidence model, within the assumed standard deviations for measurement and point noise. Measurement and point noise are taken equal to Roswinkel, variant A, were this was indeed the case. However, since the subsidence area assumed is considerably larger than Roswinkel, interpretation of precision and reliability figures should rather be in a relative than an absolute way.

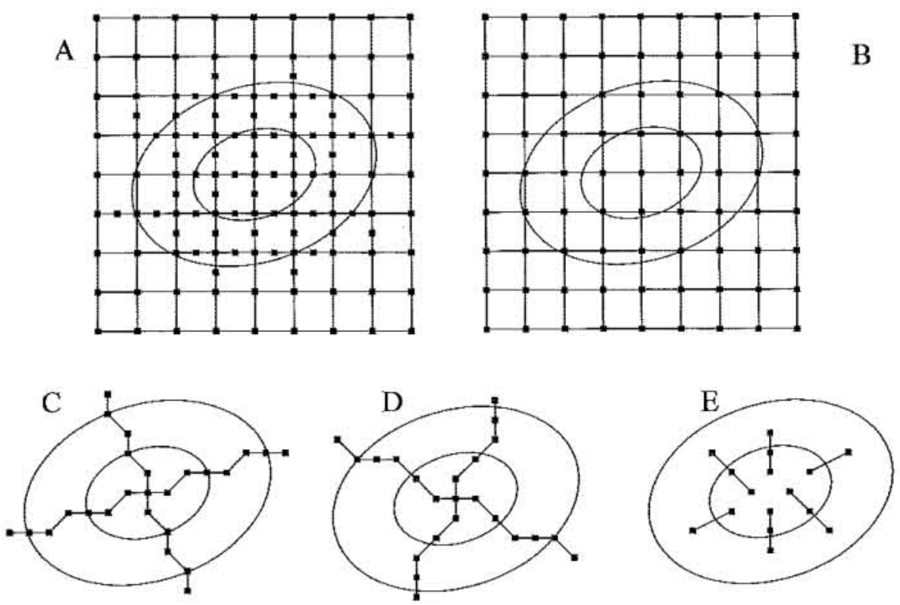

Figure 2. Five network designs A-E.

First, it was assumed that in all five epochs the *same type of network* was measured (data sets denoted e.g. as AAAAA). For network type E (dataset EEEEE) the estimability turned out to be very bad. Since the different trajectories of network E are not connected as a free network, they are only related via the spatial temporal model. This has a very negative influence on the estimability of the initial heights. This data set is left out in this part of the analysis.

In Table 3 the different data sets are compared concerning the precision of the estimated parameters of the subsidence bowl and the initial heights. Also the results of the Roswinkel data set (variant A) are given for comparison. The Minimal Detectable Bias (MDB) is the size of an error in a levelling observable that can just be identified with 50% probability by the observation test, with a level of significance α=0.1%.

Table 3. Summary of design computations for different network types.

	AAAAA (absolute)	relative to data set AAAAA			
		BBBBB	CCCCC	DDDDD	Roswinkel
σ velocity (mm/year)	0.10	1.3	1.9	1.9	2.0
σ begin subsidence (days)	40	1.1	1.6	1.6	2.0
σ X-position center (m)	51	1.3	1.8	2.2	1.0
σ Y-position center (m)	35	1.4	2.0	1.9	1.0
σ half long axis (m)	61	1.3	2.0	**5.4**	0.8
σ half short axis (m)	38	1.4	2.3	**3.6**	1.4
σ orientation (gon)	1.1	1.4	**6.7**	2.3	**3.5**
mean σ initial heights (mm)	1.0	1.1	1.3	1.3	**2.3**
mean levelling MDB (mm)	4.7	1.1	1.2	1.2	1.0
epoch levelling length (km)	250	250	43	41	38
relative redundancy	0.84	0.86	0.70	0.70	0.60

From the table it can be concluded that accurate estimation of the size of the subsidence ellipse is problematic in data set DDDDD. Thus, the levelling profiles better approximately follow the axes of the ellipse, as in data set CCCCC. Meanwhile the opposite conclusion can be drawn concerning the orientation of the subsidence ellipse. Also the Roswinkel networks are less optimal with respect to this point.

Note the reliability, expressed in MDB's of the levelling observables, is not very sensitive with regard to the network design, although the redundancy of the free networks differs considerably. Within the spatial continuous model the levelling observations of all epochs can be considered as one single levelling network, in which each levelling trajectory is measured five times since the same network design is observed in all epochs. The network types C and D have zero redundancy as a free network, but a relative redundancy of 0.70 when processed with the spatial continuous subsidence model.

To exploit the good spatial distribution of network types A and B, as well as the cost efficiency of network types C, D and E, *combinations* of them were further examined. In the first and last epoch network A is assumed, while either network type C, D or E is taken for the other epochs, thus resulting in data sets ACCCA, ADDDA and AEEEA. The dense networks cover the area in order to determine the spatial parameters and identify remaining signals. The sparse networks should confirm the trend.

Precision and reliability of the estimation are summarized in Table 4. For all combinations the precision of the spatial parameters - describing the position and shape of the subsidence ellipse - is improved considerably. The precision of the temporal parameters - velocity and beginning of subsidence - improves slightly but is still a factor 1 - 2 less than for the reference data set AAAAA. On the other hand, a precision of the estimated velocity of better than 0.2 mm/year (2% of the velocity) still seems quite impressive, considering the total length of levelling measurements is half of that of data set AAAAA.

In the last column of Table 4 the improvements are shown if an additional epoch of network E is assumed before the beginning of subsidence (data set AEEEEA). Instead, also a data set was analyzed without the third epoch (denoted as AE–EA). The precision and reliability did not differ significantly from data set AEEEA.

Table 4. Summary of design computations for network combinations.

	AAAAA (absolute)	relative to data set AAAAA			
		ACCCA	ADDDA	AEEEA	AEEEEA
σ velocity (mm/year)	0.10	**1.4**	**1.5**	**1.7**	**1.6**
σ begin subsidence (days)	40	**1.6**	**1.6**	**1.9**	**1.7**
σ X-position center (m)	51	1.0	1.1	1.1	1.1
σ Y-position center (m)	35	1.1	1.1	1.1	1.1
σ half long axis (m)	61	1.0	1.1	1.1	1.1
σ half short axis (m)	38	1.0	1.1	1.1	1.1
σ orientation (gon)	1.1	1.1	1.1	1.1	1.1
mean σ initial heights (mm)	1.0	1.2	1.2	1.1	1.1
mean levelling MDB (mm)	4.7	1.2	1.2	1.2	1.2
total levelling length (km)	1250	628	622	566	588
relative redundancy	0.84	0.66	0.67	0.65	0.66

The design study demonstrates that the increased redundancy, obtained by analysis of the levelling networks with a continuous spatial temporal subsidence model, allows for a more flexible and efficient network design. Also networks with very low free network redundancy suffice, like single profiles, conditioned the benchmarks cover the shape of the subsidence area and are occupied in multiple epochs and the direction of the levelling trajectories is approximately radial from the center of the subsidence bowl.

6. CONCLUDING REMARKS

If a reasonable continuous spatial temporal subsidence model can be specified it has certain distinct advantages for subsidence analysis, compared to the procedure based on kinematic modelling per benchmark, as used in the earlier Groningen analyses. Presently, research concentrates on the extension of the subsidence model to account for overlapping subsidence bowls of multiple gas fields and the stochastic modelling and geostatistical analysis of the remaining signal.

The continuous spatial temporal model allows for relatively easy integration of different measurement techniques. The subsidence bowl can be estimated from spatial height differences from levelling, as well as height differences in time, e.g. obtained point-wise by GPS or with high spatial resolution by SAR. It is not necessary that the different measurement techniques occupy the same points since the continuous subsidence model relates the observables. Moreover, instead of gathering the measurements in epoch networks with a single time label, the spatial temporal subsidence model can also be determined by strict kinematic deformation analysis, assuming an individual time label per observation.

Acknowledgments

This research was initiated by - and performed in close cooperation with - the Geomatics Department of the Nederlandse Aardolie Maatschappij (NAM). Both authors also wish to express their respect to their preceptor, Henk de Heus, who deceased suddenly at the beginning of this research project.

REFERENCES

Barends, F.B.J., Brouwer F.J.J., & Schröder F.H. (eds.) (1995). *Land Subsidence, Proceedings of the Fifth International Symposium On Land Subsidence (FISOLS)*, Balkema, Rotterdam.

Heus, H.M. de, P. Joosten, Martens M.H.F., & Verhoef H.M.E. (1995). Strategy for the analysis of the Groningen gas field levellings - an overview. In: *Land Subsidence, Proceedings FISOLS*, Barends, Brouwer & Schröder (eds.), pp. 301-311.

Heus, H.M. de, Martens M.H.F., & van der Marel H. (1999). Re-weighting of GPS baselines for vertical deformation analysis. *Proceedings of the 22nd General Assembly of the IUGG*, Birmingham.

Houtenbos, A.P.E.M. (2000). The quantification of subsidence due to gas-extraction in the Netherlands. In: Land Subsidence - Vol. 1, Proc. *Sixth International Symposium on Land Subsidence (SISOLS)*, September 25-29, 2000, Ravenna, Italy, Eds. L. Carbognin et al.

Krijnen, H. & de Heus H.M. (1995). Application of GPS with sub-centimeter accuracy for subsidence monitoring. In: *Land Subsidence, proceedings FISOLS* Barends, Brouwer & Schröder (eds.), pp.333-344.

Verhoef, H.M.E. & de Heus H.M. (1995). On the estimation of polynomial break-points in the subsidence of the Groningen gas field. *Survey Review*, **33** (555), pp. 17-31.

LAND SUBSIDENCE - Vol. II
Proceedings of the Sixth International Symposium on Land Subsidence
Ravenna / Italy / 24-29 September 2000

THREE DIMENSIONAL SIMULATION OF SUBSIDENCE DUE TO THE GAS PRODUCTION IN THE BARBARA FIELD AND COMPARISION WITH FIELD DATA

W. Palozzo[1(*)], G. Cassiani[2], G. Brighenti[1], and C. Zoccatelli[3]
[1]*Dipartimento di Ingegneria Chimica, Mineraria e delle Tecnologie Ambientali, University of Bologna, Italy*
[2]*Department of Environmental Science, Lancaster University, UK*
[3]*Eni, Divisione Agip, Milan, Italy*
[(*)] *currently with Proger SpA*

Abstract

The prediction of subsidence caused by hydrocarbon extraction has become an issue of considerable interest in Italy over the past five years, with special regard to an alleged risk to the Northern Adriatic coast. Numerical modelling is the tool of choice for prediction. However, models are as good as the data they are built upon. Rock compressibility is the chief parameter, and compressibility measurement from laboratory and in-situ tests (using extensimeters and radioactive markers) show considerable disagreement. In this paper a case study is presented where the predictions from a detailed 3-D finite element model are back-analysed and compared with field evidence from the Barbara field, one of the largest field operated by ENI-Agip in the Adriatic sea. The available field data include: (i) radioactive marker measurements, (ii) GPS measurements on several platforms since 1987. The simulations are performed in an uncoupled manner, using finite difference models to simulate reservoir and aquifer pressure history, and utilising a finite element geo-mechanical simulator for subsidence prediction. The results confirm that in-situ measurements provide the correct order of magnitude for compressibility value, which is considerably overestimated by laboratory oedometric tests.

Keywords: Adriatic gas field, finite element modelling, radioactive markers, subsidence, uniaxial compressibility.

1. INTRODUCTION

Subsidence has been under the spotlight of Italian mass media for a few decades, since the early evidence of man-made sinking of Venice historical city centre in late 1960s (Gambolati et al., 1973, 1974). The eastern Po Plain and the Northern Adriatic coastlines are areas of utmost concern because these areas are already slightly above, and sometimes below, mean sea level. Human activities such as the withdrawal of water and gas from the subsurface can further aggravate this already precarious situation, adding a further component to the natural subsidence rate caused by gravitational consolidation of recent sediments. Therefore, in such sensitive areas fluid withdrawal can only be carried out with great care, considering all relevant environmental impacts. As a consequence, much attention has been drawn by a new development proposed by ENI-Agip in the offshore of the Veneto Region. Fifteen gas fields located approximately 7 to 30 km from the coast and bearing gas reserves for about 30 billion standard cubic metres have been identified as the objective of a major project named "Alto Adriatico", for which Environmental Impact Assessment authorisation was requested in 1996. The proposed project had already elicited an alarmed response from the public a few years earlier. The proponent felt that a major effort in terms of time and resources was needed to reassure the media, the public and the local and central government about the impact that the development could have in terms of subsidence of the coast. One of the many activities undertaken to this end was to undergo a thorough examination of the actual subsidence, if any, produced by existing gas fields, operated by ENI-Agip, in areas of similar geological character, and especially in the Adriatic basin. The largest gas field in the Adriatic is the Barbara field, located further South from the proposed new development, but sharing with it the same formation (Asti Sands), albeit in a different setting. This paper will present the most important findings related to the study of the Barbara field in terms of predicted and measured subsidence.

The general objective of this manuscript is to study the subsidence rate caused by gas extraction in the Barbara field, via numerical modelling. The adopted model is a three-dimensional linear elastic heterogeneous soil model, having geo-mechanical parameters that vary as a function of depth. All pressure histories are simulated using state-of-the-art reservoir and aquifer simulators. The specific aim is to examine the following issues:

1. The sensitivity of the predicted subsidence to geo-mechanical and fluid dynamic parameters.
2. The importance of the aquifer influence onto the resulting subsidence.
3. An a-posterior assessment of the available methodologies for measuring the necessary geo-mechanical parameters (in situ logs and laboratory tests).

2. THE BARBARA FIELD

The Barbara Field is the largest of all shallow gas fields in the Adriatic offshore. It is located approximately 60 km from the coast, in a North-East direction from the city of Ancona (Fig. 1).

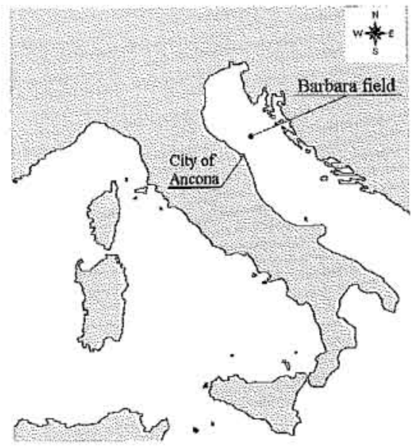

Figure 1. The location of the Barbara gas field.

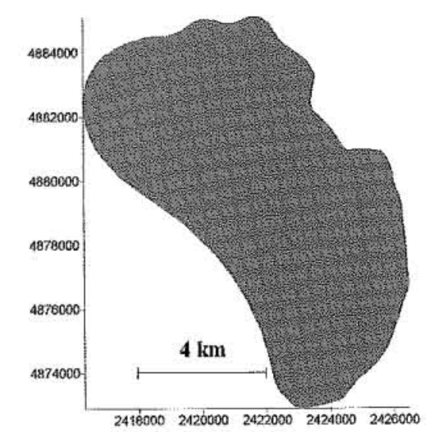

Figure 2. A map of the Barbara field showing the maximum horizontal extent of gas bearing layers.

The gas reservoir is located between 1000 m to 1500 m under sea level, with 400 m of net pay. The geometry of the reservoir is shown in Figure 2. The reservoir rock is made of 15 sand pools, not well cemented, alternated with thin clayey intercalation. The sand layers are hydraulically independent. The thickness of each sand layer varies between 5 m to 30 m. The main reservoir characteristics (formations depth, thickness and starting pressure data) are shown in Table 1.

Level name	*Depth* (m)	*Starting pressure* (bar)	*Thickness* (m)
U	1414	154.4	25
T	1404	157.9	10
S	1383	157	20
R	1351	152.6	26
Q	1330	148.8	10
O	1275	136.7	8
MN	1233	127.2	10
I	1201	124.5	15
H	1191	121.6	10
F	1159	119.1	5
DE	1159	119	24
C	1124	115.1	15
A	1093	110.8	32

Table1. Barbara reservoir characteristics.

The Barbara field has produced since early 1980s a considerable portion of the gas extracted in all the Italian fields. The production curve in thousands of standard cubic metre per year is shown in Figure 3.

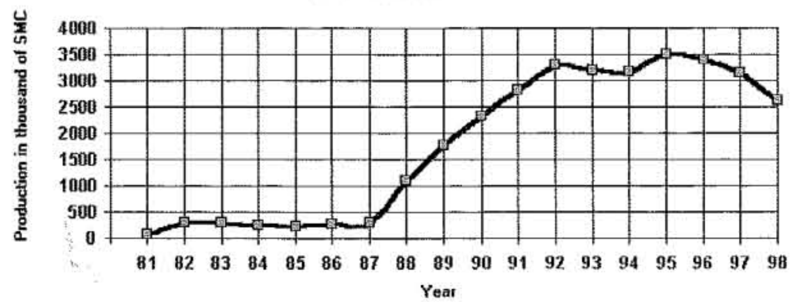

Figure 3. Production rates from the Barbara field (1981-1998)

3. AVAILABLE DATA

In order to carry out the subsidence simulation, the following input data are needed:

1) Geometric data about the reservoir, the surrounding aquifer, the overburden and the underburden.
2) Pressure history data for the reservoir and the lateral aquifer.
3) Geo-mechanical and hydrologic data such as uniaxial compressibility coefficient (C_m) Poisson ratio (v), and permeability (k) or hydraulic conductivity (K).

The geometric information has been taken from geological map, mostly originated by geophysical data. All the alternating sandy / clayey layers have been discretised, so that different properties can easily be assigned to each layer. Two geometric models have been built: a set of 3D plane grids for the fluid flow simulations and a full 3D mesh, for the geo-mechanical simulations. Pressure history in the gas reservoir has been simulated utilising a well established multiphase simulator (Eclipse™). The propagation of this pressure disturbance in the surrounding aquifer was analysed by performing a single phase flow simulation, taking the results from the reservoir simulations as an imposed boundary condition on the aquifer simulation grids. This 'uncoupled' approach to the pressure histories inside and outside the gas reservoir is justified by the fast propagation of pressure variations in the gas phase and its relative insensitivity to water drive mechanisms. The most important geo-mechanical parameter is the *uniaxial compressibility coefficient* (C_m) defined as follows:

$$C_m = \frac{\Delta H}{\Delta P \cdot H} \tag{1}$$

where H is the specimen height, ΔH is the specimen height variation, and ΔP is the pressure variation. This parameter gives a measure of material compressibility under impeded lateral deformation. This is considered to be the prevalent state of stress in depleted reservoirs (Tomasi et al., 1996). It can be measure either through (a) laboratory tests, (e.g., via *oedometric tests*), or (b) in situ well logs, i.e. via a *Radioactive Markers survey* (Bevilacqua et al., 1998). For deep sediments in the Adriatic offshore, the difference in uniaxial compressibility values between in situ and laboratory tests can amount to one order of magnitude (Cassiani & Zoccatelli, 2000). In this study the values of C_m from in-situ tests was adopted. Transmissivity (T) is the most important hydraulic parameter for aquifer simulation. It is expressed as

$$T = K\ h \tag{2}$$

where K is hydraulic conductivity (m/s), and h is the aquifer thickness (m). K is related to intrinsic permeability k by the fluid properties (ρ is fluid density, μ is fluid dynamic viscosity, g is gravitational acceleration):

$$T = K\ h \tag{3}$$

K was estimated from k values from down hole hydraulic tests and is consistent with the values inside the reservoir as used in the *Eclipse™* simulator.

4. NUMERICAL MODELLING

Two sets of numerical simulations were performed:

(a) a *fluid flow model*, where hydraulic head variations were analysed within the aquifer surrounding the reservoir.
(b) a *geo-mechanical model*, where the subsidence resulting from both reservoir and aquifer depletion was computed.

4.1 Fluid flow model

The fluid flow model is based on the well established finite difference code *Modflow*. Two-dimensional simulations were adopted (Fig. 4), one for each permeable sand layer.

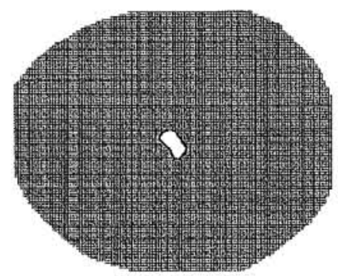

Figure 4. One of the 2-D grids used in the fluid flow simulation.

The objectives of the flow model are: *(i)* to determine the spatial and temporal variations of hydraulic head in the aquifer; and *(ii)* to define the extent needed for the geo-mechanical subsidence model, by considering the area with non-negligible pressure depletion. The grid (Fig. 4) has a 90 km radial extension so that the aquifer in practice behaves as infinite. The thickness of each simulated layer is estimated from geophysical well log profiles. The governing equation of ground water flow in an isotropic porous media are defined in terms of (a) fluid continuity equation; (b) Darcy's law; and (c) fluid and rock matrix compressibilities. The 2-D equation governing water flow in a compressible isotropic porous medium reads

$$\frac{\partial}{\partial X}\left(T\frac{\partial H}{\partial X}\right)+\frac{\partial}{\partial Y}\left(T\frac{\partial H}{\partial Y}\right)-Q=S\frac{\partial H}{\partial t} \tag{4}$$

where T and S are, respectively, the *transmissivity* and the *storage coefficient* of the aquifer, Q is the external flux, H is the hydraulic head, t is the time. The main parameters for the simulation are T and S, given by equations (2) and (5):

$$S=\rho\cdot g\ (\alpha+\phi\cdot\beta)\cdot h \tag{5}$$

where ϕ is the porosity, ρ is the water density, α is the rock matrix compressibility, β is the water compressibility, K is the rock matrix hydraulic conductivity, h is the aquifer thickness.

Boundary conditions. The external boundary of all grids has been set up as a Dirichlet boundary condition with fixed head. The internal boundary, corresponding to the water-gas interface, has been modelled as a transient hydraulic head boundary, where the varying head is derived from the gas pressure history in the reservoir, as modelled with the reservoir simulator. It is important to ensure that the amount of water crossing this internal boundary towards the reservoir does not exceed the volume made available in the reservoir itself by gas extraction. Consequently, this boundary has been modelled as a drain, or a third type boundary condition, that can provide a further resistance to flow in addition to having a certain hydraulic head. This resistance parameter has been used to calibrate the water inflow and to match the volume of extracted gas, ensuring that mass balance across the boundary is honoured.

Model calibration. It was achieved by using pressure data from wells drilled in the aquifer. These wells could provide information about pressure only at specific levels and at specific instants in time. However, they provided precious information to constraint the model parameters. It is worth to note that, from this model calibration, only hydraulic diffusivity, i.e. the ratio between transmissivity (T) and storage coefficient (S) could be determined uniquely. Consequently, some subjective judgement had to be resorted to. However, this subjective choice affects only the values of T and S, and not the pressure distribution predicted in the aquifer layers. Permeability values for the different layers are available from the reservoir study. Also, the flow rate towards the reservoir, as calibrated by the choice of the drain resistance

depends on permeability only, and allows for independent evaluation of T and S. An example of calibrated hydraulic head contours using data from well *B71-D*, is shown in Figure 5.

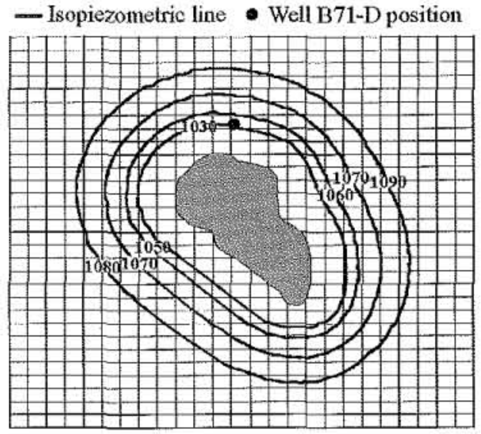

Figure 5. Example of aquifer parameter calibration.

Calibrated parameters. Using permeability data from the reservoir study, and calibrating hydraulic diffusivity to honour pressure data at specific wells, we gather information on the storage coefficient S. S depends on the fluid and porous matrix compressibility values. Consequently, values of uniaxial compressibility (C_m) can also be inferred. Well pressure data are available only in two layers, so the actual calibration was performed for those layers only. Compressibility values for the remaining layers were interpolated (Fig. 9).

Results: The results of the aquifer fluid flow simulation are shown in the Figure 6, for two of the simulated layers. The outer contour line holds the initial value of pressure for the layer. Therefore all the pressure depletion is contained within the range of this outer contour.

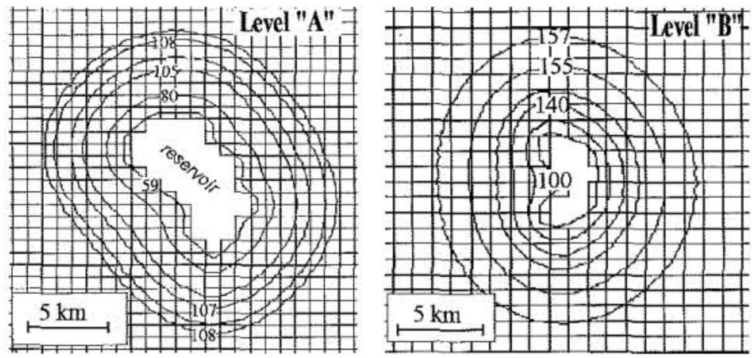

Figure 6. Pressure (bar) in 1998 from simulations of layers A and B.

4.2. Geomechanical Simulation

Geometric model. The geo-mechanical analysis has been performed by the 3D FEM code *Dynaflow* (Prevost, 1992).The 3D mesh (Fig. 7) was created from a set of geological maps showing the top and the bottom of each reservoir layer. The mesh has 9262 nodes and 17642 6-node wedge elements. The mesh is centred on the reservoir and include 30 km of the adjacent aquifer in radial direction. The total area covered by the model is about 2826 km^2.

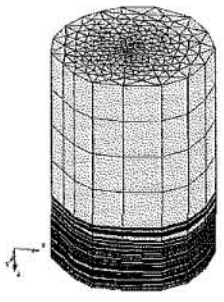

Figure 7. 3-D mesh.

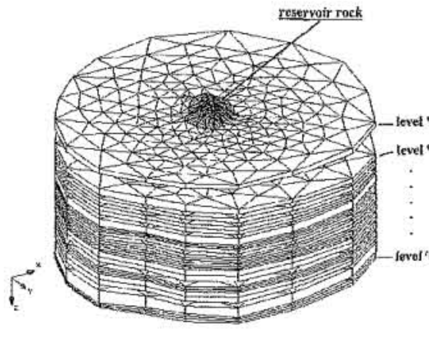

Figure 8. Reservoir levels.

The geometric model discretises the overburden (from 70 m to 1040 m deep), all the reservoir pools (from 1040 m to 1450 m) and the underburden (from 1450 m to 1550 m). 31 different element groups have been created: 15 for the rock reservoir layers, 14 for the thin clayey formations, 1 for the overburden and 1 for the underburden. All materials are assumed to be linear-elastic with the compressibility coefficient (C_m) decreasing with depth.

Boundary conditions. Free displacements have been assumed for all the nodes of the mesh except for the base. No constraint to the lateral boundary nodes has been used. By means of some simulation tests it has been proven that no interference from the boundary is detectable.

Parameters used. Pressure histories from aquifer and reservoir simulations were interpolated and attached to the elements of the geo-mechanical mesh for each time step. In Figure 8, the central part of the mesh (the grey zone) corresponds to where pressure history is taken from the reservoir simulation, while in the rest of the mesh (the aquifer zone) pressure histories come from the aquifer flow simulations. The chief geo-mechanical parameter is uniaxial compressibility (C_m). This parameter was assigned to each element group as a function of the average group depth. The curve used to estimate the C_m value has been taken from field measurements (Fig. 9, continuous curve). Poisson's ratio for all materials was chosen equal to 0.25. For C_m values coming from the surface to 1000 m, extensometer measurements and extrapolation have been used.

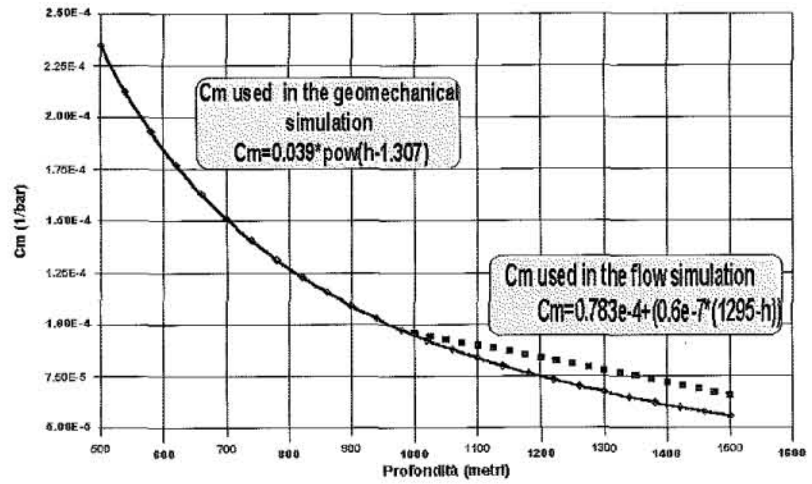

Figure 9. *Cm* value used in the simulations.

For deeper strata (1000 m to 1500 m), radioactive markers results have been adopted. It is interesting to compare (Fig. 9) this compressibility curve coming from in-situ measurements (continuous curve) with compressibility curve calibrated with fluid flow simulation (dashed curve), as explained in section 4.1. This latter curve, albeit slightly different, by and large agrees with the in-situ compressibility values from radioactive markers. Note that laboratory measurements from similar gas fields overestimate C_m of one order of magnitude or more.

Results. Two different simulations have been performed in order to assess to what extent variations of the mechanical parameter C_m with depth can influence the final results. In the first case, a unique value of C_m equal to 5.5x10^{-5} bar^{-1} has been used. This value corresponds on the curve in Figure 9 to a depth of 1250 m, average in the reservoir. With this scenario, the maximum subsidence equals 55 cm at the centre of the reservoir. The performance of the FE simulator was checked for this simulation against a semi-analytical model (Geertsma and Van Opstal, 1973), giving roughly the same results.

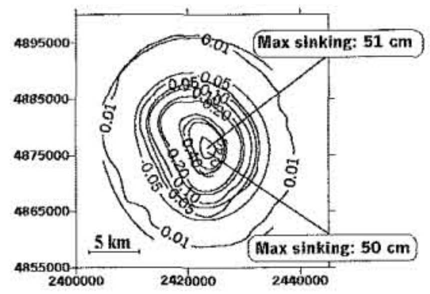

Figure 10. Subsidence resulting from Geertsma and FE model.

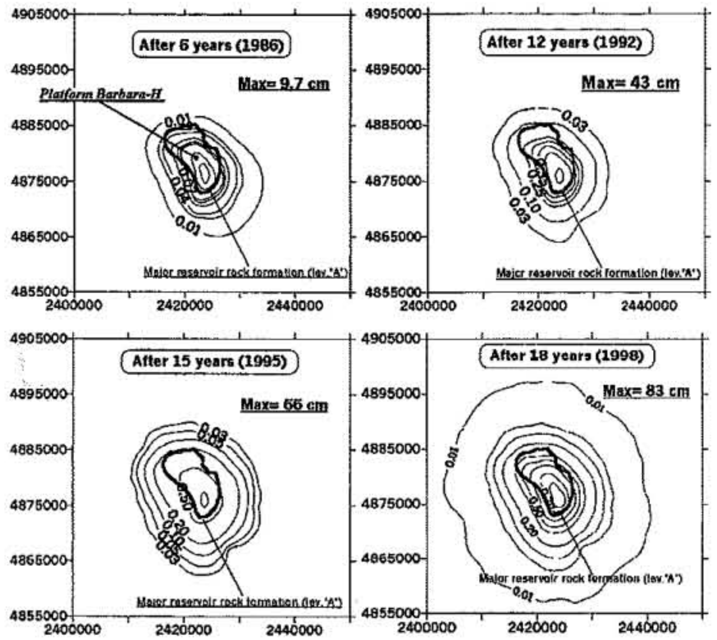

Figure 11. Simulated subsidence in 1986, 1992,1995 and 1998.

In the second simulation, the *Cm* parameter was assumed variable as a function of depth, according to Figure 9. The material hardens with depth. The relevant results are shown in Figure 10. In this scenario, the maximum land subsidence is about 83 cm at the centre of the reservoir, in the 1998 with respect to the 1981 baseline. The 1 cm subsidence contour line lies about 15 km from the reservoir border. Note also in Figure 11 the location of Barbara-H platform, where ENI-Agip has taken GPS measurements for a number of years, and recently has installed a continuous GPS system. Data from this system will allow a further calibration of the FE model results shown in Figure 12.

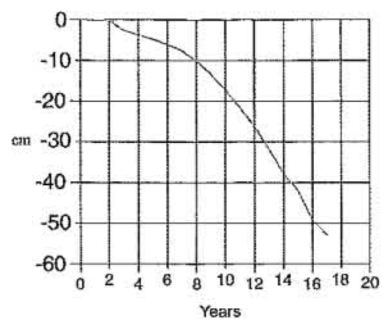

Figure 12. Simulated subsidence of platform Barbara-H

5. CONCLUSIONS

The subsidence values predicted by numerical modelling for the Barbara gas field are rather small. Indeed, the Barbara reservoir is the largest gas field in the Adriatic Sea, and one of the shallowest. Pressure decline is also substantial, reaching 60% of the original static pressure. The maximum simulated subsidence value is about 80 cm in 17 years. This value is within the range of sea tide value (about 1.5 meter) and it is therefore likely to pass unnoticed in the real world. Also, the 1 cm subsidence isoline lies about 15 km from the boundary of the field, and more than 40 km from the coast (Fig. 13), thus posing no threat whatsoever in terms of environmental impact.

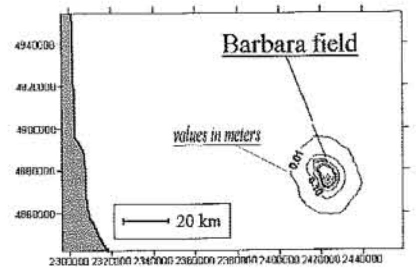

Fig.13. The extent of predicted subsidence caused by the Barbara field.

This study also highlighted the importance of accounting for the effect of the water drive in subsidence prediction. Neglecting the aquifer influence would have halved the predicted subsidence. However, a correct calibration of aquifer models is only possible when pressure data are available from wells actually drilled in the aquifer itself, a rather rare circumstance.

The main scientific result of the modelling exercise is the demonstration that using compressibility values from in-situ measurements (radioactive markers) it is possible to reproduce the likely subsidence history of a gas reservoir. Note that using compressibility values from oedometric tests, the predicted subsidence would be at least five time higher than observed. At the same time, the in-situ compressibility values can honour the fluid dynamic constraints that compressibility poses on water flow in the lateral aquifer.

Acknowledgements

The authors wish to acknowledge the support provided by ENI-Agip in terms of access to facilities, software and field data, and for the permission granted to publish the results of this study.

REFERENCES

Baù, D., Gambolati, G. & Teatini, P. (1999) Residual Land Subsidence over Depleted Gas Fields in the Northern Adriatic Basin, *Environmental and Engineering Geoscience,* V (4), 389-405.

Bevilacqua, N., Cassiani, G., Macini, P & Mesini, E. (1998) Misure di compattazione nel sottosuolo mediante marker radioattivi: tecniche ed applicazioni in Adriatico, In: *Atti Geofluid 98*, Piacenza, 77-92.

Cassiani, G. & Zoccatelli, C. (2000) Subsidence Risk in Venice and Nearby Areas, Italy, owing to Offshore Gas Fields: a Stochastic Analysis, *Environmental and Engineering Geoscience* in press.

Gambolati, G. & Freeze, R.A. (1973) Mathematical Simulation of the Subsidence of Venice, 1. Theory, *Water Resources Research*, **9**(3), 721-733.

Gambolati, G., Gatto, P. & Freeze, R.A. (1974) Mathematical Simulation of the Subsidence of Venice, 2. Results, *Water Resources Research*, **10**(3), 563-577.

Geertsma, J. & Van Opstal, G. (1973) A numerical technique for prediction subsidence above compacting reservoir, based on nucleus of strain concept, *Verhandelingen Kon. Ned. Geol. Mijnbouwk. Gen.*, **28**, 63-78

Prevost, J. (1992) *Dynaflow*: User Guide, Princeton University.

Tomasi, L., Teatini, P. & Gambolati, G. (1996) Studio agli elementi finiti del comportamento meccanico di un giacimento di gas/olio di forma cilindrica in un mezzo poro-elastico omogeneo ed isotropo, Rapporto Tecnico 55, DMMMSA, Università di Padova.

LAND SUBSIDENCE - Vol. II
Proceedings of the Sixth International Symposium on Land Subsidence
Ravenna / Italy / 24-29 September 2000

LAND SUBSIDENCE VS GAS RESERVOIR COMPACTION IN THE NORTHERN ADRIATIC BASIN

Pietro Teatini, Domenico Baú and Giuseppe Gambolati
Dept. of Mathematical Methods and Models for Scientific Applications (DMMMSA)
University of Padova, Via Belzoni 7, 35131 Padova, Italy.

Marco Gonella
MED Ingegneria S.r.l.
Riviera Ruzzante 49, 35100 Padova, Italy

Abstract

Land subsidence η above a compacting reservoir is (primarily) related to the gas pore pressure drawdown, the reservoir thickness and burial depth, the areal extent of the depleted volume, and the vertical rock compressibility. Other factors that may influence land subsidence are the stiffness of the overburden and the dynamics of an active aquifer (waterdrive) hydraulically connected to the gas-bearing formation. The present communication addresses the transference of the reservoir compaction c to the land surface for a few typical gas fields of the Northern Adriatic using a three-dimensional finite element analysis of the sedimentary basin. It is shown that the ratio η_{max}/c between the maximum land subsidence and the corresponding reservoir compaction ranges between 0.9 and 0.2 for the shallowest 1000 m deep Chioggia-Mare field and the 3000 m deep Dosso degli Angeli field, respectively. These results hold during the field production life and do not account for land settlement induced by the compaction of the waterdrive surrounding the field.

Keywords: land subsidence, reservoir compaction, rock compressibility, finite elements, Northern Adriatic gas fields.

1. INTRODUCTION

Among the several factors that influence the transference of the reservoir compaction c to the land surface are the burial depth, the areal extent of the reservoir, the stiffness of the overburden and the depletion of a lateral/bottom aquifer. Two of the above factors, *i.e.* the depth and the areal extent of the field, were analyzed by Geertsma (1973) in the simplified setting of a half-space homogeneous porous medium embedding a disk-shaped reservoir using an analytical solution. For shallow gas fields extending over large areas the maximum land subsidence h turns out to be larger than the reservoir compaction because the reservoir bottom subsides too, while for deep small fields the maximum land subsidence is only a fraction of the reservoir compaction. An infinitely rigid basement underlying the field may also affect the relation between land subsidence and reservoir compaction (Van Opstal, 1974).

At present *in situ* measurements of reservoir compaction can be performed by the radioactive marker technique (Mobach and Gusslinko, 1994) and a direct evaluation of the ratio between land settlement and reservoir compaction should be possible. However, the η /c assessment by direct measurements appears quite difficult for the gas fields located in the Northern Adriatic basin since the marker technique is implemented in boreholes drilled through gas fields which exhibit a very complex structure and span a wide range of burial depth (a few hundred of meters). At the same time levelling of the sea bottom is not available. Therefore the only way to assess the relation of interest is through a mathematical computation.

The Northern Adriatic is an example of a normally consolidated and normally pressurized basin (AGIP, 1996), where sediment compressibility decreases with depth z with the rocks becoming stiffer at a larger depth as is usually the case in a normally consolidated sedimentary basin (Chilingarian et al., 1995). In addition, the typical shape of the gas fields in the Northern Adriatic is far from that of a cylindrical reservoir, and generally the presence of an active waterdrive contributes to land subsidence. Consequently, Geertsma's (1973) simple formulation can not be used and a numerical integration, *e.g.* by the finite element method, of the poroelasticity equations governing the physical process is required.

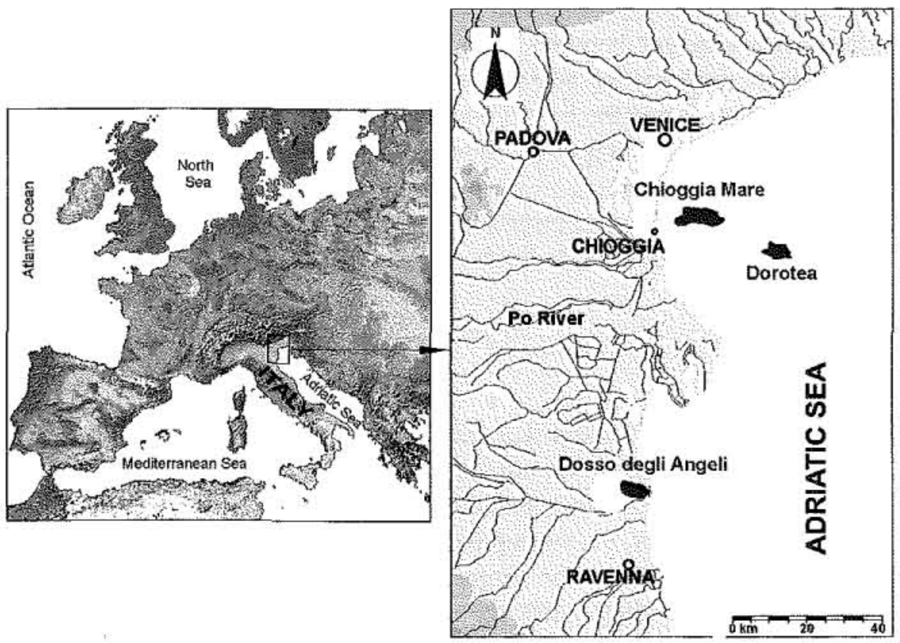

Figure 1. Location of Chioggia-Mare, Dorotea, and Dosso degli Angeli gas fields in the Northern Adriatic basin.

After a brief description of the main features of the Northern Adriatic basin and an overview of the finite element modeling approach implemented to solve the structural problem, the present paper provides the relation between the maximum land subsidence and the corresponding reservoir compaction for Chioggia-Mare, Dorotea, and Dosso degli Angeli, three major gas reservoirs located in the Northern Adriatic (Figure 1) with a different depth of burial and geometric shape. A brief discussion of the influence of the waterdrive is finally given.

2. NORTHERN ADRIATIC BASIN AND GAS FIELDS OF INTEREST

The sedimentary Northern Adriatic basin consists of a sequence of stratified deposits laid down during the Quaternary and the Upper Pliocene in different environments, from continental, lagoonal and deltaic in the upper zone to littoral and marine in the lower one. The basin is a typical case of normally consolidated sequences (AGIP, 1996) made of alternating sands, silts and clays interbedded with all possible mixture of these lithologies, with thickness that sometimes may be a few centimeters only. A detailed knowledge of the sedimentary structure of the area has been obtained with an extensive 3D seismic survey (AGIP, 1996) and log campaigns (sonic - SLS, resistivity - AIT, deepmeter - SHDT) from a number of wells.

Several gas fields have been discovered by ENI-Divisione AGIP, the Italian national oil company, in the northern part of the Adriatic basin, with a depth of burial ranging between 1000 and 4500 m. The gas-bearing formations are mostly located in the pre-Quaternary basement. A typical feature of this basin is that the gas accumulation occurs in multi-pay zone reservoirs, the pay layers consisting of sandy formations without cementative materials, and with the seal above the gas-bearing rocks made from thin beds of shale often less than 1 m thick (Marsala *et. al.*, 1994).

Three major gas reservoirs in this area are Dosso degli Angeli located 20 km north of Ravenna and underlying the Valli di Comacchio lagoon, Chioggia-Mare and Dorotea placed about 10 and 30 km offshore of Chioggia, respectively (Figure 1). Cumulative gas production from the first one amounted to $25 \cdot 10^9$ Sm^3 from 1972 to 1992 at the field abandonment. A production of $5 \cdot 10^9$ and $2.6 \cdot 10^9$ Sm^3, respectively, from the other two gas fields is planned in the near future.

Chioggia-Mare and Dosso degli Angeli are made up of 4 and 3 major pools named *C*, *C2*, *E*, *Ea* and *PL3J*, *PL2A+A1*, *PL2B+B1*, respectively. Dorotea is more complex, being formed by 8 pools located partially in units *C* and *D* of the *Sabbie di Asti* geologic formation. Since the geometric shape of the gas-bearing volumes in the two units is completely different, for the analysis that follows we have elected to consider only the 5 pools (*C*, *C2*, *C3*, *C8* and *C12*) located in unit *C* and characterized by a similar form. A three-dimensional view of the gas pools of the reservoirs is shown in Figure 2 with their main geometric features given in Table 1.

Table 1. Geometric parameters of the study reservoirs.

Reservoir	Pool	Average depth (m)	Gross volume ($\cdot 10^6$ m^3)	Average thickness (m)	Areal extent ($\cdot 10^6$ m^2)
Chioggia Mare	*C*	1071	70.4	4.0	17.6
	C2	1105	267.9	6.3	42.5
	E	1354	108.9	3.5	30.8
	Ea	1362	109.3	3.3	33.1
Dorotea	*C*	1129	27.3	4.7	5.8
	C2	1160	11.6	3.1	3.7
	C3	1172	15.0	3.4	4.4
	C8	1212	34.1	4.7	7.3
	C12	1245	24.1	3.2	7.5
Dosso degli Angeli	*PL3J*	3060	306.9	24.1	12.7
	PL2A+A1	3185	359.6	30.0	12.0
	PL2B+B1	3249	249.5	26.2	9.5

3. MODELING RESERVOIR COMPACTION AND LAND SUBSIDENCE

The poroelastic theory (Biot, 1941) is used to predict reservoir compaction and land subsidence due to gas production with the solution of the poroelasticity equations addressed by the principle of the virtual work written in incremental form.

Numerical experiments by Gambolati et al. (1999) have provided evidence that the deformation of a compacting reservoir is essentially one-dimensional and controlled by the oedometer vertical compressibility c_M:

$$c = c_M \cdot h \cdot Dp$$

where h is the (possibly non-uniform) reservoir thickness and Dp is the pore pressure decline. Moreover, the porous medium can be assumed to behave as a linear elastic body except for the reservoir where the mechanical properties are basically nonlinear due to the large pore pressure drawdown experienced by the gas-bearing rocks. An original three-dimensional approach for land subsidence simulation has been implemented coupling the one-dimensional vertical nonlinear compaction of the reservoir with a three-dimensional linear poroelastic finite element model of the remaining medium. A detailed description of the model in given in Teatini et al. (1998).

The relationships c_M vs depth z in the basin and c_M vs the effective intergranular stress s_z in the reservoir are derived from lab and *in situ* measurements as described by Baú et al. (2000a).

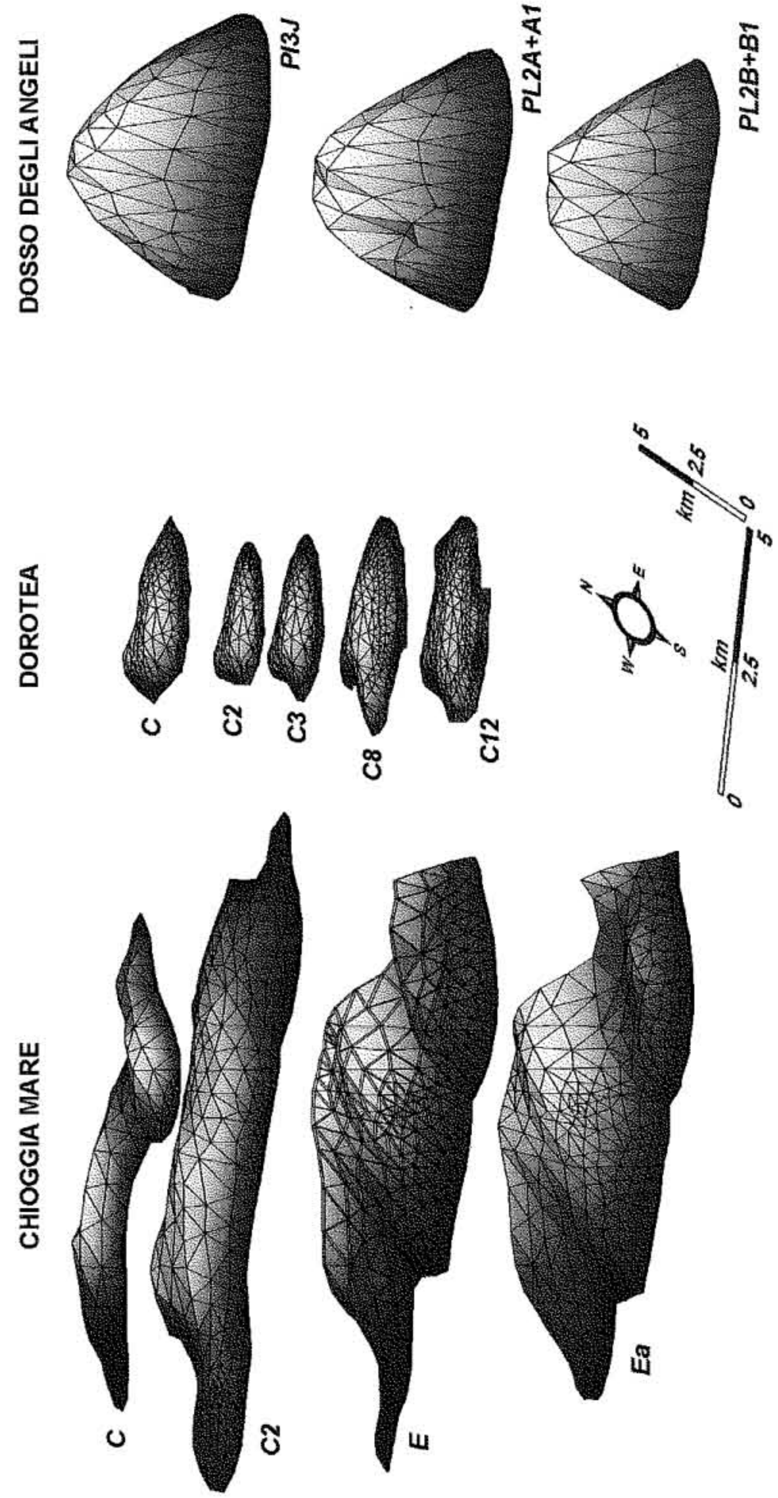

Figure 2. Three-dimensional view of the gas pools of Chioggia-Mare, Dorotea, and Dosso degli Angeli. The vertical exaggeration is 50.

The modeling approach has been applied to simulate the compaction and the land settlement induced by gas production from the three major gas fields mentioned in the previous section. A detailed representation of the geology of the basin is obtained with tetrahedral finite elements. The domain is confined by the ground surface above and a rigid basement assumed to be located at a 20000 m depth, with the three-dimensional mesh made of 53568, 56280, and 40330 nodes for Chioggia-Mare (Baú et al., 2000), Dorotea, and Dosso degli Angeli (Baú et al., 1999), respectively.

4. LAND SUBSIDENCE VS RESERVOIR COMPACTION

Reservoir compaction and related land subsidence over Chioggia-Mare, Dorotea, and Dosso degli Angeli have been simulated during the 13, 20, and 21 year production life of the gas fields, respectively, with the aid of the nonlinear finite element model mentioned in the previous section. Compaction of the waterdrive (and corresponding land settlement) is not accounted for in the present analysis. A short description of the waterdrive influence on subsidence vs compaction is given in the section that follows.

Figure 3 gives the ratio η_{max}/c between the maximum land subsidence and the related reservoir compaction, called subsidence "spreading factor" by Martin and Serdengecti (1984). At each simulated time value, c is computed as the cumulative compaction of the gas pools underlying the location where the largest land subsidence occurs over the field: η_{max}/c ranges between 0.7 and 0.9 for Chioggia-Mare and is practically constant and equal to 0.65 and 0.25 for Dorotea and Dosso degli Angeli, respectively. This is consistent with theory, which suggests that the spreading factor of a compacting reservoir decreases with the depth of burial. Values of η_{max}/c close to 1 are obtained over Chioggia-Mare due to its shallow depth and relatively large areal extent (Table 1). Although Dorotea is located at an average depth similar to that of Chioggia-Mare, the smaller value of η_{max}/c is due to the smaller horizontal size of the reservoir (Table 1). In the Dosso degli Angeli case, η_{max}/c is greatly reduced while the subsidence is spread over an area much larger than the reservoir (Figure 4).

Geertsma's (1973) analytical solution for a cylindrical field is provided by the simple expression:

$$\frac{\eta_{max}}{c} = 2\cdot(1-\nu)\cdot\left(1-\frac{\bar{z}/R}{\sqrt{1+\left(\bar{z}/R\right)^2}}\right) \qquad (1)$$

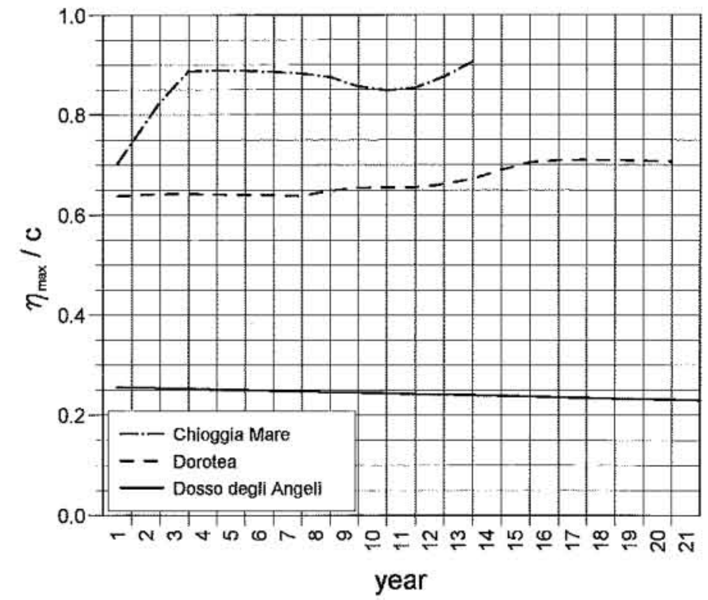

Figure 3. Ratio η_{max}/c between maximum land subsidence and related reservoir compaction vs time as obtained from the nonlinear finite element model during the production life of the Chioggia-Mare, Dorotea, and Dosso degli Angeli gas fields. The contribution from the surrounding waterdrives is not included.

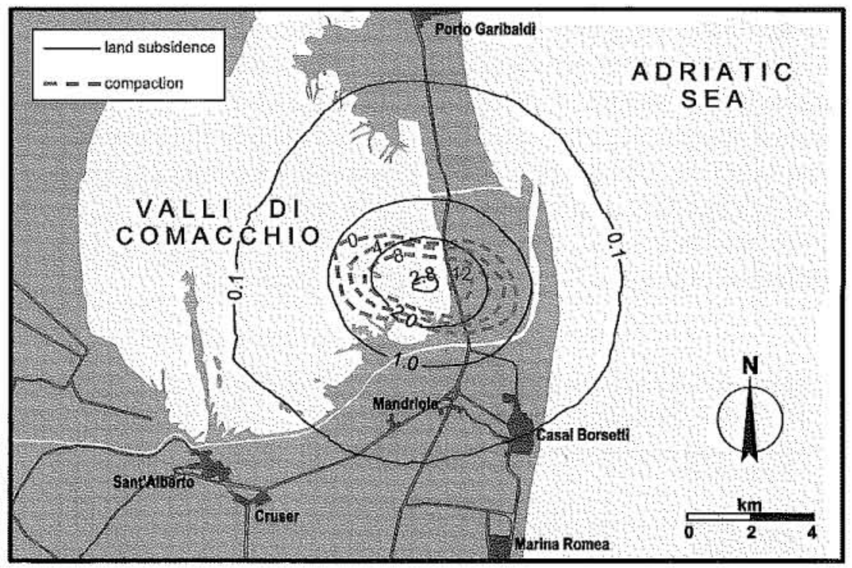

Figure 4. Land subsidence and reservoir compaction (cm) induced by gas production from the *PL3J* pool of the Dosso degli Angeli field. Land subsidence is distributed over an area significantly larger than the trace of the reservoir. The isoline of zero compaction coincides with the trace of the pool.

i.e. the subsidence spreading factor depends on the medium Poisson ratio n, the average burial depth and radius R of the disk-shaped reservoir. A comparison for each reservoir between the numerical results discussed earlier and equation (1) has been performed assuming (Table 2):

- $\nu = 0.3$, *i.e.* the most representative ν value for the Northern Adriatic sedimentary basin as used in the simulation of Chioggia-Mare, Dorotea and Dosso degli Angeli;
- $\bar{z}$ equal to the depth of the gravity center of each gas field;
- R equal to the radius of the cylinder with the cumulative gross volume V and pool thickness H as shown in Table 1.

The outcome in Table 2 (extreme right column) shows a surprisingly good agreement between the present numerical results and Geertsma's simplified solution.

4. INFLUENCE OF SURROUNDING AQUIFER

Although an active aquifer hydraulically connected to a producing gas reservoir plays a favorable role in sustaining the pore pressure in the gas-bearing formations, it may significantly contribute to spread the pressure decline and enlarge the land settlement bowl around the field. The aquifer geometry and its rock hydromechanical properties primarily control waterdrive dynamics and related compaction.

The factor that mainly affects the ratio η_{max}/c is the position of the waterdrive relative to the reservoir:

- with a lateral aquifer there may be an increase of the maximum land subsidence due to the waterdrive compaction, and hence the ratio η_{max}/c grows. This condition occurs for the Dosso degli Angeli field that is confined by a very extensive lateral waterdrive. Baú et al. (2000b), Figure 9, show that the maximum land settlement at the end of the field production life over the center of the reservoir is accounted for by the reservoir and waterdrive compaction in the ratio of 1/3 and 2/3, respectively. Since c in the present analysis denotes the reservoir compaction, η_{max}/c in Figure 3 would increase by about three times if the influence of the aquifer is included in the calculations;

Table 2. Parameters used in Geertsma's (1973) analytical solution (equation 1) to compute the subsidence spreading factor obtained for the gas fields addressed in the present study.

Reservoir	$\bar{z}$ (m)	V ($\cdot 10^6$ m^3)	H (m)	R ($\cdot 10^2$ m^2)	η_{max}/c
Chioggia Mare	1199.9	556.5	17.1	3218.5	0.91
Dorotea	1188.1	112.1	19.1	1366.8	0.48
Dosso degli Angeli	3160.6	916.0	80.3	1905.5	0.20

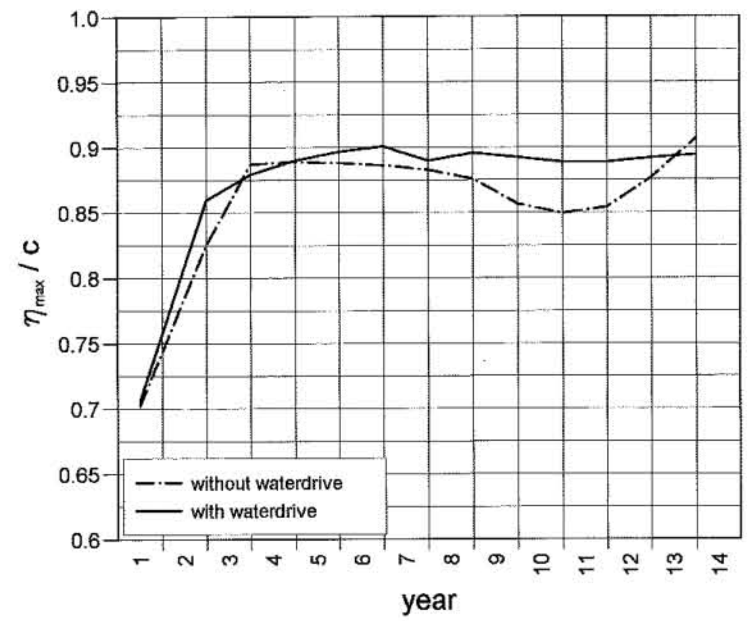

Figure 5. Ratio η_{max}/c during the production life of the Chioggia-Mare reservoir obtained from the nonlinear finite element model with and without the influence of the (bottom) waterdrive.

- with a bottom aquifer the maximum subsidence increase is associated with a similar increase of the thickness of the compacting units and hence η_{max}/c is not expected to change appreciably. Figure 5 shows that for the Chioggia-Mare gas field, which is underlain by a thick bottom aquifer (see Figures 2 and 3 by Baú et al. (2000a)), the latter does not affect the subsidence spreading factor.

5. CONCLUSIONS

The behavior of the ratio between the maximum land subsidence and the compaction of a producing gas reservoir has been investigated by a three-dimensional nonlinear finite element model for three typical reservoirs of the Northern Adriatic basin.

Consistent with theory, the results show that for shallow and large gas fields, such as Chioggia-Mare, the largest land settlement is comparable to the reservoir compaction. By contrast, for the deep Dosso degli Angeli reservoir the maximum subsidence is only a small fraction (about 20%) of the field compaction. The Dorotea gas field shows an intermediate behavior (η_{max}/c=0.65) due to its shallow depth and limited areal extent.

If the lateral aquifer surrounding the reservoir is accounted for, the ratio η_{max}/c may change. A lateral waterdrive yields a significant increase of η_{max}/c, while a thick bottom aquifer does not affect significantly the subsidence spreading factor.

Acknowledgments

The authors are indebted to the Geological Survey of the Municipality of Ravenna, the *Italian Ministero dell'Ambiente, Servizio V.I.A. (Valutazione Impatto Ambientale)*, and ENI - Divisione AGIP for making available and for the permission to publish the data used in the present analysis.

REFERENCES

AGIP (1996) Alto Adriatico. Rapporto di sintesi. Technical report, AGIP S.p.A., Milano.

Baú, D., Gambolati, G., & Teatini, P. (1999) Residual land subsidence over depleted gas fields in the Northern Adriatic basin. *Environmental & Engineering Geoscience*, **V**(4), 389-405.

Baú, D., Gambolati, G., & Teatini, P. (2000a) Can gas withdrawals from Chioggia-Mare field affect the stability of the Venetian littoral?. In: *Proc. of the VI Simposium on Land Subsidence, Ravenna, Italy, September 2000* (ed. by L. Carbognin, G. Gambolati and I. Johnson), La Garangola Publ., this issue.

Baú, D., Gambolati, G., & Teatini, P. (2000b) Waterdrive dynamics and enhanced land subsidence over productive gas fields: Application to Dosso degli Angeli reservoir, Ravenna, Italy. In: *Theory, Modeling and Field Investigation in Hydrology: A Special Volume in Honor of Shlomo P.Neuman's 60th Birthday*, Geological Society of America, In press.

Biot, M. (1941) General theory of three-dimensional consolidation. *J. Appl. Phys.*, **12**(2), 155-164.

Chilingarian, G. V., Rieke, H. H., & Donaldson, E. C. (1995) Compaction of argillaceous sediments. In: *Subsidence Due to Fluid Withdrawal* (ed. by G. V. Chilingarian *et al.*), Developments in Petroleum Science n.41, chapter 2, Elsevier Science B.V, Amsterdam, 47-164.

Gambolati, G., Teatini, P., & Tomasi, L. (1999) Stress-strain analysis in productive gas/oil reservoirs. *Int. J. Numer. Analytic. Methods Geomech.*, **23**, 1495-1519.

Geertsma, J. (1973) A basic theory of subsidence due to reservoir compaction: The homogenous case. *Verhandelingen Kon. Ned. Geol. Mijnbouwk. Gen.*, **28**, 43-62.

Marsala, A. F., Ragazzini, G., Meazza, O., Brignoli, M., & Santarelli, F. J. (1994) Basin scale rock mechanics: Logs and core measurements. In: *EUROCK'94, Rock Mechanics for Petroleum Engineering*, A. A. Balkema, Rotterdam, 105-112.

Martin, J. C. & Serdengecti, S. (1984) Subsidence over oil and gas fields. In: *Man-Induced Land Subsidence, Rev. Eng. Geol.* (ed. by T. Holzer), vol. VI, Geological Society of America, Boulder (CO), 23-34.

Mobach, E., & Gusslinko, H. J. (1994) In-situ reservoir compaction monitoring in the Gröningen field. In: *EUROCK'94, Rock Mechanics for Petroleum Engineering*, A. A. Balkema, Rotterdam, 535-547.

Teatini, P., Gambolati, G., Tomasi, L., & Putti, M. (1998) Simulation of land subsidence due to gas production at Ravenna coastline. In: *CENAS, Coastline Evolution of the Upper Adriatic Sea due to Sea Level Rise and Natural and Anthropogenic Land Subsidence* (ed. by G. Gambolati), Water Science and Technology Library n. 28, Kluwer Academic Publ., 133-150.

Van Hopstal G. H. C. (1974) The effect of base-rock rigidity on subsidence due to reservoir compaction. In: *IIIrd Conf. on Rock Mech.*, Denver (CO), 1102-1111.

CAN GAS WITHDRAWAL FROM CHIOGGIA-MARE FIELD AFFECT THE STABILITY OF THE VENETIAN LITTORAL?

Domenico Baú, Giuseppe Gambolati and Pietro Teatini
Dept. of Mathematical Methods and Models for Scientific Applications (DMMMSA)
University of Padova, Via Belzoni 7, 35131 Padova, Italy.

Abstract

A major threat to the environment as well as the economy of the Upper Adriatic coastal area is the anthropogenic land subsidence expected to occur from the prospective development of 15 gas fields recently discovered by ENI-AGIP, the Italian national oil company, north of the Po river delta in the Adriatic Sea. To evaluate the consequences of gas production on the shoreline stability, and to assist the Minister of Environment in making a decision on the sustainability of the programme, a three-dimensional finite element (FE) model is developed for the simulation of Chioggia-Mare, the largest reservoir in the area and the nearest to the Venetian littoral. Located at a depth of burial between 1000 and 1400 m in lower Pleistocene sedimentary rocks, Chioggia-Mare is planned to produce $5{\cdot}10^9$ Sm^3 of methane during the 13 year production life with a maximum pore pressure drawdown amounting to as much as 80 kg/cm^2 in the deepest pools. The model accurately accounts for the high geological complexity of the field, the extensive lateral/bottom aquifer (waterdrive) and the elasto-plastic deformation of the depleted sands based on *in situ* compaction measurements obtained with the aid of the marker technique. The prediction is extended over 12 years after the wells were shutdown and is performed under a variety of parametric scenarios intended to adequately address the parameter uncertainty. The results from the FE analysis show that under the most pessimistic assumptions the city of Chioggia may subside by 1 cm in 25 years while Venice turns out to be unaffected by a measurable settlement. If the waterdrive depletion is contrasted by two water injection wells drilled between the shoreline and the westernmost point of the reservoir the 1 cm land subsidence isoline moves 5 km offshore with Chioggia expected to rise by about 0.5 cm.

Keywords: coastland subsidence, gas production, waterdrive flux, finite elements, Venice littoral

1. INTRODUCTION

The Minister of Environment has recently initiated a procedure for the assessment of the environmental impact of the gas production planned from 15 new fields in the Upper Adriatic Sea, north of the Po River delta. In collaboration with the VIA (Valutazione Impatto Ambientale) Committee of the Ministry and ENI-AGIP, the Italian national oil company entrusted to the field development, the University of Padova, Dept. of Mathematical Models and Methods for Scientific Applications, has been given the task to develop a mathematical/numerical model for the most reliable prediction of the land subsidence expected to occur over and close to Chioggia-Mare, the largest reservoir in the programme and the nearest to the Venetian littoral (Figure 1), and to assist the Minister in making a decision on the sustainability of the plan.

Recent studies (Gambolati et al., 1996a,b) have shown that an uncoupled model of flow and stress can be safely used to simulate land settlement due to fluid withdrawal as is done in the most common geomechanical practice (Gambolati and Freeze, 1973; Gambolati et al., 1974, 1991, 1998b; Geertsma, 1973; Helm, 1975, 1976; Brutsaert and Corapcioglu, 1976; Harris Galveston Coastal Subsidence District, 1982; Narashiman and Goyal, 1984; Martin and Serdengecti, 1984; Rivera et al., 1991; Doornhof, 1992; Gonella et al., 1998; Baú et al., 1999a). A recent claim by Bolzon and Schrefler (1997) and Schrefler and Simoni (1997) that the capillary effects may play a significant role on compaction with a resulting enhanced and delayed land subsidence has been dismissed on the ground that capillary mechanism does not appear to be of some practical relevance in the sedimentary rocks of the Upper Adriatic basin (Brignoli and Figoni, 1995; Chierici, 1997; Papamichos and Schei, 1998).

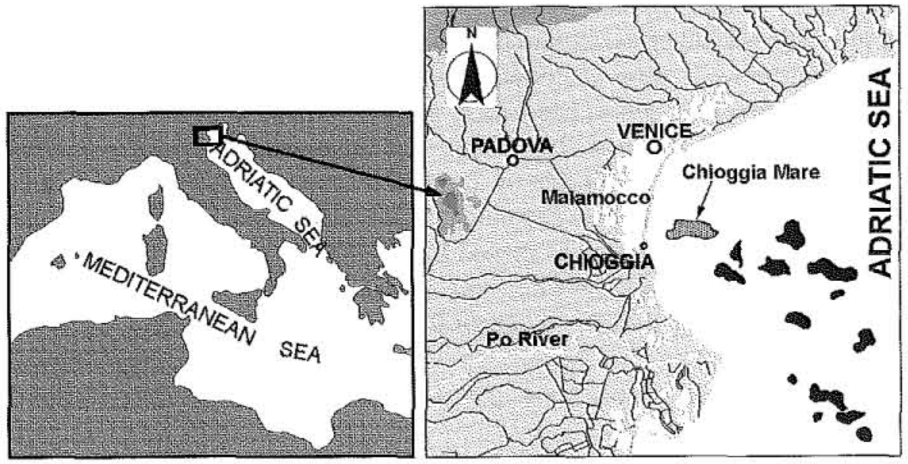

Figure 1. Map of the Upper Adriatic Sea with the trace of the major gas fields.

The greater simplification of the uncoupled approach (relative to the coupled one) allows for a very accurate three-dimensional representation of the complex geology/geometry characterizing Chioggia-Mare and the adjacent lateral/bottom aquifer (waterdrive), and for an effective finite element (FE) solution of the nonlinear equations arising from the elasto-plastic behavior of the compacting sediments and the interaction between reservoir gas dynamics and waterdrive flux during the post-production phase (Baú et al., 1999a). To cope with the uncertainty in the parameters, in particular the rock vertical compressibility c_M, several scenarios are simulated with the most pessimistic c_M values implemented into the model as well. Use is made of the *in situ* c_M below 1000 m depth as obtained from recent *in situ* compaction measurements performed with the marker technique by Schlumberger and Western Atlas in two deep boreholes of the Central Adriatic. To be more conservative in the upper 1000 m the lab c_M, typically larger than *in situ* c_M (van Hasselt, 1992; Holt et al., 1994; NAM, 1995), is used in the calculations. Moreover, other conservative assumptions are made to enhance safety including the gross pay as the reservoir compacting thickness, the lack of recharge from the lateral boundary of the aquifer and the hydraulic vertical connection between the Chioggia-Mare waterdrive and the overlying geologic units *B* and *A* below the coastland. The propagation of the depletion toward the littoral from the westernmost boundary point of Chioggia-Mare, located only 4 km from the coastline, is predicted both without and with two water injection wells intended to create a hydraulic barrier landward, as planned in the Chioggia-Mare development programme submitted by ENI-AGIP to the VIA Committee. The paper is organized as follows. A brief description of the Upper Adriatic basin and Chioggia-Mare field is first provided. Next the three-dimensional FE flow and structural models are outlined along with the constitutive mechanical rock equation used in the study for the vertical compressibility in loading and unloading conditions. Then some representative results of the expected land subsidence over and close to the field are shown and discussed. The paper closes with a set of final remarks and recommendations.

2. UPPER ADRIATIC BASIN AND CHIOGGIA-MARE FIELD

AGIP (1996) has reconstructed the geology of the Upper Adriatic basin on the basis of 2-D and 3-D seismic surveys, lithological, electrical and porosity well-logs, and sedimentology data obtained from core samples of several deep boreholes. Geologically speaking the most important formations underlying the Upper Adriatic, and of major interest for the present study, are the *Argille del Santerno* and the *Sabbie di Asti*. The former is a widespread formation comprising Pliocene and Pleistocene clay and silty clay sequences and represents a hydraulic barrier for the overlying *Sabbie di Asti* in a northeast direction. The *Sabbie di Asti* were laid down during Pleistocene starting 1.3 My BP and consist of a sequence of clayey sands, sandy clays and silts with a smooth transition from one lithology to another. The sands are mostly medium fine to fine-grained clayey sands. In the *Sabbie di Asti* formation several major units may be identified. They have been labeled using the alphabet letters *A* through *O* (AGIP, 1996). Units *A*, *B* and *C* down to 1300 m depth constitute the upper mega sequence, the remaining ones the lower mega sequence. All the units are well separated and, excluding the shallowest unit *A*, pinch out against *the Argille del Santerno* seaward. By distinction units *A*, *B* and *C* are partially intercommunicating below the coastland. This intercommunication might generate a path for the depressurization to propagate upward when the Chioggia-Mare reservoir starts to produce.

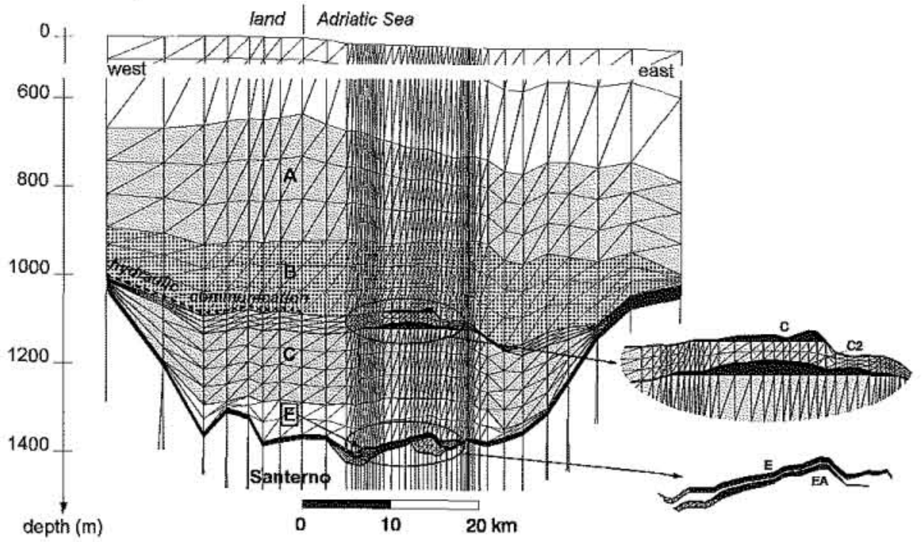

Figure 2. Chioggia-Mare gas field: vertical west east cross-section through pools *C*, *C2*, *E* and *Ea*. The dashed line denotes the interface where hydraulic communication between units *C* and *B* is permitted.

Chioggia-Mare is located between 1000 and 1400 m depth partially in units *C* and *E*. Discovered in 1985, its gravity center is about 10 km far from the city of Chioggia and 25 km from Venice (Figure 1). Chioggia-Mare is made of four pools (*C*, *C2*, *E* and *Ea*) two of which (*C* and *C2*) are formed by a structural trap while *E* and *Ea* pinch out against the *Argille del Santerno*. The cumulative gas produced from the field is estimated to be $5 \cdot 10^9$ Sm^3 during the 13 year production life with a potential maximum pressure drawdown of 78.3 kg/cm^2 in pool *Ea*. Two representative cross-sections of the Chioggia-Mare reservoir are shown in Figures 2 and 3. They have been obtained by intersecting the three-dimensional FE representation of the porous system with a west-east and a south-north plane. Figures 2 and 3 point out the high-

ly variable thickness of each pool and the large size of the waterdrive adjacent to pools *C* and *C2*, which is both a lateral and a bottom aquifer. Pools *E* and *Ea* are surrounded by the lateral aquifer southward only since northward the hydraulic communication is precluded by the Santerno formation. As was mentioned before, unit *C* is assumed to hydraulically communicate with the overlying units *B* and *A* below the coastal area. This is a pessimistic assumption intended to provide the largest possible influence of the waterdrive depletion on the depressurization of units *B* and *A*, hence on the corresponding sediment compaction and ultimately on the stability of the littoral. More detailed maps of both Chioggia-Mare and the Upper Adriatic basin may be found in Gambolati et al. (1997).

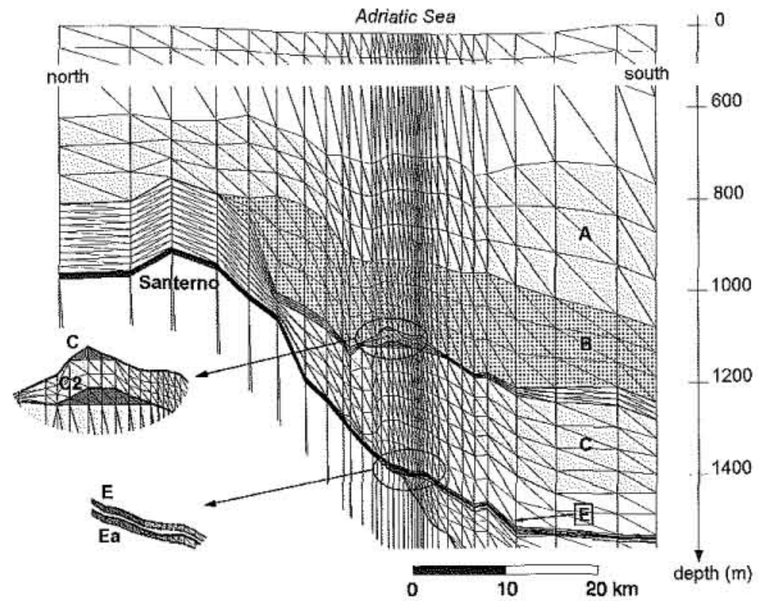

Figure 3. Chioggia-Mare gas field: vertical north-south cross-section through pools *C*, *C2*, *E* and *Ea*.

3. CONSTITUTIVE SOIL EQUATIONS

One of the most important and at the same time uncertain parameter is the vertical soil compressibility c_M which is traditionally obtained from laboratory and triaxial tests performed on sediment samples taken at depth of burial from exploratory boreholes. It is well known that the real c_M is overestimated by the lab c_M. Recently *in situ* compaction measurements by FSMT (Formation Subsidence Monitoring Tool) and CMI (Compaction Monitoring Instrument) have been performed in the deep boreholes Barbara-101 and Amelia-21 with the explored depth interval between 987-1424 m and 2750-3730 m, respectively. Available records span the time periods 1992-1994-1996-1997. The c_M values derived from these measurements have been statistically processed and properly clustered to reduce the operational and instrumental errors (Baú et al., 1999b). Although the *in situ* c_M data dispersion is rather pronounced and more experience with FSMT and CMI is needed to assess the actual deformation of productive rocks (Baú et al., 1999b), nevertheless the marker technique represent an advance in the c_M evaluation with respect to the laboratory practice.

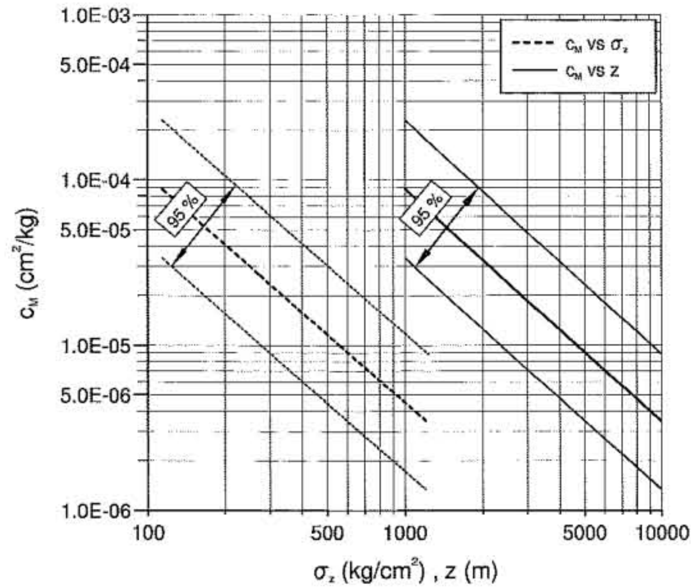

Figure 4. Upper Adriatic basin: vertical soil compressibility c_M vs effective stress σ_z and depth z (below 1000 m) along with the related 95 % confidence intervals.

Figure 4 shows the average c_M profile obtained from the statistical analysis of the *in situ* c_M along with the 95 % confidence interval below 1000 m depth. The average lab c_M in the depth interval 0-1000 m as derived from various sources by Gambolati and Teatini (1998) is given in Baú et al. (1999b, Figure 4).

A compressibility constitutive equation for reservoir unloading is required for predicting soil deformation after field abandonment, *i.e.* 13 years after the inception of development. Sediment unloading-reloading can be described by the swelling index $C_r = C_c / 3$ (AGIP, 1996) where C_c is the rock compression index defined as:

$$C_c = -\frac{de}{d\log(\sigma_z)} \qquad (\sigma_z \geq \sigma_{z_0})$$

with e the void ratio and σz_0 the pre-consolidation stress. For the c_M profile of Figure 4 C_c is variable with σz_0 with an average value of 0.2 and 0.025 for $z \leq 1000$ m and $z > 1000$ m, respectively. In expansion c_M is represented by (Baú et al., 1999a):

$$c_M = \frac{1}{1+e_f - C_r \cdot \log\dfrac{\sigma_z}{\sigma_{zf}}} \cdot \frac{C_r}{\sigma_z \cdot \ln 10} \qquad (\sigma_z \leq \sigma_{zf})$$

where e_f and s_{zf} are the void ratio and the maximum effective stress prior to unloading, respectively. The Upper Adriatic basin is normally consolidated and normally pressurized, at least down to the depth of interest for the present study, so compaction occurs on the virgin compression curve and , the pre-consolidation stress, can be easily calculated using the profile of Figure 4 according to the procedure described in Baú et al. (1999a). The Poisson ration n has been found to vary between 0.25 and 0.35 (Gambolati et al., 1997). The results shown later are obtained with n = 0.3. Finally the permeability of the waterdrive has been assessed by using the balance equation for each pool, see Gambolati et al. (1998a). Accordingly, the horizontal hydraulic conductivity K_h has turned out to be on the order of $1.6 \cdot 10^{-6}$ m/s, $5.5 \cdot 10^{-7}$ m/s and $2.1 \cdot 10^{-7}$ m/s for pools *C+C2*, *E* and *Ea*, respectively, with the anisotropy ratio $K_v/K_h = 0.1$, K_v being the waterdrive vertical permeability. For a thorough discussion of the above hydraulic calibration procedure the reader should refer to Gambolati et al. (1998a).

4. PREDICTED COASTAL LAND SUBSIDENCE

The results shown below are taken from the report handed over to the Minister of Environment (Gambolati et al., 1998a) where a much more complete discussion may be found. The most likely parametric scenario is the one called the basic "Realistic-Conservative" (RC) scenario which combines the average *in situ* rock compressibility (below 1000 m depth) with the conservative assumptions described in the Introduction. The distribution of pore pressure drawdown *Dp* in pools *C*, *C2*, *E* and *Ea* has been predicted by AGIP (1996) during the field production life and processed by Gambolati et al. (1998a). During the post-production period *Dp* is calculated by the use of coupled waterdrive flow and gas dynamic equations (Baú et al., 1999a, 2000).

Other scenarios are the "Optimistic-Conservative" (OC), the "Pessimistic-Conservative" (PC) and the "Conservative-Conservative" (CC) scenarios. In the OC and PC scenarios the lower and upper *in situ* c_M values of the 95% confidence interval, respectively, are used, while the CC scenario implement the lab c_M throughout the simulated depth down to the rigid basement (Baú et al., 1999b, Figure 4). The remaining assumptions are those of the RC scenario. Number 1 and 2 after the short label denote prediction without and with activation of the water injection wells, respectively. Figures 5a and 5b show the expected land subsidence in the 8 different scenarios described above at time t = 13 years (end of Chioggia-Mare production life) and t = 25 years along a profile orthogonal to the coastline crossing the reservoir. Note that the coastland settlement does not exceed 1 cm over 25 years. Also note that the CC scenario increases much the land sinking over the field but induces a coastline sinking smaller than that of the basic scenario.

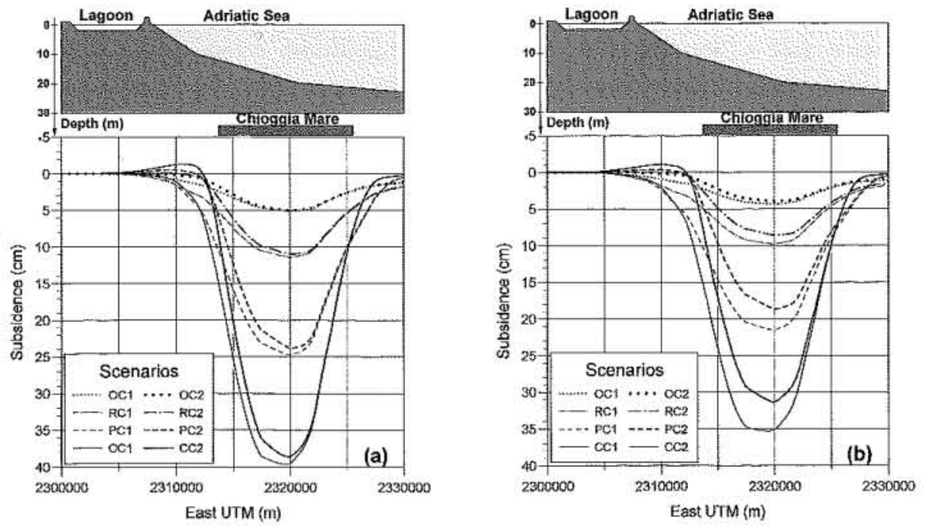

Figure 5. Chioggia-Mare gas field: expected land subsidence profiles along a west-east vertical cross-section through the reservoir (a) 13 years and (b) 25 years after the inception of field production.

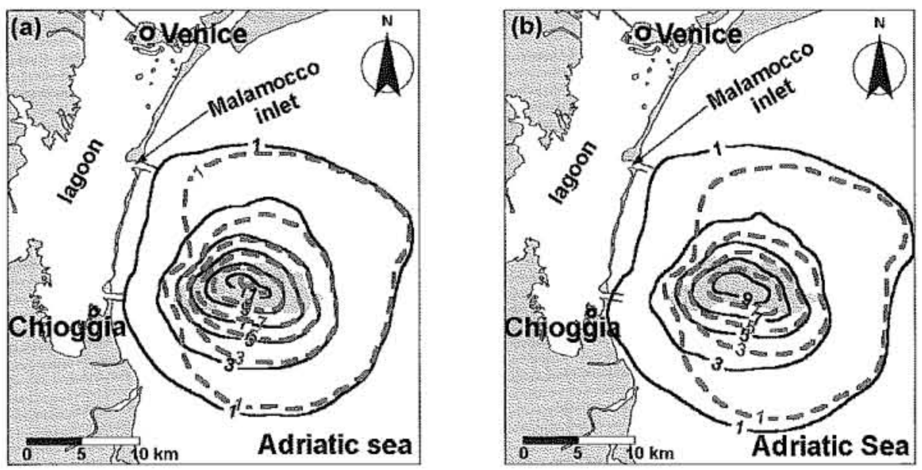

Figure 6. Chioggia-Mare gas field: expected land subsidence (cm) with the RC scenario (a) 13 and (b) 25 years after the inception of field development with (dashed line) and without (solid line) water injection.

Figures 6a and 6b provides the areal distribution of land subsidence for scenario RC at t = 13 and 25 years, respectively. In keeping with the outcome of Figure 6 the maximum settlement over the field occurs after 13 years and range between 5 cm (OC scenario) and 40 cm (CC scenario). Note that the 1 cm isoline is located about 10 km south of the historical center of Venice. Figures 5 and 6 also show how land subsidence modifies when water is injected into the waterdrive of units C and E by the injection wells (dotted lines). It is worth observing that the maximum does not change appreciably while the coastland undergoes a slight rebound on the order of 0.5 cm. This is due to the pore pressure mound generated offshore between the shoreline and the field outline by the injected water. Finally the time behaviour of the settlement of the Chioggia littoral is given in Figure 7. This figure suggests that in the RC scenario the 1 cm value can be regarded as the largest settlement the coastland is expected to experience (even beyond 25 years) because of the Chioggia-Mare field development.

5. CONCLUSIONS

From the discussion of the various simulation scenarios presented above and the inspection of the corresponding results the following conclusive remarks and recommendations can be issued as far as the impact on the coastland of the Chioggia-Mare development is concerned:

1. Stability of the Chioggia littoral is slightly affected by the gas withdrawal with 1 cm land settlement expected to occur over 25 years or more after inception of production.

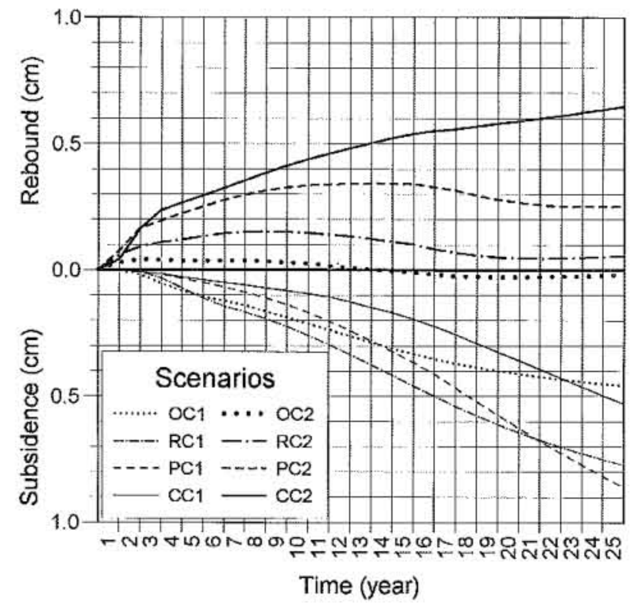

Figure 7. Expected land subsidence vs time at the Chioggia littoral.

2. Venice is not expected to subside because of the Chioggia-Mare field development. The 1 cm settlement isoline does not cross the parallel through the Malamocco inlet with its closest point located 10 km from the city historical center.
3. If water is injected into the waterdrive of units *C* and *E* through two injection wells located between the coastline and the reservoir boundary a hydraulic barrier is generated which opposes effectively the propagation of the depletion landward. As a major result the Choggia littoral may rise by 0.5 cm while the sinking over the field remains practically unchanged.
4. The results obtained in the present study are primarily based on the *in situ* compaction measurements performed with FSMT and CMI in the last few years in two deep boreholes of the Central Adriatic. The corresponding values turn out to be much scattered around the measured mean with a large standard deviation. At the same time the ratio between the average *in situ* c_M used in the present analyses and the average lab c_M is approximately equal to 5, *i.e.* twice as much as the ratio reported from similar experiments performed in The Netherlands (van Hasselt, 1992; NAM, 1995). The large data dispersion can be due to instrumental and operational errors as well as to scarcely representative compaction records. More experiences with FSMT and CMI are required to provide a less uncertain evaluation of the actual mechanical rock properties, and hence a more reliable prediction of land subsidence due to the gas production planned from Chioggia-Mare and the other fields of the Upper Adriatic basin.

Acknowledgments

The authors are indebted to the Italian *Ministero dell'Ambiente, Servizio V.I.A. (Valutazione Impatto Ambientale)*, which supported the study, and in particular to Maria Rosa Vittadini, Raffaele Ventresca and Carmela Bilanzone for their active participation. The collaboration from ENI - Divisione AGIP S.p.A. is also gratefully acknowledged.

REFERENCES

AGIP (1996) Alto Adriatico. Rapporto di sintesi. Technical report, AGIP S.p.A., Milano.

Baú, D., Gambolati, G., & Teatini, P. (1999a) Residual land subsidence over depleted gas fields in the Northern Adriatic basin. *Environmental & Engineering Geoscience*, **V**(4), 389-405.

Baú, D., Gambolati, G., & Teatini, P. (1999b) Statistical analysis of in situ compaction measurements for anthropogenic land subsidence prediction in the Northern Adriatic basin. In: *Proc. of 5th Conf. Inter. Assoc. Mathematical Geology* (ed. by A.N.S.J. Lippard and R. Sinding-Larsen), Vol. 1, Tapir Publ., 299-304.

Baú, D., Gambolati, G., & Teatini, P. (2000) Under-relaxed iterations for coupled finite element solution to gas and water dynamics in depleted reservoirs. In: *Proc. of Computational Methods in Water Resources XIII*, (ed. by L.R. Bentley et al.), Vol. 1, A.A. Balkema, 195-200.

Bolzon, G. & Schrefler, B. A. (1997) Compaction in gas reservoir due to capillary effects. In: *Computational Plasticity, Fundamentals and Applications, Proceedings of COMPLAS V - Fifth International Conference on Computational Plasticity* (ed. by D.R.J. Owen *et al.*), Barcelona, March 1997, CIMNE Publ., 1625-1630.

Brignoli, M. & Figoni, A. (1995) Compattazione in Alto Adriatico: esame critico dei dati edometrici presenti in AGIP. Technical report, AGIP S.p.A., Unità LAPO, Milano.

Brutsaert, W. & Corapcioglu, M. Y. (1976) Pumping of aquifer with visco-elastic properties. *ASCE J. Hydraul.*, **102**(11), 1663-1675.

Chierici, G. L. (1997) Nota sulla pubblicazione di B.A. Schrefler e L. Simoni "La subsidenza sopra i giacimenti di gas naturale". AGIP S.p.A., Milano, 43 pp.

Doornhof, D. (1992) Surface subsidence in The Netherlands: the Groningen gas field. *Geologie en Mijnbouw*, **71**, 119-130.

Gambolati, G. & Freeze, R. A. (1973) Mathematical simulation of the subsidence of Venice. 1. Theory. *Water Resour. Res.*, **9**(3), 721-733.

Gambolati, G. & Teatini, P. (1998) Numerical analysis of land subsidence due to natural compaction of the Upper Adriatic Sea basin. In: *CENAS, Coastline Evolution of the Upper Adriatic Sea due to Sea Level Rise and Natural and Anthropogenic Land Subsidence* (ed. by G. Gambolati), Water Science and Technology Library n. 28, Kluwer Academic Publ., 103-131.

Gambolati, G., Gatto, P., & Freeze, R. A. (1974) Mathematical simulation of the subsidence of Venice. 2. Results. *Water Resour. Res.*, **10**(3), 563-577.

Gambolati, G., Ricceri, G., Bertoni, W., Brighenti, G., & Vuillermin, E. (1991) Mathematical simulation of the subsidence of Ravenna. *Water Resour. Res.*, **27**(11), 2899-2918.

Gambolati, G., Putti, M., & Teatini, P. (1996a) Coupled and uncoupled poroelastic solutions to land subsidence due to groundwater withdrawal. In: *ASCE Engineering Mechanics Conference, Mini Symposium on Poroelasticity* (ed. by : Y.K. Lin and T.C. Su), ASCE, New York, 483-486.

Gambolati, G., Putti, M., & Teatini, P. (1996b) Land subsidence. In: *Hydrology of Disasters* (ed. by V. P. Singh), Kluwer Academic P.C., Dordrecht, chapter 9, 231-268.

Gambolati, G., Teatini, P., & Tomasi, L. (1997) Convenzione tra il Ministero dell'Ambiente e l'Universitá degli Studi di Padova per la realizzazione di un modello matematico previsivo degli eventuali effetti di subsidenza connessi alla coltivazione di giacimenti di idrocarburi in Alto Adriatico - Relazione tecnica fase I. Technical Report n. 62, Dept. of Mathematical Methods and Models for Scientific Applications, University of Padova, 55 pp.

Gambolati, G., Teatini, P., Baú, D., & Tomasi, L. (1998a) Convenzione tra il Ministero dell'Ambiente e l'Universitá degli Studi di Padova per la realizzazione di un modello matematico previsivo degli eventuali effetti di subsidenza connessi alla coltivazione di giacimenti di idrocarburi in Alto Adriatico - Relazione tecnica fase III - Rapporto finale. Technical Report 69, Dept. of Mathematical Methods and Models for Scientific Applications, University of Padova, 179 pp.

Gambolati, G., Teatini, P., & Bertoni, W. (1998b) Numerical prediction of land subsidence over Dosso degli Angeli gas field, Ravenna, Italy. In: *Land Subsidence - Current Research and Case Studies (Proceedings of the Joseph F. Poland Symposium on Land Subsidence, Sacramento (CA), October 1995)* (ed. by J. Borchers), Star Publ. Co., Belmont (CA), 229-238.

Geertsma, J. (1973) Land subsidence above compacting oil and gas reservoirs. *J. Pet. Technol.*, **25**, 734-744.

Gonella, M., Gambolati, G., Giunta, G., Putti, M., & Teatini, P. (1998) Prediction of land subsidence due to groundwater withdrawal along the Emilia-Romagna coast. In: *CENAS, Coastline Evolution of the Upper Adriatic Sea due to Sea Level Rise and Natural and Anthropogenic Land Subsidence* (ed. by G. Gambolati), Water Science and Technology Library n. 28, Kluwer Academic Publ., 151-168.

Harris Galveston Coastal Subsidence District (1982) *Water Management Study: Phase 2 and Supplement 1*. Houston, Texas, 68 pp.

Helm, D. C. (1975) One-dimensional simulation of aquifer system compaction near Pixley, California. 1. Constant parameters. *Water Resour. Res.*, **11**, 465-478.

Helm, D. C. (1976) One-dimensional simulation of aquifer system compaction near Pixley, California. 2. Stress-dependent parameters. *Water Resour. Res.*, **12**, 375-391.

Holt, R. M., Brignoli, M., Fjær, E., Kenter, C. J., & Unander, T. E. (1994) Core damage effects on compaction behaviour. In: *EUROCK'94, Rock Mechanics for Petroleum Engineering*, Paper SPE/ISRM 28027, A. A. Balkema, Rotterdam, 55-62.

Martin, J. C. & Serdengecti, S. (1984) Subsidence over oil and gas fields. In: *Man-Induced Land Subsidence, Rev. Eng. Geol.* (ed. by T. Holzer), vol. VI, Geological Society of America, Boulder (CO), 23-34.

NAM (1995) Subsidence caused by natural gas production. Report 27600, Nederlandse Aardolie Maatschappij B.V., Assen, Netherlands, 26 pp.

Narasimhan, T. N. & Goyal, K. P. (1984) Subsidence due to geothermal fluid withdrawal. In: *Man-Induced Land Subidence, Rev. Eng. Geol.* (ed. by T. Holzer), vol. VI, Geological Society of America, Boulder (CO), 35-66.

Papamichos, E. & Schei, G. (1998) Characterization of Adriatic soft weak sediments for subsidence studies. Technical Report 33.0693.00/01/98, IKU Petroleum Research, Trondheim, (Norway), 67 pp.

Rivera, A., Ledoux, E., & de Marsily, G. (1991) Nonlinear modeling of groundwater flow and total subsidence of the Mexico City aquifer-aquitard system. In: *Land Subsidence* (ed. by A.I. Johnson), IAHS Publ. no. 200, 44-58.

Schrefler, B. A. & Simoni, L. (1996-1997) La subsidenza sopra i giacimenti di gas naturale. In: *Atti e Memorie, Accademia Patavina di Scienze, Lettere ed Arti*, vol. CIX, 85-113.

van Hasselt, J. P. (1992) Reservoir compaction and surface subsidence resulting from oil and gas production. *Geologie en Mijnbouw*, **71**, 107-118.